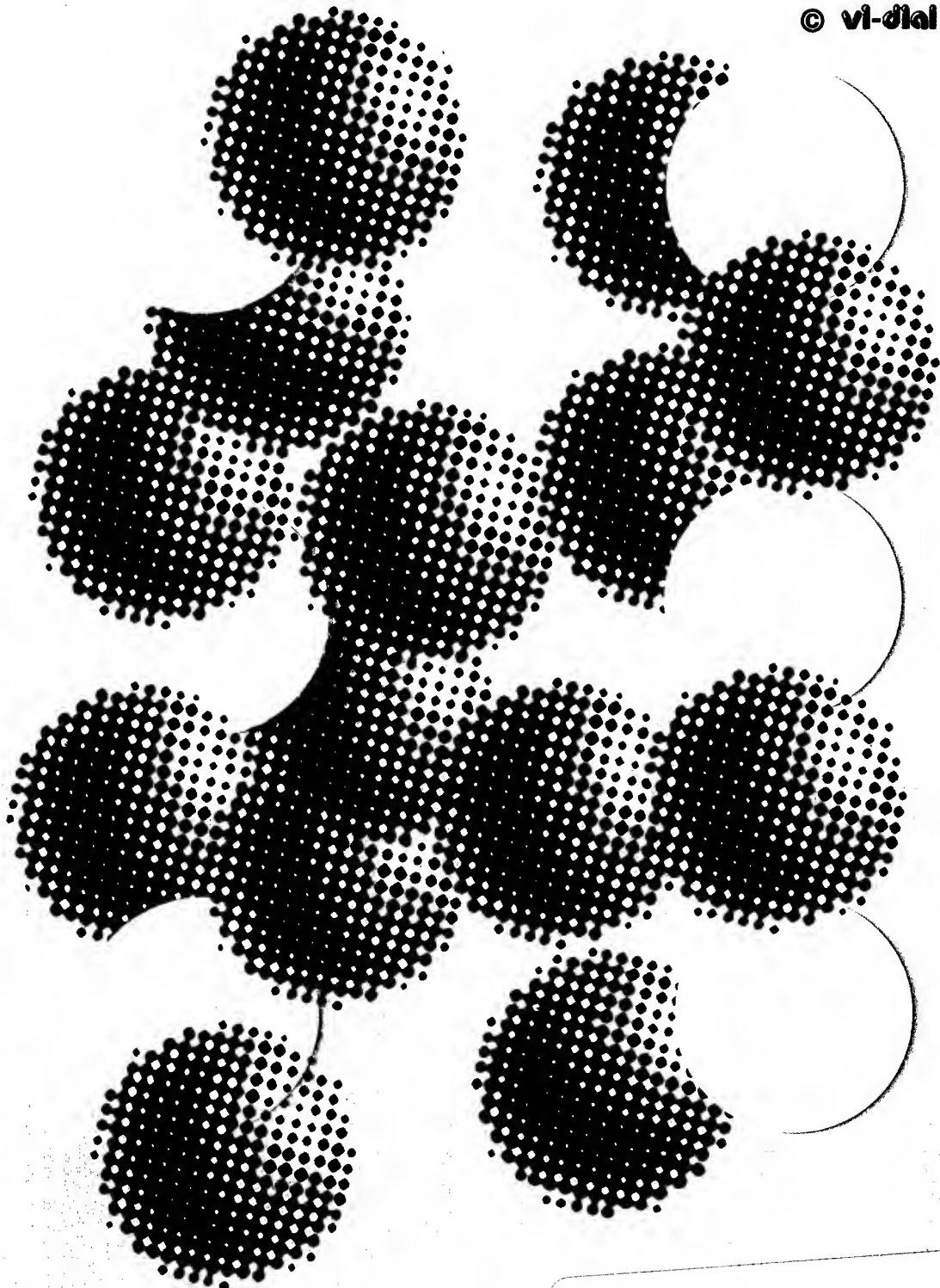


electromagnetic compatibility

© vi-dial



19980924 135



Fourteenth International
Wrocław Symposium and Exhibition
on Electromagnetic Compatibility
June 23–25, 1998

AQ F98-12-2563

The Symposium organizers gratefully
acknowledge the following organizations and
firms for their assistance to and support of this
Symposium:

NATIONAL RADIOPHONIC AGENCY

Kasprzaka 18/20, 01- Warsaw, Poland

TELEKOMUNIKACJA POLSKA S.A.

Świętokrzyska 3, 00-945 Warsaw, Poland

**PLUS GSM – DIGITAL MOBILE
TELECOMMUNICATION NETWORK**

Al. Jerozolimskie 81, 02-001 Warsaw, Poland

POLSKA TELEFONIA CYFROWA Sp. z o.o.

ERA GSM

Al. Jerozolimskie 53, 00-963 Warsaw, Poland

REPORT DOCUMENTATION PAGE

Form Approved OMB No. 0704-0188

Public reporting burden for this collection of information is estimated to average 1 hour per response, including the time for reviewing instructions, searching existing data sources, gathering and maintaining the data needed, and completing and reviewing the collection of information. Send comments regarding this burden estimate or any other aspect of this collection of information, including suggestions for reducing this burden to Washington Headquarters Services, Directorate for Information Operations and Reports, 1215 Jefferson Davis Highway, Suite 1204, Arlington, VA 22202-4302, and to the Office of Management and Budget, Paperwork Reduction Project (0704-0188), Washington, DC 20503.

1. AGENCY USE ONLY (Leave blank)		2. REPORT DATE	3. REPORT TYPE AND DATES COVERED
		29 July 1998	Conference Proceedings
4. TITLE AND SUBTITLE Fourteenth International Wroclaw Symposium and Exhibition on Electromagnetic Compatibility			5. FUNDING NUMBERS F61775-98-WE004
6. AUTHOR(S) Conference Committee			
7. PERFORMING ORGANIZATION NAME(S) AND ADDRESS(ES) Institute of Telecommunications ul. Swojczycka 38 Wroclaw 51-501 Poland			8. PERFORMING ORGANIZATION REPORT NUMBER N/A
9. SPONSORING/MONITORING AGENCY NAME(S) AND ADDRESS(ES) EOARD PSC 802 BOX 14 FPO 09499-0200			10. SPONSORING/MONITORING AGENCY REPORT NUMBER CSP 98-1001
11. SUPPLEMENTARY NOTES			
12a. DISTRIBUTION/AVAILABILITY STATEMENT Approved for public release; distribution is unlimited.		12b. DISTRIBUTION CODE A	
13. ABSTRACT (Maximum 200 words) The Final Proceedings for 14th Int'l Wroclaw Symposium and Exhibition on Electromagnetic Compatibility, 23 June 1998 - 25 June 1998 This is an interdisciplinary conference. Topics include all aspects of EMC theory and practice: antennas and propagation, biological effects, ESD, lightning, EMI reduction techniques, grounding, shielding, and absorption.			
14. SUBJECT TERMS Electromagnetics, C3I, Electronics and Electrical Engineering			15. NUMBER OF PAGES 782
			16. PRICE CODE N/A
17. SECURITY CLASSIFICATION OF REPORT UNCLASSIFIED	18. SECURITY CLASSIFICATION OF THIS PAGE UNCLASSIFIED	19. SECURITY CLASSIFICATION OF ABSTRACT UNCLASSIFIED	20. LIMITATION OF ABSTRACT UL

NSN 7540-01-280-5500

Standard Form 298 (Rev. 2-89)
Prescribed by ANSI Std. Z39-18
298-102

FOURTEENTH INTERNATIONAL
WROCŁAW SYMPOSIUM AND EXHIBITION

**ELECTROMAGNETIC
COMPATIBILITY
1998**

EDITORS:

J.M. JANISZEWSKI

W. MOROŃ

W. SĘGA

Wrocław University of
Technology
Wrocław

Institute
of Telecommunications
Wrocław

Institute
of Telecommunications
Wrocław

Published by the Institute of Telecommunications

All papers are published on responsibility of the authors

© Copyright by Wrocław Symposium on EMC

Applications for reproduction of this book or parts thereof
should be directed to EMC Proceedings Editor

Organizers address:

EMC Symposium, Box 2141
51-645 Wrocław 12, Poland
fax: +4871 728878
e-mail: emc@il.wroc.pl

ISBN 83-901999-6-3

Patron:

M. Zdrojewski
Minister of Posts and Telecommunications of
the Republic of Poland

Organizers:

The Association of Polish Electrical Engineers
The Wrocław University of Technology
The Institute of Telecommunications

Under the auspices of:

Polish Academy of Sciences (PAN)
Committee of Electronics and Telecommunication

Cosponsor:

International Union of Radio Science



Cooperating:

International Union of Radio Science (URSI); International Telecommunication Union Radiocommunication Bureau (ITU-R); Telecommunication Standardization Bureau (ITU-T) and Telecommunication Development Bureau (ITU-D); International Electrotechnical Commission (IEC); International Special Committee on Radio Interference (CISPR) and TC 77 - Electromagnetic Compatibility (IEC TC77); UNESCO International Centre for Theoretical Physics (ICTP); European Broadcasting Union (EBU); European Telecommunications Standards Institute (ETSI); Pacific Telecommunication Council (PTC); Region 8 (Europe) and Poland Section of the Institute of Electrical and Electronics Engineers (IEEE); International Amateur Radio Union (IARU) - Region 1.

Austrian Electrotechnical Association - OeVE (*Austria*); Scientific Technical Society for Radio Technology, Electronics and Electro-communications - BORES (*Belarus*); Union of Electronics, Electrical Engineering and Communications - UEEEC (*Bulgaria*); Association for the Protection against Electromagnetic Interference - EMCAS (*Czech Republic*); Estonian Electronics Society - EES (*Estonia*); Association of Electrical Engineers - AEE (*Finland*); Societe des Electriciens et des Electroniciens - SEE (*France*); Association of Electrical Engineers - VDE (*Germany*); Scientific Society for Telecommunication - HTE (*Hungary*); Association of Electrical and Electronics Engineers - AEI (*Italy*); The Institute of Electronics, Information and Communication Engineers - IEICE (*Japan*); Latvian Society of Radioelectronic and Communication Engineers - AERE (*Latvia*); Lithuanian Society of Informatics, Communications and Electronics - LIREB (*Lithuania*); Association of Electronics and Radio Engineers - NERG (*The Netherlands*); A.S. Popov Scientific Technical Society for Radio Technology, Electronics and Electrocommunications - RORES (*Russian Federation*); Slovak Electrotechnic Society - SES (*Slovakia*); Swedish Society of Electrical and Computer Engineers - SEDIR (*Sweden*); Association of Electrical Engineers - SEV (*Switzerland*); Chamber of Turkish Electrical Engineers - EMO (*Turkey*); Scientific Technical Society for Radio Technology, Electronics and Electrocommunications - UORES (*Ukraine*); Institute of Electrical and Electronics Engineers, EMC Society - IEEE EMCS (*USA*).

Symposium Council:

Chairman:
Prof. W. Majewski, *Poland*

V-chairmen:
Prof. A. Piłatowicz, *Poland*, Dr M. Rusin, *Poland*

Prof. M. Amanowicz, *Poland*; Prof. G. Balodis (AERE), *Latvia*; V. Bulavas (LIREB), *Lithuania*; Dr. M.J. Coenen (NERG), *The Netherlands*; Prof. K. Feser (VDE), *Germany*; G. Goldberg, (SEV), *Switzerland*; Dr. W. Grabowski, *Poland*; J. Grzybowski (SEP), *Poland*; Prof. S. Hahn (URSI-Nat. Com.), *Poland*; Prof. V. Heinrichsen (EES), *Estonia*; Th. Irmer, *ITU-T*; R. Jones, *ITU-R*, P.J. Kerry, *IEC-CISPR*; Dr. W. Kromołowski, *Poland*; K. Kwiecień (PAR), *Poland*; A. Laouyanne, *ITU-D*; P. Laven, *EBU*; Prof. P.E. Leuthold (EMC Symp.), *Switzerland*; Dr. F. Mayer (IEEE-EMCS), *France*; W. Nietyksza, *IARU-Region 1*; A. Peurala (AEE), *Finland*; Prof. V.V. Pilinsky (UORES), *Ukraine*; Dr. A. Radasky, *IEC-ACEC*; Prof. S.M. Radicella, *UNESCO-ICTP*; K.H. Rosenbrock, *ETSI*; P. Rzepka (Polish Telecom), *Poland*; Prof. H.R. Schmeer (EMC Congress), *Germany*; Prof. B. Smólski, *Poland*; Dr. M. Suchański, *Poland*; Dr. J. Svoboda (EMCAS), *Czech Republic*; Dr. B. Szentkuti, *IEC - TC77*; Prof. A. Świt (PAN), *Poland*; Prof. A. Wierzbicki (IŁ), *Poland*; B. Wojtyński (POLKOMTEL), *Poland*; Prof. T. Yoshino (IEICE), *Japan*; Prof. M. Zientalski, *Poland*; Dr. Yu.B. Zubarev (RORES), *Russian Federation*; Dr. E. Żernicki, *Poland*

Scientific Program Committee:

Honorary Chairman:
Prof. F.L. Stumpers, *The Netherlands*

Chairman:
Prof. R.G. Strużak, *Poland*

T. Boe, *Norway*; Prof. P. Degauque, *France*; G. Goldberg, *Switzerland*; Prof. E. Habiger, *Germany*; Prof. M. Hayakawa, *Japan*; Dr. W. John, *Germany*; Prof. A. Karwowski, *Poland*; Prof. H. Mikolajczyk, *Poland*; Prof. E. Nano, *Italy*; R.D. Parlow, *USA*; Dr. A.P. Pavliouk, *Russia*; Prof. G. Varju, *Hungary*; M.C. Vrolijk, *The Netherlands*; Prof. T. Yoshino, *Japan*.

Symposium Organization:

Prof. D.J. Bem (*Symposium Chairman*)

J. Rutkowski (*Co-chairman*)

W. Moroń (*Organizing Chairman*)

Dr. M.J. Grzybowski, Dr. J.M. Janiszewski, H. Ługowska, Prof. J. Malko, Dr. T. Niewodniczański (*Public Relations*), Dr. M. Pietranik, Z. Rabiej, Dr. W. Sęga (*Program Coordinator*), Prof. T.W. Więckowski, Dr. R.J. Zieliński (*Exhibition Coordinator*), Dr. R. Żarko

Author's index

A

- Adzinba N. 491
Ahmed K.M. 306
Alam Chowdhury N.M. 233
Allen S.M. 703
Altay B. 371
Alter L.S. 151
Altman Z. 331
Amanowicz M. 346
Aniserowicz K. 481
Aporovitch V.A. 31
Ari N. 423
Azaro R. 183, 255
Azzarone R. 687

B

- Babjak M. 170
Baquiest L. 657
Bardos P. 376
Baselli R. 193
Bater J.E. 705
Beloshapko A.A. 198
Bem D.J. 46, 188
Beria R. 491
Boe T. 3
Byahun U.M. 98
Bykhovsky M.A. 155

C

- Calamia M. 691
Canavero F. 357
Caorsi S. 183, 255
Catrysse J.A. 407, 411
Cerezzi O. 106
Cesky T. 661
Chaillou S. 331
Chavka G.G. 481
Cherkasin Y.N. 548
Chiba J. 75, 78
Chikai S. 506
Claytonsmith H. 463
Coenen M.J. 737
Cohen D.A. 705
Craig K.H. 639
Czarnywojtek P. 260

D

- D'Amico M.M. 193
Dainelli V. 621
De Schacht J. 419
Delaveau F. 264
Demoulin B. 357
Depueva A. 573, 582
Despres B. 431
Dikmarova L. 159
Dobkowski J.T. 415
Domashenko G.D. 198

- Dowden R.L. 561
Dub P. 220, 545
Dymarkowski K. 436
Dzhala R. 159

E

- Ehmann R. 334
Ene R. 357
Eremenko Z.E. 380

F

- Fedosova N.H. 98
Filcev J. 665
Filipov Y.F. 380
Finney A. 742
Flisowski Z. 500
Fogliati P. 357
Frei S. 486, 491
Fujiwara O. 268, 342, 496
Fukuda S. 88
Furst E. 625

G

- Garcia O R. 441
Gardner R.L. 10
Gazizov T.R. 353
Giachino C. 357
Glumova M.V. 362, 366
Goldberg G. 15, 121
Golebiowski L. 272
Goncharsky V.V. 467
Gonschorek K. 224, 276, 281
Gorbachev A.A. 34
Grygoriev Y.V. 362, 366
Grzebyk W.E. 203
Guimaraes Jr C.A. 441
Gula A. 127
Gulyaev A. 155
Gutschling S. 334

H

- Haga A. 446
Hallon J. 400
Hansen D. 206, 719, 747
Hanelka Z. 127
Harms H. 276
Hartansky R. 400
Hayakawa M. 553, 561
Hebert L. 419
Helmers S. 281
Hes R. 595
Hiroshima Y. 517
Homma M. 396
Hurley S. 703

I

- Inaba H. 83
Ivanov A. 143

J

- Jaekel B. 133
 Janukiewicz J.M. 203
 Jeavons P.G. 705
 Jeromin G. 721
 Jobava R. 491, 511
 Joskiewicz Z.M. 242

K

- Kanazawa M. 506
 Kang I. 496
 Karacagil P. 423
 Karkashadze D. 491, 511
 Karwowski A. 339
 Katulski R. 38
 Kawaguchi K. 268
 Kawamata K. 446
 Kawasaki Z. 566
 Kelly J. 376
 Kerry P.J. 749
 Kharkovsky S. 380
 Kikuchi H. 83, 88
 Kimura M. 396
 Kitagawa T. 561
 Kitaytsev A. 210, 385
 Kliemenko V.G. 325
 Koga H. 175
 Kogut A.E. 380
 Kolakowski J. 162
 Koledintseva M.Y. 210, 385
 Kolodziejki J. 522
 Kolomiitsev O.P. 548
 Kolosowski W. 346
 Kontorovich V.Y. 166
 Kovac K. 400
 Krechla A. 138
 Kresalek V. 388
 Krzysztofik W.J. 41, 46, 51
 Kuca B. 500
 Kucharski A.A. 56, 286
 Kuchumov L. 143
 Kudryashov V.P. 291
 Kunitsyn V.E. 548
 Kunkel G.M. 392
 Kurachi N. 268
 Kuramoto S. 506
 Kutuzov V.V. 380
 Kuwabara N. 517

L

- Lambron O. 264
 Langowski Z. 51
 Larkina V.I. 535, 540, 577
 Lascu M. 295
 Lautenbach D. 767
 Ledbetter M.R. 127
 Leese R.A. 644, 710
 Lenivenko V. 300, 306
 Leontiev N.A. 353
 Leroux E. 357
 Levin B.M. 215
 Lewicki F. 95
 Lin X. 306

- Linares y M.R. 166
 Lisitsyn V.P. 59, 198
 Loyka S.L. 311
 Lugovtsov V.M. 59
 Lutz M. 773

M

- Machczynski W. 260
 Mamchenkov P.N. 155
 Marko M. 170
 Markov V.G. 215
 Matricciani E. 64
 Mayher R.J. 600
 Mazzetti C. 500
 McGuinness S. 712
 Migulin V.V. 540
 Minegishi S. 446
 Miraj-e-Mostafa 300
 Mitchell A.C. 693
 Miyajima K. 451
 Miyoshi M. 175
 Mosin I.V. 198
 Muratov E. 155
 Murav'ev V.V. 98
 Mutoh A. 451

N

- Natale V. 621
 Nichoga V. 159, 220, 545
 Nickolaenko A.P. 553, 557
 Niewodniczanski T. 605
 Nitta S. 451
 Novitskiy A. 143

O

- Obrochta W. 436
 Ohta K. 561
 Ohtsuka M. 586
 Okayama K. 396
 Okayasu R. 517
 Ota H. 396
 Ovchinnikov E.L. 111
 Ozkan M. 247

P

- Pastor R. 657
 Pastorino M. 255
 Pavelka C. 669
 Pavliouk A.P. 609
 Pawelec J.J. 316
 Pawlowski W. 68
 Petrov S. 456
 Petzoldt J. 138
 Pilinsky V.V. 325
 Pipon F. 264
 Pommerenke D. 491, 511
 Pratt R.G. 127
 Probol C. 224
 Przybysz A. 316

Q

- Quilez M. 229

R

- Raffetto M. 255
 Raizer A. 441
 Razinkov O.G. 548
 Reich W. 625
 Rimska Z. 388
 Ristau D. 206
 Riu P. 229
 Riva C. 64
 Rochalska M. 101
 Romanchuk P.I. 111
 Rosenbrock K.H. 23
 Ruf K. 625
 Ruzhin Y.Y. 548, 573, 582

S

- Saha P.K. 233
 Sakaida S. 506
 Santiago E. 723
 Sato M. 506
 Sato R. 396, 446
 Sawdon D. 679
 Schaefer W. 238
 Schuurman J.G. 595
 Scott S.P. 724
 Seker S. 106, 371, 423
 Selivanov M. 155
 Senin B.V. 540, 577
 Sergeeva N.G. 540, 577
 Shagimuratov I.I. 548
 Shimoshio Y. 175
 Shinkov A.A. 385
 Shubitidze P.I. 491, 511
 Silva Martinez F. 229
 Simi A. 687
 Sivyakov B.K. 291
 Siwik A. 127
 Skorupski M. 522
 Skrzypczynski J. 46, 56, 64
 Slowinski M. 605
 Smiesko V. 400
 Smith D.H. 703
 Sorensen T. 376
 Sowa A.E. 188, 527
 Spoelstra T.A. 629
 Stade D. 143
 Stantchev B. 456
 Stantcheva A. 456
 Starostenko V. 362, 366
 Stewart F.M. 697
 Struzak R.G. 648
 Sukhiashvili M. 491
 Svetlichnyi V.A. 31
 Szentkuti B.T. 752

T

- Tabbara W. 331
 Tamelo A. 98

- Tanaka A. 561
 Taran E. 362, 366
 Tikhvinski V.O. 155
 Tofani G. 621
 Tokuda M. 175
 Tomassetti G. 621
 Tominaga T. 517
 Trapp B. 334
 Trufanov L.A. 111
 Trzaska H. 471

U

- Uchida S. 566
 Uczciwek J. 436
 Uryga H. 614
 Ustuner F. 247, 423
 Utiku C. 106

V

- Van den Heuvel J. 712
 Van't Klooster C.G. 621
 Vasenkova L.V. 34
 Verholt C.M. 475, 731
 Volobuev A.N. 111
 Vrolijk M.C. 733
 Vysochin V. 155

W

- Wang J. 342
 Watkins W.J. 703
 Weiland T. 334
 Wiart J. 331
 Wiecek M. 188
 Wieckowski T.W. 242
 Wieser V. 170
 Wille D. 595
 Winnberg A. 634
 Witkowski J.S. 188
 Wizimirski Z. 672
 Wnuk M. 346
 Wyderka S. 272

Y

- Yakovleva I.B. 291
 Yoshino T. 586
 Yurekli A.I. 247

Z

- Zaboronkova T.M. 34
 Zabusov V. 115
 Zajac R.P. 436
 Zaridze R. 491, 511
 Zdunek R. 527
 Zielinski R.J. 320
 Zinkovsky Y. 325

CONTENTS

PLenary PAPERS

T. BOE, <i>Norwegian Post and Telecom. Authority, Oslo, Norway: World Radiocommunications Conference 1997 - Consequences for Europe</i>	3
R.L. GARDNER, <i>Envisioneering, Inc, Fairfax, VA, USA: EM Terrorism - A Real Danger</i>	10
G. GOLDBERG, <i>Past Chairman IEC ACEC, Zurich, Switzerland: Power Quality</i>	15
K.H. ROSENBROCK, <i>ETSI, Sophia Antipolis, France: ETSI - Standards for the Global Marketplace - Radiocommunications</i>	23

II ANTENNAS AND PROPAGATION, EMC ASPECTS

V.A. APOROVITCH, V.A. SVETLICHNIY, <i>Research Institute of Automation Facilities, Minsk, Belarus: Formula for Short-Distances Propagation Loss Estimation</i>	31
A.A. GORBACHEV, T.M. ZABORONKOVA, L.V. VASENKOVA, <i>Radiophysical Research Institute, Nizhny Novgorod, Russian Federation: Features of Electromagnetic Wave Scattering by Systems of Nonlinear Oscillators</i>	34
R. KATULSKI, <i>Technical University of Gdansk, Gdansk, Poland: Antenna Aspect in EMC Analysis of a Mobile Telecommunication</i>	38
W.J. KRZYSZTOFIK, <i>Wroclaw University of Technology, Wroclaw, Poland: Antenna Self-Adapted to the EM-Environment</i>	41
W.J. KRZYSZTOFIK, D.J. BEM, J. SKRZYPczynski, <i>Wroclaw University of Technology, Wroclaw, Poland: Some Results of Long-Term Satellite Radio-Signals Monitoring in Poland</i>	46
W.J. KRZYSZTOFIK, Z. LANGOWSKI, <i>Wroclaw University of Technology, Wroclaw, Poland: Imaging & Suppresion of External Radiation on Outdoor-Field Antenna Test</i>	51
A.A. KUCHARSKI, J. SKRZYPczynski, <i>Wroclaw University of Technology, Wroclaw, Poland: Rain Induced Signal Decrease in Satellite Links</i>	56
V.P. LISITSYN, V.M. LUGOVTSOV, <i>All-Russia Electrotechnical Institute, Istra, Russian Federation: Numerical Hybrid Technique for the Analysis of Transient Electromagnetic Fields Produced by Wire Structures</i>	59
E. MATRICCIANI, C. RIVA, <i>Technical University of Milano, Milano, Italy, J. SKRZYPczynski, Wroclaw University of Technology, Wroclaw, Poland: Study of Scintillation and Simultaneous Rain Attenuation with Itsats Experiment at Wroclaw</i>	64
W. PAWLOWSKI, <i>Technical University of Gdansk, Gdansk, Poland: Propagation Conditions in the VHF and UHF Bands in the Coastal Region of Poland</i>	68

invited session: **Beverage-like Aerials and EMC**

Organizer/Chairman: H. KIKUCHI, Nihon University, Tokyo, Japan
 (URSI Commission E sponsored session)

J. CHIBA, <i>Tohoku Institute of Technology, Sendai, Japan: Effects of Trains on Fields of Wire and Wireless Communication in Tunnels</i>	75
J. CHIBA, <i>Tohoku Institute of Technology, Sendai, Japan: On the Equivalent Circuit for the G-line Above Ground</i>	78
H. KIKUCHI, H. INABA, <i>Nihon University, Tokyo, Japan: Coupling or Transition Between the Zenneck, Sommerfeld, Goubau, and K-Waves</i>	83
H. KIKUCHI, S. FUKUDA, <i>Nihon University, Tokyo, Japan: Relations of TM01, TE01, and HE11 Modes for a Conducting Wire, a Dielectric Rod, and a Dielectric Coated Cylindrical Conductor with Some Network Representations and the Effects of a Ground on Those Modes</i>	88

III BIOLOGICAL EFFECTS OF EM RADIATION

F. LEWICKI, <i>Polish Telecom, Wroclaw, Poland: Exposure of the General Public Around Polish Telecom Transmitting Stations</i>	95
V.V. MURAV'EV, A. TAMELO, U.M. BYAHUN, <i>Belarusian State University of Informatics and Radioelectronics, Minsk, N.H. FEDOSOVA, Belarusian Agricultural Academy, Gorky, Belarus: Investigation of Influence of the Non-heating Millimetre Waves Radiation on the Living Creatures</i>	98
M. ROCHALSKA, <i>Agriculture University, Warsaw, Poland: The Influence of an Alternative Magnetic Field on the Quality of Cereal Seeds</i>	101
S. SEKER, C. UTKU, <i>Bogazici University, Istanbul, O. CEREZCI, Sakarya University, Adapazari, Turkey: Power Absorption in a Multilayered Finite Length Cylindrical Model of Man Exposed by a Plane Wave at Oblique Incidence</i>	106
A.N. VOLOBUEV, E.L. OVCHINNIKOV, L.A. TRUFANOV, P.I. ROMANCHUK, <i>Samara State Medical University, Samara, Russian Federation: The Ionic Paramagnetic Resonance on the Nervous Fibre Membrane</i>	111
V. ZABUSOV, <i>Norilsk Industrial Institute, Norilsk, Russian Federation: Experimental Estimation of Electromagnetic Field Nearby High-Voltage Bus-Bars at Industrial Frequency as the Determining Factor of its Safe Services</i>	115

IV EMC IN POWER SYSTEMS

G. GOLDBERG, <i>Past Chairman IEC ACEC, Zurich, Switzerland: EMC of Signal Transmission on MV and LV Networks</i>	121
Z. HANZELKA, A. SIWIK, A. GULA, <i>University of Mining and Metallurgy, Cracow, Poland, M.R. LEDBETTER, Batelle Pacific Northwest National Lab., Portland, R.G. PRATT, Pacific Northwest Laboratory, Richland, USA: Influence of Compact Fluorescent Lamps (CFLs) on Electrical Power Quality in Distribution Networks - a PELP/DSM Program</i>	127

B. JAEKEL, <i>Siemens AG, Erlangen, Germany: Low Frequency Magnetic Fields Near Energized Components of Power Stations</i>	133
A. KRECHLA, <i>Technical University of Ilmenau, Ilmenau, J. PETZOLDT, University of Rostock, Rostock, Germany: A New Measuring Method for Low Frequency Conducted EMI in a Frequency Range 2 - 9 kHz</i>	138
D. STADE, <i>Technical University of Ilmenau, Ilmenau, Germany, L. KUCHUMOV, A. NOVITSKIY, A. IVANOV, St Petersburg Technical Institute, St Petersburg, Russian Federation: Power Flows in Electrical Power Systems Containing Non-linear and Non-symmetrical Consumers</i>	143

V EMC IN TELECOMMUNICATIONS

L.S. ALTER, <i>Radio Research and Development Institute, St Petersburg, Russian Federation: Intermodulation Interferences Analysis of Land Mobile Cellular Radio System</i>	151
M.A. BYKHOVSKY, A. GULYAEV, P.N. MAMCHENKOV, E. MURATOV, M. SELIVANOV, V.O. TIKHVINISKI, V. VYSOCHIN, <i>Radio Research & Development Institute, Moscow, Russian Federation: Experimental Investigation of Electromagnetic Compatibility Between CDMA Cellular Networks and REE of the Aeronautical Radionavigation Service</i>	155
L. DIKMAROVA, V. NICHOGA, <i>National Academy of Sciences of Ukraine, R. DZHALA, National Academy of Sciences, Lviv, Ukraine: The Influence of Medium and Constructive Parameters on the External Field of Coaxial Cables</i>	159
J. KOLAKOWSKI, <i>Warsaw University of Technology, Warszawa, Poland: Evaluation of Transient Behaviour of Radiocommunication Transmitters Using Short-Time Fourier Transform</i>	162
V.Y. KONTOROVICH, R. LINARES Y M, <i>National Polytechnic Institute of Mexico, Mexico, Mexico: An Approach for EMC Analysis of Local Communication Network</i>	166
M. MARKO, V. WIESER, M. BABJAK, <i>Military Academy, Liptovsky Mikulas, Slovak Republic: Mutual Interference in Systems With Frequency Adaptation</i>	170
Y. SHIMOSHIO, M. MIYOSHI, H. KOGA, <i>Kumamoto National College of Technology, Kumamoto, M. TOKUDA, Kyusyu Institute of Technology, Kyusyu, Japan: A New Calculation Method of LCTL for Balanced Pair Cable with Partial Unbalance</i>	175

VI EMC MEASUREMENTS AND INSTRUMENTATION

R. AZARO, <i>University of Genoa, Genoa, S. CAORSI, University of Pavia, Pavia, Italy: Electromagnetic Field Uniformity Test Using Modulated Scattering Probes</i>	183
D.J. BEM, A.E. SOWA, M. WIECEK, J.S. WITKOWSKI, <i>Wroclaw University of Technology, Wroclaw, Poland: Automated Field Calibration and Immunity Testing in Wroclaw Anechoic Chamber</i>	188
M.M. D'AMICO, R. BASELLI, <i>Technical University of Milano, Milano, Italy: TEM Cell vs. Free Space: Comparision of the Fields Inside Dielectric Spheres</i>	193

G.D. DOMASHENKO, V.P. LISITSYN, A.A. BELOSHAPKO, I.V. MOSIN, <i>All-Russia Electrotechnical Institute, Istra, Russian Federation: Method for Defining the Parameters of Transient Electric Field Sensors Using the Reciprocity Theorem</i>	198
W.E. GRZEBYK, J.M. JANUKIEWICZ, <i>Research & Academic Network in Poland - NASK, Wroclaw, Poland: Measurement of Emissions from Twisted Pair Cables Used in LAN's</i>	203
D. HANSEN, <i>EURO EMC SERVICE</i> , D. RISTAU, <i>EURO EMC SERVICE (EES), Teltow, Germany: Comparing the Measurement Results in a Fully Anechoic Chamber (FALC) to Those on Four Different OATS</i>	206
M.Y. KOLEDINTSEVA, A. KITAYTSEV, <i>Moscow Power Engineering Institute, Moscow, Russian Federation: Gyromagnetic Converter Selectivity Curve Formation for Frequency-Selective Microwave Measuring Devices</i>	210
B.M. LEVIN, V.G. MARKOV, <i>Svyazmorprojekt, St Petersburg, Russian Federation: Calculation of Fields in a Coaxial Chamber with Two Spiral Conductors</i>	215
V. NICHOGA, P. DUB, <i>National Academy of Sciences of Ukraine, Lviv, Ukraine: Measuring Sensors for Investigation of Magnetic Field on the Board of Space Apparatuses</i>	220
C. PROBOL, K. GONSCHOREK, <i>Dresden University of Technology, Dresden, Germany: Development of Field Probes Printed on Substrates for Dosimetric Assessments in the Frequency Range from 1 MHz to 18 GHz</i>	224
M. QUILEZ, F. SILVA MARTINEZ, P. RIU, <i>Universitat Politecnica de Catalunya, Barcelona, Spain: Low Cost Optical Link to Monitor EUT's Susceptibility Tests</i>	229
P.K. SAHA, <i>Bangladesh University of Engineering and Technology, Dhaka, N.M. ALAM CHOWDHURY, Bangladesh Institute of Technology, Gazipur, Dhaka, Bangladesh: Development of Fractional Loop Antenna for EMC Measurement</i>	233
W. SCHAEFER, <i>Hewlett-Packard Company, Santa Rosa, USA: Signal Processing in Radiated EMI Measurements</i>	238
T.W. WIECKOWSKI, Z.M. JOSKIEWICZ, <i>Wroclaw University of Technology, Wroclaw, Poland: Loop Antennas in the EMC Metrology</i>	242
A.I. YUREKLI, <i>TUBITAK Marmara Research Center, Gebze-Kocaeli, M. OZKAN, Bogazici University, Istanbul, F. USTUNER, Marmara Research Center, Gebze-Kocaeli, Turkey: Electromagnetic Compatibility Tests on Hearing Aids</i>	247

VII**EMC PREDICTION, ANALYSIS, MODELLING**

R. AZARO, <i>University of Genoa, Genoa, S. CAORSI, University of Pavia, Pavia, M. PASTORINO, M. RAFFETTO, University of Genoa, Genoa, Italy: Testing Numerical Codes in EMC: a Procedure for Field-Data Computation for PEC Strips and Elliptic Cylinders with Multilayer Coatings</i>	255
P. CZARNYWOJTEK, W. MACHCZYNSKI, <i>Poznan University of Technology, Poznan, Poland: SPICE - Simulation of Voltages Between Sheath and Cable Conductor due to External Excitation</i>	260

F. DELAVEAU, F. PIPON, O. LAMBRON, <i>Thomson-CSF Communications, Gennevilliers Cedex, France: Smart Antennas for Interference Resolution in Cellular Networks</i>	264
O. FUJIWARA, K. KAWAGUCHI, N. KURACHI, <i>Nagoya Institute of Technology, Nagoya, Japan: FDTD Computation Modeling for Electromagnetic Fields Generated by Spark Between Charged Metals</i>	268
L. GOLEBIOWSKI, S. WYDERKA, <i>University of Technology, Rzeszow, Poland: Modelling of Supply Transformers for Transient Overvoltages</i>	272
H. HARMS, <i>Thyssen Nordseewerke GmbH, Emden, K. GONSCHOREK, Dresden University of Technology, Dresden, Germany: Near Field EMC Analysis by a Combination of UTD and MoM</i>	276
S. HELMERS, K. GONSCHOREK, <i>Dresden University of Technology, Dresden, Germany: Determining the Coupling Parameters of Shielded Multiconductor Cables</i>	281
A.A. KUCHARSKI, <i>Wroclaw University of Technology, Wroclaw, Poland: A Body-of-Revolution Model for Calculating Electromagnetic Fields Excited Inside Human Head</i>	286
V.P. KUDRYASHOV, B.K. SIVYAKOV, I.B. YAKOVLEVA, <i>State Technical University of Saratov, Saratov, Russian Federation: Prediction and Analysis of Out-Of-Band Oscillations Spectrum of Power MW- Devices in the Pulse Working Mode</i>	291
M. LASCU, <i>"Politehnica" University Timisoara, Timisoara, Romania: Finite-Element Method Applied in Design of Absorbers</i>	295
V. LENIVENKO, <i>MITEC Ltd, Brisbane, Australia, MIRAJ-E-MOSTAFA, NOKIA Research Center, Tampere, Finland: Engineering Model for Shielding Effectiveness Evaluation</i>	300
X. LIN, K.M. AHMED, <i>Asian Institute of Technology, Pathumthanee, Thailand, V. LENIVENKO, MITEC Ltd, Brisbane, Australia: Optimized Design of Wideband Absorber for 10M EMC Test Chamber</i>	306
S.L. LOYKA, <i>Belorussian State University of Informatics & Radioelectronics, Minsk, Belarus: Detector Simulation with the Use of the Digital Technique</i>	311
J.J. PAWELEC, A. PRZYBYSZ, <i>Military Communication Institute, Zegrze, Poland: Blind Deconvolution of Spurious Signals in Noise</i>	316
R.J. ZIELINSKI, <i>Wroclaw University of Technology, Wroclaw, Poland: EMC Between Aircraft Onboard Electronic Equipment and Satellite Earth Stations</i>	320
Y. ZINKOVSKY, V.G. KLIMENKO, V.V. PILINSKY, <i>Kiev Politechnical Institute, Kiev, Ukraine: Design Procedure of Electromagnetic Fields Shielding Effectiveness</i>	325

invited session: ***Computational Electromagnetics in Wireless Personal Communications***
 Organizer/Chairman: A. KARWOWSKI, *Silesian Technical University, Gliwice, Poland*

S. CHAILLOU, J. WIART, Z. ALTMAN, W. TABBARA, <i>CNET, Issy les Moulineaux, France: Subgridding Scheme in FDTD Method to Improve the Field Resolution</i>	331
R. EHMANN, <i>CST GmbH, S. GUTSCHLING, B. TRAPP, T. WEILAND, Darmstadt University of Technology, Darmstadt, Germany: Numerical Modelling of Mobile Phone Equipment</i>	334

A. KARWOWSKI, <i>Silesian Technical University, Gliwice, Poland: Numerical Modeling of Mobile Hand-Held Cellular Telephones</i>	339
J. WANG, O. FUJIWARA, <i>Nagoya Institute of Technology, Nagoya, Japan: FDTD Computation of Temperature-Rise in the Human Head for Portable Telephones at 900 MHz</i>	342
M. WNUK, W. KOLOSOWSKI, M. AMANOWICZ, <i>Military University of Technology, Warsaw, Poland: Microstrip Antennas on Multilayer Dielectric for Mobile System Communication</i>	346

VIII**EMC RELATED TO PCB AND IC**

T.R. GAZIZOV, N.A. LEONTIEV, <i>Tomsk State University of Control Systems and Radioelectronics, Tomsk, Russian Federation: An Effect of Far-End Crosstalk Compensation in Double-Layered Dielectric PCB Interconnects</i>	353
E. LEROUX, C. GIACHINO, R. ENE, <i>High Design Technology, Torino, F. CANAVERO, Politechnic of Turin, P. FOGLIATI, CSELT, Turin, Italy, B. DEMOULIN, Lille University, Lille, France: Experimental Validation of a Hybrid Method to Predict Differential and Common Mode Radiated Emissions</i>	357
V. STAROSTENKO, M.V. GLUMOVA, E. TARAN, Y.V. GRYGORIEV, <i>Simferopol State University, Simferopol, Ukraine: Influence of Electromagnetic Fields on Integrated Microcircuits</i>	362
V. STAROSTENKO, M.V. GLUMOVA, E. TARAN, Y.V. GRYGORIEV, <i>Simferopol State University, Simferopol, Ukraine: Dynamics of Degradation Processes in Metallization of Integrated Microcircuits Under the Influence of Electromagnetic Fields</i>	366

IX**EMI REDUCTION TECHNIQUES**

B. ALTAY, S. SEKER, <i>Bogazici University, Istanbul, Turkey: Absorption Properties of Simple Shapes</i>	371
J. KELLY, T. SORENSEN, <i>University of Limerick, Limerick, P. BARDOS, Artesyn Technologies, Youghal, Ireland: The Use of SPICE Circuit Simulator to Predict Switched-Mode Power Supply Input Filter Performance</i>	376
S. KHARKOVSKY, Y.F. FILIPOV, Z.E. EREMENKO, V.V. KUTUZOV, A.E. KOGUT, <i>National Academy of Sciences, Kharkov, Ukraine: Shielding of the Dielectric Ball Resonators with Whispering-Gallery Modes</i>	380
A. KITAYTSEV, M.Y. KOLEDINTSEVA, A.A. SHINKOV, <i>Moscow Power Engineering Institute, Moscow, Russian Federation: Filtering of Unwanted Microwave Radiation by Means of Composite Gyromagnetic Thick Films</i>	385
V. KRESALEK, Z. RIMSKA, <i>VUT, Zlin, Czech Republic: Heterogeneous Dielectric Materials with High Permitivity - Electrical Properties of Carbon Fibre - Epoxy Composites in Radiofrequency Range 100 MHz - 1,8 GHz</i>	388
G.M. KUNKEL, <i>SPIRA Mfg Corp, North Hollywood, USA: The Effect of Aging on the Shielding of Electromagnetic Fields</i>	392

- H. OTA, M. KIMURA, *EMC Research Laboratories Co Ltd, Sendai, R. SATO, Tohoku Gakuin University, Tagajo, K. OKAYAMA, M. HOMMA, Tohoku University, Sendai, Japan: Analysis of Microwave Absorption and Material Properties of M-type Hexagonal Ferrites* 396

- V. SMIESKO, K. KOVAC, R. HARTANSKY, J. HALLON, *Slovak University of Technology, Bratislava, Slovak Republic: Use of the Cascade Matrix Technique in Determination of the Performance of Multi-layer Absorbing Structures Based on Ferrite Tiles* 400

invited session: ***Architectural Shielding***

Organizer/Chairman: J.A. CATTRYSSE, KHBO, Oostende, Belgium

- J.A. CATTRYSSE, *Katholieke Industriele Hogeschool, Oostende, Belgium: Architectural Shielding: From Needs into Practical Realisations* 407

- J.A. CATTRYSSE, *Katholieke Industriele Hogeschool, Oostende, Belgium: Measuring Methods for Shielded Rooms: a Practical Approach* 411

- J.T. DOBKOWSKI, *R&D Marine Technology Centre, Gdynia, Poland: Methods of Magnetostatic and Electromagnetic Shielding of Data Protection Compartments* 415

- L. HEBERT, J. DE SCHACHT, *Schlegel Bvba, Gistel, Belgium: Low Cost Shielded Rooms; From Material to Practical Realisations* 419

- P. KARACAGIL, *Marmara Research Center P. K., Gebze-Kocaeli, S. SEKER, Bogazici University, Istanbul, F. USTUNER, Marmara Research Center, Gebze-Kocaeli, Turkey, N. ARI, Ingenieurschule Zurich, Zurich, Switzerland: Theoretical and Experimental Shielding Study of Offices* 423

X EMI SOURCES & COUPLING PATHS TO VICTIM

- B. DESPRES, *France Telecom CNET DMR/RMC, Issy les Moulineaux, France: Microwave Ovens Interference Potential Between 1 & 18 GHz and Associated Standardisation Activities in CISPR* 431

- K. DYMARKOWSKI, W. OBROCHTA, J. UCZCIWEK, R.P. ZAJAC, *R&D Marine Technology Centre, Gdynia, Poland: Electromagnetic Compatibility for Impressed Cathodic Protection Systems (ICCP)* 436

- C.A. GUIMARAES JR, R. GARCIA O, A. RAIZER, *Federal University of Santa Catarina, Florianopolis SC, Brazil: Evaluation of Electromagnetic Interference from Electrosurgical Units* 441

- K. KAWAMATA, *Hachinohe Institute of Technology, Hachinohe, S. MINEGISHI, A. HAGA, R. SATO, Tohoku Gakuin University, Tagajo, Japan: Measurement of Voltage Rising Part due to Gap Discharge in Air Using Distributed Constant Line System* 446

- S. NITTA, A. MUTOH, K. MIYAJIMA, *Tokyo University of Agriculture & Technology, Tokyo, Japan: A Study on Evaluation Method of Showering Noise - From the Viewpoint of the Circuit Malfunction due to Showering Noise in Consideration of the Number of Contact Operations* 451

A. STANTCHEVA, S. PETROV, B. STANTCHEV, <i>Inst for Scientific Research in Telecom, Sofia, Bulgaria: Disturbance Voltage on Mains Terminals of the Equipment Used in Cabled Distribution Systems for Television and Sound Signals</i>	456
---	-----

invited session: ***EMC in Amateur Radio Service***

Chairman: C.M. VERHOLT, *IARU Region 1 EMC WG, Copenhagen, Denmark*
Organizer: H. TRZASKA, *Wroclaw University of Technology, Wroclaw, Poland*

H. CLAYTONSMITH, <i>RSGB, Potters Bar, Herts, UK: Residential Broadband Networking and Concomitant EMC Problems</i>	463
V.V. GONCHARSKY, <i>Safeguard Ukraine Co, Lviv, Ukraine: The EMC Problems Facing Amateur Radio Community in the Post Communist Soviet Republics and their Effect on the Future Growth of the Amateur Radio Population</i>	467
H. TRZASKA, <i>Wroclaw University of Technology, Wroclaw, Poland: EM Environment in Apartment Houses</i>	471
C.M. VERHOLT, <i>IARU Region 1 EMC Advisor & Chairman of EMC WG, Copenhagen, Denmark: EMC Work in IARU</i>	475

XI

ESD, LIGHTNING, EMP

G.G. CHAVKA, K. ANISEROWICZ, <i>Technical University of Bialystok, Bialystok, Poland: Computer Simulation of Action of Lightning Current on the Construction of Antenna Masts</i>	481
S. FREI, <i>Berlin University of Technology, Berlin, Germany: The Occurrence of Transient Fields and ESD in Typical Selected Areas</i>	486
R. JOBAVA, R. ZARIDZE, P.I. SHUBITIDZE, N. ADZINBA, D. KARKASHADZE, R. BERIA, M. SUKHIASHVILI, <i>Tbilisi State University, Tbilisi, Georgia, S. FREI, Berlin University of Technology, Berlin, Germany, D. POMMERENKE, Hewlett Packard, Roseville, USA: Aperture Penetration of Fields Radiated by ESD</i>	491
I. KANG, <i>Korea Maritime University, Pusan, Korea (Rep of), O. FUJIWARA, Nagoya Institute of Technology, Nagoya, Japan: Distance Characteristics of Electromagnetic Fields Caused by ESD Above a Ground Plane</i>	496
C. MAZZETTI, <i>University of Rome "La Sapienza", Rome, Italy, Z. FLISOWSKI, B. KUCA, Warsaw University of Technology, Warsaw, Poland: Hazard for Electronic Systems due to Effects of Lightning Electromagnetic Impulses</i>	500
M. SATO, S. CHIKAI, S. SAKAIDA, <i>NTT Technical Assistance and Support Center, S. KURAMOTO, M. KANAZAWA, NTT Multimedia Networks Laboratories, Tokyo, Japan: Voltages Induced on Switching Equipment Bus Cables by a Direct Lightning Strike</i>	506
P.I. SHUBITIDZE, R. JOBAVA, D. KARKASHADZE, <i>Tbilisi State University, Tbilisi, Georgia, D. POMMERENKE, Hewlett Packard, Roseville, USA, R. ZARIDZE, Tbilisi State University, Tbilisi, Georgia: Computer Simulation of ESD from Object with Surface Resistance</i>	511

XII**IMMUNITY**

Y. HIROSHIMA, R. OKAYASU, T. TOMINAGA, N. KUWABARA, <i>Nippon Telegraph and Telephone Corp., Tokyo, Japan: Method of Calculating Facsimile Image Quality for Immunity Testing</i>	517
J. KOLODZIEJSKI, <i>Institute of Electron Technology, Warszawa, M. SKORUPSKI, Technical-Agriculture Academy, Bydgoszcz, Poland: Effects of Electromagnetic Interferences on Operational Amplifiers</i>	522
A.E. SOWA, R. ZDUNEK, <i>Wroclaw University of Technology, Wroclaw, Poland: The Immunity of Wroclaw Town Hall Tower Fire Detection System to Atmospheric Discharge</i>	527

XIII NATURAL AND MAN-MADE EM ENVIRONMENT

V.I. LARKINA, <i>IZMIRAN, Troitsk, Russian Federation: Low Frequency Emissions Onboard "Intercosmos" Satellites Related to Ring Current Space Variations</i>	535
V.V. MIGULIN, V.I. LARKINA, <i>IZMIRAN, Troitsk, H.F. SERGEEVA, Polar Geophysical Institute, B.V. SENIN, Research Institute of Marine Geophysics, Murmansk, Russian Federation: Research of the Barents-Kara Sea Shelf by Using Low Frequency Emission Satellite Monitoring</i>	540
V. NICHOGA, P. DUB, <i>National Academy of Sciences of Ukraine, Lviv, Ukraine: Local Low-Threshold Inductive Sensors for Investigation of Natural Electromagnetic Environment</i>	545
O.G. RAZINKOV, V.E. KUNITSYN, Y.Y. Ruzhin, O.P. KOLOMIITSEV, Y.N. CHERKASIN, I.I. SHAGIMURATOV, <i>IZMIRAN, Troitsk, Russian Federation: Electromagnetic Space Disturbances Reproduced by the Method of Satellite Radiotomography</i>	548

invited session: ***Terrestrial Electromagnetic Environment***

Organizer/Chairman: M. HAYAKAWA, *University of Electro-communication, Tokyo, Japan*

A.P. NICKOLAENKO, <i>Ukrainian National Academy of Science, Kharkov, Ukraine, M. HAYAKAWA, The University of Electro-Communications, Tokyo, Japan: Electric Fields From Model Lightning Discharges</i>	553
A.P. NICKOLAENKO, <i>Ukrainian National Academy of Science, Kharkov, Ukraine: Spectra and Waveforms of Natural Electromagnetic Pulses in the ELF Range</i>	557
K. OHTA, T. KITAGAWA, A. TANAKA, <i>Chubu University, Aichi, M. HAYAKAWA, The University of Electro-Communications, Tokyo, Japan, R.L. DOWDEN, University of Otago, Dunedin, New Zealand: Mid-Latitude Multi-Path Whistlers Including a Non-Ducted Whistler</i>	561
S. UCHIDA, <i>Institute for Laser Technology, Z. KAWASAKI, Osaka University, Osaka, Japan: Laser Triggered Lightning in Field Experiments</i>	566

invited session: ***EM Emissions in High and Low Frequency Ranges Related to Earthquakes***
 Organizer/Chairman: T. YOSHINO, *Fukui University of Technology, Fukui, Japan*

A. DEPUEVA, Y.Y. RUZHIN, <i>IZMIRAN, Troitsk, Russian Federation: Large-Scale Seismoionospheric Plasma Structures and Anomalous Low-Latitude Whistlers</i>	573
V.I. LARKINA, <i>IZMIRAN, Troitsk, N.G. SERGEEVA, Polar Geophysical Institute, B.V. SENIN, Research Institute of Marine Geophysics, Murmansk, Russian Federation: Electromagnetic Emissions Over Deep Faults of the Lithosphere by Satellite Measurements</i>	577
Y.Y. RUZHIN, A. DEPUEVA, <i>IZMIRAN, Troitsk, Russian Federation: Regional (Local) Manifestation of Seismoprecursor Space Anomalies</i>	582
T. YOSHINO, M. OHTSUKA, <i>Fukui University of Technology, Fukui, Japan: The Anomaly Interference of MF Broadcast Signals in the VLF Receivers by Luxemburg Effects of Ionosphere as One of the Seismogenic Phenomena</i>	586

XIV SPECTRUM MANAGEMENT, ENGINEERING, SHARING, MONITORING

R. HES, D. WILLE, <i>Delft University of Technology, Delft, J.G. SCHUURMAN, University of Maastricht, Maastricht, Netherlands: Management of the Radio Frequency Spectrum: Towards Structured Approach for National and International Policy</i>	595
R.J. MAYHER, <i>SMILES Associates, Edgewater, USA: Review of ITU Spectrum Management Studies</i>	600
T. NIEWODNICZANSKI, <i>Institute of Telecommunications, M. SLOWINSKI, Western Bank, Wrocław, Poland: WueFem - Computer Program for Fast Analysis of Intermodulation in FM Radio Broadcasting in the Cities</i>	605
A.P. PAVLIOK, <i>Radio Research & Development Institute, Moscow, Russian Federation: International Studies of Economic Aspects of Spectrum Management</i>	609
H. URYGA, <i>France Telecom Mobiles, Paris, France: Spectrum Efficiency in Universal Mobile Telecommunication System (UMTS)</i>	614

invited session: ***Co-existence of Radio Services after 2000; a "passive" view***
 Organizer/Chairman: T.A. SPOELSTRA, *CRAF, Dwingeloo, Netherlands*
 (ESF CRAF sponsored session)

V. NATALE, G. TOFANI, <i>CAISMI-CNR, Firenze, G. TOMASSETTI, IRA-CNR, Bologna, V. DAINELLI, OERLIKON-CONTRAVES, Roma, Italy, C.G. VAN'T KLOOSTER, ESTEC, Nordwijk, Netherlands: The Cloud Radar, a Problem for the Passive Users of the mm-wave Spectrum. Tests on Proposed Filtering Structure</i>	621
K. RUF, E. FURST, W. REICH, <i>MAX-PLANCK-Institute of Radioastronomy, Bonn, Germany: At the Limits - Radioastronomical Observations with the Effelsberg 100-m Telescope</i>	625
T.A. SPOELSTRA, <i>Committee on Radio Astronomy Frequencies, Dwingeloo, Netherlands: 10 Years CRAF - An Evaluation</i>	629

A. WINNBERG, <i>Onsala Space Observatory, Onsala, Sweden: New Radio Windows: mm-Wave Astronomy</i>	634
--	-----

invited session: ***Factors and Methods in Radio Frequency Assignment***
 Organizer/Chairman: J. FINNIE, *Radiocommunication Agency, UK*

K.H. CRAIG, <i>Radio Communications Research Unit, Chilton, UK: The Role of Radiowave Propagation Models in Spectrum Planning</i>	639
---	-----

R.A. LEES, <i>University of Oxford, St Giles, UK: Mathematical Methods in Radio Frequency Assignment</i>	644
--	-----

R.G. STRUZAK, <i>Member of ITU RRB, Co-chair of URSI WGE1, Wroclaw, Poland: Computing Tools in Support of RF Spectrum Management</i>	648
--	-----

invited session: ***New Trends in Computer Support for Frequency Spectrum Management***
 Organizer/Chairman: T. CESKY, *European Radiocommunications Office, Copenhagen, Denmark*

L. BAQUIAST, R. PASTOR, <i>CRIL Ingenierie, Meudon la Foret, France: Databases for Frequency Spectrum Management Systems</i>	657
--	-----

T. CESKY, <i>European Radiocommunications Office, Copenhagen, Denmark: New Requirements and Trends in Computer Support for Frequency Spectrum Management</i>	661
--	-----

J. FILCEV, <i>CRC Data spol. s r.o., Ricany, Czech Republic: Component-based Architecture for Frequency Spectrum Management Software</i>	665
--	-----

C. PAVELKA, <i>TESTCOM PRAGUE, Prague, Czech Republic: Experience with Frequency Management Programs Based on a Component Architecture</i>	669
--	-----

Z. WIZMIRSKI, <i>National Radiocommunication Agency, Warsaw, Poland: Deployment of a Large UNIX-Based System at the Polish Administration</i>	672
---	-----

XV EMC MANAGEMENT

D. SAWDON, <i>IBM Global Services, Winchester, UK: Interference Control for IT Installations - a Practical Approach -</i>	679
---	-----

invited session: ***NATO Naval Approaches to EMC***
 Organizers: Capt. R. AZZARONE, *Ministry of Defence, La Spezia, Italy*
 Capt. A. Simi, *NATO HQ, Brussels, Belgium*
 S. Beaton, *NATO HQ, Brussels, Belgium*
 Chairman: R. AZZARONE, *Ministry of Defence, La Spezia, Italy*

R. AZZARONE, <i>Ministry of Defence, La Spezia, Italy, A. SIMI, NATO HQ International Staff, Brussels, Belgium: Armaments Cooperation and Electromagnetic Compatibility</i>	687
---	-----

M. CALAMIA, <i>University of Florence, Florence, Italy: EMI Analysis of High-Frequency Antennas on Naval Platform</i>	691
A.C. MITCHELL, <i>Ministry of Defence, Bristol, UK: Electromagnetic Compatibility in the Royal Navy</i>	693
F.M. STEWART, <i>Space and Naval Warfare Systems Command, San Diego, USA: The NATO EMI Operational Programme & Data Base (NEOP)</i>	697

Workshop: ***Mathematical Methods in Frequency Planning***

Organizers: J. FINNIE, *Radiocom. Agency, London, UK*
 R.A. LEESE, *University of Oxford, Oxford, UK*
 R.G. STRUZAK, *Member of ITU RRB, Co-chair of URSI WGE1,
Institute of Telecom., Poland*
 Chairman: J. FINNIE, *Radiocom. Agency, London, UK*
 (Workshop of URSI Commission E WG1)

S.M. ALLEN, <i>University of Glamorgan, Pontypridd, S. HURLEY, University of Wales, Cardiff, D.H. SMITH, University of Glamorgan, Pontypridd, W.J. WATKINS, University of Wales, Cardiff, UK:</i> Solving Frequency Assignment Problems	703
J.E. BATER, P.G. JEAVONS, D.A. COHEN, <i>University of London, Egham, UK:</i> Non-binary Modelling of Frequency Assignment Leads to Significant Reduction in Predicted Spectrum Requirements	705
R.A. LEESE, <i>University of Oxford, St Giles, UK:</i> Structural Features in the Construction of Good Channel Assignment	710
J. VAN DEN HEUVEL, <i>London School of Economics, London, UK, S. McGUINNESS, University of Umea, Umea, Sweden:</i> Colouring and Labelling of Planar Graphs	712

Workshop: ***European Union EMC Directive in Practice***

Organizer/Chairman: M.C. VROLIJK, *N V Philips, Eindhoven, Netherlands*
V-president of IEC – CISPR
Chairman of CENELEC SC 210A "EMC"

D. HANSEN, <i>EURO EMC SERVICE, Teltow, Germany:</i> EU EMC Directive in Practice. Analysis of the Implementation of the Directive After 2 Years by a European Competent Body	719
G. JEROMIN, <i>Regulatory Authority for Telecommunications and Posts, Mainz, Germany:</i> Enforcement of the EMC Directive in Germany: Two Years Experience with Market Surveillance	721
E. SANTIAGO, <i>European Commission, DGIII, Brussels, Belgium:</i> Implementation of the EU-EMC Directive: Added Value of the EMC Guidelines	723
S.P. SCOTT, <i>IBM (UK) Ltd, Greenock, UK:</i> The EMC Directive: A Manufacturer's Perspective	724
C.M. VERHOLT, <i>IARU Region 1 EMC Advisor & Chairman of EMC WG, Copenhagen, Denmark:</i> European Union EMC Directive in Practice. Telecommunications Equipment	731
M.C. VROLIJK, <i>N V Philips, Eindhoven, Netherlands:</i> Experiences of Industry with the EMC Directive	733

Workshop: ***EMC Quo Vadis - What Standards Will Be Need in The Future***

Organizers: P.J. KERRY, Radiocommunications Agency, London, UK

President of IEC-CISPR

B.T. SZENTKUTI, Swisscom, Corporate Technology, Bern, Switzerland

Chairman of IEC-TC77 "EMC"

M.J. COENEN, Philips Semiconductors, Eindhoven, Netherlands: Industry's view on EMC Requirements	737
A. FINNEY, ERA Technology Ltd, Leatherhead, UK: The Research Environment and its Role in Developing EMC Standards	742
D. HANSEN, EURO EMC SERVICE, Teltow, Germany: EMC Quo Vadis - What Standards Will Be Ned in the Future? Workshop Contribution: Testhouse View	747
P.J. KERRY, Radiocommunication Agency, London, UK: CISPR Standards Present and Future	749
B.T. SZENTKUTI, Swisscom Ltd, Bern, Switzerland: EMC Standards Today: Starting Point into the Future	752

Workshop: ***Practical Solution for Frequency Planning and Spectrum Management***

Organizer: L&S Hochfrequenztechnik, Lichtenau, Germany

D. LAUTENBACH, L&S Hochfrequenztechnik, Lichtenau, Germany: Practical Solution for Frequency Planning and Spectrum Management	767
--	-----

Workshop: ***Transient Immunity Tests on Different Ports, Flicker and Harmonics Measurements on Power Line Port***

Organizer: EMC PARTNER AG, Switzerland

M. LUTZ, EMC Partner AG, Laufen, Switzerland: Transient Immunity Tests on Different Ports, Flicker and Harmonics Measurements on Power Line Port	773
---	-----

Workshop: ***New Era of Communications Technologies - EMC Aspects***

Organizer: H. Kimball, Immediate Past Chairman of ITU-R SG7 "Scientific Services"

Workshop: ***EMC from Hewlett Packard***

Organizer: Hewlett Packard

Workshop: ***Penetration of EM Field Through Shielding Materials and Components***

Organizer: SPIRA Manufacturing Corp., North Hollywood, USA

PATRON'S ADDRESS



More than twenty five years ago, a group of visionary scientists in Wrocław, undertook an attempt to draw the attention of people engaged in the development of radio and wire telecommunication systems, and of other electrical and electronic equipment, generating purposely or unintentionally electromagnetic radiation, to the fact that there exists the necessity to ensure the operation of those systems without mutual harmful interference, and to protect the environment and the human against electromagnetic fields surrounding us all.

The initiative proved timely and viable, and the biennial Wrocław EMC Symposium became one of the important events in the electromagnetic compatibility considerations attracting EMC experts not only from Europe, but also from all over the world.

It is almost impossible to imagine such a broad and fast growth of the multitude of various radio and wire systems which have come into service in recent years without careful consideration of their EMC aspects. Amongst these aspects there is the more and more difficult problem of proper utilization and management of electromagnetic spectrum – the invaluable but limited resource being in the possession of mankind. The progress which has been achieved would not have been possible without considerable contributions of the EMC experts.

I would like to express here the utmost appreciation and congratulations to all those who have worked out the successful past, and the contemporary position of the Wrocław EMC Symposium.

I would also like to extend my gratitude to the Organizing Committee, Scientific Program Committee, Symposium Council and to all those whose continuous efforts have made the current event possible. I wish to stress the importance of the interest and support from EMC enthusiasts throughout the world, from the engineering societies in many countries, research entities, and international bodies.

I wish all those participating in the Symposium the best of success during their deliberations, a pleasant stay in Wrocław, and fond memories from Poland.

Marek Zdrojewski

Minister of Posts and Telecommunications
of the Republic of Poland



EMC '98

CHAIRMAN'S MESSAGE

Ladies and gentlemen, dear guests and friends,

This is for the fourteenth time that such an eminent assembly of EMC experts meets together here in Wrocław, to present and exchange information on most recent research achievements in this field. Twenty six years have elapsed since the group of 45 scientists and engineers met in Wrocław to discuss 17 papers from 4 countries. If you compare this number with the present volume of about 160 papers from 30 countries, you will easily realize the growing awareness of EMC problems.

The number of EMC Symposia held all over the world is constantly increasing. Increases also the number of people involved in EMC problems. EMC is becoming more and more essential for all aspects of our life as our electromagnetic environment keeps growing more dense, more intense, and more complex. The future of our technical civilization depends on the possibility of solving the various EMC problems.

The well reputed position of the Wrocław EMC Symposium is to a great extent the merit of active work of numerous individuals around the world, and of many scientific and professional organizations, and societies. They all are listed on the pages of the Symposium Proceedings. We owe our reputation also to the Scientific Program Committee with Professor Frans Louis Stumpers, Member of the Royal Netherlands Academy of Arts and Sciences, and Doctor Honoris Causa of the Technical University of Wrocław, who chaired it successfully for many years and now is the Honorary Chairman, and to Professor Ryszard Grzegorz Strużak - the present Chairman. Professor

R. G. Strużak was the Chairman of the Wrocław EMC Symposia in the years 1980 - 1984. I would like also to bring out the role of the Symposium Council with Professor Władysław Majewski as the Chairman. The international flavour of the Symposium has been gained with the support offered by the International Union of Radio Science URSI. The auspices granted by the Committee of Electronics and Telecommunications of the Polish Academy of Sciences with its Chairman Professor Alfred Świt, Member of the Academy, add more to the scientific atmosphere of the event.

The Symposium would not be possible without our authors who always play the most important role in such events. Special thanks must be directed to eminent specialists who have organized and chair the invited sessions. Their contribution to the success of the Symposium is appreciated very much.

The Symposium would also not be possible, and this volume would not appear, without the eminent patronage of Mr. Marek Zdrojewski, the Minister of Posts and Telecommunications of the Republic of Poland, and his kind personal support, as well as without the financial help offered by National Radiocommunication Agency, the Polish Telecommunication Co., the Plus GSM, and ERA GSM.

The objective of this Symposium is to bring together engineers and scientists who are interested in a better understanding of the origin, control, and measurements of electromagnetic influences on technical and biological systems. Our purpose in doing so is to become better informed about our current work, to appraise the status of the field, to stimulate future work, and, of course, to become better acquainted with each other.

It is up to you to decide to what extent this event, and the information presented in the Symposium Proceedings will contribute to those aims.

Most of the preparation work we owe, traditionally, to Mr. Władysław Moroń, the Organizing Chairman, and to all the members of the Organizing Committee.

I am convinced that this 14th Wrocław EMC Symposium will mark indeed a new significant step in promoting the development of EMC technology. I wish all the participants fruitful discussions during the Symposium, and a pleasant stay in the beautiful Wrocław. Thank you for your participation.



Prof. Daniel Józef Bem
Symposium Chairman

EMC '98: 14TH INTERNATIONAL WROCLAW SYMPOSIUM ON ELECTROMAGNETIC COMPATIBILITY INTRODUCTION

This volume contains some 160 papers from 30 countries selected by the Program Committee for presentation at this Symposium. Eight hundred pages of these proceedings cover significant aspects of current EMC theory and practice. They reflect, to some degree, the current research and work in industry and in major international organizations involved. EMC is understood here broadly as an ability of a device, equipment, or system to function satisfactorily in its electromagnetic environment without introducing intolerable disturbances to that environment.

Invited Lectures

Traditionally, plenary lectures and invited sessions create the nucleus of our Symposium. Their topics have carefully been selected to cover the most important issues of current interest to the EMC community and to assure balanced coverage of low- and high frequency EMC topics.

New threats and dangerous uses that could be made of electromagnetic energy are one of such issues and Dr. R. Gardner, V-Chairman of URSI-E, kindly agreed to talk about them. Another important issue of wide interest is the impact of the World Radiocommunication Conference (WRC) that was held last year to clear the way for truly global communication systems. Mr. T. Boe, Member of ITU Radio Regulation Board, will talk about that conference and Mr. K. Rosenbrock, Director General of ETSI, will discuss the ETSI work on standards on wireless systems designed for the global market. The quality of electric power is another issue of basic importance for electronic and electrical systems and Mr. G. Goldberg, Immediate Past-Chairman of IEC Advisory Committee on EMC, kindly agreed to address this problem in his plenary talk.



URSI - Related Issues

The International Union of Radio Science (URSI) sponsors three invited sessions and a workshop. Prof. M. Hayakawa, Chairman of URSI-E, will review in his session the progress made in studies of terrestrial electromagnetic environment. Prof. T. Yoshino of Fukui University will review in his session the progress made in studies of electromagnetic field associated with earthquakes and volcanic eruptions. Prof. H. Kikuchi, Past-Chairman of URSI-E, devoted his session to EMC considerations of radiating structures similar to the Beverage antenna. Dr. J. Finnie of UK

Radiocommunication Agency, Dr. R. Leese of University of Oxford and Prof. R. Struzak, Co-Chairman of URSI-WGE1, organized a workshop to review new mathematical methods in frequency planning, aimed at solving congestion problems of the radio frequency spectrum.

ITU - Related Issues

The program includes also review of relevant problems studied in ITU, a specialized Agency of United Nations. Dr. J. Finnie of UK Radiocommunication Agency organized a session on major factors and methods in radio frequency assignment. Physical radio propagation models, mathematical methods and computing tools will be discussed. Dr. T. Cesky of European radiocommunication Office organized a session on new trends in computer applications to frequency management. Dr. Th. Spoelstra, Secretary of CRAF, will discuss in his session problems of co-existence of passive and active radio services after the year 2000 when new communication technologies and systems will operate. Mr. H. Kimball, Immediate Past-Chairman of ITUSG7 on scientific services, organized a workshop on EMC aspects

WORLD RADIO CONFERENCE 1997 - CONSEQUENCES FOR EUROPE

Thormod Boe, Norwegian Posts and Telecom. Authority
Member of ITU Radio Regulations Board

Abstract

In October and November 1997 the World Radio Conference 1997 took place in Geneva, Switzerland. Such Conferences are required every second year and have become increasingly important for all users of radio; in particular those who wish to introduce new services and systems. The economic impact of the decisions taken at the conference may be severe and could determine the future development of the services dependant on radio.

The International Telecommunication Union (ITU) organise these conferences and we will describe shortly that organisation and its Radio Conferences. Furthermore, co-operation between Regional organisations will be described. Finally the preparations within Europe and the outcome of the recent conference will be discussed.

1. WHAT IS THE ITU?

The ITU with its 188 Member States is the oldest UN organisation, established in 1865 long before UN was born. The purpose of the Union is among others to maintain and to extend international co-operation and to promote development of telecommunications facilities as it is specified in the Article 1 of the ITU Constitution, taking particular account of the developing countries and their needs.

The supreme organ of the ITU is the Plenipotentiary Conference (PP) that meets every fourth year to determine the general policy and to establish the basis of the budget for the next period. The PP elect the elected officials and to take all major decisions with regard to the work of the Union.

The PP also fixes the number and timetable for the different conferences to be held in the next four

years. The ITU Council composed of 43 elected Member Countries of the Union meets once a year act on behalf of the membership between Plenipots. Every second year it decides, among others, on the bi-annual budget of the Union, directed by the financial plan set up by the PP. It also finally approve Conference agendas and give the Secretary General guidance for the work in the next year. The Headquarter of the ITU is located in Geneva, Switzerland, and employs some 800 persons.

The Headquarter consists of Secretary General, the General Secretariat and three Bureau's, the Development Bureau, the Standardisation Bureau and the Radio Communications Bureau (BR), responsible for the work in each of their Sectors, headed by an elected Director.

Without going too much in detail with regard to the tasks of the different sectors, we note that the Radiocommunications Bureau is responsible for the preparations to the Radio Conferences as well as to follow up most of the tasks coming out of the Conference Decisions. Reference is made to the ITU Convention ART. 12, which gives frame of responsibility of the BR.

The ITU Convention also identify the Radio Regulations Board (RRB), a Board consisting of nine Members elected from the five Administrative Regions of the ITU. The Board shall be independent of the Administrations and the ITU in its work, and has as a main task to prepare the Rules of Procedure to the Radio Regulations and to assist at the Radio Assembly and the WRC.

It may, if required, also serve in giving independent advice to the Director BR and the Administrations. The Board meets up to four times a year in Geneva, Switzerland, to perform its duties.

2. WHAT IS A WORLD RADIO CONFERENCE (WRC) AND WHAT IS ITS PURPOSE?

It became clear very early that some strict rules and procedures were necessary to avoid interference between services and radio stations, to assure interoperability of equipment and services and to ensure efficient use of the radio frequency spectrum.

The regulations that were first established in 1903 were named the Radio Regulations. The rapid development in radiocommunications made it necessary to regularly update and to modify the Radio Regulations in order to meet the needs of Administrations, operators and their services. With regular intervals so called "service conferences" (since the conference considered items mainly related to one service) were held in order to amend and update the regulations relevant to that particular service. Only with some 20 years intervals a general radio conference were held to undertake a more general revision of the ITU Radio Regulations to solve inter-service problems.

As the rate of development of radio communications services has increased considerably over the last years, the need arose to carry out more frequent revisions. Since 1993 therefore, the World Radiocommunication Conferences have taken place every second year. The agenda for a conference is provisionally established four years in advance, to allow a timely preparation. Two years before the conference the final agenda is agreed and the preparations are then concluded within the ITU and in the Administrations.

3. REGIONAL ORGANISATIONS

Over many years, administrations used to prepare themselves according to their national needs and requirements. As a result those administrations of the larger industrialised countries, did a lot of preparations, whereas the smaller administrations with limited resources and less industry interest and requirements very often did very little or nothing. It is easily understood that this is not a very satisfactorily situation, and in the last decade the regional co-operation has developed into a more firmly established co-operation.

Today there are a number of regional organisations where administrations co-operation in their daily work and in particular in preparations for WRC's. In Europe the CEPT is the organisation consisting of 43 European countries, extending as we use to say "from the Azores to the Vladivostok". In the Americas such a regional organisation is called CITEL, and the APT (Asian Pacific Telecommunications) co-ordinate co-operation

between Asian countries and the Arab Group and African organisations. What they have in common is that their members are also members of the ITU, and preparation to the WRC's is one of the major issues on their agendas.

4. CONFERENCE PREPARATIONS

The Radiocommunications Bureau in the ITU Headquarter support the preparations for conferences in the Study Groups. A special group, the Conference Preparatory Meeting (CPM), is established to consolidate the work done in this groups and to prepare a Technical Report to the WRC. This Report forms the technical basis for the work of the Conference.

The content of this Report consists of existing material in already prepared by the Study Groups, material developed by the Study Groups upon special request by the previous WRC and material submitted by Administrations and which is being agreed by the final CPM Meeting.

Within the CEPT co-operation has not always been as good as it should have been. At conferences in the past CEPT delegations often had divergent views, making it very difficult to achieve goals good for Europe and for the Region. In the eighties the co-operation slowly improved, recognising that there was no way Europe could achieve its goals unless a better co-ordination took place.

During the Radio Conference in 1992 the CEPT demonstrated its power by Common European Proposals (ECP's) and common CEPT Briefs for the work at the conference. This working method has since been refined and improved. In the CEPT the Radio Communication Committee has established the permanent Conference Preparatory Group (CPG), responsible for the co-ordination of the preparations for the forthcoming conference and to develop the European Common Proposals (ECP's) and the CEPT Brief.

The successful co-operation between CEPT Administrations has had the effect that most of the other Regional Organisations and Groups try to copy the "CEPT approach". Common proposals and common Briefs are being developed, and the Regional organisations and Groups become more unified and stronger counterparts. A fortunate thing is that in many cases the European draft proposals have become the basis on which many have developed their own proposals.

In the past, when "service conferences" were held with somewhat longer intervals, the available time for preparations for the conference was much longer and we had more time for better preparations of ourselves. Today, we have less than two years for

preparations. The conference now lasts only four weeks (in the past they lasted between four and eight weeks). The consequence of this is that "the conference has to go on between the conferences", i.e., there has to be a lot more co-ordination and co-operation between countries and regions than before to manage the extensive agendas at the conferences.

For many years there have been developed ever more intensive "contacts" between CEPT and other parties in order to carry out some "exchange" of views before the conferences. In the preparations for the 1992 and later conferences there have been more systematic contact meetings and exchanges of draft proposals at an early stage before the Conference. This tendency is increasing.

With such an approach many problems may at least be identified and perhaps some also resolved before the conference takes place in 1999. It is of outmost importance that conference preparatory methods are continuously improved to establish the necessary confidence between parties and to identify and hopefully align positions within as many of the problem areas as possible before the conference begin. Common preparations are not a threat to the sovereign rights of administrations. They should rather be viewed as common efforts in common interest.

5. THE CONFERENCE AGENDA

The 1997 Conference Agenda covered a wide range of items, and it would take too long to go through every item in detail at this occasion. Therefore the most significant items have been extracted from the agenda and will be discussed more in detail in the following.

5.1. Non-geostationary Fixed Satellite Systems (NGSO FSS)

By far the most prominent question at the Conference was to consolidate the proposals for allocations and regulatory framework that would enable multi-billion dollar NGSO FSS systems to develop over the next few years. These proposals covered some different bands and different regulatory approaches but will lead to systems that will offer competitive global broadband communication capacity. They include projects as "Teledesic", "Celestri" and "Skybridge" but, importantly, the Conference needed to address the problems in a non-project specific way so as to enable other systems that might emerge in the future to also be able to develop in a proper way.

In the end result the Conference was able to agree on a reasonable "package approach" that:

- a) Established the provisional application of power flux density (pfd) limits for LEO systems to protect GSO and fixed services in certain bands (particularly in 11 - 14 GHz bands). This approach was proposed as a means of overcoming the need for detailed and complex co-ordination procedures and was postulated as an approach to apply more broadly in the future. Access for LEO systems to the Broadcasting Satellite System (BSS) (bands where BSS Plans do exists) for Planned Bands was also agreed through the application of provisional pfd limits. This is clearly a break through in making possible greater use of these bands;
- b) Provided for an allocation of a total of 2 x 500 MHz of spectrum in the 20 GHz band on the basis of normal co-ordination arrangements (no application of power-flux density limits). A waiver of the normal priority given to GSO systems in this band was included, ie application of Resolution 46 and non-application of article S.22.2. (RR2613).

5.2. The Mobile Satellite Service

There were many proposals before the Conference for new allocations and for changes to existing allocations for mobile satellite services. One proposal for re-alignment of allocations at 2 GHz between Region 2 and Regions 1 and 3 was not agreed. As a result the original allocations made at WARC-92 will remain. The conference also confirmed the allocations made at WARC-92 for the world-wide satellite component for IMT 2000 at 1980-2010 MHz (uplink) and 2170-2200 MHz (downlink).

As a further recognition of the continually expanding needs for MSS, the Conference agreed to extend some allocations at 1.5/1.6 GHz from specific maritime and aeronautical satellite service bands to generic MSS bands. Moreover, priority shall be given to the requirements of the Global Maritime Distress and Safety System (GMDSS). Safety communications shall have priority over all other mobile satellite communications within a network in the specific bands involved. Similarly in specified bands at 1.5/1.6 GHz priority shall also be given to requirements of the Aeronautical Mobile Satellite (R) Service needs and protection to AGMs(R) Safety communications.

A proposal for MSS to be able to operate in the band 1559-1610 MHz (currently used by GPS and GLONASS) was not accepted but studies will be undertaken to enable this to be reconsidered at the Conference in 1999, the WRC-99.

An on-going issue for discussion is the spectrum requirements for MSS below 1 GHz (often called Little LEO Systems). The Conference made a very limited additional allocation in some bands between 454 and 460 MHz but invited further studies to enable reconsideration of this issue at the WRC-99.

I am sure that MSS spectrum requirements will continue to be a major issue in future Conferences.

5.3. Changes to HF Broadcasting

The problem of accommodating global HF broadcasting requirements has been considered by a number of Conferences in the last 50 years with little success. WRC-97 was able to reach a conclusion to this vexed problem through agreement on a system of direct co-ordination between administrations through inter-regional meetings and a voluntary co-ordination process with participation of broadcasters.

The Radio Regulations Board will develop the necessary Rules of Procedure within principles and criteria agreed by the Conference.

5.4. Broadcasting Satellite Service Plans

A significant proportion of conference time was devoted to this issue. The Conference adopted a new plan for the Broadcasting Satellite Service in Regions 1 and 3. This replaces the plan previously agreed in 1977 and accommodates the needs of new countries and new methods of service delivery. The Conference also agreed to initiate further study to provide for all countries around 10 analogue channels based on national coverage. This would need to be considered at a future conference before 2001 whether re-planning on that basis is reasonable.

5.5. High Altitude Platforms

High Altitude Platforms are stations used in the fixed service, such as those being planned by "Skystation" which operate at an altitude of 20-50 kilometres and which will deliver broadband services to urban and suburban areas. The Conference identified spectrum above 40 GHz for such stations along with other provisions in the Radio Regulations to facilitate the introduction of these services.

5.6. Maritime and Aeronautical Distress and Safety

The Conference revised the relevant parts of the Radio Regulations in preparation for the full implementation of Global Maritime Distress and Safety Systems (GMDSS), which will come into effect on 1 February 1999. This includes special

procedures: communication between GMDSS-equipped ships and those which do not yet have the new system; the use of ship information by search and rescue operations; calling procedures; licensing, and the conditions which need to be met in order to issue ship radio operator certificates.

5.7. Space Science Services

Space science services include active and passive sensing systems using satellites operating in both geostationary and low earth orbits. They are used primarily for remote sensing of Earth resources, weather forecasting, climate change, and space research.

Spectrum allocation requirements comprised:

- raising the status of the science services in many existing bands to protect them from interference existing and future satellite systems;
- new allocations in bands where observations can be made of specific physical phenomena, which allow measurements of atmospheric contaminants, land and sea surface measurements from space etc; and
- Harmonising allocations on a worldwide basis.

The WRC met nearly all of these requirements with changes and additions to 14 bands between 400 MHz and 94 GHz. Some issues were deferred pending further studies and will be considered at WRC-99.

The conference also approved Resolutions on the use of wind profiler radars and levels of spurious emissions.

5.8. Simplification of the Radio Regulations

Following the major changes of the Radio Regulations undertaken at WRC 95, WRC 97 had the task of reviewing the new arrangements for consistency, and determining the coming into effect of the new regulations.

The Conference agreed on 1 January 1999 as the date of provisional application of changes to the Radio Regulations made at WRC-95, pending final ratification by Member States.

Another aspect of "simplification" was the review of the Recommendations and Resolutions, which resulted in suppression of 65 Resolutions and 40 Recommendations. However, 16 Resolutions were revised and 56 new Resolutions were adopted by WRC-97.

5.9. Satellite Co-ordination

The Conference considered the results of studies and reports prepared by various groups in reply to a resolution of the 1994 Plenipotentiary Conference (Resolution 18). This Resolution addresses the growing problem of "paper satellites", that is, satellite systems which have been notified to the ITU, but in reality may never be launched.

The Conference adopted also called "administrative due diligence" concept that requires regular disclosure of data on the implementation of satellite systems. These data may be such as spacecraft manufacturer, the name of the satellite operator, the contractual date of delivery and the number of satellites procured, the name of the launched vehicle provider, the name of the customer and the contractual launch date.

Some Administrations felt that this development did not go far enough. It was observed that whilst the procedure adopted will place some greater discipline in the overall process, the new procedure will not have any noticeable effect for at least the 6 next years. This is due to the fact that the networks for which AP4 information was submitted prior to the WRC-97 have until 21 November 2003 to submit due diligence documentation. Some Administrations at the Conference felt that more effective steps were needed including consideration of financial due diligence measures, but the Conference did not accept to introduce such principles. It is probable that this issue will be raised again at the 1998 Plenipotentiary where a report on the results of the work of Resolution 18 will be considered.

5.10. WRC-99 Agenda

The Conference worked on a problem that is likely to worsen as time goes on. A long list of issues was proposed to be placed on the Agenda of the next two Conferences. In the result, a resolution of WRC-97 identified a list of items that it considered should be handled at WRC-99 but it also noted a supplementary list of items that could only be considered if there additional resources were provided for complementary studies. The extensive list includes some substantial issues such as requirements for IMT-2000, further MSS allocations, the results of technical sharing studies for NGSOFS, little Leo's below 1 GHz, matters relating to radionavigation satellite services, broadcasting satellite service planning, space science services and many more. It will thus be a matter for the next ITU Council meeting to consider in terms of the overall ITU Budget.

6. HOW TO TAKE THE RESULTS FURTHER IN EUROPE

In the regular day to day work in the CEPT administrations as well as in the preparations to the conferences it has always been very difficult to identify the real user requirements, those of organisations and the manufacturers. It is necessary that European Industry jointly define to a much larger extent their common interests and requirements which the CEPT would gladly use in the preparations for and negotiations at future WRC's. However, this situation has improved considerably over the last ten years in particular due to the ever-increasing transparency in the CEPT. The active participation of operators and organisations has considerably improved and to a certain extend also the industry participates, but not very enthusiastically. It has been and still is rather difficult to guess what are the requirements for the European Industry as a whole; one can certainly not fight for one or two individual or national interests in the CEPT environment.

The CEPT CPG in preparation to WRC-97 only took a particular initiative towards the Industry with limited response.

In order to cover all items at the very extensive agenda of this conference, the CEPT prepared some 287 individual proposals covering 18 major topics including proposals for 16 new Resolutions and 2 new Recommendations. These were all circulated to the 43 CEPT member Administrations for their Governments support and approval.

The major objective of the ECP's to WRC-97 was to promote and ensure the harmonious development of radio services in a competitive environment and at the same time to defend and promote European interests.

In particular, Europe placed great importance on the proposals which dealt with the improved regulatory procedures and frequency allocations needed for new fixed and mobile satellite services, and, more specifically, non-GSO systems, and the satellite feeder links. Further efforts concentrated on the protection of the terrestrial and satellite services sharing the same frequency bands to ensure efficient spectrum ever growing necessary for the escalating demand for personal communications. In developing its proposals, Europe took particular care to protect the extensive European terrestrial services when evaluating additional frequency allocations for the mobile-satellite service (MSS) and any changes in the radio regulatory provisions for the fixed-satellite service (FSS).

7. THE RESULTS FOR THE CEPT

All European Common Proposals (ECPs) submitted to WRC 97 were co-signed by most or all 43 CEPT countries and the European objectives were met on all the main issues: NGSO FSS; BSS plan; space science services; maritime; HFBC; (high altitude platforms (Sky Station); mobile-satellite; and WRC-99 agenda.

A very satisfactory outcome was achieved with virtually all-European objectives met on the main issues. The Conference proceeded in a good spirit of compromise and it must be seen as one of the most successful Conferences ever. There was no divisive voting on any major issue. This may have been due to the fact, that Europe had up to 43 votes (each member state - one vote!). This might have been an encouragement for others to reach a compromise that was satisfactory to Europe.

The regional groupings, particularly CEPT, APT and the Arab group (and to a lesser extent CITEL and African groups) were very active in promoting their proposals and proposals to the Conference, and this greatly helped in consolidating views. The bilateral meetings between regional organisations from other regions earlier in the year proved beneficial, particularly the collaboration with the Asia Pacific countries amongst which Japan played an important role. Recognising the importance of regional co-ordination, WRC 97 adopted a Resolution requesting the assistance of the Radiocommunication Bureau and the Telecommunications Development Bureau in further developing regional co-ordination and inter-regional meetings, and invited the 1998 Plenipotentiary Conference to provide for the necessary resources.

Mr Roger Smith (Australia) chaired the Conference very effectively. South Africa and Lebanon played significant mediating roles together with many other active participants.

8. THE FUTURE OF THE RADIO CONFERENCES

The resource requirement for the ITU Secretariat post WRC-97 conference work is presently estimated to 9,5 million Swiss francs, which is in a strong contrast to the 1 million Swiss franc provided to the ITU Secretariat to carry out the post WRC 1995 conference work.

In 1995 approximately 1000 delegates attended the conference whereas in 1997 more than 2000 delegates were registered. The cost of the 1995 conference was 3 million Swiss francs; the cost of the 1997 conference went up to 9 million Swiss francs. And to complete the picture of the workload in the Secretariat 7 million pages were processed in

1995 whereas in WRC -97 required over 25 million pages to be reproduced.

The 1995 conference was considered to be a large conference compared with what was normally the case for the service Radio Conferences in the past.

These figures are quite alarming and raise many questions; in particular as they cover only resources spent in the ITU Secretariat. Resources spent by the Member States are certainly even higher. If the conferences continue to grow at the same rate, they will simply not be manageable in the future. They may soon be more expensive than the Union can afford. We therefore have to be extremely pragmatic with regard to what shall be included in the agenda of the next conferences. An open question is also whether one should return to the service type conferences, which necessarily have a more limited agenda instead holding of conferences, that includes almost any issue.

Notwithstanding the success of WRC-97 there are some clear signs that there will be increasing difficulty in the future. As mentioned earlier in this presentation it is not possible to handle more issues or to do more work than was attempted at WRC-97. Apart from the budget and overall resources available from the ITU, the delegates themselves could not be expected to handle any more work. The extent and complexity of technical preparation for a Conference is a problem in particular when it is considered in parallel with the on-going work being undertaken in the ITU-R Study Groups. There is also a heavy burden on individual administrations and on Regional Groups in establishing positions and proposals sufficient time in advance to efficiently and timely inject into the Conference preparations.

No doubt the Member States of the ITU will need to consider options to improve these overall processes. When entering into a sequence of a conference every second year it was assumed that the conference, lasting for only four weeks, would have an agenda sufficient restricted to be treated during these four weeks. Since there would be an other conference in only two years time, urgent issues could be left to the next conference.

However, the real world unfortunately is different. The agenda to every conference is already completely overloaded with urgent issues; some of which stem from the previous WRC's, where they could not be resolved.

There is no other alternative to a statutory Conference process to achieve the necessary treaty status outcomes. Some have suggested an extension of time between Conferences. Whilst this would give greater preparation time it is doubtful whether it would help in dealing with the increasing volume of

issues to be addressed. Moreover, it would not be a credible reaction to the rapid developments in technology and the rapid adapted Radio Regulations.

Others will certainly have other ideas, but my own views are as follows:

- a) More discipline needs to prevail in establishing agendas and in setting priorities within future agendas;
- b) sensible assessment of the time and effort required in the administrations and the ITU Secretariat to complete studies necessary for the consideration of issues at a Conference;
- c) greater co-operation and liaison between Regional Organisations and country groupings in comparing their proposals and attempting to identify possible consolidated positions prior to a Conference;
- d) greater use of informal consultation means and mechanisms between administrations to plan for Conferences;
- e) Some improvement in the actual mechanics of Conferences themselves.

There has already been some discussion of these issues in several forums and the 1998 ITU Council and the forthcoming Plenipotentiary Conference in Minneapolis provide ideal opportunities to consider further reform.

The important bottom line is that the world communications community requires that the international radiocommunications regulatory arrangements will adequately respond to their needs on an ongoing basis. WRC-97 successfully met this requirement but it will be a challenge to repeat that success into the future.

9. FUTURE CONFERENCES

Despite the concern reflected above, the preparations to the next conference have already started. In the ITU the CPM, for which the author of this paper happens to be the Chairman, held its first meeting and organised the work among the ITU-R Study groups the week just after WRC-97. A special group to support further BSS planning activities has started its work. The Council 1998 will consider the provision of more resources at its meeting in June for more resources to make the WRC-99 able to deal with the whole of the recommended agenda proposed for that conference.

The CEPT/CPG held its first meeting in February 1998 to organise the preparations in the CEPT and an international contact group already met in January this year.

The level of activity is very high, although one should be concerned with regard to the amount of work and the substantial lack of resources in the ITU as well as in many Administrations.

Biography:

Mr. Boe has worked with the Norwegian Telecommunications Administration since 1963. He participated in CCIR since 1974, as Vice-Chairman in St.gr.1 from 1983 to 1993. He chaired many ITU meetings over the years, he was elected Vice-Chairman of CPM-97 and Chairman of CPM-99. He has been Member of the Radio Regulations Board since 1994.

He participated in CEPT since 1972 and has served as Chairman and vice-Chairman of several CEPT working groups. He chaired the CEPT preparations to the WARC-92, and served recently as Chairman of the Frequency Management Working Group from 1992 to 1998.

References: Final Acts, WRC-97 (ITU).

ELECTROMAGNETIC TERRORISM A REAL DANGER

Robert L. Gardner
Envisioneering, Inc.
5267 Pumphrey Dr.
Fairfax, VA 22032

Electromagnetic Terrorism is an outgrowth of the more familiar discipline: Electromagnetic Compatibility. In this case, however, the terrorists produce the offending currents or radiation intentionally. Accidental radiation can cause severe and inopportune damage to electronics, so certainly those fields can also be intentionally impressed on vulnerable equipment. A number of recent public statements and testimony have described potential dangers. This paper cites some of the more recent statements and uses those statements to describe the potential threat. It is not yet clear how easily or effectively such a potential weapon can be used, but it is clear that the electromagnetic compatibility community must be prepared to deal with the threat when it emerges.

1. INTRODUCTION

1.1 History

General Loborev [1] gave a plenary lecture at the AMEREM conference in Albuquerque in 1996. With that speech he coined the phrase "Electromagnetic Terrorism" and introduced into the public domain a subject that has concerned many of us in the electromagnetic compatibility community for some time. The General's comments on the use of EM techniques to defeat alarm and communication systems led to much debate within the technical community at and after the AMEREM meeting. That debate continued with committee meetings at the EMC Zurich symposium in 1997 and with a panel discussion at the North American Radio Science Meeting in Montreal in July 1997.

A US Congressional Joint Economic Committee [2] held hearings on the electromagnetic threat to the civilian infrastructure and concluded that it was an important topic. More recently the debate has continued with a panel discussion on EM Terrorism at the EUROEM 98 Symposium in Tel Aviv in June 1998 and with a similar debate I would like to encourage at this symposium.

Several articles have appeared recently in the popular press claiming that the threat from electromagnetic weapons is severe. These articles serve the purpose of encouraging public interest, but in this scientific forum our purpose is to decide on a course of action.

1.2 Application

EM Terrorism is logically part of the overall charter of the EMC community. It is our (the EMC community's) job to recommend standards for both emission and susceptibility of commercial and military electronic systems. In the case of EM terrorism, the emissions part of the equation cannot be controlled, but there are reasonable physical limits on EM weapons. In the second section of this report we will explore some of these practical limits and suggest methods of using those limits to control vulnerability of commercial systems.

1.3 Expectations

The International Union of Radio Science (URSI's) role in this debate on EM Terrorism is to stimulate scientific debate. URSI does not set standards or accomplish other regulatory tasks. At the end of this paper, we will discuss these roles more fully and make suggestions for future research and debate. From an URSI point of view, approval of a resolution by the URSI Council marks the end of the formal URSI role and the beginning of work by the members to encourage further research.

2. DEVELOPMENT OF EM TERRORISM

2.1 Loborev's Original Address

Gen Loborev gave a Plenary Lecture to the AMEREM conference in May 1996 [1]. That lecture formed the basis of our present discussions on electromagnetic terrorism and led to the public discussion of this important topic. In part of his talk on EM terrorism he discussed radio controlled explosive devices, use of EMP radiators for disabling alarm systems, pulsed sources for opening locks and the use of EM devices for suppressing radio communication.

These uses are all closely associated with criminal activity and the Russian mafia is suspected of using these tactics. Professor Loborev also discussed the potential use of electromagnetic waves for "reduction the efficiency of professional activity" in people.

2.1 Recent Congressional Testimony

On 17 June 1998 the Joint Economic Committee heard testimony from Lt Gen. Robert Schweitzer about radio frequency weapons and their effects on electronics. Since these methods and weapons could be effective against their civilian counterparts, the Committee sought testimony on the potential effects of electromagnetic weapons against the infrastructure [2]. Four scientists testified on the issue of electromagnetic threats to the infrastructure: James O'Bryon (Dept of Defense), David Schriner (Electronic Warfare Associates), Dr. Ira Merritt (Missile Defense Space Tech Center) and Dr. Alan Kehs (US Army Research Laboratories).

2.2.1 Mr. James F. O'Bryon's Statement. Mr. O'Bryon is Director of the Live Fire Range. His testimony was concerned with the role of the Live Fire Range in testing for RF weapons.

2.2.2 Mr. David Schriner's Testimony. Mr. Schriner spent most of his time describing some of the advantages of a Transient Electromagnetic Device. That device is a wideband or transient microwave transmitter. He supported the effectiveness of the device by reminding the Committee of the various reminders we hear on airplanes not to use electronic devices while the aircraft is in flight. Mr. Schriner also built a simple transient electromagnetic device in his garage for about \$500. He said that the device was effective.

2.2.3. Dr. Ira Merritt's Testimony. Dr. Merritt discussed the proliferation of a number of different types of Russian radio frequency weapons world wide. For example, he discussed the recent Swedish exploitation of Russian RF weapons. Dr. Merritt described both electrically driven and explosively driven devices. His comments on susceptibility were less precise. He did conclude that much of the required risk mitigation could be accomplished through the development of low cost, broadly-applicable mitigation techniques, similar, but not identical to those used in the EMC community.

2.2.4 Dr Alan Kehs' Testimony. Dr Kehs provided only a general outline because of classification issues. However, he did say that "the growing US dependence on sophisticated electronics for warfighting and domestic infrastructure makes us potentially vulnerable to electronic attack." [2]

2.3 Recent Articles in the Popular Press

2.3.1 New York Times. Eric Rosenberg [3] considers a scenario in which an EM terrorist team attacks a government office building full of computer equipment. In his scenario, a terrorist group uses a van full of electronic equipment to cause significant damage to a building housing government electronics. He asserts that damage may be severe. This article and others like it grew from the above cited testimony before the Joint Economics Committee Hearing . That particular scenario was not used in the testimony, but it provides a clear statement of the situation that we all fear in electromagnetic terrorism.

2.3.2 New York Review of Books. Elizabeth Scarry describes an even more serious scenario in which she suggests that a possible cause of the TWA 800 disaster was electronic interference [4]. While we do not believe that EMI was the cause of the TWA 800 explosion, Dr Scarry's summary of the potential for disaster caused by electromagnetic interference is effective and scientific. Clearly, damage or interference with electronic communications or navigation gear on aircraft could cause a very serious accident.

2.4 Panel Discussions

So far, there has not been sufficient information available at the various scientific symposia to support a complete session on electromagnetic terrorism. However, there have been meetings and panel discussions within the various scientific societies.

2.4.1 Electromagnetic Compatibility - Zurich. The meetings in Zurich were primarily organizational. URSI Commission E held an informal discussion on electromagnetic terrorism and decided to form a subcommittee on Electromagnetic Terrorism under the existing URSI Committee on EMP and Other Matters led by Dr Manuel Wik. Dr. Heinz Wipf was asked to chair the subcommittee.

2.4.2. North American Radio Science Meeting. URSI Commission E held a Panel Discussion on Electromagnetic Terrorism in Montreal during July 1997. The panel discussion generated a lot of interest and the standing room only audience overflowed into the hallway. Several members of the panel suggested scenarios in which electromagnetic terrorism could be a serious problem. One of those included the use of surplus radar equipment to threaten low flying aircraft. There was little agreement on the vulnerability of such an aircraft, despite extensive testing for EMC/EMI purposes. There was also considerable uncertainty in the vulnerability of ground equipment, particularly since the configuration of the equipment was ill-defined. Most of the audience supported additional research into electromagnetic terrorism and appropriate protection

techniques. A minority expressed the fear that discussion of the topic would encourage the use of electromagnetic means to disrupt electronics critical to the infrastructure. We have found that the discussion is already in the public domain and believe it should continue with aim of encouraging research and appropriate protection techniques.

3. QUANTITATIVE DISCUSSION

3.1 Potential Sources

An electromagnetic terrorist first requires a source, or radio transmitter. That source must be effective to a reasonable range against equipment important to the target country. In his design, the terrorist must consider all of the transfer functions indicated in fig. 1 [5].

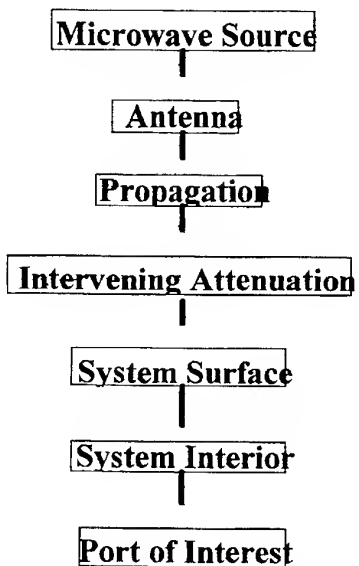


Figure 1: System Interaction for HPM [5]

Each of the layers of fig. 1 represents a change in the HPM signal generated in the source. Transition to the antenna attenuates and distorts the signal. The antenna directs the signal and narrows its focus. Distance is one of the major limiting factors for high power microwave devices and is chiefly $1/r^2$. As the intervening attenuation block indicates, however, there may be additional layers like building walls that may further attenuate the signal. System surfaces accept varying frequencies with strongly varying degrees of efficiency so the terrorist must match the source to the target geometry. The signal is further attenuated as it penetrates to the sensitive circuit element. Finally, there must be sufficient signal strength remaining to affect the device of interest.

To get an idea of the requirements for such a terrorist weapon, we can consider some of the limitations. First, antennas aperture sizes are limited for practical reasons to about 1 m^2 , say. That aperture

could, in principle, be driven at up to air breakdown which is about 10^5 W/cm^2 . That allows a total power of about a gigawatt transmitted. Assuming a 1 GHz narrowband source the relationship between the power density and range is shown in fig. 2.

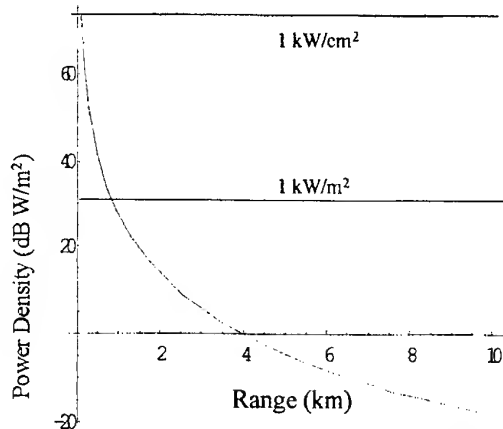


Figure 2: Power Density as a Function of Range

While this plot is just a simple $1/r^2$ plot, it demonstrates how little range some weapon concepts might have for required power levels. If one requires 1 kW/m^2 at the surface of a system to achieve lethality then our hypothetical source configuration has a range of less than a kilometer. If 1 kW/cm^2 is required then the range is only about 30 m, easily within rock throwing distance.

The attenuation of walls and other parts of a structure make up an important part of the propagation attenuation. A simple wall may attenuate a signal by 10 dB. A more complex building with metal cables and structural members may attenuate the signal many 10s of dB. These attenuators lower the curve in fig. 2 significantly.

3.2 Susceptibility

Precise statements about lethality of HPM concepts are beyond the scope of this paper, but the large variation of susceptibility levels is important to this debate. If you are a high power microwave weapon designer for a government then you would like to be able to design a weapon to affect your target and only the required target. You must attack your target whether the target has low susceptibility levels or not. The EM Terrorist does not have these restrictions. He can attempt to find a weakness in a system. Since his method of attack leaves little evidence of the attack, he can continue trying until he succeeds.

There are extreme variations in operating levels for electronic equipment. Electronic navigation equipment operates at extremely low levels, but power switchgear may operate with thousands of amps and thousands of volts. Obviously, one class of equipment is

easier to affect than the other. While susceptibility levels do not track operating levels there is a correlation. Fig. 3 shows a possible range in susceptibility levels [6] for varying exposure to high power microwaves. The figure shows the variation in lethality for a number of different systems. The x-axis is just some arbitrary system number. The y-axis is the intensity at which the system might be expected to fail. There are a couple of values outside the boundary. These bars are there to remind you that there are always targets that are not appropriate for high power microwaves.

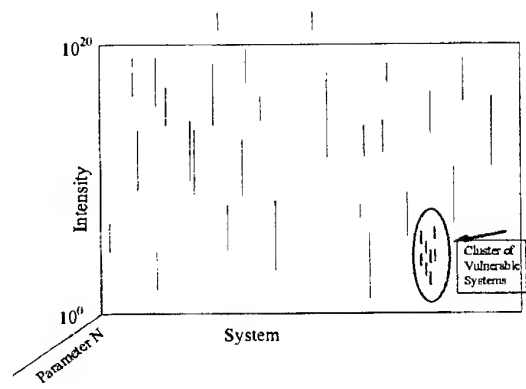


Figure 3: Intensity Levels for Possible HPM Lethality for a Variety of Systems

4. ROLES FOR FUTURE RESEARCH

During the various workshops, there was some discussion about the role of URSI in this debate about protection from EM terrorists. URSI is, by its nature a public, international organization, so all of its technical meetings are open to anyone willing to register for the conference. The details of electromagnetic interaction of particular systems are not public, however, and specific vulnerabilities, like that, should not be made public. There is still room for technical debate about the methods that should be used to protect the public from the damage that can be done to the infrastructure by EM terrorists. That brings us to the roles of the various organizations in this debate.

4.1 The Role of URSI.

URSI's home page describes the role of URSI in the following way:

"The object of the International Union of Radio Science (Union Radio-Scientifique Internationale) is to stimulate and to coordinate, on an international basis, studies in

the field of radio, telecommunication and electronic sciences, and, within these fields:....."

We are now considering the issues and members of Commission E will likely frame a resolution for consideration by the URSI Council at the next General Assembly. If the Council approves the resolution, it will be distributed. The formulation of standards of protection belongs to other parts of the electromagnetic compatibility community, however.

4.2 The Electromagnetic Compatibility Community

The IEEE web site describes the role of the Electromagnetic Compatibility Society with the words:

"The IEEE EMC Society strives for the enhancement of electromagnetic compatibility through the generation of engineering standards, measurement techniques and test procedures, measuring instruments, equipment and systems characteristics, improved techniques and components, education in EMC and studies of the origins of interference."

The IEEE EMC Society, as do other organizations, is in the business of recommending standards for EMC and that is where the real work of electromagnetic terrorism belongs.

5. CONCLUSIONS

The public should be protected from the extensive damage that could be done to vital computers in the infrastructure or to other electronic communications or navigation equipment. To protect the public the threat must first be defined. It must be assumed that terrorists do not have the resources of a major power and so will use available technology. It is then appropriate for us to survey the available surplus equipment sold by governments or by private companies. There are also physical limits on what can be done in microwave source technology, such as those suggested in section 3.

After the threat is defined, we must work to protect the electronic equipment used in vital equipment. Electromagnetic compatibility is the discipline that is designed to provide that protection to the public and to insure that the protective measures work. It is only necessary to include the potential threat from intentional microwave sources in the EMC specifications as well as those threats from unintentional sources. Some of the intentional sources may be severe and require extensive hardening. At that point, the EMC community must outline the risks and the economic trades to the public and to the owners of the electronic equipment.

6. REFERENCES

- 6.1 Loborev, V. M. "The Modern Research Problems", Plenary Lecture, AMEREM Conference, Albuquerque, NM, May 1996.
- 6.2 Saxton, J., Record of the "Joint Economic Hearing Radio Frequency Weapons and Proliferation: Potential Impact on the Economy", US House of Representatives, 25 February 1998.
- 6.3 Rosenberg, E., "New Face of Terrorism: Radio-Frequency Weapons, *New York Times*, 23 Jun 97.
- 6.4 Scarry, E., "The Fall of TWA 800: The Possibility of Electromagnetic Interference", *The New York Review of Books*, Vol. XLV, No. 6, 9 Apr 98.
- 6.5 Baum, C. E., "Maximization of Electromagnetic Response at a Distance", *IEEE Transactions of EMC*, Vol 34, No. 3, pp148-153, August 1992.
- 6.6 Gardner, R. L. and C. W. Jones, "System Lethality, Perspective on High Power Microwaves", *System Design and Assessment Notes, Note 34*, EMP Note Series, Kirtland AFB, NM, July 1995.

BIOGRAPHICAL NOTE

Dr. Robert L. Gardner received his PhD from the University of Colorado in 1980. He has been active in High Power Electromagnetics since that time. He has worked in the EMP, lightning, and high power microwave communities in a variety of positions. Dr. Gardner is currently a Senior Scientist with Envisioneering, Inc.

POWER QUALITY

G. Goldberg

Past Chairman IEC ACEC

(Advisory Committee on Electromagnetic Compatibility)

Wannerstrasse 43/61 CH - 8045 Zürich Switzerland

Abstract

The characteristics of the electricity supplied by the Utilities to the users - Power Quality - is a very topical subject. Aim of the paper is first to summarize the most important technical issues: definition (PQ should not be confused with EMC although related to it), relevant parameters, examples of limits or indicative values, role of the Utilities and users. On the other hand, it draws attention to several other aspects, e.g. subjective assessment by the users, legal or contractual responsibility.

1. Definition of Power Quality

Power Quality (PQ) is a very topical subject dealt with in numerous organizations (see Chapter 2), but it is amazing that, although they consider the same phenomena, quite different definitions of this concept exist (when a definition is given at all). In the context of this contribution it will be referred to a definition proposed by an IEC ACEC working group:

"Power quality: Set of parameters defining the properties of the electrical power supply as delivered to the user in normal operating conditions of continuity of supply and characteristics of voltage (symmetry, frequency, magnitude, waveform)."

Practically, this definition is close to the title of the relevant CENELEC Standard EN 50160 [3]. "Voltage characteristics of electricity supplied by public distribution systems."

The IEC definition is commented on by two notes:

"Note 1: PQ expresses the user's satisfaction with the supply of electricity. PQ is good if electricity supply is within satisfactory and any contractual limits and there are no complaints from users."

PQ is not only a technical operational problem of the utilities but depends on the perception of the users with regard to their applications.

Note 2: PQ depends not only on the supply but can be strongly affected by the user's equipment and installation practices."

One has to account not only for the Utilities' features but also the users' influences and the interactions between both.

The above definitions require some comments:

a) "Electricity supplied" means in fact that Electricity in this context has to be considered as a Product. This is particularly stated in the EC Directive 85/374 on Product Liability.

b) "In normal operating conditions" means that also "undisturbed" conditions and the normal ranges of variation have to be considered, not only disturbances.

c) PQ is a concept different from Electromagnetic Compatibility EMC. The latter is defined as follows:

"Electromagnetic compatibility: The ability of an equipment or system to function satisfactorily in its electromagnetic environment without introducing intolerable electromagnetic disturbances to anything in that environment."

PQ and EMC are two different concepts in that EMC concerns equipment or systems - hardware items - and only disturbances. From this last viewpoint EMC may be considered as a subpart of PQ. Obviously there is a close connection between PQ and EMC, as the voltage characteristics depend on the emission of the conducted EM disturbances and their limits. For this reason, there is often confusion between these two concepts.

d) In the context of PQ, certain limits or indicative values are specified (see Chapter 3 and Tables 1 to 3). These values should not be confused with "compatibility levels" which may be defined as follows:

"The specified levels of a particular disturbance phenomenon in a specified environment, established as a reference value for the co-ordination of emission levels and immunity requirements in order to achieve EMC"

Compatibility levels are related to the design of equipment or systems (emission and immunity), PQ levels to the actual values of the network voltage.

e) Another definition should also be kept apart from PQ: "Planning levels". Planning levels may be defined as the reference levels for the connection of equipment or a system in order that it complies with the general requirements of PQ or EMC. It is more an internal working reference value of the Utilities.

f) A technical remark concerning the disturbances phenomena: From the overall catalogue of EM

disturbances - low frequency, high frequency, conducted, radiated, ESD, HEMP, ... - it is obvious that only the conducted disturbances - at Low frequencies (LF), but also at High frequencies (HF) - have to be considered in the context of PQ.

- g) There is also to note that the term "normal operating conditions" excludes special situations like:
- exceptional weather conditions and natural disasters
 - third party interference's
 - industrial and other external actions
 - acts of public authority

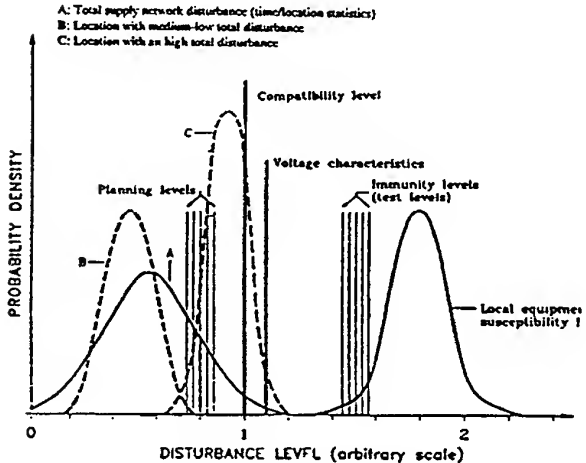


Fig. 1: Emission level, Compatibility level, Immunity level, Planning level

2. Organizations dealing with Power Quality

As already stated, PQ is nowadays a very topical subject dealt with in numerous organizations but with different purposes: general guidance, description of the phenomena, setting of limits, improvements, etc. They are:

- **Standardization bodies**
like IEC [1, 2], CENELEC [3], IEEE [7] which develop standards for limits - this in fact in the case only of CENELEC (see Chapter 3) - or mainly with regard to measurement methods:
- In IEC, SC 77A/WG 9: "Power quality measurement methods".
- In CENELEC, BTTF 68-6 "Physical Characteristics of Electrical Energy".
- In IEEE SCC 22: "Power Quality".
- **Associations of Utilities**
like UNIPEDE [4, 5, 6], EPRI which prepare detailed technical guidance documents.
- **Important utilities**
like EDF [10, 11, 12], ENEL which prepare national technical studies and sometimes offer special tariffs to their users in order to promote PQ.
- **Private bodies**
which organize symposiums with the title Power Quality but very often deal only with the EMC part of the subject, or equipment manufacturers.

3. The parameters of Power Quality

3.1. It seems appropriate to classify the parameters of PQ in three categories (which deviate from the classification of Electromagnetic phenomena):

Parameters concerning normal power supply

- voltage magnitude and normal variation range
- slow variations of the supply voltage
- long voltage interruptions ($t > 3$ min)
- frequency and normal variation range
- slow variations of the supply frequency

Parameters concerning disturbances of the voltage magnitude and symmetry

- overvoltages
- rapid voltage changes
- fluctuations of voltage magnitude (flicker) *
- voltage dips ($\Delta U < 95\%$) *
- short voltage interruptions ($\Delta U > 95\%$, $t < 3$ min) *
- unbalance of the three phase voltages *

Parameters concerning disturbances of the voltage wave

- Harmonics *
- Interharmonics *
- Signalling voltages (Ripple Control and HF up to 500 kHz) *
- Commutation notches
- Transient overvoltages (surges or oscillatory) *

The phenomena marked with an * are also considered as EM disturbances in the series of the standards IEC 61000-X-Y [14]

We assume in the context of this paper that the physical characteristics and the sources of these phenomena are well known. They are described in detail in the relevant literature [e.g. 2, 4, 7] ...

Figures 3 to 9 show typical examples or limits for the most important disturbances: voltage variations, flicker limits, harmonics, transients.

3.2. The physical characteristics of these parameters: magnitude, duration, etc. are of course primary factors for the evaluation of their importance but with regard to their nuisance for the users. The variation in course of time and the probability of occurrence play also a great role: a phenomenon which appears with a high magnitude but very seldom may be less critical than a phenomenon with a low magnitude which is more or less continuous. Measurements for the evaluation of PQ should therefore consider both aspects:

- physical characteristics, e.g. magnitude (rms or peak values, average values over a certain period), duration,
- time dependence which is accounted for by
 - a measurement period
 - an observation period

3.3. Depending on the disturbance phenomenon a Utility or the users may influence it and reduce its effects by appropriate mitigation methods; this is for example the case with slow voltage variations, harmonics, flicker, etc. It is then possible to specify disturbance limits, which should not be exceeded or only during a specified period of time.

With other phenomena the application of mitigation methods is not easily possible or unreasonably costly so that it is only possible to assess the actual disturbance characteristics and to give as reference what is called "indicative values".

Generally, like for the compatibility levels, the compliance criterion for PQ is that the specified limits or "indicative values" would not be exceeded in 95% (or 99%) of the cases or the time.

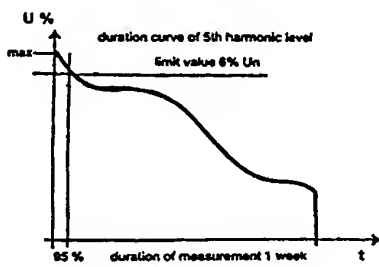


Fig. 2: Probability density curve (Example: 5th harmonics)

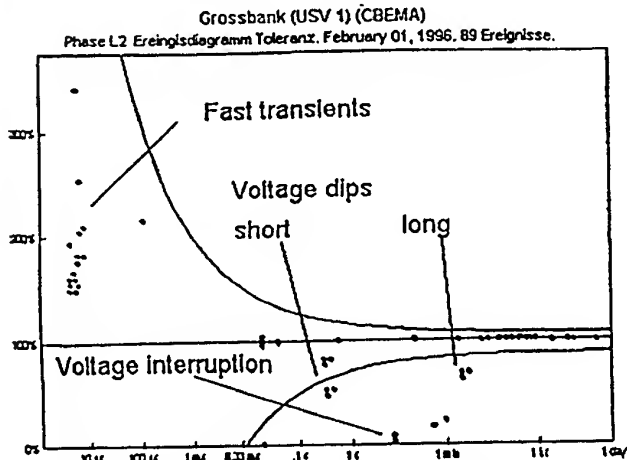


Fig. 3: CBEMA tolerance curve (voltage variation up to 1h, transients above 10 μ sec)

4. Overview on Power Quality values

Tables 1 to 3 summarize, as an example, the values specified for Europe in the CENELEC Standard EN 50160 [3] (or where more appropriate the values given in the guidance documents of UNIPEDE [4, 5, 6]). The tables show for the three categories of parameters listed in paragraph 3.1:

- the considered parameters
- the specified limits [2] or indicative values
- the compliance criteria
- the measurement rules:
 - measurement periods
 - observation periods.

It can be observed that the EM limits or indicative values of EN 50160 are often the same as the com-

patibility levels specified in IEC 61000-2-2 [2] but it shall be remembered, as explained in Chapter 1, that they correspond to two different concepts.

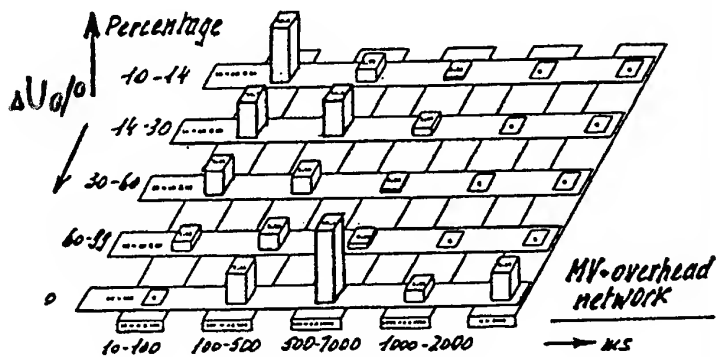


Fig. 4: Example of the distribution of voltage dips

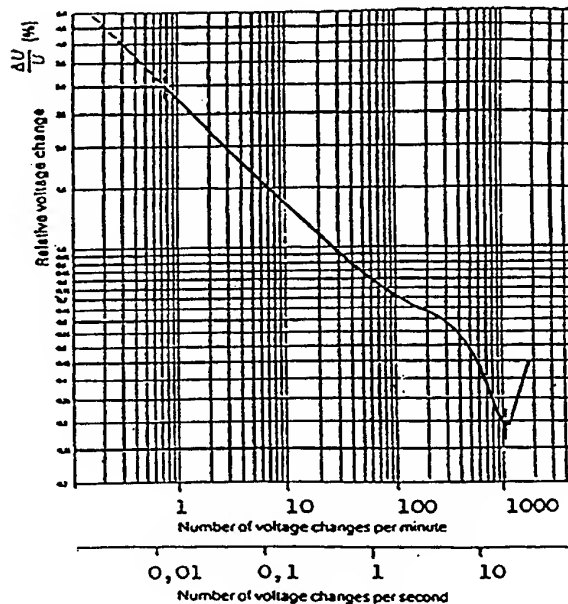


Fig. 5: Flicker tolerance curve

Other PQ standards specify in general similar values and measurement rules [7, 8, 9, 11].

It may be pointed out again that these limits or indicative values are not to be assessed just from a technical viewpoint but also from the user acceptance - or satisfaction - viewpoint (see Chapter 7).

5. Measurement equipment for Power Quality

Several manufacturers produce equipment for the measurement of the PQ parameters which go from very sophisticated apparatus for special investigations to simple apparatus for large field investigation campaigns (Note: this chapter will deal only with the PQ specific features; for all other "classical" requirements like mechanical, climatic, operational conditions, etc. it is referred to relevant standards or product descriptions).

The most sophisticated apparatus presently on the market can be characterized by the following main data [13]:

Inputs

- voltage channels: 4 (3 x Ph + N)
- current channels: 4 or 5 . (4 x Ph + N + [Ground])

Functions

- Frequency of the network
- Voltage variations (slow variations)
- Overvoltages
- Voltage dips
- Voltage interruptions
- Harmonics (THD and spectrum)
- Interharmonics
- Flicker
- Unbalance
- Remote signals (up to 148,5 kHz)
- Transients (μ sec domain)

Note: also KW, KVA, $\cos \phi$.

Parameter	Limits (L) or indicative values (I)	- Measurement period - Observation period	- Measurement period - Observation period
Harmonics (up n=40)	- THD < 8% - individual harmonics compatibility level - 95% of a week	L	- 10 min rms mean values
Interharmonics	- individual frequency < 0.2% U_n	I	- to be defined
Transients $1\mu s$ to 1ms	- generally < 6 < KV_p	I	- e.g. over one year
Mains signalling 100 Hz - 150 kHz	- diminishing with frequency 9V to 1V - 99% of a day	L	- 3 sec rms mean values - day

Table 3: Limits and indicative values for EM disturbances related to the power voltage waveform [EN 50160 or UNIPEDE Guide]

Software

- Measurement and observation periods
- Calculation of mean values
- Comparison with limits
- Fast Fourier Transform
- Flicker (IEC 868)
- Unbalance (negative sequence)
- Statistics

Display and Printer

- Data and curves (momentaneous and long periods)
- Cumulative probability curves
- Display against tolerance curve (CBEMA, etc., ...)

Remote communication

- Internet or other channels

Electronic data

- Microprocessor min. Intel 386
- Memory 4 MB RAM, 540 MB HD
- Software based on Windows 3x ...
- Sampling for power frequency ca 8 kHz
- Sampling for transients 4 MHz

It is obvious that such highly sophisticated equipment is very expensive and not appropriate for large/mass applications. Different stages of simplification may be considered:

- Limitation to just the application of EN 50160.
- Limitation to just the most important parameters [10, 11, 12]

- Voltage dips and interruptions (short and long time)

- Harmonics

- Unbalance

(KW and KVar)

Note: Other functions with specialized apparatus like Flickermeter, Transient recorders, etc.

- Limitation to one parameter
 - generally harmonics
- Optional equipment for sophisticated apparatus

In all these cases, separate data processing on a PC or central data processing via remote data

Parameter	Limits (L) or indicative values (I)	- Measurement period - Observation period
Supply voltage and slow variations	L-N: 230 V \pm 10% 95% of a week	L - 10 min. mean rms values - one week
Supply: frequency (interconnected) systems	f: 50 Hz \pm 1% 95% of a week [50 Hz \pm 4/-6% 100% of a week]	L - 10 sec. mean value - one week

Table 1: Limits and indicative values related to normal voltage conditions [EN 50160 or UNIPEDE Guide]

Parameter	Limits (L) or indicative values (I)	- Measurement period - Observation period
Overtvoltes of $U_{\phi_{LV}}$	number of events (LV fault: $U_{ph} < 440$ V) (MV fault: $U_{ph} < 1500$ V)	I - <20 msec up ...
Rapid voltage changes (<10%)	number of changes (ΔU normally < 5%, exceptionally <10%)	I - to be defined
Voltage dips 10% < ΔU < 95% t < 1 min	- number of dips (majority less 1 sec)	I - 20 msec to 1 min - e.g. 1 year
Short interruptions ΔU or ~ 100% t < 3 min	- number of interruptions (ca 70% less 1 sec)	I - 20 msec to 1 min - e.g. 1 year
Flicker	- $P_n \leq 1\%$ - 95% of a week	L - 10 min over 2 h - one week
Unbalance (negative sequence)	- majority < 2% exceptionally < 3% - 95% of a week	L - 10 min rms mean values - one week

Table 2: Limits and indicative values for EM disturbances related to the voltage magnitude [EN 50160 or UNIPEDE Guide]

transmission (continuously or at fixed periods), etc, ... can be considered: the necessary options exist.

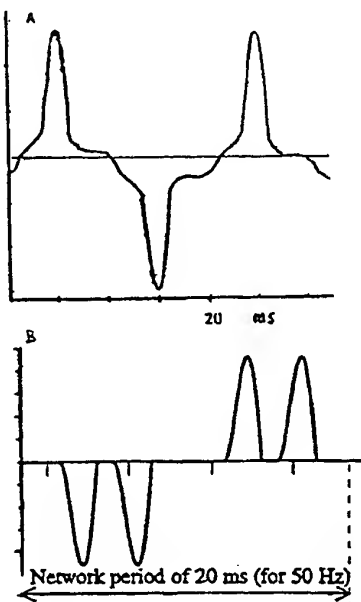


Fig. 6: Current of
a) TV set
b) speed regulated drive

Practically, sophisticated equipment may be used for technical investigations, the detection of the origin of faults, in case of user complaints. Simplified equipment is appropriate for a statistical assessment over a whole network.

6. Responsibility for Power Quality

With reference to the classification of the PQ parameters in chapter 3, the improvement of PQ means:

- stabilization of the power frequency and network voltage
- reduction of magnitude and rate of occurrence, possibly elimination, of the network voltage variations (flicker, dips, etc, ...)
- reduction of magnitude and rate of occurrence, possibly elimination, of the conducted low frequency electromagnetic disturbances, harmonics, etc, ... and transients

In practice measures have and can be taken on two levels

- measures related to the network dimensioning and operation - on the supply utility side
- measures related to the disturbing loads - on the consumer side.

A very broad technical literature exists in specialized revues or in the proceedings of EMC symposiums on these subjects. They cannot be dealt with in the context of this paper and it is referred to this literature. However, there is one aspect, which is less frequently considered: the respective responsibility of the supply utility and of the consumers for the improvement of

PQ. Let's examine the situation for the most important parameters.

- **Power frequency voltage range, slow variations**

It is the primary task of a utility to supply electricity within the normal frequency range and within the normal voltage range. This implies a correct dimensioning of the transformers and lines as well as appropriate operation rules (limits for voltage drops, voltage regulation, ...). Accordingly the Utility has to take care of slow voltage variations.

In the following it is then always assumed that the network is correctly dimensioned within the regulatory or contractual requirements.

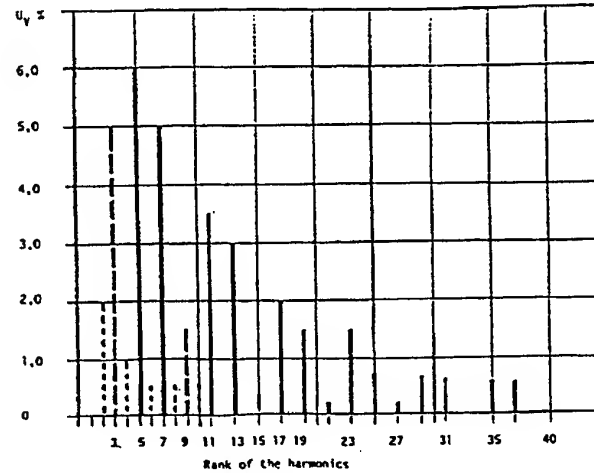


Fig. 7: Compatibility levels for harmonics
(IEC 61000-20-2)

- **Long voltage interruptions**

Long voltage interruptions are practically always caused by faults in the network for which the utility must take care.

- **Overvoltages**

Temporary overvoltages occur in the LV systems seldom (generally the LV distribution systems are operated with a solidly grounded neutral); they can arise as a consequence of a fault and switching on of power factor improvement capacitors.

- **Rapid voltage changes**

The are due

- either to tap changes in transformers on the utility side
- or to switching on/off big loads on the consumer side.

- **Voltage dips, short voltage interruptions**

Such disturbances can happen because of:

- either faults on the lines (e.g. short-circuits or earth faults followed by rapid re-cluse)
- or by faults in the consumer installation (cleared up quickly by protection devices).

The former ones depend strongly on the network characteristics: overhead or cable lines, climatic environment,

The other ones depend on the use of equipment according to quality standards and appropriate installation.

- **Voltage fluctuations and flicker**

Voltage fluctuations and the resulting flicker are due to the characteristics of the load (e.g. arc furnaces, motor switching, ...) for which the consumer is responsible and for which he has to comply with the relevant standards.

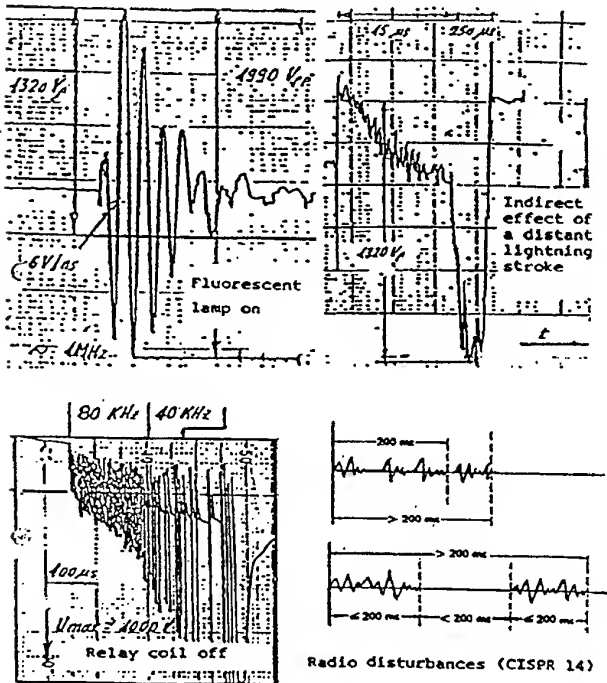


Fig. 8: Typical example of transients in LV networks

- **Harmonics, Interharmonics**

The source of harmonics is definitely on the user side which must comply with the relevant current limiting standards (e.g. for small equipment IEC 61000-3-2) or agree on the connection conditions with the utility (for large equipment IEC 61000-3-4/6)

However, as mentioned, it should be expected that the utility put at disposal a correctly dimensioned network

- **Unbalance**

Origin is mostly an unbalanced load between the three phases

- either because of a wrong distribution of the load on the three phases by the utility
- or by the consumer

- **Transients**

Transients are mostly caused by switching phenomena or in the network in the user installations. They are natural phenomena for which, for the time being, no limitation standards have been developed. For some cases mitigation rules exist.

Other transients are due to lighting but are infrequent.

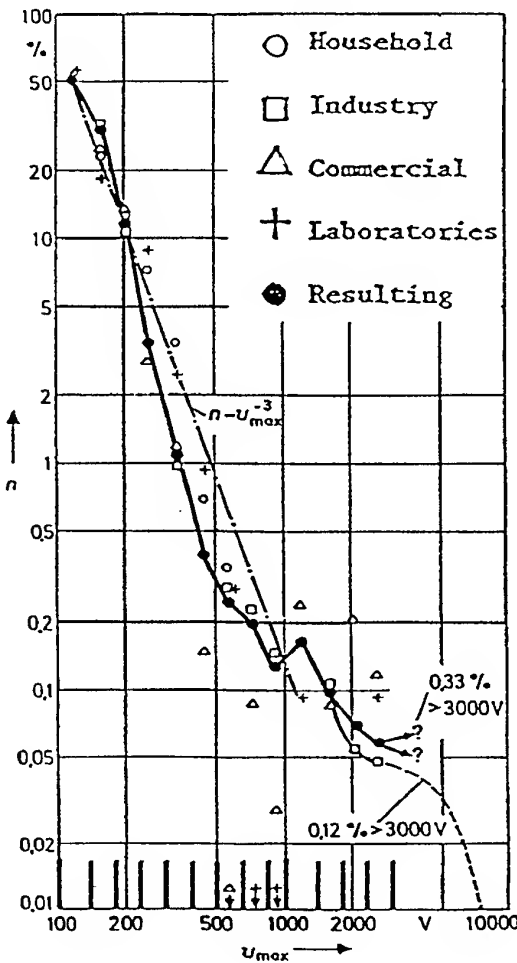


Fig. 9: Percentage of transients exceeding a given value of U_{\max} [3]

Three conclusions or remarks follow from above overview:

- The responsibility for PQ is shared between utilities and users. However, it cannot and should not be said which side bears more responsibility.
- Some of the PQ parameters can be kept under control and relevant limiting standards or installation guidelines have been or can be developed. Other PQ parameters cannot or not yet be kept under control and should be considered as natural phenomena.
- Therefore it is recommended,
 - that the utilities design and lay out their networks in order to provide good supply conditions
 - the user respect the product standards and in particular the ones related to the limitation of EM emissions.

7. Some aspects regarding the future

It can be seen from above considerations that considerable work has been already carried out with regard to PQ. Of course, all Electricity Companies will

continue their efforts to improve the quality of supply and the existing technology. In the context of this paper, this topic should not be dealt with, but rather consideration be given to some important aspects which may or may not arise in future. Let's discuss some of these items.

- **Single PQ factor**

It has been considered, if the PQ of a network could be characterized by a single factor combining all the parameters. But the actual level of each parameter depends very much on the local conditions, then how to combine harmonics and voltage dips taking into account the climatic environment? Difficult! The idea has been quickly abandoned and PQ has to be assessed parameter by parameter.

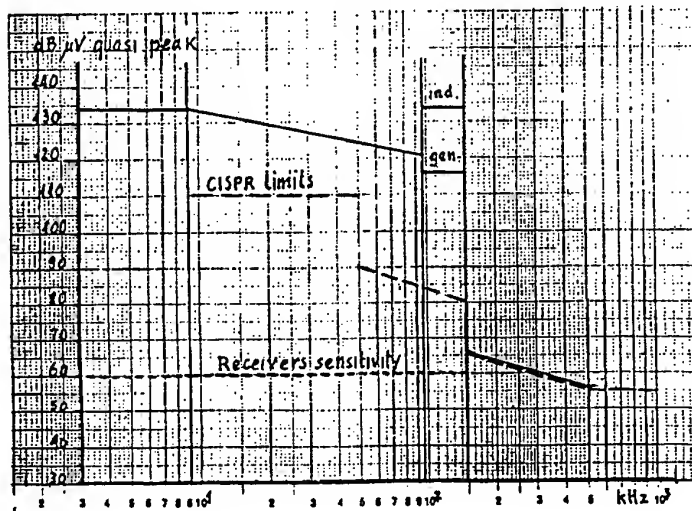


Fig. 10: Emission limits for mains signaling

- **PQ classes**

Another consideration was if it would be possible to define PQ classes. Also a very delicate intention ... which may have negative legal or psychological aspects. The idea has also been abandoned ... at least for the time being.

- **User's satisfaction**

A feature, which has slightly been alluded to in the previous chapters, is the consideration that PQ is not only a technical problem but that it should also be estimated by the level of satisfaction of the users with regard to its application.

This aspect has been considered by EdF- Electricité de France - with its project QUALIMAT which consists of two parts:

- the "physical" measurement of the voltage characteristics countrywide, with a large set of measurement apparatus QUALIMETRE associated with a statistical analysis software QUALISCOPE [10, 11, 12]
- an analysis of the "subjective" feeling of the users by means of questionnaires sent to a sample of customers.

Such a campaign can allow to clarify up which phenomena are more disturbing, up to which level

improvements are necessary, etc., ... but it requires a great effort from the supplier and is only possible in "powerful" utilities.

- **Most disturbing phenomena**

Which are the most disturbing PQ parameters? The following statements are not based on formal results of inquiries but on the literature, the utilities' opinions, the standardization work , etc., ... It seems that from the view point of the users, dips and voltage interruptions are the most unacceptable disturbances; blackouts, loss of production, breakdown of medical equipment, etc., ... From the viewpoint of the utilities the harmonics problem is the one which gives rise to more concerns with regard to a possible widespread effect on various equipment types. This does not mean that the other PQ parameters are not to be considered but just that they are easier to keep under control , that their levels are not critical presently or for the near future.

- **Power Quality contracts**

Utilities may offer to interested users - e.g. users with sensitive applications - contracts which guarantee a given level of PQ (more exactly of its main parameters). For example, EdF has launched such a policy with the "Contrat Emeraude" which addresses industrial HV, MV, ev. LV customers (the latter above a given power level). This type of contract gives guarantee with regard to frequency and voltage stability, dips and short interruptions, harmonics, etc., For this purpose EdF has developed a special meter which on the one hand carries out the usual metering functions, on the other hand measures and records all guaranteed PQ parameters. It provides local reading and remote communication to a control center. Generally the Contrat Emeraude corresponds to the relevant parts of EN 50160 [3]. EdF offers also more stringent contracts.

- **Liability of the Utility**

Electricity has to be considered as a product and this has been specifically stated in the EU Directive 85/374/EWG - AH2 on "Product liability". Laws on product liability exist also in other countries (e.g. USA) and the question arises how they apply to electricity. This is a complicated and delicate legal problem:

- How to define the quality of electricity from a legal viewpoint?

In Europe for example, CENELEC EN 50160 [3] serves as reference (possibly only for the parameters for which specific limits are defined).

In other countries, a law may exist or a decree for specifying requirements for the electricity supplied (probably limited only to the main parameters).

- How to proceed when the specified power quality is not met? For example, what is the liability of a Utility in case of loss of production or in case of disturbed medical equipment? How to judge if the necessary measures have been taken, the relevant standards fulfilled...??

- **Privatization of the Electricity Supply**

The question arises if the present move towards the privatization of the electricity supply in Europe will have consequences on the PQ level. This question is open for discussion.

Bibliography

- [1] IEC 61000-4-30 (presently new work - see 77A/205/WG and 77/183/NP): Electromagnetic compatibility (EMC) - Part 4: Testing and measuring techniques - Section 30: Power Quality measurement methods
 - [2] IEC 61000-2-2 (1990): Electromagnetic compatibility (EMC) - Part 2: Environment - Section 2: Comparability levels in public power systems
 - [3] CENELEC EN 50160 (1994): Voltage characteristics of electricity supplied by public distribution systems
 - [4] UNIPEDE Ref.: 23002 Ren 9464 (1994): Report on EMC Co-ordination in Electricity Supply Systems.
 - [5] UNIPEDE Ref.: 23002 Ren 9530 (1995): Application Guide to the European Standard EN 50160
 - [6] UNIPEDE Ref.: 23002 Ren 9531 (1995): Measurement Guide for Voltage characteristics
 - [7] IEEE Std 1159 (1995): IEEE Recommended Practice for Monitoring Electric Power Quality
 - [8] ESKOM (South Africa) (1995): Eskom Handbook on Quality of Supply
 - [9] Canadian Electricity Association: Publ. 220 D 711 and ff (1966): Power Quality Measurement Protocol
 - [10] EdF Publ. 94 NR 00001 (1993): Les outils d'appréciation de la qualité de l'électricité: Mesures physiques et perception de la clientèle - M. Suchard, N. Baumier, C. Greiveldinger
 - [11] EdF Publ. 94 NR 00079 (1994): Measurement and analysis of the quality of supply in distribution systems - N. Baumier, P. Fauquemergue, M. Suchard
 - [12] EdF Publ. 95 NR 00073 (1995): The Qualimat experiment: First results of the measurements
 - [13] Bull. SEV 1/1997: p. 29 ... 34: Integrale Messung der Netzqualität - T.Kahn
 - [14] IEC 61000-X-Y: Series of IEC standards and reports on EMC
- Note: There exist also in numerous other industrialized countries regulations concerning PQ indicative values, measurement techniques, and EMC standards, e.g. Great Britain, Japan, Poland, Hungary, Czech Republic, etc.

Biographical Note



G. Goldberg graduated as Electrical Engineer at the ETHZ - Federal School of Technology Zurich - where he began his career as Assistant to the Professor for Electrical Installations. He joined thereafter Landis & Gyr Cie where he worked in the field of Telecontrol for Electrical networks, particularly in the field of Ripple Control.

He was from 1985 to 1994 Chairman of IEC TC 77 - Electromagnetic Compatibility - and from 1990 to 1996 Chairman of ACEC - Advisory Committee on Electromagnetic Compatibility. In this capacity he initiated in IEC the work on Power Quality. He has published ca 40 papers on various subjects, particularly EMC.

ETSI - STANDARDS FOR: THE GLOBAL MARKETPLACE - RADIocommunications

Karl-Heinz ROSENBROCK
European Telecommunications Standards Institute
Route des Lucioles
06921 Sophia Antipolis Cedex, France
Karl-Heinz.Rosenbrock@etsi.fr

1. INTRODUCTON

This paper describes the activities of the European Telecommunications Standards Institute (ETSI) in the field of Radiocommunications and EMC Standardisation. It covers the purposes and organisation of the Institute, its relations with other bodies involved in the standardisation and regulation of Radiocommunications and Electromagnetic Compatibility. The paper considers the likely future developments in this area.

2. WHAT IS ETSI?

ETSI is one of the three European Standardisation organisations that are recognised by the European Commission.

The objective of ETSI is to be a regional standards body sensitive to market needs with an innovative and efficient approach to producing quality standards in a timely manner.

2.1 Membership

ETSI currently has 487 Full Members and 75 Observers coming from 34 countries within the CEPT geographical region. ETSI also has 47 Associate Members coming from 13 other countries world wide. This gives a total of 609 members from 47 Countries.

ETSI members are Manufacturers (53 %), Network Operators (16 %), Administrations (10 %), Users (6 %) and Research Bodies, Service Providers and others (15 %).

ETSI's membership composition is shown graphically in figure 1.

ETSI's membership includes 25 Full members from 12 Central and Eastern European Countries, including an Associate Member from Lithuania.

ETSI has published a total of 2849 deliverables. The number of deliverables produced annually continues to increase exponentially.

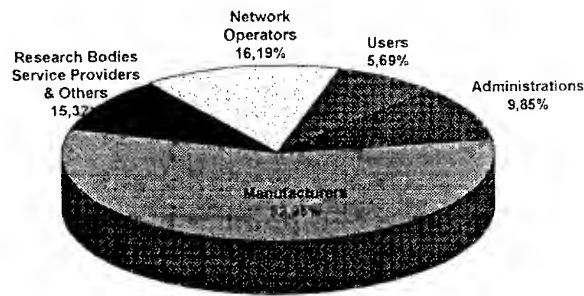


Figure 1: Composition of ETSI membership

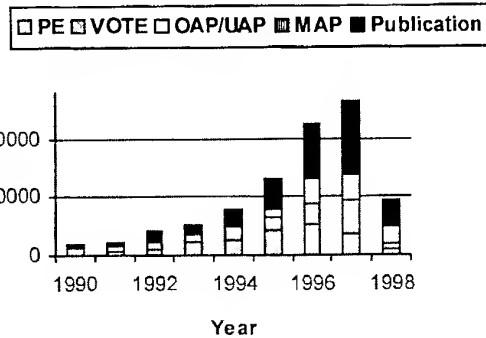


Figure 2: ETSI annual production

2.2 Structure

In 1996, ETSI adopted a new organisation. The aims of this organisation were to increase the efficiency of the standards making process in order to be able to meet the challenges brought by the changing technological environment (convergence of technologies) and the trend towards deregulation in the telecommunications sector.

The ETSI Technical Organisation is divided into Technical Committees, which provide a permanent base of expertise on matters which are common to a number of technical areas, and ETSI Projects, which are formed for the purpose of standardising a particular product, and which terminate once the standardisation project is complete.

The currently active ETSI projects are shown in figure 2.



Figure 2: ETSI Projects

The ETSI Projects relevant to Radiocommunications are: DECT, SMG, BRAN and TETRA.

The ETSI Technical Committees are shown in figure 3.

Technical Committees SES and TM include some radio aspects. The Joint Technical Committee with CENELEC and the European Broadcasting Union (EBU) also includes some radio aspects.

The principal committee for dealing with spectrum sharing and electromagnetic compatibility aspects of ETSI standards is Technical Committee ERM. This brings together all EMC and radio spectrum sharing standardisation to one place within the Institute allowing issues in this area to be resolved in an effective manner. The broad membership of ETSI puts it in a unique position to resolve the often conflicting demands of the players in the radiocommunications arena, and to come to conclusions on EMC and radio-related matters that reflect the needs of all sectors of industry.

Previously, EMC standardisation had been split between committees dealing with radio and telecommunications standards.

TC ERM is also the place where new technical areas in the radiocommunications field are developed. When an ETSI Project concerned with radiocommunications terminates its activities, the responsibility for maintenance of the standards produced moves to TC ERM.

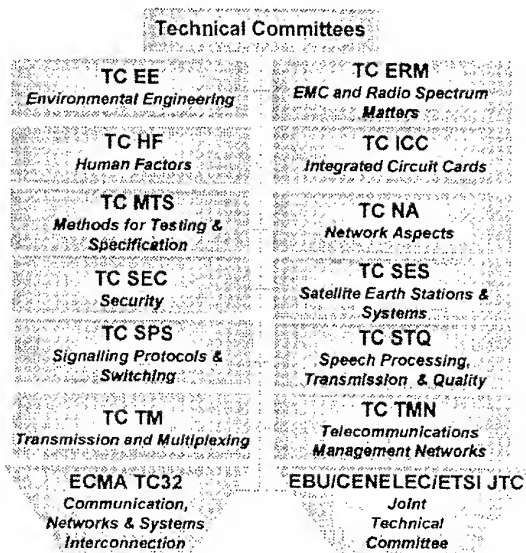


Figure 3: ETSI Technical Committees

3. THE REGULATORY ENVIRONMENT

3.1 The current position

Both EMC and Radiocommunications are areas which are regulated by Directives within the European Union (EU) Member States. For those areas where there are no EU Directives, national regulations apply. National regulations normally require type approval of radio equipment and may also require individual operator licensing. National regulations are co-ordinated through the CEPT European Radiocommunications Committee (ERC).

ETSI has a Memorandum of Understanding with the ERC in which ETSI standards are used for the type approval of radio communications equipment intended to be put into service within the CEPT countries.

Frequencies are allocated on a global basis by the ITU World Radio Conference (WRC). European positions are co-ordinated through the ERC Conference Preparatory Group (CPG). ETSI, through the Memorandum of Understanding, participates in the CPG to advise on trends in the radiocommunications industry in Europe as an input to ensure the long-term availability of the spectrum necessary for radiocommunications services.

Within the European Union, all electrical or electronic equipment is required to meet the EMC Directive [1] before being placed on the market. Telecommunication Terminal Equipment (TTE) and Satellite Earth Station (SES) equipment are also required to meet the relevant Directive [2] and [3] (recently replaced by [4]), both of which define essential requirements related to EMC and effective use of the radio spectrum.

The application of these three Directives is based on Harmonised Standards, which allow a manufacturer to construct his equipment and benefit from a

presumption of conformity with the Directives and free movement of his goods throughout the EU. ETSI is mandated by the EU to develop these Harmonised Standards.

To date, ETSI has published 44 Harmonised standards on EMC. 12 draft Harmonised Standards on EMC are on Public Enquiry or Vote and 11 drafts are at pre-Public Enquiry stage.

ETSI has also published 32 Harmonised Standards under the TTE and SES Directives (TBRs), of which 18 are in the radiocommunications sector. 7 drafts are in a pre-publication phase, of which 5 are radio equipment.

3.2 Future legislative trends

A draft Directive on Connected Terminal Equipment (also known as the Radio and Telecommunication Equipment (R&TTE) Directive) under discussion within the EU and is predicted to become mandatory around 1st January 2000.

This Directive is predicted to cover all radiocommunications equipment, as well as all equipment intended for connection to the Public Switched Telecommunications Network (PSTN).

The new Directive is predicted to include the essential requirements currently covered under the EMC Directive and the TTE and SES Directives. It is predicted to put a greater emphasis on declarations by manufacturers against Harmonised Standards, reducing the requirements for type approval prior to entry on to the market.

In this environment, ETSI expects to develop the necessary deliverables to allow manufacturers to demonstrate compliance to the essential requirements of the Directive in a time frame which is suitable for the modern telecommunications market.

4. ETSI'S ACTIVITIES IN RADIOPHONICS

4.1 ERMES

The Enhanced Radio Message System (ERMES) paging standard [5] developed by ETSI specify a high speed paging system with an ability for international roaming. Basic features standardised allow for simple "tone only" pagers, numeric, alphanumeric or "transparent data" pagers used for data transfer.

The standardised solution allows for individual and/or group calls, call diversion and a Universal Computer Protocol (UCP) for software access. It operates in Europe on a harmonised frequency band (169.4 MHz to 169.8 MHz) with a 16-channel scanning system that facilitates cross-border roaming.

Work on a two-way facility is currently underway, which will allow a further increase in traffic capacity coupled with the possibility for extended functionality.

4.2 GSM

Standardisation of the Global System for Mobile communication (GSM) started in 1984 in CEPT before the foundation of ETSI. GSM is now established as a global cellular telephone system with 233 networks on air in 105 countries / areas at the end of 1997.

GSM has been developed using a phased approach. Phase 1 offered basic services, which is being taken over by Phase 2 systems.

The modular approach is developed to allow a smooth migration path to third generation systems. GSM Phase 2+ is currently being developed, allowing circuit switched data services up to 64 kbit/s, general packet radio services, dual mode operation (GSM/DECT, GSM/DCS 1800, GSM/Mobile Satellite Services (MSS), integration of intelligent network aspects, optimised routing of calls when roaming and both half-rate and enhanced full-rate voice codecs.

4.3 UMTS

The Universal Mobile Telecommunications System (UMTS) is the ETSI third-generation wireless communication system to meet the International Telecommunications Union (ITU) requirements of the IMT-2000.

UMTS is targeted at providing globally available personalised and high quality mobile communication services. Its objectives include: integration of residential, office and cellular services into a single system and one-use equipment; speech and service quality at least comparable to current fixed networks; service capability up to multimedia; separation of service provision and network operation; UMTS user numbers independent of network or service provider; the capacity and capability to serve over 50 % of the population; seamless and global radio coverage and radio bearer capabilities up to 144 kbit/s and further to 2 Mbit/s.

The ETSI system is based on GSM. Trials are expected to be made around the turn of the century, with system introduction planned for around 2002. The fact that the system is being developed from GSM will allow a smooth introduction of new services.

4.4 DECT

The Digital Enhanced Cordless Telecommunications (DECT) standards developed by ETSI specify a cordless telephone system, the performance of which greatly exceeds that of previous systems (such as CT1, CT1+ and CT2). This is especially true regarding security aspects such as illegal interception of the radio link and protection of the use of the radio by unauthorised third parties. An overview of DECT standardisation is given in [6].

As well as providing for domestic and business cordless telephony applications, DECT is ideally suited to providing mobility services in urban areas with two-

way calling, roaming, seamless hand-over and the possibility of encryption. The automatic frequency selection capability of DECT makes it simple to install without the need for *a priori* frequency planning.

DECT also provides an effective solution for Radio in the Local Loop (RLL) applications. The wired local loop is traditionally the "weak link" in telecommunications network provision, as its installation cost is very high and its use is low. It is expensive to upgrade and is often not suitable for modern, high bandwidth communications.

DECT in the Local Loop provides a flexible, easy to install alternative to wired local loop connection. In addition to the general benefits of using radio in the local loop, it offers the user local mobility, privacy and the capability to connect to ISDN.

4.5 TETRA

Terrestrial Trunked Radio (TETRA) is a pan-European mobile radio system providing services for professional users.

Initially developed to meet the demands of emergency services, utilities and private corporations with large fleets, it offers a broad range of facilities for professional communications. Such applications require full availability of a network that can be extended in an ad-hoc fashion in emergency situations. Also required are security of information and authentication of users with capability for group call and direct mode operation.

Facilities of TETRA include dynamic group call, fast call set up and a range of security options including end to end encryption. Specific options include Direct Mode Operation (DMO), allowing mobile users to communicate in regions outside of network coverage, and Dual Watch, in which the users operating in direct mode can be accessed by the network when they enter the coverage area.

TETRA provides four TDMA channels in a 25 kHz bandwidth. In its Voice + Data application, it provides bandwidth on demand up to 28.8 kbit/s in circuit mode as well as proving capability for packet-mode data, and short message data.

TETRA also provides a mobile repeater and gateway functions, enabling the user to extend network coverage as required and give greater reliability and security.

Further information about TETRA can be found in [7].

4.6 Satellite Earth Stations

ETSI has developed standards for Very Small Aperture terminals (VSAT), satellite News Gathering (SNG) and Satellite Personal Communications Networks (S-PCN) that define the essential requirements under the Satellite Earth Station Directive [3].

In 1998 the Technical Committee SES will focus on other standardisation activities covering the interworking with terrestrial networks, in particular GSM. This activity will cover the Common Air Interface between Geostationary Satellite and the core network of GSM. The standardisation work will be carried in co-operation with ETSI SMG.

In 1998 the Technical Committee SES will start the standardization work on the Satellite Component of UMTS, in co-operation with GSM.

The standardization of Broadband Satellite Multimedia Terminals using all types of orbits and different frequency bands, will start in 1999, following the decisions achieved in WRC 97.

Prior the standardization process, the Technical Committee SES will conduct a survey in 2 Phases of the Broadband Satellite Multimedia environment.

Phase 1 for the description of the situation, and an overlook of all the Market Players. Phase 2 for the survey of the standardization objectives which are acceptable by the Market players.

4.7 Digital Broadcasting

In co-operation with the European Broadcasting Union (EBU) and CENELEC, ETSI has developed a series of standards and reports on Digital Video Broadcasting (DVB). A compete listing can be found in [8].

Standards cover baseband processing (based in the ISO/IEC MPEG-2 standards [9], transmission via satellite, terrestrial radio or cable links, conditional access systems and interactive services.

4. RELATIONSHIP WITH OTHER BODIES

In the field of EMC and radio spectrum matters, ETSI has co-operation agreements with IEC and CENELEC and is an observer to CISPR.

ETSI develops standards in co-operation with IEC for maritime radiocommunications forming part of the Global Maritime Distress and Safety System (GMDSS).

ETSI is currently develops standards for ground-based aeronautical radio, and is in discussions with EUROCAE and EUROCONTROL on the way forward for standardisation of airborne radio equipment.

6. CONCLUSIONS

ETSI is active in all areas of aeronautical, maritime and terrestrial radiocommunications and EMC, developing standards for the global market place.

ETSI is an innovative and market-driven partner in world-wide standardisation open to all telecommunications players from around the globe.

7. REFERENCES

- [1] Council Directive of 3 May 1989 on the approximation of the laws of the Member States relating to electromagnetic compatibility (89/336/EEC).
- [2] Council Directive of 29 April 1991 on the approximation of the laws of the Member States concerning telecommunications terminal equipment, including the mutual recognition of their conformity (91/263/EEC).
- [3] Council Directive 93/97/EEC of 29 October 1993 supplementing Directive 91/263/EEC in respect of satellite earth station equipment.
- [4] Directive 98/13/EC of the European Parliament and the Council of 12 February 1998 relating to telecommunications terminal equipment and satellite earth station equipment, including the mutual recognition of their conformity.
- [5] ETS 300 133: "Electromagnetic compatibility and Radio spectrum Matters (ERM); Enhanced Radio MEssage System (ERMES)".
- [6] ETR 178: "Digital Enhanced Cordless Telecommunications (DECT); A high level guide to the DECT standardization".
- [7] ETR 300-1: "Terrestrial Trunked Radio (TETRA); Voice plus Data (V+D); Designers' guide; Part 1: Overview, technical description and radio aspects".
- [8] Digital Video Broadcasting (DVB); A guideline for the use of DVB specifications and standards.

- [9] ISO/IEC 13818: "Information Technology - Generic Coding of Moving Pictures and Associated Audio Information".

BIOGRAPHICAL NOTES

Karl Heinz Rosenbrock has been the Director-General of the European Telecommunications Standards Institute, based at the ETSI Secretariat in Sophia Antipolis (South of France), since November 1990.

He was born in Hermannsburg, Germany in June 1941 and studied at the Technical University of Braunschweig, from which he received the degree of Diplom-Ingenieur in 1967.

He immediately joined the Deutsche Bundespost. Subsequently, he held the position of Head of Section for international switching at the Telecommunications Centre (FTZ) at Darmstadt. He then became project leader and Head of Section for the digitalization of the telephone network and the introduction of ISDN in the former Federal Ministry of Posts and Telecommunications in Bonn and then Head of Department back at the FTZ in Darmstadt for telephone and ISDN Technology, Planning, Operation, Testing and Services.

Before joining ETSI he was Head of the Standardization Division of the Ministry of Posts and Telecommunications (BMPT) at Bonn.

II

ANTENNA AND PROPAGATION EMC ASPECTS

FORMULA FOR SHORT-DISTANCES PROPAGATION LOSS ESTIMATION

Vladimir A. Aporovitch
Viacheslav A. Svetlichnyi

Research Institute of Automation Facilities, 117 F. Skorina Ave,
Minsk, 220600, Belarus
Phone (0-17)264 -63 -70, Ficsimile (0-17)264 -24 -50

The approach and new formula for short distance propagation loss estimation are described in this paper. This formula was created due to geometric approach to exchange of energy between transmitting and receiving antennas on short distances, include near - field zone. Formula gives valid results in range of distances from 0 and it can used for loss estimation ("worst event") in tasks of EMC on one mobile object, tower or roof.

1. INTRODUCTION

Short distances propagation loss estimation is often necessary in problems of EMC of radio means, especially in local groups, for example on mobile object (aircraft, ship), on tower or roof. But using of near field equations of wave theory is too hard because of their complexity.

Usually they used empirical formulas, based on simple formula for free space [1]

$$L = \frac{P_1}{P_2} = \frac{16\pi^2 R^2}{\lambda^2 D_1 D_2}, \quad (1.1)$$

where: L is propagation loss,

P_1 is radiated power at the input of transmitting antenna (TA),

P_2 is received power at the output of receiving antenna (RA),

R is distance between the TA and RA,

λ is wavelength,

D_1 is gain of transmitting antenna in the direction to RA,

D_2 is gain of receiving antenna in the direction to TA.

Example of similar formulas is in [2]:

$$L[\text{dB}] = 20\log f [\text{MHz}] + 20\log [m] - 28 + Sa, \quad (1.2)$$

where f is a frequency and Sa is additional factor on the length of antenna in dB.

Empirical formula (1.2) is recommended for couple of antennas on the line of sight on the board of aircraft. Similar formula is in [3]. The main feature of all listed above models is that they can't give correct result when $R \rightarrow 0$. For example, when $R=0$ we have $L=0$. It can mean that $P_1=0$, i.e. transmitter does not radiate, but it is impossible. It can mean that $P_2=\infty$, i.e. receiver receives endless power. It is impossible too. The problem is to create a model which give the mathematically and physically correct result by any short distances include zero.

2. GEOMETRIC APPROACH AND NEW FORMULA

Usually they define R as a distance between electrical centers of antennas [1,2,3]. We propose to define R as a distance between the center of TA and the absorption cross section of RA represented as a segment of sphere.

Fig.1 shows the performance of geometric approach. We propose to perform the TA as a radiating point. The point of RA is in the center of circle, which arise at the founding of a segment of sphere. The radius of the sphere is R. The square of the segment is equal to absorption cross section of RA [1]:

$$S_2 = \frac{D_2 \lambda^2}{4\pi}. \quad (2.1)$$

We have to take into account D_1 and equal cross section will be:

$$S_{2e} = \frac{D_1 D_2 \lambda^2}{4\pi}. \quad (2.2)$$

We represent this cross section as a segment of a sphere with the center in the point of TA.

Real distance between TA and RA is r . When $R \gg \lambda$ (far zone), $R \approx r$ and the segment practically is a circle – Fig. 1, a. At the short distances $R \neq r$, look Fig. 1 b, c.

So, the real distance between antennas r from TA to RA is less than R . The difference is the height of segment of sphere. Our task is to have the meaning of R . Geometry of the task is shown on Fig. 2.

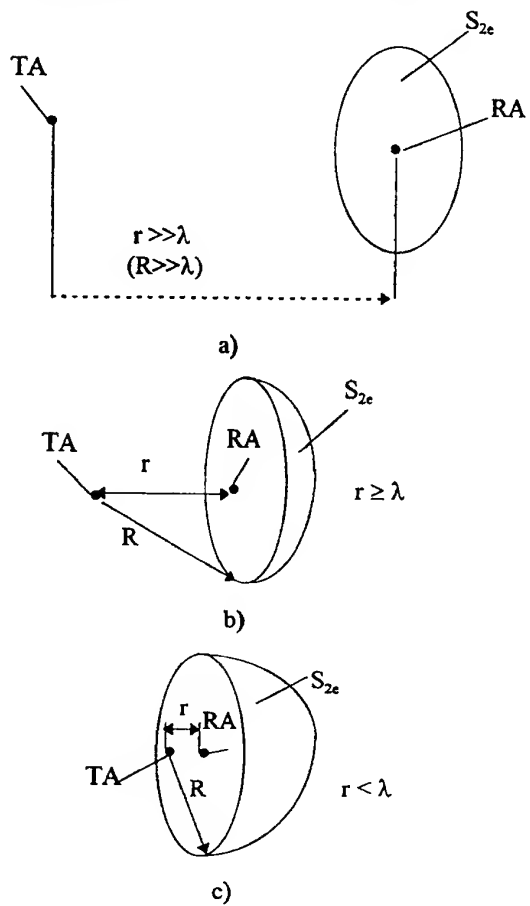


Fig. 1. Performance of geometric approach

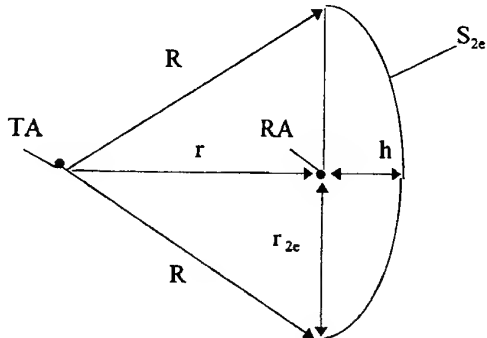


Fig. 2. Geometry of the task.

On Fig. 2 r_{2e} is a radius of the founding of segment, h is the height of segment. So,

$$R = \sqrt{r^2 + r_{2e}^2}, \quad (2.3)$$

$$r_{2e} = \sqrt{R^2 - (R-h)^2}. \quad (2.4)$$

With accordance with formula for height of segment of sphere

$$h = \frac{S_{2e}}{2\pi R}. \quad (2.5)$$

Formulas (2.3), (2.4) with formulas (2.5) and (2.2) after changes give us

$$R^2 - Rr - \frac{D_1 D_2 \lambda^2}{8\pi^2} = 0. \quad (2.6)$$

From this square equation we can have:

$$R = \frac{r}{2} + \sqrt{\left(\frac{r}{2}\right)^2 + \frac{D_1 D_2 \lambda^2}{8\pi^2}}. \quad (2.7)$$

So, we have to use formula (1.1), where the meaning of R we may have from formula (2.7). There r is a real distance between TA and RA.

3. CALCULATION OF LOSS

Results of calculations accordance with formulas (1.1) and (2.7) are shown on Fig. 3 (for $D_1=1$, $D_2=1$) and Fig. 4 (for different D_1, D_2).

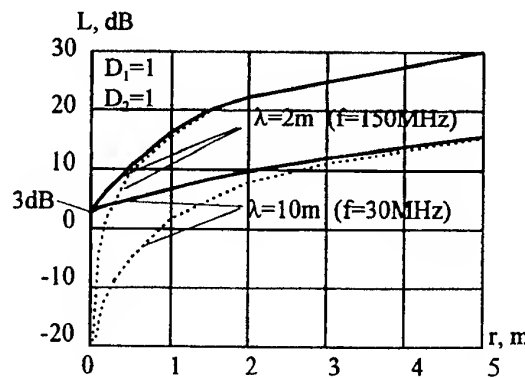


Fig. 3. Results of calculations for $D_1=1$, $D_2=1$

— formulas (1.1) and (2.7)
········· formula (1.1) with $R=r$

Results show us, that for $r=0$ the meaning of L is 3dB (2). For $r \geq \lambda$ formulas (1.1), (2.7) give us the same result that formula (1.1) with $R=r$, i.e. for far distances all models are the same. The increasing of

antennas gains leads to reducing of the loss, but at $r = 0$ L is 3dB always. This effect can be explained so, that at $r = 0$ we have electrical connection of antennas.

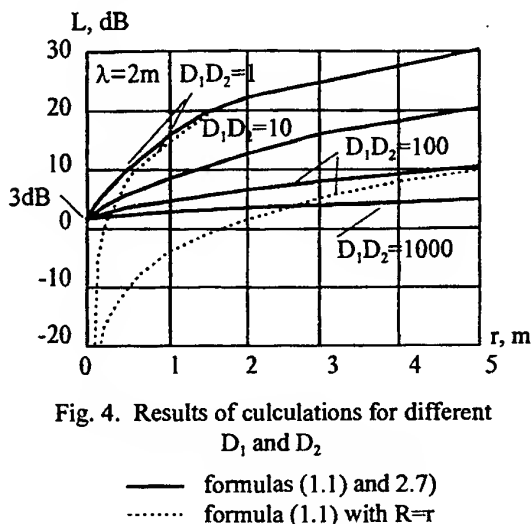


Fig. 4. Results of calculations for different D_1 and D_2

— formulas (1.1) and 2.7)
- - - formula (1.1) with $R=r$

Really, antennas "joined" and we have one antenna. Output of transmitter is connected to this united antenna and to input of receiver directly at the same time. Then naturally a half of power moves into the receiver and a half of power radiates.

4. CONCLUSIONS

After calculation accordance formula (1.1) and formula (2.7) we can do following conclusions:

1. Distance R can't be equal 0 and result of (1.1) and (2.7) always will be mathematically correct. It is very important for computer calculations.

2. Formula can give physically correct result for real distance $r=[0, \infty)$. For example, when $r=0$, $L=2$ (3dB). It means that a half of power moves into a receiver and a half radiates. It is correct if transmitting and receiving antennas "joined" each with other into single antenna.

3. When $r > \lambda$ the results of calculation accordance to formulas (1.1) with (2.7) and (1.1) with $R=r$.

4. It is obvious, that formulas (1.1) with (2.7) gives us the lowest border of loss, when we does not take into account complex coupling of antennas. But lowest border is needed in EMC-calculations often, because it is the "worst" event for EMC.

5. Coupling of antennas we can take into account by meanings of D_1 and D_2 .

We can't use new formula when sizes of antennas much more than λ , because we propose, that antenna is a point.

5. REFERENCES

1. Doluhanov M.P. Rasprostranenie radiovoln. Moscow, "Sviaz", 1972, (Russian). [Doluhanov M.P. Radio wave propagation. Moscow, "Sviaz", 1972]

2. Bull D.A. Smithers B. W. "Antenna - to - antenna coupling in aircraft radio systems" - IEEE Int. Symp. on EMC, San-Diego, CA, USA, Oct. 9-11, 1979, pp.274-281.

3. Gerbi G., Anro C. Antenna coupling analysis program - 4-th Symp. and Techn. Exh. on EMC, Zurich, March 10-12, 1981, pp.481-486.

BIOGRAPHICAL NOTES

Vladimir A. Aporovitch works as Chief Specialist of Electromagnetic Compatibility Research Center of Research Institute of Automation Facilities in Minsk (Belarus). He received the Doctor of Science degree in digital processing of information in 1984. Mr. Aporovitch is the author of 43 papers some of them were presented on international and national conferences.

Viacheslav A. Svetlichnyi works as Chief Scientific Collaborator of Research Institute of Automation Facilities in Minsk (Belarus), Doctor of Science. Mr. Svetlichnyi is the author of 47 papers.

FEATURES OF ELECTROMAGNETIC WAVE SCATTERING BY SYSTEMS OF NONLINEAR OSCILLATORS

A. A. Gorbachev, T. M. Zaboronkova, L. V. Vasenkova

Radiophysical Research Institute,
25 B. Pecherskaya st., Nizhny Novgorod 603600, Russia
Fax: +7 8312 369902; E-mail: zabr@nirfi.sci-nnov.ru

Abstract — The peculiarities of electromagnetic wave scattering at higher harmonics by the system of crossed oscillators and statistical system of nonlinear scatterers are considered. The behavior of the back scattering field at the double frequency on the distance between half-wave dipoles and location of the load in them has studied. Some polarization features of the field scattered at the higher harmonics which are absent in the field scattered at the fundamental frequency are discussed. The analysis have shown that the difference in the mean noise at the odd and even harmonics is considerable.

1. INTRODUCTION

The wide application of radio aids imposes rigorous requirement on the use of the radio range. The problem of overcrowded and contaminated state of the air is dramatized by increasing noise of different origins. Among the noise sources is the contact noise due to radio wave scattering by mechanical structures with nonlinear insertions (screw joints of case panels, places of antenna junctions and mounting, contacts of different metals, etc.). It should be noted, that the presence of such "internal" nonlinearities can be not only a reason of a high interference level at the radio reception but also may have as well a useful application, for example, the detection of hidden effects in industrial products.

The present paper deals with the investigation of the peculiarities of electromagnetic wave scattering at higher harmonics by different system of thin metallic oscillators with a nonlinear local load placed in the free space. Below we consider the system of crossed oscillators and statistical system of nonlinear scatterers. The scattering of electromagnetic waves by simple systems containing two or four parallel thin metallic dipoles with a nonlinear element has been studied in [1]. The obtained results has shown the existing a dependence of the scattered field on the distance between separate interference sources and particularly on the location of nonlinear insertion in them. One more convenient physical model to describe real nonlinear objects, permitting to solve the problem in analytical form, is a system of crossed oscillators [2]. As its nonlinear load (NL) we used to a semiconductor diode.

2. SCATTERING BY A SYSTEM OF ORTHOGONAL (CROSSED) OSCILLATORS

Let an electromagnetic wave of a circular polarization be incident on a system of two half-wave dipoles with NL disposed in mutually orthogonal planes. It is evident this polarization of the incident wave gives the maximum amplitude of the scattered field. The geometry of the problem is represented in Fig. 1.

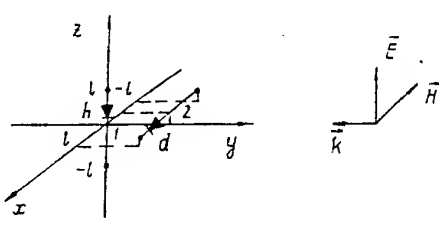


Fig.1. Geometry of the problem

Here we consider the steady-state regime of the scattering (the time dependence is assumed to be in the form $\exp(+i\omega t)$) in the approximation of weak nonlinearity, that permits us in the spectrum field representation restrict ourselves by the account of only the second harmonic, because as it is known, in the case of semiconductor contact a maximum intensity has a spectral component at frequency 2ω . The volt-ampere characteristic of semiconductor diode is approximated for rather small values V by the following expression: $I \simeq (V + \beta V^2)/R_0$, where I is the diode current, V is its voltage, R_0 is the initial diode resistance (at $V = 0$), β is the nonlinearity coefficient. The electrical circuit of the diode connection in the scatterer has been given in detail in [3]. The current at second harmonics is excited due to the lumped E.M.F. caused by the presence of the local nonlinear load (more detail see in [3]):

$$\varepsilon_{2\omega} = \frac{\beta}{2} Z_\omega^2 I_\omega^2 \quad (z = z_0) \quad (1)$$

here $Z_{N\omega} = R_0/(1 + iN\omega c R_0)$ is the load impedance ($N = 1$ or 2), $I_\omega(z)$ is the NL current at fundamental frequency ω .

A procedure to get the current expressions has been described in detail for the case of a weak nonlinearity in [3]. The electromagnetic field scattered at the frequency 2ω is represented by the sum of the emission fields created by the dipoles currents. Below, for simplicity, we give only the final expression for a back scattered field at a double frequency in the case of central disposed of NL ($z_0 = 0$, $x_0 = 0$):

$$E_{z,2\omega}^{(1)} = -\frac{Z_{2\omega} Z_\omega^2 \beta E_0^2 \sin^2 \varphi_0}{2R_0 \ln(2ka) k^2 (S^w)^2} \times$$

$$\begin{aligned} & \left[\frac{e^{-i2kr_{11}}}{r_{11}} + \frac{e^{-i2kr_{12}}}{r_{12}} + \frac{e^{-i2kr_0}}{r_0} \right], \\ E_{x,2\omega}^{(1)} &= -\frac{Z_{2\omega} Z_\omega^2 \beta E_0^2 \sin^2 \varphi_0}{2R_0 \ln(2ka) k^2 (S^w)^2} \frac{x}{x^2 + y^2} \times \\ & \left[2z \frac{e^{-i2kr_0}}{r_0} + (l+z) \frac{e^{-i2kr_{11}}}{r_{11}} - \right. \\ & \left. (l-z) \frac{e^{-i2kr_{12}}}{r_{12}} \right], \\ E_{2,2\omega}^{(2)} &= \frac{Z_{2\omega} Z_\omega^2 \beta E_0^2 e^{2ikd} \cos^2 \varphi_0}{2R_0 \ln(2ka) k^2 (S^w)^2} \times \\ & \frac{z}{(z^2 + (y-d)^2} \left[2x \frac{e^{-i2kr_{00}}}{r_{00}} + \right. \\ & \left. (l+x) \frac{e^{-i2kr_{21}}}{r_{21}} - (l-x) \frac{e^{-i2kr_{22}}}{r_{22}} \right], \\ E_{x,2\omega}^{(2)} &= \frac{Z_{2\omega} Z_\omega^2 \beta E_0^2 e^{2ikd} \cos^2 \varphi_0}{2R_0 \ln(2ka) k^2 (S^w)^2} \times \\ & \left[\frac{e^{-i2kr_{21}}}{r_{21}} + \frac{e^{-i2kr_{22}}}{r_{22}} + \frac{e^{-i2kr_{00}}}{r_{00}} \right]; \end{aligned} \quad (2)$$

where

$$\begin{aligned} r_{11} &= \sqrt{x^2 + y^2 + (z+l)^2}, \\ r_{12} &= \sqrt{x^2 + y^2 + (z-l)^2}, \\ r_{21} &= \sqrt{(y-d)^2 + z^2 + (x+l)^2}, \\ r_{22} &= \sqrt{(y-d)^2 + z^2 + (x-l)^2}, \\ r_0 &= \sqrt{x^2 + y^2 + z^2}, \\ r_{00} &= \sqrt{x^2 + (y-d)^2 + z^2}; \end{aligned}$$

$$S^\omega = \frac{k}{4\pi\omega\varepsilon_0} \left\{ \int_0^{2\pi} \frac{1-\cos t}{t} dt + i \int_0^{2\pi} \frac{\sin t}{t} dt \right\}.$$

Indices (1), (2) refer to the first and second dipoles, respectively. d is the distance between dipoles, a is the radius of the wire, $2l$ is the length of the dipoles. The first dipole is located along the z -axis, the second -- along the x -axis.

Formulas (2) have been used to calculate the electric field component $\mathbf{E}_{2\omega}$ in the plane (x, y) at an angle of 45° to axis x as dependent on distance d (ϕ_0 is also equal to 45°). Fig. 2a ($x_0 = z_0 = 0$) and Fig. 2b ($x_0 = z_0 = 0.125\lambda$) show the dependencies of

the back scattered field $|E_{2\omega}(d)|$ at the observational point $x/\lambda = z/\lambda = 0.25, y/\lambda = 10, a/\lambda = 1.5 \cdot 10^{-3}$.

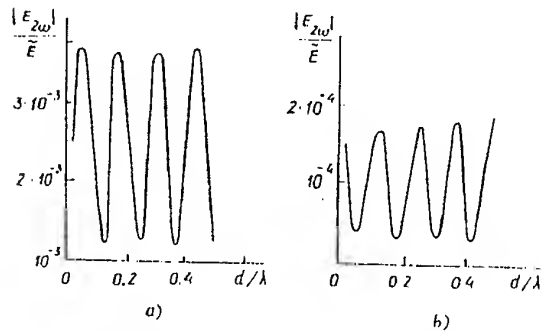


Fig.2. Dependencies of the back scattered field at the double frequency versus d

These dependencies have a periodical character with period $T_d/\lambda = 0.125$. As expected, for a plane-polarized wave incident under angles $\varphi_0 = 0$ or $\varphi_0 = \pi/2$ the dependence of the back-scattered field on distance d has a quasimonotone character.

From this expression at the observation point $x = z = 0, y \neq 0$ (for $y \gg \max\{d, l\}$ and $\varphi_0 = 45^\circ$) we have for a radial component of the electromagnetic field at the double frequency the following simple expression ($\mathbf{r}^0 = \mathbf{x}^0 \cos \varphi + \mathbf{z}^0 \sin \varphi$)

$$|E_r|^2 = \frac{|D|^2}{y^2} (1 - \sin 2\varphi \cos 4kd) \quad (3)$$

where $D = -\frac{Z_{2\omega} Z_\omega^2 \beta E_0^2}{R_0 \ln(2ka)(S^\omega)^2 k^2}$. The change of polarity of one of dipoles leads to the change of sign in the round brackets of formula (3).

It should be noted that when an electromagnetic wave is incident on a system of two crossed dipoles containing NL we may observe new polarization effects at second harmonic which are absent at the fundamental frequency. It will be remembered that the polarization diagram is the dependence of received power on angle φ when the polarization plane of a linear receiving antenna is rotated. Let the initial position of the polarization plane of the incident wave be vertical, then as it follows from (4) the polarization of the received signal at frequency 2ω

changes from vertical ($d = 0$) to elliptic one ($d_1/\lambda_0 = 1/32$) then circular ($d_2/\lambda_0 = 1/16$), elliptic with another ellipse slope ($d_3/\lambda_0 = 3/32$), horizontal (at $d_4/\lambda_0 = 1/8$) and so on. Hence, from (4) it follows that in a period of $T_d = \lambda_0/4$ the polarizations recurs completely. The change of the diode polarity, as it has been already mentioned, changes the polarization type to the opposite one (for example, the vertical to the horizontal). the fundamental frequency. Therefore, in this case it is possible to produce the preassigned polarization if the signal at the double frequency using dipole space diversity and directivity of NL. Fig. 3 shows the dependencies of the scattered field at double frequency on the azimuthal angle φ for the different values of the distance d between dipoles. So the theoretical results has a good experimental confirmation.

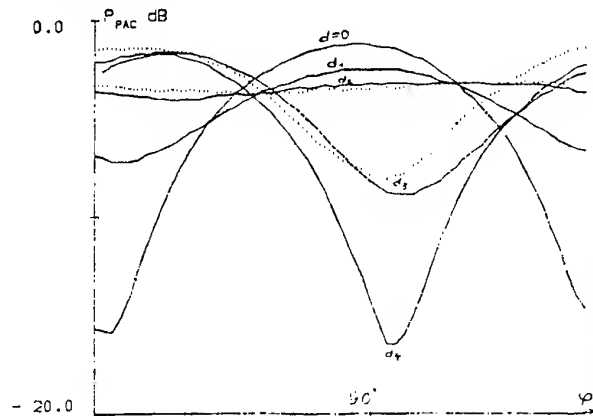


Fig.3. Dependencies of the field intensity at the double frequency versus φ

3. STATISTICAL SYSTEM OF NONLINEAR SCATTERERS

Here consider more realistic and complicate case of the scattering of higher harmonics by a statistical system of N identical simple nonlinear scatterers (NS) when a monochromatic electromagnetic wave of frequency ω is incident upon them. Assume that each NS has an isotropic scattering diagram. The NS are arranged randomly in two-dimensional space with characteristic length $L \ll R$, where R is the distance from the center of gravity of the system to the reception point.

The wave scattering by conventional NS, such as a half-wave dipoles using diodes as nonlinear load, is rather specific. The point is that the phase of the scattered signal, if the latter is a nonlinear product of even order, will depend on the switching direction of the nonlinear element of NS [4]. As mentioned earlier (in section 2) the scattering signal phase is changed by π by reversal of the nonlinear load switching direction. The analysis shows that the difference in the mean noise at the odd and even harmonics is considerable. The investigation of system of randomly placed NS show also that the electric length of this system (for even higher harmonics) as well as the positions of its phase center is determined not only by the system geometry, but also by the direction of diode connection into NS. This analysis makes it possible to conclude that there exist situations when the mean by realizations (or the system sounding angle) scattering cross-section at higher harmonics of the system decreases with reduction of the size of an area occupied by the system. This is a result of the presence of opposite oriented NS in the system. It is note, that in the linear case the signal vanishing with the system contraction is possible only due to the anisotropy of its back scattering diagram.

4. CONCLUSION

An essential new moment (describing in the section 2) is the fact that the polarization diagram of the signal at the double frequency depends on the spatial configuration of dipoles (distance d) and in this way it may differ from the polarization of the incident field at fundamental frequency. Thus, the analysis shows that the difference in the mean noise at the odd and even harmonics is considerable in the case of extended sets of NS as well as the NS are arranged in determinate fashion. In the latter case, the level of nonlinear products can be reduced by appropriate arrangement of their sources.

This work is supported by RFFI under grant No 96-02-18570

5. REFERENCES

- [1] N. Yu. Babanov, A. A. Gorbachev, T. M. Zaboronkova, S. V. Lartsov, "Investigation of a system of nonlinear interference sources" *Proc. of the 12-th Int. Wroclaw Symposium on EMC*, Wroclaw, Poland, June, 1994, pp. 214-216.
- [2] A. A. Gorbachev, S. V. Lartsov, "Polarization properties of two-vibration model of the nonlinear scatterers", *Radiotekhnika i Electronika*, vol. 40, No. 12, 1995, pp. 1761-1766, (in Russian).
- [3] A. A. Gorbachev, T. M. Zaboronkova, S. P. Tarakankov, "Scattering of electromagnetic waves by nonlinear antennas in the presence of a two media boundary" *Journal of Electromag. Waves and Applic.*, vol. 9, No. 10, 1995, pp. 1285-1299.
- [4] A. A. Gorbachev, "Peculiarity of sounding by electromagnetic waves in media with nonlinear insertions" *Radiotekhnika i Electronika*, vol. 41, No. 2, 1996, pp. 152-157, (in Russian).

BIOGRAPHICAL NOTES

Andrei A. Gorbachev received the PH.D from Nizhny Novgorod Polytechnical Institute, Russia in 1957, Doctor of Science from NIRFI in 1974 and Professor attestate in 1994. He is the head of the Department of Radiophysical Research Institute (NIRFI). His research interests include signal detection, nonlinear scattering of the electromagnetic waves and EMC.

Tatiana M. Zaboronkova received the PH.D from N. Novgorod State University in 1979, Doctor of Science from NIRFI in 1994 and Professor attestate in 1996. She is the leading scientific worker at NIRFI. In recent years she has investigated mainly nonlinear theory of electromagnetic waves diffraction.

Larisa V. Vasenkova is the research scientist at NIRFI. Her research interests are in the field of EMC and the theory of nonlinear scattering.

ANTENNA ASPECT IN EMC ANALYSIS OF A MOBILE TELECOMMUNICATION

Ryszard J. Katulski

Technical University of Gdańsk, PL-80-952 Gdańsk, Poland

The subject of this paper is the influence of an adaptive antenna aspect on emc condition of a mobile telecommunication. The results of directivity properties investigations of an adaptive circular array are presented. First, the problem of interference effects reduction in aspect to mobile communication is introduced. The multi-beam circular adaptive array is described. Next, the theoretical investigations obtained results of dependences between directivity properties and structural parameters of the adaptive circular array are presented. The researches carried out show that the optimal from emc condition of a mobile radio link point of view value of the spacing between antenna sensor elements is between from 0.5 to 0.75 wavelength.

1. INTRODUCTION

The cellular networks to realize a land wireless communication are very modern form of the mobile telecommunication systems. A radio link is a main element of each mobile wireless system. The radio link consists of a base station and a mobile unit between which a radiowave propagation medium is existed. Antennas installed in both the base station and the mobile unit are the interfaces between the propagation medium and the base or mobile unit equipments. Properties of these antennas influence on electromagnetic compatibility (emc) condition of the mobile radio link. Moreover, important questions connected with the emc condition of the mobile cellular network are the limitation of frequency band and interference problem due to a reflection phenomena. These emc condition depend of the follow design parameters of the antennas [1]:

- a height of the base station antenna,
- a length of the mobile unit antenna,
- and especially, a shape and mobility of these antennas radiation patterns.

Taking into account the structure and the emc conditions of the mobile radio link, the different shapes of the antennas radiation patterns are applied in the base station and mobile units. The movement of the mobile units requires to apply simple and not expensive these antennas forms with omnidirectional

radiation patterns. But the omnidirectional forms are not optimal from emc point of view because produce high value of an interference field, especially from a base station working in high capacity cellular network. The interference problem require to use in the base station an antenna system with directional shape of their radiation pattern, which can be in two options:

- as one-beam radiation pattern in which the beam illuminates the mobile unit,
- as multi-beams radiation pattern for multi-channels operation.

The above mentioned radiation patterns can be realized by sectorized antennas with fixed beam or by adaptive antenna systems with mobile beams [2].

In this paper the directivity properties of the adaptive base station antenna system in circular form of a multi-beams scanning phased array are analysed. First, the multi-beams adaptive system short description is presented. Next, the influence of the circular array form diameter and the number of antenna sensor elements on directivity properties - the values of a beamwidth and a sidelobe level - of the adaptive antenna system are discussed. Finally, properties observed from emc conditions point of view are summarized.

2. THE MULTI-BEAMS ADAPTIVE SYSTEM

The multi-beams adaptive antenna system consists of a base station controller with exchange radio interface and circular array of antenna sensor elements with adaptive control unit. The base station controller coordinates and controls the operation of the cell site. The exchange radio interface manages communication between the mobile telephone switching centre and the base station. The adaptive control unit is used to perform the phase shifting necessary to form and steer the forward radio channel beams.

Often the total number of radio channel available to a mobile telecommunication system will not provide satisfactory service based on large coverage area. In high capacity cellular network the number of users can be increased by spatial reuse of the radio channels. But, if the distance between the mobile units is reduced the co-channel interferences increase.

The circular array consists of identical antenna sensor elements equally spaced around a cylinder of radius a - exemplary circular structure for eight antenna sensor elements is shown in Fig. 1. The typically spacing between antenna sensor elements is about halfwavelenght.

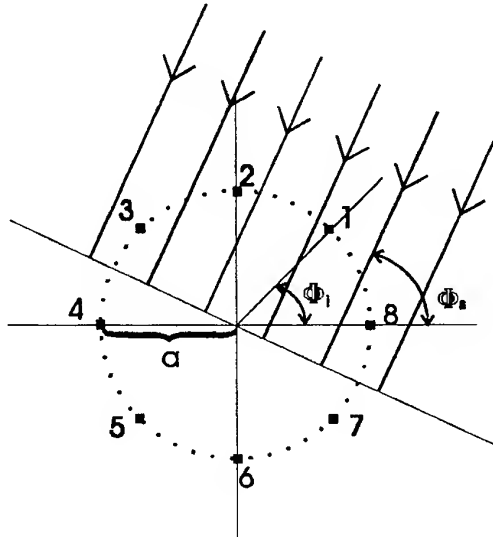


Fig. 1. Antenna sensors circular array

The far-field radiation pattern $F(\theta, \phi_i)$ can be written as:

$$F(\theta, \phi_i) = SF(\theta) \cdot AF(\theta, \phi_i), \quad (1)$$

where:

$SF(\theta)$ - space factor, which for typical monopole antenna elements is described as:

$$SF(\theta) = \frac{\cos\left[\frac{\pi}{2} \cdot \sin(\theta)\right]}{\cos(\theta)}, \quad (2)$$

$AF(\theta, \phi_i)$ - normalized array factor, which for N antenna elements is noticed as:

$$AF(\theta, \phi_i) = \frac{\sin\left\{\frac{N}{2} \cdot [\pi \cdot \sin(\theta) - \phi_i]\right\}}{N \cdot \sin\left\{\frac{1}{2} \cdot [\pi \cdot \sin(\theta) - \phi_i]\right\}}, \quad (3)$$

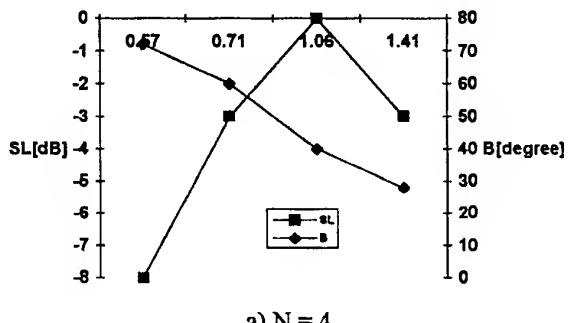
ϕ_i - the linear phase shift between adjacent antenna elements for

i-th channel operation.

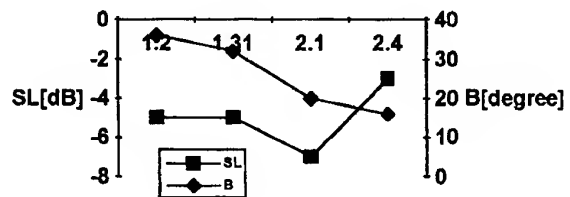
A value of the phase shift will be channel dependent because the beam will be positioned on the mobile which is operating on the channel.

3. THE THEORETICAL INVESTIGATIONS

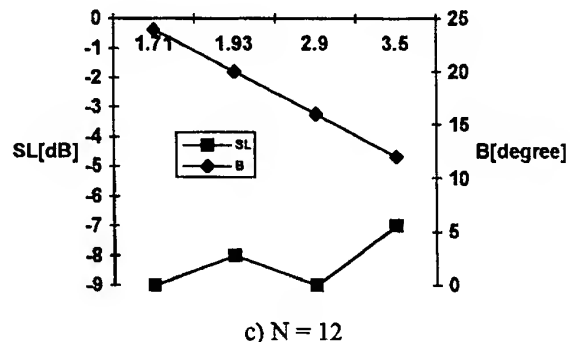
The directivity properties of the circular antenna array were investigated at frequency value equals 900 MHz by use LMS adaptive procedure. The number of antenna sensor elements changes from four to thirty and the circular array form diameter from one to eight wavelenght. Taking into account the evolution of the obtained radiation patterns the influences of the above mentioned structural parameters of the antenna array on the array directivity properties are shown in Figs. 2. In these figures the sidelobe levels and beamwidths versus the antenna array diameter for different number of antenna sensor elements are presented.



a) $N = 4$



b) $N = 8$



c) $N = 12$

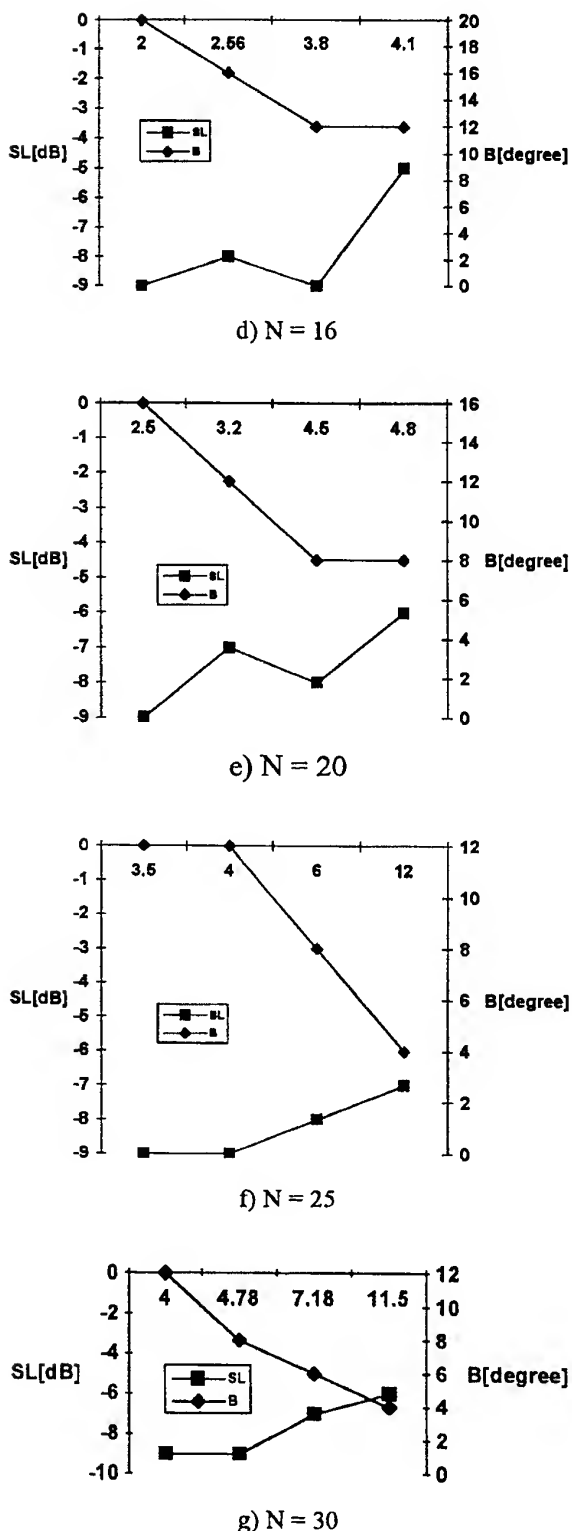


Fig. 2. The dependences of the sidelobe levels SL and beamwidths B vs. the antenna array diameter for different number N of antenna sensor elements

Additionally, taking into account the results presented in Figs 2, the values of sidelobe levels vs. number of antenna sensor elements for optimal emc condition of investigated mobile radio link are presented in Fig. 3 - the numbers in parenthesis are the antenna circular array diameter.

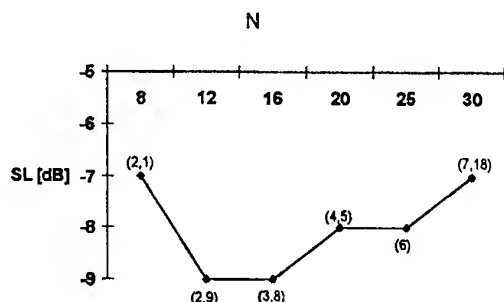


Fig. 3. The dependences of the sidelobe levels SL vs. number N of antenna sensor elements for optimal emc conditions

4. CONCLUSION

The adaptive circular array with LMS optimization has been tested theoretically by use numerical modelling. The researches carried out show that the optimal from emc condition of mobile radio link point of view value of the spacing between antenna sensor elements is between from 0.5 to 0.75 wavelenght. The obtained results show the usefulness of the antenna system for base station of the cellular mobile telecommunication systems to degradation of interference signals, especially to reduce the influence of co-channel interferences.

5. REFERENCES

- [1] R.J. Katulski, "Investigations of an Adaptive Array for Mobile Telecommunication", *Proc. of the Int. Conf. on Telecommunications*, pp. 473-476, Istanbul-Turkey - 1996.
- [2] R.J. Katulski, "Base Station Antenna System for Cellular Network", *Proc. of the Int. Wiss. Colloq.*, pp. 904-909, Germany - 1992.

BIOGRAPHICAL NOTE

Ryszard J. Katulski graduated at the Technical University of Gdansk in 1975, and received Ph.D. degree from the Technical University of Wroclaw in 1984. Since 1968 he is with the Technical University of Gdansk, working on wireless communication with special interest in antenna theory and techniques with electromagnetic compatibility aspects.

ANTENNA SELF-ADOPTED TO THE EM-ENVIRONMENT

Wojciech J. Krzysztofik

Wroclaw University of Technology
Institute of Telecommunication & Acoustics
The Radio Department
Wybrzeże Wyspiańskiego 27, 50-370 Wrocław, POLAND
Email: wojka@zr.ita.pwr.wroc.pl

The paper reviews a number of applications where antenna characteristics are made to adopt dynamically to the environment. Somewhat surprisingly, perhaps, it is broadcast and communications rather than the military domain that has the most wide-ranging examples in common use.

1. INTRODUCTION

The vast majority of antennas in use are simple, passive, fixed mechanical structures that have a constant directional radiation pattern. Where required, as in most radar systems, mechanical rotation or sector scanning of the antenna is used to enhance its sensing capabilities over a wide range of angular directions. In such systems, however, the mechanical control of antenna takes no account of the information being obtained, or information rate. The antenna operates open loop, controlled in fixed and predetermined manner.

The first attempts to make an antenna in any way adopt to its electromagnetic environment (EM) involved the use of secondary antenna. By suitably combining the signals from the two antennas in appropriate amplitude and phase [3], a variety modifications to the primary antenna may be made. This technique (the diversity reception method) has been particularly useful in the cancellation of multipath signals on communication links and in producing a directional null to cancel interference in radar systems.

Phased array antennas offer the possibility of much greater flexibility, however. Electronic control of the amplitude and phase of signals in the array elements spread across the total antenna aperture allows near instantaneous change of the antenna beam direction and beamwidth. It also allows control of the sidelobe pattern of the antenna, and notably the direction of multiple nulls.

There exists, therefore, the capability to configure a closed loop system in which now the properties of the antenna are modified in response to information obtained by the antenna in such a way as to optimize a parameter such as signal-to-interference plus noise ratio (SINR). Such systems may be thought of as the first step in making antennas „intelligent”. New developments which include the application of heuristic reasoning and learning from past experience in such systems are bring closer the concept of the intelligent antenna.

2. PRINCIPLES

Digital beam forming (DBF) represents a quantum step in antenna performance and complexity [1]. The approach preserves the total information available at the aperture. This, coupled with digital processing, offers tremendous flexibility.

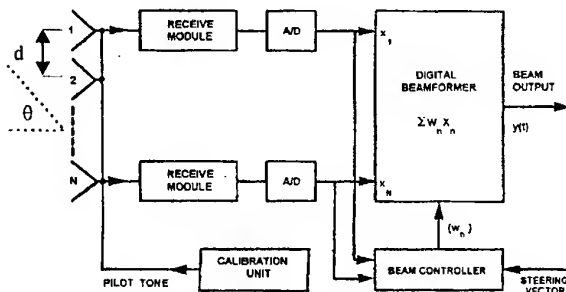


Fig. 1 Generic System of a Self-Adopted to EM-Environment Antenna

In the generic system (Fig. 1), the digital processing has been broken up in two parts: the actual beamformer, which accepts the digitized element signals (x_n) and the weights (w_n) to form the sum $\sum w_n x_n$, that constitutes the beam, and the beam controller that determines the

proper weights. One of the major applications of DBF is adaptive pattern nulling for jammer suppression.

2.1. Null Steering

Communications and radar antenna systems are susceptible to degradation in performance because of interference received through their sidelobes. The interference may be deliberate electronic counter measures, accidental RF interference (RFI), clutter returns or natural noise sources. Typical interference signals received by RF systems are from point sources radiating a coherent wavefront for at least the signal gathering time of the antenna. The antenna operating in its far field will receive a plane coherent wavefront. In order to prevent interference of this type entering receiver it is necessary to arrange for null in antenna's polar response to coincide with angle of incidence. The existence of plane coherent wavefront can be identified through the use of an array of receiving elements. Once identified, the angle of incidence of the signal can be readily determined. The directional pattern of an N -element linear array may possess up to $(N-1)$ independent zeros. There are obvious advantages in having the ability to independently steer the zeros in the array's directional pattern in order to reduce interference signals normally received by the sidelobes.

In order to independently control the angular location of the zeros it is necessary to control both the phase and amplitude [3] of signals in the feed system of each element.

2.1.1. Multiple Nulls

Schelkunoff showed [2] that the directional pattern of an N -element linear array may be expressed as polynomial of order $(N-1)$. Hence for the N -element linear array itself (without the beamformer), shown in Fig. 1 the polynomial is

$$D(\theta) = W_1 + W_2 z + W_3 z^2 + \dots + W_N z^{N-1} = \sum_{k=1}^N W_k z^{k-1} \quad (1)$$

where $z = \exp(j2\pi d \sin\theta/\lambda)$, d = element spacing, and the phase reference is taken as the first element in the array. The coefficients of the polynomial may be complex, thus representing the amplitude and phase weighting of each array element. Thus:

$$W_k = A_k \exp(j\phi_k) \quad (2)$$

The polynomial may be factorised into $(N-1)$ roots and each of these represent a zero of the polynomial

$$D(\theta) = W_N(z-b_1)(z-b_2)(z-b_3) \dots (z-b_{N-1}) \quad (3)$$

In general, these roots are complex numbers and may therefore be represented as points in complex z -plane. Since z is simply a phasor, $|z| = 1$; so roots located on the unit circle represent true zeros of the directional pattern (i.e. $D(\theta) = 0$).

The relationship between the zeros, the radiation pattern and the element weights W is sometimes difficult to visualize. Consider the pattern of the uniformly

illuminated array and assume that there is a jammer in the sidelobe as shown in Fig. 2.

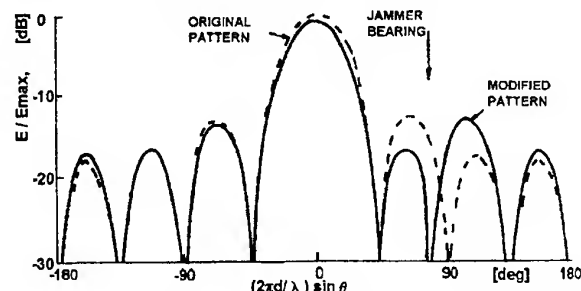


Fig. 2. Effect of Moving One Zero on the Pattern of an 8-Element Uniformly Illuminated Array

It would be sensible to move the zero closest to jammer on to the jammer bearing. In z -plane terms this is easy. The root b_p corresponding to the closest zero is simply replaced by B_j , where

$$B_j = \exp(j2\pi d \sin\theta_j / \lambda) \quad (4)$$

and θ_j is the jammer bearing.

The modified radiation pattern can be expressed as

$$D_j(\theta) = D(\theta) (z - B_j) / (z - b_p) \quad (5)$$

and it is clear that the disturbance of the pattern is mainly in the region of the jammer. However, the effect upon the element weights W is quite complicated and it will be appreciated that every weight must be modified in order to achieve the new pattern. The situation becomes more complicated if there is more than one jammer to be dealt with.

In cases where interfering signals are received by the array from specific directions, multiple zeros are useful in preventing the unwanted signals entering the receiver. However, it is not always advantageous to overlay nulls on existing nulls. Superior performance can often be achieved by locating zeros between existing ones, especially when signals with a wide bandwidth are being received.

Many null steering applications are limited to systems where it is possible to derive a feedback signal to verify the locations of the nulls. Such a system may use an operator to apply the necessary corrections or processor designed to automatically steer nulls. Such systems are termed adaptive.

2.1.2. Adaptive Null Steering

A major disadvantage of the open-loop null steering arrays is that the angular locations and depth of the nulls is extremely sensitive to phase and amplitude errors in the power splitting networks. In order to avoid this limitation, an automatic control system is required which steers zeros in desired directions and which compensates for any errors due to tolerances in the array construction or due to mutual coupling effects [2].

Data on the desired null directions is invariably obtained by processing some form of measured covariance matrix which defines the mean values of the cross-products of the voltages received by the elements

of the system. In the case of a 2-element isotropic system illuminated by a single narrow-band jammer at angle θ , the co-variance matrix M reduces to

$$M = \begin{bmatrix} \overline{V_1^* V_1} & \overline{V_1^* V_2} \\ \overline{V_2^* V_1} & \overline{V_2^* V_2} \end{bmatrix} = \begin{bmatrix} P_j + Q_n & P_j \exp(j\phi) \\ P_j \exp(-j\phi) & P_j + Q_n \end{bmatrix} \quad (6)$$

where the asterisk stands for the complex conjugate and an overbar indicates a time averaged value, and V_1, V_2 = voltage received by element number 1, 2, respectively, P_j =mean jammer power at each element, Q_n =receiver noise at each element, $\phi = 2\pi d \sin\theta / \lambda$.

In this case it is evident that the angle of arrival of the jamming signal can be deduced immediately from the ratio of two terms of the co-variance matrix, since

$$\exp(j\phi) = (\overline{V_1^* V_2} / \overline{V_2^* V_1}) \quad (7)$$

In principle, the NxN co-variance matrix of N-element system can be manipulated to provide angle of arrival data up to (N-1) jamming sources. This involves analysing the incident signals into N eigenbeam components. In the simple adaptive arrays, angle of arrival data is rarely evaluated explicitly, since it transpires that the optimum element weights demanded by the widely-used maximum SINR algorithm can be found simply by inverting the co-variance matrix.

In the absence of interference, it is generally required that the radiation pattern of the array should revert to a fixed quiescent pattern. For radar and fixed point-to-point communications antennas the quiescent pattern will usually be a single narrow beam with low sidelobes. For mobile communication applications, where directions of wanted signals are unknown a priori, this pattern may be omnidirectional. When interference occurs, the radiation pattern is required to adopt to present nulls in the directions of interference, but it is essential that the adaptive circuits do not attempt to cancel wanted signals.

2.2. Adaptive Arrays

Adaptive beamforming for receiving the signal in a specified direction, while canceling the interference signals without the a priori knowledge of the interference environments has been widely used in any areas [1], [2], [4], [5].

The concept of sidelobe canceling can be extended to arrays with many elements, each additional element allowing an extra null to be steered. In situation which an N-element array is receiving the remaining N-J-1 nulls to be adjusted so as to optimize the performance according to some predetermined criteria. Of course, the number of jammers is rarely known in advance (and may even exceed the number of elements), and the most widely adopted criterion is simply that of optimizing the ratio of signal power-to-interference plus receiver noise power (SINR).

For array beamforming with full adaptivity, we consider an array with N isotropic sensor elements. Let the received data vector be $x(t)$ and the output of the array be $y(t)=w^*x(t)$. The optimal weight vector w_0 is

found by minimizing the array output power subject to L linear or derivative constraints as follows [5]

$$\text{Minimize } E[y(t)^2] = w^* R_x w \quad \text{Subject to } C^* w = f \quad (8)$$

where the autocorrelation matrix $R_x = E[x(t)x^*(t)]$, C is the NxL constraint matrix, and f is the Lx1 response vector.

The optimal solution for (8) is given by

$$w_0 = R_x^{-1} C (C^* R_x^{-1} C)^{-1} f \quad (9)$$

If a constraint unit gain in the desired signal direction is imposed, then (9) becomes

$$w_0 = \kappa R_x^{-1} s_d \quad (10)$$

where s_d denotes the desired signal direction vector and κ a constant given by $\kappa^{-1} = s_d^* R_x^{-1} s_d$.

Each of (10) reveals that a matrix inversion is required to compute the optimal solution. Consequently, the required computation loads are about $O(N^3)$.

To obtain better resolution and interference cancellation, we generally increase the size of adaptive arrays. As a result, the required computational burden and the convergence speed for adaptation become two severe problems. Moreover, the resulting high-resolution capability of using a large array makes the array's sensitivity to imperfections more severe.

Many techniques have been presented to alleviate these drawbacks of using large adaptive arrays. A widely considered one is the partially adaptive processing technique which utilizes a fraction of the available array weights for adaptation.

Let the desired signal be the source incident from directional angle θ_1 and the other $J=P-1$ sources be the undesired interferences. For the case of correct steering, $s_d = A(\theta_1)$ ($A(\theta_i)$ =the response vector of the i th signal) with steering angle $\theta_0 \neq \theta_1$. The theoretical SINR on the output of uniform N-elements linear array is given by [5]

$$\text{SINR} \approx \frac{\pi_1 |A^*(\theta_0) A(\theta_1)|^2}{\frac{\pi_1^2}{\pi_2} |A^*(\theta_0) A(\theta_2)|^2 + \frac{1}{N} |A^*(\theta_0) A(\theta_1)|^2} \quad (11)$$

π_i =is the i th variance

if there is only one interferer falling outside the mainlobe of the beam pattern. From (11) we note that the output SINR approaches zero when the desired signal is impinging on the array near to the mainlobe edge or $|A^*(\theta_0) A(\theta_1)|^2 \approx 0$. Figure 3 shows the curves of the output SINR versus θ_1 for an array of $N=10$ or 20 or 30 elements, respectively.

There are multiple SINR nulls, because the values of the angle θ_1 which make $|A^*(\theta_0) A(\theta_1)|^2 \approx 0$ satisfied are equal to the multiple of the beamwidth. To cure this problem, an efficient technique is proposed in [5] to enhance the robust capabilities of the adaptive beamformer.

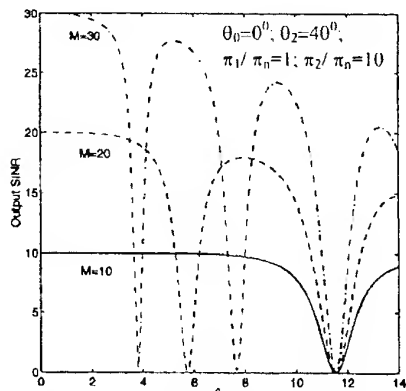


Fig. 3. SINR on the Output of N-Element Adaptive Beamforming Linear Array Versus θ_1 .

3. PERFORMANCE EVALUATION

Performance of an adaptive antenna operating in communication system is judged by the ratio of the directive gain D_d , in the direction of the desired signal S_d source (or sources), to the directive gain D_u in the direction of the undesired signal S_u sources. The system designer needs to know the ratio D_d/D_u so that he may set S_d large enough to guarantee uninterrupted communication even in presence of undesired and/or unexpected interference. Unfortunately, it is not always possible to specify the location and strength of all S_u ; consequently, the system designer might consider the "worst case" performance characteristics in specifying the antenna performance. This could lead to an antenna system much too large, too complicated, or perhaps even impractical. Hence the system designer must compromise, or trade-off, the system performance. He might do this by specifying the antenna performance on statistical basis; that is, $D_d/D_u > X$ for Y % of the communication system operating hours. In short, an intelligent quantitative means of trading off system performance characteristics can be very useful.

In response to the foregoing, consider a figure of merit (FOM) as shown in Fig. 4, which consists of first dividing the angular field of view (FOV) into grid of cells.

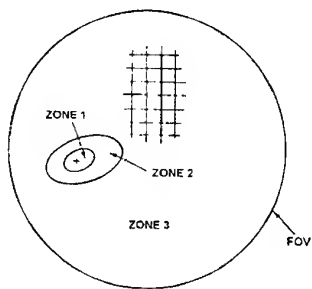


Fig. 4. Figure of Merit

Next select a particular location and strength of desired and undesired signal sources and allow the adaptive antenna under test to adopt. Then the directive gain is

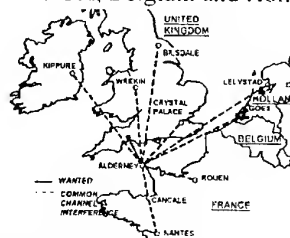
determined at each cell in FOV and the cells are grouped according to their angular separation from the undesired signal sources. The values of directive gain would be sorted in accordance with their associated zone. In the case of more than one interfering source S_u , a cell may be in more than one zone. In this case, the cell would be assigned to the zone closest to an undesired signal source. Now the new scenario is selected, the antenna is allowed to adopt, and the directive gain is determined and sorted as described before. This procedure is repeated until all important scenarios have been considered, or a data base, sufficient for statistical analysis, has been accumulated. Using this data base, one can determine the probability of realising D_d/D_u greater than a selected value, in any of the zones. In those instances when the strength of undesired signal is known, the ratio D_d/D_u can be used to determine the effective isotropic radiated power (EIRP) required by desired signal source to overcome that signal radiated by undesired signal source. In those cases where more than one interfering source of different intensity is present, one could determine an effective $D_{u\text{eff}}$ in accordance with [2]

$$D_{u\text{eff}} = \left(\sum_{i=1}^I D_i P_i \right) / \left(\sum_{i=1}^I P_i \right) \quad (11)$$

4. EXAMPLES OF APPLICATION

4.1. UHF TV-Broadcasting System

The most successful example of an intelligent antenna is the UHF TV broadcast antenna developed specifically to cope with the difficulties of providing television service to the Channel Islands [6]. In this case the closest point to the UK is Alderney and the relevant UK main transmitter is the one at Stockland Hill. There was difficulty with co-channel interference arising from nearby French transmitters and more distant transmitters in the UK, Belgium and Holland (Fig. 5).



Note: All the transmitters shown are on the same channel and are potential sources of interference

Fig. 5. Map Showing the Rays of Possible Interference of UHF TV-Broadcasting Station at Alderney (UK)

An adaptive antenna (16x4 array of printed dipole elements) was developed and applied. The output of each element is connected to a network which controls the amplitude and phase of that output, prior to summation of the array signals. An adaptive control unit provides the logic for control of the amplitude and phase weighting. The system has satisfied its performance objectives by achieving 50 dB nulls on at least three

sources of interference, though at lower rejection levels it can cope with up to 12 sources of interference.

4.2. Mobile Cellular Communication System

Mobile radio communication systems are currently characterized by an ever-growing number of users, which however is coupled with limited available resources, in particular in terms of usable frequency spectrum. Research is therefore oriented towards developing new access techniques, for more efficient employment of available frequency bands. The Space Division Multiple Access (SDMA) technique allows to enhance the capacity of a cellular system by exploiting spatial separation between users [7]. In this method the base station does not transmit the signal throughout the area of the cell, as in the case of conventional access techniques, but rather concentrates power in the direction of the mobile unit the signal is meant to reach, and reduces power in directions where other units are present (Fig. 6).

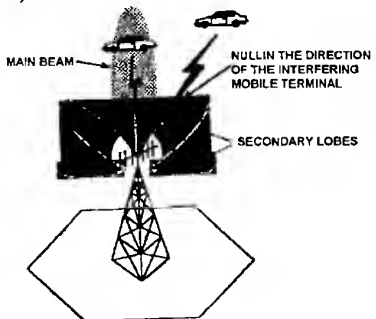


Fig. 6. Radiation Beam Pattern Adapted for a Single User of a Mobile Cellular Communication System

The radiation pattern of the base station, both in transmission and reception, is adopted to each different user so as to obtain the highest gain in direction of the mobile user. Simultaneously, radiation nulls shall be positioned in the directions of interfering mobile units. In this case an adaptive antenna array (Fig. 1) of base station helps to carry out spatial filtering. The use of an adaptive antenna array increases system capacity, i.e. the number of users it can handle due to reduction in co-channel interference. It allows to reduce frequency reuse distance and cluster size, what means if each cell can be assigned a higher number of channels.

5. CONCLUSIONS

The self-adapted to the EM-environment antenna system is developed to meet the following requirements: automatic adjustment of the antenna pattern to give minimum interfering signal; no prior knowledge of direction of interfering signals; ability to handle multiple sources of interference; ability to track changes in direction of interference resulting from propagation effects; ability to provide nulls at least 45 dB on interference sources.

The amount of information received by a full-scale DBF antenna system is formidable and, therefore, it may prove desirable to incorporate artificial intelligence to control the processing of these data so as to extract the essential features and present a comprehensible image of the electromagnetic environment under changing conditions. This constitutes the fifth generation antenna: the first being the reflector with dipole fed, the second the phased array, the third the printed circuit antenna, and the fourth the monolithic array. It involves a community of people from widely different domains. The intelligent antenna will be a natural concept to the next generation of antenna engineers.

REFERENCES

1. Steyskal H. „Digital Beam Forming Antennas”, *Microwave Journal*, January 1987, pp. 107-22
2. Rudge A.W., Milne K., Olver A.D., Knight P. (ed.), „The Handbook of Antenna Design”, Peter Peregrinus Ltd., London, UK, 1983
3. W.J. Krzysztofik, „Modern Methods of Microwave Antenna Measurements”, *Quarterly of Electronics & Telecommunications*, vol. XXVI, 1, PWN, Warsaw, Poland, 1990, pp. 51-74.
4. Spinger J., „Digital Beam Forming Antenna of the Radar”, M.Sc. Thesis, Wrocław University of Technology, Wrocław, 1996
5. S.-J. You, J.-H. Lee, „Adaptive Array Beamforming Based on Efficient Technique”, *IEEE Trans. on Antennas & Prop.*, vol. 44, no. 8, Aug. 1996, pp. 1094-1101
6. Forrest J.R., „The Intelligent Antenna. A Smart Solution to Improved Performance”, *Ann. Telecommun.*, 42, no 3-4, 1987, pp. 135-9
7. E. Buracchini, „SDMA in Mobile Radio Systems: Capacity Enhancement in GSM & IS-95”, Proceedings of the Workshop on Smart Antenna Design and Technology, COST Action 260 Smart Antennas, Dubrovnik, Croatia, Dec. 1997. Pp.2.8-2.17

BIOGRAPHICAL NOTE



Wojciech J. Krzysztofik was born in Świdnica Poland on March 28, 1949. He received the M.Sc., and Ph.D. degrees from Wrocław University of Technology, Wrocław, Poland, both in electrical engineering, in 1974 and 1983, respectively. Since 1974 he has been a member of the Department of Electronics Engineering, the Institute of Telecommunications & Acoustics of the Wrocław University of Technology, where he is currently an Assistant Professor.

In 1988 he was a Visiting Professor at the Chalmers University of Technology, Sweden. Since 1988 to 1990 he was engaged as a Professor of Telecommunications at the College of Engineering of Mosul University, Iraq.

His research interest are in microwave remote sensing, and microwave application in communication, the electromagnetic theory of numerical methods applied to scatterers and antennas of arbitrary shape in complex environments. Recently he was a manager of a project entitled „Investigation of Satellite Signal Reception in Poland” supported by the Polish Council of Scientific Research.

SOME RESULTS OF LONG-TERM SATELLITE RADIO-SIGNALS MONITORING IN POLAND

Wojciech J. Krzysztofik, Daniel J. Bern, Jacek Skrzypczyński

Wrocław University of Technology
Institute of Telecommunication & Acoustics
The Radio Department
Wybrzeże Wyspiańskiego 27, 50-370 Wrocław, POLAND
Email: wojka@zr.ita.pwr.wroc.pl

This paper reports some results of the Ku-band satellite radio-signals observation. The communication (TV-SAT) and telemetric (beacon) signals received from the geostationary satellites: ASTRA, EUTELSAT, and INTELSAT have been collected over ten-month period from April 1997 to March 1998. The elevation angle from the receiving site in Wrocław, Poland to the satellites was about 31.5 (ASTRA, EUTELSAT), and 18.0 (INTELSAT 601/602) degrees. The analyzed database consists of power levels for both type of signals, and a carrier-to-noise ratio for the communication signals.

1. INTRODUCTION

Recently, during the 1970-98th period, in Poland the increase use of satellite links for broadcasting, telecommunication and data acquisition systems has been observed. Unfortunately, the past political relationship situated us, in term of satellite systems planning and realization, in quite different condition than Western European countries. For most satellites the Poland territory is a long way apart of beam-center. Information concerning most satellites, available on common market, are insufficient for systems designer. The World Satellite Almanac does not guarantee that the values expressed therein will necessarily correspond to performance levels found in the field. So, more data have been still needed to characterize the propagation impairments for satellite systems planning.

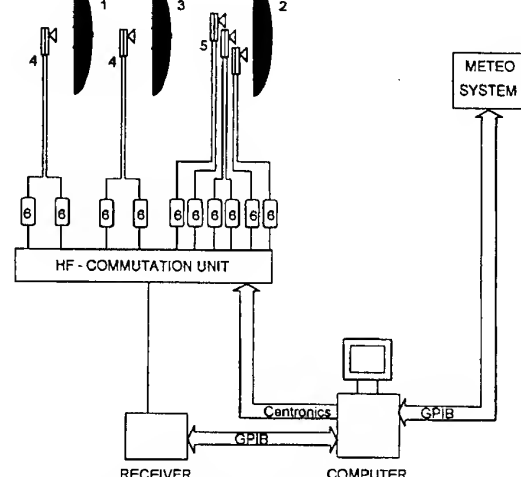
Broadcasting by satellites leads to propagation considerations that are not entirely comparable with those occurring in the fixed-satellite service. Attenuation data for space-to-Earth direction are needed in the form of statistical averages and/or contour maps of attenuation and depolarization for large areas. Specific coordination problems may arise at the margin of the

service area between satellite broadcasting systems and terrestrial or other space services. In the case of space-to-Earth paths for broadcasting systems, several propagation effects (e.g. tropospheric absorption, attenuation, and depolarization; ionospheric scintillation and Faraday rotation; local environmental effects, including attenuation by buildings and vegetation) may require consideration. Each of these contributions has its own characteristics as a function of frequency, geographic location and elevation angle.

This paper discusses some of these effects and refers them to experimental results were done.

2. EXPERIMENT DESCRIPTION

2.1. Measuring set up



1-, 3-, 2-: parabolic dishes of INTELSAT 601 , 602, and ASTRA/EUTELSAT (multi-beam antenna) receivers, respectively;
4-, 5-: front-end PLL receivers/down-converters; 6 - DC/HF- coupler
Fig. 1. Block diagram of the satellite signals receiving and data acquisition system

Measuring setup consists of three parabolic-dishes, two for INTELSAT (601 - 27.5° W and 602 - 62.9° E) satellites reception and one - multi-beam antenna for ASTRA19.2°E, and EUTELSAT 13E and 16° E satellites reception. Antennas are fixed on a terrace, at XI-th floor of the Wrocław University of Technology building. The receiving system was constructed to take advantage of the frequency coherence of the beacons.

Some characteristics of the receiving system are given in Table I.

TABLE I.
Characteristics of satellite monitoring system at
Wrocław University of Technology, Poland

Terminal	Commun.	Beacon INTELSAT
Frequency [GHz]	10.9 to 11.7	11.198
Bandwidth [Hz]	$27\ 10^6$	300
Polarization	X or Y	RHCP
Switching loss [dB]	0.2	0.2
Switching time [ms]	15	15
EIRP, toward Wrocław [dBW]	45 to 50	7 to 10
Antenna diameter [m]	1.8	1,8
Gain [dB]	43.8	43.8
Beamwidth [deg]	1.1	1.1
LNB Noise Factor [dB]	0.94	0.94
Local Phase Noise [dBc]	-95	-65

The signal in receiver was processed by a RF section (front-end PLL-LNB), spectrum analyzer (TEK 2710) and was monitored by a PC-based data acquisition system. The satellite signals from each RF-section are combined in the RF-multi-position switch, which connects randomly selected one of eight satellite signals to the analyzer input. It allows to make sequentially observation of signals from different satellites, received by fixed antennas.

The outputs of the receiver and RF-switch were continuously monitored by a PC-based data acquisition system via GPIB and CENTRONICS interfaces, steered by remote control program (RCP). The RCP provides control of all receiver function: frequency tuning, bandwidth adjusting, time of sweeping, input level, the acquisition procedure of the computer, as well as the RF-switch switching order.

2.2. Satellite constellation under investigation

The main assumption of our investigation was determination of satellite signal reception and qualification in Poland. So, we wish to estimate communication signal behaviour during long-time rather, than propagation condition itself as they were done in many research before [1], [2], [3]. The problem is how to elect satellite candidates to be representative from such point of view. At first we decided to monitor all satellites which carry the Polish TV Programs, they are: EUTELSAT HOT BIRD, and EUTELSAT II F2.

Second condition, had taken under consideration was popularity of TV programs broadcasted via satellite. In this competition ASTRA satellite was the winner. At last we chose satellites are on extreme position with respect to receiving site, having in mind the propagation condition (lowest elevation angle, slant-path length, etc.). From that reason the INTELSAT satellites, No 601 and 602 were the best choose (Fig. 2).

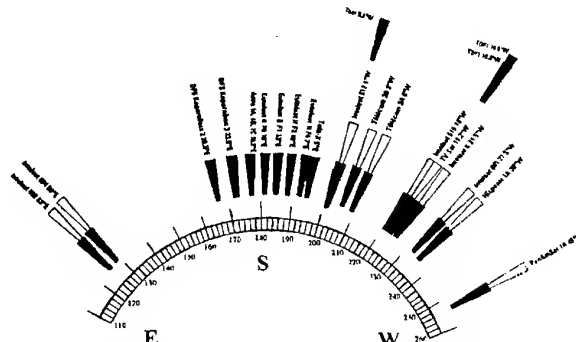


Fig. 2. Azimuth position of on a geostationary orbit satellites with respect to Wrocław, Poland

2.3. Measurement of satellite communication signals

Observation of communication signals (e.g. carrier spectrum line) as a data for the satellite signals quality estimation have some disadvantages:

- most of the satellite transponders are operated in multi-carrier environment (Fig. 3). It means that the level of each received carrier can be affected very much by variations in the other carriers in the same transponder. These variations would limit the accuracy of measurements.

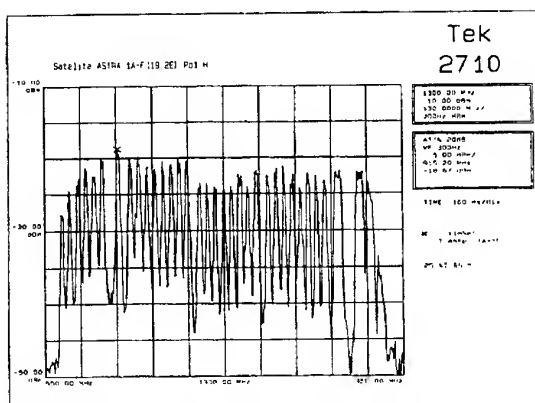


Fig. 3. Measured power spectral density of the downlink communication signals of all ASTRA satellite transponders

- the communications carriers themselves do not have a constant amplitude. This is particularly so if we wish to receive an FM-TV signal in a limited bandwidth (Fig. 4).

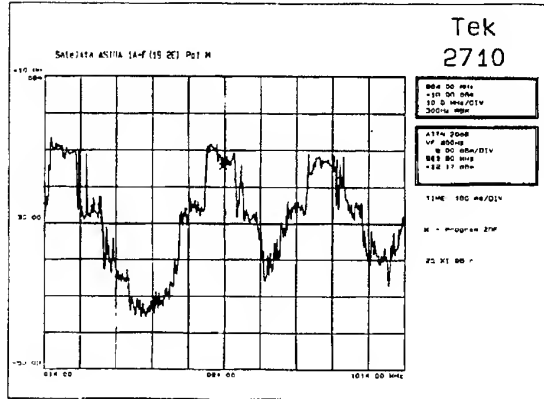


Fig. 4. Spectra of ASTRA satellite TV ZDF channel

- the dynamic range of the received signals (from a carrier) would generally be less than if we were receiving a beacon which usually contains all of its energy in less than 100 Hz bandwidth.
 - the communications carriers can be re-assigned at short notice, particularly if the transponder is leased out and satellite has no day-to-day control over the content of that transponder.
 - if we are going to detect a digital carrier, only one or two dB in level can cover the range from an acceptable performance to a degraded performance (or even an outage). In other words, the detection level would be too sensitive.

Concluding above remarks, we should carefully interpret some variations of a real communication signal. They can not depend only on propagation effects. From that reason it is useful to observe, as a reference, the telemetric beacon signals, which are radiated by most satellites in use.

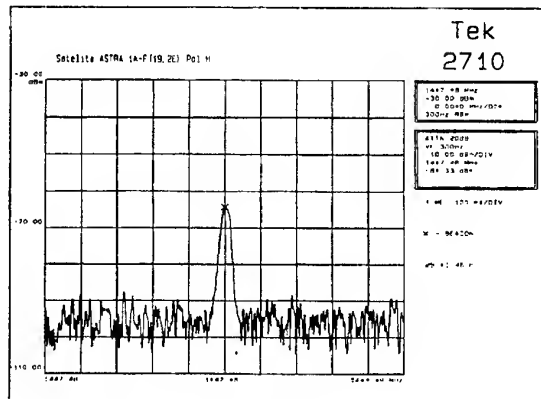
2.4. The telemetric beacon measurement

A satellite beacon (Fig. 5) measurement can be made with generally simple equipment. A 2m in diameter antenna, a system noise temperature of about 200K, and phase lock-loop (or equivalent) bandwidth of 200 Hz would enable a fade margin of 20 dB to be achieved with the global (or zone) Ku-band beacons that most satellites radiate.

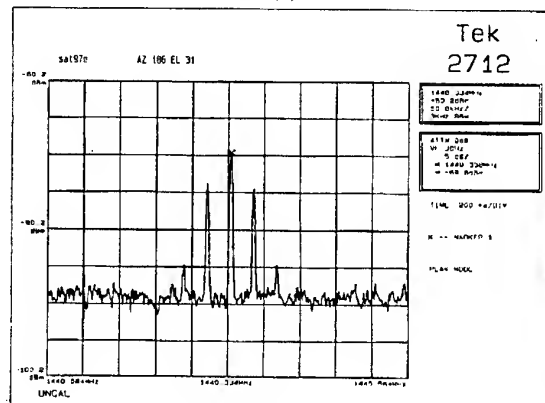
The station-keeping tolerance on the satellite fleet is very tight, being better than $\pm 0.1^\circ$ both E-W and N-S, so no one should have problems with a fixed antenna with diameter of about 2 m.

All satellites carry global- or zone-beam Ku-band beacons, with very similar specifications. Once beacon is on, it is very unlikely that the beacon frequency will be changed, except for reasons of failure in the operating beacon.

The Ku-band beacons are characterized by following parameters:



(a)



(b)

Fig. 5. Telemetric beacon signal ($f=11447.48$ MHz) received from ASTRA satellite (a); modulated by telemetry and/or ranging signal beacon from EUTELSAT-Hot Bird satellite ($f_c = 11451.83$ MHz) (b)

Frequencies: 11.198 GHz (INTELSAT), 11.447 GHz (ASTRA); 11.451 GHz (EUTELSAT).

Polarization: RHCP (INTELSAT); X-LP (ASTRA, EUTELSAT).

Minimum EIRP: 9 dBW to the rim of spot coverage,
Power Stability: < 1dB variation between -10 and +50 °C on the satellite; < 2 dB variation over 7 years; both values peak-to-peak; ±0.5 dB variation over any 24 hours; ±0.2 dB variation over any 2 minutes

Frequency Stability: short-term: 90% the total radiated power falls within a 5 Hz bandwidth centered on the beacon frequency. If a phase-lock loop approach is used in the beacon receiver design, a good compromise between search time and depth of fade during which lock can be maintained is 100 Hz; long-term: $\pm 3 \cdot 10^{-6}$; long-term refers to the spacecraft design life which is e.g. 10 years for an INTELSAT VI.

Modulation: there is no modulation on the Ku-band beacons, they are „pure” CW tones (see Fig. 5a) on ASTRA and INTELSAT satellites. Sometimes they are modulated by the telemetry and/or ranging signal, as on EUTELSAT satellite is (Fig. 5b).

3. SOME MEASURED DATA

3.1. Long-term of satellite signal observations

The Radio Department of Wrocław University of Technology has been carrying out a systematic measurements and monitoring of the communication satellite signals both in fixed place in Wrocław [7], and in different locations, uniformly distributed all over the Poland [8] since 1997. The preliminary results from fixed site are presented below. We present time dependence of communication signals power level and carrier-to-noise ratio along with the beacon power level. As an example we choose, the continuous measurements, were doing during a few weeks, from December 19, 1997 to January 8, 1998.

In Fig. 6 the EUTELSAT signals behaviour are shown.

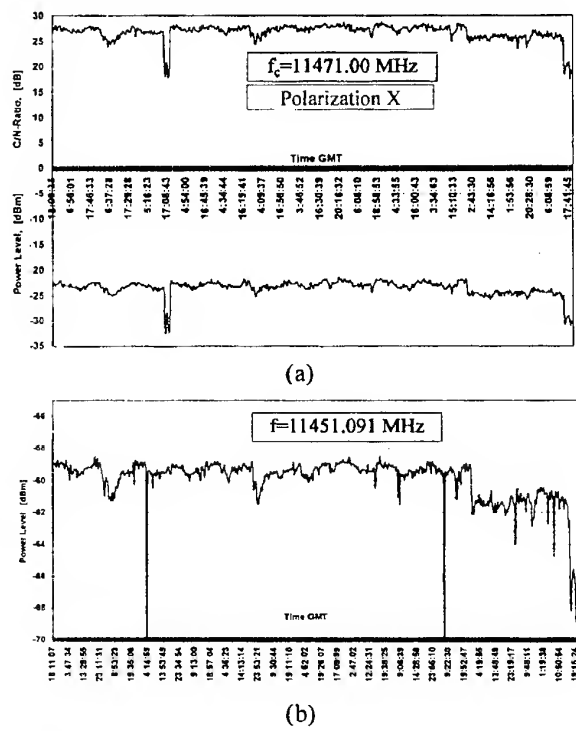


Fig. 6. Time-variations of communication signal carrier-to-noise ratio and power level (a); and telemetric beacon signal power level (b) received from the EUTELSAT II F1 13°E satellite during December 19, 1997 to January 8, 1998 period

Horizontally polarized communication signal has -23 dBm an average power level and about 27 dB carrier-to-noise ratio. The two events was observed during whole period. First, was observing on December 22 afternoon, between 15:29 and 18:44 GMT. That time power level and C/N-ratio decreased over 10dB. Second event presented on January 8, 1998 had shallow decrease, about 6 dB. It's worth to note that on the beacon diagram only second event coincide with communication signal, the first did not registered. Most

of time all over observation period beacon power level changes less than ± 0.5 dB.

On next few pictures variations of measured signals from ASTRA and INTELSAT satellites are shown.

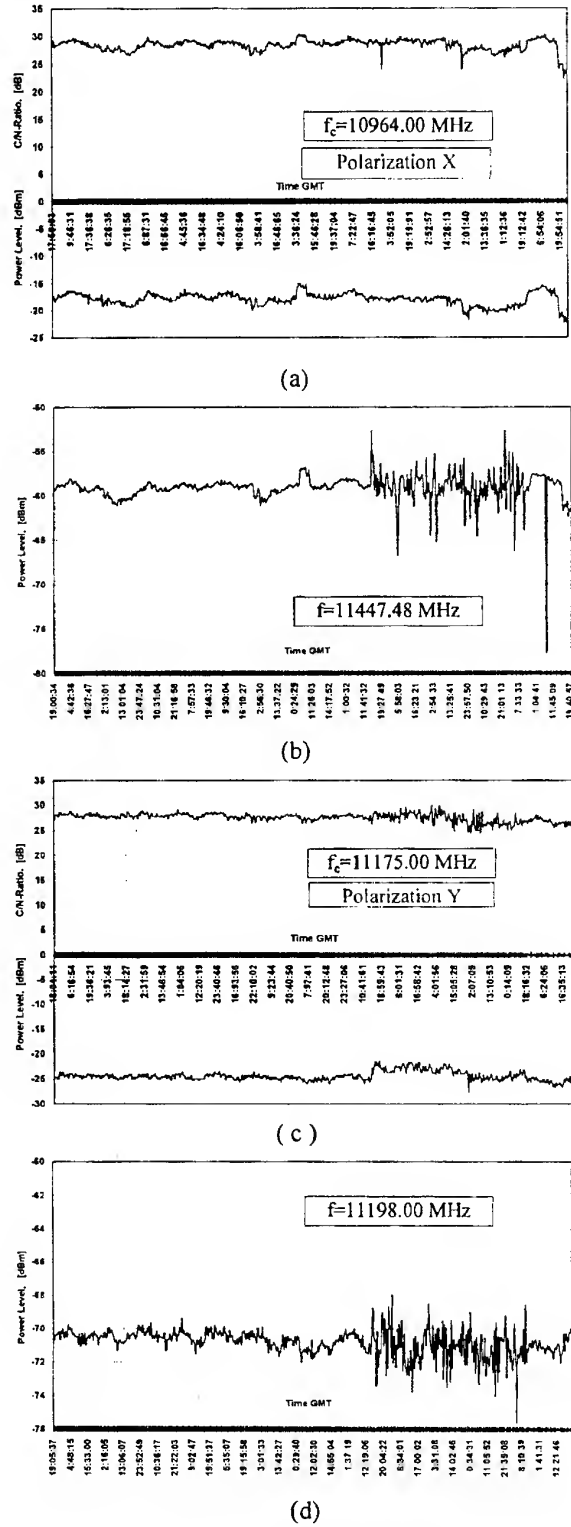


Fig. 7. Time-variations of communication and telemetric beacon signals received from ASTRA (a), (b), and INTELSAT601 satellites (c), (d) (period as in Fig.6)

Above results permit roughly estimate satellite signal behaviour during assumed period of time. One cycle of observation some ten signals, from seven satellites were registered. Each communication signal was observed, averaged and memorized about 3:30 min, and beacon signal from this same satellite - about 1:20 min. The whole acquisition process consumes 31 minutes. It acts as a sampling time of the monitoring procedure.

Such rare sample data could not show subtle distinction of satellite signals due to at the moment propagation conditions (e.g. short-time rain event, scintillation effects, etc.). For such data only beacon signals were observed, with sample rate 1:2 seconds.

3.2. Scintillation and multipath effects

Rapid signal variations caused by small-scale variations of refraction are called scintillations. Tropospheric effects in absence of precipitation are unlikely to produce serious fading in space communication systems operating at frequencies below about 10 GHz and at elevation angles above 10°.

The magnitude of tropospheric amplitude scintillations depends on the amplitude and structure of the refractive index variations. The magnitude of scintillations increases with frequency and with the path length through the medium and decreases as the antenna beamwidth reduces. An example of our observation of attenuation effect due to scintillation is shown in Fig. 8.

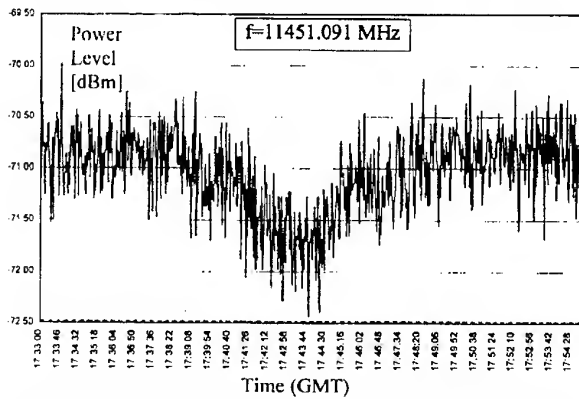


Fig. 8. A representative propagation event of May 19, 1997 observed at Wrocław, Poland on the EUTELSAT II F1 13°E beacon signal level

4. SUMMARY AND CONCLUSIONS

This paper described an experimental campaign for collecting Ku-band propagation data using ASTRA, EUTELSAT, and INTELSAT satellites. The objective to the experiment is to characterize satellite communication channels received in Poland. The campaign consists of a single fixed (on the roof of the Wrocław University of Technology) measuring site, and the mobile terminal. Only the measurements using the fixed site were addressed in this paper. Reference 8 describes the mobile experiment.

The site began collecting data in March 1997 and data analysis began late that year. Sample measurements and preliminary results have reported in Figures 2-8.

Basing on the collected data, up to date many refined statistics and results, that have never been done in Poland before, are expected to be developed.

A number of years of observations are needed for a single path to provide a reliable estimate of actual attenuation distribution. To obtain an uncertainty of less than 10% r.m.s., a minimum of four years of observation are needed.

The variation from year-to-year of the measured path attenuation from the long-term average is of interest to system designers if additional margin (or safety factor) is required to perfect sensitive links that require extremely high availability, such as telemetry, command, control, and monitoring functions.

ACKNOWLEDGMENTS

This work was supported by the Polish Government Committee of Scientific Research, Warsaw, Poland, under Grant KBN No 2 Z6Z6 012 03p37.

5. REFERENCES

- [1] ITU-R Section 5F, „*Propagation Data and Prediction Methods Required for Earth-Space Telecommunication Systems*”, Report 564-4, Geneva, Switzerland, 1990
- [2] ITU-R Section 5F, „*Propagation Data for Broadcasting from Satellites*”, Report 565-4, Geneva, Switzerland, 1990
- [3] L.W. Stutzman, et al., „*Results from the Virginia Tech Propagation Experiment Using Olympus Satellite 12, 20, and 30 GHz Beacons*”, IEEE Trans. Vol. AP-43, No 1, January 1995, pp. 54-62
- [4] J. Skrzypczyński, “*Determination of satellite signal reception through the Poland*”, M.Sc. Thesis, Wrocław University of Technology, Wrocław, Poland, 1993.
- [5] W.J. Krzysztofik, D.J. Bem, J. Skrzypczyński, „*The Ground Station for Satellite Signals Monitoring at the Wrocław University of Technology*”, Workshop on Satellite Propagation Experiments, Politecnico di Milano, Italy, 1995.
- [6] W.J. Krzysztofik, J. Skrzypczyński, „*Monitoring & Qualification of Satellite Signals Reception in Poland*”, International Broadcasting Convention, Amsterdam, Holland, 1995
- [7] W.J. Krzysztofik, „*Estimation of the Satellite Communication Signals Level & Quality on the Base of the Experimental Investigation*”, Report, Wrocław University of Technology, Wrocław, Poland, 1998 (to be in press)
- [8] W.J. Krzysztofik, „*Mobile Measurements of Satellite Signals all over the Poland Territory*”, Report, ibid.

IMAGING & SUPPRESSION OF EXTERNAL RADIATION ON OUTDOOR-FIELD ANTENNA TEST

Wojciech J. Krzysztofik, Zygmunt Langowski

Wrocław University of Technology
Institute of Telecommunication & Acoustics
The Radio Department
Wybrzeże Wyspiańskiego 27, 50-370 Wrocław, POLAND
Email: wojka@zr.ita.pwr.wroc.pl

The antenna outdoor-range is optimized according to IEEE Recommendation with respect to external radiation (interference) and/or acceptable levels of unwanted reflections from the ground and some scattering artifacts presented in surrounding space to measuring set up. Electromagnetic radiation hazard in the vicinity of antenna range is taken into account and some precautions to the personnel are indicated.

1. INTRODUCTION

A fundamental property of an antenna is its radiation pattern. The working environment in which an antenna is installed may substantially modify the intrinsic pattern. Consequently measurements *in situ* are frequently required.

A classical problem encountered when measuring the far-field radiation pattern of an antenna in a medium distance range is the degradation that occurs when undesirable reflections (from the ground or nearby objects) are present. To reduce this problem, the source and test antennas are often installed on towers to remove them from reflective objects, radio-frequency (RF) absorptive materials are used to reduce the amplitude of the reflected signals and diffraction fences and/or a longitudinal ramp are installed in the range in order to null out the reflections and „clean up” the range. These solutions are often limited in their effectiveness and can be prohibitively expensive to implement.

Outdoor ranges provide an uncontrolled environment. They are usually subjected to interference from signal sources outside the range area. These sources can be mobile communications, radar, and/or common broadcasting systems operating in VHF-band. The use of filters can often suppress the effect of these interfering signals but not eliminate them. We should be

able to control external radiation before and during measuring procedure on test set up.

Another concern to the antenna engineer is that of radiation hazards. It is well known that RF-fields of sufficient intensity can cause damage of biological tissue. Therefore it is usually necessary to determine the level of the radiation intensity in the vicinity of antennas radiating high RF-power so that appropriate safety precautions can be taken before personnel enter area.

The purpose of this contribution is to present a means of evaluating the performance of an antenna test range from diagnostics of the wave front incident on the region to be occupied by the antenna under test.

2. ANTENNA-RANGE MEASUREMENTS OF RADIATION PATTERN

Antenna range has been developed for the purpose of measuring the radiation patterns of antennas in the frequency range between 0.06 and 26 GHz, independent of their operational environment. The antenna range consists of the appropriate instrumentation and the physical space required for the measurements (Fig. 1).

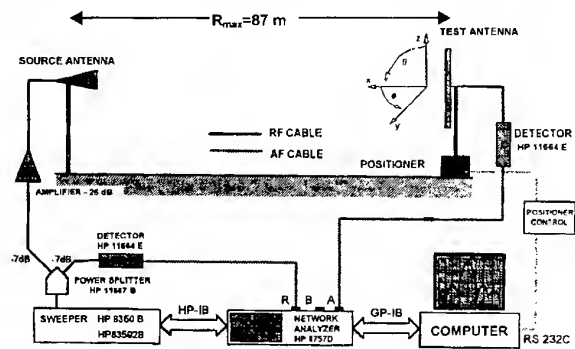


Fig.1. Outdoor antenna-test setup on the roof of Wrocław University of Technology building [4], [5]

The ideal incident field for measuring the radiation characteristics of the antenna is that of a uniform plane wave. In practice it is only possible to approximate such a field. Attempts to do this have led to development of *free-space range* - designed in such a manner that all the effects of the surroundings are going to be suppressed to acceptable levels.

There are two basic range configurations that accomplish the position requirement for θ and ϕ cuts [1], [2], [3]. One is the fixed-line-of-sight configuration, the other one is called the movable-line-of-sight configuration. Here, in our case, the former setup is being used in which the test antenna and its associated coordinate system are rotated about a z-axis (usually passing through the phase center of the test antenna).

When the broadband antenna patterns are measured at discrete frequencies over their operating bands, it is possible to miss significant variations in their amplitude patterns. These variations are typically frequency dependent and narrow band. They are often referred to as „anomalies” in the pattern. For that reason the swept-frequency technique is employed on presented setup.

The range is designed over an approximately flat area, on the roof of the University building (C-3/4), and the effects of the surroundings are suppressed: by careful choice of the source antenna with regard to directivity and side-lobe level; - by clearance of the line of sight along range surface.

Some experimental results of different antenna radiation patterns measured on our setup are shown in Fig. 2.

3. ANTENNA-RANGE EVALUATION

Once an antenna-pattern range has been designed, constructed, and instrumented, it is necessary to experimentally determine the state of the illuminating electromagnetic field over the test region, that is, the region where the test antenna is to be mounted.

The illuminating field over the test region will deviate from that predicted from calculations based upon a highly ideal range geometry because of reflections from various mounting structures, cables, obstacles on or near the range surface, and from irregularities in the range surface itself. In addition RF interference is often a cause of difficulty.

It is convenient to investigate separately that part of the field which is incident from the general direction of the source antenna and that which arrives from wide angles with respect to the line drawn from the center of the test region toward the phase center of the source antenna. The former is often referred to as the near-axis incident field, and the latter as the wide-angle incident field. The near-axis incident field may be determined from a field-probe measurement over a plane perpendicular to the range axis and coincident with the expected location of the test antenna. This plane is called the test aperture.

The two most commonly used techniques for the evaluation of wide-angle fields [2] are the antenna-

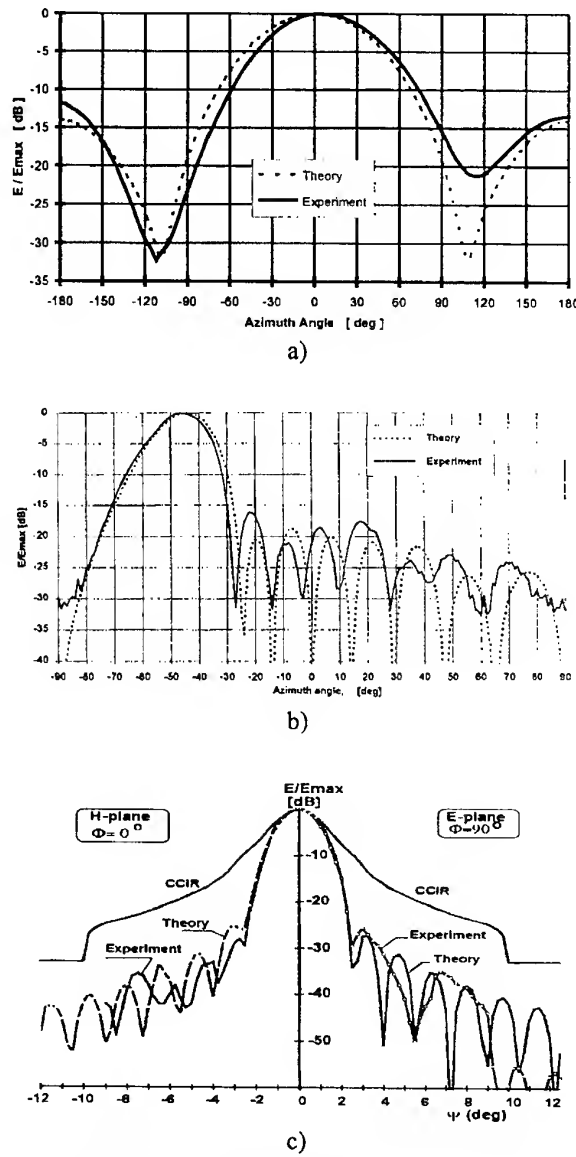


Fig.2. Radiation pattern of various antenna: a) screen-backed dipole, $f=87$ MHz, b) microstrip phased antenna array $f=5.02$ GHz, c) an offset parabolic reflector of diameter 0.9 m., $f=11.4$ GHz

pattern-comparison method and the longitudinal-field-probe method. The *antenna-pattern-comparison* method is based upon the premise that in the absence of any reflected or extraneous signals the measured azimuthal antenna patterns of the test antenna will be unchanged with small changes in the test antenna's position with respect to the source antenna. If the other hand, antenna patterns are measured for several different positions of the test antenna and the patterns exhibit changes from position to position, then this indicates the presence of reflected or extraneous signals. The *antenna-pattern-comparison* method then consists of recording the azimuthal patterns of a test antenna for enough different positions along the range axis so that the maximum excursions of the side lobe levels are obtained. It is convenient to record all patterns on a single chart from

which the apparent direction of the incoming wave and its relative level can be determined. An example of such a measurement is shown in Fig.3.

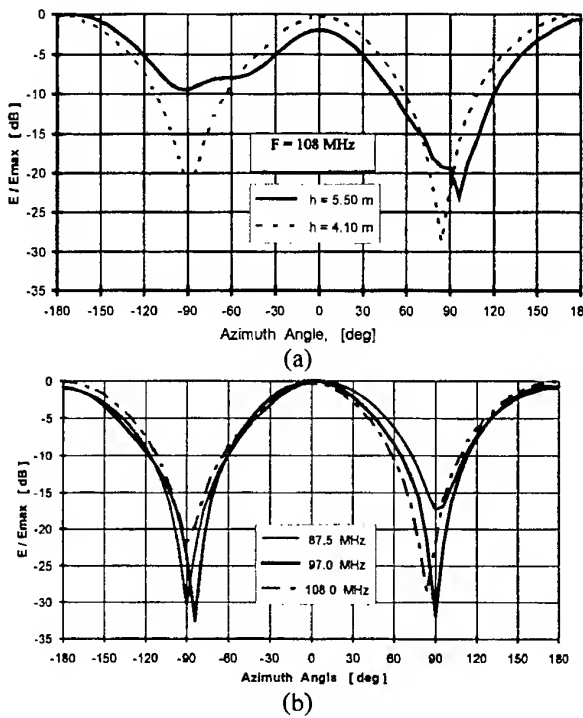


Fig. 3. Azimuthal dipole-antenna pattern comparisons for incremental longitudinal displacements (a) height, h of the center of rotation (a), and for fixed optimal height (4.1 m) versus frequency (b)

Note that there is a variation of approximately 3 dB in main-lobe of the patterns and 5 to 12 dB at the azimuth angle $\pm 90^\circ$. If the direct and major reflected waves were both received on the „minimum”-direction, this would mean that the reflected wave is more than 5 dB below of the direct wave. Since the variation occurred on 90 degree are approximately 20 dB below the peak of main beam, the reflected wave is at least - 25 dB relative to the level of the direct wave.

Observable results of antenna pattern measurements exhibits some discrepancy and asymmetry in their shapes. It means if the measuring environment covers some distortions. We try to minimize and/or eliminate them in following manner: - by redirection or absorption of energy reaching the range surface or obstacles that cannot be removed; - by special signal-processing techniques such as modulation tagging of the desired signal; - by use the time-domain gating (three-step procedure: frequency-domain (measurements)-to-time-domain (signal processing) -and-back-to-frequency-domain (visualization) transformation) [6], [7].

4. TIME-DOMAIN AND GATING

To reduce the effects of reflected signal paths in an antenna measurement and determine the response of the

antenna to the main path signal only, without costly range modifications it possible measuring the swept frequency response of the antenna and compute the inverse Fourier transform to give the time domain impulse response. The time domain response allows to user to identify the reflected signal path responses in time and then remove them with the gating feature. In converting back to the frequency domain, the effects of the responses outside the gate are removed.

The first step of the three-fold process begins with automatically controllable phase and amplitude measurement of the antenna under test with respect to a reference antenna or RF source signal. The equipment required is quite similar to presented on frequency-domain setup (Fig.4).

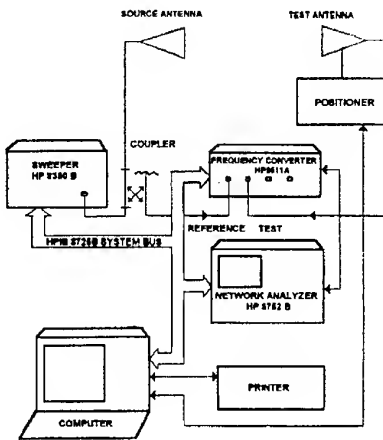


Fig. 4. Antenna measurement configuration employing time-gating technique

The principal difference is that if a complex E-field (amplitude and phase) have to be measured, so now the vector network analyzer is required. This is done by using network analyzer to measure the swept frequency response of the antenna to the main path signal only. The emitting antenna and the reference one are fixed. The direction of the tested antenna is controlled in elevation and azimuth by variable positioner. The measurement cycle is fully controlled by computer which also records the measured phase and amplitude for every specified antenna direction at each frequency point.

The second step of the procedure (the signal processing) takes place on quite powerful computer for an off-line analysis. The mathematical analysis is based on Fourier transform from frequency domain (measurement) to the time domain. Parasitic reflections are hence easily canceled in time domain using numerical gate filtering.

The usual antenna radiation pattern is then obtained in the third step (visualization) after a reverse Fourier transform back to the frequency domain (Fig. 5) [6].

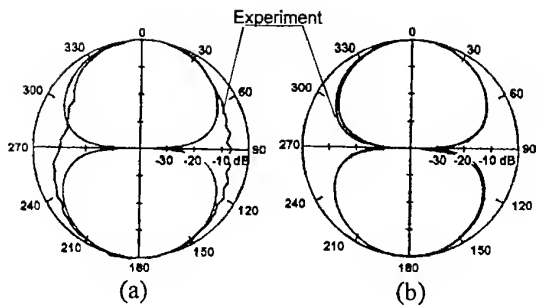


Fig. 5. Dipole antenna pattern : measured on actual setup, $f=125$ MHz (a), and after time-gating procedure (b), together with theoretical one

The dipole was measured with 201 points from 50 to 300 MHz at each 5 degree increment of azimuth rotation (72 sets of 201 point data). In this case, the gating technique has improved the measurement of the nulls by better than 25 dB.

The distance between the main impulse (directly incident wave) and the parasitic impulses (reflected waves) must be large enough to apply gating in time domain. The time domain width is determined by the obstacle distances in the surrounding frame. The measurement frequency span must be inversely proportional to the desired time impulse width $T_{\max}[\text{ns}] = f^{-1}$ [GHz]. So, the wider the necessary time domain width, the narrower the frequency span and the greater the number frequency points will be. In this measurement, the effect of any signals that are picked up from reflections from the antenna positioner or other close in reflective objects will not be removed.

This method is very suitable for wide band centimeter wavelength antennas, generally measured in anechoic chambers, because the phase delays between the directly incident wave and the reflected waves allow a quite efficient cancellation of parasitic reflections by gating in time domain. A quite good accuracy can be obtained with 512 frequency points by gating per octave (typical number) and the necessary storage capacity is achievable on most of usual personal computers. A program using fast Fourier transform (FFT) has been especially designed for this application. It computes the actual radiation pattern of the studied antennas along with interesting information about the quality of the test equipment used (e.g. the parasitic reflection level versus space direction or the obstacle distances).

A good accuracy can be reached with quite short computation time (a few seconds are necessary to compute all the radiation patterns in the measurement frequency range).

The program allows to plot the measured antenna pattern with gating or without gating and the parasitic reflections pattern: for a fixed elevation with variable azimuth, for any space direction (contour plot).

5. ELECTROMAGNETIC RADIATION HAZARDS

Individuals involved in the generation of electromagnetic signals and the testing of antenna shall consider carefully the potential hazard of exposure of humans to excessive electromagnetic radiation. The spectrum of nonionizing radiation covers the frequency range up to ultraviolet-light region.

This section presents brief comments pertinent to health and safety precautions, which apply primarily to radiant energy in the RF region. The purpose is to alert those engaged in testing antennas, microwave components, and so on, to potential RF radiation hazards. In addition to radiation damage, burns may be incurred when contact is established by arcing between the body and exposed components of a system operating at high RF power levels.

The principal factors which affect the amount of RF energy absorbed by human body are the frequency, polarization and power flux density of the incident wave, the exposure time, and the electrical properties of the body.

The American National Standards Institute (ANSI) has published recommendations concerning safety levels with respect to human exposure to electromagnetic fields in the frequency range from 300 Hz to 100 GHz. The ANSI RF protection guides (RFPG) are intended to apply to both occupational and nonoccupational exposure. These guide specify maximum allowable levels as a function of frequency in terms of the mean squared E- and H-fields, respectively, and the equivalent free-space plane-wave power density. To determine adherence to this RFPG, the power density or squares of the field strengths should be averaged over any 0.1-h period with all measurements to be made at distance 5 cm or greater from any object. Table 1 is a summary of the ANSI C95.1-1982 RFPG.

Table 1.

RADIO-FREQUENCY PROTECTION GUIDES
by ANSI C95.1-1982 RFPG (U.S.A)

Frequency Range [MHz]	Mean Squared E ² -field [V ² /m ²]	Mean Squared H ² -field [A ² /m ²]	Power Density [mW/cm ²]
30-300	4000	0.025	1.0
300-1500	4000(f/300)	0.025(f/300)	f/300
1500-100000	20000	0.125	5.0

Note: f = frequency in MHz

The frequency dependency of the maximum allowable equivalent plane-wave power density and of the mean squared field strengths is based on research results which show that the whole-body-average specific absorption rates approach maximum values when the long axis of the body is parallel to the E-field vector and is approximately 0.4λ in length where λ is the free-space wavelength of the incident field. This resonance occurs at a frequency of about 70 MHz for man of average size.

The allowable incident intensities increase above 300 MHz. The levels in Table I may be exceeded if the input power to a radiating device at RF between 300 kHz and 1GHz is seven watts or less.

The Polish Government Regulations recommends slightly different levels of electromagnetic radiation hazard for personnel engaged in maintenance of the electromagnetic fields sources. They are presented in Table 2.

Table 2.

RADIO-FREQUENCY PROTECTION GUIDES
by Dz.U. No 3, 1995 (Poland)

Frequency Range, [MHz]	10 - 300	300 - 300000	
Zone	E-field Strength [V/m]	Power Density [W/m ²]	
		Stat. Fields	Nonstat. Fields
Safety	<7	< 0.1	<1.0
Intermediate	7 -20	0.1 - 2.0	1 - 10
Danger	20-300	2 -100	10 -100
Hazardous	> 300	> 100	> 100

Having in mind the above recommendations and taking into account the gain of source antenna frequency-dependence, the whole frequency range of measurement was divided on few bands, and some numbers of electromagnetic radiation hazard on antenna range were estimated (see Table 3).

Table 3.
ELECTROMAGNETIC RADIATION HAZARD
ON OUTDOOR ANTENNA-TEST RANGE

Band	I	II	III	IV	V	VI	VII
F MHz	60 to 140	180 to 230	300 to 1000	1000 to 3000	3000 to 6500	6500 to 12000	12000 to 18000
E V/m. R=20m	1.22	1.95	1.72	-	-	-	-
S mW/m ² R=20m	1.99	5.06	3.95	0.31	0.397	1.98	0.70
S mW/m ² R=87m	-	-	-	0.016	0.021	0.105	0.037

Note: Source Power=13 dBm; Amplifier Gain=26 dB
(for frequency range 60 to 1000 MHz)

Determined radiation hazards are well below permissible levels, for all frequency bands. However some exceptions may happen when VHF (1st-band) antenna are measured. In this case a high-level of interference radiation are produced by broadcasting stations. To overlap them sometimes some increased powers of source have been used. On a longitudinal axis of antenna test range it produces radiation hazard

extending permissible level of 7 V/m, which may even reach a danger-zone.

6. CONCLUSIONS

The modern outdoor antenna test range, working in 0.06 to 26 GHz frequency range, and fully controlled via computer was designed [4], [5] and evaluated. The external radiations (interference) were suppressed by means of tuned filters and careful monitoring before and during measurements. To omit reflected waves on antenna site the double Fourier transform and time-gating of measured signal processing was considered. This method improves rejection of reflected products even over 25 dB. The electromagnetic radiation hazard was taken into account. The estimated radiation are well below permissible levels. However, sometimes they may be exceeded, during a VHF antenna measurements, as a result of higher level of source signal applications on a test site, in order to overlap of external emission produced by broadcasting stations.

It is concluded that at present time the minimum measurable levels on the site are on the level -25 to -30 dB with respect to the peak of main beam.

ACNOWLEDGMENTS

This work was partially supported by the Polish Government Committee of Scientific Research (KBN), Warsaw, Poland, under Grant No22 150 92 03p38.

7. REFERENCES

1. G.E. Evans, „Antenna Measurement Techniques”, Artech House, Inc., Boston, London, 1990
2. IEEE Std., „Test Procedures for Antennas”, 1979
3. W.J. Krzysztofik, „Modern Methods of Microwave Antenna Measurements”, (in Polish) Quarterly of Electronics & Telecommunications , vol. XXVI, I, PWN, Warsaw, Poland, 1990, pp. 51-74.
4. Z. Langowski (ed.), “The outdoor automatic antenna test set up”, (in Polish) cht. 1 in Report I28/S-005/96, Wrocław University of Technology, Wrocław, Poland, 1996.
5. R. Borowiec, P. Słobodzian, Far-Field Antenna Test in the Frequency Domain - the Outdoor Range”, (in Polish) National Symposium on Telecommunication, KST-96, September, 1996, Bydgoszcz, Poland, pp. 155-64
6. J.W. Boyles, „Measuring a Dipole Antenna Radiation Pattern Using Time Domain and Gating”, RF Design, September 1985, pp. 44-2
7. S. Wijkowski, M. Budnik, „Time-Domain Measuring Setup of Antenna Radiation Pattern & Power Gain”, (in Polish) M.Sc. Thesis, Wrocław University of Technology, Wrocław, Poland, 1994

RAIN INDUCED SIGNAL DECREASE IN SATELLITE LINKS

Andrzej A. Kucharski, Jacek Skrzypczyński

Wrocław University of Technology, Wybrzeże Wyspiańskiego 27
50-370 Wrocław, Poland

In this paper concepts of theoretical and measurement investigation for predicting signal decrease in satellite links due to the rain are presented. Measurement set-up for measuring statistics of signal rain induced attenuation is described. A method of theoretical prediction of electromagnetic waves scattering by rain particles is outlined.

1. INTRODUCTION

In satellite communications with frequencies over 10 GHz rain induced effects play a fundamental role in determining the margin to be implemented in the system's link budget.

This problem for Ku band (12 - 14 GHz) has been investigated in details in the Institute of Telecommunications by the team under supervision of A. Kawecki. For higher frequencies (Ka band: 20 - 30 GHz) up to now there has been no research of this phenomenon for polish climate.

At the Institute of Telecommunications and Acoustics of Wrocław University of Technology there has been developed measurement system for propagation studies on satellite link in 20 GHz band. The system consists of satellite beacon receiver to measure attenuation and scintillation of electromagnetic waves in satellite link. In order to investigate climatic characterization of Wrocław region meteorological station in vicinity of satellite antenna has been established. The data obtained from measuring devices are automatically collected in the digital computer in the format proposed by European Space Agency (ESA). This allows to exchange data with other research institutes and universities in the world. The obtained data will be used to validate existing slant path attenuation prediction methods and to develop new models.

In parallel, the advanced research concerning numerical prediction of attenuation and scattering by rain particles is carried out. This concerns development of new models, which allow computing fields scattered by raindrops in so called resonance region, which covers frequencies under investigation.

Described research program will allow presenting the scientific background of the propagation effect and practical aspects of link planning. The research results will be given to ITU-R database in order to compare with results from other geographical locations, which will give inside into the regional and seasonal differences of rain attenuation.

2. MEASURING SET-UP

The measuring set-up is presented in Figure 1. The system consists of a computer controlled 20 GHz signal receiver, a rain measuring sub-system and a workstation with analysis software.

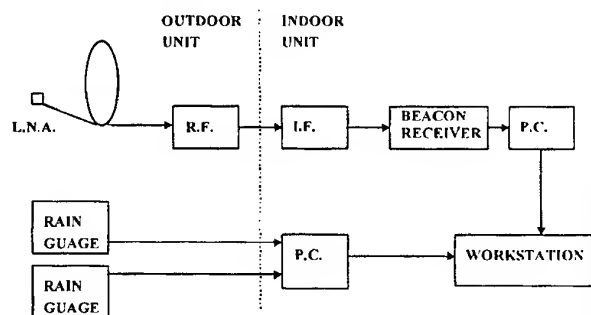


Fig. 1. The measuring system simplified layout.

Propagation terminal continuously measures level of the satellite signal transmitted by the Italsat F2 (20 GHz beacon). The signal is received by a reflector antenna, then processed by a RF section, an IF section, and an analog/digital receiver monitored by a PC-based data acquisition system. The RF section of the receiver includes a waveguide switch for injection of a calibration signal into the beacon path, a low noise amplifier, and a mixer-preamplifier which downconverts the RF signal to an IF frequency. The IF section provides two stages of frequency downconversion and produces 10 kHz signal. The 10 kHz carrier is sampled at a 1 kHz rate by a 12-bit A/D converter. This 1-kHz data stream is filtered in a 3-Hz

bandwidth and then recorded every 0.1 s by the data acquisition system.

The rain measuring sub-system collects data from two rain gauges. The rain gauges are of tipping bucket type with a collecting area of 1000 sqcm and a rain height of 0.03 mm for each tip. The number of tips are stored every minute by dedicated PC system equipped with hard disk.

The other environment data necessary for analysis and modelling such as a temperature of air, humidity, and a barometric pressure are collected in nearby meteo station of Meteorological Institute (located 2 km to East).

Data from the experiment will be first pre-processed to ensure that only valid data are analysed. Then a set of beacon and weather data will be processed to obtain statistical results for rain rate, beacon attenuation, fade duration, and fade slope. The most important results are cumulative statistics of attenuation. The majority of that attenuation is caused by a rain. The most significant parameters of a rain are both its extent along the path and its intensity (or rain rate). Obtained cumulative statistics of attenuation will be then compared with the annual statistics of point rain rate. The agreement with the CCIR recommended rain zone and attenuation prediction tools would be then checked.

All obtained data and statistic results will be transferred into the digital format proposed by European Space Agency (DAPPER format). This would allow to exchange data with other research institutes and universities in the world.

3. COMPUTER MODELING

The problem of prediction of electromagnetic fields attenuation due to propagation through rain regions plays extremely important role in designing both satellite and terrestrial microwave radio links. The scattering phenomena depend very strongly on frequency range of electromagnetic waves. Three main frequency regions are usually defined when considering scattering by rain particles:

- 1) Rayleigh-scattering region, when rain particles can be considered both as electrically small, and phase shifts across particles are small;
- 2) Optical-scattering region, when the incident wavelength is much less than the diameter of scattering particle;
- 3) Resonance region, which lies between Rayleigh and optical regions.

In the resonance region no simple asymptotic techniques could be used in order to describe field-rain interactions. In fact, the description of scattering problem requires rigorous solution of Maxwell

equations. Unluckily, when investigating the 20 GHz frequency band that is considered in this paper this third attitude must be used.

In this work, a new simple and efficient numerical method has been applied to predict scattering by hydrometeors for the resonance region.

The method makes an extensive use of the rotational symmetry of rain particles, which allows to decouple the solution into so called azimuthal modes which considerably reduces the number of unknowns used in the solution scheme. The method of moments scheme is used to solve the modal volume integral equations.

Using this method it is possible to calculate for example radar or extinction cross sections against drops diameter and frequency.

3.1. Method of moments solution

The rain particle can be understood as a small dielectric body, usually with rotational symmetry, immersed in the incident field, which, in most cases, can be approximated with the plain wave.

There are two commonly known methods of dealing with dielectrics in electromagnetic theory. Both make an extensive use of some equivalence principles. One of them leads to so called surface integral equation (SIE), which is applicable to homogeneous objects and uses both electric and magnetic equivalent surface currents. The second one uses volume integral equation (VIE) and volume equivalent electric currents.

While dealing with general three-dimensional geometries usually surface approach is preferred because of computer resource related matters. In the present case however, if we take into account rotational symmetry of the body, in authors opinion, volume integral equation approach has advantages that overrides its drawbacks. First, we use only electric currents, which makes all formulas and operators much simpler. Second, it allows to easily model heterogeneous objects.

The method of electric field integral equation (EFIE) construction is similar to that used in another paper in this proceedings [1], so in this place we only outline the main steps in solution process:

- 1) the solution process is decoupled into azimuthal modes;
- 2) special basis and testing functions are developed, with the property of being divergenceless, which enables further reduction of the number of unknowns;
- 3) the corresponding set of algebraic linear equation is obtained and solved;
- 4) far or near field solutions are obtained via adding solutions for particular modes.

3.2. Validation of the method

To validate the procedure especially for far field calculations we applied the method to the case for which SIE solution by other authors was available [2,3].

The comparison of the results is shown in Figure 2.

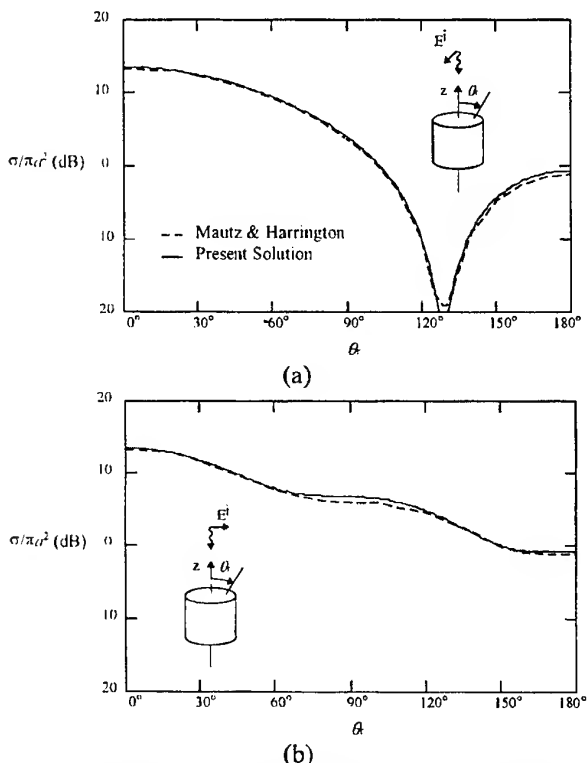


Fig. 2. Plane wave scattering patterns for dielectric cylinder of radius a and height $2a$. $a = 0.25 \lambda_0$, $\epsilon_r = 4$.

(a) $\phi\phi$ -polarization. (b) $\theta\theta$ -polarization.

From above figures, it can be found that the agreement of results is excellent and method can be directly used in other investigations.

Of course while investigating rain particles as objects of interest more sophisticated shapes have to be used instead of simple cylinder. Especially important is the case of dielectric sphere. The authors have made some comparison of resonance frequencies of spherical dielectric objects calculated with present method and with semi-analytical method available in the literature [4]. In all cases the agreement of results was within 0.5 per cent.

The full analysis of rain-drop scattering phenomena will be presented on EMC'98 conference in Rome [5].

4. CONCLUSIONS

In the paper concepts of both practical and theoretical investigations concerning scattering and signal decreasing due to rain phenomena have been presented. The measurement set-up is now under construction in Institute of Telecommunications and Acoustics, Wrocław University of Technology. It is hoped, that it will allow to perform first in Poland

investigation of propagation through the rain in 20 GHz frequency band. In parallel theoretical models with the use of method outlined above are under construction.

5. REFERENCES

- 5.1. A.A. Kucharski, "A Body-Of-Revolution Model For Calculating Electromagnetic Fields Excited Inside Human Head", Proceedings of the 14th International Symposium on EMC, Wrocław, 1998.
- 5.2. J.R. Mautz and R.F. Harrington, "Electromagnetic scattering from a homogeneous material body of revolution," *Arch. Elec. Übertragung.*, vol. 33, pp. 71-80, Feb. 1979.
- 5.3. A.W. Glisson and D.R. Wilton, "Simple and efficient numerical methods for problems of electromagnetic radiation and scattering from surfaces," *IEEE Trans. Antennas Propagat.*, vol. AP-28, pp. 593-603, Sept. 1980.
- 5.4. P.W. Barber, J.F. Owen, and R.K. Chang, "Resonant scattering for characterization of axisymmetric dielectric objects," *IEEE Trans. Antennas Propagat.*, vol. AP-30, pp. 168-172, Mar. 1982.
- 5.5. A.A. Kucharski, "A method of moments solution of scattering by hydrometeors in resonance frequency region", accepted for publication in the Proceeding of the International EMC Symposium, Rome, 1998.

BIOGRAPHICAL NOTES



Andrzej A. Kucharski received M. Sc. and Ph. D. degrees from Wrocław University of Technology in 1988 and 1994, respectively. Since 1993 he is with the Radio Department, Institute of Telecommunications and Acoustics, Wrocław University of Technology where he is currently an Assistant Professor. His research interests are primarily in computational electromagnetics, antennas and propagation and electromagnetic compatibility.



Jacek Skrzypczyński received M. Sc. degree from Wrocław University of Technology in 1994. Since 1994 he is with the Radio Department, Institute of Telecommunications and Acoustics, Wrocław University of Technology. His research interests are primarily in satellite communication, electromagnetic compatibility, antennas and propagation.

NUMERICAL HYBRID TECHNIQUE FOR THE ANALYSIS OF TRANSIENT ELECTROMAGNETIC FIELDS PRODUCED BY WIRE STRUCTURES

V.P. Lisitsyn, V.M. Lugovtsov

High-Voltage research Center of Russia Electrotechnical Institute
143500, RUSSIA, Istra, Moscow Region, tel/fax: (095)560-34-38

A new general technique is suggested for numerical analysis of transient electromagnetic response of large-scale wire structures. The basic idea is to advance of practical ability of well-known integral equation method in the time-domain by combine it with a traveling waves current approximation approach. The specification hybrid technique is illustrated on an example of the wire plate EMP simulator. In many practical cases hybrid technique provide accuracy similar to one the traditional method of moments and significant reduce the computational cost.

1. INTRODUCTION

The transient electromagnetic fields radiated by wire structures (antennas, scatterers, EMP simulators and others) can be calculated by the numerical method of moments for the integral equations in the time-domain (TD MoM) [1-3]. MoM is perhaps the most universal, accurate and developed numerical technique for solving scattering and radiation problems in EMC. However, this method is intractable for the large-scale structures because an excessive number of unknowns are required in formulation and computers resources are limited.

On the other hand the transient current on the same wire structures can be approximated by the traveling waves (TW) [4,5]. Advantages of this approach are simplicity of program realisation and minimum requirements to resources of the computers. In many practical cases TW approach gives good results. However, in problems where the structure contains various irregularities (curved wires, complex wire junctions, resistive load and etc.), the behaviour of a current can poorly be described by a sum of traveling waves. In these cases the TW gives only rough estimation of electromagnetic characteristics.

In this paper a new hybrid technique is enunciated. This technique combine the TD MoM with TW in single algorithm. The presentation is organised as follow. In section 2 and 3 we briefly formulate our form of TD MoM and TW. In section 4 we will introduce hybrid method. In section 5 numerical results based on hybrid approach are presented and discussed.

2. SPLINE MOM FORMULATION

Using thin-wire approximation, the time-domain integro-differential electric field equation we used has the general form [1].

$$(1) \quad Z(s)I(s,t) + \frac{\mu_0}{4\pi} \int_S \left[\left(\frac{\vec{s} \cdot \vec{s}' \frac{\partial}{\partial \tau} + c \frac{\vec{s} \cdot \vec{R}}{R^2} \frac{\partial}{\partial s'}}{R} \right) I(s',\tau) - c^2 \frac{\vec{s} \cdot \vec{R}}{R^3} Q(s',\tau) \right] ds' = \vec{s} \cdot \vec{E}^0(s,t), \quad 0 \leq t \leq T_{\max}, \quad s \in S + \rho,$$

where I is the current to be found, \vec{E}^0 is the known incident electric field, $\rho=\rho(s)$ is the wire radius, \vec{s} and \vec{s}' are unit tangent vectors to wire axis contour S at position $s = s(\vec{r}) \in S + \rho$ and $s' = s'(\vec{r}') \in S$ respectively, $\vec{R} = \vec{r} - \vec{r}'$, $R = |\vec{R}|$, c is the velocity of light in vacuum, $\tau=t-R/c$ is the retarded time, Z is the resistive load (in Ohms/m), μ_0 is the vacuum permeability, Q is the charge distribution that can be expressed in terms of current using the equation of continuity

$$(2) \quad Q(s,t) = - \int_0^t \frac{\partial}{\partial s} I(s,\xi) d\xi.$$

In addition to (1), (2) the initial-value conditions we used

$$(3) \quad I(s,0) = \frac{\partial}{\partial t} I(s,t)|_{t=0} = Q(s,0) = \frac{\partial}{\partial t} Q(s,t)|_{t=0} = 0, \quad s \in S.$$

We shall now define the numerical scheme to resolve problem (1) - (3).

Let us introduce the time gridpoints by $t_m = (m-1/2)\delta$, $m=0,1,\dots,M+1$, where $\delta=T_{\max}/M$. We assume that geometry of structure can be modeled using straight wires. Then the structural geometry for S is described in terms of location of first and second wire nodes at each wire making up the structure. Let us assume that K is the number of straight wires and that k -th wire, $1 \leq k \leq K$ is strings from node $u_{k,1}$ to node $u_{k,2}$ and local wire coordinate s such that $0 \leq s \leq L_k$, where L_k is the length of k -th wire. Let us introduce the wire (spatial) mesh through division of a wire into segments of identical length with centers

$$s_n = (i-1/2)h_k, \quad i=1,2,\dots,N_k, \quad (i \text{ - local wire index});$$

$$n=n_{k,1}+i-1, n_{1,I}=1, n_{k,I}=1+\sum_{l=1}^{k-1} N_l, \quad 1 < k \leq K;$$

(n - global structure index); $h_k=L_k/N_k$, $k=1,2,\dots,K$.
In result we get wire structure in N segments form

$$(4) \quad S = \bigcup_{n=1}^N S_n, \quad N = \sum_{k=1}^K N_k.$$

For each segment S_n , $1 \leq n \leq N$ we denote by $J_{n,1}$ and $J_{n,2}$ the set of segments connected to the first and to the second end of segment respectively and connection coefficients such that:

$$\text{if } S_p \in J_{n,1}, \text{ then } \sigma_{np} = \begin{cases} 1, & \text{if } S_n \in J_{p,2}, \\ -1, & \text{if } S_n \in J_{p,1}; \end{cases}$$

$$\text{if } S_p \in J_{n,2}, \text{ then } \sigma_{np} = \begin{cases} 1, & \text{if } S_n \in J_{p,1}, \\ -1, & \text{if } S_n \in J_{p,2}. \end{cases}$$

Observe that $\sigma_{np}=\sigma_{pn}$.

Let us introduce the current on structure (4) at $0 \leq t \leq T_{\max}$.

$$(5) \quad I(s, t) = \sum_{n=1}^N \sum_{m=0}^{M+1} I_{n,m} V_n(s) B_m(t),$$

$$I_{n,0} = I_{n,1} = 0, \quad n=1,2,\dots,N;$$

$$B_m(t) = \frac{2}{3\delta^2} \begin{cases} 3\delta^2/2 - 2(t-t_m)^2, & |t-t_m| \geq \delta/2, \\ (3\delta/2 - |t-t_m|)^2, & \delta/2 \leq |t-t_m| \leq 3\delta/2, \\ 0, & |t-t_m| \geq 3\delta/2; \end{cases}$$

$$V_n(s) = \gamma_n \begin{cases} \sigma_{np} \frac{\mu_{n,I}}{\Delta_p} (s - s_p + \sigma_{np} \Delta_p / 2)^2, & s \in S_p \in J_{n,1}, \\ -\frac{1}{\Delta_n} (\mu_{n,I} + \mu_{n,2}) [(s - s_n)^2 + \Delta_n^2 / 4] + \\ + (\mu_{n,I} - \mu_{n,2})(s - s_n) + 1, & s \in S_n, \\ \sigma_{np} \frac{\mu_{n,2}}{\Delta_p} (s - s_p - \sigma_{np} \Delta_p / 2)^2, & s \in S_p \in J_{n,2}, \\ 0, & s \in S_p \notin D_n = J_{n,1} \cup S_n \cup J_{n,2}, \end{cases}$$

$$\mu_{n,I} = 1 / (\Delta_n + \sum_{S_p \in J_{n,I}} \Delta_p), \quad I=1,2,$$

$$\gamma_n = 4 / [4 - \Delta_n (\mu_{n,I} + \mu_{n,2})], \quad n=1,2,\dots,N.$$

Charge at $|t-t_m| \leq \delta/2$, $m=1,2,\dots,M$ we determine in a form:

(6)

$$Q(s, t) = Q(s, t_m - \delta/2) - \sum_{n=1}^N \sum_{l=-1}^I I_{n,m+l} \frac{d}{ds} V_n(s) \bar{B}_{m,l}(t),$$

were

$$\bar{B}_{m,l}(t) = \int_{t_m-\delta/2}^t B_{m+l}(\xi) d\xi, \quad l=-1,0,1;$$

$$Q_{n,l} = 0, \quad Q_{n,m} = Q_{n,m-1} - \frac{2}{9} \delta (I_{n,m} + 4I_{n,m-1} + I_{n,m-2}), \\ n=1,2,\dots,N; m=2,3,\dots,M.$$

Functions $B_m(t)$ and $V_n(s)$ are the well-known polynomial B -splines of order two. Note that $V_n(s)$ has a specific form near the wire ends (junctions) only. Charge distribution (6) is the polynomial spline function of order one on spatial and order three on time.

Current (5) and charge (6) have the following properties:

- 1). Current, charge and their temporal and spatial derivatives included in (1)-(3), are continuous at $0 \leq t \leq T_{\max}$ on each wire i.e. at $0 \leq s \leq L_k$, $k=1,2,\dots,K$;
- 2). In wire junctions at $0 \leq t \leq T_{\max}$ Kirchoff's law for a current is satisfied and charge is continuous;
- 3). Equation of continuity (2) and initial conditions (3) are satisfied.

Hence, the current and charge approximations (5), (6) correspond to a physical nature of a current and charge and are coordinated on a level of continuity with a mathematical formulation (1)-(3).

The delta-functions used as weighting functions are situated at the centers of the space segments $s=s_n$ and at the temporal gridpoints $t=t_m$ for MoM formulation in a point-matching form. These weighting functions and current and charge approximations (5), (6) allows us to transform the integral equation (1) into the linear system of equations. In operator notation

$$A \bar{I}_m = F(\bar{I}_{m-i}; \bar{Q}_{m-i}; 1 \leq i \leq m-1) + \bar{E}_{\tan}^0(t_m), \\ m=2,3,\dots,M,$$

where $\bar{I}_j, \bar{Q}_j \in R^N$ are vectors of current and charge spline-coefficients, $\bar{E}_{\tan}^0(t_m) \in R^N$ is the vector of tangential incident field at time $t=t_m$.

The matrix A is a matrix of interaction, whose elements are time independent. They depend only on the geometry and on the resistive loading of the structure. This $N \times N$ matrix has a large number zero elements (sparse matrix). This factor is very important for solving the linear system of equation by the direct or iterative techniques.

Finally we get the time-stepping procedure to determine induced currents. The induced currents are then used to find the time-depended radiated or scattering fields.

Spline TD MoM method is realised in computer program WIRES [3]. This code allows to compute current and charge distribution, radiated or scattered transient fields, frequency characteristics and etc. for an arbitrary thin-wire structure which has been excited with a specified time-varying field.

3. TW FORMULATION

The transient electromagnetic field produced by traveling wave of current on linear wires is considered

in number of work [4,5]. However, we shall fulfill all calculations, anew to receive more simple and physically evident formulas, in additions we shall use a usual method of potentials.

We shall find an electromagnetic field of a piece of a linear filament with traveling along an axis z wave of a current. The vector of volume density of a current is determined by following expression

$$\vec{j}(x, y, z, t) = \begin{cases} \bar{z}_0 I(ct - z)\delta(x)\delta(y), & 0 \leq z \leq L; \\ 0, & z < 0, z > L; \end{cases}$$

where \bar{z}_0 - unite vector along an axis z ; $I(ct-z)$ - traveling wave of a linear current; $I(x)$ - arbitrary continuous function, $I(x \leq 0) = 0$.

Linear density of charge along a filament includes end dot charges:

$$Q(z, t) = - \int_0^t \frac{\partial I(ct - z)}{\partial z} dt = \\ = \begin{cases} \frac{1}{c} I(ct - z) - q(ct)\delta(z) + q(ct - L)\delta(z - L), & 0 \leq z \leq L; \\ 0 & z < 0, z > L; \end{cases}$$

$$\text{where } q(ct) = \frac{I}{c} \int_0^{ct} I(x) dx.$$

We shall find electrical and magnetic fields with the help of traditional potentials, but we shall separate terms from a traveling wave and dot charges.

$$\vec{E} = \vec{E}_{tw} + \vec{E}_q, \quad \vec{E}_{tw} = -\frac{\partial \vec{A}}{\partial t} - \text{grad} \varphi_{tw}, \quad \vec{E}_q = -\text{grad} \varphi_q,$$

$$\vec{H} = \frac{I}{\mu_0} \text{rot} \vec{A},$$

$$\vec{A} = \frac{\mu_0}{4\pi} \bar{z}_0 \int_0^L \frac{I(ct - s - r)}{r} ds,$$

$$\varphi_{tw} = \frac{1}{4\pi\epsilon_0} \frac{1}{c} \int_0^L \frac{I(ct - s - r)}{r} ds,$$

$$\varphi_q = \frac{I}{4\pi\epsilon_0} \frac{1}{c} \int_0^L \left[-q(ct - r)\delta(s) + q(ct - L - r)\delta(s - L) \right] ds,$$

where $r = r(s) = \sqrt{x^2 + y^2 + (z - s)^2}$ - distance between a point of observation and point of integration.

By carrying out operation of differentiation and integration there, where it is possible, we shall receive

$$\vec{E}_q = \frac{-I}{4\pi} \sqrt{\frac{\mu_0}{\epsilon_0}} \left[\left(\frac{I(ct - r_0)}{r_0} + \frac{cq(ct - r_0)}{r_0^2} \right) \frac{\bar{r}_0}{r_0} - \left(\frac{I(ct - L - r_L)}{r_L} + \frac{cq(ct - L - r_L)}{r_L^2} \right) \frac{\bar{r}_L}{r_L} \right],$$

$$\vec{H} = \frac{I}{\mu_0} \text{rot}(\bar{z}_0 A) = \frac{I}{\mu_0} [\text{grad} A \times \bar{z}_0] = \\ = \frac{I}{\sqrt{\mu_0/\epsilon_0}} [\text{grad} \varphi_{tw} \times \bar{z}_0] = \frac{I}{\sqrt{\mu_0/\epsilon_0}} [\bar{z}_0 \times \vec{E}_{tw}],$$

where \vec{r} , $\vec{r}_0 = \vec{r}(s=0)$, $\vec{r}_L = \vec{r}(s=L)$ - vectors of distances, drawn accordingly from a points of integration, beginning and end of a segment in a point of observation.

Expression for \vec{E}_{tw} we shall transform as follows.

We shall present \vec{r} as $\vec{r} = \rho \vec{p}_0 + (z - \bar{s}) \bar{z}_0$, where $\rho = \sqrt{x^2 + y^2}$ and \vec{p}_0 - an unite radial vector in cylindrical system of coordinates. For each of two components of a vector

$$\vec{E}_{tw} = (\vec{E}_{tw}, \vec{p}_0) \vec{p}_0 + (\vec{E}_{tw}, \bar{z}_0) \bar{z}_0$$

we shall carry out change variable $u = s + r = s + \sqrt{\rho^2 + (z - s)^2}$ and shall integrate in parts terms, containing derivative of a current, thus the integral members will be reduced. In result we shall receive:

$$\vec{E}_{tw} = \frac{1}{4\pi} \sqrt{\frac{\mu_0}{\epsilon_0}} \left[\frac{I(ct - r_0)}{r_0} \left[\frac{\rho \vec{p}_0}{r_0 - z} - \bar{z}_0 \right] - \frac{I(ct - L - r_L)}{r_L} \left[\frac{\rho \vec{p}_0}{r_L - (z - L)} - \bar{z}_0 \right] \right].$$

The expression for $\vec{E} = \vec{E}_{tw} + \vec{E}_q$ is transformed to known one of [4] and [5], if to take into account, that

$$\frac{\rho \vec{p}_0}{r - (z - s)} - \bar{z}_0 = \frac{\vec{r} - r \bar{z}_0}{r - (z - s)} = \frac{\vec{r}}{r} + \frac{z \vec{r} - r^2 \bar{z}_0}{r(r - (z - s))}.$$

The derived formulas are realised in the program module TWW, which can be used as in structure of other programs and separately.

It allows to calculate a transient electromagnetic field of wire structure with given traveling waves of currents.

For structures as the wire plate simulator the determination of cross distribution of currents in TWW is made otherwise than in [5], and is not prescribed but calculated. We assume, that in the region of excitation wires of the simulator have the conic form and converge to the dot voltage generator. A position and the cross sizes wires are set. The distribution of charges and currents in spherical TEM wave is found from the decision of an electrostatic problem for an equivalent cylindrical line. Such method allows more precisely to take into account peculiarities of wire structure of the simulator.

The impulses of fields, calculated with the help TWW are only the first estimation. However the initial part of impulses of fields, which determines front and amplitude and which is formed by a section of a uniform conic line, is calculated quite correctly and coincides with MoM solution.

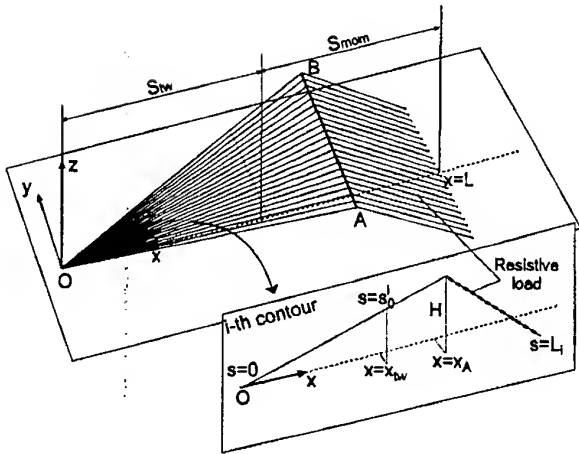


Fig. 1. Structural geometry of the simulator

Testing the program TWW by data from [5] has shown complete concurrence of results.

4. HYBRID FORMULATION

Hybrid method combine the TDIE with TW-approach. The wire structure is divided in two part. First TW-part include generator and regular part of structure. All irregularities (curved wires, wire junctions, resistive load and other) are on second or MoM-part of structure. Currents on the TW-part are approximated by a sum of the primary (propagating from the generator) and reflected traveling waves.

We shall formulate a method for structures as the wire plate EMP simulator, shown on fig. 1. The simulator is composed of two flat-plate transmission-line sections which are approximated by N_s longitudinal thin wire contours and located on perfectly conducting ground plane. Each wire contour is excited at point O. Resistive load is distributed on a second flat-plate.

On an example of this structure a principle of division on TW and MoM part is well illustrated. From physical reasons follows, that TW approach well corresponds to a first conical-plate of structure S_{tw} , fig. 1. The current on a second part S_{mom} in general can be determinated by MoM only.

We shall now define the formal description of a hybrid method using section 2 designation. Let the structure S is divided into two adjoining parts

$$S = S_{tw} \cup S_{mom}, S_{tw} \cap S_{mom} = \{s_0^i, i = 1, 2, \dots, N_s\}.$$

If s is a local coordinate of i -th contour, then part $0 \leq s \leq s_0^i$ belongs S_{tw} and other part $s_0^i \leq s \leq L_i$ belongs S_{mom} . Current at S_{tw} we determine in a form

$$(7) \quad \begin{aligned} J(s, t) &= a_i f(t - s/c) + \\ &+ I(s_0^i, t + (s - s_0^i)/c - a_i f(t + (s - 2s_0^i)/c)) \\ &0 \leq s \leq s_0^i, i = 1, 2, \dots, N_s \end{aligned}$$

where $f(\tau)$ is the known function, $a_i, i = 1, 2, \dots, N_s$ are the amplitudes, which get out according to static

charge distribution at region of source-point O (see section 3). The current at S_{mom} is the spline (5). Hence, $J(s, t)$ is the sum of a primary and reflected wave. The form of a reflected wave is defined through the spline-current on S_{mom} . Using above results (section 3) and by substituting (7) in (1) we get the integral equation (1), which stands on S_{mom} only. In this equation

$$\tilde{E}^0(s, t) = \tilde{E}_{tw}(s, t) - \tilde{E}_{tw}^*(s, t),$$

where

$$\begin{aligned} \tilde{E}_{tw}(s, t) &= \frac{1}{4\pi} \sqrt{\frac{\mu_0}{\epsilon_0}} \left\{ f(ct - r_0) \sum_{i=1}^{N_s} a_i \frac{\bar{r}_0 / r_0 - \bar{s}_i^i}{r_0 - \bar{r}_0 \bar{s}_i^i} - \sum_{i=1}^{N_s} [a_i f(ct - \eta_{i,i}) \times \right. \\ &\times \left. \frac{\bar{r}_{i,i} / r_{i,i} - \bar{s}_i^i}{r_{i,i} - \bar{r}_{i,i} \bar{s}_i^i} + (I(s_0^i, t - \eta_{i,i}/c) - a_i f(ct - \eta_{i,i})) \frac{\bar{r}_{i,i} / r_{i,i} + \bar{s}_i^i}{r_{i,i} + \bar{r}_{i,i} \bar{s}_i^i}] \right\}, \end{aligned}$$

where $\bar{r}_0 = \bar{r}_0(s, 0)$, $\bar{r}_{i,i} = \bar{r}_{i,i}(s, s_0^i)$, $i = 1, 2, \dots, N_s$ are vectors of distances up to a source and up to points of continuity s_0^i , \tilde{E}_{tw}^* is a similar expressions for a field of image of structure.

A condition of current continuity at $s = s_0^i$ we used has the form

$$(8) \quad \begin{aligned} \left[\frac{\partial}{\partial s} - \frac{1}{c} \frac{\partial}{\partial t} \right] (I(s, t) - f(t - s/c)) &= \\ = \left(\frac{\partial I}{\partial s} - \frac{1}{c} \frac{\partial I}{\partial t} + \frac{2}{c} f'(t - s/c) \right) \Big|_{s=s_0^i+0} &= 0 \end{aligned}$$

Using representation of a current (5), we get

$$\left(\frac{\partial I}{\partial s} - \frac{1}{c} \frac{\partial I}{\partial t} \right) \Big|_{\substack{s=s_0^i \\ t=t_m-\delta/2}} = \frac{1}{\Delta_i} (I_{1,m-1} - I_{0,m}),$$

where δ is the temporal grid step, Δ_i is the spatial grid step at i -th wire. Then the condition (8) will be transformed to

$$I_{0,m} = I_{1,m-1} + \frac{2\Delta_i}{c} f'(t_m - s_0^i/c).$$

Is thus determined all, that it is necessary for the solution of a problem (1)-(3) on a S_{mom} .

It is known, that the MoM in cases, when it to be applied, gives good results with high accuracy. In principle, goal of a hybrid method is a good approximation of the solution, received by a MoM. The initial part of a fields in the working area of the simulator is defined by TW-current on S_{tw} and is calculated analytically quite correct. The basic source of an error of a hybrid approach is form reflected wave. In general, this error grows with grown of a share, which makes a S_{tw} from S . Therefore at application of a hybrid method it is important to lead correct division of the structure.

5. RESULTS

In this section we present same results obtained by hybrid approach.

Structure studied was a simulator (fig. 1) of length $L=90$ m, height $H=15$ m, width $AB=20$ m, number of

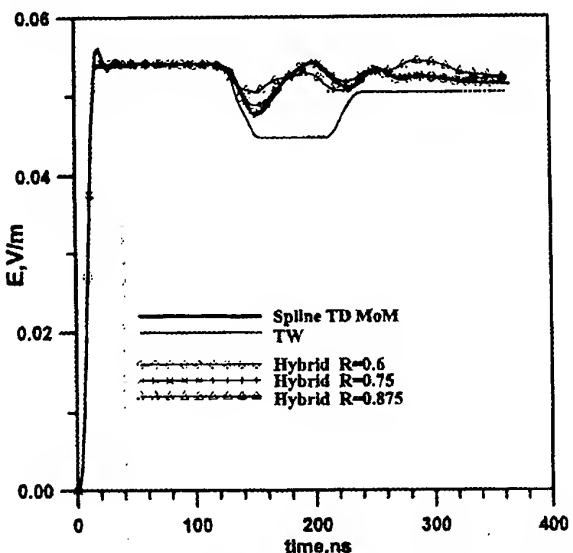


Fig. 2. Vertical electric-field pulse in working region : $x=65$ m, $y=0$ m, $z=0$ m.

longitudinal wires $N_s=6$. The simulator was mounted on a perfectly conducting plane and fed at point O by a source voltage of a form $V(t)=\exp(-\alpha t)$, $\alpha=2.7 \cdot 10^8$ 1/s.

On a fig.2 calculated vertical electrical-field pulses in the working region $x=65$ m, $y=0$, $z=0$ are shown. The pulses are calculated by various method: spline MoM for all structure, TW for all structure, hybrid method with various division on TW and MoM parts i.e. with various $R=x_{tw}/x_A$.

From these data follows that a hybrid method provide accuracy similar to one the MoM for all structure if $R<0.7$. The number of unknowns at the solving of the integral equation decreases about 40% and computer CPU time decreases more than twice.

REFERENCES

1. E.K. Miller, A.J. Poggio and G.J. Burke, "An integro-differential equation technique for time-

domain analysis of thin wire structures", J. Comput. Phys., Vol 12, No. 24, 1973, p. 48.

2. R.G. Martin, A. Salinas and A. Rubio Bretones, "Time-domain integral equation method for transient analysis", IEEE Antennas Propagat. Mag., Vol. 34, No. 3, 1992, pp. 15-23.

3. V.M. Lugovtsov, "Spline-collocation technique for numerical analysis of time-domain electromagnetic response from thin-wire structures" (Russian), J. Radiotekhnika I Electronika, Vol. 38, No. 38, 1993, pp. 1559-1569.

4. S.A. Podosenov, Y.G. Svekis, A.A. Sokolov, "Transient radiation of traveling waves by wire antennas", IEEE Trans. Electromagn. Compat., Vol 37, No. 1, 1995, pp. 367-383.

5. J.J.A. Klaasen, "An efficient method for the performance analysis of bounded-wave nuclear EMP simulator", IEEE Trans. Electromagn. Compat., Vol. 35, No. 3, 1993, pp. 329-338.

BIOGRAPHICAL NOTES

Vladislav P.Lisitsyn was born in 1940 in Kostroma, Russia. In 1963 he graduated from Moscow Aviation Institute, Radio Engineering Facility. He received the Ph. D. degree from Moscow Energy Institute in 1978. Presently he is working in the field of non-stationary electrodynamics.

Viacheslav M. Lugovtsov. In 1983 he graduated from Moscow State University Computational Mathematics and Cybernetics Faculty. His research deals mainly with numerical method for transient electromagnetic scattering and propagation , applied mathematics and computer modeling.

STUDY OF SCINTILLATION AND SIMULTANEOUS RAIN ATTENUATION WITH ITALSAT EXPERIMENT AT WROCŁAW

Emilio MATRICCIANI¹, Carlo RIVA², Jacek SKRZYP CZYŃSKI³

1 Dipartimento di Elettronica e Informazione – CSTS/CNR
Politecnico di Milano - Piazza L. da Vinci 32, 20133 Milano (Italy)
Tel.: +39-2-2399.3639 - Fax: +39-2-2399.3413 - E-mail: matricci@elet.polimi.it

2 Dipartimento di Elettronica e Informazione – CSTS/CNR
Politecnico di Milano - Piazza L. da Vinci 32, 20133 Milano (Italy)
Tel.: +39-2-2399.3611 - Fax: +39-2-2399.3413 - E-mail: riva@elet.polimi.it

3 Institute of Telecommunications and Acoustics, Wrocław University of Technology
Wybrzeże Wyspianskiego 27, 50-370 Wrocław (Poland)
Tel.: +48-71-320.3074 - Fax: +48-71-22.3473 - E-mail: jacek@zr.ita.pwr.wroc.pl

Abstract. In satellite communications at carrier frequencies above 10 GHz, scintillation when superposed to rain attenuation may play a significant role in determining the power margin, especially for low availability systems with low elevation angle and low gain antennas. The assessment of the linkage between rain attenuation and scintillation during rain are then necessary to better use a given system capacity. Matricciani et al. found that the statistical relationship between 1-s averaged rain attenuation (A , in decibels) and standard deviation (σ , in decibels) of simultaneous tropospheric scintillation in 1-s intervals can be fitted by the power law $\sigma = CA^{5/12}$ derivable from a turbulent-thin layer model. This relationship has been validated by using high-resolution (50 samples/s) experimental 12.5 and 19.77 GHz attenuation time series recorded at Spino d'Adda (45.4°N) in a 30.6° slant path to satellite Olympus during an observation time of approximately 1 year. In this contribution we describe the analysis procedure we intend to apply to the time series which will be recorded in Wrocław with Italsat experiment in 1998 and 1999 to validate the turbulent-thin layer model in the case of smaller gain antenna in a new climate region.

I. INTRODUCTION

The propagation studies concerning satellite communications have been recently more and more deeply involved in the scintillation characterisation. Using frequencies above 20/30 GHz and low elevation

angle for earth-to-space link, especially in low-availability systems, it becomes mandatory to consider the influence of the tropospheric turbulence, to correctly determine the margin in the system's link budget.

So far, the exact correlation between rain and scintillation is not clearly assessed in the literature. Filip and Vilar [1] assume that rain attenuation and scintillation are statistically independent. Karasawa and Matsudo [2] conclude that the two phenomena might be treated independently, though they find a weak dependence. On the contrary, Matricciani et al. [3, 4] prove theoretically, and verify experimentally, that the two phenomena are statistically linked at a carrier frequencies (12.5 and 19.77 GHz) for which scattering due to hydrometeors is not yet comparable to turbulence scintillation [5]. They theoretically derived the following statistical relationship between rain attenuation, A (dB), averaged over 1 second, and the standard deviation of simultaneous tropospheric scintillation, σ (dB), calculated for 1 s intervals by using 50 samples:

$$\sigma = CA^{5/12} \quad (1)$$

The constant C has been determined using 1 sample/s time-series of simultaneous scintillation standard deviation and rain attenuation recorded at Spino d'Adda (45.4°N), with a 3.5 m diameter antenna, in a 30.6° slant path to satellite Olympus, during an observation time of approximately 1 year, and has been found equal to 0.068 at 12.5 GHz and to 0.039 at 19.77 GHz.

The model of equation (1) (*turbulent-thin layer model*) still needs a validation in experimental conditions where scintillation effects are more important, such as for

smaller gain antennas. To this purpose, the ItalSat propagation experiment which will be carried out in Wroclaw (Poland) using an earth-terminal of 1.2 m diameter and at an elevation angle of 31.4° (practically equal 30.6° to satellite Olympus at Spino d'Adda) is very significant. It is also interesting to verify the model in a new climate region.

In Section 2 we describe the analysis procedure which will be used (after Matricciani et al. [3, 4]) to further validate the turbulent-thin layer model experimentally, by means of the ItalSat attenuation time series to be recorded at Wroclaw. In Section 3 we outline the experimental set-up of the ItalSat propagation experiment at Wroclaw, while in Section 4 we will present a schedule of the experiment. In Section 5 some conclusions are drawn.

2. DATA PROCESSING

To distinguish between rain attenuation (i.e. signal amplitude variation caused by absorption and scattering by hydrometeors) and scintillation (i.e. signal amplitude variation caused by tropospheric turbulence), we must separate the two effects as much as possible by filtering the experimental time series. To this purpose a spectral analysis is needed. With the power spectra of attenuation time series it is possible to assess the frequency range in which there is a change in the nature of the physical phenomenon causing amplitude fluctuations. As rain attenuation has most of its power at the lowest frequencies and in this range this power is much larger than that of scintillation, 1 sample/s time series, i.e. the conventional rain attenuation time series usually recorded, is sufficient for the spectral study. The average power spectra of several events is given by the following equation

$$\bar{S}(f) = 10^{\frac{1}{N} \sum_{i=1}^N \log_{10} S_i(f)} \quad (2)$$

which maintains constant the logarithmic slopes and thus allows to compare the experimental results with theory (equation also used in [3]). An example of average power spectrum of attenuation time series at 12.5 GHz is shown in Figure 1. Notice that the theoretical -20 dB/decade slope due to rain [6] is valid up to about 0.02 or 0.03 Hz, beyond which other effects are prevalent, as confirmed by the change in spectrum slope.

Figure 2 shows an example of power spectrum of a single event, in which turbulence with a spectrum slope of $-80/3$ dB/dec (i.e., $f^{-8/3}$ in natural units, [2, 7]) is evident.

It is then possible to estimate bulk rain attenuation time series, referred to as "rain attenuation", from the original time series by a low-pass filter with a cut-off frequency equal to the spectral component separating

the rain and turbulence effects (0.025 Hz in the case of Figure 1).

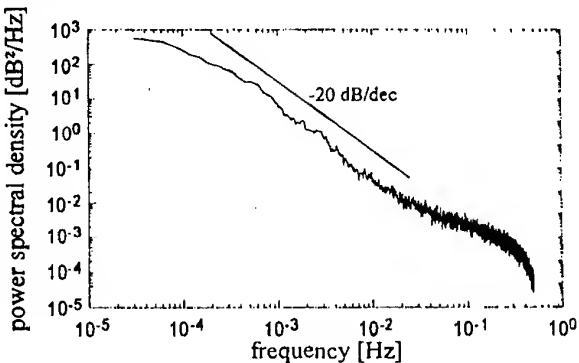


Figure 1. Average power spectral density of 31 events (original data averaged over 1 second; satellite: Olympus; frequency: 12.5 GHz; antenna diameter 3.5 m; slant path elevation: 30.6°); total time is 92.18 hours [4].

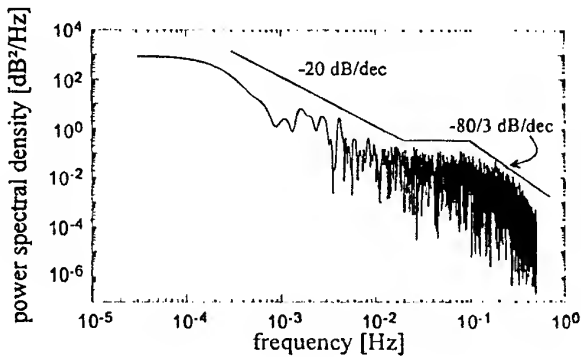


Figure 2. Power spectral density of attenuation (original data averaged over 1 second; satellite: Olympus; frequency: 12.5 GHz; antenna diameter 3.5 m; slant path elevation: 30.6°) for one event; date 21 September 1992 [4].

To complement the previous analysis and to obtain scintillation time series, the original time series must be filtered by high-pass filter with cut-off frequency equal to that of low-pass filter used for rain attenuation. Intervals of scintillation stationarity should then be identified by visual inspection, for each interval, of the probability distribution of the amplitude, to assess that it is well modeled by the Gaussian probability distribution with zero mean, as predicted by the theory and experiments [7-9]. Finally with the average power spectrum of scintillation, calculated according to equation (2), the possible high frequency components due to receiver noise can be filtered out. In Figure 3 an example of average spectrum of 50 samples/s high-pass filtered time series is shown. We notice that the receiver carrier-to-noise ratio permits observation of frequency components up to about 3 Hz, beyond which the

receiver (white) noise appears. We also notice decay very close to the theoretical $f^{-8/3}$ above 0.03 Hz while the smoother decay below 0.03 Hz is likely due to changes in the scintillation spectrum from one event to another [3].

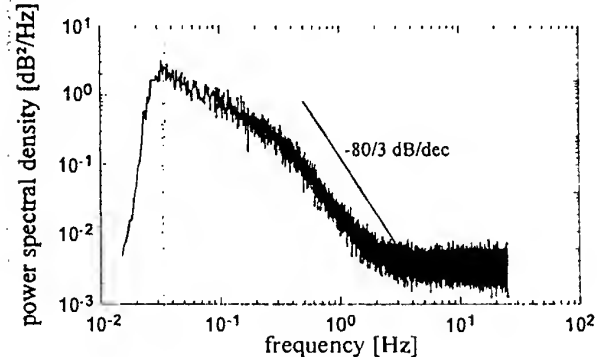


Figure 3. Average power spectral density of scintillation for the 71 intervals of stationarity. Original time series at 50 samples/s high-pass filtered with cut-off frequency 0.025 Hz; satellite: Olympus; frequency: 12.5 GHz; antenna diameter 3.5 m; slant path elevation: 30.6° [4].

In the end we can produce two concurrent time series, one for "rain attenuation" only, and one for "scintillation" standard deviation only, the latter obtained by the band-pass time series. At this step, it is then possible to verify the relationship of equation (1) also for the Wroclaw data.

3. EXPERIMENTAL SET-UP AT WROCLAW

Wroclaw measurement system is prepared for reception of the ITALSAT F2 beacon transmitted with linear vertical polarisation at frequency of 18.6 GHz.

The main functions of the system are:

- evaluation of the attenuation and scintillation relative to the changes of the beacon signal level due to atmospheric phenomena
- measurement of the actual rainfall intensity.

The system can be divided into the following subsystems:

- receiving subsystem
- rain rate measuring subsystem
- gain calibration subsystem
- data processing subsystem.

The receiving subsystem consists of:

- 1.2 m dual reflector antenna
- 18.6 GHz low noise front end (LNA)
- down converter
- beacon detector
- personal computer (PC)

The beacon detector provides PC with received signal level in digital format. The data are acquired and stored continuously on hard disc of PC.

The rain rate measuring subsystem consists of:

- two rain gauges (tipping bucket type)
- PC.

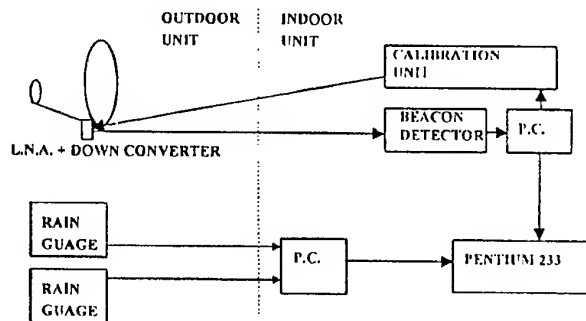


Figure 4. The measuring system layout.

The rain gauges are placed in the vicinity of receiving antenna. Two rain gauges are used to ensure unfailing work of the system. The rain gauges are of tipping bucket type with a collecting area of 1000 sqcm and a rain height of 0.03 mm for each tip. The numbers of tips are stored every minute by dedicated PC system equipped with hard disk. The data are stored in a special, memory saving, format.

Gain calibration subsystem is used to evaluate the correction of receive chain gain with respect to the nominal gain value. During the calibration phase the reference level signal is injected at the LNA input and then correction factor is established.

Both PCs work independently and are connected by local network with Pentium 233 computer used for the data processing functions, error correction and statistical analysis.

4. PROPAGATION EXPERIMENT AT WROCLAW

The first stage of propagation experiment in Wroclaw is planned to start in March of 1998. The rain rate measuring subsystem will be set up on the roof of WUT C-5 building. The beacon receiving subsystem is to start working in June 1998. The other significant physical parameters necessary for modelling, such as local temperature and humidity will be taken from meteo station of Meteorological Institute located 2 km East to C-5 building.

The data will be processed, as they are collected. Then propagation database with statistics of main propagation parameters will be created. The software for generation, keeping and using the database is the one developed at ESA-ESTEC for the Olympus Propagation Experiment. The main results of propagation experiment at Wroclaw will be a cumulative distribution of rain intensity and total attenuation of the Italsat beacon for the period of measurements. A detailed study of slant path scintillation will be also performed by analysing the

experimental data to determine statistics for fading and enhancement of the satellite signals.

5. CONCLUSION

The main purpose of 20 GHz telemetry beacon of ITASAT F2 is to relay to ground telemetry data and spacecraft tracking by earth stations. But thanks to its high EIRP and coverage of large part of Europe ITASAT F2 satellite offers possibility of characterisation of satellite radio channel by attenuation and scintillation measurements. The data collected in as many as possible locations are fundaments for working out universal designing tools necessary for the future advanced satellite systems.

Wroclaw measurement campaign will contribute to the improvement of the existing model in the following area

- the separation of rain attenuation and scintillation
- the turbulent-thin layer model validation
- the evaluation of statistics of rain attenuation and scintillation for various sites
- the prediction of rain attenuation and scintillation from ground meteorological measurements.

6. REFERENCES

- [1] M. Filip and E. Vilar: Optimum utilization of the channel capacity of a satellite link in the presence of amplitude scintillations and rain attenuation, *IEEE Transactions on Communication*, Vol. 38, pp. 1958-1965, 1990.
- [2] Y. Karasawa and T. Matsudo: Characteristics of fading on low-elevation angle earth-space paths with concurrent rain attenuation and scintillation, *IEEE Transactions on Antennas and Propagation*, Vol. 39, pp. 657-661, 1991.
- [3] E. Matricciani, M. Mauri and C. Riva: Relationship between scintillation and rain attenuation at 19.77 GHz, *Radio Science*, Vol. 31, pp. 273-279, 1996.
- [4] E. Matricciani, M. Mauri and C. Riva: Scintillation and simultaneous rain attenuation at 12.5 GHZ to satellite Olympus, *Radio Science*, Vol. 32, pp. 1861-1866, 1997.
- [5] J. Haddon and E. Vilar: Scattering induced microwave scintillations from clear air and rain on earth space paths and the influence of antenna aperture, *IEEE Transactions on Antennas and Propagation*, Vol. 34, pp. 646-657, 1986.
- [6] E. Matricciani: Physical-mathematical model of the dynamics of rain attenuation with application to power spectrum, *Electronics Letters*, Vol. 30, pp. 522-524, 1994.
- [7] V.I. Tatarski: 'Wave propagation in a turbulent medium', McGraw-Hill, New York, USA, 1961.
- [8] G. Ortgies G.: Probability Density Function of Amplitude Scintillations, *Electronics Letters*, Vol. 21, pp. 141-142, 1985.
- [9] O.P. Banjo and E. Vilar: Measurement and Modelling of Amplitude Scintillations on Low-Elevation Earth-Space Paths and Impact on Communication Systems, *IEEE Transactions on Communications*, Vol. 34, pp. 774-780, 1986.

PROPAGATION CONDITIONS IN THE VHF AND UHF BANDS IN THE COASTAL REGION OF POLAND

Wiktor Pawłowski

Technical University of Gdańsk, PL-80-952 Gdańsk, Poland

The subject of this paper are the results of investigations of the influence of the synoptic situation on propagation conditions of VHF and UHF radio waves in the south of the Baltic Sea and the coastal region of Poland. The obtained results show that the influence of the so called character of atmospheric circulation on the field strength is substantial to a high degree. Also the air mass affect essential the propagation conditions of the above mentioned radiowaves, especially in summer.

1. INTRODUCTION

The atmospheric refraction is one of the phenomena in the troposphere which affect the propagation conditions of VHF and UHF radio waves. The atmospheric refraction depends essentially on the climate of a given region. That is why regional properties of atmospheric refraction are still investigated [1], [2]. Results of studies in that field are of great importance for fulfilling of EMC conditions in radiocommunication systems.

A comprehensive study of the radio climate of the coastal region of Poland has been carried out at the Technical University of Gdańsk during last years [3]. The attention was fixed on such problems related to atmospheric refraction as the following subjects:

- regional reference atmospheres [4],
- radiometeorological parameters,
- the gradient of the radio refractive index in a near the ground layer of the troposphere, and
- the influence of the radio refractivity on coverage in the coastal zone of Poland.

It follows from the obtained results that the radio climate within the coastal region of Poland differs from the average ITU-R data [5]. So one should use regional data originating from the area of interest when analysing radio systems in the VHF and UHF bands.

In the above mentioned study propagation conditions of radio waves in the VHF and UHF

bands were investigated, too. The subject of interest was the influence of the synoptic situation on the distributions of the field strength. The aim of this paper is to present some results obtained in that study elaborated from that point of view.

2. THE RESEARCH METHOD

In the study records of the field strength of radio broadcasting stations operating in the 100 MHz band in the region of the south of the Baltic Sea were analysed. The presented below results were obtained on a 320 km over horizon path (in majority a sea path) Emmaboda - Gdańsk at the frequency of 96,7 MHz, shown in Fig.1. The profile of the propagation path is drawn in Fig.2. These measurements were carried out in the summer season because of the large variability of the atmospheric refractivity in that period. The presented results were acquired analysing an about 250 records set.

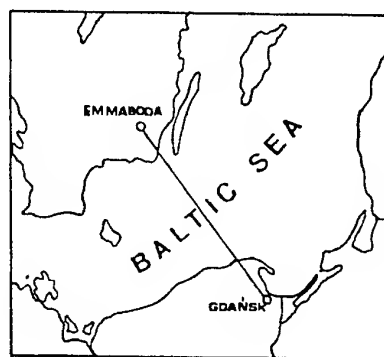


Fig.1 The region of the propagation path

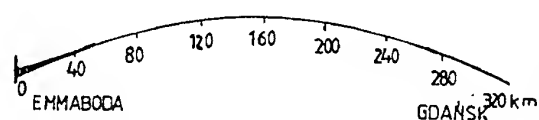


Fig.2. The profile of the propagation path

Each individual record was 30 minutes long in time. The outcome of the statistical analysis of a single record were among other statistical parameters the mean value, as well as the standard deviation of a 30-minute field strength value distribution.

The fluctuations of the field strength were examined, too. The frequency of the field strength fluctuations in a single 30-minutes record was defined as the number of passages of the field strength course through the field strength mean level of that record.

Parameters characterising the 30-minutes individual records formed the general population analysed by means of statistical methods.

The influence of the synoptic situation was studied taking into account the so called character of the atmospheric circulation and the air mass. The distributions of the field strength parameters had been investigated by means of variance analysis, taking into account the day cycle, too. It was found that the influence of the character of the atmospheric circulation on distributions of field strength parameters is particularly important.

The character of the atmospheric circulation was classified taking into account the location of the main atmospheric circulation areas, i.e. the anticyclone (high) and the cyclone (low) in relation to the propagation path. The following 3 characters of the atmospheric circulation were applied:

- AA - the region of the propagation path is covered by the centre of a anticyclone,
- A - the propagation path is under the influence of an anticyclone area and
- C - the propagation path is under the influence of a cyclone area or the propagation path is covered by the centre of a cyclone.

Situations in which a centre of a cyclone covered the region of the propagation path appeared very rarely in the analysed period. For that reason atmospheric situations with cyclone circulation were not differentiated.

2. INFLUENCE OF THE CHARACTER OF THE ATMOSPHERIC CIRCULATION

2.1 Distributions of field strength values

The influence of the character of the atmospheric circulation on the distributions of statistical parameters of the field strength records, as mentioned above, had been investigated by means of variance analysis for different hours. The obtained object mean values of the field strength means for different characters of atmospheric circulation are given in Table 1. The following

measurement hours were taken into account: 6⁰⁰, 12⁰⁰ and 18⁰⁰ UT. The mean values are given in dB and the reference level was the value of 1 μ V/m. The obtained average mean value, i.e. without differentiating the character of the atmospheric circulation, equalled 16 dB.

Table 1. Field strength means taking into account the character of the atmospheric circulation

hour	character of atmospheric circulation		
	AA	A	C
6 ⁰⁰	23	19	12
12 ⁰⁰	21	17	13
18 ⁰⁰	24	16	13

Results of variance analysis of the distributions of the means of the field strength records show that the influence of the character of the atmospheric circulation is substantial to a high degree. The comparison of calculated and tabulated F-test values testify to the mentioned above conclusion. The calculated F-test values, as well as tabulated F-test values, are presented in Table 2.

Table 2. Calculated and tabulated F-test values (distributions of field strength values)

hour	F-test values	
	calculated	tabulated (0.05)
6 ⁰⁰	18.55	3.11
12 ⁰⁰	5.80	3.11
18 ⁰⁰	7.94	3.13

The next question was: which of the examined objects differ substantial from the average conditions, i.e. when the character atmospheric circulation objects is left out of account. This question was analysed by means of the d-test. There was found that objects AA and C differ from the average conditions, at least on significance level of 0.05. Similar results were obtained when examining the differentiation of object pairs by means of the Student's t-test.

On the contrary, the carried out investigations show that the influence of the character of the atmospheric circulation on the distributions of the standard deviations of the field strength records is not essential, in the light of variance analysis. The standard deviation of 30-minutes field strength

distributions varied from 4.5 dB to 5.3 dB and average equalled 4.8 dB.

The study confirmed that there is a substantial influence of the atmospheric circulation on the propagation conditions of ultra short radio waves. The best propagation conditions, i.e. larger field strength values should be expected when in the region of the propagation path is the centre of a stable anticyclone, while small field strength values - when the propagation path is under the influence of a cyclone.

2.2. Field strength fluctuations

A significant dependence of the field strength fluctuations on the character of the atmospheric circulation is observed, too. The object mean values of the frequency of field strength fluctuations for different characters of the atmospheric circulation and different hours are shown in Table 3. The mean value of the frequency of the field strength fluctuations for average conditions, i.e. when the character of the atmospheric circulation was left out of account, equalled about 40.

Table 3 Influence of the character of the atmospheric circulation on field strength fluctuations

hour	character of atmospheric circulation		
	AA	A	C
6 ⁰⁰	13	37	83
12 ⁰⁰	15	42	70
18 ⁰⁰	11	54	76

Results of variance analysis of the distributions of the frequency of the field strength fluctuations showed that the influence of the character of the atmospheric circulation is substantial. The obtained calculated and tabulated F-test values on significance level 0.05 are presented in Table 4.

Table 4 Calculated and tabulated F-test values (distributions of field fluctuations)

hour	F-test values	
	calculated	tabulated (0.05)
6 ⁰⁰	15.53	3.11
12 ⁰⁰	5.79	3.11
18 ⁰⁰	5.20	3.13

The dispersions of the distributions of the frequency of the field strength fluctuations were greater than observed in the case of dispersions of field strength values distributions. Nevertheless, the object distributions differentiated substantial from the general population distribution, in the light of a analysis by mean of the d-test. That investigation show that the object AA, as well as the object C differ from the average distribution, i.e. when the character of the atmospheric circulation and the day time are left out of account, at least on the significance level of 0.05.

3. INFLUENCE OF THE AIR MASS

An study of the influence of the air mass on the taken into consideration parameters of the 30-minutes field strength records were carried out, too. The classification of air masses used by the Polish Meteorological service was applied:

PA_s - the old arctic air,
PPm - the polar maritime air,
PPm_s - the old polar maritime air,
PPm_c - the warm polar maritime air,
PPK - the polar continental air, and
PZm - the tropic maritime air.

In the reported research study different polar air masses were observed mostly. The sample sizes in the case of other air masses were to small to form separate objects. The object means of field strength values are given in Table 5.

Table 5 Influence of air masses on field strength means

hour	air mass		
	PPm	PPm _s	PPm _c
6 ⁰⁰	13	20	18
12 ⁰⁰	14	19	17
18 ⁰⁰	12	20	17

A significance dependence of the field strength mean values on the air mass is observed, in the light of variance analysis. That show the Table 6, which contains calculated F-test values and tabulated F-test values on the significance level of 0.05.

The air mass object distributions differ from the distribution of the general population not so distinctly as it was in the case of object distributions of the character of the atmospheric circulation. Similar results were obtained when the influence of the air mass on the frequency of field strength

fluctuations was examined. The similarity of properties of different polar air masses is the reason for smaller differentiation of air mass object distributions, than object distributions in the case of the character of the atmospheric circulation.

Table 6 Calculated and tabulated F-test values (polar air masses)

hour	F-test values	
	calculated	tabulated(0.05)
6 ⁰⁰	5.37	2.76
12 ⁰⁰	3.40	2.72
18 ⁰⁰	7.04	2.74

4. FINAL REMARKS

In the light of the obtained results, both the character of the atmospheric circulation and the air mass, can be applied for differentiation of the synoptic situation, when investigating the influence of the synoptic situation on parameters of field strength distributions.

The investigation results confirmed that the influence of the character of the atmospheric circulation on propagation conditions of VHF and UHF radio waves in the south of the Baltic Sea, substantial to a high degree. One should expect greater field strength values and smaller frequencies of field strength fluctuations when anticyclones are dominating in the region of the propagation path. On the contrary, smaller field strength values and greater field strength fluctuations will be observed when the region of the propagation path is under the influence of a cyclone.

The study will be continued. The data base will be enlarged - on one hand each individual field strength record will be characterised by a greater number of parameters, on the other hand, the file of records will be more numerous.

The aim of that work will be to explore the possibility of increase of the accuracy of prediction field strength values through taking into consideration the influence of the synoptic circulation, for example in the well known method using the recommended by the ITU-R radiometeorological parameters [6]. That may make possible better fulfilling of EMC conditions in radiocommunication systems.

5. REFERENCES

- 5.1. K.H.Craig, "Refractivity parameters and prediction modelling", Proc. of the XXIVth General Assembly of URSI Symp., Kyoto, 1993, F8-3,p.251
- 5.2. S.K.Sarkar et al., "Recent advances in the climatological studies over the Indian subcontinent", Proc.of the ICAP Third Int.Conf. on Antennas and Prop., UK, 1985, pp.248-252
- 5.3. W.Pawlowski, "Radio climate of the coastal region of Poland", Proc. of the Int. Wrocław EMC Symp. on Electromagnetic Compatibility, Wrocław, Poland, 28.06.- 01.07.,1994, pp. 53-57
- 5.4. W.Pawlowski, "Regional reference atmospheres for the north of Poland", Proc. of the XIth Int.Wrocław EMC Symp. on Electromagnetic Compatibility, Wrocław, Poland, 1992, pp. 40-44
- 5.5. CCIR, Rep.563-3, "Radiometeorological data"
- 5.6. CCIR, Rec.470-5, "VHF and UHF propagation curves for frequency range from 30 to 1000 MHz"

BIOGRAPHICAL NOTE

Wiktor Pawłowski was born 1933. He graduated at the Technical University of Gdańsk 1957 and received the Dr. Ing. degree in Electronics from the Technical University of Warsaw in 1966. Since 1957 he is with the Technical University of Gdańsk, working on radio communication with special interest in propagation of radio waves in nonionised media.

II

ANTENNA AND PROPAGATION EMC ASPECTS

Beverage-like Aerials and EMC

URSI Commission E sponsored session

Invited session organized by

Prof. H. Kikuchi - Japan

Effects of Trains on Fields of Wire and Wireless Communication in Tunnels

Jiro Chiba

Tohoku Institute of Technology

35-1 Yagiyama Kasumi-cho, Sendai 982 JAPAN

Tel +81-22-229-1151 FAX +81-22-229-2570

Effects of trains in an arched tunnel on the cutoff frequency and field were determined at the range of VHF, UHF, and SHF bands by the finite-element method (wireless communication) and the boundary element method (wire communication).

The field is represented by contour lines. Thus, its change is clearly shown by a change in the distribution of the lines caused by the train in the tunnel. In underground environments, communicability is vital in emergency cases such as fires, as well as in routine management operations. This study aims at establishing a basis for solving such problems.

1. INTRODUCTION

The effects of trains in tunnels on fields are yet to be clarified. In addition, the cross section of an actual tunnel is not of the typical rectangular or arched shape.

Trains in the tunnel complicate its cross section further. This study uses the following assumptions as the first step in determining the characteristics involved in such a complicated problem : the tunnel is replaced by a model which is a conductor with an infinite length and has the same cross section as that of the tunnel; trains are regarded as a rigid conductor, with a fixed cross section, the length of which is infinite in the direction of the

wave propagation.

Thus, this model can be regarded as "uniform cross section". Therefore, the complicated problem is reduced to a two-dimensional one in which electromagnetic fields can be determined by the finite-element method or boundary element method.

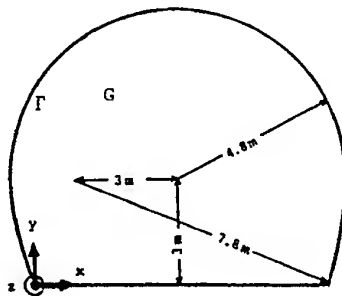
2. EFFECTS OF TRAINS

2.1 Wireless systems

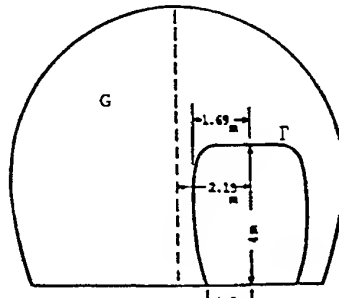
The tunnel is assumed to be straight and infinitely long, and the tunnel wall is assumed to be perfect conductors. Fig. 1. shows a model for tunnel. The cross section of the tunnel is taken as the X-Y plane and the direction of radio wave transmission as the Z axis. The internal region of the tunnel is expressed as G and the boundary of G (the walls of the tunnel and the trains) as Γ . With this notation, the TE_{nm} modes and the TM_{nm} modes are expressed by the following Helmholtz equation :

i) TE_{nm} modes

$$\begin{aligned} \nabla^2 H_z + k^2 H_z &= 0, && \text{in } G \\ \partial H_z / \partial n &= 0, && \text{on } \Gamma \end{aligned} \quad (1)$$



(a)



(b)

Fig. 1 The model of the tunnel. (a) The empty tunnel, (b) The boundary of the tunnel which train enters in one row.

ii) TM_{nn} modes

$$\nabla^2 \text{Ez} + k^2 \text{Ez} = 0, \quad \text{in } G \\ \text{Ez} = 0, \quad \text{on } \Gamma \quad (2)$$

where Hz is Z component of the magnetic field, Ez is the Z component of electric field, k is the cutoff wave number, and $\partial / \partial n$ is the partial differentiation along a normal line against the boundary Γ .

The functional $I[\phi]$ corresponding to the above Helmholtz equation is expressed as follows :

$$I[\phi] = \iint_G \left(\left(\frac{\partial \phi}{\partial x} \right)^2 + \left(\frac{\partial \phi}{\partial y} \right)^2 \right) dx dy - k^2 \iint_G \phi^2 dx dy \quad (3)$$

where $\phi = \text{Hz}$ (or Ez).

This function is solved for each set of boundary conditions by applying the finite element method [1].

The elements used are triangular ones on which ϕ is approximated as a quadratic function.

If each eigenvalue (k)² is determined, the cutoff frequency f_c is obtained from the following formula :

$$f_c = k / 2\pi\sqrt{\epsilon_0 \mu_0} \quad (4)$$

ϕ (Hz or Ez) is determined as eigenvector of each eigenvalue.

The inside of the tunnel is divided into over 176 elements.

2. 1. 1 Accuracy of numerical analysis. The relative errors for up to the TE_{11} mode and for up to the TM_{11} mode are less than 0.05 percent and 0.3 percent, respectively.

2. 1. 2 Effects of trains on fields. Fig. 2 shows field pattern of the TE_{11} mode in empty tunnel and Fig. 3 shows field pattern of the TE_{11} mode which train entered in one row. In these figures, the maximum value of field

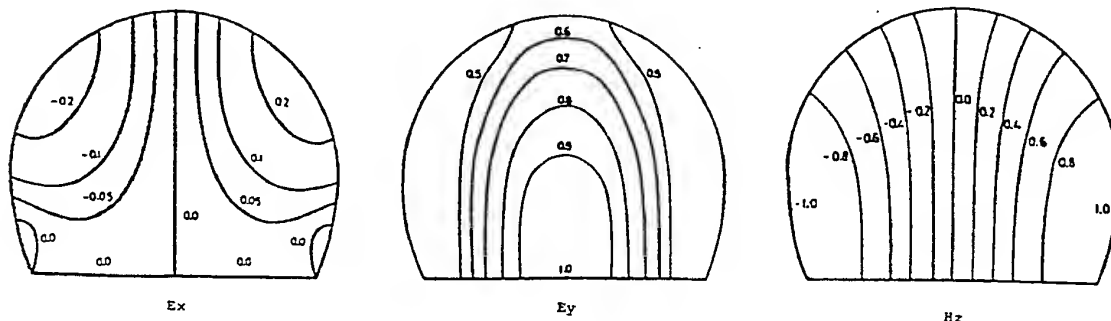


Fig. 2 Field pattern of the TE_{11} mode in empty tunnel.

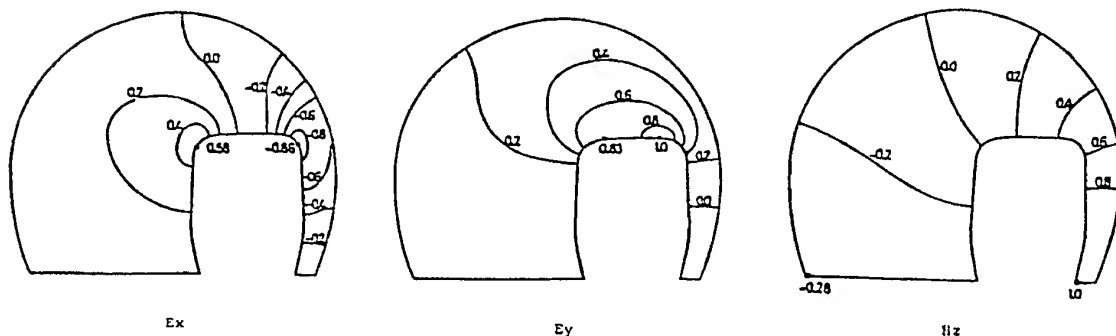


Fig. 3 Field pattern of the TE_{11} mode which train enters in one row.

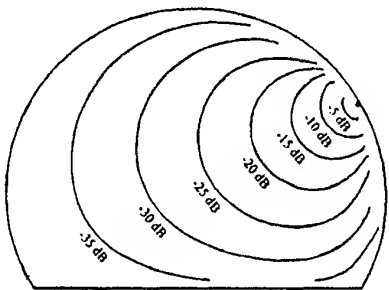


Fig. 4 Field pattern of the E_z in empty tunnel

intensity is specified as 1.

2. 1. 3 Effects of trains on cutoff frequency. TABLE 1 gives cutoff frequency changed by train for TE_{11} mode.

The results have revealed that cutoff frequencies for ordinary empty tunnels are in the higher region of the HF band. The trains in the tunnel lower the cutoff frequency for the TE_{11} modes and raise that for the TM_{11} modes.

TABLE 1-Effects of trains on cutoff frequency in arched tunnel.

	Empty tunnel	Tunnel with train
cutoff frequency	17.2 MHz	9.6 MHz

2.2 Wire systems

2. 2. 1 Effects of trains on fields. We used boundary

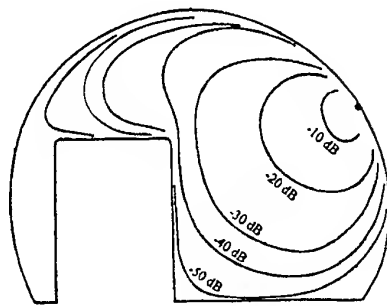


Fig. 5 Field pattern of the E_z which train enters in one row

element method. The boundary is divided into over 72 elements.

The source is a surface wave cable. Fig. 4 shows field pattern of the empty tunnel and Fig. 5 shows field pattern of the E_z which train entered in one row. In these figures, the maximum value of field intensity is specified as 0 dB.

3. CONCLUSION

This study analyzed the effects of trains in tunnels on the basis of certain assumptions and elucidated part of the basic characteristics. The field distribution in the tunnel depends on the train as shown in Figs.2, 3, 4 and 5. The trains in the tunnel lower the cutoff frequency for the TE_{11} mode.

4. REFERENCES

- [1] S. Kagawa, "The introduction of finite element method for electron and electricity", Ohm Company, Japan, 1978.

ON THE EQUIVALENT CIRCUIT FOR THE G-LINE ABOVE GROUND

Jiro Chiba

Tohoku Institute of Technology

35-1 Yagiyama Kasumi-cho, Sendai 982 JAPAN

Tel +81-22-229-1151 FAX +81-22-229-2570

Based on the field theory, the primary transmission line constants of the Goubau line (G line) above ground (R, L, C and G) and the secondary transmission line constants ($\gamma_0 = \alpha_0 + j\beta_0$ and Z_0) were obtained, and then the equivalent circuit for the G line above ground was given. The behavior of the line from an engineering standpoint is now completely determined by the usual simple circuit theory. The transition of the G line from a ground return transmission line of a surface-wave transmission line was proved experimentally.

1. INTRODUCTION

This paper outlines the Equivalent Circuit for the G-line Above Ground.

In practice, the G line [1] is installed at a certain height above ground. We have a classic theory of the propagation of the electromagnetic waves along overhead wires developed by Carson and by Pollaczek as early as 1926 [2], [3]. Thirty years after that, remarkable advances in the theoretical aspects have been achieved through the studies of Kikuchi [4]-[5] and Amamiya [6]. Kikuchi was the first to give the transition theory (from ground return transmission line to surface-wave transmission line) for the Sommerfeld line above ground. We can say that great interest is focused on the earth's problem. Various authors (Wise [7], Sunde [8], Wait [9], Coleman [10], and Knyazev [11]) have studied the earth's problems, and recent research in this area has been promising (Wait [12], [13], Dos Santos [14] and Kikuchi [15]).

The objectives of the present paper are to derive expressions for the primary transmission line constants of the G line above ground (R, L, C and G) and the secondary transmission line constants ($\gamma_0 = \alpha_0 + j\beta_0$ and Z_0), and to find the equivalent circuit for the G line above ground.

2. SERIES IMPEDANCE Z AND PARALLEL ADMITTANCE Y OF THE G LINE IN THE PRESENCE OF THE EARTH

2.1 The coordinate system

Assume that a line of infinite length and of sufficiently small diameter is installed at height h above ground and carries a current $Ie^{-\gamma_0 z+j\omega t}$, (I = total axial current in wire, γ_0 = propagation constant of the transmission line, ω = angular frequency = $2\pi f$, f = frequency). The diameter of the wire $2a$ is much smaller than h .

As shown in Fig. 1 in rectangular coordinates, the surface of the earth is the plane at $y = 0$. Beneath the surface or, in the region $y < 0$, the plane wave propagation constant is $k_2 (= \omega\sqrt{\mu_0\varepsilon_2(1-j\sigma_2/\omega\varepsilon_2)})$, Re

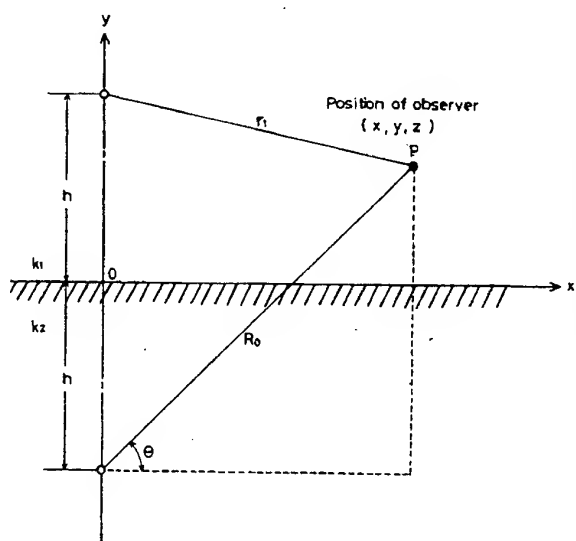


Fig. 1. The coordinate system.

$k_2 > 0, \operatorname{Im} k_2 < 0$. μ_0 = permeability of free space
 $\epsilon_2 = \epsilon_1 \cdot \epsilon_0$ = dielectric constant of the earth, σ_2 = conductivity of the earth, while above the surface, or in the region $y > 0$, the plane wave propagation constant is $k_1 (= \omega \sqrt{\mu_0 \epsilon_1} = \omega \sqrt{\mu_0 \epsilon_0})$.

2.2 FORMULATION FOR Z AND Y

From Maxwell's equation,

$$E_x = -\operatorname{grad}\phi_c - j\omega A_z \quad (1)$$

where E_x is Z component of the electric field at the wire surface ($x = 0, y = h - a$) ϕ_c and A_z account for the scalar potential at the wire surface ($x = 0, y = h - a$) and for the z component of the vector potential at the wire surface ($x = 0, y = h - a$), and are represented by

$$\begin{aligned} A_z &= \mu \epsilon (\hat{c} \Pi / \partial t) \\ \phi &= -\nabla \cdot \Pi \end{aligned} \quad (2)$$

given in [16] part 2 of (6). We introduce the series impedance Z and the parallel admittance Y of the transmission line above the plane earth by the following equations :

$$\begin{aligned} Z &= \frac{1}{I\zeta} [E_x + j\omega A_z] \\ Y &= -\frac{\partial I\zeta}{\partial z} \frac{1}{\phi_c} = \frac{\gamma_0 I\zeta}{\phi_c} \end{aligned} \quad (3)$$

The following assumptions have been made in working out the theory of the transmission line : $a \ll h, b \ll h, a \ll \text{wavelength}, b \ll \text{wavelength}$.

From (2), (3)

$$\begin{aligned} Z &= R + j\omega L = \frac{(1+j)}{2\pi a \sqrt{2}} \sqrt{\frac{\omega \mu_0}{\sigma_c}} + \frac{j\omega \mu_0}{2\pi} \left[\frac{j\pi}{2} \{H_0^{(1)}(\lambda_1 a) \right. \\ &\quad \left. - H_0^{(1)}(\lambda_1 R_1)\} \right] + \frac{j\omega \mu_0}{\pi} S_1 \end{aligned} \quad (4)$$

$$Y = G + j\omega C$$

$$= \frac{j\omega 2\pi \epsilon_0}{\frac{\ln(b/a)}{\epsilon_d (1-j\tan\delta)} + \frac{j\pi}{2} \{H_0^{(1)}(\lambda_1 b) - H_0^{(1)}(\lambda_1 R_1)\} + 2S_2} \quad (5)$$

where σ_c is the conductivity of the wire, $R_1 = 2h - a$, ϵ_d is the specific inductive capacity of coated dielectric, $\lambda_n = \sqrt{k_n^2 + \gamma_0^2}$, $\operatorname{Re} \sqrt{u^2 - \lambda_n^2} > 0, n = 1, 2$

$$S_1 = \int_0^\infty \frac{e^{-R_1 \sqrt{u^2 - \lambda_1^2}}}{\sqrt{u^2 - \lambda_1^2} + \sqrt{u^2 - \lambda_2^2}} du \quad (6)$$

$$S_2 = k_1^2 \int_0^\infty \frac{e^{-R_1 \sqrt{u^2 - \lambda_1^2}}}{k_2^2 \sqrt{u^2 - \lambda_1^2} + k_1^2 \sqrt{u^2 - \lambda_2^2}} du \quad (7)$$

R, L, G and C are series resistance, series inductance, parallel conductance, and parallel capacitance in the presence of the earth. The part $H_0^{(1)}(\lambda_1 R_1)$ stands for a contribution from the image of the line at $y = -h$. S_1 and S_2 are supplementary terms which take into account the effects of finite conductivity of the earth.

In a practical G-line, we can assume $\lambda_1 = j\lambda_u$.

The integration forms of equation (6), (7) are as follows :

$$S_1 = \frac{\lambda_u}{\lambda_u + \sqrt{\beta_0^2 - \omega^2 \mu_0 \epsilon_2} + j\omega \mu_0 \sigma_2} \frac{1}{2} \sqrt{\frac{2\pi}{\lambda_u R_1}} e^{-\lambda_u R_1} \quad (8)$$

$$\begin{aligned} S_2 &= \frac{\lambda_u}{\lambda_u \left(\epsilon_2 - j \frac{\sigma_2}{\omega \epsilon_0} \right) - j \sqrt{\omega^2 \mu_0 \epsilon_2 - \beta_0^2} - j\omega \mu_0 \sigma_2} \\ &\quad \cdot \frac{1}{2} \sqrt{\frac{2\pi}{\lambda_u R_1}} e^{-\lambda_u R_1} \end{aligned} \quad (9)$$

Equations (8) and (9) are applicable to the region $\lambda_u R_1 \geq 1$.

3. CHARACTERISTIC EQUATION OF THE G LINE ABOVE GROUND

From (1), (2) and (3), the characteristic equation is

$$\begin{aligned} &\frac{\gamma_0}{\omega \epsilon_0} \left[\frac{\ln(b/a)}{\epsilon_d (1-j\tan\delta)} + \frac{j\pi}{2} \{H_0^{(1)}(\lambda_1 b) - H_0^{(1)}(\lambda_1 R_1)\} + 2S_2 \right] \\ &+ \omega \mu_0 \left[\frac{j\pi}{2} \{H_0^{(1)}(\lambda_1 a) - H_0^{(1)}(\lambda_1 R_1)\} + 2S_1 \right] \\ &= j \frac{(1+j)}{a \sqrt{2}} \sqrt{\frac{\omega \mu_0}{\sigma_c}}. \end{aligned} \quad (10)$$

In order to simplify the characteristic equation, we assume that a wire is a perfect conductor, $\lambda_1 = j\lambda_u$ and $S_1 = S_2 = \tan\delta = 0$. Then result is as follows :

$$k_1 = \frac{\lambda_u}{\sqrt{\frac{K_0(\lambda_u a) - K_0(\lambda_u R_1)}{\{ \ln(b/a)/\epsilon_d \} + \{ K_0(\lambda_u b) - K_0(\lambda_u R_1) \}} - 1}} \quad (11)$$

This is in agreement with the result of Section 5 [see (19)] according to circuit theory.

4. PRIMARY TRANSMISSION LINE CONSTANTS OF THE G LINE ABOVE GROUND

The following equations are applicable to the

$$R + j\omega L = Z = \left\{ \frac{(1+j)}{2\pi a \sqrt{\sigma_e}} \sqrt{\frac{\omega \mu_0}{\sigma_e}} \right\} + \left\{ \frac{j\omega \mu_0}{2\pi} [K_0(\lambda_u a) - K_0(\lambda_u R_i)] \right\} + \left\{ \frac{j\omega \mu_0}{2\pi} \frac{\lambda_u}{\lambda_u + \sqrt{\beta_0^2 + \omega^2 \mu_0 \epsilon_2} + j\omega \mu_0 \sigma_2} \sqrt{\frac{2\pi}{\lambda_u R_i}} e^{-\lambda_u R_i} \right\} \\ = \{R'_e + j\omega L'_e\} + \{R''_e + j\omega L''_e\} + \{R_g + j\omega L_g\} \quad (\Omega) \quad (12)$$

$$G + j\omega C = Y = \frac{j\omega 2\pi \epsilon_0}{[K_0(\lambda_u a) - K_0(\lambda_u R_i)] + \left[\frac{\ln(b/a)}{\epsilon_s (1 - j \tan \delta)} \right] \left[\frac{\lambda_u}{\lambda_u \left(\epsilon_2' - j \frac{\sigma_2}{\omega \epsilon_0} \right) + j \sqrt{\omega^2 \mu_0 \epsilon_2 - \beta_0^2} - j\omega \mu_0 \sigma_2} \cdot \frac{1}{2} \sqrt{\frac{2\pi}{\lambda_u R_i}} e^{-\lambda_u R_i} \right]} \\ = \frac{1}{\frac{j\omega 2\pi \epsilon_0}{\{K_0(\lambda_u a) - K_0(\lambda_u R_i)\}}} + \frac{1}{\frac{j\omega 2\pi \epsilon_0}{\frac{\ln(b/a)}{\epsilon_s (1 - j \tan \delta)}}} + \frac{1}{\frac{j\omega 2\pi \epsilon_0}{\lambda_u \sqrt{2\pi / \lambda_u R_i} e^{-\lambda_u R_i}}} \\ = \frac{1}{\frac{1}{G_c + j\omega C_c} + \frac{1}{G_d + j\omega C_d} + \frac{1}{G_g + j\left(\omega C_g - \frac{1}{\omega L_g'}\right)}} \quad (S/m) \quad (13)$$

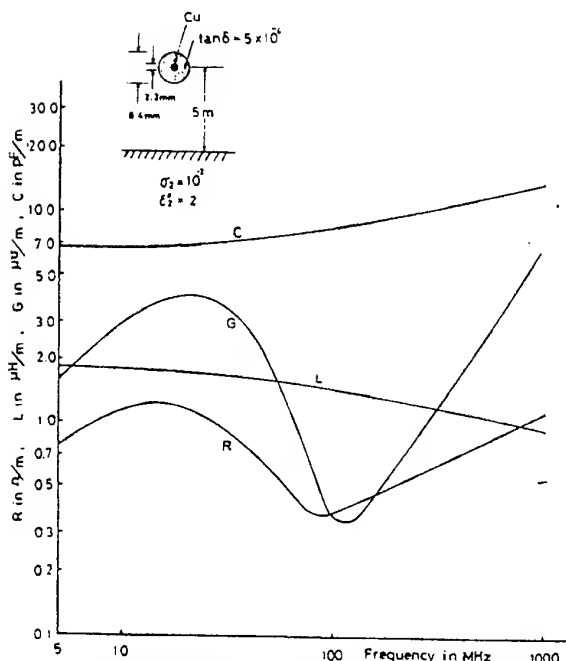
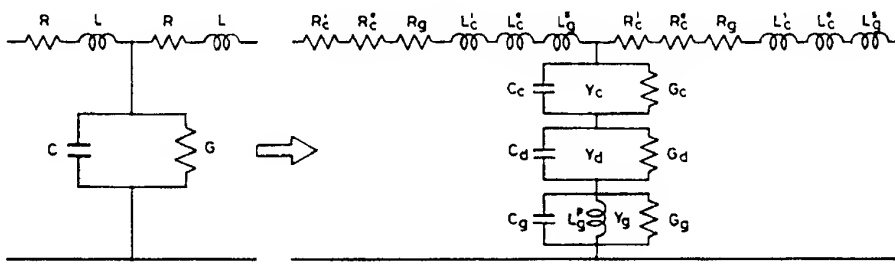


Fig. 2. Series resistance R , series inductance L , parallel capacitance C , and parallel conductance G of the G line above ground.

region $\lambda_u R_i \geq 1$. From (4), (5), (8), (9) and the hankel function formula,

where R'_e , R''_e and R_g are the wire resistance and the equivalent resistance for the ground, respectively ($R = R'_e + R''_e + R_g$). L'_e , L''_e and L_g' are the wire internal inductance, external inductance, and the equivalent series inductance for the ground, respectively ($L = L'_e + L''_e + L_g'$). C_e and G_e are the wire capacitance and the wire leakage conductance, respectively ($Y_e = G_e + j\omega C_e$). C_d and G_d are the equivalent capacitance for the dielectric coat and the equivalent leakage conductance for the dielectric coat respectively ($Y_d = G_d + j\omega C_d$). C_g , L_g' , and G_g are the equivalent capacitance, the equivalent parallel inductance for the ground, and the equivalent leakage conductance for the ground, respectively ($Y_g = G_g + j(\omega C_g - (1/\omega L_g''))$).

In Fig. 2 R , L , C and G are indicated according to (12) and (13).



$$Z = R + j\omega L = (R_c' + R_d' + R_g) + j\omega(L_c' + L_d' + L_g)$$

 Ω/m

$$Y = G + j\omega C = \frac{1}{\frac{1}{Y_c} + \frac{1}{Y_d} + \frac{1}{Y_g}} = \frac{1}{G_c + j\omega C_c + G_d + j\omega C_d + G_g + j\left(\omega C_g - \frac{1}{\omega L_g'}\right)}$$

 S/m

Fig. 3. Equivalent circuit of the G line above ground and items of the primary transmission line constants \$R\$, \$L\$, \$C\$, and \$G\$.

From these relations [see (12) and (13)] the equivalent circuit of the G line above ground is as shown in Fig. 3.

5. SECONDARY TRANSMISSION LINE CONSTANTS OF THE G LINE ABOVE GROUND

By (12) and (13) the characteristic impedance \$Z_0\$ is

$$Z_0 = \sqrt{\frac{Z}{Y}} = \sqrt{\frac{R + j\omega L}{G + j\omega C}} \quad (14)$$

$$\approx \sqrt{\frac{L}{C}} = 60 \sqrt{\frac{\left\{ \ln(b/a)/\epsilon_d + K_0(\lambda_u b) - K_0(\lambda_u R_i) \right\}}{\left\{ K_0(\lambda_u a) - K_0(\lambda_u R_i) \right\}}} \quad (\Omega) \quad (15)$$

Equation (15) holds to a very good approximation in the VHF and UHF regions. In Fig. 4 \$Z_0\$ is indicated [according to (15)].

By (12) and (13) the phase constant and the attenuation constant are

$$\gamma_0 = \alpha_0 + j\beta_0 = \sqrt{(R + j\omega L)(G + j\omega C)} = \sqrt{Z \cdot Y} \quad (16)$$

$$\alpha_0 = \frac{R}{2Z_0} + \frac{GZ_0}{2} \quad (\text{Np/m}) \quad (17)$$

$$\beta_0 = k_1 \sqrt{\frac{K_0(\lambda_u a) - K_0(\lambda_u R_i)}{\left\{ \ln(b/a)/\epsilon_d + \{K_0(\lambda_u b) - K_0(\lambda_u R_i)\} \right\}}} \quad (\text{rad/m}). \quad (18)$$

From (18) and \$\lambda_i = \sqrt{k_1^2 + \gamma_0^2}\$ the characteristic equation is

$$k_1 = \frac{\lambda_u}{\sqrt{\frac{K_0(\lambda_u a) - K_0(\lambda_u R_i)}{\left\{ \ln(b/a)/\epsilon_d + \{K_0(\lambda_u b) - K_0(\lambda_u R_i)\} \right\}} - 1}}. \quad (19)$$

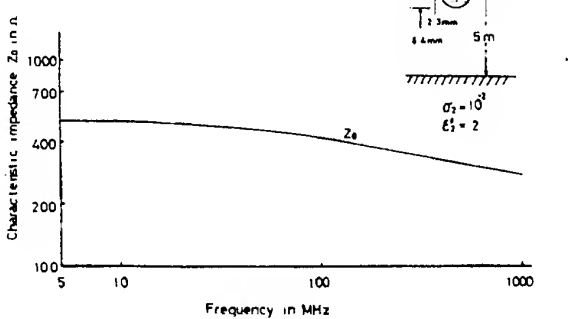


Fig. 4. Characteristic impedance of the G line above the ground.

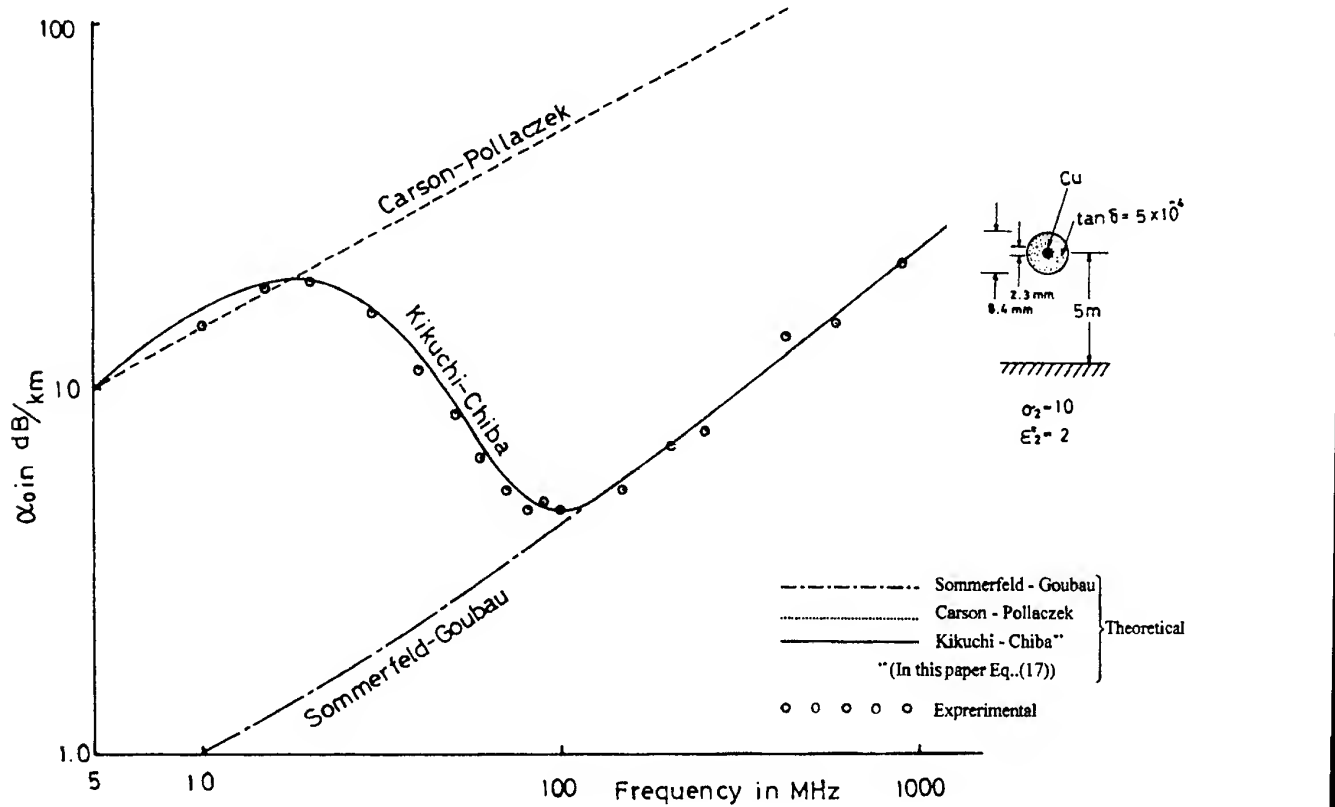


Fig. 5. Attenuation constant of the G line above ground. Ground return transmission line mode is transformed into surface-wave transmission line mode by elevation of frequency with a rise in degree of electromagnetic field concentration.

Equations (17) and (18) hold to a very good approximation in the VHF and UHF regions. In Fig. 5 α_0 is indicated [according to (17)].

6. CONCLUSION

The features of the paper which seem to present results are as follows:

- 1) evaluation of transmission line parameters (R , L , C , G , Z_0 , α_0 , β_0 , γ_0) for the model;
- 2) presentation of a reasonable equivalent circuit as a passive line which involves the plane ground;
- 3) the extension of the theory to a dielectric-coated wire;
- 4) the verification of the transition theory which Kikuchi proposed first by experimental work.

7. REFERENCES

- [1] G. Goubau, "Surface waves and their application to transmission line," *J. Appl. Phys.*, vol. 21, pp. 1119-1128, Nov. 1950.
- [2] J. Carson, "Wave propagation in overhead wires with ground return," *Bell Syst. Tech. J.*, vol. 5, pp. 539-554, Oct. 1926.
- [3] F. Pollaczek, "Über das Feld einer unendlich langen wechselstromdurchflossenen Einfachleitung," *Elek. Nachr.*, vol. 3, pp. 339-359, Sept. 1926.
- [4] H. Kikuchi, "On a ground return circuit at high frequencies," *J. Inst. Elec. Eng. Japan*, vol. 75, pp. 1176-1187, Oct. 1955
- [5] —, "Propagation coefficient of the Beverage aerial," *Proc. IEE (London)*, vol. 120, pp. 637-638, June 1973.
- [6] Y. Amamiya, "On the field of a ground-return circuit in the medium-frequency region," *J. IEE Japan*, vol. 77, pp. 7-14, June 1957.
- [7] W. H. Wise, "Propagation of high frequency currents in ground return circuits," *Proc. Inst. Radio Eng.*, vol. 22, pp. 522-527, Apr. 1943
- [8] E. Sunde, *Earth Conductance Effects in Transmission Line Systems*. New York: Van Nostrand, 1949, ch. 1-5, pp. 8-63.
- [9] J. R. Wait, *Electromagnetic Waves in Stratified Media*. New York: Pergamon, 1962, ch. 2, pp. 1-168.
- [10] B. L. Coleman, "Propagation of electromagnetic disturbances along a thin wire in a horizontally stratified medium," *Phil. Mag. Ser. 7*, vol. 41, pp. 276-288, Mar. 1950.
- [11] A. S. Knyazev, "Engineering computation of the resistance of line conductors taking into account the earth's influence," *Radiotekhnika*, vol. 15 (a), pp. 21-32, 1960.
- [12] J. R. Wait, "On the impedance of a long wire suspended over the ground," *Proc. Inst. Elec. Eng. (London)*, vol. 49 (10), p. 1576, 1961.
- [13] —, "Theory of wave propagation along a thin wire parallel to an interface," *Rad. Sc.*, vol. 7, pp. 675-679, June 1972.
- [14] A. F. Dos Santos, "Electromagnetic wave propagation along a horizontal wire above ground," *Proc. IEE (London)*, vol. 119, pp. 1103-1109, Aug. 1972.
- [15] H. Kikuchi, "Active distributed parameter lines with ground return", *EMC '84 INTERNATIONAL WROCLAW SYMPOSIUM ON ELECTROMAGNETIC COMPUTABILITY*, pp. 153-161, 1984.
- [16] Jiro Chiba, "Studies in Overhead Wire-Goubau Line Above Ground", *IEEE Trans. vol. MTT-25, No. 2, pp. 83-93, Feb. 1977.*

COUPLING OR TRANSITION BETWEEN THE ZENNECK, SOMMERFELD, GOUBAU, AND K-WAVES

H. Kikuchi and H. Inaba

Nihon University, College of Science and Technology
8, Kanda Surugadai, 1-chome, Chiyoda-ku, Tokyo 101, Japan

The K-wave is a natural wave associated with a bare wire with finite conductivity or dielectric coated conducting wire above a ground and can be a quasi-TEM, hybrid (EH-type) or TM wave, depending on the frequency and medium parameters of the ground (conducting, semiconducting, or dielectric).

Mutual relations between the Zenneck, Sommerfeld, Goubaud, and K-waves are investigated on the basis of their propagation characteristics in frequency. The Z-wave couples to neither the S- nor G-wave, since the former is a fast wave, while the latter, S or G, is a slow wave. However, the Z-wave couples weakly to the K-wave for a bare conducting wire at a certain frequency where attenuation characteristics both waves cross each other and where the phase velocity of the K-wave tends to a fast wave from a slow wave at lower frequencies, approaching but never reaching the phase velocity of the faster Z-wave. For a dielectric coated conducting wire, however, there is no coupling between the Z- and K-waves unless its dielectric layer is extremely thin.

The K-wave can be both a slow and a fast wave for a bare conducting wire; a fast wave in the so-called 'transition region' and a slow wave in the rest range of frequencies, and transfers smoothly to a TEM-type of the Carson-Pollaczek wave with decreasing frequency and to the S- or G-wave in a TM-type of surface wave with increasing frequency.

All the above statements are confirmed theoretically, providing some numerical examples and experimental evidence.

1. INTRODUCTION

The Zenneck wave is a TM wave along the surface of a medium of finite conductivity and is considered an inhomogeneous plane wave or a fast surface wave whose phase velocity is faster than the velocity of light. This type of wave has been extended to a general medium, including a semiconductor or dielectrics, since Zenneck was mainly concerned with a conducting medium [1].

The Sommerfeld or Goubaud wave is a cylindrical TM wave along the surface of a bare wire with finite conductivity or dielectric coated conducting wire, respectively [2], [3], and is considered a slow surface wave whose phase velocity is slower than the velocity of light.

The K-wave is a hybrid Zenneck-Sommerfeld or -Goubaud wave arising from the presence of ground and its

low frequency side is related to a TEM type of the Carson-Pollaczek (C-P) wave [4, 5] and to the so-called 'Beverage aerial' [6]. Since its anomalous propagation characteristics for high frequencies were discovered by the first author in 1956 [7, 8, 9, 10], interest in this aerial has been renewed and the problem is still in active investigations in a variety of extended or modified forms (for example, [11, 12]).

In Sec.2, the propagation characteristics of the Z-wave are presented in an extended form over an entire range of frequencies on the basis of an analytical solutions of Maxwell's equations.

In Sec.3, exact expressions for the propagation characteristics of the K-waves are summarized for a dielectric coated conducting wire above the ground [13, 14]. On this basis, some numerical examples of propagation characteristics and circuit parameters are shown over an entire range of frequencies. It is rephrased that the K-wave possesses a maximum and a minimum attenuation, the so-called 'transition' from a TEM-type of the C-P wave to the G-wave in a TM-type of surface wave.

In Sec.4, the K-wave for a bare conducting wire above the ground is specifically investigated with particular reference to the problem of its coupling to the Z-wave, adding new results obtained from purely numerical solutions. It has been found that there may be a weak coupling between the K- and Z-waves at a certain frequency where attenuation characteristics of both waves cross each other and where the phase velocity of the K-wave tends to a fast wave from a slow wave at lower frequencies, approaching but never reaching the phase velocity of the faster Z-wave. For a dielectric coated conducting wire, however, there is no coupling between them unless its dielectric layer is extremely thin.

In contrast, there may be a strong coupling between the K-wave for a bare conducting wire and a plane wave of grazing incidence at a certain angle in the transition region where the K-wave becomes a fast wave and its phase velocity coincides exactly with the front velocity of the plane wave along the interface. Based on this principle, Sec.5 briefly describes a new type of travelling antenna [15] similar in construction to and different in function from the Beverage antenna, since this problem is to be discussed elsewhere.

2. PROPAGATION CHARACTERISTICS OF THE ZENNECK WAVE

Consider a TM wave propagating along a plane interface of a semi-infinite medium and choose a rectangular coordinate system x, y, z as shown in Fig.1. Then, assuming the temporal and spatial factor $\exp[-ux-\Gamma z]$

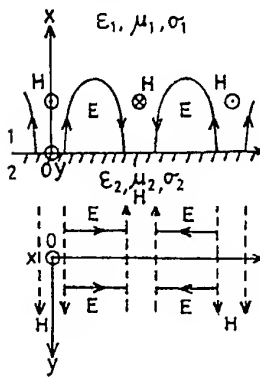


Fig. 1. Z-wave.

+ $j\omega t$], the relations between x, y , and z components of electric (E) and magnetic (H) fields are written from Maxwell's equations, putting $E_y = H_x = H_z = 0, \partial/\partial y = 0$, as

$$\Gamma H_y = (\sigma + j\omega\epsilon) E_x, \quad (1)$$

$$-uH_y = (\sigma + j\omega\epsilon) E_z, \quad (2)$$

$$-\Gamma E_x + uE_x = -j\omega\mu H_y, \quad (3)$$

$$-(u^2 + \Gamma^2) = k^2 = \omega^2\epsilon\mu - j\omega\sigma\mu, \quad (4)$$

where ϵ, μ, σ , and k are dielectric constant, permeability, conductivity, and wave number, respectively. Substituting the boundary conditions: $E_{1z} = E_{2z}, H_{1y} = H_{2y}$ (subscript 1 or 2 refers to medium 1 or 2, respectively) in Eq.(2), we obtain the relation

$$u_1 / (\sigma_1 + j\omega\epsilon_1) = u_2 / (\sigma_2 + j\omega\epsilon_2). \quad (5)$$

Substituting Eq.(5) in Eq.(4), the propagation constants, Γ and u are written as

$$\Gamma = \alpha + j\beta = jk_1 k_2 / (k_1^2 + k_2^2)^{1/2}, \quad (6)$$

$$u_i = a_i + jb_i = j k_i^2 / (k_1^2 + k_2^2)^{1/2}, \quad (7)$$

where α and β are the attenuation and phase constants of the Zenneck wave.

2.1. The Z-wave for a semi-infinite conducting medium

Consider the Z-wave along a surface of a semi-infinite conducting medium when the above medium 1 is air. Then, putting $\epsilon_1 = \epsilon_0, \epsilon_2 = \epsilon, \mu_1 = \mu_2 = \mu_0, \sigma_1 = 0, \sigma_2 = \sigma \gg \omega\epsilon$, $k_1 = k_0 = \omega(\epsilon_0\mu_0)^{1/2}, |k_2|^2 \gg |k_0|^2$, we obtain from Eqs.(6) and (7)

$$\alpha = \omega^2\epsilon_0/2\sigma = (k_0^2/2\sigma)(\epsilon_0/\mu_0)^{1/2} = k_0^2/(2\sigma Z_0) = k_0^2 Y_0/2\sigma, \quad (8)$$

$$\beta = k_0 \{1 - (\omega^2\epsilon_0\epsilon/2\sigma^2)\} \quad \text{or}$$

$$v = \omega / \beta = c / \{1 - (\omega^2\epsilon_0\epsilon/2\sigma^2)\} \equiv c \{1 + (\omega^2\epsilon_0\epsilon/2\sigma^2)\}, \quad (9)$$

$$u_1 = a_1 + jb_1 = k_0^2(1-j)/(2\omega\sigma\mu_0)^{1/2} = k_0^2\delta(1-j)/2, \quad (10)$$

$$u_2 = a_2 + jb_2 = -(1+j)(\omega\sigma\mu_0/2)^{1/2} = -(1+j)/\delta, \quad (11)$$

$$\delta = (2/\omega\sigma\mu_0)^{1/2}, \quad (12)$$

where δ is the skin depth, Z_0 and Y_0 are the intrinsic impedance and admittance in free space, respectively.

2.2. An extended Z-wave for a semi-infinite dielectric medium

Consider an extended Z-wave along a surface of a semi-infinite dielectric medium instead of a conducting one discussed in Subsec.2.1, namely $\sigma_2 = \sigma \ll \omega\epsilon, \epsilon_2 = \epsilon_0\epsilon_s$. Then, we have from Eqs.(6) and (7)

$$\alpha = \sigma k_0 \epsilon_s^{1/2} / \{2\omega\epsilon(1+\epsilon_s)^{3/2}\} = \sigma Z_0 / \{2(1+\epsilon_s)^{3/2}\}, \quad (13)$$

$$\beta = k_0 [\epsilon_s / (1 + \epsilon_s)]^{1/2} \quad \text{or}$$

$$v = \omega / \beta = c[1 + (1/\epsilon_s)]^{1/2} \quad (14)$$

$$u_1 = a_1 + jb_1 = \sigma k_0 / \{(2\omega\epsilon_0)(1+\epsilon_s)^{3/2}\} - (jk_0) / (1+\epsilon_s)^{1/2}, \quad (15)$$

$$u_2 = a_2 + jb_2 = \{k_0 \epsilon_s / (1+\epsilon_s)^{1/2}\} [(\sigma/2\omega\epsilon) \{(2+\epsilon_s)(1+\epsilon_s)\} + j]. \quad (16)$$

2.3. Numerical results for propagation characteristics

Figs.2 and 3 represent attenuation and phase characteristics of the Z-wave for $\sigma_2 = \sigma = 10^{-2}$ S/m, $\epsilon_2 = \epsilon_1 = \epsilon_0$ and $\epsilon_2 = \epsilon = 10\epsilon_0; \sigma_2 = \sigma = 4$ S/m, $\epsilon_2 = \epsilon = 80\epsilon_0$ (seawater), obtained from Eq.(6). It is seen that the Z-wave is a fast wave whose phase velocity is faster than the velocity of light and increases with increasing frequency, approaching $c[1 + (1/\epsilon_s)]^{1/2}$ and its attenuation also increases with increasing frequency, approaching $\sigma Z_0 / \{2(1+\epsilon_s)^{3/2}\}$. In general, attenuation decreases in a conductive region but increases in a dielectric region with increasing conductivity, while the phase velocity decreases in a dielectric region with increasing permittivity.

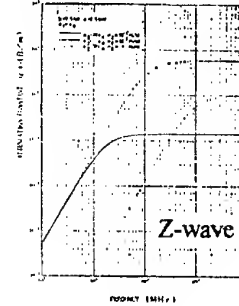


Fig. 2. Attenuation.

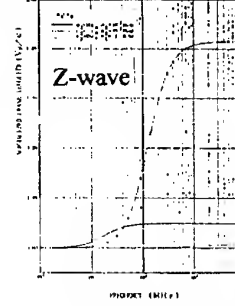


Fig. 3. Normalized phase velocity.

3. PROPAGATION CHARACTERISTICS AND CIRCUIT PARAMETERS OF THE K-WAVE FOR A DIELECTRIC COATED CONDUCTING WIRE

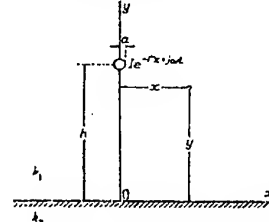


Fig. 4. Wire above ground.

Consider a TM wave propagating along an infinite bare or dielectric coated cylindrical conductor above the ground and choose a rectangular coordinate system x, y, z as shown in Fig.4. According to the results obtained by one of the authors [13, 14], propagation characteristics are still expressed in terms of a generalized lossy transmission line with dispersive distributed parameters, as follows

$$\Gamma = \alpha + j\beta = (ZY)^{1/2}, \quad Z_0 = R_0 + jX_0 = (Z/Y)^{1/2}, \quad (17)$$

$$Z = Z_i + Z_e = [(1+j)/(2^{3/2}\pi a)](\omega\mu_c/\sigma_c)^{1/2}$$

$$+ (j\omega\mu_c/2\pi) \{1 - (\epsilon_1/\epsilon_i)(1 + j\tan\delta_i)\} \ln(a'/a)$$

$$+ (j\omega\mu_i/2\pi) \{ \ln 2j / (\gamma\lambda_1 a') - j(\pi/2)$$

$$- H_0^{(1)}[\lambda_1(2h-a')] + 2(Q-jP)\}, \quad (18)$$

$$Y = j2\pi\omega\epsilon_i / \{ \ln 2j / (\gamma\lambda_1 a') - j(\pi/2) H_0^{(1)}[\lambda_1(2h-a')] + 2(Q'$$

$$- jP')\}, \quad (19)$$

where

$$Q_0 - jP_0 = p \int_0^\infty \exp[-(2h-a')(u^2 - \lambda_1^2)^{1/2}] / \{p(u^2 - \lambda_2^2)^{1/2} + q(u^2 - \lambda_1^2)^{1/2}\} du$$

$$= \int_0^\infty \exp[-(2h-a')(u^2 - \lambda_1^2)^{1/2}] / \{(u^2 - \lambda_2^2)^{1/2} + \eta(u^2 - \lambda_1^2)^{1/2}\} du$$

$$= Q - jP \quad \text{for } p=q=1 \text{ or } \eta=1, \quad (20)$$

$$= Q' - jP' \quad \text{for } p=k_1^2, q=k_2^2 \text{ or } \eta=k_2^2/k_1^2, \quad (21)$$

$$\lambda_1^2 = k_1^2 + \Gamma^2, \quad \lambda_2^2 = k_2^2 + \Gamma^2 = k_2^2 - k_1^2 + \lambda_1^2, \quad (22)$$

and $\Gamma = \alpha + j\beta$ is the propagation constant along the wire (α : attenuation constant; β : phase constant), $Z_0 = R_0 + jX_0$, the characteristic impedance, and Z and Y are the series impedance and the parallel admittance, respectively. On the right-hand side of Eq.(18), the first and second terms refer to Z_i , the internal impedance, and the remaining term refers to Z_e , the external impedance, respectively. ($H_0^{(1)}$: Hankel function of the first kind and zeroth order, λ : transverse wavenumber, $\gamma = e^C = 1.781$, C : Euler's constant, a : radius of conductor, a' : outer radius of dielectric coated wire, h : height of wire, $\omega = 2\pi f$: angular frequency, k : wavenumber, σ : conductivity, μ : permeability, ϵ : dielectric constant, $\tan \delta = \sigma/\omega\epsilon$: loss factor). The subscripts, c , i , 1 , and 2 refer to the conductor, dielectric, air, and earth. The extended Carson's function ($Q - jP$) and the first-author's function ($Q' - jP'$) [13, 14] arise from the earth's finite conductivity and permittivity, and are considered as corrections for the series impedance and parallel admittance, respectively.

In an exact manner, Γ is to be determined numerically by employing successive approximations which lead to a self-consistent solution [13, 14].

As an typical example, Figs.5 to 8 represent the frequency characteristics of the propagation constant and circuit parameters as a dispersive distributed parameter line for a polyethylene-coated copper ($a = 1.15$ mm, $a' = 4.2$ mm, $\epsilon_1 = 2.3\epsilon_0$, $\tan \delta_1 = 3 \times 10^{-4}$, $\mu_1 = \mu_0$; the subscript i refers to polyethylene dielectric) 5 m high above the ground ($\sigma_2 = \sigma = 10^{-2}$ S/m, (a): $\epsilon_2 = \epsilon_1 = \epsilon_0$ and (b): $\epsilon_2 = 10\epsilon_1 = 10\epsilon_0$). The dashed and solid lines refer to the first approximation and a final exact solution, respectively. The chain line provides case of a single G-line without ground. As a whole, there is a little effect of the difference in the earth's dielectric constant.

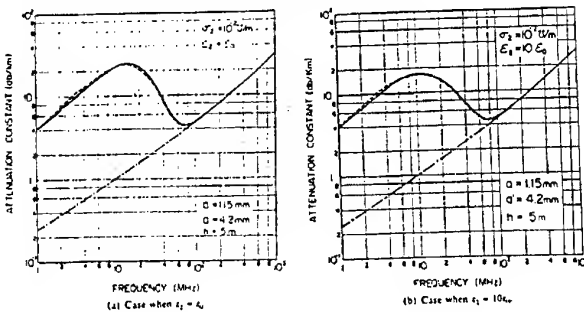


Fig. 5. Attenuation (G-line above ground).

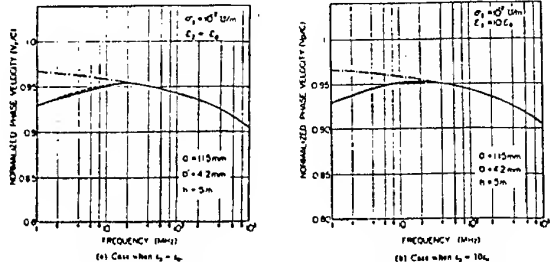


Fig. 6. Normalized phase velocity (G-line above ground).

As seen in Fig.5, the attenuation takes a maximum around 10 MHz and a minimum around 100 MHz, and indicates a mode transfer from a quasi-TEM (or ground-return) region at low frequencies to a TM surface-wave (or G-wave) region at high frequencies via an intermediate transition region where the wave becomes hybrid (HE type).

Fig.6 indicates that the wave is a slow wave over an entire range of frequencies, although its phase velocity approaches the velocity of light as close as 0.955c at a frequency near 20 MHz. This is in contrast to case of bare conducting wire that can become a fast wave in a transition region as discussed in the next section. Actually a dielectric coating tends to make the phase velocity slower. Accordingly, it can be said that a fast wave is almost impossible for a dielectric coated wire unless its dielectric layer is extremely thin.

Fig.7 shows the complex characteristic impedance. Its resistance R_0 possesses a low-frequency limit of about 500 Ω , decreasing monotonically with increasing frequency, while its reactance X_0 is capacitive in the ground-return region and tends to be slightly inductive in the transition region, but diminishing in surface-wave region.

Fig.8 represents the frequency characteristics of the series impedance and the parallel admittance. Among them line-loss parameters, R and G , are both similar in shape to attenuation characteristics in the sense that they possess both a maximum and a minimum in the transition region. Further, the parallel conductance G is more similar to attenuation characteristics in the sense that

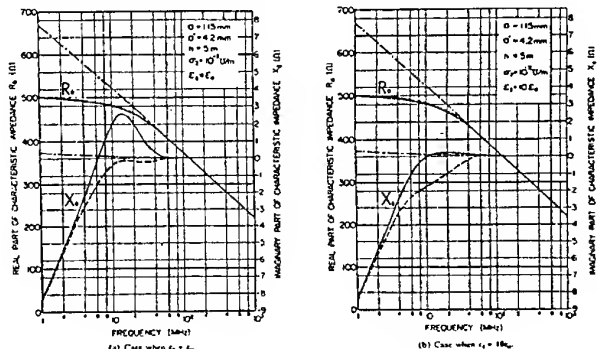


Fig. 7. Characteristic impedance.

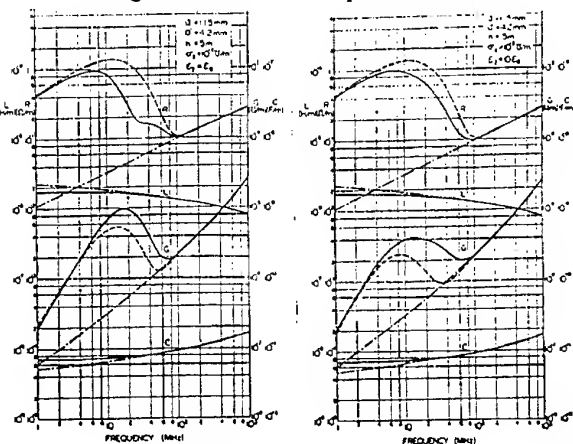


Fig. 8. Circuit parameters.

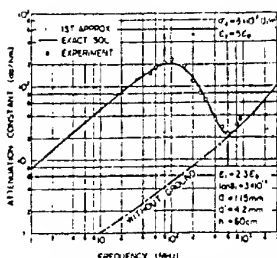


Fig. 9. Attenuation (theory and experiment)

parallel capacitance exhibit far less dispersion over a whole range of frequencies, though the former and the latter slightly decreases and increases, respectively in a monotonous manner with increasing frequency.

Finally, Fig.9 represents a comparison of theory and experiment for a polyethylene-coated copper wire mentioned above but for 60 cm high above the ground. The theory is in satisfactory agreement with experiment.

In summary, it can be stated that attenuation characteristics are best correlated with the parallel conductance and that a decrease in attenuation in the transition region is due entirely to the first-author's function $Q' - jP'$ introduced as a correction to the parallel admittance, which plays a crucial role in propagation characteristics.

4. THE K-WAVE FOR A BARE CONDUCTING WIRE AND ITS WEAK COUPLING TO THE ZENNECK WAVE

In the preceding section, we have been concerned with the K-wave for a dielectric coated wire or a G-line above the ground. The present section is to elucidate the effects of dielectric coating by dealing with a bare conducting wire in particular reference to its coupling to the Z-wave, although the study of the K-wave actually started with this case when a 'transition phenomenon' was discovered as early as 1950s [7, 8, 9, 10].

Let $a'=a$ for Eqs.(18) to (21). Then, the second term of the right-hand side of Eq.(18) is canceled out. We assume that the wave phase velocity would slightly deviate from c , the velocity of light, holding the approximations $\lambda_1 \approx 0$, $\lambda_2^2 \approx k_2^2 - k_1^2$. To evaluate Γ , one takes $\lambda_1 = 0$ as a zeroth order quantity and proceeds to the first approximation. Then the substitution of Eq.(18) in the first of Eq.(17) leads to a simple but accurate expression for Γ [14] in spite of the first approximation, usually over ground-return and transition regions as seen hereafter, namely

$$\alpha = (\omega/c) \cdot \{(\delta_c/4a) + P - P'\} / \ln\{(2h-a)/a\}, \quad (23)$$

$$\beta = (\omega/c) \cdot [1 + \{(\delta_c/4a) + Q - Q'\} / \ln\{(2h-a)/a\}], \text{ or}$$

$$\nu = \omega/\beta = c [1 - \{(\delta_c/4a) + Q - Q'\} / \ln\{(2h-a)/a\}], \quad (24)$$

where

$$\delta_c = (2/\omega\sigma_c\mu_r)^{1/2}, \quad (25)$$

the skin depth of wire.

In particular, let $P' = Q' = 0$ in Eqs.(23) and (24). Then, the Carson-Pollaczek theory in the ground-return region is recovered.

From Eq.(24), we notice that

$$\nu = \omega/\beta < c \quad \text{for } Q - Q' + (\delta_c/4a) > 0, \quad (26)$$

$$\nu = \omega/\beta > c \quad \text{for } Q - Q' + (\delta_c/4a) < 0. \quad (27)$$

In other words, the K-wave can be a fast wave in a range of frequencies for Eq.(27), actually in the transition region as seen below. According to the Carson-Pollaczek theory, however, the wave is always a slow wave by putting $Q' = 0$ in Eq.(26), since $Q > 0$.

Figs.10 and 11 represent attenuation and phase characteristics obtained from a purely numerical solution for a bare conducting wire (radius: 2.5 mm) with various height, $\sigma_2 = \sigma = 10^{-2} \text{ S/m}$, $\epsilon_1 = \epsilon_0$, and $\epsilon_2 = 10\epsilon_0$, while the open circles represent purely analytical solutions. One notices that beyond a certain height of wire ($0.5 \sim 1 \text{ m}$) numerical results exhibit a discontinuity in both attenuation and phase velocity at a certain frequency where the attenuation curve of the K-wave should cross that of the Z-wave and where the K-wave tends to become a fast wave from a slow wave at lower frequencies, approaching but never reaching the phase velocity of the Z-wave. Such a discontinuity arises from difficulties in performing numerical integration for $Q' - jP'$ because of singularities around that frequency, although analytical solutions do not exhibit discontinuities. This indicates that there may be a weak coupling between the K- and Z-waves at a lower edge of the transition region and that the K-wave keeps a fast wave throughout the transition region. It is seen that both the ground-return and transition regions tend to shift to higher frequencies and the K-wave in the transition region tends to become faster with decreasing height of the wire. However, the K-wave in the ground-return region is always a slow wave.

On the other hand, it is also seen that the K-wave tends smoothly to a TEM-type of the C-P wave in the ground-return region or to the Sommerfeld TM_{01} wave in the surface region with decreasing or increasing frequency, respectively, while the K-wave transfers to the S-wave with increasing height of the wire.

From Secs.3 and 4, it should be summarized that in contrast to a possible weak coupling for a bare conducting wire, there is no coupling for a dielectric coated conducting wire between the K- and Z-waves, since the K-wave is a slow wave over a whole range of frequencies unless its dielectric layer is extremely thin.

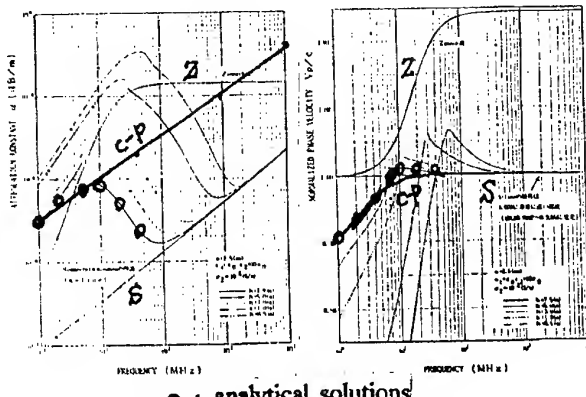


Fig. 10. Attenuation. Fig. 11. Normalized phase velocity.
(S-line above ground)

5. COUPLING BETWEEN A PLANE WAVE AND THE K-WAVE AND A NEW TRAVELLING WAVE ANTENNA

In contrast to a weak coupling between the K- and Z-waves described in the preceding section, it is possible to obtain a strong coupling between the K-wave for a bare conducting wire and a plane wave of grazing incidence in the transition region by making the front velocity of the plane wave along the interface equal to the phase velocity of the K-wave. This can be done by changing the angle of incidence of the plane wave. Based on this principle, one can construct a new type of travelling-wave antenna [15] similar in construction to and different in function from the Beverage antenna. Actually, the induced wave on the Beverage antenna is a TEM type of a slow wave in the ground-return region, while the front velocity of the incident sky wave along the wire is higher than the velocity of light (fast wave) for oblique incidence and is equal to it for horizontal incidence. Due to this difference in velocity between the line and sky waves, the phase difference increases as both waves progress, resulting in the decrease of the line current. In other words, the induced line wave couples only weakly to the sky wave in contrast to a strong coupling and consequently a much higher gain for the new antenna. This is an essential difference between the Beverage and the new antenna. Details of the new antenna are not aimed in this article but are to be discussed elsewhere.

6. CONCLUSIONS

The K-wave is a natural hybrid Zenneck- Sommerfeld or -Goubau wave arising from the presence of ground and its low frequency side is related to a TEM type of the Carson-Pollaczek wave and the Beverage aerial. In the transition region, its attenuation has a maximum and a minimum and it becomes a fast wave, although it is a slow wave in the rest range of frequencies, namely in both the ground-return and the surface-wave region. Consequently, the K-wave transfers smoothly to the C-P wave with decreasing frequency and to the S- or G-wave with increasing frequency.

There may be a weak coupling between the K- and Z-waves at the lower edge of the transition region where the phase velocity of the K-wave tends to become closest to that of the Z-wave but never reaching it.

Finally, it is indicated that there may be a strong coupling between an incident plane wave and the K-wave for a bare conducting wire under certain conditions.

7. REFERENCES

- 7.1. J. Zenneck, "Über die Fortpflanzung ebener elektromagnetischer Wellen langs einer ebenen Leiterfläche und ihre Beziehung zur drahtlosen Telegraphie", *Ann. d. Phys.*, Vol.23, No.9, 1907, pp.846-866.
- 7.2. A. Sommerfeld, "Fortpflanzung elektrodynamischer Wellen an einem zylindrischen Leiter", *Ann. Phys. Chem.*, Vol.67, 1899, pp.233-290.
- 7.3. G. Goubau, "Surface Waves and Their Application to Transmission Lines", *J. Appl. Phys.*, Vol.21, No.11, 1950, pp.1119-1128.
- 7.4. J.R. Carson, "Wave Propagation in Overhead Wires with Ground Return", *Bell System Tech. J.*, Vol.5, 1926, pp.539-554.
- 7.5. F. Pollaczek, "Über das Feld einer unendlich langen wechselstromdurchflossenen Einfachleitung", *Elek. Nachr. Tech.*, Vol.3, 1926, pp.339-359.
- 7.6. H.H. Beverage, C.W. Rice, and E.W. Kellogg, "A New Type of Highly Directive Antenna", *Transactions A.I.E.E.*, Vol.42, No.2, 1923, pp.215-266.
- 7.7. H. Kikuchi, "Wave Propagation along Infinite Wire above Ground at High Frequencies", *Electrotechnical J. Japan*, Vol.2, No.3/4, 1956, pp.73-78.
- 7.8. H. Kikuchi, "On the Transition from a Ground Return Circuit to a Surface Waveguide – étude de la transition entre un circuit de retour la terre et un guide d'onde de surface", *L'onde Elec.*, Vol.38 (Special Suppl.), 1957, pp.39-45.
- 7.9. H. Kikuchi, "Electromagnetic Fields on Infinite Wire above Plane-Earth at High Frequencies", (Japanese), *J. Inst. Elec. Eng. Japan*, Vol.77, No.6, 1957, pp.721-733.
- 7.10. H. Kikuchi, "Propagation Coefficient of the Beverage Aerial", *Proc. IEE*, Vol.120, No.6, 1973, pp.637-638.
- 7.11. M. D'Amore, "Field-Excited Multi-Conductor Transmission Lines", *Proc. of th International Symp. on Electromagnetic Compatibility*, September 17-20, 1996, Rome, Italy.
- 7.12. J. Chiba, "On the Equivalent Circuit for the G-line above Ground", to appear in *Proc. of the Wroclaw Symp. on Electromagnetic Compatibility*, June 23-25, 1998, Wroclaw, Poland.
- 7.13. H. Kikuchi, "Propagation Characteristics along a Dielectric Coated Cylindrical Conductor above the Ground", *Proc. IEEE*, Vol.66, No.3, 1978, pp.351-352.
- 7.14. H. Kikuchi, "Power Line Transmission and Radiation", in *Power Line Radiation and Its Coupling to the Ionosphere and Magnetosphere*, H. Kikuchi (ed.), D. Reidel, Dordrecht, 1983, pp.59-80.
- 7.15. H. Kikuchi, "Parametrically Amplifying Traveling-Wave Antenna", *US Patent 5,469,179*, 1995; *UK Patent 2276985*, 1996; *French Patent 9404020*, 1997; *Japan Patent 2636164*, 1997.

BIOGRAPHICAL NOTES

Hiroshi Kikuchi received Ph. D. degree from University of Tokyo in 1959 and was Chief, Ultramicrowave Laboratory of Electrotechnical Laboratories, MITI until 1961. Before his return to Japan as Professor of Nihon University, Tokyo in 1973, he worked with University of Oxford and several Institutes. He was Chairman, URSI Commission E (1987-1990) and is Life Fellow of IEEE.

Hiroshi Inaba received M.S. degree from Nihon University in 1991 and now works with Toshiba Co., Tokyo.

RELATIONS OF TM₀₁, TE₀₁, AND HE₁₁ MODES FOR A CONDUCTING WIRE, A DIELECTRIC ROD, AND A DIELECTRIC COATED CYLINDRICAL CONDUCTOR WITH SOME NETWORK REPRESENTATIONS AND THE EFFECTS OF A GROUND ON THOSE MODES

H. Kikuchi and S. Fukuda

Nihon University, College of Science and Technology
8, Kanda Surugadai, 1-chome, Chiyoda-ku, Tokyo 101, Japan

Mutual relations of the lowest three modes, TM₀₁, TE₀₁, and HE₁₁ modes for three different lines, S-, D-, and G-lines, are elucidated on the basis of the general characteristic equations of a dielectric coated cylindrical conductor with the aid of mode distribution and characteristic charts which are still not well-known, since a S- or D-line is regarded as a limiting case of a G-line with diminishing dielectric layer ($s \rightarrow 1$ or $s = 1$, $s = a_0/a_1$, a_0 : conductor radius, a_1 : dielectric radius) or with diminishing conductor radius ($s \rightarrow 0$ or $s=0$). In particular, exact, simple solutions and a network representation are given of the TM₀₁ mode for a lossy G-line with thick dielectric layer and are compared with Goubau's solution. In addition, the field extent of TM₀₁, TE₀₁, and HE₁₁ modes for three different lines are estimated with the aid of a 'scale radius' as a measure of the effects of a ground to be investigated in detail in the future except for the TM₀₁ modes of S- and G-lines.

1. INTRODUCTION

While a dielectric rod (D-line) is so familiar in connection with optical fiber communications, it is closely related to a thickly dielectric-coated conducting wire, the so-called 'G-line' and can be treated as its special case when its conductor radius shrinks to zero. At the same time, a single conducting wire, the so-called 'S-line' is also considered its special case when the dielectric thickness shrinks to zero. It is therefore interesting to investigate the most general case of G-line as initiated by one of the authors [1, 2] and to relate it to D- and S-lines.

A general theory of G-line is presented on the basis of the characteristic equations in Sec.2., and propagation modes are discussed in Sec.3, particularly on TM₀₁, TE₀₁, and HE₁₁ modes with the aid of mode distribution and characteristic charts. Numerical results are given of phase and attenuation characteristics. It is stressed that a G-line possesses two no-cutoff modes, TM₀₁ and HE₁₁, since this is still not well-known. It is noted, however, that the TM₀₁ mode of a G-line does not approach that of a D-line for $s \rightarrow 0$, since the conducting wire still remains with infinitesimal radius. Actually, a D-line

with $s=0$ has a finite cutoff TM₀₁ mode different from that of the G-line. The TM₀₁ and TE₀₁ modes of a G-line, however, tend smoothly to those of the S-line for $s \rightarrow 1$, while the scale radius of the HE₁₁ mode of a G-line rapidly increases for $s \rightarrow 1$, indicating its transfer to a plane wave.

The field extent of TM₀₁, TE₀₁, and HE₁₁ modes for three different lines are estimated with the aid of a 'scale radius' as a measure of the effects of a ground.

2. CHARACTERISTIC EQUATION FOR A DIELECTRIC COATED CYLINDRICAL CONDUCTOR

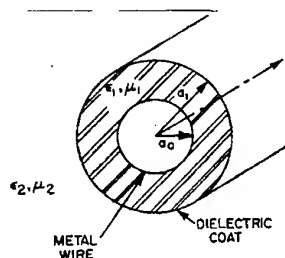


Fig. 1. Dielectric coated conductor

Consider an infinitely long, lossless, dielectric coated wire with a cylindrical coordinate system ρ, θ, z as shown in Fig. 1. Then the longitudinal z components of E (electric) and H (magnetic) fields in medium 1 (dielectric layer) and 2 (air) are expressed, assuming the temporal and spatial factor $e^{j(\omega t - \beta z)}$, as:

$$E_{1z} = A Z_{En}(pp/a_1) \cos n\theta e^{j(\omega t - \beta z)}, \quad (1)$$

$$H_{1z} = B Z_{Hn}(pp/a_1) \sin n\theta e^{j(\omega t - \beta z)}, \quad (2)$$

$$E_{2z} = C K_n(qp/a_1) \cos n\theta e^{j(\omega t - \beta z)}, \quad (3)$$

$$H_{2z} = D K_n(qp/a_1) \sin n\theta e^{j(\omega t - \beta z)}, \quad (4)$$

where K_n is the modified Bessel function of the second kind, and Z_{En} and Z_{Hn} are the following linear combinations of the Bessel functions of the first and second kinds chosen so as to satisfy the boundary conditions on the surface of medium 0 (conducting wire):

$$Z_{En} = J_n(pp/a_1) Y_n(sp) - Y_n(pp/a_1) J_n(sp), \quad (5)$$

$$Z_{Hn} = J_n(pp/a_1) Y_n'(sp) - Y_n(pp/a_1) J_n'(sp), \quad (6)$$

where $s = a_0/a_1$, a_0 and a_1 are the conductor and the dielectric radius, respectively. Then, the following rela-

tions hold:

$$k_1^2 = \omega^2 \epsilon_1 \mu_1 = \beta^2 + p^2/a_1^2, \quad (\epsilon_1 = \epsilon \epsilon_2, \mu_1 = \mu \mu_2) \quad (7)$$

$$k_2^2 = k_0^2 = \omega^2 \epsilon_2 \mu_2 = \beta^2 - q^2/a_1^2, \quad (\epsilon_2 = \epsilon_0, \mu_2 = \mu_0) \quad (8)$$

where k_n is the wave number; ϵ_n and ϵ the absolute and relative dielectric constants; μ_n and μ the absolute and relative permeabilities; β is the phase constant. Eliminating β from Eqs.(7) and (8), we obtain

$$2\pi a_1/\lambda_0 = [(p^2+q^2)/(\epsilon\mu-1)]^{1/2}. \quad (9)$$

where λ_0 is the free space length given by

$$\lambda_0 = 2\pi/k_0 = 2\pi/[\omega(\epsilon_0\mu_0)^{1/2}] = 2\pi c/\omega, \quad (10)$$

where c is the velocity of light in free space. Putting

$$\beta = 2\pi/\lambda_g = k_0 U = (2\pi/\lambda_0)U, \quad (11)$$

where λ_g is the guide wavelength, we obtain from Eqs.(7) and (8)

$$U = \lambda_0/\lambda_g = [(p^2+\epsilon\mu q^2)/(p^2+q^2)]^{1/2}. \quad (12)$$

Then, one obtains the phase velocity

$$v_p = \omega/\beta = \lambda_g f = c \lambda_g / \lambda_0 = c/U, \quad \bar{v}_p = v_p/c = \lambda_g / \lambda_0 = U^{-1} \quad (13)$$

A relation between the parameters p and q , namely characteristic equation is obtained by fulfilling the boundary conditions at $\rho = a_1$ as follows:

$$n^2[(\epsilon\mu/p^2)+(1/q^2)][(1/p^2)+(1/q^2)] = (\epsilon f_{En} + g_n)(\mu f_{Hn} + g_n), \quad (14)$$

where

$$f_{En} = Z_{En}'(p)/pZ_{En}(p), \quad f_{Hn} = Z_{Hn}'(p)/pZ_{Hn}(p), \quad (15)$$

the primes denoting differentiation. For given values of ω , n , ϵ , and μ , Eqs.(10) and (14) yield a pair of values, p and q , defining a mode propagating along the guide. It is convenient to introduce two more abbreviations:

$$V_1 = \eta_0 B/A, \quad V_2 = \eta_0 D/C, \quad (16)$$

where $\eta_0 = (\mu_0/\epsilon_0)^{1/2}$ is the intrinsic impedance of free space. Then, we have from the boundary conditions of the electric and magnetic field components at $\rho = a_1$

$$C/A = Z_{En}(p)/K_n(q), \quad D/B = Z_{Hn}(p)/K_n(q), \quad (17)$$

$$V_1/V_2 = Z_{En}(p)/Z_{Hn}(p), \quad (18)$$

$$V_2 = [(\epsilon f_{En} + g_n)/(\mu f_{Hn} + g_n)]^{1/2}. \quad (19)$$

By solving Eqs.(9) and (14) simultaneously, we obtain the relations, p , q , and λ_0 . Since q can take the values from 0 to ∞ from Eq.(8), the range of values of

the wavelength is given, from Eq.(12), by

$$\lambda_0 \geq \lambda_g \geq \lambda_0/(\epsilon\mu)^{1/2} \quad \text{or} \quad 1 \leq U \leq (\epsilon\mu)^{1/2}, \quad (20)$$

where $q = 0$ or $U = 1$ ($\lambda_g = \lambda_0$) corresponds to cutoff and the cutoff wavelength is given from Eq.(9) by

$$\lambda_{gc} = 2\pi a_1(\epsilon\mu-1)]^{1/2}/[p]_{q=0}. \quad (21)$$

In order to see the field extent around a line, it is convenient to introduce a parameter of 'scale radius', ρ_s as a measure of it, which may be defined as

$$\rho_s = a_1/q, \quad (22)$$

since the asymptotic expression of all the electric and magnetic field factor can be expressed as

$$K_n'(qp/a_1) \sim (\pi a_1/2qp)\exp(-qp/a_1) \quad \text{for large } \rho. \quad (23)$$

3. TRANSMISSION MODES OF DIELECTRIC COATED CYLINDRICAL CONDUCTOR AND APPLICATIONS TO DIELECTRIC ($s=0$) AND CONDUCTING WIRES ($s=1$)

In order to investigate the characteristics of the transmission modes, and particularly to make clear the properties near the cutoff, it is convenient to rewrite Eq.(14) by using the recurrence formula

$$g_n = K_n'(q)/qK_n(q) = -K_{n-1}(q)/qK_n(q) - n/q^2 \\ \equiv -G_n(q) - n/q^2. \quad (24)$$

This yields

$$(n^2/p^2)[(\epsilon\mu/p^2)+(1/q^2)] = \{\epsilon f_{En}(p)-G_n(q)\}\{\mu f_{Hn}(p) \\ - G_n(q)\} - (n/q^2)\{\epsilon f_{En}(p)+\mu f_{Hn}(p)-2G_n(q)\} \quad (25)$$

3.1. Symmetrical modes ($n = 0$): E_{0m} (TM_{0m}) and H_{0m} (TE_{0m})
Eq.(25) or Eq.(14) separates into two parts:

$$\epsilon f_{E0}(p)-G_0(q)=\epsilon f_{E0}(p)+g_0(q)=0, \quad (26)$$

$$\mu f_{H0}(p)-G_0(q)=\mu f_{H0}(p)+g_0(q)=0. \quad (27)$$

The solutions of Eqs.(26) and (27) give E_0 (TM₀) and H_0 (TE₀) modes, respectively, because the former corresponds to $V_2=0$ ($D=H_{2z}=0$) from Eqs.(16) and (4), and the latter to $1/V_2=0$ ($C=E_{2z}=0$) from Eqs.(16) and (3).

Since q moves from zero to infinity, the frequency varies from cutoff to infinity. Then, referring to

$$g_0(q) = -G_0(q) = K_0'(q)/qK_0(q) = -K_1(q)/qK_0(q) \\ \rightarrow 1/[q^2 \{ln(q/2) + C\}] \rightarrow (-\infty) \quad \text{for } q \rightarrow 0 \quad (28)$$

$$\rightarrow -1/q \rightarrow -0 \quad \text{for } q \rightarrow \infty \quad (29)$$

from Eq.(21), p varies in each interval between zeros of $1/f_{E0}$ and f_{E0} from Eq.(26) for the E_{0m} (TM_{0m}) modes and

$1/f_{110}$ and f_{110} from Eq.(27) for the H_{0m} (TE_{0m}) modes. If we denote the m th zeros of $1/f_{p0}$ and $1/f_{110}$ by p_{E0m} and p_{H0m} , respectively, the cutoff wavelength of each mode is given from Eq.(21) by

$$\lambda_{E0m} = 2\pi a_1 (\epsilon \mu - 1)^{1/2} / p_{E0m}, \quad \lambda_{H0m} = 2\pi a_1 (\epsilon \mu - 1)^{1/2} / p_{H0m}. \quad (30)$$

Since $p_{E01} = 0$, $p_{H01} \neq 0$, only the E_{01} (TM_{01}) mode has no cutoff frequency as is well-known for the G-line.

3.2. Hybrid modes for $n \geq 1$: HE_{nm} and EH_{nm}

In the vicinity of the cutoff for $q \rightarrow 0$, Eq.(25) becomes

$$n(\epsilon \mu + 1)/p^2 + \epsilon f_{En}(p) + \mu f_{Hn}(p) = 2G_n(q) \rightarrow 2K_0(q) \text{ for } n=1 \\ \rightarrow 1/(n-1) \text{ for } n \neq 1 \quad (31)$$

for both HE_{nm} (for larger V_2) and EH_{nm} (for smaller V_2) modes. Since we have from Eqs.(15)

$$f_{En} \rightarrow (n/p^2)[(1+s^{2n})/(1-s^{2n})], \quad (32)$$

$$f_{Hn} \rightarrow (n/p^2)[(1-s^{2n})/(1+s^{2n})] \quad (33)$$

for $p \rightarrow 0$, Eq.(31) holds for $n=1$ when $p \rightarrow 0$ and $q \rightarrow 0$, simultaneously, but it does not hold for $n > 1$ when $p \rightarrow 0$. In other words, the HE_{11} mode has no cutoff frequency for $0 \leq s < 1$, but all the modes for $n > 1$ always possess finite cutoff frequencies. The upper limits of p of each mode must satisfy the equation:

$$n^2/p^4 = f_{En}(p)f_{Hn}(p), \quad (34)$$

which is obtained by making $q \rightarrow \infty$ in Eq.(25).

3.3. Numerical results

In this section, some numerical results for TM_{01} , TE_{01} , and HE_{11} modes are given for $\epsilon = 2.3$ and $a_1 = 4.2$ mm.

3.3.1. Chart of mode distributions

Based on 3.1. and 3.2., it is convenient to introduce a chart of mode distributions in a range of p for s . Fig.2 shows a distribution chart of TM_{01} , TE_{01} , and HE_{11} modes for various $s = a_0/a_1$, where the lower limit of p corresponds to cutoff. It is clear that TM_{01} and HE_{11} modes coexist as no cutoff modes ($p=0$) for $0 < s < 1$, although the upper limit of p value of each mode is different from other. With vanishing s ($s \rightarrow 0$), the characteristics of TE_{01} and HE_{11} modes approach asymptotically those of pure dielectric rod ($s=0$); the TM_{01} is still a no cutoff mode because of the current flowing in an infinitesimally thin conducting wire and does not approach that of pure dielectric rod. This is an essential difference between a dielectric coated conductor and a dielectric rod. In fact, for $s=0$

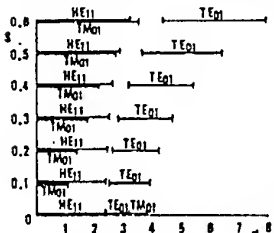


Fig. 2. Chart of mode distributions.

(pure dielectric rod), the TM_{01} mode possess a finite $p=j_{01}=2.40$ with the same range of p as the TE_0 mode, namely $j_{01} \leq p \leq j_{11} = 3.83$, although the HE_{11} mode is still a no cutoff one. In summary, the TM_{01} wave for $0 < s < 1$ and the HE_{11} wave for $0 \leq s < 1$ are no cutoff modes, and the TE_{01} mode has different cutoff wavelengths proper for different s values.

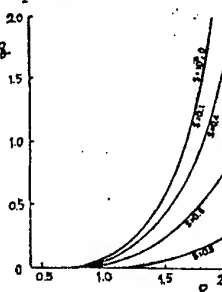


Fig. 3. HE_{11} (M-C).

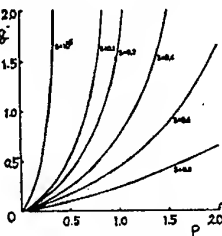


Fig. 4. TM_{01} (M-C).

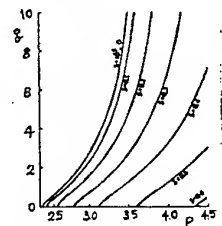


Fig. 5. TE_{01} (M-C).

3.3.3. Scale radius

Fig.6 shows an example of the scale radius - $2a_1/\lambda_0$ for TM_{01} , TE_{01} , and HE_{11} waves, assuming $a_0=1.15$ mm and $\sigma=5.8 \times 10^7$ S/m: conductivity of copper. It is seen that the degree of concentration of the HE_{11} wave is much lower than that of the TM_{01} wave in such a way that its transmission energy tends rapidly to leak into the air with decreasing frequency from about 9 GHz ($2a_1/\lambda_0 = 0.25$) and its extent rapidly increases, eventually approaching a plane wave. For the TE_{01} wave, electromagnetic energy tends to expand to all the space below $2a_1/\lambda_0=0.76$ and to become a plane wave, but beyond the cut-off its degree of concentration increases abruptly as seen in Fig.6.

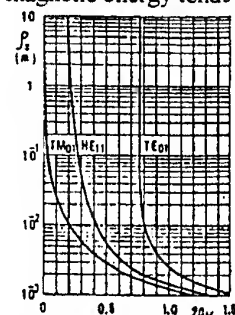


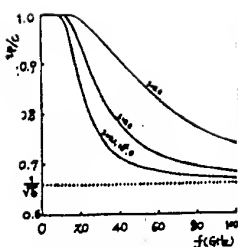
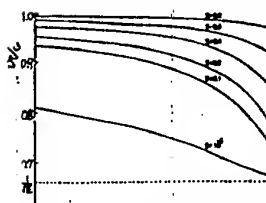
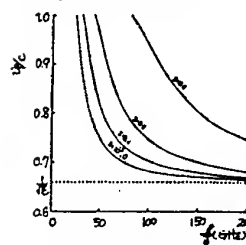
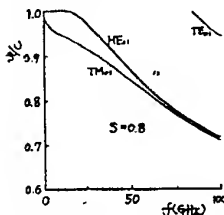
Fig. 6. Scale radius.

3.3.2. Chart of mode characteristics (M-C)

Figs.3~5 shows the characteristic p - q curves with parameter s for HE_{11} , TM_{01} , and TE_{01} modes obtained by solving Eq.(14) or (25) numerically. From these curves, one can compare a degree of field extent around the line, since q also becomes its measure, larger q indicating better concentration of the fields from the relation to the scale radius $p_s = a_1/q$ in Eq.(23). Thus, with increasing dielectric thickness, the field concentration becomes better for all three modes.

While the characteristic curves of HE_{11} and TE_{01} modes for $s=10^{-5}$ in Figs.3 and 5 coincide with those of a pure dielectric rod, respectively, the p - q curve of TM_{01} mode for $s=10^{-5}$ in Fig.4 does not agree with that of a pure dielectric rod ($s=0$), because a thin conductor still exists for $s=10^{-5}$ and a current flows in it.

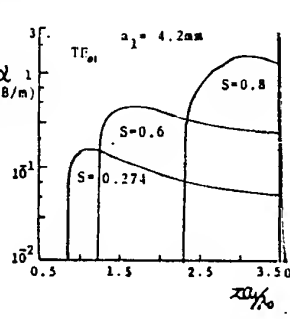
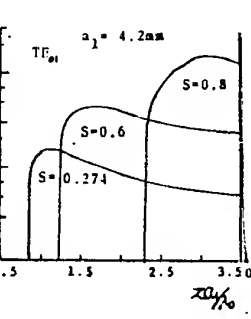
For both G- and D-lines, the scale radius increases with decreasing frequency; for a G-line, more rapidly for the HE_{11} than the TM_{01} and most rapidly for the TE_{01} mode with approaching

Fig. 7. HE₁₁(P.V.).Fig. 8. TM₀₁(P.V.).Fig. 9. TE₀₁(P.V.).Fig. 10. P.V. for $s=0.8$.Fig. 11. P.V. for $s=0.4$.

cutoff modes and their phase velocities tend to become closer with approaching a millimeter wave range.

3.3.5. Attenuation characteristics

The loss can be calculated by a perturbation method and exact formulas are lengthy and given in Ref.[1,2].

Fig. 12. P.V. for $s=0.1$. Ref.[1,2].Fig. 13. Attenuation
(conductor+dielectric losses).Fig. 14. Attenuation
(conductor loss only)

its cutoff; for a D-line, more rapidly for the TM₀₁ than the TE₀₁ with approaching a common cutoff and most rapidly for the HE₁₁ mode.

3.3.4. Phase velocity (P.V.)

Figs. 7~9 shows frequency characteristics of normalized phase velocities with a parameter s for HE₁₁, TM₀₁, and TE₀₁ modes. For each mode, the lower the frequency or the thinner the dielectric layer, the greater the field extent, the phase velocity approaching that of a plane wave, c in the air. Conversely, the higher the frequency or the thicker the dielectric layer, the better the field concentration, the phase velocity approaching that of a plane wave $c/(\epsilon\mu)^{1/2} = c/(e)^{1/2}$ in the dielectric.

Figs. 10, 11, and 12 show the phase velocities for $s=0.8$, 0.4, and 0.1, respectively, for HE₁₁, TM₀₁, and TE₀₁ waves. HE₁₁ and TM₀₁ waves are no

Figs. 13 and 14 show the attenuation characteristics for HE₁₁, TM₀₁, and TE₀₁ modes for $a_0=1.15$ mm and $a_1=4.2$ mm, including both conductor and dielectric losses ($\sigma=5.8\times 10^7$ S/m, $\tan\delta=3\times 10^{-4}$) and for the TE₀₁ mode with parameter s (changing a_0) taking into account only conductor loss with no dielectric loss. It is interesting to see in Fig. 14 that the conductor loss of the TE₀₁ mode exhibits a maximum just beyond the cutoff and tends to decrease with increasing frequency in contrast to a conducting circular tube. Practically, however, the attenuation increases monotonically with increasing frequency due to an additional dielectric loss for the TE₀₁ mode as well as for TM₀₁ and HE₁₁ modes, as shown in Fig. 13.

4. TM₀₁ MODE OF G-LINE WITH A THICK DIELECTRIC LAYER AND ITS DISTRIBUTED PARAMETER LINE REPRESENTATION

Goubau's solution of the TM₀₁ mode is only an approximation for a thin dielectric layer. In this Section, more exact solutions for a thick dielectric layer are given analytically and numerically and compared with his solution. A distributed parameter line representation of the TM₀₁ mode is also given for a lossy G-line.

4.1 Characteristic equation and exact solutions

A rigorous characteristic equation of the TM₀₁ mode for a lossy G-line with a thick dielectric layer can be written, instead of Eq.(26), as

$$qK_0(q)/K_1(q) = -j2\pi a_1^2 \omega \epsilon_2 Z_i, \quad (35)$$

where Z_i is the internal impedance of the line and can be expressed, taking into account the conductor and dielectric losses, as

$$Z_i = [(1+j)/(2^{3/2}\pi a_0)](\omega\mu_0/\sigma_0)^{1/2} + (j\omega\mu_0/2\pi)\{1-(\epsilon_0/\epsilon_1)(1+j\tan\delta)\}/\ln(a_1/a_0). \quad (36)$$

When the dielectric is not too thick, i.e. $|q| \ll 1$, Eq.(35) is simply written as

$$\xi \ln \xi = \eta, \quad (37)$$

where

$$\xi = \xi_r - j\xi_i = (\gamma q/2)^2, \quad \eta = -\eta_r + j\eta_i = j\pi r^2 \omega \epsilon_1 a_1^2 Z_i, \quad (\eta_i \ll \eta_r) \quad (38)$$

and there is a relation between q and the propagation constant Γ :

$$\Gamma = \alpha + j\beta = jk_0[1+(q/k_0 a_1)^2]^{1/2}. \quad (39)$$

Substitution of Eqs.(38) in Eq.(37) yields

$$\xi_r \ln \xi_r = -\eta_r, \quad (40)$$

$$\xi = \xi_r + (j\eta_i)/(\ln \xi_r + 1) = \xi_r - (j\xi_r \eta_i)/(\eta_r - \xi_r), \quad (\xi_r < \eta_r). \quad (41)$$

Substituting Eqs.(38) in Eq.(39), we obtain

$$\alpha = (2/\gamma^2) \cdot (\xi_r \eta_i) / \{ k_0 a_1^2 (\eta_r - \xi_r) \}, \quad (42)$$

$$\beta = k_0 [1 + (2/\gamma^2) \cdot \{ \xi_r / (k_0 a_1)^2 \}] \text{ or}$$

$$v_p = c [1 - (2/\gamma^2) \cdot \{ \xi_r / (k_0 a_1)^2 \}]. \quad (43)$$

4.2. Equivalent distributed parameter line

Incorporating the external impedance of the line, Z_e to Eq.(36), the series impedance and the parallel admittance of the line for the TM_{01} mode can be expressed as

$$Z = R + j\omega L = Z_i + Z_e = Z_i + \{j\omega \mu / (2\pi)\} \ln \{2 / (\gamma q)\}. \quad (44)$$

$$Y = G + j\omega C = j2\pi\omega\epsilon / ln \{2 / (\gamma q)\}, \quad (45)$$

$$\Gamma = \alpha + j\beta = (ZY)^{1/2}, \quad Z_0 = (Z/Y)^{1/2}, \quad (46)$$

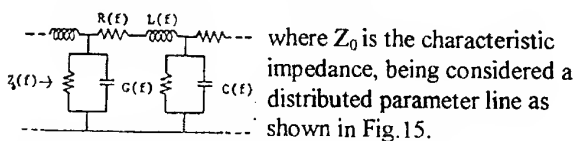


Fig. 15. Equivalent circuit. Figs. 16 and 17 shows frequency characteristics of the attenuation and normalized phase velocity of the TM_{01} mode obtained from various solutions in comparison for a polyethylene coated copper

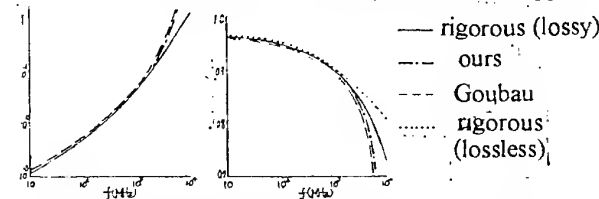
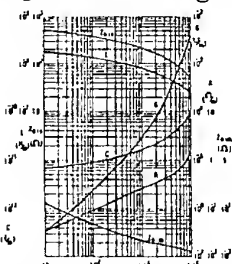


Fig. 16. Attenuation. Fig. 17. Normalized phase velocity. wire ($\epsilon = 2.3$, $\tan\delta = 10^{-3}$, $a_0 = 1.15$ mm, $a_1 = 4.2$ mm, $\sigma_c = 5.65 \times 10^7$ S/m). The solid and chain lines refer to a rigorous solution obtained from Eq.(35) and our exact solution from Eqs.(42) and (43) and the large broken line refers to Goubau's solution, while the small broken line in Fig. 16 refers to a rigorous solution for lossless case.



It is seen that our exact solution well coincides with a rigorous solution below 2 GHz, while Goubau's solution is somewhat larger in attenuation and somewhat smaller in phase velocity, deviating from a rigorous solution with increasing frequency.

Fig. 18. Circuit parameters. In contrast to his rather tedious procedure of re-peating several graphical solutions, our method is extremely simple, since the analytical solution is already available in Eqs.(42) and (43) and a graphical solution is also obtained immediately by using a sheet of graph. Fig. 17 represents the frequency characteristics of various circuit parameters, R , L , G , C , and Z_0 .

7. CONCLUSIONS

A unified treatment for S-, D-, and G-lines is now a-

available on the basis of a rigorous theory of thickly dielectric-coated conducting wire (G-line) where ($s = 0$ or $s \rightarrow 0$) or ($s = 1$ or $s \rightarrow 1$) goes to a D- or S-line, respectively.

It has been proved that charts of mode characteristics and distributions are most useful for a comparative survey of various modes for different lines in size and structure.

While a thickly dielectric coated G-line has two no-cutoff modes, TM_{01} and HE_{11} , an exact and simple solution and a network representation have been obtained for the TM_{01} mode.

Although the field extent around lines can be estimated from the 'scale radius' and the effects of a ground on the TM_{01} mode have been well established for both S- and G-lines, its effects on the HE_{11} mode are still largely open for both G- and D-lines and on both TM_{01} and TE_{01} modes for a D-line.

8. REFERENCES

- 8.1. H. Kikuchi and E. Yamashita, "Theory of Dielectric Waveguides and Some Experiments at 50 GHz", *Proc. of the Symposium on Millimeter Waves*, Polytechnic Institute of Brooklyn, New York, March 31, April 1-2, 1959, pp.619-638.
- 8.2. H. Kikuchi and E. Yamashita, "Hybrid Transmission Modes of Goubau Line" (Japanese), *J. of the Institute of Electrical Communication Engineers of Japan*, vol.43, No.1, 1960, pp.39-45.
- 8.3. G. Goubau, "Surface Waves and Their Application to Transmission Lines", *J. Appl. Phys.*, Vol.21, No.11, 1950, pp. 1119-1128.
- 8.4. D. Hondros and P. Debye, "Elektromagnetische Wellen an dielektrischen Räumen", *Ann. d. Phys.*, Vol.32, No.6, 1910, pp.465-476.
- 8.5. H. Kikuchi and E. Yamashita, "Theory of Dielectric Rod Waveguide and Its Experiment at 50 GHz" (Japanese), *Bulletin of the Electrotechnical Laboratory of Japan*, Vol.22, No.10, 1958, pp. 752-768.
- 8.6. A. Sommerfeld, "Fortpflanzung elektrodynamischer Wellen an einem zylindrischen Leiter", *Ann. Phys. Chem.*, Vol.67, 1899, pp.233-290.

BIOGRAPHICAL NOTES

Hiroshi Kikuchi received Ph. D. degree from University of Tokyo in 1959 and was Chief, Ultramicrowave Laboratory of Electrotechnical Laboratories, MITI until 1961. Before his return to Japan as Professor of Nihon University, Tokyo in 1973, he worked with University of Oxford and several Institutes. He was Chairman, URSI Commission E (1987-1990) and is Life Fellow of IEEE.

Shuichi Fukuda received M.S. degree from Nihon University in 1976 and now works with Soga Patent Office, Tokyo.

III

**BIOLOGICAL EFFECTS
OF EM RADIATION**

EXPOSURE OF THE GENERAL PUBLIC AROUND POLISH TELECOM TRANSMITTING STATIONS

Fryderyk Lewicki
Polish Telecom, R & D Division, Powstancow Slaskich 134
50-940 Wroclaw, Poland

Exposure on electromagnetic radiation is a big public problem in our times. In the last years all Polish Telecom Transmitting Stations (PTTS) have launched new additional emissions: FM, UHF TV and mobile systems. In the result the levels of radiation around PTTS are increased.

Polish Telecom (TP S.A.) as the biggest FM and television broadcast operator in Poland, carry an extensive program of complex analysis of radiation situations around (PTTS). In this program resultant electric field strength (in the frequency range 10 MHz + 300 MHz) and power flux density (in the frequency range 300 MHz + 300 GHz) are calculated for the purpose of comparing the results with Polish environmental protection regulations.

Such analysis brings TP S.A. knowledge how many new additional emissions can be held on each PTTS also.

In this paper it is shown that exposure limits around PTTS are satisfied, but in many cases it was achieved by modification of the antenna system radiation patterns. Earlier it was necessary to find out the antenna system which is mostly responsible for the exceeding permitted level of radiation. Modifications were done for the purpose to decrease the radiation near antenna towers with no changes of coverage areas.

1. INTRODUCTION

Radio frequency radiation can cause health hazards. In Poland occupational and public exposure limits are stronger than in other countries. Limits for public exposure are: 2 V/m of resultant field strength in the frequency range 10 + 300 MHz, and 0,025 W/m² of resultant power flux density in the frequency range 300 MHz + 300 GHz [1, 2, 3, 5]. According to Polish regulations in each frequency range resultant radiation should be considered separately.

Typical high power PTTS carry more than ten emissions: FM in OIRT and CCIR bands (from 3 + 10 emissions), television in VHF (usually one emission) and UHF (from 1 to 6 emissions). Additionally Base Stations of Paging, Trunking and Cellular systems are in operations on PTTS. All this emission has to be taken into account in resultant radiation calculation [5]. Such a situation in which more than 10 emissions are radiated from one antenna tower is not typical in other countries. If we add very restricted regulation of environmental protection for radiation limits, situation in Poland is unusual.

Resultant radiation around each PTTS is calculated and measured. Calculations are performed in the TP S.A. Research & Development Division, and they are important specially before any new investment process. After antenna system construction any modification in emission parameters (in most

case's modification of the antenna systems radiation patterns) is very difficult or impossible. If the problem with too big radiation on existing PTTS appears, such a consideration is very useful too.

Measurements are very important in order to verify calculation, and according to Polish regulations are done in all cases by independent to TP S.A. authorities.

2. RADIATION AROUND TYPICAL PTTS

On figure 1 example of resultant field strength (and each of its radiation components) around one of the PTTS is shown for the frequency range 10 + 300 MHz (originally each component is drawn in different colour). Field strength was calculated on 2 m above terrain level, in the distance from 10 m to 1400 m from the antenna tower, on the one azimuth direction.

We can see that FM emissions have highest influence on the resultant field strength. Emissions from the mobile systems have comparatively low level and can be neglected. In the distances about 100 m from the antenna tower level 2 V/m is exceeded.

On figure 2 example of resultant power flux density, around one of the PTTS is shown for the frequency range 300 MHz + 300 GHz. Power flux density was calculated on 2 m above terrain level, in the distance from 10 m to 1400 m from the antenna tower, on the one azimuth direction.

We can see that TV UHF emissions have highest influence on the resultant power flux density, but in all range of distances' exposure limits are not exceeded. The ranges of distances in which radiation level is relatively high are very short (in oppositions to FM emissions shown on fig 1). Maximum of each emission is placed in different distance from the antenna tower, that is additionally very profitable from the environmental protection point of view. Emissions from the mobile systems can be neglected as in lower frequency range.

Diagrams shown on figures 1 and 2 are very useful. They allow to consider which component of radiation brings highest influence on the resultant radiation. In case in which radiation is higher than limit for public exposure, diagrams show which antenna system should be modified to meet the regulations. For example in fig. 1 it is obvious that FM CCIR antenna system should be modified. Computer simulation of many modifications of the antenna system (its vertical radiation pattern) is possible and allows to find the best solution.

Results of calculations were compared with results of the measurements done by independent to TP S.A. authorities. Compliance results of calculations and measurements are better than good.

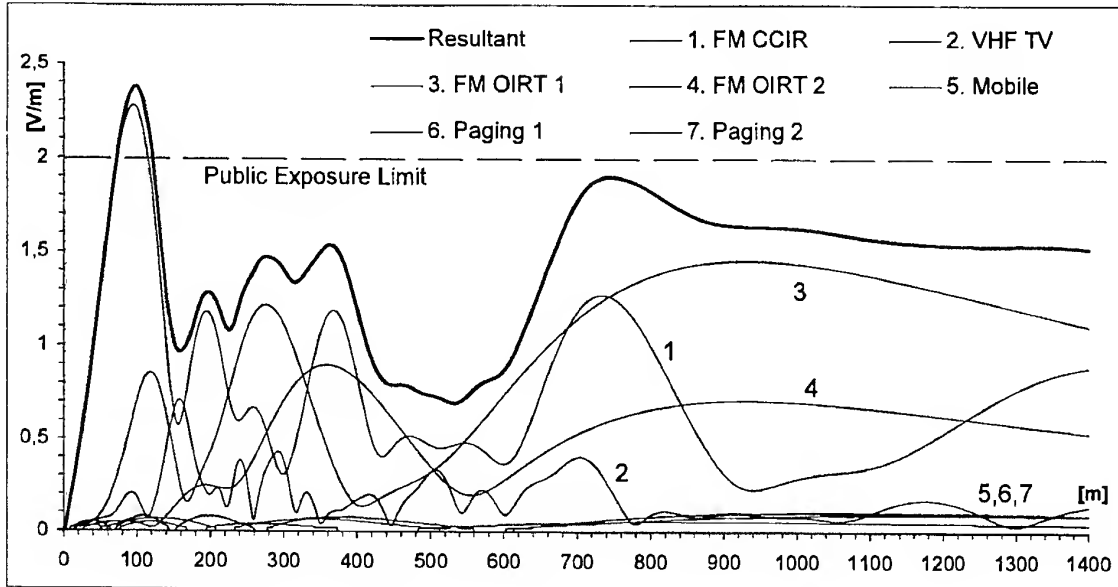


Fig. 1. Radiation around PTTS (10-300 MHz).

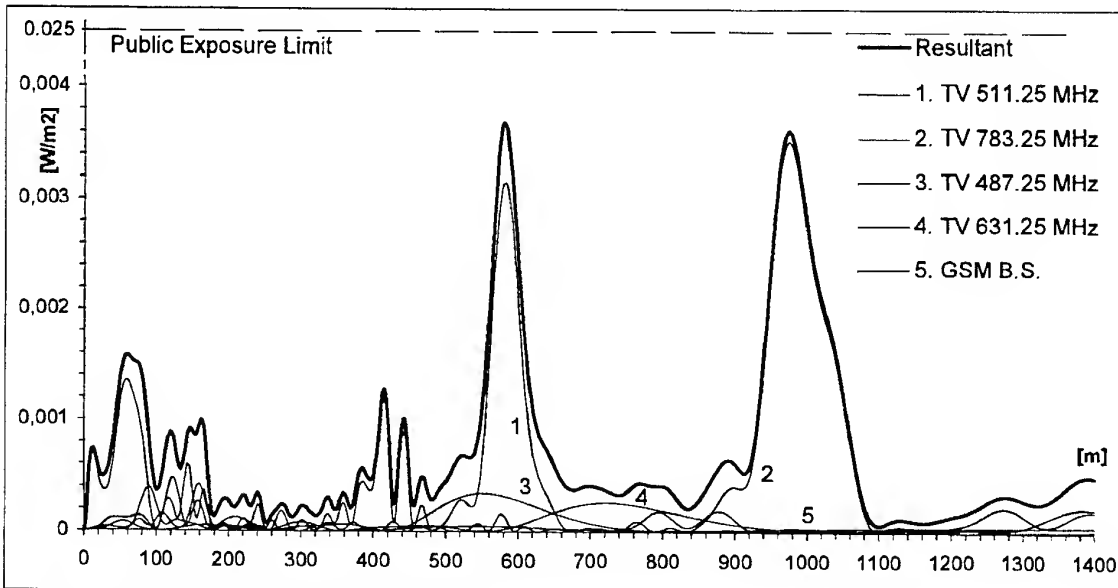


Fig. 2. Radiation around PTTS (300 MHz-300 GHz).

3. COMPARISON FOR CONSIDERED PTTS

During last five years detailed calculations were done for more than 25 PTTS. In this number are high and low powers transmitting stations. Because of complexity of the electromagnetic field that has to be considered, with many radiation's on many different frequencies, radiated from many different antenna systems, each case had to be considered separately.

It is interesting that highest level of radiation's not always appear around high power PTTS. High power antennas have high gain and bigger part of the energy is radiated above terrain around antenna tower to the horizon. Low power PTTS has mainly low gain antenna systems and comparatively big part of energy is radiated in the area near antenna tower.

All considered cases can be divided into three categories dependent of resultant radiation level:

- it is lower then limits in national regulations
- it is higher then limits, but only in the area with no residents
- it is higher then limits in area with residents.

Last cases are required changes of emission parameters.

Comparison of the results from analysis done until now, gives very interesting information about exposure of general public around PTTS. In the table 1 and 2 results of considerations are put together for both frequency ranges.

Results contained in the tables 1 and 2 show that in the frequency range 10 - 300 MHz problems with to high resultant radiation level is much grater. In this range many emissions have big and similar influence on the resultant field strength. (see fig. 1). Configurations of the antenna systems on six PTTS were modify only for the reason to meet national regulations on health hazards. One antenna system was replaced by new one. Two other cases are still under considerations.

Table 1. Frequency range 10 ÷ 300 MHz

Number of PTTS		
Radiation lower than national limit	Radiation exceed limit, but in area with no residents	Radiation exceed limit in area with residents
7	11 6*	2**

* - after modification of the antenna systems according to TP S.A.
R & D projects

** - antenna systems under modification

Table 2. Frequency range 300 MHz ÷ 300 GHz

Number of PTTS		
Radiation lower than national limit	Radiation exceed limit, but in area with no residents	Radiation exceed limit in area with residents
22	4 2*	-

* - after modification of the antenna systems according to TP S.A.
R & D project

Changes in feeding arrangements of the antenna system in many cases are sufficient modifications of antenna system configuration. In this way vertical radiation pattern is modified. In more complex cases, new bays are added to existing antenna systems in purpose to increase antenna gain and to radiate more energy above area around antenna tower. In such a case additionally transmitter power is decreased with no changes with ERP, so effect of changes is doubled, but such a solution is expensive and needs free space on the tower.

Much better situations is in the 300 MHz ÷ 300 GHz frequency range. It is mainly because in this range only UHF television emissions have substantial influence on resultant power flux density (see fig. 2). In this range only two antenna systems needed modifications, one of them during earlier planned replacement (after 25 years of operations).

Program is not finished yet and new results are coming all the time. New calculations are needed also, because licences for new additional emissions are still issued.

Measurements around PTTS were done by the independent to Polish Telecom authorities. Results of measurements and calculations are very close to each other, so implemented methodology of calculation is good.

After so many examples of problems with health hazards around transmitting stations, TP S.A. now consider each new investment very carefully from health hazards point of view. Calculations of resultant radiation level in area around antenna systems are carried for each new planned antenna system before technical specification for tender is prepared. During tender procedure level of antenna system radiation in the area near the antenna tower is one of the most important factors.

From the other hand problems with health hazards around transmitting stations in Poland are so big because of very strong limits of radiation. If the national regulations in Poland are closer to INIRC guideline [1] or European proposals [2], problem will be not so important.

4. CONCLUSIONS

Polish Telecom has many (high and low power) transmitting stations. In Research and Development Division of Polish

Telecom the radiation levels in area around antenna towers are calculated. Comparison with measurements done by independent authorities proofs that calculation methodology is proper.

Results obtained for area around many PTTS shows, that in many cases' antenna systems need modifications, because radiation levels are exceeded limits in national, very restricted regulations. Such modifications were done successfully in all considered until now cases. Results are good because calculation methodology makes possibility to find which emission is mostly responsible for exceeding the allowed level of radiation.

Problems are bigger in 10 ÷ 300 MHz frequency range, because of much more broadcast emission in this band. Emissions from the mobile systems base stations are comparatively very low and can be neglected.

New emissions are still issued in Poland and in many cases optimal localisation of them is on existing PTTS. For many PTTS strong national limits of radiation made it expensive (antenna systems modification or even replacement) or even impossible. Change of the exposure limits (to make them close to suggested in INIRC guidelines) is reasonable, because in the literature we have no justification for such restrictive regulations.

5. REFERENCES

- 5.1. Guidelines on Limits of Exposure to Radio Frequency Electromagnetic Fields in the Frequency Range 100 kHz to 300 GHz, Health Physics, Vol. 54, No 1, Jan. 1988, pp 115-123.
- 5.2. ENV 50166-2, Human exposure to electromagnetic fields. High frequency (10 kHz to 300 GHz), CENELEC, Brussels 1995
- 5.3. IEC 61566, Measurement of exposure to radio-frequency electromagnetic fields - Field strength in the frequency range 100 kHz to 1 GHz, Geneva 1997.
- 5.4. W. Segal, A. Marszałek, An Environment Analysis of Broadcasting Network in VHF/UHF Band Based on Test Points Concept, XI International Wrocław Symposium on EMC, Wrocław, Poland 1992.
- 5.5. F. Lewicki, Solutions of the Problem with Assigned ERP Utilisation, XIII International Wrocław Symposium on EMC, Wrocław, Poland 1996.

BIOGRAPHICAL NOTE

Dr. Fryderyk Lewicki was born in 1956. He received M.Sc., and Ph.D. degrees from the Technical University of Wrocław, Poland in 1980 and 1985 respectively. He is also a graduate at seven telecommunication programs provided on the United States Telecommunication Training Institute in Washington. Since 1985 he has been employed at the Research and Development Division of Polish Telecom where at present he is Wrocław Branch Manager. His main interest concern: telecommunication systems, antenna systems, computer aided technique in telecommunication and health hazards caused by electromagnetic fields. He is the author of several technical papers and reports. He is a member of the IEEE.

INVESTIGATION OF INFLUENCE OF THE NON-HEATING MILLIMETRE WAVES RADIATION ON THE LIVING CREATURES

Valentin V. Murav'ev¹, Alexander A. Tamelo¹,
Ulazimir M. Byahun¹, Nina H. Fedosova²

¹ Belarusian State University of Informatics and Radioelectronics,
vul. Petrusya Broiki 6, BLR-220027 Minsk, Republic of Belarus

² Belarusian Agricultural Academy,
BLR-223015 Gorky, Republic of Belarus

Experimental results of the non-heating millimetre wave influence at cow embryos' transplantation are describe. Results of the cow's treatment mastitis are describe also. The author's hypothesis about parametric millimetre wave influence is discussing.

Nowadays, many proprieties of millimetre wave including its vital influence on the living beings have been invent. This vital influence on the living beings is also mention. The energy of quantum of wave band is being compared with the energy gaps of cell spectral characteristic. At influence of the non-heating millimetre wave number of settle down cow's embryos is 71.43 per cent. Using this method for 4 days we have gotten milk of quality according to standard. The author's hypothesis concerning parametric millimetre wave influence was confirm.

INTRODUCTION

Still in the 18th century the german physiologist Virhov discovered that the illnesses of all organs begin with the illness of the cells. The mammal's organism consists of more than $10^{14} \dots 10^{15}$ cells. Brain cannot operate efficiently such great number of cells. This fact proposed an idea that the cell brings itself into the healthy state. Inspire of the fact that the way to the treatment is in the cell itself, effective of the treatment has the sense when the cell is capable of its functions' renewal.

The professor of the Liverpool University Fröhlich supposed that the ill cell radiates accost-electric vibrations in the wide frequency spectrum including millimetre wave. The first experiments were make with the yeast culture. Yeastes were radiate with the electromagnetic waves (EMW) of 42 GHz freelance. It was founding out that the speed of the cell's division increased. When the cell is ill,

electromagnetic vibrations appeared in the surface of the membrane. Interaction of the millimetre outside oscillation with the membrane surface process resulted in spatial extraction of the albumen structures from the cell's depth. This process returns cell to its natural statement.

During the evaluation, development of the animate nature, nature used electromagnetic vibrations for the information exchange on the cell's level. The electromagnetic vibrations of the millimetre diapason are maximum reduced in passing through the Earth's troposphere. On the surface of the body the millimetres waves reduce 10^{12} times (120dB). The experiments of the millimetre oscillation influence were make on the mice and rats. The mice and rats were process with the non-heating dozes of millimetres waves and they survived after they had been expose to the X-rays. The application of the microwaves' oscillations gives positive results in the treatment of such man's illnesses as stomach and duodenum ulcer, immune system illness, anaemia, stenocardia, some other illnesses. Thus, the using only non-heating dozes of millimetres waves is not always effective for the treatment. That is why complex influence of the low frequency (LF), of the extremely high frequencies (EHF) for both millimetre wave and infrared frequency (IF) oscillations' ware proposed.

Mentioned influence is very effective. The cell's energy balance, except energy transformation from one state to another, contains also small part or the losses and energy spent for the radiation. The part of the radiation energy increases if the cell is ill. In the literature there is some information about complex influence of the EMW radiation, in particular complex using of the IF, EHF and LF oscillations. The joint using of IF, EHF and LF oscillations as the biological influence is very effective method in the treatment of

many illnesses and growing of the high-productive strains of cattle.

1. WORKING OUT OF THE HYPOTHESIS CONCERNING INFLUENCE OF THE EMW THERAPY

The scientific and practical research in the sphere of the EMW therapy began with the treatment of the cow's mastitis. The problem concerning mentioned illness is still actual and difficult. In spite of the constant improvement of the milking equipment and working out of the new methods of prevention, diagnostics and therapy, this illness is consider to be one of the most spread.

The most spread form of the mastitis is mastitis without showed symptoms or closed form. According to the International milking federation, only 3 per cent of ill cows has shown symptoms and 52.0 per cent of ill cows does not have any symptoms of mastitis.

The milk gland processing was make in the morning and in the evening for 3 days. The sample of milk was take before and artier processing. Received results were process with the help of the statistic and correlation analysis. The cows are continue to be observe and clinic examination and milk analyses are take place.

During the microbiological examination of the cow's milk gland was found out that 17-38 per cent of all the micro-organisms is of spherical form, 3-42 per cent — staphylococcus, 58...80 per cent — milk-lactic micro-organisms. At the examination of the cow's without shown symptoms putrefactive microflora was founding also.

After the first processing the composition of the gram-negative forms of the micro-organisms decreased. The concentration of the micro-organisms was decreasing constantly and on the 3rd day the single gram-positive forms of the micro-organisms appeared.

That means, that after processing of the cow's milk gland with our devices positively influenced on the microbiological composition of the milk gland and promotes its recovery. *On the 4th day it is possible to receive milk of good quality.*

2. WORKING OUT THE WAYS OF THE QUALITY AND VIABILITY IMPROVEMENT OF THE CATTLE'S EMBRYOS

One of the modern achievements in the field of biology that attracting scientists of the world is embryoengineering. Embryoengineering is the active recombination of the cattle's genom at early stages of the ontogenesis. This method includes embryo's

reconstruction by the merging or direct injection of the strange genes to their nucleus.

An important role of the embryo's transplantation in the cattle-breeding belongs to the opportunity of receiving the great number of the progeny from females of high genetic potential. The hormone donors processing — the condition of the superovulation— has made possible receiving dozens of the calves from the one female a year. The embryo's transplantation method is very important because of the following genetic programs realisation:

- rapid receiving of the valuable families;
- rapid receiving of the lines and types in the usual herds;
- spreading of the mutant genes in the strains of cattle (illness resistance, for instance);
- extracting of the "bad" genes out of the herds.

2.1. The ways of raising of the viability and getting accustomed to the receptor's organisms

The most difficult problem in the sphere of the embryo's transplantation is receiving the great number of the embryos from the genetically valuable cows-donors. Cultivation and fecundating of the oocytes in vitro and further receiving of the cow-donor embryos are possible method of solving this problem

Three series of the experiments' ware put. All embryos were divide into two groups. First group are contain of the embryos of an excellent and good quality. Second group was satisfactory quality. Each group was divide into two sub-groups. First subgroup was process by the EMW for 2 minutes (1st series), than 5 minutes (2nd series) (Fig.1) and 10 minutes (Fig.2). Second subgroup was not process by EMW. Criterion of the effectiveness of the EMW influence was embryos' estimations that included morphological indices and being accustomed to the receptor's organism. The estimations were compare with the estimations of the resembling parallel groups without EMW influence(control).

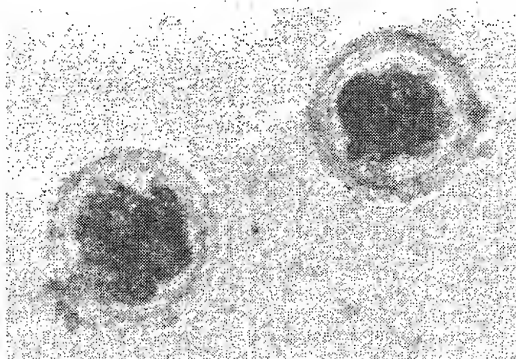


Fig. 1.

influence of the EMW on biosystems what means that regeneration processes take place in the cells.

REFERENCES

- [1]. Valentin V. Murav'ev, Alexander A. Tamelo, Uladzimir M. Byahun, Nina H. Fedosova. Investigation of Action of the Non-Heating Millimetre Wave Radiation on Animal.// IEEE AP-S/URSI International Symposium, Montreal, Canada, July 13-18, 1997, p.660.

Fig. 2.

Indices that efficiency of the embryo's transplantation after 10 minutes EMW influence is excellent.

Groups	Embryo's quantity	Embryo's quality	Receptors quantity	Cow with calf in 3 months quantity / per cent
experiment	14	excellent and good	14	10 / 71.42%
control	12	excellent and good	12	8 / 66.6%
experiment	9	satisfactory	9	4 / 44.4%
control	10	satisfactory	9	3 / 33.3%

We found out the tendency of rising embryos' viability and being accustomed after using EMW. The effectiveness depends on embryo's quality. This fact assures us to continue research work in this direction.

SUMMARY

The methods of the complex influence of the electromagnetic fields for embryos cultivating, their quality improvement was work elaborate. The device appreciated in practise for cows with high indices' reproduction was elaborate. This device uses non-heating millimeter wave. The index of fecundating after which 46.2 per cent of the oocytes could be transplant is reach. Influence of the EMW on the embryos increased their being accustomed to the receptor's organism. Index of embryos being accustomed of 71.42 per cent was receive. Our experiments confirmed our hypothesis about parametric

THE INFLUENCE OF AN ALTERNATIVE MAGNETIC FIELD ON THE QUALITY OF CEREAL SEEDS

Małgorzata Rochalska

Department of Plant Breeding and Seeds Science
Warsaw Agricultural University, Nowoursynowska 166 02-787 Warszawa.

In this paper the results of experimental investigation of biological effects of alternating magnetic field on the seeds of wheat and triticale are presented. Stimulating effect of seeds irradiation in laboratory condition and field experiment is shown.

1. INTRODUCTION.

Both the increasing competition on the seed market and the increase of demands of the seeds customers create necessity of continual improvement of seeds quality. This implicates the research on new ways of improving of the quality of sowing material. On the other hand seed collections are looking for the way of prolongation of the vivacity of kept seeds to avoid the necessity of frequent sowing. A lot of different methods of improvement the quality of sowing material after harvest were worked out (for example washing, conditioning) [1]. One of the factors was a magnetic field. Magnetic field was used in general for improvement of cereal seeds quality but also for seeds of oil plants or potatoes [2,3,4]. The effect of magnetic field was generally profitable but in some cases it was no effect at all and even a decrease of the yield [5]. Therefore it seems to be necessary to do the further research on the influence of the magnetic field on the quality of agricultural plants seeds. It concerns in particular seeds with low quality parameters (for example old seeds).

2. MATERIALS AND METHODS.

Commercial seeds of spring wheat cultivar Sigma and spring triticale cultivar Jago were used for experiment. Seeds were harvested in 1991 and 1994 year. Air-dry seeds were treated with alternative magnetic field of low frequency (16 Hz or 50 Hz) during 2 hours. Magnetic flux density was 5 mT. Magnetic field generator was constructed by Technical University in Wrocław. Generator pro-

duces a homogenous magnetic field of frequency 16 Hz or 50 Hz and strictly determined magnetic flux density. The construction of this generator allows to eliminate electric component of field and enables treatment of seeds only with alternative magnetic field. Seeds previously treated with magnetic field were examined with following laboratory tests:

- laboratory germination test according to Polish Standard PN 79/R-65950,
- indication of mean time of germination of single kernel (Pieper's coefficient),
- indication of length of epicotyl and hypocotyl of seedlings grown from treated seeds at optimal temperature (20°C) and optimal quantity of water in germination substrate in roll test.

Tests started 19 days after seeds treatment with alternative magnetic field.

Kernels of the same species, cultivars and years of harvest not treated with alternative magnetic field were used as the control. Kernels of examined species and cultivars 19 day after irradiation with alternative magnetic field were sown in the experimental field of Department of Plant Breeding and Seeds Science in Żelazna (nearby Skierniewice) in the spring of 1995 year in plot experiment. There were sown 100 kernels for each plot in 3 replications.

During vegetation season following characteristics were examined:

- rate of emergence,
- mean time of emergence of single kernel (Pieper's coefficient),
- time of individual phase of development of plant (for example tillering and heading),
- biometrical characteristics of plant during vegetation such as length of plants, number of culms and length of ears,
- characteristics measured after harvest important for crop such as number of productive ears, number of kernels per plant, weight of kernels per plant, thousand kernel weight.

After harvest characteristics measured earlier biometrically during vegetation were examined for the plants.

Plants were harvested and threshed by hands. Plants of the same species, cultivars grown from the kernels of the same year of harvest not treated with alternative magnetic field, grown in the same field were used as a control.

The time between irradiation with magnetic field and experiments - 19 days- was chosen on

the base of literature date concluding the fact that optimal influence of magnetic field for kernel appears from ten to twenty days after irradiation the same as in preliminary self-experiments.

The results were elaborated statistically with using the ANOVA 1 program. The lowest significant differences (LSD) were calculated with Student's test at the significance level $p = 0,01$ for laboratory experiments and the significance level $p = 0,05$ for field experiments.

3. RESULTS AND DISCUSSION.

Table 1

Seeds germination and seedlings growth of spring wheat Sigma and spring triticale Jago after treatment of seeds with alternating magnetic fields (19 days after treatment).

Year of seed harvest and treatment conditions	Laboratory germination capacity (%)		Pieper's coefficient (days)	Length of epicotyl (cm.)	Length of hypocotyl (cm.)
	4 days	7 days			
Sigma 1991 control	96.33	97.33	2.31	14.16	9.99
16Hz	97.33	97.33	2.06*	15.50*	12.08*
50Hz	99.00	99.00	2.13*	15.58*	11.89*
LSD	5.01	2.68	0.16	1.19	1.03
Sigma 1994 control	92.00	94.00	2.25	13.20	11.05
16Hz	95.33	96.67	2.17	12.53	12.68
50Hz	95.67	96.33	2.16	13.19	11.67
LSD	8.13	6.64	0.21	0.78	2.34
Jago 1991 control	93.33	94.44	2.26	14.60	23.95
16Hz	100.00*	100.00*	1.71*	17.26*	29.89*
50Hz	100.00*	100.00*	1.91*	18.79*	33.39*
LSD	4.36	2.96	0.30	1.95	2.09
Jago 1994 control	100.00	100.00	2.10	15.76	26.82
16Hz	95.20	97.10	2.19	18.35*	37.41*
50Hz	100.00	100.00	1.77*	19.06*	34.66*
LSD	5.07	4.22	0.39	0.69	1.61

*- statistically significant differences

LSD- lowest significant differences

Table 1 presents the results of laboratory tests of spring wheat cultivar Sigma and spring triticale cultivar Jago. As you can see from these results alternative magnetic field did not influence germination capacity of wheat fresh kernels (harvested in 1994 year) as well as old kernels (harvested in 1991 year). Magnetic field on the other hand shorted the mean time of germination of single kernel of old seeds and lengthened epicotyl and hypocotyl of seedlings grown out from them. There was influence on these characteristics of fresh kernels. Old kernels (harvested in year 1991) of

spring triticale cultivar Jago irradiated with alternative magnetic field germinated better in comparison to the control. Germination capacity of fresh kernels did not differ significantly from the control. In both fresh and old seeds the treatment with magnetic fields shortened of the time of germination of single kernel and lengthen of epicotyl and hypocotyl of seedlings grown out of them. Kernels examined 1 day after irradiation with alternative magnetic field did not differ from the control in all described characteristics. It concerned fresh seeds as well as old seeds both of examined species.

Table 2.

Rate of emergence and development of plants of spring wheat Sigma and spring triticale Jago grown from seeds sown 19 days after irradiation.

Year of seeds harvest and treatment conditions	Rate of emergence (%)			Pieper's coefficient (days)	Tillering (%)		Heading (%)	
	7 days+	14 days+	20 days+		29 days+	35 days+	46 days+	64 days+
Sigma 1991 control	47.33	51.83	53.17	7.92	7.67	27.33	44.00	52.33
16Hz	75.11*	80.44*	82.00*	7.70	22.67*	56.67*	81.11*	87.78*
50Hz	73.87*	78.00*	79.78*	8.06	11.11*	41.11*	68.44*	78.00*
LSD	6.72	5.02	6.83	1.94	8.94	11.15	7.31	9.19
Sigma 1994 control	67.67	69.00	69.50	7.32	10.50	28.83	62.83	64.33
16Hz	74.00	79.11	81.56	7.46	24.44*	58.44*	80.22*	85.33*
50Hz	70.22	74.22	77.56	7.91	13.34	45.33*	67.33	82.44*
LSD	17.09	17.26	18.19	0.85	8.62	12.26	11.27	11.34
Jago 1991 control	15.33	16.17	18.00	8.63	9.67	19.67	6.67	19.50
16Hz	25.33*	30.89*	34.44*	9.40	21.55*	29.11*	9.33	30.89*
50Hz	25.55*	31.33*	33.34*	9.26	17.78*	25.11*	10.89	33.33*
LSD	6.88	5.24	5.92	1.98	5.87	4.36	5.31	4.73
Jago 1994 control	52.17	56.17	59.33	8.17	42.50	52.33	6.00	53.83
16Hz	63.11*	72.67*	76.22*	8.43	43.56	63.55	13.11*	70.67*
50Hz	67.56*	73.11*	79.78*	8.57	52.44	58.89	11.11*	77.98*
LSD	8.37	5.62	6.82	0.89	12.20	16.20	7.16	15.54

+- days after sowing

*- statistically significant differences

LSD- lowest significant differences

Table 2 shows the results of examination of field emergence and on the bases of tillering and heading plants development phases of spring wheat cultivar Sigma and spring triticale cultivar Jago grown out of seeds sown 19 days after irradiation with alternative magnetic field. It is visible the increase of the emergence in comparison from the control is significant. In the case of spring wheat statistically significant increase concerned only old kernels. In the case of spring triticale this concerned both old and fresh kernels. The increase of emergence of old kernels was more than 50% for both examined species. Date of the time of tillering and heading indicated that plants obtained from seeds treated with alternative magnetic fields developed faster than plants grow out of non treated seeds. Likewise as in the case of emergence this effect is clearer for the plants grown out of old seeds although for heading concerned also plants grown out of fresh seeds.

Weather condition during vegetation season of 1995 year (when plot experiments were made) were not suitable for crop vegetation. There was a spring drought: significant deficit of water in the soil during emergence and long periods of time (in the area of experimental field in Żelazna several weeks) without rains together with high air temperature during the summer [6]. Increase of emergence and acceleration of entering following development phases of plants growing in unfavorable for them weather conditions is the best evidence of profitable influence of alternative magnetic field on seed kernels and plants obtained from them. Not shortened mean time of emergence of single kernel (Pieper's coefficient) observed in this experiment instead of increase of total emergence could also be a result of the wrong weather condition (soil dryness) prolongating the emergence of examined seeds.

Table 3.

Crop characteristics of spring wheat Sigma and spring triticale Jago grown from seeds sown 19 days after irradiation.

Year of seed harvest and treatment conditions	Length of plants (cm)	Number of productive culms per plant	Length of ears (cm)	Number of kernels per plant	Weight of kernels per plant (g)	Weight of 1000 kernels (g)
Sigma 1991 control	88.17	2.23	9.30	54.00	1.63	28.19
16Hz	89.97	2.67	9.60	64.67	2.28	34.98*
50Hz	84.43	2.20	9.47	56.47	2.01	35.12*
LSD	3.85	0.61	0.48	23.82	0.84	5.27
Sigma 1994 control	80.23	2.20	8.77	29.97	1.01	34.58
16Hz	83.93	2.87*	9.73*	70.30*	2.54*	35.14
50Hz	81.90	3.10*	9.46*	76.13*	2.97*	37.12
LSD	3.74	0.70	0.53	22.15	0.83	4.57
Jago 1991 control	115.50	2.20	9.97	150.68	4.93	32.12
16Hz	110.00	4.30*	11.80*	311.97*	10.61*	35.18
50Hz	110.80*	4.30*	11.40*	321.83*	11.13*	36.96
LSD	5.15	0.82	0.90	63.77	2.16	6.97
Jago 1994 control	122.80	3.80	11.13	201.07	7.31	35.64
16Hz	116.60*	4.67*	11.50	259.00*	8.99	36.96
50Hz	116.10*	4.67*	11.93	263.90*	8.51	39.13
LSD	5.58	0.87	5.91	58.03	1.96	4.60

*- statistically significant differences

LSD- lowest significant differences

Table 3 presents the results of a biometric measurements of examined plants made during field vegetation and selected crop characteristics of these plants measured after harvest. As you can see magnetic field did not influence significantly on examined characteristics of plants growing from the old seeds. In the case of plants grown from fresh seeds productive tillering (number of culms with ear containing kernels), length of ears , number and weight of kernels per plant increased. This indicates clearly an increase of the yield from one plant and also from the field. In the case of triticale plants obtained from irradiated seeds were shorter, what is an advantage in modern breeding experiments of this species. Also an increase of productive tillering and number of kernels per plant was visible. In the case of plant growing from old seeds additionally there was also observed ear's prolongation and increase of kernels weight per plant. Similarly to wheat it is connected to the increase of yield. The values of presented characteristics of control plants did not differ from mean values typical for examined varieties [7]. Both frequencies of magnetic field seem to have the same influence on seeds and plants grown from them although some results may suggest more profitable influence o magnetic field frequency of 16 Hz. Profitable influence of alternative magnetic field is more clear in the case of

seeds of lower quality (harvested in year 1991) than seeds of high quality. Such a „restitutional” influence of magnetic field was observed earlier [8,9]. Probably difficult vegetational conditions in the year when presented experiments were led enabled to notice profitable influence of alternatic magnetic field also on growth and yield of plants growing from fresh seeds of high quality. For the agricultural practice not only increase of field emergence rate is a factor a great importance out also an acceleration of plant development (quicker entering early development phases) which remain more time for forming and mature of kernels and in consequence improves the yield. It also can help the plants to avoid disadvantageous weather conditions often appearing in our country during the second half of summer. Presented results show that different species reveal different response to the magnetic field. This factor influenced much more features in triticale than in wheat. That is probably a result of genetic differences (causing physiological differences) between both of these species. Differences in magnetic field influence for different genotypes was observed previously for some wheat species [10]. Presented results concern only one vegetation season which is too short period for field experiment for general conclusions and need to be continued. But obtained results maintain an opinion

about profitable influence of alternating magnetic field on the seeds of cereals and plants growing from these seeds. This profitable influence can be seen not only in laboratory but what is more important for agricultural practice confirmed also in the field.

4. REFERENCES.

1. S. Podlaski , „Modern ways of improving of seeds quality. Seed-conditioning” (Nowoczesne sposoby poprawy jakości materiału siewnego) (in Polish), Hod. Roślin i Nas., 1,1992, 21-25
2. V.J. Pittman , „Effect of magnetic seeds treatment of yields of barley, wheat and oats in Southern Alberta” J. Plant. Sci. ,57, 1977, 37-54.
3. G.H. Gubbels , „Seedlings growth and yield response of flax, buckwheat, sunflower and field pea after magnetic treatment” J. Plant. Sci., 62, 1982, 61-64.
4. W.J. Miszczenko „Presowing seed treatment with electromagnetic field”, (in Russian) Elect. Obr. Mat. 6, 1980 ,68-69.
5. S. Pietruszewski „Effect of magnetic seeds treatment on yield of wheat”, Seeds Sci and Technol.,21,1996, 621-626.
6. A. Orzeszko „Effect of incubation of sugar beet seeds in water at 25 C on emergence and yielding” (Wpływ inkubacji nasion buraka cukrowego w wodzie o temperaturze 25 C na wschody i plonowanie) (in Polish), Zeszyty Problemowe Post. Nauk Roln., 439, 1997, 25-30.
7. M. Behnke, L. Kaczyński, B. Lewandowska, J. Zych „ Synthesis of the results of varieties evaluation” (Synteza wyników doświadczeń odmianowych), Z 1060, 1995, 12-19 and 66-68.
8. M. Rochalska „The influence of power supply frequencies magnetic field on the quality of seeds of agricultural crops” (Wpływ pól magnetycznych o częstotliwościach sieciowych na własności nasion roślin rolniczych)(in Polish), Proc. VIII National Symposium of Radio Science, 1996, 291-294.
9. M.P. Alexander, S.D. Doijode "Electromagnetic field a novel tool to increase germination and seedling vigour of conserved onion (*Allium cepa L.*) and rice (*Oryza sativa L.*) seeds with low viability, Plant Genetic-Resources Newsletter, 104, 1995, 1-5.
10. H. Kilasińska „The influence of alternating magnetic field of industrial frequency on the seeds of spring wheat at different ploidy level”(Wpływ zmiennego pola magnetycznego o częstotliwości przemysłowej na nasiona pszenicy jarej o różnym stopniu ploidalności)(in Polish), Master Thesis SGGW Warszawa 1996.

5. BIOGRAPHICAL NOTES

Rochalska M. (48) Dr, received the M.Sc degree at Warsaw University. Received the doctor degree in the Institute of Nuclear Chemistry and Technology. At present she works at Agricultural University in Warsaw. The main field of her activity is an improvement of seeds quality, especially using electromagnetic fields.

POWER ABSORBTION IN A MULTILAYERED FINITE LENGTH CYLINDRICAL MODEL OF MAN EXPOSED BY A PLANE WAVE AT OBLIQUE INCIDENCE

S.S Seker

Bogazici University, Dept. of Electrical-Electronic Eng.
80815 Bebek , Istanbul-Turkey

Cuneyt Utlu

Istanbul Technical University, Dept. of Electrical-Electronic Eng.
80626 Maslak,Istanbul-Turkey

Osman Cerezci

Sakarya University, Department of Computer Eng.
Adapazari-Turkey

The absorption characteristics of multilayered cylindrical model of man exposed to electromagnetic (EM) plane wave with oblique incidence has been investigated. In literature the results obtained are valid for only exposure with normal incidence. General field expressions induced inside a multilayered infinite length lossy cylinder by a plane wave with oblique incidence have been derived for both vertical and horizontal polarizations. These expressions are used to investigate the effect of angle of incidence of the EM wave on the average SAR of a human modelled by a finite length multilayered lossy cylinder between the frequency range 10 MHz. to 10 GHz. The fields induced inside the finite length lossy multilayered cylinder are approximated by those of the infinite length lossy multilayered cylinder having the same radial dimensions, orientation and electrical properties for corresponding layers. The effect of the length of the model on the average SAR is also investigated. The average SAR versus frequency plots for a plane EM wave with normal incidence for both vertical and horizontal polarizations are compared with those in literature and good agreement is obtained.

1. INTRODUCTION

The absorption characteristics of multilayered cylindrical model of man exposed to electromagnetic plane (EM) wave has been investigated in literature using a variety of methods. Such a multilayered model has been taken to consideration by Massoudi et al. [1]. In their study effects of layering on average SAR is investigated and the skin-fat-muscle arrangement for the triple layer is considered for changing frequency of range 10 MHz. to 10 GHz. The results are compared with those of the homogenous (single layer) cylindrical model. The effects of wet and dry clothing are also taken into account in their work. But the angle of incidence for the EM waves in their work and others is taken to be at right angles to the cylinder axis (normal incidence) which greatly reduces formulation and computational complexity. In their work, they made use

of the field expressions obtained in [2]. In this paper the EM wave is considered to be coming with oblique incidence to the multilayered finite length cylinder.

A brief account on the formulation is given. General expressions for the field components induced inside the layers of the multilayered cylinder are given for oblique incidence. The model considered here is of finite length and the fields induced inside are approximated by those of the infinite length multilayered cylinder having the same radial dimensions, orientation and electrical properties for corresponding layers. Such an approximation is assumed to be valid under the assumption that the length of the cylinder is comparable or greater than the wavelength of the incident wave. This assumption holds for the frequencies considered herein.

Numerical results are obtained for the single, triple and five layer models of man for the average SAR versus frequency for different angles of incidence of the plane EM wave and the effects of oblique incidence on average SAR is observed. The results obtained for normal incidence are compared with those of Massoudi et al. [1]. The effect of length on the average SAR has also been considered.

2. FORMULATION

We consider a planar monochromatic electromagnetic wave to be oblique incident upon a dielectric multilayered cylinder of length ℓ of M layers having permittivity ϵ_m , permeability μ_o , conductivity σ_m and radius r_m at the m'th layer. Furthermore

$$\epsilon_m = \epsilon_0 \epsilon_{rm} = \epsilon_0 (\epsilon'_{rm} - j\epsilon''_{rm}) \quad , \quad \epsilon''_{rm} = \frac{\sigma_m}{\omega \epsilon_0}$$

and ω is the radial frequency.

The geometry of the problem is shown in Fig. (1). We represent the total field outside the cylinder (incident fields plus the scattered fields) by

$$E_z = \sum_{n=0}^{\infty} E_0^{TM} j^n \sin \theta_i J_n(\lambda_0 \rho) \cos(n\phi) e^{k_z z} + S_n H_n^{(2)}(\lambda_0 \rho) \cos(n\phi) e^{k_z z} \quad (1)$$

$$H_z = \sum_{n=0}^{\infty} H_0^{TE} j^n \sin \theta_i J_n(\lambda_0 \rho) \cos(n\phi) e^{k_z z} + Z_n H_n^{(2)}(\lambda_0 \rho) \cos(n\phi) e^{k_z z} \quad (2)$$

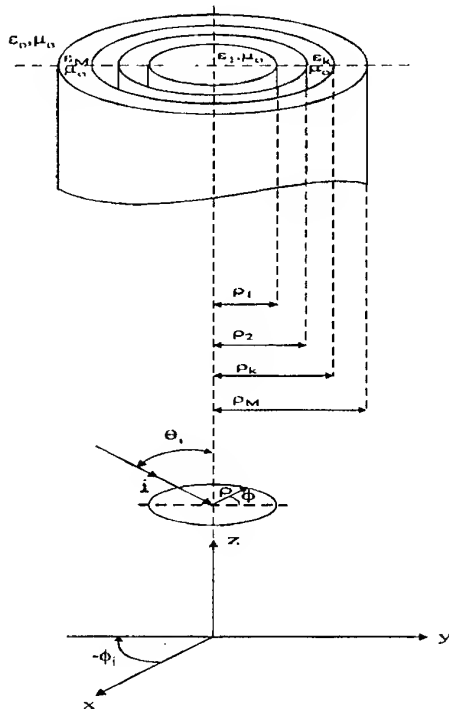


Fig. 1. A plane electromagnetic wave incident with oblique incidence on a multilayered cylinder

for TM (electric field with z component) and TE (electric field with no z component) polarizations respectively. In Eqs. (1) and (2) $k_z = k_0 \cos \theta_i$, $\lambda_0 = k_0 \sin \theta_i$ and $k_0 = \omega \sqrt{\mu_0 \epsilon_0}$ is the free space wave number and E_0^{TM} and H_0^{TE} are the magnitudes of the incident TM and TE fields respectively. The z , ϕ and ρ components of electric field induced inside the m 'th layer are expressed respectively by

$$E_{z,m}^q = \sum_{n=0}^{\infty} [A_{mn}^q J_n(\lambda_m \rho) + B_{mn}^q N_n(\lambda_m \rho)] \cos(n\phi) e^{k_z z} \quad (3)$$

$$E_{\phi,m}^q = -\frac{k_z}{\lambda_m^2 \rho} \sum_{n=0}^{\infty} [A_{mn}^q J_n(\lambda_m \rho) + B_{mn}^q N_n(\lambda_m \rho)] n \cos(n\phi) e^{k_z z} + \frac{j\omega \mu_m}{\lambda_m} \sum_{n=0}^{\infty} [C_{mn}^q J_n(\lambda_m \rho) + D_{mn}^q N_n(\lambda_m \rho)] \cos(n\phi) e^{k_z z} \quad (4)$$

$$E_{\rho,m}^q = \frac{j k_z}{\lambda_m} \sum_{n=0}^{\infty} [A_{mn}^q J'_n(\lambda_m \rho) + B_{mn}^q N'_n(\lambda_m \rho)] \cos(n\phi) e^{k_z z} + \frac{j\omega \mu_m}{\lambda_m^2} \sum_{n=0}^{\infty} [C_{mn}^q J'_n(\lambda_m \rho) + D_{mn}^q N'_n(\lambda_m \rho)] n \cos(n\phi) e^{k_z z} \quad (5)$$

where $\lambda_m = k_0 \sqrt{\mu_0 \epsilon_m - \cos^2 \theta_i}$ and $q \in \{v, h\}$ and v stands for vertical (TM) and h stands for horizontal (TE) polarization. The primes over the Bessel and the Neumann functions in Eqs. (4) and (5) mean derivative with respect to the argument. The constants S_n and Z_n is Eqs. (1) and (2) and the constants A_{mn}^q , B_{mn}^q , C_{mn}^q , D_{mn}^q in Eqs. (3), (4) and (5) can be obtained by solving for each layer the boundary conditions on each layer boundary of the multilayered cylinder [3]. By the aid of the boundary conditions the field coefficients can be expressed in a recursive manner.

$$\begin{bmatrix} A_{m+1,n} \\ B_{m+1,n} \\ C_{m+1,n} \\ D_{m+1,n} \end{bmatrix} = [\beta_{mn}] \begin{bmatrix} A_{mn} \\ B_{mn} \\ C_{mn} \\ D_{mn} \end{bmatrix} \quad (6a)$$

and

$$\begin{bmatrix} A_{mn}^q \\ B_{mn}^q \\ C_{mn}^q \\ D_{mn}^q \end{bmatrix} = \prod_{k=1}^{m-1} [\beta_{kn}] \begin{bmatrix} A_{1n}^q \\ 0 \\ C_{1n}^q \\ 0 \end{bmatrix}, \quad q \in \{h, v\} \quad (6b)$$

The matrix multiplication is carried on from left to right in Eq. (6 b). The elements of the matrix $[\beta_{mn}]$ are given in [3] where $X_m = \lambda_m p_m$ and $X_{m+1} = \lambda_{m+1} p_m$. The coefficients A_{1n}^q and C_{1n}^q in Eq. (6 b) are determined to be [3]

$$A_{1n}^v = A_{1n}^{TM} = \frac{j^{-n}}{\Delta} \Psi_{11} E_0^{TM}, \quad A_{1n}^h = A_{1n}^{TE} = \frac{j^{-n}}{\Delta} \Psi_{12} H_0^{TE}$$

$$C_{1n}^v = C_{1n}^{TM} = \frac{j^{-n}}{\Delta} \Psi_{21} E_0^{TM}, \quad C_{1n}^h = C_{1n}^{TE} = \frac{j^{-n}}{\Delta} \Psi_{22} H_0^{TE} \quad (8)$$

with

$$[\Psi] = \begin{bmatrix} \gamma_{33} - j\gamma_{43} & -\gamma_{13} + j\gamma_{23} \\ -\gamma_{31} + j\gamma_{41} & \gamma_{11} - j\gamma_{21} \end{bmatrix}$$

$$\Delta = (\gamma_{11} - j\gamma_{21})(\gamma_{33} - j\gamma_{43}) - (\gamma_{13} - j\gamma_{23})(\gamma_{31} - j\gamma_{41})$$

$$[\gamma] = \prod_{k=1}^M [\beta_{kn}]$$

With A_{1n}^q and C_{1n}^q determined the rest of the remaining coefficients for each layer can be obtained by Eq. (6 b).

The specific absorption rate (SAR) of the cylinder for both polarizations is

$$\text{SAR} = \sum_{m=1}^M \frac{S_{a,m}}{v_m} \quad (\text{W/m}^3) \quad (8)$$

where

$$S_{a,m} = \int_{v_m} \sigma_m |\tilde{E}_m|^2 dv_m \quad (9)$$

is the power absorbed by the m 'th cylinder layer of volume v_m of the m 'th layer. Thus the total average SAR is the sum of average SARs of each individual layer. The explicit form of Eq. (9) can be expressed as

$$S_{a,m} =$$

$$2\pi\ell \sum_{n=0}^{\infty} \int_{\rho_{m-1}}^{\rho_m} [|E_{z,mn}(\rho)|^2 + |E_{\phi,mn}(\rho)|^2 + |E_{p,mn}(\rho)|^2] \rho d\rho \quad (10)$$

3. SIMULATION RESULTS

Curves of average SAR versus frequency are plotted for single, triple and five layer models of man exposed to plane electromagnetic wave with oblique incidence for both vertical and horizontal polarizations. The effect of length on the average SAR is also depicted for both polarizations.

In the following simulations the incident power is taken to be 1 mW/cm^2 for both vertical and horizontal polarizations.

Table 1. gives the parameters used for each tissue layer of man [4], considered in simulations. For the five layer model of man the fourth layer is considered to be air of thickness 6 mm. and the fifth layer is taken to be wet clothing with complex permittivity $\epsilon_r = 10 - j5$ for all frequencies [1].

In Fig.(2) the effect of length at normal incidence on the average SAR is considered for both polarizations. Simulations for two different lengths of 1.7 mt. and 1.0 mt. are made.

In Figs. (3)-(5) average SAR versus frequency plots for different layers in modeling man, are given for vertical and horizontal polarizations. Incidence angles (namely $\theta_i = 30^\circ$, $\theta_i = 60^\circ$ and $\theta_i = 90^\circ$) are taken as parameters in all figures. Normal incidence ($\theta_i = 90^\circ$) corresponds to the cases depicted in [1].

Table 1. Parameters of the different tissue layers.

	ϵ_r (F/m)	σ (S/m)	Thickness (m)
Skin	29.10	2.08	0.002
Fat	5.61	0.112	0.01
Muscle	50.63	1.56	0.1008

From Fig.(2) it can be seen that length has no effect on the average SAR. Although this is what was expected from the approach used in this work, it is deceiving. In the cylindrical modeling of man, the

internal fields are assumed to be the same as those of an infinite cylinder having the same physical and electrical properties and orientation with respect to the incident field. This assumption will disguise the effect of length since in reality the fields inside the finite cylinder differ from those of the infinite cylinder and also change with length.

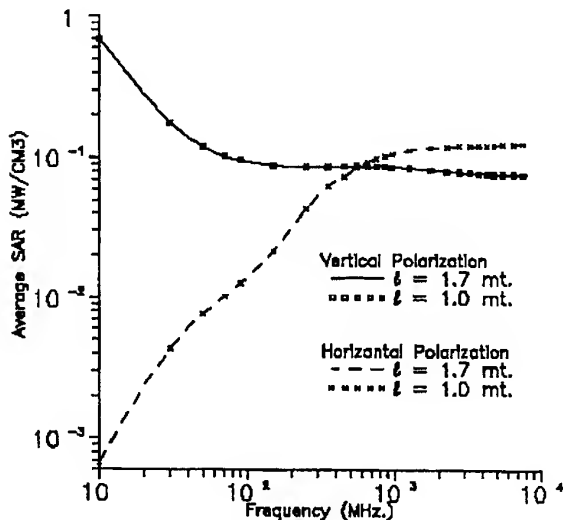


Figure 2 : The effect of length on the average SAR versus frequency curves for the single layer model for both vertical and horizontal polarizations.

It is seen that for normal incidence the results obtained in Figs. (3)-(5) are in good agreement with those of [1]. For oblique incidence, up to around 400 MHz, average SAR appears to be higher for skewer angles of incidence. This may be due to the cross polarization terms appearing in the field expressions. In the 400 - 600 MHz. frequency range there is a cross-over between the normal and oblique incidence curves and this takes place close to the frequency where the muscle tissue is distinguished between behaving as a good conductor and a good dielectric ($\sigma_{\text{muscle}} / 2\pi\epsilon_0\epsilon_r^{\text{muscle}} = 1$). For frequencies above approximately 600 MHz. the average SAR for incidence with skewer angles are lower for both vertical and horizontal polarizations.

It is apparent from the given figures that the average SAR depends on the angle of incidence, polarization, frequency and the constitutive parameters of man. The effect of layering is the addition of extra peaks for all angles of incidence. For frequencies above 8 GHz. the effect of layering decreases and the average SAR curves tend to the single layer model. But we do not see why this should be due to the low depth of penetration at frequencies above 8 GHz, as mentioned in [1], since at these frequencies the loss tangent is very small and all tissue layers act as good dielectrics and the attenuation factors of all layers settle to constant values determined by their conductivities and relative permittivities. Since other layers are very thin compared to the muscle layer, the muscle layer will play a dominant role at frequencies above 8 GHz.

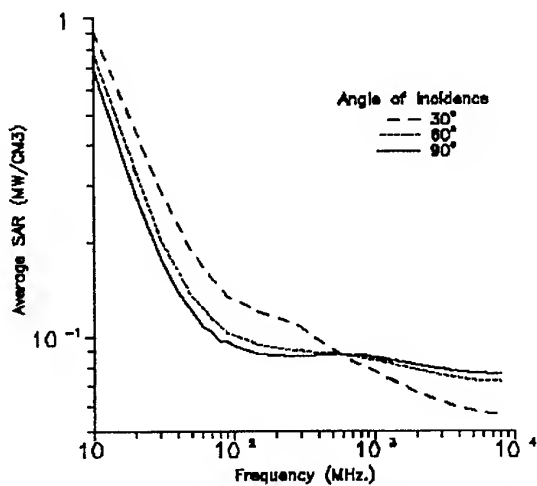


Figure 3 a: Average SAR versus frequency for the single layer model for vertical polarization.

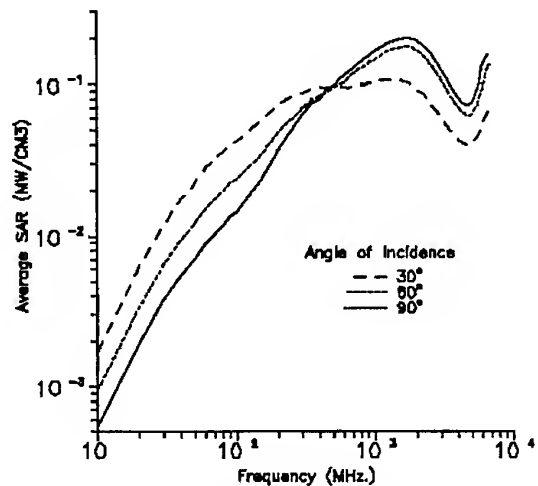


Figure 4 b: Average SAR versus frequency for the triple layer model for horizontal polarization.

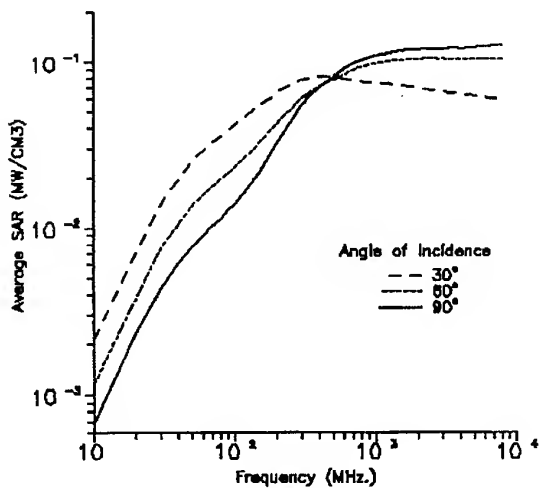


Figure 3 b: Average SAR versus frequency for the single layer model for horizontal polarization.

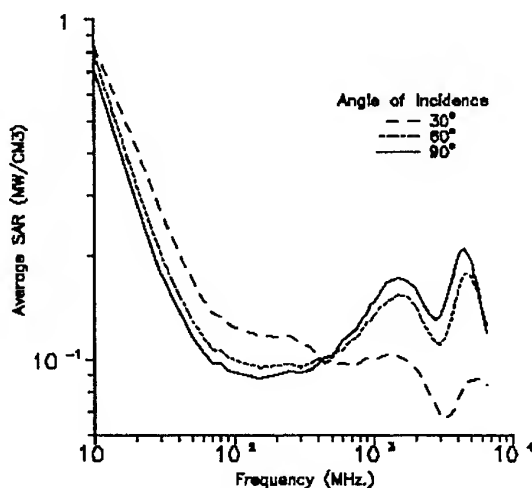


Figure 5 a: Average SAR versus frequency for the five layer model for vertical polarization.

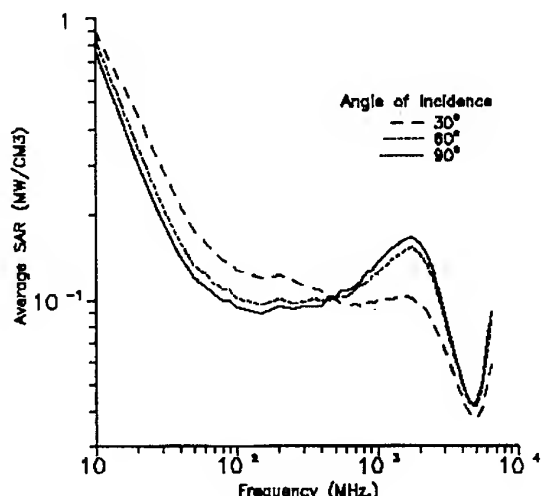


Figure 4 a: Average SAR versus frequency for the triple layer model for vertical polarization.

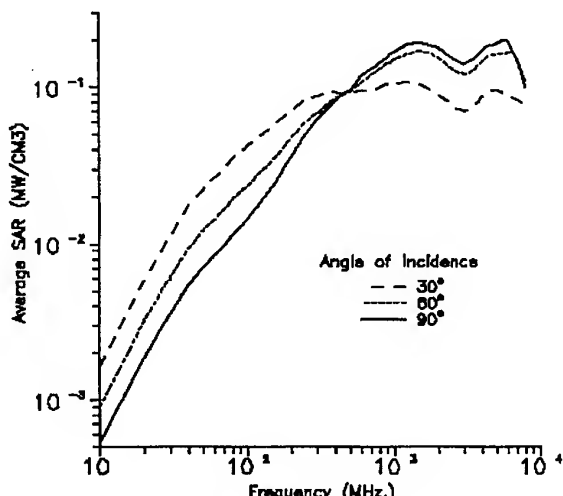


Figure 5 b: Average SAR versus frequency for the five layer model for horizontal polarization.

4. CONCLUSIONS

The results depicted gives a more general picture of the behavior of the average SAR in human body. For normal incidence they are in good agreement with the results obtained in [1].

It is seen that for skewer angles of incidence the average SAR increases in the frequency range where the dominant tissue layers act as good conductors. For the frequency range where the dominant tissue layers act as good dielectrics the average SAR decreases as the angle of incidence gets skewer.

It was not possible to observe the effect of length on average SAR with the present approximation for the internal fields of the finite cylinder since it does not reflect the dependence of these internal fields on the cylinder length.

5. REFERENCES

- 5.1. H. Massoudi, C.H. Durney, W. Barber and M.F Iskander, "Electromagnetic Absorption in Multilayered Cylindrical Models of Man", IEEE Trans. Microwave Theory Tech., Vol. MTT-27, No.10, Oct. 1979, pp. 825 – 830.
- 5.2. H.E. Bussey and J.H. Richmond, "Scattering by a Lossy Dielectric Circular Cylindrical Multilayer, Numerical Values", IEEE Trans. Antennas Prop., Vol AP 23, Sept. 1975, pp. 723-725.
- 5.3. S. Seker, I. Akkaya, C. Utku, "Differential Cross Section of Multi-Layered Lossy Cylinder of Finite Length", Progress in Electromagnetics Research, Pier 18, 1998, pp. 151-171.
- 5.4. J.C. Lin, "Handbook of Biological Effects of Electromagnetic Fields", CRS Press, 1979.

BIOGRAPHICAL NOTES

Selim Seker: Received his M.S. and Ph.D. degrees in 1978 and 1982 from George Washington University. In the summer of 1984, 1985 and 1987 he joined the CyberCom Corporation, VA, U.S.A. to do research in Electromagnetic Wave Propagation through forests. In 1986 he worked at Baden, Switzerland on the problem of absorbers. He has publications on Microwave Remote Sensing, Scattering and Propagation through Random Media. Currently he is a full time faculty member of the department of Electrical Engineering at Bogazici University in Istanbul, Turkey.

Cuneyt Utku: Received his B.S. degree in Electronics and Communication engineering in 1993 and M.S. degree in 1996 from Istanbul Technical University . Currently he is a research assistant in Electromagnetic Waves and Microwave Engineering in Istanbul Technical University and is studying for his Ph.D. degree in the same university.

THE IONIC PARAMAGNETIC RESONANCE ON THE NERVOUS FIBRE MEMBRANE

A.N. Volobuev, E.L. Ovchinnikov, L.A. Trufanov, P.I. Romanchuk
Samara State Medical University, 443079, box 1423, Samara, RUSSIA

Abstract

The ionic spread through the membrane of the nerve fibre placed axially into the constant magnetic field (CMF) is considered. It is shown that the circulating currents appear during the propagation of the Action potential along the fibre due to Lorentz force. Magnetic moments of the circulating currents precess round the external CMF direction.

The ionic paramagnetic resonance (IPR) appears during the alternating current passing through the nerve fibre (*in vivo* consisting of the organ) at coincidence of the current frequency and precession frequency. The impedance of biotissues is increasing greatly at that moment. The IPR method allows to selective determine the intensity of the ion flow, because the resonance frequency depends on the type of ions moving through the membrane.

1. INTRODUCTION

Spreading of the nerve impulse along the nerve fibre is the process accompanied by the movement of the ions through the fibre membrane. In the main they are the Na^+ and K^+ ions. Also the Cl^- ions for which the membrane is enough permeable, constantly move through the membrane by simple diffusion. Besides there are other ions moving through the membranes of the nerve and muscle fibres during the varoius physiological processes. Penetration of the H^+ -ions through the mitochondria membrane is the most important and in particular for ATP synthesis.

Functional state of the nerve and muscle fibre membranes depends on intensity of the ion transfer. Decrease of the intensity of the ion transfer testifies to metabolic inhibition, lower level of the energy processes and that is the reason of the various pathology. On the other hand increase of the intensity of the ion transfer more than normal testifies to disturbanse of the barrier function of the membranes. The latter also leads to the pathologic processes. Therefore making more precise the intensity of the ion transport both active and passive and comparision it with normal one is the important diagnostic problem. Selective determination of the ion transport intensities for individual kind of ions appeals to diagnostic aims.

2. BIOPHYSICS BASIS OF THE IPR

The problem raised here can be solved by ion paramagnetic resonance appearing on the setting of the organism into the CMF.

The essence of the resonance rise is as follows (Fig.1). Let us look at the spreading of the nerve impulse along the nerve fibre 1 which is acted by CMF. Induction B_0 of the external CMF is directed axially to the fibre. That situation takes place in the sciatic nerve of the human being which lower extremities are placed along the axis of the solenoid creating CMF. Ions 2 moving perpendicularly to the neuromembrane at the velocity V are acted by LORENTZ force F which directed along the membrane surface and perpendicularly to the fibre axis. That force creates the tangential components of the movement velocity of the ions both diffusible between lipid molecules and moving within the ionic channels.

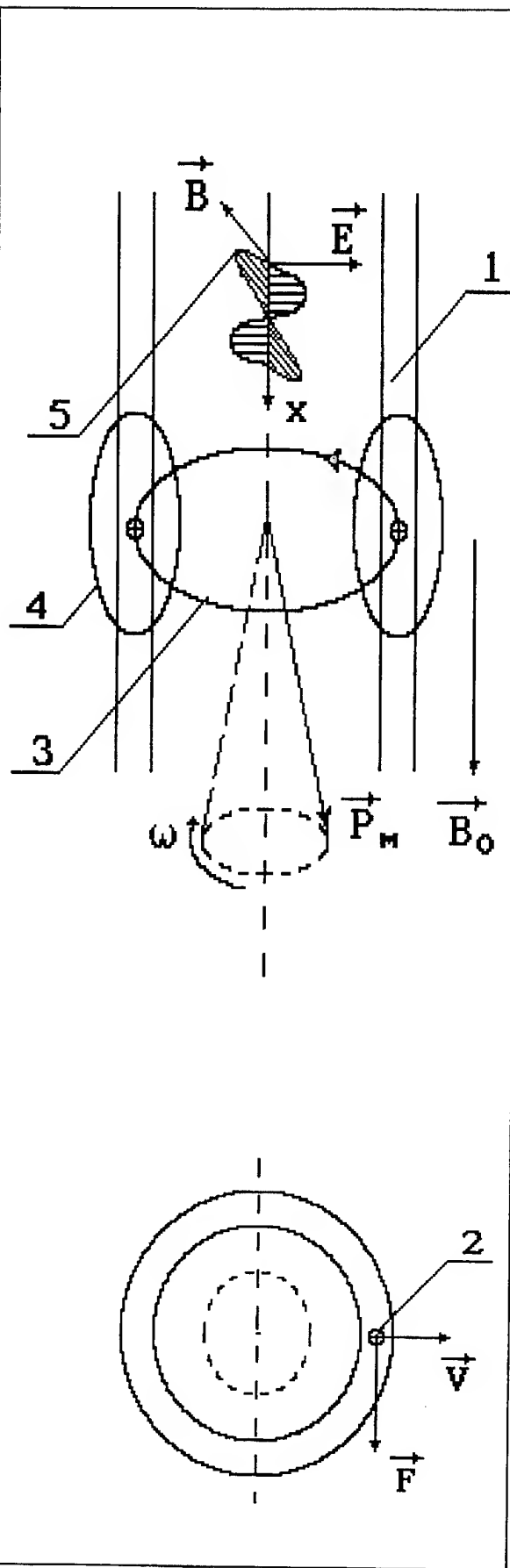
Tangential movement of the ions creates the circulating current 3 inside the nerve fibre. The current has maximal value at acrossing the action potential because the ion transfer is the most intensive exactly at that moment. Current circle 3 and its magnetic field 4 having a tore form move along the fibre in common with the action potential. The magnetic moment P_m may be the characteristic of the magnetic field bound to the current circle.

According to principles the quantum mechanics, the magnetic moment P_m cannot coincide the direction, allocated by the external magnetic field [1].

According to the LARMOR theorem magnetic moment P_m will precess round the vector of the external magnetic field induction B_0 with LARMOR frequency ω which may be calculated from the formula:

$$\omega = \frac{q B}{2 m}$$

where q is the charge of the ion creating the circulating current, m is the ion mass. It is important to note that the common magnetic moment of the circulating current P_m represents the vector sum of the magnetic moments determined by movement of various kinds of ions across the neuromembrane.



The certain precess LARMOR frequency corresponds to every kind of ions.

The LARMOR frequencies $\nu = \omega/(2\pi)$ calculated for various kind of ions for external CMF $B_0=10$ mT are given in the table 1.

Table 1

	Ion	ν, Hz
1	Na^+	3340
2	K^+	1970
3	H^+	76836
4	Cl^-	2195
5	Ca^{++}	3841
6	Mg^{++}	6403

The induction $B_0 = 10$ mT is in the range of values usually being applied to the magnitotherapeutic procedure.

3. USE OF THE IPR FOR ANALYSIS OF MEMBRANEOUS PROCESSES

If the nerve fibre is placed in an electromagnetic field 5, paramagnetic resonance arises at coincidence of the frequency of magnetic moment P_m precession round the external CMF and electromagnetic field frequency of precession. The resonance frequency corresponds to the LARMOR precession frequency and it is a individual characteristic of the ion penetrating through the membrane.

Electromagnetic field inside the organ may be created by conducting alternating current with changing frequency.

Fig. 1: Biophysical principle of IPR:

- 1 - nervous membrane,
- 2 - ion moved trough membrane,
- 3 - circle current,
- 4 - toroidal magnetic field,
- 5 - external electromagnetic field.

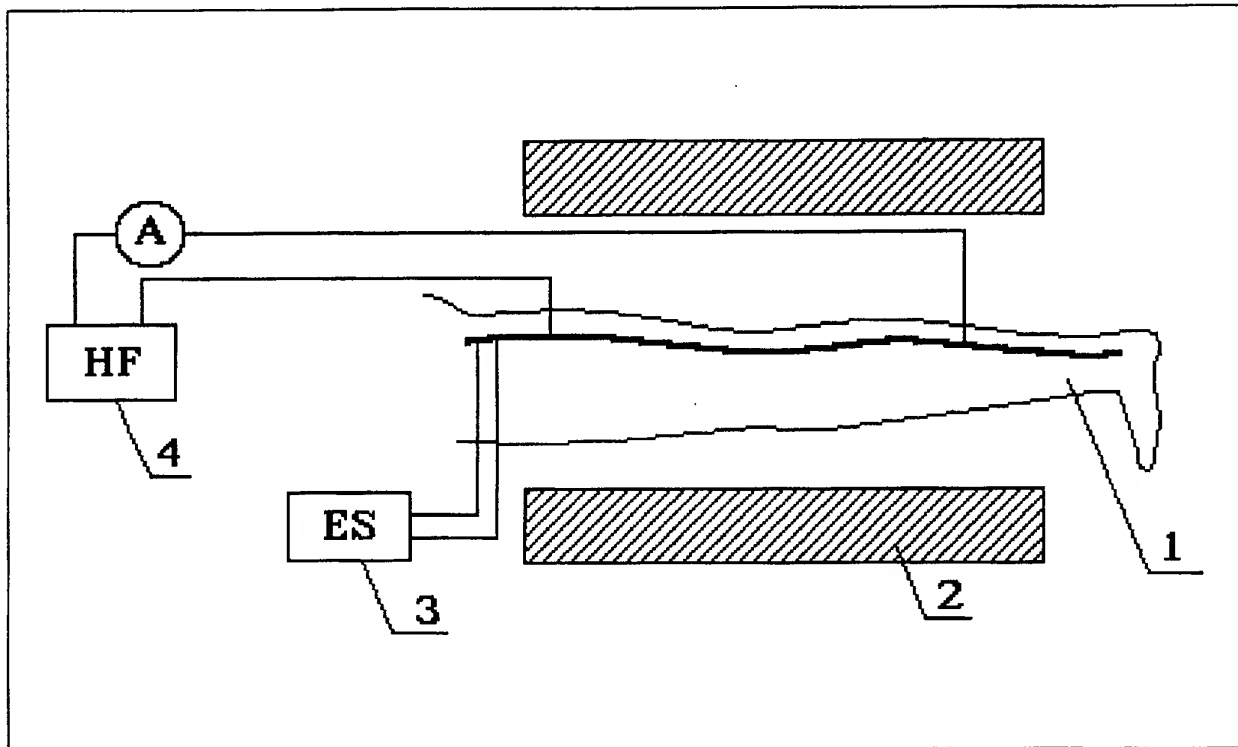


Fig. 2: The block-scheme of device for research IPR:

- 1 - organ with research nerve,
- 2 - solenoid for creation of constant magnetic field,
- 3 - electrostimulator,
- 4 - generator for creation high-frequency current.

Resonance appearing at coincidence of the alternating current frequency and LARMOR one leads to increase the absorbtion the electromagnetic field energy by organ tissue and as consequence to increase of the tissue impedance.

It leads to decrease the alternating current value at the resonance LARMOR frequency under that voltage.

The frequency at which the great decrease of the alternating current being conducted takes place allows to determine the kind of the ions passing through the membrane, the value of the current change allows to see the change of the ion transport intensity comparatively to normal.

It may be noted some formal analogy between ion paramagnetic resonance and electron paramagnetic resonance [2].

4. APPLICATION OF THE IPR IN THE NEUROPHYSIOLOGY

The scheem of registration which of ion paramagnetic resonance on the human sciatic nerve is shown in Fig.2.

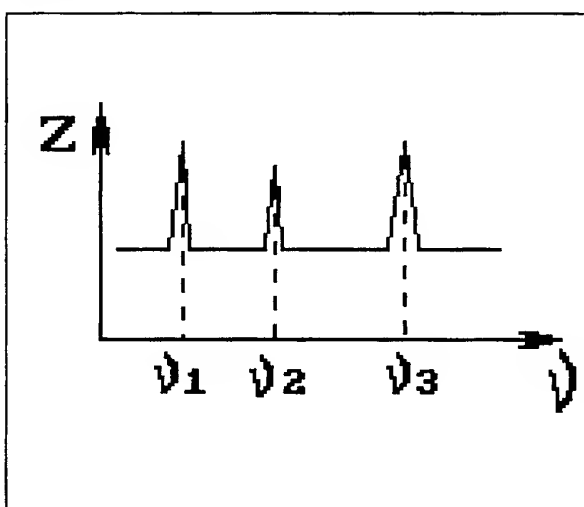


Fig. 3: Example of IPR-gram:

- Z - impedance of tissue,
- v - resonance frequency.

The lower extremity 1 is placed inside the solenoid 2 which creates the CMF with the necessary induction. Electrostimulator 3 creates the skinover single nerve impulses spreading along the sciatic nerve. Generator 4 is intended for creation of the alternating current with changing frequency. The current value is registered by measuring device A.

The approximate form of the impedance spectrum, i. e. dependence of the tissue impedance value Z during the passing of the nerve impulse on a frequency v is shown on Fig. 3. Ion paramagnetic resonance for various kinds of ions is observed at frequencies v_i .

5. THE IPR PUTING INTO MEDICAL PRACTICE

A lot of pathological states of organism occur because of ion-penetration running through the cell membrane breach. These breaches may be different. First of all it is because the protective function of membrane is changing for the worse. It gives the opportunity either to enter the superfluous Na^+ ions to the cell or the superfluous K ions leave it. In consequence of it membrane electrochemical potential falls down and a cell stops functioning. So the nerve fibre stops functioning as well; a secretive cell doesn't supply the organism with the necessary substances.

The membrane worse conductivity may depend on bad functioning of ion canal and different kinds of transfers. This leads to reducing of ion flows which are necessary for a normal cell life.

The cell accumulates slags and starts anomalously functioning, therefore structural damages take place. All these damages could be diagnosed with the help of the ionic paramagnetic resonance.

Thus this method gives a new possibility to diagnose the causes of many diseases and creates the conditions for the most suitable treatment which depends not only on the disease symptoms. For a wider inculcation of this method into practice it is

necessary to go on further research work to reveal the connection between the concrete pathology and the intensity of ion transfers in organ tissue.

6. CONCLUSION

Experimentally [3] the magnetic parametrical resonance of ions Ca^{++} and Mg^{++} in the biosystems is found out. Therefore the submitted method presented here allows to create the apparatus which can be used to diagnose *in vivo* the selective intensity of the ion transport through the cell membrane. It will help to ascertain the true reasons of many pathology and create active methods for their treatment.

7. REFERENCES

- 7.1. I.V. Saveljev, "Course of general physics". V.3, Moscow, 1971, p.355.
- 7.2. A.B. Rubin, "Modern methods of biophysical investigation", Moscow, 1988, pp.226-258.
- 7.3. V.V. Lednev et al., "Magnetic parametric resonance in biosystems", Biophysics, No.4, 1996, pp. 815-825.

BIOGRAPHICAL NOTES

Andrey N. Volobuev, Prof., Head of the chair Medical and biological physics of Samara State Medical University.

Eugeniy L. Ovchinnikov, Dr., teacher of this chair.

Lev A. Trufanov, Prof. of the chair Surgery.

Peter I. Romanchuk, Dr., Head of the laboratory of Research Institute Computer ElectroStructurography.

EXPERIMENTAL ESTIMATION OF ELECTROMAGNETIC FIELD NEARBY HIGH-VOLTAGE BUSBARS AT INDUSTRIAL FREQUENCY AS THE DETERMINING FACTOR OF ITS SAFE SERVICE

V. Zabusov
Norilsk Industrial Institute
Norilsk, Russia.

Intensive electromagnetic field (EMF) arising in the space around busbars in the operating high voltage electrical plants is one of the factors determining hazard and unhealthy conditions of works. Maintenance personnel of the plants gets the disturbance of the nervous and cardio-vascular systems, high fatiguability, low attention concentration, the change of blood pressure and pulse that causes arrhythmia, etc. [1].

It should be pointed out that negative influence of EMF of electrical plants with voltage more than 220 kV as well as equipment operating at high and ultra-high frequencies was understood best of all. But estimation of EMF at up-to-date industrial enterprises full of equipment operating on different voltages (less than 110kV, as a rule) and frequencies (50 Hz and 200 Hz) was not carried out yet. This problem is the most topical in the Far North where environment determines conditions of work and state of health. Factors of environment are: drastic atmospheric pressure and air humidity differentials, negative radiation balance, intensive geomagnetic disturbances, strong static charges (especially in winter) and aeroionizatoin [2]. These climate and geographical features of northern areas essentially change the psycho-physical state of the personnel, its response to external imitants and, as consequence, determine safe service of the electrical equipment.

In order to define the most dangerous places where personnel can be the experimental investigations of EMF parameters in service areas situated in special galleries along the mains three phases busbars of 10kV voltage at one of the enterprises of Norilsk Mining Metallurgical Works was carried out. Busbars are made in the form of tubular symmetric steelworks. Busbars of different phases are arranged at the corners of the equilateral triangle. They are suspended by special brackets. Full transmitting power on voltage ratings U=10.5 kV is 91.7-165.5 MVA. Allowable amperages within heating conditions of busbars is 5.04-9.1 kA respectively.

Generally, the electrical field has adverse effect on the human body in electrical plants operating at industrial frequency. According to GOST (Russian state standards system) the instrument "NFM-1" was used for measurements. Its application sphere is measurements of the electrical field tensity (E) at 50 Hz (with probe of E type). The maximum scale limits are 10, 30, 100, 300 and 1500 V/m. Maximum error is $\pm 20\%$.

Two busbars service area is the special central passage of 1.8 m width. It's partitioned off the busbars by metal nettings and partially asbestos-cement slabs of 2.1m height. Investigations of this area were carried out in devised methods. The following have been done:

- study of arrangement plan of busbars to define the target sections and target points for measurement E;
- provisional analytical estimation of E in the service area at familiar technological operating mode parameters;
- setting the instrument for measurements;
- measuring E and representing of results as distribution plots (fig. 1) and diagrams (fig. 2) of E in the space of central passage;
- analysis of the results.

According to GOST [3] measurements of air temperature were carried out before and after measurements of E; its values are 0°C and +2°C respectively. Also there was amperage defined: $I_{min} = 1.4 \text{ kA}$, $I_{max} = 3.06 \text{ kA}$.

The results of the investigations show the following:

- maximum value of E in height (axis Y) is defined above barrier of busbars ($h=2.1\text{m}$). It does not exceed 1.5 kV/m.
- values of E in width of service area (axis Z) from zero point to $h=1.5\text{m}$ do not exceed 0.15 kV/m. E_{max} is defined at height $h=2.1\text{m}$ directly above the barrier. When moving to the center of the gallery at this height the value of E is decreasing very quickly and does not exceed 0.2 kV/m in the passage.

Section through the service area at the
Heat and power plant №3

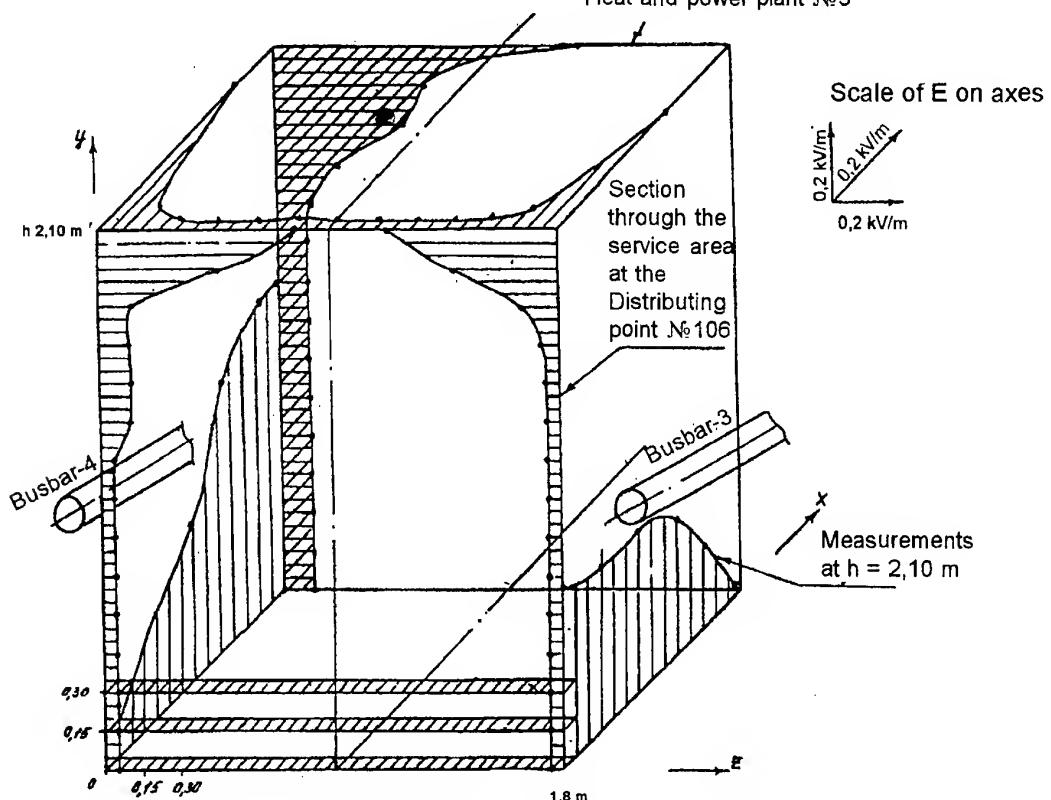


Fig.1. Diagrams of E distribution in space nearby busbars B-3, B-4 along the straight part of the gallery

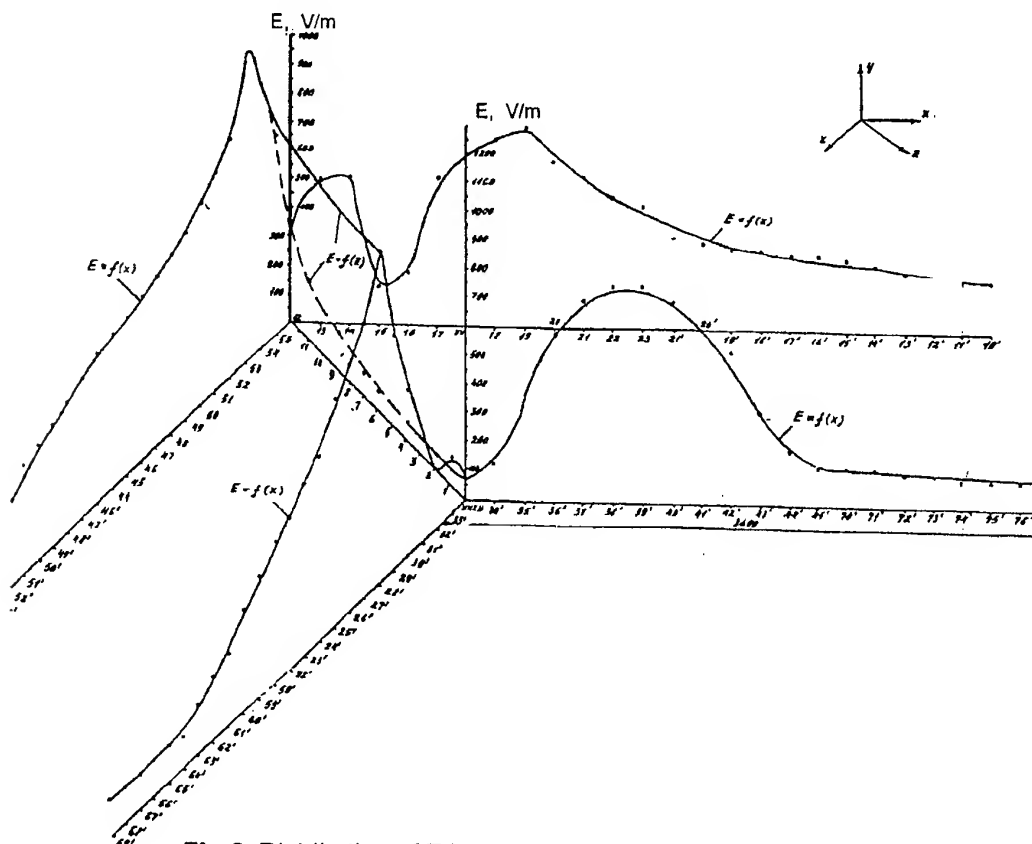


Fig.2. Distribution of E in space nearby busbars B-3, B-4 at the turn 2

- E_{max} in inspection direction (axis X) is defined in the center of the distance between reinforced concrete columns at height $h=2.1m$. When moving to these columns the value of E is decreasing to $0.15-0.2\text{ kV/m}$.
- E_{max} along straight parts of the gallery is almost the same as E_{max} at the turns. They are 1.2 kV/m and 1.45 kV/m respectively.
- EMF tensity of two busbars tends to decrease in direction from the energy source (heat and power plant) to distributing points.
- two symmetric lines of three phases busbars at the both sides of the passage do not sufficiently increase the value of E in service area in comparison with one line of busbars. Difference between E_{max} in these cases is tenth fractions of kV/m .

CONCLUSIONS

- Values of E in service area of busbars on 10 kV voltage at one of the enterprises in the Far North do not exceed a limiting value of 5 kV/m at busbars amperage $I=3.5\text{ kA}$.
- Defined values of E do not limit the duration of personnel staying in service area.
- The increasing of busbars amperage causes the increasing of E. It is necessary to make extra investigations of EMF parameters when amperage is more than 5 kA . The most dangerous places are ones above the barrier (in its plane) at the center of the distance between adjacent columns.

BIBLIOGRAPHY

1. P.A. Dolin, "Basis of electrical safety in electrical plants" (Russian), Energoatomizdat, Moscow, 1984.
2. I.S. Kandror, "Essays about psychology and hygiene of human in the Far North" (Russian), Meditsina, Moscow, 1968.
3. GOST 12.1.002-84. "Electrical fields of industrial frequency. Limiting values of electrical tensity and requirements to controlling of working places" (Russian), State standard committee of USSR, Moscow, 1984.

BIOGRAPHICAL NOTES

Vladimir Zabusov is the professor of Norilsk Industrial Institute (NII). He defended his thesis for the degree of the Candidate of Science of Electrical Engineering on speciality "Electrotechnical complexes and systems including its controlling and adjusting" in 1990. Since 1986 he conducts the course "Theoretical Basis of Electrotechnics" at the chair "Electrotechnics and Electrical Machines". He published 50 scientific works on problems of reliability and safety supplying in electrical plants exploitation in the extreme climatic conditions, ecology of power engineering and labour protection.

IV

EMC IN POWER SYSTEMS

EMC OF SIGNAL TRANSMISSION ON MV AND LV NETWORKS

G. Goldberg, Past Chairman IEC ACEC

Wannerstrasse 43/61, CH - 8045 Zürich - Switzerland

ABSTRACT

The transmission of signals on power networks is a quite difficult problem. The so called Mains signalling systems meet with a wide range of EMC features. Particularly the power lines are strongly disturbed channels. The paper gives a general overview on these EMC features, the relevant standardization and rationales hereto.

1. BACKGROUND

1.1. The 50/60 Hz power network is designed to transport electrical energy but already by the end of the 19th century the idea arose to use it for the transmission of information with superimposed signals at a higher frequency. The realization of the idea started actually only in the twenties with the so-called Ripple Control Systems. They developed well, in the very low frequency range of 110 Hz to 1(3) kHz as one way systems for utilities with a downwards signal transmission from the substations to the LV customers. They are used mainly for load control, the control of watt-hour meters and other remote switching operations.

With the tremendous progress in the last thirty years in the field of (micro) electronics and signal transmission techniques (modulation, coding, ...) and with the trend towards increasing automation of the network services, new two way systems are being developed in a higher frequency range of 3 to 150 (even 525) kHz.

Three kinds of application should now be considered:

- two way systems for Utilities, with downwards signalling for the same control functions as Ripple Control and upwards signalling for data transmission like remote meter reading, network status information, etc., ... With regard to the difficult transmission of high frequencies on power networks (see below), the tendency seems to prevail now - at least in Europe - to transmit the signals only on the LV level and to go from the MV/LV distribution transformers stations by means of telecommunication channels (telephone, radio) to the central controller.
- two way systems for Utilities for Network Automation functions mostly in the MV networks,

e.g. remote control of MV switches, data transmission (load, voltage, etc. ...). For these functions, signal transmission is required only on the MV level. Such systems are also called Distribution line carrier systems, DLC systems.

- two way systems for private users in the consumer premises, either residential houses (switching operations, alarms, etc.) or in commercial and industrial plants. Signal transmission occurs only on the LV level within the limited area of the user.

1.2. Signal transmission on the power network - "Mains Signalling" (MS) - is a quite difficult problem:

- the network is built for the power frequency and at higher, even much higher frequencies, great voltage drops can occur along the line inductances network or user capacitors absorb the signals or create resonances, etc. ... Particularly the short-circuit impedance of the MV/LV transformers causes great voltage attenuations. After the original attempt to transmit the signal on two power voltage levels - MV and LV - the tendency is now to remain only on one level and it is appropriate to consider independently the MV and LV levels.
- the power network is a strongly disturbed medium
- however, the transmitter power is quite small, at the user site in the range of some watts. Accordingly, the signal level is very low.
- several independent systems (for utilities or private users) may be installed in the same network. Mutual influences must be avoided.
- the equipment has to comply with all safety and EMC requirements, e.g. the EU directives.

Aim of this paper is to present a short but comprehensive overview of the EMC features of Mains Signalling. Three basic problems of Mains Signalling are not directly related to EMC and will not be dealt with in this paper: signal transmission in the networks, signal modulation and coding. They will just shortly be considered in relation with EMC. As this technique is subject of a comprehensive standardization it will be widely based on it.

Note: the paper will deal only with new systems in the 3 to 500 kHz frequency band and will not consider the previous well-established Ripple Control Systems.

2. TERMINOLOGY

Generally IEC 50(161) - IEV chapter on Electromagnetic Compatibility - is applied in this paper, but some terms need a more specific definition.

- **EM INFLUENCE OR DISTURBANCE:** cause of an EM effect, in the present case also the signals on the mains
- **EM INTERFERENCE:** degradation caused by an EM disturbance
- **FUNCTIONAL IMMUNITY:** correct operation of a Mains Signalling System in the presence of EM noise
- **EQUIPMENT IMMUNITY:** no degradation of the Mains Signalling apparatuses (components, etc., ...)
- **IN-BAND FREQUENCY RANGE:** frequency range within which the Mains Signalling System operates
- **OUT OF BAND FREQUENCY RANGE:** frequency ranges outside - below or above - the in-band range

For simplification, in the following, the term System will mean a Mains Signalling System unless otherwise specified.

3. THE EMC PROBLEMS OF MAINS SIGNALLING

Mains signalling should not be considered just as a collection of single apparatuses but consist of a complex system of various elements: the central control and emission items, the MV or LV network as transmission channels, the receivers/emitters (transceivers) at the user sites, the external world, ... whereby these elements frequently interfere with each other.

There are numerous problems related to EMC:

- allocation of frequency bands or choice of appropriate frequencies (Chapter 4)
- permissible signal level (Chapters 5 and 7)
- effects of external EM disturbances - functional immunity (Chapter 6)
- limitation of disturbance emissions (Chapter 7)
- mutual influences between systems (Chapter 8)
- equipment immunity (Chapter 9)

4. FREQUENCY BANDS

Several factors influence the selection of the mains signalling frequency(ies) and have to be considered:

- a sufficiently reliable signal propagation: this leads to a relatively low frequency
- a sufficient functional immunity against network disturbances
- avoiding of interferences of other equipment from line conducted or radiated effects
- avoiding of mutual interference with neighbouring installations

The frequencies bands allowed for mains signalling have been standardized by IEC [1] and CENELEC [2]. The lower limit has been set above the Ripple Control frequencies at 3 kHz. As for the upper limit, the critical factor is to avoid disturbances of the radio

communication services, more exactly of the long wave broadcasting frequencies. The upper limits became therefore:

- in Europe - ITU Region 1 - where there are several LW stations: 148,5 kHz (150 kHz less the sideband AM modulation) [1] [2]
- outside Europe - ITU Regions 2 or 3 - 500 kHz respectively 525 kHz. [1]

In order to avoid mutual influences, it appeared appropriate to split the frequency band at 95 kHz into two parts, the lower part 3 to 95 kHz being allocated to Utilities and their licensees (better signal transmission over long lines), the upper part 95 to 148,5 kHz being allocated to private users. Furthermore, a share of the upper part 125 to 140 kHz is reserved for systems with an access protocol, in order to avoid mutual influences between private systems (see Chapter 8).

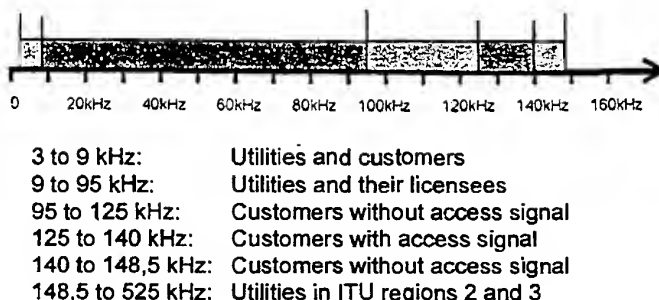


Fig 1 - Frequency allocation for Mains Signalling

It should be noted that in the frequency band 3 to 148,5 kHz there are still some LW radio stations, e.g. for Standard Frequency and Time Signals (for example, in Switzerland at 20 kHz) or for Navigation purposes (LORAN). It is advisable to avoid such frequencies.

5. SIGNAL LEVEL

Somewhat similar considerations as for the frequency bands should be made for determining the signal level

- on the one hand a sufficiently high signal level should be provided in order to allow a good functional immunity on a very disturbed channel, the power network
- on the other hand, the signal level should remain sufficiently low in order to avoid interferences with other equipment, particularly with radio services.

Experience gained during long trials, have shown that in for a correct operation of the receivers, assuming an appropriate signal modulation (see Chapter 6), a signal level in the range of $60 \text{ dB}\mu\text{V} \sim 1 \text{ mV}$ is appropriate. Further on the LV level it can be reckoned with an average signal attenuation on the utilities' LV lines of ca. 60 dB (in home networks 20 to 40 dBs) so that a minimum signal emission level in the range of $120 \text{ dB} \sim 1\text{V}$ (in home networks $100 \text{ dB} \sim 0,1 \text{ V}$) is necessary. These levels depend on the frequency. Higher levels will assure a more secure operation.

A particular feature of MS is that the output impedance of the emitters, the LV or MV network impedance at the signal frequency varies in a very large range. In a LV network, this output impedance can vary between 1Ω up to 200Ω depending on the momentary load, the load represented by the receivers, the length of the lines, etc., ... MS emitters have to be designed accordingly.

A problem arises with testing and in case of certification as for comparable and reproducible results, identical measurement conditions have to be specified. For understandable reasons, it has been tried to use existing CISPR equipment. The testing arrangement defined by the relevant standards [1], [2] prescribes the use of artificial mains V-networks with $50 \Omega / 50 \text{ mH} + 5 \Omega$ according to CISPR 16-1, Annex F as standardized loads (as the standard CISPR network is designed for frequencies above 150 kHz, it has a too high impedance at the lowest mains signalling frequencies. Either the 5Ω resistance must be replaced by $1,6 \Omega$ or the equipment must be extended by an adaptive network). The use of a standard CISPR network offers the advantage that it allows the measurement of out-of-band spurious disturbances with the same arrangement (see Fig 2).

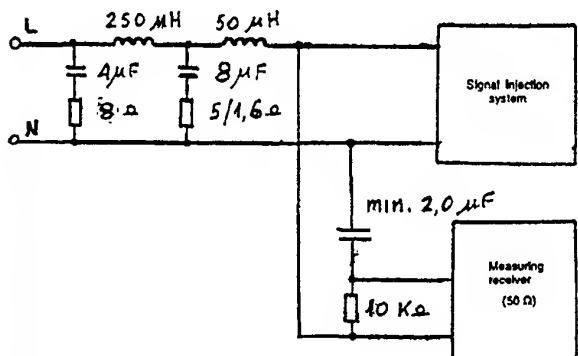


Fig 2 - Measuring arrangement for MS Signals

The signal limits and the detailed measurement procedures for the different kinds of systems are described in the relevant standards [1], [2]. For general information we shall consider in this paper the systems normally used with injection between phase and neutral (differential mode). With regard to the very short signals (see Annex B), peak values shall be measured with an appropriate spectrum analyzer.

In the testing arrangement the following levels should not be exceeded (see Fig 3):

- 3 to 9 kHz
 - 9 to 95 kHz
 - 95 to 148,5 kHz
 - 134 dB μ V/5.0 V
 - Narrow band signals:
decreasing from 134 dB μ V/5.0 V to 120 dB μ V/1.0 V with the logarithm of the frequency
 - Wide band signals:
134 dB μ V/5.0 V, but no single frequency shall exceed 120 dB μ V/1.0 V
 - General use: 116 dB μ V/0.8 V
 - Particular applications
(industrial) 134 dB μ V/5.0 V

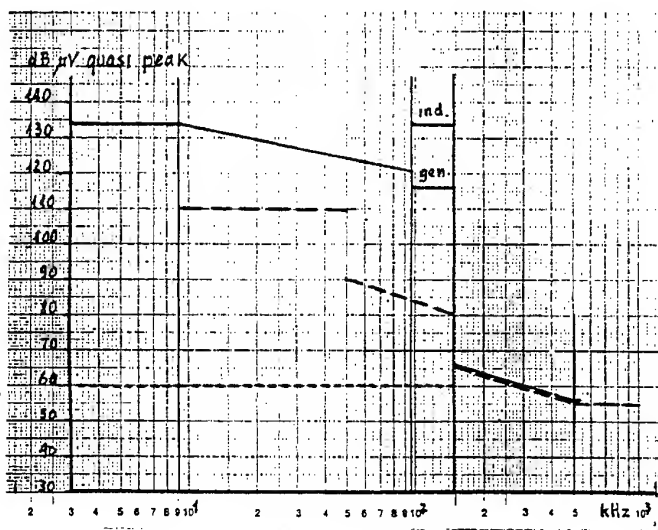


Fig 3 - Mains signalling levels and CISPR limits

- Mains signalling emission level
 - - - Range of magnitude of Mains signalling receiving level
 - CISPR limits for induction appliances

It should be noted that in practice the emitters generally send their signals on a mismatched network impedance and that the actual emission voltage may be quite different from the above nominal values: higher or lower. Furthermore, resonances may occur.

6. EFFECTS OF EM DISTURBANCES ON MAINS SIGNALLING SYSTEMS - FUNCTIONAL IMMUNITY

MS Systems are exposed to various external radiated or conducted EM disturbances, which may prevent a correct functioning.

As for radiated disturbances, two main sources are of importance:

- radio broadcast in the frequency range of MS like Time Signal Transmitters (e.g. in Switzerland 20 kHz, in Germany 75 kHz) or Maritime Navigation Transmitters (LORAN) with high field levels (up to 1 V/m near the stations)
- unintentional industrial disturbances (e.g. induction ovens) or residential (e.g. induction cooking appliances in the frequency band 20 to 40 kHz)

These radiated disturbances may influence MS apparatus either directly or by induced currents. As for the broadcast transmitters, the easiest way to avoid interferences is to avoid these frequencies. As for unintentional disturbances, no general recommendation exists for limits, but maximum field values are specified in CISPR 11 for induction appliances which may deal as reference. The limits of the magnetic field measured in a 2 m loop antenna should not exceed 108 to 73 μ A/m, decreasing from 9 to 148,5 kHz.

Conducted disturbances originate from various sources, e.g.:

- induction cooking appliances (20 to 40 kHz)
- light dimmers (periodic spikes)
- TV sets (sweep frequency)
- induced voltages (e.g. from industrial equipment)
- random switching phenomena

Fig 4 shows a typical record of conducted disturbances in the range 10 to 100 kHz. Generally, and in this example, three kinds of disturbances may be differentiated:

- Gaussian noise (switching operations)
- specific frequencies (e.g. induction applications)
- periodic impulse noise (e.g. light dimmers)
- random impulses

One can note that the Gaussian noise seems to remain quite high below 50 to 60 kHz and to be lower above. Similar values are shown in [9] for MV networks

General limits for conducted disturbances in the frequency band of MS have not (yet) been specified but there exists again information in CISPR 11 for induction appliances which may serve as guidance (also in CISPR 15, for lightning equipment). They are shown in Fig 3.

The functional immunity of a MS System in such a disturbed environment must be achieved by the use of a sophisticated signal modulation methods associated with sophisticated coding. This problem is very complex, has been subject of thorough studies and cannot be dealt with in the context of this paper. All the

classical modulation methods - or keying - are used: Amplitude Modulation Keying AMK, Phase Shift Keying PSK, Frequency Shift Keying FSK, Spread Frequency Keying ... Recent developments led to a combined Method: Spread Frequency Shift Keying S-SFK [9] whereby two frequencies are used for data 0 or 1, the two frequencies are separated by great distance (> 10 kHz) and each one is frequency modulated. Such a method combines the advantages of the two single methods.

In order to check the functional immunity of MS Systems to above conducted disturbances, specific test methods are proposed.

In IEC, for Distribution Automation Systems the following tests are specified [9]:

- the receivers are operated with a reference message at signal in the range of 2 mVrms to 20 Vrms.
- three kinds of disturbances are added:
 - Gaussian noise with increasing energy
 - Specific continuous frequencies ($P_N/P_S < 30$ dB)
 - periodic impulses 5 Vp.p, 100 to 1000 Hz, signal at 20 ms.
- with all these tests, a bit error rate BER of $< 10^{-5}$ should be achieved.

In CENELEC, the immunity requirements specify only a test with narrow frequencies in the out-of-band frequency ranges. The disturbance signals should have an unmodulated amplitude

- for Utility systems of 134 dB μ V/5.0 V
- for private systems of 134 to 120 dB μ V/5.0 to 1.0 V

 It is required, according to the case, that the tested equipment continues to operate normally or that only a temporary loss of function occurs.

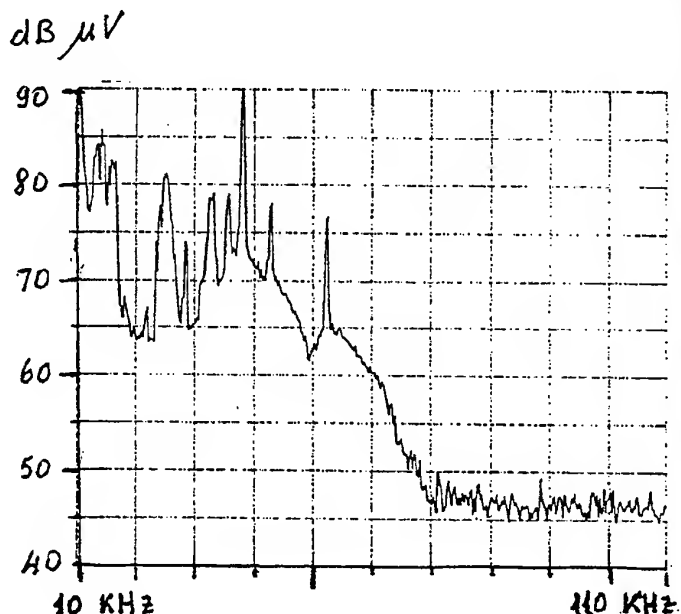


Fig 4 - Example of conducted disturbances in the frequency range 10 to 100 kHz

7. EM DISTURBANCES FROM MAINS SIGNALLING SYSTEMS

MS Systems are also a source of radiated or conducted disturbances in the frequency range 3 to 148,5 (525) kHz and of out-of-band spurious radiations at higher frequencies. They could influence other devices, particularly electronic equipment and radio services.

A main concern could arise from the EM fields generated by the signal voltages or currents circulating on the power lines. The worst case is probably the one of an overhead line near a emitter influencing a radio receiver at a distance of 10 to 20 m. Accurate field calculations or even adequate approximations seem quite difficult (near-field conditions, earth return, etc., ...). In the context of this paper, the task is not to carry out a general study of these fields but to make an assessment of acceptable limits.

We refer, rather than to a theoretical approach, to a thorough, practical measurement of EdF [10] measurements in a MV network (the results are also valid for LV lines). They led to the following ranges of magnitude of the EM fields, with 1.0 V injection level, near the injection point, between 10 and 100 kHz:

- E field ca. 90 dB μ V/m / 30 mV/m \pm 20%
- H field ca. 40 dB μ V/m / 0,1 mA/m \pm 20%

With the allowed nominal voltage of 5.0 V/m (+ 14 dB). E fields of ca. 150 mV/m and more would be expected. These fields are much higher than the sensitivity of radio receivers for time signals. For this reason also, these frequencies should be avoided. Fortunately the field is reduced with increasing distance to the lines, but they are anyway much lower in cable networks, and mains signalling transmission duration are very short.

With regard to conducted disturbances, limits in the considered frequency range are specified in CISPR 11 for induction appliances (induction cooking) which can serve as reference (see Fig.1):

9 to 50 kHz:	110 μ V peak / 200 mVrms
50 to 148,5 kHz:	90 to 80 μ V peak / 30 to 10 mVrms decreasing linearly with the logarithm of frequency

These limits are lower than the mains signals.

It appears that generally there is not yet concordance between the Mains Signalling Standardization and the CISPR limits (CENELEC SC 205A has invited CISPR 205A to discuss this problem).

Out of band conducted or radiated disturbances - above 148,5 or 525 Hz - shall be limited according to usual values specified by the Generic Standards [12] of CISPR 14.

8. MUTUAL INFLUENCE BETWEEN NEIGHBOURING SYSTEMS

This problem is not directly EMC related, but is still dealt with in the MS standards, e.g. [2]. Several systems could be installed in the same LV network and should not of course influence one another. Different methods can be used for this purpose:

- a) separation by frequency bands. That is the method used to separate Utilities Systems from private systems,
- b) allocate different frequencies to different systems,
- c) install filters to prevent the signal propagation (CENELEC SC 205A prepares relevant standards),
- d) make use of an acces or signal protocol; such a signal is sent by the first emitter to operate and is received by the "slave" emitters so that further emissions are avoided. In the EU this procedure is specified for the private systems in the sub-band 125 to 140 kHz [2].

The access control consists of an impulse of 4 ms at a frequency of $132 \pm 0,5$ kHz and 80 dB μ V/10

9. EQUIPMENT IMMUNITY

IEC has not (yet) developed specific standards concerning the EM immunity of MS equipments for low voltage but the general specifications of the IEC 6100-4-x [11] and 6100-6-x [12] may be applied.

In the EU countries, in principle and as far as relevant, MS equipment should comply with the EMC directive and CENELEC is preparing relevant standards [2 to 5]. With regard to the immunity standard, there is to note:

- requirements for private systems are based on the classical generic standards for residential/commercial environments or "normal" industrial environments [12]
- requirements for utility systems are based on the generic standards for industrial environments, but with some more severe test values, in particular for the magnetic field tests and the electrostatic discharge test.

10. FINAL REMARKS

Mains Signalling Systems are an interesting example of how far a complex electronic system, a comprehensive approach of all EMC features is necessary: frequency, signal level, functional immunity, limitation of emitted disturbances, co-ordination of several systems, apparatus immunity, ... Relevant standards are available or being prepared in IEC and CENELEC. Not dealt with in this paper, and not clear, is the question how these technical features interact with the economic ones.

ANNEX A: STANDARDIZATION ORGANIZATIONS

At international level, the following bodies deal with EMC standardization in the field of Mains Signalling.

IEC SC 77B = Basic standards concerning frequency bands, signal levels, etc., ...

CISPR B = Limitation of radio frequency disturbances

IEC TC 57 = Distribution automation using distribution line carrier systems

CENELEC SC 205A = Mains communication systems

ANNEX B: MAINS SIGNALLING SYSTEMS - EXAMPLES OF SIGNAL CHARACTERISTICS

Example: Modulation method - Frequency(ies) - speed
Emission levels → Receiver level

SYSTEMS FOR UTILITIES

System A: S-SFK - 47/62 kHz - 600 Bd

1 V_{rms} → 1 mV_{rms}

System B: FSK - 82 ± 0,3 kHz - 600 Bd

2 V_{rms} → 3 mV_{rms}

SYSTEMS FOR PRIVATE USERS

System X: S-SFK - 105,6/115,2 kHz - up 1200 Bd

0,8 V_{rms} → 1 mV_{rms}

System Y: ASK - 97 kHz - 300 Bd

0,8 V_{rms} → 2 mV_{rms}

BIBLIOGRAPHY

- [1] IEC 61000-3-8/Ed.1 (1997): Electromagnetic Compatibility - Part 3: Limits - Section 8: signalling on low voltage electrical installations - Emission levels, frequency bands and electromagnetic disturbance levels (IEC SC 77B)
- [2] CENELEC EN 50065-1 (1991/2/5): Signalling on low voltage electrical installations in the frequency range 3 kHz to 148,5 kHz - Part 1: General requirements, frequency bands and electromagnetic disturbances (CENELEC SC 205A)

[3] CENELEC draft EN 50065-2-1: Signalling on low voltage electrical installations in the frequency range 3 kHz to 148,5 - Part 2-1: Immunity requirements for Mains Communications Equipment and systems operating in the range of frequencies 95 to 148,5 kHz and intended for use in Residential, Commercial and Light Industrial Environments (CENELEC SC 205A)

[4] CENELEC draft EN 50065-2-2: like [3] but intended for use in Industrial environment (CENELEC SC 205A)

[5] CENELEC draft EN 50065-2-3: like [3] but for the frequency range 3 to 95 kHz and intended for use by Electricity Suppliers and Distributors (CENELEC SC 205A)

[6] IEC 61334-1-1/TR3 (1995): Distribution automation using distribution line carrier systems - Part 1: General conditions - Section 1: Distribution automation system architecture (IEC TC 57)

Note: This document includes in Annex B a comprehensive list of all the documents of the IEC 61334 series

[7] IEC 61334-3-1 (CDV): Distribution automation using distribution line carrier systems - Part 3: Mains signalling requirements - Section 1: Frequency bands and output levels (IEC TC 57)

[8] IEC 61334-1-4/TR3 (1995): Distribution automation using distribution line carrier systems - Part 1: General conditions - Section 4: Identification of date transmission parameters concerning MV and LV distribution mains (IEC TC 57)

[9] IEC 61334-5-1/TR2 (1996): Distribution automation using distribution line carrier systems - Part 5: Low layer profiles - Section 1: Spread frequency shift keying (S-FSK) profile (IEC TC 57)

[10] EdF Report 93 NR 00020 (1993): Analysis of radiation characteristics of distribution line carrier with NEC Code - N. Recrosio

[11] IEC 6100-4-X: Electromagnetic compatibility (EMC) Part 4: Testing and measurement techniques - Whole set (IEC TC 77)

[12] IEC 61000-6-1/2: Electromagnetic Compatibility (EMC) Part 6: Generic Standards - Whole set. (IEC TC 77)

INFLUENCE OF COMPACT FLUORESCENT LAMPS (CFLs) ON ELECTRICAL POWER QUALITY IN DISTRIBUTION NETWORKS - A PELP/DSM PROGRAM

Zbigniew Hanelka*, Adam Siwik*, Adam Gula*, Marc R. Ledbetter**, Robert G. Pratt***

*University of Mining and Metallurgy, 30-059 Cracow, Al. Mickiewicza 30, POLAND

** Battelle Pacific Northwest National Laboratory, SW Main Street, Suite 815, Portland, OR 97204-3216, USA

*** Pacific Northwest Laboratory, Battelle Boulevard, Richland, Washington 99352, USA

Due to the expanding application of energy-saving loads such as radio and TV equipment, lighting sources, computers, etc. the power of nonlinear loads in electrical installations is continuously growing. In 1997 this phenomenon was further enhanced by a very intense promotional campaign for energy-saving compact fluorescent lamps (CFLs) in three cities of Poland (part of the PELP/DSM program). Measurements of a wide range of electrical power parameters were carried out before and after the promotional sale of the CFLs in all the three cities. The results of these measurements demonstrated that despite the significant numbers of CFLs installed, the level of voltage distortions in the supply network did not increase significantly.

1. INTRODUCTION

The main goal of the currently implemented DSM programs is to improve the efficiency of energy utilization in commonly used loads at the same (or even enhanced) level of user's convenience. The most frequently implemented contemporary DSM programs in various countries focus on:

- promotion of energy- and material-efficient drives and electrical motors
- promotion of energy-efficient lighting systems. The potential energy gain can reach very significant values. For example in 1995 there were 10,418,000 registered households in Poland consuming 18.1 TWh of electrical power. There is significant potential for a reduction in energy consumption. It is estimated that electrical lighting accounts for about 55% of energy consumption in residential space (9.94 TWh) [6.4].

The above mentioned data were, among others, the basis for a decision made in 1997 on the creation of the Polish Efficiency Lighting Project (PELP/DSM). The objective of this program was to promote energy-efficient lighting sources - the compact fluorescent lamps (CFLs).

The key advantages of CFL units are a nearly 75% reduction in electrical power consumption at equivalent lighting rates (as compared to conventional incandescent lighting sources) and an eight to ten fold extension of operating life. As in many other cases, CFLs have some disadvantages, which are the price to pay for the improvement of energy efficiency. These disadvantages

are the sensitivity of the devices to supply voltage disturbance and the fact that CFLs themselves generate distortions into supply network. The PELP/DSM program team considered these issues as an integral part of the program. Numerous studies and measurements carried out by the team members aimed at answering the question on the extent of harmful effects of the new energy-efficient lighting systems (CFL) offered by the PELP/DSM program.

The power sector should perceive this problem as an important element of the DSM program and take the eventual costs related with the reduction of these harmful effects into account in the global economic assessment of power distribution management.

After a detailed analysis of all the aspects (technical, economic, sociological, etc.) three cities were selected for a trial implementation of the program: Chełmno, Ełk and Żywiec. The objective of the first phase of the PELP/DSM project was to reach, in a relatively short period of time, a „saturation” of households and some public buildings (such as schools) with energy-efficient CFLs. For the needs of the experiment, the prices of CFL units in these three cities have been significantly reduced (subsidized) and the sales were based on namely coupons. During the first few weeks almost 20,000 CFLs were sold in the three cities. Thanks to the efficient marketing campaign the program reached a very high degree of saturation, measured by the number of CFL units per statistical household (family houses in the urban area). The saturation degrees were 5.34 in Chełmno, 3.67 in Ełk and 9.0 in Żywiec. Such a situation contributed to a very advantageous environment for energy quality measurements. The intense sales of CFLs were initiated at precisely determined dates. To assess the impacts of CFLs on power supply conditions the situation before the sales program and after installation of the energy-efficient units were compared.

2. ENERGY-EFFICIENT CFL UNITS

There are two main types of CFL units, differing by the design of the starter circuit: magnetic and electronic ballast CFLs. The CFLs have numerous obvious advantages but also some disadvantages:

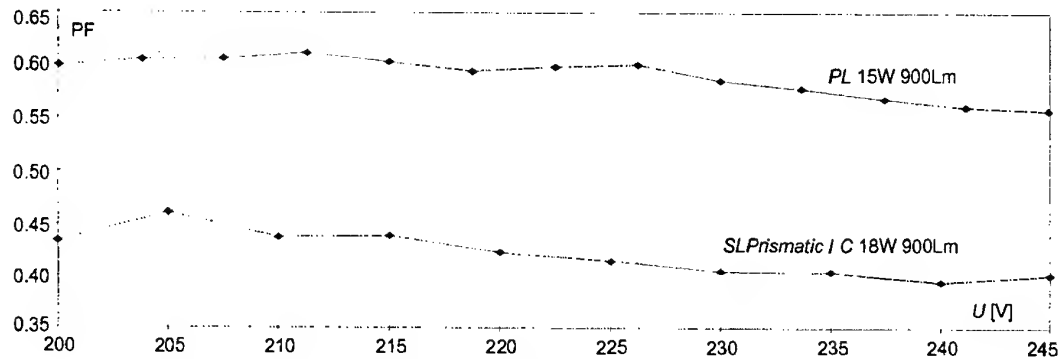


Fig. 1 Examples of relations between the power factor of CFL units and the supply voltage

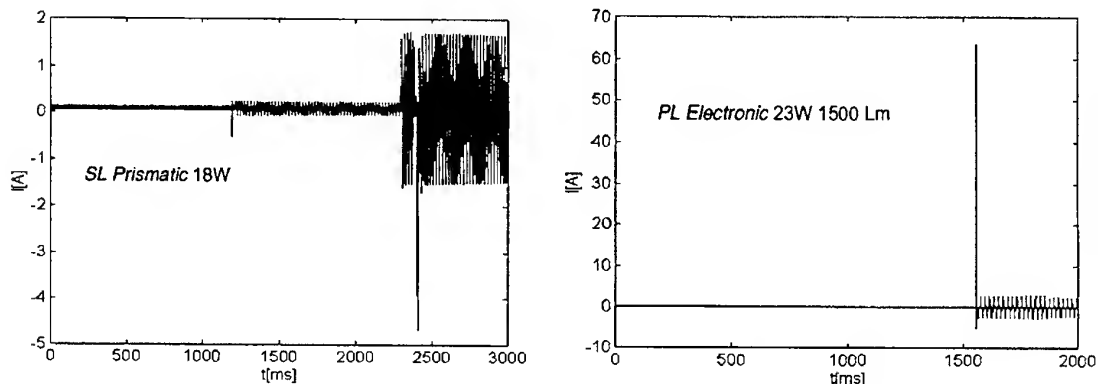


Fig. 2 Time waveforms of the start-up current of two selected types of CFLs (magnetic and electronic start-up circuits)

- low value of the power factor
- unfavorable course of the start-up process
- flicker phenomena
- generation of current higher harmonics (hh).

2.1 Power factor (PF)

The average PF value for the CFL units with magnetic ballast (SL) is about 0.4 to 0.5 versus 0.55 to 0.65 in CFLs with electronic starters (PL). The low value of this factor mainly results from current distortions. It should not be forgotten that there is a difference between the power factor and the coefficient of displacement between the basic voltage and current harmonics (displacement power factor - DPF). The DPF value is significantly higher for both types of CFLs (Table I).

Figure 1 shows examples of the relations between the power factors of selected CFL units and the value of the supply voltage. It is clearly discernible that the values of this factor are significantly higher in the case of magnetic ballast CFLs (due to lower current distortions).

2.2 Starting-up of the CFL units

Due to the specific design of the starter circuit, the process of switching-on a CFL unit may become a source of distortions in the supply network and cause discomfort to the users. Figure 2 shows examples of CFL start-up currents waveform plots. There is a discernible very short (ms) current overload, with a peak value 20 times higher than the nominal current level. There are two discernible

phases in magnetic ballast CFL start-up current waveforms. During the first phase, the current reaches about 50% of the nominal value and during the second phase it increases up to the nominal value.

In the case of CFL units with electronic start-up circuits these phases are not discernible. The negative effects are particularly dramatic in the situation when many CFLs are turned on simultaneously (i.e. in public buildings, offices, schools, etc.). There is a real threat of contact welding in installation switches when the contactor's Joule integer is not adapted to the thermal effect accompanying connection.

2.3 Flicker phenomena

Fluorescent light sources have a significantly lower thermal time constant (as compared to conventional incandescent light sources). Thus they are much faster in reacting to any change in the supply conditions (i.e. change in the shape of the supply voltage). The measurements performed demonstrated, that the time constant of a 60W/220V incandescent bulb was approx. 18.6 ms whereas the same parameter for a fluorescent lamp was about four times shorter. Laboratory tests showed that CFL units with electronic start-up circuits are much better in terms of sensitivity to voltage variations and generation of flicker. For a voltage variation frequency below 25 Hz CFLs cause less flicker than incandescent light sources (this relation is strongly dependent on the type of the CFL, manufacturer and even the individual specimen of the product). This situation changes when the frequency increases.

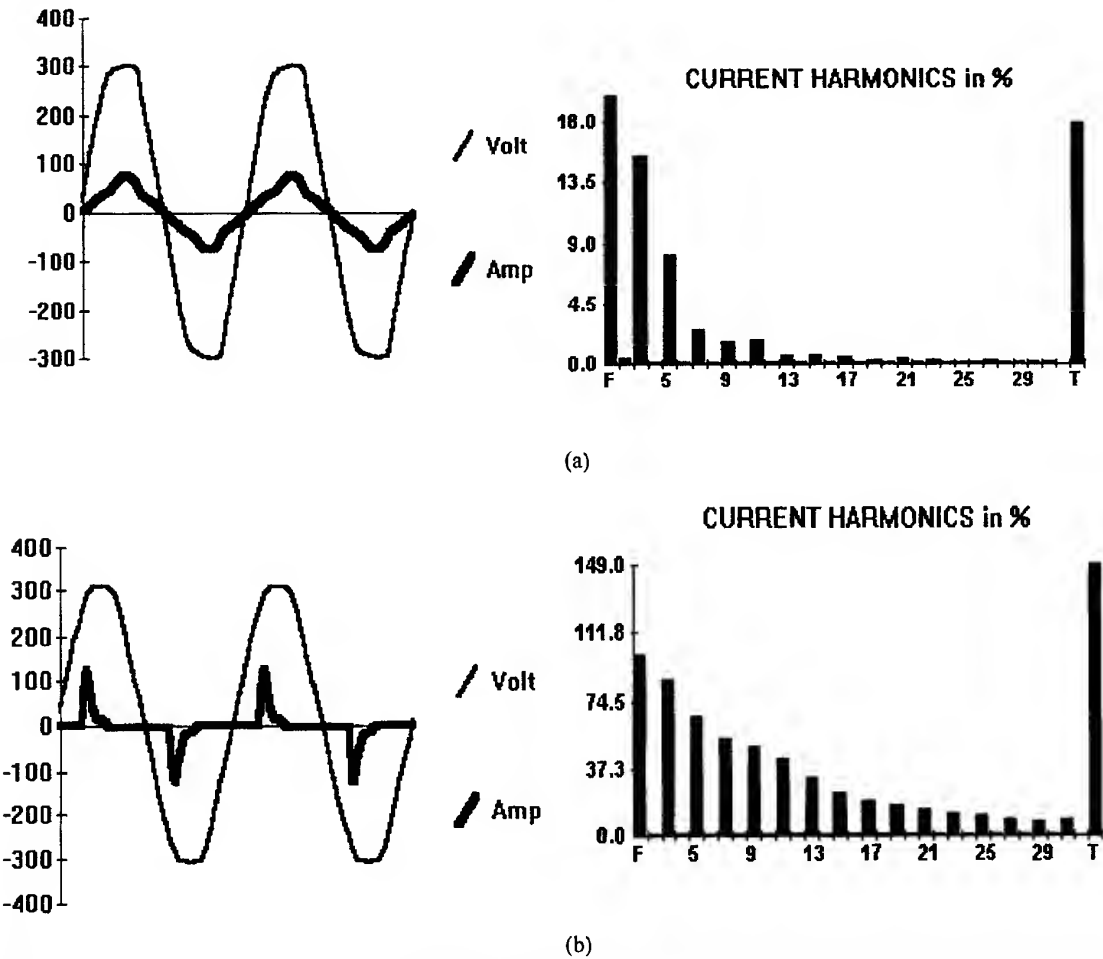


Fig. 3 Waveform and spectrum of the current in a) magnetic CFL unit, and b) PLC23 electronic CFL unit (current scaled 200:1); F - basic harmonic, T-THD₁

2.4 Higher order current harmonics

The introduction of electronic ballast circuits allowed energy saving but simultaneously caused an expansion of the waveband of distortions (due to the application of a 20-25 kHz converter in the electronic circuit). According to [6.9] the promotion of energy-efficient light sources in the USA lead to several cases of problems with electromagnetic compatibility. There were a few cases of interference with the operation of nearby electrical equipment and devices due to conduction and radiation interference of CFLs (disturbed operation of clocks, noise in walkman headphones, malfunctioning of wireless phones, interference of CFL's infrared radiation with household remote control devices).

2.5 Influence of the electromagnetic environment on the operation of CFL units

The major part of CFL-related publications known by the authors address the issue of their harmful effects in supply networks and interference with the operation of nearby loads. The problem of the influence of operating environment on the functioning of the CFL units is very seldom addressed. Some rare exceptions to be mentioned are papers [6.1 and 6.6]. The laboratory tests performed

(on a limited pool of CFL units of both magnetic and electronic ballast type) demonstrated that in both types of CFL units an increase in voltage distortion ("flattening" of the voltage sinusoid near the peaks) had a positive influence on the CFL current spectrum and the THD value. In current waveforms this process was illustrated by longer current flow times during subsequent half-periods of the supply voltage. It was found that the extent of this influence varies depending of the manufacturer, power rating and individual specimen of the CFL.

2.6 Lower order current harmonics

Figure 3 shows examples of waveforms and plots of spectrum analyses of currents supplying magnetic CFL units (Figure 3a) and electronic CFLs (Figure 3b). The spectrum remains broad in both cases (more particularly in the case of electronic CFLs). It can be assumed that in such cases the analysis should take into account nearly 29 harmonics. Odd harmonics are dominant (third, fifth, seventh and ninth). The spectrum of CFL current varies depending on the manufacturer, power rating and type of ballast circuit. In the case of magnetic CFL a typical value of the THD coefficient is approx. 20% and in the case of electronic units the THD value exceeds 100%. Phase shifts between harmonic currents marks of various

CFL units indicate that they sum up geometrically (not arithmetically). It was found that an increase in CFL's power rating causes an increasing variability of current shapes, values of particular harmonics and their phase angles, leading to a diversification of the THD values.

3. PARALLEL OPERATION OF CFLS AND OTHER ELECTRICAL DEVICES

Figures 3b and 4 show the harmonic spectrum of example single-phase low-power nonlinear loads most frequently installed by individual users (personal computer and CFL unit). The level of hh in the 220 V

supply voltage did not exceed $\text{THD}_U \approx 3.5\%$ during the test. Figure 5 shows the corresponding waveforms plotted during simultaneous operation of the above mentioned receivers (also see Table 1).

It is worth noticing that simultaneous operation of different types of loads, due to different phase shifts of current hh, causes a spontaneous reduction of certain harmonics in the resultant current spectrum.

From the standpoint of a low voltage supply network, so-called „triple harmonics” are particularly significant. These are harmonics of orders being integral multiples of three. They form a zero-order symmetrical component, thus increasing the loading of the neutral wire (PEN).

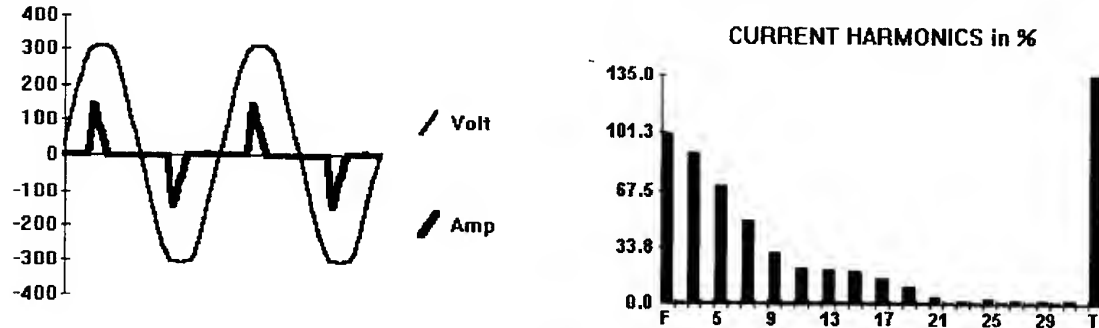


Fig. 4 Waveforms of the voltage and current (current scaled 100:1) and the spectrum of current harmonics for the personal computer; F - basic harmonic, T- THD_I

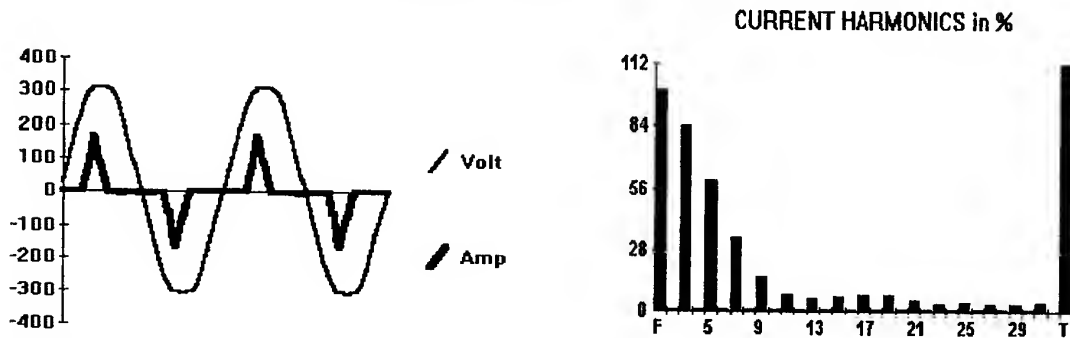


Fig. 5 Current (x100) and voltage waveforms and spectrum of the harmonics with PC (Fig. 4) and PLC23 (Fig. 3b)) operating simultaneously

Table 1: Some electrical features in power supply lines during operation of selected nonlinear loads

Type of load	I_{rms} A	P W	Q VAr	PF	DPF	Angles [°el] of n-th current harmonics to fundamental					THDI %
						n = 3	5	7	9	11	
PC	0.44	56.5	11.1	0.57	0.98	-153	59	-84	142	26	134.6
PLC 23	0.17	19.9	8.8	0.51	0.91	-125	120	16	-91	158	148.8
PC+PLC23	0.54	77.4	19.6	0.64	0.97	-147	71	-67	166	57	112

P - active power (basic harmonic)

Table 2: Selected results of measurements of the influence of nonsymmetrical and quasisymmetrical power loads on three-phase networks with phase nonlinear loads (PC+PLC23+PLC20)

Type load	I_{L1} A	I_{L2} A	I_{L3} A	I_{PEN} A	THDI [%]				Harmonic ratio HR% in vires L1/PEN				
					L1	L2	L3	PEN	n=3	5	7	9	
Nonsymmetrical	0,63	0,78		0,94	98	90		172	80	49	20	4	
									153	67	14	19	
Quasi-symmetrical	0,61	0,72	0,68	1,16	94	87	83	940	78	46	16	4	
									894	167	125	131	

Table 2 shows example results of measurements performed on selected lines of a three-phase four-wire supply network after connection of a symmetrical power load or an asymmetrical connection of the same set of nonlinear loads.

In this case, a two-phase asymmetrical load increases the rms value of the current in the neutral wire by approx. 50% (as compared to the phase wires). The level of harmonics in the PEN wire is two times higher than in any of the phase wires. It is obvious that in this case, currents of the third and ninth harmonics (as well as of the other harmonics of zero order) add up in the neutral line.

In the situation of a practically symmetrical loading of the network with nonlinear loads, according to Table 2, the rms value of the current in the neutral wire is higher than in any of the phase wires (a difference reaching as much as 70%). Also the higher harmonics of zero order are more discernible than in the case of nonsymmetrical load (this particularly applies to the third harmonic). The higher harmonic content coefficient in the PEN wire is close to 1000%. In the case of a symmetrical power loading of a three-phase network the neutral wire is exposed to the presence of all the current harmonics, therefore the rms current value in this wire is higher than in the case of nonsymmetrical loads. This last observation may become useful in future assessment of potential malfunctioning of differential-current switches commonly applied in electrical shock prevention systems for low-voltage installations.

4. HIGHER HARMONICS OF LOWER ORDERS IN SUPPLY NETWORKS

There is a very large number of publications addressing the issue of CFL impacts on energy quality, particularly focusing on voltage distortions in distribution networks. The information provided in these publications certainly does not reflect the complete knowledge in this field. In many cases data are contradictory and do not allow any synthesis or conclusion to be drawn. Most of the publications are rather focused on the potential for distortions and not on real cases of such threats.

Maybe this results from a low saturation of this type of loads in the networks analyzed by the authors. In most cases these publications refer to American power supply networks, and the main research method applied is simulation and static modeling. The results obtained are, according to the authors of [6.2.] „unrealistically high” in terms of harmonic contents.

Figure 6 shows examples of typical waveforms of the selected harmonics in a power line supplying a residential building (75 flats in Chełmno). The changes in the value of the third harmonic (dominating the analyzed spectrum) can be considered as a basis to conclude on the extent of nonlinear load saturation (and thus on the saturation with CFL units). There is a very well discernible increase in the value of „triple” harmonics, resulting from the application of CFLs but also other electronic devices used in household conditions. The current and voltage waveforms were recorded over several days of the experiment. By comparing the measurement results obtained before and after intense promotion of the CFLs

it was found that the increase in third harmonic levels reached a maximum of a dozen percent (in all measured cases). No significant increase in THD value was observed. The graphs presented on Fig. 6 are typical for the analyzed types of electrical loads and indicate:

- a load asymmetry between particular phases of the supply system
- a high value of THD coefficient in the neutral wire
- a significant (but „safe” in terms of permissible load levels) content of the „triple” harmonics, most particularly third harmonic in the neutral wire (PEN). The value of this harmonic varies along with the changes in daily load.

5. CONCLUSIONS

The amount of nonlinear loads (including CFLs) installed and operated in public buildings in Poland is rather small and linear loads account for a very significant part of the supplied power. Therefore the probability of supply voltage distortion in power distribution systems of public and residential buildings is yet rather low.

ACKNOWLEDGEMENTS

The authors acknowledge the unique opportunity to perform the measurements in field conditions made available by the Polish Efficient Lighting Project (PELP) sponsored by Global Environment Facility (GEF) and administered by International Finance Corporation (IFC). They also acknowledge the financial support of the University of Mining and Metallurgy (UMM Grant no. 21.210.07).

6. REFERENCES

- 6.1. Arseneau R., Quellette M. „The effects of supply harmonics on the performance of compact fluorescent lamps” IEEE Trans. on Power Delivery, 8, 2, 1993
- 6.2. Brauner G., Wimmer K. „Nefzruckwirkungen durch Kompaktleuchtstofflampen in Niederspannungsnetzen” Technische Universität Wien, Institut für Elektrische Anlagen Juli 1995 Chazottes B., Fauquemberque P., Lachaume J. „Harmonic disturbances caused by compact fluorescent lamps” PQA '94, Amsterdam
- 6.3. Drożdż M. „Effects of introducing energy-efficient light sources on the national power system” (polish), Power Quality and Utilization, 2, 2, 1996,
- 6.4. Emanuel A. E., Peretto L., The response of fluorescent lamp with magnetic ballast to voltage distortion, IEEE Trans. on Power Delivery, 1997, 12,
- 6.5. Etezadi – Amoli M., Florence T. „Power factor and harmonic distortion characteristics of energy efficient lamp” IEEE Trans. on Power Delivery, 4, 3, 1989.
- 6.6. Guła A., Hanzelka Z., Ledbetter M., Pratt R., Rudek R., Siwik A., Stana P., Reducing residential peak power loads with compact fluorescent lamps (CFLs), 4 th Intern. Conf. Electrical Power Quality and Utilization, Cracow, Sept 23-25, 1997.

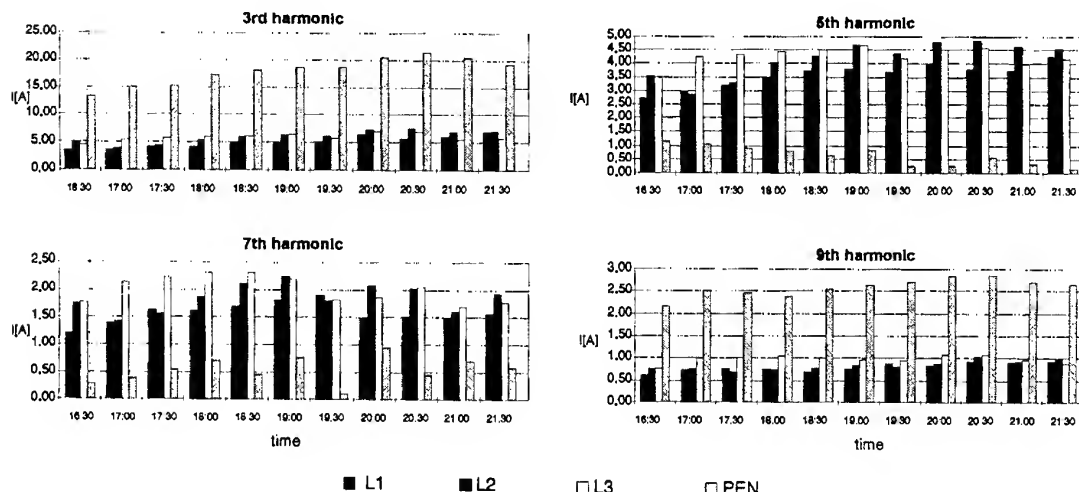


Fig. 5 Examples of results of current harmonics and nonsymmetry measurements in a selected measuring point (building with 75 flats and 373 CFLs with a total power rating of 5,910W)

- 6.7. Kataoka S., Atagi K., Preventing IR interference between infrared waves emitted by high-frequency fluorescent lighting systems and infrared remote controls, IEEE Trans. On Industry Applications, 1997, 33, 1
- 6.8. Lachaume J., Fauquemberque P., „Harmonics in distributions systems generated by lucompact lamps” Fifth Alberta Exposition and Conference on Power Quality, Calgary October 19-22, 1993
- 6.9. Pileggi D.J., Gulachenski B.M., Gentile T.J., Emanuel A.E., „The effect of modern compact fluorescent lights on voltage distortion”, IEEE Transaction on Power Delivery, 8, 3, 1993
- 6.10. Rudek R., Stana P., „Influence of the energy-saving light sources on the residential load characteristics and electrical power quality”, Faculty of Electrical Engineering, Automatics and Electronics Univ. Of Mining & Metall., 1997
- 6.11. Siwik A.: „Energy-saving discharge lamps as a sources of disturbances in the low-voltage power networks” (polish), Power Quality and Utilization, 2, 2, 1996, pp.3-8
- 6.12. Topalis F.V., Effiency of energy saving lamps and harmonic distortion in distribution systems, IEEE Transaction on Power Delivery, 8, 4, 1993
- 6.13. Vederber R., Morse O.C., Alling W.R., „Harmonics from compact fluorescent lamps” IEEE Transaction on Ind. Appl., 29, 3, 1993.

Zbigniew Hanzelka, Ph.D. Eng, Associate Professor of the Institut of Electrical Drive and Industrial Equipment Control, UMM, phone: (+4812) 617 28 78; fax: (+4812) 633 83 44; e-mail: hanzel@uci.agh.edu.pl

Adam Siwik, Ph.D. El. Eng. at UMM in Cracow. Faculty of Electrical Engineering, Automatics and Electronics, phone: (+4812) 617 28 25; fax: (+4812) 634 57 21; e-mail: asiwik@uci.agh.edu.pl

Adam Gula, Professor of UMM, Faculty of Fuels & Energy; phone: (+4812) 421 37 81 or 421 39 89; fax: (+4812) 421 30 70; e-mail: gula@novell.fj.agh.edu.pl; gigula@cyf-kr.edu.pl

Marc Ledbetter, phone: (503) 417 75 57; fax: (503) 413 21 75; e-mail: mr_Ledbetter@ccmail.pnl.gov

Robert G. Pratt, phone: (509) 375 36 48; fax: (509) 375 36 14; e-mail: rg_pratt@pnl.gov

LOW FREQUENCY MAGNETIC FIELDS NEAR ENERGIZED COMPONENTS OF POWER STATIONS

Bernd Jaekel, Siemens AG A&D GT 6, P.O. Box 3220, D-91050 Erlangen, Germany
e-mail: Bernd.Jaekel@erl6.siemens.de

Abstract

Energized components of power stations are basic sources for the radiation of low frequency magnetic fields. Measurements of the field strengths in the close vicinity of generators, transformers, converters and the generator leads in combined cycle gas turbine power stations are described. The measurements were performed for both the situation of steady-state power station operation and for the process of starting the generator during which time period some energized components are working wholly or in part beyond their nominal rates. An overview of typical magnetic flux density levels which have to be taken into account in the power station environment is presented. The measured levels are evaluated and compared with limits regarding the personnel safety. They can also be used as a basis to determine the required susceptibility of electrical apparatus against low frequency magnetic fields which are to be installed close to energized components.

Keywords

EMC, Magnetic Fields, Measurements, Power Station, Combined Cycle Gas Turbine, Personnel Safety

1. INTRODUCTION

1.1 Experience in the area of low frequency magnetic fields

The occurrence of low frequency magnetic fields with significant levels is closely connected with the operation of energized components like transmission power lines, electric power substations or power stations. The electromagnetic fields generated by them are of great interest to the electric utility industry not only because of recent public concerns regarding perceived health affects caused by magnetic fields but also because of the increasing need to identify steady-state and

transient field levels to which sensitive electronic equipment may be exposed.

There are several papers dealing with field investigations of electric power substations [1, 2] and transmission lines [3], in which results of measurements and calculations of magnetic fields are described. But there are only few data available dealing with the situation in power stations.

1.2 Energized components of power stations

Power stations typically have several components in which the electrical energy is produced, transmitted and distributed. Since there are current densities up to several ten kA in these components they are producing low frequency magnetic fields in addition to their intrinsic function. Particularly in the close vicinity of energized components like the generator, magnetic field strengths of relatively high levels are expected to occur. Thus, basically sensitive equipment which may be installed in the vicinity may be influenced. In addition, the field strength levels could act as a source of influencing or endangering personnel particularly people wearing sensitive equipment such as pacemakers. This might be relativized by the fact that this kind of environment is normally not accessible to the public. But nevertheless the situation for workers or occasional visitors should be clarified. Therefore, knowledge of typical field strengths in this environment is becoming more and more important.

Figure 1 shows a section of an example of a power station layout consisting of several combined cycle gas turbine modules each with an electrical power of 225 MW. Power stations of this type and a module size of about 200 to 400 MW are becoming more and more wide-spread on one hand due to the increasing substitute for old coal plants, and on the other hand due to their special technical features of high reliability and of an excellent

efficiency which finally resulting in low fuel consumption [4].

The relevant energized power station components leading to significant low frequency magnetic field strengths are assumed to be the components carrying high current densities such as generators, transformers or converters. Some of them are in operation only during a short period when starting the generator but in which the components are working about several ten percents beyond their nominal rates.

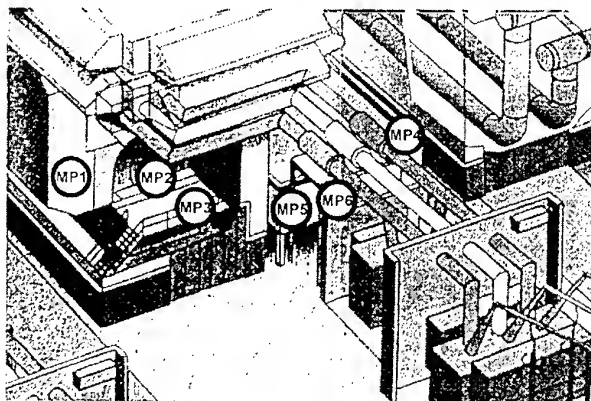


Fig. 1: Schematic layout of a combined cycle gas turbine power station with the measurement points MP (Section)

1.3 Purpose of Investigation

The main intention of these investigations was to get an impression of typical magnetic field strengths at low frequencies in the power station environment. Obtaining data by numerical simulations, however, will require detailed modelling of the energized components as well as of the metallic structures of the station in order to include induced current effects. Such simulations would be very extensive and complicated. Therefore the measurement method was preferred.

Naturally these measurements cannot give an entire description of the field strength distribution all over the power station due to technical and logistical restrictions. Therefore, the measurements were concentrated to particular measurement points.

2. MEASUREMENTS

2.1 Measurement Setup

The measurements were carried out at several combined cycle gas turbine modules of two power stations located at Didcot, with an electrical power of 225 MW per module, designated in the following

as type 1, and at King's Lynn with an electrical power of 347 MW, designated as type 2. Both are situated in Great Britain. The measurements took place during the commissioning period since there was the possibility of several generator starting processes.

The magnetic field strengths were measured with an arrangement of several field probes each consisting of a set of three orthogonally oriented field coils which are constructed of 318 turns with an effective area of 100 cm^2 per turn [5]. The time dependent signals from each coil of a total of five probes, e.g. 15 coils, were recorded using a digital audio tape recorder (DAT-Recorder TEAC RX 8016) with 16 input channels.

The setup is schematically shown in Fig. 2. It allows the field strength at different test points for every field orientation at the same time and also the behaviour of the field strengths over a defined time period to be measured and recorded. This was useful in the case of obtaining data during the start-up of the generator where the field strengths show a strong time dependent behaviour and where due to the converter operation a relatively broad frequency band of radiated magnetic fields is produced. The frequency range under investigation reached from several Hz to several kHz. The recorded signals were evaluated using a spectrum analyzer as well as by means of Fourier analysis of the original time data. Using the frequency dependent correction factors for the receiving coils, the frequency spectra of the magnetic field strengths at different moments in time, different measurement points and for different operation modes could be obtained.

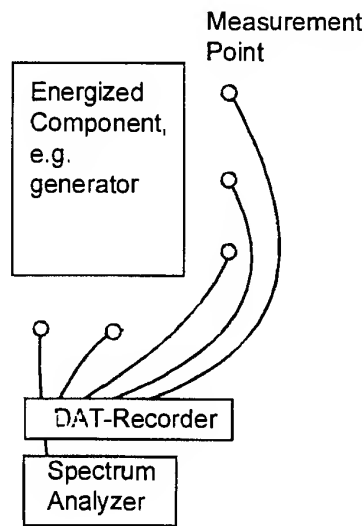


Fig. 2: Schematic Measurement Setup

2.2 Measurement Points

Suitable measurement points were chosen according to two criteria: what are the energy components producing the highest field strengths and where are critical points in the vicinity of these components? These points were derived during extensive preliminary investigations and the field strengths at these points were then recorded in detail. They are listed below where their designation used in the following is added in brackets:

- the generator and its slipring (MP 1),
- the coupling of the generator leads to the generator (MP 2),
- the coupling of the generator leads to the leads of the starting converter via a breaker (MP 3),
- the generator lead breaker (MP 4),
- the transformer for the excitation converter (MP 5) and
- the transformer for the starting converter (MP 6).

Typical measurement distances to the surface of these components are about 20 cm. There is, indeed, a strong increase of the field strengths at smaller distances but they finally do not represent realistic distances for installations or longer stays of personnel. Only measurement points were considered which might be possible locations for electrical apparatus and which might be spatially accessible to personnel.

3. RESULTS

3.1 Field Strengths at Steady-State Operation

The field strength measurements during the gas turbine and the generator steady-state operation could not be performed in any cases at the specified nominal power. However, measurements at several points for different power ratings showed that there is a linear correlation between the generator power rate and the detected field strength. This is due to the linear increase of current densities in the energized components and therefore of the magnetic field strengths with increasing power, because the voltage terms are primarily not affected by power rate changes. An extrapolation of the measured field strengths to ones at nominal power is therefore justified and allows the comparison of the results at different measurement points.

Fig. 3 shows the spectrum of the magnetic flux density in the range of the generator near the coupling of the generator leads (MP 2). The results are for a power rating of 49 % of the nominal power. The magnetic flux density with the

significant highest level of about 50 999 occurs at the fundamental power frequency of 50 Hz. There is a very strong decay of the flux density with increasing frequency. The identifiable but relatively small amplitudes at harmonics of 300 Hz may be attributed to the converter which supplies the generator exciter.

Magnetic Flux Density [μ T]

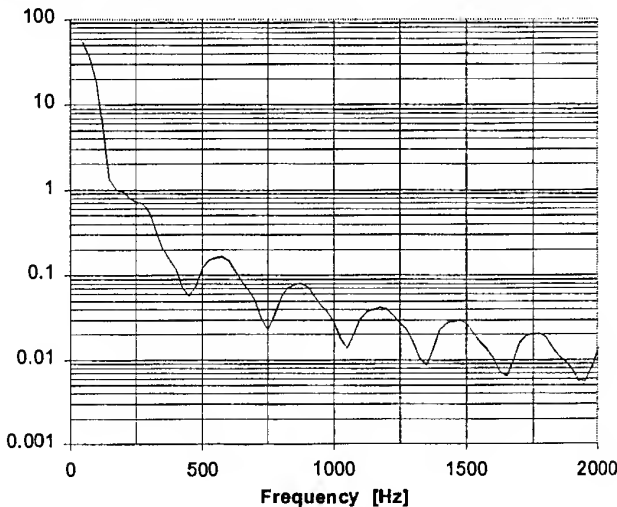


Fig. 3: Measured magnetic flux density versus frequency near the generator at the measurement point MP 2 (Power Station Type 2)

Magnetic Flux Density [μ T]

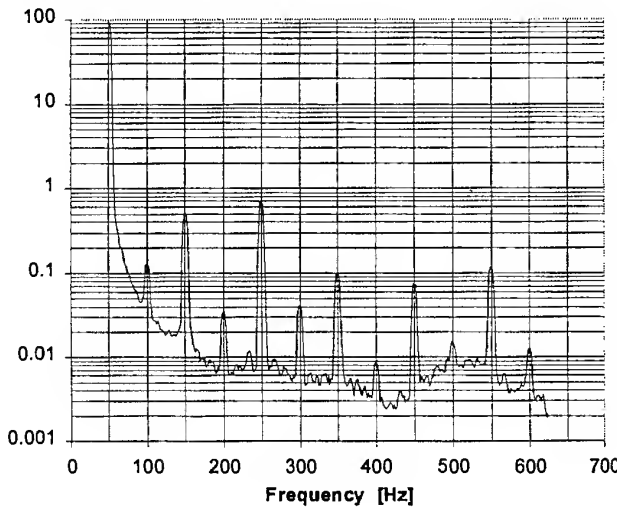


Fig. 4: Measured magnetic flux density versus frequency near the generator lead breaker at the measurement point MP 4 (Power Station Type 2)

A typical spectrum of the magnetic flux density near the generator lead breaker is shown in Fig. 4. The results are for a power rating of 59 % of the

nominal electrical power. A current of about 6700 A is flowing through the breaker. Flux density levels in the magnitude of order of 100 μT at the power frequency of 50 Hz occur. Levels with significant lower amplitudes could also be detected at harmonics of the power frequency where amplitudes at odd harmonics dominate.

The maximum flux densities measured in the range of the different energized components and extrapolated to the nominal power of each of the modules are listed in Table 1. As can be seen, flux density levels up to 700 μT have to be taken into account in the power station environment during steady-state operation. The significant differences between the different types of power stations are due to the different layouts and arrangements of the stations as well as due to the different possible access of personnel to energized components. So far these levels should be taken for representative ones.

Table 1: Magnetic flux density levels near energized components during steady-state generator operation

Measurement Point	Power Station Type 1	Power Station Type 2
MP 1, MP 2	61 μT	151 μT
MP 4	41 μT	698 μT
MP 5, MP 6	14 μT	137 μT

3.2 Field Strengths during Generator Start-ups

Energized components of special concern in the case of generator starts are the generator starting converter, its supplying transformer and the coupling of the converter output leads to the generator leads via a breaker which is opened after the starting process of several minutes. For further information the field strengths at the previous measurement points were also investigated but they do not show levels higher than during the steady-state operation mode.

Fig. 5 shows the spectrum of the magnetic flux density measured near the breaker between the starting converter output leads and the generator leads (MP 3). This spectrum represents all the maximum frequency dependent density levels occurring during the starting process which levels however are not all present at the same time. The spectrum corresponds in principle to the display of a spectrum analyzer which continuously records and saves the input signal during the starting process in the peak-hold detection mode. Now in contrast to the previous spectra shown in Figs. 3 and 4, it is a quasi continuous spectrum with no discrete spectral lines. This is due to the fact that during generator starting current frequencies

increasing from several Hz up to 50 Hz as well as their respective harmonics are produced at the converter output. Thus, finally there are in principle discrete flux density spectra for short moments but they have continuously varying spectral lines. Only adding these spectra leads to a quasi-continuous one which finally represents the flux density conditions from a worst case point of view, i.e. what maximum flux density levels must be expected in the entire frequency range up to 1 kHz during the generator starting process.

Magnetic Flux Density [μT]

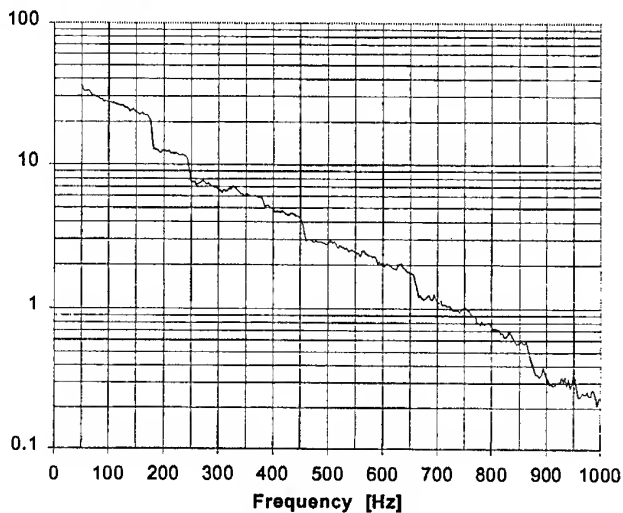


Fig. 5: Measured magnetic flux density versus frequency near the breaker between the generator leads and the starting converter at the measurement point MP 3 (Power Station Type 1)

Magnetic Flux Density [μT]

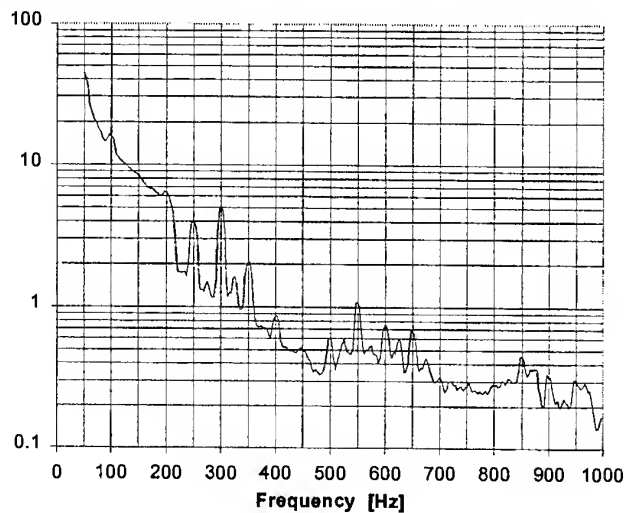


Fig. 6: Measured magnetic flux density versus frequency near the converter for the generator start at the measurement point MP 6 (Power Station Type 2)

A modified situation could be detected on the starting converter input side. The flux density spectrum near the converter is shown in Fig. 6 and is recorded in the same way as the previous one. It does not have such a continuous form as that from Fig. 5.

The rectifier at the converter input which is connected to a three phase system predominantly shows the typical behaviour with harmonics at the 5th and 7th, 11th and 13th etc. of the power frequency. Only some peaks occur at normally nontypical frequencies of 100 Hz, 150 Hz and 200 Hz. They might be due to the unbalanced load conditions during the starting process.

4. CONCLUSIONS

When evaluating the results from a human risk point of view the fact that several standards exist which give limits for human exposure in low frequency magnetic fields must be considered. These standards state limits for the public as well as for professionally exposed people. The spectrum of standards reaches from national standards [6] over European standards [7] to international recommendations which are given by the International Radiation Protection Association IRPA [8]. Table 2 shows a comparison of the several limits at the power frequency of 50 Hz including the limits for persons with pacemakers derived from [9].

Table 2 : Exposure limits according various standards

Standard	Workers	Public
DIN VDE 0848	1360 µT (4240 µT)	420 µT
ENV 50166-1	1600 µT	640 µT
IRPA	500 µT(5000 µT)	100 µT
DIN VDE 0750 (People with pacemakers)	53 µT	53 µT

A comparison of the measurement results with a maximum of 400 µT with the limits for workers shows that the measured values remain below the limits. As the results at different measurement points show the possibility of influencing or endangering people with pacemakers in a power station environment should always be taken into account.

5. REFERENCES

- [1] W. K. Daily and F. Dawalibi, *Measurements and Computations of Electromagnetic Fields in Electric Power Substations*, IEEE Transactions on Power Delivery, Vol. 9, No. 1, 1994, pp. 324-333
- [2] D. G. Kasten, S. A. Sebo and R. Caldecott, *Development of a Computer Program for Modeling of Magnetic Fields in High Voltage AC Substations*, Proc. of the 6th International Symposium on High Voltage Engineering, New Orleans, USA, August 28 - September 1, 1989, No 24.05.
- [3] IEEE Magnetic Fields Task Force, *Magnetic Fields from Electric Power Lines - Theory and Comparison to Measurements*, IEEE Transactions on Power Delivery, Vol. 3, No. 4, 1988, pp. 2127-2136
- [4] Newest KWU-technique of combined gas cycle in Great Britain (German), Elektrizitätswirtschaft, Jg. 95, Heft 13, 1996, pp. 909-911
- [5] DIN VDE 0107, *Electrical Installations in Hospitals and Locations for Medical Use Outside Hospitals* (German), VDE Verlag, Berlin und Offenbach, November 1989, pp. 12-21
- [6] DIN V VDE 0848-4 A3, *Safety in electromagnetic fields, limits of exposure of persons in the frequency range from 0 to 30 kHz*, Vornorm, (German), VDE oder Beuth Verlag, März 1994
- [7] ENV 50166-1, *Human Exposure to Electromagnetic Fields – Low-frequency (0 Hz to 10 kHz)*, Prestandard, CENELEC, Brussels, January 1995
- [8] IRPA/ICNIRP, *Interim Guidelines on limits of exposure to 50/60 Hz electric and magnetic fields*, Health Physics, Vol. 58, No. 1, 1990, pp. 113-122
- [9] DIN VDE 0750-9 A1, *Safety of pacemakers, Safety against Electromagnetic Disturbances*, Draft, (German), VDE Verlag, Berlin und Offenbach, August 1992

BIOGRAPHICAL NOTE

Bernd W. Jaekel was born in Erlangen, Germany, and received the B.S. and Ph.D. degrees in physics from the University of Wuerzburg in 1985 and 1989 respectively. Since 1989 he has been with the EMC center of the Siemens automation and drives group. He is presently involved in planning EMC of electrical power components with the emphasis on performing numerical simulations and on-site measurements.

A NEW MEASURING METHOD FOR LOW FREQUENCY CONDUCTED EMI IN A FREQUENCY RANGE 2 - 9 KHZ

A. Krechla *, J. Petzoldt **

* Technical University of Ilmenau, Dept. of Power Electronics, PO BOX 0565, D-98684 Ilmenau, Germany
Phone: (++49) (3677) 691554, Fax: (++49) (3677) 691552
Mail: andreas.krechla@e-technik.tu-ilmenau.de

** University of Rostock, Dept. of Power Electronics, Albert-Einstein-Str. 2, D-18051 Rostock, Germany
Phone: (++49) (381) 4983477, Fax: (++49) (381) 4983479,
Mail: jp@rex.e-technik.uni-rostock.de

1. ABSTRACT

This paper focuses on fundamental investigations and simulations of conducted electromagnetic interference emissions produced by power electronic circuits in a frequency range from 2 to 9 kHz. The emissions of different power converters were measured and compared with another. The influence of different conditions at the altitude of the EMI are represent.

2. INTRODUCTION

In order to understand the principles of origin and expansion of the disturbances, it is necessary to analyze these by using simple models. The high frequently currents of high power electronic instruments cause a voltage drop at the impedance of the mains supply (low-voltage network, communication network etc.).

This voltage drop is called the interference voltage. The impedance depends on the specific environments, such as an industrial residential area. So it can be that an and the same instrument produce varying interference voltages at the mains connexion. There are two possibilities to measure these interferences:

- measuring the current
- measuring the voltage drop across a known impedance

This determination of conducted electromagnetic interference emissions produced by power electronic circuits is divided into two frequency ranges as shown in figure 1. Both frequency ranges are set by standards.

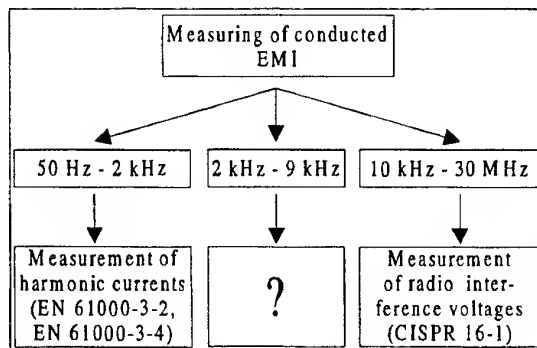


Fig. 1: Division of the frequency range from 50 Hz to 30 MHz

2.1. Measurement of harmonics (EN61000-3-2)

The measurement of current harmonics in the frequency range from 50 Hz to 2 kHz is governed by European Standard 61000-3-2 and 61000-3-4 (for currents > 16A per phase). The currents are measured across a current sensing part. The resulting voltage are presented in the frequency range through different processes like frequency domain measurements or time domain measurements [5], [6]. In this standard considers time domain measuring systems as well as frequency domain measuring systems as equally good.

2.2. Measurement of interference voltages

The measurement of low frequently disturbances in instruments over the frequency range from 10 kHz to 30 MHz is specified in the CISPR 16-1. It is based on the determination of the voltage drop across a LISN (LISN - Line Impedance Stabilization Network) [3], [4]. These LISN allow for reproducible measuring

results independent of the internal resistance of the network. They also prevent the invalidation of the measurements due to disturbances already present in the network. There are three essential characteristics of the LISN:

- a) recreates the internal impedance of the mains supply
- b) decouples the measuring system from the network
- c) a damping of the 50 Hz-voltage

3. ERROR ANALYSIS

The impedance of the network increases with rising frequency. In the frequency range from 10 kHz to 30 MHz the impedance may be recreated by a network of $(50 \mu\text{H} + 5 \Omega) \parallel 50 \Omega$. It can be seen, that with increasing frequency, a constant current amplitude will induce a higher voltage drop. In other words, the same voltage drop will result from lower currents at higher frequency. Since the operating currents are included in the measurement, measurements in the higher frequency ranges cannot be considered to be accurate. This will be shown more clearly later on.

3.1. Measuring error of the current measurement

For the measurement of current harmonics there are concrete limits up to the 40th Harmonics of the fundamental frequency specified in the European Standard 61000-3-2. These limits apply to instruments of the class A (for genuine three-phase equipment's). In this standard is fixed also a maximum measuring error: 5 % of the allowed limit or 0,2 % of the input current (which ever value is larger) [5].

That means, a set error limit is specified in European Standard 61000-3-2. This limit has a value of $\pm 32 \text{ mA}$ at a input current of 16 A . The limit for the 40th Harmonic in EN61000-3-2 for a mains current of 16 A is given with 46 mA . This corresponds to a 69 % tolerance for the 46 mA current. Assuming that the threshold values for the frequency range from 2 kHz to 9 kHz lie well below the limits of the European Standard 61000-3-2, a current measurement by this procedure does not appear to be accurate. The measuring error of the powermeter with integrated FFT used for this researched project was specified as follows:

$$\Delta I = \pm (0.05 \% \text{ of the measured value} + 0.05 \% \text{ of the measurement range})$$

At a nominal current of 16 A and a measuring range of 30 A , there is a measuring accuracy of

$$\Delta I = \pm (0.008 \text{ A} + 0.015 \text{ A}) = \pm 0.023 \text{ A} = \pm 23 \text{ mA}$$

The resulting measuring error relative to the smallest threshold value of the harmonic current of $I_{40} = 46 \text{ mA}$ is thus:

$$I\%_{\text{meas}} = \frac{\Delta I}{I_{40}} = \frac{0.023 \text{ A}}{0.046 \text{ A}} = 50\% \quad (1)$$

The measuring accuracy of the powermeter is also relativ bad.

3.2. Measuring error of the voltage measurement

The error occurring in measurements of the interference voltage is determined by the measuring accuracy of the measuring receiver. This measuring accuracy is specified by the producer as $\Delta V = \pm 1 \text{ dB}$ maximum.

If a voltage is calculated from the threshold value of the 40th harmonic (46 mA) and the mains impedance at 2 kHz (approximate $|Z_{\text{Mains}}| = 2 \Omega$), according to

$$\hat{V}_1 = |Z_{\text{Mains}}| \cdot \hat{I}_{\text{Harmonic}} \quad (2)$$

The amplitude of the interference voltage is 92 mV . This corresponds to a tension of $V_s = 99.3 \text{ dB}(\mu\text{V})$. There is a relative measuring error in the measurement of the interference voltage of:

$$V\% = \frac{\Delta V_I}{V_I} = \frac{103.2 \text{ mV} - 92 \text{ mV}}{92 \text{ mV}} = 12.2\% \quad (3)$$

This accuracy is a result of the strong damping of the 50 Hz component by the LISN. There fore, the measuring receiver can be very sensitively. These differences in the measuring accuracy between the two procedures is of the main reasons measuring the interference voltage across a standard LISN.

4. MEASURING SYSTEM

The existing LISN's for the measurement of interference voltages differ greatly in the construction. Functionally however, they are all equivalent. From this consideration it makes sense, to modified the LISN specified in CISPR16-1 based on the function they should accomplish.

4.1. Modification of the LISN

a) high frequently decoupling from the mains

The decoupling from the power supply is usually done by a low-pass filter. Each power lead has its own decoupling choke, which isolates the equipment from high frequently currents in the mains. In order to guarantee a decoupling for the frequency range to be examined, the cut off frequency of the low-pass filter must be shifted into the range below 2 kHz. This can be accomplished by adding a further CR-combination at the mains port of the LISN. An exact design of the low-pass filter can be seen in figure 3.

b) recreation of the mains impedance

The European Standard CISPR16-1 specifies a impedance of the LISN of $(50 \mu\text{H} + 5 \Omega) \parallel 50 \Omega$ for the frequency range from 10 kHz to 30 MHz. In the frequency range to be examined, however the actual impedance $|Z|$ is below 5Ω [2]. In order to recreate the impedance more accurately, a further impedance ($540 \mu\text{H} + 40 \mu\text{F} + 2,3 \Omega$) was added to the LISN.

c) decoupling and/or damping of the mains voltage

The LISNs commonly used all recreate the impedance of the mains equally. Since the full power of the 50 Hz fundamental would destroy the measuring equipment it had to be attenuated by using a high-pass filter. In the frequency range from 10 kHz to 30 MHz the output attenuation is either zero or has a set value. According to CISPR 16-1, a CR-high-pass filter is used for decoupling the low-frequently signals. The damping of the filter is non-negligible over the frequency range from 2 kHz to 9 kHz and can be calculate with equation 4.

$$|G(j\omega)| = 20 \cdot \log \left(\frac{1}{\sqrt{1 + \left(\frac{1}{\omega C \cdot R} \right)^2}} \right) \quad (4)$$

The result of this three modifications can bee seen in figure 3.

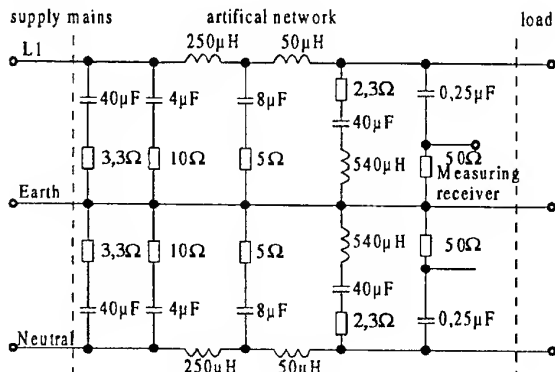


Fig. 3: Modification of CISPR16-1 network [1]

5. MEASURING RESULTS

The conducted EMI caused by the switching frequency of different three-phase power converter were measured in the frequency range from 2 to 9kHz. Besides the investigated converters were divided into the following basic types:

- a) three phase pulsed rectifier with DC Voltage Link
- b) three phase rectifier with capacitive load and following three phase pulsed converter

An example for both types can be seen in figures 4 - 5.

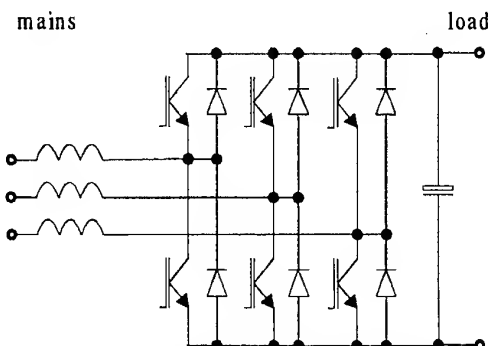


Fig. 4: Three phase pulsed rectifier with DC Voltage Link

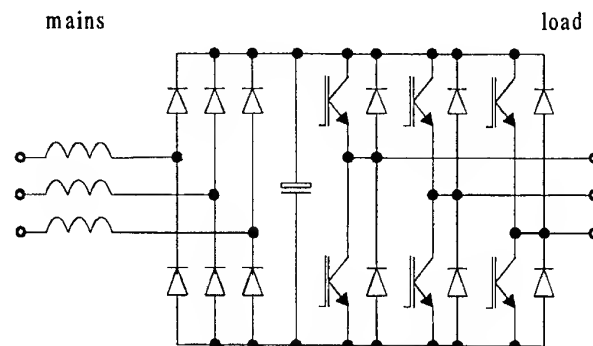


Fig. 5: Three phase rectifier with capacitive load and following three phase pulsed converter

5.1. Influence of the load current

To see the influence of the load current, the emissions of all converters were measured with no-load and full load (pure resistive load).

The highest emissions are produce by three phase pulsed rectifiers with DC Voltage Link.

The altitude of emissions of all three phase pulsed rectifiers with DC Voltage Link aren't dependent on the load current. An example is shown in figure 6.

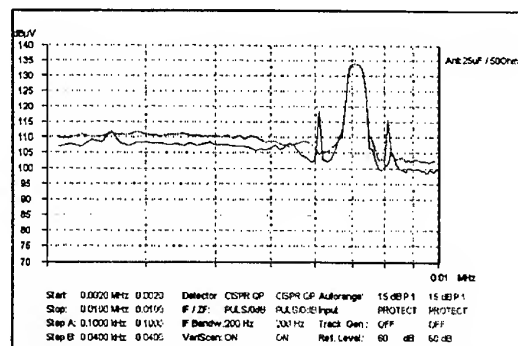


Fig. 6: Emissions of three phase pulsed rectifier with DC Voltage Link (influence of load current)

The emissions of the three phase rectifiers with capacitive load and following three phase pulsed rectifier depend on the load current (figure 7).

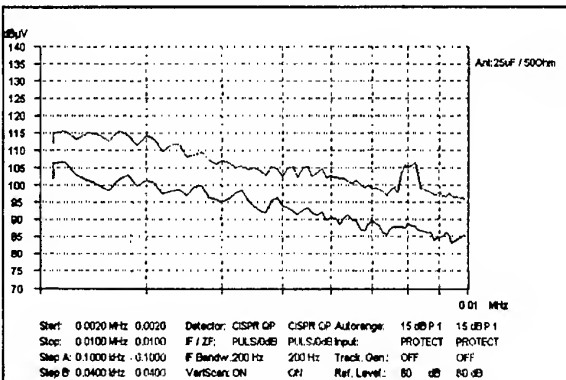


Fig. 7: Emissions of three phase rectifier with capacitive load and following three phase pulsed converter (influence of load current)

The emissions of three phase pulsed rectifiers with DC Voltage Link depend on three important facts:

- the altitude of the voltage DC Link
- the impedance of the converter choke
- the impedance of the supply mains

5.2. Influence of the kind of load

To see the influence of the load the emissions of the converter were measured with pure resistive load and with motor load. In figure 8 it can be seen that the emissions of three phase pulsed rectifiers with DC Voltage Link aren't dependent on the kind of load.

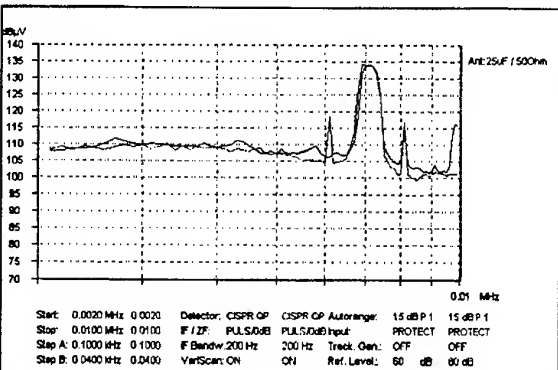


Fig. 8: Emissions of three phase pulsed rectifier with DC Voltage Link (influence of kind of load)

Unlike, as opposed to figure 8 the emissions of the three phase rectifiers with capacitive load and following three phase pulsed converter depend on the kind of load. The emissions with connected motor load are higher than with resistive load (figure 9).

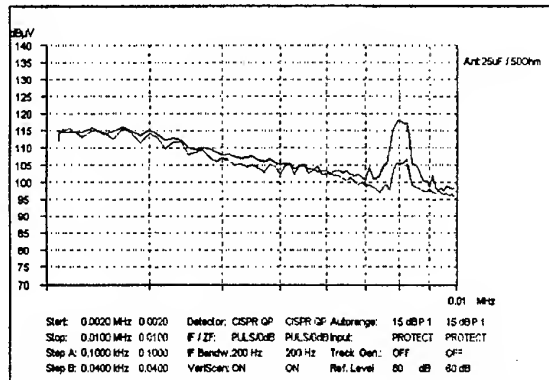


Fig. 9: Emissions of three phase rectifier with capacitive load and following three phase pulsed converter (influence of kind of load)

5.3. Highest emissions

The highest emissions of all converters were measured and placed in figure 10. The converters are subdivided in three parts:

- Group a: three phase pulsed rectifiers with DC Voltage Link - $I > 16A$
- Group b: three phase pulsed rectifiers with DC Voltage Link - $I \leq 16A$
- Group c: three phase rectifiers with capacitive load and following three phase pulsed converter - $I > 16A$

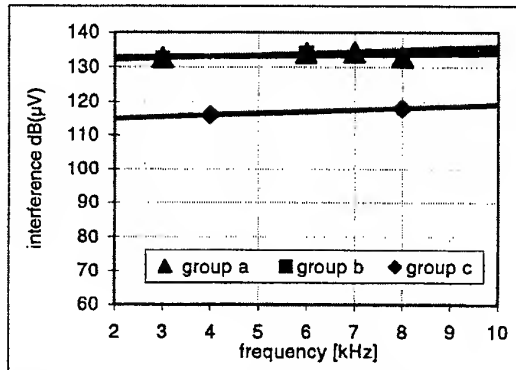


Fig. 10: Highest emissions of investigated converters

The group "three phase rectifier with capacitive load and following three phase pulsed converter - $I \leq 16A$ " can not be seen in figure 10 because no converter for this group was in existence.

As well, it was measured that the highest level of the emissions are not situated in the centre of the pulsed frequency but 50 Hz or 100 Hz beside this frequency. This is the result of the different modulation techniques of the converters.

6. CONCLUSION

This paper deals with the selection of a suitable measuring procedure for the measurement of conducted EMI in a frequency range 2 to 10 kHz. Because

of the higher accuracy of the voltage measurement using an LISN as opposed to current measurements this method was judged superior for determining interferences. Since the required LISNs, are not standardized for the frequency range from 2 kHz to 10 kHz, this paper suggest a modification to the existing LISN's.

7. REFERENCES

- [1] A. Krechla, J. Petzoldt, "Measuring techniques and analysis of conducted EMI of power converters in a frequency range 2 to 9 kHz" (german), Forschungsvereinigung Elektrotechnik beim ZVEI e.V., 01/1998
- [2] R. Gretsch, M. Neubauer, "Investigation of the mains impedance in a frequency range 2 to 9 kHz", Lehrstuhl für Elektrische Energieversorgung der Universität Erlangen Nürnberg, 10/1996
- [3] CISPR 16-1, "CISPR specification for radio interference measuring apparatus and measurement methods
- [4] EN55011, "Radio interference suppression of electrical operating machinery and equipment, limits and measuring techniques for Radio interference suppression of industrial, scientific and medical (ISM) and similar purposes", DIN VDE 0875 Teil 11, 07/92
- [5] EN 61000-3-2 (draft IEC1000-3-2), "Limits for harmonic current emissions (equipment input current ≤ 16 A per phase)
- [6] EN 61000-3-4 (draft IEC1000-3-4), "Harmonic limits for connection of equipment with input current exceeding 16 A to the public low voltage supply system, 03/1995

BIOGRAPHICAL NOTES

- Prof. Dr. Ing. habil. J. Petzoldt (1952)
 - studied electrical engineering at the Ilmenau University, 1976 - Dipl. Ing., 1980 - Dr.-Ing., 1976 - Dept. of Power Electronics at the University Ilmenau, 1991 - 1995 Leader of Dept. of Power Electronics, 1995 - guest professorship at University of Rostock, Dept. of Power Electronics
- Dipl. Ing. A. Krechla (1971)
 - studied electrical engineering at the Ilmenau University, 1996 - Dipl. Ing., since 1996 scientific assistant at the Ilmenau-University (Dept. of Power Electronics)

POWER FLOWS IN ELECTRICAL POWER SYSTEMS CONTAINING NON-LINEAR AND NON-SYMMETRICAL CONSUMERS

Dietrich STADE

Technical University of Ilmenau

D-98684 Ilmenau P.O.B. 10 05 65 Germany

Leonid KUCHUMOV Alexander NOVITSKIY Alexei IVANOV

St.Petersburg State Technical University

195251 St.Petersburg Polytechnicheskaya 29 Russia

Abstract - Method of the analysis of the spread of distortion in an electrical network containing non-linear and non-symmetrical loads is suggested in the offered paper. On the basis of investigation it is shown that contrary directed power flows exist simultaneously in an electrical power system containing distortion sources. Theoretical approach, results of experimental measurements and results of mathematical modelling of non-sinusoidal and non-symmetrical states in electrical power system are described in the paper.

1. INTRODUCTION

Modern electrical power systems contain a lot of high-power non-linear and non-symmetrical loads. When connecting a new non-linear or non-symmetrical consumer with an electrical network it is necessary to take into account the electromagnetic compatibility. It is necessary to determine the permissible level of distortion for every distortion source in the Point of Common Coupling (PCC) in the electrical network. This means that it is necessary to locate distortion sources, to analyse the interaction between different distortion sources, and to analyse the spread of the distortion in electrical power system. There is not a universally agreed-upon theory of power spread under distorted conditions in networks [1 - 4], but this paper attempts to make some contribution, based on a fundamental electrotechnical approach. Some aspects of it were published in [5].

2. THEORETICAL APPROACH

Let us consider a simple three-phase electrical network with insulated neutral containing only one non-symmetrical and non-linear consumer (distortion source) which is supplied from bus with the ideal symmetrical non-distorted fundamental harmonic voltage U_s as is shown on the Fig.1.

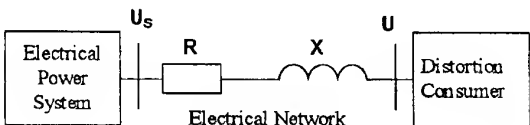


Fig.1

In a common case for the current in each phase of a three-phase system exist in the following relations:

$$i_l(t) = \sum_k \{ I_{kpos} \sin(k\omega_0 t + \Psi_{kpos} - \frac{2\pi}{3}(l-1)) + I_{kneg} \cos(k\omega_0 t + \Psi_{kneg} - \frac{2\pi}{3}(l-1)) \} \quad (1)$$

where

$l = 1, 2, 3$ - index of phases in three-phases system

$k = \nu \pm \frac{\Omega \beta}{\omega_0}$ - combination frequency

$\nu = 0, 1, 2, \dots$ - order of harmonic

ω_0 - fundamental frequency

$\Omega \beta = \beta \Omega$ - modulation frequency

Ω - basis modulation frequency

$\beta = 1, 2, \dots$ - order of modulation frequency

pos, neg - positive, negative sequence index

The same relations exist for the voltage:

$$u_l(t) = \sum_k \{ U_{kpos} \sin(k\omega_0 t + \Psi_{kUpos} - \frac{2\pi}{3}(l-1)) + U_{kneg} \cos(k\omega_0 t + \Psi_{kneg} - \frac{2\pi}{3}(l-1)) \} \quad (2)$$

According to Tellegen's theorem [5] can write for every harmonic frequency k the following relations can be written for power:

$$\underline{S}_{s,k} - \underline{S}_k = I_k \underline{U}_{s,k}^* - I_k \underline{U}_k^* = I_k^2 R + j I_k^2 \omega_k L = \Delta P_k + j \Delta Q_k \quad (3)$$

where

$\Delta P_k, \Delta Q_k$ - active, reactive losses in the network on the harmonic frequency k

As the supply voltage on the system bus contains only positive sequence fundamental harmonics $U_s = U_{s1pos}$, follows from equations (3) :

$$P_{s,1pos} - P_{1pos} = \Delta P_{1pos}$$

$$-P_{1neg} = \Delta P_{1neg}$$

$$-P_k = \Delta P_k$$

$$Q_{s,1pos} - Q_{1pos} = \Delta Q_{1pos} \quad (4)$$

$$-Q_{1neg} = \Delta Q_{1neg}$$

$$-Q_k = \Delta Q_k$$

Here are the equations for both sequences:

$$P_k = I_k U_k \cos(\Psi_k U - \Psi_k I) \quad (5)$$

$$Q_k = I_k U_k \sin(\Psi_k U - \Psi_k I)$$

From equations (4) follows that **normal power flow** (1st harmonic positive sequence), directed from power source to consumer, and contrary **anomalous power flow** (1st harmonic negative sequence and all other harmonics) exist in the electrical network. Only normal power flow exists on the system bus.

Anomalous power flows are

$$P_{an} = P_{1neg} + \sum_{k \neq 1} P_k \quad (6)$$

$$Q_{an} = Q_{1neg} + \sum_{k \neq 1} Q_k$$

The middle power on the load bus is

$$P_m = \sum_{k=1} (P_{kpos} + P_{kneg}) \quad (7)$$

$$Q_m = \sum_{k=1} (Q_{kpos} + Q_{kneg})$$

By substituting (6) in (7) follows:

$$P_m = P_{1pos} - P_{an} \quad (8)$$

$$Q_m = Q_{1pos} - Q_{an}$$

This means that a part of power consumed from load bus P_{1pos} , Q_{1pos} transforms into anomalous power flow which is injected back into the electrical network. This part of energy is lost for the consumer. Also anomalous power flows cause additional energy losses $\Delta(\Delta P_{an})$, $\Delta(\Delta Q_{an})$ in the electrical network.

If a non-distortion (linear and symmetrical) load on the load bus is coupled then non-distorted consumer uses the following power:

$$P_{cn} = P_{1pos} + P_{an} \quad (9)$$

$$Q_{cn} = Q_{1pos} + Q_{an}$$

Consumed anomalous power flows cause additional energy losses and deteriorate technological conditions.

In Fig.2 the diagram of power flows in electrical network for the common case, with both distortion and non-distortion consumers, is shown.

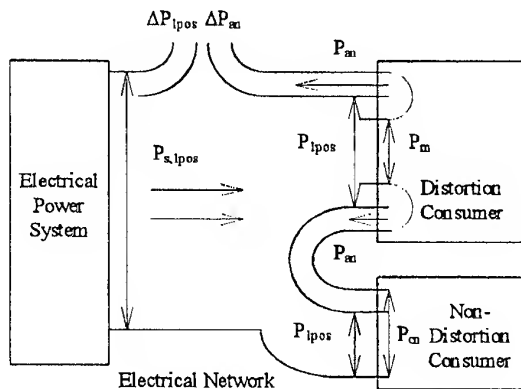


Fig.2.

3. COMPUTATIONAL RESULTS

Simple tests of the theory presented above were carried out by PC program system SALOMON [6] on the three-phase mathematical model.

Example 1. Non-symmetrical linear load.

Fig.3 shows us the simplified circuit diagram of an electrical network containing one non-symmetrical linear load, which was used in computations. In this case only power flows on the fundamental frequency exist. The impedances of every phase are symmetrical.

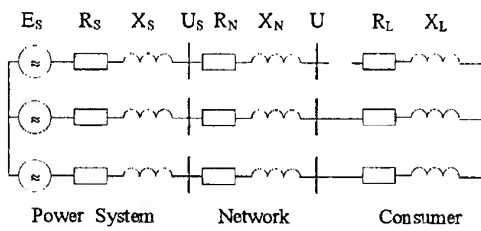


Fig.3.

Results of computations of power consumed on the load bus are presented in the Table 1.

Table 1.

P_{1pos} kW	Q_{1pos} kVar	P_{1neg} kW	Q_{1neg} kVar
30244,34	32143,97	-53,20	-1984,44

It is shown that power of negative sequence $P_{1neg} < 0$, $Q_{1neg} < 0$. This means that power flows of negative sequence are directed contrary to power flows of positive sequence. Also it is shown

that power of negative sequence $P_{1neg} < 0$, $Q_{1neg} < 0$.

that power of negative sequence is significantly less than power of positive sequence. At last,

$$Q_{1\text{neg}} \gg P_{1\text{neg}}$$

Example 2. Non-linear symmetrical load.

Fig.4 shows the simplified circuit diagram of an electrical network, containing one non-linear symmetrical load, which was used in computations.

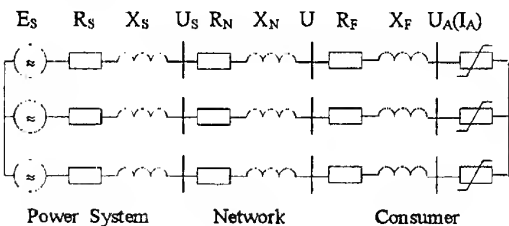


Fig.4.

The three-phase electrical arc, which was modelled according to their v-i characteristic as it is shown on the Fig.5, was taken as the non-linear element. The v-i characteristic is typical for electrical arc furnace [6]. For every phase symmetrical v-i characteristics were taken.

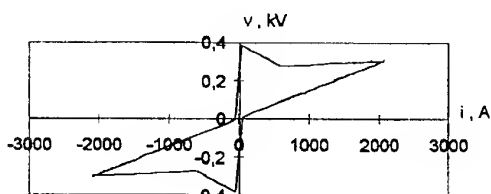


Fig.5.

Results of computations of load flows are presented in Table 2.

In this case power flows exist on both the fundamental frequency and on odd harmonics, except 3rd and multiple. Because of symmetry of phase parameters and symmetry of distortion sources only positive sequence power flows exist on harmonics 1, 7 and negative sequence power flows on harmonic 5. Harmonic flows on harmonics order 11, 13, etc. are not presented in Table 2.

Table 2.

k	P _{kpos} kW	Q _{kpos} kVar	P _{kneg} kW	Q _{kneg} kVar
1	32201,55	10059,59	-	-
5	-	-	-4,78	-92,40
7	-0,77	-37,25	-	-

Conclusions for Example 1 are true also for Example 2.

It is shown that $Q_k \gg P_k$, by $k \neq 1$.

Example 3. Non-linear non-symmetrical load.

Circuit diagram Fig.4. was used for modelling of non-linear non-symmetrical load. Non-symmetrical v-i characteristics of electrical arc were taken.

Results of computations of load flows are presented in Table 3.

Table 3.

k	P _{kpos} kW	Q _{kpos} kVar	P _{kneg} kW	Q _{kneg} kVar
1	31650,43	11585,73	-3,46	-114,16
5	-1,51	-17,52	-17,41	-128,49
7	-5,35	-63,432	-5,24	-3,13

It is shown that under non-symmetrical conditions (non-symmetrical distortion source) power flows for both positive and negative sequences for every harmonic k exist. All power flows of negative sequence are directed from distortion source into electrical network. Positive sequence power flows on harmonics $k > 1$ are also injected into the electrical network.

The following is true for the majority of anomalous power flows $Q_k \gg P_k$.

4. EXPERIMENTAL MEASUREMENTS

For experimental check-up of the main aspects of theory presented above on-site measurements in electrical networks containing distortion consumers were carried out.

In Fig.6. power supply scheme of a steel plant is shown. Arc furnaces are high power distortion sources. Measurements were done by means of the measuring system DIGIS, recording the instantaneous values of voltages and currents with a sampling rate of 6400 Hz. On the basis of experimental results power flows were calculated.

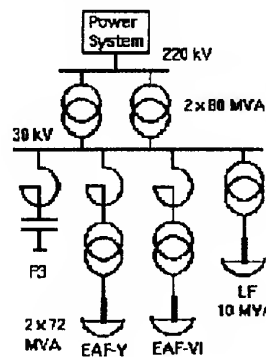


Fig.6.

In Fig.7 load flow behaviours of only one working arc furnace EAF-V (main melting) are presented. The 30 kV voltage on the busbar and the current of arc furnace in three-phases were measured. The other load was switched off from the busbar.

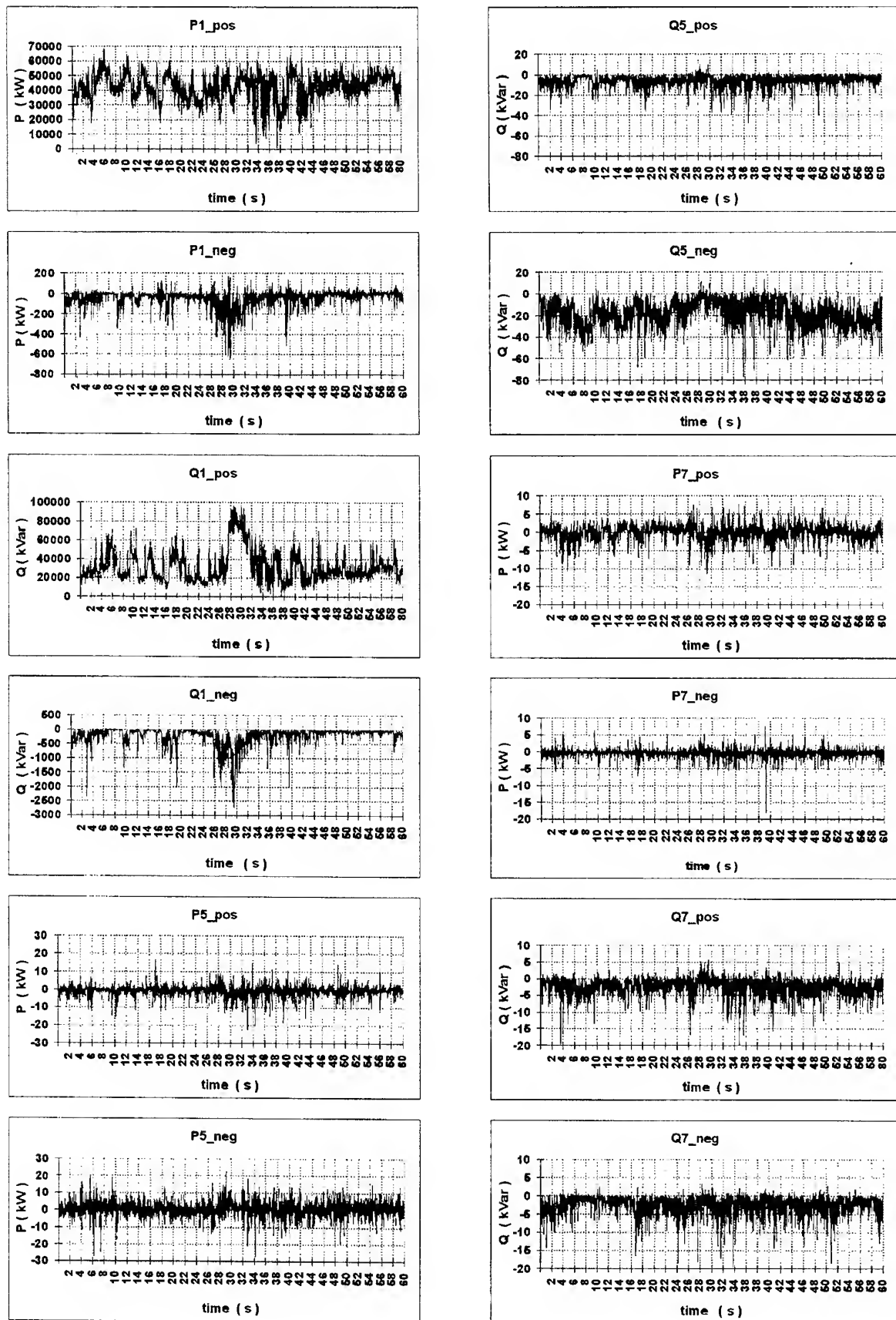


Fig.7.

Measuring results confirm main aspects of described power theory. It is shown that measured negative sequence power flow on the fundamental frequency is directed from consumer to electrical network. Measured reactive power flows on harmonics are also directed into the electrical network. Variable direction of measured harmonic active power flows can be explained by a presence of harmonic distortion in the supply voltage, and a significant level of active losses on harmonics in the electrical arc furnace circuit. There are $Q_k \gg P_k$.

5. CONCLUSIONS

1. This paper suggests power flows theory under distorted conditions in an electrical network.
2. Mathematical modelling and experimental measurements confirmed existence of contrary directed normalous and anomalous power flows in the electrical network.
3. Measurements of anomalous power flows can be recommended for location of distortion sources in the electrical network.

ACKNOWLEDGEMENTS

The authors would like to express their appreciation to the German Academic Exchange Service and to the Technical University of Ilmenau, Germany for financial support.

REFERENCES

1. J.L.Willems, „Mathematical Foundations of the Instantaneous Power Concepts: A Geometrical Approach“ (in English), ETEP, Vol. 6, No. 5, 1996, pp. 299-304.
2. L.Czarnecki, „What is Wrong with the Budeanu Concept of Reactive and Distortion Power and Why it Should be Abandoned“ (in English), IEEE Transactions on Instrumentation and Measurement, Vol. IM-36, No. 3, 1987, pp. 834-837.
3. A.Tugulea, „Power-flows under non-sinusoidal and non-symmetric periodic and almost periodic steady-states of electrical power systems“ (in English), Proceedings of the Conference IEEE ICHPS VI, Bologna, Italia, 1994, pp. 388-395.
4. Z.Kusmirek, „Influence of a nonlinear receiver on power system“ (in English), Proceedings of the Conference EPQU'97, Cracow, Poland, 1997, pp. 375-380.
5. Л.А.Кучумов, Л.В.Спиридонова, „Потоки мощности и энергии в электрических сетях с нелинейными потребителями и их использование при учете электроэнергии и оценке добавочных потерь“ (in Russian), Proceedings of the Conference 28 Intern. Wiss. Koll. TH Ilmenau, Ilmenau, GDR, 1983, pp.155-158.

6. D.Stade, H.Schau, M.Malsch, A.Novitskiy, „Dissipation of voltage fluctuations and flickers caused by arc furnaces in the H.V. distribution system“ (in English), Proceedings of the Conference UPEC'97, Manchester, England, 1997, pp. 859-862.

BIOGRAPHICAL NOTES

Prof. Dr.Sc. Dietrich Stade

was born in 1939 in Suhl, Germany. He received his M.S., Ph.D. and Dr.Sc. degrees from Technical University of Ilmenau, where he works as a professor. His area of interest include Power Quality and Electromagnetic Compatibility.

Mailing address:

Technical University of Ilmenau
Faculty of Electrical Engineering and Information Technique,
Division of Electric Power Systems and Appliances
P.O.B. 10 05 65
D-98684 Ilmenau Germany
phone ++49 3677 2840
fax ++49 3677 1496
e-mail: krueger@e-technik.tu-ilmenau.de

Prof. Dr. Leonid Kuchumov

was born in 1935 in Leningrad, Russia. He received his M.S. and Ph.D. degrees from St.Petersburg State Technical University, where he works as a professor. His area of interest include Power Quality and Electromagnetic Compatibility.

Dr. Alexander Novitskiy

was born in 1965 in Leningrad, Russia. He received his M.S. and Ph.D. degrees from St.Petersburg State Technical University, where he works as an associate professor. In 1997 he was a fellow at the Technical University of Ilmenau, Germany. His area of interest include Power Quality and Harmonic Modelling.

Alexei Ivanov

was born in 1974 in Leningrad, Russia. He received his M.S. degree from St.Petersburg State Technical University, where he works as a researcher. In 1997 he was a fellow at the Technical University of Ilmenau, Germany. His area of interest include Power Quality and Harmonic Analysis.

Mailing address:

St.Petersburg State Technical University
Electrical Engineering Faculty
Electrical Power Systems & Networks Chair
Polytechnicheskaya 29
195251 St.Petersburg Russia
phone: (007)(812) 2473735
fax: (007)(812) 2473735
e-mail: kuchumov@garm.hop.stu.neva.ru

V

EMC IN TELECOMMUNICATIONS

INTERMODULATION INTERFERENCES ANALYSIS OF LAND MOBILE CELLULAR RADIO SYSTEM

L.ALTER. Radio Research and Development Institute (LONIIR),
Bolshoy Smolensky pr.,4, 193029 St.-Petersburg, Russian Federation

An analysis of third order intermodulation (RIM) interference which are made by two or three unwanted signals in base station (BS) receiver is performed. As a result we obtain an equation where the interference zone radius is a function of BS receiver parameters , unwanted transmitters parameters, wanted signal field strength and standard deviations of unwanted and wanted signals. For example the calculations show that mobile stations situated in vicinity of BS of about $R \leq 1$ km can generate RIM interference in NMT-450 cellular system.

INTRODUCTION

It is known that two or three strong unwanted signals affecting a receiver can generate intermodulation (RIM) interference . The frequency requirement of third order RIM interference existing is [1]:

$$2F_i - F_j \leq Fr \pm Br/2, \quad (1)$$

$$F_i + F_j - F_q \leq Fr \pm Br/2, \quad (2)$$

where F_i, F_j, F_q - unwanted signal frequencies ; Fr - victim receiver frequency; Br - bandwidth receiver. Such situation may occur in BS receiver of cellular system when unwanted mobile stations are situated in the vicinity of BS . In this case the service zone will be reduced. Wellknown papers consider two-signal RIM interference only [1...5,12].

This paper presents the method and results of interference zone calculations with two- and three-unwanted-signal affects.

1. AMPLITUDE REQUIREMENT OF RIM INTERFERENCE

Amplitude requirement for third order RIM interference existing is [2,4,6,11]:

$$2P_i + P_j > 3W_2, \quad (3)$$

$$P_i + P_j + P_q > 3W_3, \quad (4)$$

where P_i, P_j, P_q - unwanted signals at receiver input, dBW; W_2 and W_3 - receiver susceptibility for two- and three-signal interference of the third order, dBW. They are determined by two (three) equal levels $P_i = P_j$ ($P_i = P_j = P_q$) of unwanted signals which cause SINAD ratio decreasing by 3 dB at receiver output.

Theoretical studies have shown - and this has been verified by experimental work - that magnitude W_2 (W_3) is function of frequency diversity of unwanted and wanted signals $\Delta F_i(j,q)$, level of wanted signal at the input of receiver P_s and receiver susceptibility parameters [6]. At special case for cellular system when mobile station unwanted signals are in preselector band, i.e. $\Delta F_i(j,q) < Br_f$, where $\Delta F_i(j,q) = [F_i(j,q)-Fr]$;

Br_f - preselector bandwidth, we can write

$$W_2 = S_2 + P_{so} + d_2(P_s - P_{so}), \quad (5)$$

$$W_3 = S_3 + P_{so} + d_3(P_s - P_{so}), \quad (6)$$

P_{so} - receiver sensitivity, dBW; S_2, S_3 - RIM susceptibility for two and three signal interference, dB. They are determined by ratio between two or three equal levels of unwanted signals $P_i(j,q)$, which cause SINAD ratio

decreasing by 3 dB at receiver output, and P_{so} ; d_2, d_3 - parameters of RIM susceptibility model (d_2, d_3 show how W_2 and W_3 vary in case of P_s varying).

In terms of field strengths amplitude requirements (3), (4) are [1,2]

$$2E_i + E_j \geq 3[S_2 + E_{so} + d_2(E_s - E_{so})], \quad (7)$$

$$E_i + E_j + E_q \geq 3[S_2 + E_{so} + d_3(E_s - E_{so})], \quad (8)$$

where E_i, E_j, E_q - unwanted and wanted signal field strengths at receiver antenna location, $\text{dB}\mu\text{V/m}$; E_{so} - field strength which corresponds to P_{so} .

Then (7), (8) can be represented as

$$2E_i + E_j - 3d_2 \cdot E_s \geq 3[S_2 + E_{so}(1 - d_2)], \quad (9)$$

$$E_i + E_j + E_q - 3d_3 \cdot E_s \geq 3[S_3 + E_{so}(1 - d_3)]. \quad (10)$$

To determine service and interference zones the wanted and unwanted path loss model is formed taking into account the fading with normal distribution law at measurement units in dB, [2,9].

Left parts (9), (10) are the sum of three (or four) independent random values with overall standard deviation:

$$\sigma_{2\Sigma} = \sqrt{4\sigma_i^2 + \sigma_j^2 + 9d_2^2\sigma_s^2}; \quad (11)$$

$$\sigma_{3\Sigma} = \sqrt{\sigma_i^2 + \sigma_j^2 + \sigma_q^2 + 9d_3^2\sigma_s^2}. \quad (12)$$

and median values:

$$E_{M2\Sigma} = 2E_{Mi} + E_{Mj} - 3d_2E_{Ms}, \quad (13)$$

$$E_{M3\Sigma} = E_{Mi} + E_{Mj} + E_{Mq} - 3d_3E_{Ms}, \quad (14)$$

where $\sigma_i, \sigma_j, \sigma_q, \sigma_s, E_{Mi}, E_{Mj}, E_{Mq}, E_{Ms}$ - standard deviations and median values of wanted and unwanted signals.

Median values $E_{Mi}, E_{Mj}, E_{Mq}, E_{Ms}$ near BS receiver antenna which is at the distance R to signal source are

$$E_m = 107,2 + P_\Sigma - L(R) + 20\lg F, \quad (15)$$

$$P_\Sigma = Pt + Gt - Ba,$$

where Pt - unwanted signal of mobile station transmitter, dBW; Gt -transmitter antenna gain, dB; Ba -antenna feeder path loss, dB; F -transmitter frequency, MHz; $L(R)$ - unwanted and wanted signal path loss at distance R , dB.

Interfering zone of mobile stations will be maximum in case of minimum wanted signal level. This takes place at the distance $R=R_o$ between mobile station and BS where R_o -radius of service zone.

Probability of interference appearing , i.e. eq.(10) requirement complying for three unwanted signals due to fading

$$P_{pr} = 1 - \Phi \left(\frac{3S_3 + 3E_{so}(1 - d_3) - E_{m3\Sigma}}{\sigma_{3\Sigma}} \right), \quad (16)$$

where $\Phi(Z_3)$ - probability integral;

$$Z_3 = \frac{3S_3 + 3E_{so}(1 - d_3) - E_{m3\Sigma}}{\sigma_{3\Sigma}}. \quad (17)$$

Using approximation of $\Phi(Z_3)$ [7] we receive:

$$\Phi(Z_3) = 0,5[1 \pm \sqrt{1 - EXP(-0,619536 \cdot Z_3^2)}]$$

Substituting it into eq.(16) we receive:

$$1 - P_{pr} = 0,5[1 \pm \sqrt{1 - EXP(-0,619536 \cdot Z_3^2)}]$$

Solving this equation for Z_3 we receive:

$$Z_3 = \sqrt{-1,6141 \cdot \ln[4P_{pr}(1 - P_{pr})]} \quad (18)$$

Denoting

$$A_1(P_{pr}) = \sqrt{-1,6141 \cdot \ln[4P_{pr}(1 - P_{pr})]} \quad (19)$$

and equating right parts of eq. (17) and (18) we receive:

$$\frac{3S_3 + 3E_{so}(1 - d_3) - E_{m3\Sigma}}{\sigma_{3\Sigma}} = A_1(P_{pr}). \quad (20)$$

Substituting $E_{m3\Sigma}$ from eq.(15) to (20) we receive:

$$Li + Lj + Lq \leq A_1(Ppr) \times \sigma_{3\Sigma} - 3[S_3 + Eso(1 - d_3) - 107,2 - P_\Sigma - 20\lg F + d_3Ems]. \quad (21)$$

Similarly for RIM interference caused by two unwanted signals we have:

$$2Li + Lj \leq A_1(Ppr) \times \sigma_{2\Sigma} - 3[S_2 + Eso(1 - d_2) - 107,2 - P_\Sigma - 20\lg F + d_2Ems]. \quad (22)$$

Equations (22) and (21) allow to calculate max path loss $2Li + Lj$ and $Li + Lj + Lq$ which correspond RIM interference formed by 2 or 3 unwanted signals with given probability Ppr .

2. PATH LOSS

The median values of path loss L of wanted and unwanted signals are function of distance R . The calculation for a distance of $R < 1$ km was made using "Lustgarten model" [8]. For $F = 450$ MHz

$$L = 91 + 20 \log R. \quad (23)$$

When using this model the path loss are 5,5 dB more than in free space, but many less than that of "Hata model" [9].

3. CALCULATION OF INTERFERENCE ZONE FOR 2Fi - Fj FORM

In the case when radius of service zone in large city is $R_o=3...4$ km, space signal fluctuation is approximated by normal distribution law with $\sigma_s = 6...12$ dB [9,11].

For calculation of interference zone let's use next parameters of system NMT-450: $F = 450$ MHz ; $Pt = 0.15W$; $Ga=5$ dB; $Ba=1$ dB; $d_2 = 0.33$; $Eso = 9.3$ dB μ V/m (where Eso corresponds to sensitivity $Pso = -117$ dBm or $U=-4$ dB μ V emf); $Ppb=0.1$; $\sigma_s = 8$ dB. Here Pt is minimum transmitter power. Let the

fading of unwanted signals $\sigma_i(j,q) \approx 0$ ($R < 1$ km). In this case $\sigma_{2\Sigma} = 3d_2\sigma_s = 8$ dB.

Calculation of interference zone as function of IM-susceptibility S_2 and median value of wanted signal field strength Ems for a pair of unwanted signals F_i and F_j with substituting the NMT-450 parameters in (22) can be made using:

$$2Li + Lj \leq 460,2 - 3S_2 - E_{ms}. \quad (24)$$

Let $S_2=70$ dB [10] and $Ems = 25$ dB μ V/m. Values R_i and R_j satisfy eq. (23), (24) are presented in table 1. So for this parameters of system the interference zone radius is about 1 km.

Table 1

Interference zone radii			
R_i , km	0.065	0.15	0.25
R_j , km	1.0	0.18	0.065

This is a significant distance when the servise zone radius is $R_o = 3...4$ km.

4. CALCULATION OF INTERFERENCE ZONE FOR Fi+Fj-Fq FORM

The values of S_3 , d_3 are absent in specification and may be calculated [6] or measured. The measurements gave $d_2 = d_3 = 0.33$. Substituting NMT-450 parameters in (21) we receive:

$$Li + Lj + Lq \leq 460,2 - 3S_3 - E_{ms}.$$

Let $S_3=70$ dB and $Ems = 25$ dB μ V/m. RIM interference exists when $R_i = R_j = R_q = 0.16$ km. RIM interference also exists when $R_i = R_j = 0.065$ km and $R_q = 1.0$ km .

If we use "free space" model for calculation of path loss, large number of pairs and triplets of unwanted signals and $Pt > 0.15W$ the interference zone will be increased.

CONCLUTION

At radius of about 1 km far from BS the interference of third order, which are generated by two or three unwanted signals, may exist. Therefore when frequency assigning for a site of land mobile network it is necessary to take into consideration the RIM interference of three unwanted signals not only two.

REFERENCE

- 1.CCIR.1990.Report 739 - 1.
- 2.CCIR.1990.Rep.655-2.
- 3.CCIR.1990.Rep.842-2.
- 4.CCIR.1990.Rep.522-2.
5. ITU Doc. 1/ 1009-E. Intermodulation interference calculation in the land mobile service.
6. L.Alter,H.Rubinshtein. A mathematical model of the receiver susceptibility to intermodulation interference of three sources. Trudy NIIR, no.4, 1982, p.91-94 (Russian).

7. A.Gitnik. Simple function approximation of the probability integral. Elektrosvyaz, 1981, no.8 , p.61. (Russian).

8. M.Lustgarten. An empirical propagation model. IEEE Trans. on EMC,v.19, aug.1977,no.3,p.301-309.

9.CCIR. 1990.Rep.567.

10.CCIR.1990.Recom.478-4.

11. W.Lee. Mobile Communication Design Fundamentals, Second Edition. John Wiley and Sons, Inc., N.Y., 1995.

12.G.K.Chan, S.Bartlett. Identification of land mobile denied spectrum due to radio interference. 10th International Zurich Symposium on EMC, 9-11 March, 1993, p.538.

Leonid Alter - received the MS from St.-Petersburg Telecom. University (1968) and PhD from Moscow Telecom. University (1987). He is head of sector, an expert in the field of radio system planning and system EMC simulation on base of PC, an author of 23 papers and patents.

EXPERIMENTAL INVESTIGATION OF ELECTROMAGNETIC COMPATIBILITY BETWEEN CDMA CELLULAR NETWORKS AND REE OF THE AERONAUTICAL RADIONAVIGATION SERVICE

*Dr. M. Bykhovski, A. Gulyaev, P. Mamchenkov, Dr. E. Muratov, M. Selivanov,
Dr. V. Tikhvinski Dr. V. Vysochin, ,*

**Radio Research & Development Institute (NIIR),
16, Kazakova str., 103064, Moscow, Russia, Fax: + 7 095 267-8430
E-mail: mark@niirad.msk.ru**

The paper deals with EMC problems between the (IS-95) CDMA public land mobile networks and radio electronic equipment (REE) of the aeronautical radionavigation service (ARNS) resulting from the national special features of frequency allocations in Russia. The following items are observed:

- the results of bench testing aimed on determination of the signal-to-interference ratio at the ARNS aircraft receiver input in the presence of harmful interference from CDMA network REE;*
- based on the mentioned background an original procedure of calculation the permissible number of base stations (BS) IS-95 and their performance in order to provide EMC with REE ARNS while operating in shared band;*
- an example of practical application of the procedure.*

1. INTRODUCTION

The distinguishing feature of the national frequency allocations in the Russian Federation, CIS countries and certain East European countries is the use of the band 873-1000.5 MHz by the aircraft REE of the ARNS. The above-mentioned REE supports aircraft navigation and landing operations using ground radiobeacons which provide a nation-wide radionavigation field for short range navigation purposes.

However a widespread introduction of cellular mobile radio (CMR) in Russian Federation, in view of an inconformity of the national (federal) allocations of the RF spectrum and the international allocations, has aggravated EMC problems with ARNS REE, namely, with airborne REE of short range radionavigation and landing systems sharing the same frequency band [1]. Airborne REE will receive interference from the transmitting equipment of the base stations of IS-95 CDMA networks. The receiving equipment of IS-95 CDMA subscriber's terminals will be affected by the transmitting devices of ARNS ground radiobeacons. The problem is currently being tackled through a rational frequency planning of shared frequency band in particular areas on the basis of

evaluated and experimentally obtained protection ratios for ARNS receivers interfering with IS-95 CDMA radio electronic equipment [1].

In view of the fact that the procedure of the EMC estimation between ARNS and IS-95 CDMA REE was developed in 1996 in the absence of actual CDMA systems, operational constraints on IS-95 CDMA systems on the territory of the Russian Federation proved to be rather conservative. The required expansion of cellular networks of the IS-95 CDMA networks in Russia while providing compatibility with existing ARNS short range navigation system induced the more sophisticated investigations. In order to obtain the correct protection ratios the bench tests were organized.

2. BENCH TESTING

The bench tests were aimed to determine:

- the amount of potential harmful interference from the transmitting equipment of base stations of IS-95 CDMA cellular networks to ARNS airborne receivers in the Navigation and Landing modes;*
- the minimum permissible level of harmful interference from the transmitters of base stations of the IS-95 CDMA cellular networks at the input of ARNS airborne receivers in the Navigation and Landing modes.*

Since ARNS airborne radio electronic equipment becomes more sophisticated, the bench test was conducted for ARNS aircraft receivers of new generations. The latter are noted for higher sensitivity and powerful digital processor which offers a higher accuracy of determination of the navigation parameters.

The bench test was performed using a special-purpose laboratory setup intended to check operability and accuracy of measurements of ARNS airborne equipment. Fig.1 shows a block diagram of the laboratory setup used for bench testing of EMC compatibility between the ARNS airborne REE of the azimuth mode and IS-95 CDMA REE.

The following measuring equipment was used in the bench test :

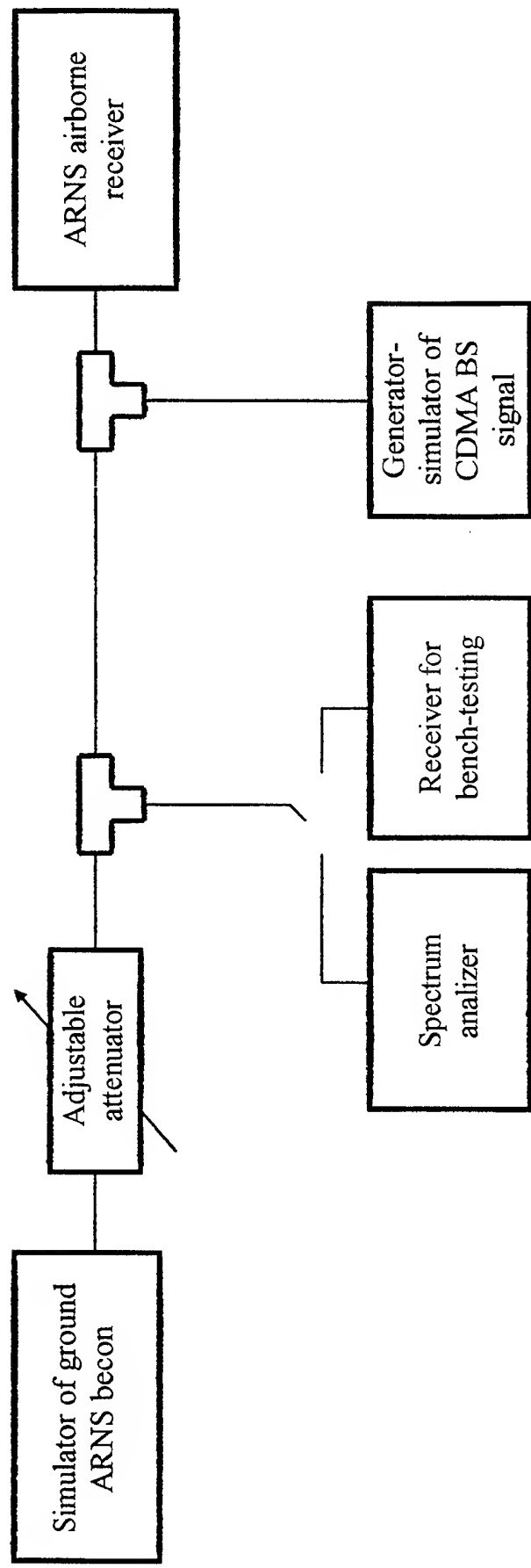


Fig. 1. Block-diagram of the laboratory setup used for researching of EMC between ARNS and IS-95 REE

- simulator of IS-95 CDMA base station transmitters;
- simulator of ARNS ground radionavigation beacons;
- adjustable attenuator;
- operation/maintenance kit.

The bench test involved the following stages:

1. ARNS aircraft receiver sensitivity was measured in the Navigation mode.
2. The prescribed operational mode and required frequency-code channel were set in the simulator of ARNS ground radio beacons. Following this the ARNS airborne equipment was connected to the simulator and correct readings of simulated navigation parameters were recorded by aircraft indicators.
3. By the use of the adjustable attenuator the required wanted signal power was set at the ARNS receiver input. Then the IS-95 CDMA transmitter carrier frequency was tuned to the frequency of the ARNS frequency code channel.
4. The IS-95 CDMA transmitter simulator was connected to the signal simulator and ARNS airborne receiver using an HF coupler.
5. By increasing level of harmful interference from the IS-95 CDMA transmitter the change in the reception quality performance of ARNS wanted signals was recorded. The harmful interference level was further increased to the point of a breakdown of ARNS airborne indicator readings that corresponded to the failure of Navigation Azimuth channel.
6. The level of harmful interference was recorded for several gradations of an azimuth error. For the given wanted signal power level the signal-to-interference ratio was determined.
7. The tests as described in 5 and 6 were successively repeated for several frequency offsets for different ARNS azimuth frequency code channels.

The results of bench testing confirmed potential harmful interference from the transmitting equipment

of base stations of IS-95 CDMA cellular networks [2] to ARNS aircraft receivers in the Navigation mode.

The effect of harmful interference to ARNS airborne receivers from base station transmitters of IS-95 CDMA cellular networks can make itself evident both in an intolerable deterioration in accuracy of measurements of navigation parameters in the Navigation mode and in switching ARNS airborne receivers to the Failure mode with the appropriate indication to the aircraft crew.

The experimentally obtained signal-to-interference protection ratios at the input of the ARNS airborne receivers for co-carrier frequencies (co-channel) are 0 .. 2 dB for the azimuthal channel in Navigation mode.

The above-mentioned signal-to-interference protection ratios were obtained for the cases of switching on the airborne failure indicators of the Navigation channels of the ARNS equipment.

3. PROCEDURE OF THE EMC ESTIMATION BETWEEN ARNS AND IS-95 CDMA SYSTEM

The obtained values of protection signal-to-interference ratios can be used in the original procedure which allows to calculate the permissible number of BS (IS-95) and their performance in order to provide EMC with REE ARNS while operating in shared band. The core of the procedure is as follows:

1. Calculation of the useful signal power at the airborne receiver azimuth channel input (fig.2):

$$P_r = \frac{P_t \cdot G_t \cdot G_r \cdot \lambda^2 \cdot \beta_t \cdot \beta_r}{(4\pi \cdot R_s)^2},$$

where P_r – power measured at an airborne receiver input, W;

P_t – land beacon transmitter power, W;

G_t – land beacon antenna gain;

G_r – airborne antenna gain;

λ – wave length, m;

β_t – transmitter cable losses factor;

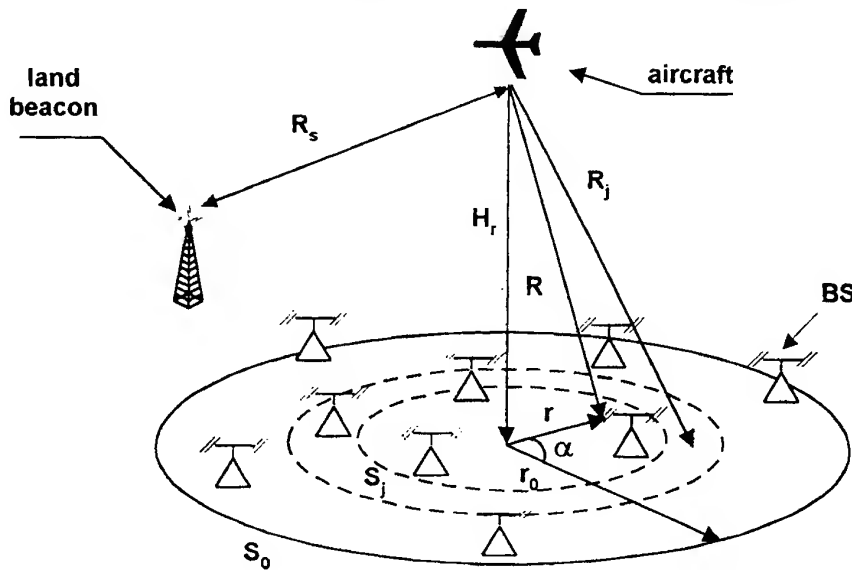


Fig.2

β_r – factor of losses, caused by receiver and transmitter mutual antenna patterns fluctuations;

H_r – height of airborne receiver, m;

R_s – distance between land beacon and an aircraft ($R_s = 3600 \cdot \sqrt{H_r}$), m.

2. Calculation of the maximum integral BS interfering power P_Σ measured at an airborne receiver input. At worst an aircraft is situated at H_r height above the center of the S_0 area with uniformly deployed base stations (fig.2). This follows from the fact that in this case the sum of distances between the corresponding BS and an aircraft would be minimum.

Let's divide the total coverage S_0 into k concentric rings with S_j area of each ones, $j=1\dots k$. Then P_Σ can be defined as:

$$P_\Sigma = \sum_{j=1}^k B \cdot \frac{N_{BS} \cdot S_j}{S_0 \cdot R_j^2},$$

where

$$B = \frac{P_{tBS} \cdot G_{tBSj} \cdot G_r \cdot \lambda^2 \cdot K_{pol}}{(4\pi)^2};$$

Here

P_{tBS} – BS transmitter power (the same for all BS), W;

G_{tBSj} – BS (j) antenna gain in the direction of an aircraft (assume them approximately equal to each other);

K_{pol} – polarization factor;

N_{BS} – the total number of BS;

R_j – distance between the center of (j) ring and an aircraft, m.

S_0 – BS network coverage, m^2 ;

S_j – square of (j) ring, m^2 .

Let's $S_j \rightarrow 0$. Then the limit of sum can be defined as (fig.2):

$$\begin{aligned} \lim_{S_j \rightarrow 0} \sum_j B \cdot \frac{N_{BS} \cdot S_j}{S_0 \cdot R_j^2} &= \int B \cdot \frac{N_{BS}}{S_0 \cdot R^2} dS = \\ &= \int_{r=0}^{r_0} \int_{\alpha=0}^{2\pi} B \cdot \frac{N_{BS} \cdot r}{\pi r_0^2 \cdot (r^2 + H_r^2)} d\alpha dr, \end{aligned}$$

where Ω – the surface of S_0 square;

r – radius-vector, changes from 0 to r_0 , m;

α – angle between the initial and current position of radius-vector, changes from 0 to 2π , rad.

Accomplishing this integral we obtain the final expression for P_Σ :

$$P_\Sigma = \frac{B \cdot N_{BS}}{r_0^2} \cdot \ln\left(\frac{r_0^2}{H_r^2} + 1\right)$$

Let's denote the protection signal-to-interference ratio as A . Equating $A P_\Sigma$ to the given useful signal power at an airborne receiver input P_r we have the following equation:

$$A P_\Sigma(P_{tBS}, N_{BS}) = P_r$$

Solving this equation considering N_{BS} to be an unknown quantity and given values of P_{tBS} and other parameters we can determine the maximum permissible number of simultaneously working BS (the sources of interference) within network coverage S_0 .

4. CONCLUSIONS

Taking into consideration the described procedure and protection ratios there was developed the system design of IS-95 network in Moscow and Moscow region. It was obtained that there can be deployed 26 BS with 13dB ERP of each ones on non-interfering basis with REE ARNS equipment.

5. REFERENCES

- [1] Table of Frequency Band Allocations to Radio Services of the Russian Federation in the Frequency Range from 3 kHz to 400 GHz. -Moscow, State Commission on Radio Frequency Management of the Russian Federation. 1996.
- [2] IS-95. "Mobile Station – Base Station Compatibility Standard for Dual-Mode Wideband Spread-Spectrum Cellular Systems", TR-45, PN-3115, Electronic Industries Association Engineering Department, March 15, 1993.

BIOGRAPHICAL NOTES

Dr. M. Bykhovski was born in Moscow, Russia, in 1938; a graduate of Moscow Electrotechnical Institute of Communications (1962), the chief of EMC department in Radio Research & Development Institute (NIIR) since 1998. He has over 100 scientific papers. His interests: theory of information, methods of EMC analysis in mobile communications, frequency planning.

A. Gulyaev was born in Tambov, Russia in 1973; a graduate of Jukovski Air-Force Engineering academy (1996, Moscow), master of informatics (1996). Presently, he works at NIIR, Russia and deals with EMC in mobile communications.

P. Mamchenkov was born in Moscow, Russia, in 1969. He received the degree of Radio Engineer of the Aviation Engineering Institute in Kiev, 1986. Presently he is the leading expert of the EMC department of NIIR, Russia.

Dr E. Muratov was born in 1946 in Moscow, Russia. He works in "Personal Communications" company.

M. Selivanov was born in Gorky, Russia in 1974. He works at Radio Research & Development Institute (NIIR).

Dr. V. Tikhvinski was born in Moscow, Russia, in 1958. He is a graduate of the Aviation Engineering Institute in Kiev (1980); since 1996 the head of the sector of the EMC department in NIIR, Russia. He is engaging in EMC problems in mobile communications.

Dr. V. Vysochin was born in Poltava, Ukraine in 1955; graduated from the Aviation Engineering Institute in Kiev, 1977. He works at Radio Research & Development Institute (NIIR).

THE INFLUENCE OF MEDIUM AND CONSTRUCTIVE PARAMETERS ON THE EXTERNAL FIELD OF COAXIAL CABLE

Liudmyla Dikmarova, Vitalij Nichoga, Roman Dzhala

Karpenko Physico-Mechanical Institute of National Academy of Sciences of Ukraine
5 Naukova str., Lviv, 290601, Ukraine

The external field of coaxial cable under various conditions was examined. New analytic dependencies for the components of the external electromagnetic field, produced by the spread currents and eccentricity of conductors, were obtained. The field features of coaxial cable with the slot on the external wire were examined. The data of the experimental verification of the obtained results is given.

1. INTRODUCTION

In the classical literature the theory of signals transmission via coaxial cables is worked out completely enough [1,2]. But the external electromagnetic field of coaxial cables (CC) and its characteristics are very often not analyzed and only those its parameters, that allow to evaluate the influence on the nearby other electric circuits, communication lines or the circuit formed by the external wire of CC and the medium, where it is located, are examined. Coupling resistance Z_C , that depends on the features of the shielding cover of the cable and is measured in linear resistance units, is one of these parameters. But, solving the problems of electromagnetic compatibility, it is not always efficient to use such parameters as coupling resistance Z_C , because in this case the influence of CC should be analyzed conformably to the specific second circuit of line. Such approach eliminates the possibility of parasitic emissions, the analysis of their features and level. Such problem can be solved by evaluation of the CC external field.

The theory of signals transmission accepts, that CC is a highly-shielded electromagnetic system, that doesn't possess the external field. The last may take place only in the case if CC possesses superconducting external cylindrical conductor (shield), the axis of which concurs with the axis of the internal (central) conductor and CC itself is located in the non-conducting medium (e.g.: in the air). Some aspects, concerning the CC external field, are examined in [3,4], but in these works the influence of the medium parameters, where CC is located, is not considered.

In the report the CC external field, depending upon the medium influence, where CC is located, and

constructive technological heterogeneity of the cable, is examined. The solution of such problem takes into consideration such factors, which were not considered before, and allows to examine both coinfluence of CC and other circuits and defining of their shielding in the mediums with various feature, where CC is located.

The solution are obtained on the basis of examination of the number of extreme electrodynamics problems. The simplifications used in every model allowed to define the mechanism of forming and the type of external field distributions under different conditions. The following models were examined: axis-symmetric CC in the conducting medium, CC with technologic eccentricity of the conductors, CC with the slot in the external conductor. The analysis was done for the frequency range $10^4 \div 10^7$ Hz. It was assumed, that medium conductivity may equal up to 4 S/m, what corresponds the cable location in the soil, ground saturated with highly mineralized water or sea water [2].

2. THEORETICAL ANALYSIS

The examination of the axis-symmetric CC in the semiconducting medium with the cable and medium parameters taken into consideration, when the currents in the cable conductors are not equal, what differs from the approach used in the classical literature, allowed to define, that the external field is formed by the spread of currents from the external cable conductor to the medium. The external field then is circular-symmetric and is described by the H_ϕ , E_Z , and E_r components. For the calculation of the external electromagnetic field components under $f > 10^5$ Hz to within +10% it is possible to use the following approximate formulas:

$$\begin{aligned} H_\phi &= IA H_1^{(1)}(\sqrt{j k_m r}) e^{-j\omega t}, \\ E_Z &= IA \frac{\sqrt{j k_m}}{\sigma_m} H_0^{(1)}(\sqrt{j k_m r}) e^{-j\omega t}, \\ E_r &= IA \frac{j}{\sigma_m} H_1^{(1)}(\sqrt{j k_m r}) e^{-j\omega t}, \end{aligned} \quad (1)$$

where

$$A = \frac{2\sqrt{\frac{r_2\sigma_m}{r_3\sigma_c}} e^{-x+j\phi}}{\pi r_2 \sqrt{1 + (0.88 - 1.27 \ln \Gamma k_m r_2)^2}},$$

$$\varphi = \operatorname{arctg} \frac{\cos x - (0.88 - 1.27 \ln \Gamma k_m r_2) \sin x}{\sin x + (0.88 - 1.27 \ln \Gamma k_m r_2) \cos x},$$

$$t = r_3 - r_2, x = \frac{k_c t}{\sqrt{2}}, k_c = \sqrt{\omega \mu_0 \sigma_c}, k_m = \sqrt{\omega \mu_0 \sigma_m}.$$

In this case k_m , σ_m is a wave number and conductivity of medium; k_c , σ_c - the same parameters of the external cable conductor; γ - field distribution constant; I - current in the cable; $H_0^{(1)}$, $H_1^{(1)}$ - Hankel functions of the first level of zero and first degree; r_2 , r_3 , r_4 - radiiuses of the cable external wire and of its isolation.

The conducted quantitative analysis by the formulas (1) and the formulas obtained for CC without isolation of the external wire, showed, that under $f > 1$ MHz in the semiconducting medium ($\sigma_m \approx 1$ S/m), the high frequency grounding of the external wire takes place and the external field doesn't depend upon the isolation of the external conductor.

The examination of the CC in the semiconducting medium allowed to define the presence of two own waves in it, that possess the distribution constants γ and γ_m . The obtained formulas for γ and γ_m showed that γ is close to the CC distribution constant used in the literature [1], and γ_m is close to wave number of the medium k_m and in the semiconducting medium is higher a number degrees than γ . Constant γ_m affects noticeably on field distribution only near the ends of the cable and heterogeneity, where due to wave superposition field distribution along the cable is of unmonotonous, pulsating type. On Fig.1 such dependence for CC 1 km long in the semiconducting medium under some fixed frequencies is given.

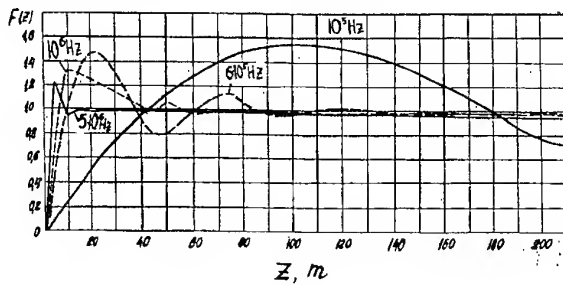


Fig. 1

To define the influence of the constructive heterogeneity on the CC external field the cable with conductors eccentricity under the condition of equality of direct and reverse currents in the cable conductors was examined. The external field then is not axially symmetric and is defined by the H_ϕ , E_z , and H_r components. In this case the external field of CC in the air is equivalent to the field of two-wired line with the distance between the wires equal to some calculated eccentricity:

$$\varepsilon' = \frac{2\varepsilon}{\Delta_1 r_2}, \quad (2)$$

where

$$\begin{aligned} \Delta_1 = & \frac{\nu_c + 1}{\xi_c} \cos \alpha \cdot \operatorname{sh} \alpha + \frac{\nu_c - 1}{\xi_c} \sin \alpha \cdot \operatorname{ch} \alpha - \\ & - \frac{r_2 + r_3}{r_3 \sqrt{r_2 r_3}} \cos \alpha \cdot \operatorname{ch} \alpha + j \left(\frac{\nu_c - 1}{\xi_c} \cos \alpha \cdot \operatorname{sh} \alpha - \right. \\ & \left. - \frac{\nu_c + 1}{\xi_c} \sin \alpha \cdot \operatorname{ch} \alpha + \frac{r_2 + r_3}{r_3 \sqrt{r_2 r_3}} \sin \alpha \cdot \operatorname{ch} \alpha \right), \end{aligned}$$

$$\nu_c = \omega \mu_1 \sigma_c r_2 r_3, \alpha = ik_c, \xi_c = r_3 k_c \sqrt{2r_2 r_3},$$

ε - cable conductors eccentricity.

As the CC with the slot on the external wire the cable, the external wire of which has the slot in the shape of sector cut (Fig.2) was used. It is rather hard to

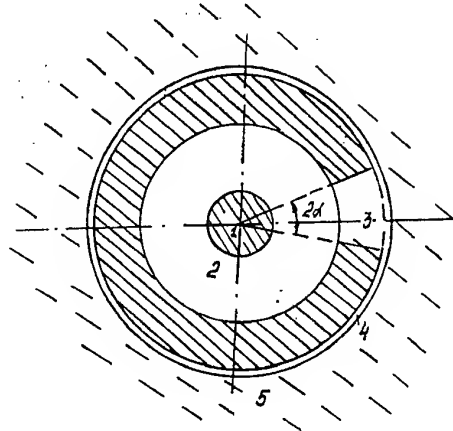


Fig. 2

obtain field distribution in such model, so the number of particular cases were examined. Cable conductors were considered ideally conductive. The algorithms for the field components were obtained as an unlimited system of linear algebraic equations, which is solved by the method of successive approximation [5,6]. The obtained algorithms allowed to define amplitude-frequency parameters of the field, that goes through the slot. It is shown, that near the slot the zone of higher level of the field increases to some extent when the frequency increases; this shows qualitative change of frequency dependence of the cable external field in this case. Field level is defined, generally, by the width of the clearance. Azimuthal field distribution is unmonotonous and the more complicated, the higher frequency is and the closer it is to the cable axis. The field is defined by H_ϕ , H_r , E_z , E_ϕ , E_r components. Depending upon the distance r , the field on the side of the slot is decreasing as $1/r^2$, and on the opposite side - much slower. The general scheme of field distribution is shown on Fig.3. The conducted calculations showed, that under the frequency $f > 1$ MHz CC has the emission through the slot. The

resulting CC external field is defined by the influence of all examined factors. Any of the factors can perform

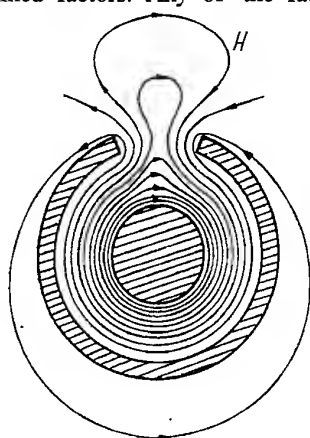


Fig.3

major influence depending upon frequency range, medium parameters and cable constructive parameters.

3.EXPERIMENTAL RESEARCH

The result given were partially proved by the experiments. The measured values of H_ϕ component of the cable external field (RK-75-9-11 in the air) under the frequencies $0,01 \div 10$ MHz gave a good coincidence with the formula (2) calculation results for the CC with conductors eccentricity. The conducted measurements of frequency dependencies H_ϕ component of the CC field in the conducting medium with the frequency range $0,1 \div 10$ MHz showed good coincidence with the formula (1) calculated data for the CC field formed by spread currents. The scheme of spatial field distribution of the CC with the slot in the semiconducting medium was also experimentally proved.

4.CONCLUSIONS

1.The CC external electromagnetic field may be formed by spread currents, eccentrical conductors placement or emission through the slot on the external conductor, depending upon the operating frequency range, medium parameters and constructive heterogeneity of the cable conductors. The levels of this field components and its spatial-frequential parameters are defined by the new analytic dependencies, obtained in this work, which were partially checked experimentally. Especially, in the air the CC external field might be formed by its conductors eccentricity or emission through the slots in the external wire, depending upon the operating frequency range.

2. When CC is located in the semiconducting medium the existence of parts near the end and heterogeneity along the cable length, where the pulsating of the field components, because of the presence of two own waves in such cable takes place.

3. When there is a slot on the CC external conductor the qualitative change of frequency dependencies of the field is observed, i.e. near the slot field components in the zone of higher level increase to some extent with the increasing of frequency.

5. REFERENCES

1. I.I.Grodnev, L.A.Frolov, "Coaxial Transmission Lines" (Russian), Svyaz, Moscow, 1977, 311p.
2. E.F.Vance, "Coupling to Shielded Cables", John Wiley and Sons, New York, 1982, 220 p.
3. S.A.Schelkunof, "The Electromagnetic Theory of Coaxial Transmission Lines and Cylindrical Shields", Bell System Techn. J., Vol.13, No. 4, p.532.
4. Yung-Ping Yoh, "Shielding Theory of Coaxial Cylindrical Structures", IEEE Transactions on Electromagnetic Compatibility, Vol. EMC-10, No.1, 1968.
5. R.M.Dzhala,, L.P.Dikmarova, " Main Wave of Partly Shielded Double-Phase Line" (Russian), Teoreticheskaiia Elektrotehnika, Vol.26, Lviv University Press, Lviv, 1980, pp. 80-87.
6. R.M.Dzhala, "Cylindrical Shield with Longitudinal Slot and with Finite Thickness and Conductivity" (Russian), Radiotekhnika i Elektronika, Vol.XXX, No.1, 1985, pp.1-7.

BIOGRAPHICAL NOTES

Vitalij Nichoga is a leading scientific researcher and the manager of laboratory of primary measuring transducers of Karpenko Physico-Mechanical Institute of National Academy of Sciences of Ukraine. He graduated Radio Engineering Faculty of State University "Lvivska Politehnika" in 1960, obtained his Dr. ing. degree in 1966 and Dr. hab. degree in 1996. Investigation of electromagnetic fields and manufacturing of instrumentation for their measuring are his main scientific interests.

Liudmila Dikmarova is a senior scientific researcher of Karpenko Physico-Mechanical Institute of National Academy of Sciences of Ukraine. She graduated Electric Engineering Faculty of State University "Lvivska Politehnika" in 1950, obtained his Dr. ing. degree in 1954 and Dr. hab. degree in 1989. Investigation of electromagnetic fields concerning geophysics, communication lines and testing of underground pipelines corrosion is her main scientific interest.

Roman Dzhala is a senior scientific researcher of Karpenko Physico-Mechanical Institute of National Academy of Sciences of Ukraine. He graduated Physical Faculty of Lviv State University in 1969, obtained his Dr. Phys.-math. degree in 1984. Radiophysics, theory of diffraction, electromagnetic methods of measurements, corrosion inspections, physical methods of non-destructive testing are his main scientific interests.

EVALUATION OF TRANSIENT BEHAVIOUR OF RADIOPHONIC TRANSMITTERS USING SHORT-TIME FOURIER TRANSFORM

Jerzy Kołakowski

Institute of Radioelectronics, Warsaw University of Technology
ul. Nowowiejska 15/19, 00-665 Warszawa
tel/fax +48 22 6607635 e-mail j.kolakowski@ire.pw.edu.pl

Abstract

The paper deals with measurements of signals emitted by a radiophonic transmitter during transient states. Traditional measures and measurement methods are briefly described. The method for transients evaluation based on Short-time Fourier Transform (STFT) is presented and its features are discussed. The paper contains results of simulations as well as measurements of exemplary transmitter.

1. INTRODUCTION

Recently we can observe a rapid development of radiophonic equipment from simple radiotelephones to sophisticated terminals working in cellular networks. Many of them work in systems requiring frequent switching the transmitter on and off. After switching the transmitter we can observe its transient behaviour i.e. RF power and carrier frequency are changing towards their nominal values. Moreover a rapid growth of RF power makes the output signal spectrum broader. Transient state duration depends on a kind of transmitter and in case of radiophonic transmitters can last from few μ s to tens of milliseconds.

During this, relatively short, period the transmitter can be a source of interference. This is the reason for detailed investigation of transients and for development of advanced methods and instrumentation for radiophonic transmitter testing [4].

2. MEASURES AND METHODS FOR TESTING TRANSIENTS

Phenomena occurring in the transmitter during transient state cause changes of output spectrum and emitted power. This is the reason that measures describing transmitter behaviour are based on these quantities. The way these values

are changing in time, specific to particular transmitter is usually investigated. Curves corresponding to these changes are the basis for attack and release time determination and give answer to the question if instantaneous carrier frequency and power values do not exceed the appropriate limits. An example of test arrangement traditionally used for transmitter transient measurements is shown in figure 1 [6].

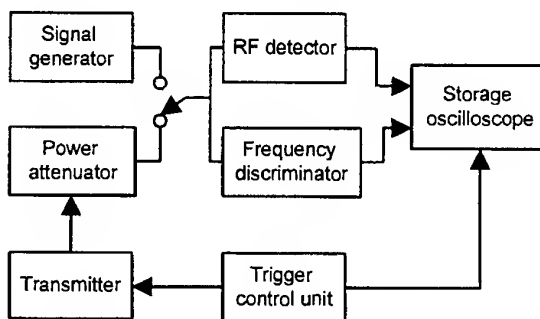


Fig. 1. Traditional measurement arrangement for transients evaluation

Another aspect of transients is RF power delivered to the adjacent channel. The intensity of this emission is estimated by adjacent channel transient power. Generally, the point of the method is to catch a peak value of RF power detected in adjacent channel during transient state. The signal is measured at the output of the intermediate frequency filter specified in standard [6].

3. APPLICATION OF STFT FOR EVALUATION OF TRANSIENTS

Great advances in signal processing and development of computer equipment are stimuli for development of measurement methods and instruments.

The essence of proposed method is the calculation

of required parameters using set of transmitter output signal samples. Generally there is no problem with determination of RF power behaviour. Digital detection and low-pass filtering will do. More problems can be encountered with calculation of frequency behaviour.

The proposed method is based on Short-time Fourier Transform. STFT can be described by equation (1) [3].

$$STFT(n, \omega) = \sum_{m=-\infty}^{\infty} x(m)w(n-m)e^{-j\omega m} \quad (1)$$

where:

- $x(n)$ – discrete time signal
- $w(n)$ – analysis window

Transformation maps one-dimensional function of time into the two-dimensional function of time and frequency. From the processing point of view STFT calculation depends on evaluation of FFT for subsets of samples falling into the window $w(n)$ that is sliding along set of signal samples. From the signal image in the time-frequency plane, frequency behaviour can be easily determined.

Properties of measured signal have great influence on the method. Transmitter signal spectrum components usually are lying in the vicinity of nominal carrier frequency. In such case standard FFT algorithm does not provide enough resolution for signal frequency determination. The signal should be moved to lower frequencies (fig 2) thus FFT resolution can be changed from

$$df_1 = f_{s1}/N_1 \quad (2)$$

to

$$df_2 = f_{s2}/N_2 \quad (3)$$

where: N_1, N_2 – window lengths

There is a contradiction concerning length of the window. Longer one provides better frequency resolution but location in time is worse.

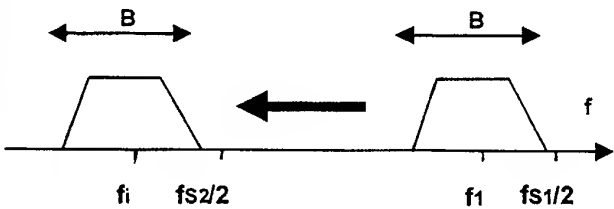


Fig. 2. Moving the spectrum to lower frequencies

- f_1 – signal carrier frequency,
- f_i - intermediate frequency,
- B - signal bandwidth,
- f_{s1}, f_{s2} – sampling frequencies

A choice of intermediate frequency (f_i) and thus new sampling frequency (f_{s2}) (Nyquist criterion) should be based on a type of transmitter or should be preceded by preliminary estimation of the band (B) occupied by the signal.

The operation of down-conversion is done in digital complex mixer (fig 3). Besides increase in frequency resolution there is another advantage, the length of the signal record is significantly reduced. It is done by resampling (retaining only samples corresponding to new sampling frequency).

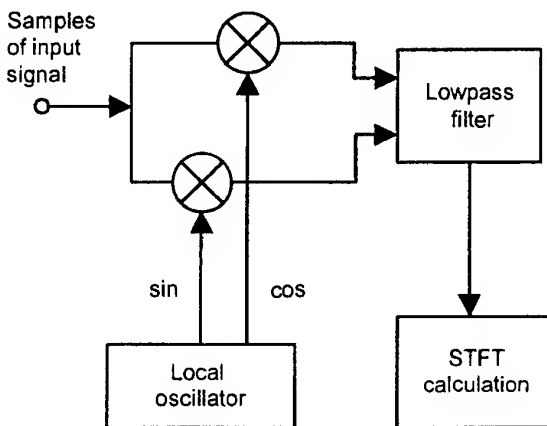


Fig. 3. Signal processing according to proposed method

FFT results are further refined by zero-padding i.e. extending set of samples with zeros. This way the accuracy of estimating the frequency of spectral peaks (df_z) is enhanced.

$$df_z = f_{s2}/N_z \quad (4)$$

where N_z – total number of analysed signal samples and padding zeros.

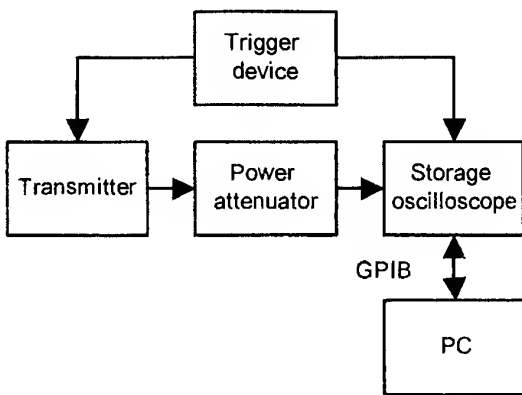


Fig. 4. Test arrangement for measurement of transients

Test arrangement that have been used for signal acquisition (fig. 4) is simpler than the traditional one (fig. 1). In both cases investigation of transmitter working at higher frequencies requires use of additional mixing stage.

4. FEATURES OF THE METHOD

Features of the method were investigated by carrying out software simulations. Obtained results should be referred to requirements that can be found in standards dealing with measurement of transients in radiocommunication transmitters [5],[6].

Standards require RF power and frequency evaluation for levels above -30 dBc . This requirement can be easily fulfilled for oscilloscopes providing effective 8-bit resolution.

Required uncertainty of transient frequency measurement is equal to 250 Hz [5]. If we assume $f_{\text{S2}}=100 \text{ kHz}$ and $N_z=512$ (values that have been used for measurements) the accuracy of frequency determination is about 200 Hz.

Another demand concerns capability of measurement of signals with fast frequency changes. In some standards discriminator fast enough to display the frequency deviations ($1 \text{ kHz}/\mu\text{s}$) is required [6]. Dynamic features of the method have been investigated with the use of simulated signals. Test signal carrier frequency has been equal to 30 MHz. Signal has been down-converted to 20 kHz and resampled at 100 kSa/s. STFT has been calculated for 16 and 32 sample sets (Barlett window was used). In both cases signal record has been zero-padded to 512 samples.

Figure 5 presents frequency deviation of test signals. Results of calculations are shown in figures 6 and 7.

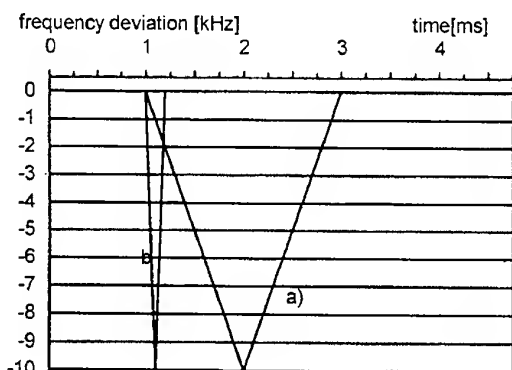


Fig 5. Test signals: a) $10 \text{ Hz}/\mu\text{s}$, b) $100 \text{ Hz}/\mu\text{s}$

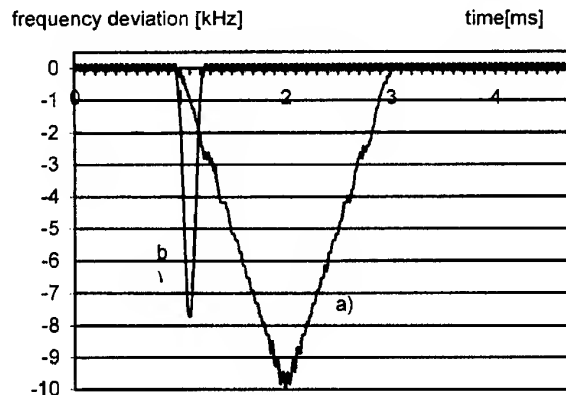


Fig 6. Results of calculations performed for test signals (window covered 16 signal samples)

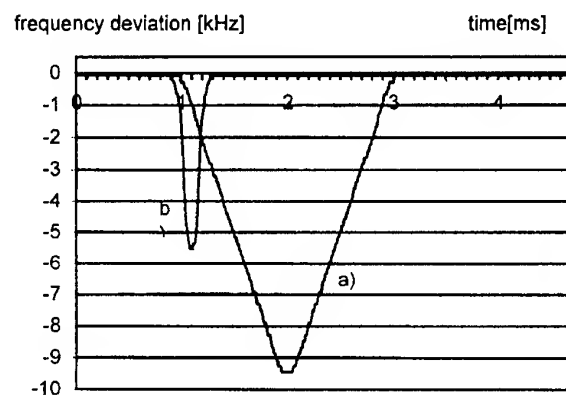


Fig 7. Results of calculations performed for test signals (window covered 32 signal samples)

The method with chosen signal processing parameters does not fulfil requirement that is mentioned above. For these settings error of frequency evaluation will be less than 5% for signals whose frequency is changing slower than $10 \text{ Hz}/\mu\text{s}$.

Responses to test signal are shifted in time. The main reason for this "timing advance" is the length of the window.

5. EXEMPLARY MEASUREMENTS AND RESULTS

Proposed test setup has been used for estimation of frequency changes during transient state of CB transmitter working at 27 MHz. The signal acquisition has been made using HP 54645A (8 effective bits, 100 MSa/s). Parameters used for STFT evaluation have been the same as for described simulations. Spectrogram obtained

during measurement is presented in fig. 7.

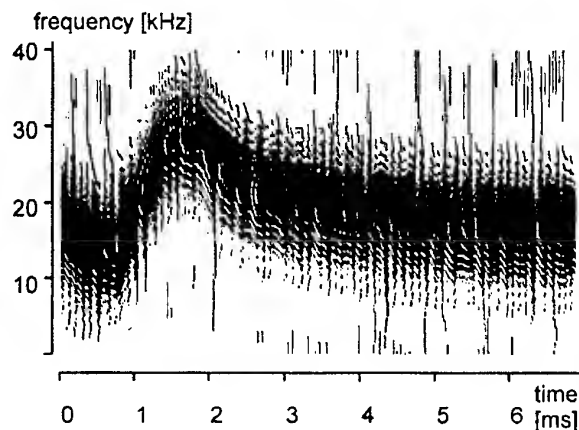


Fig. 7. Spectrogram of output signal of investigated CB transmitter

The results of frequency behaviour measurement have been verified by means of modulation analyzer HP 53310A. Obtained results are presented in figures 8 and 9.

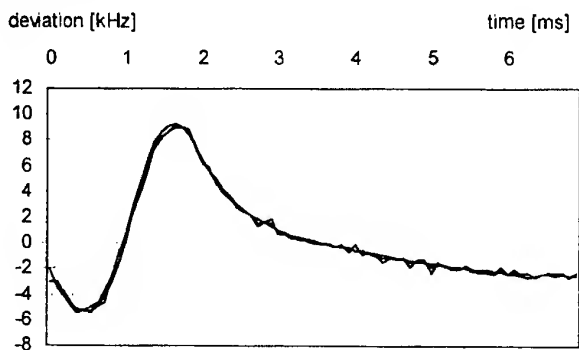


Fig. 8. CB transmitter transient frequency behaviour - results from modulation analyzer and proposed method

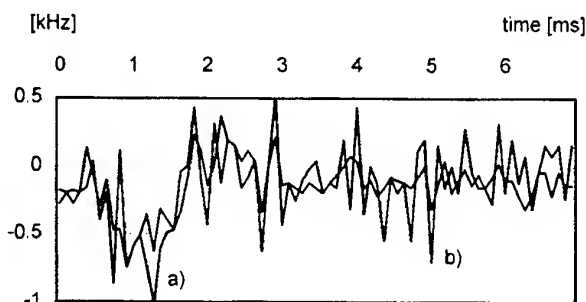


Fig. 9. CB transmitter transient frequency behaviour (difference of readings from modulation analyzer and proposed method) a) STFT - 32 samples b) STFT - 16 samples

6. CONCLUSIONS

The method seems to be a good solution for preliminary estimation of transmitter behaviour during transient state. Proposed measurement arrangement is significantly simplified in comparison with traditional one. Signal acquisition requires use of instrument equipped with fast A/D converter and large memory for collected samples. This barrier can be omitted by utilisation of additional mixing device in front of storage oscilloscope. Software for calculation of parameters can be run on a standard Pentium class PC.

7. REFERENCES

1. S. L. Marple, "Digital Spectral Analysis", Prentice-Hall Inc., 1987
2. L. B. Jackson, "Digital Filters and Signal Processing", Kluwer Academic Publishers, 1986
3. A. D. Poularikas (ed) "The Transforms and Applications Handbook", CRC Press & IEEE Press, 1996
4. A. J. Fiok, J. Cichocki, J. Kołakowski, K. Kwiecień, S. Żmudzin, "Systems for measuring radiocommunication equipment. Selected problems." Proceedings of the XII IMEKO World Congress, Torino, 1994, v.1, pp.576-581.
5. ETSI 300086; Technical characteristics and test conditions for radio equipment with an internal or external RF connector intended primarily for analogue speech; ETSI standard January 1991
6. ETSI 300113; Technical characteristics and test conditions for radio equipment intended for the transmission of data (and speech) and having an antenna connector; ETSI, June 1996.

BIOGRAPHICAL NOTE

Jerzy Kołakowski received his MSc degree in 1988 from Warsaw University of Technology. Since 1988 he is with Institute of Radioelectronics. His activity concerns methods and systems for measurements of radiocommunication equipment.

AN APPROACH FOR EMC ANALYSIS OF LOCAL COMMUNICATION NETWORK

V. Ya Kontorovich

CINVESTAV, México, Research and Advanced Studies Center of National Polytechnic Institute of Mexico, Electrical Engineering Department, Telecommunication Section, Av. IPN # 2508, Esquina con Av. Ticomán, Col. San Pedro Zacatenco, C.P. 7000, México, D. F., Tel+Fax: (011525) 747-7088. E-mail: valeri@mvax1.red.cinvestav.mx

R. Linares y M.

ESIME-SEPI-IPN; Becario COFAA, National Polytechnic Institute of Mexico, Unidad Profesional Adolfo López Mateos, Edif. 5, 3er. Piso, Col. Lindavista, C.P. 07738, México, D. F. Tel+Fax: (011525) 729-6000 ext. 54622. E-mail: rlinares@maxwell.esimez.ipn.mx

ABSTRACT

Major demand of services in telecommunication systems are taking place at local network and at the same time Electromagnetic Compatibility (EMC) problems are growing. In this paper an approach for the EMC analysis of local network is developed on the basis of queuing systems. With this approach the noise immunity evaluation is rather realistic, it can be used for weak point identification of the system and determine of interference tolerance level.

Keywords: Communication network, Measurement Systems, Noise immunity.

I. INTRODUCTION

Industrial processes efficiency is leaning on communications systems and the network local is growing because major changes are taking at the same time in related measurement, computing, communications technologies [1]. Electromagnetic Compatibility (EMC) problems do not wait and some analysis have done on this matter that including digital communications systems [2, 3]. In any local network, there are many storage devices and behavior of them depend on the interaction of the system workload and of the system resources. This problem basically is called traffic queues, which interact in the sense that messages departing from a node can enter one or more other queues, which in turn can simultaneously be accepted traffic from other queues. This analysis for communication networks has received much attention [4], but EMC problems are often not fulfilled for instance at high frequency the level of radiation and

susceptibility are not defined about all high traffic of acquisition data systems in measurement process.

The purpose of this paper is to develop an approach for analysis of noise immunity in presence of multitude of interference at network local using queues theory.

II. RADIAL LOCAL NETWORK ANALYSIS

Let us investigate the network, illustrated on the figure 1. The system depicted there represents the conventional multichannel measurement set, radial local network for computer communications, etc.

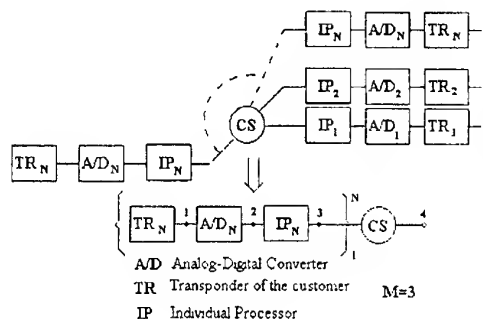


Figure 1. Radial structure of the communication network

For many practical cases the structure shown in the previous figure is adapted together with the following assumptions.

- Customers can be modeled by mean of the transponder set with band-path $\{\Delta F_i\}_1^N$
- Individual processors (IP_i) can be modeled by a queuing system GI/G/1, with intensity

for demands $\{\lambda_i\}_1^N$ and intensity for processing $\{\mu_i\}_1^N$;

- c) Capacities of $\{IP_i\}_1^N$ are sufficient and its results with probabilities (θ_i) are passed to central server (CS), which is modeled by a queuing system;
- d) The structure of the figure 1 is corrupted by statistically independent electromagnetic interference sources, mainly of man-made nature, which are modeled as pulse interference Poisson streams with intensities $\{v_e\}_1^M$ and with Log-Normal amplitude distribution:

$$W(V) = \frac{1}{\sqrt{2\pi}\sigma_e} \exp\left(-\frac{\ln^2 \frac{V}{b_e}}{2\sigma_e^2}\right)$$

where V -random amplitude of the interference pulse;

$\{b_e\}_1^M$, $\{\sigma_e\}_1^M$ -distribution parameters

Now, the problem is the noise immunity analysis of the whole system in the output terminal in nontrivial conditions, when the interference sources are distributed along the network stages.

III. ANALYSIS OF NOISE IMMUNITY

For the evaluation of the noise immunity of the local network in the mentioned environment, an approach is proposed with following basic ideas.

Work discipline of the set $\{IP_i\}_1^N$ together with CS can be described by means of queuing system with random structure, (and in each arbitrary k -state it can be modeled by mean of G1/G/1 with λ_k , μ_k , $k = 1, M$, where M -number of Random States of the system ($M \neq N$) is given by:

$$\sum_{k=1}^N C_N^K = M \quad (1)$$

The qualitative parameter for system evaluation is:

$$\Psi = 20 \log_{10} \frac{\bar{Q}_1}{\bar{Q}} / \forall v_e, \mu_e, \tau_e \equiv 0, \quad (2)$$

Where \bar{Q} - average length of the queue (waiting line); ψ -represents the increment of waiting line in presence of interference in different points of the system, comparing with the interference absence conditions.

Due to interference affecting each processor, or set of processors, CS (central server) can be in two general states: working or breakage (not working) and transformation from one to another (and vice-versa) follows to Poisson law with intensities v_{12} and v_{21} respectively.

Note: One not have to be confused with this process and do not mix it with random structure conditions, which depends only to information from the sensors and follows the rules of the way, how the CS is serving together with IP_i : (random structure regime in the previous sense has nothing to do with interference)

IP_i 's errors include arbitrary interference and error correcting codes with the proper margin range; then, it is necessary to consider in number of observation point, that is given by:

$$v_{12} = \sum_{j=3}^L \bar{n}; L = 3,4 \quad (3)$$

$$v_{21} = \sum_{j=3}^4 \frac{1}{T_j - \Delta T} \quad (4)$$

Where $-\Delta$ - margin range of the code; T -symbols internal; T_i - average burst interval.

Then, assuming that in point 1 to point 2 of the figure 1, one has aggregate interference to desired signal and if pulses interference succession are statistically independent, the distribution parameters are:

$$\mu_1^2 = k_o \mu_1, \quad \sigma_1^2 = \sigma_1, \quad v_1^2 = v_1;$$

In general case k_o can be evaluated from

$$k_o / k_{max} \leq \sqrt{\Delta f_{eff} \bar{\tau} p}, \\ k_{max} = \max|k(j\omega)|,$$

$k(j\omega)$ transfer function of the amplifier.

In case of bursts of interference, while they are passing through TR_N , pulses in the burst get to be overlapped.

The number of overlapped pulses are:

$$n_{o/e} \sim \frac{1}{\Delta f_{eff} \bar{\tau}_p}, \text{ then } \mu_1^{(2)} \sim \mu_1 \bar{n}_{o/e}; \quad (5)$$

$$\bar{n}_1^{(2)} \sim \bar{n}_1$$

At the A/D input we have interference, which get there from point 1 and passed from point 2 directly; assuming A/D as an uninertial devices one has for intensity for demands in point 3:

$$\lambda^{(3)} \equiv v_1 + v_2 + \bar{n}_1 + \bar{n}_2 + \lambda_2 \quad (6)$$

where λ_2 signal demands in point 2.

In absolutely similar way one can make an evaluation of the set of $\{IP_i\}$ with CS in k regime, where

$$\lambda_k^{(4)} = \sum_{i=0}^k b_i^{(3)} \sigma_i$$

For analysis of system GI/G/1 (obviously it depends to point 3) with random structure in k state, one also can use SDE approach for so-called diffusion approximations of GI/G/1 [5]. If q_k instantaneous number of demands at the set of $\{IP_i\}$ and CS in k state, then [6]:

$$q^k = (L_k + \xi_{INP,K})^{1(qk+0)} - (b_k + \xi_{s,k})^{1(qk-0)} \quad (7)$$

where $k=1, M$; $\xi_{INP,K}, \xi_{s,k}$ independent white noise with power spectrum densities: $L_k m_{INP,K}^2, b_k m_{INP,K}$ respectively;

$m_{INP,K}^2, m_s^2$ variances of the intervals between demands and between services periods respectively; $1(\bullet)$ -unit step function.

Let us rewrite (7) in the canonical form which is stochastically equivalent to (57) taking $M = 1$ (for simplicity); one has [5]:

$$q_k = f(q) + g(q)\xi(t) \quad (7a)$$

$$f(q) = \lambda 1(q+0) - b 1(q-0),$$

$$\text{Where } g(q) = \sqrt{m_{INP}^2 + b m_s^2}, \xi(t) \text{ white noise}$$

of unique intensity.

According to [6] one has for probability density function in stationary conditions:

$$W_{ST}(q) = \frac{2\beta \exp\left(-\frac{2\beta q}{\alpha}\right)}{\alpha(1-\pi_0) + \pi_0 \delta(q-0)} \quad (8)$$

where π_0 probability for the event of $q=0$; $\alpha = \lambda m_{INP}^2 + b m_s^2$; $\beta = b - \lambda$ assuming full load i.e. $\pi_0 = 0$

For $m_r(q)$ one can get from (8):

$$m_r(q) = (1-\pi_0) \frac{\Gamma(\gamma+1)}{(2\beta/\alpha)^2} \leq \frac{\Gamma(\gamma+1)}{(2\beta/\alpha)^2} \quad (9)$$

For $\gamma = 1$, what is practically important.

$$\bar{q} \leq \frac{1}{(2\beta/\alpha)^2} (M=1)$$

For $M > 1$ one can get [8]:

$$\begin{aligned} \sum_{k=1}^M P_k (\lambda_k - b_k) &= 0 \\ \sum_{k=1}^M Q_{1k} (b_k - \lambda_k) &= 0.5 \sum (\lambda_k m_{INP,k}^2 + b_k m_{s,k}^2) \end{aligned} \quad (10)$$

Where

$\bar{Q}_{1k} = P_k \bar{q}_k, \{P_k\}_1^M$ probabilities for each "k" state, which have to satisfy (10).

$$\bar{Q}_1 = \sum_{k=1}^M \bar{Q}_{1k} \quad (11)$$

Formula (11) concern to point 3

Therefore, from (11) one has

$$\bar{Q}_1^{(5)} = \frac{1}{M} \sum_{k=1}^M \bar{Q}_1^{(3)} + \bar{Q}_1^{(4)}, \quad (12)$$

Where $\bar{Q}_1^{(4)}$ is the average length of queue (waiting line) for CS it self (point 4), $\lambda_k^{(4)}$ can be format as.

$\lambda_k^{(4)} = \sum_{i=0}^k b_i^{(3)} \theta_i$ and CS can be modeled by M/M/1 system with $v_1 = \gamma$ and $v_{21} = \delta$ (see (4)), then from (10) one get ($M=2$):

$$\begin{aligned} \bar{Q}_1^{(4)} \leq & \lambda^{(4)} \left(m_{INP}^2 + m_s^2 \right) \left(1 + \frac{\gamma}{\delta} \right) + \\ & \frac{b^{(4)} \gamma / \delta}{(\delta + \gamma) 2 b^{(4)} \left[1 - \lambda^{(4)} / b^{(4)} \left(1 + \gamma / b^{(4)} \right) \right]} \end{aligned} \quad (13)$$

Let us take advantage of numerical example, with the following dates (neglecting interference at point 4)

$$\Delta f_{eff} = 10 kHz, v_1 = 10^2 P/s,$$

$$\tau_4 = 1 \mu s, k_{max} = 1; \mu_e = 1/e = 1.3;$$

$$T = 1 \mu s, \bar{n}_e = 10^4 \frac{burst}{s};$$

$$T_e = 10 \mu s/e = 2.3; \lambda^{(3)} / b^{(3)} = 0.3;$$

$$\bar{n}_2 + v_1 + v_2 = 0.1\delta; m_{INP}^2 + m_s^2 = 2;$$

$$\gamma / \delta = 0.1$$

Then from (3), (10), (4), (6), (13), and etc. $\Psi = 1.6$ dB, which show, that the average length of queue increases insignificantly.

IV CONCLUSION

The main advantages of the proposed approach are:

1. Noise immunity for communication systems depends in general to $v_1, \bar{n}_i, \mu_i, \sigma_i |k_i(j\omega)|$;
2. Total noise immunity evaluation in local network with rather realistic assumptions;
3. Determination of the system "weak points" which are not protected against interference influence.

REFERENCES

1. Joel S. Birnbaum, "Communications Challenges of the Digital Information Utility," HP Journal Vol. 48, No 15, pp 6-10, Dec. 1997
2. S. Methley, "Recent Emissions Measurements for 2 -TP and Higher Speed VG," IEEE 802.12, Nov. 1995.
3. S. Methley, "Recent Emissions Measurements for 2 -TP and Higher Speed VG," IEEE 802.12, January . 1996
4. P. R. Kumar, "A tutorial on some new methods for performer evaluation of queuing networks," IEEE Transaction on Selected Areas in Communications, Vol 13, No 6, p 970-980, 1995
5. D. Middleton, *Introduction to Statistical theory of communications.*, Peninsula Publishing, Los Altos California, 1987.
6. H. Risken *The fokker Plank Equation*, 2end Springer, Berlin , 1989

MUTUAL INTERFERENCE IN SYSTEMS WITH FREQUENCY ADAPTATION

Martin MARKO, Vladimír WIESER, Marián BABJAK

Military Academy in Liptovský Mikuláš, P.O.Box 76, 03101 Liptovský Mikuláš, Slovak Republic

Tel.: +421-849-22234/422 209, Fax :+421-849-249 59, E-mail : marco@valm.sk

ABSTRACT

Fundamental theoretical problems of a potential efficiency of frequency adaptive radio systems in high frequency band are indicated in this contribution. A probability of the mutual interference in frequency adaptive radio system with N radio links is determined with respect to spatial correlation.

1. INTRODUCTION

Effective utilization of the frequency spectrum is one of evolution trends on the fields of system conceptions and radiocommunication systems technical realization. Utilization of the higher frequency bands with aim to render new kind of the telecommunication services is characteristic for nowadays.

In spite of that the utilization of the short-wave band plays unsubstitutable role in radiocommunication through it has limited throughput capacity, especially as strategic insurance.

Physical characteristics of this band and their time instability have led to automation and higher form of equipment's technical parameter adaptation.

2. CLASSIFICATION OF ADAPTIVE RADIO SYSTEMS

Various variants of a technical support for radio link adaptation to changing connection's conditions make possible to classify adaptive systems according:

- regulated parameter (power, frequency, type of modulation, data rate and combination of about mentioned),
- object of regulation (transmitter, receiver, transmitter and receiver),

- method of the regulation (threshold, extreme, and combined),
- method for achieving of wanted quality parameter (searching, analytical, or combination),
- method for transmission of control commands (without transmission, in information channel, in special channel, combinations), and these channels can be narrow bandwidth or wide bandwidth.

Due to contribution extent, only frequency adaptive radio systems are addressed. Frequency adaptation is decisive for reliable communication in short-wave band, mainly if sky wave propagation is used.

3. POTENTIAL EFFICIENCY OF FREQUENCY ADAPTIVE RADIO SYSTEMS

Think to adapt frequency has been born earlier, in time when group of Q frequencies has been used for increasing of communication reliability in classical radio systems.

If we assume that

- all frequencies from group of Q frequencies are suitable from radio-wave propagation point of view,
- frequency spacing is sufficient to assume that levels of defects are independent,
- levels of signal and noise are the same on all frequencies,
- probability of connection on one frequency p_{si} is known,
- transition from one frequency to another is instantaneous,

then resultant probability of connection on group of frequencies will be [2]

$$P_{sQ} = 1 - (1 - p_{s1})^Q. \quad (1)$$

This relation is displayed on Fig.1 for various

Q. It is seen that although probability of connection on one frequency p_{s1} is quite low, if group of frequencies is used, for example Q=10, high probability of connection is achieved.

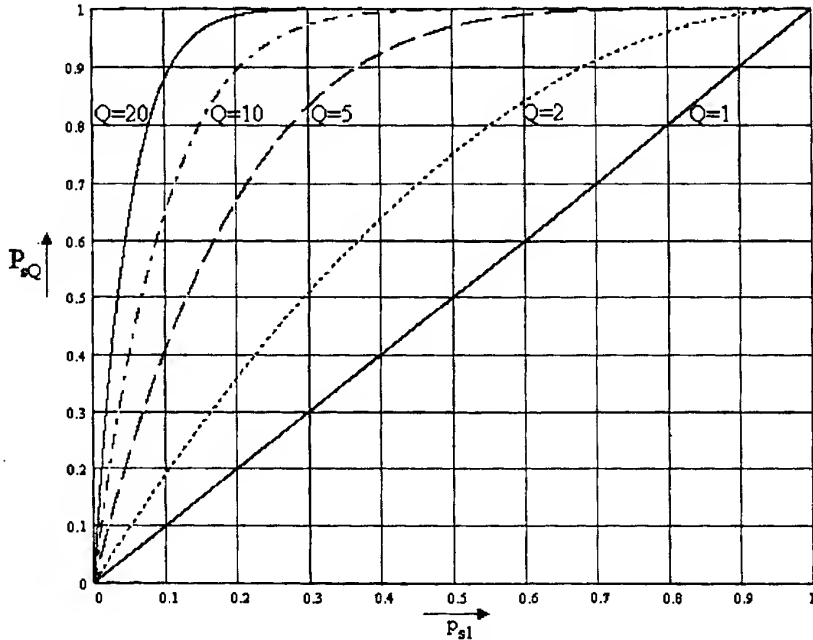


Fig.1. Resultant probability of connection on group of Q frequencies.

Transition from one frequency to other is not instantaneous in real system, but it takes a time interval τ_{prel} . This interval itself contains, the time needed for the working channel analyze from criteria for selection of working frequency on the base signal to noise ratio ($z \geq z_{\text{dov}}$) point of view, and the time needed for technical retuning of radio connection to new suitable frequency. The time needed to analyze the reserve channels may not be assumed, because this analyze is done parallel with operation of radio links. Probability of connection over this condition is

$$P_{sQ}(z \geq z_{\text{dov}}) = \frac{\bar{T}_{\text{spr}} - \bar{T}_{\text{prel}}}{\bar{T}_{\text{spr}} - \bar{T}_{\text{por}}}, \quad (2)$$

where \bar{T}_{spr} is average interval of the correct operation, \bar{T}_{prel} is average time of retuning during average interval of the correct operation and \bar{T}_{por} is average interval of system fault.

Average time of retuning during interval \bar{T}_{spr} can be written in form

$$\bar{T}_{\text{prel}} = \bar{T}_{\text{spr}} \cdot \bar{\lambda} \cdot \bar{\tau}_{\text{prel}}, \quad (3)$$

where $\bar{\lambda}$ is average number of retuning during unit of time and $\bar{\tau}_{\text{prel}}$ is average time of retuning.

After substitutions and arrangements we obtained

$$P_{sQ}(z \geq z_{\text{dov}}) = \frac{\bar{T}_{\text{spr}}}{\bar{T}_{\text{spr}} - \bar{T}_{\text{por}}} \cdot (1 - \bar{\lambda} \cdot \bar{\tau}_{\text{prel}}), \quad (4)$$

further

$$P_{sQ}(z \geq z_{\text{dov}}) = P_{iQ} \cdot (1 - \bar{\lambda} \cdot \tau_s). \quad (5)$$

The connection dynamic and the time intervals of the system states are displayed on Fig.2. Besides time intervals, which have been discussed above, it is in Fig.2 labeled time interval of the useful information transmission τ_s (time of real communication).

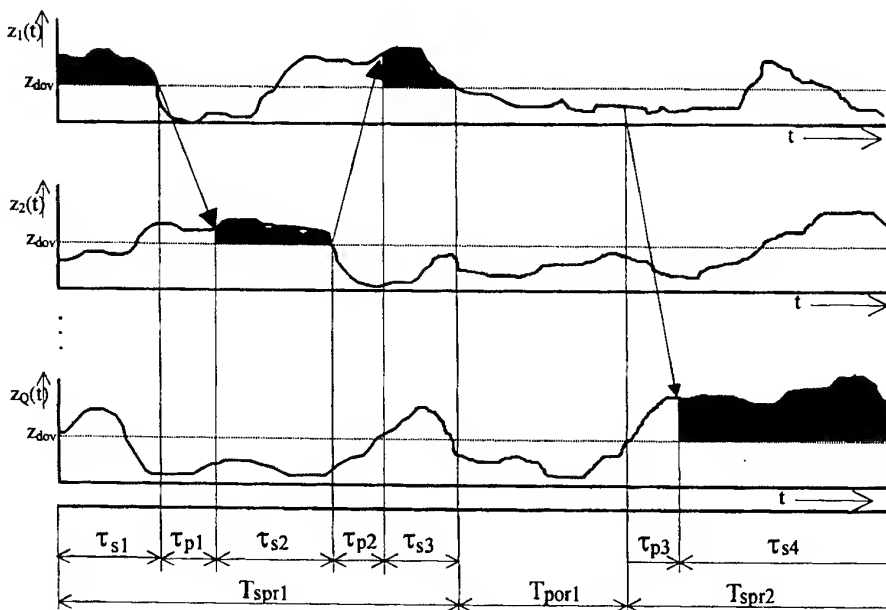


Fig.2. The operation dynamics on group of frequencies.

The longer are intervals $\bar{\tau}_s$ a $\bar{\tau}_{prel}$ the thinner will be retunings and fewer retunings will be done in unit of time. So stream of the work frequency changes will be

$$\bar{\lambda} = \frac{1}{\bar{\tau}_s + \bar{\tau}_{prel}} \quad (6)$$

Substituting equation (6) into (5) we will obtain

$$P_{sQ}(z \geq z_{dov}) = P_{iQ} \cdot \left(\frac{\bar{\tau}_s}{\bar{\tau}_s + \bar{\tau}_{prel}} \right). \quad (7)$$

From this is easy to find how long may be average time of retuning $\bar{\tau}_{prel\ dov}$, if we know the required probability of connection

$$\bar{\tau}_{prel\ dov} = \frac{\bar{\tau}_s (P_{iQ} - P_{sQ\ dov})}{P_{sQ\ dov}}. \quad (8)$$

For example, if the required probability of connection is $P_{sQ}=0,9$, $\bar{\tau}_{prel}=10$ min a $Q=10$, then

$$\bar{\tau}_{prel\ dov} = \frac{10(1-0,9)}{0,9} \approx 1\text{min}$$

and P_{iQ} is equal to one.

From what it was discussed follows, that for high values of $\bar{\tau}_{prel}$ neither will not be achieved required reliability nor will be obtained no gain in

comparison to operation on fixed frequency.

Last statement hint at fact, that successful realization of operation on group of frequencies is not possible without complex solution for automatization of the working and reserve channel's analyze process and without solution for process of the transmitter and receiver equipment's retuning.

This requirement has led to the considerable technical changes in receivers and transmitters construction. As example, the present time transmitters of middle power are able to realize a frequency maneuver about 1 to 1.5 seconds and transmitters of low power about 0.5 seconds. Retuning of receivers is about a few milliseconds [1].

4. PROBABILITY OF MUTUAL INTERFERENCE OF FREQUENCY ADAPTIVE RADIO SYSTEMS

Next actual problem connected with using frequency adaptive radio systems is determination of mutual interference in radio system with N autonomy radio connections.

These problems are solved in [3,4]. With respect to the considerable extent of calculations are addressed only assumptions and solution results in this contribution.

A mutual correlation is respected in problem analyzed by definition of the spatial correlation coefficients for each pair of receive points which are

arranged into matrix

$$\|k_{i,j}\| = \begin{vmatrix} 1 & k_{1,2} & \dots & k_{1,n} \\ & 1 & \vdots & \vdots \\ & & 1 & k_{m-1,n} \\ & & & 1 \end{vmatrix}. \quad (9)$$

Some simplifications are made in solution, which make able to assume disturbance levels on the individual frequencies as uncorrected. Retuning to new

Probability of mutual interference P_{vzr} after change of working frequencies in time interval Δt is

$$P_{vzr}(\Delta t) = P_{\text{prel } i,j}(\Delta t) \cdot P_{\text{zhody } f_{i,j}} = \binom{N}{2} \cdot (\lambda_{\text{prel } i,j} \cdot \Delta t)^2 \cdot (1 - \lambda_{\text{prel}} \cdot \Delta t)^{N-2} \cdot \left[\frac{1 + k_{i,j} \cdot (Q - N - 1)}{Q - N} \right] \quad (11)$$

An example of relationship between probability of mutual interference P_{vzr} and number of radio links N with $k_{i,j} = 0,5$ is on Fig.3.

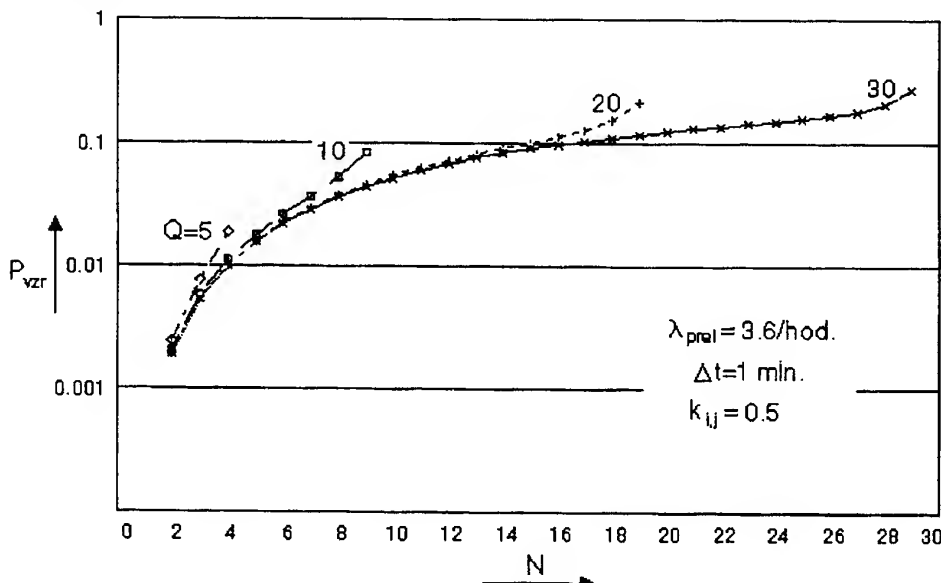


Fig.3. Relationship between probability of mutual interference P_{vzr} and number of radio links N , $k_{i,j} = 0,5$.

5. CONCLUSIONS

From above mentioned analyze of the potential efficiency of the frequency adaptive radio systems the following conclusion can be made.

The following problems must be solved in process of the frequency adaptive radio systems design and calculation:

- selection of subbands in HF band which are suitable from radio-wave propagation point of view,

frequency is performed on the base of minimal disturbance level. The transition streams from one frequency to other at all N radio links can be with sufficient accuracy assumed as Poisson stream.

As interference is assumed to be used the same frequencies after process of retuning in time interval Δt in j -th and an i -th receive points.

$$P_{\text{zhody } f_{i,j}} = (Q - N) \cdot P(A_i, A_j) = \frac{1 + k_{i,j} \cdot (Q - N - 1)}{Q - N} \quad (10)$$

$$P_{vzr}(\Delta t) = P_{\text{prel } i,j}(\Delta t) \cdot P_{\text{zhody } f_{i,j}} = \binom{N}{2} \cdot (\lambda_{\text{prel } i,j} \cdot \Delta t)^2 \cdot (1 - \lambda_{\text{prel}} \cdot \Delta t)^{N-2} \cdot \left[\frac{1 + k_{i,j} \cdot (Q - N - 1)}{Q - N} \right] \quad (11)$$

$\lambda_{\text{prel}} = 3.6/\text{hod.}$

$\Delta t = 1 \text{ min.}$

$k_{i,j} = 0.5$

- choice of the optimal statistic criteria for selection of working frequencies,
- connection establishment and transmission of control commands,
- retuning of transmitters and receivers,
- to assume level of mutual interference.

From the effective utilization of radio systems point of view it is necessary to solve them with multiparameter adaptation.

The discussed theory is applicable in higher frequency bands too (for example VHF), mainly for increasing of the resistance to interference or for

throughput optimization of the frequency adaptive radio links.

6. REFERENCES

- [1] J.GOODMAN-J.W.BALLARD-E.SHARP: "Practical method for highly reliable HF communication" (English). In: IEEE Communications Conference - „Milcom 95“, San Diego, November 1995, Vol.2, pp.1076-1082.
- [2] J.P.KALININ: "Adaptive automatic military radio systems" (Russian). VAS Leningrad, Russia 1978.
- [3] M.MARKO: "Compatibility of frequency adaptive radio connections in communication with the common frequency group" (Slovak). Proceeding SPOJAR, No.2, 1990, pp. 11-18.
- [4] M.MARKO-M.BABJAK: "Mutual interference of frequency adaptive communication system" (Slovak). Proceeding of Military Academy Liptovský Mikuláš, No.1, 1996, pp.89-95.

BIOGRAPHICAL NOTE

Martin Marko received the M.Sc. degree in electrical engineering from Military Academy Brno and PhD. degree from the same school in 1983. His interests include the mobile radio systems, frequency hopping systems and frequency adaptation in mobile radio.

Vladimír Wieser received the M.Sc. degree in electrical engineering from Military Academy Brno and Ph.D degree at Military Academy Liptovský Mikuláš, Department of Radiocommunication Systems. He is interesting in mobile radio communication systems and spread spectrum systems.

Marián Babjak graduated Military Academy Liptovský Mikuláš at 1992 and terminated his dissertation in 1997. His interests include mobile radio channel, digital modulations and coding, propagation and antennas.

A NEW CALCULATION METHOD OF LCTL FOR BALANCED PAIR CABLE WITH PARTIAL UNBALANCE

Y.Shimoshio[†], M.Miyoshi[†], H.Koga[†] and M.Tokuda^{††}

[†]Dept. of Information and Communication Engineering, Kumamoto National College of Technology ,
2659-2 Suya, Nishigoshi-machi, Kikuchi-gun, Kumamoto-ken, 861-1102 (Japan)

^{††}Kyusyu Institute of Technology, 1-1 Sensui, Tobata-ku, Kitakyusyu-shi, Fukuoka-ken, 804-0015 (Japan)
(E-mail address:yshimo@knetta.tc.knct.ac.jp)

ABSTRACT A new calculation method of LCTL has been proposed for a balanced pair cable circuit which consists of a balanced pair cable and terminal equipment. Generally, actual balanced cable has some unbalance about earth and terminal equipment also. The balanced pair cable is represented as a cascade connection of many short cables. Each short cable consists of a perfectly balanced short cable and a lumped elements circuit. The lumped elements circuit simulates unbalance to the perfectly balanced cable and it shows unbalance of the actual balanced pair cable. If the unbalance of terminal equipment is also represented by the lumped elements circuit, then a transmission matrix for the whole of the balanced pair cable circuit is derived. Thus, LCTL of the circuit is obtained from the matrix. Several LCTLs are examined and experimental results for them well coincided with calculated ones.

1. INTRODUCTION

A balanced pair cable circuit in communication system consists of a balanced pair cable and terminal equipment. An actual balanced pair cable has unbalance about earth because of nonuniform diameter of the conductors, inhomogenous dielectric constant, geometrical configuration and so on. Not only that, there are some partial unbalances caused by impedance unbalance of terminal equipment, by water penetration in the cable, etc. LCTL(Longitudinal conversion transfer loss) which represents unbalance about earth is defined in the ITU-T recommendation[1],[2] and it is an important characteristic in a design of communication systems[3]. Nevertheless, LCTL of the balanced pair cable circuit has been only investigated experimentally and analyzed roughly in theory. Thus, some of LCTL characteristics, such as LCTL for unbalanced impedance in arbitrary location of a balanced pair cable and LCTL of the balanced pair cable with test splicing, have not been clarified theoretically.

In this paper, we have proposed a new LCTL calculation method using a transmission matrix for six terminal circuits and have analyzed some LCTLs. In the

proposed method, it is assumed that the balanced pair cable circuit itself consists of N-sections and each section contains two kinds of parts; a perfectly balanced short pair cable part and a lumped elements circuit part, as shown in Fig.1. The unbalance of actual balanced pair cable is represented by the perfectly balanced cable with the lumped elements circuit. That is, each lumped element in the lumped elements circuit means unbalance component of the actual balanced cable. Two kinds of transmission matrices for these two parts are derived. A transmission matrix for the partial unbalance circuit such as terminal equipment is also derived. Then, a transmission matrix for the balanced pair cable circuit is derived and all of voltages and currents of the circuit are obtained from a equation by the transmission matrix of the balanced pair cable circuit. Thus, a common mode and a normal mode voltage is derived from the voltages and LCTL is represented by an simple equation which consists of components in the transmission matrix.

We examined several LCTL characteristics for unbalanced impedance and the balanced pair cable with test splicing. As a result, it is clarified that the proposed method is useful for LCTL calculation.

2. Theory

We propose a LCTL calculation method for balanced pair cable circuit. In this method, actual balanced cable is treated as a cascade connection of many short cables which consists of a perfectly balanced short cable and a lumped elements circuit as shown in Fig.1. Here, we derive a transmission matrix for the perfectly balanced cable, one for the lumped element circuit, one for the whole of the balanced pair cable circuit and LCTL equation.

2.1 Transmission matrix for perfectly balanced pair cable

Here, we derive a transmission matrix for three conductor lines which consists of balanced pair lines("1" and "2") and a ground("3") as shown in Fig. 2. In Fig. 2, there are a real circuit and a longitudinal circuit. Next

differential equations are derived for Fig. 2[4].

$$\begin{aligned} -\frac{dv_n}{dx} &= Z_n i_n + Z_m i_c & -\frac{dv_c}{dx} &= Z_m i_n + Z_c i_c \\ -\frac{di_n}{dx} &= Y_n v_n + Y_m v_c & -\frac{di_c}{dx} &= Y_m v_n + Y_c v_c \end{aligned} \quad (1)$$

where

$Z_n = R_n + j\omega L_n$: Primary impedance of real circuit

$Z_c = R_c + j\omega L_c$: Primary impedance of longitudinal circuit

$Y_n = G_n + j\omega C_n$: Primary admittance of real circuit

$Y_c = G_c + j\omega C_c$: Primary admittance of longitudinal circuit.

Z_m : Mutual impedance between longitudinal circuit and real circuit

Y_m : Mutual admittance between longitudinal circuit and real circuit

If $Z_m = 0$ and $Y_m = 0$, then the three conductor lines become the perfectly balanced cable. Figure 3 shows the matrix representation of the perfectly balanced cable and Eq.(2) for Fig. 3 is derived from Eq.(1).

$$\begin{bmatrix} V_{11} \\ V_{21} \\ I_{11} \\ I_{21} \end{bmatrix} = \begin{bmatrix} a_{11} & a_{12} & b_{11} & b_{12} \\ a_{21} & a_{22} & b_{21} & b_{22} \\ c_{11} & c_{12} & d_{11} & d_{12} \\ c_{21} & c_{22} & d_{21} & d_{22} \end{bmatrix} \begin{bmatrix} V_{12} \\ V_{22} \\ I_{12} \\ I_{22} \end{bmatrix} \quad (2)$$

where,

$$a_{11} = a_{22} = d_{11} = d_{22} = \frac{1}{2}(\cosh \sqrt{Z_c Y_c} x + \cosh \sqrt{Z_n Y_n} x)$$

$$a_{12} = a_{21} = d_{12} = d_{21} = \frac{1}{2}(\cosh \sqrt{Z_c Y_c} x - \cosh \sqrt{Z_n Y_n} x)$$

$$b_{11} = b_{22} = \frac{1}{2}\left(2\sqrt{\frac{Z_c}{Y_c}} \sinh \sqrt{Z_c Y_c} x + \frac{1}{2}\sqrt{\frac{Z_n}{Y_n}} \sinh \sqrt{Z_n Y_n} x\right)$$

$$b_{12} = b_{21} = \frac{1}{2}\left(2\sqrt{\frac{Z_c}{Y_c}} \sinh \sqrt{Z_c Y_c} x - \frac{1}{2}\sqrt{\frac{Z_n}{Y_n}} \sinh \sqrt{Z_n Y_n} x\right)$$

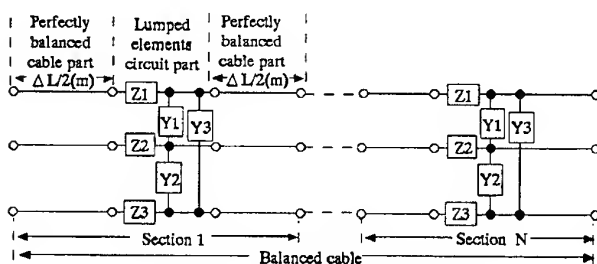


Fig. 1 Model of balanced pair cable.

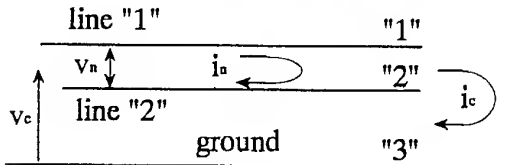


Fig. 2 Three conductor lines.

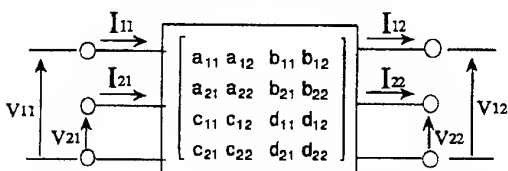


Fig. 3 Matrix representation of perfectly balanced pair cable.

$$c_{11} = c_{22} = \frac{1}{2}\left(\frac{1}{2}\sqrt{\frac{Y_c}{Z_c}} \sinh \sqrt{Z_c Y_c} x + 2\sqrt{\frac{Y_n}{Z_n}} \sinh \sqrt{Z_n Y_n} x\right)$$

$$c_{12} = c_{21} = \frac{1}{2}\left(\frac{1}{2}\sqrt{\frac{Y_c}{Z_c}} \sinh \sqrt{Z_c Y_c} x - 2\sqrt{\frac{Y_n}{Z_n}} \sinh \sqrt{Z_n Y_n} x\right)$$

2.2 Transmission matrix for lumped elements circuit

Here, we derive a transmission matrix for the lumped elements circuit in Fig. 1. As each element in the circuit is represented by simple transmission matrix for six terminals circuit, the transmission matrix of the circuit is derived as Eq.(3). When there is a partial unbalance in the balanced pair cable circuit by impedance unbalance of terminal equipment etc., the same way can be used to obtain a transmission matrix for the partial unbalance circuit.

$$\begin{bmatrix} 1 & 0 & Z_1 + Z_3 & Z_3 \\ 0 & 1 & Z_3 & Z_2 + Z_3 \\ Y_1 + Y_3 - Y_1 & 1 + Z_1 \cdot Y_1 + Z_1 \cdot Z_3 + Z_3 \cdot Y_3 & Z_3 \cdot Y_3 - Y_1 \cdot Z_2 \\ -Y_1 & Y_1 + Y_2 & Y_2 \cdot Z_3 - Z_1 \cdot Y_1 & 1 + Y_1 \cdot Z_2 + Z_2 \cdot Y_2 + Y_2 \cdot Z_3 \end{bmatrix} \quad (3)$$

2.3 Transmission matrix for balanced pair cable circuit

Figure 4 shows a matrix representation of a balanced pair cable circuit. Since the circuit consists of balanced pair cable and partial unbalance circuit, a transmission matrix of the circuit is obtained by a multiplication of many transmission matrices. Equation (4) shows the circuit equation for the circuit and each F_i shows matrix for perfectly balanced pair cables, lumped elements circuits and partial unbalance circuits, respectively. M is the total number of matrices in the balanced pair cable circuit.

$$\begin{bmatrix} V_{1i} \\ V_{2i} \\ I_{1i} \\ I_{2i} \end{bmatrix} = \begin{bmatrix} A_{11} & A_{12} & B_{11} & B_{12} \\ A_{21} & A_{22} & B_{21} & B_{22} \\ C_{11} & C_{12} & D_{11} & D_{12} \\ C_{21} & C_{22} & D_{21} & D_{22} \end{bmatrix} \begin{bmatrix} V_{1o} \\ V_{2o} \\ I_{1o} \\ I_{2o} \end{bmatrix} = \prod_{i=1}^M F_i \begin{bmatrix} V_{1o} \\ V_{2o} \\ I_{1o} \\ I_{2o} \end{bmatrix} \quad (4)$$

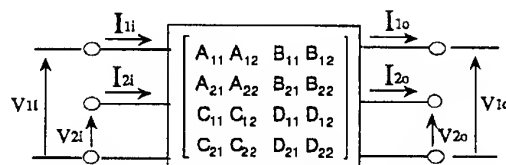


Fig. 4 Matrix representation of balanced pair cable circuit.

2.4 Longitudinal conversion transfer loss

We define LCTL as a ratio of the common mode voltage at the output terminal to the normal mode voltage at the input terminal in Fig. 4. The definition is same with $LCTL_{21}$ in reference[3] and LCTL is represented as Eq.(5) by matrix components in Eq.(4).

$$\begin{aligned} LCTL &= 20 \log \frac{V_{out \text{ common}}}{V_{in \text{ normal}}} = 20 \log \frac{(V_{1o} + V_{2o})/2}{V_{1i} - V_{2i}} \\ &= 20 \log \left| \frac{1}{2} \frac{(C_{12} + C_{22})(C_{11} + C_{21})}{(A_{11} - A_{21})(C_{12} + C_{22})(A_{12} - A_{22})(C_{11} + C_{21})} \right| [\text{dB}] \quad (5) \end{aligned}$$

3. Experiment results

3.1 Unbalance of actual balanced pair cable

Figure 5 shows the LCTL measurement circuit for the balanced pair cable. The transformer at the input terminal is a balun which is used for conversion from balance to unbalance. We used a CCP-AP(Color-coded polyethylene insulated aluminum polyethylene sheathed) cable containing 10 pair lines as the balanced pair cable. The ground line in Fig. 5 is the aluminum sheath of the CCP-AP cable. In our measurement system, the minimum detection level of the signal is -107dBm.

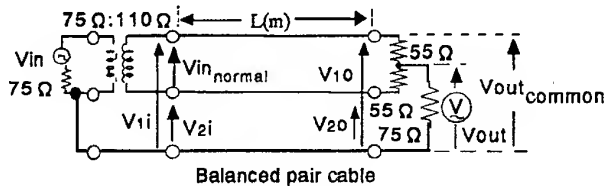


Fig.5 Measurement circuit of balanced pair cable.

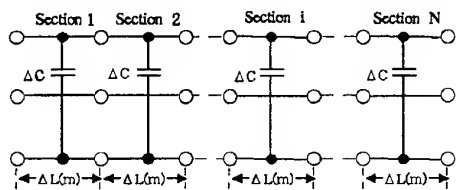


Fig.6 Model of balanced pair cable.

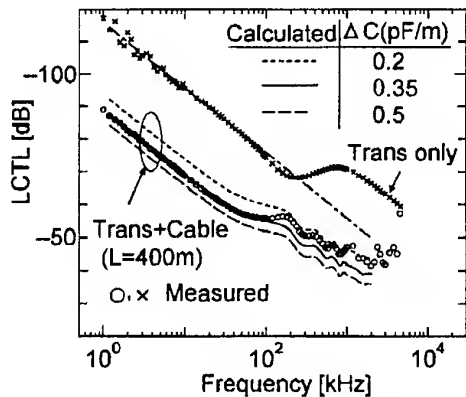


Fig.7 LCTL characteristics for capacitive unbalance of cable.

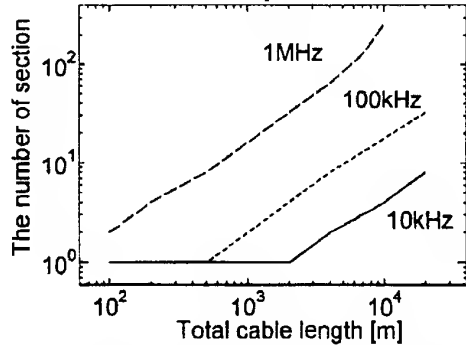


Fig.8 The number of sections necessary for LCTL calculation.

Figure 6 shows a model of an actual balanced pair cable for LCTL calculation. In Fig.6, each line has capacitance to the ground. The capacitance ΔC in Fig.6 represents the difference between each capacitor. Figure 7 shows the measured and calculated LCTLs for Fig.5. The cross mark(×) in Fig.7 shows the measured LCTL for the balun only, that is $L=0m$, in Fig.5. The white circle(○) in Fig.7 shows measured LCTL for the balanced pair cable with balun. Three lines in Fig.7 show the calculated LCTLs when the ΔC has the values of 0.2, 0.35 0.5pF/m, respectively. When ΔC is 0.35pF/m, the measured LCTL(○) well coincides with the calculated one(solid line) so that the capacitive unbalance of the balanced cable should be 0.35pF/m. When we calculate LCTL for $L=0m$ and $\Delta C=5pF$, the LCTL curve well fits to the one of balun. The dotted dash line in Fig.7 shows this calculated LCTL. It means that the unbalance capacitor of the balun is around 5pF.

Figure 8 shows the number of sections which is enough to obtain accurate LCTL of the balanced pair cable at the specified frequency.

3.2 LCTLs for parallel capacitive unbalance, parallel resistive unbalance, and series resistive unbalance

Figure 9 shows an experimental circuit which is used to measure LCTL of the balanced pair cable circuit with partial unbalance by C13, R13 and R11. C13, R13 and R11 simulate the parallel capacitive unbalance, parallel resistive unbalance and series resistive unbalance at the output terminal, respectively.

Figures 10(a), (b), and(c) show measured and calculated LCTL characteristics for parallel capacitive unbalance, parallel resistive unbalance and series resistive unbalance, respectively. As shown in Fig.10(a), LCTL for parallel capacitive unbalance decreases 20dB every decade of frequency and increases 6dB every twice of parallel capacitance value. From Fig.10(b), it is shown that LCTL for parallel resistive unbalance increases 6dB every half of parallel resistance. The difference between measured LCTLs and calculated ones in the range of higher frequency than 100kHz in Fig.10(b) occurs from the capacitive unbalance of the balun and the balanced pair cable itself. From Fig.10(c), LCTL for series resistive unbalance shows similar characteristic with the one for parallel capacitive unbalance. The difference between measured LCTLs and calculated ones in Fig.10(c) comes from the capacitive unbalance of the balun and the balanced pair cable itself. In the calculation of LCTL in here, we didn't use the model of Fig.6 to show ideal LCTL.

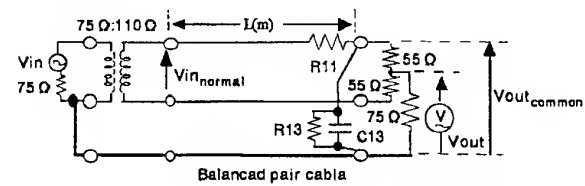


Fig.9 Experimental circuit for terminal unbalance.

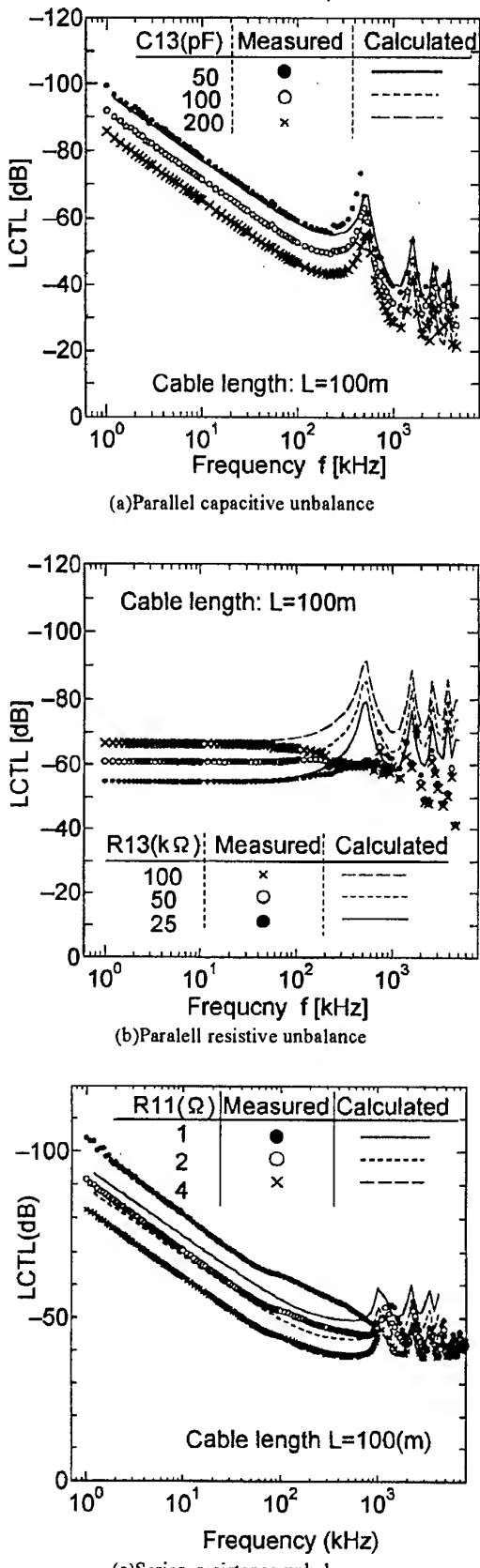


Fig.10 LCTL characteristics for parallel capacitive, series resistive unbalance and ground resistance.

3.4 LCTL for test splicing

Test splicing is used to equalize the unbalance of the balanced pair cable itself. Here, we examine LCTL for various cable configuration in test splicing. Figure 11 shows three kinds of cable configurations which are used in 3.4. Figure 12 shows an experimental circuit for Fig.11(b). Figure 13 shows measured and calculated LCTL for each of Fig.11. In Fig.13, LCTL for the cable configuration of Fig.11(a) shows the best LCTL characteristic because the capacitive unbalance at the input terminal side has less effect to the output terminal side's one. In Fig.13, calculated LCTLs well coincide with measured ones. Thus, it is shown that LCTL for test splicing can be also calculated by the proposed method.

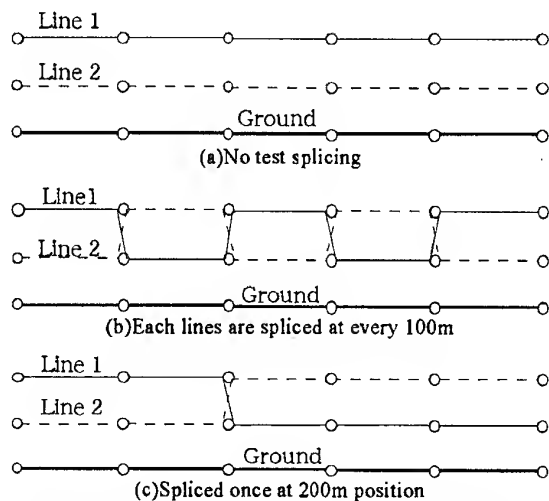


Fig.11 Test splicing to cancel the unbalance of balanced pair cable itself.

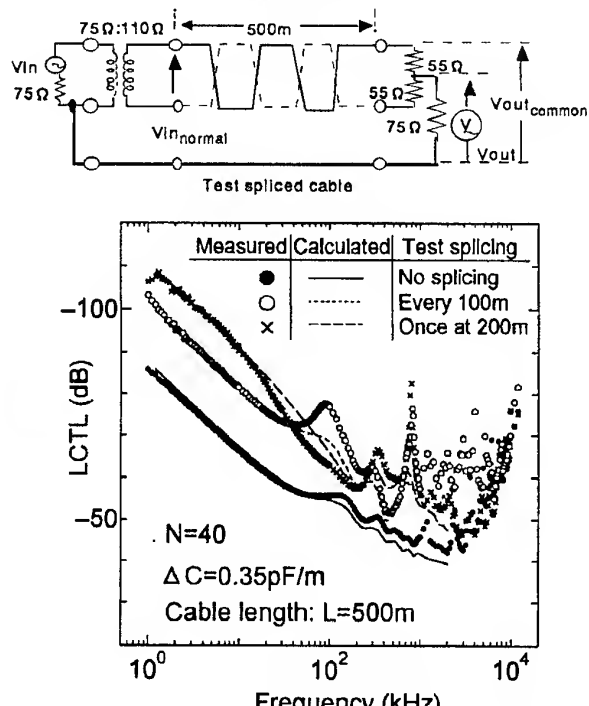


Fig.13 LCTL for balanced pair cable with test splicing.

4. Conclusion

We have proposed a new LCTL calculation method for the balanced pair cable circuit with partial unbalance and examined some LCTLs for the balanced pair cable under various terminal conditions and test splicing. In conclusion,

(1) We derived the transmission matrix for three conductor lines which consists of balanced pair lines and ground when the pair lines are perfectly balanced. This matrix can be easily obtained from the measured primary impedance and the measured primary admittance of real circuit and longitudinal circuit.

(2) We also derived the transmission matrix for the lumped elements circuit which represents unbalance of the balanced pair cable or partial unbalance by terminal equipment.

(3) It has been clarified that LCTL characteristics for a balanced pair cable with partial unbalance is easily calculated by using these transmission matrices.

Acknowledgments

This work was supported in part by a grant-in-aid for scientific research C(08650453) from the Ministry of Education in Japan.

References

- [1]ITU-T Recommendation K.10;"Unbalance about earth of telecommunication installation," 1993.
- [2]ITU-T Recommendation;"Transmission aspects of unbalance about earth," Rec.G.117,1980.
- [3]M.Hattori,T.Ideguchi;"Electromagnetic Interference and Countermeasures on Metallic Lines for ISDN,"IEICE Trans.Commun.,vol.E75-B,no.1,Jan.1992.
- [4]Natsuo Kobayashi;"Tushin senro densou riron,"IEICE, pp.141-145,1959(in Japanese).

Yoshifumi Shimoshio received the B.E. in Telecommunications from University of Electro-Communications, Tokyo, Japan in 1975. In 1975, he joined the Dept. of Radio Communications of KNCT(Kumamoto National College of Technology, Kumamoto), Japan, where he is now Associate Professor in the Department of Information and Communication Engineering.

Masazumi Miyoshi received the B.E. in Telecommunications from University of Electro-Communications, Tokyo, Japan in 1976. In 1976, he joined the Dept. of Radio Communications of KNCT, where he is now Associate Professor in the Department of Electronics Engineering.

Hiroaki Koga received the B.E. and M.E. degrees in Electric Engineering from Kagoshima University,Kagoshima, Japan in 1968 and 1970 respectively, and Dr.E. from Tohoku University, Sendai, Japan in 1988. He joined Electrical Communications Laboratories of Nippon Telegraph & Telephone Corporation(NTT) until 1991 and In 1992 he is engaged in the Dept. of telecommunication Engineering of KNCT, where he is now Professor.

Masamitsu Tokuda(Member of the IEEE) received the B.E. and the M.E. degrees in Electric Engineering in 1967 and 1969, respectively, and the Dr.E. degree in Electronics in 1983, from Hokkaido University, Sapporo-shi, Japan. He joined NTT Laboratory, and engaged in research and development of many kind of telecommunication cables, especially optical fiber cables from 1969 to 1986, and moved in studies of electromagnetic compatibility for telecommunication systems in 1986. Presently, he is Professor of Kyushu Institute of Technology, Kitakyusyu, Japan. He had been chairman of the Technical Group on EMC of IEICE of Japan from 1991 to 1993. He received the Achievement Award of IECE of Japan in 1986.

VI

EMC MEASUREMENTS AND INSTRUMENTATION

ELECTROMAGNETIC FIELD UNIFORMITY TEST USING MODULATED SCATTERING PROBES

R. Azaro*, S. Caorsi**

*DEPT. OF BIOPHYSICAL AND ELECTRONIC ENG. - UNIVERSITY OF GENOA
Via Opera Pia 11/A, 16145 GENOVA - ITALY

**DEPT. OF ELECTRONICS - UNIVERSITY OF PAVIA
Via Abbiategrasso 209, 27100 PAVIA - ITALY

The use of the Modulated Scattering Technique (MST) for electromagnetic field uniformity test is proposed. Measurement times associated with the conventional technique employing mechanical positioning of a single probe, are usually long. By using an array of modulated scattering probes, electronically driven, the technique allows a dramatic reduction in measurement time.

In the paper the theoretical basis of the technique are discussed, the prototype system is described and some measurement data are presented.

1. INTRODUCTION

According to IEC 1000-4-3 (*Electromagnetic Compatibility - Part 4: Testing and measurement technique - Section 3: Radiated, radio-frequency, electromagnetic field immunity test*), this verification must be periodically carried out, in all the frequency range 80 - 1000 MHz, to ensure a "uniform area", which is a hypothetical vertical plane in which field intensity variations are acceptably small. This uniform area is 1.5 m × 1.5 m and, during electromagnetic field immunity test, the equipment under test (EUT) shall have its face to be illuminated coincident with this plane.

Measurement times associated with the conventional technique prescribed by IEC1000-4-3 standard, employing mechanical positioning of a single probe, are usually long; in fact this standard requires that a single probe will be positioned in 16 calibration grid points and measurement must be performed in frequency steps no greater than 10% of the start frequency (and thereafter the

preceding frequency) for both horizontal and vertical polarization.

Modulated Scattering Technique was first proposed by Richmond [1], Justice and Ramsey [2], Cullen and Parr [3] in 1955 for the measurement of antenna near-field distribution at centimeter wavelength, in order to eliminate the transmission line from the receiving antenna to the receiving apparatus.

The general formulation for the back-scattered field from loaded object, in particular from small dipole and small loop, was given by Harrington [4], and the scattering properties of antennas were discussed, by using the generalized scattering matrix, by Green [5] and Collin [6]. Besides a complete system capable of measuring amplitude, phase and polarization of microwave field distribution was described by King [7].

In the past the Modulated Scattering Technique, in the *monostatic* and *bistatic* set-up, was proposed as a fast characterization method of antennas and complex radiating systems by Bolomey [8] [9] and other authors [10] [11], as a fast electromagnetic field measurement technique for biomedical imaging [12], as a tool for the characterization of microwave circuits [13] and, in general, as a near-field measurement method.

The Modulated Scattering Technique is essentially a free space perturbation technique; so it is not the signal delivered by the measuring probe which is measured, but it is the field scattered by the measuring probe which is collected and measured by the transmitting antenna itself (in the monostatic setup), or an auxiliary antenna (bistatic setup).

As can be shown, in the Modulated Scattering Technique the signal resulting from the

introduction of the probe at a given site is related to the electric field at that point. In the monostatic case the signal is proportional to $E^2 \cdot e^{j2\varphi}$ while in the bistatic case it is proportional to $E \cdot e^{j\varphi}$, where E and φ are the amplitude and the phase of the electric field.

The scattering of each element of a probe array, loaded with a nonlinear element such as a diode, may be modulated successively by a low frequency signal, so that the resulting signal, related to the field in the modulated probe position, is an AC signal of the same frequency. Low frequency modulation of the scattering of the probes is impressed in order to distinguish the weak signal scattered by the desired probe from all other reflected field contributes.

2. THE MONOSTATIC MST RELATIONSHIP

The basic relations existing between received voltage and the electric field in the point where the probe is located, has been derived by many authors. In particular the relationship for the monostatic setup of the MST has been derived starting from the application of the reciprocity theorem [10] [14]. However this relation may also be derived, under some hypothesis and in a less rigorous way, directly from the particular measurement system considered.

The basic monostatic configuration, as shown in figure 1, is composed of a sinusoidal wave generator, a dual directional coupler, a transmitting-receiving antenna and a scattering probe.

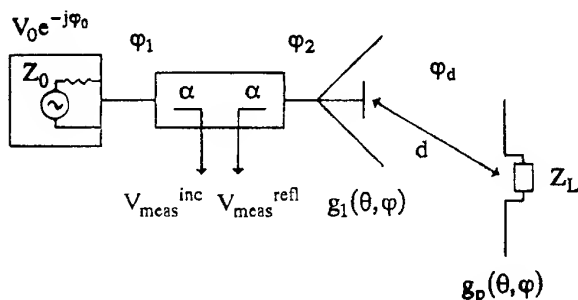


Fig. 1 The basic monostatic Modulated Scattering setup.

In this scheme $V_0e^{-j\varphi_0}$ is the complex value of the sinusoidal voltage delivered by the source to the measurement system, V_{meas}^{inc} and V_{meas}^{refl} are the voltages measured at the coupled arms of the

dual directional coupler, φ_1 and φ_2 are the phase delays due to interconnecting transmission lines, φ_d is the phase delay due to the propagation of the electromagnetic field starting from the transmitting-receiving antenna input port to the probe position, α is the coupling coefficient (the same in both the directions) of the dual directional coupler, $g_1(\theta, \varphi)$ and $g_p(\theta, \varphi)$ are the power gains of the transmitting-receiving antenna and of the probe antenna respectively, Z_0 is the characteristic impedance of the transmitting-receiving system and Z_L is the load connected to the probe antenna.

Besides let's assume the following hypothesis:

- there is impedance matching in all the sections of the transmitting-receiving system,
- probe antenna is a small electric dipole,
- there is impedance matching between the probe antenna and its load,
- probe antenna is in the far-field of the transmitting-receiving antenna,
- the dual directional coupler has an infinite directivity and very small coupling coefficients α .

Under this hypothesis the complex value of the electric field generated by the transmitting-receiving antenna in the position of the probe can be written as:

$$E = \sqrt{\frac{\eta P_{TX}^{inc} g_1(\theta_p, \varphi_p)}{4\pi d^2}} e^{-j(\varphi_0 + \varphi_1 + \varphi_2 + \varphi_d)} \quad (1)$$

where $P_{TX}^{inc} = \frac{V_0^2}{4Z_0}$ is the power delivered by

the signal source to the transmitting-receiving antenna, η is the wave impedance in free space, d is the distance between the transmitting-receiving antenna and the probe, and $g_1(\theta_p, \varphi_p)$ is the power gain of transmitting-receiving antenna in the direction toward the probe.

Since there is impedance matching on the probe antenna port, the received power can be written as:

$$P_{RX} = P_{TX}^{inc} g_1 g_p \frac{\lambda^2}{(4\pi d)^2} \quad (2)$$

where g_1 and g_p stand for the power gain of the transmitting-receiving antenna and of the probe in the joining direction (in the concerning angular positions).

If the probe is a short electric dipole, one can show that, when matched, it scatters as much power as is absorbed. This can be shown describing the probe with the generalized scattering matrix and expressing the electric field under measurement, assumed to be solenoidal, in spherical vector wave functions [6].

So, if there is impedance matching in all the section of the MST measurement system, at the reflected arm of the dual directional coupler, can be detected an amount of power equal to:

$$P_{\text{meas}}^{\text{refl}} = \alpha \frac{V_0^2}{4Z_0} \left[g_1 g_p \frac{\lambda^2}{(4\pi d)^2} \right]^2 \quad (3)$$

corresponding to a measured voltage that can be written as:

$$V_{\text{meas}}^{\text{refl}} = \frac{V_0}{2} \sqrt{\alpha} g_1 g_p \frac{\lambda^2}{(4\pi d)^2} e^{-j(\varphi_0 + \varphi_1 + 2\varphi_2 + 2\varphi_s)} \quad (4)$$

Besides (4) can also be written as:

$$V_{\text{meas}}^{\text{refl}} = \sqrt{\alpha} \frac{Z_0 g_p \lambda^2}{V_0 2\pi\eta} e^{j(\varphi_0 + \varphi_1)} \left[\eta \frac{V_0^2}{4Z_0} \frac{g_1}{4\pi d^2} e^{-j2(\varphi_0 + \varphi_1 + \varphi_2 + \varphi_s)} \right] \quad (5)$$

In the relation (5) we can identify the part in square brackets with the square of the expression (1) of the electric field at the probe position. So (5) can be written as:

$$V_{\text{meas}}^{\text{refl}} = \sqrt{\alpha} \frac{Z_0 g_p \lambda^2}{V_0 2\pi\eta} e^{j(\varphi_0 + \varphi_1)} E^2 \quad (6)$$

The expression (6) is the basic relationship for the monostatic Modulated Scattering Technique setup; it allows one to evaluate the electric field in the probe position by means of the measurement of the reflected voltage in the transmitting system.

Besides the same results can be expressed for the reflection coefficient, normalizing the reflected coupled voltage to the incident coupled voltage

$$V_{\text{meas}}^{\text{inc}} = \sqrt{\alpha} \frac{V_0}{2} e^{-j(\varphi_0 + \varphi_1)}. \text{ So we obtain the}$$

expression of the reflection coefficient due to the presence of the probe:

$$\begin{aligned} \Gamma_{\text{meas}} &= \frac{V_{\text{meas}}^{\text{refl}}}{V_{\text{meas}}^{\text{inc}}} = \\ &= \frac{g_p \lambda^2}{\pi\eta} \frac{V_0}{Z_0} e^{j2(\varphi_0 + \varphi_1)} E^2 \end{aligned} \quad (7)$$

3. DESCRIPTION OF THE EXPERIMENTAL SETUP

To verify the applicability of the Modulated Scattering Technique to electromagnetic field uniformity test, a monostatic setup, in accordance with the basic scheme shown in figure 1, was prepared inside an anechoic shielded chamber. The field distribution under measurement was radiated from a logperiodic antenna on a 1.5×1.5 m uniform area, on which were placed 16 modulated scattering probes, coinciding with 16 calibration grid points; so the distance between the neighboring probes was equal to 0.5 m. According to IEC 1000-4-3 the RF source, the MST receiver and the traditional measurement receiver were placed outside the chamber.

The array of Modulated Scattering Probes was made with 16 probe; each probe was supplied with a modulating circuit and powered by means of a little battery. So the automatic scanning of the probe was carried out by means of 16 optical links connecting the remote scanning system with the modulating circuits of the probes. Besides the optical links was made with 16 optic fibers in order to minimize perturbation of the field distribution.

Modulating sequentially the MST probes, by means of the remote scanning system placed outside the anechoic shielded chamber, output scattered signals were measured, stored and subsequently converted to electromagnetic field intensity level.

In figure 2 an example of the comparison between the data obtained both using a standard probe and our MST measurement system is shown for a single frequency.

The obtained data allow to verify the uniformity of the electromagnetic field and, if necessary to repeat measurements after the introduction of site modification (introducing or moving optional anechoic material to reduce floor reflections, for example).

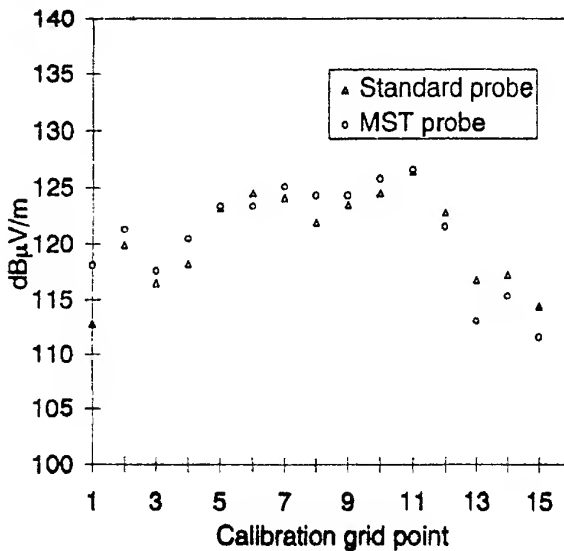


Fig. 2 Uniformity field test: electric field amplitude ($f = 900$ MHz, horizontal polarization).

In order to evaluate the perturbation of the field distribution due to the contemporaneous presence of the 16 MST probes, each one equipped with its modulating circuit and battery, the electric field measured in a grid point of the MST array with a standard probe, replacing the corresponding MST probe, was compared with the values measured in the same point by means of the same standard probe when the MST array was removed.

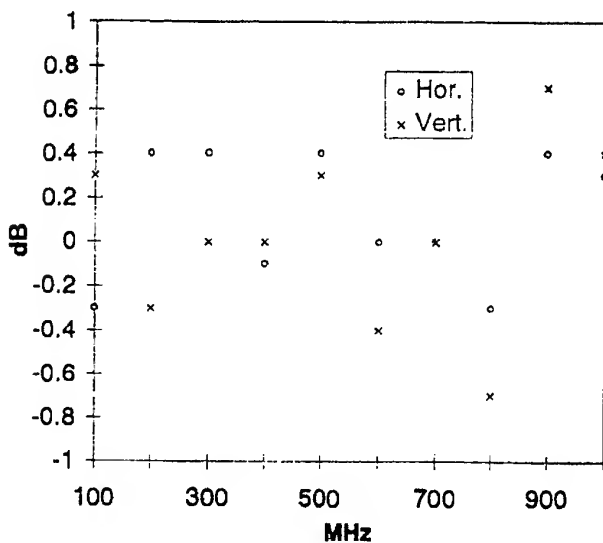


Fig. 3 Perturbation of the field distribution due to the presence of the MST array.

This procedure has been done for some frequencies and the difference between the two sets of measurements is shown in figure 3. The results reported point out a moderate field perturbation in all the frequencies considered, both for the horizontal and the vertical polarization.

Besides a calibration procedure of the measurement system based on the Modulated Scattering Technique allowed to estimate its behavior for different frequencies. Figure 4 shows the calibration factor of the system, denoting a sensitivity that is fairly uniform for the considered frequencies.

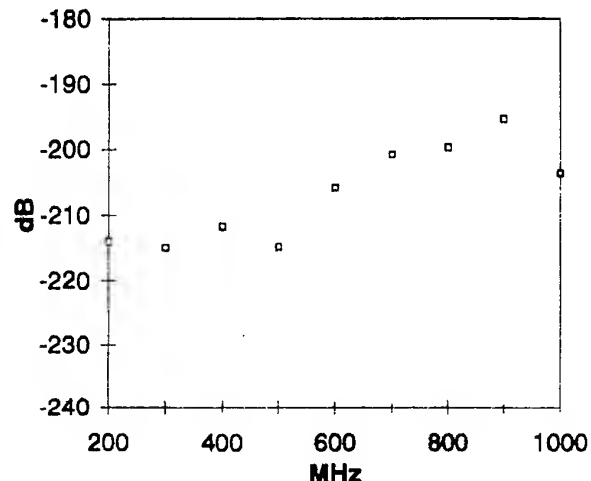


Fig. 4 Calibration factor versus frequency.

4. CONCLUSIONS

The use of the Modulated Scattering Technique (MST) for electromagnetic field uniformity test has been proposed. Since the measurement procedure must be performed for a lot of frequency step and for vertical and horizontal polarization, times associated with the conventional technique employing mechanical positioning of a single probe, are usually long. A measurement system based on the Modulated Scattering Technique allowed a dramatic reduction in measurement time. Besides experimental results obtained via laboratory prototype system, carried out inside an anechoic shielded chamber, have denoted a moderate field perturbation due to the presence of the MST array, and a fairly uniform sensitivity in a broad frequency range.

5. REFERENCES

- 5.1. J. H. Richmond, "A modulated scattering technique for measurement of field distributions," Inst. Radio Eng. Trans. Microwave Theory Tech. MTT-3, 1955, pp. 13-15.
- 5.2. R. Justice, V. H. Ramsey, "Measurement of electric field distributions," Inst. Radio Eng. Trans. on Antennas and Propagat. AP-3, 1955, pp. 177-180.
- 5.3. A. L. Cullen, J. C. Parr, "A new perturbation method for measuring microwave fields in free space," IEE Proceedings part B 102, 1955, pp. 836-844.
- 5.4. R. F. Harrington, "Small resonant scatterers and their use for field measurements," Inst. Radio Eng. Trans. Microwave Theory Tech. MTT-10, 1962, pp. 165-174.
- 5.5. R. B. Green, "Scattering from conjugate-matched antennas," IEEE Trans. on Antennas and Propagat., AP-14, 1966, pp. 17-21.
- 5.6. R. E. Collin, "The receiving antenna" in R. E. Collin, F. J. Zucker, "Antenna Theory - Part 1" McGraw-Hill, New York, 1969, pp. 123-133.
- 5.7. R. J. King, "Probing amplitude, phase, and polarization of microwave field distributions in real time," IEEE Trans. on Microwave Theory and Techniques, MTT-29, 1981, pp. 225-1231.
- 5.8. M. Mostafavi, J. C. Bolomey, D. Picard, "Far-field accuracy investigation using modulated scattering technique for fast near-field measurements," IEEE Trans. on Antennas and Propagat., AP-33, 1985, pp. 279-285.
- 5.9. J. C. Bolomey, B. Cown, G. Fine, L. Jofre, M. Mostafavi, D. Picard, J. Estrada, P. Friederich, and F. Cain, "Rapid near-field antenna testing via arrays of modulated scattering probes," IEEE Trans. on Antennas and Propagat., AP-36, 1988, pp. 804-814.
- 5.10. G. Hygate, J. F. Nye, "Measuring microwave fields directly with an optically modulated scatterer," Meas. Sci. Technol. 1, 1990, pp. 703-709.
- 5.11. W. Liang, G. Hygate, J. F. Nye, D. G. Gentle, R. J. Cook, "A probe for making near-field measurements with minimal disturbance: the optically modulated scatterer," IEEE Trans. on Antennas and Propagat., AP-45, 1997, pp. 772-780.
- 5.12. J. C. Bolomey, C. Pichot, "Microwave tomography: from theory to practical imaging systems," International Journal of Imaging System and Technology, Vol. 2, 1990, pp. 144-156.
- 5.13. T. P. Budka, S. D. Waclawik, G. M. Rebeiz, "A coaxial 0.5-18 GHz near electric field measurement system for planar microwave circuits using integrated probes," IEEE Trans. on Microwave Theory and Techniques, Vol. 44-12, 1996, 2174-2184.
- 5.14. J. C. Bolomey, D. Picard, M. Mostafavi, "Evaluation of near-field measurement rates using modulated probes," Annales des Télécommunications, Vol. 40, n. 1-2, 1985.

BIOGRAPHICAL NOTES

Renzo Azaro received the "laurea" degree in Electronic Engineering from the University of Genoa, Italy, in 1992. At present he is a Ph. D. student in "Computer science, applied electromagnetics and telecommunication engineering" at the same University. His main research interests are in electromagnetic compatibility and measurements.

Salvatore Caorsi is a full professor of Electromagnetic Compatibility at the Department of Electronics of the University of Pavia, Italy and he is also teaching the course of Antennas at the University of Genoa. He is the Past-President and founding member of the Inter-university Research Center for Interactions Between Electromagnetic Fields and Biological Systems (ICEMB). His primary activities are focused on applications of electromagnetic fields to telecommunications, artificial vision and remote sensing, biology, medicine and electromagnetic compatibility. Prof. Caorsi is a member of the AEI, EBEA and ESHO.

AUTOMATED FIELD CALIBRATION AND IMMUNITY TESTING IN WROCLAW ANECHOIC CHAMBER

D.J.Bem, A.E.Sowa, M.Więcek, J.S.Witkowski

Wroclaw University of Technology
Institute of Telecommunication and Acoustics
Wybrzeze Wyspianskiego 27
50-370 Wroclaw, Poland

phone: (+4871) 3203276, fax: (+4871) 3203189, e-mail: asowa@zr.ita.pwr.wroc.pl

The paper presents a new site for immunity testing located in Wroclaw Anechoic Chamber. Testing equipment and in particular a uniform area scanner developed by the authors are described. The way of solving site automation problems is defined.

1. INTRODUCTION

The method of testing the immunity of electrical/electronic equipment to strong electromagnetic RF fields is described by IEC-1000-4-3 [9]. The best place to perform immunity tests is an anechoic chamber placed in a screened room [2]. A chamber like this gives adequate separation from electromagnetic environment and allows a measurement field uniform to the standard to be obtained.

Wroclaw Anechoic Chamber (WAC), described in the Proceedings of previous Wroclaw Symposia [1], was used as a location for a measurement site for immunity testing to electromagnetic noise.

The cubicoidal chamber internal dimensions are 4.9x4.7x2.2m (length x width x height) between tips of the largest absorbers. The size of the chamber enables a 3m site for immunity testing in accordance with IEC-1000-4-3 to be placed in it, although with some difficulty. Dismantable floor absorbers allow the measurement site to be arranged along the symmetry axis of the chamber, along the diagonal or along other directions. The site for immunity testing was equipped with the equipment necessary for measurement automation.

There is an adjacent control room accessible from the chamber through a shielded door and a special panel for connecting installation cables.

2. TEST SITE EQUIPMENT

Fig.1 shows a sketch of test site for field calibration and immunity measurement. The basic equipment of the site is described below.

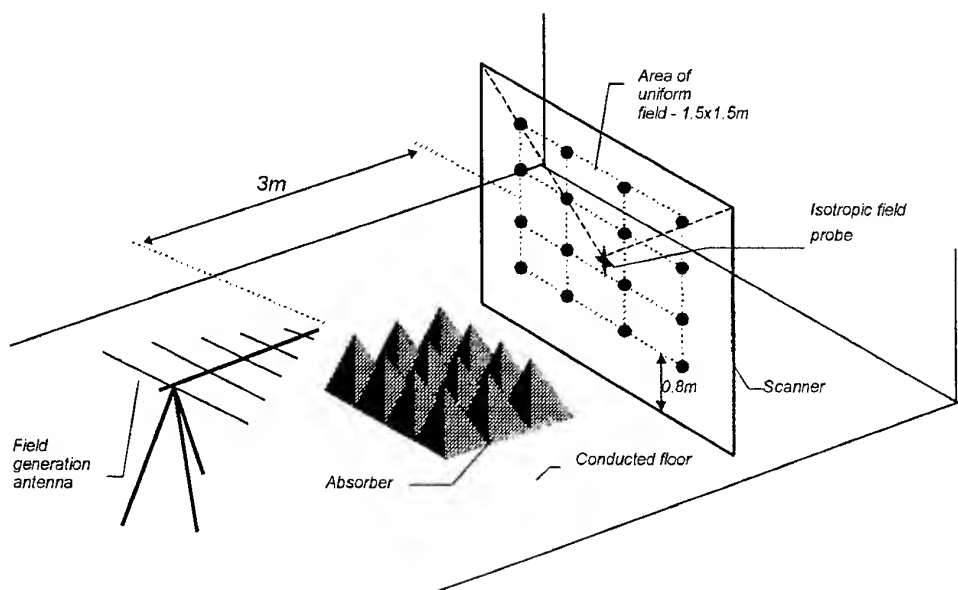


Fig. 1. Sketch of test site for field calibration and immunity measurement

2.1. Field generating antenna

Commercially available antennas were researched according to their size (because the chamber is small) and the amplifier power required [3]. The most interesting antennas were found to be combination antennas („bilog” type). An antenna manufactured by Frankonia (type BTA-L Fig.2), measuring 1.134m. x 1.709m. was selected. The small length of the antenna and its relatively big width show that it is suitable for small anechoic chambers. The antenna works in the range of 26MHz to 1300MHz.

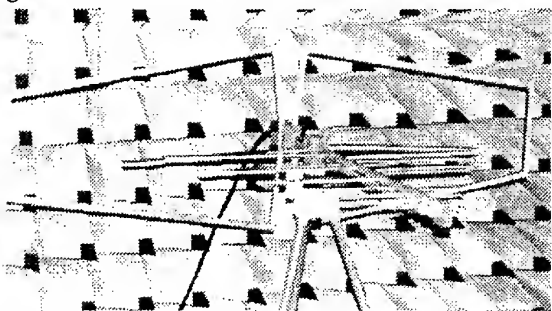


Fig. 2. Field generating antenna BTA-L (Frankonia)

The amplifier power required to drive the antenna (ca 65W for 10V/m at 3m) is bigger than the power needed for a logperiodic antenna (for the range of 80 to 1000MHz), but the dimensions of the antenna selected are significantly smaller. The antenna with appropriately larger amplifier power will work in the range starting from 26MHz.

2.2. Power amplifier

The site was equipped with a broadband 100W power amplifier (SMX100 -IFI USA) which, with the above-mentioned antenna, gives a measurement field of 10V/m in the range of 80 to 1000MHz. The amplifier can be fully controlled by GPIB interface.

2.3. Field strength sensor

Commercially available electromagnetic field strength sensors were compared in detail. A PMM8052 field strength meter manufactured by PMM (Italy) equipped with EP-115 E-field probe (Fig.3) for the range of 100kHz to 1,5GHz was chosen. The system enables isotropic field measurement (RMS) and X,Y,Z axis field measurement to be carried out. The probe is relatively small (sphere 140mm) and features an entirely symmetrical construction (3 symmetrical dipoles), autonomous power supply (battery) and a fibre optic communication link to the meter, not interfering with the measured field. The meter is linked to a PC by RS232C interface.

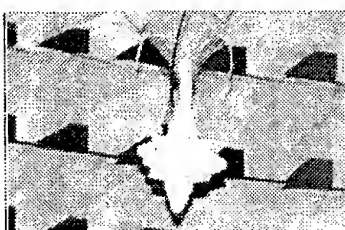


Fig.3. Field sensor EP-115 (PMP)

2.4. Scanner

As is well known in accordance with IEC-1000-4-3 [9] a test field calibration is conducted on a 1.5m. square area (“uniform field area”) situated on a vertical measurement plane 3m. away the tip of the antenna. Calibration measurements are conducted in 16 sensor positions (equally spaced) located every 0.5m. for every measurement frequency in the range of 80MHz to 1GHz. For speed, accuracy and convenience, calibration measurements should be automated. Automatic adjustment of a field sensor placement on the measurement plane is particularly useful. A scanner allowing an arbitrary field sensor placement on the measurement plane was designed (Fig.4). A sensor is suspended on a dielectric frame by the use of dielectric cables whose length (and also the position of the sensor) can be adjusted by stepping motors. This allows the sensor placement to be controlled with an accuracy higher than 1cm. Stepping motors together with their control module may be placed inside the chamber far away from the measurement field or even outside of the chamber. It should be stressed that the calibration installation is entirely dielectric and that only a probe is suspended in the measurement field area.

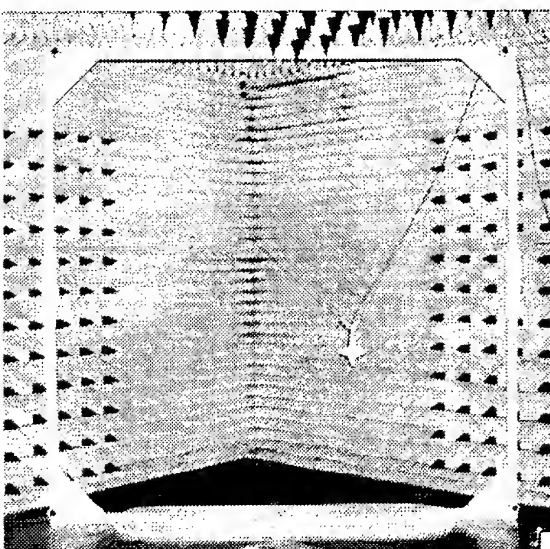


Fig. 4. Scanner of uniform field area.

3. AUTOMATION OF CALIBRATION AND TEST PROCEDURES

Field immunity tests should be carried out in accordance with the standards [4,5,6,7,8,9]. Based on these standards the following procedure may be recommended:

1. Place the field generation antenna in the distance of 3m from the uniform area (as measured to the tip of the antenna).
2. Check the uniformity of the electromagnetic field strength at 16 measurement points of the uniform area (Fig.1). The uniform area should be calibrated for every measurement frequency without placing the

EUT in the measurement field. The measurement signal should not be modulated. The field is considered uniform if its strength lies within -0dB to +6dB of nominal value for at least 12 of the 16 measurement points. The detailed calibration procedure is as follows [9]:

- a) Position the field sensor at one of the 16 points in the grid (see Fig 1).
 - b) Apply a forward power to the field generating antenna so that the field strength obtained is in the range 3V/m to 10V/m and record power and field strength readings.
 - c) With the same forward power, measure and record the field strength at the remaining 15 points.
 - d) Taking all 16 points into consideration, delete a maximum of 25% (i.e. 4 of the 16) of those with the greatest deviation.
 - e) The remaining points shall lie within ± 3 dB.
 - f) Of the remaining points, take the location with the lowest field strength as reference (this ensures the -0dB to +6dB requirement is met).
 - g) From knowledge of the input power and the field strength, the necessary forward power for the required test field strength can be calculated. This is recorded.
 - h) Repeat steps a) to g) in frequency steps no greater than 10% of the start frequency (and thereafter the preceding frequency) for both horizontal and vertical polarisation.
3. Position the EUT at the height of 0.8m above the floor level and with one face coincident with the uniform area (calibration plane). The arrangement of wiring should be in accordance with the standards [4,5,6,7,8,9].

4. Install the EUT measurement instrumentation. Only the test levels are defined by the standard [9]. A functional description and a definition of performance criteria shall be provided by the manufacturer or the user of the equipment tested. The EUT measurement instrumentation may consist of variety of testing devices, both electrical and mechanical. A video camera is also used for visual observation of the EUT.

5. Test the immunity within frequency range from 80 to 1000MHz. The product specification may require other frequency range (e.g. from 26 to 1000MHz). The signal is 80% amplitude modulated with a 1kHz sinewave. Moreover for certain EUTs [8] the signal is pulse modulated in the range 900+-5MHz. The duty cycle is 50% and repetition frequency is 200Hz. The step of frequency shall not exceed 1% of the previous frequency. To obtain the required field strength the previously calculated generator and amplifier settings should be used (see point 2g). For each frequency step the EUT performance should be checked.

6. Perform the test on all sides of the EUT as described in points 3 to 5.

The above described method of testing shows that the calibration (point 2) and testing procedure (point 5) are the most labour intensive and time consuming. The automation of both of them is possible.

Fig.5. shows a diagram of a system for testing of immunity to strong electromagnetic fields developed for WAC. The system consists of a main computer which controls the signal generator and power amplifier (by GPIB) and the field strength sensor and sensor scanner (by RS 232C). This computer registers fail/pass signals from the EUT measurement

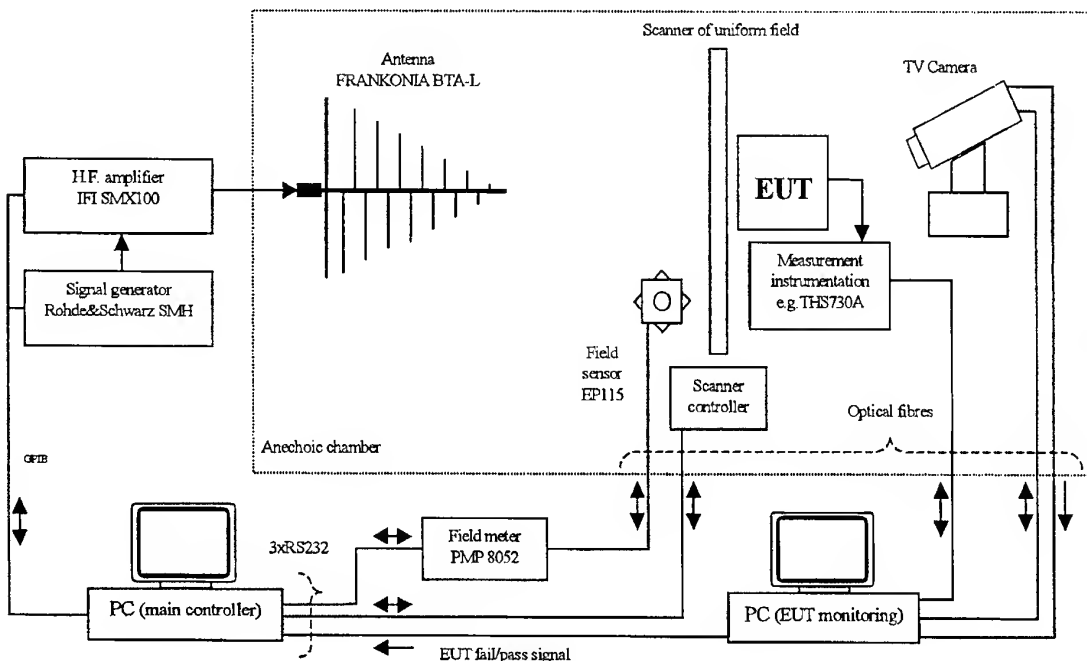


Fig. 5. Diagram of a system for testing of immunity to strong electromagnetic fields in WAC

instrumentation and enables creation of a test report. There is also a second computer monitoring the EUT. This computer for reasons of having a variety testing tasks is capable to communicate directly with the EUT using measurement interface (e.g. GPIB, RS232C), as well as to gather information from the EUT measurement instrumentation. The computer must be programmed for each EUT separately.

This computer also supervises the television system installed in the anechoic chamber.

The main features of the television system constructed for the chamber are:

- remote control of all important settings and movements of the camera (communication with a PC by RS232C),
- observation, recording and processing of pictures using a PC equipped with a high performance video card.,
- immunity to strong electromagnetic fields.

A special computer program enabling the automation of field calibration and immunity testing was developed for the main computer. Fig.6 shows the main window of the program and Fig.7 shows the window during the field calibration.

The calibration process of the measurement site is entirely automatic. The frequency and the output level of a generator, the power amplifier gain, the probe position on the calibration plane and the probe read-out are controlled and memorised automatically. During immunity measurement the frequency and adequately

corrected output level of the generator and the power amplifier gain are set automatically, allowing the required field strength to be obtained. If the test indicates incorrect EUT functioning, an immunity level definition procedure is initiated. The generator output level is reduced to a minimum and then, if EUT starts functioning normally the generator output level is gradually increased to the level where malfunctioning occurs. The results are decided by the operator on the basis of the adequately configured measurement instrumentation and visual monitoring or automatically on the basis of the information supplied by the second (specially programmed) PC monitoring the EUT performance (Fig.5).

4. FIELD CALIBRATION IN WAC

Tab.1 shows the results of the field calibration in WAC for two polarities of the antenna, which axis is parallel to the symmetry axis of the chamber, for several measurement frequencies Shaded fields show values rejected in the calibration process (according to the standard [9]).

5. CONCLUSIONS

The immunity measurement site in WAC fulfils requirements of IEC-1000-4-3 and enables automatic field calibration and immunity testing. The site makes possible the immunity testing in the frequency range from 80 to 1000MHz with the field strength up to 10V/m and the test distance of 3m

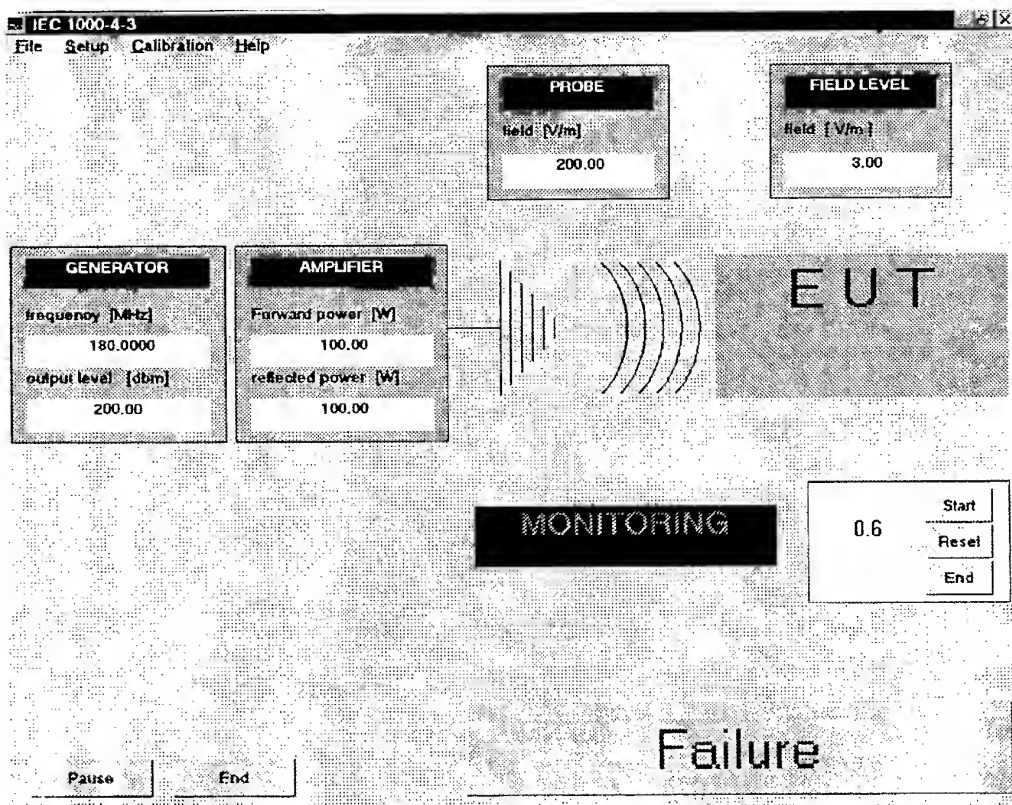


Fig. 6. Main window of the immunity testing program.

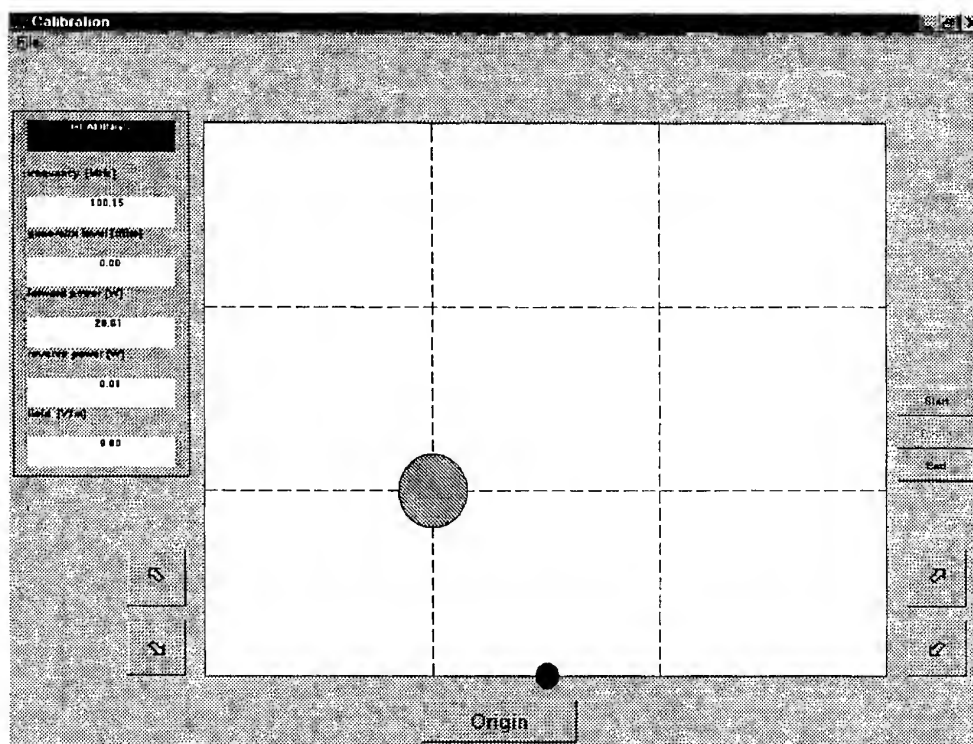


Fig. 7. Program during field calibration process.

Tab. 1. Calibration results ([V/m] for P_r=20W).

Horizontal polarisation			
f=26MHz			
1.3	1.4	1.6	2.0
1.4	1.6	1.9	2.0
1.6	1.7	1.8	2.0
1.7	1.6	1.6	1.7
f=80MHz			
10.9	12.4	12.7	11.1
12.1	15.2	15.7	13.5
12.2	14.6	15.5	13.4
9.5	11.3	11.3	6.5
f=200MHz			
10.4	11.8	12.1	10.8
12.6	13.5	13.8	14.4
10.1	12.2	13.0	11.7
7.8	9.7	10.3	9.5
f=500MHz			
11.0	11.3	11.5	10.3
10.5	10.6	10.3	9.5
7.5	8.1	8.0	7.7
7.2	6.9	6.7	6.4
f=1000MHz			
7.2	8.3	8.0	7.6
8.5	8.7	8.8	8.4
7.8	8.0	8.3	8.1
7.6	8.5	9.5	9.5

Vertical polarisation			
f=26MHz			
5.1	5.4	5.0	5.0
4.6	4.8	4.8	4.3
4.7	4.9	4.8	4.3
5.6	5.5	5.6	4.8
f=80MHz			
7.5	9.2	9.7	8.4
5.3	6.0	6.7	6.0
4.4	4.2	5.0	4.7
4.4	3.2	4.0	5.0
f=200MHz			
7.6	7.2	7.6	8.3
9.5	7.9	11.8	12.5
9.2	9.0	11.2	13.9
6.6	7.0	9.2	7.7
f=500MHz			
12.1	11.7	11.1	12.2
11.6	9.5	8.8	11.3
9.7	8.7	9.0	9.4
4.9	10.1	9.7	11.3
f=1000MHz			
8.2	8.5	8.1	8.4
7.4	7.4	6.9	8.4
6.6	7.8	8.0	8.3
5.8	7.6	7.3	6.7

6. REFERENCES.

1. Bem D. J., Kucharski A.A, Sowa A. E., Więcek M., "Wrocław anechoic chamber", Intern. Symp. on EMC, Wrocław, 28 June – 1 July, 1994.
2. Bem D.J., Sowa A.E., Więcek M., Witkowski J.S., "The immunity testing of equipment to strong electromagnetic RF fields in an anechoic chamber" (in Polish), Proc. of KST'96, Bydgoszcz 11-13.09.1996, t.B.
3. Bem D.J., Sowa A.E., Więcek M., Witkowski J.S., Michałak.M., "Selection of antennas for immunity testing" (in Polish), Proc. of KST'97, Bydgoszcz 10-12.09.1997.
4. EN 50082-1, Electromagnetic compatibility. Generic immunity standard. Part 1: Residential, commercial and light industry. 1996.
5. EN 50082-2, Electromagnetic compatibility. Generic immunity standard. Part 2: Industrial environment. March 1995.
6. EN 61000-4-3 Electromagnetic compatibility (EMC). Part 4: Testing and measurement techniques- Section 3: Radiated, radio-frequency, electromagnetic field immunity test., 1996
7. ENV 50140. Electromagnetic compatibility. Basic immunity standard. Radiated, radio-frequency electromagnetic field – immunity test. 1993.
8. ENV 50204 - Radiated electromagnetic field from digital radio telephones - Immunity test (Basic immunity standard)
9. IEC 1000-4-3, Electromagnetic compatibility (EMC). Part 4: Testing and measurement techniques- Section 3: Radiated, radio-frequency, electromagnetic field immunity test., Feb.1995

TEM CELL VS. FREE SPACE: COMPARISON OF THE FIELDS INSIDE DIELECTRIC SPHERES

Michele M. G. D'AMICO, Roberto BASELLI

Dipartimento di Elettronica e Informazione,
Politecnico di Milano
Piazza L. Da Vinci 32, Milano 20133, Italy
E-Mail:damico@elet.polimi.it

Abstract

The Crawford cell is a very convenient equipment for generating high intensity Transverse Electromagnetic fields; it has a straightforward design, and it is inexpensive to be built. Unfortunately, when an object is placed inside the cell, the field distribution can be significantly distorted. To date there is no definite answer on whether the (loaded) Crawford cell is a good approximation of (loaded) free space. In this work a typical Crawford cell is considered, properly designed to obtain a uniform TEM field when empty. A dielectric hemisphere is then assumed to be placed on the central conducting septum; this hemisphere is equivalent (for the images' theorem) to a dielectric sphere in the free space. The field inside the dielectric hemispheres is numerically evaluated, using a 3D E.M. simulator; this field is then compared with that inside the corresponding sphere in free space, illuminated by a plane wave, for which the analytical solution is known. Comparisons are carried out at several frequencies, for (hemi)spheres of different sizes and refractive indices.

1 Introduction

The Crawford cells, a particular kind of TEM cell, have been widely used since their formal introduction in 1974 [1]; they offer the undeniable advantages of being inexpensive and capable of generating quite large values of electromagnetic fields with little effort, with arbitrary wave impedances (e.g. E/H ratio) [2]. Moreover, the generated fields are confined inside the cell, thus reducing the risks of interference.

On the other hand, they have several serious drawbacks: their size dramatically influences the maximum usable frequency; when an object (DUT) is placed inside the cell, the configuration of the EM field can be significantly different from that in the free space. For this reason the Crawford cells

are normally used in the range of frequencies where the TEM mode dominates; accurate studies of the higher order mode cutoff frequencies have been carried out in the past by several researchers [3] [4]. The electromagnetic field configuration inside the cell has also been widely investigated, for the unloaded as well as for the loaded TEM cell [5] [6] [7] [8].

However, it is recognized that the question is whether the test object when placed in a TEM cell is stressed as in free space [9]. That is, the proper comparison is not loaded versus unloaded TEM cell, but rather fields inside the object when located in the TEM cell versus fields when in free space.

In this paper we will investigate how close the E-field inside an object placed into a TEM cell resembles that inside the same object in free space. For this purpose we will design a TEM cell using the standard formulas that can be found in the open literature; the cell's cutoff frequency is set to 200 MHz. We then place a dielectric object inside the cell, on the central conducting septum. The shape of the object is chosen so that the field inside the object can be analitically computed, when the object is illuminated by a plane wave propagating in free space.

In this respect, it is worthwhile noting that if the object is placed directly on the central conductor, it is not possible to neglect the presence of the conductor itself when deriving the free-space equivalent; i.e. the images' theorem has to be applied.

After discussing briefly the general properties of the empty cell, we will evaluate the fields inside the object along longitudinal lines, using a commercial 3D Electromagnetic Wave simulator (HFSS). The computed fields are then quantitatively compared with that obtained using the analytical solution.

Comparisons are carried out at several frequencies, for objects of different sizes and refractive indices, in order to investigate how closely (and under which conditions) a TEM cell can reproduce,

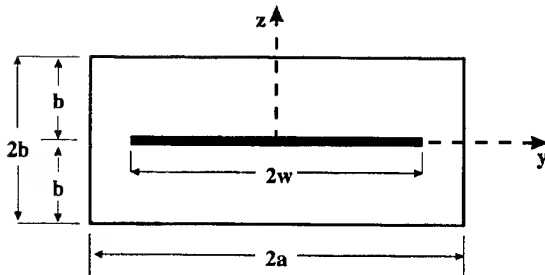


Figure 1: Cross-sectional view of the Crawford cell.

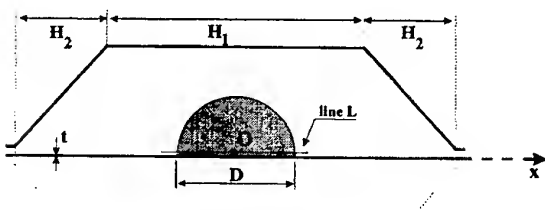


Figure 2: Longitudinal section of the Crawford cell, with the DUT in place.

within the DUT, the effects of a plane TEM wave.

2 The Crawford cell

The cell is designed to have a cutoff frequency of 200 MHz for the first non-TEM mode. Moreover, the cell has to be symmetrical and its characteristic impedance (when empty) has to be $Z_0 \approx 50 \Omega$. For the calculation of the characteristic impedance Z_0 we use the equations proposed by [10], while for the calculation of the higher order modes cutoff frequencies we refer to [3]. Using jointly the conditions on Z_0 and the cutoff frequency, we obtain the following dimensional values (see fig. 1 and 2): $2a = 48.2$ cm, $2b = 43.4$ cm, $2w = 39$ cm, $H_1 = 48.2$ cm, and $t = 1.5$ mm. As far as the length H_2 of the tapered transitions is concerned, we assume with [11] $H_2 = H_1/2 = 24.1$ cm.

With the dimensions above, the characteristic impedance evaluated with HFSS is 53.5Ω , very close to the desired value. The TEM cell has been closed on its ideal load through a short piece (10 cm) of transmission line (coaxial).

The lowest cutoff frequencies evaluated with the equations proposed by [3] are collected in table 1; the first non-TEM mode to be excited is the TE_{01} , whose cutoff frequency is 200 MHz. Being the TEM cell a high-Q cavity, very sharp resonances can appear at certain frequencies; for our geometry the first significant resonance (evaluated with HFSS) is around 610 MHz, well outside the frequency range considered in this work.

Mode	Frequency
TE_{01}	200.0
TE_{10}	311.2
TE_{11}	417.8
TE_{02}	691.6
TE_{12}	758.4
TM_{12}	758.4
TE_{20}	622.4
TE_{21}	1056.5

Table 1: Cutoff frequencies (in MHz) of the higher-order modes for the empty TEM cell.

Object	Size D (cm)	ϵ_r	$\sigma, S m^{-1}$
A	9	6	0
B	9	12	0
C	9	12	10
D	16	6	0
E	16	12	0
F	16	12	10

Table 2: Geometrical and electrical characteristics of the test objects.

3 TEM cell versus free-space

Our objective is to investigate the E-field *inside* a dielectric object (Dut, or Device Under Test) placed on the central septum of the Crawford cell, and to compare it with that found when the object is illuminated by a plane wave propagating in the free space. In the real world there is an almost unlimited choice for Dut's shape and dielectric characteristics; we wanted to consider a non-trivial shape, and at the same time to have an analytical solution for the fields inside the object in free-space.

In this respect the spherical shape seems to be a good choice, since a rigorous scattering theory exists [12] (Mie theory). As said, being the DUT placed directly on the central conducting septum, its free-space equivalent has to be found by applying the images' theorem. For our purposes, we placed a dielectric hemisphere on the central conductor inside the cell, that corresponds to a dielectric sphere in free-space.

We consider two different values for the diameter D , specifically 9 cm ("small" DUTs) and 16 cm ("large" DUTs); with a choice of three different values for the dielectric constant we get a total of 6 different objects (A to F, see table 2). Simulations and calculations are carried out at the frequencies of 100, 200 and 400 MHz; for the first two frequencies only the TEM mode can propagate; at 400 MHz at least two higher order modes (TE_{01} and TE_{10}) can exist.

To compare in a quantitative way the values of the electromagnetic fields inside the object, it is

Freq. (MHz)	DUT	E(HFSS) (V m ⁻¹)	E(Mie) (V m ⁻¹)	ΔE (dB)
100	A	30.7	25.4	1.65
100	B	18.1	14.6	1.87
100	C	18.0	14.6	1.81
100	D	30.5	25.9	1.42
100	E	17.9	15.1	1.48
100	F	17.9	15.1	1.48
200	A	29.2	26.1	0.97
200	B	17.1	15.3	0.97
200	C	17.3	15.3	1.07
200	D	30.4	28.2	0.65
200	E	19.0	17.5	0.71
200	F	19.1	17.5	0.76
400	A	28.5	29.0	-0.15
400	B	18.1	18.4	-0.14
400	C	18.0	18.5	-0.24
400	D	24.2	38.9	-4.12
400	E	17.9	32.3	-5.13
400	F	17.9	32.2	-5.10

Table 3: . Absolute values of the E-field, evaluated in O , for the different DUTs. Input power to the cell is 4 W.

necessary to establish a correspondance between the power injected into the TEM cell and the power density associated with a TEM wave propagating in free-space. Crawford and Workman [13] propose the following very simple expression for the evaluation of the E-field E_0 in an empty TEM cell:

$$E_0 = \frac{\sqrt{P/G_c}}{b} \quad (\text{V m}^{-1}) \quad (1)$$

where P is the net input power to the cell, G_c is the real part of the characteristic admittance of the cell, and b is the separation distance between the center conductor and the upper wall of the cell. This value of E_0 in the empty cell can be associated to the value of the E-field of a TEM wave propagating in free-space and illuminating the object.

All the simulations have been carried out assuming an input power to the cell $P=4$ W; using this value in eq. (1) we obtain $E_0=67.2$ V m⁻¹. This is only an average value; in fact, the E-field is not constant along the z-axis, being higher on the central septum: using HFSS we obtain $E_0=77.1$ V m⁻¹ for $z=0$, and $E_0=57.5$ V m⁻¹ for $z=21.7$ cm.

The E-field inside the DUTs is evaluated along line L (fig. 2), very close to the central septum (1 mm). The center of the hemisphere is coincident with the origin O of the reference frame. The absolute value of the E-fields in O , for the different DUTs at the various frequencies, are collected in table 3.

Figures 3 to 8 show the ratio (in dBs) between the E-field theoretically evaluated using Mie theory (solid lines) and that obtained from 3D simulations

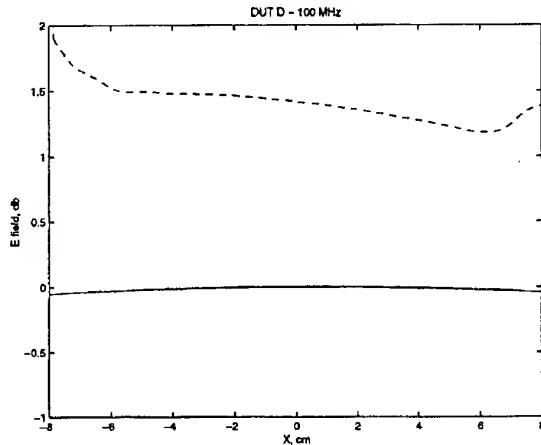


Figure 3: E-field inside DUT D at 100 MHz, evaluated using Mie solution (continuous line) or HFSS (dashed line).

(dashed lines), at different frequencies, along line L . The fields are referred to that calculated with Mie at the origin O .

From these figures it is clear that below 200 MHz the discrepancy between theoretical (free-space) and measured (TEM cell) E-fields is mainly due to the underestimation of E_0 in the empty cell, introduced by eq. (1): the actual value for E_0 , close to the septum, is 77.1 V m⁻¹, about 1.2 dB higher than that obtained through eq. (1). Unfortunately this “offset” can be quantified only through simulation; if it were possible to compensate for it, the difference between free-space and TEM cell fields would be smaller than 1 dB.

Things start to change at 200 MHz, and at 400 MHz the discrepancies are definitely not negligible: the general behaviour of the E-field in free-space is similar to that of the field in the cell, but differences of several dBs can be observed. As expected, these differences tend to increase for increasing values of the dielectric constant; for a large beryllium ($\epsilon_r = 6$) sphere (DUT D) the maximum difference is about 3 dB (4.2 dB is the offset in E_0 is taken into account); this difference increases to about 5 dB (6.2 dB) if silicon is considered ($\epsilon_r = 12$). Only minor changes can be observed when silicon is slightly doped, as shown in fig. 8.

4 Conclusions

In this work we have investigated how close the E-field *inside* a dielectric hemisphere placed on the central septum of a Crawford (TEM) cell resembles that inside the equivalent object in free space. The fields evaluated along longitudinal lines, using a 3D electromagnetic wave simulator, have been quantitatively compared with that obtained using an analytical solution.

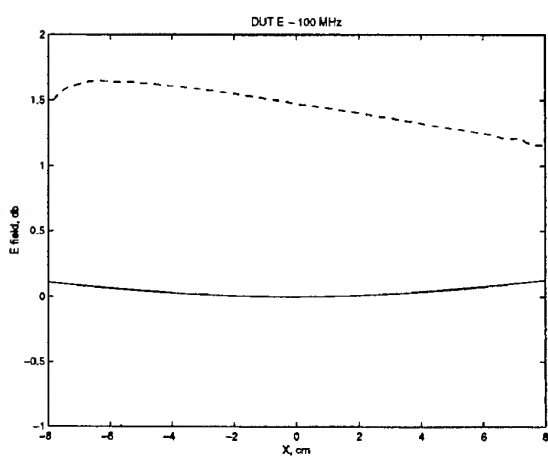


Figure 4: As fig. 3, but for DUT E at 100 MHz.

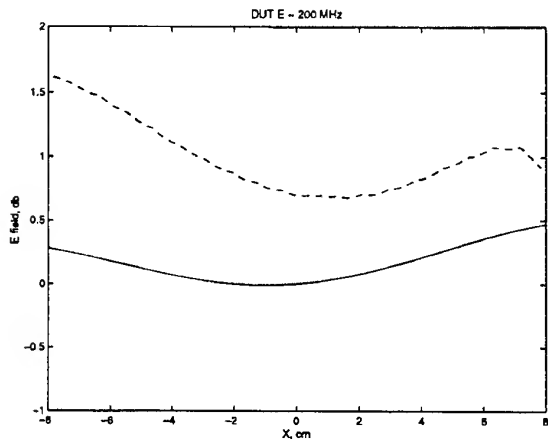


Figure 5: As fig. 3, but for DUT E at 200 MHz.

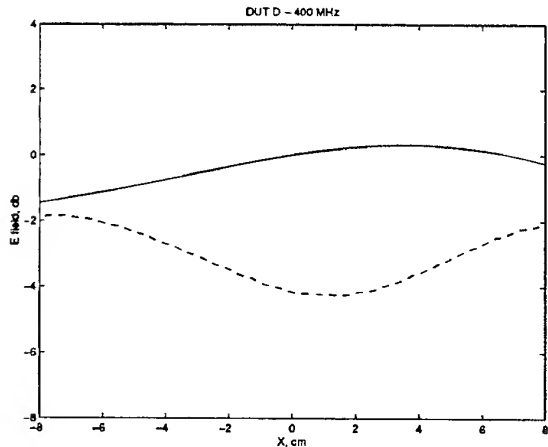


Figure 6: As fig. 3, but for DUT D at 400 MHz.

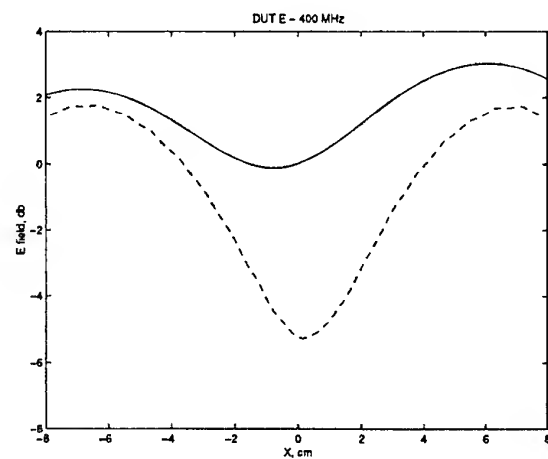


Figure 7: As fig. 3, but for DUT E at 400 MHz.

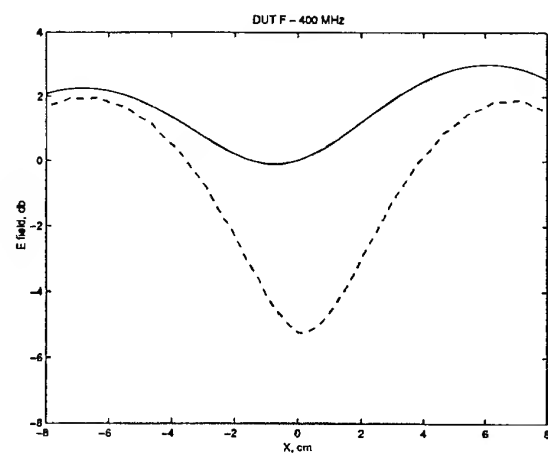


Figure 8: As fig. 3, but for DUT F at 400 MHz.

A good agreement between theoretically-derived and measured fields is found, when the cell is operated below the cutoff frequency of the first higher-order mode; the discrepancy is less than 1 dB, provided that the E_0 field in the empty cell is correctly evaluated. Beyond this frequency limit the difference increases sharply; the general behaviour of the E-field in free-space is similar to that of the field in the cell, but discrepancies of several dBs can be observed.

Far from being an exhaustive study for the qualification of loaded TEM cells (nature and shape of possible DUTs are extremely variable), this investigation gave us some insight on the real usability of the Crawford cell. A natural extension of this work is the investigation of the fields inside DUTs suspended in the centre of the cell, on dielectric stays; in this case it won't be necessary to consider the image of the DUT.

5 Acknowledgments

The authors are grateful to Prof. M. Politi for his valuable suggestions and help during the development of this work.

References

- [1] Crawford M.L. Generation of Standard EM Fields Using TEM Transmission Cells. *IEEE Trans. on EMC*, 16(4):189–195, November 1974.
- [2] Ma M.T., E.B. Larsen, and M.L. Crawford. Electromagnetic Fields with Arbitrary Wave Impedances Generated Inside a TEM Cell. *IEEE Trans. on EMC*, 33(4):358–362, November 1991.
- [3] Wilson P.F., and M.T. Ma. Simple Approximate Expressions for Higher Order Mode Cut-off and Resonant Frequencies in TEM Cells. *IEEE Trans. on EMC*, 28(3):125–130, August 1986.
- [4] Jingjun Z., and F. Junmei. Higher Order Mode Cutoff Frequencies in TEM Cells with Calculated TLM Method. *IEEE Trans. on EMC*, 30(4):563–567, November 1988.
- [5] Kanda M. Electromagnetic-Field Distortion Due to a Conducting Rectangular Cylinder in a Transverse Electromagnetic Cell. *IEEE Trans. on EMC*, 24(3):294–301, August 1982.
- [6] Kucharski A. Electromagnetic Field Inside Loaded TEM Cells. In *Proc. Intl. Wroclaw Symp. on EMC*, pages 345–349, Wroclaw, Poland, June 1990.
- [7] De Leo R., A. Lobascio, and V. Mariani Primiani. Rigorous Analysis of Diffraction in a TEM Cell. In *Proc. Intl. Wroclaw Symp. on EMC*, pages 319–323, Wroclaw, Poland, June 1990.
- [8] Wilson P., and F. Gassmann. Theoretical and Practical Investigation of the Field Inside a Loaded/Unloaded GTEM Cell. In *Proc. 10th Intl. Zurich Symp. on EMC*, pages 595–598, Zurich, Switzerland, March 1993.
- [9] Wilson P. A Review of TEM Cell Development. In *Proc. Intl. Wroclaw Symp. on EMC*, pages 206–209, Wroclaw, Poland, June 1994.
- [10] Tippet J.C., and D.C. Chang. A New Approximation for the Capacitance of a Rectangular Coaxial Strip Transmission Line. *IEEE Trans. on MTT*, pages 602–604, September 1976.
- [11] Decker W.T., M.L. Crawford, and W.A. Wilson. Construction of a Transverse Electromagnetic Cell. Technical report, U.S. Dept. of Commerce, November 1978. NBS Technical Note 1011.
- [12] Van De Hulst H.C. *Light Scattering by Small Particles*. John Wiley & Sons, Inc., 1957.
- [13] Crawford M.L., and J.L. Workman. Using a Tem Cell for Emc Measurements of Electronic Equipment. Technical report, U.S. Dept. of Commerce, 1981. NBS Technical Note 1013.

Biographical Notes

Michele D'Amico was born in Italy in 1965; he received his degree in Electronic Engineering from Politecnico di Milano in 1990; in 1997 he received his Ph.D. from the University of Essex (UK). He has been Assistant Professor at DEI since 1993. Teaching duties include lectures and classes on Antennas and Electromagnetic Fields. Research activities include radar investigation of the atmosphere, electromagnetic wave propagation in the troposphere, and electromagnetic compatibility.

Roberto Baselli received his degree in Electronic Engineering from Politecnico di Milano in 1998.

Method for Defining the Parameters of Transient Electric Field Sensors Using the Reciprocity Theorem.

G.D.Domashenko, V.P.Lisitsyn, A.A.Beloshapko, I.V.Mosin

Fast Electromagnetic Processes Department, High-Voltage Research Center of All-Russia Electrotechnical Institute, Istra, Moscow Region, Russia, 143500. Phone/Fax: (095) 560-34-38.

Abstract: In the paper we suggest the two- or three-parameters models for sensor signal reconstruction. For calculation of the sensor parameters the two-dimensional radiation problem is solved by the FDTD technique. Comparisons of computed and measured sensor responses are presented.

1. INTRODUCTION

For the last 15-20 years the techniques for measuring transient electromagnetic fields in nanosecond and sub-nanosecond ranges have got significant development due to works of C.E. Baum, R.W.P.King, M.Kanda and others [1,2]. At the moment the problem of field sensors elaboration is still urgent owing to development of ultra-wideband short-pulse electromagnetics [3].

This work is concerned with passive electrical field sensors having axisymmetric shapes and resistive loads. Three variants of geometry are examined: disk, cone, rod. The sensors with such configurations are traditional and widely used in practice.

2. EQUIVALENT CIRCUIT MODELS FOR THE SENSORS

The transient response (i.e. response to step excitation) provides complete information about the sensor. When applied to sensor signal processing, this response will allow reconstruction of any exciting field pulse very accurately. As a rule, the sensor transient response is rather complex. Therefore for the signal processing it is preferable to use some simplified algorithms, following from representation of the sensor as an equivalent circuit of lumped elements.

In the most general form the problem of determination of sensor's equivalent circuit is solved by the SEM-method [4,5]. In this method the sensor response is considered as a combination of damped sinusoids, complex frequencies and the amplitudes of which are determined by solution of a spatial homogeneous integral equation. In general, the

sensor has series of its own frequencies (modes), each of which corresponds to a branch in the equivalent circuit (Fig.1). The first mode, whose equivalent circuit is shown in fig.2 has the most essential contribution to output signal.

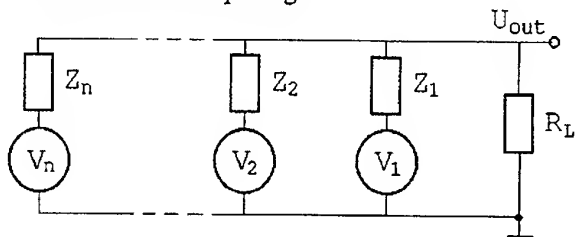


Fig. 1. Thevenin's equivalent circuit representation of a sensor in general case.

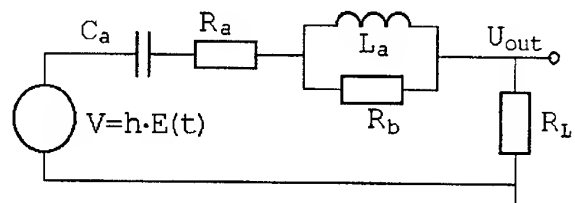


Fig. 2. The sensor's equivalent circuit considering the first mode only.

It follows from this circuit that the algorithm of an incident field pulse reconstruction from output signal of the sensor is:

$$kE(t) = \int_0^t U_{out}(t') dt' + \tau U_{out}(t) + \frac{1}{\omega^2} \frac{dU_{out}}{dt} + f(U_{out}) \quad (1)$$

where

$$k = R_L C_a h, \tau = (R_L + R_a) C_a,$$

$$\begin{aligned} f(U_{out}) &= -L_a C_a e^{-\frac{R_b}{L_a} t} \int_0^t \frac{d^2 U_{out}(t')}{dt'^2} e^{\frac{R_b}{L_a} t'} dt' = \\ &= \sum_{n=2}^{\infty} a_n \frac{d^n U_{out}(t)}{dt^n}, \end{aligned}$$

$$f(U_{out}) \rightarrow 0 \text{ for } R_b \rightarrow \infty.$$

Predominance of one or another term in (1) is set by choice of forms, sizes and loads of the sensor. Therefore several variants of the algorithm are possible:

- 1) "Differentiating sensor" model including the first term on the right side of (1) only.
- 2) "Self-integrating sensor" model including the second term only.
- 3) Two- or three-parameter models using two or three terms in (1).

It is the first two models that are mainly used in practice due to simplicity of their realization [1]. However at today's level of hardware and digital signal processing it is quite possible to use models with large number of parameters. It might be expected that it results in expanding of sensor's frequency range.

The parameters of the algorithm (1) k, τ, ω may be determined during experimental calibration of the sensor. However it is faster and cheaper to make electromagnetic computing using the technique described below replacing, in a sense, the calibration procedure.

3. METHOD FOR COMPUTING TRANSIENT RESPONSE USING THE RECIPROCITY THEOREM

The direct account of the transient response of a sensor to the incident plane wave is a three-dimensional electrodynamic problem requiring significant computing resources. However for sensors with axially symmetric geometry it is possible to reduce the three-dimensional problem of reception to the two-dimensional problem of radiation. To make it, we use the well known principle of reciprocity [6, 7].

The sensor can be either monopole located over a conducting plane or dipole located in free space. The geometry of the antenna for cases of reception and transmission is schematically represented in fig. 3.

Being based on the known general ratios in the frequency domain [6], we shall receive the calculation formulae, valid both for dipole and for monopole antennas.

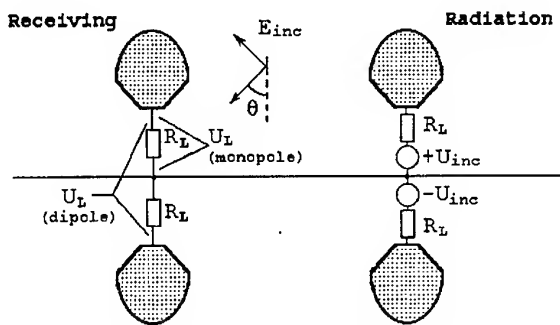


Fig. 3. Schematic of the antenna for cases of reception and transmission.

Spectral density of voltage on the sensor load in case of reception is:

$$U_L(\omega, \theta) = 2E_{inc}(\omega)h_e(\omega, \theta) \frac{R_L}{Z_A(\omega, \theta) + 2R_L}$$

where ω - the circular frequency; $E_{inc}(\theta)$ - the electrical field spectral density of an incident vertically polarized wave; θ - the incidence angle of the wave; h_e - the dipole effective length; Z_A - the input impedance of the dipole antenna; R_L - the load resistance (in our case $R_L = 50 \Omega$).

If the sensor is the transmitting antenna, the spectrum of the electrical field strength in the far-zone region is:

$$E_{rad}(\omega, \theta) = \frac{j\omega U_{inc}(\omega)h_e(\omega, \theta)Z_0}{\pi c r(Z_L(\omega) + 2R_L)} e^{-jkr},$$

where Z_0 - the characteristic wave impedance of the free space; $k = \omega/c$; c - the speed of light; r - the distance from the sensor to the observation point.

Let the time forms and, hence, spectra of incident waves in cases of reception and transmission are the same:

$$U_{inc}(\omega, \theta) = r_d E_{inc}(\omega, \theta),$$

where r_d - some auxiliary factor introduced for coordination of dimensions, for example, $r_d = 1m$. From the formulae mentioned above it follows:

$$U_L(\omega, \theta) = \frac{\pi c r E_{rad}(\omega, \theta) R_L}{2 j \omega r d Z_0} e^{+jkr}.$$

Passing with the help of Fourier transformation to the time domain, we shall receive:

$$U_L = \frac{\pi c R_L}{2 r d Z_0} \int_0^t E_{rad}(t + r/c, \theta) dt.$$

The far-zone radiation field of the sensor is calculated from fields on some surface S , enclosing the sensor, with the help of known integral ratios [8]. Carrying out analytical integration with respect to time, we shall receive:

$$U_L(t, \theta) = \frac{R_L}{2r_d Z_0} \vec{\theta}_0 \cdot \int_S \{Z_0 [\vec{n} \times \vec{H}(\vec{s}, \tau)] - [\vec{n} \times \vec{E}(\vec{s}, \tau) \times \vec{r}_0]\} ds,$$

$$\tau = t + \vec{r}_0 \cdot \vec{s}.$$

where \vec{n} - the external unit vector normal to the surface S ; \vec{E} and \vec{H} - the vectors of electrical and magnetic radiation fields; $\vec{\theta}_0, \vec{r}_0$ - the unit vectors in

the spherical coordinate system; \vec{s} - the radius-vector specifying a point position on the surface S .

In the work the radiation fields in some vicinity of the sensor were calculated with the help of the finite difference time domain method (FDTD) [9]. At the boundary of the calculation area the second order local absorbing conditions were used. For the space cell size of 0.25 mm the calculation of one antenna geometry on the computer with Pentium-166 processor required about 5-6 hours.

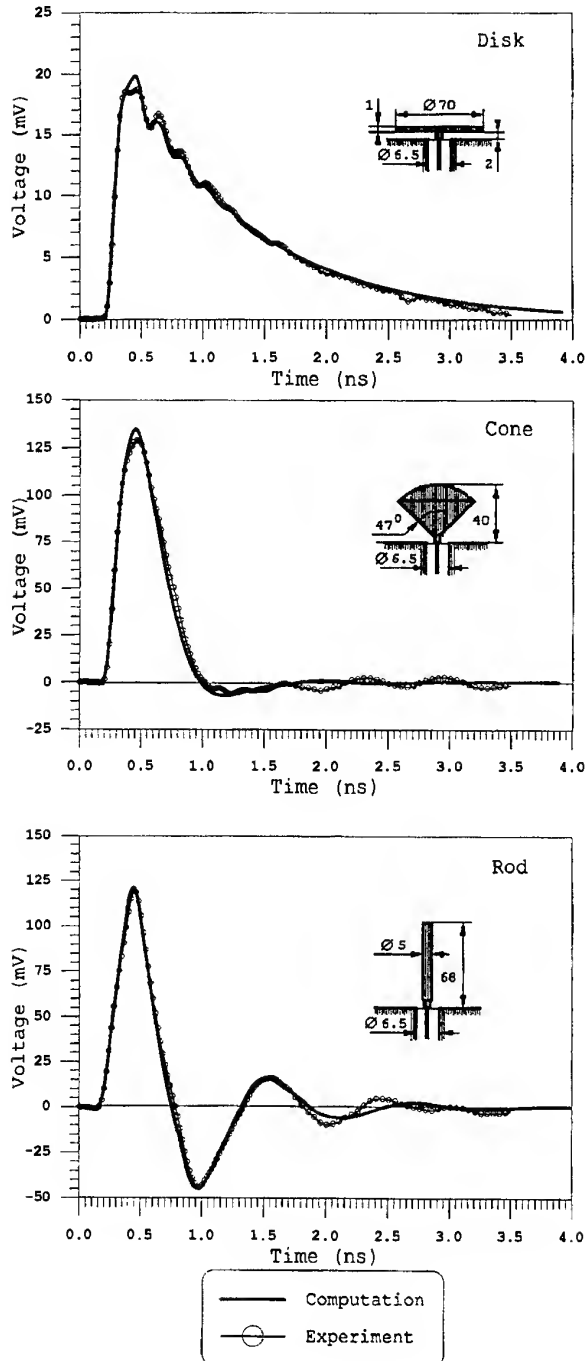


Fig.4. The transient responses of the sensors.

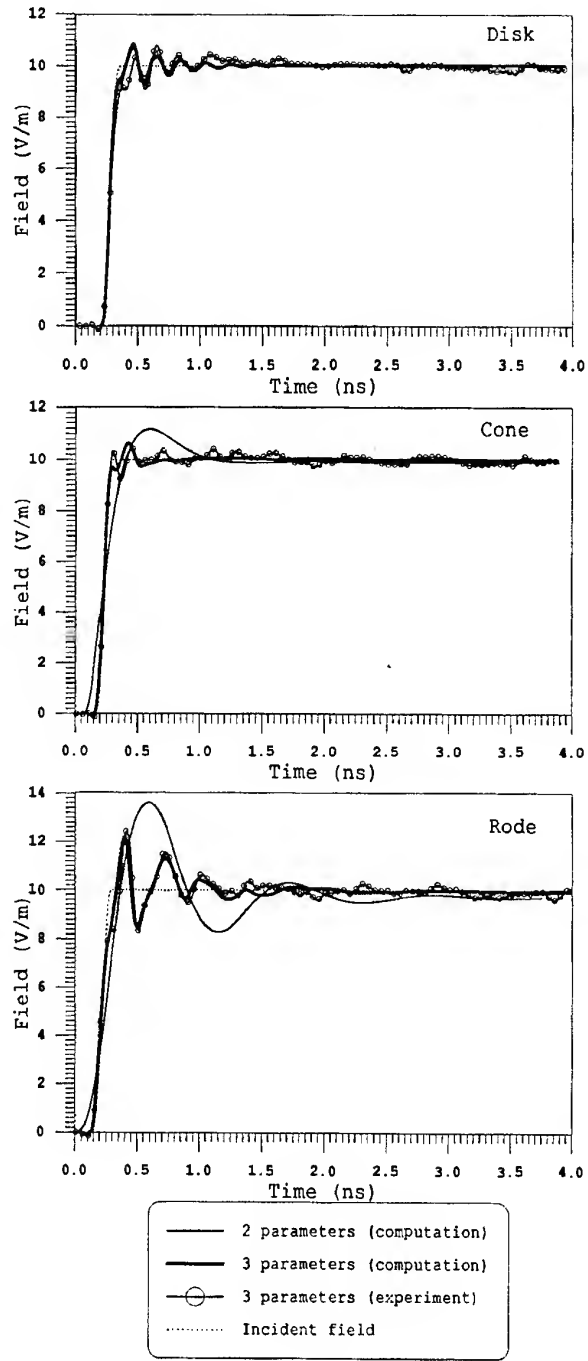


Fig.5. The reconstructed field pulses.

Table 1. The parameters of the sensors

		Disk		Cone		Rod	
		Computation	Experiment	Computation	Experiment	Computation	Experiment
3-param model	k (ns \times mm)	2.218	2.220	5.008	5.207	2.630	2.719
	τ (ns)	1.047	1.005	0.2347	0.2500	0.0884	0.0964
	$\omega/2\pi$ (Hz)	0.8867	1.078	0.8949	0.8560	1.002	0.9823
2-param model	k (ns \times m)	2.221	2.222	5.051	5.251	2.692	2.777
	τ (ns)	1.024	0.9893	0.1712	0.1872	-1.05×10^{-3}	2.80×10^{-4}

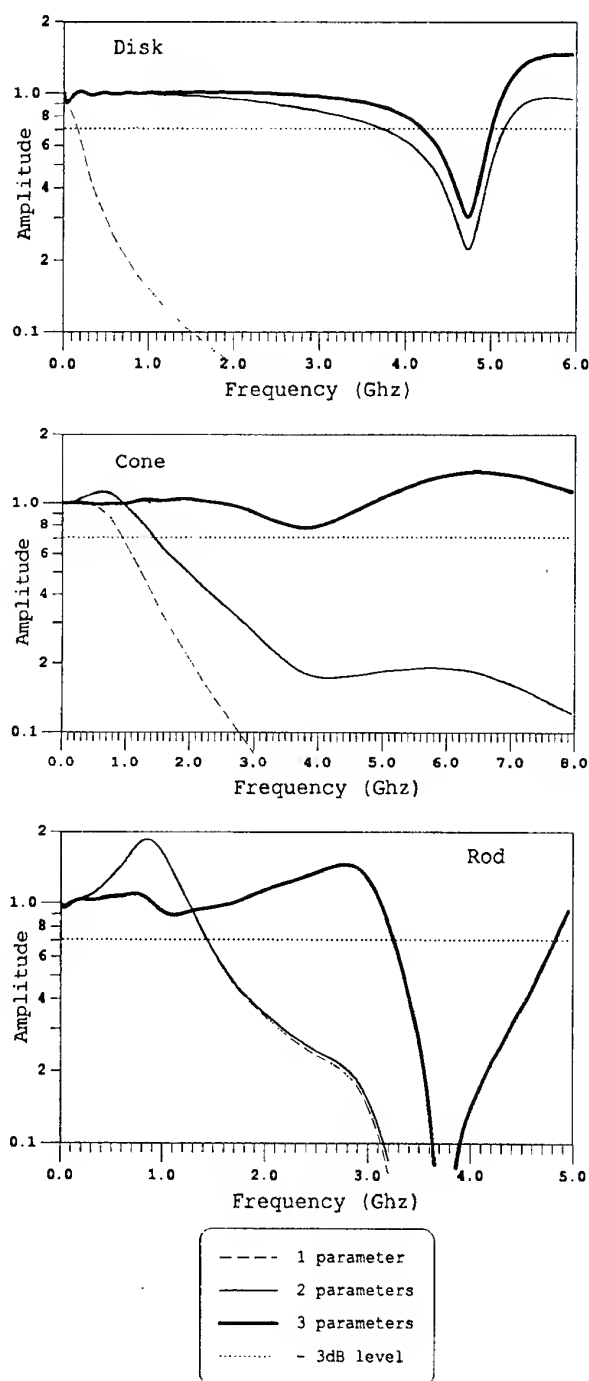


Fig. 6. The normalized transfer functions of the sensors after the signal reconstruction.

4. COMPUTED RESULTS AND THEIR EXPERIMENTAL CONFIRMATION

For confirmation of the method's correctness the numerical results were verified by experiment. For simplicity in experiment and in calculations "monopole" sensors and horizontal direction of incident wave only were examined. The sensors under test were placed in the field formed by the conic asymmetrical TEM-line. The field pulse in the TEM-line had the rectangular form with rise time of about 80 ps. The output signal of the sensors was registered with help of digital sampling oscilloscope S9-9 connected with computer. The small non-uniformity of the excited pulse top was corrected by subsequent processing of results.

The results of calculations and experiment are shown in fig. 4. The agreement between the results is good for all the sensors. The sensor geometries are also depicted in fig. 4.

The transient responses of the sensors were processed by the algorithm (1) with two or three terms. Fitting the processed responses with an initial pulse $E(t)$ according to the least squares method the optimum values of parameters k, τ, ω were determined. In fig. 5 one can see field pulses reconstructed with use of known parameters. The parameters of the sensors obtained from measured and calculated data in two- and three-parametrical approximations are given in table 1.

Analysis of the results allows us to make several conclusions. The reconstruction by the 3-parameter algorithm provides the highest accuracy for the cone. But when 2-parameter model is applied it is preferable to use the disk. For the rod the reconstruction errors are very large in both approximations. This is, apparently, caused by excitation of the next (third) mode of the antenna, whose description would complicate the equivalent circuit.

In fig. 6 the frequency transfer functions of the sensors are shown after signal reconstruction by using the algorithms with different numbers of parameters. The figures demonstrate that the use of two or three-parametrical models results in sufficiently increasing bandwidth of measurements in comparison with simple (one-parametrical) integration.

By means of modern electronics it is possible to create analog devices for hardware realization of the algorithm (1). The sample of similar broadband

"pseudo-integrator", made in our laboratory and working according two-parametrical algorithm with $\tau = 2$ ns, has its own rise time of about 100 ps and maximum duration of reconstructed signal of about 300 ns. When adjusting such devices for input signal formation, it is possible to use the sensor equivalent circuits, which is implemented physically.

5. CONCLUSION

For increasing measurement bandwidth by passive field sensors it is possible to use two- or three-parameter algorithms of signal reconstruction following from representation of a sensor as some equivalent circuit of lumped elements. The parameters of algorithms may be determined from the transient response of the sensor by the least squares method.

For electrical field sensors having an axisymmetric form the response can be computed quickly due to reducing, according to the reciprocity theorem, the three-dimentional reception problem to two-dimensional radiation problem. The latter is solved numerically in time domain by the FDTD method.

For the disk-sensor one can restrict oneself to the 2-parameter signal reconstruction model, which is quite simple for hardware realization. In case of the 3-parameter model the cone-sensor is the most broadband one.

6. REFERENCES

1. C. E. Baum, E. L. Breen, J. C. Giles, J. P. O'Neill, G. D. Sower, "Sensors for electromagnetic pulse measurements both inside and away from nuclear source regions", IEEE Trans. on Antennas and Propagation, Vol. 30, No. 4, 1982, pp. 657-660.
2. M. Kanda, "Time-domain sensors and radiators", in " Time-domain measurements in electromagnetics" Ed. E. K. Miller, 1986, Van Nostrand Reinhold Company, Ney York, ch. 3, pp.122-174
3. "3rd international conference on ultra-wideband short-pulse electromagnetics ", Albuquerque, 27-31 May, 1996.
4. C. E. Baum and B.K. Singaraju, "The singularity and eigenmode methods with application to equivalent circuits and related topics", IEEE Trans. on Antennas and Propagation, Vol. 30, No. 4, 1982, pp. 657-660.
5. L. W. Pearson and D. R. Wilton, "Theoretical aspects of the physical realizability of broad-band

equivalent circuits for energy collecting structures", in "Acoustic, electromagnetic and elastic wave scattering-focus on T-matrix approach", Ed. V. K. Varadan, Pergamon Press, New York, 1980, pp. 431-452.

6. C. W. Harrison, Jr. and C.S. Williams, Jr., "Transients in wide-angle conical antennas", IEEE Trans. on Antennas and Propagation, Vol. 13, No. 2, 1965, pp. 236-246.

7. D. M. Sazonov, "Microwave circuits and antennas" (english), Mir Publishrs, Moscow, 1990, ch. 8, pp. 242-262.

8. R. Mittra (Ed.), "Computer techniques for electromagnetics", Pergamon Press, 1973, ch. 4.

9. A. Taflove and K.R. Umashankar, "The finite-difference time domain method for numerical modeling of electromagnetic wave interactions with arbitrary structures", in "Finite element and finite difference methods in electromagnetic scattering", Ed. M. A. Morgan, Elsevier Science Publishing Co. New York, ch. 8, pp. 287-373.

BIOGRAPHICAL NOTES

Gennadi D. Domashenko was born in 1960 in Stavropol Territory, Russia. In 1984 he graduated from Moscow State University, Physical Faculty. Since 1984 he has been working at the All-Russian Electrotechnical Institute on the problems of EM-pulses propagation and measurements.

Vladislav P.Lisitsyn was born in 1940 in Kostroma, Rusia. In 1963 he graduated from Moscow Aviation Institute, Radio Engineering Faculty. He received the Ph. D. degree from Moscow Power Institute in 1978. Presently he is working in the field of non-stationary electrodynamics.

Alexander A. Beloshapko was born in 1959 in Bryansk region, Russia. In 1985 he graduated from Moscow State University, Physical Faculty. Since 1985 he has been working at the All-Russian Electrotechnical Institute. Presently he is working on the problems of EM-pulses generation, propagation and interaction with losses materials.

Ivan V. Mosin was born in 1950 in Tula region, Russia. In 1973 he graduated from Moscow Power Institute, Electrophysical Faculty. Since 1973 he has been working at the All-Russian Electrotechnical Institute. Presently he is working in the field of EM-pulses measurements and instrumentation.

MEASUREMENT OF EMISSIONS FROM TWISTED PAIR CABLES USED IN LAN'S

Waldemar E. Grzebyk, Jaroslaw M. Janukiewicz

Research & Academic Network of Poland, Telecommunication Department,
ul. Janiszewskiego 7/9, 50-372 Wroclaw, Poland
Phone: +48 (71) 219259, Fax: +48 (71) 219259

1. INTRODUCTION

Intra- and inter cable crosstalks may be treated as a measure of twisted pair cables emission. The objective of our study was to investigate the crosstalk between pairs of twisted wires in the same cables and between the cables. The measured crosstalk may be an indication of the ability to detect information.

The copper cables used in computer networks are sources of electromagnetic radiation associated with the transmission of electric signals. Electromagnetic radiation covers a frequency range which depends on the transmission technique applied (Ethernet, FastEthernet, ATM).

2. MEASUREMENT OF EMISSIONS

The volume of crosstalks as a function of frequency (measured in the cable and between the cables of the network, as well as the attenuation of electromagnetic scattering as a function of frequency (measured with an antenna in the vicinity of the cable system), may be a clear sign of emission from symmetric cables. To check the levels of emission from symmetric cables we measured both the attenuation characteristics.

2.1. Crosstalks in symmetric cables

The tests were carried out in a structural cabling system made of four twisted pair cables (two of UTP type, category 5, and two of S/UTP type, category 5), which had been laid in parallel along a section of about 85 m. Shielded cables were earthed on the side of the floor distributor (FD), and measurements were performed with an HP8711A network analyser (Fig. 1). The measurements were repeated, using a standard wiring tester (PentaScanner 350), made by Microtest (Fig. 4). PentaScanner 350 was used to check the utility of structural wiring testers in preliminary measurements of emission from twisted pair cables. Crosstalk levels were measured between pairs in the same cable and between pairs in different cables.

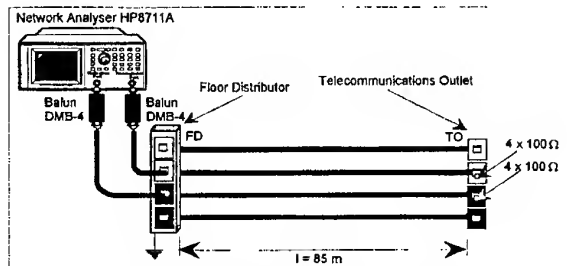


Fig. 1. Measuring setup using a network analyser

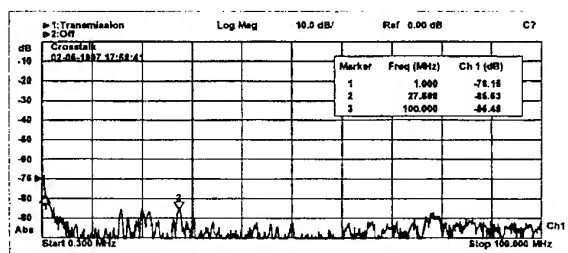


Fig. 2. Crosstalk level measured between pairs 1-2 and 1-2 in two different shielded cables (S/UTP), using an HP8711A

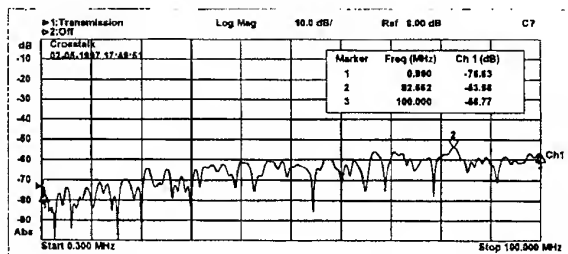


Fig. 3. Crosstalk level measured between pairs 1-2 and 1-2 in two different unshielded cables (UTP), using an HP8711A

Intra-cable crosstalks were measured with a PentaScanner 350 tester. The measured data were verified in a measuring procedure performed with an HP8711A network analyser for selected pairs. Inter-cable crosstalks were measured using both an

HP8711A network analyser and a PentaScanner 350 tester.

When use was made of the HP8711A network analyser, the output and input signals were sent via DMB-4 baluns ($100\Omega/50\Omega$) made by EG&G, which were very well balanced with respect to mass (above 50 dB) in the entire range of the investigated frequencies (300kHz-100MHz). Each cable pair ended with a matched load of a 100Ω impedance.

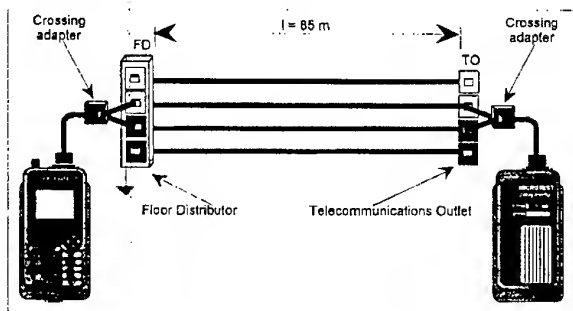


Fig. 4. Measuring setup using a PentaScanner 350 tester

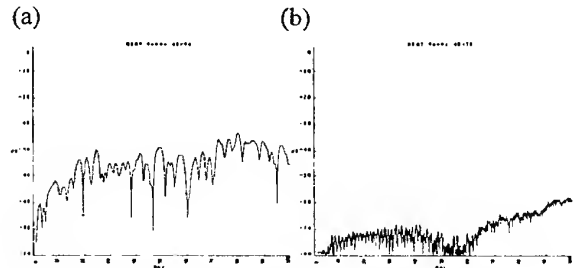


Fig. 5. Crosstalk level measured with a PentaScanner 350 tester:

- (a) - between pair 1-2 and pair 3-6 in the same shielded cable (S/UTP),
- (b) - between pair 1-2 and pair 1-2 in two different shielded cables (S/UTP),

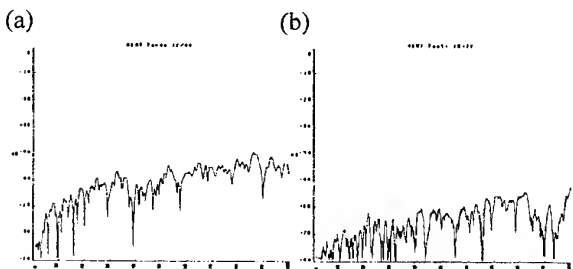


Fig. 6. Crosstalk level measured with a PentaScanner 350 tester

- (a) - between pair 1-2 and pair 3-6 in the same unshielded cable (UTP),
- (b) - between pair 1-2 and pair 1-2 in two different unshielded cables (UTP),

2.2. Measurement of signal attenuation characteristics in the vicinity of the cable network with the use of an active antenna

Signal attenuation was measured in the same structural cabling system as were crosstalks. Use was made of two measuring antennas (a magnetic antenna of BBH-1100/A type and an electric antenna of ADA-120/A type made by Antenna Research Associates) and a network analyser (of HP8711A type) (Fig. 7). The output signal of the HP8711A network analyser was passed by the DMB-4 balun to a pair of the shielded or the unshielded cable.

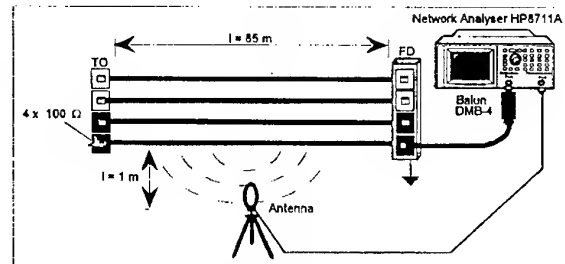


Fig. 7. Setup for attenuation characteristic measurements

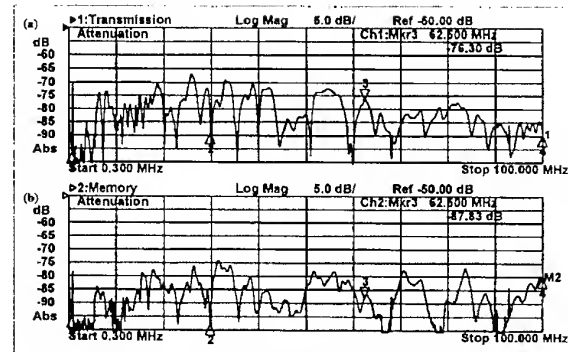


Fig. 8. Attenuation measured with a BBH-1100/A antenna, for (a) an unshielded cable (UTP), and (b) a shielded cable(S/UTP)

3. POSSIBILITY OF INFORMATION DETECTION

When the characteristics of the transmitted signals and propagation phenomena are known, there is a strong possibility that the source signal can be reconstructed.

To verify the possibility of information detection the electromagnetic field in the vicinity of the structural cabling system was measured in the time domain. The source signal (in the form of Ethernet-type frames) was generated from a protocol analyser of HP J2302B type to a network cable connected with another device. Use was made of a BBH-1100/A antenna connected to a TDS640 digital oscilloscope made by Tektronix. The measurement was synchronized with the signal of the Ethernet frame controlled by a current-difference probe.

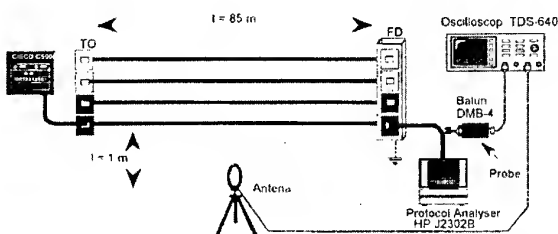


Fig. 9. Setup for signal measuring in the detection circuit

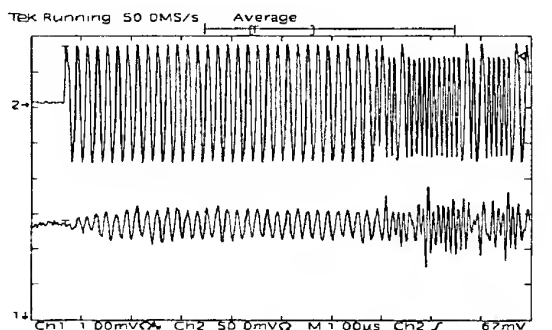


Fig. 10. Preamble to an Ethernet-type frame, measured with an oscilloscope: in an unshielded cable (UTP) (top of the chart) and in the listening-in channel (bottom of the chart)

4. CONCLUSIONS

When use in made of circuit methods and field methods, it is possible to assess the desired dynamics of the measuring setup for the determination of emissions from twisted pair cables which are used in LAN's. As shown by the measured data, in a standard network the dynamics of 100 dB is sufficient (Fig. 2, Fig. 3, Fig. 8). Measurements in the time domain by the field method (Fig. 10) have revealed that even a slight processing of the measured signal makes it possible to find out what kind of information is being transmitted by the network.

Comparison of qualitative differences between shielded and unshielded twisted pair cables (Fig. 8) has led to the following findings. Emission from unshielded cables is higher than that from the shielded ones. In adequately constructed networks the shielded system provides a larger „safety margin” which makes the detection of useful information more difficult than does the „safety margin” provided by the unshielded system. However, even an appropriately designed network will not be able to meet such an emission requirement that provides sufficient protection of useful information. The compatibility of the system is affected by each component of the network. In a shielded network, a lack of continuity may result in that the screen begins to act as an antenna. In an unshielded network, an unbalanced transmitter or receiver in the network card may cause that the level of the emitted electromagnetic field will rise dramatically.

5. REFERENCES

1. EN 50173 European Standard, Information technology. Generic cabling systems, CENELEC, Brussels, 1995.
2. Grzebyk W.E., Janukiewicz J.M., Pulse method for EMC testing of symmetrical cables, Thirteenth International Wroclaw Symposium on EMC, Wroclaw, 1996.

BIOGRAPHICAL NOTES

Waldemar E. Grzebyk is with the Telecommunication Department of Research and Academic Network in Poland, where he works as the Network Analyst. A graduated M.Sc. in 1985 from the Wroclaw University of Technology

Jaroslaw M. Janukiewicz is with the Telecommunication Department of Research and Academic Network in Poland, where he works as the Network Analyst. A graduated M.Sc. in 1988 from the Wroclaw University of Technology

COMPARING THE MEASUREMENT RESULTS IN A FULLY ANECHOIC CHAMBER (FALC) TO THOSE ON FOUR DIFFERENT OATS

Diethard Hansen and Detlef Ristau
EURO EMC SERVICE Dr. Hansen GmbH
Potsdamer Str. 18A, D-14513 Teltow, Germany
Fax: +49 3328 430142, http://www.euro-emc-service.de

An investigation of the performance between four EN 45001 accredited 10m OATS in Germany is conducted. Starting with the ± 4 dB NSA criterion of the empty calibration for each site a small battery driven test radiator resulted in deviations of ± 6 dB of the mean value from the four sites. A specially prepared desktop computer system with cables driven by the test radiator source and not powered by the mains caused deviations of up to ± 12 dB. The test results were repeated in a 7m x 4m x 3m FALC and compared to the mean values of the four OATS. The 3m FALC results demonstrated excellent agreement with the 10m OATS for both EUTs.

1. INTRODUCTION

One requirement for an accredited EMC lab under EN 45001 and ISO 25 in order to establish its measurement uncertainty is the participation in round robin tests. This comparison is important to determine the absolute precision and the repeatability to meet legal criteria. Further more having a small uncertainty may help the customer to save money in preventing costly over designs. Experience teaches radiated emissions to be a major obstacle to reach CE compliance. This is normally measured on open area test sites (OATS) or in alternative facilities (e.g. FALC). FALCs are relatively new in the standards and easier to operate because of less ambients. A major benefit is the cost reduction in building expenses and testing time, due to neglecting the height scan [1], [2].

To verify and explain the often found discrepancies between fully accredited OATS (NSA empty calibration ± 4 dB) and using them with the same EUT, we performed round robin tests among four 10m OATS without weather protection. These OATS were situated in various parts of Germany and belonged to government accredited test houses.

2. COMPARISON OF DIFFERENT OATS

2.1. NSA

In order to validate the 10m accredited OATS the normalized site attenuation (NSA) of ± 4 dB according to CISPR 16 and ANSI C-63.4/1992 was rechecked on each site. These sites belong to different BAPT or DATECH officially accredited EMC test labs according to EN 45001 scattered all over Germany. On our own EES 10 m reference site with wire mesh ground plane dimensions 18 m x 21 m we measured the following NSA (fig. 1 and fig. 2). The 27 measurement values are well within the ± 4 dB tolerance band, which is marked in the figures.

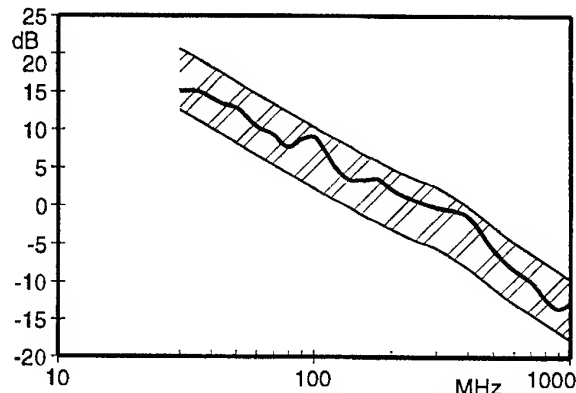


Fig. 1: Vertical NSA of the 10 m Reference Site

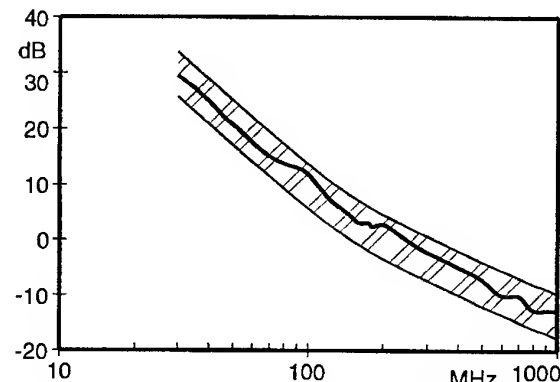


Fig. 2: Horizontal NSA of the 10 m Reference Site

2.2. Using a Small Test Radiator

Fulfilling the ± 4 dB NSA criterion for the empty site does not necessarily mean that real objects (EUT) are correctly measured within the same error limits. For the actual test we used a 40 cm long symmetrically driven broad band dipole. The generator was a small, stable, battery operated 10 MHz spectral line source. The test radiator was measured according to EN 55022 class B. Consequently a full height scan was executed. In order to save time only four positions on the turn table where typically checked. The peak and not the quasi-peak detector mode was used because of the known stable characteristics of the test radiator.

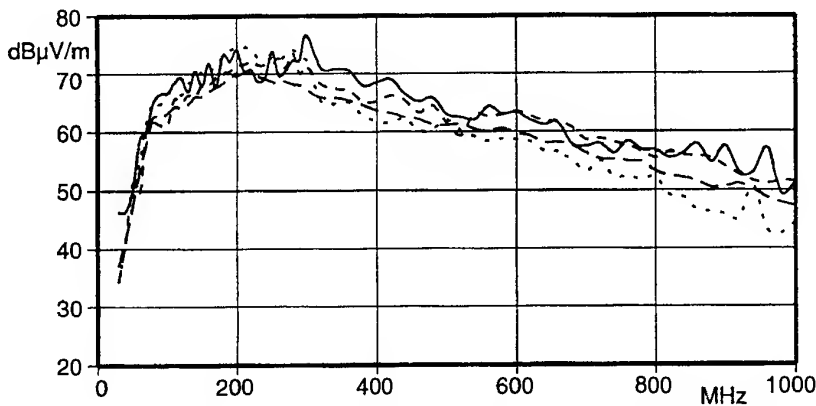


Fig. 3: Measurement Results of the Small Test Radiator on Four Different 10 m OATS

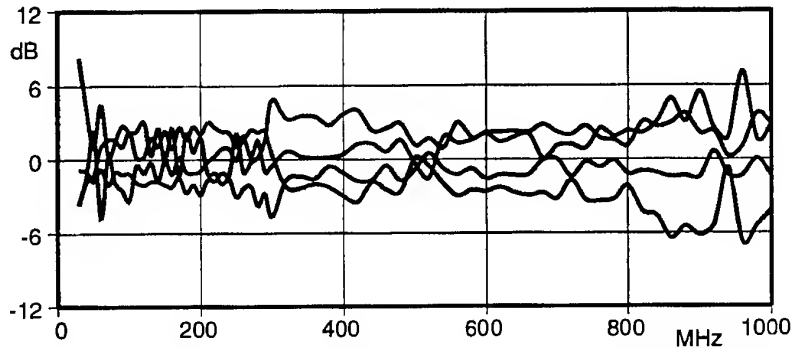


Fig. 4: Deviation Results for the Small Test Radiator on the Four Different 10 m OATS

In the low frequency range we used a biconical antenna and measured each peak, spaced 10 MHz apart. Above 200 MHz we used a logarithmic periodic antenna at 20 MHz intervals. This resulted in typical test times of one to two days per site.

The measurements were performed over several months in summer and autumn 1997. We used the existing equipment and site of the very organization with always the same EES test engineer, supervising the measurements. As expected many problems with ambient signals on the OATS according to their specific and permanently changing environment (GSM at 900 MHz) were experienced, resulting in degraded signal noise ratio.

Before and after each test the test radiator was rechecked in our accredited, traceable test lab in Teltow. We tested the 50

Ohm generator output between 30 and 1000 MHz, regarding the spectral distribution and amplitude. The spectrum generator characteristics stated by the manufacturer is:

- frequency error: $< 1 \times 10^{-6}$
- discrete line stability: $< \pm 0.2 \text{ dB} (20^\circ \text{ C})$
- temperature drift $< \pm 0.5 \text{ dB} (+10^\circ \text{ to } 30^\circ \text{ C})$

As shown in Fig. 3 the typical radiation characteristic of the test radiator exhibits a resonance around 200 MHz. The deviation is investigated by calculating the mean value of the four sites. This compares favorably with the absolute values of the EES reference site. The deviation of the OATS from the mean value is given in fig. 4. This results in an overall deviation of about $\pm 6 \text{ dB}$. Such values are within the known errors listed in the international literature [3], [4], [5].

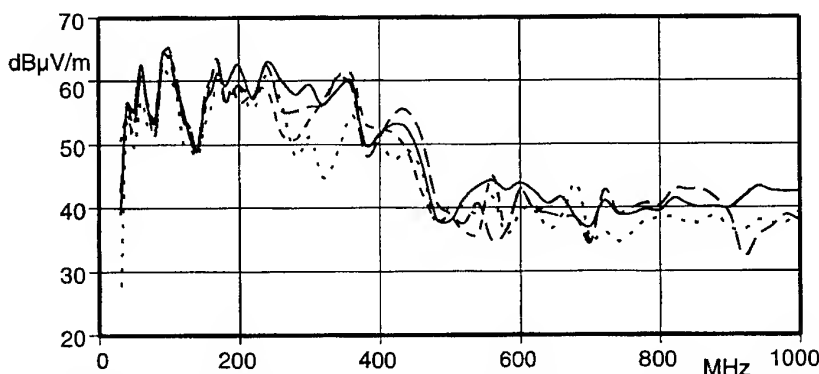


Fig. 5: Measurement Results of the Special System with Cables on the Four OATS

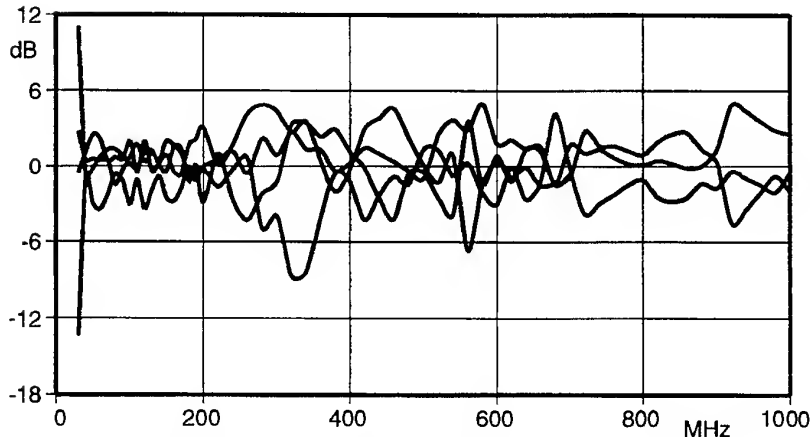


Fig. 6: Deviation Results for the Special System on the Four Different 10 m OATS

2.3. Special Desktop System with Cables

Below 150 MHz cables play a very important role in radiated emission measurements. Therefore a generic object, representing a typical ITE EUT, a desktop computer system, was subjected to basically the same procedure as under chapter 2.2.

Due consideration was given to create a stable source, however, fully representative of real devices including cables. This is why we mounted a video display unit, a desktop PC, including mouse and power supply cable in the same way, as normally being used, on a wooden platform, giving all cables a fixed horizontal and vertical position. The big difference to the real live system is the installation of our stable test generator inside the computer chassis between the boards. The generator output was directly connected to the DC power supply system cable, feeding all boards. The power cord was not connected to the usual 230V AC. This procedure results in a realistic, but stable scenario of RF leakage currents through out the PC system.

Fig. 5 illustrates the measured results of this system on all four sites. The deviation can be depicted from fig. 6, resulting in about ± 12 dB. The strongest deviation appears near 30 MHz. The deviation seems to be high, but is not unusual between laboratories. Similar results have been obtained in the first round robin tests several years ago in the UK by NAMAS.

3. CALIBRATION RESULTS IN FALCS

As listed in [1] we used a 7m x 4m x 3m fully anechoic chamber lined with ferrite tiles and a 3 m test distance, including a special electromagnetically "non-reflecting" turn table. The previous paper outlines the conversion procedures to 3m, 10m and 30m test distances over metallic ground planes. The same results are obtained in [6], however, using a different method.

Additionally it is pointed out to potentially existing errors, extrapolating even 10m ground plane sites to 30m sites, using exactly the prescribed method as in the CISPR standard. Using only the inverse distance law, adding 10 dB, may result in additional errors for ground plane sites of up to +8, -6.9 dB. This fact disqualifies 10m semi-anechoic chambers to be used under EN 55011: 10/97 for group 1 class A ISM equipment.

This disadvantage does not exist in the fully anechoic chamber, because the indirect path shouldn't be existing.

The calibration results for our FALC are shown in fig. 7 and 8 for vertical and horizontal polarization, converted to the 10m ground plane equivalent.

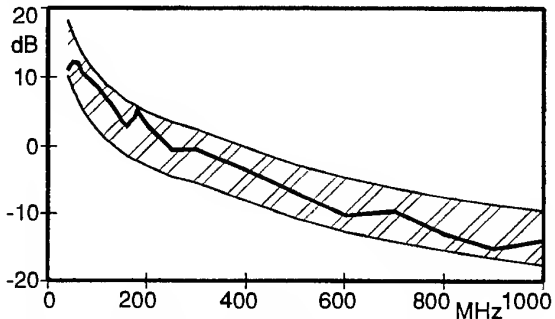


Fig. 7: Equivalent 10 m OATS vertical calibration for our 7m x 4m x 3m FALC

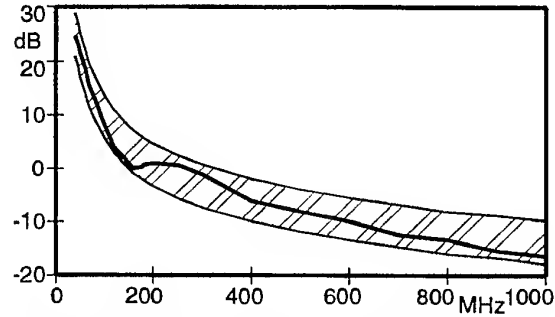


Fig. 8: Equivalent 10 m OATS horizontal calibration for our 7m x 4m x 3m FALC

4. COMPARISON OF OATS AND FALC DATA

4.1. Using a Small Test Radiator

The reference radiator was used with the results as demonstrated in fig. 9. The error band is derived from the mean value of the four OATS adding ± 4 dB. The result is almost perfect. Only around 300 MHz one data point is slightly off.

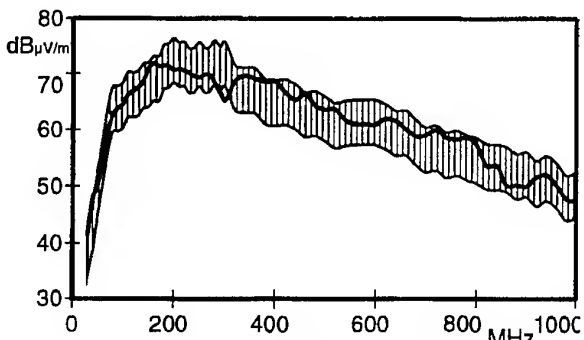


Fig. 9: Comparison of OATS and FALC for the Small Radiator

4.2. Special Desktop System with Cables

We repeated the system tests in the same way as described before on the turn table at 3 m antenna distance in our FALC. The same antennas, turn table and receiver as on the EES reference site were used. Fig. 10 reveals the interesting truth. The error band represents the OATS data of the special system with cables (mean value ± 4 dB). The overall result for the FALC is in very good agreement to the OATS result.

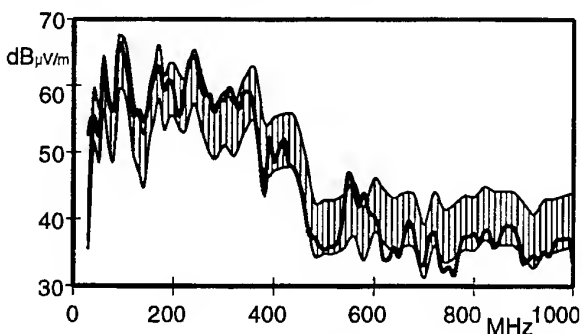


Fig. 10: Comparison of OATS and FALC for the Special System with Cables

5. CONCLUSIONS

OATS to FALC correlation can be performed with good agreement. The advantages of the FALC, however, are evident:

- no ambients
- practically no antenna height scan
- much better repeatability
- emission and immunity testing with the same test setup
- cost and time savings

Furthermore the received and stored raw data can be post processed and correlated to any OATS distance.

In the second part of 1998 the German accreditation planes a mandatory round robin test for all 100 EMC labs.

6. REFERENCES

- [1] D. Ristau, D. Hansen: "Correlating Fully Anechoic to OATS Measurements", Proceedings of the EMC 96 Wroclaw Symposium, Wroclaw, Poland, 1996, pp. 402-405
- [2] D. Hansen, S. Moessler: "NSA o.k. is now all o.k." (German: "Normgerecht ist nicht gleich Normen gerecht"), EMV-ESD, No. 4, 1997, by EMP Verlag, Boeblingen, pp. 26-29
- [3] L. E. Kolb: "Statistical Comparison of Site-to-Site Measurement Reproducibility", Proceedings of the 1996 IEEE Int. Symposium on EMC, Santa Clara, CA, USA, 1996, pp. 241-244
- [4] D. Steinbach: "A comparison of results of GTEM emission measurements" (German: "Vergleichbarkeit von Ergebnissen aus GTEM-Emissionsmessungen") in HF-Report, No. 2, May/June 1997
- [5] J. DeMarinis: "The Antenna Cable as a Source of Error in EMI Measurements" Proceedings of the 1988 IEEE Int. Symposium on EMC, Seattle, WA, USA, 1988, pp. 9-14
- [6] T. Jahn, D. Hansen: "Are Fully Anechoic Emission Measurements in Compliance with the Standards" in International Product Compliance, No. 1, 1998, by James&James, London, pp. 25-29

[1], [2] and [6] available from <http://www.euro-emc-service.de>

ACKNOWLEDGMENT

The authors have to thank Dipl.-Ing. Stefan Moessler for excellence in performing the majority of the measurements and the data processing.

BIOGRAPHICAL NOTES



Dr.-Ing. Diethard Hansen is president of the EES company group, specializing in EMC test products, consulting, training, testing and R&D. Further areas: LVD, radio, automotive and medical. He is holding a BS/MS in electrical engineering from Germany and a Ph.D. degree from TU Berlin. More than 20 years of industrial EMC/EMI experience, 35 patents (GTEM, EUROTEM, Poyntor) and 130 professional publications as well as chairmanships are assigned to him. He is the manager of the EES Competent Body and member of the board of European Competent Bodies ACB - Brussels. Memberships: IEEE/EMC, CENELEC, ETSI and IEC.



Dr.-Ing. habil. Detlef Ristau is vice president of EES Teltow near Berlin. He is leading the EES R&D division. Dr. Ristau is holding all engineering, Ph.D. and lecturer degrees from the university of transport Dresden, Germany. He has published numerous scientific contributions in major professional journals and symposia and he is one of the inventors of the EUROTEN, Poyntor. His particular interest includes sophisticated electromagnetic field problems. He is a member of the IEEE EMC society of the United States.

Both authors may be reached by phone +49 3328 430 141 or e-mail: euro.emc.service@t-online.de.

GYROMAGNETIC CONVERTER SELECTIVITY CURVE FORMATION FOR FREQUENCY- SELECTIVE MICROWAVE MEASURING DEVICES

Koledintseva M.Yu.*, Kitaytsev A.A.

Moscow Power Engineering Institute (Technical University)

Krasnokazarmennaya, 14, Moscow, 111250 Russia

Tel. (095)362-79-58, fax: (095)362-89-38, e-mail: koled@home.orbita.ru

The principle of operation of microwave frequency & power gyromagnetic converter (GC) using stable non-linear phenomena at ferromagnetic resonance in monocrystal ferrite resonators (FR) is discussed. The GC are used in microwave panorama devices for frequency-selective measurements of the signals power parameters (wideband noise spectrum power density, integral density in the given frequency band, peak power of the pulses, power of the deterministic signal at the certain frequency).

The method of formation the necessary selectivity curve (SC) of the gyromagnetic converter (GC) used in microwave panorama frequency-selective measurers of power parameters is presented. This method using multi-channel scheme of the weighted summation of the FR magnetization components at the harmonics of the modulation frequency leads not only to the possibility of the SC shape control, but even to increasing the GC conversion coefficient.

1. INTRODUCTION

Development of methods and equipment for frequency-selective power parameters measurement of radiation produced by microwave active devices of middle and high power level (10^{-3} - 10^3 W) is an urgent problem. Modern EMC Standards demand the levels of active electronic devices being detected and controlled up to the third harmonic of the main oscillation. Microwave measuring devices need high-quality tunable filters-preselectors (or a set of filters) at their input with the suppression of spurious signals more than -60 dB. It is a complicated technological problem, especially when coming to mm-waveband. There are a lot of problems

connected with waveguide path calibration and identification of spurious reception channels of standard microwave heterodyne analyzers, especially in multi-signal regime of active devices operation, when level of irradiation intensity and its frequency range are not clear beforehand.

For evaluating the electromagnetic situation in wide frequency range (more than two octaves), visualization of wideband signals spectrum envelopes and measuring power parameters of microwave signals the panorama frequency-selective devices on base of gyromagnetic converters (GC) have found their application [1]. Various constructions of the GC in cm and dm wave bands permit to operate at 10^{-7} - 10^3 W of continuous power at linear dynamic range of a GC 25 dB [2]. Due to the non-heterodyne principle of frequency and power conversion [3] in the GC, they are free from spurious channels of reception, connected with combination frequencies. They have constant conversion coefficient in wide operation frequency band (about 10 mV/W), and due to their frequency selectivity (determined by the ferrite resonator quality) can measure rather small signal spectrum density in presence of intense electromagnetic interference. The demands to the pre-selectors at the input of measuring devices (-60 dB losses outside the passband and minimum possible losses in the passband) may be less strict when using the GC.

GC is designed on base of the ferrite resonator (FR) with element for its resonance frequency modulation and the converted signal output (spiral microcoil or Hall-element) [1,2]. In dm and cm waveband there are usually used monocrystal ferrogarnet resonators with narrow resonance line (units of MHz). The FR is magnetized by the external magnetic system, being also used for the resonator

tuning in wide frequency range. Ferrogarnets are not used in mm waveband, because they need field of FR magnetization, increasing with the operating frequency, and thus the external magnets become too massive. But application of prospective hexagonal monocrystal ferrites with internal magnetic field of crystallographic anisotropy leads to the possibility of GC design for mm waveband without massive external magnets [2,4].

2. PRINCIPLE OF THE GYROMAGNETIC CONVERTER OPERATION

The principle of the GC operation is based on non-linear stable effects at ferromagnetic resonance (FMR) in the FR [5]. At the interaction of microwave field with the GC having modulated resonance frequency 'cross-multiplication' regime takes place. It means that at the harmonic input microwave signal the voltage in the output element (spiral microcoil or Hall-element) contains only harmonics of modulation and does not depend on the carrier of the input signal [3].

The modulation frequency Ω is rather low compared to the carrier of the microwave signal ω and comparable or even less than that of the FR relaxation at FMR (RF band). Modulation of the FR resonance frequency can be either 'field' (by modulation of the magnetization field) or 'angular' (by modulation of the uniaxial hexagonal ferrite angle of crystallographic magnetic axis orientation relatively to the constant magnetization field direction) [6].

The longitudinal component of any FR magnetization vector M_z is proportional to the sum of squares of the transversal components and is determined by the formula, generalized from that valid for the ferrogarnet with zero crystallographic field of magnetic anisotropy [7]:

$$M_z = M_s - A^2 \times \sum_{n=0}^{\infty} \Psi_n(a, p, q) \cos(n\Omega t - \varphi_n);$$

$$A^2 = \left(\frac{\omega_M^2 \cos \theta_M J_0(\Delta \theta_M) + b^2}{2M_s} \right) \left(\frac{h_{xm} + h_{ym}}{2\delta} \right)^2,$$

$$\delta = \omega_r (1 + N_t \chi_0 / \mu_0);$$

$$b = \omega_r \chi_0 / \mu_0$$

$$q = \omega_m / \Omega;$$

$$p = \Omega / \delta;$$

$$a = \frac{\omega - \omega_0}{\delta}.$$

$$\Psi_n = \sqrt{A_n^2 + B_n^2};$$

$$\varphi_n = \operatorname{arctg} \frac{B_n}{A_n},$$

where $A_n = \sum_{n=-\infty}^{+\infty} J_n(q) \frac{\cos \Delta \omega_n t + a_n \sin \Delta \omega_n t}{a_n^2 + 1}$,

$$B_n = \sum_{n=-\infty}^{+\infty} J_n(q) \frac{\sin \Delta \omega_n t - a_n \cos \Delta \omega_n t}{a_n^2 + 1},$$

$$a_n = \frac{\Delta \omega + n\Omega}{\delta}.$$

These formulae use the following notations: M_s is the saturation magnetization of the FR, $\omega_M = \mu_0 M_s$; $J_0(\Delta \theta_M)$ is Bessel function of the zero order of argument $\Delta \theta_M$, deviation of the FR angle of crystallographic axis orientation (for the uniaxial hexagonal ferrite resonator at 'angular' modulation of the resonance frequency); δ determines the half of the FR line width, ω_r is the ferrite relaxation frequency, χ_0 is the FR static susceptibility, N_t is the FR transversal demagnetization factor; h_{xm}, h_{ym} are the amplitudes of the transversal microwave magnetic field; p is the relative frequency of modulation; q is the normalized amplitude of modulation (with ω_m - amplitude of the FR resonance frequency modulation at either 'field' or 'angular' control), a is the relative detuning of the FR resonance frequency ω_0 from the carrier of the microwave signal ω .

Thus, in the vicinity of the FMR the longitudinal component of the FR magnetization vector contains the harmonics of the modulation frequency $\Psi_n(a, p, q)$, and so does the voltage in the output element (microcoil or Hall-element) $E_n(a, p, q)$. Each harmonic can be selected by the proper filter of the converted signal at intermediate frequency. The amplitude of the harmonic depends on the microwave signal and the FR parameters, as it is seen from the listed above formulae.

3. THE GYROMAGNETIC CONVERTER SELECTIVITY CURVE

The frequency-selective properties of the GC are characterized by its selectivity curve (SC). It is determined by the dependence of the output signal on the detuning of the FR central resonance frequency ω_0 from the signal carrier ω . As the second harmonic $\Psi_2(a)$ is the most intense one

with maximum at zero detuning, it is usually used in practice (the 1-st harmonic is not used, because it is necessary to separate the modulation signal and the converted signal in one output element, and when using the 2-nd or other harmonics special filter is applied). The SC has the form of this harmonic versus detuning, and it is similar to the second derivative of the resonance curve.

Optimum parameters of modulation (normalized amplitude of modulation $q = \omega_m / \Omega = 3.55$, relative modulation frequency $p = \Omega / \delta = 0.8$) [8], when the second harmonic is maximum $\Psi_2(0) = 0.32$ can be found, and the conversion coefficient of the GC is maximum, too. But at these parameters the SC has inhomogeneous shape with two side lobes. This is an unwanted situation for the signals determination and resolution when there are several signals with different intensities in the panorama view.

By choosing the modulation parameters ($q=1.6, p=1.8$), we can get rid of the inhomogeneities in the form of the SC on base of the second harmonic [9], but this is known to reduce the conversion coefficient and broaden the SC width, thus leading to worse resolution of the microwave signals.

On the other hand, for accurate measuring of the irradiation intensities it is necessary to obtain flat top of the SC. Then the impact of destabilizing factors on the FMR frequency is essentially less. But it is impossible to get flat top when using only the second harmonic at any modulation parameters.

The presented method of SC control makes it possible to form the needed shape of the SC for the mentioned above problems solution. This method is based on selecting several harmonics of modulation in the output voltage E_n and weighted summation of their square amplitudes with certain coefficients K_n [10]:

$$S(a) = \sum_{n=2}^N E_n^2 K_n,$$

where

$$E_n = np\Psi_n$$

The formula, convenient to the SC calculation is the following:

$$S(a) = (\Psi_2(a))^2 \pm (\Psi_3(a)R_3)^2 \pm \dots \pm (\Psi_n(a)R_n)^2$$

where

$$R_n = n\sqrt{|K_n|} / 2$$

Certain vector of the weight coefficients $\bar{R} = [1, R_3, R_4, \dots, R_n]$ corresponds to each SC, and its form can be optimized by choosing the proper coefficients at the most typical modulation parameters, corresponding to the maximum of the second harmonic, for example, $p=0.8, q=3.5$. If some harmonic is subtracted, corresponding coefficient is

written as R_i . The calculation results are represented on Fig.1-3.

Fig.1 shows the normalized SC $S(a)/S(0)$ at the summation of the squares of the 2-nd, 3-rd and 4-th harmonics with different coefficients. At $[R] = [1, 2, 5, 4, 0]$ we get the most "smooth" SC with the corresponding conversion coefficient twice as big as in the case of only the second harmonic at $p=1.8, q=1.6$ and 10 per cent more than at $p=0.8, q=3.5$. Summation of only 2-nd and 4-th harmonic squares, as well as of the 2-nd and 4-th doesn't lead to reduction of inhomogeneities. But optimization with

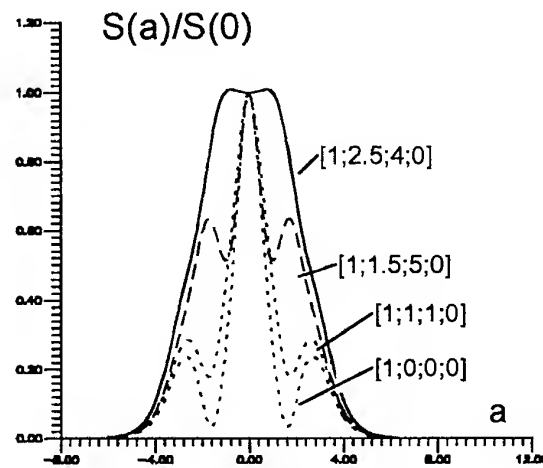


Fig.1

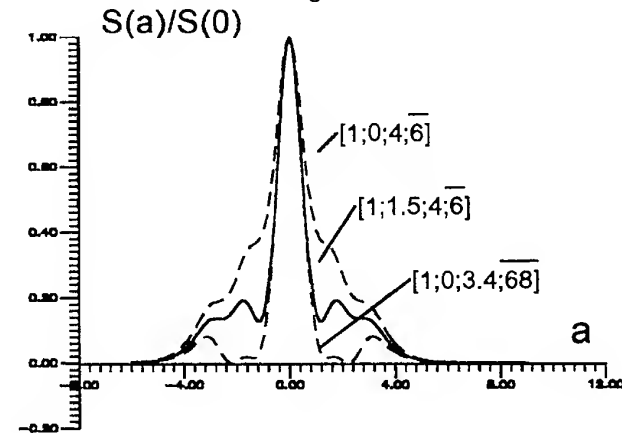


Fig.2

the 5-th harmonic at $[R] = [1,0,3,4,6,8]$ allows to minimize side lobes and lessen the SC width, too (Fig.2). Fig.3 represents for the comparison SC formed by various ways.

Thus, one-signal narrow SC, formed using the presented algorithm, leads to the better signal resolution, than the SC, formed only on base of the 2-nd harmonic.

The scheme of this method apparatus realization is shown in Fig.4. There are used the following notations: GC - gyromagnetic converter, M-modulator, F_i - filter of the i -th harmonic; K_i - multiplication coefficients; SD- square detectors; Σ - summator; SR-square root block.

Now let's consider two signals at frequencies ω_1, ω_2 with powers P_1, P_2 correspondingly. Fig.5,6 show signals resolution at different ways of SC formation (the signals are taken, for instance, equal in their amplitude). At the ordinary way with only the 2-nd harmonic it is difficult to identify two signals even at large difference their carriers (Fig.5). When the SC being wide and flat at the top we get uniqueness of signals determination and measurement of their intensities, but resolution is rather low (Fig.6). We can see good resolution of the signals due to the special form of the SC with $[R] = [1,0,4,6]$.

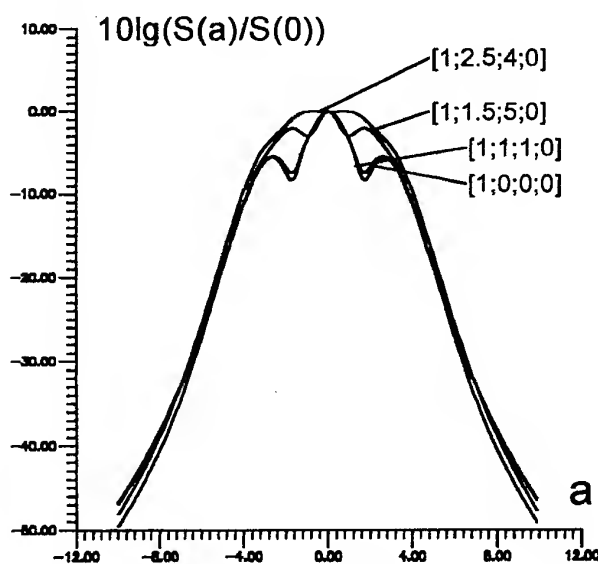


Fig.3

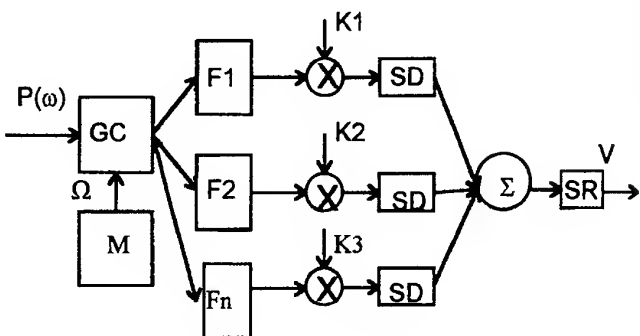


Fig.4

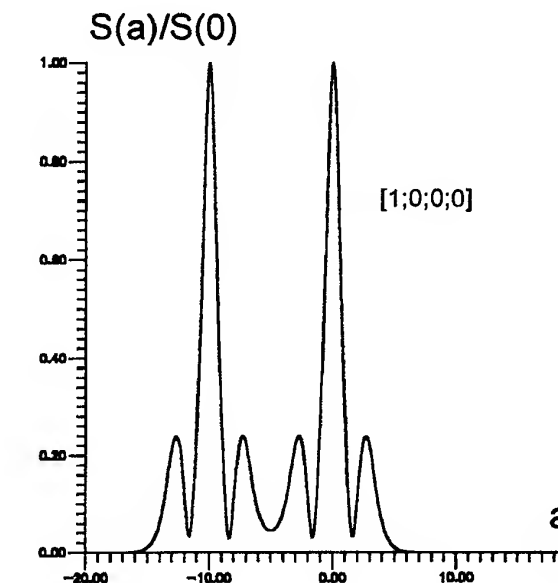


Fig.5

The presented method has an advantage: it doesn't demand high accuracy of the coefficients realization. The form of the SC doesn't essentially depend on the accuracy of the coefficients mounting (20 percent deviation is quite admissible), except $R_2=1$, which is satisfied in any case due to normalization.

CONCLUSION

Previous papers dealt with the GC selectivity curve optimization for getting maximum conversion coefficient at using only the second harmonic of the modulation frequency. This was done by choosing the proper modulation amplitude and frequency according to the resonance line of the FR in the GC. But the SC has inhomogeneities in the form of the side lobes in this case, and this leads to the

ambiguity of the signal determination. Changing the parameters of modulation, one can form the SC with small side lobes at the 2-nd harmonic, but this regime reduces the conversion coefficient and broadens the SC width.

The presented method of formation the necessary selectivity curve of the gyromagnetic converter used in microwave panorama frequency-selective measurers of power parameters is based on the summation of weighted harmonics of the GC ferrite resonator longitudinal magnetization component. The FR resonance frequency is modulated by the signal of intermediate radio frequency. The narrow SC without side lobes for the uniqueness of the signals determination and resolution in multi-frequency regime in the waveguide path can be formed, as well as wide SC with flat top for accurate measuring of the intensities of high-power radiation in order to reduce the influence of destabilizing factors on the FMR.

The presented method leads not only to the possibility of the SC shape control, but even to increasing the GC conversion coefficient.

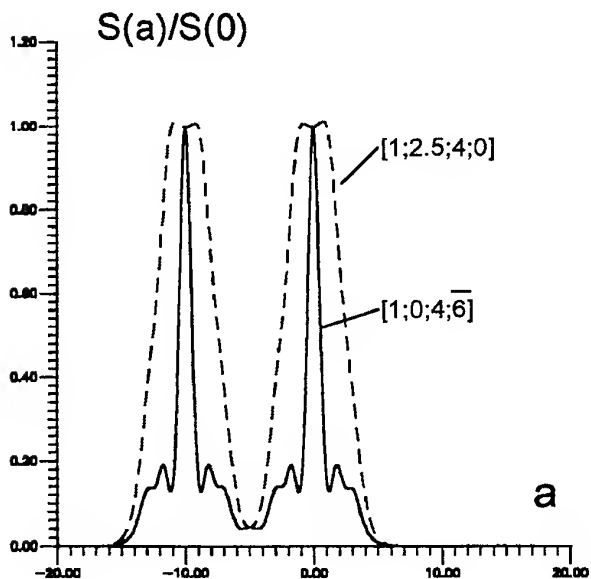


Fig.6

REFERENCES

- [1] Application of gyromagnetic effects in the ferrite monocrystals for electromagnetic signals parameters measurement (in Russian)/ Balakov V.F., Kartsev V.A. et al./ Proc. 5th Int. Conf. On Microwave Ferrites, ICMF'80. Moscow. V.3, p.86-99.

[2] Kitaytsev A.A., Koledintseva M.Yu. Prospective frequency-selective methods of power conversion in mm-waveband using hexagonal ferrites. Proc. 5th Int.

Symp. On the recent advances in microwave technology ISRAMT'95. Kiev. Ukraine, 11-16 Sept. 1995. V.1. P.71-74.

[3] Mikhailovsky L.K. Cross-modulation frequency conversion on the ferrite// "Physical properties of the ferrite". Minsk: "Nauka i Technika". 1967, p. 235-241.

[4] Elaboration, research and application of monocrystal hexagonal ferrites - novel microwave materials (in Russian)/ Medvedev S.A., Pollak B.P. et al./ Reports of the Conference on the results of the research work in 1968-1969. Radioengineering Section. Ferrite Microwave Radiophysics. Moscow. 1969, p.80-89.

[5] Koledintseva M.Yu., Kitaytsev A.A. Application of stable non-linear resonance effects in monocrystal hexagonal ferrites for electromagnetic compatibility problems solution. Proc. ICCSE'97. Moscow. 1997. P. 141-153.

[6] Kitaytsev A.A., Koledintseva M.Yu. Interaction between mm-wave oscillations and monocrystal hexagonal ferrites with modulated resonance frequency. 6th Int. Conf. "Mathematical methods in electromagnetic theory" MMET'96, Sept.10-13. 1996. Lviv. Ukraine, p.88-91.

[7] Kitaytsev A.A., Savchenko N.I. Characteristics of monocrystal ferrite ellipsoid at alternating magnetization. Proc. 2 Int. Conf. On Microwave Ferrites ICMF'74, Zuhl, GDR. 1974. P.205-213.

[8]. Kitaytsev A.A., Savchenko N.I. Influence of the external magnetic field variation velocity on the oscillation of the longitudinal magnetization component of the ferrite at the FMR (in Russian) // Proceedings of the Conference of electronic engineering. 1969. Issue 25. P.77-79.

[9]. Savchenko N.I. Frequency-selective properties of the gyromagnetic frequency cross-multiplier of electromagnetic oscillations (in Russian) // Moscow Power Engineering Institute Transactions No 437. Moscow. MPEI.1979, p.29-33.

[10] Adouevsky I.A., Balakov V.F., Kitaytsev A.A., Koledintseva M.Yu. Method of frequency-selective peak power measuring at microwaves.//Author Certificate of the USSR No 1800377, priority 24.04.90.

CALCULATION OF FIELDS IN A COAXIAL CHAMBER WITH TWO SPIRAL CONDUCTORS

B. M. Levin, V. G. Markov

Svyazmorprojekt Design Office, 14, M. Morskaya ul., St. Petersburg, 190000, Russia

A coaxial chamber for calibration of magnetic field strength meters in a conducting medium is considered. Its central conductor is built of two spiral wires with opposite winding directions, while the meter is installed inside a tank with a conducting liquid placed within the space contained by the spiral.

The wave propagation constant in the chamber and the wave impedance of an equivalent long line are determined. The capacitance between the spiral conductors placed on the dielectric cylinder (a tank with a conducting liquid) with the permittivity different than that of the air is calculated.

1. INTRODUCTION

As shown in [1], the results of the electromagnetic field measurements in conducting media are dependent on the medium conductivity, that is, a preliminary calibration of meters is necessary. An efficient way to calibrate meters is to place them in coaxial chambers [2].

The chamber (Fig. 1a) is a segment 1 of a coaxial line of an increased size where a transverse electromagnetic wave is established. The conic junctions 2 at the line ends provide for the output to standard coaxial connectors, one of which (input 3) is connected to the oscillator 4 and the other (output 5) – to the matching

load 6. The coaxial line and the conic junctions are built so that the wave impedance would be unchanged.

The meter 7 under calibration is placed inside the chamber. The signal from the meter is fed through the preamplifier 8 and the communication link 9 to the recording device 10.

Of the most complex design is the coaxial chamber for calibration of magnetic field strength meters in a conducting medium (Fig. 1b). Its central conductor is a cylindrical spiral, while the meter is installed inside a tank 11 with a conducting liquid placed within the space contained by the spiral. In order to remove the spurious radial component of the magnetic field, which corrupts the measurement results, the central conductor of the chamber should be built of two spiral wires 12 and 13 with opposite winding directions, one of them being connected to the oscillator via a phase inverter 14 changing the phase of the current by π .

The traveling wave in a line which is equivalent to a coaxial chamber takes place only if the line is homogeneous and the matching load at its end is equal to the wave impedance of the line. The introduction of a tank with a conducting liquid into the chamber causes the wave impedance of the line to be frequency dependent. A similar effect is produced by the self-capacitance of the spiral wire. This makes it necessary to adjust the matching load of the coaxial chamber with changing frequency, and, theretofore, to calculate the fields inside the chamber and the chamber parameters.

2. A CHAMBER WITH TWO SPIRAL WIRES

The equivalent circuit of a chamber with two spiral wires excited in anti-phase is given in Fig. 2. It is an unsymmetrical line of two wires situated above the ground (external sheath). However, as distinct from electrically connected lines (their theory has been resolved by A. A. Pistolkors [3]), in this case, additional per-unit-length impedance $jQ = Z_1 Z_2 / [2\pi a_1 (Z_1 + Z_2)]$, which is due to the surface impedance, is connected in each wire. Here Z_1 is the surface impedance of a spiral wire, Z_2 is that of the conducting liquid, a_1 is the spiral radius.

Impedance Z_1 is introduced as follows. The outside surface of the spiral is mentally metallized and turned

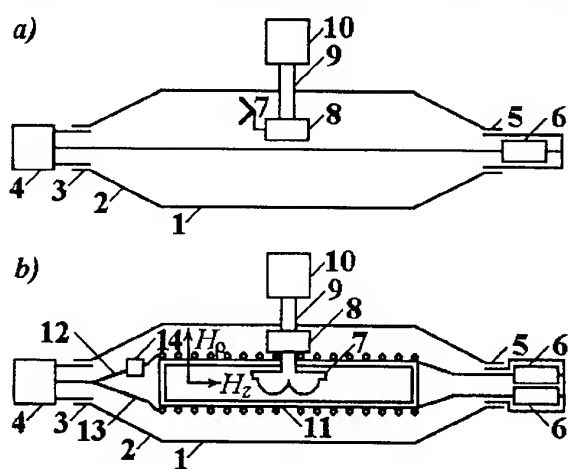


Fig. 1. Coaxial chambers for meter calibration
(a) for the electric field in the air;
(b) for the magnetic field in a conducting liquid

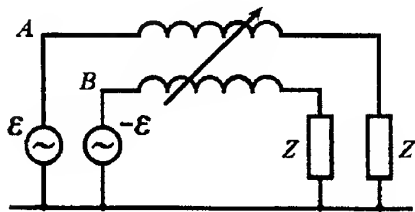


Fig. 2. Equivalent circuit of a chamber with two spiral wires

into a cylindrical wire of radius a_1 . To account for the effect of the wave deceleration along it, a per-unit-length impedance, assumed to be purely reactive (without regard to losses in the spiral wire), is connected in the resulting wire. At lower frequencies the impedance is inductive in its behavior: the surface impedance of a spiral wire is $Z_1 = j2\pi a_1 \omega L_1$ where ω is the circular frequency, $L_1 = \pi \mu_0 w^2 a_1^2 K_a / L^2$ is the per-unit-length inductance of the spiral, μ_0 is the magnetic permeability of free space, w is the number of turns, L is the length of the winding, K_a is a factor which equals one for $a_1 \ll L$ and decreases smoothly with growing a_1/L [4].

As frequency increases, the self-capacitance of the spiral starts to have an effect, i. e. the spiral behaves as a parallel circuit with resonant circular frequency ω_0 :

$$Z_1 = j2\pi a_1 \omega L_1 / [1 - (\omega/\omega_0)^2].$$

If a tank with a conducting liquid is placed within the space contained by the spiral, this is tantamount to the connection of an additional surface impedance Z_2 in the wire, the former is parallel to impedance Z_1 and equals $Z_2 = k_1 J_0(k_1 a_1) / [\sigma_1 J_1(k_1 a_1)]$ where k_1 is the wave propagation constant in the conducting liquid, σ_1 is the specific conductivity of the liquid. The tank radius is assumed to be the same as the spiral radius.

As shown in [5], the system of two wires, having different surface impedances and located above ground, exhibits two different propagation constants. In the particular case of identical wires with the same surface impedance, regardless of boundary conditions (at the ends of the line), the components of currents and voltages with propagation constant k_c are the same in both wires (cophasal wave), while the components with propagation constant k_a are the same in magnitude and opposite in sign (anti-phase wave). Here

$$k_c = [k_2^2 + \omega Q(\beta_{11} + \beta_{12})]^{1/2}, k_a = [k_2^2 + \omega Q(\beta_{11} - \beta_{12})]^{1/2},$$

where k_2 is the wave propagation constant in the medium between the spiral wires and the external sheath, and β_{11} and β_{12} are the factors of electrostatic induction, the self-induction one (for each of the wires) and the mutual one (between the wires), respectively.

In the circuit in Fig. 2, two spiral conductors are excited by two voltages which are the same in magnitude and opposite in sign, i. e. there is only the anti-phase wave, and impedance Z_{AB} at points AB is the

input impedance of a two-wire line with the propagation constant k_a and wave impedance

$$W_a = 2k_a / [\omega(\beta_{11} - \beta_{12})].$$

By converting from the electrostatic induction factors to partial capacitances C_{ik} , we get:

$$k_a = [k_2^2 + \omega Q(C_{11} + 2C_{12})]^{1/2}, W_a = k_a / [\omega(C_{12} + C_{11}/2)].$$

Here, quantity C_{12} is the mutual per-unit-length capacitance between the wires and C_{11} is that between each wire and the ground (external sheath). For the traveling wave mode to take place in a line of two wires, the load impedance $2Z$ of the latter must equal wave impedance W_a .

As seen from the formulas given, to calculate the wave impedance and propagation constant of a long line, one has to know the values of capacitances C_{11} and C_{12} . Capacitance C_{11} is calculated simply enough. With a close winding, it is the per-unit-length capacitance between coaxial circular cylinders with radii equal to those of the shield and of the winding. With a sparse winding, it is the per-unit-length capacitance of an equivalent straight wire to a plane at a distance, equal to the difference of the shield and spiral radii, from it.

The problem of calculation of capacitance C_{12} breaks down in two. The first one is to calculate the capacitance between the wires located in a homogeneous medium (the air). This has an importance of its own, since its solution is needed to calibrate magnetic field strength meters in the air, and to establish relevant basic standards (coaxial chambers).

The second problem is to take account of the medium inhomogeneity, since inside the spirals there is, in actual fact, a dielectric cylinder (the tank with a conducting medium) with the permittivity different than that of the air. In addition, the problem becomes more involved if the wires are raised above the media interface, the surface of the dielectric cylinder.

3. CAPACITANCE BETWEEN THE WIRES OF A DOUBLE-START SPIRAL

The first problem is solved by the method of average potentials (to be more precise, Howe's method [6, 7]). The linear charge density τ of the spiral wire is assumed to be the same along its length: $\tau = q/l$, where q is the total charge of each wire, l is its length. The wire diameter $2a$ is small as compared to the transversal and longitudinal dimensions of the spiral. As the system consists of two identical wires, their charges adding up to zero, the capacitance between the wires coincides with the partial capacitance

$$C_l = 1 / [2(\alpha_{11} - \alpha_{12})]. \quad (1)$$

Here α_{11} and α_{12} are the self-potential and mutual potential coefficients of wires, respectively.

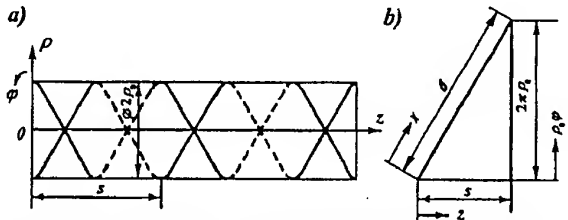


Fig. 3. (a) Double-start cylindrical spiral with opposed windings and (b) developed view of its one turn

We shall use a cylindrical coordinate system (ρ, ϕ, z) with z axis along the spiral axis and point O in the plane passing through the starting points of wires (Fig. 3a). We let x denote the coordinate measured along the wire. Then, in an arbitrary point of the spiral wire, we have $x = (z^2 + \rho_0^2 \phi^2)^{1/2}$ where ρ_0 is the radius of the cylindrical surface, around which the spiral is wound, and ϕ is the total rotation angle from the starting point of a wire to the point with coordinate z .

Fig. 3b shows the developed view of the first turn of a spiral wire. As seen from the figure, $z/x = s/b$, $\rho_0 \phi / x = 2\pi \rho_0 / b$, where s is the spiral lead and $b = [s^2 + (2\pi \rho_0)^2]^{1/2}$. Hence,

$$x = zb/s, \phi = 2\pi x/b. \quad (2)$$

If L is the spiral length, the length of each spiral wire is $l = Lb/s$.

The potential at point M with coordinates (ρ_0, ϕ', z') , created by charge τdx of wire element dx , is

$$dU_M = \tau dx / (4\pi\epsilon_0 R_1)$$

where ϵ_0 is the dielectric permittivity of free space and R_1 is the distance from point M to element dx with coordinates (ρ_0, ϕ, z) . To simplify, potential is assumed to be determined by a filamentary charge situated on the wire axis, that is,

$$\begin{aligned} R_1 &= \{(z - z')^2 + [2\rho_0 \sin(\phi - \phi')/2]^2 + a^2\}^{1/2} \\ &= (s/b)\{(x - x')^2 + [(2\rho_0 b/s) \sin\pi(x - x')/2]^2 + (ab/s)^2\}^{1/2} \end{aligned} \quad (3)$$

The total potential of entire charge q at point M is

$$U_M(x') = \frac{q}{4\pi\epsilon_0 l} \int_0^l \frac{dx}{R_1}.$$

Taking its average over the wire length,

$$U_{11} = \frac{1}{l} \int_0^l U_M(x') dx'.$$

we find self-potential coefficient α_{11} :

$$\alpha_{11} = \frac{1}{q} U_{11} = \frac{1}{4\pi\epsilon_0 l^2} \int_0^l dx' \int_0^l \frac{dx}{R_1}. \quad (4)$$

Calculating α_{12} , one should take into account that the spiral wires are wound in opposite directions. Besides, their ends in the starting cross-section are shifted

round the periphery of the section by π relative to each other. Therefore, if Eqs. (2) are valid for one wire, we have for another one (at observation point M): $x' = z'b/s$, $\phi' = \pi - 2\pi x'/b$. Accordingly, for distance R_2 from point M to element dx we get, instead of Eq. (3):

$$R_2 = (s/b)\{(x - x')^2 + [(2\rho_0 b/s) \cos\pi(x + x')/b]^2 + (ab/s)^2\}^{1/2}.$$

Calculating the total potential of entire charge q of the next wire at point M and taking its average over the wire at hand, we find:

$$\alpha_{12} = \frac{1}{4\pi\epsilon_0 l^2} \int_0^l dx' \int_0^l \frac{dx}{R_2}. \quad (5)$$

Integrals (4) and (5) are not expressible in terms of elementary functions, since the radicands in their integrands involve, along with $(x - x')^2$, the squares of trigonometric functions with arguments also dependent on x and x' . Therefore, they can be found only numerically.

Here the double integral (4) can be reduced to a single one. Denote

$$\begin{aligned} A &= 1/(4\pi\epsilon_0 L), \\ f(t) &= \{t^2 + [(2\rho_0 b/s) \sin\pi t/b]^2 + (ab/s)^2\}^{-1/2}. \end{aligned}$$

$$\text{Then we have } \alpha_{11} = A \int_0^l dx' \int_0^l f(x - x') dx'.$$

As the function $f(t)$ has even symmetry in argument t and the domain of integration is a square of side l , so

$$\alpha_{11} = 2A \int_0^l dx' \int_0^{x'} f(t) dt.$$

By changing the order of integration, we find:

$$\alpha_{11} = 2A \int_0^l f(t) dt \int_t^l dx' = 2A \int_0^l (l - t) f(t) dt. \quad (6)$$

If the wire radius is small, then, when $t \rightarrow 0$ ($x \rightarrow x'$), the integrand in expression (4) grows sharply, making numerical integration difficult. The reduction of the double integral to a single one simplifies the calculations considerably.

As an alternative to the numerical technique, an approximate technique can be suggested, which is based on the capacitance between wires being due to their multiple crossing each other, i.e. being equal to the sum of capacitances of intersection nodes. We represent an intersection node as two wire segments at angle γ to one another and of length $l_0 = l/2w$ where w is the number of spiral turns. To simplify, the segments are assumed to be straight lines. Then

$$C_l = 2w C_{10}^{(n)} \quad (7)$$

where $C_{10}^{(n)}$ is the capacitance between two intersecting wires of the n -th node.

Similar to Eq. (1),

$$C_{10}^{(n)} = 1/[2(\alpha_{11}^{(n)} - \alpha_{12}^{(n)})] \quad (8)$$

where $\alpha_{11}^{(n)}$ and $\alpha_{12}^{(n)}$ are the self-potential and mutual potential coefficients of the n -th node wires, respectively.

If radii a of the wires are small as compared to their lengths l_0 , then

$$\alpha_{11}^{(n)} = \frac{1}{2\pi\epsilon_0 l_0} [\ln(2l_0/a) - 1]. \quad (9)$$

The value of $\alpha_{12}^{(n)}$ is found by calculating the potentials at points of the left and right segments of one of the wires and taking the average of the potentials over the entire wire length:

$$\alpha_{12}^{(n)} = \frac{1}{2\pi\epsilon_0 l_0} [\operatorname{arcsinh}(\tan \gamma/2) + \operatorname{arcsinh}(\cot \gamma/2)] \quad (10)$$

From Eqs. (7)-(10), it follows that

$$C_l = \pi\epsilon_0 / [\ln(l/aw) - 1 - \operatorname{arcsinh}(\tan \gamma/2) - \operatorname{arcsinh}(\cot \gamma/2)]^{-1} \quad (11)$$

Here, as is easily seen, $w = l/s$, $\tan \gamma/2 = 2\pi\rho_0/s$.

Fig. 4 shows the results of computation and measurement of the capacitance between the wires of spiral with parameters (in m): $L = 0.32$; $2a = 1.5 \cdot 10^{-3}$, $\rho_0 = 0.045$ – for different numbers of turns w . Curve 1 is obtained by the numeric technique in accordance with Eqs. (1), (5) and (6); curve 2 – by the approximate technique in accordance with Eq. (11). The measured values are given by circles. As seen from the figure, both computational techniques yield close results (a difference from 2 to 4 %) in good agreement with the experiment, which is an evidence of applicability of the approximate technique to calculation of the capacitance between the wires of a spiral.

The technique accuracy decreases with growing wire diameter.

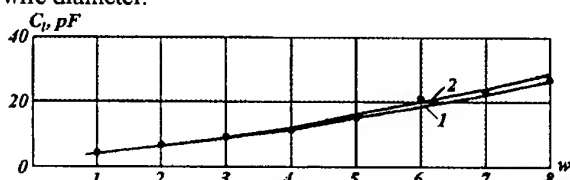


Fig. 4. Spiral capacitance against the number of turns

4. THE EFFECT OF MEDIUM INHOMOGENEITY

Underlying the solution of the second problem in the calculation of capacitance C_{12} is the fact that the electrostatic field of a system of arbitrarily shaped wires located in a piecewise homogeneous medium coincides with the one in a homogeneous medium, provided the invariance condition holds, i. e. the media interfaces coincide with the surfaces of equal field strength in the homogeneous medium and with the wire surfaces [8, 9]. Accordingly, for the capacitance between two wires in a piecewise homogeneous medium, we get

$$C_l = \sum_{n=1}^N \frac{\epsilon_n}{\epsilon_0} C_{n0} \text{ where } n \text{ is the medium number, } N \text{ is the count of media; } \epsilon_n \text{ is the dielectric permittivity of the } n\text{-th medium; } C_{n0} \text{ is the capacitance between the wire segments adjoining the } n\text{-th medium, if the wires are located in a homogeneous medium with dielectric permittivity } \epsilon_0.$$

This means that, when calculating the capacitance between two wires, dielectric permittivity ϵ_0 of a homogeneous medium is to be replaced with equivalent permittivity ϵ_{eq} which is equal to $\epsilon_{eq} = \frac{1}{2\pi} \sum_{n=1}^N \epsilon_n \Delta\phi_n$, where $\Delta\phi_n$ is the length of the arc of wire circumference adjoining the n -th medium. For a line of two wires along the generatrices of a circular dielectric cylinder, the invariance condition holds, the angular width of both media adjoining each wire is equal to π , i. e. the capacitance in a piecewise homogeneous medium equals a half-sum of values of capacitances between the same wires in homogeneous media. Since this is valid for any length of an arc between generatrices, this is also valid for spiral wires, i. e. the quantity $\epsilon_{eq} = (\epsilon_1 + \epsilon_2)/2$ is to be substituted for ϵ in the expressions for α_{11} and α_{12} , ϵ_1 and ϵ_2 being the dielectric permittivities of the ambient space and the dielectric cylinder (the tank with a conducting medium), respectively.

If the wires are raised above the media interface, this result needs to be refined. Making use of the known expression for the capacitance per unit length of a line of two wires located in a dielectric near the cylindrical interface of two media [6], and assuming the distance h between each wire axis and the interface to be small (on the order of radius a of a wire), we get

$$\epsilon_{eq}(R) = \epsilon_1 [1 + k \ln(R/2h)/\operatorname{Arccosh}(R/a)]^{-1}.$$

Here $k = (\epsilon_1 - \epsilon_2)/(\epsilon_1 + \epsilon_2)$; ϵ_1 is the dielectric permittivity of the medium the wires are located in, ϵ_2 is the permittivity of the dielectric cylinder, and R is the distance between the wire segments. Then, for the self-potential coefficient we get, instead of Eq. (4),

$$\alpha_{11} = \frac{1}{4\pi l^2} \int_a^l dx' \int_a^l \frac{dx}{\epsilon_{eq}(R_1) R_1},$$

or, having reduced the double integral to a single one,

$$\alpha_{11} = \frac{1}{4\pi L l} \int_a^l \frac{(l-t)}{\epsilon_{eq}(sR_1/b) R_1} dt \quad (12)$$

where $R_1 = \sqrt{t^2 + [(2\rho_0 b/s) \sin \pi t/b]^2 + (ab/s)^2}$.

The lower integration limit in above expressions is taken to be a , which allows to get rid of the physically nonsensical singularity due to the second term of the integrand.

Accordingly, for the mutual potential coefficient we get, instead of Eq. (5),

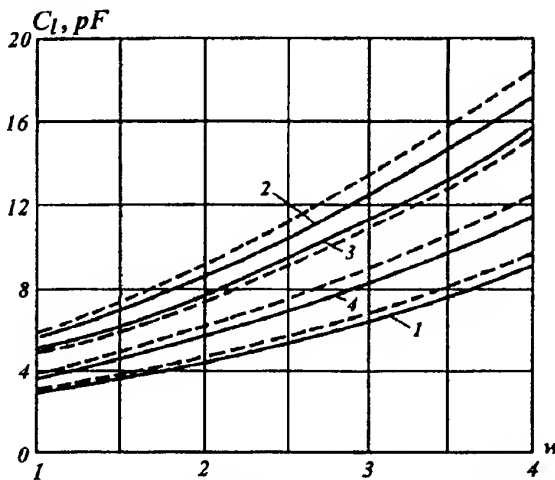


Fig. 5. Capacitance of a spiral wound around a dielectric cylinder

$$\alpha_{12} = \frac{1}{4\pi l^2} \int_a^l dx' \int_a^l \frac{dx}{\epsilon_{eq}(R_2)R_2}. \quad (13)$$

The value of C_l is found, as usual, from Eq. (1).

Fig. 5 shows the results of computation of capacitance C_l between the wires spiral with parameters (in m): $L = 0.3$; $2a = 1.8 \cdot 10^{-3}$; $\rho = 0.03$ – for different numbers of turns w . Solid curves are obtained in accordance with Eqs. (1), (12) and (13). Curve 1 is plotted for a spiral located in free space, curve 2 – for a spiral wound around a cylinder with relative dielectric permittivity $\epsilon_r = 2.8$ (wire axes coincide with the media interface) and curves 3 and 4 – for wires raised above the interface at height $h = 0.75 \cdot 10^{-3}$ and $2.25 \cdot 10^{-3}$, respectively.

Described above was the approximate technique of calculation of the capacitance between coaxial cylindrical spirals located in the air, which is based on the capacitance being equal to the sum of capacitances of intersection nodes. To get an approximate estimate of the capacitance between spirals raised above the cylindrical interface, the said capacitance should be increased $\epsilon_1/(1 + Bk)$ times where

$$B = 1 - \ln(4h/a)/\ln(4\rho\sqrt{a}).$$

The results of such estimation are given in Fig. 5 by dash lines.

The frequency dependencies of the propagation constant and wave impedance of the chamber for calibration of the magnetic field meters in conducting liquid are given in [1].

5. CONCLUSION

A coaxial chamber can be efficiently used for the calibration of field strength meters in conducting media. The proposed technique allows to calculate the

parameters of such chambers.

6. REFERENCES

- 6.1. V. G. Markov, B. M. Levin, "Measurement of the HF Electromagnetic Field in Conducting Media", Proceedings of the 13th Symposium on Electromagnetic Compatibility, Wroclaw, Poland, 25-28.06.1996, pp. 375-379.
- 6.2. M. Kanda *et al.*, "Standards for Electromagnetic Field Measurements", Proceedings of the IEEE, Vol. 74, No. 1, 1986, pp. 120-128.
- 6.3. A. A. Pistolkors, "Antennas" (Russian), Svyazizdat, Moscow, 1947, ch. 2, pp. 59-68.
- 6.4. P. L. Kalantarov, L. A. Cheitlin, "Calculation of Inductances" (Russian), Energoizdat, Leningrad, 1986, ch. 6, pp. 247-253.
- 6.5. B. M. Levin, "Impedance Folded Dipole" (Russian), Antennas, No. 23, 1976, pp. 80-90.
- 6.6. Yu. Ya. IosseI, E. S. Kochanov, M. G. Strunsky, "Calculation of Electrical Capacitance" (Russian), Energoizdat, Leningrad, 1981, ch. 1, 8, pp. 24-31, 257-261.
- 6.7. G. W. O. Howe, "The Capacity of Rectangular Plates and a Suggested Formula for the Capacity of Aerials", The Radio Review, Dublin, 1919-1920, Vol. 1.
- 6.8. Yu. A. Bakhvalov, L. A. Panyukov, "Invariance Condition for Static Fields Strength in Piecewise-homogeneous Media" (Russian), Izvestiya Vuzov SSSR/ Electromekhanika, No. 4, 1982, pp. 408-410.
- 6.9. B. M. Levin, V. G. Markov, "The Method of Complex Potential and Antennas" (Russian), Sudovaja Elektrotehnika i Svyaz, 1997, ch. 2, pp. 9-16.

BIOGRAPHICAL NOTES



Levin Boris Mironovich is an engineer of Svyazmorprojekt Design Office, a graduate of Leningrad Polytechnic Institute (1960). Candidate of Technical Sciences since 1969. Doctor of Physical and Mathematical Sciences since 1993. The field of scientific interest is the vibrator antennas and technical electrodynamics.



Markov Vladimir Glebovich is an engineer of Svyazmorprojekt Design Office, a graduate of Leningrad Institute of Electrical Engineering (1974), specializes in antenna measurements in conducting media.

MEASURING SENSORS FOR INVESTIGATION OF MAGNETIC FIELD ON THE BOARDS OF SPACE APPARATUSES

Vitalij Nichoga, Petro Dub

Karpenko Physico-Mechanical Institute of National Academy of Sciences of Ukraine
5 Naukova str., Lviv, 290601, Ukraine

The paper is devoted to manufacturing of high sensitive sensors for investigation of magnetic fields in space and for control of electromagnetic compatibility in the modules of space stations. The basic requirements to such sensors are formulated and the ways of their realization are examined. Technical parameters of the elaborated series of "Kaskad" and "Ekran" inductive sensors are considered. Some results of magnetic field measurements are presented.

1. INTRODUCTION

When carrying out modern electronic devices it is necessary to guarantee low level of interference created by these devices to satisfy the requirements of electromagnetic compatibility with other apparatuses. This question is especially actual when these interference can improve on human organism either directly or as the result of functioning disturbances of electronic apparatuses and personal computers under influence of other devices radiation. During the manned flights on the space stations it is necessary to carry out the regular biophysical and hygienic estimations of spectral composition levels and to measure temporal characteristics and spatial distribution of low-frequency interference magnetic field in the inhabited modules of the station. Besides, diagnostics of electromagnetic field created by orbital complex on-board systems must be carried out for the crew and Earth services to obtain some additional information about these systems state and functioning. Such investigations permit to make operatively structural alterations in devices when interference exceeds permissible level. Successful realization of these investigations is possible only in the case when magnetic field sensors (MFS) with sufficiently low threshold are used for level measuring and spatial distribution definition of magnetic fields. This paper is devoted to designing of such sensors, which can also be used for measuring outer natural fields when carrying out scientific experiments on the boards of rockets, satellites and orbital stations.

2. BASIC REQUIREMENTS TO MAGNETIC FIELD SENSORS

MFS is a principal part of the whole data-measuring system for magnetic fields investigation. This device is also responsible for its quality.

The basic requirements to the MFS for such investigations are as follows: linear and high-accuracy conversion of the measured magnetic field, high sensitivity, wide-band performance, maximum information content, adequate speed of response, high temperature and time stability, quick availability for service, wide dynamic range, simplicity of service and exploitation, high spatial resolution, short recovery period after high pulse overloads, high reliability in severe mechanical and environmental conditions, low mass and small dimensions, low energy consumption. Additional requirements to amplitude-frequency (AFC) and phase-frequency (PFC) characteristics are formulated if minimal distortions of interference are needed.

It is only natural, that all above requirements are not to be satisfied in every designed sensor. By contrast the task is to rationally use relevant characteristics at the expense of some others. Practical implementation of these requirements is an important stage in the MFS development and design. It should be noted, that the idea that implementation of some requirements to the MFS is not very important since it can be changed for optimization of secondary converters following the MFS (i.e. amplifiers, filters and processing devices) is basically incorrect.

It is necessary to consider more carefully the above mentioned requirements. We preferred inductive sensors (IS) of magnetic fields in our investigations and manufacturing. It is caused by low level of most of electronic devices "parasite" radiation. Their fields are low-impedance magnetic in the nearness of majority of investigated devices, i.e. such field energy is concentrated mainly in magnetic components. That is why the investigations of such apparatuses are

necessary to carry out with IS, which have some advantages as it was mentioned above.

It is preferably to use IS for measuring the magnetic fields for mentioned above purposes in frequency band 1 Hz÷30 MHz. Out of this band the sensors based on other physical principles must be used, for example short electrical sensors. IS are elaborated in most cases as winding on the permalloy or high permeability ferrite core for low frequency and low permeability ferrite for high frequency. Sometimes the IS as air frames are used.

It is necessary to have constant ("flat") AFC and linear PFC of IS in needed band for signals transformation without distortion. In particularly phase shifts, which are approximately equal to zero, are often used. The requirements to PFC are often very hard to realize. But during definition of interference level the peak, quasi-peak and root-mean-square magnitudes are measured. The PFC form have not sufficient importance in such cases. Sometimes, especially in lower part of the band, it is necessary to use linear AFC. Non-ideal frequency characteristics can be corrected with the help of additional devices.

We shall now consider the basic requirements to sensors for electromagnetic compatibility control in frequency band 1 Hz÷150 kHz.

We can make on the base of analyzed literature the conclusion that magnetic field threshold must be equal (with some reserve) to $1 \text{ nT}\cdot\text{Hz}^{-0.5}$ ($\sim 10^3 \text{ A}\cdot\text{m}^{-1}$) in band $1+10 \text{ Hz}$, $10^1+10^2 \text{ nT}\cdot\text{Hz}^{-0.5}$ ($\sim 10^4+10^5 \text{ A}\cdot\text{m}^{-1}$) in band $10+10^3 \text{ Hz}$ and $10^2+10^3 \text{ nT}\cdot\text{Hz}^{-0.5}$ ($\sim 10^5+10^6 \text{ A}\cdot\text{m}^{-1}$) in band $10^3+1,5\cdot10^5 \text{ Hz}$. Lower magnitudes of IS discrimination threshold are not of great interest on the electromagnetic compatibility point of view. Dynamic range, which is needed for magnetic interference levels measuring, is equal approximately to $100+120 \text{ dB}$. This range is in practice defined by dynamic range of pre-amplifier (PA) because sensor range is not limited. But it should be mentioned that the phenomenon of sufficient delay of transient processes can arise when very strong magnetic field impulse influence on sensors with ferromagnetic core.

Study of spatial distribution of magnetic field interference is possible if IS dimension are comparatively small. To our mind length of IS with ferromagnetic cores should not exceed $200+400 \text{ mm}$ and their diameters should not exceed $10+40 \text{ mm}$. Mass within $300+800 \text{ g}$ and energy consumption less than $0,25 \text{ W}$ are desirable (for one component sensor).

The definite directional diagram is needed to carry out component measuring, for example in the form of figure 8. Such diagram is easily realized for IS.

It is necessary also to take into consideration the problem of high stability of sensitivity, especially in the case of temperature changes.

3. SOME CALCULATION EXPRESSIONS FOR DETERMINATION OF INDUCTIVE SENSORS PARAMETERS

The choice of IS constructive parameters is determined first of all by necessity of maximum frequency band and low discrimination threshold. These requirements are often contradictory and must be considered more carefully.

Flat AFC can be realized by application of shunt. In this case IS hasn't PA and is named passive IS. Also the voltage or field negative feedback (NF) is often used to enlarge the flatness band of AFC. Field feedback have advantages as for discrimination threshold and possibility of enlarging flatness band at the low frequencies. This variant of IS is used with PA and is named active IS

Let's consider IS with field NF. In presented below formulae ω - field frequency, μ - core magnetic permeability, w - turn number, S - core section area, L, C, r - inductance, conductivity, pure resistance of IS, R_a, C_a - input impedance of PA, K_u - coefficient of amplification, e_c - electromotive force of IS, w_{bf}, L_{bf}, R_{bf} - turn number, inductance, pure resistance of feedback network, e_n, e_n, i_n, e_{nbf} - noise sources. All these parameters are the complicated functions of IS constructive parameters (core dimensions, turn number wire diameter and others). If correlation between noise sources are disregarded and $\omega L_{bf} \ll R_{bf}$ the following expressions for sensitivity G and discrimination threshold B_m can be obtained [1,3]:

$$G = \omega \mu w S K_u \left[\left(1 + \frac{r}{R_a} - \omega^2 L(C + C_0) \right)^2 + \omega^2 \left[\frac{L}{R_a} + r(C + C_a) + \frac{L K_u W_{bf}}{w R_{bf}} \right]^2 \right]^{-\frac{1}{2}}, \quad (1)$$

$$B_m = \frac{1}{\omega \mu w S} \left\{ 4kT \left(r + \frac{\omega^2 L^2 W_{bf}^2}{w^2 R_{bf}} \right) + i_n^2 (r^2 + \omega^2 L^2) + e_n^2 \left[(1 - \omega^2 LC)^2 + \omega^2 C^2 r^2 \right] \right\}^{\frac{1}{2}}. \quad (2)$$

IS parameters are chosen to minimize both B_m and deflection of $G(\omega)$ from its maximum

$$G_{\max} = \frac{\mu w^2 S R_{bf}}{L W_{bf}}. \quad (3)$$

Some compromises have to be done if requirements to AFC and B_m can not be realized with limited mass and dimensions. For example, linear AFC is used sometimes in lower part of frequency operating band, where

$$G = \omega \mu \nu S K \frac{R_a}{r + R_a}. \quad (4)$$

4. EXAMPLES OF MAGNETIC FIELD SENSORS FOR ON-BOARD INVESTIGATION

We have elaborated two series of IS ("Ekran" and "Kaskad") for space apparatuses and orbital stations.

"Ekran" series of IS [9] are active inductive sensors which include integrated preamplifier. These IS are intended for application out of space apparatuses. Theoretical estimation showed that it is rather hard to ensure required value of discrimination threshold by one sensor within the whole frequency band ($1\text{--}10^5$ Hz) and to realize at the same time the necessary form of AFC. That is why we had to use IS with combined AFC: linear at the beginning of operating range and then - flat (frequency independent).

In "Ekran-1" sensor, which is intended for work in band $1\text{--}30000$ Hz, linear part of AFC is disposed within band $1\text{--}3000$ Hz and flat - within $3\text{--}30$ kHz. Linear part of AFC has frequency proportional sensitivity G , which equals $3.86 \cdot 10^5 f V \cdot T^1 \cdot Hz^{-1}$ with deflection not exceeded $\pm 10\%$. Discrimination threshold of "Ekran-1" is characterized by curve 1 at Fig.1. Sensor together with PA is covered with cylindrical shielded body, which length l is 370 mm, diameter d is 45 mm and mass m is 900 g.

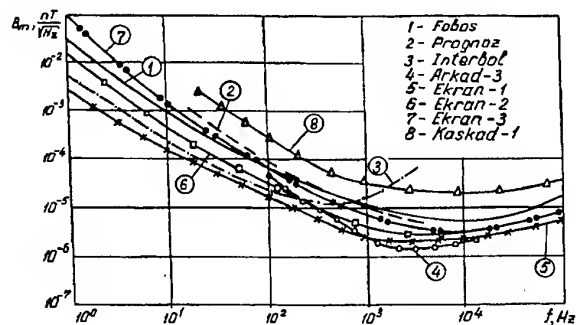


Fig.1

"Ekran-2" and "Ekran-3" sensors are intended for exploitation in $1\text{--}10^5$ Hz and have practically similar AFC: within the band $1\text{--}700$ Hz sensitivity is proportional to frequency and equals $1.4 \cdot 10^5 V \cdot T^1 \cdot Hz^{-1}$, within the band $10^3\text{--}10^5$ Hz sensitivity is constant and equals $8 \cdot 10^8 V \cdot T^1$.

"Ekran-3" is a three-dimensional sensor (higher sensor at Fig.2). The three components of "Ekran-3" have equal discrimination threshold, which is

characterized by curve 2 at Fig.1. Every component have its own PA and required AFC is formed by field NF. Dimensions of this sensor are 480-370-355 mm and mass is equal to 800 g.

One-component "Ekran-2" sensor differs from each sensor of "Ekran-3" in less discrimination threshold at frequencies lower than 10^4 Hz (see curve 3 at Fig.1). Longer core was used in order to realize this threshold. It permitted to improve the signal-to-noise ratio. "Ekran-2" has cylindrical shielded body with $d=22$ mm $l=770$ mm and mass which equals 370 g. Within the $10^4\text{--}10^5$ Hz band the thresholds of "Ekran-2" and "Ekran-3" are practically identically (see Fig.1).

Dependencies $B_m(f)$ for space sensors "Prognoz" [2,7] ($20\text{--}16000$ Hz, $l=300$ mm, $d=20$ mm and $m=1000$ g, curve 4 at Fig.1), "Fobos" [2,7] ($1\text{--}10000$ Hz, $l=400$ mm, $d=20$ mm and $m=300$ g, curve 5 at Fig.1), "Interbol" [2,7] ($0.1\text{--}1000$ Hz, $270\text{--}150\text{--}65$ mm and $m=280$ g, curve 6 at Fig.1), "Arkad-3" [8] ($100\text{--}20000$ Hz, $l=250$ mm, $d=30$ mm and $m=400$ g, curve 7 at Fig.1) are shown at Fig.1. to compare them with "Ekran" sensors. It is must be mentioned that "Prognoz" is also three-dimensional sensor.

"Kaskad" sensors were elaborated for carrying out the regular biophysical and hygienic estimations of spectral composition level, and for measuring temporal and spatial distribution of low-frequency interference magnetic fields in the inhabited modules of the orbital station "Mir" station [2,4,5,6].

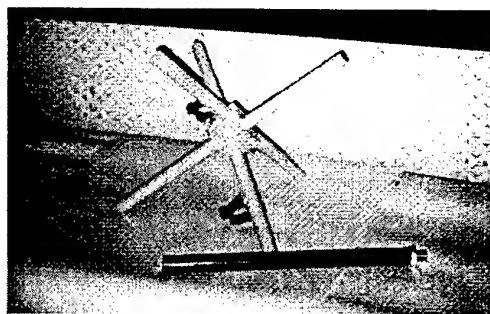


Fig.2

High accuracy is reached thanks to application of up-to-date magnetic materials, low-noise electronic components and new methods of structural and electrical parameters optimization. "Kaskad" sensor have permalloy pivot core manufactured by special technology. It is intended for frequency band $1Hz \text{--} 100kHz$. It has the same characteristics as "Ekran-3" but dimensions and mass are less.

Another type of "Kaskad" ("Kaskad-1", lower sensor at Fig. 1) has not PA because measured on-board fields isn't to weak. AFC is flat within range 20 Hz ± 50 kHz and it has lower sensitivity $G = 1.7 \cdot 10^5 V/T$. "Kaskad-1" has twice as much threshold as "Ekran-3" (curve 8 at Fig.1).

5. MAIN RESULTS OF INVESTIGATIONS

"Ekran" sensors are widely used for measurements of magnetic fields when carrying rocket and satellite experiments.

Investigations of low-frequency magnetic field distribution in the modules of «Mir» orbiting station have been carried out with the help of "Kaskad" sensors since 1993. These investigations which aim is to discover the influence of electromagnetic emission of apparatuses and equipment on human physiological condition have been accomplished for the first time in the world practice.

Measured spectral and spatial distribution of fields is taken into consideration when location of instrumentation, which is sensitive to magnetic fields, is chosen. It is very important for solving the problems of electromagnetic compatibility. The recommendations which permit to remove interference have been formulated.

It is interest to reveal zones in which artificial fields are weaker than natural ones. It can enable to extend investigations of outer space magnetic fields by apparatuses placed in hermetic modules of orbiting station.

On the base of carried out investigations the optimal places for rest and work in space station inhabited modules have been recommended. It have permitted to remove the discomfort sensations during sleep. The investigations of physiological condition of astronauts, which are carried out simultaneously with magnetic field measurements, will enable to formulate or to make more precise space flight sanitary standards, which can sufficiently differ from Earth's ones.

6. CONCLUSIONS

The ways of elaboration of mobile low-threshold wide-band inductive sensors for investigation of magnetic fields when carrying rocket and satellite experiments, for biomedical explorations and control of electromagnetic compatibility on orbiting stations are considered in the paper. The formulae which permit to optimize sensors structural and electrical parameters for minimizing discrimination threshold and for maximum widening of frequency band are presented. Some types of sensors intended for functioning on space apparatuses and stations are described.

7. REFERENCES

1. P.Dub, L.Mizuk, V.Nichoga, "Optimization of Constructive Parameters of Low-frequency Induction Sensor with the Aim of Achievement of the Lowest Discrimination Threshold" (Russian), Selecting and Processing of Information, Vol.3, 1989, pp.64-68.
2. V.Tsybulsky, V.Nichoga, A.Gnatyuk, P.Dub,

A.Yasinov, "Wide-band Component Converters for Magnetic Field Measurements in Space", Proceedings of the IV-th International Seminar on Manufacturing of Scientific Space Instrumentation, Frunze, USSR, 1989, Vol.VIII, pp.3-14.

3. I.Gontar, P.Soprnyuk, "Optimization of Low-band Sensors of Magnetic Fields", Ibid., pp. 25-32.
4. 4.A.Aleksandrov, S.Bronnikov, V.Shabelnikov, V.Nichoga, P.Dub, G.Trokhym, "Investigation of Spatial Distribution of Magnetic Fields and Their Integral Level Definition on "Mir" Space Station Board During Manned Flight" (Russian), Proceedings of the Conference on Control of Technologies, Wares and Environments by Physical Methods, Russia, Yekaterinburg, 1996, pp.60-61.
5. V.Nichoga, P.Dub, G.Trokhym, "Manufacturing of Instrumentation and Procedure of Operative Magnetic Monitoring" (Ukrainian), Proceedings of the Conference on Automatic Control, Sevastopol, Ukraine, 9-14. 09. 1996, Vol. III, pp.168-170.
- 6.V.Nichoga, P.Dub, "High Sensitive Microlocal Sensors for Investigation and Control of Electromagnetic Compatibility of Precision Electrotechnical and Electronic Devices", Proceedings of the I-st International Symposium on Microelectronics Technologies and Microsystems, Rzeszow, Poland, 1997, p. 37-42.
7. V.Nichoga, "Measurment of Very Weak Low-Frequency Magnetic Fields in Geophysics and Space Investigation", (Russian), Selecting and Processing of Information, Vol.9, 1993, pp.70-77.
- 8 "Electromagnetic Compatibility of "Arkad-3" Scientific Space Complex"(Russian), Nauka, Moscow, 1984, 190 p.
9. M.Afanaseko, B.Bondaruk, V.Nichoga, "Peculiarities of Designing of Super Wide-Band High-Sensitivity Inductive Antennas with Frequency Independent Amplitude Response"(Russian), Proceedings of Conference on Application of Super Wide-Band in Radio Engineering and Geophysics, Krasnoiarsk, Russia, 1991, pp.56-57.

BIOGRAFICAL NOTES

Vitalij Nichoga is a leading scientific researcher and the manager of laboratory of primary measuring transducers of Karpenko Physico-Mechanical Institute of National Academy of Sciences of Ukraine. He graduated Radio Engineering Faculty of State University "Lvivska Politehnika" in 1960, obtained his Dr. ing. degree in 1966 and Dr. hab. degree in 1996.

Petro Dub is a leading engineer of the same Institute. He graduated Automatics Faculty of State University "Lvivska Politehnika" in 1977.

Investigation of electromagnetic fields and manufacturing of instrumentation for their measuring are both V. Nichoga and P.Dub main scientific interests.

DEVELOPMENT OF FIELD PROBES PRINTED ON SUBSTRATES FOR DOSIMETRIC ASSESSMENTS IN THE FREQUENCY RANGE FROM 1 MHz TO 18 GHz

C. Probol

K.-H. Gonschorek

Dresden University of Technology
ETI/ EMV Electromagnetic Compatibility Division
01062 Dresden, Germany

email: probol@gmx.de

The electric and magnetic fields in the proximity of strong sources of radiation (e.g. RADAR and broadcasting) can exceed the limits mentioned in the national standards for the exposition of persons. Several field probes have been developed to ensure that people working close to these sources of radiation will not be exposed to energy densities above the limit. However, many field probes have disadvantages in the everyday use by people that are not experienced in measuring electromagnetic fields.

The limits for power density, electric and magnetic field strength depend on the frequency. In contrary, field probes covering a large frequency range e.g. 1 MHz to 18 GHz or even larger normally have a flat frequency response. Therefore, the person using the field probe has to know the frequency of the electromagnetic field and to evaluate the fieldstrength with respect to the frequency dependent legal limit value. Human mistake while making that evaluation can lead to expositions above the legal limit value and therefore possibly lead to an accident. On the other hand, the evaluation of the power density in the presence of multiple strong sources of radiation at different frequencies with different limit values leads to measurement problems too.

Some design principles are described in this paper that allow the development of an electric field probe covering the large frequency range from 1 MHz to 18 GHz with a shaped frequency response, shaped with respect to a legal limit value.

1 PRINCIPLE OF RECTIFYING FIELD PROBES

A rectifying field probe consists of three main parts: antenna and detector, resistance line, DC voltmeter (see Fig. 1).

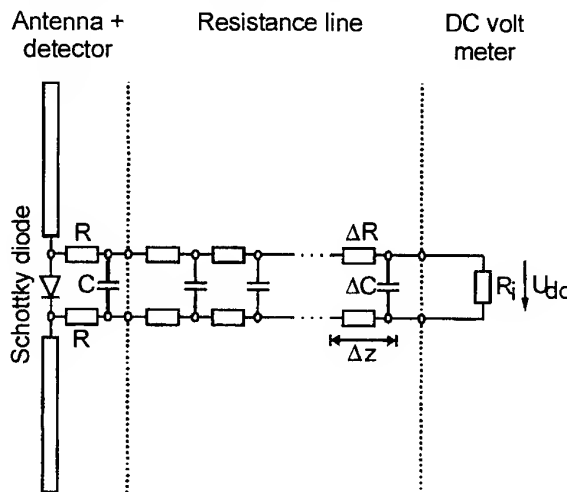


Fig. 1: Principle of rectifying electric field probe

The field probe works on the following principle. An electric field induces a voltage over a slot at the midpoint of an antenna. For frequencies far below the first resonance a simple metal dipole terminated by a load that is dominated by a capacitance would lead to a flat frequency response, so that the output DC voltage of the detector is approximately constant over a certain frequency range. The induced RF-voltage is rectified by the detector diode [2]. The frequency response can be shaped for low frequencies using discrete elements. E.g. the sensitivity for low

frequencies can be reduced using a low pass filter in parallel to the detector diode. Usually, the dipole antenna is made of resistive material to obtain a flat frequency response up to the first resonance frequency of a metal dipole of the same size [1], [3].

The rectified voltage is lead via a high resistance transmission line to a DC volt meter [4]. The resistance per unit length of the transmission line and the capacitance per unit length have to be high enough to cause only a small field distortion and a sufficient HF-attenuation. The DC-voltage drop on the resistance line can be reduced by choosing a large internal resistance of the DC volt meter.

2 DESIGN OF A SHAPED FREQUENCY RESPONSE CONSIDERING THE INFLUENCE OF THE SUBSTRATE

Broadband field probes normally cover a large frequency range with a flat frequency response while the limit value for the exposition of human beings depends on the frequency. Using such field probes the personnel has to compare the limit value for each frequency with the reading of the field probe to evaluate the fieldstrength. The limit values of the German standard DIN VDE 0848 for electric fields, exposition area 1, time of exposition longer than 6 min. and frequencies between 1 MHz and 18 GHz are shown in Fig. 2 [7].

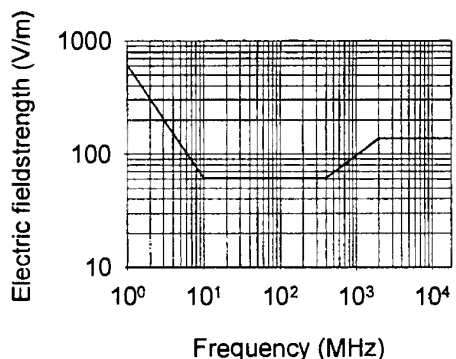


Fig. 2: Limit of the electric fieldstrength for the safety of persons, DIN VDE 0848, exposition period > 6 min., exposition area 1

If the field probe provides a shaped frequency response, that means a sensitivity reciprocal proportional to the limit value, the electronics of the probe can compare the signal direct to the limit value. In that case it is not longer necessary for the person to compare the reading with the limit value. A high signal compared to the limit value can be indicated by an acoustical and optical signal. One possible reason for accidents - mistake of a human

being when comparing the reading of the field probe with limit value - has been eliminated.

The design of an antenna providing a shaped frequency response (see Fig. 3) is possible using the recent advances made in numerical field computation.

Some field probes are designed neglecting the influence of the substrate and using expensive techniques to make the influence of the substrate as small as possible. On the other hand the design on low-cost substrates is possible if the influence of the substrate is carefully taken into account using state-of-the-art numerical field computation programs.

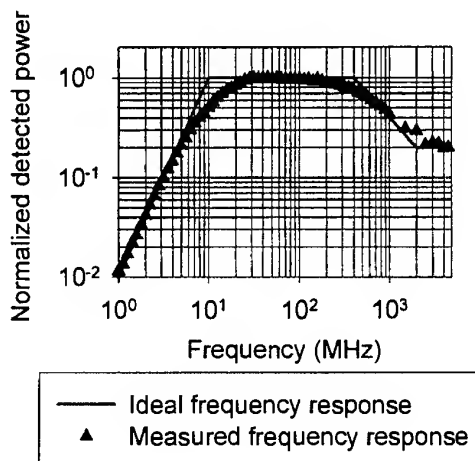


Fig. 3: Ideal and measured frequency response

The results described in this paper were computed on HP 9000 workstations with 64 MB of RAM using the field-computation-software CONCEPT [2] that is based on the method of moments. The computations were carried out using approximately 1500 - 4000 unknowns at each frequency. Most of the unknowns are due to the modelling of the substrate. Taking into account the electromagnetic behaviour of the substrate allows the use of low-cost substrates like Alumina (Al_2O_3 , e.g. 96 %) without loosing accuracy.

A CONCEPT-model of the dipole on the substrate is shown in Fig. 4. The numerical effort has been reduced for some field orientations by considering the symmetry to the xz-plane.

Calculations where made using Al_2O_3 -substrate of the dimensions 20 mm x 40 mm x 0.625 mm and 8 mm x 10 mm x 0.625 mm. The dielectric constant was 10.

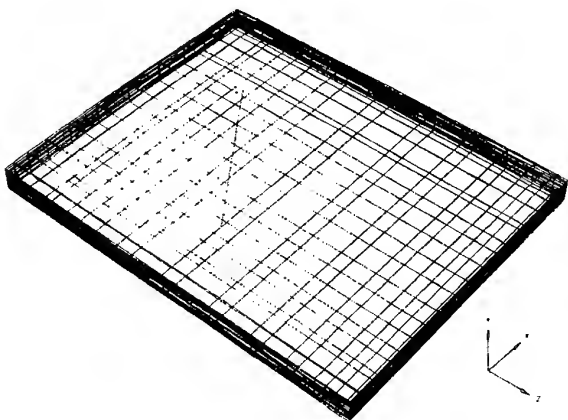


Fig. 4: CONCEPT-model of the dipole on the Al_2O_3 -substrate

The angle between the x-axis and the antenna equals to 54.7° . It was shown in paper [8] that the angle between each two antennas in a three-antenna-arrangement equals to 90° , if the substrates are arranged in an angle of 60° to each other.

A development of the probe without taking the influence of the substrate into account can lead to unacceptable deviations in the frequency response. The calculated frequency response with and without substrate is shown in Fig. 5.

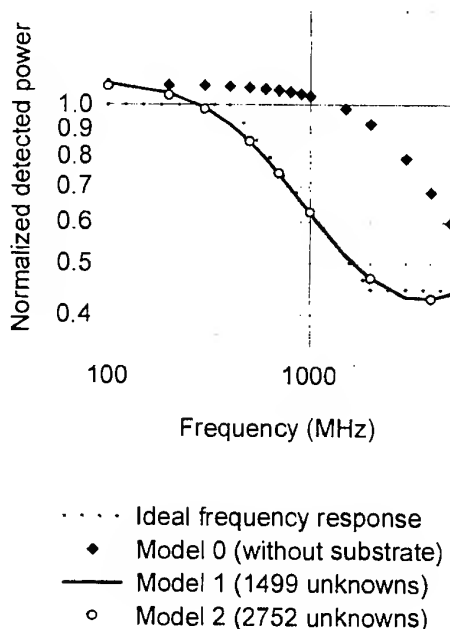


Fig. 5: Computation results, neglecting (model 0) and considering (model 1 and 2) the influence of the substrate

The differences between the shapes of the frequency response for the models with and without substrate can reach up to 6 dB. The calculations were made with two different segmentations of the substrate. The maximum differences between the results of model 1 (1499 unknowns) and model 2 (2752 unknowns) was 0,06 dB (1.3 %).

For wavelengths much greater than the dimensions of the substrate the sensitivity of the dipole is increased due to the field concentration within the dielectric material (Fig. 6, arrows represent the fieldstrength at the middle of each arrow).

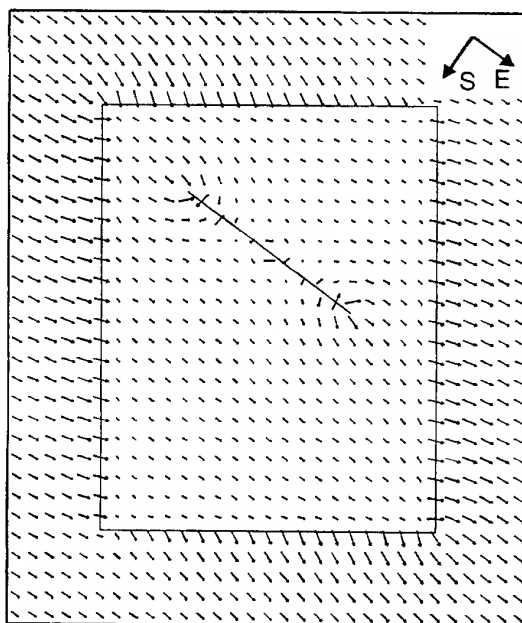


Fig. 6: Distribution of the electric field, $f = 1 \text{ MHz}$, $\varphi = 0^\circ$

Somehow, the field distribution is more complex for higher frequencies so that a precise numerical calculation is advantageous for the design of the geometrical dimensions, orientations and the dimensions and values of the resistive parts of the antenna.

3 INCREASE IN DYNAMIC

Some legal limit values for expositions of human beings refer to the power density [7]. A detector with an output signal that is proportional to the power density has to have a square-law characteristic concerning the electric field:

$$U_{dc} \sim S \sim E^2. \quad (1)$$

U_{dc} : output signal of the detector diode, DC voltage over the diode.

The AC voltage U_i over a slot at the midpoint of the antenna is proportional to the electric fieldstrength. The DC voltage U_{dc} is given by equation (2):

$$U_{dc} = -mU_T \cdot \ln \left(\sum_{n=0}^{\infty} \left(\frac{U_i}{2mU_T} \right)^{2n} \cdot \left(\frac{1}{n!} \right)^2 \right), \quad (2)$$

- U_i : antenna voltage of the dipole, AC voltage over the detector diode.
 U_T : voltage equivalent of thermal energy, 25.7 mV at $T = 25^\circ\text{C}$,
 m : reality factor, e.g. $m = 1$,

if the detector diode has the following characteristic:

$$i(t) = I_0 \cdot \left(e^{\frac{u(t)}{mU_T}} - 1 \right) \quad (3)$$

- $i(t)$: current through the detector diode,
 I_0 : saturation current of the diode,
 $u(t)$: total voltage over the diode.

The characteristic of the detector diode is shown in Fig. 7.

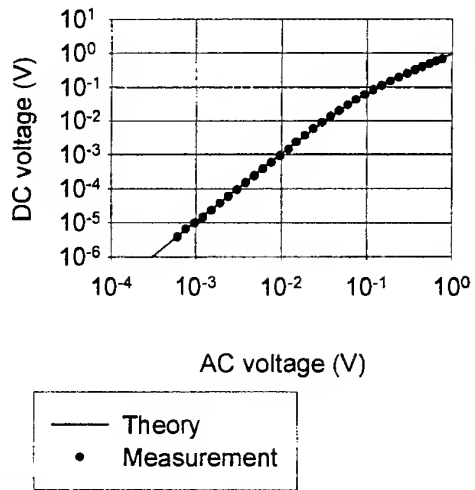


Fig. 7: Characteristic of single diode detector, $m = 1$

For low AC voltages the detected DC voltage approximately is given by:

$$U_{dc} = -\frac{U_i^2}{4mU_T}. \quad (4)$$

For higher amplitudes the detector exceeds the square-law region and therefore the range of correct power density measurement.

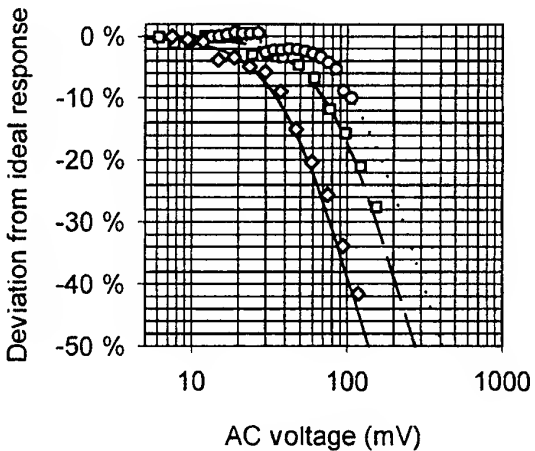
The range of correct power density measurement of a dipole with detector diode can be increased by several techniques:

1. measurement of smaller dc voltages,
2. correction factors for high amplitudes,
3. several diodes in series.

The measurement of smaller dc voltages is combined with increased sensitivity to environment influences like change of temperature, shock, humidity and internal influences like the bias current through the detector.

The characteristic of the detector can be used to employ correction factors. For some signals (e.g. pulsed RADAR), that correction leads to deviations of the measured power density from the real power density. An additional correction factor for pulse modulation has to be considered in that case.

The third way increasing the dynamic range with correct power density measurement is to use two or more diodes in series. Using more than one detector diode in series can increase the range of correct power density detection as shown in Fig. 8 without introducing one of the above-mentioned disadvantages.



- | |
|-------------------------------|
| Calculation, 1 diode detector |
| Calculation, 2 diode detector |
| Calculation, 3 diode detector |
| Measurement, 1 diode detector |
| Measurement, 2 diode detector |
| Measurement, 3 diode detector |

Fig. 8: Amplitude response of some diode detectors, theoretical and measured results

The maximum deviation between the measured and the calculated results equals to 2.3 % at 30 mV AC for a 3 diode detector. A deviation of the DC voltage of 2.3 % corresponds to a deviation in the fieldstrength of 0.1 dB.

Two diodes in series lead to 3 dB, three diodes in series lead to 4.8 dB increase in dynamic.

The diodes used in our investigations, were manufactured in beam-lead package and have been bonded thermosonically. Their capacities, which have to be low to get a medium sensitivity, had a typical value of about 100 - 200 fF. Putting more than one diode in series does no lead to a large reduction of the detected voltage and therefore to a reduced sensitivity because of the reduction of the overall capacity of the detector.

4 CONCLUSION

The development of electric field probes on substrates with a defined frequency response can be efficiently supported by using numerical field computation considering the influence of the substrate. The paper describes the results of such computations. Furthermore, it is shown that the range of correct power density detection can be increased by using more than one diode in series for the detection.

5 REFERENCES

- [1] R. Bitzer, H. Keller, M. Schaller, "Field Strength Measurement System up to 18 GHz" ("Feldstärkemeßsystem bis 18 GHz"), EMV 97, Wehrtechnisches Symposium, Mannheim, 1997, pp. 5.1-5.8.
- [2] K.-H. Gonschorek/ H. Singer, "Electromagnetic Compatibility" ("Elektromagnetische Verträglichkeit"), B. G. Teubner, Stuttgart, 1992, pp. 471.
- [3] S. Hopfer, Z. Adler, "An Ultra Broad-Band (200 kHz - 26 GHz) High-Sensitivity Probe", IEEE Transactions on Instrumentation and Measurement, Vol. IM-29, No. 4, Dec. 1980, pp. 445-451.
- [4] M. Kanda, "An Isotropic Electric-Field-Probe with Resistive Dipoles for Broad-Band Use, 100 kHz to 18 GHz", IEEE Transactions on Microwave, Vol. 35, No. 2, Feb. 1987, pp.124-130.
- [5] Meinke/ Gundlach, "Handbook of High Frequency Technology" ("Taschenbuch der Hochfrequenztechnik"), Springer-Verlag, Berlin, Chap. Q4, 5. Aufl., 1992.
- [6] Th. Schmid, O. Egger, N. Kuster, "Automated E-Field Scanning System for Dosimetric Assessments", IEEE Transactions on Microwave Theory and Techniques, Vol. 44 , No. 1, Jan. 1996, pp 105-113.
- [7] DIN VDE 0848, "Safety in electromagnetic fields" ("Sicherheit in elektromagnetischen Feldern"), German Standard, part 1, 2, 4, Beuth-Verlag, Berlin, 1991-1995.
- [8] M. Kanda, "Standard Antenna for Electromagnetic Interference and Methods to Calibrate Them", IEEE Transactions on Electromagnetic Compatibility, Vol. 36, No. 4, Nov. 1994, pp.261-273.

BIOGRAPHICAL NOTES

Carsten Probol was born in Hamburg, Germany, in June 1967. He received the Diploma in Electrical Engineering from the Technical University of Hamburg-Harburg in 1994 and continued his working on Electromagnetic Compatibility within the MAZ Hamburg GmbH. He joined the Dresden University of Technology in 1996 where he is involved in the development of measurement techniques to ensure the safety of persons in the presence of strong electromagnetic fields.

Karl-Heinz Gonschorek was born in a small village close to Hanover in September 1946. He studied electromagnetics, concentrating on high frequencies, at the University of Hanover. In 1980 he wrote his doctor thesis about electromagnetic coupling of arbitrarily located thin electrodes. From 1980 to 1988 he was with Siemens, working in a R&D-group handling questions of EMC. 1988 he became professor for electromagnetic influences at the Technical University of Hamburg-Harburg. Since 1995 he is the holder of the Siemens-foundation chair on EMC at the Dresden University of Technology.

LOW COST OPTICAL LINK TO MONITOR EUT'S SUSCEPTIBILITY TESTS

Marcos Quilez, Ferran Silva and Pere Riu

Departament d'Enginyeria Electrònica. Universitat Politècnica de Catalunya.

Gran Capità s/n. Edifici C-4. 08034 Barcelona. SPAIN.

tel: 343-401-7826 fax:343-401-6756 E-mail: marcos@eel.upc.es

The high immunity level to electromagnetic disturbances of fiber optic links makes them very useful to transmit signals during radiated and transient susceptibility tests. The present design widens the bandwidth of a low cost LED and allows sending analog signals up to 100 MHz over a fiber-optic link.

1. INTRODUCTION.

External disturbances are applied to equipment under test (EUT) in radiated and transient electromagnetic susceptibility (EMS) tests. In radiated susceptibility tests, the EUT is illuminated with electromagnetic fields and it must work properly under the radiation to pass the test. This kind of test takes place inside an anechoic chamber or any other specific site as TEM or GTEM enclosures. Some EUT responses must be transmitted outside the enclosures during the test because the test engineers must follow the effects of radiation on the EUT features. Shielded video systems, fiber-optic links for digital signals and coaxial cables for analog signals are frequently used. The analog signal coaxial cable link is susceptible to the electromagnetic fields inside the enclosure and sometimes it is impossible to separate the signal generated by the equipment from the signal coupled to the cable. Similar problem arises in transient susceptibility tests. The transients coupled to EUT cause radiated disturbances that may produce interference in any near coaxial cable link.

The high immunity level to external disturbances fiber-optic links feature make them very suitable for this application, not only to transmit digital signals as usual, but also analog ones. Transmission of low bandwidth analog signals does not present any difficulty, because analog to digital conversion at low frequency is easy and a digital LED based fiber-optic link fits well. However, the disturbances applied in EMS tests are large bandwidth signals. For that reason, high frequency links are needed to follow how disturbances interfere with the signals in the EUT.

Two alternative techniques are frequently used when the analog signal bandwidth is high. The first one uses high

speed A/D converters. The second one allows high bandwidth links based on the direct modulation of a linear LASER. Systems based on both techniques take benefit of fiber optics links, but present the disadvantage of the high cost of A/D converters at high frequencies and linear LASERS.

The design that we present in this paper allows sending analog signals up to 100 MHz over a fiber-optic link using low cost components. A voltage to current conversion and an equalized gain amplifier allows a LED-based emitter to work at these frequencies in analog mode.

2. CIRCUIT DESCRIPTION

Figure 1 shows the link block diagram. The transconductance amplifier in the emitter section is the heart of this design, as it performs the voltage to current conversion and the frequency response equalization.

The transconductance amplifier and the emitter circuit operation are described next.

One of the basic desired features of an analog transmission system is linearity. The relation between input LED and output photodiode current is given by [1]

$$i_{\text{photodiode}} = I_{\text{photodiode}} \left(1 + \frac{i_{\text{LED}}}{I_{\text{LED}}} \right)^n \quad (1)$$

where I 's are the polarization currents and i 's are the signal currents. The exponent n is the non-linearity factor, which depends on the LED, and tends to 1 when I_{LED} increases. In these conditions, n is the only reason for non-linearity when the LED is current excited.

If the LED is voltage-excited then linearity becomes worse: the relation between voltage and current in a LED is

$$i_{\text{LED}} = I_0 \left(1 - e^{-\frac{V_{\text{LED}}}{V_t}} \right) \quad (2)$$

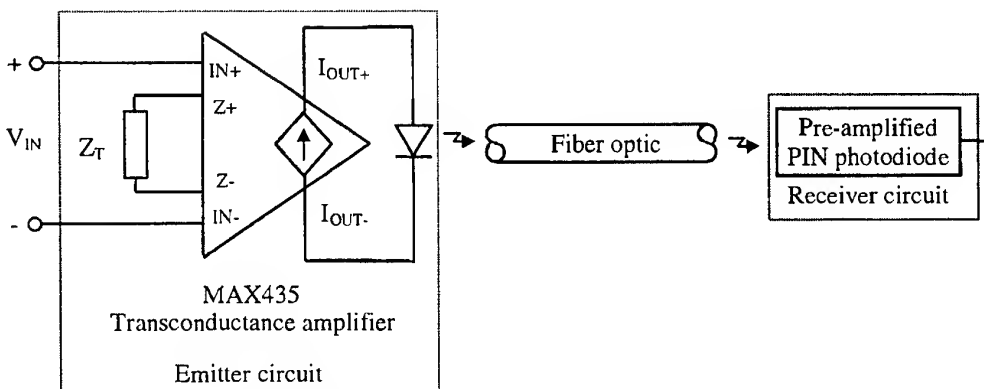


Figure 1. Block diagram of the optical link.

where v_{LED} is the signal voltage, I_0 is the reverse saturation current and $V_T = KT/q$ with K the Boltzman constant.

Combining equations (1) and (2) the voltage input at the LED and voltage output at the photodiode relation is

$$v_{photodiode} = Z \cdot I_{photodiode} \left(1 + \frac{I_0 (1 - e^{\frac{v_{LED}}{V_T}})}{I_{LED}} \right)^n \quad (3)$$

where Z is the impedance that gives $v_{photodiode} = Z \cdot i_{photodiode}$.

When a LED is voltage excited, equation (3) shows clearly the non-linearity. Therefore, current LED excitation is the best option to improve the optical link linearity. An amplifier based on two current conveyors (see figure 1) [2] implements a V-I converter to be used with a voltage source.

A low-cost LED has a small bandwidth when it is excited by a current signal. So, equalization in the voltage-current amplifier response has been used to widen the LED bandwidth (patent application filed). This equalization performance has been obtained with a simple passive R-C circuit.

The decreasing gain in the LED response near the cut-off frequency can be approximated by a single pole circuit, that is, a -20 dB/dec gain decrease. The adopted solution equalizes the V-I converter amplification to compensate the LED response. By placing a zero at the amplifier at the same frequency where the LED-photodiode pair presents the pole, the system presents a flat response. At high frequencies, however, LED response is not well represented by a single pole circuit and, on the other hand, the amplifier gain cannot be incremented continuously so the system is not completely equalized, but cut-off frequency is increased.

The response of V-I converter amplifier from Figure 1 can be calculated by

$$I_{out} = \frac{V_{in}}{Z_T} \quad (4)$$

To include a zero in the amplifier response, feedback impedance Z can be configured as a simple resistor-capacitor parallel pair (R_C is set to avoid feedback oscillation, see Figure 2). This net presents an impedance:

$$Z_T = \frac{1/C_T}{s + \frac{1}{R_T C_T}} \quad (5)$$

so the amplifier output current is

$$I_{out} = k C_T \left(s + \frac{1}{R_T C_T} \right) \quad (6)$$

The receiver circuit is based on a pre-amplified PIN photodiode (Honeywell HFE4211) and follows the application note provided by its manufacturer.

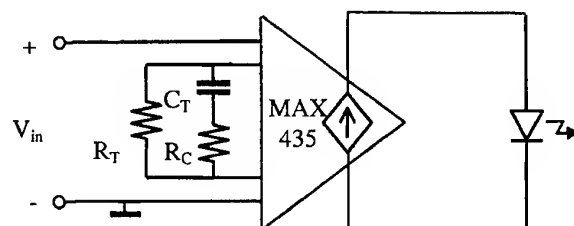


Figure 2. Amplifier gain equalization with an R-C net feedback.

3. TECHNICAL CONSTRUCTION ASPECTS

Good linearity and wide enough bandwidth are fundamental in analog transmission systems, but some other additional features must be considered to obtain an optical link suitable for EMS susceptibility test.

The led polarization current is directly related to link behaviour, because the non-linearity factor in equation (1) and LED bandwith depend on it. For these reasons, this current must be set properly to obtain the best linearity and bandwidth figures. For the LED used in our design, the manufacter recommends a 50 mA polarization current to get the maximun bandwith.

Since changes in polarization affect link performance and diode characteristics are very sensitive to temperature, an independent current source has been used to adjust polarization current. This source allows to set the polarization current avoiding inestability of the LED working-point due to temperature changes.

Equalization of LED response involves finding the exact frequency at where the zero due to Z_T must be placed to match the frequency pole. Dispersion of responses in the same LED family due to manufacturing process makes necessary to use slightly different Z_T for each LED unit. So, to obtain a maximum flat response, the R-C equalization net must be designed for each unit and must be redesigned if the LED has to be replaced.

This unpleasant situation can be avoided by using a fixed value of Z_T and moving slightly the LED pole position until it fits the zero provided by Z_T . Effectively, LED bandwidth, and so its pole frequency, depend on the polarization current. In this situation, the R-C net

that provides the gain equalization is set for the typical pole frequency, then the LED polarization current is adjusted to move the LED pole at the frequency of the amplifier zero.

This way, the LED polarization current and the correct equalization of its frequency response are set with only one adjustment.

The layout of the printed circuit board has been accurately designed to reduce the effects that appear when signals frequency increase because of parasitic capacitors and inductances, as well as to improve the immunity of the system against external disturbances.

Using this optical-link in EMS tests involves that emitter and receiver circuits, but especially at the emitter side, must be able to work under radiated electromagnetic fields. So, the emitter and the receiver circuits have been protected by a shield. Both circuits have been enclosed in a metallic case connected to a fixed potential. This way, good electric field protection is achieved. But, at low frequencies, this shield is ineffective for magnetic field. To get additional protection against magnetic fields at the emitter section, the inner side of the case was covered of ferromagnetic material. In these conditions, the optical link has been tested to work properly inside a semi-anechoic chamber under radiated fields of 10 V/m amplitude and 80 MHz to 1 GHz frequencies.

To obtain all the benefit of the fiber-optic link, shielding and bounding techniques are nor enough. Since external disturbances couple to power cables, emitter must be powered locally without using any external conductor cable. A battery-operated emitter is the adopted solution.

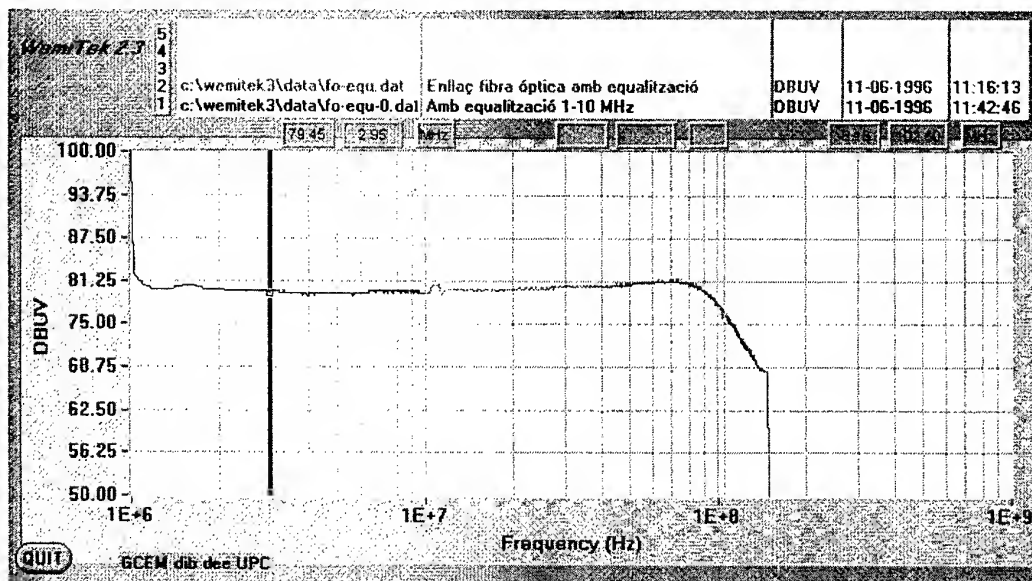


Figure 3. Frequency response of a LED-photodiode pair (Honeywell HFE 4211 & HFD 3216) with equalized current LED excitation.

In this situation, the high energy demand to polarize the LED (50 mA for the LED considered in this application) presents a problem and discards the use of small cell batteries to obtain long autonomies.

Low battery charge produces a power supply drop that affects the emitter behavior. This power supply drop must be detected to avoid errors in measurements. Since the operator and the measurement instrumentation usually stay beside the receiver, power supply drops in the emitter should be automatically detected. In our design, power supply drops are controlled. When battery charge can not guarantee the proper emitter function, the led polarization current is cut off, avoiding led emission and no signal arrives to the receiver.

4. RESULTS

Figure 3 shows the frequency response of the optical link. The LED used in this design has its -3 dB cut-off frequency at 45 MHz when it is directly excited. By using the equalized amplifier described, the cut-off frequency is increased up to 100 MHz.

Linearity has been determined measuring the harmonic distortion due to the optical link. A sinusoidal signal has been applied at the input and the level of the harmonics that appear at the output signal has been measured. The level of harmonics due to distortion is expressed in dBc

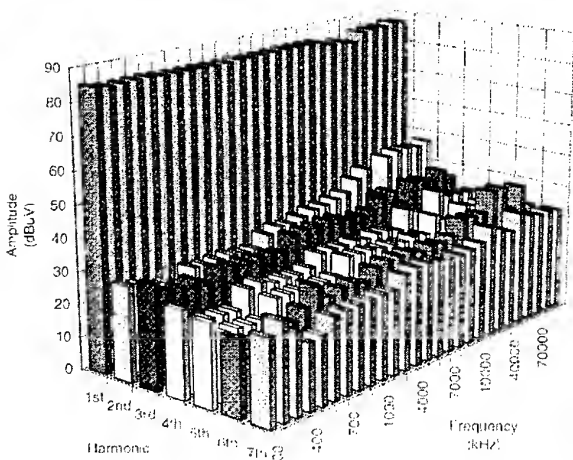


Figure 4. Harmonics level for 100 mVrms input signals.

(dB to carrier) referred to the level of the fundamental harmonic.

In order to have a good characterization of link linearity, first seven harmonics were measured for a total of 1134 input signals, making a frequency sweep through the whole bandwidth and an amplitude sweep between 100 mVrms and 300 mVrms. Measurements for 100 mVrms input signals are plotted in Figure 4. This figure shows,

for instance, that the harmonics level referred to the level of the fundamental frequency signal is less than -50 dBc for a 10 MHz and 100 mVrms input signal.

The noise floor was obtained measuring the output signal level with a spectrum analyzer while no input signal is applied. The input was ended with an adapted charge. The spectrum analyzer input impedance and the resolution bandwidth (RBW) are known parameters. So, noise power spectral density is given by

$$N = \frac{V_n^2 / R_{in}}{RBW} \quad (7)$$

The measured noise floor is below $4.2 \cdot 10^{-10}$ $\mu\text{W}/\text{Hz}$.

Electromagnetic immunity was tested by transmitting a known signal form inside a semi-anechoic chamber. The link worked properly under a radiated field of 10 V/m, in the conditions set for IEC-100-4-3 standard susceptibility tests.

These measured features show that this low-cost analog optical link is suitable for motoring equipment under electromagnetic susceptibility tests.

5. CONCLUSIONS

This design proves that current excitation of LEDs based on current conveyors is very effective to transmit analog signals over fiber optic links. Especially because this technique allows to include equalization in the transconductance amplifier, and widen the LED bandwidth, using few passive components.

Another important point is the use of the current polarization to correct the dispersion of the LED pole frequency. This feature allows a single adjustment design to set the current polarization and the correct equalization of LED response.

Referring to the link features, the results show that it is a suitable optical-link to monitor equipment during electromagnetic susceptibility tests. So, this low cost optical-link covers the empty segment between high performance but high cost optical-links and other low cost optical-links with very poor performance.

6. REFERENCES

- [1] P. Vettiger. "Linear signal transmission with optocoupler", IEEE Journal of Solid State Circuits, Vol. 12, No. 3, 1977, pp. 298-302.
- [2] F. Silva, M Quilez, R. Bragos. "Circuit Widens optocouplers response 10-1 MHz", EDN Magazine, 21 Dec. 1995.

DEVELOPMENT OF FRACTIONAL LOOP ANTENNA FOR EMC MEASUREMENT

P. K. SAHA AND N. M. ALAM CHOWDHURY*

Dept. of Electrical & Electronic Engineering
Bangladesh University of Engineering and Technology (BUET)
Dhaka-1000, Bangladesh
E-mail : sahapk@eebuet.bdmail.net
*Bangladesh Institute of Technology (BIT) Dhaka, Gazipur - 1700
E-mail : bitdhaka@bangla.net

A fractional loop (one sixth of a complete loop) in front of 60° corner reflector is proposed in this paper to simulate a highly directive standard EM wave. Field equation of the proposed antenna is developed. Various parameters such as loop radius, wire diameter and reflector size which are to be considered in developing the proposed antenna are well described in this paper. The proposed fractional loop antenna is constructed and the radiation pattern of the antenna is measured to compare the theoretical radiation pattern. Comparison shows a very good agreement with the theoretical pattern.

1. INTRODUCTION

The simplest way of reducing Electromagnetic Interference (EMI) problem of the electrical and electronic equipment is by enclosing the equipment using conducting materials. The level of shielding of the enclosure against EMI is usually determined by the measurement of Shielding Effectiveness (SE) of the material used for the enclosure. Standard field simulation is the starting point of any SE measurement technique. Thus it is necessary for an antenna which could simulate standard EM waves. In this paper a fractional loop antenna has been proposed which can be employed to simulate standard EM wave for magnetic-field shielding effectiveness measurement of the planar sheet.

The paper is organised as follows. The development of field equation of the fractional loop antenna presented in section-2. Directivity and gain of the developed antenna is also given in this section. Size and shape of the fractional loop and the corner reflector are selected in section-3. Computation of the antenna parameters and measurement of radiation pattern of the designed antenna are presented in section-4. Section-5 contains the concluding remarks.

2. FIELD EQUATION

Field equation for the fractional loop antenna in front of 60° corner reflector has been developed by using the image theory and the theory of pattern multiplication [1]. One sixth of loop in front of a 60° corner reflector produces five image loops of the original one as shown in Fig.1. Image theory straightway refers to the two images at A₂ and A₃ because of the reflectors OR₁ and OR₂. If we take the corner line as a reflector then the third image A₆ is to be considered. Again, another two images A₄ and A₅ images are produced due to the image reflector OR₄ and OR₃ respectively. Therefore, each infinitesimal dipole element of the arc would have five images. The effect of these images on the field of the original fractional loop are then superimposed by a method similar to pattern multiplication. Thus, the one sixth of loop in front of the corner reflector can act as a complete loop in free space.

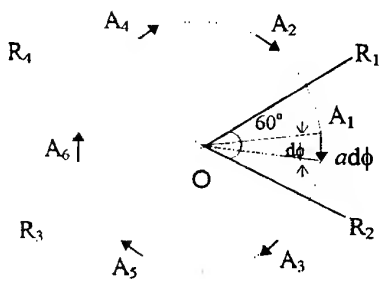


Fig. 1 Image produces by an infinitesimal dipole of one sixth of loop in front of a 60° corner reflector.

The fractional loop antenna can be considered an array of coplanar three pair of dipoles shown in Fig. 2. Each pair of dipoles are parallel to each other carrying equal and out of phase current. The far field is computed from the vector potential of coplanar hexad dipoles and the vector potential of the one sixth of loop element.

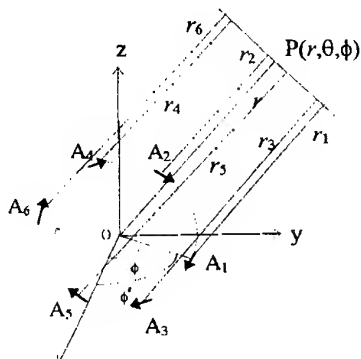


Fig. 2 Geometry of fractional loop and its images.

For $\lambda \gg a$ and $\beta a \ll 1$, the resultant vector magnetic potential due to the three pair of dipoles at the far field point $P(r, \theta, \phi)$ can be obtained as [2]

$$\vec{A} = \hat{\phi} 3j\beta a \sin\theta \times \vec{A}_{arc} \quad (1)$$

$$\text{where } \vec{A}_{arc} = \frac{\mu [I]a}{4\pi r} \cdot \frac{\pi}{3} \hat{\phi}, \quad [I] = I_o e^{j(\omega t - \beta r)}$$

The term $3j\beta a \sin\theta$ is known as the array factor.

If the co-ordinate axes are chosen so that the loop is in the x-y plane and the reflectors in the x-z and y-z plane respectively then the net field expressions valid for azimuth angle ϕ of 0 to $\pi/3$ and the polar angle θ of 0 to π (i.e. in front of the reflector). Reflector is assumed as an infinite ground plane. Thus neither magnetic nor electric field is present behind the

reflector. The radiated field expressions can then be obtained as [2]

$$E_\phi = \frac{\mu \omega [I]a}{4r} \beta a \sin\theta \quad \text{for } 0 \leq \phi \leq \pi/3 \text{ and } 0 \leq \theta \leq \pi \\ = 0 \quad \text{elsewhere} \quad (2)$$

$$H_\theta = \frac{[I]a}{4r} \beta a \sin\theta \quad \text{for } 0 \leq \phi \leq \pi/3 \text{ and } 0 \leq \theta \leq \pi \\ = 0 \quad \text{elsewhere} \quad (3)$$

From the field expressions of the quarter loop and those of the complete loop which are given in the literature's [3,1], it can be seen that the radiation pattern of the fractional loop is similar to that of a quarter loop and that of a complete loop but the radiated field area is different from each other.

2.1 Antenna parameters

The directivity of an antenna is the ratio of maximum radiation intensity (U_m) to average radiation intensity (U_v). These radiation intensities are related to the total power radiated (P_r) by the antenna. For fractional loop antenna

$$P_r = \frac{5\pi^2 \beta^4 a^4 I_o^2}{3}, \quad U_m = \frac{9}{4\pi} P_r, \quad U_{av} = \frac{P_r}{4\pi} \quad (4)$$

Hence, the directivity of fractional loop antenna (D_H) will be 9.

The gain of the fractional loop antenna (G_H) can be obtained by multiplying the directivity D_H with radiation efficiency (η).

$$\text{where } \eta = \frac{R_r}{R_r + R_{ohmic} + R_{ref}} \quad (5)$$

Here, R_r is the radiation resistance, R_{ohmic} is the ohmic resistance of the loop and R_{ref} is the reflector resistance.

The input impedance of the fractional loop antenna can be obtained from the equivalent circuit of the antenna as described in the literature [4].

3. SELECTION OF SIZE AND SHAPE OF ANTENNA

3.1 Design consideration of fractional loop

Antenna parameters such as the radiation efficiency and radiated power depends on the design

parameters such as the loop radius, the size and the shape of the loop arc. A loop antenna of constant gain and maximum radiation efficiency in the frequency range of interest (30MHz to 1000MHz) is desirable. Gain and radiation efficiency are computed at various loop radius. Gain and radiation efficiency at various frequencies as a function of loop radius are shown in figs. 3 and 4 respectively.

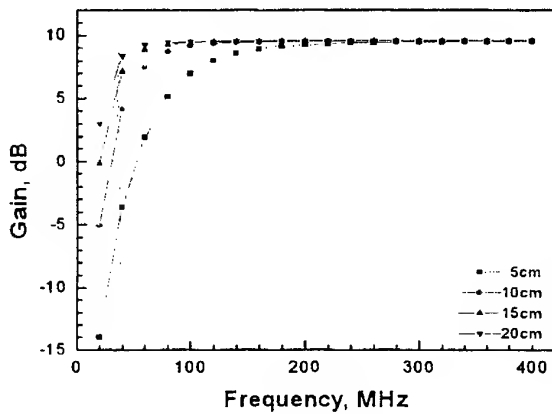


Fig. 3 Gain vs Frequency curve at various loop radius.

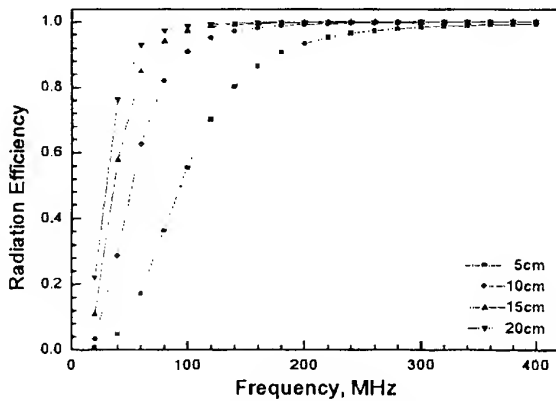


Fig. 4 Radiation Efficiency vs Frequency curve at various loop radius.

The Figs. 3 and 4 show that, the gain and radiation efficiency both increases with the increase of loop radius at frequencies below 100MHz. Above 100MHz, the gain and efficiency both are almost constant at all loop radius. However, maximum gain and radiation efficiency are found at frequency above 40MHz at a loop radius of 15cm. Thus, it is decided to select the loop radius of 15cm, because it can provide enough arc length for easy to bending at a 60° arc.

Cross-sectional dimension of the loop wire is an important factor for the radiation efficiency at a fixed loop radius. In this work a wire of circular cross-section is chosen to construct the fractional loop. The radiation efficiency of 85% is found at frequency above 40MHz at a wire radius of 8mm as describe in

literature[2]. Thus a wire radius of 8mm is selected because it can provide enough space for mounting the connectors at the end of fractional loop, where it meets with the sides of the corner reflector.

3.2 Design consideration for the reflector

A square corner reflector is used to improve the directional property as well as gain of the fractional loop antenna. The length of the reflector is to be large as compared to the antenna-to-corner spacing (i.e. the length of the loop radius), so that the reflector can be considered as an infinite ground plane to hold the image theory. The minimum length of each side of the square-corner reflector is considered to be the three times of the antenna-to-corner spacing (i.e. loop radius) [1]. Therefore, in this work each side of the reflector is assumed to be the four times of the loop radius (i.e. $4 \times 15 = 60\text{cm}$).

The region behind the sheet reflector would not be a full shadow region due to the sharp edge of the reflector. Thus the diffracted radiated field is found into the shadow region[5]. However, this diffracted radiation can be reduced by converting the sharp edges of the reflectors into the rolled edges[6], which have a curvature of radius greater than $\lambda/4$. Thus in this work, the edges of the reflector are curved with a curvature radius of greater than 75cm to reduce the diffracted field at frequencies above 100MHz. The reflector should be strong enough so that it remains straight in any orientation. In this work an aluminum sheet of 2mm thickness is used in order to construct the reflector.

3.3 Construction of the designed antenna

The fractional loop is fixed onto the reflector by the plastic screw. A diagram of the fractional loop with end connection is shown in Fig. 5.

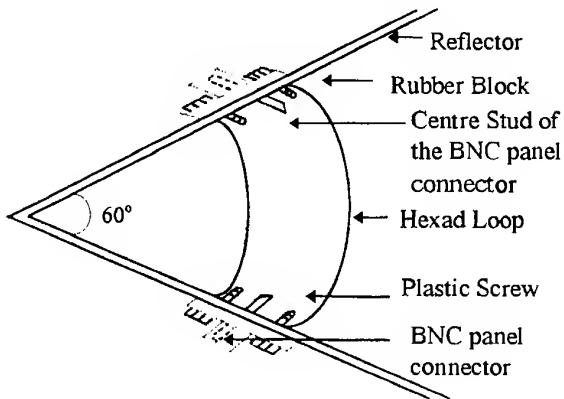


Fig. 5 Fractional loop antenna in front of 60° corner reflector.

4. COMPUTATION AND MEASUREMENT

4.1 Computation of antenna parameters

Radiated fields and gain of the designed fractional loop antenna have been computed. Predicted gain of the proposed fractional loop antenna has been compared with that of the quarter loop antenna and a complete loop antenna. This comparison is shown in Fig. 6. Fig. 6 shows that the gain of the proposed antenna is higher than that of the quarter loop[3] and that of a complete loop[1]. It is also found that the directivity of fractional loop antenna is 1.5 times of that of a quarter loop[3] and 6 times of that of a complete loop[1] antenna.

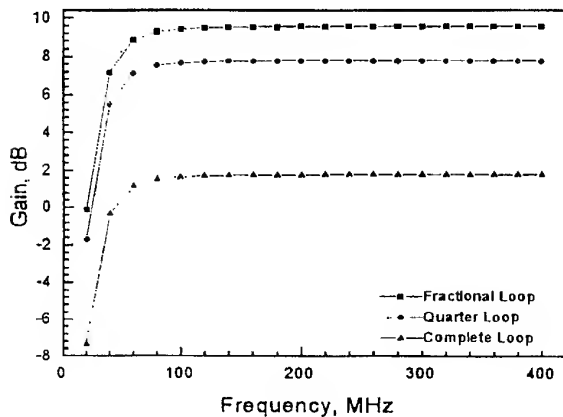


Fig. 6 Gain vs frequency curve.

4.2 Radiation pattern measurement

Throughout the measurement of radiation pattern, it is assumed that the developed fractional loop antenna is treated as a passive, linear and reciprocal

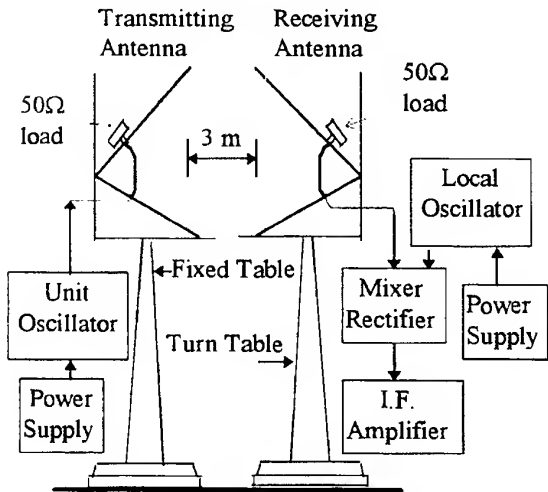


Fig. 7 Schematic block diagram of test set-up.

devices. Thus the two fractional loop antennas are used to observe the radiation pattern of the developed antenna. One is used as a transmitting antenna while the other is used as a receiving antenna. Schematic block diagram of the test set- up is shown in Fig. 7.

Field measurement is done at a radial distance of 3m and at a frequency of 250MHz. Measurement procedures are well described in the literature[2]. In order to obtain horizontal pattern, the receiving antenna is rotated in the horizontal plane (i.e. $\theta = 90^\circ$) where the azimuth angle (ϕ) varies from 0 to 180° .

The maximum field strength is found at $\phi=90^\circ$, and $\theta = 90^\circ$. The position of maximum field strength is then considered as the reference position for the present task. The measurement are also repeated for other frequencies.

4.3 Test results and Comparison

It has already been mentioned that the fractional loop antenna radiates in the azimuth angle (ϕ) varying from 0 to 60° in the horizontal plane (i.e. $\theta = 90^\circ$). In this work the reference position is considered at $\phi = 90^\circ$ and $\theta = 90^\circ$. Therefore, the presence of the radiated field is to be expected in between $\phi \geq 60^\circ$ and $\phi \leq 120^\circ$ in the same plane. The measured field strength at different positions of the transmitting antenna are normalized by the maximum field strength which is obtained at the reference position. Polar plot of the measured radiated fields is shown in Fig. 8(a). The computed normalized field pattern of the developed antenna in the horizontal plane ($\theta = 90^\circ$) has been shown in Fig. 8(b). Fig. 8 shows that though the theoretical pattern and the measured pattern are identical but a weak field is found in the shadow region. These may be due to the reflections from the metallic objects present in the room and associated cabling, radiation from the instruments, reception of other EM noise by both the receiving and transmitting antenna, the leakage current flowing through the reflector which also contributes to radiation, the edge diffraction, and the change in amplitude of the local oscillator during measurement.

5. CONCLUSION

This paper discusses the proper selection of designed data of newly developed fractional loop antenna. It is found that both the directivity and gain of the developed antenna remains constant at all frequencies above 60 MHz.

Measured radiation pattern has been found nearly identical to that of the computed pattern. Measurement of antenna parameters such as directivity,

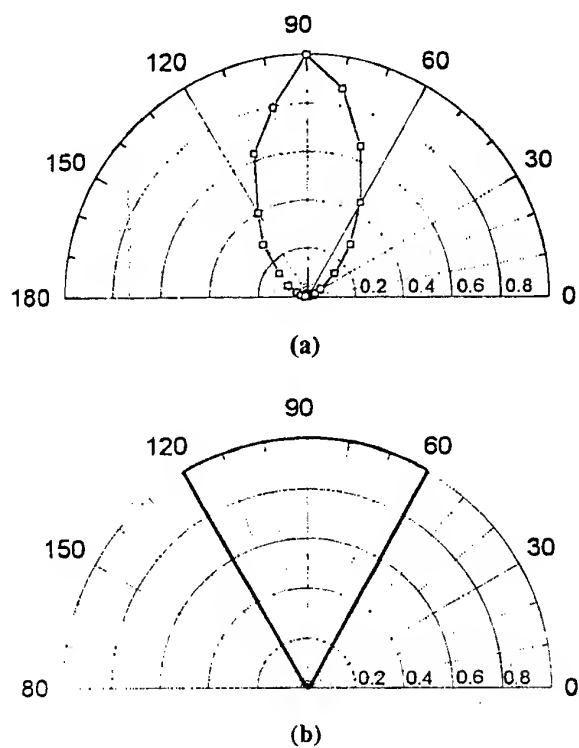


Fig. 8 (a) Radiated field pattern (b) theoretical field pattern.

gain and input impedance of the developed antenna was not done due to the non standard test environment.

Two fractional loop antenna (one acts as a transmitting antenna while the other acts as a receiving antenna) can be used to measure the low impedance magnetic field SE of a planar sheet like conductive material. The test sheet and the receiving antenna has to be positioned strictly in the near field region of the transmitting antenna. The field in and around the test location will be predominantly reactive not radiative. Thus measuring the SE using this type of antenna has to be calibrated to take into account correction factor for indirect path signal infringement.

6. REFERENCES

6.1 J.D. Krauss, *Antennas*, 2nd ed., McGraw Hill Inc., Singapore, 1988.

6.2 N. M. Alam Chowdhury, "Development of Fractional Loop Antenna in Front of 60° Corner Reflector", *M.Sc. Engg. Thesis*, Department of Electrical & Electronic Engg., Bangladesh University of Engineering and Technology, Dhaka, Bangladesh, June 1997.

6.3 H. Rahman, "Development of EMC Antenna and their Application in On-line SE Measurement of Conductive Composite Plastic Materials", *Ph.D. Thesis*, School of Electronic Engineering, Dublin City University, Ireland, March 1994.

6.4 P.K.Saha, N.M.Alam Chowdhury and Z.Alam, "Hexad Loop (H-Loop) Antenna in Front of 60° Corner Reflector for EMC Measurement", Proceedings of the International Conference on Electromagnetic Interference and Compatibility '97, Hyderabad, India, 3-5 Dec., 1997, pp. 65-70.

6.5 J. D. Krauss, *Radio Astronomy*, 2nd edition, Cygnus Quasar, 1986, pp. 642-646.

6.6 W.D. Burnside et al., "Curved edge modification of compact range reflectors," *IEEE Transaction on Antenna & Propagation*, AP-35, Feb. 1987, pp. 176-182.

BIOGRAPHICAL NOTE(S)

Dr.P.K.Saha is with the department of Electrical & Electronic Engineering of the Bangladesh University of Engineering & Technology (BUET), since 1986. His research interest include EMC CAD Package and EMC antenna.



N. M. Alam Chowdhury (Member, IEEE, IEB, BCS) received the B.Sc. Engg. degree in Electrical & Electronic Engg. from Bangladesh Institute of Technology (BIT), Dhaka and the M.Sc. Engineering Degree in Electronics & Communication from Bangladesh University of Engineering & Technology, Dhaka in 1992 & 1997 respectively. Presently he is with the Dept. of EEE of BIT Dhaka. His research interest includes EMC equipment & antennas, Microwave Engineering.

SIGNAL PROCESSING IN RADIATED EMI MEASUREMENTS

Werner Schaefer
Hewlett-Packard Company
Santa Rosa Systems Division
1400 Fountaingrove Parkway
Santa Rosa, CA 95403-1799, USA

Abstract - Overall test times can be reduced significantly by using signal processing algorithms on data collected during EMI measurements. This is especially true for commercial radiated EMI compliance tests, which usually require signal maximization by scanning the antenna tower over a defined height range, changing the antenna polarization, and turning the table on which the equipment under test (EUT) is set up. By varying these three parameters, the highest amplitude at each detected EUT emission is determined, which can be a lengthy process. Additional complexity is added when the measurement is made on an open area test site (OATS). Then, extra measurement steps must be used to discriminate between ambient signals and EUT emissions. Software tools can automate parts of the measurement or provide assistance during interactive testing. In this paper, some algorithms and their implementation in a commercial radiated EMI software package are discussed and sample applications are presented.

1. Introduction

During the course of a conducted or radiated EMI compliance measurement different types of signals are detected, depending on the EUT. Often, the spectrum measured in a conducted test contains broadband emissions, caused, for example by the brushes of the EUT's electric motor. The determination of the frequency of this signal is rather complex, because this information cannot be directly derived from the EMI receiver's display. Some further analysis is required to identify related spectral components and to calculate the actual emission frequency. Furthermore, the interception of broadband signals, especially those with low repetition rates, is complicated because the EMI receiver has to either dwell at the tuned frequency for a certain time or sweep across a band at an adequate sweep rate. In either case, prior knowledge of the characteristics of the signal to be measured is necessary to select the appropriate receiver settings. A solution to these specific problems is provided by so-called "trace-based" software packages, which re-

cord complete measurement traces of swept receivers and compare this data against one or multiple limit lines. Usually, the EMI receiver sweep time and the number of sweeps per frequency band are selectable to ensure intercept of broadband signals. By taking this approach, the actual frequency determination of signals in these traces is avoided. When amplitudes exceed the applied limit line, the receiver is swept across this small frequency segment using a different detector. The result is documented as a graph showing the measurement traces along with limit lines. No signal lists are provided containing the emission's frequency, amplitude and other attributes, because this demands a frequency determination and might require manual interaction. With radiated EMI measurements the emissions are predominantly narrowband. Therefore, an algorithm can be applied to the measurement traces to discern actual signals in the spectrum. In this way, signal information can be separated from measured broadband noise, which reduces the number of emissions that must be maximized during compliance testing. To ensure the shortest test time possible, only the significant signals should be maximized.

The ability to discern signals in traces usually leads to a "list-based" software product, which provides signal lists as a basis to store, process and present signal data. These lists also serve as the input information for the maximization and measurement procedures. In addition, these lists provide powerful data comparison capabilities, which can be used in many different ways. For instance, the discrimination between ambient and EUT signals on an OATS is simplified by comparing two lists, where one contains ambient signals only and the second holds both ambient and EUT signals. The comparison of signal amplitudes against limit lines, as well as the sorting of lists by a specified attribute or selection of emissions meeting a definable criterion contributes to a shorter overall test time. However, the list-based measurement approach introduces a new set of technical challenges, mainly related to signal processing. In the following paragraphs, the focus will be on radiated EMI measurements and the

issues related to signal discernment in traces and data handling.

2. Discernment of Signals in Traces

A swept EMI receiver has a definite advantage over a stepped receiver: the optimization of the probability of signal detection. The receiver has to be swept as fast as possible and multiple sweeps over the same frequency range have to be taken. This multi-sweep test strategy results in a lot of measurement traces, which require special data handling in the controlling software. It is not feasible to save all digital points because of the amount of memory needed. More importantly, a lot of trace points are only associated with the measurement system's noise floor, and many data points adjacent to signal maxima do not provide new information. Using such a set of data as the input of a maximization or measurement procedure would cause measurements at irrelevant frequency points and thus lengthen the test time considerably. Signal processing is necessary to discern signals in traces. This requires an algorithm capable of detecting signals by evaluating adjacent frequency points and assigning the appropriate amplitude and frequency to a dis-

Limited access to these parameters is essential, because a change has a dramatic impact on the measurement result. For instance, change of the *Peak Excursion* criterion from a lower to a higher value will usually result in a smaller number of signals discerned in the same trace. Furthermore, results of signal comparisons as well as list manipulation operations are impacted by the signal matching criteria shown in the interface.

The algorithm that discerns the signals processes traces by using two Boolean variables, *PSF* ("Positive Slope Found") and *NSF* ("Negative Slope Found"), and a variable, *Peak Value*, which stores the maximum trace amplitude based on the state of *PSF*. Both *NSF* and *PSF* are set to False before the actual trace processing starts. The leftmost point, which represents the start frequency of the trace, initially serves as a reference point for the determination of a rise in the trace as defined by the *Peak Excursion* criterion. The algorithm processes the data points from the start frequency toward the stop frequency, checking simultaneously for an amplitude lower than the initial reference point and the first rise in the trace (Figure 2). If an amplitude that is lower than the current reference point is found, the lower amplitude becomes the new reference value. When an amplitude meets or exceeds the *Peak Excursion* criterion relative to the current reference point, *PSF* is set to True. From this point on, the amplitudes of all following trace points are stored in the *Peak Value* variable until a fall in the trace is detected according to the *Peak Excursion* criterion. The storage procedure for trace amplitudes in the *Peak Value* variable utilizes a "maximum hold" function to retain the maximum value found during the analysis. Whenever data is stored in the variable (*PSF*=True, *NSF*=False), the reference for the detection of a fall in the trace is set to the currently processed point. If a fall is detected, *NSF* is set to True. The maximum amplitude retained in the variable *Peak Value* is associated with a frequency in the trace data array. This frequency and amplitude will be reported as a discerned signal and stored in a list. Now, both *PSF* and *NSF* are set to False and the processing starts over again from the current data point on.

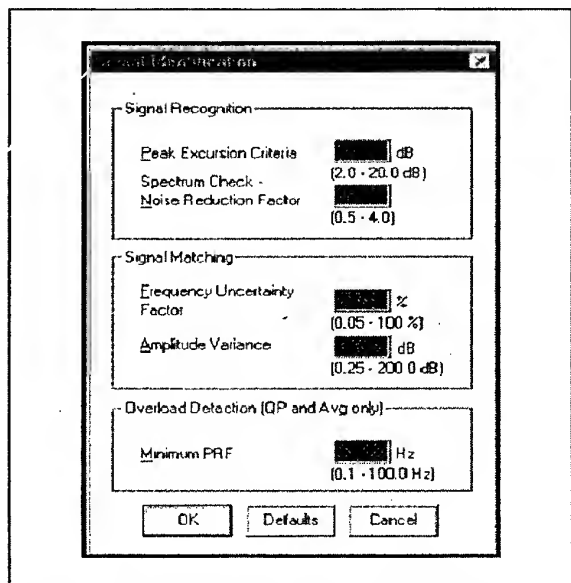


Figure 1: Signal identification parameter interface

cerned signal. This information, along with other signal attributes like antenna height and turntable angle at the time of measurement, can be stored in a list.

A key parameter used by the discernment algorithm is the *Peak Excursion* entry in the software interface shown in Figure 1. Other significant criteria related to signal processing are also part of this central interface to ensure ease of use and to provide protection against unwanted modifications of these values by non-qualified personnel.

The trace shown in Figure 2 is processed by the algorithm in the following way: the first data point is used as the reference and retained, since now lower values are found before the first rise in the trace as defined by the *Peak Excursion* criterion. At this point *PSF* is set to true and data storage of amplitudes in the *Peak Value* variable occurs as long as increasing amplitudes are encountered. The amplitude of the first maximum, D_1 , will be retained; the following data points are discarded because their amplitudes are lower than the value at D_1 . No storage into *Peak Value* takes place until data point D_3 is processed and higher amplitudes are detected. The drop between point D_1 and D_2 does not meet or exceed the

Peak Excursion criterion and thus is ignored. The maximum amplitude at data point D₄ is stored and the refer-

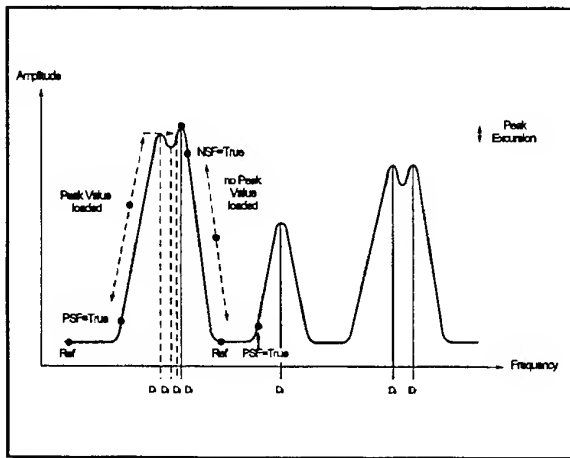


Figure 2: Signal discernment in traces

ence moved to this trace element. Thereafter, only lower amplitudes are detected while processing adjacent points. When a fall that meets or exceeds the *Peak Excursion* criterion is found, amplitude D₄ is related to its frequency in the trace array and saved in a list. *PSF* and *NSF* are set to False and the processing starts over again from this point on. The reference is now moved along the trace as long as consecutively lower amplitudes are found.

The algorithm detects four signals in the example trace at data points D₄, D₅, D₆ and D₇. The impact of the *Peak Excursion* value, which is user definable, is obvious; a smaller value would have caused the discernment of an additional signal at point D₁. A higher value will cause fewer signals to be discerned; for example, the signal at point D₆ might have been discarded. A careful selection of this value is necessary to ensure proper measurement results.

3. Signal Matching Parameters

It is often desirable to identify two signals as duplicate signals; for example, to avoid multiple storage in a list. Since no signal has a perfectly stable frequency and amplitude, a signal comparison cannot just include a check of their nominal frequency and amplitude values; frequency uncertainty, amplitude variations and signal characteristics must be used during the comparison of two signals to identify them as "the same signal". Even if their nominal values differ from each other, the algorithm has to be able to identify them as duplicate signals. Furthermore, the EMI receiver has a limited frequency and amplitude accuracy, which both contribute to the signal ambiguity and therefore demand a more sophisticated comparison algorithm. For example, a signal

might be found in the first trace at 150 MHz with an amplitude of 60 dB μ V and in the following trace at 150.5 MHz with a 59 dB μ V signal level. If duplicate signals are not desired, a decision must be made to either retain both signals in case they are truly different signals, or discard one signal. In the latter case, an additional decision is required to determine which of the two signals to retain. This process, known as signal matching, involves two parameters, frequency uncertainty and amplitude

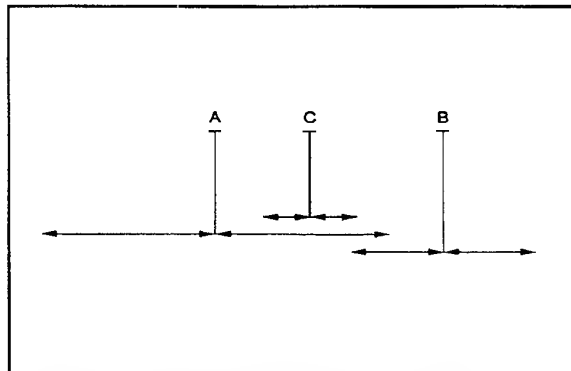


Figure 3: Frequency uncertainty specification

variance, which can be specified by the user in a dedicated interface (Figure 1).

The application of the frequency uncertainty parameter is shown in Figure 3. Three signals, - A, B and C - were discerned in three different traces and have identical amplitudes. Their individual frequency uncertainties, indicated by the arrows, are different. In the first step of the matching process, possible duplicate signals ("candidates") are determined, based on the nominal frequency and frequency uncertainty. Two signals are candidates if the nominal frequency of one signal lays within the uncertainty range of the reference signal. This does not mean that the frequency uncertainty of one signal has to be fully contained in the reference signal's range. In the example, signal A is the reference for the comparison and signal C lies within A's uncertainty range; therefore A and C are candidates. The nominal frequency of signal B is not contained in signal A's frequency uncertainty. B does not qualify as a candidate, even though their uncertainty ranges overlap. For that reason B will be retained, because it is not considered a duplicate signal. In the next step, a decision is made about which candidate signal, A or C, to keep. The most accurate signal, C in this case, will be kept because it has a smaller frequency uncertainty associated with it. If two candidates have identical frequency uncertainties, the reference signal will be kept. It should be noted that the order of the comparison is very important because the results may differ. If signal B is chosen as a reference, neither signal A's nor C's nominal frequency lays within B's uncertainty range. Therefore, no candidates are identified and all three signals are retained. The signal matching algorithm applies the fre-

quency uncertainty criterion first, then uses the amplitude variation for further identification.

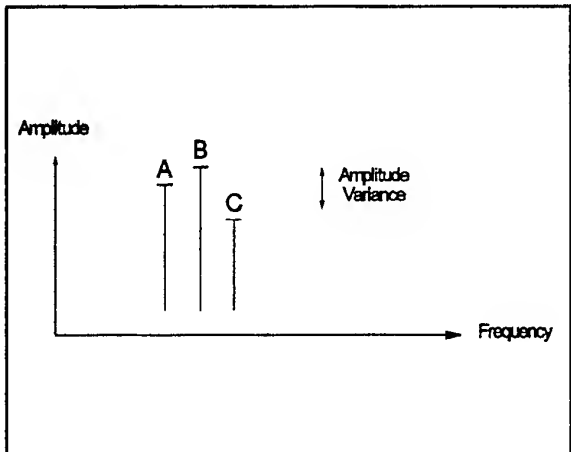


Figure 4: Amplitude variance specification

In Figure 4, the use of the amplitude variance is shown. The nominal frequencies of signals B and C are assumed to lie within the frequency uncertainty of reference signal A, and all three signals have the same frequency uncertainty but different amplitudes. The frequency uncertainty check determines that all three signals are candidates. The amplitude variance specification is applied to determine which signals to discard. Since signal B's amplitude is within the amplitude variation range of reference signal A, they are identified as candidates. The matching algorithm retains the signal with the higher amplitude, in this case signal B. If candidates have identical amplitudes, the reference signal will be kept. The amplitude of signal C is considerably lower and does not lie within the amplitude variation window. Therefore, signal C will be stored as a separate signal. In general, the most accurate signal with the lowest frequency uncertainty will be retained. If the candidate signals have iden-

tical amplitudes, the amplitude variation is used to determine the resultant signal. In this case, the candidate with the highest amplitude will be used.

If multiple signals are contained within the uncertainty window of the reference signal, as shown in Figure 5, a determination of the candidate closest to the reference has to be made. Each distance between the reference and all other signals is calculated and the candidate with the shortest distance is retained. All other signals in the uncertainty window will be discarded and not used by the matching algorithm. In Figure 5, signal C and the reference will be kept and the algorithms described above are applied to these two signals only.

4. Summary

List-based EMI software packages offer distinct advantages over trace-based products. Signal lists provide powerful comparison, selection, and sorting processes needed to complete many different tasks. For example, discrimination between ambient signals and EUT emissions is greatly simplified by comparing two lists containing the appropriate information. Sorting signals in a list by turntable angle instead of frequency can considerably speed up an interactive maximization process. The discernment of signals in EMI receiver traces requires a powerful algorithm, which must be flexible enough to accommodate different measurement needs and test environments. Signal matching, a fundamental capability necessary for list comparisons, must take different attributes of signals into account when attempting to identify duplicate emissions. A software product can perform these tasks, but the selection of key parameters used by these algorithms has to be made by the user.

5. References

1. W. Schaefer, "New Advances in Radiated EMI Measurements", Proceedings of the 1994 international EMC/ESD Symposium, Atlanta, GA, USA.

Biography

Werner Schaefer holds a degree of Diplom-Ingenieur and an MBA. His professional experience has been in the areas of microwave measurements, application software development and EMC measurements. He is an active member of ANSI C63, SC1, SC3, SC6 and a US representative to CISPR A, involved in the development of EMI standards, and a NARTE-certified EMC engineer. He has published numerous papers on EMC and microwave topics in Europe and the USA, and has co-authored a book on microwave measurement techniques.

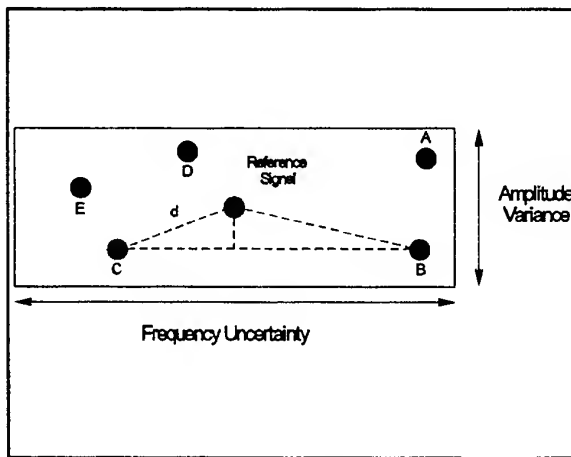


Figure 5: Multiple signal matching

LOOP ANTENNAS IN EMC METROLOGY

Tadeusz W. Więckowski, Zbigniew M. Jóskiewicz

Technical University of Wrocław
Institute of Telecommunication and Acoustics
Wybrzeże Wyspiańskiego 27, 50-370 Wrocław, POLAND
Phone: +48 71 214998, Fax. +48 71 223473

A new method is proposed for determining the emissions from small-sized devices (sources of interference). In the method use is made of an array of three orthogonally arranged double-loaded loop antennas, at frequencies above 30 MHz. With the measured values of the currents flowing across each load it is possible to determine the parameters of the source (equivalent electric and magnetic dipole moments) placed in the centre of the measuring system. Knowing the parameters of the source, we can determine the radiation pattern for the device under test in an arbitrary environment.

1. INTRODUCTION

In the past few years, more and more interest has been focused on the problem of how to reduce unwanted emissions of electromagnetic fields from electric and electronic devices. This is a key problem not only in electromagnetic compatibility, but also in transmitting or processing top secret information. To reduce unwanted emission it is necessary to perform reliable measurements with adequate methods.

For preliminary emission measurement, alternative methods to those being used in open area test site (OATS) measurements seem to be best situated. They consist in determining the parameters of the radiation sources for the device under test (DUT) instead of measuring the strength of the radiated electromagnetic field. An electrically small source of interference can be described in terms of equivalent dipoles - an electric dipole of moment (\bar{p}) and a magnetic dipole of moment (\bar{m}) [1]. Once the moments of the equivalent dipoles have been determined, it is possible to establish the radiation pattern of the DUT in an arbitrary environment. In some instances, these may be measuring conditions resembling those of an open-area test site.

There are three alternative methods of emission measurement - the one involving an array of three double-loaded loop antennas arranged perpendicularly to one another, the TEM cell technique and the GTEM

cell approach. The array of three loops, arranged orthogonally to one another (CISPR 15), which enables determination of the magnetic field strength components, has found wide acceptance in engineering. It makes use of transfer function relating the currents across each load to the components of electromagnetic field strength. The method proposed by Kanda and Hill [2] involves an array of three double-loaded loops with orthogonal arrangement to determine the moments of equivalent dipoles, both electric and magnetic. However, because of the adopted simplifications, the method does not work with frequencies higher than 30 MHz. In our study, those simplifications were modified to make the technique workable at higher frequencies as well.

2. CURRENT IN THE LOOP ANTENNA

To determine the function that relates the components of the equivalent electric dipole moment and the equivalent magnetic dipole moment to the currents across the loads of double-loaded loop antennas it is sufficient to consider one out of the three antennas belonging to the array and to generalize the results onto the remaining two.

Let us now consider a loop antenna of a radius b . The antenna lies on a plane xy , and has been situated so that its centre coincides with origin of the co-ordinate system xyz (Fig. 1). The antenna is loaded with two identical impedances Z_L at two opposite points: ($\varphi = 0$) and ($\varphi = \pi$)

The DUT introduced into the centre of the antenna can be substituted by an equivalent electric dipole of a moment (\bar{p}) and by an equivalent magnetic dipole of a moment (\bar{m}). For a Cartesian co-ordinate system the two moments take the form:

$$\bar{p} = \bar{I}_x p_x + \bar{I}_y p_y + \bar{I}_z p_{zx} \quad (1)$$

$$\bar{m} = \bar{I}_x m_x + \bar{I}_y m_y + \bar{I}_z m_{zx} \quad (2)$$

where: $\vec{I}_x, \vec{I}_y, \vec{I}_z$ are unit vectors. The time dependence $e^{j\omega t}$ is suppressed.

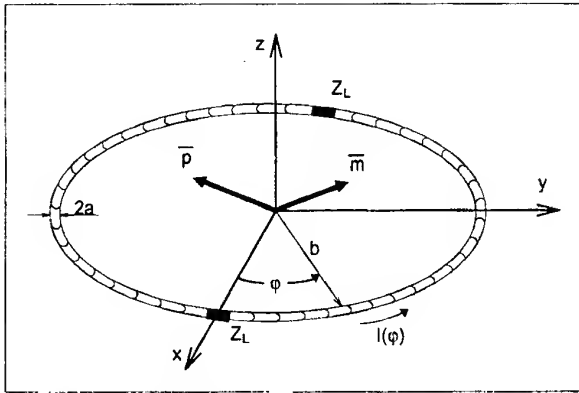


Fig. 1. Double-loaded loop antenna with indicated moments of equivalent electric dipole and equivalent magnetic dipole

The electric field component (tangential to the surface of the loop antenna), induced by the equivalent electric dipole and by the equivalent magnetic dipole, is described by following relation:

$$E^i(b, \varphi) = A_0 + A_1 \cos \varphi + B_1 \sin \varphi \quad (3)$$

where

$$A_0 = m_z g_m, \quad A_1 = p_y g_e, \quad B_1 = -p_x g_e, \quad (4)$$

$$g_m = \frac{k^2 \cdot \zeta_0}{4\pi} \cdot \left[1 - \frac{j}{k \cdot b} \right] \cdot \frac{e^{-jk \cdot b}}{b}, \quad (5)$$

$$g_e = -\frac{j \cdot k \cdot \zeta_0}{4\pi} \cdot \left[1 - \frac{j}{k \cdot b} - \frac{1}{(k \cdot b)^2} \right] \cdot \frac{e^{-jk \cdot b}}{b}. \quad (6)$$

If we make use of the boundary condition for the components of the electric field tangential to the surface of the wire of which the antenna has been made:

$$E^i(b, \varphi) + E(b, \varphi) = 0, \quad (7)$$

where $E^i(b, \varphi)$ denotes the electric field component induced by the equivalent electric dipole and by the equivalent magnetic dipole, and $E(b, \varphi)$ is the electric field component induced by the current flowing in the antenna, than we can write [3]:

$$\sum_{n=-\infty}^{\infty} \left[\frac{j\zeta}{2} \cdot a(n) \cdot I(n) - b E_b^i(n) \right] \cdot e^{-jn\varphi} = -Z_L I(0) \delta(\varphi) - Z_L I(\pi) \delta(\varphi - \pi) \quad (8)$$

where

$$a(n) = a(-n) = \frac{kb}{2} [\mu(n+1) + \mu(n-1)] - \frac{n^2}{kb} \mu(n) \quad (9)$$

$$\mu(n) = \mu(-n) = \frac{1}{2 \cdot \pi} \int_{-\pi}^{\pi} \frac{b \cdot e^{-jk \cdot R_n}}{R_b} \cdot e^{jn \cdot (\varphi - \varphi')} d\varphi \quad (10)$$

$$R_b = \sqrt{4b^2 \sin^2 \left(\frac{\varphi - \varphi'}{2} \right) + a^2} \quad (11)$$

where $I(n)$ is the coefficient of Fourier series expansion for the current flowing in the antenna; $E_b^i(n)$ denotes the coefficient of Fourier series expansion for the electric field component (tangential to the surface of the antenna wire) induced by both equivalent electric and equivalent magnetic dipoles; a stands for the radius of the cross-section of the wire of which the antenna has been made; b represents the radius of the antenna, and $\delta(\varphi)$ is Dirac delta function.

Solving equation (8) with respect to $I(n)$ and incorporating the expression obtained for the coefficient $I(n)$ into:

$$I(\varphi) = \sum_{n=-\infty}^{\infty} I(n) e^{-jn\varphi} \quad (12)$$

we derive the relation describing the current flowing in the antenna, which takes the form

$$I(\varphi) = \sum_{n=-\infty}^{\infty} \frac{e^{-jn\varphi}}{a(n)} [2\pi b E_b^i(n) - I(0) Z_l - I(\pi) Z_l e^{jn\pi}] \quad (13)$$

Substituting argument (φ) by the values of the angles which describe the positions of the antenna loads, we obtain a set of equations. Their solutions with respect to $I(0)$ and $I(\pi)$ lead to the equations that define the currents flowing across the antenna loads. Hence, we have

$$I(0) = \frac{2\pi b}{j\pi\zeta} \left[\frac{m_z \cdot g_m}{a(0) \cdot (1 + 2 \cdot Y_0 \cdot Z_L)} + \frac{2 \cdot p_y \cdot g_e}{a(1) \cdot (1 + 2 \cdot Y_1 \cdot Z_L)} \right] \quad (14)$$

$$I(\pi) = \frac{2\pi b}{j\pi\zeta} \left[\frac{m_z \cdot g_m}{a(0) \cdot (1 + 2 \cdot Y_0 \cdot Z_L)} - \frac{2 \cdot p_y \cdot g_e}{a(1) \cdot (1 + 2 \cdot Y_1 \cdot Z_L)} \right] \quad (15)$$

where

$$Y_0 = \frac{1}{j\pi\zeta} \left[\frac{1}{a(0)} + \sum_{n=1}^{\infty} \frac{1}{a(2n)} \right] \quad (16)$$

$$Y_1 = \frac{2}{j\pi\zeta} \left[\sum_{n=1}^{\infty} \frac{1}{a(2n-1)} \right] \quad (17)$$

The admittances Y_0 and Y_1 incorporated in the relations of (14) and (15) represent the admittances for magnetic and electric field, respectively. They can be calculated in terms of (16) and (17). For antennas which are small in size as compared to the wavelength of the electromagnetic field radiated by the DUT (and this condition is fulfilled in the frequency range of up to 30 MHz), it is possible to confine oneself to the initial terms of the Fourier series incorporated in the relation of

(16) and (17). Because of the potentiality for promoting considerable errors, it is not advisable to make use of such simplifications when frequencies higher than 30 MHz are involved.

3. TRANSFER FUNCTION

Addition of the currents flowing across the two antenna loads situated at two opposite points ($\varphi = 0$) and ($\varphi = \pi$) gives the resultant current I_s , which depends only on the component of the equivalent magnetic dipole moment m_z (perpendicular to the surface of the antenna):

$$I_s = 4 \cdot \pi \cdot b \cdot \frac{m_z \cdot g_m}{j \cdot \pi \cdot \zeta \cdot a(0) \cdot (1 + 2 \cdot Y_0 \cdot Z_L)} . \quad (18)$$

Subtraction of the currents flowing across the two antenna loads yields the current I_d , which depends only on the component of the equivalent electric dipole moment p_y (tangential to the surface of the antenna and perpendicular to the line passing through the antenna loads):

$$I_d = 4 \cdot \pi \cdot b \cdot \frac{2 \cdot p_y \cdot g_e}{j \cdot \pi \cdot \zeta \cdot a(0) \cdot (1 + 2 \cdot Y_1 \cdot Z_L)} . \quad (19)$$

Thus, knowing the sum and difference of the currents across the antenna loads it is possible to determine the components of the equivalent magnetic dipole moment and of the equivalent electric dipole moment. Hence we can write

$$m_z = \frac{j \cdot \pi \cdot \zeta \cdot a(0) \cdot I_s \cdot (1 + 2 \cdot Y_0 \cdot Z_L)}{4 \cdot \pi \cdot b \cdot g_m} \quad (20)$$

$$p_y = \frac{j \cdot \pi \cdot \zeta \cdot a(0) \cdot I_d \cdot (1 + 2 \cdot Y_1 \cdot Z_L)}{8 \cdot \pi \cdot b \cdot g_e} \quad (21)$$

The remaining components (m_x, m_y, p_x, p_z) of the equivalent magnetic dipole moment and of the equivalent electric dipole moment can be determined by an array (instead of one double-loaded loop) involving three loop antennas arranged perpendicularly to one another.

For the loop antenna situated in the xz plane we can establish the components m_y and p_x , whereas for the one situated in the yz plane the components m_x and p_z . It is convenient to re-write the relations of (20) and (21) in the following form:

$$m_z = F_m \cdot I_s \quad (22)$$

$$p_y = F_e \cdot I_d \quad (23)$$

where

$$F_m = \frac{j \cdot \pi \cdot \zeta \cdot a(0) \cdot (1 + 2 \cdot Y_0 \cdot Z_L)}{4 \cdot \pi \cdot b \cdot g_m} \quad (24)$$

$$F_e = \frac{j \cdot \pi \cdot \zeta \cdot a(0) \cdot (1 + 2 \cdot Y_1 \cdot Z_L)}{8 \cdot \pi \cdot b \cdot g_e} \quad (25)$$

The relation of (24) is a transfer function which relates the component of the equivalent magnetic dipole moment (normal to the surface of the antenna) to the sum of the currents across the two loads. The relation of (25) is a transfer function which relates the component of the equivalent electric dipole moment (tangential to the surface of the antenna and perpendicular to the line passing across the loads of the antenna) to the difference of the currents across the two loads.

Assuming that the effect of the DUT size on the input impedance of the antenna is negligibly small, it may be anticipated that the functions F_m and F_e depend only on the geometry of the antenna, as well as on the values of impedance Z_L and frequency. It should be noted that if we determine the admittances Y_0 and Y_1 , the number of elements in the series must fulfil the condition

$$n > k \cdot b . \quad (26)$$

If the condition of (26) is satisfied, the determination of the admittances Y_0 and Y_1 for each frequency will be correct. Thus, during measurements, it is possible to make use of transfer function calculated only one. Figures 2 and 3 shows examples of transfer functions calculated for double-loaded loop antenna with impedances $Z_L=50 \Omega$. The antenna had a diameter 2m. and a cross-section radius $a = 0.01$ m. The transfer function can be determined experimentally by introducing into the measuring volume an electrically small loop antenna of a known magnetic dipole moment and by measuring the currents in individual antennas or the voltages across the loads. The procedure is repeated for an electrically small linear antenna of a known electric dipole moment.

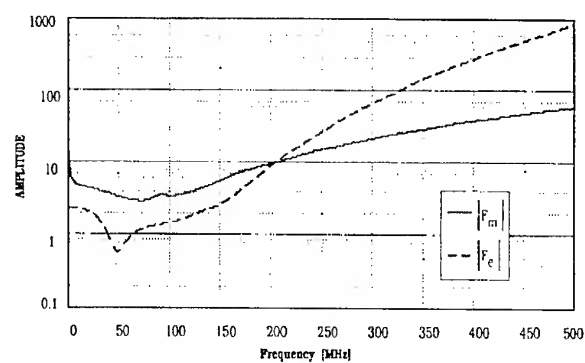


Fig. 2. Modules of functions F_m and F_e in frequency domain

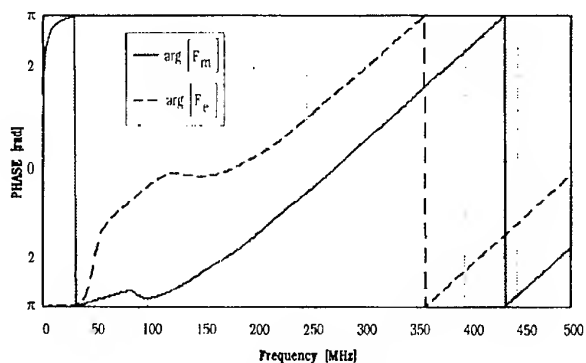


Fig. 3. Arguments of functions F_m and F_e in frequency domain

The values of the loading impedance Z_L exerts an influence on the transfer functions F_m and F_e and, consequently, on the sensitivity of the loop antenna to the field induced by the equivalent electric dipole and by the equivalent magnetic dipole. This influence is shown in Figs. 4 + 7. The choice of the Z_L value is a kind of compromise, but in most instances the value of Z_L corresponds with that of the input impedance for the measuring circuit.

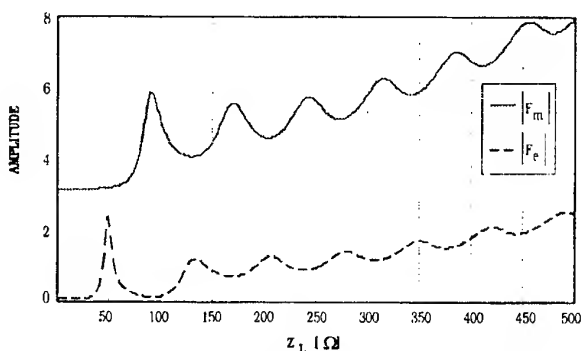


Fig. 4. Modules of functions F_m and F_e versus impedance Z_L (for frequency 20 MHz)

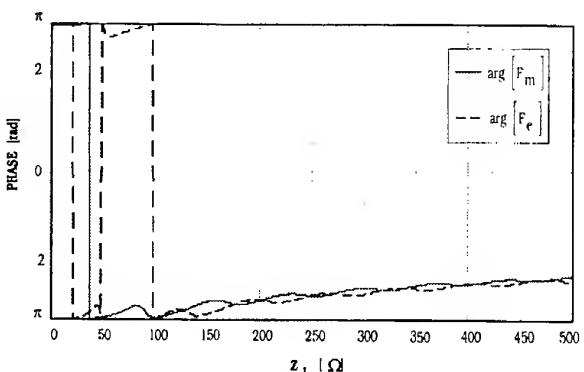


Fig. 5. Arguments of functions F_m and F_e versus impedance Z_L (for frequency 20 MHz)

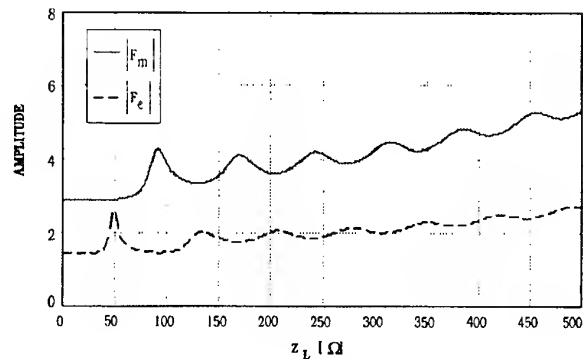


Fig. 6. Modules of functions F_m and F_e versus impedance Z_L (for frequency 100 MHz)

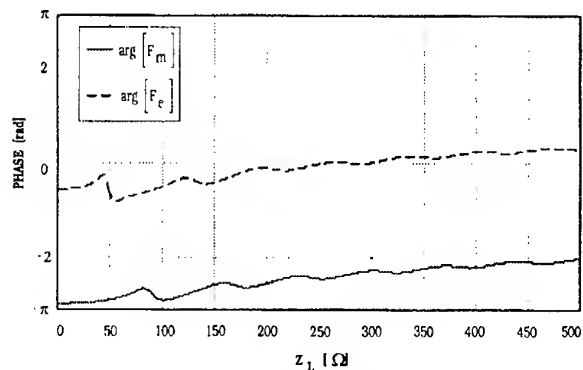


Fig. 7. Arguments of functions F_m and F_e versus impedance Z_L (for frequency 100 MHz)

If the components of the equivalent electric dipole moment and equivalent magnetic dipole moment are known, we can determine complete radiation patterns of the DUTs in an arbitrary environment.

4. MEASURING SET-UP

A measuring set-up involving three circular, double-loaded loop antennas arranged orthogonally to one another has the inherent advantage of providing appropriate conditions for the measurement of an electromagnetic field induced by equivalent electric and magnetic dipoles, and - consequently - for the determination of their moments.

On placing the DUT in the measuring volume of the set-up, we determine the components of the equivalent magnetic and equivalent electric dipole moments by making use of the following: the transfer functions presented earlier, as well as the measured sums and differences of the currents across the loads of the three loop antennas. To determine the parameters of the radiation source we can also use the values of the voltages across the antenna loads.

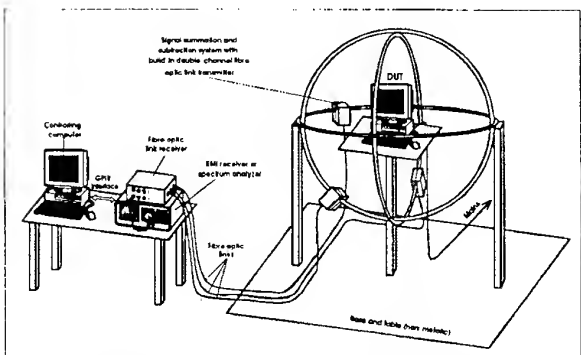


Fig. 8. Example of a set-up using an array of three double-loaded loop antennas arranged orthogonally to one another to enable measurement of the radiated electromagnetic field

Figure 8 shows a set-up which measures the emission produced by electric and electronic devices. The set-up consists of three loop antennas arranged perpendicularly to one another, so there is no need to revolve it in order to measure all the parameters of the radiation source. The feeding wires remain in one place and do not change the values of the components of the measured magnetic and electric dipole moments. To eliminate propagation of errors by the measured values (which is due to the influence of the electromagnetic field induced by the DUT on the measuring cables) it is advisable to use fibre optic links.

There are two variations of the measuring set-up. In one of them the information about the current across the loads is sent to the system of signal summation and subtraction (placed far away from the measuring set) via fibre optic links. In the other one the signal summation and subtraction system is an integral part of the loop antenna array. Information about the sum and difference of the currents or voltages across the loads is passed through the fibre optic links. Relevant signals (measured at the output of the system with EMI receiver or a spectrum analyzer) make it possible to determine the components of the equivalent magnetic and equivalent electric dipole moments. To determine the emission of the DUT in an arbitrary environment numerical calculations are carried out, using an equivalent model describing the radiation of the DUT.

Under the Project financed by the Committee for Scientific Research, a new set-up is being constructed, which will be used for the verification of the method proposed.

5. SUMMARY

Measuring set-ups involving alternative methods for determining emission from electric and electronic devices have found wide acceptance in the past few years. Compared to open area test site method, they are more cost-effective. Another advantage of the measuring set-up presented here is the potentiality for determining the emission from the DUT in an arbitrary environment on the basis of a defined equivalent radiation model.

Such an analysis can be carried out with no additional measurements. Like TEM or GTEM cells, the array of three double-loaded loop antennas arranged perpendicularly to one another may be of utility in preliminary measurements of the emission. Even though the method proposed has not been verified, it can be anticipated that the results obtained via this route will propagate smaller errors than the other available methods. In our method the frequency range is smaller than in the GTEM cell approach, but it may be expected that our method will apply to frequencies much higher than 30 MHz.

Despite their unquestionable advantages, the set-ups using alternative methods do not allow emission measurements for very electric or electronic devices - unlike the measurements in OATS which do. For this reason it is advisable to equip EMC laboratories with standard measuring set-ups as well.

6. REFERENCES

- [1] H. Koepke, M. T. Ma, „A New Method for Determining the Emission Characteristics of Unknown Interference Source”, 5th Symposium and Exhibition on EMC, Zurich, March 1983, pp. 35-40.
- [2] M. Kanda, D. A. Hill, “New Emission Measurement Method for an Electrically Small Source: a Three Loop Method and TEM Cell Method”, 13th Symposium and Exhibition on EMC, Wrocław, June 1992, pp. 310-312.
- [3] T. W. Więckowski, “Loop antennas in electromagnetic field metrology”: Scientific Papers of the Institute of Telecommunication and Acoustics of the Technical University of Wrocław, No. 34, Wrocław 1992 (monograph)

BIOGRAPHICAL NOTES

Tadeusz W. Więckowski is with the Institute of Telecommunication and Acoustics of the Technical University of Wrocław (Poland), where he works as an Professor in the field of communications systems and electromagnetic compatibility. He received the MSc and PhD degrees in telecommunication in 1976 and 1980, respectively. He is a member of Association of Polish Electrical Engineers and Organizing Committee of the Wrocław Syposia. Mr Więckowski is the autor of some 80 papers presented on international and national conferences.

Zbigniew M. Jóskiewicz received the MSc degree in telecommunications in 1994 from the Technical University of Wrocław (Poland). Since 1994 is with the Institute of Telecommunication and Acoustics of the Technical University of Wrocław, where he works as an Assistant Professor in the field of electromagnetic compatibility.

ELECTROMAGNETIC COMPATIBILITY TESTS ON HEARING AIDS

Ali Ihsan YUREKLI

TUBITAK Marmara Research Center

National Electronics and Cryptology Research Institute, 41470 Gebze-Kocaeli, Turkey

Phone:+90-262-6412300, Fax:+90-262-6412309, E-mail: yurekli@mam.gov.tr

Mehmed OZKAN

Bogazici University, Institute of Biomedical Engineering, 80815 Istanbul, Turkey

Phone: +90-212-2631500, Fax:+90-212-2575030, E-mail: mehmed@boun.edu.tr

Fatih USTUNER

TUBITAK Marmara Research Center

National Electronics and Cryptology Research Institute, 41470 Gebze-Kocaeli, Turkey

Phone:+90-262-6412300, Fax:+90-262-6412309, E-mail: ustuner@mam.gov.tr

Radio transmitter emissions that have intensity variations in audio frequencies cause interference on sensitive electronic equipment. Hearing aid user complaints caused by this kind of interference were increased by the introduction of digital mobile phones in recent years. In order to understand this interaction, the electromagnetic compatibility of 16 different hearing aid types was measured for high-frequency electromagnetic fields, particularly for those emitted by digital mobile phones. An automated PC-controlled test setup was developed for testing. The setup consisted of a GTEM cell where high frequency fields were generated. Draft version of IEC 118-13 standard was utilized as a basis for the test methodology. All of the hearing aids showed susceptibility to some degree. Six of the hearing aids were found to produce levels above the level proposed by the standard. Additionally, increasing levels of the electric field strength were found to cause a quadratic increase in sound pressure levels produced at the hearing aid output.

1. INTRODUCTION

Digital mobile phones, also known as cellular phones, were introduced to the public use only about ten years ago but their commercial and social benefits have quickly caused them to be accepted as an indispensable adjunct to modern life. However, digital mobile phones, with their portability and pulsed transmissions, have created a new class of interference issues. This interference typically presents itself as a buzz in the effected audio electronic equipment especially when the intensity of the radio wave transmitted from the digital

phone varies at an audible rate. Interference to other equipment is also possible.

In the digital system known as GSM (Global System for Mobile communications) which is used widely in many European countries the voice information is digitally encoded. The GSM phones transmit to the base station in the frequency band 890 to 915 MHz. There are a number of power ranges for the GSM system, but for the handheld mobile phones only 0.8 and 2.0 W peak power levels are available. The GSM transmission is pulsed with a repetition frequency of approximately 217 Hz and a pulse width of approximately 0.6 ms. This has several advantages, one of which is the instantaneous transmitted power can be greater, giving better reception, although the average power is still low enough to conserve battery life. Unfortunately, the level of electromagnetic interference (EMI) depends on the instantaneous power and engineers would therefore intuitively expect more interference problems from digital phones than with analogue phones.

Hence, the interference problem with hearing aids is due to the essential nature of the pulsed emissions from the GSM transmitter, and is not an incident by-product which might, for example, be solved by improved shielding of the digital phones.

This study involves an objective approach to the hearing aid - digital mobile phone interaction problem with appropriate test methodology and setup.

2. HEARING AID SELECTION

In order to understand the interaction between hearing aids and digital mobile phones, tests were

performed on 16 Behind-the-Ear (BTE) hearing aids from 7 different producers. There are approximately 15 brand names in hearing aid market of Turkey and 16 hearing aids which are selected include most widely used types. Hearing aids tested cover a range of electroacoustical characteristics as shown in Table 1. Note that SPL represents the sound pressure level in dB with reference to 20 μ Pascal.

Table 1. Hearing aids tested for immunity.

HA No	Frequency Range (Hz)	Max. Output (dB SPL)	Gain at 1 kHz (dB SPL) *
1	110 - 4800	133	68 / 57
2	270 - 5800	126	48 / 38
3	120 - 4500	140	73 / 56
4	320 - 4800	137	57 / 50
5	125 - 4300	140	56 / 51
6	300 - 5700	122	56 / 41
7	150 - 5000	140	62 / 53
8	150 - 5000	134	56 / 50
9	200 - 6200	132	55 / 50
10	225 - 6000	133	51 / 33
11	215 - 4300	133	47 / 37
12	75 - 4800	139	55 / 39
13	325 - 6000	126	33 / 27
14	900 - 7100	134	45 / 39
15	50 - 6200	129	49 / 46
16	110 - 4800	133	57 / 51

* Left-hand side gives the acoustic gain measured with 25mm tubing length whereas right-hand side gives that measured with 500 mm tubing length.

3. TEST ENVIRONMENT AND SETUP

In order to measure immunity of hearing aids, tests have to be carried out in an RF controlled environment. The hearing aid must be isolated from other sources of interference and exposed to only one type of source that is of interest.

Using standard digital wireless telephone as an RF source is not feasible due to reflections, telephone power switching, variation in carrier frequency, etc. Instead, simulating the emissions using a RF signal source and generating it inside a GTEM cell is preferred. A GTEM cell associated with proper RF signal source is a suitable platform to perform the tests.

In order to apply specific field strength levels on the hearing aids, a closed loop control system is used. The applied power is controlled through a power meter to obtain and maintain a specific field strength along the frequency range.

Generating a specific electromagnetic (EM) field in a controlled area is one end of the immunity test setup. At the other end lies the acquisition of data at the hearing aid output as a result of electromagnetic field exposure. In this part of the setup acoustic output is measured and recorded. The first element of this end is a 500 mm long plastic tubing of 2 mm inner diameter that is connected to the horn of a BTE type hearing aid under test. This tubing extends till it connects to the 2 cc coupler which is a standard device used in hearing aid

testing for simulating the ear cavity [1,2]. Since the coupler and the microphone are metallic and can distort the electromagnetic field around the hearing aid, both must be kept at a distance from the hearing aid. Keeping the microphone away from the test space is furthermore beneficial since the microphone itself can also be affected from the field. That is why we use a tubing of such length, i.e. 500 mm instead of conventional 25 mm used hearing aid testing. The plastic tubing is taken outside the test area through the honeycomb waveguides installed for ventilation purposes under GTEM. This resulted in the shift of test volume nearer to the input port and new calculation for the electric field generated since the septum height is changed.

Microphone precedes its preamplifier and both are connected to their power supply which also acts as a signal output port of the microphone-preamplifier system. The signal output is then connected to a lock-in amplifier in order to measure the sound pressure levels and to an oscilloscope to monitor the interference signal. Lock-in amplifiers need an internal or an external reference frequency and they measure the component of the input signal only at that specific reference frequency. This reference frequency (i.e. 1 kHz) is provided by the signal generator which also uses this 1 kHz frequency as a modulation frequency of its carrier wave. The data obtained from the lock-in amplifier are read by the computer via GPIB and saved to analyze them later.

Generation of field with specific characteristics using signal generator and power meter and acquisition of interference data from the lock-in amplifier are both are automatically controlled by means of a program developed for this study. The software has a user interface for appropriately setting of the test parameters, starting the measurement and saving the data after measurement. Equipment used in the experiment is listed in Table 2 and a schematic of the test setup is illustrated in Figure 1.

4. TEST PROCEDURE

There are two types of tests performed on hearing aids. The first test is based on draft version of IEC 118-13 where hearing aids are exposed to a constant field level in 800-960 MHz range. However, the method followed in this study has a few differences. The second test involves exposure of hearing aids to increasing levels of EM field at a constant carrier frequency.

As a first step in the first test, gain of hearing aid at 1 kHz is measured according to IEC 118-7. The same 500 mm tubing is used for comparability of the measurements. Hearing aid under test is placed on the test platform inside GTEM. Every hearing aid is tested for 4 orientations in the horizontal plane (with 90 degrees separation) and 1 orientation in the vertical plane. Input of the hearing aid is adjusted to microphone, telecoil or MT. In the user interface of the software, frequency range of the EM field and step size is determined. Also parameters of the hearing aids

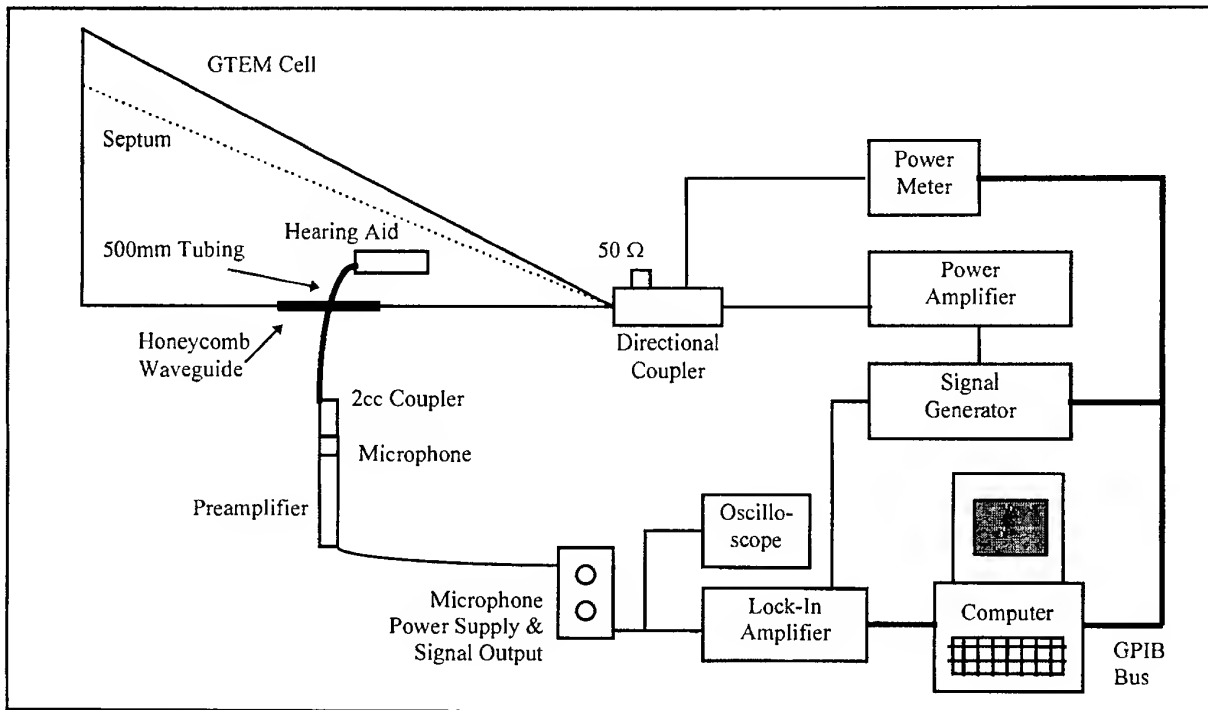


Figure 1. Experimental setup for immunity testing of hearing aids.

Table 2. Equipment used in testing.

Equipment	Manufacturer / Model
GTEM cell	Messelektronik Berlin / 1750
Signal Generator	Rohde & Schwarz / SMY 01
Power Amplifier	Amplifier Research / 50W1000A
Power Meter	Rohde & Schwarz / NRVS
Directional Coupler	Messelektronik Berlin / RK 100
Acoustic 2-cc Coupler	According to IEC 126
Microphone	Brüel & Kjaer / 4134
Mic. Preamplifier	Brüel & Kjaer / 2639
Mic. Power Supply	Brüel & Kjaer / 2804
Lock-In Amplifier	Stanford Research Sys. / SR 850
Oscilloscope	Hewlett-Packard / 54615 B
Computer	Tulip / Pentium 100
GPIB card	National Instruments / AT-TNT+
Software	National Inst./LabWindowsCVI

specific to that test are given for data recording. EM field applied is 80% AM modulated at 1 kHz in the 800-960 MHz range with at most 16 MHz steps. IEC 118-13 draft [3] proposes a 3 V/m (unmodulated carrier) field level for bystander situation where hearing aid user is supposed to be 2 m away from the interference source. However, we applied 6 V/m as a standard level since our first attempts at lower levels did not create measurable interference. (Yet, this does not turn out to be a problem since we also performed the second test where we investigated the dependence of interference on the magnitude of the EM field level applied). In order to determine the electromagnetic compatibility of hearing aids with digital mobile phones "Input Related Interference Level (IRIL)" is used as a performance

criterion. IRIL is found by subtracting the acoustic gain of the hearing aid at 1 kHz from the interference levels produced at the hearing aid output because of AM modulated (80% at 1 kHz) EM field exposure. Decreasing values of IRIL indicate increasing immunity. IEC 118-13 imposes a maximum of 55 dB SPL IRIL under 3 V/m.

5. TEST RESULTS

Sixteen hearing aids were tested for 5 orientations and 2 input positions (or 3 for those having MT input also) under 6 V/m field level. As a sample graph, Figure 2 shows the interference levels produced in one hearing aid (HA4) along 800-960 MHz range. Note that negative IRIL values in some orientations refer to interference levels less than the gain of the hearing aid.

The results for 6 V/m test level can be summarized as follows:

- Output related interference levels up to 140 dB SPL were created by just exposing the hearing aid to electromagnetic fields and without any sound input.
- Of all the 5 orientations tested, vertical orientation resulted in highest interference levels for each hearing aid with a few exceptional cases.
- 90° and 270° orientations on the horizontal plane produced lowest interference levels and were often near the noise level.
- Interference levels produced at horizontal 0° and 180° orientations were correlatable in many instances. The response of the hearing aid at these

orientations were nearly the same only with a shift of a few dB SPLs along the 800-960 MHz range.

- Microphone input generally produced higher interference levels than the telecoil input. But for the hearing aids with MT input also, microphone input showed up lower levels than the telecoil and MT inputs.
- Mini type hearing aids showed lowest interference levels with one exception.

The second test involved testing of hearing aids at a specific carrier frequency but exposing them to increasing field levels. Figure 3 illustrates a typical

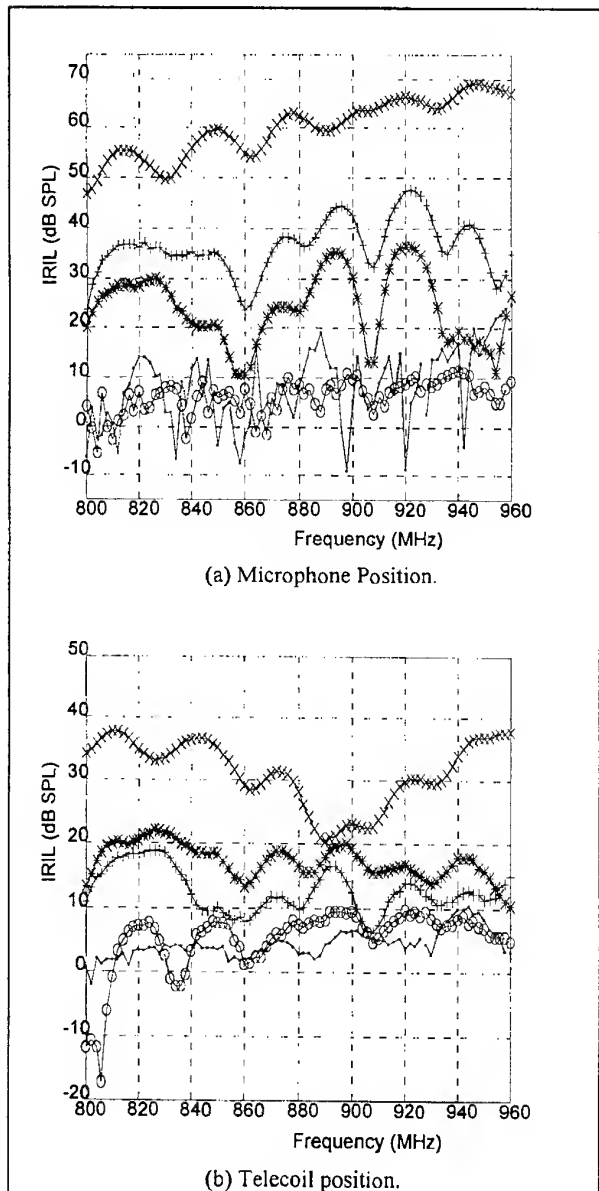


Figure 2. Interference levels measured at HA4 output when exposed to 6 V/m field level for (a) microphone and (b) telecoil position.

(xxxx) Vertical (****) Horz. 0 deg (----) Horz. 90 deg
 (++++) Horz. 180 deg (eeee) Horz. 270 deg

relationship between field strength and interference level for one hearing aid (HA1). Note that this time we have expressed the electric field strength in dB with reference to 1 V/m.

Figure 3 implies a linear relationship between the applied field strength and hearing aid output. The slope of the line is 2, i.e. every 1 dB increase in the field level corresponds to 2 dB increase in interference level provided that hearing aid output is not masked by the noise level or is not saturated. This holds for frequencies other than 900 MHz also. These results are consistent with previous studies [4,5,6].

Thus we can make an interpolation to 3 V/m field level from 6 V/m after expressing both in dB units. Halving the field level corresponds to a 6 dB decrease and this corresponds to 12 dB SPL decrease in interference levels.

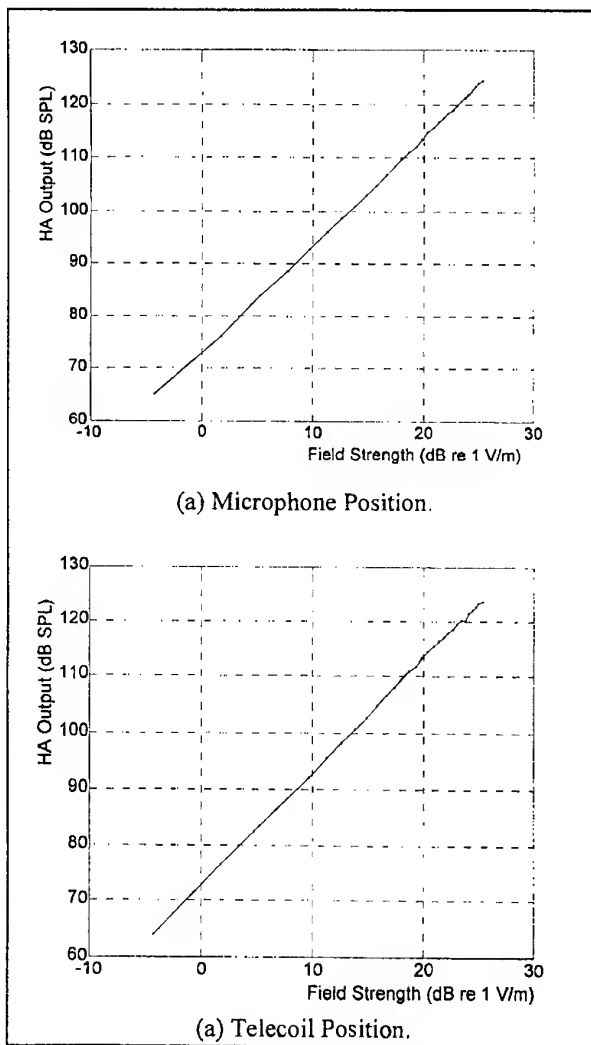


Figure 3. Output interference level of HA1 as a function of field strength for different inputs at 900 MHz carrier frequency.

6. CONCLUSION

Objective tests were performed in order to understand the interaction between hearing aids and digital mobile phones. Sixteen hearing aids were tested for immunity along 800-960 MHz range at 6 V/m test level. All of the devices produced acoustic output to some degree when they were exposed to amplitude modulated electromagnetic fields. Interference level depended on many parameters like the electromagnetic field level, input of the hearing aid and the orientation of the hearing aid in the test volume.

Interference levels up to 140 dB SPL were measured in the 800-960 MHz range of the carrier frequency. Six of the hearing aids were found to produce levels above the level proposed by the standard (55 dB SPL IRIL).

Particularly, a 1:2 dB ratio between the electric field strength and hearing aid interference level has been proved. In other words, whenever we increase field strength in 1 dB, hearing output increases in 2 dB. This 1:2 dB ratio proves to be a helpful tool in interpolating for any field strength level that was not tested.

Methodology followed and test setup developed in this study together with the results can be used to evaluate the electromagnetic compatibility of hearing aids to high frequency electromagnetic fields.

7. REFERENCES

- [1] IEC 126:1973, IEC Reference Coupler for the Measurement of Hearing Aids Using Earphones Coupled to the Ear by Means of Ear Inserts, International Electrotechnical Commission, Geneva, 1973.
- [2] IEC 118-7:1983, "Hearing Aids, Part-0: Measurement of the Performance of the Hearing Aids for Quality Inspection for Delivery Purposes", International Electrotechnical Commission, Geneva, 1973.
- [3] IEC 118-13:1995, "Hearing Aids, Part-13: Electromagnetic Compatibility Product Standard of Hearing Aids (Draft)", International Electrotechnical Commission, Geneva, June 1995.
- [4] G. Ravn and O.H. Soerensen, "Hearing Aids and GSM Mobile Telephones: Interference Problems, Methods of Measurement and Levels of Immunity", EHIMA GSM Project Final Report, 1995.

- [5] J.S.L. Strange, D. Byrne, K.H. Joyner and G.L. Symons, "Interference to Hearing Aids by the Digital Mobile Telephone System, Global System for Mobile Communications, (GSM)", National Acoustic Laboratories, NAL Report No.131, Australia, May 1995.
- [6] U. Richter and M. Schaedler, "EMV-Messungen an Hörgeräten" (German), Physikalisch-Technische Bundesanstalt, PTB Bericht-MA-51, Braunschweig, Germany, November 1996.

ACKNOWLEDGEMENTS

The authors gratefully acknowledge the considerable efforts of Dr. Ferda Akdas and Dr. Sezer Kulekci, Marmara University Faculty of Medicine, for providing the hearing aids and technical information on them.

BIOGRAPHICAL NOTES

Ali İhsan Yürekli has received his BS degree in Physics (1994) and MS degree in Biomedical Engineering (1997) both in Bogazici University. He works as a researcher in TUBITAK National Electronics and Cryptology Research Institute and he has been involved in EMC tests and measurements for two years.

Mehmed Özkan, after graduated from Bogazici University Electrical Engineering Department in 1986 with an honor degree, continued his graduate studies at Vanderbilt University in Nashville, USA. In 1988 and in 1991 he received MS and PHD degrees respectively. Dr. Özkan was specialized on AI, Robotics and applications of these in the medical field. Between the years 1992-95 Dr. Özkan moved to Japan to join Bridgestone R&D team in Tokyo as a senior research associate to develop mechatronic systems. In 1995 he became a faculty member of Bogazici University Biomedical Engineering Institute in Istanbul, as an assistant professor. In 1996 he became an associate professor and assistant director of the same institute where he is currently teaching graduate courses.

Fatih Üstüner was graduated from Middle East Technical University Electrical Engineering Dept. (1991) where he also received his MS degree (1994). He has 3 years of experience on RF/MMIC design. He works as a senior researcher in TUBITAK National Electronics and Cryptology Research Institute. His current interests include EMC tests, measurements and their automation.

VII

EMC PREDICTION, ANALYSIS AND MODELING

TESTING NUMERICAL CODES IN EMC: A PROCEDURE FOR FIELD-DATA COMPUTATION FOR PEC STRIPS AND ELLIPTIC CYLINDERS WITH MULTILAYER COATINGS

Renzo Azaro[†], Salvatore Caorsi[†], Matteo Pastorino[‡], and Mirco Raffetto[‡]

[†] Department of Electronics, University of Pavia,
Via Abbiategrasso 209, I-27100 Pavia, Italy

[‡]Department of Biophysical and Electronic Engineering, University of Genoa,
Via Opera Pia 11A, I-16145 Genoa, Italy

Phone: + 39 10 3532243 Fax: +39 10 3532777

E-mail: donaz@dibe.unige.it, caorsi@dibe.unige.it, pastorino@dibe.unige.it, raffetto@dibe.unige.it

In this paper we provide the solutions to some electromagnetic scattering problems. The considered scatterers are conducting elliptic cylinders or strips coated by multilayer dielectric materials. These results can be used for testing other numerical codes well suited for more complicated situations, which typically arises in electromagnetic compatibility.

1. INTRODUCTION

This paper deals with the interaction between electromagnetic waves and conducting and/or dielectric materials. In the field of the electromagnetic compatibility this represents, as is well known, a classic problem. In the open literature, such problem has been addressed both numerically and analytically depending on the particular configuration one has to analyse.

The particular importance of the analytical solutions, in case of canonical bodies, is due, above all, to the necessity to check the accuracy of the solutions calculated by using numerical techniques.

In this context, we address the problem of the scattering by a dielectrically coated conducting cylinder. In particular, the coating is assumed to be inhomogeneous, as it is made up of a multilayer elliptic cylinder, and the metallic core can be a strip or an elliptic cylinder. This scatterer is rather complex to be a quite challenging test for the numerical techniques used in electromagnetic compatibility, such as the finite-difference time-domain (FDTD) method [1], the finite element method (FEM) [2], the moment method (MoM) [3], the transmission line method (TLM) [4], etc.

As a matter of facts, the considered scatterer contains both dielectric and conducting materials, the former being inhomogeneous and it does not exhibits a circular symmetry. Finally, it is worth noting that the conducting strip is one of the few scattering problems

with sharp edges for which the solution can be calculated analytically [5].

The solution of the scattering problem due to a perfectly conducting or a homogeneous dielectric elliptic cylinders is well known [6][7]. It makes use of the so-called Mathieu functions [8][9]. The scattering by a perfectly conducting elliptic cylinder dielectrically coated by a single homogeneous lossless dielectric layer is known as well [10].

However the multilayer dielectric case is much more complicated. This is due to the lack of orthogonality of the angular Mathieu functions in adjacent dielectric materials. This prevents the development of a recursive procedure analogous to the one devised by Bussey and Richmond [11] for the multilayer circular cylinder. For this reason, the above problem has been considered to be "relatively intractable" [10]. Nevertheless a solution for the two-medium problem has been given in [5].

Finally, a recursive procedure for the exact solution to this multilayer scattering problem has been proposed in [12]. It has been generalised in [13] in order to deal with cylinders having a perfectly conducting core.

The recursive computation proposed in [12] requires the solution of a matrix equation having dimensions independent of the number of layers of the dielectric coating. For this reason, it seems computationally very efficient.

In the present paper, by applying the recursive solution proposed in [12] and modified in [13], we will provide several solutions of the scattering problem due to a conducting elliptic core or strip coated by multilayer dielectrics. These results will be provided in terms of both the behaviour of the electromagnetic field and the bistatic radar cross-sections per unit length.

The details of the mathematical formulation for the expansion of the electromagnetic field in terms

of Mathieu's functions in the various layers have been provided in [12][13] and are not repeated here in order to save space. However the main steps of the computational procedure are given. In the above mentioned papers, several comparisons have been performed with existing results in order to validate and check the proposed series solution.

2. MATHEMATICAL FORMULATION

2.1 Mathematical model

In this paper we will consider scatterers made up of perfect electric conducting (PEC) elliptic cylinders or strips coated by elliptic dielectric layers. For these problems the natural reference system is the elliptic cylinder coordinate system (u, v, z) , which is described for example in [9], where the relation between (u, v, z) and the Cartesian coordinates system (x, y, z') is also given.

It is assumed that the interfaces between different media are confocal elliptic cylinders, that all the quantities varies sinusoidally in time and that the electromagnetic fields "illuminating" the scatterers are transverse magnetic plane wave.

In these hypotheses the field equations can be treated by using the separation of variables. Following this procedure and by assuming that all the quantities does not depend on z , one can convert the equations for the electric fields in the different layers (Helmholtz equation) into Mathieu's equations. These equations admit denumerable sets of solutions (Mathieu's functions) which allow the expansion of all the quantities of interest in infinite series. However in order to manage the problems we have to truncate the infinite series and deal with finite sum. The unknowns are now a finite number of coefficients appearing in the truncated series considered. In the i -th layer, z -component of the electric field can be written as [12]

$$\begin{aligned} E_{z,i}(u,v) = & \sum_n [e_{m1,i} M c^{(0)}_m(q_i, u) + \\ & + e_{m2,i} M c^{(2)}_m(q_i, u)] c e_m(q_i, v) \\ & + \sum_n [o_{m1,i} M s^{(0)}_m(q_i, u) + o_{m2,i} M s^{(2)}_m(q_i, u)] s e_m(q_i, v) \quad (1) \end{aligned}$$

where $M c^{(j)}_m(q_i, u)$, $M s^{(j)}_m(q_i, u)$, $c e^{(j)}_m(q_i, u)$, and $s e^{(j)}_m(q_i, u)$, $j=1, 2$, denote Mathieu functions, and q_i is given by the product between the propagation constant for the i -th layer and the semi-focal distance.

For the external medium, analogous expressions can be written involving Mathieu functions of the 4-th order. Analogous relations can be written for the u - and v -component of the magnetic field.

In order to solve the indicated problems in terms of (truncated) series of Mathieu's functions the boundary conditions (i.e. the continuity of the tangential components of the electric and magnetic fields) are to be enforced. If these condition were applied at the same time the resulting system of equations would have a dimension growing linearly with the number of layers. However it has already been shown [13] that it is possible to implement a procedure for the calculation of the electromagnetic fields scattered by PEC elliptic cylinder coated by multilayer dielectrics whose computational complexity is almost independent of the number of layers of the coating. For this reason, a problem which was considered to be relatively intractable can now be solved quite efficiently.

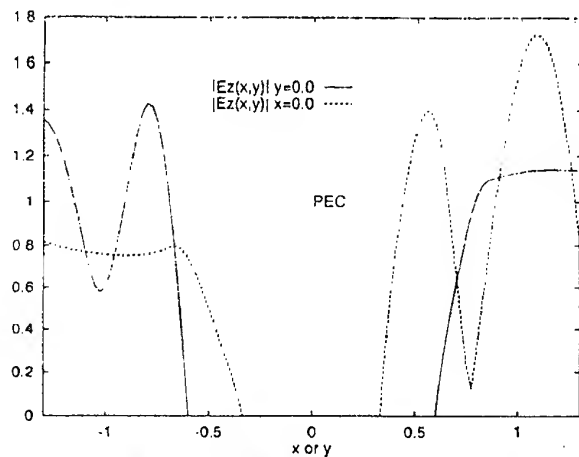


Fig. 1. Scattering by a thick PEC core coated by a multilayer dielectric: amplitudes of the z -component of the electric field along the x and y axes.

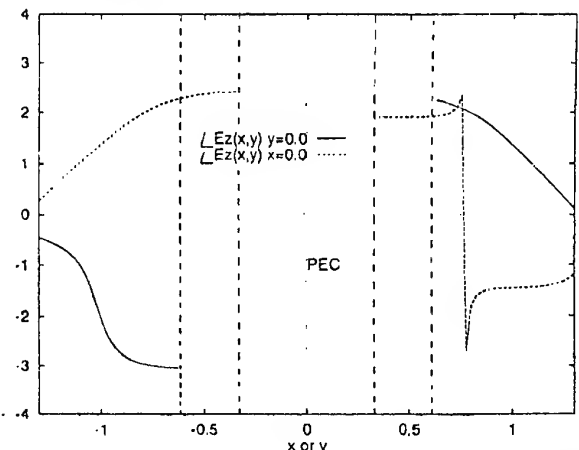


Fig. 2. Scattering by a thick PEC core coated by a multilayer dielectric: phases of the z -component of the electric field along the x and y axes.

2.2 Computational recursive procedure

Let us outline the salient points of the indicated procedure, whose details can be found in [12][13]:

- 1) for all dielectric interfaces but the external one compute the matrices involved in the equations enforcing (in a weak sense) the continuity of the tangential components of the electric and magnetic fields;
- 2) by using the equations found in 1) determine an explicit expression of the coefficients of the i -th layer in terms of those of the $(i-1)$ -th layer;
- 3) apply point 2) recursively and find an expression of the unknown coefficients of the external layer of the scatterer in terms of the unknown coefficients of the first dielectric layer;
- 4) substitute the calculated expression in the equations enforcing the continuity of the tangential components of the electric and magnetic fields at the outermost interface.
- 5) solve the obtained equation and find the coefficients of the innermost dielectric layer and of the medium surrounding the scatterer;
- 6) Go back to point 2) and 3) and calculate the expansion coefficients of all the other layers.

3. NUMERICAL RESULTS

In this section, we provide several results concerning the scattering due to PEC strips and elliptic cylinders coated by multilayer dielectrics.

In the first example, an elliptic cylinder with a PEC core is coated by three dielectric layers. The semifocal distance is equal to 0.5 m and the semimajor axes of the four interfaces are equal to 0.6 m (conductor-dielectric interface), 0.65 m (first dielectric-dielectric interface), 0.75 m (second dielectric-dielectric interface), and 0.85 m (external dielectric-dielectric interface). The relative dielectric permittivities of the three layers coating the metallic core are 3.0 (innermost dielectric layer), 1.5 (intermediate dielectric layer), and 2.0 (outermost dielectric layer). The external medium is assumed to be the free space. All the dielectric layers considered are lossless and are characterised by a relative magnetic permeability equal to unity. In this case we have considered an incident transverse-magnetic plane of unit amplitude (i.e. the electric field is of unit amplitude) and propagating along the straight line forming an angle of 135° with the positive x-axis.

In Figure 1, the amplitudes of the z-component of the electric field along the x and y axes are reported. For the scatterer considered the length of the semiminor axis is about 0.332 m. Figure 2 reports the phases of the electric field along the same axes. Finally, in Figure 3 the bistatic scattering width is provided.

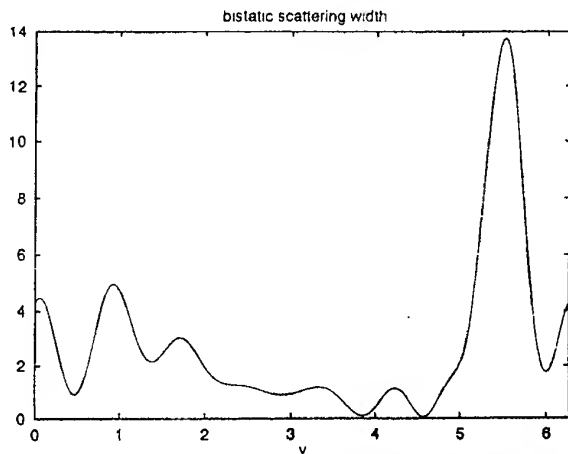


Fig. 3. Scattering by a thick PEC core coated by a multilayer dielectric: bistatic scattering width or radar cross section per unit length.

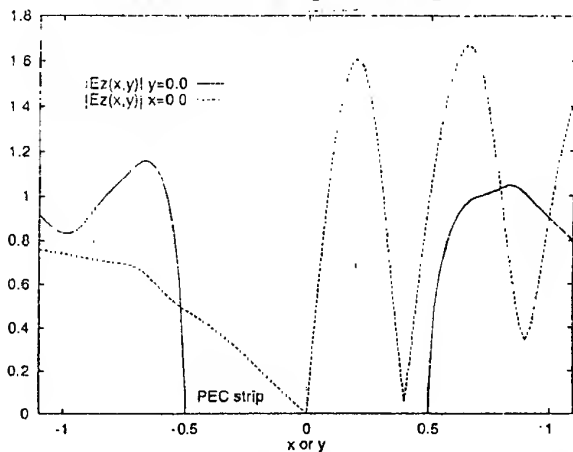


Fig. 4. Scattering by a PEC strip coated by a multilayer dielectric: amplitudes of the z-component of the electric field along the x and y axes.

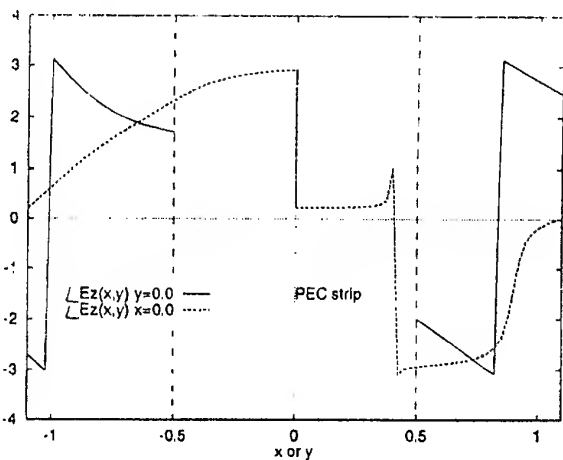


Fig. 5. Scattering by a PEC strip coated by a multilayer dielectric: phases of the z-component of the electric field along the x and y axes.

In another example, a PEC strip is coated by four dielectric layers. The semifocal distance considered is 0.5 m, and the semimajor axes of the ellipses constituting the cross section are given by: 0.6 m, 0.7 m, 0.8 m and 0.9 m. The relative dielectric permittivities of the four dielectric layers are (from the innermost layer to the outermost one) 2.0, 1.5, 1.0, and 1.4.

The direction of propagation of the incident plane wave forms an angle of 120° with the positive x-axis. In this case too, the dielectric layer are lossless and nonmagnetic and the medium outside the cylinder is the free space.

The amplitudes of the z-component of the electric field along the x and y axes are shown in Figure 4. Figure 5 reports the phases of the electric field along the same axes. Finally, in Figure 6 the bistatic scattering width is reported (in a polar format: the angular variable is the coordinate v).

As a final remark, it is important to note that all the indicated results are calculated by using a number of terms in the truncated series which guarantee very good approximations. In particular, by considering more terms in the finite sum would not provide a significant improvement in the quality of the results shown in this paper.

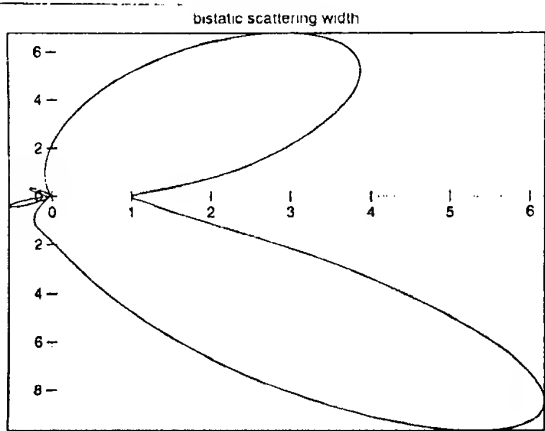


Fig. 6. Scattering by a PEC strip coated by a multilayer dielectric: bistatic scattering width or radar cross section per unit length.

4. CONCLUSIONS

In this paper the electromagnetic scattering problems in which a conducting elliptic cylinder or strip is coated by a multilayer dielectric material is considered. Results concerning both near-field and far-

field data are provided. These results can be important in order to test general numerical codes for the analysis of more practical electromagnetic compatibility problems.

5. REFERENCES

- 5.1. C. E. Brench, "Creating practical FD-TD models for EMC analysis," Proceedings of the 1995 IEEE International Symposium on Electromagnetic Compatibility, Atlanta, USA, 14-18 August 1995, pp. 174-178.
- 5.2. J. R. Brauer and B. S. Brown, "Mixed-dimensional finite-element models of electromagnetic coupling and shielding," IEEE Transactions on Electromagnetic Compatibility, vol. 35, pp. 235-241, March 1993.
- 5.3. E. H. Newman and M. Kragalott, "Moment method analysis of the electric shielding factor of a conducting TM shield at ELF," IEEE Transactions on Electromagnetic Compatibility, vol. 37, no. 3, August 1995, pp. 400-408.
- 5.4. C. Christopoulos, "Advanced simulation techniques in EMC based on the TLM method," Electromagnetics, vol. 16, no. 5, September-October 1996, pp. 567-590.
- 5.5. R. Holland and V. P. Cable, "Mathieu functions and their applications to scattering by a coated strip," IEEE Transactions on Electromagnetic Compatibility, vol. 34, no. 1, February 1992, pp. 9-16.
- 5.6. J. S. Avestas and R. E. Kleinman, "The strip," in J. J. Bowman, T. B. A. Senior, and P. L. E. Uslenghi, Eds., "Electromagnetic and acoustic scattering by simple shapes," North-Holland Publishing Company, Amsterdam, 1969.
- 5.7. C. Yeh, "The diffraction of waves by a penetrable ribbon," Journal of Mathematical Physics, vol. 4, January 1963, pp. 65-71.
- 5.8. G. Blanch, "Mathieu Functions," in M. Abramowitz and I. A. Stegun, Eds., "Handbook of Mathematical Functions," Dover Publications, New York, 1965.
- 5.9. P. M. Morse and H. Feshback, "Methods of theoretical Physics," Mc Graw-Hill, New York, 1953.
- 5.10. J. H. Richmond, "Scattering by a conducting elliptic cylinder with dielectric coating," Radio Science, vol. 23, November-December 1988, pp. 1061-1066.
- 5.11. H. E. Bussey and J. H. Richmond, "Scattering by a lossy dielectric circular cylindrical multilayer, numerical values," IEEE Transactions on Antennas and Propagation, vol. 23, September 1975, pp. 723-725.
- 5.12. S. Caorsi, M. Pastorino, and M. Raffetto, "Electromagnetic scattering by multilayer elliptic cylinder under transverse-magnetic illumination: series solution in terms of Mathieu functions," IEEE Transactions on Antennas and Propagation, vol. 45, no. 6, June 1997, pp. 926-935.

5.13. S. Caorsi, M. Pastorino, and M. Raffetto, "Scattering by a Conducting Elliptic Cylinder with a Multilayer Dielectric Coating," *Radio Science*, vol. 32, no. 6, November-December 1997, pp. 2155-2166.

ACKNOWLEDGEMENT

The authors would like to thank Prof. Johan Wettergren for having very kindly provided the subroutines for computing Mathieu functions.

BIBLIOGRAPHICAL NOTES

Renzo Azaro received the "laurea" degree in Electronic Engineering from the University of Genoa, Italy, in 1992. At present he is a Ph. D. student in "Computer science, applied electromagnetics and telecommunication engineering" at the same university. His main research interests are in electromagnetic compatibility and measurements.

Salvatore Caorsi is a full professor of Electromagnetic Compatibility at the Department of Electronics of the University of Pavia, Italy and he is also teaching the course of Antennas at the University of Genoa. He is the Past-President and founding member of the Inter-university Research Center for Interactions Between Electromagnetic Fields and

Biological Systems (ICEMB). His primary activities are focused on applications of electromagnetic fields to telecommunications, artificial vision and remote sensing, biology, medicine and electromagnetic compatibility. Prof. Caorsi is a member of the AEI, EBEA and ESHO.

Matteo Pastorino is an assistant professor of Electromagnetic Fields in the Department of Biophysical and Electronic Engineering and, since 1995, he has taught the university courses of Electromagnetic Fields 1 and Remote Sensing and Electromagnetic Diagnostic. His main research interests are in electromagnetic direct and inverse scattering, microwave imaging, wave propagation in presence of nonlinear media, and in numerical methods in electromagnetism. Dr. Pastorino is a senior member of IEEE, and a member of AEI and EBEA.

Mirco Raffetto received the "laurea" degree in Electronic Engineering ("summa cum laude") from the University of Genoa, Italy, in 1990, and the Ph. D. degree in "Models, Methods and Tools for Electronic and Electromagnetic Systems" from the same university, in 1997. Presently he is a postdoc research assistant. His main research interests are in electromagnetic direct scattering, microwave boundary value problems, and numerical methods in electromagnetism.

SPICE - SIMULATION OF VOLTAGES BETWEEN SHEATH AND CABLE CONDUCTOR DUE TO EXTERNAL EXCITATION

P. Czarnywojtek, W. Machczyński

Poznan University of Technology, Institute of Industrial Electrical Engineering,
ul. Piotrowo 3A, 61-138 Poznań, Poland
tel.: (+4861) 8782383, fax: (+4861) 8782389, e-mail: mawo@sol.put.poznan.pl

The paper considers the SPICE (Simulation Program with Integrated Circuit Emphasis) simulation of cable response to external excitation. The objective of the paper is to model both inductive and conductive power line steady-state and transient effects on underground cable. The response of the cable (voltage between sheath and cable conductor) to the transient d.c. and the sinusoidal components of the power line earth - fault current is simulated assuming that the homogenous cable section may be modeled by an equivalent circuit consisting of two two-ports representing the cable conductor - cable sheath and the cable sheath - earth loops, respectively. The SPICE simulation is a useful and an alternative approach to the analysis of the EMI problems in earth return circuits, when compared with the solutions in the frequency and time domains, respectively. The SPICE simulation has been illustrated by examples.

1. INTRODUCTION

The effects of electric lines and installations on nearby underground metal conductors with earth return result mainly in hazards of accident for persons in contact with the conductors, damage to the insulating coating as well as the metal itself, and destruction of the equipment connected to the conductor.

The methods of calculation of the electromagnetic interference (EMI) on underground cables have already been presented in a number of places, e.g. [1, 2]. Some of the publications of the authors have been also devoted to these problems [3, 4, 5]. The objective of the paper [3] was to analyse power line transients effects on earth return circuits using the simulation program SPICE (Simulation Program with Integrated Circuit Emphasis). In the paper the response (potential to the remote earth) to the transient d.c. and the sinusoidal components of the power line earth - fault current, inductive and conductive coupled to a pipeline has been simulated. In the paper [4] a modified method of characteristic has been presented and illustrated by an example of simulation transient effects in earth return circuits. This method of calculation of the pipeline potential to the remote earth has been verified by the

SPICE simulation according to [3]. The purpose of the paper [5] was to present an analytical - numerical solution for the voltage between sheath and cable conductor of buried cable due to quasistationary conductive effects from nearby complex earthing arrangements. The present paper considers the SPICE simulation of voltages between sheath and cable conductor due to external excitation.

The objective of the paper is to model both inductive and conductive power line steady - state and transient effects on underground cable. Using the program SPICE the excitation by ac signals and transients may be performed, assuming that the homogeneous cable section with uniform exposure to the interfering electric field may be modeled by equivalent two ports. It should be noted that the equivalent circuit of the cable section with distributed external excitation and the driving voltage controlled voltage source is presented for the first time. It is also assumed in the paper that the reaction of currents in the subjected cable on the primary electric field may be disregarded, and that the system considered is linear. Such assumptions are accepted in many publications dealing with earth currents. In the paper the response to the transient d.c. and the sinusoidal components of the power line earth-fault current, which is assumed to be known, inductive and conductive coupled to an underground cable has been simulated.

2. GENERAL CONSIDERATIONS

2.1. Equivalent circuit of a cable conductor - sheath loop

An element of an underground cable of differential length is shown in Fig. 1, where Z_C - unit-length impedance of cable conductor, Y_C - unit-length leakage admittance of cable insulation, Z_S is the unit length internal-surface impedance of cable sheath, and I_S is the sheath current due to external excitation [2, 5].

The knowledge of the current I_S flowing along the sheath is essential for the determination of the voltages in the cable conductor - sheath loop.

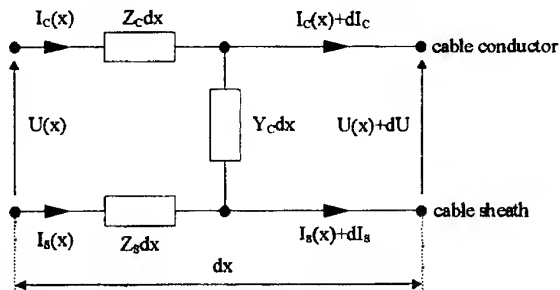


Fig. 1. Equivalent circuit of a cable conductor - sheath loop.

2.2. Equivalent circuit of a cable sheath - earth loop

The current I_s flowing along the sheath of the cable may be calculated using the equivalent circuit involving the cable sheath and the earth, Fig. 2 [2, 3, 4, 5].

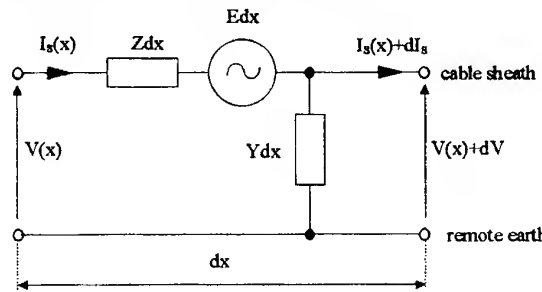


Fig. 2. Equivalent model of an elementary section of a cable (earth return circuit) with external excitation

The circuit of the differential length dx , consists of a unit - length series impedance $Z = \gamma Z_0$ and a unit - length shunt admittance $Y = \gamma / Z_0$, where γ is the propagation coefficient and Z_0 is the characteristic impedance of the earth return circuit. E represents the external influence. Generally E , the electric intensity impressed at every point of the cable, is the sum of an induced and a static component

$$\bar{E} = \bar{E}_i + \bar{E}_s \quad (1)$$

The induced electric field is associated with the inductive, whereas the static electric field with the conductive influence of the cable.

In the case of the inductive interference

$$\bar{E}_i = -\frac{\partial \bar{A}}{\partial t} \quad (2)$$

where \bar{A} is the vector potential along the cable due to the current in an overhead conductor of a power line under normal or fault conditions.

During a phase-to-ground fault large currents may enter the ground through the earthing arrangements. These currents produce significant electric flow field in the surrounding earth, characterised by scalar earth potential, which is proportional to the current flowing through the electrode to the earth.

In the case of the conductive interference

$$\bar{E}_s = -\text{grad } V_E \quad , \quad (3)$$

where V_E is the scalar potential of the electric flow field along the cable.

3. SIMULATION USING SPICE

Theoretically there are two approaches possible for earth return circuit network simulation, one based on the transmission line model, and the other on the large multinode electrical equivalent circuit containing active and passive elements. The SPICE package handles only lossless transmission lines with one propagation mode, therefore is not adequate for the earth return circuit such as a cable with the contact with the earth through a leakage insulation.

The response of the cable to transient effect may be simulated using SPICE, when a basic circuit consisting of two two-ports shown in Fig. 3 is applied.

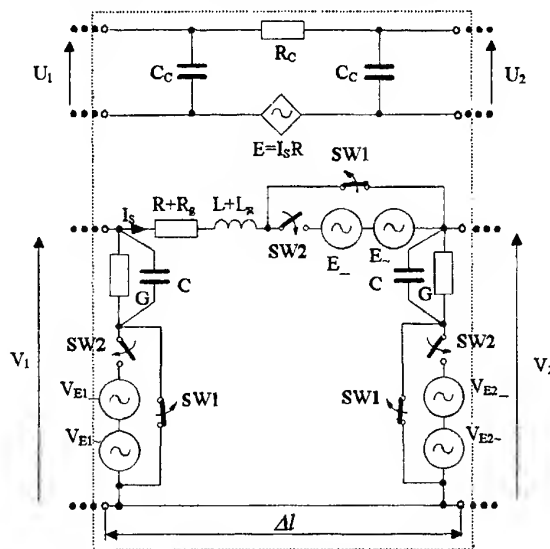


Fig. 3. Basic circuit - model of the segment of the inductively and conductively subjected cable

The inductive effect of the sinusoidal component of the fault current in a power line is represented in the lower circuit by the voltage sinusoidal source E_- , whereas the inductive effect of the transient d.c. component is modeled by the voltage source E_- . The voltage sources V_{E-} and V_{E_-} represent the conductive effects of the fault current on the cable. The source V_{E-} models the conductive sinusoidal component and the source V_{E_-} models the conductive d.c. component of the cable excitation. Voltage controlled switches SW1 and SW2 are applied to model the finite time of earth fault duration. The switches operate synchronously. When switch SW1 opens, switch SW2 closes and vice versa. We begin by assuming that the switch SW1 has been closed for a long time. At $t = 0$ (instant of the ground fault in the power line), switch SW1 opens. At $t = 0.2$ s the switches are thrown to the opposite positions.

The upper circuit in the Fig.3 represents the cable conductor - sheath loop. The driving voltage controlled voltage source $E = I_s R$ produces the voltage U between the sheath and cable conductor, whereas I_s is the current flowing along the cable sheath. The objective of the simulation is to find the voltages between sheath and cable conductor of the upper circuit for the time $0 \leq t \leq 0.2$ s.

For the simulation each element of the individual basic circuit should be defined in the enter data file.

4. EXAMPLES OF SIMULATION

4.1. Inductive interference

In the first example the simulation of the cable responses to transients in a power line, has been carried out for the case of inductive interference (the earth fault is remote from the approach section of the power line), so that $V_{E_+} = 0$ and $V_{E_-} = 0$ in the circuit shown in Fig.3. An underground cable is subjected to a phase-to-ground current ($i_- = 132.9\sqrt{2} \sin(\omega t - 77^\circ)$ A, $f = 50$ Hz, $i_-(0) = 129$ A) in a power line, which is parallel to the cable. The parameters of the line: $R = 0.118 \Omega/\text{km}$, $L = 0.05 \text{ mH/km}$, $\tau = L/R = 423.7 \mu\text{s}$.

The length of the cable with the parameters $\gamma = 4.92\exp(j0.834) \text{ S/km}$, $Z_O = 1.27\exp(j0.698) \Omega$ is $l = 15 \text{ km}$. The cable is terminated internally and externally through the characteristic impedances. The parameters of the cable conductor and the insulation between the conductor and the cable sheath are $Z_C = 10 \Omega/\text{km}$, $Y_C = 3.141\exp(j\pi/2) \text{ mS/km}$, and $Z_S = 1.6 \Omega/\text{km}$.

The mutual impedance (50 Hz) between the cable and the overhead conductor of the power line is $Z_M = 0.05 + j0.228 \Omega/\text{km}$.

The cable has been modeled as a chain of 6 basic circuits shown in Fig. 3. The initial conditions in this circuit have been assumed to be zero. In Fig. 4 and in Fig. 5 the voltages between sheath and cable conductor at the end point of the cable ($U(x=15\text{km})$) are plotted as function of the time. In the Fig.4 the dashed curve is related to the d.c. transient response and the solid curve represents the sinusoidal response of the cable, inductively affected.

In the Fig.5 the total cable response to the transient effects for the inductive interference is shown. As expected the transient d.c. component of the cable response (voltage) has a minor effect when comparing with the sinusoidal component of the response. The maximum value of the total transient voltage is 200% of the amplitude of the steady - state voltage. The steady - state condition is practical reached immediately in the cable conductor - sheath loop.

4.2. Conductive interference

In the second example the conductive effects of a fault current in a power line has been simulated. For the case of a conductive influence of the cable, the

voltage sources representing the scalar potential in the earth adjacent to the cable, have been applied in shunt branches of the basic circuit, Fig. 3, whereas $E_+ = 0$ and $E_- = 0$.

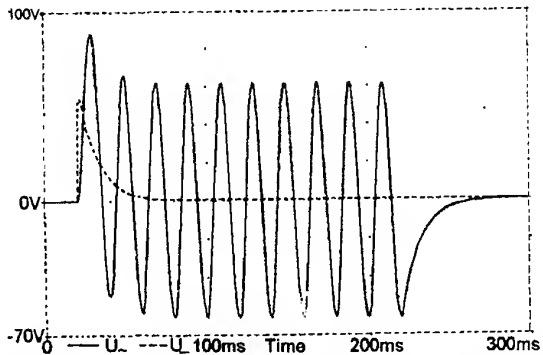


Fig. 4. Components of the voltage between sheath and cable conductor simulated for the case of inductive effects

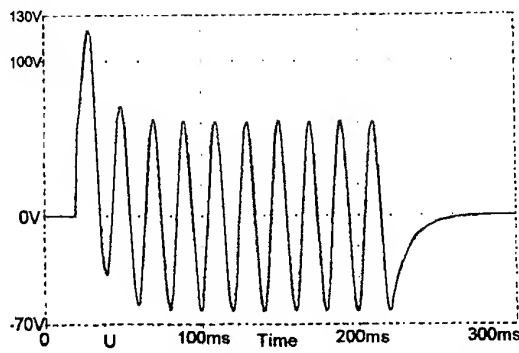


Fig. 5. Total voltage between sheath and cable conductor (inductive interference)

In the example it is assumed that the cable is buried perpendicular to the route of the power line. The conductivity of the earth is $\sigma = 0.01 \text{ S/m}$. The earth fault current flows into the earth through the point earth electrode, which is a model of the tower grounding. The distance between the point earth electrode and the cable is $s = 10 \text{ m}$. The electrical parameters of the cable and the value of the components of the earth fault current are the same, as in the first example.

The cable has been modeled as a chain of 56 basic circuits shown in the Fig.3. The initial conditions in this circuit have been assumed to be zero. In the Fig.6 and Fig.7 voltages between sheath and cable conductor at the cable point $x = 7.5 \text{ km}$, lying opposite to the point earth electrode are plotted vs time.

It follows from the simulation, that the transient d.c. component of the cable response may be neglected when comparing with the sinusoidal response of the cable conductively effected. Similary, as in the case of the inductive influence on the cable, the steady - state condition is reached immediately in the loop conductor - cable sheath.

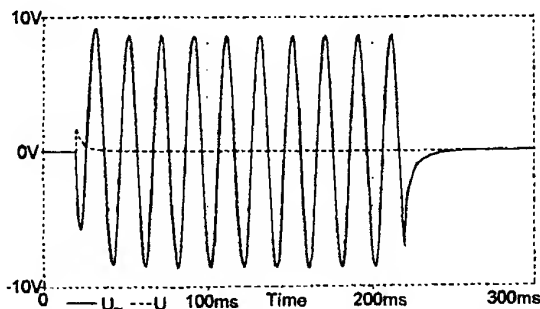


Fig. 6. Components of the voltage between sheath and cable conductor simulated for the case of conductive effects

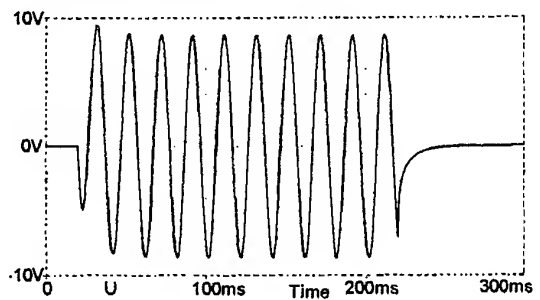


Fig. 7. Total voltage between sheath and cable conductor (conductive interference)

5. FINAL REMARKS

The analysis of transient as well as steady-state inductive and conductive effects of power lines on nearby underground cables is possible using the simulation program SPICE. The basic circuit-model of the segment of the cable, consisting of two coupled two ports, representing the cable sheath - earth loop and the cable conductor - sheath loop, respectively, has been presented for the first time. The computer simulation of effects of both component of the phase-to-ground fault current in a power line, permit to analyse these phenomena with greater accuracy, especially for the case of the d.c. transient component. The transient on the cable may be handled by techniques developed previously for the steady state coupling calculations, when considering the sinusoidal (50 Hz) component of the transient.

The application of the simulation program SPICE may be useful in understanding and quantifying the transient effects on underground cables. The extensive parametric analysis to examine the roles of various factors which affect the electrical and magnetochemical interference levels caused in underground cables by nearby power line under fault conditions may be performed using the simulation program.

AC and transient excitation effects can be evaluated at the design stage of a new power line on an existing network of underground cables, thus enabling potential EMI problems to be identified before site testing becomes practicable or possible.

Acknowledgement

This work has been sponsored by the grant 42-539/98-BW.

6. REFERENCES

- [1] E.F. Vance: "Coupling to shielded cables", A. Wiley - Interscience Publication, N. York, 1978.
- [2] M. Krakowski: "Mathematical study of voltages between sheath and cable conductor due to currents from nearby earth electrodes", Proc. IEE, Vol. 116, No. 10, October 1969, pp. 1701-1706.
- [3] P. Czarnywojtek, W. Machczyński: "Analysis of power line transients on earth return circuits using simulation programs", 11th International Zurich Symposium on Electromagnetic Compatibility, Zurich, March 7-10, 1995, pp. 69-72.
- [4] W. Bandurski, P. Czarnywojtek, W. Machczyński: "Simulation of transient effects in earth return circuits", 13th International Wroclaw Symposium on Electromagnetic Compatibility, Wroclaw, June 25-28, 1996, pp. 264-267.
- [5] W. Machczyński: "Voltage between sheath and cable conductor due to conductive effects on underground cable", EMC'96 ROMA, Roma, September 17-20, 1996, pp. 786-789.

BIOGRAPHICAL NOTES

Piotr CZARNYWOJTEK was born in Poland in 1968. He received the M.S. degree in electrical engineering from the Poznan University of Technology in 1993. From 1993 to the present he has been with the Poznan University of Technology, where he is now Assistant in Institute of Industrial Electrical Engineering. He is interested in studies and research in earth return circuits.

Wojciech MACHCZYŃSKI was born in Poland in 1947. He received the M.S., Ph.D. and D.Sc degrees in electrical engineering from the Poznan University of Technology in 1971, 1976 and 1989, respectively. From 1971 to the present he has been with the Poznań University of Technology, where he is now Professor and the Head of the Division of Electrical Engineering Basics. He is engaged in studies and research in earth return circuits.

SMART ANTENNAS FOR INTERFERENCE RESOLUTION IN CELLULAR NETWORKS

F. Delaveau*, F. Pipon**, O. Lambron*, THOMSON-CSF COMMUNICATIONS

*RadioSurveillance and COMINT Systems Unit

**Common Technics and Technologies Unit

66, rue du Fossé Blanc, 92231 Gennevilliers Cedex – France

ABSTRACT

This paper introduces a new method to identify harmful interference in cellular networks, using smart antenna techniques and signalling channel decoding to retrieve interfering station identifiers even under highly negative C/I conditions (-15 dB) and in the presence of multiple signals. Experiments in the Paris area demonstrated the effectiveness of the method to evidence both co-channel and adjacent channel interference, whether it is caused by frequency reuse, multipath or a non-cellular signal. This technology is the basis of SMART AIR, the new generation of cellular network coverage and interference measurement systems introduced by THOMSON-CSF Communications.

1. PURPOSE OF INTERFERENCE ANALYSIS

Cellular operators nowadays face a new phase of network deployment by which they have to provide both higher traffic capacity and higher quality of service in terms of coverage and call disruption rate. Division of cells into micro- or even pico- cells, repeaters and extensive frequency reuse are factors that make internal interference more likely and difficult to evidence using traditional methods such as plain field strength measurements or test receivers. In many cases, calls cannot be set-up despite apparently high signal levels, a situation resulting in dissatisfied subscribers. A common source of problems is the simultaneous reception of signals broadcast by several base stations, at levels sufficient enough to disrupt the reception of the best server station by the handset of the subscriber, but low enough to make their identification impossible through conventional methods.

Operators have tried various technologies, such as field strength and channel impulse response

measurement systems, with little success to evidence problems other than multipath. GSM operators facing severe service quality problems in urban areas need new technologies to perform network quality control and in-situ correction of planning data, able to perform:

- measurement, analysis and identification of internal and external interference sources independently of planning data
- planning and network deployment support, particularly in urban or mountainous zones (presence of several high-level sources, multipath, etc.) by identifying base stations
- aid to frequency management (presence of several networks, frontier zones, etc.).

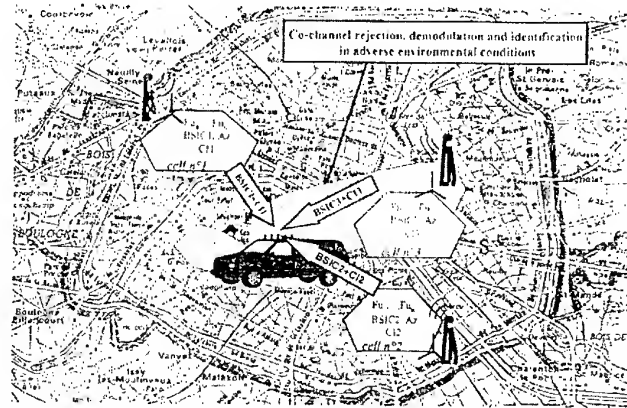


Fig. 1: Principle of use

2. RECEPTION AND PROCESSING

Reception and processing are performed with five quarter-wave antennas, a five-channel high-sensitivity receiver and acquisition system (5 x 300

kHz), and a computer for signal processing, receiver management, and analysis of results.

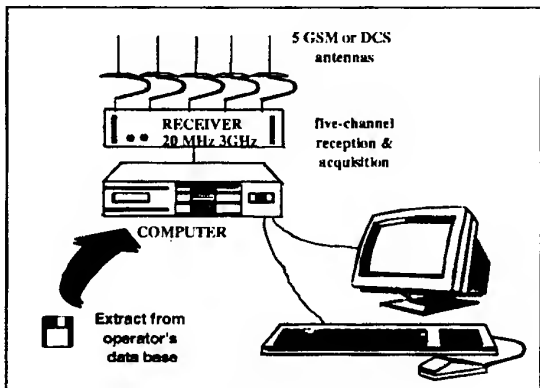


Fig. 2: Equipment structure

3. PRINCIPLE OF INTERFERENCE ANALYSIS

The equipment identifies all types of adjacent and co-channel interference sources with Wiener space-time matched filtering and

- demodulation and decoding of relevant identification parameters (BSIC, TSC, LAC, LAI, CI, MNN, MNC, etc.) on beacon frequencies,
- estimation of C/I and E_b/N_0 ratios.

3.1. BCCH-BCCH interference situation

BCCH-BCCH adjacent and co-channel interference situations are analysed in three steps :

a- Multi-channel detection of Broadcast Channel (BCCH) and multi-channel synchronisation on Synchronisation Channel training sequence (SCH included in BCCH) are performed with a same algorithm described in section 4.3. The 300 kHz bandwidth signal is acquired on 5 channels, digitised and recorded.

b- Multi-channel reception, including channel and noise estimation and equalisation, is performed with a second algorithm described in section 4.4.

c- Demodulation and decoding of BCCH are then performed to extract base station, cell and network identification parameters (see section 4.4.).

3.2. BCCH-TCH interference situation

BCCH-TCH adjacent and co-channel interference situations are analysed in five steps:

a'- Multi-channel detection of Traffic Channel (time slot TCH) with level estimation and selection of a given TCH (operator's choice). The TCH selected is defined by its training sequence.

b'- Multi-channel detection of Broadcast Channel (BCCH) in the total GSM band (with multi-channel synchronisation as in a step a-).

c'- Automatic selection of Broadcast Channels (BCCH) that are time-correlated with a given TCH.

d'- Multi-channel reception of previously selected BCCH, including channel estimation noise estimation for each of them as in step b-

e'- Demodulation and decoding of selected BCCH, extraction of base station, cell and network identification parameters.

Thus, carrier sources and interference sources are detected and identified either for BCCH-BCCH and BCCH-TCH interference situations.

Matched space-time filtering has some advantages:

- no antenna calibration is required,
- location of interfering base stations is simply performed through identification and planning data (automatic look-up in database would be possible with digital map display).

4. SIGNAL PROCESSING

4.1. Signal model

GSM uses a GMSK modulation with index $h=0.5$, $BT=0.3$, $L=3$. Ref [1] shows that the transmitted GMSK signal can be expressed in the linear form hereafter :

$$s(t) = \exp \left[2i\pi h \sum_{n=-\infty}^q s_n v(t - nT) \right] \approx \sum_{n=-\infty}^q j^n a_n C_0(t - nT)$$

where :

- $(s_n)_{n=-\infty, q}$ is the symbol stream
- $a_n = s_n a_{n-1}$
- C_0 is the first pulse modulation function:

$$C_0(t) = \frac{\sin[\psi(t)]}{\sin(h\pi)} \quad 0 \leq t \leq 2LT$$

$$0 \leq t \leq LT ; \psi(t) = \varphi(t)$$

$$LT \leq t \leq 2LT , \psi(t) = h\pi - \varphi(t - LT)$$

$$\varphi(t) = [2\pi h \cdot v(t)] : \text{signal phase during } 2L \text{ symbols.}$$

So the input signal $x(t)$ on the 5-channel array is the 5-vector

$$x(t) = \sum_{n=-\infty}^q a_n g(t - nT) + (b + j)(t)$$

where

- $g(t) = [G * C_0](t)$ is the convolution result of C_0 function above with channel filter G (including Nyquist filtering)
- b is the contribution of ambient noise and j is the contribution of interference
- $x(t)$, $g(t)$, $b(t)$ and $j(t)$ are 5-vectors.

4.2. Some definitions

For further developments, we call K the length of the training sequence d , N_L the length of channel response and we define

- the 5-channel sampled vector $x_{(n)}$, $g_{(n)}$, $b_{(n)}$ and $j_{(n)}$
- the $5 \times N_L$ arrays : $D(k) = (d_{(k)}, \dots, d_{(K+N_L)})$,
- the 5×1 correlation array

$$r_{xd}(n) = \frac{1}{K} \sum_{k=1}^K x_{(n+k)} d_{(k)}^*$$

- the 5×5 correlation arrays :

$$R_{xx}(n_0) = \frac{1}{K} \sum_{k=1}^K x_{(n_0+k)} x_{(n_0+k)}^T$$

$$R_{xD}(n_0) = \frac{1}{K} \sum_{k=1}^K x_{(n_0+k)} D_{(k)}^T$$

$$R_{dd} = \frac{1}{K} \sum_{k=1}^K D_{(k)} D_{(k)}^T$$

4.3. Multi-channel detection and synchronisation

It follows from Wiener theory that the sample n for which multi-channel synchronisation is achieved maximises the function $C(n)$ hereafter (see ref. [2] for more details) :

$$C(n) = (r_{xd}(n))^T [R_{xx}(n)]^{-1} [r_{xd}(n)]$$

4.4. Multi-channel reception and demodulation

After synchronisation processing, performed either on SCH and TCH training sequences, the multi-channel reception algorithm is composed of a

purely spatial part w , followed by a temporal matched filter.

The principle is to minimise the mean square error between the output $y=w^T x$ of a spatial matched filter w and a channel filtered version $\hat{g}^T d$ of the training sequence d . For this we search w and \hat{g} that realise

$$\text{Min} \left\{ E \left[\left| w^T x \right| - \left| \hat{g}^T d \right| \right]^2 \right\}$$

with the constraint $\hat{g}^T \hat{g} = 1$.

The optimal choice of w and \hat{g} is given by

\hat{g} : eigenvector corresponding to the smallest

eigenvalue of matrix $F = R_{dd} - R_{xx}^T R_{xx}^{-1} R_{xD}$

w : matched filter defined hereafter:

$$w(\hat{g}) = R_{xx}^{-1} R_{xD} \cdot \hat{g}$$

This single channel output is then sampled at symbol rate and a Viterbi algorithm is chosen for symbol decision (because of residual symbol interference) as shown hereafter.

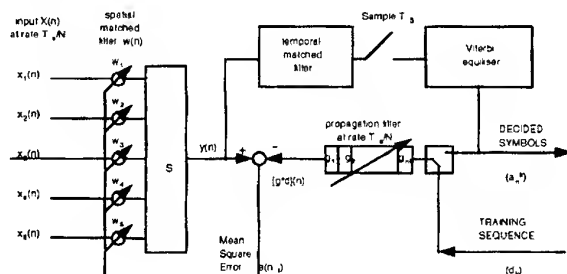


Fig. 3: Reception and demodulation

Extraction and decoding of identification parameters are then performed. Signal power, C/I and E_b/N_0 ratio are estimated from filter outputs and arrays defined above.

5. RESULTS AND EXPERIMENTATIONS

Figure 4 hereafter explains the result of processing for co-channel interference situations.

Figures 5 and 6 show experimental results obtained in Paris region (France).

The symbols xx and zzz are the codes of the GSM channel, the symbol y identifies the operator:

these parameters and the precise location of measurements are not given in this paper to respect operators' data confidentiality.

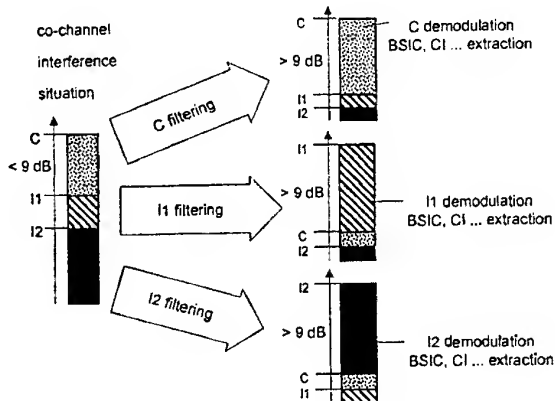


Fig. 4: Illustration of processing results

Type Station	FU1	BSIC	LAC	CI	E _b /N ₀	TCH
Carrier BCCH	xx	y2	4300	17581	20 dB	105
Interference BCCH	xx	y6	14300	7508	7 dB	120, 84
Interference BCCH	xx	y3			9 dB	

Fig. 5: Experimental measurement of 3 BCCH signals: although the first interferer is 13 dB below the wanted carrier, it was demodulated, decoded and identified

Type Station	FU1	BSIC	LAC	CI	E _b /N ₀	TCH
Carrier BCCH	zzz	y3	4300	17576	20 dB	66
Interference BCCH	zzz	y7	4200	17514	8 dB	68, 107
Interference TCH	zzz	y0			6 dB	

Fig. 6 : Experimental measurement of 2 BCCH signals and one TCH signal 14 dB below the wanted carrier

The LAC and CI parameters were not extracted every time because of an acquisition duration limited to 0.5 second for the experiment (instead of 2 seconds in SMART AIR to extract these parameters with 100% probability).

6. CONCLUSION

The results above show that GSM channel decoding and parameter identification can be performed with matched space-time filtering, under highly disturbed reception conditions (multiple sources, multipath, highly negative C/I ratio - down to -15 dB and less).

These filtering techniques have thus proved very efficient for measurement and interference analysis,

and for planning support and service quality control of cellular networks when regular instrumentation is not sufficient. Above principles could be extended to other TDMA and CDMA wave forms, such as NADC, IS95, UMTS, etc.

7. REFERENCES

[1] P.A. LAURENT: "Exact and approximate Construction of digital Phase Modulation by Superposition of Amplitude Modulated Pulses (A.M.P)" (English), IEEE trans. on Com. vol. COM-34 N°2 feb. 1986.

[2] P. CHEVALIER, F. PIPON & al: "Antenne intelligente pour le système GSM: résultats expérimentaux pour une réception mobile" (French), Proceedings of IEEE Veh. tech. Conf., Vanves, 11 June 1996.

[3] P. CHEVALIER, F. PIPON & al: "Multichannel Receiver Performance Comparison in presence of ISI and CCI - Application to a GSM link" (English). Paper presented at the Santorini Congress, Paris, 1997.

[4] PATENT France 15/07/97 nr 97 089554: "Interférences en radiocommunication cellulaires"

BIOGRAPHICAL NOTES

After an Engineering degree (ENSTA, Paris) and Mathematics degree (Paris VII University), F. DELAVEAU developed simulation models about propagation, diffusion, and optimisation problems. He joined the product department of THOMSON CSF Communications where he took the responsibility of cellular product line and drove the development of SMART AIR.

After an Engineering degree (Polytechnique School and ENSTA, Paris), F. PIPON joined the study department of THOMSON CSF Communications where he develops advanced smart antennas technologies for military and civilian applications. He is the author of numerous patents and publications for applications of these techniques to propagation and reception problems in mobile radio systems.

After an Engineering degree (ENST, Paris) and a MSc. in Communications (Imperial College, London), O. LAMBRON was involved in infrastructure telecommunication projects world wide. He joined THOMSON-CSF Communications where he developed the spectrum management and monitoring activities.

FDTD COMPUTATION MODELING FOR ELECTROMAGNETIC FIELDS GENERATED BY SPARK BETWEEN CHARGED METALS

Osamu FUJIWARA, Kei KAWAGUCHI and Nobunari KURACHI
Faculty of Engineering, Nagoya Institute of Technology,
Gokiso-cho, Showa-ku, Nagoya 466, Japan.

The occurrence electromagnetic fields caused by the electrostatic discharge (ESD) between the charged metals can be affected by the presence of the metal itself, whereas the effect has not previously been examined. In this paper the finite-difference time-domain (FDTD) method was used to compute the occurrence electromagnetic fields due to the spark between the metal spheres. Comparison was made between the FDTD computation results and the analytical results obtained from a dipole model. The effect of the metal on the ESD field level was also shown.

1 INTRODUCTION

The occurrence electromagnetic fields due to electrostatic discharge (ESD) include broad-band frequency spectra over a microwave region[1], which cause serious damage to high-tech information devices. For this kind of electromagnetic interference (EMI), it is well-known as a peculiar phenomenon[2]-[4] that an indirect ESD happening at a location far from the device gives the stronger EMI than a direct ESD does and also that the EMI level is not always proportional to the ESD voltage. For the indirect ESD, we have previously proposed a dipole model[5]-[7] having a spark current, which could qualitatively explain the peculiar ESD event. In the above model, however, the presence of the metal has not been considered, and its effects on the occurrence electromagnetic fields are not well understood. In order to numerically examine the effect of the metal presence on the ESD field, we analyzed the occurrence electromagnetic fields generated by the spark between the metal spheres, using the finite-difference time-domain (FDTD) technique. The computed results were also compared with those analytically obtained from our previously proposed dipole model[6].

2 ESD SOURCE MODEL AND FDTD COMPUTATION ALGORITHM

Figure 1(a) shows a fundamental ESD model for the spark between the metal spheres with a radius of

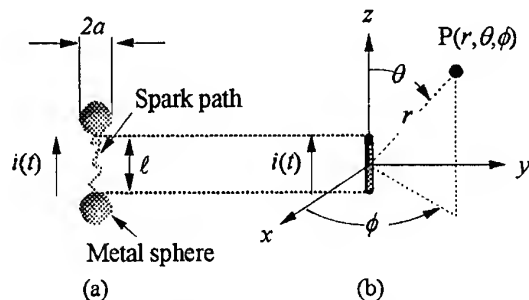


Figure 1 (a)Spark discharge between metal spheres, and (b)dipole model.

a whose gap length is ℓ . When the radius a of the metal sphere is sufficiently small compared with the gap length ℓ , the charged metal sphere is assumed to be a point charge and thus Figure 1(a) is modelled as a dipole model which is shown in Figure 1(b), so that the occurrence electromagnetic fields in this case can theoretically be obtained. Consider the ESD current as a single shot impulsive current, when the spark discharge occurs between the gap. Then the current $i(t)$ flowing through the gap can be expressed as

$$i(t) = I_m \cdot F(t/\tau), \quad (1)$$

where I_m and τ are the current peak and nominal duration period, respectively, and $F(\cdot)$ is the non-dimensional function that represents the waveform of the spark current and the following relation holds:

$$\int_0^\infty F(x)dx = 1. \quad (2)$$

The occurrence electromagnetic fields at a location $P(r, \theta, \phi)$ in Figure 1(b) are given from Reference [6] by

$$E_r(t) \simeq \frac{\cos\theta}{2\pi} \cdot \left[\left(\frac{c\tau}{r} \right)^3 \int_{t/\tau}^\infty F(\xi - \frac{r}{c\tau}) d\xi + \left(\frac{c\tau}{r} \right)^2 F\left(\frac{t}{\tau} - \frac{r}{c\tau}\right) \right] \cdot \frac{\ell}{c\tau} E_0 \quad (3)$$

$$\begin{aligned}
E_\theta(t) &\simeq \frac{\sin \theta}{4\pi} \cdot \left[\left(\frac{c\tau}{r} \right)^3 \int_{t/\tau}^{\infty} F(\xi - \frac{r}{c\tau}) d\xi \right. \\
&+ \left(\frac{c\tau}{r} \right)^2 F\left(\frac{t}{\tau} - \frac{r}{c\tau}\right) \\
&\left. + \frac{c\tau}{r} \frac{\partial}{\partial t/\tau} F\left(\frac{t}{\tau} - \frac{r}{c\tau}\right) \right] \cdot \frac{\ell}{c\tau} E_0 \quad (4)
\end{aligned}$$

$$\begin{aligned}
H_\phi(t) &\simeq \frac{\sin \theta}{4\pi} \cdot \left[\left(\frac{c\tau}{r} \right)^2 F\left(\frac{t}{\tau} - \frac{r}{c\tau}\right) \right. \\
&+ \left. \frac{c\tau}{r} \frac{\partial}{\partial t/\tau} F\left(\frac{t}{\tau} - \frac{r}{c\tau}\right) \right] \cdot \frac{\ell}{c\tau} H_0 \quad (5)
\end{aligned}$$

$$E_0 = Z_0 \cdot H_0 \quad (6)$$

$$H_0 = \frac{I_m}{c\tau} \quad (7)$$

where $c = 1/\sqrt{\mu_0 \epsilon_0}$ is the speed of light and $Z_0 = \sqrt{\mu_0/\epsilon_0}$ is the intrinsic impedance of free space.

When the radius a of the metal sphere is large compared with the gap length ℓ as shown in Figure 2(a), the dipole model in Figure 1(b) is no longer applicable to calculation of the occurrence electromagnetic fields, which must numerically be obtained. The FDTD method is used here to compute the occurrence electromagnetic fields due to the spark between the metal spheres. Rizvi and Vetri also used the FDTD method to compute the ESD fields[8], whereas they did not consider the presence of the metal.

Figure 2(b) shows a FDTD computation model of the metal spheres shown in Figure 2(a), which were composed of small cubic cells. For the implementation of the spark path, only one cell was used. Denote by $\delta x = \delta y = \delta z = \delta$ the difference interval of space, and by δt the difference interval of time. Let the difference function of $W = W(x, y, z, t)$ be $W^n(i, j, k) = W(i\delta x, j\delta y, k\delta z, n\delta t)$. On the assumption that the spark discharge between the metal spheres as shown in Figure 2(a) happens in the z -direction, the z -component of the electric field normalized to $Z_0 H_0$, for example, is given by

$$\begin{aligned}
E_z'^{n+1}(i, j, k + \frac{1}{2}) = & \frac{2\epsilon_r(i, j, k + \frac{1}{2}) - \delta t' \tau \sigma(i, j, k + \frac{1}{2}) / \epsilon_0}{2\epsilon_r(i, j, k + \frac{1}{2}) + \delta t' \tau \sigma(i, j, k + \frac{1}{2}) / \epsilon_0} E_z^n(i, j, k + \frac{1}{2}) \\
& - \frac{1}{\delta^2} \frac{2\delta t' F^{n+1}(i, j, k + \frac{1}{2})}{2\epsilon_r(i, j, k + \frac{1}{2}) + \delta t' \tau \sigma(i, j, k + \frac{1}{2}) / \epsilon_0} \\
& + \frac{1}{\delta^2} \frac{2\delta t'}{2\epsilon_r(i, j, k + \frac{1}{2}) + \delta t' \tau \sigma(i, j, k + \frac{1}{2}) / \epsilon_0} \\
& \cdot \left[H_y'^{n+1/2}(i + \frac{1}{2}, j, k + \frac{1}{2}) - H_y'^{n+1/2}(i - \frac{1}{2}, j, k + \frac{1}{2}) \right. \\
& \left. + H_z'^{n+1/2}(i, j - \frac{1}{2}, k + \frac{1}{2}) - H_z'^{n+1/2}(i, j + \frac{1}{2}, k + \frac{1}{2}) \right], \quad (8)
\end{aligned}$$

where $E' = E/(Z_0 H_0)$, $H' = H/H_0$, $\delta t' = \delta t/\tau$, and $\delta' = \delta/c\tau$. Similar expressions can be ob-

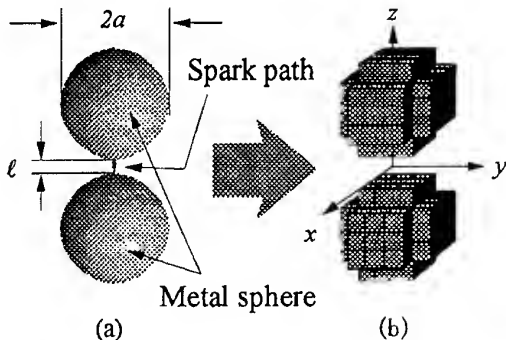


Figure 2 (a) ESD model of charged metal sphere and (b) block model for FDTD computation.

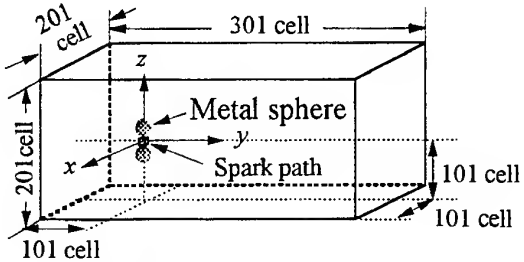


Figure 3 FDTD computation region and arrangement of metal spheres.

tained for E'_x and E'_y . The function F^{n+1} , which is the second term of the right-hand side of the above equation, is given by $F^n(i, j, k) = F(n\delta t/2)$ for the cell through that the spark current flows, but 0 for other cells. Permittivity $\epsilon_r(i, j, k)$ and conductivity $\sigma(i, j, k)$ have numerical values corresponding to the medium of the cell. The first order Mur absorbing boundary condition[9] was applied to the boundary surface of the computational region to simulate an unbounded region.

3 NUMERICAL COMPUTATIONS AND DISCUSSION

Figure 3 shows the FDTD computation region and arrangement of the metal spheres. The region consisted of $(201 \times 301 \times 201)$ cells with $\delta = 1.2$ mm. The radius of the metal sphere was taken as $a = 3.0$ mm ($= 2.5\delta$). As a material of the metal sphere, brass (conductivity: $\sigma = 2.0 \times 10^7$ S/m) was used.

For the spark current, $I_m = 7.4$ A and $\tau = 0.49$ ns were used, which were obtained from our spark experiments for the metal spheres having a gap of 1.2 mm. For such a case the function $F(\cdot)$ can theoretically be derived in a closed form[6], which is given by

$$F(t/\tau) = \frac{3\sqrt{3}}{2} \cdot \exp \left\{ 3\sqrt{3}(t/\tau - x_0) \right\}$$

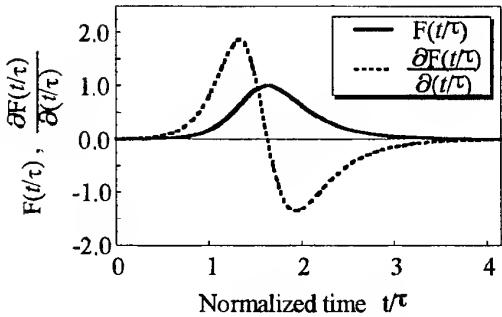


Figure 4 Waveforms of nondimensional function $F(\cdot)$ for spark current and its derivative.

$$\cdot \left[1 + \exp \left\{ 3\sqrt{3}(t/\tau - x_0) \right\} \right]^{-1.5} \quad (9)$$

$$\frac{\partial F(t/\tau)}{\partial t/\tau} = \frac{27}{4} \cdot \exp \left\{ 3\sqrt{3}(t/\tau - x_0) \right\}^{-2.5} \cdot \left[1 + \exp \left\{ 3\sqrt{3}(t/\tau - x_0) \right\} \right]^{-2.5} \cdot \left[2 - \exp \left\{ 3\sqrt{3}(t/\tau - x_0) \right\} \right] \quad (10)$$

where x_0 is the integral constant and was taken here as 1.5. The waveforms of the function $F(\cdot)$ and its derivative are shown in Figure 4.

Figures 5(a) and 5(b) show the computed waveforms of the occurrence magnetic fields on the y -axis at locations of $(0, 0.082c\tau, 0)$ and $(0, 0.90c\tau, 0)$, respectively. The abscissa is the time normalized to τ . The ordinate is the magnetic field normalized to $H_0 = I_m/c\tau$. The solid lines and dashed line are the waveforms computed by the FDTD method and the dipole theory, respectively. The thin line is the FDTD computed result without the metal spheres, which agrees well with the result calculated from the dipole theory. This validates our FDTD computation code. The thick line is the waveform computed for the metal spheres, which shows that the magnetic field peak for the metal spheres is considerably higher compared to the case without the metals.

Figure 6 shows the dependence of the first and second peaks of the magnetic field waveform on the distance from the spark portion. The abscissa is the distance on the y -axis normalized to $c\tau$. The ordinate is the absolute value of the magnetic field peak normalized to $H_0 = I_m/c\tau$. Since the second peak appears in the radiated field proportional to $\partial F(t/\tau)/\partial(t/\tau)$, its distance dependence corresponds to that of the radiated field. The crosshatching part shows the region of $y/c\tau \leq a/c\tau \approx 0.02$, which is near the spark portion. The distance dependence of the first peak, therefore, corresponds to that of the inductive field.

For the case without the metals, the FDTD computed peaks agree well with those calculated from

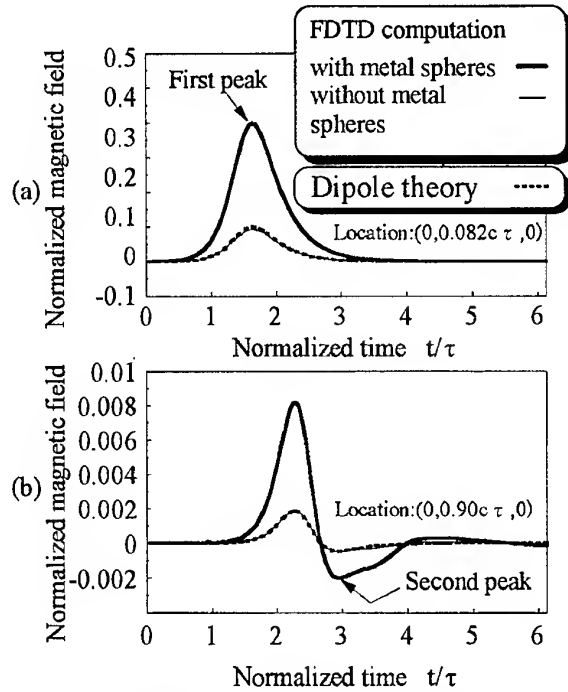


Figure 5 Computed waveforms of occurrence magnetic field.

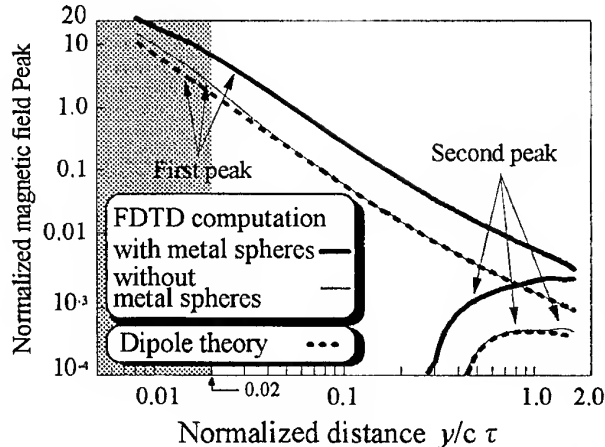


Figure 6 Dependence of magnetic field peak on distance.

the dipole theory. The thick lines are the peaks computed for the metal spheres, which shows that both the field peaks in the region of $y/c\tau > 0.02$ are higher at a constant rate than those calculated from the dipole theory. This means that the presence of the metal spheres enhances the field level and thus increases the radiated field.

4 CONCLUSIONS

The effect of the charged metal itself on the ESD field has not previously been examined. In this paper, we have computed the occurrence electromagnetic fields generated by the spark between the metal

spheres, using the FDTD technique. As a result, we have found that the presence of the metals enhances the ESD field level according to the metal dimensions.

Future subjects include experimental confirmation of the ESD field enhancement effect described here, and computation of the occurrence electromagnetic fields due to the spark between metals having a complicated shape.

5 REFERENCES

- [1] for instance, G.Cerri, R.DeLeo and V.Mariani Primiani, "ESD Indirect Coupling Modeling", IEEE Trans. Electromagnetic Compatibility, Vol.**38**, No.3, pp.274-281, August 1996, pp.274-281.
- [2] P.F.Wilson and M.T.Ma."Field radiated by electrostatic discharges",IEEE Trans. Electromagnetic Compatibility, EMC-**33**,1, Feb.1991, pp.10-18.
- [3] M.Honda."A new threat-EMI effect by indirect ESD on electronic equipment", IEEE Trans. Ind. Appl., Vol.**25**, No.5, May 1989, pp.939-944.
- [4] Greason, W.D.: "Indirect effect of ESD: modeling and measurement", Proc. 11th Int. Zurich Symp. Tech. & Exh. on EMC, 116R1, Mar.1995, pp.613-618.
- [5] O.Fujiwara and N.Andoh:"Analysis of transient electromagnetic fields radiated by electrostatic discharges",IEICE Trans. Commun., Vol.E**76-B**, No.11, Nov.1993, pp.1478-1480.
- [6] O.Fujiwara:"An analytical approach to model indirect effect caused by electrostatic discharge",IEICE Trans. Commun., Vol.E**79-B**, No.4, Apr.1996, pp.483-489.
- [7] O.Fujiwara:"A source model and experiment for explaining peculiar event due to electrostatic discharge", Proc. Inst. Wroclaw Symposium on Electromagnetic Compatibility, EMC96 Wroclaw, Poland, June 1996, pp.480-483.
- [8] M.Rizvi and J.L.Vetri:"ESD source modeling in FDTD", Proc.1994 IEEE Int. Syposium on Electromagnetic Compatibility, Chicago, USA, Aug.1994, pp.77-82.
- [9] G.Mur:"Numerical solution of initial boundary value problems involving Maxwell's equations in isotropic media", IEEE Trans., Vol.AP-**14**, No.8, May 1966, pp.302-307.

BIOGRAPHICAL NOTE

Osamu FUJIWARA received the B.E. degree in electronic engineering from Nagoya Institute of Technology , Nagoya , Japan , in 1971 , and the M.E. and the D.E. degrees in electrical engineering from Nagoya University, Nagoya, Japan, in 1973 and in 1980, respectively. He is presently a professor at Nagoya Institute of Technology. His research interests include measurement and control of electromagnetic interference due to discharge, bioelectromagnetics and other related areas of electromagnetic compatibility.

Kei KAWAGUCHI received the B.E. and M.E. degrees in electrical and computer engineering from Nagoya Institute of Technology, Nagoya, Japan, in 1996 and 1998, respectively. He is presently working for Matsushita Electric Works, Ltd.

Nobunari KURACHI received the B.E. degree in electrical and computer engineering from Nagoya Institute of Technology, Nagoya, Japan, in 1997. He is with Suzuki, Ltd.

MODELLING OF SUPPLY TRANSFORMERS FOR TRANSIENT OVERVOLTAGES

Lesław Gołębowski, Stanisław Wyderka
Rzeszów University of Technology
35-959 Rzeszów, ul. W. Pola 2, Poland
e-mail: swyderka@prz.rzeszow.pl

The paper presents a simple procedure of modelling of supply transformers for transient overvoltages. Proposed model of one-phase transformer was created using ATP-EMTP and its analogue module MODELS. To do that, first the transformer admittances were calculated in MATLAB basing on measurements of voltage and current impulses in transformer windings. Then, the model was built up as a four-terminal network comprising controlled current sources.

1. INTRODUCTION

Transformers are ones of the most familiar components of electrical supply systems. They are ones of the most difficult to model accurately. This concerns both middle-to-low voltage three-phase transformers and low-to-low voltage one-phase transformers. Supply transformers are the devices with the complex arrangement of coils around an iron core. Because of close spacing of coils, transformers have significant stray capacitances and inductances which come into effect at higher frequencies. Then, models of transformers created for power system frequency analysis are not suitable for accurate simulation of propagation of lightning and switching overvoltages through a transformer.

Supply transformers behave linearly for higher frequencies (essentially above 1 kHz) and an iron core does not play a significant role [1]. Transformer winding behaves as a linear system (without saturation effects) for lightning overvoltages, also the magnetic effects of hysteresis can be neglected since the hysteresis loop of supply transformers is very narrow [2].

Two main trends can be distinguished in modelling of transformers for overvoltage transfer analysis [3]. The first of them concerns the detailed internal winding models. The second trend concerns the terminal models.

Detailed internal winding model consists of large networks of inductances and capacitances obtained as a result of discretisation of distributed self and mutual winding inductances and capacitances. Determination of values of such network elements requires information on the construction details of the transformer and the solution of complex field problems. Such models are mainly suitable for determination of voltage distribution along a winding as a result of impulse excitation.

Terminal model is that where the wide range of frequency response at the transformer terminals is reproduced by means of equivalent networks. The model is constructed basing on special tests and measurements. The main task is to carry complicated numerical calculations for determining the parameters of equivalent networks. In this case transformers are often tested using low voltage impulses.

Practical procedure of terminal model creation often proceeds as follows [3]. First the diagram of a π -equivalent of transformer model should be established. To determine the transformer short circuit admittance functions the low voltage technique [2] is often used. Voltage impulses used for excitation of the transformer at one of the terminals and the consequent current waveforms are simultaneously recorded.

In the second step the nodal equations relating to the voltages and currents at the terminals of the transformer must be established. Then, the elements of the nodal admittance matrix should be approximated in the frequency domain with rational functions consisting of real as well as complex conjugate poles and zeroes. The fitting technique used to the approximation is often based on a least squares curve fitting process performed with the use of suitable computer program. As the result of this complicated process the parameters of equivalent RLC networks are determined. Each admittance of the π -equivalent of transformer model comprises one such RLC network.

Terminal model of a transformer achieved according to above procedure can be implemented into one of the computer programs enabling the simulation of overvoltage transfer through a transformer. For that purpose the world-wide known ATP-EMTP (Alternative Transients Program - Electromagnetic Transients Program) [4] is often used.

Presented procedure of transformer terminal model creation for overvoltage transfer study is difficult and time consuming. Many steps of mathematical operations with simplifying assumptions are the reason for reduction of model accuracy.

In this paper the simpler procedure of transformer terminal model creation is proposed. This digital model is created using the ATP-EMTP and its analogue module MODELS [5].

2. PROPOSED MODEL

For presentation of creation procedure of the proposed new transformer model for simulation of transfer of steep fronted overvoltages a one-phase low-to-low voltage (220/24 V) transformer was chosen.

The four-terminal network as a model of such transformer is presented in fig. 1. It can be described according to the network theory with the admittance parameters:

$$\begin{aligned} I_1 &= Y_{11}V_1 + Y_{12}V_2 \\ I_2 &= Y_{21}V_1 + Y_{22}V_2 \end{aligned} \quad (1)$$

where: Y_{11} , Y_{12} , Y_{21} , Y_{22} - admittance parameters of the four-terminal network.

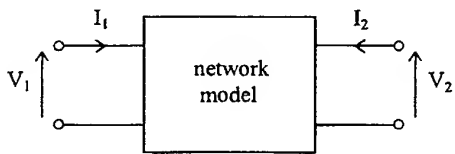


Fig. 1. General four-terminal network model of one-phase transformer

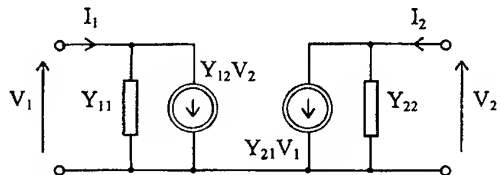


Fig. 2. Model of one-phase transformer including two current sources

Such four-terminal network model can be realised in digital form in ATP-EMTP by replacing it with two two-terminal source networks as it is presented in fig. 2. The admittance parameters Y_{11} , Y_{12} , Y_{21} and Y_{22} of a transformer are frequency dependent functions. Then, digital models of current sources as well as admittances Y_{11} and Y_{12} must be created using current sources (type 60) controlled with analogue module MODELS.

The model presented in fig. 1 can be naturally described also using the impedance or hybrid parameters, but when such model is to be realised in digital form in ATP-EMTP in the way proposed above, only its representation with admittance parameters can be taken into account. This is because in ATP-EMTP the one of the two nodes of modelled voltage or current sources controlled with MODELS must be grounded.

3. MEASUREMENTS AND CALCULATIONS

For determination of admittance parameters of the proposed model (fig. 2) the appropriate time functions of voltage and current for examined transformer were measured and digitally recorded. In each case, as an

input function the low voltage impulses of double exponential type were used. The simple impulse generator was developed which has a continuously adjustable output between 0 and 200 V in order to be able to make efficient use of the oscilloscope vertical resolution.

For the measurements a digital storage oscilloscope was used. Its nominal parameters are as follows: effective storage frequency bandwidth: 100 MHz, maximum effective sampling rate: 100 MS/s, vertical resolution: 8 bits, horizontal resolution: 12 bits, saving memory: 4096 words for each of 2 channels.

For data processing and communication between the oscilloscope and microcomputer (PC) the RS232C version interface and special program was used. This program enables the transfer of recorded waveforms from the oscilloscope to PC.

Selected voltage input waveform and resulting current waveforms in transformer primary and secondary windings are presented in fig. 3. These waveforms were measured when the primary winding was excited with the voltage impulse and the secondary winding was shorted ($V_2 = 0$). Registered, in this case, time functions enable the determination of admittances Y_{11} and Y_{21} - see equations (1).

In order to determine the admittances Y_{12} and Y_{22} similar measurements were conducted but in this case the voltage impulse generator was connected to the secondary winding and the primary winding was shorted ($V_1 = 0$).

On the base of achieved results the admittance parameters of the model in fig. 2 were calculated as the functions of the Laplace operator s . For identification of these admittances the MATLAB, well known computer program, was used. On the base of measured voltage time function as an excitation impulse, and current time function in given transformer winding as the answer to this excitation, special identification tool of the program gives the admittance (self or mutual) as the rational function of variable s .

All four identification methods (arx, armax, bj, iv4) available in Identification Toolbox of Matlab 4.2 were used and the best results were chosen for creation of transformer model. In the case of conducted investigations polynomials of fourth order regarding the variable s (both for the numerator and denominator) for each of four calculated admittances have proved as adequate for the model.

Schematic diagram of the proposed digital model of one-phase supply transformer is presented in fig. 4. Electrical elements of the model (current sources) were realised in basic module of ATP-EMTP. For this purpose the controlled current sources type 60 have been used. Each source is controlled by the one of terminal voltages (V_1 or V_2). In the individual case the controlling voltage value in each time step is modified by proper admittance function. Controlling elements of the model were realised in analogue module MODELS of the ATP-EMTP.

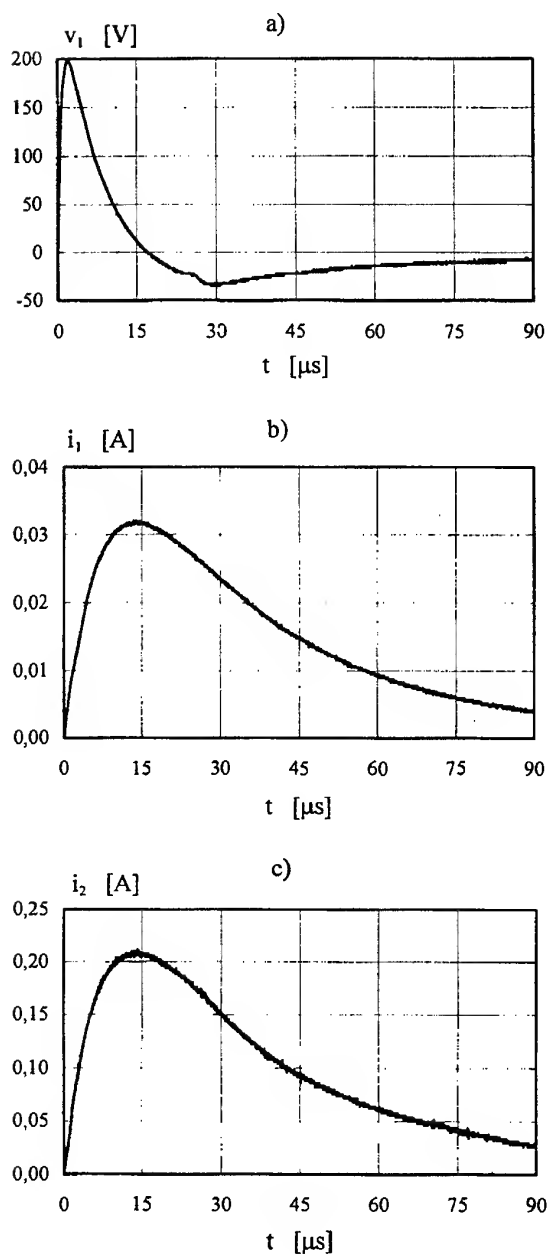


Fig. 3. Results of measurements for secondary winding shorted: a) voltage impulse at primary winding, b) and c) current waveforms in primary and secondary winding respectively

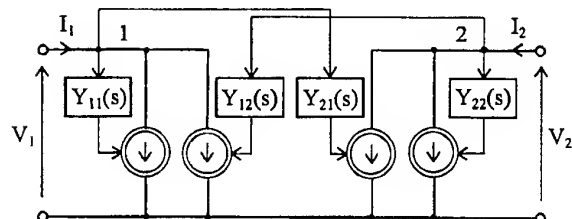


Fig. 4. Schematic diagram of the proposed digital model of one-phase transformer

For verification of proposed model of one-phase transformer the measurements and simulations were conducted. Selected results of this verification are shown in figures 5 and 6. During measurements primary winding of the examined unloaded transformer was excited with voltage impulse presented in fig. 5a. As the response the voltage waveform at open secondary winding was measured and presented in fig. 5b.

For comparison with results of measurements the simulations were performed in ATP-EMTP using digital model of examined transformer created according to the proposed procedure. To simulate the same working state of the transformer as in the case of measurements the voltage impulse presented in fig. 6a was selected as the input function. It should be noted that voltage impulses in fig. 5a and fig. 6a are almost identical. As the output function the voltage waveform at open secondary winding of the transformer model was calculated and presented in fig. 6b.

Measured (fig. 5b) and simulated (fig. 6b) functions of secondary voltage of unloaded transformer as the answers to voltage impulses at primary winding are similar in amplitude and shape. Some small differences between these functions especially in the falling parts are the results of errors which can not be avoided during measurements and calculations. Fortunately these differences are not of essential importance.

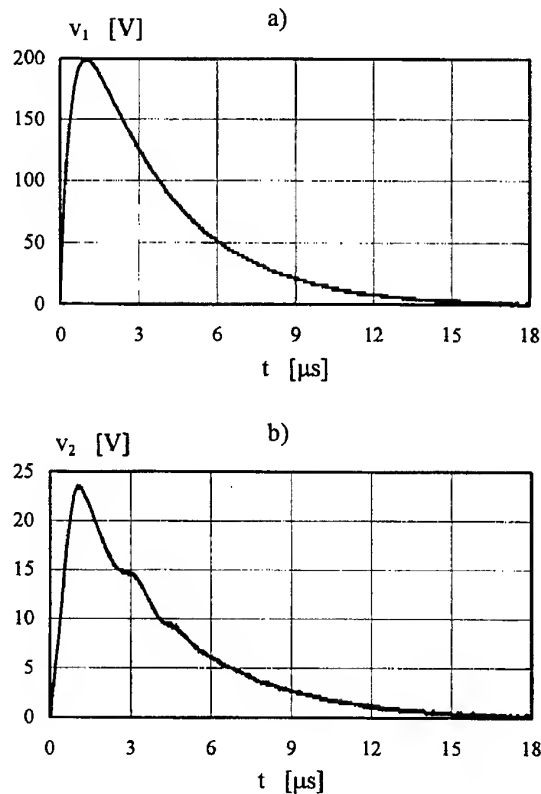


Fig. 5. Results of measurements for unloaded transformer: a) voltage impulse exciting primary winding, b) voltage waveform at secondary winding

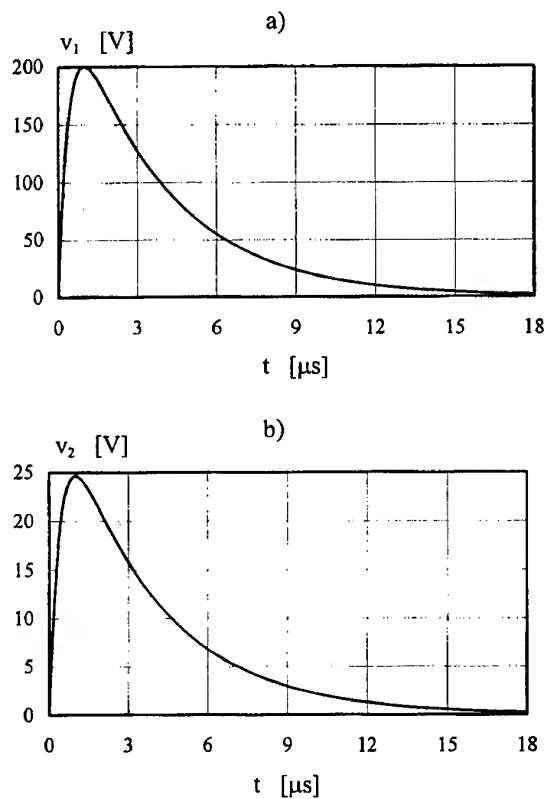


Fig. 6. Results of simulation for unloaded transformer:
a) input voltage function, b) output voltage function

4. CONCLUSIONS

Presented above the proposal of a simple procedure of modelling of supply transformers for transient overvoltages should be treated as initial. Further investigations should determine precisely its advantages and shortcomings. Nevertheless general advantages of this procedure can be evaluated basing on the analysis conducted during creation of the model.

The main advantage of the proposed procedure of modelling of one-phase transformers for high frequencies is its simplicity. The method is easy in realisation and created model can be implemented into most of network models built in ATP-EMTP.

The hybrid (analogue-digital) character can be counted as the disadvantage of the proposed model. But this problem is not of essential importance as number of computer programs which enable modelling of analogue

modules increases quickly. Proposed model created in ATP-EMTP can be easily adapted to other computer programs.

5. REFERENCES

- 4.1. P.T.M. Vaessen, E. Hanique, „A new frequency response analysis method for power transformers”, IEEE Transaction on Power Delivery, Vol. 7, No. 1, January 1992, pp. 384-391.
- 4.2. R.A. Kelly, J.M. Van Coller, A.C. Britten, „Propagation of lightning surges from MV to LV distribution networks”, 23rd International Conference on Lightning Protection, Italy, Firenze, 23-27 September 1996, pp. 630-635.
- 4.3. A. Morched, L. Marti, J. Ottavangers, „A high frequency transformer model for the EMTP”, IEEE Transaction on Power Delivery, Vol. 8, No. 3, July 1993, pp. 1615-1626.
- 4.4. H.W. Dommel, „Electromagnetic Transients Program - Reference Manual” Bonneville Power Administration, Portland, USA 1986.
- 4.5. L. Dubé, „Models in ATP - language manual”, Internet, 1996.

BIOGRAPHICAL NOTES

Lesław Golębiowski was born in Rzeszów, Poland on November 4, 1946. He received a M. Sc. degree in electrical engineering from Academy of Mining and Metallurgy in Kraków in 1970, and a Ph. D. degree from the same Academy in 1974. Since 1970 he works for Engineering College in Rzeszów, and since 1974 for Rzeszów University of Technology as lecturer and researcher. In 1997 he received a D. Sc. degree from Academy of Mining and Metallurgy in Kraków. His fields of interest include calculation methods in electrical engineering and dynamic states of electrical machines.

Stanisław Wyderka was born in Jasło, Poland on January 24, 1949. He received a M. Sc. degree in electrical engineering from Warsaw University of Technology in 1994, and a Ph. D. degree from Electrical Engineering Institute in Warsaw in 1982. Since 1972 he is lecturer and research worker at Rzeszów University of Technology. His fields of interest include high voltage engineering, surge protection of electrical equipment and digital modelling of surge arresters.

NEAR FIELD EMC ANALYSIS BY A COMBINATION OF UTD AND MOM

Harm-Friedrich Harms, Thyssen Nordseewerke GmbH, P. O. Box 2351, D-26703 Emden, Germany
 Karl-Heinz Gonschorek, Technical University Dresden, Helmholtzstr. 9, D-01069 Dresden, Germany

A combination of Geometric Theory of Diffraction (UTD) and Method of Moments (MoM) called Hybrid Method (HM) will be presented. This combination makes it possible to derive benefits from the advantages of both methods, UTD and MoM. One advantage of the HM, the extended possibilities for near field calculation, will be presented.

1 INTRODUCTION

The Uniform Geometric Theory of Diffraction (UTD) is a very efficient tool for EMC field analysis in high frequency (HF) region. In technical arrangements the UTD is used for frequencies starting at 1 GHz. So UTD is especially used for EMC problems in arrangements with radar antennas. For many other methods it is necessary to discretise the space, the bodies or the surface of the bodies in the field region. For using UTD no discretisation is necessary.

Therefore the storage and the calculation time are independent of the electric size of the bodies (size in terms of the wave length λ). One problem is that near to field sources longitudinal field components appear. UTD cannot calculate them. EMC analysis in near field is not possible.

Another powerful tool for HF field analysis is given by the Method of Moments (MoM) [1, 7]. For using MoM the surface of the bodies in field region has to be modeled by patches. The discretisation has to be small in terms of the wave length. With MoM near field analysis is possible. One disadvantage of this method is caused by the discretisation, when changing the frequency f . The impedance matrix describing the coupling process increases $\sim f^4$, the calculation time increases $\sim f^6$ [2, 8]. The application of MoM to complex arrangements is mostly limited by computer power. Electrically large arrangements cannot be examined.

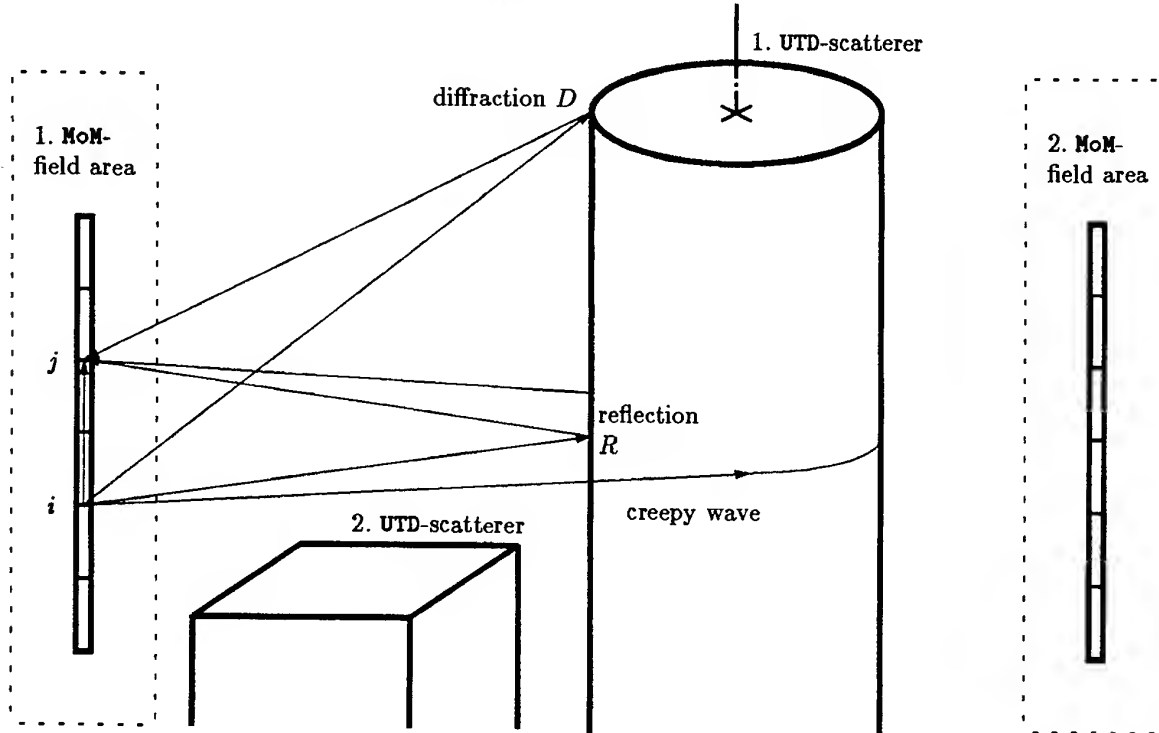


Fig. 1: Principle of the Hybrid Method.

Combining both methods, UTD and MoM, delivers the possibility to calculate arrangements of both, electrically small and electrically large bodies. Especially field calculations near to antennas can be performed. This combination, called Hybrid Method (HM), was founded by Ekelman and Thiele [3]. More investigations were made by the authors [4] and other scientists [6, 9].

2 HYBRID METHOD

In the arrangement which has to be analysed by HM (Fig. 1), there can be several MoM field areas and several large bodies (UTD-scatterer). For explanation only MoM area 1. and the cylinder will be regarded. In a first step of the calculation the large bodies are ignored. Their influence will be considered by UTD in a second step. The MoM area is handled as usual in MoM. The antenna wires have to be discretised and an equation system is built up. The elements of the impedance matrix $[Z]_{N,N}^{MoM}$ describe the direct influence of the current basis functions on the segment voltages (Eq. 1):

$$[Z]_{N,N}^{MoM} \cdot [I]_{N,1} = [U]_{N,1}^{MoM}. \quad (1)$$

The rest of the arrangement is given by electrically large bodies. They cannot be handled by MoM. Their influence on the current distribution will be calculated by UTD. These bodies will be called UTD scatterers. The current basis functions cause fields which are reflected, diffracted and propagated as creeping waves on the surface of the UTD scatterers. Maybe these scattered fields hit again the MoM structure (Fig. 1). They produce an additional segment voltage. For that reason an additional equation system with an second impedance matrix $[Z]_{N,N}^{UTD}$ is built up:

$$[Z]_{N,N}^{UTD} \cdot [I]_{N,1} = [U]_{N,1}^{UTD}. \quad (2)$$

The direct field components are neglected. They are already considered in the impedance matrix $[Z]_{N,N}^{MoM}$. To take into account all couplings the equation systems are added:

$$[U]_{N,1}^{MoM} + [U]_{N,1}^{UTD} = [U]_{N,1}, \quad (3)$$

$$([Z]_{N,N}^{MoM} + [Z]_{N,N}^{UTD}) \cdot [I]_{N,1} = [U]_{N,1}. \quad (4)$$

After solving the resulting equation system the currents on the MoM structures are known. Now it is possible to calculate the field at every point in space by a superposition of the field parts of every current basis function. For doing that, the scattering of the fields at the UTD bodies have to be considered again. More detailed information can be found in [3, 4].

3 NEAR FIELD ANALYSES

Many comparisons have been made between results of MoM field analyses, HM field analyses and mea-

surements [5]. There has always been a good agreement between the results.

Usually these comparisons have been made made for far field. It still remains the question whether this good agreement of the results of MoM and HM can also be found in the near field. To answer this question in a first step the fields of MoM and HM for a single current basis function are compared. The results (not given here) show good agreements between both methods.

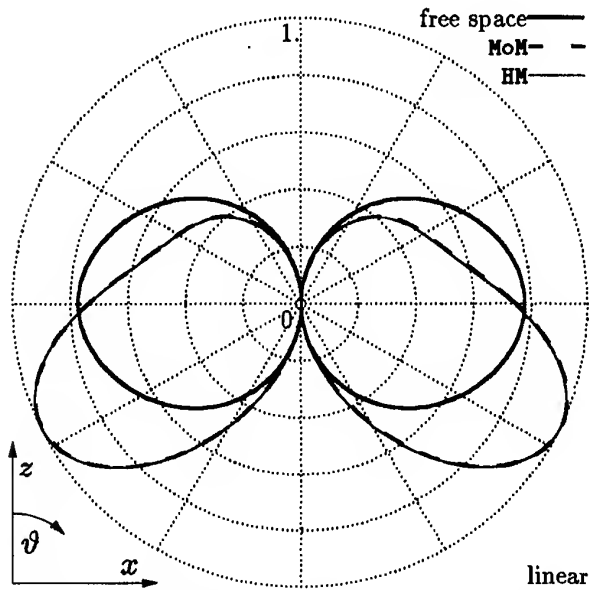


Fig. 2: Vertical antenna diagrams of a $\lambda/2$ -dipole in a distance of λ parallel above the surface of an infinite plane. The diagrams present the radial or respectively the longitudinal field components for a distance of $s = 0.5 \lambda$.

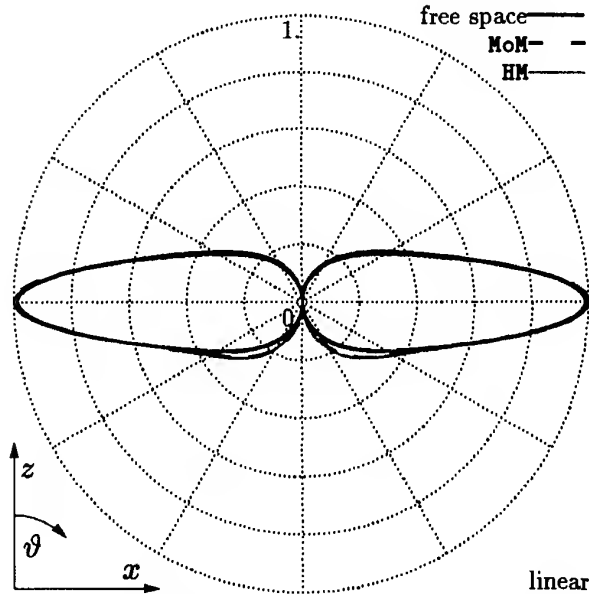


Fig. 3: Vertical antenna diagrams of a $\lambda/2$ -dipole in a distance of λ parallel above the surface of an infinite plane. The diagrams present the radial or respectively the longitudinal field components for a distance of $s = 0.3 \lambda$.

3.1 Dipole above infinite plane

In a next step, a discretised structure and a scattering process is used for the test. The arrangement is chosen as follows: A $\lambda/2$ -dipole is positioned in a distance of λ above an infinite plane. The field is calculated at cycles around the loading point of the dipole. The radiiuses of the cycles are 0.5λ and 0.3λ . Fig. 2 and Fig. 3 show the results of the calculations. The diagrams represent the radial or respectively the longitudinal field components. As a reference the radial field of the dipole in free space is shown (—). The results of MoM (—) and HM (—) are nearly the same. No difference can be seen in the diagrams.

3.2 Yagi-Uda antenna with scatterers

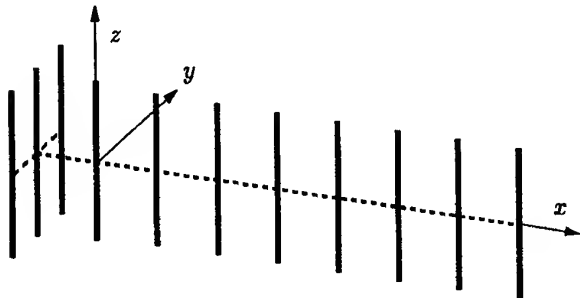


Fig. 4: Model of Yagi-Uda antenna.

Now results for a complex arrangement are presented. A Yagi-Uda antenna according to Fig. 4 is built up. It is loaded by a voltage source of 1 V at a frequency of 1 GHz. For demonstration the main loop of the free space antenna diagram points in the direction of different scattering objects. In the first example an infinite plane is used as a scatterer (Fig. 5). The distance between the loaded dipole and the surface is 3λ .

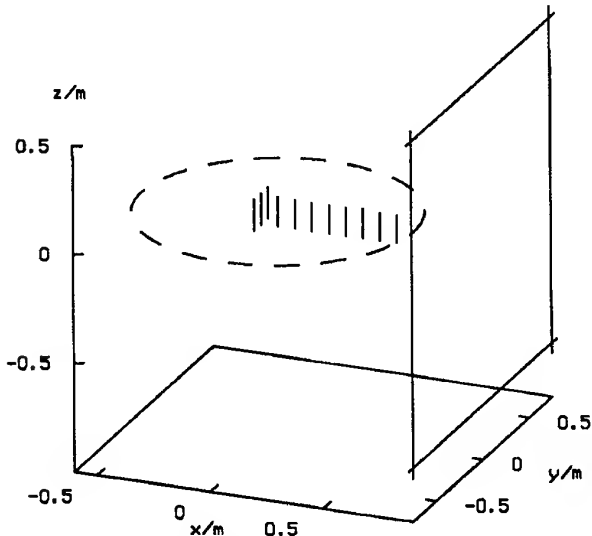


Fig. 5: Yagi-Uda antenna in front of an infinite plane.

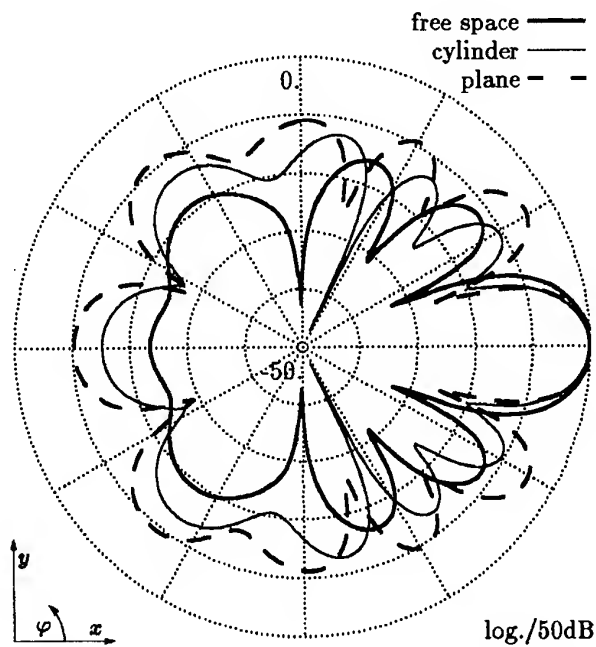


Fig. 6: Horizontal antenna diagrams of the Yagi-Uda antenna for a distance of 2λ , scaled to the maximum of the field in free space.

Horizontal antenna diagrams for this arrangement are calculated (Fig. 6 and Fig. 7). The loaded dipole is in the center of the cycle for the field calculations. The first cycle has a radius of 2λ in order to be in the near field of the antenna. These results are presented in Fig. 6. As a reference the thick solid line (—) represents the field of the antenna in free space. The results are scaled to the maximum of this curve. Line (—) represents the field distribution for the antenna in front of the infinite

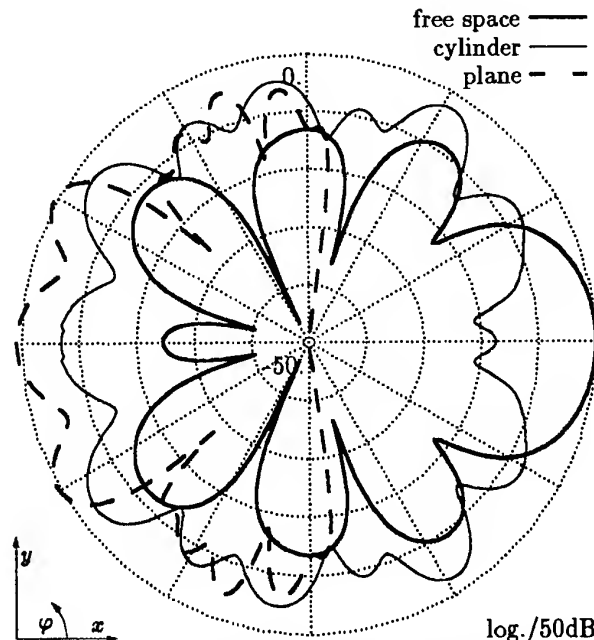


Fig. 7: Horizontal antenna diagrams of the Yagi-Uda antenna for a distance of 20λ , scaled to the maximum of the field in free space.

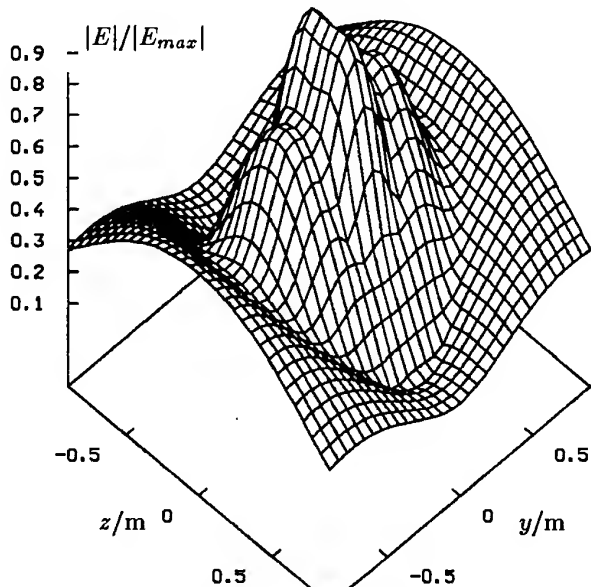


Fig. 8: Yagi-Uda antenna, main loop pointed on an infinite plane. Field strength in a plane ($6\lambda \times 6\lambda$) 0.5λ above the surface of the body. Maximum field strength $E_{max} = 5.33$ V/m. HM result.

plane. This arrangement can be calculated by the HM as well as by the MoM using the mirror principle. The thick dashed line (— —) represents the fields of both methods, the results are equal.

As pointed out it is not possible for MoM to solve problems with complex large bodies. Therefor an HM-analysis was done with the Yagi-Uda antenna in front of a cylinder instead of the plane. In the first example the cylinder has a radius of 10λ and a length of 8λ . Nearly no difference for the near field of the antenna was found compared to the example with the infinite plane (of course the far field diagram is very

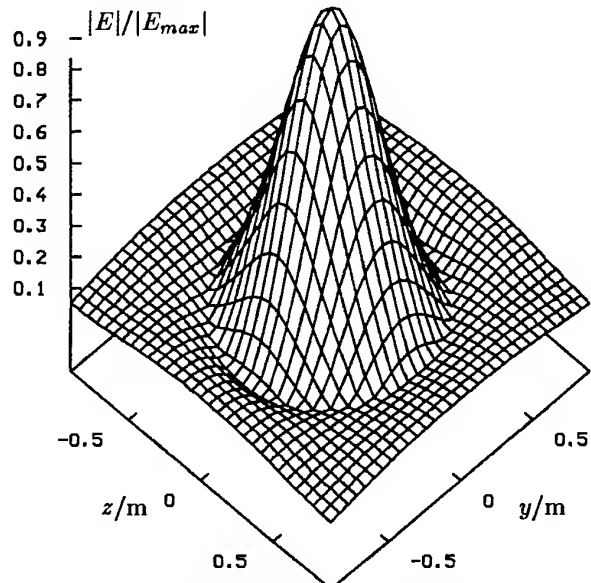


Fig. 10: Yagi-Uda antenna, main loop pointed on a cylinder. Field strength in a plane ($6\lambda \times 6\lambda$) 0.1λ above the surface of the body. Maximum field strength $E_{max} = 11.28$ V/m. HM result.

different). For that reason a cylinder with a radius of λ and a length of 8λ was chosen. A clear difference can be seen between the curve for the plane and the curve for the cylinder (—).

To complete the comparisons diagrams have also been calculated for a distance of 20λ which are shown in Fig. 7. Again the fields are scaled to the results of the antenna in free space. Because of the larger distance from the antenna the scattered field component and the direct field component have nearly the same value. So the influence of the scattered field on the field distribution is much bigger, greater

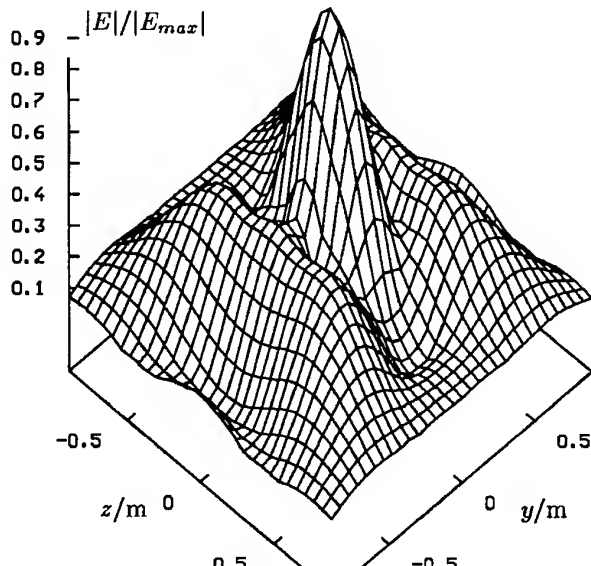


Fig. 9: Yagi-Uda antenna, main loop pointed to a cylinder. Field strength in a plane ($6\lambda \times 6\lambda$) 0.5λ above the surface of the body. Maximum field strength $E_{max} = 5.82$ V/m. HM result.

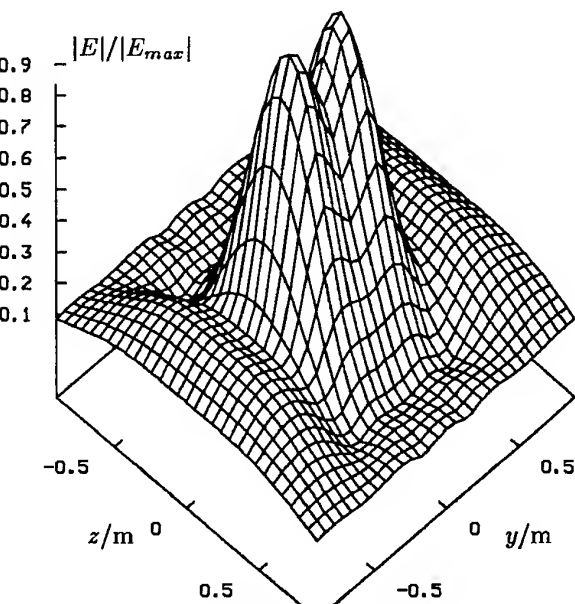


Fig. 11: Yagi-Uda antenna, main loop pointed to a cylinder. Field strength in a plane ($6\lambda \times 6\lambda$) 0.1λ above the surface of the body. Maximum field strength $E_{max} = 10.90$ V/m. HM result.

difference can be seen between the three curves.

The diagrams of Fig. 6 and Fig. 7 represent the near field of the MoM-field area. In the following a look on the near field of the UTD bodies will be done. The field strength in a plane of $6\lambda \times 6\lambda$ parallel to the surface of the scattering body is calculated.

The distance between the calculation plane and the surface of the body is 0.5λ (Fig. 8, Fig. 9) and 0.1λ (Fig. 10, Fig. 11). The calculations are also carried out for the antenna in free space to have a reference. Comparisons are made between the results of MoM and HM for the arrangement with the infinite plane. No difference can be seen in the diagrams. The results for the field calculation with the cylinder (Fig. 9 Fig. 11) can only be done by HM.

4 CONCLUSION

The simple example of the dipole shows that it is possible to calculate near fields for arrangements of antennas and electrically large bodies by the Hybrid Method. The example with the Yagi-Uda antenna demonstrates, that near field calculations are also feasible for arrangements which are much more complicated. In realistic applications normally there would be no scatterer in the direction of the main radiation direction. But also a scattering body in the side loops will have influence on the antenna parameters.

The restrictions for HM near field analyses are especially given by the MoM part. The discretisation has to be small in terms of the distance to the MoM-field area and the thin wire model has to be valid for this part.

REFERENCES

- [1] H.-D. Brüns. *Pulserregte elektromagnetische Vorgänge in dreidimensionalen Stabstrukturen*. PhD thesis, Universität der Bundeswehr, Hamburg, 1985.
- [2] Guido Bürger. Lösung des linearen Gleichungssystems in CONCEPT durch optimierte Out-Of-Core Gauß-Elimination. CONCEPT Internal Working Note 02, Arbeitsbereich Theoretische Elektrotechnik, Technische Universität Hamburg-Harburg, 1995.
- [3] E. P. Ekelman and G. A. Thiele. A hybrid Technique for Combining the Moment Method Treatment of Wire Antennas with the GTD for curved Surfaces. *IEEE Transactions on Antennas and Propagation*, AP-28(6), November 1980.
- [4] Harm-Friedrich Harms. *Hybridmethode - Erweiterung der Momentenmethode um das Verfahren der Einheitlichen Geometrischen Beugungstheorie*. PhD thesis, Technische Universität Hamburg-Harburg, 1996. Shaker Verlag GmbH, Aachen.

Hamburg-Harburg, 1996. Shaker Verlag GmbH, Aachen.

- [5] Harm-Friedrich Harms and K.-H. Gonschorek. Berechnung hochfrequenter EMV-Probleme durch die Kombination der Momentenmethode mit der Geometrischen Beugungstheorie. In *EMV'94 Tagungsband*, pages 311–320, 1994. VDE-Verlag.
- [6] Christian Kieviet, H.-F. Harms, H. Wagner, and K.-H. Gonschorek. Generalized Formulation for Raytracing in GTD/UTD. In *Workshop Electromagnetic Light and Scattering: Theory and Application, Moscow 1997*, pages 43–47, 1997.
- [7] Thomas Mader. *Berechnung elektromagnetischer Felderscheinungen in abschnittsweise homogenen Medien mit Oberflächenstromsimulation*. PhD thesis, Technische Universität Hamburg-Harburg, 1992.
- [8] E. K. Miller and F. M. Tesche. Impact of continued computer development on em modeling. In *9th International Zurich Symposium and Technical Exhibition on EMC*, March 1991.
- [9] Holger Wagner, H.-F. Harms, and K.-H. Gonschorek. Der Einsatz von Punktquellen zur Nachbildung stückweise linearer Strombasisfunktionen in der Kombination vom MoM und GTD. In *EMV'96 Karlsruhe Tagungsband*, pages 251–258, 1996. VDE-Verlag.

BIOGRAPHICAL NOTE

Harm-Friedrich Harms was born in Aurich, Germany on January 11, 1960. In 1979 he finished his vocational education (Funkelektroniker, radio engineer). He received the Dipl.-Ing. (MSEE) degree from the University of Hanover in 1990 and the Dr.-Ing. (PhD EE) degree from the Technical University Hamburg-Harburg in 1996. He wrote his doctor thesis about the Hybrid Method - The Combination of MoM and UTD. Since 1996 he has been working for the Thyssen Nordseewerke Emden (shipyard) in the naval department. His field of work is the Electromagnetic Compatibility on ships and submarines.

Karl-Heinz Gonschorek was born in a small village close to Hanover in Sept. 1946. he studied electrotechniques, concentrating on high frequencies, at the University of Hanover. In 1980 he wrote his doctor thesis about electromagnetic coupling of arbitrarily located thin electrodes. From 1980 to 1988 he was with Siemens, working in R & D-group handling all questions of EMC. 1988 he became professor of for electromagnetic influences at the Technical University of Hamburg-Harburg. Since 1995 he is the holder of the Siemens-foundation chair on EMC at the Technical University of Dresden.

DETERMINING THE COUPLING PARAMETERS OF SHIELDED MULTICONDUCTOR CABLES

Sven Helmers Karl-Heinz Gonschorek

Dresden University of Technology
ETI/EMV Electromagnetic Compatibility Division
01062 Dresden, Germany

Abstract The coupling of electromagnetic fields to shielded cables is to be considered as one of the most important aspects in EMC (Electromagnetic Compatibility) system analysis. Normally, the shielding quality of a shielded multiconductor cable is best described by its peculiar vectors of transfer impedances and transfer admittances. To determine both of these coupling parameter vectors, a straightforward method which is based on combining the method of moments and transmission line analysis with experimentally obtained data is presented in this paper. Thereby, the role of transfer admittances or radial electric coupling coefficients, respectively, is focused.

1. INTRODUCTION

A lot of contributions have been made by the scientific community to investigate the coupling of electromagnetic fields to shielded cables. Due to the difficulty of the underlying physical principles, experimental methods of measuring the coupling parameters have become increasingly important. Unfortunately, a majority of the workers restrict themselves to the contribution of the transfer impedances to the coupling process. For this reason, a lack of certainty remains about the influence of transfer admittances under these circumstances.

Here, a new approach is presented taking into account both sets of parameters Z'_T and Y'_T . Following a proposal from Broydé et al [1], a vector of radial electric coupling coefficients ζ_R is put forward to replace the vector of transfer admittances Y'_T in the range of high frequencies. The outer electromagnetic impact on the shield of the cable within a clearly defined test fixture is computed using the method of moments (MoM) and, secondly, included into transmission line theory. In this way, the main equation

for the evaluation of both coupling parameter vectors Z'_T and ζ_R is derived. This theory is summarized in the second chapter. The third section is directed to the description of the experimental fixture. Finally, in chapter 4 the results obtained so far are discussed while concentrating on the quality of the cable shield on the one hand and the geometry of the inner conductors on the other hand.

2. MODELING

In the following, the analytical description of the coupling process is developed. All equations refer to the frequency domain with sinusoidal field excitation. Applying the definition of transfer impedance and transfer admittance from Vance [2] to a shielded multiconductor cable yields:

$$Z'_T = \frac{1}{I_S} \cdot \left. \frac{d\mathbf{V}(z)}{dz} \right|_{\mathbf{I}=0}, \quad (1a)$$

$$Y'_T = -\frac{1}{V_S} \cdot \left. \frac{d\mathbf{I}(z)}{dz} \right|_{\mathbf{V}=0}. \quad (1b)$$

Z'_T and Y'_T denote two vectors of the dimension N while N refers to the number of inner conductors of the cable. In this way, one transfer impedance and one transfer admittance is assigned to each of the inner conductors. The two vectors $\mathbf{V}(z)$ and $\mathbf{I}(z)$ symbolize the N voltages between the inner conductors and the shield or the N currents running on these conductors of the cable, respectively. The common-mode current I_S runs on the shield of the cable and the voltage between the shield and the reference ground is named V_S .

According to [1] a vector of dimensionless radial electric coupling coefficients ζ_R is defined by:

$$\zeta_R = \frac{Y'_T}{j\omega C'_S} = \frac{1}{I'_D} \cdot \left. \frac{d\mathbf{I}(z)}{dz} \right|_{\mathbf{V}=0}. \quad (2)$$

By relating the transfer admittances \mathbf{Y}'_T to the per-unit-length capacitance C'_S between the shield and the reference ground, a vector ζ_R is defined which solely depends on the type of cable being considered. Alternatively, ζ_R is figured out from the division of the per-unit-length induced currents $\frac{d}{dz} \mathbf{I}(z)$ by the per-unit-length displacement current I'_D impinging the shield. See Fig. 1 for the details of the coupling interaction to a coaxial cable.

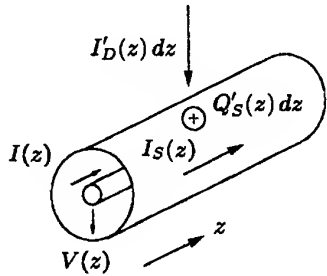


Figure 1: Coupling to a coaxial cable

As shown in the figure a short section of the cable within an exterior electromagnetic field is influenced by the per-unit-length displacement current $I'_D(z)$ impinging the shield as well as by the current $I_S(z)$ running on the shield. Both currents $I'_D(z)$ and $I_S(z)$ are related by the continuity equation:

$$\frac{d}{dz} I_S(z) = -j\omega Q'_S(z) = I'_D(z) . \quad (3)$$

The coordinate z extends along the the cable while Q'_S stands for the total per-unit-length surface charge density on the shield. The induced voltages $\mathbf{V}(z)$ and currents $\mathbf{I}(z)$ on the inner conductors are got from the transmission-line equation [3]:

$$\frac{d}{dz} \begin{pmatrix} \mathbf{V}(z) \\ \mathbf{I}(z) \end{pmatrix} = \underbrace{\begin{pmatrix} 0 & -Z' \\ -Y' & 0 \end{pmatrix}}_A \cdot \begin{pmatrix} \mathbf{V}(z) \\ \mathbf{I}(z) \end{pmatrix} + \begin{pmatrix} \mathbf{V}'_F(z) \\ \mathbf{I}'_F(z) \end{pmatrix} , \quad (4)$$

which leads to the solution [3]:

$$\begin{pmatrix} \mathbf{V}(l) \\ \mathbf{I}(l) \end{pmatrix} = \underbrace{\exp(A l)}_{\Phi(l)} \cdot \begin{pmatrix} \mathbf{V}(0) \\ \mathbf{I}(0) \end{pmatrix} + \int_0^l \underbrace{\exp(A(l-z))}_{\Phi(l-z)} \cdot \begin{pmatrix} \mathbf{V}'_F(z) \\ \mathbf{I}'_F(z) \end{pmatrix} dz . \quad (5)$$

The distributed voltage sources $\mathbf{V}'_F(z)$ and current sources $\mathbf{I}'_F(z)$ along the transmission line are dependent on the coupling parameters Z'_T and ζ_R and the currents $I'_D(z)$ and $I_S(z)$:

$$\mathbf{V}'_F(z) = Z'_T \cdot I_S(z) , \quad \mathbf{I}'_F(z) = \zeta_R \cdot I'_D(z) . \quad (6)$$

The outer influence $I_S(z)$, $I'_D(z)$ on the cable is assumed to be calculable from numerical analysis using the MoM. Actually, modern computer implementations of the MoM will cover almost every arrangement of direct electromagnetic field coupling to cables. Therefore, evaluating the second part on the right-hand side of equation (5) yields:

$$\begin{pmatrix} \mathbf{V}(l) \\ \mathbf{I}(l) \end{pmatrix} = \Phi(l) \cdot \begin{pmatrix} \mathbf{V}(0) \\ \mathbf{I}(0) \end{pmatrix} + \Theta(l) \cdot \begin{pmatrix} \mathbf{Z}'_T \\ \zeta_R \end{pmatrix} , \quad (7)$$

using the abbreviation:

$$\Theta(l) = \quad (8)$$

$$\begin{pmatrix} \int_0^l \Phi_{11}(l-z) I_S(z) dz & \int_0^l \Phi_{12}(l-z) I'_D(z) dz \\ \int_0^l \Phi_{21}(l-z) I_S(z) dz & \int_0^l \Phi_{22}(l-z) I'_D(z) dz \end{pmatrix} .$$

Measuring the voltage vectors $\mathbf{V}(0)$ and $\mathbf{V}(l)$ and evaluating equation (7) give way to the determination of both coupling parameter vectors Z'_T and ζ_R . Therefore, a appropriate experimental fixture is to be designed. These aspects are covered by the following section.

3. MEASUREMENT SET-UP

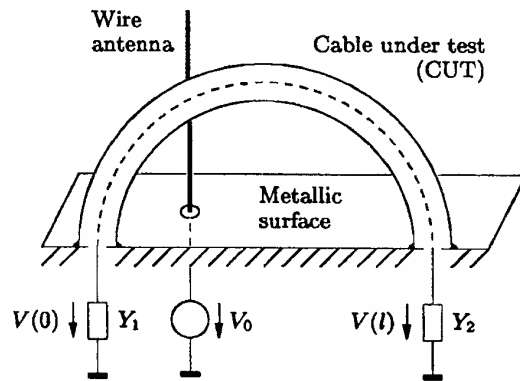


Figure 2: Experimental set-up

The experimental set-up is shown in Fig. 2. For the sake of simplicity, again, the cable under test (CUT) being displayed is a coaxial one. The CUT forms a semicircle with a diameter of about 50 cm over a conducting plane. The cable is terminated at its beginning and its end by the two admittances Y_1 and Y_2 , repectively. A simple implementation of the arrangement is achieved by using the metallic wall of a shielded room for the reference plane. So, the coupling between the test fixture and the measurement equipment is minimized [4].

The structure is excited by a wire antenna of about 30 cm height which is positioned at a distance of about 25 cm from the left connection point

of the CUT. The ratio of the voltages $V(0)/V_0$ and $V(l)/V_0$, respectively, is measured using a HP 4195 A network analyser over a frequency range from 1 MHz up to 100 MHz. The maximum of the voltage V_0 at the feeding-point of the antenna is about 1 V, effectively.

A corresponding model of the set-up is built for analysis using the MoM. Thereby, the CONCEPT II computer code from the Department of Theoretical Electrical Engineering at the University of Hamburg-Harburg is utilized. The resulting representation consists of 19 wires (modeling the semicycle by use of a polygon) with 58 unknowns for the current. Coming next, the current distribution $I_S(z)$, $\frac{d}{dz} I_S(z)$ on the shield of cable is extracted from the output data of CONCEPT II. After the matrix $\Theta(l)$ has been computed numerically from equation (8), the coupling parameters are finally obtained from equation (7).

Considering a shielded multiconductor cable with a number of N inner conductors, overall $2 \cdot N$ measurements have to be made. Step by step, the induced voltage between each of the inner conductors and the shield is measured at both ends of the cable while all other inner conductors are open circuited. Consequently, a system of linear equations of the dimension $2 \cdot N^2$ is derived from equation (7). Solving that system numerically yields the $2N \cdot (N-1)$ voltages of the open circuited inner conductors at the beginning of the cable. Additionally, both coupling parameter vectors Z'_T and ζ_R are obtained.

4. RESULTS

Two major issues are discussed within this section. In the first place, the scalar coupling parameters Z'_T and ζ_R of coaxial cables are investigated for their dependency upon the optical coverage K of the shield. The measured values of the radial electric coupling coefficients ζ_R are compared with those obtained from analytical formulas.

Secondly, the vector of radial electric coupling coefficients ζ_R of a LiYCY $7 \times 0.14 \text{ mm}^2$ shielded multiconductor cable are displayed.

Name	K	N_S	G	α
RG 58-0	76 %	5	16	27°
RG 58-1	65 %	4	16	27°
RG 58-2	52 %	3	16	27°
RG 58-3	37 %	2	16	27°
RG 213-0	90 %	8	24	24°
RG 213-1	84 %	7	24	24°
RG 213-2	76 %	6	24	24°
RG 213-3	67 %	5	24	24°
RG 213-4	57 %	4	24	24°

Table 1: Properties of the modified shields

4.1 Coupling to lousy shielded coaxial cables

A sample of coaxial cables of the type RG 58 and RG 213 has been modified in order to reduce the optical coverage K of the shield. The particular shielding properties of each of the cables are shown in Table 1.

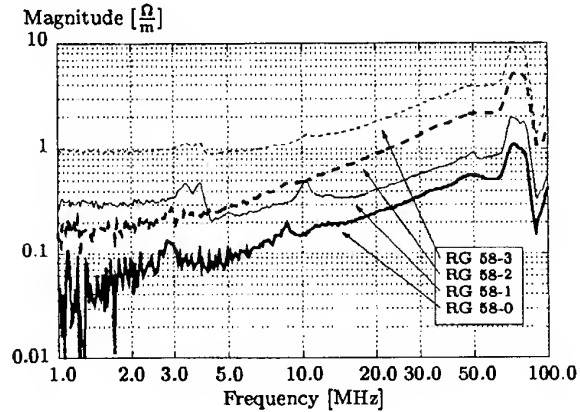


Figure 3: Magnitude of the transfer impedance Z'_T , coaxial cables with modified shield

Here, N_S refers to the number of strands per carrier, G denotes the number of carriers itself and α denotes the weave angle. The magnitude of the transfer impedances Z'_T belonging to the cables of the type RG 58- x is shown in Figure 3. (x denotes the number of strands removed from each carrier.) It can be clearly seen, how the magnitude of the transfer impedance Z'_T increases while the optical coverage K of the shield decreases.

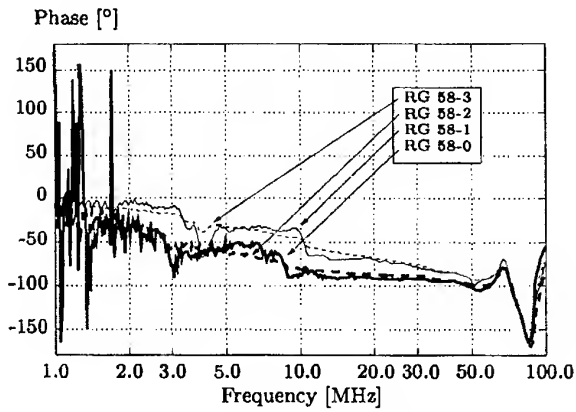


Figure 4: Phase of the transfer impedance Z'_T , coaxial cables with modified shield

Generally, the corresponding phase which is shown in Fig. 4 varies from 0°, approximately, at 1 MHz to between -80° and -100° at 40 MHz. Above the latter frequency the values are influenced by resonance phenomena which are difficult to compensate. Considering the RG 58-0 and RG 58-1, at frequencies below 2 MHz the signal intensity falls below the

noise level.

Nevertheless, the obtained values are showing good agreement with the results obtained by other authors. The signal to noise ratio might be improved by injecting the current I_S directly to the shield of the cable [5]. But doing so, the influence of the transfer impedance Z'_T will not be separated that easily from the influence of the radial coupling coefficient ζ_R .

The magnitude of the radial electric coupling coefficient is shown in Fig. 5. Again, the magnitude of the coupling parameter ζ_R is much increased by reducing the optical coverage K of the shield. Different from the transfer impedance Z'_T , the magnitude of the radial coupling coefficient ζ_R is constant from 1 MHz to 40 MHz, approximately. The deviation at higher frequencies above 40 MHz is due to the resonances of the test set-up.

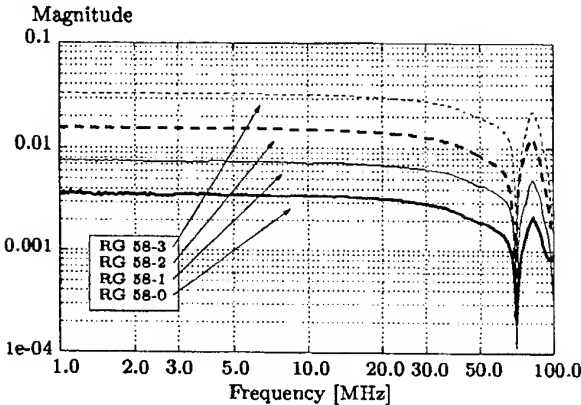


Figure 5: Magnitude of the radial electric coupling coefficient ζ_R , coaxial cables with modified shield

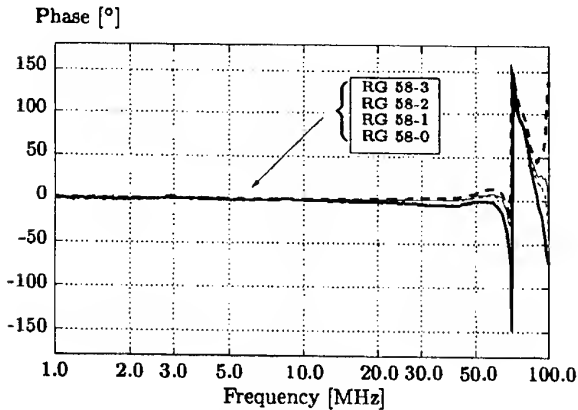


Figure 6: Phase of the radial electric coupling coefficient ζ_R , coaxial cables with modified shield

Additionally, Fig. 6 shows that the phase of the radial electric coupling coefficient ζ_R equals 0° up to frequencies above 50 MHz. Recalling that:

$$Y'_T = j\omega C'_a \cdot \zeta_R , \quad (9)$$

the real part of the transfer admittance Y'_T becomes zero. This observation fully complies with literature [2].

A comparison of the measured values of the radial electric coupling coefficient ζ_R with the analytical formula from [6] is shown in Fig. 7. The average of the measured results concerning the cables of the type RG 58-x (marked as "+") and RG 213-x (marked as "◆") have been computed. Although the overall concurrence is poor, the analytical expression yields an upper limit for the radial electric coupling coefficient to be expected actually.

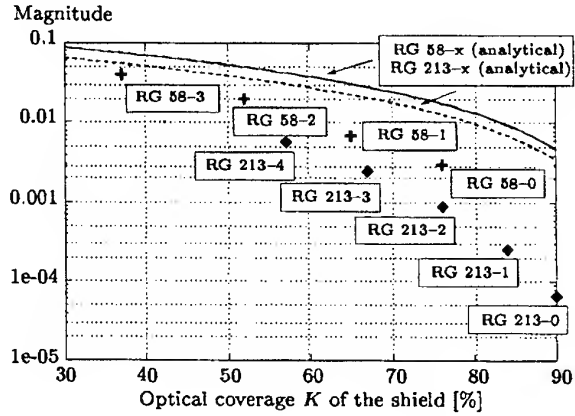


Figure 7: Comparison of the measurement results with the analytical formula for the calculation of the radial electric coupling coefficient ζ_R from [6]

4.2 Coupling to a shielded multiconductor cable

In the second place, the radial electric coupling coefficients ζ_R of a LiYCY $7 \times 0.14 \text{ mm}^2$ shielded multiconductor cable are investigated.

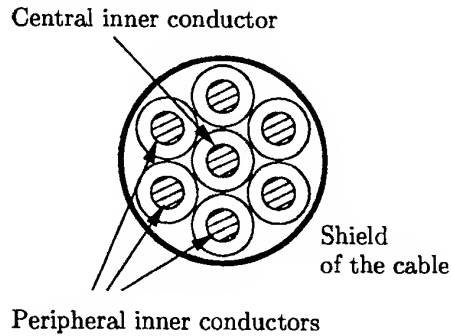


Figure 8: Cross-sectional structure of the cable LiYCY $7 \times 0.14 \text{ mm}^2$

The cross-sectional structure of the cable is shown in Fig. 8. Six peripheral inner conductors are spiral-wound on the circumference of one central inner conductor. For this reason, the central inner conductor gets extra shielding with respect to external fields.

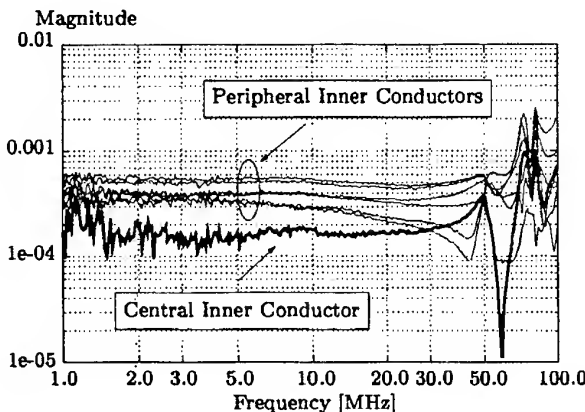


Figure 9: Magnitude of the radial electric coupling coefficients ζ_R , LiYCY $7 \times 0.14 \text{ mm}^2$ shielded multi-conductor cable

These circumstances are clearly represented by the measured results. The magnitude of the coupling parameter vector ζ_R is displayed in Fig. 9. The element of the vector ζ_R which is associated with the central inner conductor is considerably less compared with the other elements.

Additionally, Fig. 9 shows that the remaining elements of the vector ζ_R are far from being the same. These elements are grouped together in pairs of the peripheral inner conductors opposing with regard to the central inner conductor. At present, this phenomenon is still under investigation.

5. CONCLUSIONS

A forthright method of determining the coupling parameter vectors of shielded multiconductor cables has been presented. Both vectors of the transfer impedances Z'_T and the transfer admittances Y'_T or the radial electric coupling coefficients ζ_R , respectively, are obtained from one unique test set-up. Due to the widespread availability of elaborated computer codes realizing the MoM (e. g. CONCEPT, NEC) and the uncomplicated implementation of transmission line theory the seemingly disadvantageous need of numerical field calculation is fully repaid by a robust test fixture. The application to shielded multiconductor cables is fully covered by this method.

The dependence of the capacitive coupling to a shielded cable on the quality of the shield has been investigated. A new set of radial electric coupling coefficients ζ_R has been found which might give way to an improved analytical modelling of the coupling interaction.

Future investigations will examine the influence of discontinuous sections along the cable such as connectors and imperfections of the shield.

REFERENCES

- [1] F. Broyd  , E. Clavelier, D. Givord, P. Vallet, "Discussion of the Relevance of Transfer Admittance and Some Through Elastance Measurement Results", IEEE Transactions on Electromagnetic Compatibility, Vol. 35, No. 11, November 1993, pp. 417-422
- [2] E. F. Vance, "Coupling to Shielded Cables", Robert E. Krieger Publishing Company, Inc., Malabar, Florida, USA, 1987, pp. 111-132
- [3] C. R. Paul, "Analysis of Multiconductor Transmission Lines", John Wiley & Sons, Inc., New York, USA, 1994, pp. 405-407
- [4] S. Helmers and K.-H. Gonschorek, "Measuring the Complex Transfer Admittance of Shielded Coaxial Cables" (in German), Proceedings of the International Symposium on Electromagnetic Compatibility, D  sseldorf, Germany, 1998, pp. 129-137
- [5] F. Sattler and K.-H. Gonschorek, "Measurement and Computation of Cable Coupling in Arbitrary Environment", Proceedings of the IEEE International Symposium on Electromagnetic Compatibility, Chicago, USA, 1994, pp. 5-10
- [6] F. M. Tesche, M. V. Ianoz, T. Karlsson, "EMC Analysis Methods and Computational Models", John Wiley & Sons, Inc., New York, USA, 1997, pp. 466-468

About the Authors

Sven Helmers was born in Hamburg, Germany, in September 1967. He studied electrical engineering focusing on electromagnetic compatibility at the Technical University of Hamburg-Harburg from 1987 to 1994. In 1995 he joined the EMC Division at the Dresden University of Technology. Today, his major research interests are in the field of electromagnetic field coupling to shielded cables and EMC modeling.

Karl-Heinz Gonschorek was born in a small village close to Hanover in September 1946. He studied electromagnetics, concentrating on high frequencies, at the University of Hanover. In 1980 he wrote his doctor thesis about electromagnetic coupling of arbitrarily located thin electrodes. From 1980 to 1988 he was with Siemens, working in a R & D-group handling questions of EMC. 1988 he became professor for electromagnetic influences at the Technical University of Hamburg-Harburg. Since 1995 he is the holder of the Siemens-foundation chair on EMC at the Dresden University of Technology.

A BODY-OF-REVOLUTION MODEL FOR CALCULATING ELECTROMAGNETIC FIELDS EXCITED INSIDE HUMAN HEAD

Andrzej A. Kucharski

Wrocław University of Technology, Wybrzeże Wyspiańskiego 27
50-370 Wrocław, Poland

In this paper a new method for calculating electromagnetic fields inside human body is presented. The method is based on method of moments (MoM) solution applied to so called Mixed Potential Integral Equation (MPIE) developed for a Body-Of-Revolution (BOR) case. The simplification concerning assuming rotational symmetry of the body allows to significantly reduce the number of unknowns involved in the solution process via well-known mode decomposition scheme. Verification of the method together with sample results is presented.

I. INTRODUCTION

The problem of theoretical prediction of electromagnetic fields induced inside human head has been recently extensively studied by many authors because of its importance in, for example, mobile telephones applications. Various numerical techniques are used to more or less exactly model human head, which include finite elements methods (FEM), finite-differences-time-domain (FDTD) method, transmission-line-matrix (TLM) method and the method of moments (MoM).

It must be remembered that in high frequency applications only rigorous solutions of Maxwell equations are acceptable, therefore no simple asymptotic techniques could be used.

The existing solutions could be groped into two main classes:

- 1) Homogeneous models, in which the human body is considered as consisting of one type of lossy dielectric material with medium dielectric permittivity and conductivity;
- 2) Heterogeneous models in which complex dielectric constant is the function of observation point position inside the body.

In the first attitude usually surface integral equations (SIE) are applied which are typically solved by the method of moments. Such solutions do not require a great computational power, they however give rather crude estimation of real fields inside human body.

The second attitude gives the perfect field prediction, however it requires very fast computers with big memory resources. Usually supercomputers or at least high-class workstation must be used, however even then computation times may reach several hours or even days.

In this work some kind of intermediate solution is proposed. The author makes a simplification, which assumes rotational symmetry of the human head, which is of course far from realistic model. However heterogeneous distribution of dielectric parameters is allowed, which allows for example to distinguish different tissue layers. With the use of above assumptions simple and efficient method is constructed which enable modeling of human head with extremely small number of unknown coefficients. The procedure is validated by comparisons with analytical solutions, which exist for simple shapes, like dielectric spheres or layered dielectric spheres.

Sample calculations for typical model human head are presented.

2. METHOD OF CALCULATIONS [7]

2.1. Volume Integral Equation

Let us assume, that a lossy, inhomogeneous, dielectric body with the volume V and complex dielectric constant $\hat{\epsilon}(\mathbf{r}) = \epsilon(\mathbf{r}) - j\sigma(\mathbf{r})/\omega$ where ϵ and σ are the medium permittivity and conductivity at position \mathbf{r} , is illuminated by an incident field \mathbf{E}^i , defined as the field in the absence of the body. In the presence of the body the total electric field consists of „incident” and „scattered” field:

$$\mathbf{E}(\mathbf{r}) = \mathbf{E}^i(\mathbf{r}) + \mathbf{E}^s(\mathbf{r}) \quad (1)$$

the former being excited by the polarization current \mathbf{J} ,

$$\mathbf{J}(\mathbf{r}) = j\omega[\hat{\epsilon}(\mathbf{r}) - \epsilon_0]\mathbf{E}(\mathbf{r}). \quad (2)$$

The scattered field \mathbf{E}^s is related to the polarization current \mathbf{J} through the following formulas:

$$\mathbf{E}^s(\mathbf{r}) = -j\omega \mathbf{A}(\mathbf{r}) - \nabla \Phi(\mathbf{r}) \quad (3)$$

$$\mathbf{A}(\mathbf{r}) = \frac{\mu_0}{4\pi} \int_{\Gamma} \mathbf{J}(\mathbf{r}') G(\mathbf{r}, \mathbf{r}') d\Gamma' \quad (4)$$

$$\Phi(\mathbf{r}) = \frac{1}{4\pi\epsilon_0} \int_{\Gamma} q(\mathbf{r}') G(\mathbf{r}, \mathbf{r}') d\Gamma' \quad (5)$$

where

$$G(\mathbf{r}, \mathbf{r}') = \frac{e^{-jk_0|\mathbf{r}-\mathbf{r}'|}}{|\mathbf{r}-\mathbf{r}'|} \quad (6)$$

$$k_0 = \omega/\sqrt{\epsilon_0\mu_0} = 2\pi/\lambda_0. \quad (7)$$

The charge density $q(\mathbf{r})$ is related to the polarization current in (2) by the continuity equation:

$$\nabla \cdot \mathbf{J}(\mathbf{r}) = -j\omega q(\mathbf{r}). \quad (8)$$

Equation (1) is in fact the integro-differential equation for the polarization current \mathbf{J} . However, following [3], it is convenient to take as the unknown quantity the electric flux

$$\mathbf{D} = \hat{\epsilon} \mathbf{E} \quad (9)$$

which has a continuous normal component at media interfaces and is divergenceless. This second feature will be extensively used in the construction of basis and testing functions.

We can now express \mathbf{J} in terms of \mathbf{D} :

$$\mathbf{J}(\mathbf{r}) = j\omega\kappa(\mathbf{r})\mathbf{D}(\mathbf{r}) \quad (10)$$

where we define the *contrast ratio*:

$$\kappa(\mathbf{r}) = \frac{\hat{\epsilon}(\mathbf{r}) - \epsilon_0}{\hat{\epsilon}(\mathbf{r})} \quad (11)$$

which accounts for discontinuities in the normal component of \mathbf{J} at media interfaces.

2.2. Expansion of VIE into modes

Up to this point we have made no use of the fact the body of interest has a rotational symmetry.

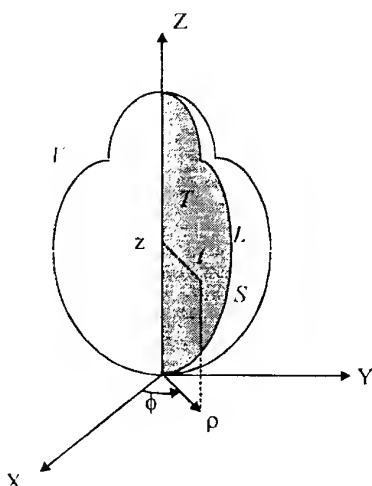


Fig. 1. Body of revolution and coordinate system.

Taking advantage of this feature, we can expand all currents, fields and scalar Green's functions in Fourier series in ϕ . Thus, we have

$$\mathbf{E}' = \sum_{m=-\infty}^{\infty} \mathbf{E}'_m(\rho, z) e^{im\phi} \quad (12)$$

$$\mathbf{J} = \sum_{m=-\infty}^{\infty} \mathbf{J}_m(\rho, z) e^{im\phi} \quad (13)$$

$$\mathbf{D} = \sum_{m=-\infty}^{\infty} \mathbf{D}_m(\rho, z) e^{im\phi} \quad (14)$$

$$G(\rho, z, \rho', z', \phi - \phi') = \frac{e^{-jk_0 R}}{R} = \frac{1}{2\pi} \sum_{m=-\infty}^{\infty} G_m(\rho, z, \rho', z') e^{im(\phi - \phi')} \quad (15)$$

$$G_m(\rho, z, \rho', z') = \int_0^{2\pi} G(\rho, z, \rho', z', \alpha) e^{-im\alpha} d\alpha \quad (16)$$

The expansion (15) follows from the fact, that $R=|\mathbf{r} - \mathbf{r}'|$ is periodic in the variable $(\phi - \phi')$.

Substituting the expansions into formulas (1) to (10) and invoking the orthogonality of azimuthal harmonics, we get

$$\mathbf{E}_m(\rho, z) = \mathbf{E}_m^i(\rho, z) + \mathbf{E}_m^s(\rho, z) \quad (17)$$

$$\mathbf{J}_m(\rho, z) = j\omega[\hat{\epsilon}(\rho, z) - \epsilon_0] \mathbf{E}_m(\rho, z) \quad (18)$$

$$\mathbf{E}_m^s(\rho, z) = -j\omega \mathbf{A}_m(\rho, z) - \nabla_m \Phi_m(\rho, z) \quad (19)$$

where

$$\mathbf{A}_m = \frac{\mu_0}{4\pi} \int_T \bar{\Gamma}_m \mathbf{J}_m \rho' d\Gamma' \quad (20)$$

$$\bar{\Gamma}_m = \begin{bmatrix} \Gamma_{\rho\rho}^m & \Gamma_{\rho z}^m & \Gamma_{\rho\phi}^m \\ \Gamma_{z\rho}^m & \Gamma_{zz}^m & \Gamma_{z\phi}^m \\ \Gamma_{\phi\rho}^m & \Gamma_{\phi z}^m & \Gamma_{\phi\phi}^m \end{bmatrix} =$$

$$\begin{bmatrix} \frac{G_{m-1} + G_{m+1}}{2} & 0 & \frac{G_{m-1} - G_{m+1}}{2j} \\ 0 & G_m & 0 \\ \frac{G_{m+1} - G_{m-1}}{2j} & 0 & \frac{G_{m-1} + G_{m+1}}{2} \end{bmatrix}. \quad (21)$$

In the above formulas vector components are taken in the (ρ, z, ϕ) order. The integration in (20) is on the transverse surface of the BOR (see Figure 1).

The scalar potential is defined as

$$\Phi_m = \frac{1}{4\pi\epsilon_0} \int_T q_m G_m \rho' d\Gamma' \quad (22)$$

where the electric charge density q_m is related to the current \mathbf{J}_m through the equation

$$q_m = -\frac{1}{j\omega} \nabla_m \cdot \mathbf{J}_m = -\frac{1}{j\omega} \left[\frac{1}{\rho'} \frac{\partial (\rho' J_m^\rho)}{\partial \rho} + \hat{z} \frac{\partial J_m^z}{\partial z} + \frac{jm}{\rho'} J_m^\phi \right] \quad (23)$$

In equation (23) we introduce the harmonic divergence. Additionally we define the harmonic gradient operator

$$\nabla_m \Phi_m = \hat{\rho} \frac{1}{\rho} \frac{\partial (\rho \Phi_m)}{\partial \rho} + \hat{z} \frac{\partial \Phi_m}{\partial z} + \hat{\phi} \frac{jm}{\rho} \Phi_m \quad (24)$$

2.3. Basis functions

As mentioned before, the electric flux has been chosen as the unknown quantity in the moment method solution. Thus, we have:

$$\mathbf{D}(\mathbf{r}) = \sum_{i=1}^N D_i \mathbf{f}_i(\mathbf{r}) \quad (25)$$

or, for the m -th mode:

$$\mathbf{D}_m(\rho, z) = \sum_{i=1}^N D_{mi} \mathbf{f}_{mi}(\rho, z). \quad (26)$$

where N is the total number of basis functions.

The main purpose in the process of basis functions development is to impose on the basis set the condition, that \mathbf{D} is divergenceless. Satisfying this condition allows to reduce the total number of unknowns.

Thus, we have:

$$\nabla_m \cdot \mathbf{f}_m = \frac{1}{\rho} \frac{\partial(\rho f_m^\rho)}{\partial \rho} + \frac{\partial f_m^z}{\partial z} + \frac{jm}{\rho} f_m^\phi = 0. \quad (27)$$

It is easy to find, that for all modes except $m=0$ we can derive the ϕ component of \mathbf{f}_m taking:

$$f_m^\phi = -\frac{\rho}{jm} \left[\frac{1}{\rho} \frac{\partial(\rho f_m^\rho)}{\partial \rho} + \frac{\partial f_m^z}{\partial z} \right]. \quad (28)$$

It means that in the process of solution of (17) we can deal only with „transverse” components. It is the desired feature of number of unknowns reduction. The zero-th mode has to be treated separately and the solution for this case will be discussed later on.

Because of space limitations the full (complicated enough) formulas describing basis functions will not presented here. We shall only state that two kinds of basis functions have been developed during this investigation, depending on the shape of surfaces they are defined on. These are basis functions on rectangles and basis functions on triangles. The “triangle” basis functions are better suited for modeling complicated shaped, but require much more computation effort, and thus computer time.

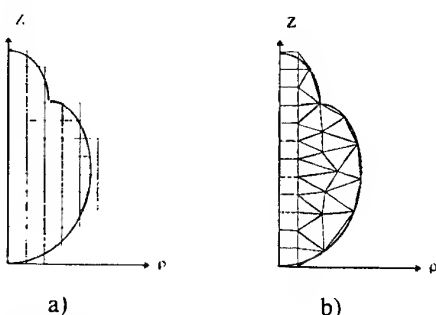


Fig. 2. Discretization of the transverse plane of the body; (a) rectangular basis functions; (b) rectangular and triangular basis functions.

2.4. Testing Procedure

In order to get unknown coefficients of the electric flux expansion equation (17) must be tested to reduce it to the set of simultaneous linear equations. In this work the Galerkin procedure has been applied, together with the scalar product defined as:

$$\langle \mathbf{f}, \mathbf{g} \rangle = \int_V \mathbf{f} \cdot \mathbf{g}^* dV \quad (29)$$

For a given mode we can perform azimuthal integration and the volume integral in (29) becomes a surface integral on “transverse” area of the body shown in Fig. 1.

The equation (17) after “testing” takes the form:

$$\begin{aligned} & \left\langle \frac{\mathbf{D}_m}{\hat{\epsilon}}, \mathbf{f}_{mj} \right\rangle + j\omega \left\langle \mathbf{A}_m, \mathbf{f}_{mj} \right\rangle + \left\langle \nabla_m \Phi_m, \mathbf{f}_{mj} \right\rangle = \\ & = \left\langle \mathbf{E}_m^i, \mathbf{f}_{mj} \right\rangle \end{aligned} \quad (30)$$

which, represents the desired matrix equation with the vector of unknown coefficients.

It is well known [4], [5], that modal Green’s function G_m has an integrable singularity. Thus, while calculating „self terms” in (30) the integrations in the immediate vicinity of singular points must be performed analytically.

2.5. Zero-th mode

The technique of basis function construction presented above cannot be used in the case of $m=0$. In this case however it can be noted that:

- 1) there is no charge associated with the azimuthal field component,
- 2) $G_{,1} = G_1$, so the $p\phi$ and ϕp components of $\bar{\Gamma}$ matrix (21) are zero.

Thus, for zero-th mode, equation (17) decouples into two independent equations concerning transverse and azimuthal field components. These equations can then be solved separately.

Solving the equation for transverse field components the author has used the same transverse field representation as in the previous subsection. However, one must remember, that basis functions constructed in this manner are no longer divergenceless. This condition must now be enforced numerically.

The equation for the azimuthal mode has very simple form, because it does not have the scalar potential term. In present work it has been solved numerically using pulse basis functions and the Galerkin testing scheme.

Note, that because of the equations decoupling, we never have to solve system of linear equation with more unknowns, than in the case of non-zero modes. It means that the main advantage of the method is in this case preserved.

3. VERIFICATION OF THE METHOD

In order to check the method described in the previous section, it has been applied to some problems, for which solutions, either analytical or numerical, obtained by other authors are available. Most of those solutions concern homogeneous or partially homogeneous bodies. In all calculations basis functions defined on rectangular domains have been used. The results presented here are repeated after [7].

As first example homogeneous dielectric sphere has been considered. Next, layered sphere has been modeled.

In both examples the incident field has been assumed to be the plane wave. This requires applying formulas for plane wave expansion into modes. Formulas for these expansions can be easily obtained from those presented for example in [4] or [5] and will be not repeated here.

Simple sphere model, with discretization similar to that of Fig. 2a, has been used to calculate the electric field inside the dielectric sphere. First, the axial incidence of the incident field has been assumed which requires performing computations only for -1 and +1 modes. Field calculations for low frequencies have shown that the electric field is within 5 percent of $3/(\epsilon_r + 2)$ times the incident field, which is the theoretical value.

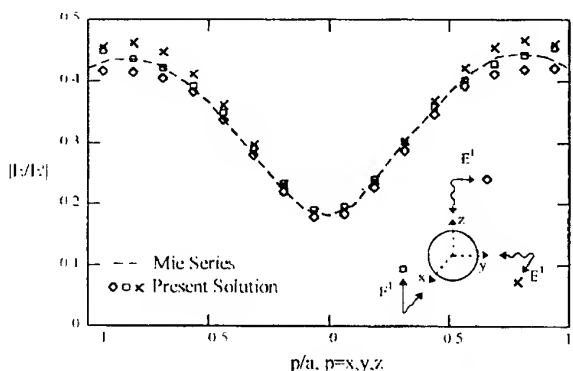


Fig. 3. Field along axis of incidence inside dielectric sphere; $\epsilon_r = 36$, $k_0a = 0.408$.

At higher frequencies the typical standing wave behavior has been observed. In Fig. 3 the comparison of results with analytical solution [3] is presented for the sphere with $ka=0.408$. One can see that the agreement is excellent. In order to verify procedures for zero-th mode and more sophisticated modal expansions, the same calculations for different angles of incidence and polarizations have been performed. Again very good agreement has been obtained which validates all procedures described in the previous section.

Field distributions for the layered sphere are presented in Fig. 4. The calculations have been done for two grids.

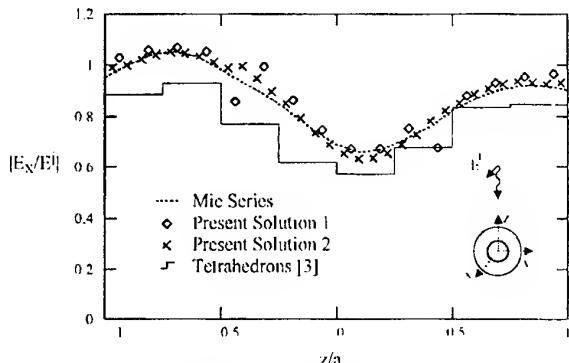


Fig. 4. Fields inside inhomogeneous sphere: $\epsilon_{r1} = 36$, $k_0a_1 = 0.3738$, $\epsilon_{r2} = 9$, $k_0a_2 = 0.8168$.

The solution 1 and 2 denote 8 and 16 squares per sphere radius, respectively. The solution 1 gives some error in the vicinity of the boundary of materials. It is because of non-precise model of the inner sphere. Solution 2 gives a very good field prediction. It proves improvement of accuracy when the investigated body is modeled using smaller volume elements.

Finally, some calculations of resonant frequencies of dielectric spheres and cylinders have been performed and compared to analytical and numerical results given by Barber, Owen and Chang [6]. In all cases resonant frequencies predicted with the present method were within 0.5 percent from those of Barber et al.

For more examples showing good numerical properties of the method the reader is referred to [7].

4. MODEL OF THE HUMAN HEAD

To illustrate applying the method to the point of interest it has been used to calculate the electric field inside simple human head model presented in Fig. 5. Step discontinuities of particular borders result from the simple rectangular basis functions used in this case.

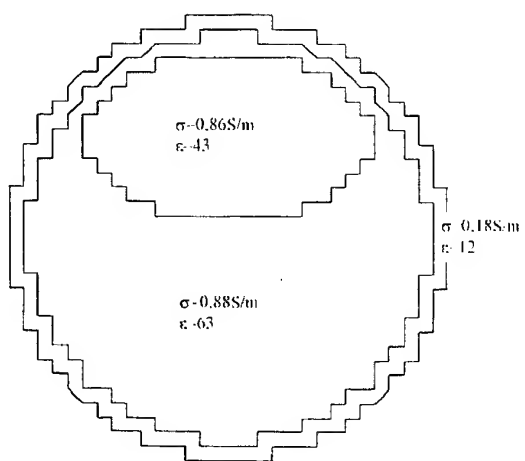


Fig. 5. Simplified model of the human head

Calculated field distribution inside the head model is presented in Fig. 6. In the example the object is illuminated by a plane wave with unit amplitude and frequency 450 MHz (from the right side of the picture).

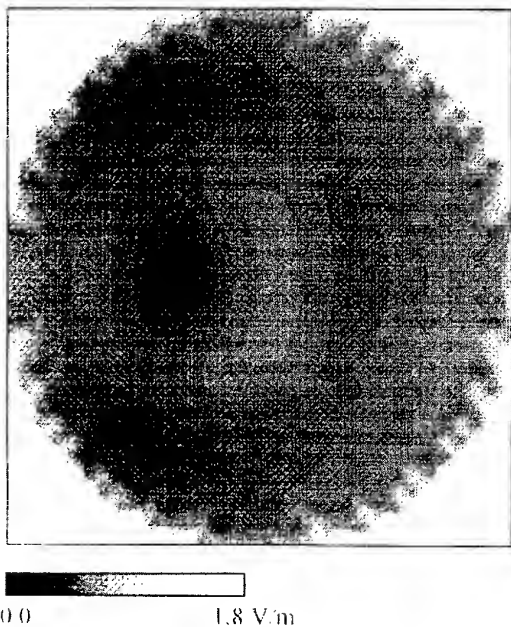


Fig. 6. Computed field distribution inside the human head model

5. CONCLUSIONS

In the paper a method of calculating fields inside human head has been presented. The key element of the method is the assumption about rotational symmetry of the object of interest which enables applying a convenient mode-by-mode solution scheme.

In the paper only plane wave excitation was used however other forms of excitation are also possible. Of particular interest are methods which enable modeling coupling of BOR geometries to non-BOR ones.

Next step in the investigation could also concern applying iterative solution scheme (like Conjugate Gradient Method) in which there would be no necessity of storing large interaction matrices.

6. REFERENCES

- 6.1. J.R. Mautz and R.F. Harrington, "Electromagnetic scattering from a homogeneous material body of

revolution," *Arch. Elec. Übertragung.*, vol. 33, pp. 71-80, Feb. 1979.

- 6.2. A.W. Glisson and D.R. Wilton, "Simple and efficient numerical methods for problems of electromagnetic radiation and scattering from surfaces," *IEEE Trans. Antennas Propagat.*, vol. AP-28, pp. 593-603, Sept. 1980.
- 6.3. D.H. Schaubert, D.R. Wilton, and A.W. Glisson, "A tetrahedral modeling method for electromagnetic scattering by arbitrarily shaped inhomogeneous dielectric bodies," *IEEE Trans. Antennas Propagat.*, vol. AP-32, pp. 77-85, Jan. 1984.
- 6.4. M.G. Andreasen, "Scattering from bodies of revolution," *IEEE Trans. Antennas Propagat.*, vol. AP-13, pp. 303-310, Mar. 1965.
- 6.5. J.R. Mautz and R.F. Harrington, "Radiation and scattering from bodies of revolution," *Appl. Sci. Res.*, vol. 20, pp. 405-435, June 1969.
- 6.6. P.W. Barber, J.F. Owen, and R.K. Chang, "Resonant scattering for characterization of axisymmetric dielectric objects," *IEEE Trans. Antennas Propagat.*, vol. AP-30, pp. 168-172, Mar. 1982.
- 6.7. A.A. Kucharski, "A Method of Moments Solution for Electromagnetic Scattering by Inhomogeneous Dielectric Bodies of Revolution", submitted for publication in *IEEE Trans. Antennas Propagat.*

BIOGRAPHICAL NOTE



Andrzej A. Kucharski received M.Sc. and Ph. D. degrees from Wrocław University of Technology in 1988 and 1994, respectively. Since 1993 he is with the Radio Department, Institute of Telecommunications and Acoustics, Wrocław University of Technology where he is currently an Assistant Professor. His research interests are primarily in computational electromagnetics, antennas and propagation and electromagnetic compatibility.

PREDICTION AND ANALYSIS OF OUT-OF-BAND OSCILLATIONS SPECTRUM OF POWER MW-DEVICES IN THE PULSE WORKING MODE

V.P.Kudryashov, B.K.Sivyakov, I.B.Yakovleva.
Saratov State Technical University, Politehnicheskaya, 77
Phone: (845-2)257-744. Fax: (845-2)506-740.
E-mail: siv@star.sstu.runnet.ru
410054 Saratov-54, Russia

The methods of prediction and the theoretical and experimental investigation results of out-of-band oscillation spectra of power vacuum MW-devices such as TWT and klystron in the pulse working mode are considered. The description of amplitude- and phase-modulated pulse signals spectrum analysis program making possible high-speed calculation of tens and hundreds of thousands of spectral components is given. The presentation of analytical technique of plotting the limitation spectrum line is offered.

I. INTRODUCTION

Power vacuum MW-devices such as TWT and klystron are widely used in radiolocation, in transmitting communication systems and electronic countermeasures equipment, etc. The pulse working mode with modulating pulses applied between the device cathode and anode (the interaction space) is typical for them. For all that a strong phase modulation, caused by the electron flow velocity variations, accompanies the amplitude modulation of the carrier frequency. On account of this out-of-band oscillations spectrum is more complex than in case of a pure amplitude modulation. The spectrum asymmetry, its envelope overshoots and fluctuations that have a great influence on the electromagnetic compatibility of the transmitting devices are experimentally observed.

The numerical spectrum analysis of MW-devices pulse signals technique for prediction of out-of-band oscillations spectrum is worked out. It allows with small consumption of machine time to calculate tens and hundreds of thousands of spectral components with the levels up to -100 dB and to determine the spectrum envelope.

The developed spectrum analysis technique is realized in the IBM PC program SPECTR, included in the problem-orientated package SIGNAL [1] of applied

programs for computer simulating of TWT and klystron spectral and information characteristics and parameters.

With the help of the program SPECTR the numerical analysis of the influence of the carrier amplitude and phase modulation at the pulse front, top and droop on the out-of-band oscillations spectrum up to the level -100 dB has been carried out.

The analytical method of envelope calculation and plotting a limitation spectrum line has been developed. It can be used for estimating engineering out-of-band oscillations spectrum calculations of MW-devices with spurious phase modulation of the carrier frequency.

2. SPECTRUM ANALYSIS OF AMPLITUDE- AND PHASE-MODULATED PULSE SIGNALS TECHNIQUE

Amplitude- and phase-modulated microwave signal can be presented in the form of:

$$a(t) = A(t) \cos[\omega_0 t + \Phi(t)] = \operatorname{Re} A(t) e^{j\Phi(t)} e^{j\omega_0 t}, \quad (1)$$

where $A(t)$ and $\Phi(t)$ are amplitude and phase of the carrier oscillation with frequency ω_0 .

If $A(t)$ and $\Phi(t)$ are periodic functions with repetition frequency of modulating signal Ω then the functions may be expanded in a Fourier series:

$$A(t) e^{j\Phi(t)} = \sum_{n=-\infty}^{\infty} A_n e^{jn\Omega t}, \quad (2)$$

where

$$A_n = \frac{1}{2\pi} \int_0^{2\pi} A(t) e^{j\Phi(t)} e^{-jn\Omega t} d(\Omega t) \quad (3)$$

is a complex amplitude.

Substitution (2) into (1) gives the following form of a :

$$\begin{aligned} a(t) &= \operatorname{Re} \sum_{n=-\infty}^{\infty} |A_n| e^{j\varphi_n} e^{j(\omega_0+n\Omega)t} = \\ &= \sum_{n=-\infty}^{\infty} |A_n| \cos [(\omega_0+n\Omega)t + \varphi_n], \quad (4) \end{aligned}$$

where $|A_n|$, φ_n - are absolute value and phase of spectral harmonic.

Hence, the expression (4) determines radio signal spectrum with the given amplitude $A(t)$ and phase $\Phi(t)$ periodic modulation functions.

Accurate and high-speed method of evaluating the integral (3) is needed as the oscillations spectrum analysis often requires a large number of high orders modulation harmonics with small amplitudes determination. Filon's method [2] meets to all above requirements with greater degree among well-known methods of spectrum analysis. The method is one of the variety of Simpson's method, which allows to evaluate integrals of the following types:

$$\int_a^b f(t) \cos(kt) dt \quad \text{and} \quad \int_a^b f(t) \sin(kt) dt. \quad (5)$$

The interval $[a,b]$ is divided up into even numbers of subintervals $2N$. Function $f(t)$ is approximated by the second order polynomial in every double subinterval similar to Simpson's method. After that integrals (5) are evaluated analytically.

Standard working formulas for Filon's method are presented in [2]:

$$\begin{aligned} \int_a^b \frac{f(t) \cos kt}{\sin kt} dt &= h \left\{ \pm \alpha \left[f(b) \frac{\sin kb}{\cos kb} - f(a) \frac{\sin ka}{\cos ka} \right] + \right. \\ &\quad \left. + \beta \frac{C_{2n}}{S_{2n}} + \gamma \frac{C_{2n-1}}{S_{2n-1}} \right\}, \end{aligned}$$

where

$$\alpha = \frac{\theta^2 + \theta \sin \theta \cos \theta - 2 \sin^2 \theta}{\theta^3};$$

$$\beta = \frac{2[\theta(1 + \cos^2 \theta) - 2 \sin \theta \cos \theta]}{\theta^3};$$

$$\gamma = \frac{4(\sin \theta - \theta \cos \theta)}{\theta^3}; \quad \theta = kh; \quad h = \frac{b-a}{2N};$$

$$\begin{aligned} C_{2n} &= \frac{1}{2} f(a) \frac{\cos}{\sin} ka + f(a+2h) \frac{\cos}{\sin} k(a+2h) + \\ &\quad + f(a+4h) \frac{\cos}{\sin} k(a+4h) + \dots + f(b) \frac{\cos}{\sin} kb; \end{aligned}$$

$$\begin{aligned} S_{2n-1} &= f(a+h) \frac{\cos}{\sin} k(a+h) + f(a+3h) \frac{\cos}{\sin} k(a+3h) + \\ &\quad + f(b-h) \frac{\cos}{\sin} k(b-h). \end{aligned}$$

To apply Filon's method integral (3) is transformed to the following form:

$$\begin{aligned} \operatorname{Re} A_n &= \frac{1}{2\pi} \int_0^{2\pi} A(t) \cos \Phi(t) \cos n\Omega t d(\Omega t) + \\ &\quad + \frac{1}{2\pi} \int_0^{2\pi} A(t) \sin \Phi(t) \sin n\Omega t d(\Omega t); \end{aligned}$$

$$\begin{aligned} \operatorname{Im} A_n &= \frac{1}{2\pi} \int_0^{2\pi} A(t) \sin \Phi(t) \cos n\Omega t d(\Omega t) - \\ &\quad - \frac{1}{2\pi} \int_0^{2\pi} A(t) \cos \Phi(t) \sin n\Omega t d(\Omega t). \end{aligned}$$

The received integrals are evaluated according to standard working formulas for Filon's method. Then amplitude and phase of spectral harmonics are determined

$$|A_n| = \sqrt{(\operatorname{Re} A_n)^2 + (\operatorname{Im} A_n)^2} \quad \varphi_n = \arctg \frac{\operatorname{Im} A_n}{\operatorname{Re} A_n}.$$

As integrals are evaluated analytically, the error of spectrum calculation according to technique is determined only by the accuracy of second order polynomial amplitude and phase modulation functions approximation on the double subinterval. The needed accuracy is obtained by choosing the subintervals number.

3. PACKAGE OF APPLIED PROGRAMS SPECTR

The described technique of spectrum analysis is realized in a package of programs SPECTR.

The user may calculate spectrum or the spectrum envelope of microwave signal.

The calculation may be carried out by given pulse MW-signal amplitude and phase envelopes or by given device modulation characteristics, the modulating pulse form and input signal amplitude and phase envelopes.

While preparing the calculation task the user separates the characteristic time intervals corresponding to the front, top, its oscillations, droop and other signal peculiarities from the MW-signal envelopes or the modulating pulse form. The number and time coordinates of such intervals are specified in program. Every characteristic interval in the turn is divided up into even numbers of subintervals.

MW-signal amplitude and phase envelopes or the modulating pulse form and the input signal envelopes are determined by their values in the interpolation nodes.

Amplitude and phase modulation device characteristics are tabulated for given values of input signal amplitude.

During simulation of the device modulation phenomena the output MW signal envelopes are formed as the result of input signal envelopes and modulating pulse function transformation at the modulation characteristics set. The linear interpolation is used for determining intermediate values of output signal amplitude and phase that don't coincide with the table nodes.

Depending on the program task the following results may be received:

- amplitude and phase of the harmonic spectrum components from zero, corresponding the carrier frequency, till maximum (positive or negative) components with a given interval, determined by harmonic numbers;
- spectrum envelope determined by maximum harmonic amplitude in the group (the number of harmonics in group is determined by user).

The program may be used also to find amplitude and phase envelopes of output microwave signal and its spectrum by given amplitude and phase characteristics of amplifier and input signal amplitude envelope which are given correspondingly instead of amplitude and phase modulation characteristics and modulating pulse function.

4. ANALYSIS OF PULSE FRONT, DROOP AND TOP PHASE MODULATION INFLUENCE UPON THE OUT-OF-BAND OSCILLATIONS SPECTRUM

The rigorous numerical analysis of pulse front, top and droop modulation processes influence is carried out by program SPECTR. The variations of the carrier oscillation phase at the pulse front and droop to the value of approximately 1000 degrees, accepted in the calculations, are typical for TWT with anode modulation and agree with experimental data.

Fig.1 presents spectrum envelopes of out-of-band oscillations for rectangular pulse and trapezoidal pulses with linear pulse front and droop amplitude and phase modulation. The rectangular pulse spectrum envelope rolls off linearly with the velocity -20 dB/dec. The trapezoidal pulse spectrum envelope has two characteristic side maxima. The maximum in the positive tuning frequency region is caused by modulation processes on the pulse front and in the negative tuning region - on its droop.

Thus it is ascertained that modulation processes at the trapezoidal pulse front and droop cause a noticeable boosting of spectra envelope in the side maxima region above the rectangular pulse spectrum envelope.

Symmetric change in pulse front and droop durations causes symmetric spectrum envelope change.

The calculation showed that the spectrum envelope is not noticeably influenced by pulse top phase change and by the appearance of characteristic overmodulation pulse top distortions.

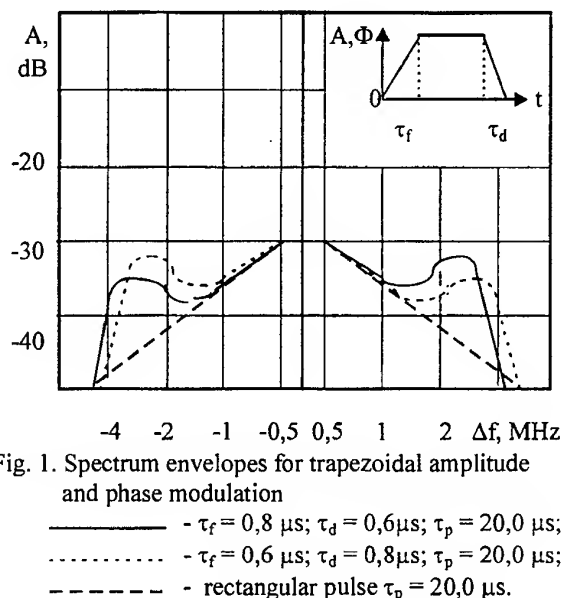


Fig. 1. Spectrum envelopes for trapezoidal amplitude and phase modulation

— $\tau_f = 0.8 \mu s; \tau_d = 0.6 \mu s; \tau_p = 20.0 \mu s$
 - - - $\tau_f = 0.6 \mu s; \tau_d = 0.8 \mu s; \tau_p = 20.0 \mu s$
 - - - - rectangular pulse $\tau_p = 20.0 \mu s$

Fig. 2 presents calculation spectrum envelope of power TWT out-of-band oscillations. Experimental amplitude and phase modulation device characteristics and output radio pulse amplitude envelope were the initial data for determination of radio pulse phase modulation and further calculations. Good agreement of calculation results and experimental data received by means of spectrumanalyser is observed. Calculations were carried out up to the level -100dB, every tenth of 120000 spectral components was determined. The spectrum envelope was built by the maxima of components in the group of 24.

5. TECHNIQUE OF PLOTTING THE LIMITATION SPECTRUM LINE

The offered technique is used for pulse signal front and droop phase changes more than 2 rad (115°).

The initial data:

τ_p - pulse duration;

τ_f, τ_d - pulse front and droop durations;

U_{min} - minimum value of modulating parameter corresponding to the output signal amplitude of $0.1 A_m$, where A_m is maximum output signal value;

$\delta\phi_{mean} = (\delta\phi_{max} + \delta\phi_{min})/2$ - mean value of MW device relative phase sensitivity (rad/%) in the range of modulating parameter variations from U_{min} till U_{max} .

Calculating relations:

1. The horizontal section.

$$A_0 = 0 \text{ dB}; \pm \Delta f_A = 1/\pi\tau_p.$$

2. The first sloping section.

The coordinates of its final points:

$$A_{f,d} = 20 \lg (\tau_{f,d} / \tau_p) \text{ dB}; \Delta f_{f,d} = \Delta\Phi / 2\pi\tau_{f,d}$$

where

$$\Delta\Phi = 2.3 \cdot 10^2 \delta\varphi_{mid} \lg (U_{max} / U_{min})$$

3. The second sloping section.

The limitation line is drawn from the point with coordinates $\Delta f_{f,d}, A_{f,d}$ with a slope of -40 dB/dec.

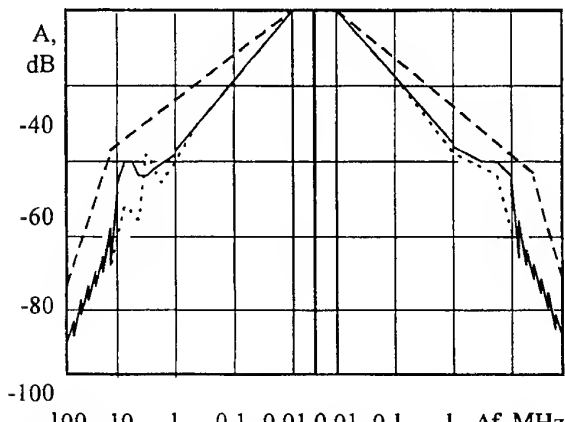


Fig. 2. Radio pulse spectrum envelopes of power TWT
 ——— — calculation; - - - - - - experiment;
 - - - - - limitation line.

The offered technique of plotting a limitation line is simple and doesn't need in computer calculations. For all that it represents the main mechanisms of out-of-band oscillations spectrum formation and involves sufficiently simply measured device and pulse parameters.

Fig.2 presents the limitation spectrum line plotted according to the given technique. It describes well the

peculiarities of the envelope caused by the presence of phase modulation at the pulse front and droop.

6. CONCLUSION

The developed package of applied programs SPECTR and analytical technique of plotting the limitation spectrum line allow to solve efficiently problems of analysis and prediction of out-of-band oscillations spectrum of power MW-devices with linear electron flow in the pulse working mode.

7. REFERENCES

1. B.K.Sivyakov, I.B.Yakovleva, D.A. Yakimov "Integrated package of programs for simulating of TWT and klystron spectral and information characteristics"(rus), Proceedings of the International Conference on Actual Problems of Electron Devices Engineering, Saratov, Russia, Sept.10-12, 1996, pp.16-17.
2. R.W. Hamming "Numerical Methods for Scientists and Engineers"(rus), Nauka, Moscow,1972, pp.400.

BIOGRAPHICAL NOTES

Kudryashov Valeri Pavlovich, Dr.T.Sc, Deputy Director of Vacuum Devices Department of State Scientific Industrial Enterprise "Almaz", Saratov. Specialist in the field of power MW-devices.

Sivyakov Boris Konstantinovich, Professor, Dr.T.Sc., professor of the chair of electronic devices and instruments of Saratov State Technical University. Since 1973 has been specializing in the field of numerical simulation of MW electronics.

Yakovleva Irina Borisovna, Docent, Cd.T.Sc., docent of the chair of electronic devices and instruments of Saratov State Technical University. Since 1973 has been working in the field of MW devices.

FINITE-ELEMENT METHOD APPLIED IN DESIGN OF ABSORBERS

Mihaela Lascu

"Politehnica" University Timișoara

Faculty of Electronics and Telecommunications
Measurement and Optical Electronics Department
Bv. Vasile Pârvan Nr.2, RO-1900 Timișoara, Romania
Tel: 0040-56-204332 or 0040-56-190608

Fax: 0040-56-190608

Email: mihaela@ee.ut.ac.ro

This paper will develop the formula for the reflection coefficient ρ from multilayered media in order to use it in case studies about absorbers, such as those used in electromagnetically anechoic rooms.

The Finite Element Method (FEM) will be applied upon a hypothetical, planar, multilayered absorber made from 50 layers of non magnetic material ($\mu_r=1$).

The main use of large wideband absorbers is in the building of electromagnetically anechoic and screened rooms for experimental purposes.

1. INTRODUCTION

In order to make materials which absorb electromagnetic radiation and not just reflect it back into the environment, they must be lossy so that the energy in the wave can be dissipated within the material. One way out to solve this problem is to compromise and make layered materials which have variable properties, such that their surface impedance is as close as possible to the incident wave impedance, but then change their intrinsic impedance inside by gradually increasing their conductivity, keeping the reflection coefficient at the boundary of each layer as low as possible but allowing Joule heating to dissipate progressively the energy in the wave.

The paper will examine an idealised model of a layered absorber, with a view to understanding how to do the necessary calculations, and get a feeling for such parameters as their thickness and effectiveness.

The Finite Element Method (FEM) will be applied upon a hypothetical, planar, multilayered absorber made from 50 layers of non magnetic material ($\mu_r=1$).

Some important factors that have to be obeyed in practical and simulation design are:

- any successful absorber has a thickness of order of one wavelength;
- scattering from a surface depends not only on its absorbing properties but also on its shape;

- the skin depth plays an important role in describing the distance waves penetrate into conductors;

- absorbers are often mounted on the walls of screened rooms which have metal walls; if this is the case the conductivity of the layers adjacent to the walls should be high to obtain better impedance matching at that boundary and not contribute unnecessarily to any reflection.

In the following it is of great interest to find the reflection coefficient and the total thickness of the absorber. Once the electrical properties are chosen, using the computer model, that means the FEM-model of the absorber it is possible to determine the propagation constant for each layer and the wave impedance at each boundary.

The study will be then extended to see how the performance of absorbers is changing at different frequencies. It is clearly of great practical importance to know how a given absorber, with its parameters fixed, performs at different frequencies.

2. THE REFLECTION COEFFICIENT FROM MULTI-LAYERED MEDIA

In this section we determine the formula for the reflection coefficient ρ from multilayered media in order to use it in case studies about absorbers, such as those used in electromagnetically anechoic rooms.

Consider a planar, multi-layered, structure consisting of layers numbered 1 to k , each with thickness

d_i , different conductivities σ_i , permittivities ϵ_i , and permeabilities μ_i as shown in Fig.1. Each layer has different intrinsic impedances $Z_i(\omega)$ and propagation constants $\gamma_i(\omega)$. Layer k is taken to be semi-infinite. A TEM wave with wave impedance Z_0 travelling in the $+x$ direction is incident on the layer 1. The reflection coefficient is:

$$\rho = \frac{Z_{w1} - Z_0}{Z_{w1} + Z_0} \quad (1)$$

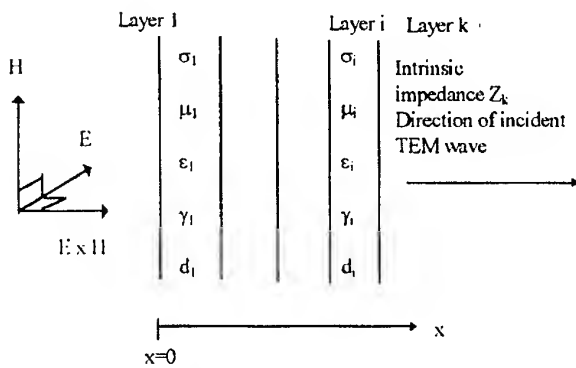


Fig. 1. A multi-layer medium where the electrical properties and thickness of each layer i is different. The final layer, layer k , is assumed to be semi-infinite. A free-space TEM wave is incident onto the surface of layer 1 at $x=0$.

where Z_{w1} is the wave impedance at the first boundary, which from [2] is just

$$Z_{w1} = Z_1 \frac{\{Z_{w2} + Z_1 \tanh(\gamma_1(\omega)d_1)\}}{\{Z_1 + Z_{w2} \tanh(\gamma_1(\omega)d_1)\}} \quad (2)$$

where Z_{w2} is the wave impedance at the second boundary,

$$Z_{w2} = Z_2 \frac{\{Z_{w3} + Z_2 \tanh(\gamma_2(\omega)d_2)\}}{\{Z_2 + Z_{w3} \tanh(\gamma_2(\omega)d_2)\}} \quad (3)$$

where Z_{w3} is the wave impedance at the third boundary.

$$Z_{w3} = Z_3 \frac{\{Z_{w4} + Z_3 \tanh(\gamma_3(\omega)d_3)\}}{\{Z_3 + Z_{w4} \tanh(\gamma_3(\omega)d_3)\}} \quad (4)$$

and so on up to the last but one layer, layer $k-1$,

$$Z_{wk-1} = Z_{k-1} \frac{\{Z_k + Z_{k-1} \tanh(\gamma_{k-1}(\omega)d_{k-1})\}}{\{Z_{k-1} + Z_k \tanh(\gamma_{k-1}(\omega)d_{k-1})\}} \quad (5)$$

where in this final term Z_k is the intrinsic impedance of the last layer.

To calculate ρ one proceeds as follows:

- assign values of σ , ϵ , μ and thickness d to each layer;
- choose a value for ω and the wave impedance Z_0 of the incident wave;
- calculate the propagation constant γ_i and intrinsic impedance Z_i for each layer at this frequency;
- begin working backwards for finding first the wave impedance of the last but one layer $k-1$, then use this impedance for finding the impedance for layer $k-2$, and so on until we find the impedance for layer 1;
- calculate ρ .

3. DESIGN OF ABSORBERS

3.1. Some factors in absorber design

In any practical absorber a large number of factors are important, but in order to examine the general properties it is worth bearing the following points in mind.

- It is a general principle in physics that waves are unaffected by structures considerably smaller than a wavelength. This means that any successful absorber is likely to have a thickness of order of one wavelength.
- The skin depth plays an important role in describing the distance waves penetrate into conductors. After 1 skin depth the wave amplitude which has survived is $E_0 e^{-1}$.
- Dielectric materials have intrinsic impedances $= \frac{Z_0}{\sqrt{\epsilon_r}}$. As most dielectrics have $\epsilon_r \geq 2$ this makes it difficult to have an impedance big enough to Z_0 . The effective dielectric constant may be layered to $\epsilon_r \approx 1$ by having a foam of material with low average density, but low mechanical strength.
- Absorbers are often mounted on the walls of screened rooms which have metal walls. If this is the case the conductivity of the layers adjacent to the walls should be high to obtain better impedance matching at that boundary and not contribute unnecessarily to any reflection.

3.2. A hypothetical absorber

For the problem under test, we shall consider the following model of a hypothetical, spherically, multilayered absorber made from 45 to 50 layers of non magnetic ($\mu_r=1$) with the following properties:

- ϵ_r varies from 1.5 in layer 1 to 2.56 in the last one.
- The conductivity of the layers varies from $\sigma \approx 0$ in layer 1 to $\sigma \approx 5.8 \times 10^5 \text{ S m}^{-1}$ in the last one.
- The thickness d_k of each layer is made equal to 2 'skin depths' [2], where the skin depth is calculated at a frequency of 1 GHz.

Using this recipe, it is of interest to find the reflection coefficient and the total thickness of the absorber. This question can best be answered by building a computer model of the absorber. In such a computer model the conductivity and dielectric constant of layer k could be parametrised by the formulae:

$$\sigma_k = 5.8 \times 10^5 \left(\frac{k}{k_{max}} \right)^5 \quad (6)$$

and

$$\epsilon_k = 1.5 + 1.06 \log_{10}(k) / \log_{10}(k_{max}) \quad (7)$$

so in the last layer where $k=k_{max}$, $\sigma=5.8 \times 10^5 \text{ S m}^{-1}$.

4. FEM APPLIED TO MODELING ABSORBERS

In the finite-element approach, an electromagnetic problem is solved by dividing the studied region into a set of arbitrary shapes, known as finite elements, and finding an approximate solution for each of the subregions that satisfies the governing equations of the problem. The most common shape used for two-dimensional problems is a triangle [1]. The electrostatic field distribution can be obtained from the scalar potential $\phi(x, y)$ satisfying the Laplacian equation:

$$\frac{\partial^2 \phi(x, y)}{\partial x^2} + \frac{\partial^2 \phi(x, y)}{\partial y^2} = 0 \quad (8)$$

with associated Dirichlet and Neumann boundary conditions. The problem has an inhomogeneous domain where the permittivity is a function of position. The Dirichlet boundary condition is the voltage on each pyramid shaped absorber [2]. In practice the absorbers are pyramid shaped, with variable conductivity throughout, and have a size which depends on the longest wavelength that is required to be absorbed. The hypothetical absorber has a spherically layered structure, which approximates better the pyramid shaped absorber, than a hypothetical, planar, multi-layered absorber.

Three reasons for choosing these shapes are:

- specular reflection from the side of an absorber will direct the reflected component further into the absorbing structure rather than back into the environment;
- there is more surface area available;
- in the vicinity of the sharp point, averaged over the whole wavefront the impedance will be almost the same as the incident wave.

The potential distribution is obtained by solving the partial differential equation given in (8) with the above Dirichlet boundary condition. This can be done if an appropriate functional proportional to the energy of the system per unit length is associated to (8), the Euler equation of the functional [3]. The appropriate functional, proportional to the energy, to be minimized in this situation is

$$F(\phi) = \frac{1}{2} \int_D \epsilon(x, y) \|\nabla \phi(x, y)\|^2 dx dy \quad (9)$$

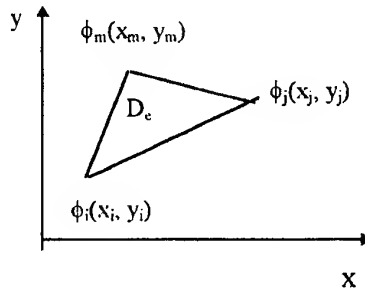
where the finite-element region D includes the dielectric substrate. Because FEM discretizes the solution domain with finite elements, it requires a finite domain. The selection of an external boundary B far away from the absorber, in our case the spherically multilayered absorber, with a zero potential will truncate the domain and is a relatively simple solution to implement. Another alternative is to use an appropriate absorbing boundary condition [3]. The infinite region above the board is truncated by the artificial Dirichlet boundary B characterized by $\phi=0$.

After the solution region D is divided into finite elements, the potential distribution $\phi(x, y)$ is approximated by linear combinations of local

interpolation polynomials. A typical triangular element is shown in Fig.2. The finite element is characterized by the

node potentials ϕ_i, ϕ_j, ϕ_m and node coordinates (x_i, y_i) ,

Fig.2. Typical triangular element



$(x_j, y_j), (x_m, y_m)$. The potential distribution is defined within each triangle and varies over the finite element as a function of position. The trial function, written in terms of the node potentials and the local interpolation polynomials is given by

$$\phi_e(x, y) = \phi_i \alpha_i(x, y) + \phi_j \alpha_j(x, y) + \phi_m \alpha_m(x, y). \quad (10)$$

For a first-order approximation, the interpolatory polynomials $\alpha_i, \alpha_j, \alpha_m$ known as shape functions, are related to the node coordinates and are given by

$$\alpha_i(x, y) = \frac{1}{2A} \left\{ (x_j y_m - x_m y_j) + (y_j - y_m)x + (x_m - x_j)y \right\} \quad (11)$$

$$\alpha_j(x, y) = \frac{1}{2A} \left\{ (x_m y_i - x_i y_m) + (y_m - y_i)x + (x_i - x_m)y \right\} \quad (12)$$

$$\alpha_m(x, y) = \frac{1}{2A} \left\{ (x_i y_j - x_j y_i) + (y_i - y_j)x + (x_j - x_i)y \right\} \quad (13)$$

where A denotes the area of the triangle when the i, j, m nodes are numbered in the counterclockwise sense and the negative of the area when numbered in the clockwise sense. In both cases, A is given by

$$A = \frac{(x_j y_m - x_m y_j + x_m y_i - x_i y_m + x_i y_j - x_j y_i)}{2} \quad (14)$$

The above trial functions are calculated for each triangle and replaced into the functional, which becomes a function of node potentials. The contribution from the functional integral over the domain of a single triangle with nodes (i, j, m) and $\epsilon=1$ to the total functional can be written as

$$F_e = \int_{D_e} \left\{ \left(\frac{\partial \phi_e}{\partial x} \right)^2 + \left(\frac{\partial \phi_e}{\partial y} \right)^2 \right\} dx dy \quad (15)$$

where D_e represents the domain (area) of a single triangle; and F_e is the functional evaluated for a single triangle. The constant factor of $\frac{1}{2A}$, appearing in (9) has been dropped as the final system of equations is obtained by minimizing the functional and this constant can be simplified. To obtain the values for the node potentials ϕ_i , ϕ_j , ϕ_m and equated to zero to find the optimum. The differentiation with respect to the node potential ϕ_i is given by

$$\begin{aligned} \frac{\partial F_e}{\partial \phi_i} &= 2 \int_{D_e} \left\{ \frac{\partial \phi_e}{\partial x} \frac{\partial}{\partial \phi_i} \left(\frac{\partial \phi_e}{\partial x} \right) + \frac{\partial \phi_e}{\partial y} \frac{\partial}{\partial \phi_i} \left(\frac{\partial \phi_e}{\partial y} \right) \right\} dx dy \\ &= 2 \int_{D_e} \left\{ \frac{\partial^2 \phi_e}{\partial x^2} \left(\frac{\partial \phi_e}{\partial \phi_i} \right) + \frac{\partial^2 \phi_e}{\partial y^2} \left(\frac{\partial \phi_e}{\partial \phi_i} \right) \right\} dx dy = 0 \end{aligned} \quad (16)$$

The first term in the integral can be evaluated as follows:

$$\frac{\partial \phi_e}{\partial \phi_i} = \alpha, \quad (17)$$

so that

$$\frac{\partial}{\partial x} \left(\frac{\partial \phi_e}{\partial \phi_i} \right) = \frac{\partial \alpha}{\partial x} \quad (18)$$

and

$$\frac{\partial \phi_e}{\partial x} = \phi_i \frac{\partial \alpha_i}{\partial x} + \phi_j \frac{\partial \alpha_j}{\partial x} + \phi_m \frac{\partial \alpha_m}{\partial x}. \quad (19)$$

Repeating the above operations for the second term in (16) and then assembling the results, we get

$$\begin{aligned} \frac{\partial F_e}{\partial \phi_i} &= 2 \int_{D_e} \left\{ \left[\left(\frac{\partial \alpha_i}{\partial x} \right)^2 + \left(\frac{\partial \alpha_i}{\partial y} \right)^2 \right] \phi_i \right. \\ &\quad + \left[\frac{\partial \alpha_i}{\partial x} \frac{\partial \alpha_j}{\partial x} + \frac{\partial \alpha_i}{\partial y} \frac{\partial \alpha_j}{\partial y} \right] \phi_j \\ &\quad \left. + \left[\frac{\partial \alpha_i}{\partial x} \frac{\partial \alpha_m}{\partial x} + \frac{\partial \alpha_i}{\partial y} \frac{\partial \alpha_m}{\partial y} \right] \phi_m \right\} dx dy \end{aligned} \quad (20)$$

The derivatives of the interpolatory functions can be obtained from (11)-(13) and for α_i , they reduce to

$$\frac{\partial \alpha_i}{\partial x} = \frac{y_j - y_m}{2A}, \quad \frac{\partial \alpha_i}{\partial y} = \frac{x_m - x_j}{2A}. \quad (21)$$

Because of the simple form of the first-order interpolation functions and the fact that the integral

$$\int_{D_e} dx dy = A, \quad (20) \text{ becomes}$$

$$\begin{aligned} \frac{\partial F_e}{\partial \phi_i} &= \frac{1}{2A} \left[\left[(y_j - y_m)^2 + (x_j - x_m)^2 \right] \phi_i \right. \\ &\quad - \left[(y_i - y_m)(y_j - y_m) + (x_i - x_m)(x_j - x_m) \right] \phi_j \\ &\quad \left. + \left[(y_i - y_j)(y_m - y_j) + (x_i - x_j)(x_m - x_j) \right] \phi_m \right] \end{aligned} \quad (22)$$

The same procedure can be followed to derive the expressions for $\frac{\partial F_e}{\partial \phi_j}$ and $\frac{\partial F_e}{\partial \phi_m}$. If the equations for the three derivatives are assembled in matrix form, the single-element contribution to the total system of linear equations minimizing the functional F is given by

$$2[S][\phi] = 2 \begin{bmatrix} S_{ii} & S_{ij} & S_{im} \\ S_{ji} & S_{jj} & S_{jm} \\ S_{mi} & S_{mj} & S_{mm} \end{bmatrix} \begin{bmatrix} \phi_i \\ \phi_j \\ \phi_m \end{bmatrix} \quad (23)$$

where the entries S_{ii} and S_{jj} are given by

$$S_{ii} = A \left[(y_j - y_m)^2 + (x_j - x_m)^2 \right] \quad (24)$$

$$S_{jj} = A \left[(y_i - y_m)(y_j - y_m) + (x_i - x_m)(x_j - x_m) \right]$$

and any other combination obtained by permutations of i, j, m .

The final system obtained from assembling all the element contributions given by (23) can be written as

$$[S][\phi] = [b] \quad (25)$$

where $[S]$ now represents contributions from all triangular elements; and $[b]$ is a result of replacing the known node potentials with their Dirichlet values.

Applying the above mentioned FEM model we shall obtain the following graphics concerning the strength and displacement distributions. The model can be applied also for different forms of absorbers. Making the comparison between the different kind of absorbers it is possible to choose that kind of absorber which absorbs the most electromagnetic radiation. The study can be made for a loaded and an unloaded border.

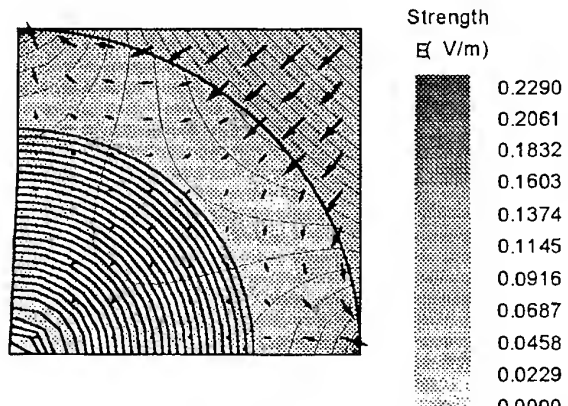


Fig.3. Distribution of E inside the hypothetical absorber

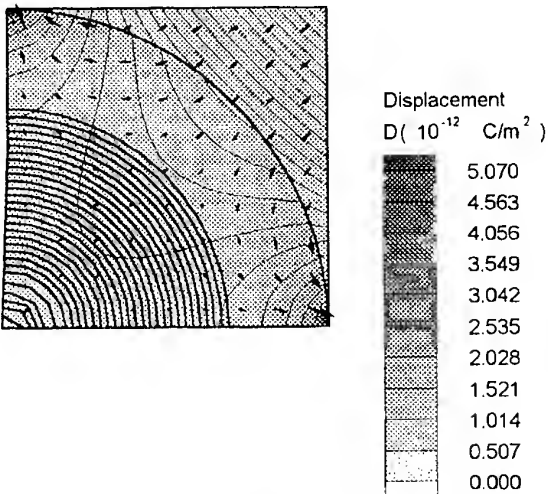


Fig.4. Distribution of D inside the hypothetical absorber

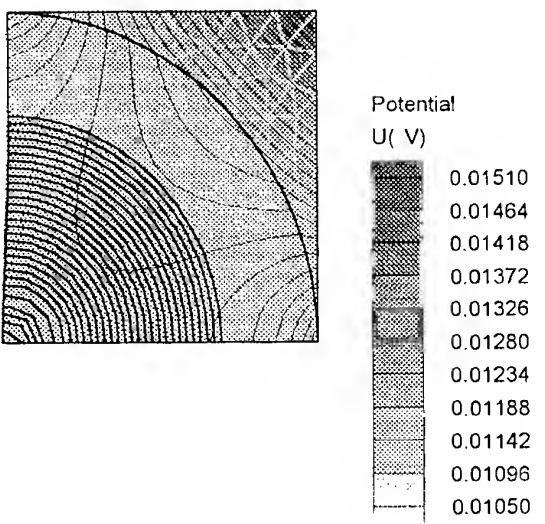


Fig.5. Meshed absorber and distribution of U inside the hypothetical absorber

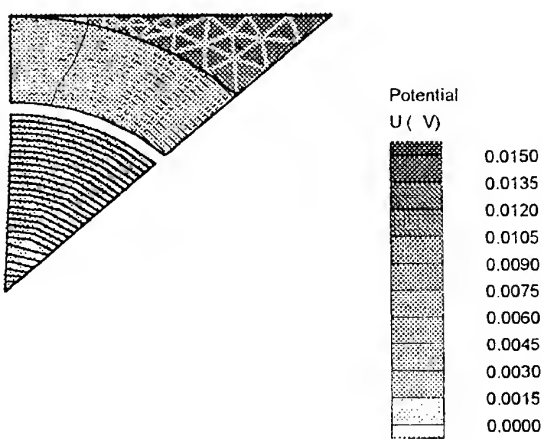


Fig.6. A thinner meshed absorber

The potential absorbed in this case is lower than in the upper case. In these situations it is better to use the absorber from Fig.5.

5. CONCLUSIONS

In this paper the FEM has been applied in modeling absorbers. One tool extensively used in characterizing parasitic effects has been the finite element method. The FEM, which is a numerical method, offers an attractive alternative to solve the problem in all its aspects. This technique is first applied to obtain the field distribution lengthways the absorber. The result is a method to evaluate the field levels at any desired point on the absorber. An integral absorbing boundary condition derived from the integral solution to the wave equation was implemented to truncate the FEM domain.

This now can help in fully defining the operation of the design of absorbers and the correction of any defaults early in the design stages.

The approach is a general approach that can be applied to homogeneous or inhomogeneous domains surrounding the equipment under test.

6. REFERENCES

- 6.1. R. Laroussi and G.I. Costache, "Finite element method applied to EMC problems", IEEE Trans. On Electromagn. Compat., Vol.35, No.2, May 1993, pp.178-183.
- 6.2. P.A. Chatterton and M.A. Houlden, " EMC Electromagnetic Theory to Practical Design", John Wiley & Sons, West Sussex, England, 1992.
- 6.3. Ghi. Mîndru and M.M. Rădulescu, "Numerical analysis of electromagnetic field" (Romanian), Editura Dacia, Cluj, România, 1986.
- 6.4. D.S. Jones, "Methods in Electromagnetic Wave Propagation", Oxford University Press Inc., New York, 1992.
- 6.5. A. K. Bhattacharyya, " Electromagnetic Fields in Multilayered Structures", Artech House, Norwood, England, 1994.

BIOGRAPHICAL NOTE(S)

Mihaela Ruxandra Lascu was born in Timișoara, Romania, on May 7, 1962. She received the degree in electrical engineering from the "Politehnica" University of Timișoara in 1986, where she is presently pursuing the Ph.D. degree in electromagnetic compatibility.

Since 1990 she was appointed Assistant at the University of Timișoara. Her main interest is in numerical techniques applied in electromagnetic compatibility, such as finite-element analysis and finite-difference time-domain methods, and their application to interference problems in steady-state and time-domain applications.

ENGINEERING MODEL FOR SHIELDING EFFECTIVENESS EVALUATION

Vladimir A. Lenivenko, MITEC Ltd., 532 Seventeen Mile Rocks Road,
Sinnamon Park Brisbane, QLD 4073, Australia
Miraj-E-Mostafa, NOKIA Research Center, PO Box 100, FIN 33721, Tampere, Finland

This paper presents results of the modeling of Shielding Effectiveness for modular type shielding enclosures of 3-m and 10-m EMC chambers. Propagation of electromagnetic waves inside and outside the shielding enclosure was analyzed. Engineering models based on the equivalent circuit approach and mode matching solution were employed. Results of the two approaches compared with each other and with experimental data. Influence of structural configuration and mechanical tolerances on the overall Shielding Effectiveness of the chamber was studied based on the typical enclosure design. Frequency band from 1 to 20 GHz was taken under consideration though results might be applicable for other frequency bands as well.

1. SHIELDING EFFECTIVENESS OF THE EMC CHAMBER

Shielding effectiveness (SE) is among several important parameters specified for shielded enclosures. SE measurement is certainly one of the main parts of the acceptance test during the implementation and certification of EMC measurement facility. Due to the nature of electromagnetic processes, when it's coming to the real project implementation, actually measured SE may vary significantly depending on the configuration of the enclosure and surrounding structures, guaranteed tolerances and assembling technology used during the implementation stage as well as the way test engineers evaluate SE during the acceptance test. Additional and rarely mentioned problem is the process of aging which may become critical in the harsh climate conditions. The problem, therefore, has variety of aspects from pure technological up to the level of understanding required from test engineers in order to make sure measurement procedures properly followed and compliance to the EMC standards achieved.

In order to address the problem and guarantee cost efficient and time saving implementation of shielded enclosure a kind of inexpensive but still enough adequate computer simulation tool is developed. Propagation of the electromagnetic waves inside and outside the shielding enclosure

was modeled using well established modeling approaches in order to describe the entire picture of the electromagnetic environment inside and outside the enclosure.

2. VARIETY OF THE FACTORS INFLUENCING SE PERFORMANCE

2.1 Electromagnetic environment inside and outside shielding enclosure

Propagation pass during the SE measurement include internal region inside the enclosure, external region outside the enclosure and wall region characterizing all possible ways of electromagnetic leakage through the enclosure walls. Internal region is treated as a resonator excited by transmitting antenna. Strong standing waves encountered inside metal enclosure to be taken into consideration in this region. Resulted electromagnetic field in the vicinity of the internal wall surface is an input source for all the leakage channels taken into consideration by test engineer when modeling "real life" design of the enclosure. Outside region characterized by pronounced multipass propagation between the ensemble of radiating apertures, excited by all possible leakage channels, and receiving antenna. Effects of multiple reflection may be encountered here due to presence of massive metal or concrete structures in the vicinity of the shielded enclosure.

2.2 Propagation through the walls of enclosure

Analysis of the possible leakage channels in the wall region shows two distinctively different leakage models have to be applied. These are low frequency and high frequency leakage channels encountered. The low frequency channel exists due to direct coupling through the metal walls allowing electromagnetic coupling under condition the enclosure is infinitely thin metal layer. This is applicable in the very low frequency band where any imperfection of the wall structure is under cutoff and no radiating apertures formed. Contribution of this leakage channel is rapidly decreasing with frequency and affecting relatively narrow portion of the band. Appropriate modeling

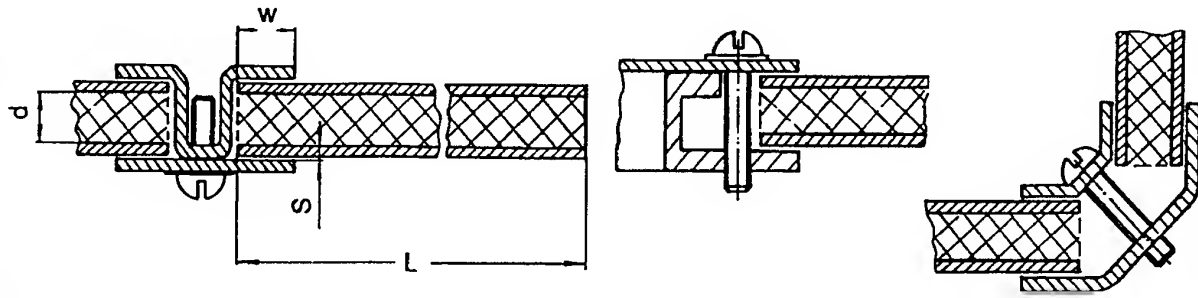


Fig. 1. Mechanical configuration of the wall sections

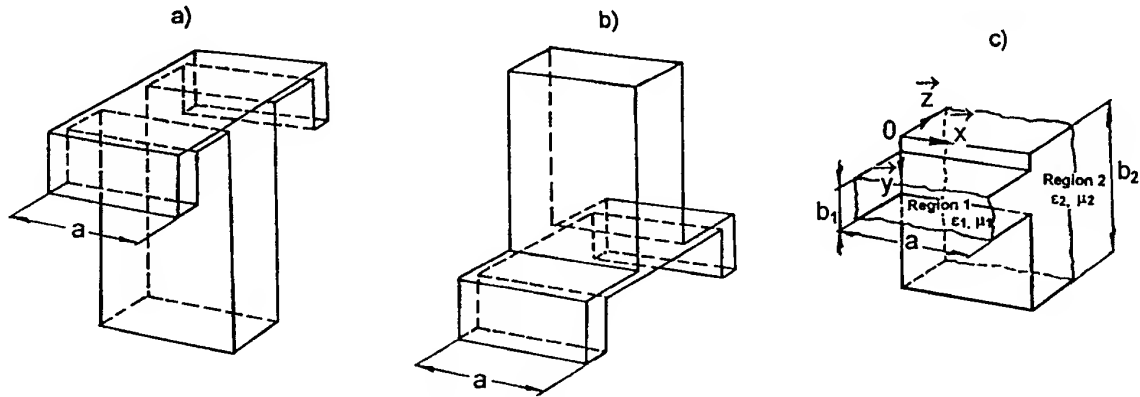


Fig. 2. Equivalent waveguide structures

approach developed in [1] and not considered in this paper. The second leakage channel engages as soon as structural imperfections become comparable to the wavelength creating multiple leakage channels through the wall structure and radiating apertures on the external surface of the enclosure.

3. MODELING APPROACH

The modeling approach is based on the decomposition of the actual complex propagation problem to the partial problems simplified enough to be treated applying appropriate models.

3.1 Modeling of structural imperfections

Waveguide model was applied treating each structural imperfection as a coupling slot. Fig. 1 shows mechanical configurations of the wall sections for typical commercially available modular shielding enclosure. Wall panel is a layered structure containing two metal sheets spaced by dielectric (ply wood). Junction between panels made using metal framing joined with screws. Critical dimensions are shown in Fig. 1: panel size L, spacing inbetween metal sheets d, clamp overlapping W. The distance between screws is typically of about 10 to 15 cm. The configuration guarantees perfect contact in the vicinity of screws. Due to various structural

tensions tiny gap is formed unavoidably between screws. Dimension S, depicting its size, is shown in Fig. 1. Following equivalent waveguide structures allowing quite close approximation of the real mechanical design are shown in Fig. 2(a), (b). These structures have common dimension a determined by the distance between screws.

3.1.1. Electrical response of the waveguide structures Fig. 2(a), (b) may be analyzed using equivalent circuit approach. Necessary equivalent circuits – for uniform waveguide section, steps, bends and T-junctions of rectangular waveguides are available from the literature [2]. The structure then recomposed by cascading T matrices of separate junctions.

3.1.2. More elaborated study of the structures Fig. 2(a), (b) involves mode matching analysis. Key building block element suitable for this purpose is shown on the Fig. 2(c). Modal analysis of such junction is well presented in the literature [3]. The fields on either side of the discontinuity are treated as a sum of the modal fields in rectangular waveguide. Application of the condition of continuity for the fields at the interface results in the integral equation which can be converted to a system of linear algebraic equations using method of moments.

As far as dimension a is fixed by distance between screws (rivets), it's the same for all the

junctions. Evaluating coupling coefficients between H_{mn} and E_{mn} modes, it's possible to show that all coupling coefficients between waves having different indexes m , are equal to zero. This means no mode conversion takes place between waves with different indexes m .

The entire structure then recomposed by combining generalized S-matrices of all key-building blocks and intermediate uniform waveguide sections between them. The generalized S-matrix technique [4] was applied. In fact, attenuation factor of the elementary wall structure may be calculated as well as excitation amplitudes and phases for radiating apertures found.

3.2. Modeling areas inside and outside the enclosure for SE evaluation

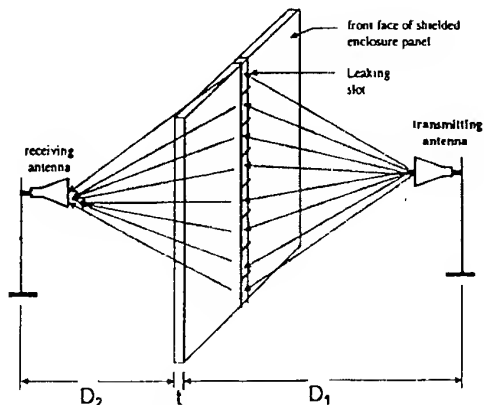


Fig. 3. Configuration for SE test

Phase array model was applied to describe the propagation of waves inside and outside shielding enclosure. All previous discussion is focused on one specific leaking slot (micro level consideration), while the practical case involves leakage through many leaking slots within the beamwidth of the transmitting antenna. So, taking into account each possible leaking slot within the beamwidth of transmitting antenna and superimposing the effect of each of these considered slot to the receiving antenna gives the macro level consideration of the whole scenario. This scenario for only one series of panel to panel joints and one face of enclosure is shown in Fig. 3. Considering all the leaking slots as an array by setting constant phase difference between the consecutive slots will be applicable for individual measurement position of any enclosure and the process will not be a close representation of the whole scenario. Taking different slots individually and superimposing their effect at the receiving antenna would make the scenario more general, making the computation model more versatile and closer to the actual case. There are following assumptions made:

- only the shielded enclosure front face effect is considered while calculating SE, neglecting all forms of reflection from other faces in the process;
- while calculating radiation from transmitting antenna to leaking slots only the far-field pattern is taken into account;
- while radiating from different slots toward the receiving antenna, coupling between different slots is neglected;
- for calculating the radiation pattern from the slots, the conducting shield was approximated to be extended to the infinite length in both the transverse directions.

SE test is simulated using procedures from the applicable documents including MIL-STD 285 taken as a guideline [5,6]. Test procedures taken as recommended by the enclosure producer [7]. Typical design of the commercially available shielded enclosure was analysed.

4. CONVERGENCE AND ACCURACY

The convergence of the magnitude of insertion loss ($|S_{21}|$) of the configuration Fig. 2 (a) is shown in Fig. 4. For this convergence investigation number of modes taken into account in the Region 1, is $N = 1$. Number of modes taken in Region 2 (M) is variable. Dotted curve is calculated using one mode in the Region 2 ($M = 1$). Dashed curve shows effect of two modes taken in Region 2 ($M = 2$). Solid curve is calculated with 14 modes ($M = 14$). Another solid curve refer to the reflection loss (module of S_{11}). Calculated results may be compared to the measured data taken for experimental structure. Actual dimensions of measured structure were: $a = 34.92$ mm, $s = 2.02$ mm, $W = 6.0$ mm, $d = 5.98$ mm, $L = 28.02$ mm. Measured results (insertion loss) presented in Fig. 5.

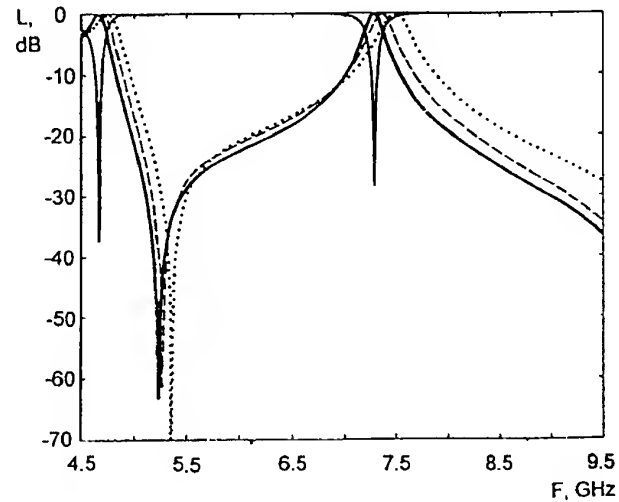
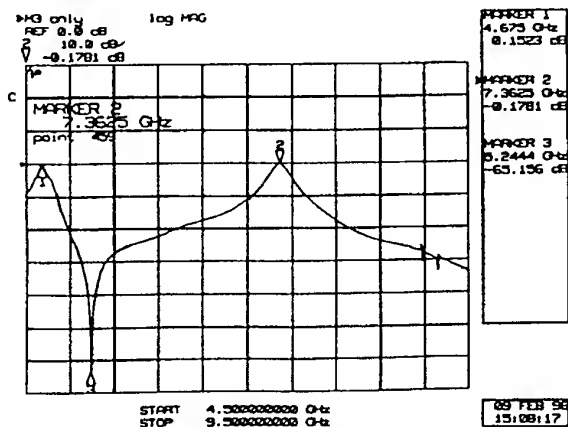


Fig. 4. Calculated $|S_{21}|$ and $|S_{11}|$.

Fig. 5. Measured $|S_{21}|$.

For more detailed consideration Table 1 shows frequency location of the first null measured (position of Marker 3 in Fig. 5) and calculated using various number of modes in Region 2.

Table 1

Number of modes taken in Region 2	Calculated location of the first null of S_{21} , GHz	Measured location of the first null of S_{21} , GHz	Relative difference, %
1	5.35	5.2444	2.0
2	5.27	5.2444	0.5
3	5.2486	5.2444	0.08
5	5.2394	5.2444	-0.09
7	5.2384	5.2444	-0.11
14	5.23824	5.2444	-0.12
19	5.23828	5.2444	-0.12

Results presented in Table 1 illustrate the existence of optimum ratio of the number of modes taken into consideration in the Region 2 and Region 1 $M/N \approx b_2 / b_1$ as known from the literature [8].

Peculiar feature of this study is that dimensions of practical structures used in actual design of shielded enclosure lead to considerably high ratios $M/N = 1_{102} \dots 1_{103}$ due to the fact that coupling slot is narrow. Because of the actual geometry of the structure Region 1 may support only one propagating mode while Region 2 is strongly overmoded. For actual size of the panel 240 cm and inter-screw distance about 12.5 cm there are 45 propagating modes in the gap between metal sheets already at 3GHz. Fig. 6 illustrates the effects of mode conversion in case of strongly overmoded Region 2.

As every next mode becomes propagating, the H_{10} (dominant one in the Region 1) loosing part of its energy in favour of the new one. Fig. 6 clearly show increasing of the partial energy of higher

order modes with frequency and simultaneous growth of e-waves contribution.

Convergence of solution for considerably high ratio M/N is shown in Fig. 7-9 where the calculated

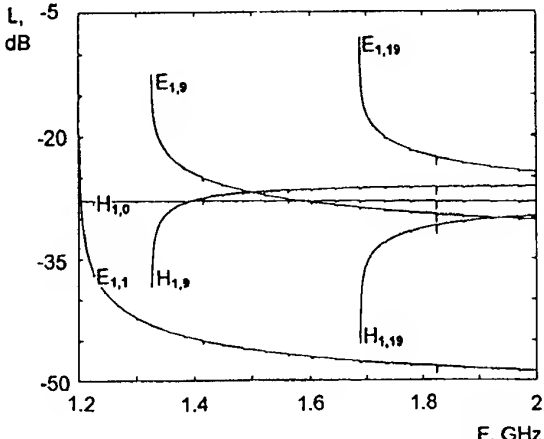


Fig. 6. Mode conversion of overmoded junction.

incertion loss (module of S_{21}) is plotted for the structure having $a = 12.5$ cm, $s = 1.0$ mm, $W = 1.5875$ cm, $d = 1.905$ cm, $L = 240$ cm. Fig. 7 is calculated with $M = 2$, Fig. 8 – with $M = 99$. Fig. 9 is plotted for $M = 2399$. In all cases $N = 1$. Comparison show much slower convergence for this structure with highly overmoded Region 2, especially in the higher frequency range. To keep optimum ratio M/N several thousand modes needed to be taken into consideration.

5. RESULTS

This modeling approach was applied for analysis of actual SE performance for modular design. Fig. 10 presents SE of enclosure having following critical dimensions of panels: $a = 12.5$ cm, $W = 1.5875$ cm, $d = 1.905$ cm, $L = 240$ cm. Solid curve shows SE for $s = 0.01$ mm, dashed curve – for $s = 0.05$ mm, dotted curve – for $s = 0.6$ mm – all plotted the results obtained using mode matching analysis. Corresponding results of equivalent circuit approach shown by smooth solid curves and appropriately marked. The analysis show two areas of possible excessive leakage – in the vicinity of 10 GHz and slightly below 20 GHz. Results were compared to the actual measurements of SE. There are certain technical difficulties of measuring very low level of attenuation in the conditions of construction site. Accuracy of measurement can not be made very high as measured value is close to the limits of dynamic range available for the measurement setup and normally measured at single frequencies. Actual values of SE depend on the measurement position as well. Available measured data for SE presented in Fig. 10 as rectangular boxes – result of averaging of

measured values from several measurement positions obtained according to test procedure MIL STD 285. Specified SE for this modular design is -100 dB in the microwave frequency range. Mention, that equivalent circuit approach can not

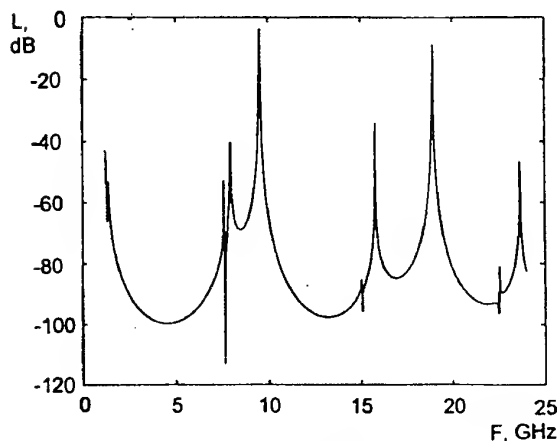


Fig. 7. $|S_{21}|$ calculated with $M = 2$.

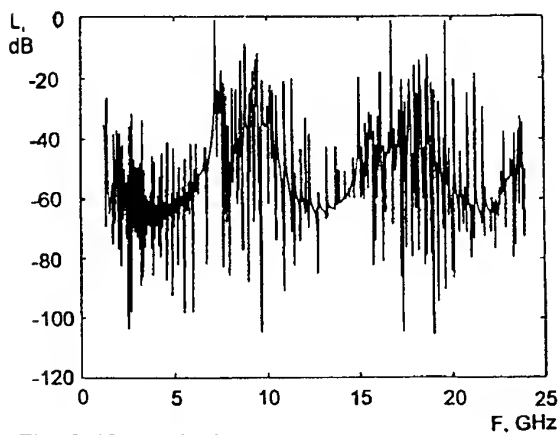


Fig. 8. $|S_{21}|$ calculated with $M = 99$.

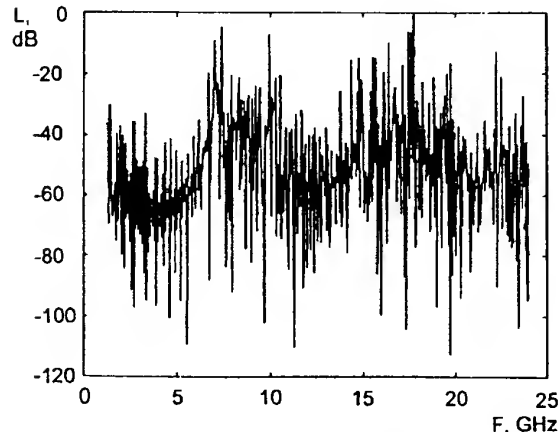


Fig. 9. $|S_{21}|$ calculated with $M = 2399$.

be applied for calculations, but still could be useful for qualitative estimations.

Numerical investigation show the possibility of further improvement of SE performance by optimizing the structure's geometry using different approaches. Direct CAD synthesis is possible though complicated by considerable computation time and multiple sharp resonances caused by overmoded nature of the problem. Fruitful

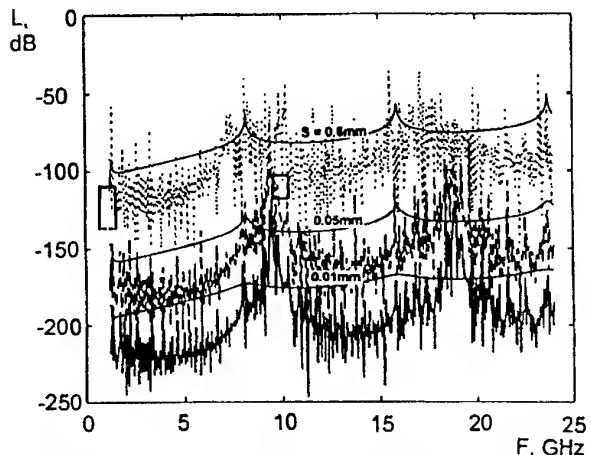


Fig. 10. Comparison of predicted and measured values of SE

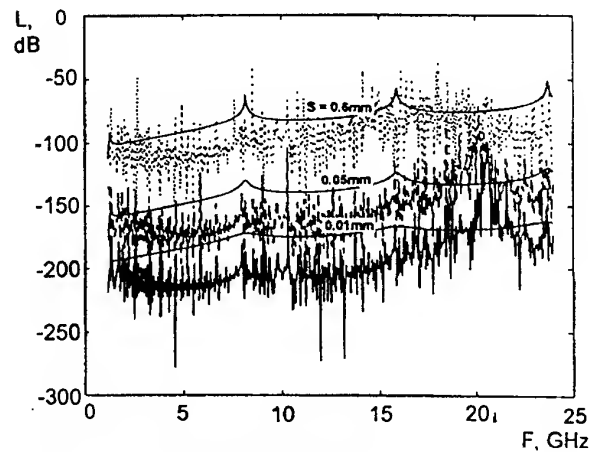


Fig. 11. SE of modified structure

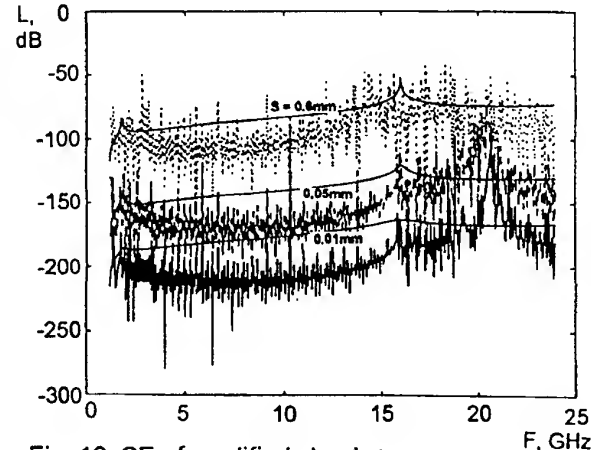


Fig. 12. SE of modified structure

approach might be discovered when using well established filter design techniques. Simple changes in structure's geometry allow reduction of resonances causing excessive leakage and increasing the overall frequency band of the enclosure while keeping that same mechanical tolerances. Fig. 11 shows SE performance of the modified structure having $a = 12.5$ cm, $W = 7.26$ mm, $d = 1.905$ cm, $L = 240$ cm. The first resonance was suppressed by about 50 dB. Number of resonances in the frequency band of interest may be reduced if the layered structure made more thin. Fig. 12 shows SE performance of the modified structure having $a = 12.5$ cm, $W = 7.26$ mm, $d = 9.525$ mm, $L = 240$ cm.

6. CONCLUSION

Flexibility of computer simulation allows the actual configuration of the enclosure to be easily changed as well as measurement setup to be modified and surrounding structures to be taken into account, if necessary, leaving enough possibilities to the test engineer for quick investigation and understanding of the main factors contributing to the results of SE measurement. Practical examples of possible applications of the model considered above include purposes of enhancing confidence during the construction phase, for final evaluation and acceptance test as well as for maintenance of the shielded enclosure. Effects of painting and aging may be simulated using this approach. Express analysis of SE performance is especially valuable for final enclosure evaluation when preparing for the acceptance test, in the case of reconfiguration / structural modification of measurement facility, for troubleshooting and maintenance as well as training of personnel.

7. ACKNOWLEDGEMENT

Authors are thankful to Bill Giacone of Lindgren R.F. Enclosures Inc. for helpful discussions and data on SE acceptance test. This work was conducted in connection with project involving implementation of five shielded enclosures of the EMC facility for Thai Industrial Standard Institute.

8. REFERENCES

1. A. Aiello, et al., "A theoretical model for thin shield effectiveness for rectangular cases", *International Wroclaw Symposium on Electromagnetic Compatibility - EMC 96*, Wroclaw, Poland, 1996.

2. K. C. Gupta, et al., "Computer aided design of Microwave Circuits", Artech House, Inc., 1981.

3. A. Wexler "Solution of Waveguide Discontinuities by Modal Analysis", *IEEE Trans. Microwave Theory Tech.*, vol. MTT-9, pp. 508 - 517, Sep. 1967.

4. Nikolskii, V. V. et al., "Decomposition approach to the problems of electromagnetics" (Russian), Nauka Press, Moscow, 1983, ch. 1.5, pp. 30 - 32.

5. MIL-STD-285. Method of Attenuation Measurements for Electromagnetic Shielding Enclosures for Electronic Test Purposes, June 1956.

6. Standard Committee of the IEEE EMC Society, IEEE Standard Method for Measuring the Effectiveness of Electromagnetic Shielding Enclosures, The Institute of Electrical and Electronics Engineers, Inc., March 1991.

7. Lindgren Test Plan RF Shielding Effectiveness Measurements, No.12677, February 19, 1997

8. R. Mittra and S.W. Lee, "Analytical Techniques in the Theory of Guided Waves", Macmillan, NY, 1971.

BIOGRAPHICAL NOTES

Vladimir A. Lenivenko received the M.Sc. and Ph. D. degrees from the Kiev Polytechnical Institute, Kiev, Ukraine, in 1983 and 1989, respectively. Since 1997 he's been with MITEC Ltd., Brisbane, Australia. His areas of interests include antennas, filters and waveguide structures with applications in microwave engineering and EMC. He is the author of some 20 papers presented in international and national conferences.



Md. Miraj-E-Mostafa received the B. Sc. degree in electrical engineering from Bangladesh University of Engineering and Technology, Dhaka, Bangladesh in 1995. He's got M. Sc. degree in telecommunication in Asia Institute of Technology, Bangkok, Thailand in 1997. His research activities involve several areas in telecommunications.

OPTIMIZED DESIGN OF WIDEBAND ABSORBER FOR 10M EMC TEST CHAMBER

Xu Lin

Telecommunications Program
Asian Institute of Technology
P.O. Box 4, Klong Luang,
Pathumthani 12120, Thailand
Email: lulu66@iname.com

Kazi M Ahmed

Telecommunications Program
Asian Institute of Technology
P.O. Box 4, Klong Luang,
Pathumthani 12120, Thailand
Email: ahmed@cs.ait.ac.th

Vladimir A. Lenivenko

MITEC Ltd.,
532 Seventeen Mile Rock Rd.,
Sinnamon Park
Brisbane, QLD 4073
Australia

In this paper, hybrid absorbers are optimized for specific range of incident angles encountered in the test chambers. It is found that absorbers optimized for small incident angles for front and back walls and absorbers optimized for large incident angles in side walls and ceiling, site attenuation test criteria can be achieved for a wide frequency range. Optimization procedure and results obtained are presented in this paper. The usefulness of this optimization idea is demonstrated by the results obtained.

1. INTRODUCTION

Semi-anechoic chambers are often used for EMC measurements as an alternative to ideal open area test site. Site attenuation test and field uniformity test have to be performed to determine whether the chamber is suitable to be used for radiation test and immunity test. Compared to field uniformity test, the requirement of absorber in site attenuation test is more strict, because the standards for site attenuation test (ANSI C63.4 [1] and CISPR 16 [2]) restrict the deviation between measured results and ideal value while field uniformity test just restrict the deviation measured at test points. Between 3-meter test chamber and 10-meter test chamber, the requirements for absorber used in 10 meter chamber is more limiting. This can be explained explicitly by ray tracing theory.

In ray tracing theory, the field strength at receiving antenna are considered to be the total effect of waves arrived through different paths. Those rays which reflect only once from the absorber are most significant here. From a one-bounce model introduced in [3], it is evident that the angle of incidence for side wall and ceiling is quite large. In 10m test, as the distance between transmission antenna and receiving antenna are longer than the distance between antennas in 3m test, the incident angle to the side wall will be even greater than that of in 3m test. Many studies have

already indicated that as the angle of incidence approaches grazing, the performance of absorber is degraded. So for 10m test chamber, special care must be taken for the large incidence occurring on the side wall and ceiling.

In a recent paper [4], a general guideline for absorber reflectivity has been given. It states that for 10m chamber, the reflectivity for normal incidence should be less than -20 dB and for 45° incidence, the reflectivity should be less than -15 dB. According to this guideline, we examined different absorbers. It is found that reflectivity less than -20 dB in normal incidence doesn't guarantee that the reflectivity for 45° incidence is lower than -15 dB. And the reflectivity less than -15 dB for 45° incidence may be achieved while the reflectivity for normal incidence may not reach -20 dB. By adjusting the absorber structure, the absorber can be optimized for different incident angle range.

In our study, hybrid absorbers are optimized for the specific incident angle range it faces. By installing the absorber, optimized for small incident angles, in the front wall and back wall, and installing the absorber, optimized for large incident angles, in the side wall and ceiling, the ±4 dB criteria in site attenuation test can be achieved in a wide frequency range.

Optimization procedure and results obtained will be introduced in this paper. The simulated normalized site attenuation for a semi-anechoic chamber constructed by the newly designed hybrid absorber will also be presented. The usefulness of this optimization idea is demonstrated by the results we obtained. Same designing idea can be implemented in designing absorber, placed on the floor, for field uniformity test.

2. ABSORBER OPTIMIZATION APPROACH

A cost function proposed in [5] has been applied here. It is given as

$$e = \sum_{i=1}^{NF} \sum_{j=1}^{NA} \left(|R_{0i}^{\parallel}(\theta_j)|^N + |R_{0i}^{\perp}(\theta_j)|^N \right) \quad (1)$$

where NF is the number of frequencies in the optimization bandwidth;

NA is the number of angles in the angular optimization range;

R_{0i}^{\parallel} is the absorber reflection coefficient for parallel polarization;

R_{0i}^{\perp} is the absorber reflection coefficient for perpendicular polarization;

N is chosen as an integer greater than 2, so that the large reflection coefficient will have more weight than the small reflection coefficient. Generally, N should not be more than 4.

By minimizing the cost function in certain angular range, the optimized design of absorber structure can be obtained.

3. CALCULATION OF ABSORBER COEFFICIENT

Homogenization model proposed in [6,7] provides a simple way of calculating absorber reflection coefficient from absorber structure and properties. Here, we will take advantage of this method.

By utilizing homogenization model, geometrically shaped absorber can be modeled as an planar in-homogenous material. The reflection coefficient of the equivalent in-homogenization medium can be calculated by using multi-layer approximation, i.e. dividing the effective absorber medium into N layers and assigning each the bulk parameter value at the layer midpoint, and applying Kong's formula.

The equivalent material properties of a pyramid absorber are :

$$[\epsilon] = \begin{bmatrix} \epsilon_t & 0 & 0 \\ 0 & \epsilon_t & 0 \\ 0 & 0 & \epsilon_z \end{bmatrix} \quad (2)$$

$$[\mu] = \begin{bmatrix} \mu_t & 0 & 0 \\ 0 & \mu_t & 0 \\ 0 & 0 & \mu_z \end{bmatrix} \quad (3)$$

$$\epsilon_t = \sqrt{\epsilon_x \cdot \epsilon_y} \quad (4)$$

$$\mu_t = \sqrt{\mu_x \cdot \mu_y} \quad (5)$$

$$\epsilon_x(z) = \epsilon_y(z) = \epsilon_0 \left[1 - g(z) \frac{2(\epsilon_a - \epsilon_0)}{[1+g(z)]\epsilon_0 + [1-g(z)]\epsilon_a} \right] \quad (6)$$

$$\mu_x(z) = \mu_y(z) = \mu_0 \left[1 - g(z) \frac{2(\mu_a - \mu_0)}{[1+g(z)]\mu_0 + [1-g(z)]\mu_a} \right] \quad (7)$$

$$\epsilon_z(z) = [1 - g(z)]\epsilon_0 + g(z)\epsilon_a \quad (8)$$

$$\mu_z(z) = [1 - g(z)]\mu_0 + g(z)\mu_a \quad (9)$$

where ϵ_a is the permittivity of the absorber material;

μ_a is the permeability of the absorber,

$g(z) = \frac{z}{L}$, L is the length of absorber.

For the grid ferrite tile, the equivalent material properties are :

$$[\epsilon] = \begin{bmatrix} \epsilon_t & 0 & 0 \\ 0 & \epsilon_t & 0 \\ 0 & 0 & \epsilon_z \end{bmatrix} \quad (10)$$

$$[\mu] = \begin{bmatrix} \mu_t & 0 & 0 \\ 0 & \mu_t & 0 \\ 0 & 0 & \mu_z \end{bmatrix} \quad (11)$$

$$\epsilon_t(z)^{-1} = \epsilon_a + \frac{1-g(z)}{1} + \frac{g}{(\epsilon_0 - \epsilon_a) + 2\epsilon_a} \quad (12)$$

$$\mu_t(z)^{-1} = \mu_a + \frac{1-g(z)}{1} + \frac{g(z)}{(\mu_0 - \mu_a) + 2\mu_a} \quad (13)$$

$$\epsilon_z(z) = [1 - g(z)]\epsilon_0 + g\epsilon_a \quad (14)$$

$$\mu_z(z) = [1 - g(z)]\mu_0 + g\mu_a \quad (15)$$

$$\text{where } g(z) = \frac{z}{L}.$$

The reflection coefficient of a planar in-homogenous uniaxial lossy material can be computed numerically, or approximately in terms of integral expression. However, a much simpler approach here is to divide the effective absorber medium into N layers and assign each the bulk parameter values at the layer midpoint [8], then applying the layered media

equations to calculate the reflection coefficient of the layered homogeneous medium (Fig. 1). If N is chosen reasonably large, such that the layer thickness are small compared to the wavelength in the medium then the results will be accurate and the computation time will be much less than using equivalent in-homogenous transmission line theory.

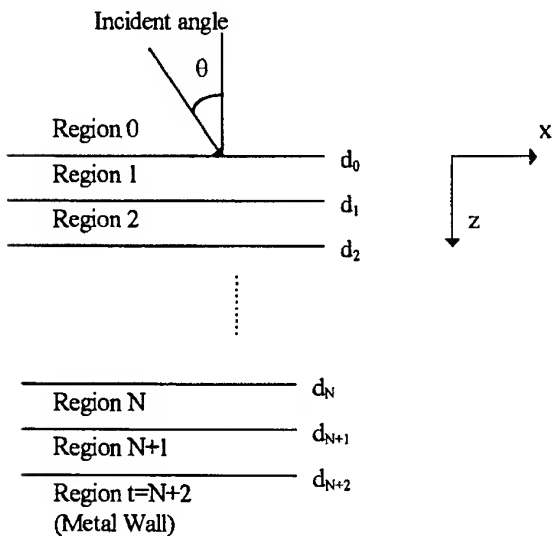


Fig. 1. Ray incident on a layered medium

The calculation algorithm for a layered medium is given as following:

1. Calculating the effective permittivity and permeability

The effective permittivity and permeability for each layer (including the air layer) are:

for perpendicular polarization (TE),

$$\varepsilon_{\text{eff}}(\theta) = \varepsilon_y - \frac{\mu_0 \varepsilon_0 \sin^2 \theta}{\mu_z} \quad (16)$$

$$\mu_{\text{eff}} = \mu_x \quad (17)$$

and for parallel polarization(TM).

$$\mu_{\text{eff}}(\theta) = \mu_y - \frac{\mu_0 \varepsilon_0 \sin^2 \theta}{\varepsilon_z} \quad (18)$$

$$\varepsilon_{\text{eff}} = \varepsilon_x \quad (19)$$

2. Calculating the reflectivity by using Kong's formula:

a) calculating z directed propagation constant of region n:

$$k_{nz}(\theta) = \omega \sqrt{\mu_{\text{eff}}(\theta) \varepsilon_{\text{eff}n}(\theta)} \quad (20)$$

b) calculating $p_{(n-1)n}$

$$\text{for TE wave, } p_{(n-1)n} = \frac{\mu_{(n-1)z} k_{nz}}{\mu_{nz} k_{(n-1)z}} \quad (21)$$

$$\text{for TM wave, } p_{(n-1)n} = \frac{\varepsilon_{(n-1)z} k_{nz}}{\varepsilon_{nz} k_{(n-1)z}} \quad (22)$$

c) calculating the reflection coefficient between regions n-1 and n

$$\Gamma_{(n-1)n} = \frac{1 - p_{(n-1)n}}{1 + p_{(n-1)n}} \quad (23)$$

d) using iteration to calculate the reflectivity of multi-layer medium

$$R_{(N+1)} = \Gamma_{(N+1)t} e^{j2k_{nz}d_n} \quad (24)$$

$$R_n = \frac{e^{j2k_{nz}d_n}}{\Gamma_{n(n+1)}} + \frac{\left[1 - \left(1 / \Gamma_{n(n+1)}^2 \right) \right] e^{j2(k_{(n+1)z} + k_{nz})d_n}}{\left(1 / \Gamma_{n(n+1)} \right) e^{j2k_{(n+1)z}d_n} + R_{n+1}} \quad (25)$$

$$\text{Reflectivity: } \Gamma(\theta) = \frac{1}{R_0} \quad (26)$$

where $\Gamma_{(N+1)t}$ is the reflection coefficient between N+1 layer and t layer. If t layer is metal wall,
for TE wave $\Gamma_{(N+1)t} = -1$,
for TM wave $\Gamma_{(N+1)t} = 1$.

4. OPTIMIZED DESIGN OF ABSORBER FOR 10M CHAMBER

During the study of multi-bounce anechoic chamber model, it is found that for chamber lined with good absorber, i.e. its reflection coefficient is close to or less than -20 dB at normal incidence, only the ray reflected once from absorber need to be considered. Since in 10m anechoic chamber, the incident angle for a one-bounce ray reflected from ceiling and side wall is generally within 35-55 degree and the incidence angle for a one-bounce ray reflected from front wall and back wall is generally within 0-15 degree, absorber optimization should be performed for 0-15 degree incident angle and 35-55 degree incident angle individually.

The absorber used in our study is an hybrid absorber constructed by pyramid foam, grid ferrite tile and a plywood (dielectric) layer (Fig. 2). The permittivity of carbon load pyramid foam is shown in Fig.3 and the permeability of ferrite tile is shown in Fig. 4.

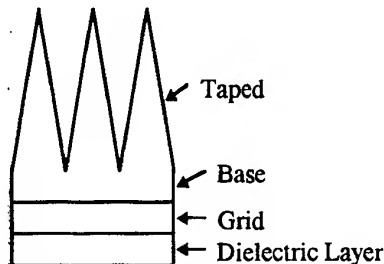


Fig. 2. Structure of a hybrid absorber used in this study

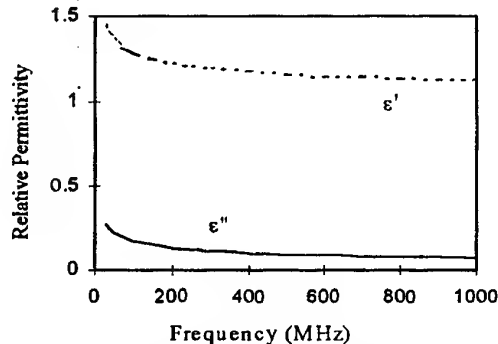


Fig. 3. Relative permittivity of absorber used in this study ($\epsilon = \epsilon' + \epsilon''$)

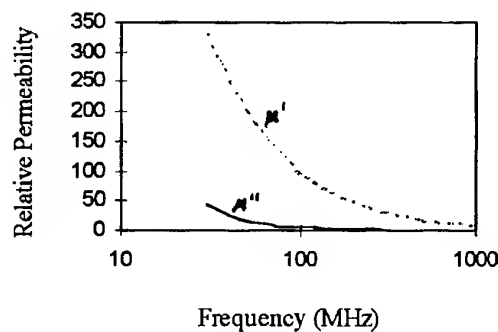


Fig. 4. Relative permeability of grid ferrite tile used in this study ($\mu = \mu' + \mu''$)

In order to minimize absorber size, the length of taped foam is kept within 0.45m and its base is kept within 0.1m. By using optimization approach, it is found that the optimal dimension of absorber for 0-15 degree incidence wave and for 35-55 incidence wave is given as Tab.1.

Table 1: Optimal Dimension of Absorber for Different Angles of Incidence

	Optimized for 0-15 degree incident angle	Optimized for 35-55 degree incident angle
grid ferrite tile g value*	0.82	0.92
grid ferrite tile thickness	0.0053m	0.0053
thickness of plywood layer	0.009m	0.01

* g is the fraction of space occupied by absorber

Reflectivity (dB)

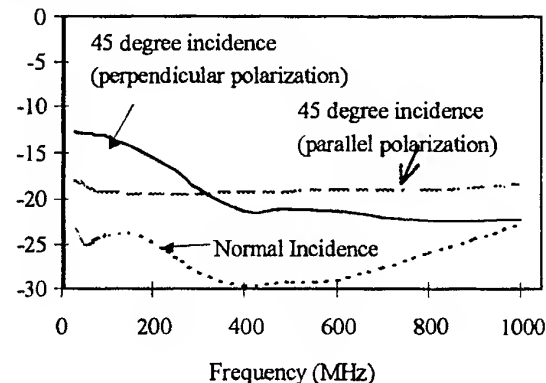


Fig. 5. Calculated reflectivity of absorber optimized for 0-15 degree incidence

Reflectivity (dB)

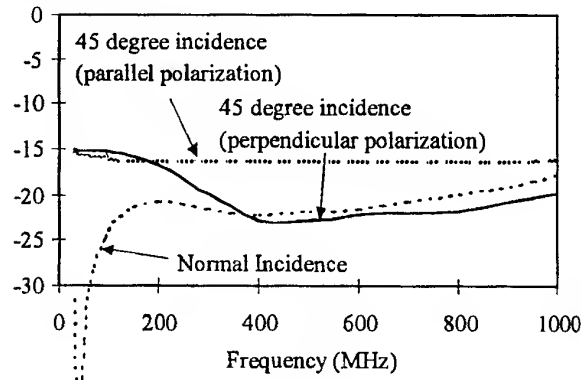


Fig. 6. Calculated reflectivity of a hybrid absorber optimized for 35-55 degree incidence

The results in Fig. 5 shows that the absorber optimized for 0-15 degree incidence can not satisfy the -15 dB guideline at 45 degree incidence [4] in low frequency range and the results in Fig. 6 shows the absorber optimized for 35-55 degree incidence can not satisfy -20 dB guideline at normal incidence in high frequency range. However, by installing absorber optimized for small incident angle on front and back wall and installing absorber optimized for large incident angle at side wall and ceiling, the chamber's performance is very well (Fig.7).

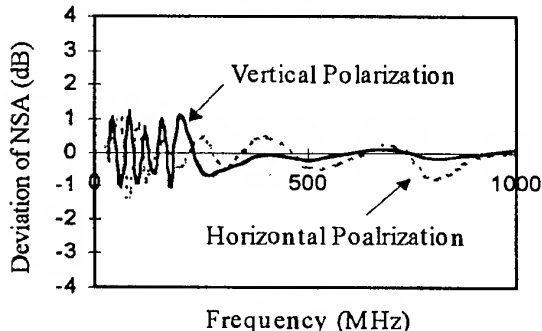


Fig. 7. Calculated deviation of NSA in a chamber lined with newly designed material

5. CONCLUSIONS

This paper introduced an optimized new design of wideband absorber for 10M EMC test chamber. The design procedure and results obtained showed that the absorber lined on anechoic chamber can be tailored according to the wave it mainly encounters.

The absorber designed for large incident angle in this study can be used in field uniformity test.

6. REFERENCES

1. American National Standards Institute, "American National Standard for electromagnetic compatibility - radio-noise emissions from low voltage electrical and electronic equipment in the range of 9kHz to 40GHz", ANSI C63.4., 199
2. International Electrotechnical Commission, "Specification for Radio Disturbance and Immunity Measuring Apparatus and Methods - Part 1: Radio Disturbance and Immunity Measuring Apparatus", CISPR 16-1., 1993
3. C. L. Holloway and E. F. Kuester, "Modeling Semi-Anechoic Electromagnetic Measurement Chambers", IEEE Transaction on Electromagnetic Compatibility, Vol. 38, No. 1, 1996, pp 79-84.
4. C. L. Holloway, R. R. Delyser, R. F. German, P. McKenna and M. Kanda, "Comparison of Electromagnetic Absorber Used in Anechoic and Semi-

Anechoic Chambers for Emission and Immunity Testing of Digital Devices", IEEE Transaction on Electromagnetic Compatibility, Vol. 39, No. 1, Feb. 1997, pp.33-47.

5. J. Perini and L. S. Cohen, "Design of Broad-Band Radar-Absorbing Materials for Large Angles of Incidence", IEEE Trans. on Electromagnetic Compatibility, Vol. 35, No. 2, May 1993, pp. 223-230.
6. E. F. Kuester and C. L. Holloway, "A Low-Frequency Model for Wedge or Pyramid Absorber Arrays-I: Theory", IEEE Transaction on Electromagnetic Compatibility, Vol. 36, No. 4, 1994, pp. 300-306.
7. E. F. Kuester and C. L. Holloway, "A Low-Frequency Model for Wedge or Pyramid Absorber Arrays-II: Computed and Measured results", IEEE Transaction on Electromagnetic Compatibility, Vol. 36, No. 4, 1994, pp. 307-313.
8. P. Wilson, H. Garbe and D. Hansen, "Simulation of Site Attenuation of Site Attenuation in Anechoic Chambers: Try before you Buy", 9th Int. Aurich Symposium and Technical Exhibition on EMC, 1991, pp. 311-316.

BIOGRAPHICAL NOTES

Ms. Xu Lin finished her BE degree in Radio Engineering from Southeast University, Nanjing, China. In December 1997, she finished her ME degree in Telecommunications from Asian Institute of Technology, Thailand. Presently, she is to join Nokia Telecommunications in Finland.

Kazi M. Ahmed had his ME in Communications from Leningrad Prof. Bonch Bruevitch Electrical Engineering Institute of Communications (Russia) in 1978 and Ph.D. in Electrical Engineering from University of Newcastle, NSW, Australia, in 1983. He was an Associate Professor at Bangladesh University of Engineering and Technology, Dhaka, Bangladesh and currently he is an Associate Professor in Telecommunications at Asian Institute of Technology, Bangkok, Thailand.

Vladimir A. Lenivenko graduated in 1983 from Kiev Polytechnic Institute, Kiev, Ukraine, in Radioengineering. He obtained his Candidate of Technical Science degree in 1989. With 10 years of professional experience in microwave engineering, he joined SAMART COMTECH Co. Ltd., in Bangkok, Thailand, in 1994. Since June 1997, he has been working for MITEC Ltd., Brisbane, Australia.

DETECTOR SIMULATION WITH THE USE OF THE DISCRETE TECHNIQUE

Sergey L. Loyka,

Belorussian State University of Informatics & Radioelectronics, P. Brovki Str. 6, Minsk
220027, Republic of Belarus, e-mail: loyka@nemc.belpak.minsk.by

This paper presents a functional-level detector simulation technique which is based on the Hilbert Transforms and can be used together with the Discrete Technique. AM-detector simulation as well as its constrains, improvements and validation has been discussed in detail. It has been shown that the RC-circuit at the detector output should be ignored during the simulation. The technique proposed can be used for a rapid nonlinear EMC/EMI modeling at the system/subsystem level.

I. INTRODUCTION

Numerical modeling of a radio electronic system is a very useful tool for electromagnetic compatibility/interference (EMC/EMI) analysis, in that it allows for the simulation of system behavior for a wide variety of initial conditions, excitations and system configurations in a rapid and inexpensive way [1]. A system can often reveal nonlinear behavior and nonlinear phenomena (intermodulation, cross-modulation, gain compression/expansion etc.) has profound effect on EMC/EMI in some cases [2]. A nonlinear modeling tool must be used in order to carry out EMC/EMI analysis in such a case.

A nonlinear modeling technique (so called 'discrete technique') for numerical EMC/EMI simulation at the system level has been proposed in [3]. This technique allows one to carry out rapid numerical EMC/EMI analysis of a complex system or subsystem (i.e. receiver, transmitter etc.) or a set of systems/subsystems in a wide frequency range taking into account nonlinear effects (including spurious responses of a receiver). Such an analysis is, for instance, a very important part of EMC/EMI modeling of a mobile communication system [4,5].

The basis of the discrete technique [3,6] is a representation of the equivalent block diagram of a system as linear filters (LF) and memoryless nonlinear elements (MNE) connected in series (or in parallel). Thus a stage which employs a nonlinear element, for example, a radio frequency amplifier, can be represented as a typical radio stage, which employs the linear filter at the input, the memoryless nonlinear element and the linear filter at the output [2], see Fig.1.

The process of signal passage through linear filters is simulated in the frequency domain using the complex transfer factor of the filter,

$$S_{out}(f_n) = S_{in}(f_n) \cdot K(f_n), \quad (1)$$

where $S_{out}(f_n)$ - is the signal spectrum at the filter output, $S_{in}(f_n)$ - the signal spectrum at the filter input, $K(f_n)$ - is the complex transfer factor of the filter, f_n - are sample

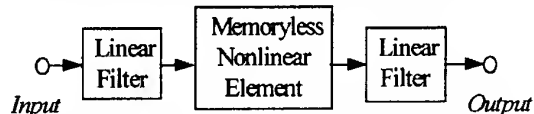


Fig.1. Representation of a typical radio frequency stage

frequencies. The process of signal passage through a nonlinear memoryless element is simulated in the time domain,

$$u_{out}(t_k) = \sum_{i=1}^I a_i u_{in}^i(t_k), \quad (2)$$

where $u_{out}(t_k)$ - is the instantaneous value of the signal at the MNE output, $u_{in}(t_k)$ - is the same for the MNE input, t_k - are sample points in time, a_i - are coefficients of the high-order polynomial which describes the transfer characteristic of the nonlinear element; I - is order of the polynomial. The transition from the time domain to the frequency domain and vice versa is made with the use of the direct and inverse Fast Fourier Transform (FFT and IFFT):

$$S = FFT(u), \quad u = IFFT(S). \quad (3)$$

The determination of the sampling rate, the sample frequency interval, the number of samples as well as a polynomial synthesis technique have been discussed in [6]. Using this technique, a radio receiver can be simulated in a wide frequency range with a very high frequency resolution (up to 10^6 - 10^7 sample frequencies) on a modern PC in dozens of minutes (a conventional circuit-level simulation would require several years for such an analysis).

The essential limitation of this technique is that (1) the nonlinear element is to be memoryless (or, at least, the non-zero memory of the nonlinear element must

allow an assignment to the linear filters), (2) the succeeding element in the functional block diagram does not influence the preceding one (in some cases, this influence can be taken into account by the use of the equivalent transfer factor). Therefore this technique cannot be directly applied to the detector simulation, which is an essential limitation on its possibilities - the simulation of a radio receiver can be carried out only as far as the output of the intermediate frequency (IF) path (the detector input) and, correspondingly, baseband signal processing cannot be simulated. But the detector and baseband signal processing can substantially influence the EMC/EMI situation, so it's desirable to have an appropriate simulation technique.

This article presents several methods used so as to simulate various (amplitude (AM), frequency (FM) or phase (PM)) detectors at the system (functional) level, which can be used together with the discrete technique. The method of an amplitude detector simulation, which is based on the Hilbert transforms, as well as its constraints, improvements and validation has been discussed in detail.

2. AM DETECTOR SIMULATION

Since the primary function of an AM detector is to generate output signal which is proportional to the amplitude of an input signal, it's necessary to calculate the input signal amplitude in order to carry out the simulation. A signal at the input of a radio receiver detector is, as a rule, a narrowband one, so the Hilbert transform can be used for this purpose (we should note that the requirement for the input signal to be narrowband is dictated by not Hilbert transform itself which can be applied to a broadband signal too, but by the RC-circuit present at the detector output. Further this issue will be discussed in detail).

For the sampled spectrum which is used in the discrete technique, the Hilbert transform takes the simplest form [7]:

$$S_n^* = -j \cdot S_n, \quad (4)$$

where $S_n = S(f_n)$ - is a sampled spectrum, S_n^* - is the spectrum of the Hilbert conjugate signal, j - is the imaginary unit. The input signal amplitude can be obtained with the use of the well-known ratio [7,8]

$$A_k = \sqrt{u_k^2 + (u_k^*)^2}, \quad (5)$$

where $u_k = u(t_k)$ - is the sampled input signal, u_k^* - the Hilbert conjugate signal of u_k . u_k^* is obtained from S_n^* by means of inverse FFT

$$u_k^* = IFFT(S_n^*). \quad (6)$$

In the simplest simulation technique, A_k can be used in order to obtain the detector output signal

$$u_{out,k} = k_d \cdot A_k \quad (7)$$

where k_d - is the detector transfer factor. This approach works quite well in some practical cases. But, as a detailed consideration shows, there are two constraints for this approach:

(1) the bandwidth of the input signal must be smaller than the cut-off frequency of a low-pass filter (RC-circuit) at the detector output,

$$\Delta f_{in} < F_{cut}, \quad (8)$$

(in some cases this constraint can be relaxed, see below), and

(2) the input signal must be large enough so that the detector operates in the large signal mode,

$$A_k > A_{min}, \quad (9)$$

where A_{min} - is a threshold level which is determined by the volt-ampere characteristic of the nonlinear device used in the detector (for a diode detector, $A_{min} \approx 0.2 \div 0.7V$).

The second constraint is rather obvious - only in the large signal mode the output signal in an AM detector is proportional to the input signal amplitude (k_d is a constant). In the small signal mode, k_d is a function of A_k and the spectral content of the output signal is much richer than that of A_k . This technique doesn't "feel" the difference between the small and large signals modes since the Hilbert transform is linear relative to the input signal amplitude

$$u_k^*(c \cdot u_k) = c \cdot u_k^*(u_k), \quad (10)$$

where c - is a constant, and, correspondingly, $A_k(c \cdot u_k) = c \cdot A_k(u_k)$. By this reason, this technique cannot predict harmonics of the modulating signal, which always are present at the detector output (fortunately, for most of practical detectors, they level are rather low and may be disregarded in EMC problems).

To discuss the first constraint in detail, let us consider the detector shown in Fig. 2.

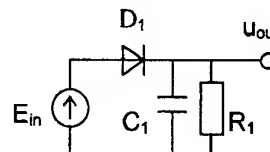


Fig. 2. AM diode detector

If the bandwidth of the input signal E_{in} (which contains interference as well as a required signal) is smaller than the cut-off frequency of the RC-circuit at the detector output, the output signal u_{out} repeats the amplitude of the input signal at the same moment of time - the detector is said to be memoryless. If not, the output signal doesn't repeat the amplitude of the input signal and depends on its levels at the preceding moments of time - the detector is said to have memory. To determine the boundary between these two modes, let's consider the input signal shown in Fig. 3. This signal consists

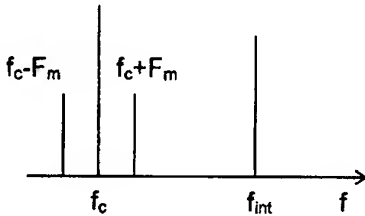


Fig. 3. Spectrum of the input signal. f_c - carrier frequency, F_m - modulating frequency, f_{int} - interference frequency.

of the required AM signal and the interference signal. The required signal bandwidth is always smaller than the cut-off frequency (the design constrain). The interaction between the interference and the required signal will result in beat. So, we must consider the difference between the interference frequency and the required signal frequencies (the beat frequencies). Taking into account that the side frequencies levels are, as a rule, smaller than that of the carrier and for the sake of simplicity, we shall consider further the beat between the carrier and the interference (beat between the side frequencies and the interference can be considered in a similar way). Then the signal bandwidth is equal to the beat frequency

$$\Delta f_{in} = f_{beat} = f_{in} - f_c , \quad (11)$$

where f_{beat} - is the beat frequency. If condition (8) is true, then the output signal repeats the input signal amplitude and the technique works quite well. Otherwise, the output signal doesn't repeat the input signal amplitude because capacitor C_1 has not managed to discharge with the beat frequency: the rate of the capacitor discharge v_C is smaller than the rate of the change of the beat signal amplitude v_{beat} . Let's assume for simplicity that $u_{int} < u_c$, where u_{int} - interference level, u_c - required signal level without modulation (the opposite case can be considered in a similar manner). Then, taking into account the exponential law for the capacitor discharge, we obtain the following assessment for v_C :

$$v_C \approx \frac{u_c}{\tau} , \quad (12)$$

where $\tau = R_1 C_1$ - is the RC-circuit constant. In a similar way we obtain the following assessment for the average value of v_{beat} :

$$v_{beat} \approx \frac{u_{int}}{4T_{beat}} , \quad (13)$$

where $T_{beat} = 1/f_{beat} = 1/\Delta f_{in}$ - is the beat period, since the beat amplitude equals the interference amplitude. Our simulation technique will predict the correct output signal if $v_C > v_{beat}$, or, using (12) and (13)

$$u_{int} < \frac{4u_c}{\tau \cdot f_{beat}} , \quad (14)$$

From this condition we can conclude the following: if the interference level is rather low, then the output interference level (at the beat frequency) is not affected

by the RC-circuit even if the beat frequency is larger than the cut-off frequency of the RC-circuit (this conclusion is also confirmed by the PSpice simulation - see below).

Thus, it's absolutely unacceptable to model the AM detector as the series connection of a nonlinear element (or a frequency transformer) and a low-pass filter, as it has been proposed by some authors. Physically it can be explained as follows: the capacitor is discharged through the resistor R_1 and is charged through the direct diode resistance which is much smaller than R_1 , so the discharge time constant and the charge time constant are quite different.

From the practical viewpoint, spectral components of the detector input signal, which lie outside of the IF path bandwidth, will be strongly attenuated by the IF path, so that condition (14) will be fulfilled. If, nevertheless, it is not, it means that these spectral components have very large level at the receiver preselector and the receiver is completely blocked.

If condition (14) is not true, then the output interference signal will be attenuated by the RC-circuit. But the attenuation factor will be smaller than the transfer factor of the RC-circuit. Thus, the optimal decision is to ignore the RC circuit during the simulation at all.

Taking into account all considerations given above, we can present the AM detector simulation scheme as on Fig.4.

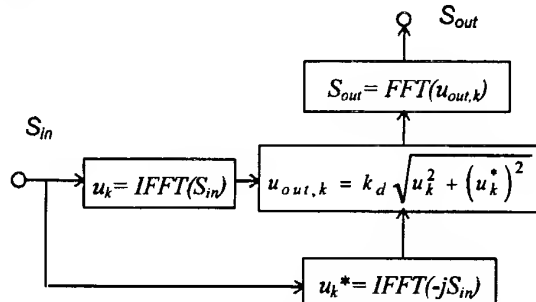


Fig.4. AM-detector simulation scheme. S_{in} - input signal spectrum, S_{out} - output signal spectrum.

We should note that if an additional low-pass filter is connected to the detector output (as on Fig.5) then this filter must be taken into account (since the capacitor C_2 charge and discharge time constants are the same)

$$\bar{S}_{out} = S_{out} K(f) , \quad (15)$$

where \bar{S}_{out} - spectrum at the filter output, $K(f)$ - complex transfer factor of the filter. The scheme on Fig. 4 must be corrected too.

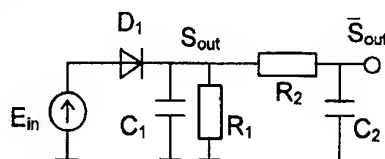


Fig. 5. AM diode detector with a low-pass filter

The technique proposed can be used to simulate an AM detector in the small-signal mode. In this case, k_d must be considered as a function of A_k . An appropriate approximation to this function can be found, for instance, in [9]. Harmonics of the modulating signal can also be predicted in this way.

Let's consider determination of the sampling rate, the sample frequency interval and the number of samples. It's similar to the determination of these quantities for the discrete technique [3,6]. The maximum sample frequency $f_{n,max}$ must be higher than the highest input spectrum frequency $f_{in,max}$ with some margin,

$$f_{n,max} = k f_{in,max} \quad (16)$$

where k - is a margin factor ($k=2\dots10$). The sample frequency interval Δf_n must be lower with some margin than the lowest input beat (or modulating) frequency $f_{beat,min}$ which should be modeled,

$$\Delta f_n = k_1 f_{beat,min} \quad (17)$$

where k_1 - is a margin factor ($k_1=0.1\dots0.5$). Using (16) and (17), we find the number of samples

$$N = 2 \frac{f_{n,max}}{f_{beat,min}} \quad (18)$$

We must round off this number to a power of two (in order to use FFT)

$$\bar{N} = 2^m, \quad m = [\log_2 N] + 1 \quad (19)$$

where $[*]$ - is the whole part. Further we recalculate Δf_n for constant $f_{n,max}$ (or $f_{n,max}$ for constant Δf_n) using equations (16)-(18).

3. SIMULATION TECHNIQUE VALIDATION

In order to validate the technique proposed, an extensive circuit-level simulation of the diode AM-detector given on Fig.2 (the cut-off frequency $F_{cut}=30kHz$) has been carried out by means of well-known simulation tool PSpice [10]. The input signal used in the simulation is as that on Fig.3. Some results of this simulation and the comparison with the technique proposed are presented on Fig. 6 and 7. For Fig.6, the interference frequency is within the required signal bandwidth (parameters of the input signal: $f_c=1MHz$, $F_m=10kHz$, modulation index $m=0.3$, $u_c=3V$, $u_{int}=3V$, $f_{int}=1015kHz$). As it can be seen from this figure, the agreement between our technique and PSpice predictions is quite well for levels not smaller than -20 ... -30dB relative to the maximum. All effects known from the theory (signal compression, beat generation at the frequencies $f_{int} - f_c$, $f_{int} - f_c - F_m$, $f_{int} - f_c + F_m$ etc.) are predicted quite well. We should note that the technique proposed works more than ten times faster than PSpice.

For Fig.7, the interference frequency lies outside of the required signal bandwidth (parameters of the input signal: $f_c=1MHz$, $F_m=10kHz$, $m=0.3$, $u_c=3V$, $u_{int}=1V$, $f_{int}=1100kHz$). As it can be seen from this figure,

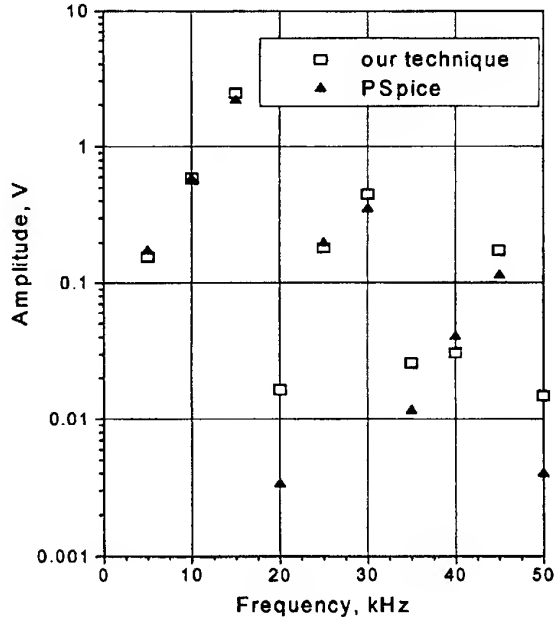


Fig.6 Spectrum at the detector output (input signal - as shown on Fig.3). The interference lies within the required bandwidth.

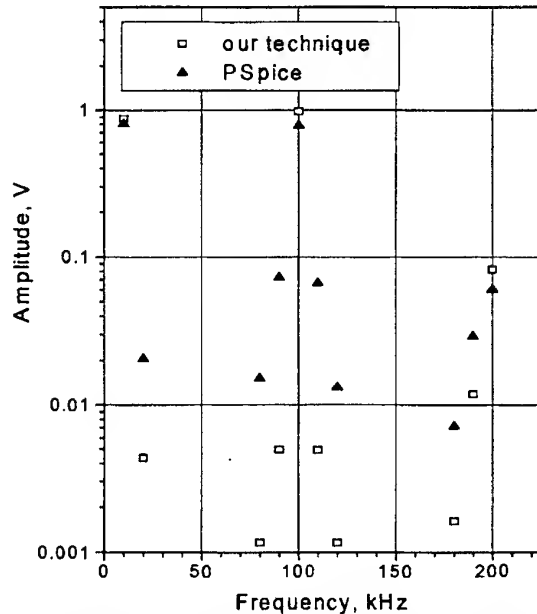


Fig.7 Spectrum at the detector output (input signal - as shown on Fig.3). The interference lies outside the required bandwidth.

the largest beat level at the frequency $f_{int} - f_c = 100kHz$ is predicted quite well. It proves our conclusion that the RC-circuit must be discarded during the simulation (for the present case, $(f_{int} - f_c)/f_{cut} \approx 3$ so if the RC-circuit had operated as an usual low-pass filter, three-fold attenuation would have been expected for this beat frequency, which is not observed in reality). To predict small spectral components more accurately, it's

necessary to use an appropriate approximation for $k_d(A_k)$ instead of a constant.

4. FM DETECTOR SIMULATION

A similar approach can be used in order to simulate an FM or PM detector. Using the Hilbert Transform, we find instant angular frequency of the detector input signal [8]

$$\omega_k = \frac{\hat{u}_k \cdot \hat{u}_{k-1} - \hat{u}_{k-1} \cdot \hat{u}_k}{\Delta t \cdot A_k^2}, \quad (20)$$

where Δt - is the time sample interval. Output signal of an FM detector is proportional to the difference between the instant frequency and the detector resonant frequency ω_0

$$u_{out,k} \approx k_d(\omega_k - \omega_0) \quad (21)$$

This equation is valid for the linear part of the detector input-output characteristic when

$$|\omega_k - \omega_0| \leq \Delta\omega, \quad (22)$$

where $\Delta\omega$ - is the linear part width, and for a sufficiently large input signal when its amplitude is constant due to the limiter which is connected in front of the detector,

$$A_{lim,in} \geq A_{th,in}, \quad (23)$$

where $A_{lim,in}$ - is a signal amplitude at the limiter input, $A_{th,in}$ - its threshold level (the saturation level). In other cases, this equation should be generalized to take into account the nonlinearity of the detector characteristic and its dependence on the input signal amplitude

$$k_d = k_d(\omega_k - \omega_0, A_k). \quad (24)$$

Appropriate approximations for the dependence of k_d on $\omega_k - \omega_0$ can be found in [9]. The dependence of k_d on A_k can be approximated by

$$k_d \approx c \cdot A_k, \quad c - \text{constant} \quad (25)$$

for an FM detector with tuned-off circuits or similar, and by

$$k_d \approx c \cdot A_k^2, \quad c - \text{constant} \quad (26)$$

for an FM detector with a multiplier.

As practical experience shows, this simulation technique predicts the required signal compression and the threshold effect quite well. Predicted interference levels are smaller than in reality since the nonlinearity of the detector amplitude characteristic is not taken into account.

5. CONCLUSION

We can conclude that the technique proposed predicts output spectral components which are not smaller than -20dB relative to the maximum level quite well. The feasible improvements of the technique, which

have been discussed above can increase the analysis dynamic range.

Further reduction in the computational time can be achieved by decreasing the sampling rate (i.e. computing the output signal samples $u_{out,k}$ not for every k , but only for some k) at the output due to the fact that the output spectrum is a baseband one

An PM detector can be simulated in a way similar to the FM detector simulation.

6. REFERENCES

1. F.M. Tesche "Numerical Modeling for EMC", Proc. of 12th Inter. Zurich Symp. On EMC, Zurich, Switzerland, Feb. 18-20, 1997, pp.269-274.
2. D.D. Weiner "Nonlinear Interference Effects in EMC", Supplement to the Proc. of 10th Int. Zurich Symp. On EMC, Zurich, March 1993, pp.114-127.
3. V.I. Mordachev "Express analysis of electromagnetic compatibility of radio electronic equipment with the use of the discrete models of interference and Fast Fourier Transform", Proc. of IX Inter. Wroclaw Symp. on EMC, Poland, Wroclaw, 1988, Part 2, pp.565-570.
4. S.W.Chen, W. Panton and R. Gilmore "Effects of Nonlinear Distortion on CDMA Communication Systems", IEEE Trans. On MTT, vol. 44, No. 12, Dec. 1996, pp.2743-2750.
5. B. Gallagher "Estimating and Measuring C/I in a GSM Wireless Local Loop Receiver", Microwave Journal, vol.40, No. 10, Oct. 1997, pp.70-83.
6. S.L. Loyka, V.I. Mordachev "Computer-aided nonlinear simulation at the system level", Proc. of 5th Inter. Confer. On EMC/EMI (INCEMIC'97), Hyderabad, India, Dec. 3-5, 1997, pp. 93-98.
7. S.I. Baskakov "Radio engineering circuits and signals", Vysshaj Shkola, Moscow, 1988. (in Russian)
8. "Computer-aided circuit design", Editor V.N. Il'in, Radio I Cvjaz, Moscow, 1987. (in Russian).
9. "Radio receivers", Editor V.I. Siforov, Sovetskoe Radio, Moscow, 1974. (in Russian).
10. "MicroSim PSpice & Basics. User's Guide." MicroSim Corporation, Irvine, California, 1996.

BIOGRAPHICAL NOTES

Dr. Sergey L. Loyka was born in Minsk, Republic of Belarus on August 6, 1969. Since 1995 he is Senior Researcher of the Electromagnetic Compatibility Laboratory, Belorussian State University of Informatics and Radioelectronics. Dr. Loyka is a member of the New York Academy of Sciences and IEEE EMC Society. He has about 40 publications in the area of electromagnetic compatibility, active and self-phased antenna arrays, nonlinear circuit analysis, computer-aided modeling and design.

BLIND DECONVOLUTION OF SPURIOUS SIGNALS IN NOISE

Józef Jacek Pawelec, Artur Przybysz

Military Communication Institute, 05-130 Zegrze, Poland (e-mail: przybysz@cc.wil.waw.pl)

Abstract - Two methods of reconstruction of digital signals, distorted by nonlinear phase of channel and corrupted by AWG noise has been proposed. The first method is based on 3-rd order cumulant function, the second -on 4-th order moment function. The both utilize adaptation techniques. Some simulation results relating to Bernoulli-Gauss and bipolar signals ± 1 are included. Their deconvolution consistency is 0.98 and 1, resp.

1. INTRODUCTION

The paper deals with the so-called spurious emissions, generated by the digital equipment such as printers, displays and others. Because of the very wide spectrum of such emissions and of poor channel characteristics, the shape of signal at the receiving point is deeply distorted. We usually do not dispose the unit impulse response function $h(k)$. If however the medium of emanation presents a linear time invariant system (LTIS), it is possible to recover the input signal - to some degree of consistency - on the basis of higher-order statistics (HOS) and adaptation techniques. The fundamental works on this field have been laid by Swami, Mendel, Nikias, Cadzow and Haykin [1,3,5,7].

The general approach to the problem is illustrated in Fig.1. An independent digital series $s(n)$ is led to the input of LTIS channel. In our experiments it is represented by a physical or theoretical all-pass filter. If $s(n)$ is a random sequence of bipolar signals (± 1) and the phase characteristics of LTIS is nonlinear, the output $x(n)$ is no longer a binary series - rather some nearly uniform distribution random series

If we knew the unit impulse response function $h(k)$, the output $x(n)$ would be as follows

$$x(n) = \sum h(k) s(n-k) \quad k=0, 1, 2, \dots \quad (1)$$

This is however not the case. So we have to look for another method. Since the distortions of signal are caused by a linear system, it is reasonable to use -for the recovering operation -also some linear system. The simplest one is a finite impulse response (FIR) filter. The farther procedure includes an adaptation process. It consists of two phases, Fig.1. In the first one we choose the proper criterion function - a measure of difference between $s(n)$ and its estimate $s'(n) = y(n)$. At the second phase we elaborate an algorithm, which matches the filter coefficients $\beta(k) \Leftrightarrow h^{-1}(k)$ to the values of criterion function.

In the present paper we consider two methods: the first one is based on cumulant function of the 3-rd order and the second - on normalized 4-th order moment function. The moment is a derivative of characteristic function, the cumulant -a derivative of normal logarithm of this function.

2. FOUNDATIONS OF CUMULANT METHOD

The cumulant function (in the biased form) is defined as follows [1]

$$c(m, n) = \frac{1}{L} \sum_{k=L+mx(0, m, n)}^{L-mx(0, m, n)} y(k)y(k+m)y(k+n) \quad (2)$$

where $y(k)$ is a data series; L - a number of samples; m, n - the mutual displacements (lags) of series, $m, n = 0, \pm 1, \pm 2, \dots$

We recognize that distortion process is linear, so the output and input signals y and x should be related by a linear operation

$$\sum \beta_i x(k-i) = y(k) \quad i = 0, 1, 2, \dots K \quad \beta_0 \equiv 1 \quad (3)$$

where K is an order of FIR filter and β_i is a vector of its coefficients.

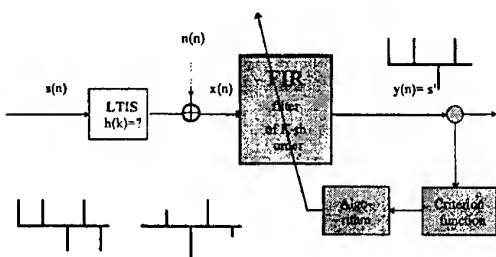


Fig.1. The diagram of experiment

Let us multiply eq. (3) by $x(k+m)x(k+n)$ and take the expectation values. So, we obtain

$$\begin{aligned} \beta_0 E\{x(k)x(k+m)x(k+n)\} + \\ \beta_1 E\{x(k-1)x(k+m)x(k+n)\} + \dots = \\ \beta_0 c_x(m,n) + \beta_1 c_x(m+1,n+1) + \dots \\ + \beta_K c_x(m+K,n+K) = c_{xy}(m,n) \end{aligned} \quad (4)$$

where c_x is a cumulant function and c_{xy} - a cross-cumulant function

$$c_{xy} = E\{y(k)x(k+m)x(k+n)\} \quad (5)$$

It has been shown that for causal filters the cross-cumulant function is identically zero for $m \leq 0$ or $n \leq 0$ [2].

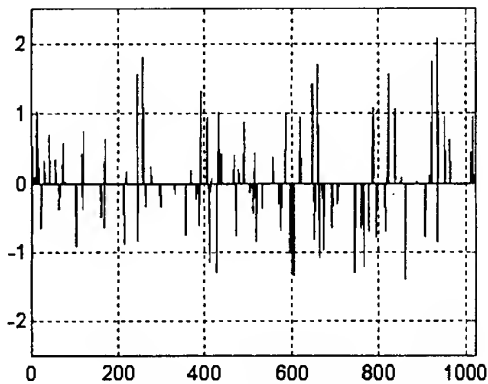


Fig. 2. The original input signal

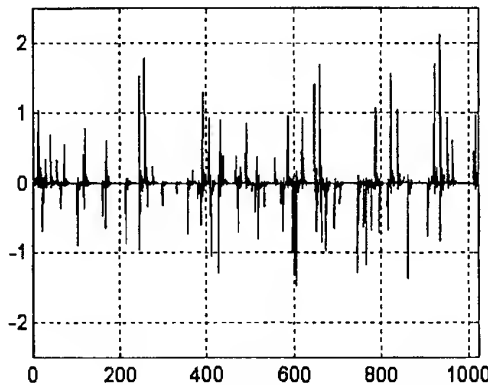


Fig. 3. The recovered signal

Then we obtain

$$\begin{aligned} c(m+1,n+1)\beta_1 + c(m+2,n+2)\beta_2 + \dots \\ + c(m+K,n+K)\beta_K = -\beta_0 c(m,n) \end{aligned} \quad (6)$$

for $m \leq 0$ or $n \leq 0$

This may be expressed in a matrix form

$$C_H \beta_K = -\beta_0 c \quad (6a)$$

where β_K - a vector of FIR coefficients

$$\beta_K = [\beta_K, \beta_{K-1}, \dots, \beta_1]^T; c - \text{a cumulant vector}$$

$$\begin{aligned} c = [c(-1,-K), c(-2,-K), \dots, c(-1,-K+1) \\ c(-2,-K+1), \dots, c(-1,0), c(-2,0), \dots, c(-K,0)]^T \end{aligned}$$

C_H - Hankel matrix (the same components along diagonals 45°).

Henkel matrix may be received from cumulant matrix. Let us consider a simple example:

$$x(n) = [2 -2 -2 2 2 -2 -2 2], K=2.$$

Then, according to eq. (2) the cumulant matrix is as follows

$$C = \begin{bmatrix} c(-2,-2) = 0 & c(-2,-1) = 2 & c(-2,0) = 0 \\ c(-1,-2) = 2 & c(-1,-1) = -1 & c(-1,0) = -1 \\ c(0,-2) = 0 & c(0,-1) = -1 & c(0,0) = 0 \\ c(1,-2) = -1 & c(1,-1) = 2 & c(1,0) = -1 \\ c(2,-2) = 0 & c(2,-1) = -1 & c(2,0) = 0 \end{bmatrix} \quad (7)$$

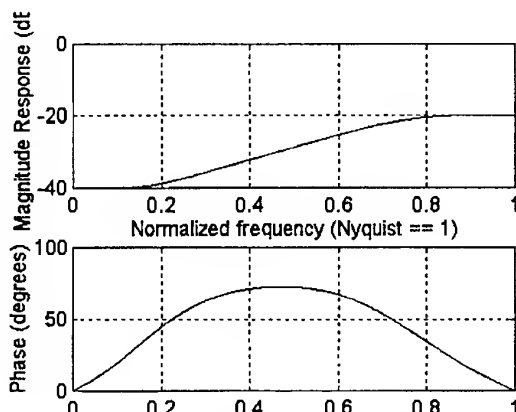


Fig. 4. LTIS characteristics

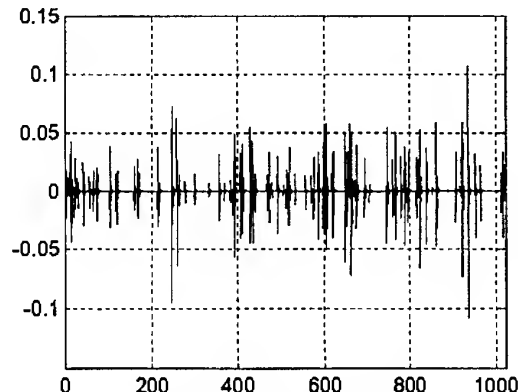


Fig. 5. The distorted signal

The Hankel matrix is then formed by taking the second, third and fourth component of each column of matrix C and arranging them in a rectangle, as below

$$C_H = \begin{bmatrix} 2 & 0 & -1 & -1 & -1 & 0 \\ 0 & -1 & -1 & 2 & 0 & -1 \end{bmatrix}^T \quad (8)$$

The vector c is formed by taking the last two components of each column of C

$$c = [-1 \ 0 \ 2 -1 \ -1 \ 0]^T \quad (9)$$

Having done C_H and c we may calculate β_K due to eq. (6a) $\beta_K = -\beta_0 C_H^{-1} c$. The inversion of matrix C_H is performed in an adaptation process [3]. The final result is as follows: $\beta_2 = 0.375$, $\beta_1 = 0.625$. We add to them the coefficient $\beta_0 \equiv 1$.

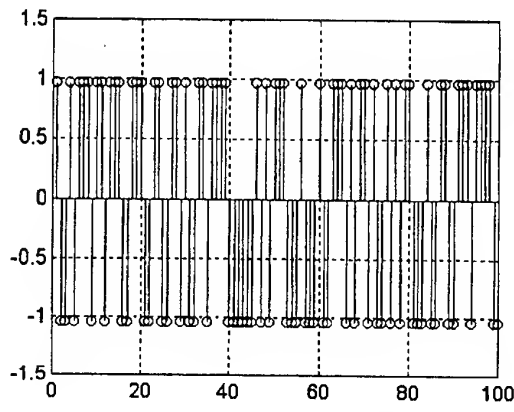


Fig. 6. A binary random series

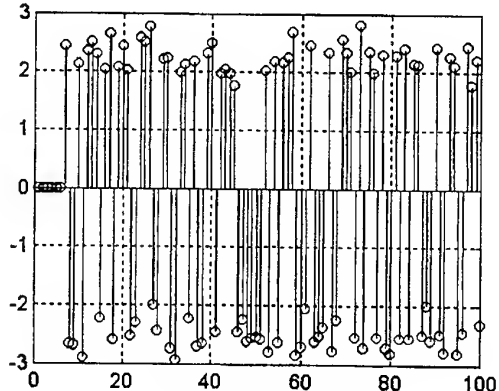


Fig. 7. The recovered series

3. AN EXPERIMENT

The signal transformation and reconstruction procedures are illustrated in Fig.2, 3, 4, 5. In Fig.2 we see the input signal s : 1024 samples of Bernoulli-Gauss process [3]. Fig.4 presents a magnitude and phase characteristics of transmission channel [4]. The Nyquist frequency is 10 MHz. In Fig.5 we see the output distorted signal x . Its mean value is very small as a result of attenuation phenomenon. The more severe feature is however its weak correlation to input signal,

what is an effect of nonlinear phase influence (Fig.4b). In Fig.3 we see the recovered signal y . Its correlation coefficient (to input s) is greater than 0.98. There is also evident a small Gaussian noise but it is unavoidable result of signal transmission through the band-pass filter. The other parameters of the experiment are as follows: the order of FIR filter $K=6$, the vector $\beta = [1 \ 1.15 \ 0.75 \ 0.31 \ 0.21 \ 0.20 \ 0.12]$. The correlation coefficient is calculated due to equation

$$r = \text{mean}(s^*y) / (\text{std}(s) * \text{std}(y)). \quad (10)$$

Up to now we do not use evidently the adaptive procedures. One is, however used within the matrix inversion algorithm C_H^{-1} . Moreover a simple adaptation loop is also applied in selecting the optimal order of FIR filter (K_{opt} for r_{max}).

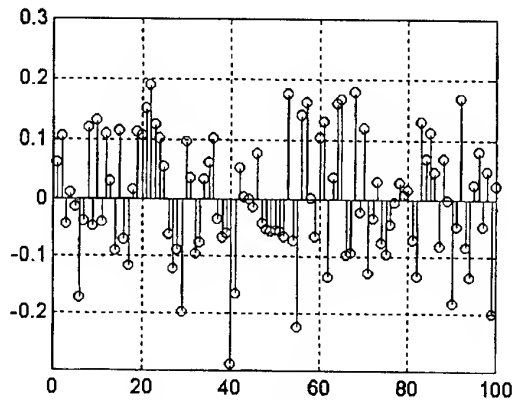


Fig. 8. An additive Gaussian noise

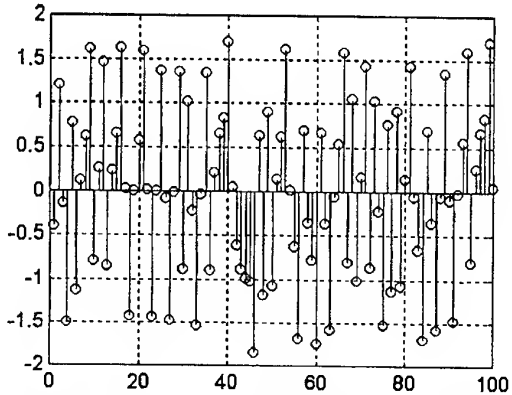


Fig. 9 A replica of binary series at the output of filter

4. FOUNDATIONS OF MOMENT METHOD

This method is aimed to large class of binary signals. As it is known, the odd order (central) moments of the typical binary series (equally likely distributions of ± 1 states) is equal zero, while the even order moments are equal 1. If we transfer such a binary series through an

all-pass filter, then its second moment at the output is also equal 1; because $H(z) = 1$. However, the forth order moment is no longer 1, and six order moment is much more higher than 1 (for uniform distribution $u(4)=1.8$ and $u(6)\approx 3.85$). Then the higher order moments may be used as a good criterion function in adaptation process: the lower the value of moment, the smaller the distance to the optimum, $u(4) \approx 1$. We will choose the so-called normalized forth order moment $\mu(4) = u(4)/u^2(2)$ to achieve the stable magnitude of signal during the transformation process [5].

The general scheme of deconvolution is the same as previously (Fig.1). The central normalized moment is calculated according to the following formulas

$$\begin{aligned} u(0) &= u = \frac{1}{N} \sum [y(n)] \quad n = 1, 2, 3, \dots, N \\ u(2) &= \frac{1}{N} \sum [y(n) - u]^2 \quad u(4) = \frac{1}{N} \sum [y(n) - u]^4 \\ \mu(4) &= u(4) / u^2(2) \end{aligned} \quad (11)$$

The transformation of signal $x(k)$ into $y(k)$ is done by
 $y(n) = \sum \beta(k)x(n-k) \quad k = 1, 2, \dots, K \quad (12)$

The iterative equation is as follows

$$\beta_m = \beta_{m-1} - \varepsilon \nabla_\beta(\mu) \quad (13)$$

where $\varepsilon = (1 - 1/M)^m$

$$\nabla_\beta(\mu) = [\partial\mu / \partial\beta_1, \dots, \partial\mu / \partial\beta_K] \quad (14)$$

$$\begin{aligned} \partial\mu / \partial\beta_k &\approx [4 / N\mu^2(2)] \sum [y(n) - u]^3 [x(n-k)] \\ &- [4\mu(4) / N\mu^3(2)] \sum [y(n) - u][x(n-k)] \end{aligned}$$

m - is an iteration number; M - the overall quantity of iterations; N - the quantity of signal samples

The procedure of deconvolution runs as follows. We take K random values of vector $\beta(k)$. Then we transform the distorted signal $x(n)$ in $y(n)$ due to eq. (12). On the basis of obtained $y(n)$ series the normalized moment $\mu(4)$ and its gradient ∇ are calculated due to eq. (11) and (14), resp. Then a new vector $\beta(k)$ is computed due to eq (13). By M repetition of this procedure it is possible to achieve nearly a full agreement between input s and output $y=s'$ series. The results are given in Fig. 6, 7, 8 and 9.

In Fig. 6 we see the input signal s , in Fig.9- its distorted counterpart x and in Fig.8- the noise n . The recovered signal s' is presented in Fig.7. We see there is a full consistency between s and s' , that is $r = \text{mean}(\text{sign}(s) * \text{sign}(s')) = 1$

6.CONCLUSIONS

Two methods of reconstruction of phase distorted and noise corrupted digital signals have been proposed.

The first cumulant function method is more general and brings the moderate degrees of reconstruction quality (correlation coefficient is of order 0.95). The second - moment function method is aimed especially to the class of binary signals. Here the degree of consistency may reach 1 for a heavy distorted and noise corrupted series. For all-pass filter ($H(z) = [-a+z^{-1}] / [1+az^{-1}]$, $a < 1$) the noise level may reach more than 40% of the signal level (7 dB) and thousands of bits may be processed in a fraction of minute without any error. For physical filters (low-pass, 3 dB) the results are yet better. The only weak point of the method is a phase ambiguity (starting series $\beta_0(k)$). This will be analyzed elsewhere [6].

7.REFERENCES

1. A. Swami and J. Mendel "Identifiability of AR parameter of ARMA process using cumulants" IEEE -Automatic Control, 37, 268-273, Feb 1992
2. A. Al-Smadi and D. Wilkes "On estimating ARMA model orders" IEEE Int. Symp. on Circuits and Systems '96, Atlanta, Georgia, May 1996
3. Higher-Order Spectral Analysis Toolbox, The Math Works Inc. 1995
4. S. Musial "Attenuation of radio signals in office buildings" Private communication 1998.
5. J. Cadzow "Blind deconvolution via cumulant extrema" IEEE Signal Processing Magazine, May'96
6. J. Pawelec "Adaptive deconvolution of binary noisy series" MILCOM '98 (in preparation)
7. S. Haykin "Blind deconvolution" Prentice Hall 1994

BIOGRAPHICAL NOTES



Jozef Pawelec is associate professor of Military Communication Institute -MCI (formerly -Military Academy of Technology -MAT). He received Ph.D. and Hab. degrees from MAT in 1975 and 1982, respectively. His main interests are: radio communication systems, reception techniques, noise cancellation and compatibility. Recently he has joined the group of adaptation methods and H.O.S. in MCI



Artur Przybysz received the M.S. degree from Military Academy of Technology in communications (1995). Since that time, he is with Military Communication Institute. His research interests include: reception techniques, signal processing and higher order statistics (HOS)

EMC BETWEEN AIRCRAFT ONBOARD ELECTRONIC EQUIPMENT AND SATELLITE EARTH STATIONS

Ryszard J. Zielinski

The Wroclaw University of Technology, Institute of Telecommunication and Acoustics
Wybrzeze St. Wyspianskiego 27, 50-370 Wroclaw, Poland
Phone +48 71 214 998, Facsimile +48 71 223 473, Email: Dick@zr.ita.pwr.wroc.pl

This paper provides an analysis of the risk of interference resulting from aircraft exposure to the main beam of a Satellite Earth Station (SES) of various types. Presented analysis aimed at determining: the path of the aircraft in the wanted radiation area, distance between the SES and the point at which the main beam of the antenna and the path of approach of the aircraft intersect, duration of aircraft travel through the wanted radiation area and levels of electromagnetic exposure experienced by an aircraft during landing approach.

1. INTRODUCTION

With the ever increasing use of very small aperture terminals (VSAT) and satellite news gathering transportable earth stations (SNG TES) - to say nothing of the general tendency to unify and simplify relevant licenses procedures - there is an urgent need to define the potential threats to aircraft passing through the main beams of such stations.

This paper provides a detailed analysis of the threats resulting from aircraft exposure to the main beam of a Satellite Earth Station (SES). Since some of the cases considered in our study pertained to the near-field zone of the antenna, we made use of the near-field radiation model described in [1]. The following SESs has been analysed:

- VSAT - typical terminal working in Skystar Plus system (GTE Spacenet Corp.),
- SNG - typical vehicle mounted SNG TES type VMA - 2.6/73/25 (Dornier GmbH),
- Hub VSAT - hub station of Skystar Plus system,
- fixed TV - large SES used for transmission of television signals by Polish TV.

Major parameters of these SESs are listed in Table 1. Their analysis aimed at determining the levels and duration of electromagnetic exposure experienced by an aircraft during landing approach.

2. AIRCRAFT EXPOSURE TO THE MAIN BEAM

To determine how long the aircraft is exposed to the main beam radiation of the SES antenna during landing, it is necessary to establish the beam width (angle 2γ in Fig. 2.2) and to know the path of approach when use of the instrument landing system (ILS) is made. For a given station type it is possible to define precisely the width of the area in which the field strength exceeds the set value [1].

Table 1. Basic parameters of the SESs

	VSAT	SNG	Hub VSAT	Fixed TV
Power P [W]	5	490	125	700
Aperture D [m]	1,8	2,6	5,6	9,0
Frequency f [MHz]	14,125	14,125	14,125	14,125
D/λ ratio	85	122	264	424

Beam width can also be defined in terms of the relations $\beta=2,442/D$ which describes the zero places of the radiation pattern for an antenna with a uniform field distribution in the aperture. But taking into account the need of analysing the least advantageous variant independently of the station parameters, we can determine the width of the wanted radiation area, using relevant international standards. The ITU-R 465-3 Recommendation for the radiation pattern of the SES antenna outside the main beam limits on the pattern envelope from the 1° angle to the beam axis. Thus, a 2° -wide area which has not been included in the recommendation, is conventionally adopted as the main beam area. The ITU-R 580-2 extends this angle to low-gain antennas. The area outside the main beam for antennas of a D/λ ratio varying between 35 and 100 begins with the angle of $100/(D/\lambda)^\circ$. According to the definitions of the ETS 300 159 ETSI standard for VSAT terminals and the ETS 300 327 standard for SNG TES, the area of wanted radiation has a width of 5° (2.5° from the axis of the main beam). As shown by these data, it is difficult to select one out of the recommended values which would best describe the main beam width. Such a choice is a compromise between the adoption of the highest possible number of potential cases that might occur and the best possible description of the real situation. From the considerations presented earlier it follows that, irrespective of the recommended value we have chosen, the beam, in fact, is always much narrower.

A SES produces particular threat to a landing aircraft which make use of the electronic landing system (ILS). Any interference that might affect the variety of measuring and receiving devices involved can lead to a catastrophe. For this reason, our analysis concentrates on this part of the flight.

Figure 2.1 shows a typical path of approach when the ILS is used. For the needs of analysis we adopted the most common elevation angle of the path of approach in the ILS, which amounts to $\phi=3^\circ$. Irrespective of its type, the aircraft becomes exposed to the beam of the ILS at the distance from 18 to 13 km (10 to 7 nm). At the height $h_{cr}=300$ m (1000 ft) the pilot has to decide whether he is landing or pulling off the machine. Once the decision has been made, the pilot cannot change it. And that is why this altitude is regarded as the most neuralgic point of the landing operation - misinformation coming from the deck part of the ILS may lead to a catastrophe. The height of 300 m has been taken to analyse the potentiality for a SES-induced interference to the ILS. For simplification, analysed is the location of the station on the extension of the airstrip, as shown in Fig. 2.2.

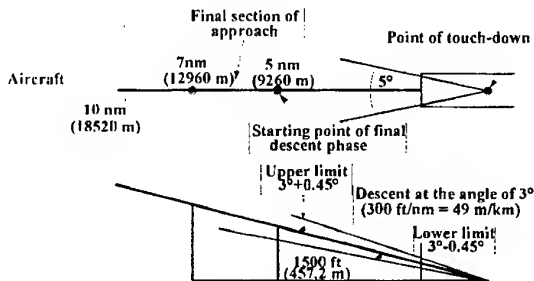


Fig. 2.1 Path of approach in the ILS.

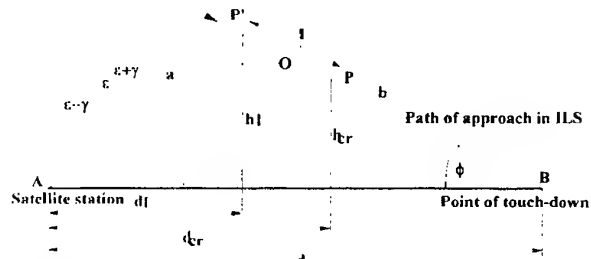


Fig. 2.2 Duration of exposure to the radiation in the main beam.

For the given value of h_{cr} from the ABP triangle, the distance d_{cr} and $d-d_{cr}$ can be calculated as follows:

$$d_{cr} = \frac{h_{cr}}{\tan(\varepsilon - \gamma)} \quad (2.1)$$

$$d - d_{cr} = \frac{h_{cr}}{\tan(\phi)} \quad (2.2)$$

The distance between the SES and the touch-down point is defined by

$$d = d_{cr} + \frac{h_{cr}}{\tan(\phi)} = \frac{h_{cr}}{\tan(\varepsilon - \gamma)} + \frac{h_{cr}}{\tan(\phi)} \quad (2.3)$$

To calculate the length of the path of approach getting into the area of wanted radiation it is necessary to consider two triangles which have a common side, ABP and ABP'. Thus the difference between the length of the side BP' and the length of the side BP describes the length l of the path which was to be found:

$$l = BP' - BP \quad (2.4)$$

The length of BP' and BP can be calculated by virtue of the law of sines:

$$BP' = \frac{d \sin(\varepsilon + \gamma)}{\sin(180^\circ - \phi - \varepsilon - \gamma)} \quad (2.5)$$

$$BP = \frac{d \sin(\varepsilon - \gamma)}{\sin(180^\circ - \phi - \varepsilon + \gamma)} \quad (2.6)$$

$$\text{Hence } l = d \left(\frac{\sin(\varepsilon + \gamma)}{\sin(180^\circ - \phi - \varepsilon - \gamma)} - \frac{\sin(\varepsilon - \gamma)}{\sin(180^\circ - \phi - \varepsilon + \gamma)} \right) \quad (2.7)$$

To determine the radiation level at the intersection point of the path of approach and the main-beam axis of the antenna we have to calculate the distance of the intersection point from the satellite station AO. After that, according to the type of the station, we have to read and take appropriate values from the earlier established plots of energy flux or field strength vs. distance curves.

The length of the side AO in the AOB triangle can be calculated in terms of the law of sines:

$$AO = \frac{d \sin(\phi)}{\sin(180^\circ - \phi - \varepsilon)} \quad (2.8)$$

The time of aircraft travel through the area of wanted radiation during landing approach is

$$t = \frac{l}{v} \quad (2.9)$$

where v denotes aircraft speed during approach. For the purpose of analysis we assumed that $v=77$ m/s (150 knots). We calculated two widths of the wanted radiation area for varying values of the antenna elevation angles ε . The results are plotted in Figs. 2.3, 2.4 and 2.5.

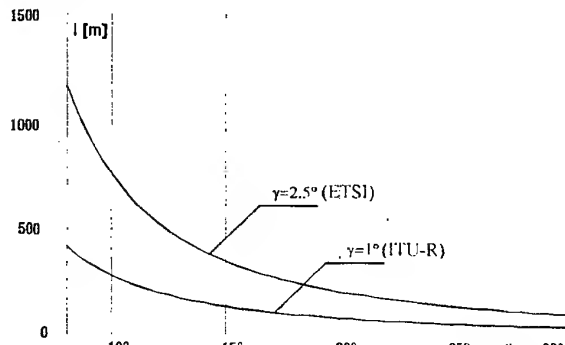


Fig. 2.3 Path of the aircraft in the wanted radiation area at beamwidth 2γ of 2° and 5° .

The calculated results show that the aircraft takes about 0.5 to about 5 s and about 1.25 to 15 s to travel through the wanted radiation area of 2° width and 5° width, respectively.

An exact determination of the time during which the aircraft travels through the main beam of the antenna requires consideration of the electrical parameters of the antenna (radiation pattern) which vary from one station type to another.

To achieve a better approximation it can be anticipated that the main beam is limited by the zero places of the radiation pattern. The width β of the beam defined via this route for an antenna with a uniform field distribution in the aperture is described by the relation $\beta=2.44\lambda/D$ (radians). Calculations were carried out

for a station characterised by the parameters of table 1. The results are plotted in Fig. 2.6.

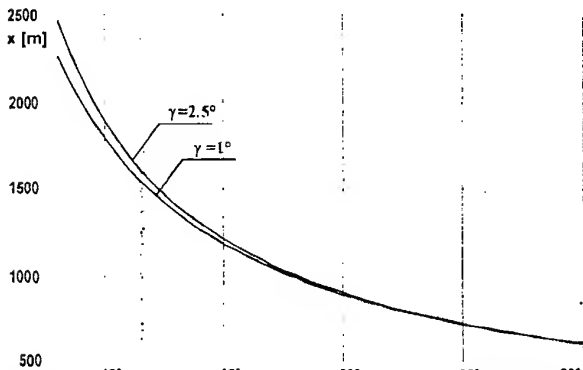


Fig. 2.4 Distance of the SES from the point at which the main beam of the antenna and the path of approach of the aircraft intersect.

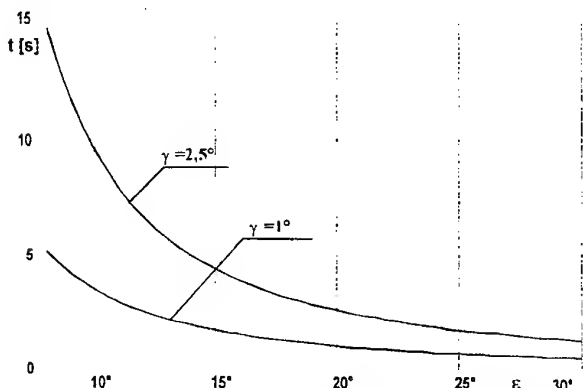


Fig. 2.5 Duration of aircraft travel through the wanted radiation area of the SES versus elevation angle of the antenna ϵ (for two widths of wanted radiation area, 2° and 5°).

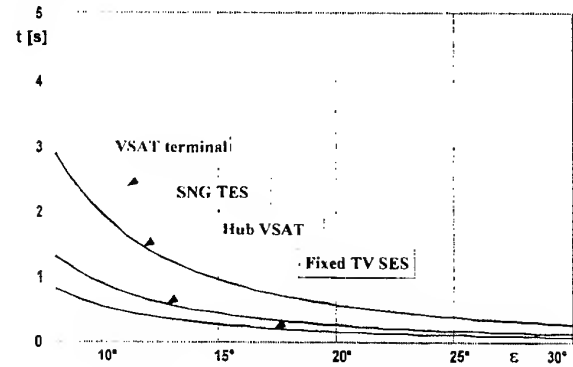


Fig. 2.6 Duration of aircraft travel through the main beam of the SES antenna.

3. ELECTROMAGNETIC FIELD IN THE MAIN BEAM OF THE ANTENNA

The member countries of the European Community direct their efforts towards a widespread application of VSAT and SNG systems by liberalising their licence policies. Operators providing such services have been authorised to install VSATs and SNGs wherever necessary or possible. Advertisements claim that such

systems can work at the user's or that they can provide communication from an arbitrary point in Europe (which is of importance in the case of SNG). Hence, it cannot be excluded that stations of that kind will be located at a point where the antenna „illuminates“ the path of approach immediately before reaching the critical height at which the pilot has to decide whether to land or to make a re-approach. For this phase of landing approach, the variations in the amplitude of the electromagnetic field strength (to which the aircraft is exposed) will be determined.

Taking into account the difference in field strength determination between the near zone and the far zone of the antenna radiation, the calculations will involve models for both the zones. If we use the far zone model, initial dissipation of energy in the antenna aperture becomes negligible. But if use is made of the near zone model, the physical dimensions of the antenna aperture must be considered.

3.1. Analysis of field strength distribution in the far zone

Figure 3.1 shows the geometry of the configuration which is used for analysing the field strength amplitude in the final section of the landing approach located in the far-zone of the SES antenna.

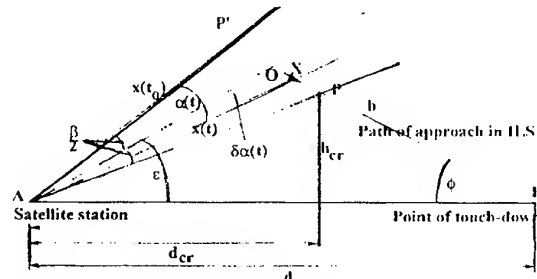


Fig. 3.1 Geometry of the configuration in the far zone (the antenna being a point source).

For the purpose of analysis it has been anticipated that the aircraft enters the area of the main beam determined by its upper edge (the station is a point source) at point P', time $t=t_0=0$, and distance $x(t_0)$ from the SES.

Energy flux density in the far zone can be expressed as:

$$S(t)_d = \frac{G_u(t)P_{cf}}{4\pi x^2(t)} \quad (3.1)$$

where $x(t)$ denote the distance to the point under analysis, and

$$G_u(t) = G_f F_{n,u}^2(t) \quad (3.2)$$

where G_i is antenna gain determined by virtue of $G_i = \left(\frac{\pi D}{\lambda}\right)^2$, and the standardised radiation pattern can

be calculated in terms of the following relation:

$$F_{n,u}(t) = 2 \left| \frac{J_1(u(t))}{u(t)} \right| \quad (3.3)$$

Function $\mu(t)$ takes the form of

$$u(t) = \frac{\pi D}{l} \sin(\delta\alpha(t)) \quad (3.4)$$

The distance $x(t)$ between the aircraft and the station varies with time and can be determined at an arbitrary point of time t :

$$x(t) = \sqrt{d^2 + (b - vt)^2} - 2d(b - vt)\cos(\phi) \quad (3.5)$$

The off-axis angle $\delta\alpha(t)$ can be defined in terms of the following conditions:

$$\begin{array}{lll} \text{if } \alpha(t) \leq \beta/2 & \text{then} & \delta\alpha(t) = \beta/2 - \alpha(t), \\ \text{if } \alpha(t) > \beta/2 & \text{then} & \delta\alpha(t) = -\alpha(t) - \beta/2. \end{array}$$

where:

$$\alpha(t) = \arcsin\left(vt \frac{\sin\left(\pi - \varepsilon - \frac{\beta}{2} - \phi\right)}{x(t)}\right) \quad (3.6)$$

The relationship between field strength in the far zone and energy flux density is defined as $E = \sqrt{120 \cdot \pi \cdot S}$.

3.2. Analysis of field strength distribution in the near zone

Figure 3.2 presents the geometry of the configuration which is used for analysing the field strength amplitude in the final section of the landing approach located in the near zone of the SES antenna. The condition that the lower edge of the beam should pass through the critical point P must be fulfilled.

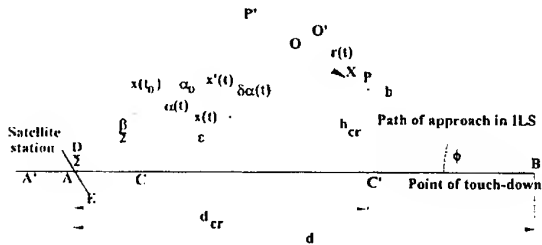


Fig. 3.2 Geometry of the configuration in the near zone (antenna of an aperture diameter D).

The maximum energy flux density S_{max} in the cross-section situated at distance $x'(t)$ from the antenna is defined by the relation [1]

$$S_{max}(x) = \frac{12}{\pi} \frac{P_{ef}}{D_{oo}(x)^2 + D_{ef}(x)D_{oo}(x) + D_{ef}(x)^2} \quad (3.7)$$

The energy flux density $S(r)$ at a distance r from the main beam can be calculated as follows [2]:

$$S(x_o, r) = S_{max}(x_o) \quad \text{for } r \leq D_{ef}/2 \quad (3.8)$$

$$S(x_o, r) = 2 \frac{S_{max}(x_o)}{D_{oo}(x_o) - D_{ef}(x_o)} \left(\frac{D_{oo}(x_o)}{2} - r \right) \quad (3.9)$$

for $D_{ef}/2 < r \leq D_{oo}/2$

after having determined the values of $D_{oo}(x'(t))$ and $D_{ef}(x'(t))$ [1].

When use is made of the field strength distribution model for the near zone, it is necessary to know the distance $x'(t)$ (AO') from the antenna to the cross-section in which the analysed point is found, as well as the distance $r(t)$ ($O'X$) from this point to the beam axis. These values can be obtained by virtue of

$$x'(t) = x(t)\cos(\delta\alpha(t)) \quad (3.10)$$

$$r(t) = x(t)\sin(\delta\alpha(t)) \quad (3.11)$$

where:

off-axis angle $\delta\alpha(t)$ of the aircraft position at time t is defined by the following conditions:

$$\text{if } \alpha(t) \leq \alpha_0 - \varepsilon \quad \text{then} \quad \delta\alpha(t) = \alpha_0 - \varepsilon - \alpha(t),$$

$$\text{if } \alpha(t) > \alpha_0 + \varepsilon \quad \text{then} \quad \delta\alpha(t) = -\alpha(t) - \alpha_0 + \varepsilon,$$

where:

$$\alpha(t) = \arcsin\left(\frac{vt}{x(t)} \sin(\pi - \alpha_0 - \phi)\right) \quad (3.12)$$

$$\alpha_0 = \arcsin\left(\frac{b}{x(t_0)} \sin(\phi)\right) \quad (3.13)$$

$$x(t_0) = \sqrt{AA'^2 + a^2 - 2AA'ac \cos\left(\varepsilon + \frac{\beta}{2}\right)} \quad (3.14)$$

4. RESULTS OF SIMULATION

Making use of the models described in an earlier paper [1], calculations were carried out for SESs characterised by the parameters listed in Table 1. Two elevation angles ε were adopted, 30° and 10° . These are, respectively, the approximately maximum and the approximately minimum elevation angles for the SESs located throughout Poland and co-operating with geostationary satellites [3]. Figures 4.1a to 4.3a show the calculated results obtained with the 30° elevation angle values. Figures 4.1b to 4.3b provide the distance between the antenna and the points under analysis. Included are also the distances to the far zone. The speed with which the aircraft travels during landing approach was assumed to be 77 m/s (about 280 km/h) in every instance.

SNG TES differ from one another in their electrical parameters. Hence, there might be doubt whether or not the parameters of the Dornier station (which is the subject of analysis) can be regarded as typical. A Dornier station is installed on a Mercedes chassis and serves for the transmission of TV signals. Stations of "fly-away" type are also made use of in SNG but their design makes them suitable for air transport. Another type of SNG serves for voice transmission alone. Such stations involve comparatively small antennas (e.g. umbrella-like in shape) and produce low-energy radiation. Their electrical parameters are similar to those of the VSATs. And that is why the result obtained for the SNG station under analysis are not valid for every type of stations belonging to that category.

As far as the SNG TES is concerned, the points of interest were located in the near zone at the elevation angle of 30° . The maximum value of the electric field strength is 42 V/m, whereas the duration of aircraft exposure to the main beam is 0.35 s.

When analysing the radiation levels produced by the hub station of the VSAT system, we made use of the parameters of the station which had been installed at TS S.A. Bielsko-Biala, Poland. The station is classified as a large one. In engineering, hub stations of a VSAT system are smaller, both in antenna size and in radiated energy. In that particular case it is also

inadvisable to regard the adopted parameters as being typical.

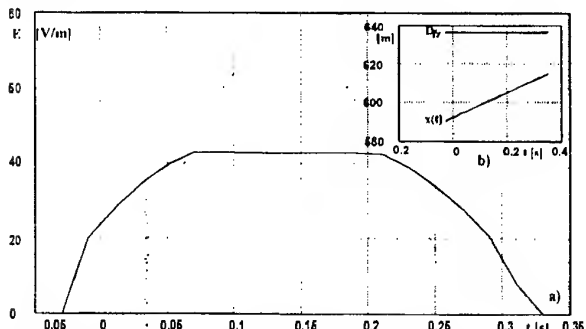


Fig. 4.1 a) Amplitude of electromagnetic field strength during aircraft travel through the main beam - a typical SNG TES ($\varepsilon=30^\circ$), b) distance $x(t)$ to the analysed points and distance D_{fZ} to the far zone.

The hub station of the VSAT system analysed in this study had the points of interest in the near zone. The maximum value of the electric field strength is 25 V/m, whereas the time of aircraft exposure to the main beam is 0.26 s.

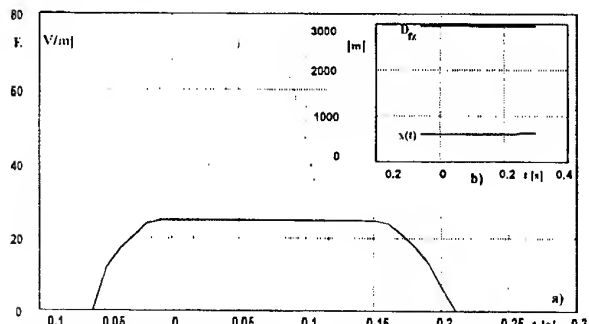


Fig. 4.2 a) Amplitude of electromagnetic field strength during aircraft travel through the main beam - a VSAT hub station ($\varepsilon=30^\circ$), b) distance $x(t)$ to the analysed points and distance D_{fZ} to the far zone.

To determine the level of radiation produced by a fixed satellite station which serves for the transmission of TV signals we adopted the parameters of the station located at J.P. Woronicza Street, Warsaw, Poland.

The points under analysis were situated in the near zone. The maximum value of the electric field strength is 50 V/m, whereas the duration of aircraft exposure to the main beam is 0.3 s.

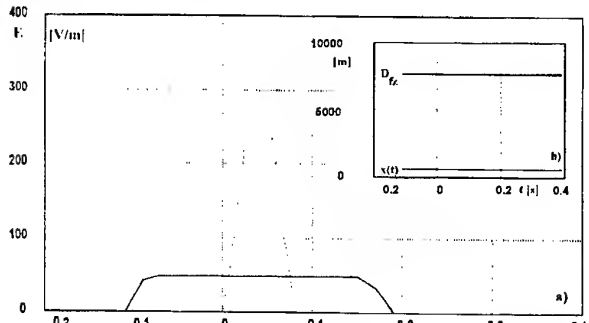


Fig. 4.3 a) Amplitude of electromagnetic field strength during aircraft travel through the main beam - a typical fixed TV satellite station ($\varepsilon=30^\circ$), b) distance $x(t)$ to the analysed points and distance D_{fZ} to the far zone.

Compared to the vulnerability levels of the electronic equipment on board, the values of the maximum field strength obtained for all three examples were of the same order. This is an indication of a serious threat of such satellite stations to air traffic. This finding has been taken seriously by some European countries, and adequate authorising procedures for transmitting station operators have been implemented [9]. Problem of the VSAT terminals has been discussed in [5].

5. REFERENCES

- [1] Bem D.J., Janiszewski J.M., Więckowski T.W., Zieliński R.J., „Simple model of reflector antennas for evaluation power flux density in the vicinity of antenna for EMC purposes” (English), 13th International Wroclaw Symposium and Exhibition on EMC, Wroclaw, Poland, 25-28 June 1996, pp. 419 - 424.
- [2] Bem D.J., Janiszewski J.M., Więckowski T.W., Zieliński R.J., „Coordination of Satellite Earth Station with aeronautical services and airborne equipment” (English), 12th International Wroclaw Symposium and Exhibition on EMC, Wroclaw, Poland, June 28, July 1, 1994, pp. 466 - 471.
- [3] Zieliński R.J., „Satellite Earth Stations with small antenna (VSAT) as a source of interference” (English), 12th International Wroclaw Symposium and Exhibition on EMC, Wroclaw, Poland, June 28, July 1, 1994, pp. 235 - 239.
- [4] Zieliński R.J., „EMC analysis of Satellite Earth Stations with small antenna (VSAT)” (English), Euro Electromagnetics - EUROEM '94, Bordeaux, France, May 30-31, June 1-2-3, 1994, pp. 702 - 709.
- [5] Zieliński R.J., „Risk of interference to aircraft from VSAT and SNG terminals”, Euro Electromagnetics - EUROEM'98, Tel-Aviv, Israel, June 14 - 19.
- [6] Colwell B., „Earth Stations/Aircraft Instrument Landing System EMC study” (English), Final Report, ERA Technology, March 1992.
- [7] Stevens E.G., Watkins P.J., „EMC study phase II - Earth Station/Aircraft Instrument Landing Systems” (English), Archival Report, ERA Technology, April 1993.
- [8] „Site Clearance Manual of Code of Practice No. 1, The Clearance Procedure Followed in Order to obtain authorisation for operation of Transportable Earth Stations and Mobile Satellite Terminals”, RA 172, August 1991, Radiocommunications Agency, United Kingdom.

BIOGRAPHICAL NOTE

Ryszard J. Zieliński received the M.S. and Ph.D. degrees in Telecommunications from the Wroclaw University of Technology in 1978 and 1984, respectively. He has been involved in electromagnetic compatibility issues e.g. spectrum management, methods of measurement broadcasting antennas, emc of ITE, emc in satellite systems. Currently his main interest is in VSAT networks. He actively participates in the international standardization works of ETSI as an expert and member of TC SES. He is a member of Organizing Committee of The Wroclaw EMC Symposium and Polish Electrical Engineers Association. Mr Zieliński is the author of some 40 papers and publications.

DESIGN PROCEDURE OF ELECTROMAGNETIC FIELDS SHIELDING EFFECTIVENESS

Zinkovsky Yu.F., Klimenko V.G., Pilinsky V.V.

National Technical University of Ukraine «Kiev Polytechnic Institute» 37 Peremogy Av. 252056, Kiev-56, Ukraine

The approach to the calculation of shielding factor in the near field is considered. The process of diffuse interaction of electromagnetic fields with the metallic materials of the shields is the basic here. The streams of electrons are involved by the shielding fields into the semichaotic movements, that forms weakly chanalized eddy currents, providing shielding effect. The numerical methodics to calculate shielding factor are developed.

1. INTRODUCTION

Dimensions of components and equipment devices allow to estimate the processes within equipment on the frequencies from hundreds kHz up to tens GHz having reactive nature. Therefore near field processes should be considered.

«Wave» analytical methods in quasistatic and electrodynamic shielding modes (electromagnetic shielding) become semianalytical or approximate ones, their results being badly conformed with experimental data (overestimated values of shielding factor or very small thickness of shield, etc.).

To increase shielding efficiency the methods of numerical fields simulation were developed. The numerical models of processes are adapted to approach for program models and computer-aided simulation. These models allow to investigate the processes into the depth of shields material. The accuracy of simulation can be increased by means of increasing level of discretization which is limited by the computer's RAM [1, 2].

2. THEORETICAL PART

Let us consider simulation of shielding process for the most typical conditions, when closed shields, made of nonmagnetic metallic material, and components, being shielded (HF coils) are coaxial situated. The axial symmetric system in two dimensions is considered.

Let us separate in the shield section the circular line via points with axial coordinates (R, ϕ, z), via which a circular line of current runs along, having length l_q and radius R_q with the center on the axis z (fig1).

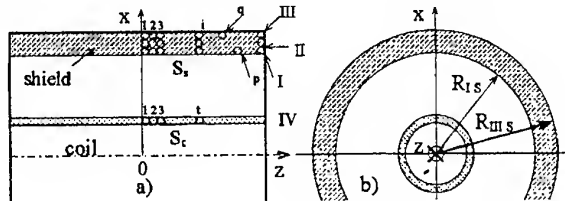


Fig 1. The sections of the system - HF-coil within the shield (a) and side view (b):

I - near boundary of the shield, II - shield, III - distant boundary of the shield, IV - coil being shielded, n - number of layers for shield model, q, p - discrete elements of the shield model, S_s, S_c - cross sections of shield and coil, accordingly, $R_I s$ - inner radius of the shield, $R_{III} s$ - outer radius of the shield.

For complex value of the density of current J in the point q it is possible to write:

$$\rho_q * J = E_q, \quad (1)$$

where E_q - electric intensity along the line l_q , ρ_q - specific resistance of shield material in the point q .

Let us separate circular elements p in the shield and t in the coil with small sections accordingly. Then for the ring l_q of the shield in accordance with the Kirchhoff's law it is possible to write an equation:

$$2\pi R_q E_q = -j\omega (M_{qp} J_p \Delta S_p + M_{qt} J_q \Delta S_t), \quad (2)$$

where M_{qp}, M_{qt} - factors of mutual inductance of rings l_q, l_p, l_t ; R_q - rings radius; $\Delta S_p, \Delta S_t$ - elementary sections of shield and coil.

Substituting (1) to (2) and integrating along sections of shield S_s and coil S_c , we obtain integral Fredholm's equation of the second kind relative to unknown density of eddy current

$$2\pi R_q \rho_q J_q + j\omega \int_{S_s} M_{qp} J_p dS_p = -j\omega \int_{S_c} M_{qt} J_t dS_t. \quad (3)$$

If configuration of both coil and shield and current density are known $J_t = I_c w / S_c$ (I_c - complex quantity of the current in each turn; w - coil turns), then kernel of integral equation (3) M_{qp} and free term

$$f_q = -j\omega \int_{S_c} M_{qp} J_p dS_p \quad (4)$$

are known functions. Then substituting (4) into (3), we obtain:

$$2\pi R_q \rho_q J_q + j\omega \int_{S_s} M_{qp} J_p dS_p = f_q. \quad (5)$$

So far as there are reflected impedance from shield to coil, then current density distribution along the section of the coil is unknown. Then, distributing discrete points p and q to the coil, transform (3) to the equation

$$2\pi R_q \rho_q J_q + j\omega \int_{S_s} M_{qp} J_p dS_p = \mathcal{E}_q, \quad (6)$$

where \mathcal{E}_q - circular EMF for the ring l_q . Value of \mathcal{E}_q is equal to zero for all rings within shield, and in the coil $\mathcal{E}_q = \mathcal{E}_{HF}/w$, where \mathcal{E}_{HF} - feeding HF EMF of the coil being shielded.

When integral equations (3), (6) are being solved, it's necessary to calculate mutual inductance factors M_{qp} for coaxial rings. There are detailed tables and formulas for the circular rings of cylindrical shields [3].

The method of numerical solution for integral equation (6) is a replacement the integral by the sum as a result of discretization the area S_s by squares ΔS_q , in which the condition $J_q = \text{const}$ takes place. It gives the system of algebraic equations:

$$r_q I_q + j\omega \sum_s M_{qp} I_p = \mathcal{E}_q, \quad (7)$$

where $r_q = 2\pi \rho_q R_q / \Delta S_q$ - active resistance of ring l_q ; I_q , I_p - currents in the rings l_q and l_p accordingly.

Taking into consideration an axial-symmetrical type of the shielding problem on RF, it is possible to perform discretization of the sections S_s , S_c by the squares ΔS_q , localized by definite geometrical places as concentric cylindrical surfaces (strait lines in section), satisfying equations $R_q = \text{const}$, $z > 0$ (fig. 1). It gives possibility to result the task of field simulation to one-dimensional variant of summarizing by linear element of sections S_s , S_c

$$r_q I_q + j\omega \sum_l M_{qp} I_p = \mathcal{E}_q; \quad l \in S_s, S_c \quad (8)$$

and to obtain a set of algebraic equation of lower order in matrix form:

$$I * Z = \mathcal{E}, \quad (9)$$

were:

$$I = \begin{bmatrix} I_{p1} & I_{q1} & I_{n1} & I_{f1} \\ \vdots & \vdots & \vdots & \vdots \\ I_{pk} & I_{qk} & I_{nk} & I_{fk} \end{bmatrix}, \quad \mathcal{E} = 0, \mathcal{E}_q,$$

$$Z = \begin{bmatrix} r_{p1} & j\omega(M_{12}^p \dots M_{1k}^p M_{21}^{q_1} \dots M_{1k}^{q_1} M_{21}^{f_1} \dots M_{1k}^{f_1}) \\ \dots & \dots \\ r_{pk} & j\omega(M_{k1}^p \dots M_{kk}^p M_{k1}^{q_k} \dots M_{kk}^{q_k} M_{k1}^{f_k} \dots M_{kk}^{f_k}) \\ \dots & \dots \\ r_n & j\omega(M_{12}^f \dots M_{1k}^f M_{21}^{q_1} \dots M_{1k}^{q_1} M_{21}^{f_1} \dots M_{1k}^{f_1}) \\ \dots & \dots \\ r_k & j\omega(M_{k1}^f \dots M_{kk}^f M_{k1}^{q_k} \dots M_{kk}^{q_k} M_{k1}^{f_k} \dots M_{kk}^{f_k}) \end{bmatrix}$$

Taking into consideration correlation between densities of currents, currents and field intensities in circular elements, shielding factor is determined:

$$B_q = E_q / E_{qIII} = J_q / J_{qIII} = I_q / I_{qIII}, \quad (10)$$

where E_q , J_q , I_q , E_{qIII} , J_{qIII} , I_{qIII} - fields intensities, densities of eddy currents, eddy currents in circular elements accordingly, which are situated symmetrically on inner and outer surfaces of shield.

Substituting (6) into (10), it is possible to obtain integral form expression for shielding factor

$$B_q = \frac{(\mathcal{E}_q - j\omega \int_{S_s + S_c} M_{qp} J_p dS_p) R_{qIII}}{(\mathcal{E}_q - j\omega \int_{S_s + S_c} M_{qIII} J_p dS_p) R_{qI}}, \quad (11)$$

where R_{qIII} and R_{qI} - inner and outer radius of cylindrical shield.

Taking into account axial symmetry of the systems task conditions, it is possible to obtain numerical model of shielding factor as expression

$$B_q = \frac{(\mathcal{E}_q - j\omega \sum_{l_1} M_{qp} I_p) r_{qIII}}{(\mathcal{E}_q - j\omega \sum_{l_m} M_{qIII} I_p) r_{qI}}, \quad (12)$$

where r_{qI} , r_{qIII} - active resistance's of inner and outer circular element, l_1 , l_m - inner and outer perimeter lines of the shield section S_s .

Numerical model (12) may be represented in form, suitable for computer calculation.

3. METHODICS OF COMPUTER SIMULATION

Model of the coil is formed as a system of linear equations (9), where $Z = [z_{ij}]$ - square matrix of circular impedance's of the coil and shield;

$\mathcal{E} = [\mathcal{E}_1, \mathcal{E}_2, \dots]^t$ - vector of circular EMFs, which is equal to zero for shield rings and nonzero for coil rings; $I = [I_1, I_2, \dots]^t$ - vector of the currents in the rings of coil and shield, to be found.

Matrix Z contains the coefficients of the equations set in the form:

$$(r_q + j\omega L_q)I_q + \sum_{p=1; p \neq q}^k (r_p + j\omega M_{qp})I_p = E_q, \quad (13)$$

where r_q - resistance of the q -th ring; I_q , I_p - the currents of q -th and p -th ring accordingly; E_q - rings EMF; k - total number of rings (points of discretization) of the shield and coil.

Self-inductance of the circular ring with rectangular section is determined:

$$L = \mu_0 R \{ \ln[8R/(a+b)] - 0.5 \}, \quad (14)$$

where μ_0 - magnetic constant; R - mean radius of the ring; a , b - thickness and width of the ring.

Mutual inductance of near situated coaxial circular outlines of the same radius is determined by expression:

$$M = \mu_0 R [(1+3\xi^2/4-15\xi^4/64+35\xi^6/256+\dots) \ln(4/\xi) - 2\xi^2/4+31\xi^4/128-274\xi^6/1536+\dots], \quad (15)$$

where $\xi = x/2R \ll 1$, x - distance between mean lines.

Mutual inductance of far situated outlines of the same radius:

$$M = \mu_0 \pi R \gamma^3 (1-3\gamma^2/4+75\gamma^4/128-\dots-245\gamma^6/512+6615\gamma^8/16386-\dots)/16, \quad (16)$$

where $\gamma = 2R/x = 1/\xi$.

Mutual inductance of coaxial circular outlines with nonequal radiiuses:

$$M = \mu_0 \pi (2 \cdot R_1 \cdot R_2)^{1/2} q^{3/4} \{ 1 + q^2/4 + 2q^4/64 + \dots + A_n q^{2n} + \dots + q/2 + 3q^3/16 + \dots + (2n+1)A_n q^{2n+1}/[2(n+1)] \} / (1+q)^{1/2}, \quad (17)$$

where $q = [(b_1^{1/2} - b_2^{1/2})/(b_1^{1/2} + b_2^{1/2})]^2$; $A_n = \{(1 \cdot 3 \cdot 5 \dots [2n-1])/(2 \cdot 4 \cdot 6 \dots 2n)\}^2$.

Mutual inductance of circular rings with angle (θ) between planes of rings:

$$\begin{aligned} M = & (\pi/2) \mu_0 \delta R_2 \{ P_1(\cos\theta) + [3\delta^2 P_3(\cos\theta)]/8 + \\ & + [15\delta^4 P_5(\cos\theta)]/64 + [175\delta^6 P_7(\cos\theta)]/1024 + \dots + \\ & + [(2n!)^2 (2n+1) \delta^{2n} P_{2n+1}(\cos\theta)]/[2^{4n} (n!)^4 (n+1) + \dots] \}, \quad (18) \end{aligned}$$

where R_1 , R_2 - large and small ring radiiuses; $\delta = R_2/R_1 < 1$; $P_1(\cos\theta)$, $P_2(\cos\theta)$, ... - Legandre polynoms.

At $\theta = 0$ $P_i(\cos\theta) \equiv 1$ ($i = 1, 2, 3, \dots$), then expression (18) transforms to:

$$\begin{aligned} M = & (\pi/2) \mu_0 \delta R_2 [1 + 3\delta^2/8 + 15\delta^4/64 + 175\delta^6/1024 + \dots + \\ & + (2n!)^2 (2n+1) \delta^{2n} / (2^{4n} (n!)^4 (n+1) + \dots)]. \quad (19) \end{aligned}$$

Algorithm diagram of coil with the shield modeling is presented in fig. 2.

Block 1: input of frequency, dimensions and parameters of the coil with shield:

R_{oc} , R_{os} - initial dimensions of the coil and shield accordingly;

N_{lc} , N_{ls} - number of layers of the coil and shield; N_{rc} , N_{rs} - number of rings in a layer of coil and shield; H_{rc} , H_{rs} - height of the rings of coil and shield; D_{rc} , D_{rs} - width of the rings of coil and shield.

Block 2: the model of the coil as extended matrix of impedance's Z (9); calculation of mutual inductance's (15...19).

Block 3: solution of the system of linear algebraic equation by the method of Hauss elimination.

Block 4: the investigations results - values of currents in coil's and shield's rings as well as shielding factor dependence's from the number of rings in a layer of coil and shield.

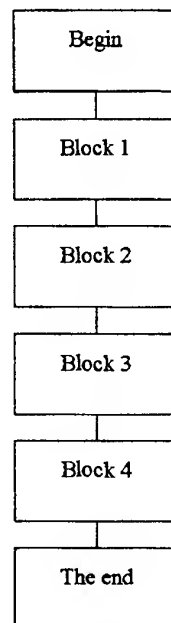


Fig. 2. Generalized algorithm diagram of the methodics.

4. RESULTS & CONCLUSION

Experiments were carried out on breadboard models in quasistatic and electrodynamics modes at frequencies from tens kHz up to some hundreds MHz.

An example of application of the proposed methodics is illustrated in fig. 3: the variation of shielding factor B from the number N_r of the shield layer, which is measured from the center of a system: shield - HF-coil. As the shield the cylinder of aluminium alloy with height about 20 mm and thickness 1 mm was used; HF - coil parameters: diameter and height - 10 mm. The calculations were performed within frequency range 30 kHz - 3 GHz.

Experimental investigations of the coil without ferrite core, with single - layer and multiplex - layer windings at frequency 465 kHz give the results, corresponding to simulation.

With the methodics described it is possible to

calculate the shields reactions, Q changing, resistance's and reactance's of the circuits with great accuracy.

The method advantage consists in possibility to define shielding factors of inhomogeneous materials, taking into account gaps and holes. The accuracy of such calculation is much more then with the traditional methods.

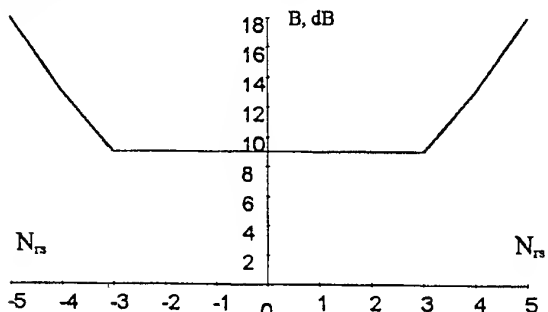


Fig.3. Dependence of shielding factor B from number of rings N_r in shield layer by axis z.

4. REFERENCES

1. O. V. Tozoni «The computer methods of analysis of electromagnetic fields» (Rus), Kiev, Technics, 1967.- 252 p.
2. Yu. F. Zinkovski, V. G. Klimenko, «Investigation of the processes of diffuse interaction of electromagnetic fields and the shielding» (Rus), Izvestija VUZov - Radioelectronics, №5, 1994; pp. 18-24.
3. P. L. Kalantarov, L. A. Ceytin «Calculation of coils». - (Rus.), L.: Energy, 1970. - 416 p.

BIOGRAPHICAL NOTES

Zinkovsky Yuri - Doctor of Science, professor, Head of Department of Radioengineering at National Technical University of Ukraine «Kiev Polytechnic Institute». He was graduated from NTUU KPI in 1956; PhD - 1964. , DSc - 1974, Professor - 1981; Meritorious worker of Science and Technology of Ukraine -1989; Laureate of State Prize of USSR - 1976. He is the author of 270 works, his science interests are in area of radioengineering.

Klimenko Vadim - Assistant professor of the Department of Radioengineering of National Technical University of Ukraine «Kiev Polytechnic Institute». He was graduated from NTUU KPI in 1965, PhD - 1975. His science interests are in area of radioengineering. He is the author of about 70 works.

Pilinsky Vladimir – Professor of the Department of Audio Technics and Registrations of Information, was graduated from Kiev Polytechnic Institute in 1963; PhD - 1973, Professor - 1993. Area of science interests: Power Electronics, Telecommunications, Electromagnetic Compatibility (EMC), CAD Electronics Systems with EMC support. He is the author of about 200 works including 6 books; He is the Head of Power Supply Group and Member of EMC Section of Scientific Technical Society for Radiotechnology, Electronics and Telecommunications of Ukraine, Member of Audio Engineering Society and IEEE EMC Section.

VII

EMC PREDICTION, ANALYSIS AND MODELING

**Computational Electromagnetics
in Wireless Personal Communications**

Invited session organized by

Prof. A. Karwowski - Poland

SUBGRIDDING SCHEME IN FDTD METHOD TO IMPROVE THE FIELD RESOLUTION

S. CHAILLOU*, J. WIART, Z. ALTMAN, W. TABBARA

*stephane.chailiou@cnet.francetelecom.fr

ABSTRACT

A new subgridding approach based on mesh nesting is presented. This scheme is numerically stable, accurate, easy to implement and allows high reduction factor. The stability and accuracy of the approach are illustrated by analyzing the scattered near field from a conducting sphere and the field near a radiating dipole.

1. INTRODUCTION

Since the late sixties the Finite Difference Time Domain (FDTD) [1] has been extensively used to solve various problems in electromagnetic. A major drawback of the standard uniform FDTD is its difficulty to handle geometries with fine structures since a dense mesh is required all over the computational domain, which often implies unrealistic memory requirements. To overcome this problem two avenues can be considered : the non-uniform FDTD and the subgridding method for the local mesh refinement in conjunction with the FDTD. The non-uniform FDTD is easy to implement however it is still limited [2]. The main advantage of the subgridding method is its ability to locally improve the field resolution, without modifying the rest of the computational domain. Thus, it enables us to considerably reduce the memory and computational time requirements for various problems with fine structures.

In the last few years, several techniques have been developed to include locally refined mesh in the FDTD. In 1981 Kunz and Simpson [3] have introduced a method to model small objects based on a double run approach. Later on the subgridding method has been introduced, and different techniques have been developed to recover the missing components at the interface between the coarse and the local meshes, based on the wave equation [4 - 6], the matrix approach [7], and Courant Law [8].

Recently, several subgridding techniques based on interpolation schemes have been proposed. Okoniewski and Stuchly [9] have developed a technique based on interpolations in space and time with an offset of the local grid. Chevalier and Luebbers [10] have introduced the co-located fields. In both cases the idea is to reduce the number of interpolations to minimize the error. In [8, 10] it has been proposed to reduce the error

due to interpolation process by smoothing the fields at the interface using weighting operations.

In most of the subgridding algorithm described in the literature the reduction factor is still limited. The purpose of this paper is to present a stable and accurate subgridding technique based on nested submeshes which allows a high reduction factor of 16. The performances of this scheme are illustrated through two examples of near field calculations.

2. IMBRICATION SUBGRIDDING TECHNIQUE

The building block of the nested subgridding scheme we propose in this paper is based on Okoniewski scheme [9]. This scheme has been chosen for its low reflection coefficient even with simple linear interpolations. It uses a reduction factor of two which is insufficient in some applications where objects with fine structures are present.

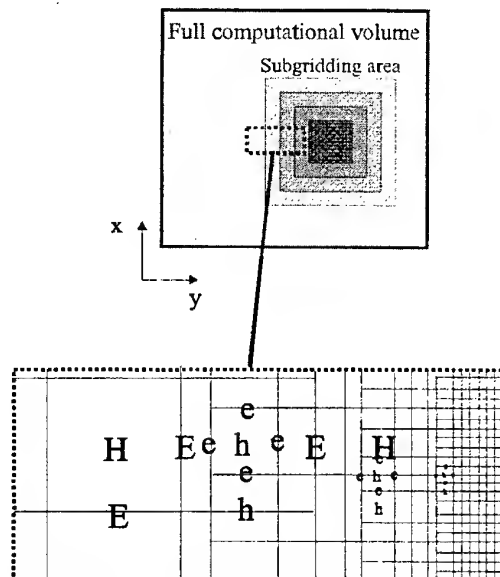


Fig. 1. Nested mesh configuration.

We have found that the error due to the local grid in Okoniewski's scheme decreases with the reduction of the cell size. This feature has motivated us to develop an nested subgridding technique based on nested meshes as shown on Figure 1.

The nested subgridding technique consists in adding local grids one into another, thus permitting to multiply by two the reduction factor for each extra local grid. A few cells are left between each nested grid so that the use of the standard FDTD between each local grid operates as a kind of weighting operator that ensures the stability and the accuracy of the scheme.

To analyze the scheme we consider a local mesh of $20 \times 20 \times 20$ cells inside a coarse mesh of $30 \times 30 \times 30$ cells. The local mesh is illuminated by a TE incident plane wave perpendicular to one of its faces that is generated by a Huygens box surrounding it. The proposed scheme has been tested up to 60,000 time steps where it was still stable for four nested grids which means a reduction factor of 16. To evaluate the accuracy of the scheme we have calculated the reflection coefficient (RC) from the subgridding volume. The reflected E-field is sampled outside the Huygens box. The magnitude of the RC depends on the spatial and time steps. The test has been performed for a spatial step of $\lambda/10$ which is the worst case.

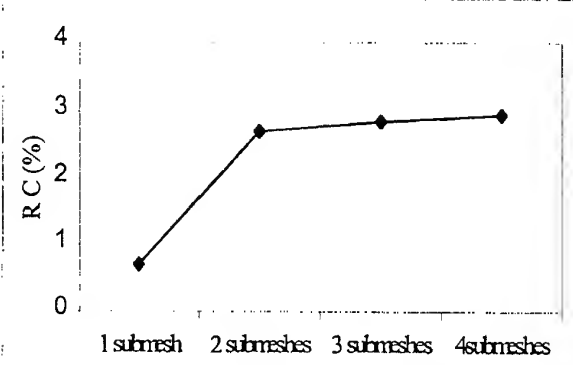


Fig 2. Reflection Coefficient for various nested grids.

Figure 2 shows the behavior of the error due to successive nested grids. As expected, we can see that additional error due to each new nested grid decreases rapidly. We have also analyzed the influence of the number of cells between each nested grids. In the previous test, we left three cells on each side of each nested grid. For a number of cells superior to three, the behavior of the RC is similar so it is useless and costly in memory to use more than three cells. Numerical experiments show that the scheme becomes unstable for less than three separating cells between each nested grid. For a reduction factor of 32 we have noticed that instability appears after 20,000 time steps of the main grid.

3. NEAR FIELD CALCULATION

To illustrate and validate the nested subgridding scheme we analyze two examples : scattering from a perfect conducting sphere and the near field calculation of a $\lambda/2$ dipole.

3.1 Scattered near field from a conducting sphere

In the first example we consider a conducting sphere of 2 cm diameter which is about $\lambda/16$. The sphere is placed inside a Huygens box which generates a sinusoidal plane wave at 900 MHz propagating along the X axis. The sphere is successively meshed for a reduction factor of 4, 8 and 16 with the same main grid. The results for the field magnitude are presented in Figure 3.

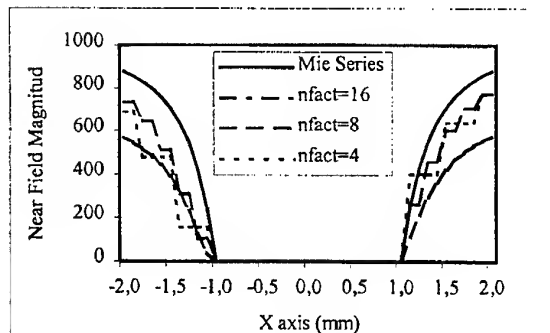


Fig 3. Scattered near field from a perfect conducting sphere centered at the origin. The scattered field is calculated using the nested subgridding method using different reduction factors, 4, 8 and 16, and an analytical solution.

The results obtained from the subgridding technique are compared with analytical results obtained using the Mie series. We note that the error is minimal for a reduction factor of 8. The error for a reduction factor of 4 is more important since the mesh is not fine enough to accurately describe the sphere.

For a reduction factor of 16 the error due to the high reduction factor becomes predominant in the sense that the gain in accuracy due to further refining the mesh cannot compensate the additional error. This example shows the duality between the interest of a high reduction factor and the error it entails.

3.2 Near Field of a dipole

In the second example we compare the near radiating field of a half wave length dipole at 900 MHz to quantify the error due to the local grids. The results using the nested subgridding method with a reduction factor of 16 is compared with those obtained using the standard FDTD with a mesh size of $60 \times 60 \times 250$ cells and a cell size of 1 mm corresponding to that of the local grid. The dipole is located at the center of the inner nested mesh, with a size of $56 \times 56 \times 232$ cells which corresponds to a coarse mesh of $30 \times 30 \times 30$ cells. The inner cubic cell size is $(\lambda/300)^3$ and that of the coarse mesh is $(\lambda/19)^3$.

Figure 4 shows the field near the dipole. The computational domain described in the figure is entirely included in the inner nested grid. At 2 mm from the dipole the difference between the two curves is of 20 percent, and it rapidly decreases. From 1 cm from the

dipole, vis., $\lambda/30$, the two curves are practically identical.

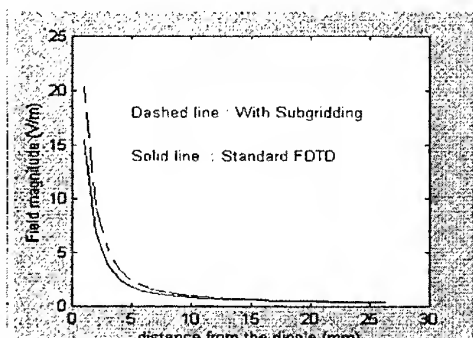


Fig 4. Comparison of the near field of a dipole using standard FDTD and the nested subgridding scheme with a reduction factor of 16.

This results is most satisfactory and it illustrates the efficiency of the proposed scheme.

4. CONCLUSION

In this paper we have presented an nested subgridding scheme which is numerically stable and accurate. The importance of the proposed scheme is that it enables one to drastically reduce the memory storage and the computational time. This scheme allows to use a reduction factor of 16 to locally improve the precision of the FDTD method. It is well suited for problems with fine structures or for problems which require fields with high resolution.

The stability of the scheme is based on two major upsets: Small interpolation error and implicit weighting operations due to the use of standard FDTD between each nested grid. The simplicity of this scheme makes it easy to implement in a standard FDTD code. Two examples of near field calculation illustrate the accuracy of the proposed scheme. Important application of the nested subgridding scheme such as wire antenna analysis and the study of near field interaction between a human head and mobile phone can be envisaged.

5. REFERENCES

5.1 K. Yee, "Numerical solution of initial boundary value problems involving Maxwell's equations in

isotropic media," *IEEE Trans. Antennas and Propagat.*, Vol. AP-16, pp. 302-307, May 1966.

5.2 J. A. Svilapl, "Efficient solution of Maxwell's equations using the nonuniform orthogonal finite difference time domain method," PhD Thesis, University of Illinois at Urbana-Champaign, 1995.

5.3 K. Kunz and L. Simpson, "A technique for increasing the resolution of finite-difference solution of the Maxwell equation," *IEEE Trans. Electromagn. Compat.*, Vol. ENC-23, Nov. 1981.

5.4 S. Zivanovic and K. Yee, "A subgridding method for the Time-Domain Finite-Difference method to solve Maxwell's equations," *IEEE Trans. Microwave Theory Tech.*, Vol. 39, pp. 471-479, Mar. 1991.

5.5 D. Prescott and N. Shuley, "A method for incorporating different sized cells into the Time-Domain Finite-Difference analysis technique," *IEEE Microwave Guided Wave Lett.*, Vol. 2, pp. 434-436, Nov. 1992.

5.6 M. White, M. Iskander and Z. Huang, "A three dimensional multi-grid FDTD code for modeling microwave sintering of materials," *IEEE AP-S International symposium*, Maryland, USA, pp. 120-123, July 1996.

5.7 P. Thomas and T. Weiland, "A consistent subgridding scheme for the Finite Difference Time Domain method," *Int. J. Numerical Model. Electronic Networks, Devices and fields*, Vol. 9, pp. 359-374, 1995.

5.8 M. White and M. Iskander, "A new 3D multi-grid technique with dielectric-traverse capabilities," *URSI International symposium*, Montreal, Canada, July 1997.

5.9 M. Okoniewski, E. Okoniewska and M. Stuchly, "Three-Dimensional Subgridding Algorithm for FDTD," *IEEE Trans. Antennas and Propagat.*, Vol. 45, pp. 422-429, Mar. 1997.

5.10 M. W. Chevalier and R. J. Luebbers, "FDTD local grids with Materials Traverse," *IEEE Trans. Antennas and Propagat.*, Vol. 45, pp. 411-421, Mar. 1997.

BIOGRAPHICAL NOTES

S. Chaillou, J. Wiart and Z. Altman are with CNET, National Center of Telecommunication Studies of France Telecom, 92794 Issy les Moulineaux, France.

W. Tabbara is with the Laboratoire des Signaux et Systèmes - CNRS / SUPELEC, 91192 Gif-sur-Yvette, France.

NUMERICAL MODELLING OF MOBILE PHONE EQUIPMENT

R. Ehmann¹, S. Gutschling², B. Trapp², T. Weiland²

¹CST GmbH
 Lauteschlägerstr. 38, D-64289 Darmstadt, Germany
 Phone:+49(0)6151/717057, Fax:+49(0)6151/718057,
 e-mail: ehmann@temf.tu-darmstadt.de

²University of Technology Darmstadt, Theorie Elektromagnetischer Felder,
 Schloßgartenstr. 8, D-64289 Darmstadt, Germany
 Phone:+49(0)6151/162461, Fax:+49(0)6151/164611,
 e-mail: trapp@temf.tu-darmstadt.de

The influence of using a cellular phone inside a car on the radiated electromagnetic field is analyzed numerically. The specific absorption rate (SAR) inside the head and the antenna characteristics are considered for a simulation with and without car. For the computations the Finite Integration Technique in time domain implemented in the Software Package MAFIA¹ is used.

1. INTRODUCTION

The energy absorption inside a human head caused by electromagnetic near fields of a cellular phone has been analyzed in several publications [3],[5]. For all these studies the human head was located in free space. In practice cellular phones are used under various circumstances, e.g. inside cars. The influence of that electric conducting environment on the antenna characteristics, farfield and impedance, and the energy absorption inside the human head is considered in numerical simulations. The method used for the simulations is the Finite Integration Technique, in time domain equivalent to FDTD. For a realistic modelling of the structure to be analyzed, CAD data of a car and a human head model extracted out of NMR-measurements are imported into the software package MAFIA. Due to the complexity of the whole simulated structure local mesh refinements and a PML boundary condition are used to improve the accuracy and the numerical efficiency of the computation.

2. NUMERICAL METHOD

¹MAxwells Finite Integration Algorithm

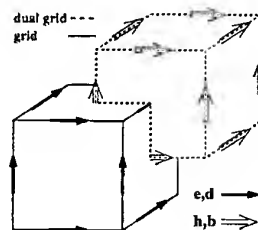


Figure 1: Allocation of the field components in the mesh

2.1 Finite Integration Technique (FIT)

The method used for our calculations is the FI-method [2], which in the time domain formulation becomes equal to Yee's [4] scheme.

Maxwell's Equations are transformed one to one from the continuous domain to a discrete space by allocating electric fields on a grid G and magnetic fields on a dual grid \tilde{G} [1]. The allocation of the field components on the grid can be seen in Fig.1.

$$Ce = -\dot{b} \quad (1) \quad d = D_e e \quad (5)$$

$$\tilde{C}h = j + \dot{d} \quad (2) \quad b = D_\mu h \quad (6)$$

$$Sb = 0 \quad (3) \quad j = D_\kappa e + j_A \quad (7)$$

$$\tilde{S}d = q \quad (4)$$

The discrete equivalent of Maxwell's equations are shown in Eqs.(1)-(4), where e and h are the electric voltages between grid points and the magnetic voltages between dual grid points, respectively. d , b

and \mathbf{j} are fluxes over grid or dual grid faces. The discrete analogon of the coupling between voltages and fluxes is represented by the diagonal material matrices \mathbf{D}_ϵ , \mathbf{D}_μ and \mathbf{D}_κ . So far Maxwells Equations are mapped on a discrete space and can be simplified regarding special problem types. The time domain formulation is equivalent to FDTD and is performed by using the well known leap-frog-scheme [4], which leads to an explicit algorithm to solve the electromagnetic field problem. For the lossless case the scheme is described in Eqs.(8)-(11) [2].

$$\mathbf{f}^{i+1} = \mathbf{A}\mathbf{f}^i + \mathbf{s}^i \quad (8)$$

with

$$\mathbf{A} = \begin{pmatrix} \mathbf{I} & -\Delta t \mathbf{C} \\ \Delta t \mathbf{D}_\epsilon^{-1} \tilde{\mathbf{C}} \mathbf{D}_\mu^{-1} & \mathbf{I} - \Delta t^2 \mathbf{D}_\epsilon^{-1} \tilde{\mathbf{C}} \mathbf{D}_\mu^{-1} \mathbf{C} \end{pmatrix} \quad (9)$$

$$\mathbf{f}^i = \begin{pmatrix} \mathbf{b}^i \\ \mathbf{e}^{i+1/2} \end{pmatrix} \quad (10)$$

$$\mathbf{s}^i = \begin{pmatrix} \mathbf{0} \\ -\Delta t \mathbf{D}_\epsilon^{-1} \mathbf{j}^i \end{pmatrix} \quad (11)$$

The maximum stable time-step inside an equidistant grid is restricted by the Courant criterium to

$$\Delta t \leq \frac{1}{c \sqrt{\frac{1}{\Delta x^2} + \frac{1}{\Delta y^2} + \frac{1}{\Delta z^2}}} \quad (12)$$

and is not affected by taking additionally electric losses into consideration.

2.2 Local Mesh Refinement

To achieve an accurate modelling e.g. of the small details inside the human head a consistent three-dimensional subgridding scheme is used (Fig.2). With such a scheme it is possible to reduce the total number of gridpoints in less sensitive areas, whereas the necessary resolution in and around the human head is ensured ([7]). In contrast to other subgridding methods the one used in this work guarantees energy and divergence conservation and therefore long term stability. A local time step inside the subgrids allows a further reduction of the computation time.

The subgrid algorithm in MAFIA enables the use of subgrids inside subgrids (Fig.2). The number of subgrids put into one another is not limited. The grading factor for the mesh step size of each subgrid is always two.

2.3 PML Open Boundary Condition

The theoretically boundless space extension of the whole structure is simulated by the Perfectly Matched Layer (PML) boundary condition. This technique was first published by Berenger [8] and bases upon a splitting of the electric and magnetic fields in combination with assigning individual losses

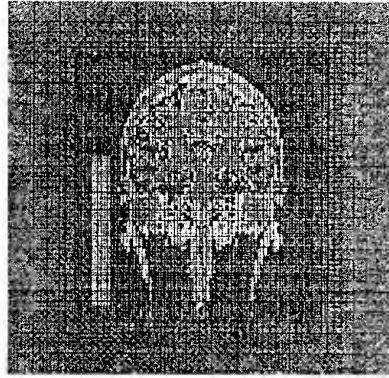


Figure 2: Subgridding in and around the human head

to the splitted components. Outgoing waves of any frequency and any incident angle are absorbed with rather low reflections. The layer used for the simulation has a thickness of 6 cells; the losses inside are quadratically graded with the depth. The theoretical reflection coefficient for perpendicular outgoing waves is set to 0.01%.

3. SIMULATED STRUCTURE

3.1 Human Body Model

One main issue of our considerations is the penetration of the electromagnetic field into the human head, since the head is located nearest to the antenna and seems to be the most sensitive part. For

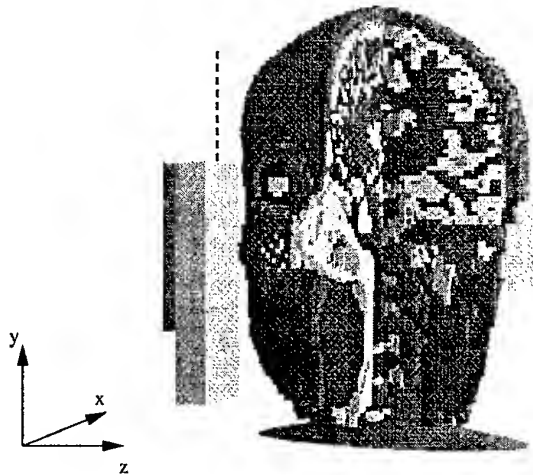


Figure 3: The human head modelled out of NMR-data with the mobile phone aside

the head an advanced model has been extracted out of NMR-data consisting of 55 slices with 100x100 voxels and with a single voxel dimension of 2.5mm x 2.5mm x 3.3mm [3]. 7 different tissue types for gray and white brain, skin, bone, muscle, gristle, and fat are used. Additionally the eyes, the aorta, air gaps and liquid areas are modelled. The material properties are taken from [5]. Figure 3 shows the

human head model used for the simulation. The human body is created out of elementary shapes with homogeneous material parameters.

3.2 Car Model

As shown in Figure 4 the model of a Honda Accord is imported via a CAD-Interface into the code MAFIA. The car model consists of the outer body-

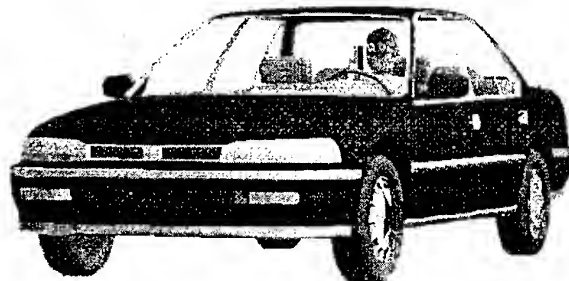


Figure 4: The Honda Accord with human body inside and the fine resolution head model (Fig.3)

work and a complete interior with seats, dashboards and further details, which may influence the electro-magnetic fields inside the car. The car itself is positioned with the tires upon an electric conducting ground. The outer body of the car is perfectly electric conducting, whereas the inner synthetic parts and the seats were modelled with a permittivity of 2 and a neglectable conductivity.

3.3 Computational Model and Efforts

For the discretization of the complete structure a base grid, which is extended to the outer boundaries of the computation domain with about 1.4 million mesh cells is used. The maximum mesh step size in that grid is 2.2 cm, $\lambda/15$ at the operation frequency of 900 MHz. The phone, a conducting case with antenna on top and a current source in between is positioned aside the head at a distance of 2.5 mm. The distance between the head and the antenna on top of the phone case is 2 cm. Three submeshes put into one another are used to reach the resolution of 2.5mm required for the human head (Fig.2). The innermost submesh contains the human head with the cellular phone. Just this single submesh has about 900000 meshpoints. The complete structure including all submeshes consists of 2.47 million mesh cells. The memory required for the computation is 162 MB for a computation with a first order open boundary operator. Additionally 65 MB are necessary for the PML boundary condition with a thickness of 6 layers. The calculation time for the structure with car and human is 24 h on an Ultra-Sparc II with 167 MHz for the broadband computation and 40 h for the monochromatic computations,

respectively. For the comparison computation without car, just with human body, the calculation domain is reduced to an outer boundary of one wavelength around the human body. The total number of mesh cells for that computation is about 1.37 million. Due to the applied algorithm the computation time scales down linear e.g. to 13 h for the broadband computation.

4. RESULTS

The cellular phone used for the excitation is positioned at the right side of the head (Fig.2,3,4). The quarter wave antenna on top of the handy is excited at a frequency of 900 MHz with a smooth switch-on slope for the monochromatic computations, whereas for the broadband results a sinusoidal modulated gaussian pulse is excited with a middle frequency of 900 MHz and a 60dB bandwidth of 600 MHz.

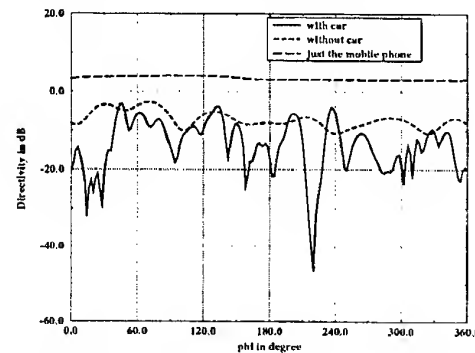


Figure 5: The directivity for the three simulated cases

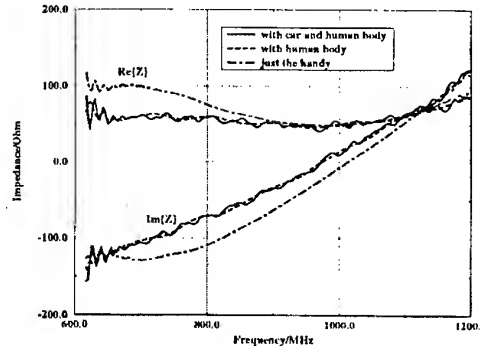


Figure 6: The real and imaginary part of the base impedance for the three simulated cases

Three different arrangements are considered to compare the antenna characteristics, impedance and farfield. The first structure contains the car, the human and the fine resolution head model. For the second structure the human is considered in free space without car but also with the fine resolution head model. In the third simulation only the mobile phone is taken into account.

Fig.6 shows the real and imaginary part of the impedance for the three analyzed arrangements.

Table 1: Energy Absorption P in % of the radiated power; SAR-values in mW/cm^3 for 1W radiated power; Results are given for the simulation with and without car

	with car	without car
P _{brain} [%]	17.19	16.92
P _{eye} [%]	0.04	0.03
P _{head} [%]	60.35	57.88
SAR _{peak}	22.71	21.31
SAR _{1ccm}	3.70	3.66

The resonance frequency just for the phone without human aside is at about 1 GHz, whereas for the simulations with head it is shifted to values much closer to the interesting frequency of 900 MHz. The influence of the car and the human on the directivity is shown in Fig.5. Due to the energy absorption inside the head the levels of the directivity for the simulation with and without head differ obviously, the influence of the car on the characteristic is not neglectable as well.

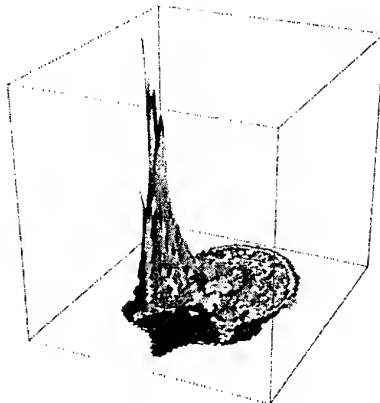


Figure 7: The difference between the SAR values for the simulation with and without car in a y-cutplane

Further investigations deal with the influence of the electromagnetic fields on the human head. In the following only the computation with and without car are considered. Table 1 shows the energy absorption inside the human head for the both simulated cases. The energy absorption in % of the radiated power as well as the SAR peak and averaged values in mW/cm^3 for 1 W radiated power are listed. The totally absorbed power in the head is about 3% higher for the usage of the phone inside the car. The difference for the SAR peak value is about 6.5%, whereas the maximum averaged values over $1 cm^3$ are comparable.

Fig.7 and Fig.8 show the SAR distribution difference: $SAR_{with\ car} - SAR_{without\ car}$ in x- and y- cutplanes (Fig.3). For nearly all areas in that cutplanes

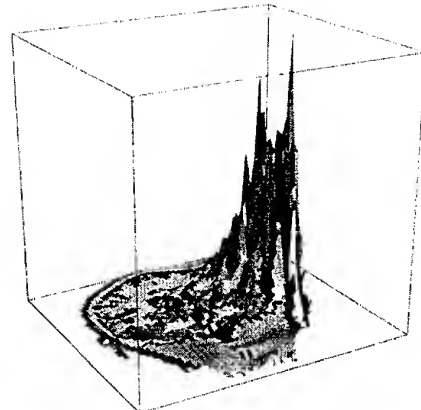


Figure 8: The difference between the SAR values for the simulation with and without car in a x-cutplane (Fig.3)

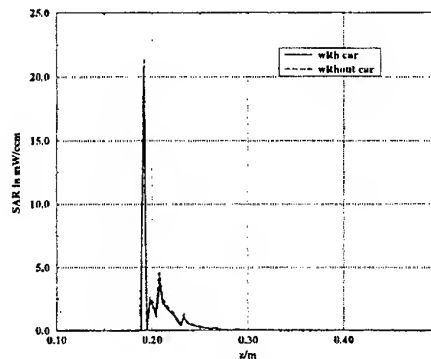


Figure 9: The SAR values versus z for constant x and y at the height of the current source; The values correspond to 1W radiated power

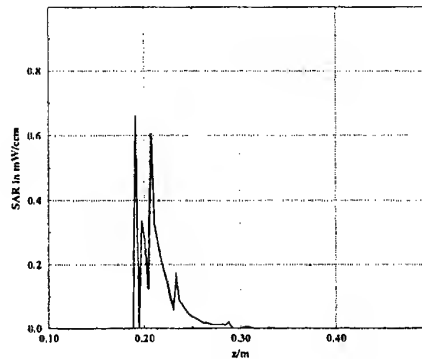


Figure 10: The difference between the SAR values for the simulation with and without car corresponding to 1W radiated power (same line as in Fig.9)

the absorption for simulation with car is higher. Fig.9 and Fig.10 confirm that result. They show the SAR distribution versus the z-coordinate for constant x and y at the height of the current source.

5. CONCLUSION

Using a cellular phone inside a car is compared to using it in free space. Two different kind of quantities are considered, the antenna characteristics farfield and impedance and the energy absorption in different parts of the human head. The main influence on the impedance is given by the human head, which shifts the resonance frequency by about 50 MHz. As expected the directivity of the mobile phone shows differences between the computation with and without car, although the main influence is given by the human head and the absorption of about 60% of the radiated energy. The differences between the absorbed energy for the simulations with and without car differ only about 3%, also the SAR peak value is just 6% higher for using the phone inside the car. The capability of the MAFIA code to handle structures extended to several wavelengths with complex details has been proved. A further advance to treat EMC relevant problems with numerical methods has been achieved.

6. REFERENCES

- [1] T. Weiland : "A Numerical Method for the Solution of the Eigenwave Problem of Longitudinally Homogeneous Waveguides", *Electronics and Communication (AEÜ)* Vol.31(1977),pp.308.
- [2] T. Weiland : "Time Domain Electromagnetic Field Computation with Finite Difference Methods", *Numerical Modelling, Electronic Networks, Devices and Fields*, Vol.9, 295-319 (1996).
- [3] S. Gutschling, T. Weiland; Resonance Effects Inside a Human Head Exposed to a Cellular Phone; *3rd International Conference on Computation in Electromagnetics; CEM'96 Bath*, No. 420, pp.62-66.
- [4] K.S.Yee : "Numerical Solution of Initial Boundary Value Problems Involving Maxwell's Equations in Isotropic Media", *IEEE, AP-14*, 1966, pp. 302-307.
- [5] V. Hombach, K. Meier, M. Burkhardt, E. Kühn, N. Kuster, "The Dependence of EM Energy Absorption Upon Human Head Modeling at 900 MHz", *IEEE Transactions on Microwave Theory and Techniques*, Vol. 44, No. 10, 1996, pp. 1865-1873.
- [6] R. Ehmann, B. Wagner, T. Weiland, "Farfield Calculations for Car Antennas at Different Locations", *IEEE Transactions on Magnetics*, Vol.33, No.2, March 1997, pp. 1508-1511.
- [7] P. Thoma, T. Weiland, "A Consistent Subgridding Scheme for the Finite Difference Time Domain Method", *International Journal of Numerical Modelling: Electronic Networks, Devices and Fields*, Vol. 9, 1996, pp. 359-374.
- [8] J. P. Berenger, "A Perfectly Matched Layer for the Absorption of Electromagnetic Waves", *Journal of Computational Physics*, Vol. 114, 1994, pp. 185-200.



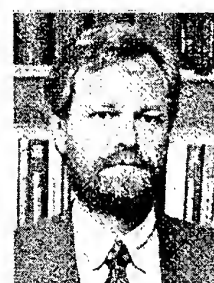
Ralf Ehmann, born in 1967 in Neunkirchen, Germany, received the Dipl.-Ing. degree in electrical engineering from the University of Technology Darmstadt in 1994. In the same year he joined the Institute for Theory of Electromagnetic Fields. Since 1996 he has been with CST GmbH in Darmstadt. He is working towards the Ph.D. His main interests include time domain simulation and farfield calculations.



Stefan Gutschling was born in Berlin, Germany, in 1965. He received the Dipl.-Ing. degree in electrical engineering from the University of Technology Darmstadt in 1993. In the same year he joined the Institute for Theory of Electromagnetic Fields where he is currently working towards the Ph.D. His main research interest is in the time domain simulation of dispersive materials.



Bernd Trapp was born in Fulda, Germany, in 1971. He received the Dipl.-Ing. degree in electrical engineering from the University of Technology Darmstadt in 1996. In the same year he joined the Institute for Theory of Electromagnetic Fields where he is currently working towards the Ph.D. His main research interest is in examination of boundary operators in time domain simulation.



Thomas Weiland, born in 1951, received his Ph.D. in 1977. He received several national and international research prizes: In 1986 the 'Physics Prize' of the German Physical Society, the 'Prize for Achievements in Accelerator Physics and Technology' of the US Particle Accelerator School and the 'Leibniz Prize' from the German Research Association in 1987. In 1993 he was elected a full member of the Academy of Science and Literature at Mainz, Germany. In 1995 he received the Max Planck-Research Prize for International Collaboration and in 1997 the Phillip Morris Research Price. Since 1989 he has been a full professor at the University of Technology Darmstadt, Germany.

NUMERICAL MODELING OF MOBILE HAND-HELD CELLULAR TELEPHONES

(Prolog to the session "Computational Electromagnetics in Wireless Personal Communications")

Andrzej Karwowski

Silesian Technical University, Akademicka 16, 44-101 Gliwice, Poland
e-mail: akarw@victrix.iele.polsl.gliwice.pl, www: <http://157.158.1.241/~akarw>

This short paper presents some general, introductory remarks on two subjects, namely, SAR calculation via FDTD, and subgridding algorithms in FDTD, dominating in the papers included in the session "Computational Electromagnetics in Wireless Personal Communications". Also, the papers are briefly introduced.

1. INTRODUCTION

Wireless cellular telephony and other mobile personal communication services are the fastest growing field in the telecommunications world. In personal mobile communications, a key consideration is the electromagnetic (EM) interaction between a portable handset (hand-held mobile terminal equipment (MTE)) and the human body. Hand-held and body-mounted devices operate in close proximity to the user's body, and this results in that the presence of the user has a significant, usually undesirable, influence on the handset antenna parameters (radiation pattern, gain, and input impedance). This effect seems to deserve thorough investigation, since a detailed understanding of the handset-user EM interaction mechanism provides basis for designing antennas whose performance is potentially less affected by the presence of the human.

Another important consideration resulting from the handset operation in close proximity of the user's body involves the interaction of the radiated EM energy with the nearby biological tissues. A certain amount of the EM energy is absorbed by the body and converted to heat. This results in public concern about possible health effects of human exposure to electromagnetic energy emitted by mobile telecommunication equipment, and, generally, about the safety of wireless personal communications.

2. SAFETY LIMITS AND SAR CALCULATION

In the frequency range of mobile communications, the electromagnetic absorption effects on the human tissues are consistent with responses to induced heating and are commonly referred to as thermal effects. Consequently, the basic limits of exposure are expressed by the quantity called "specific absorption rate" (SAR). SAR is the time rate at which EM energy is absorbed by (dissipated in) an element of biological body mass, and is expressed in units of watts per kilogram. The safety standards recommend limits on the whole-body averaged SAR, and the mass-normalized maximum local SAR. These quantities must be averaged over a defined time interval. The threshold for effects considered detrimental to health is observed at SAR of about 4 W/kg, averaged over the whole body. For the general public, a safety factor of 50 against the threshold of 4 W/kg is introduced, resulting in a SAR value restriction of 0.08 W/kg, averaged again over the whole body. The limitations for the whole body averaged SAR value are not sufficiently restrictive, since the distribution of the absorbed energy in the human body can be very inhomogeneous, and the maximum value of a local SAR, i.e., the peak SAR value can be excessively high even when the whole body averaged SAR does not exceed 0.08 W/kg. In order to avoid excessive local heating, additional restrictions of local SAR are introduced. Specifically, the European Prestandard [1] sets the basic limit for the peak SAR value at 2 W/kg, as averaged over any 10 g of tissue in any 6-min time interval. The U.S. ANSI/IEEE standard [2] requires spatial peak SAR value not exceeding 1.6 W/kg, as averaged over 1 g of tissue in any 30-min time period. Hence, knowledge of the SAR distribution in the human body as a result of exposure to the electromagnetic field radiated by nearby source is of fundamental importance for the hazard assessment of thermal effects to the persons, and for test-

ing compliance of handheld MTE with safety limits. The maximum local SAR, which is the most critical quantity in the context of potential health effects of RF energy radiated by handheld MTE, depends on a large number of factors, such as: 1) design of MTE, its operational frequency and antenna input power; 2) orientation of the telephone with respect to the human head; 3) the characteristics of the head, i.e., its size, external and internal geometry, and electric properties of the different tissues within the head.

Because of difficulties of direct measurements of SAR distribution in living biological systems (humans), several numerical techniques have been developed for SAR calculation, allowing detailed modeling of the human body and its anatomical properties. Of the several approaches, the finite difference time domain (FDTD) technique [3]–[10] is often regarded as the most successful and the one with the greatest scope for the future. Basically, the approach involves solving Maxwell's curl equations using a finite-difference approximation to both space and time derivatives. While FDTD is very well suited to computing transient responses, the technique can also be employed to obtain continuous wave (CW) steady-state solution by allowing the time-domain solution to run for a period of time enough to achieve steady-state conditions.

The SAR can also be used to evaluate the time rate of change of temperature provided the heat exchange characteristics, including the thermoregulatory responses of the organism under consideration is known.

2. SUBGRIDDING IN FDTD

In applying FDTD, one of the most critical points is the choice of the cell size. In general, the accuracy of the numerical solution becomes better as the cells become smaller, since smaller cells result in better representation of the geometry ("staircase" effects), and better approximation to space derivatives. On the other hand, the cell size must be large enough to keep the computer storage requirements reasonable. Usually, a maximum FDTD cell size is set to 10–15 cells per minimum wavelength for which accurate results are desired. There are situations, however, that require far more higher mesh resolution in only small subvolumes of the entire mesh space. This is the case, for example, when there are small portions of the entire mesh space that contain dielectric material with high dielectric constant. By applying mesh refinement only to these subvolumes, the resolution can be locally increased without modifying the rest of the mesh space (computational domain). The principal advantage of this approach, called "subgridding method" [11], [12], [13], is that it offers considerable memory and computation time saving compared to those required if the entire FDTD computational space were meshed with the local-grid cell size.

3. PAPERS INCLUDED IN THE SESSION

The first paper in the Session, co-authored by Chaillou, Wiart, Altman, and Tabbara, proposes a subgridding technique based on nested submeshes which allows a high reduction factor of 16. The usefulness of the proposed technique is illustrated by the examples of near field calculations. The intended application of the technique is in the analysis of near field interaction effects between the human head and a mobile phone.

The paper by Ehmann, Gutschling, Trapp, and Weiland reports the results of the study of the handheld mobile phone radiating inside a car at 900 MHz.. Anatomically correct model of the human head, and a precise numerical model of a car are employed in the analysis. Numerical simulation is performed with the use of the software package MAFIA with implementation of the local mesh refinement (subgridding) technique.

In the paper by Wang and Fujiwara, the temperature rise in the anatomically correct model of the human head due to the absorption of EM energy radiated by a nearby hand-held telephone is computed using FDTD. The results of numerical simulation show that the maximum temperature rise in the brain is 0.1°C when the ICNIRP safety limit for the peak spatial SAR is not exceeded.

The paper by Wnuk, Kolosowski, and Amanowicz presents two new types of microstrip antennas for mobile terminal equipment with reduced radiation towards the user (operator) head. The Method-of-Moment theoretical results are presented and compared with the experimental results.

REFERENCES

- [1] CENELEC, European Prestandard ENV 50166-2, Human Exposure to Electromagnetic Fields. High Frequency (10 kHz to 300 GHz), January 1995.
- [2] ANSI/IEEE C95.1-1992, Safety Levels with Respect to Human Exposure to Radio Frequency Electromagnetic Fields, 3 kHz to 300 GHz.
- [3] K. S. Kunz, R. J. Luebbers, "The Finite Difference Time Domain Method for Electromagnetics", CRC Press, 1993.
- [4] A. Taflove, "Computational Electrodynamics: The Finite-Difference Time-Domain Method", Artech House, 1995.
- [5] M. A. Jensen, Y. Rahmat-Samii, "EM interaction of handset antennas and a human in personal communications", *Proc. IEEE*, vol. 83, pp. 7-17, Jan. 1995.
- [6] P. J. Dimbylow and S. M. Mann, "SAR calculations in an anatomically realistic model of the

- head for mobile communication transceivers at 900 MHz and 1.8 GHz", *Physics in Medicine Biology*, vol. 39, pp. 1537-1553, 1994.
- [7] M. Okoniewski and M. A. Stuchly, "A Study of the handset antenna and human body interaction", *IEEE Trans. Microwave Theory Tech.*, vol. 44, pp. 1855-1864. Oct. 1996.
- [8] V. Hombach, K. Meier, M. Burkhard, E. Kuhn, and N. Kuster, "The dependence of EM energy absorption upon human head modeling at 900 MHz", *ibid.*, pp. 1865-1873.
- [9] S. Watanabe, M. Taki, T. Nojima, and O. Fujiwara, "Characteristics of the SAR distributions in a head exposed to electromagnetic fields radiated by a hand-held portable radio", *ibid.*, pp. 1874-1883.
- [10] O. P. Gandhi, G. Lazzi, and C. M. Furse, "Electromagnetic absorption in the human head and neck for mobile telephones at 835 and 1900 MHz" "Characteristics of the SAR distributions in a head exposed to electromagnetic fields radiated by a hand-held portable radio", *ibid.*, pp. 1884-1897.
- [11] M. W. Chevalier, R. J. Lubbers, and V. P. Cable, "FDTD local grid with material transverse", *IEEE Trans. Antennas Propagat.*, vol. 45, pp. 411-421, Mar. 1997.
- [12] M. Okoniewski, E. Okoniewska, and M. A. Stuchly, "Three-dimensional subgridding algorithm for FDTD", *ibid.*, pp. 422-429.
- [13] M. J. White, M. F. Iskander, and Z. Huang, "Development of a multigrid FDTD code for three-dimensional applications", *IEEE Trans. Antennas Propagat.*, vol. 45, pp. 1512-1517, Oct. 1997.

BIOGRAPHICAL NOTE

Andrzej Karwowski received M. Sc. and Ph. D. degrees, both in electrical engineering, from the Wroclaw Technical University in 1969 and 1976, respectively. Since 1987 he has been affiliated with the Department of Automatic Control, Electronics and Computer Science, Silesian Technical University, where he currently holds the position of Professor. His research interests are primarily in computational electromagnetics.

FDTD COMPUTATION OF TEMPERATURE-RISE IN THE HUMAN HEAD FOR PORTABLE TELEPHONES AT 900 MHZ

Jianqing WANG and Osamu FUJIWARA

Faculty of Engineering, Nagoya Institute of Technology,
Gokiso-cho, Showa-ku, Nagoya 466, Japan.

In this paper, temperature-rises in the human head for portable telephones were computed with an anatomically based head model. The specific absorption rate (SAR) in the human head was determined using the finite-difference time-domain (FDTD) method, while a bioheat equation, which takes into account various heat exchange mechanisms such as heat conduction, blood flow and electromagnetic heating, was numerically solved also using the FDTD method. Computed results show that, for an uncontrolled environment, application of the ANSI/IEEE safety guidelines restricting the one-gram-averaged peak SAR to 1.6 W/kg results in a maximum temperature-rise in the brain of 0.05 °C, and application of the ICNIRP/Japan safety guidelines restricting the ten-gram-averaged peak SAR to 2 W/kg results in a maximum temperature-rise in the brain of 0.10 °C at 900 MHz.

1 INTRODUCTION

With the recent rapid increase in the use of portable telephones, public concern regarding potential health hazards due to the absorption of electromagnetic (EM) energy emitted by these telephones has been growing. Safety guidelines for protecting the human body from radio frequency exposure have been issued in various countries. These safety guidelines are based on the findings from animal experiments that the biological hazards due to radio waves result mainly from the temperature-rise in tissue and that a whole-body-averaged specific absorption rate (SAR) below 0.4 W/kg are not hazardous to human health. In contrast to a wealth of data available on the whole-body-averaged SAR threshold, very little is known about possible biological effects of localized SAR. For the human head exposed to RF fields from portable telephones, there may be a high localized peak SAR in parts of the head as a portable telephone is brought extremely close to the head. A localized spatial peak SAR not exceeding 1.6 W/kg averaged over any one-gram of tissue [1] or 2 W/kg averaged over any ten-grams of tissue [2][3], which are specified in uncontrolled environments, has been recommended. However, the physiological ground

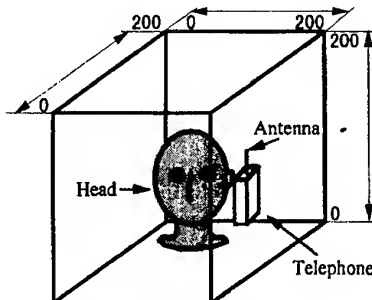


Fig.1 Geometry of head-telephone model.

of these safety guidelines for near-field exposure is still unclear. Since the SAR is a physical quantity which causes the tissue heating due to RF exposure, the safety guidelines on localized SAR for portable telephones should be determined in relation to temperature-rise in the head, especially in the brain because of its critical control function.

From this point of view, the temperature-rise in the human head for portable telephones is computed in this paper. The human head is modeled as an anatomically based head model and the portable telephone is modeled as a monopole antenna on a metal box. The temperature-rise is computed in two steps [4]. The first step is to compute the SAR distribution in the human head using the finite-difference time-domain (FDTD) method, while the other step is to determine the temperature-rise by solving a bioheat equation which takes into account various heat exchange mechanisms such as heat conduction, blood flow and EM heating also using the FDTD method.

2 COMPUTATION METHOD

2.1 SAR Computation

Figure 1 shows the human head and portable telephone model for the present study. The head model was constructed by our groups on the basis of an anatomical chart of a Japanese adult head [5]. It consists of 273 108 cubical cells with a resolution of $2.5 \times 2.5 \times 2.5$ mm. Six types of tissues are involved in this model. The electrical properties of tissues at 900 MHz are given in Table 1 in which ϵ_r

and σ are the relative permittivity and conductivity, respectively. The portable telephone was considered to be a 1/4-wavelength monopole antenna mounted on a rectangular metal box. The metal box was 12 cm tall, 4 cm wide and 2.5 cm deep. The monopole had a radius of 0.5 mm and was located at the center of the top surface of the metal box.

The FDTD method was used for the SAR computation. The parameters for our FDTD computation were as follows. A space domain enclosing the human head and the portable telephone had $200 \times 200 \times 200$ cells. Each cell had a size of $\delta = 2.5$ mm. The time step was set to $\delta/\sqrt{3}c$, where c is the speed of light, to ensure the numerical stability. The time-stepping was performed for about seven sinusoidal cycles in order to reach a steady state. To absorb the outgoing scattered waves, the second order Mur absorbing boundaries acting on electric fields were used. The monopole antenna was approached by thin-wire approximation. An antenna excitation was introduced by specifying a voltage across the 1-cell gap between the monopole and the top surface of the metal box.

Table 1 Dielectric properties of tissues

Tissue	ϵ_r	σ [S/m]
Bone	17.4	0.19
Brain	44.1	0.89
Muscle	51.8	1.11
Eyeball	74.3	1.97
Fat	10.0	0.17
Skin	39.5	0.69

2.2 Temperature-Rise Computation

The normal human body temperature is kept in a thermal equilibrium state based on the balance of chemically thermal generation and physically thermal dissipation. When a human head in such a thermal equilibrium state is exposed to the EM fields, the resultant temperature-rises may be obtained from a bioheat equation which takes into account such heat exchange mechanisms as heat conduction, blood flow and EM heating [6]. The bioheat equation is given by

$$\rho \cdot C_p \frac{\partial T}{\partial t} = K \nabla^2 T + \rho \cdot SAR - b \cdot (T - T_b) \quad (1)$$

with the boundary condition

$$K \frac{\partial T}{\partial n} = -h \cdot (T - T_a) \quad (2)$$

where $T = T(x, y, z, t)$ is the temperature [$^\circ$ C] at time t , C_p is the specific heat [$J/kg \cdot ^\circ C$], K is the thermal conductivity [$W/m \cdot ^\circ C$], b is a constant [$W/m^3 \cdot ^\circ C$] related to the blood flow, T_b is the blood temperature, T_a is the ambient temperature, n is the unit vector normal to the surfaces of head or internal cavity, h is the convective heat transfer coefficient

[$W/m^2 \cdot ^\circ C$], and the SAR is the input EM heating source into the bioheat equation. For simplicity in solving the bioheat equation, the parameters C_p , K and b are taken to be independent of temperature and time, and assumed constant within each tissue.

The discretization of the bioheat equation follows that of the FDTD cell used to determine the SAR. By expanding the bioheat equation in its finite difference approximation, Eqs.(1) and (2) can be written as

$$T^{m+1}(i, j, k) = T^m(i, j, k) + \frac{\delta_t}{C_p(i, j, k)} SAR(i, j, k) \\ - \frac{\delta_t}{\rho(i, j, k)C_p(i, j, k)} b(i, j, k)[T^m(i, j, k) - T_b] \\ + \frac{\delta_t}{\rho(i, j, k)C_p(i, j, k)\delta^2} [T^m(i+1, j, k) \\ + T^m(i, j+1, k) + T^m(i, j, k+1) \\ + T^m(i-1, j, k) + T^m(i, j-1, k) \\ + T^m(i, j, k-1) - 6T^m(i, j, k)] \quad (3)$$

$$T^{m+1}(i_{min}, j, k) = \frac{KT(i_{min}+1, j, k)}{K+h\delta} + \frac{T_a h \delta}{K+h\delta} \quad (4)$$

where the finite difference approximation of Eq.(2) is given only along the x-directed line. Similar approximations can be obtained along y- and z-directed lines. In order to ensure the numerical stability, δ_t was chosen to satisfy

$$\delta_t \leq \frac{2\rho C_p \delta^2}{12K + b\delta^2} \quad (5)$$

which was derived by us from the Von Neumann's condition.

Values of the thermal properties are required for each of tissues to solve the bioheat equation. Table 2 gives the values of ρ , C_p , K , and b used in our computation. They are taken from [6] and [7]. As for the convective heat transfer coefficient h , two values were adopted. One was h_a , the convective heat transfer coefficient from the head surface to the ambient temperature, which was taken to be $10.5 W/m^2 \cdot ^\circ C$ [8]. The other was h_b , the convective heat transfer coefficient from the internal surface to the cavity, which was taken to be $50 W/m^2 \cdot ^\circ C$. The ambient temperature and the blood temperature were set to be $20^\circ C$ and $37^\circ C$, respectively.

Table 2 Thermal properties of tissues

Tissue	ρ [kg/m ³]	C_p [J/kg \cdot $^\circ$ C]	K [W/m \cdot $^\circ$ C]	b [W/m ³ \cdot $^\circ$ C]
Bone	1810	1300	0.30	1401
Brain	1040	3500	0.60	37822
Muscle	1040	3500	0.60	3488
Eyeball	1010	3900	0.50	0
Fat	920	2300	0.22	816
Skin	1010	3500	0.50	8652
h_a			10.5 [W/m ² \cdot $^\circ$ C]	
h_b			50 [W/m ² \cdot $^\circ$ C]	

The temperature-rise due to the EM field exposure from portable telephones was obtained from the difference between the temperature $T(x, y, z, t)$ and $T(x, y, z, 0)$ where $T(x, y, z, 0)$ is the normal temperature distribution in the unexposed head (with SAR = 0) at thermal equilibrium.

3 NUMERICAL RESULTS AND DISCUSSION

For the computation of temperature-rise due to portable telephones, two source geometries, denoted by NE and PE (NE is short for normal ear and PE for pressed ear), were considered. The NE geometry represented a normal position of a portable telephone in ordinary use. A separation of 1.5 cm between the monopole antenna and the head was considered. The PE geometry represented a more practical use of a portable telephone. The ear was pressed by the telephone so that the shape of the ear was changed. Both of the two source geometries had a vertical alignment at the side of the head by the ear. The hand holding the portable telephone was removed here for considering a worst case of temperature-rise.

3.1 Transient Temperature-Rise

In the practical use of portable telephones, the steady-state temperature-rise may not give a realistic picture of the temperature-rise distribution within the head since the communicate time by portable telephone is generally not so long. So it is informative to consider how quickly the temperature in the head is elevated. Figure 2 shows the transient peak temperature-rise in the ear, brain and eye. It is found that the peak temperature-rises for all of them increase exponentially with time. The temperatures increase rapidly over the first 6 ~ 7 minutes, and the rate of temperature-rise then slows down and the steady-state is achieved after approximately 30 minutes of exposure. A communicate time of 3 minutes yields temperature-rises over 60% of the steady-state value, and a communicate time of 6 ~ 7 minutes yields temperature-rises of approximately 90% of the steady-state value. It is known that the thermal time constant, obtained from the cross point of the tangent line of temperature-rise curve and the steady-state value, for human, is approximately over 6 minutes. For our present computation, the thermal time constants for all of tissues are verified to be approximately between 6 and 8 minutes. This fact provides a ground for the reliability of our temperature computation.

3.2 Steady-State Temperature-Rise

The steady-state temperature computation provides information on the maximum temperature-rise within the human head. Figure 3 shows the computed temperature-rise distributions in the steady-

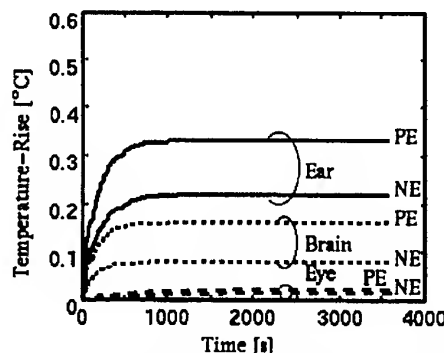


Fig.2 Transient temperature-rises in the head.

The antenna output power is 1W.

state which are observed in a horizontal cross section through the eyes. It can be found that the temperature-rise distributions are similar to the SAR ones and the peak temperature-rises occur in the region of ear close to the portable telephone. Figure 4 shows the one-gram-averaged and ten-gram-averaged peak SARs, and Figure 5 shows the peak temperature-rises for the whole head and brain. With an antenna output power of 1 W, the maximum temperature-rises of 0.22 °C for NE geometry and 0.33 °C for PE geometry have been observed at 900MHz. All of them occur in the ear region.

For the brain which has the largest blood flow rate in the head, the maximum temperature-rises are 0.16 °C at 900 MHz for PE geometry with an antenna output of 1 W. They are located at the outward appearance of the brain close to the telephone. With deepening into the brain tissue, the temperature-rise slows rapidly down. Anderson and Joyner have calculated the maximum temperature-rise in the brain using a perfusion model in which the effect of heat conduction was lumped with the heat-exchanger effect of blood perfusion in a single heat sink term [9]. They gave a maximum temperature-rise of 0.034 °C in the brain for a measured localized one-gram-averaged SAR of 0.83 W/kg at 835 MHz. For the same localized SAR value, scaling our results at 900 MHz can obtain the maximum temperature-rises of 0.041 °C ~ 0.046 °C in the brain. For an uncontrolled environment, application of the ANSI/IEEE safety guidelines restricting the one-gram-averaged peak SAR to 1.6 W/kg results in a maximum temperature-rise in the brain of 0.05 °C, and application of the ICNIRP/Japan safety guidelines restricting the ten-gram-averaged peak SAR to 2 W/kg results in a maximum temperature-rise in the brain of 0.10 °C at 900 MHz. These values have a safety margin of at least 35 relative to a temperature-rise threshold of 3.5 °C which is considered not to cause physiological damage to the brain.

4 CONCLUSION

Temperature-rises in the human head for portable

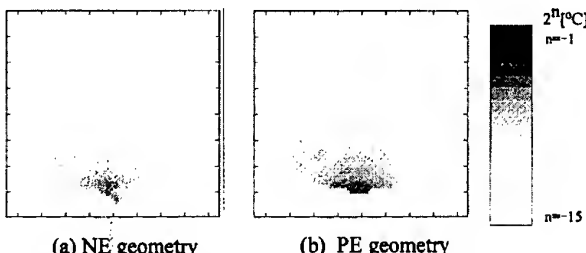


Fig.3 Temperature-rise distributions in a horizontal cross section through the eyes for a 900 MHz portable telephone with an antenna output of 1 W.

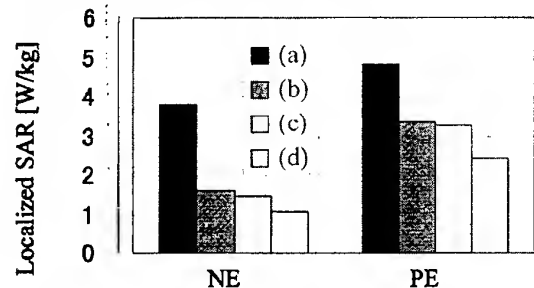


Fig.4 Localized SARs. (a) one-gram-averaged SAR in the whole head, (b) ten-gram-averaged SAR in the whole head, (c) one-gram-averaged SAR in the brain, (d) ten-gram-averaged SAR in the brain. The antenna output power is 1W.

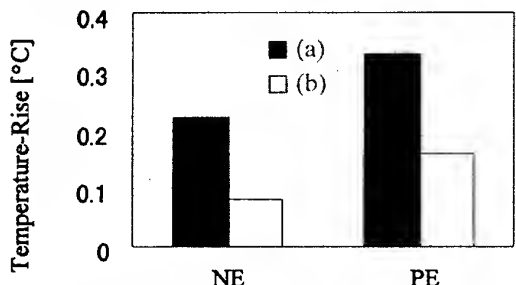


Fig.5 Peak temperature-rises (a) in the whole head, (b) in the brain. The antenna output power is 1W.

telephones have been computed using the FDTD method with an anatomically based human head model. Computed results show that, for an uncontrolled environment, application of the ANSI/IEEE safety guidelines restricting the one-gram-averaged peak SAR to 1.6 W/kg results in a maximum temperature-rise in the brain of 0.05 °C, and application of the ICNIRP/Japan safety guidelines restricting the ten-gram-averaged peak SAR to 2 W/kg results in a maximum temperature-rise in the brain of 0.10 °C at 900 MHz. Further works are required for experimental evaluation.

5 REFERENCES

- [1] ANSI/IEEE C95.1-1992, "American national standard - Safety levels with respect to exposure to radio frequency electromagnetic fields, 3 kHz to 300 GHz", New York, IEEE, 1992.
- [2] ICNIRP, "Health issues related to the use of hand-held radiotelephones and base transmitters", *Health Physics*, vol.70, pp.587-593, 1996.
- [3] Telecommunications Technology Council for the Ministry of Posts and Telecommunications, Deliberation no.89, "Radio-Radiation Protection Guidelines for Human Exposure to Electromagnetic Fields", Tokyo, 1997.
- [4] A. Taflove and M.E. Brodwin, "Computation of the electromagnetic fields and induced temperatures within a model of the microwave-irradiated human eye", *IEEE Trans. Microwave Theory Tech.*, vol.23, pp.888-896, 1975.
- [5] O. Fujiwara and A. Kato, "Computation of SAR inside eyeball for 1.5-GHz microwave exposure using finite-difference time-domain technique", *IEICE Trans. Commun.*, vol.E77-B, pp.732-737, 1994.
- [6] A.W. Guy, J.F. Lehmann and J.B. Stonebridge, "Therapeutic applications of electromagnetic power", *Proc. IEEE*, vol.62, pp.55-75, 1974.
- [7] N. Haruyama, M. Fujii, K. Sakamoto and H. Kanai, "Basic study on magnetically induced hyperthermia for brain heating", *Japanese J. Med. Electron. Biol. Eng.*, vol.34, pp.230-237, 1996.
- [8] H.N. Kritikos, K.R. Foster and H.P. Schwan, "Temperature profiles in spheres due to electromagnetic heating", *J. Microwave Power*, vol.16(3&4), pp.327-344, 1981.
- [9] V. Anderson and K.H. Joyner, "Specific absorption rate levels measured in a phantom head exposed to radio frequency transmissions from analog hand-held mobile phones", *Bioelectromagnetics*, vol.16, pp.60-69, 1995.

BIOGRAPHICAL NOTE

Jianqing WANG received the B.E. degree in electronic engineering from Beijing Institute of Technology, China, in 1984, and the M.E. and D.E. degrees in electrical and communication engineering from Tohoku University, Japan, in 1988 and 1991, respectively. He is currently a Research Associate at Nagoya Institute of Technology, Japan. His research interests include electromagnetic compatibility and bioelectromagnetics.

Osamu FUJIWARA received the B.E. degree in electronic engineering from Nagoya Institute of Technology, Japan, in 1971, and the M.E. and the D.E. degrees in electrical engineering from Nagoya University, Japan, in 1973 and in 1980, respectively. He is presently a professor at Nagoya Institute of Technology. His research interests include measurement and control of electromagnetic interference due to discharge, bioelectromagnetics and other related areas of electromagnetic compatibility.

Microstrip antennas on multilayer dielectric for mobile system communication

Marian Wnuk, Władysław Kołosowski, Marek Amanowicz

Military University of Technology, Electronics Faculty

Str. .Kaliskiego 2, 01-489 Warsaw, Poland

phone: (+48 22) 685-92-28 fax: (+48 22) 685-90-38

E-mail: mwnuk@wel.wat.waw.pl.

Abstract - Intensive development of cellular personal communications system has been observed lately. Thus, protection of a man, and especially protection of his head against non-ionizing electromagnetic radiation generated by cellular telephones is becoming one of the most important problems. The results of elaborated microstrip antennas which have minimized radiation towards the user's head are presented in this paper.

1. INTRODUCTION

In portable cellular personal communication devices which are used at present, a considerable part of radiation energy (up to 30 %) is absorbed by the user's head. It may have a harmful effect on his health.

- limitation to the necessary minimum of electromagnetic fields power emitted towards the user's head
- limitation of the time for people staying in these electromagnetic fields.

The second principle that is, the length of a telephone call time, depends mainly on the speaker itself.

The first principle concerning the limitation of electromagnetic power absorbed the user's head may be based on changing of the radiation pattern which can be obtained by using a new type of antenna. The quarter-wave dipole which has been used so far, has an omnidirectional pattern (plane \vec{H}).

2. REQUIREMENTS FOR THE ANTENNA RADIATION PATTERN

Actually, there is lack of formal requirements (or practically implemented solutions) for the desired radiation pattern. The matter is complicated by the fact that the user's head is in the area of the near zone antenna. Therefore, it is necessary to find a compromise between the requirements for the availability of signals received by the antenna from all directions on the one hand , and the protection of a human head from radiation on the other hand.



Fig.1. Omnidirectional handset antenna radiation patterns

Therefore, protection of a man against the radiation of radio communications system is an important problem. Protection from this radiation may be carried out on the basis of two principles:

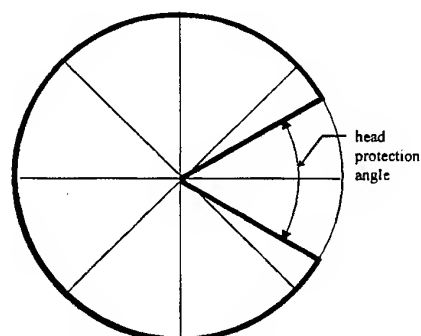


Fig.1. Ideal radiation pattern (horizontal plane)

The elaborated microstrip antennas on the multilayer dielectric which realise the dipole and path pattern (fig 4, 5 and 7) are presented in this paper.

We assume that the radiation pattern in the plane \vec{H} should be defined as it is shown in fig.2, and the space pattern as in fig.3. It is assumed that in the vector of \vec{H} plane the radiation level in the whole area, except the area defined by the head protection angle within the range of 360° , should be uniform. The problem of reverse radiation is disputable.



Fig.3. Requirements for antenna radiation pattern

On the one hand it is necessary to receive the signals emitted by a base station located in the operator head direction, but then the human head, especially some of its elements like bones, brain and skin which are characterized by high level of thermal conductivity (14.6, 8.05, 4.42 mW/cm²°C respectively), should be exposed to transmitter radiation with minimal radiation power.

The radiation pattern shown in fig.2 and 3 has been accepted for practical analyses of the designed antenna systems.

3. MODELLING OF MICROSTRIP ANTENNAS

The thorough analysis of microstrip antennas which takes into account the structure of the layer and which is true for each frequency, is based on Green function and on moment method. This method is based on solving the integral equation which concerns the electric field generated by the currents flowing in the antennas elements and its feeding systems. These currents are unknown. We simulate the flow of induced current by means of distribution for base and test currents, next we test their mutual reaction by means of these functions. According to [L-8.7] the reaction has the form of:

$$\langle \vec{E}^i(\vec{J}_m); \vec{J}_i \rangle = - \sum_n I_n \langle \vec{E}^s(\vec{J}_m); J_n \rangle \quad (1)$$

The unlimited sequence of these functions is necessary for exact solution. We assume the limited number of these functions and, thus we obtain approximate solution. The mutual reaction of the whole analysed system can be expressed in the form of a matrix equation:

$$[z_{mn}] [I_n] = [V_m] \quad (2)$$

By solving this equation we define the distribution of the currents flowing along the analysed structure on condition that we have defined the elements of general matrix impedance, which in our case has the form of:

$$z_{mn} = -\frac{1}{\pi^2} \int_0^\infty \int_0^\infty F[G(k_x, k_y)] \{F[J_0(k_x)]\}^2 \cos[k_x(x_m - x_n)] \cdot \cos[k_y(y_m - y_n)] dk_x dk_y \quad (3)$$

where:

$F[G(k_x, k_y)]$ - Fourier transform of Green function

$F[J_0(k_x)]$ - Fourier transform of base current

x_n, y_n, x_m, y_m - respectively, the coordinates of the means of base and testing functions.

With the defined current distribution we can express the radiation pattern in the dipole plane by the following equation:

$$\vec{E}(\varphi) = \sum_{n=1}^N I_n [\vec{E}(\vec{J}_n)] \quad (4)$$

where:

I_n - coefficient of current distribution

The microstrip antennas patterns (presented in fig. 9a, 10a,) have been calculated on the basis of these relationships

4. MICROSTRIP DIPOLE ANTENNA

Microstrip dipole antenna has been designed for GSM hand-held unit which operates at 900 MHz band. It can also be easily implemented for DCS system which operates at 1800 MHz.

The structure of the dipole antenna with coaxial feeding is presented in figure 4. The microstrip dipole radiator is excited by the microstrip resonator which is coupled with the handset input. There are two possibilities of feeding the dipole antenna i.e. using coaxial feedline (fig.4) or unsymmetrical stripline - USL (fig.5).

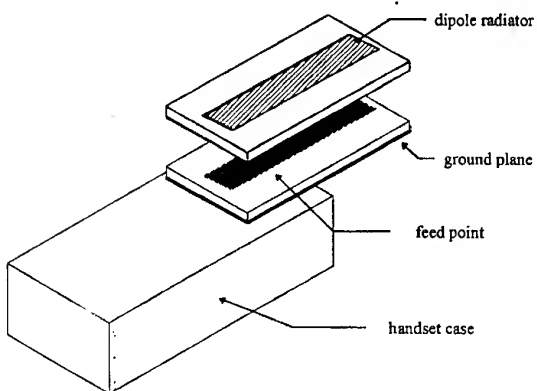


Fig. 4. Microstrip dipole antenna with coaxial feedline

Typically, the microstrip radiator is excited directly from the feedline when USL is used for feeding the antenna, as it is shown in figure 5.

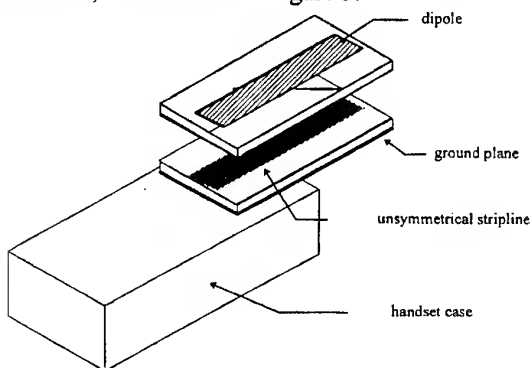


Fig. 5. Microstrip antenna with unsymmetrical stripline

The multilayer technology used for dipole antennas is described here. This structure was selected to obtain the necessary bandwidth of the antennas (about 10%) which is necessary for GSM application.

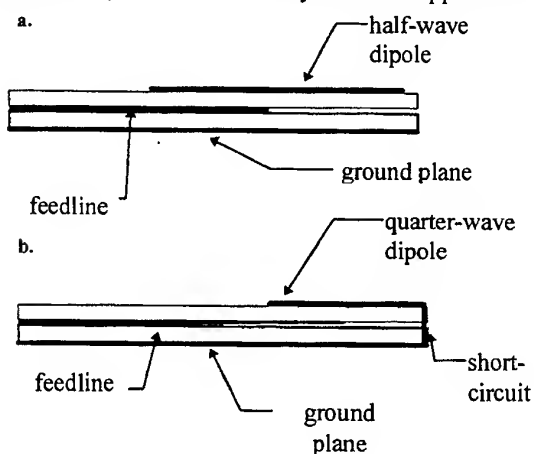


Fig. 6. Half-wave (a) and quarter-wave (b) dipole

Taking into account the requirements for the small size antenna for GSM application, two types of multilayer microstrip dipole antennas were manufactured and tested i.e. :

- open-circuit half-wave dipole,
- short-circuit quarter-wave dipole.

The structure of these antennas is presented in figure 6. Special attention should be paid to a quarter-wave dipole antenna due to its size which is especially important for 900 MHz band application. This antenna is approximately half the size of the half-wave antenna. It can be expected that the radiation pattern of a quarter-wave antenna in the E-plane may be sufficiently wide to achieve the optimal values of the antenna parameters antennas

5. MICROSTRIP PATCH ANTENNA

The application of a patch antenna for mobile communications is possible when higher frequency bands are considered (e.g. $f > 1 \text{ GHz}$). The structure of a multilayer microstrip patch antenna is presented in figure 7. The upper rectangular patch radiator of L in length and W in width is excited by a slot placed on the upper side of the lower layer of the antenna. This slot is coupled with unsymmetrical feedline. The dimensions L and W as well as the slot location were selected empirically in accordance with the bandwidth criterion.

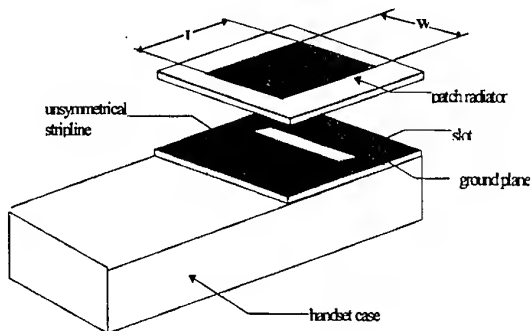


Fig. 7. Structure of patch microstrip antenna

Next we optimize the dimensions of the patch that is its resonance length and the length of the slot in order to make the real part of the input impedance and the wave impedance of the feeding line equal. In case of a multilayer structure the process of designing is more complicated due to greater manipulation freedom. The requirements for a small size of a handset antenna makes this structure effective at a higher frequency band (e.g. for DCS 1800 system).

6. MEASUREMENTS RESULTS

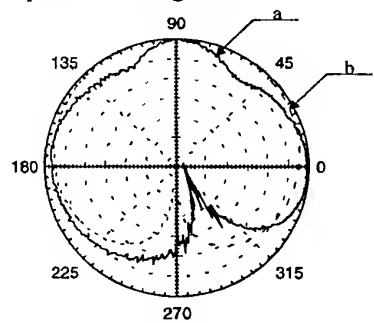
The construction of a microstrip antenna on a multilayer dielectric is presented in fig.8.



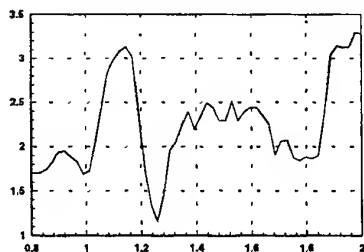
Fig.8. Microstrip dipole antenna with GSM handset

The empirical verification of dipole and patch microstrip antennas characteristics was performed.

Measurements were made in free space and in user presence to investigate the influence of handset antenna radiation on the user's head. During the experiments the user was standing on a rotary platform and was holding a GSM handset at 45° to the ground. Some results of quarter-wave dipole antenna measurements are presented in figure 10 i.e.: standing wave ratio, radiation pattern in free space. The similarly measured characteristics of microstrip patch antenna are presented in figure 9.

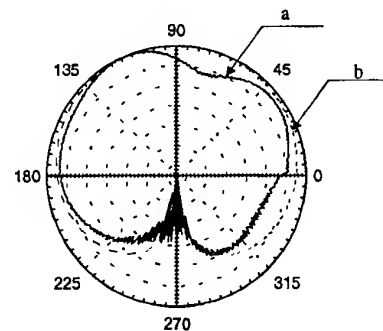


a. Radiation pattern in free space
b. Theoretical characteristic

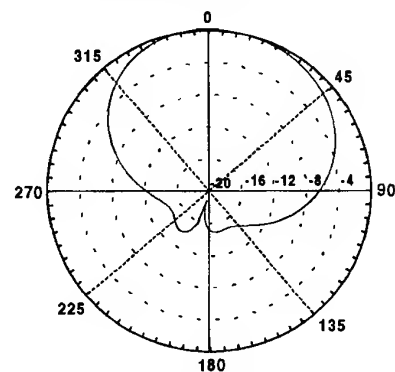


c. Standing wave ratio

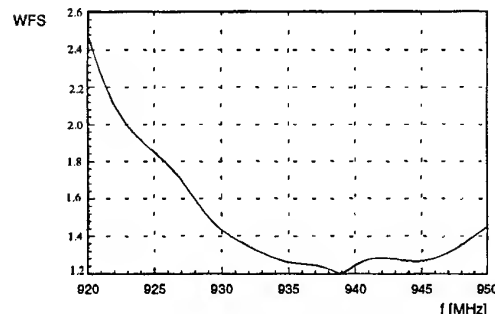
Rys.9. Patch antenna measurements results



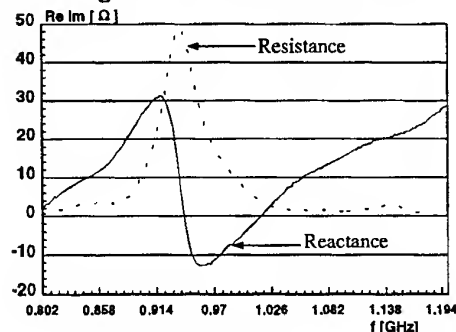
a. Radiation pattern in free space
b. Theoretical characteristic



c. Radiation pattern with man presence



d. Standing wave ratio measurement results



e. Input impedance

Rys.10. Dipole antenna measurements results

7. CONCLUSION

Two types of microstrip antennas for mobile communications were presented in the paper. The experimental results showed that a compromise between the requirements for radiation pattern and the protection of human head from this radiation is possible. Both antenna have the reduced radiation towards handset operator head and they ensure reliable communication regardless of the antenna orientation. Dipole antenna is preferable to GSM 900 applications while patch antenna may be used effectively when cellular system operates at the frequencies above 1 GHz.

8. REFERENCES

- 8.1 M. Arnanowicz, W. Kołosowski, M. Wnuk, A. Jeziorski „Microstrip antennas for mobile communications” Proc. Of the Conference VTC'97 Phoenix , May. 1997, USA.
- 8.2 Bahl I.J Microstrip antennas with paper-thin dimensions. Microwaves No. 10.1979
- 8.3 Guy A.W, Lehmann J.F, Stonebridge J.B. Therapeutic applications of electromagnetic power. Proceedings of the IEEE vol. 62 No. 1. 1974
- 8.4 Jensen M.A, Rahmat-Samii Y, Performance analysis of antennas for hand-held transceiver using FDTD. IEEE_Transactions on antennas and propagation. vol. 42 No 8. 1994
- 8.5 R.J.Mailloux, J.F.McIlvenna, N.P.Kernweis: Microstrip Array Technology, ” IEEE Trans. Antennas and Propagat. AP-29, No.1, January 1981.pp.25-38
- 8.6 Xiao-Hai Shen,A.E. Vandebosch, A.R.Van de Capelle: Study of Gain Enhancement Method for Microstrip Antennas Using Moment Method, ” IEEE Trans. Antennas and Propagat. AP- 43 No 3, 1995.pp. 227-231
- 8.7 W. Kołosowski, M. Wnuk „Impedancia wzajemna anten liniowych umieszczonych na podłożu dielektrycznym” Biuletyn WAT 1988 Nr 11.



Dr Marian Wnuk was born in Lublin, Poland in 1943. He studied measure systems at Technical University of Warsaw, Poland, where he received the MSc degree in 1968. In 1987 he received Ph.D. degree in communication system from Military University of Technology. Dr Wnuk specialises in problem concentration of the antenna field analyses and

construction of the antenna on a dielectric layer as well as in the electromagnetic compatibility of communications systems. He has received awards of the Minister of National Defence for his outstanding scientific achievements and practical application of their results. He is a member of many research councils of Polish universities and of research industrial institutes



Prof. Włodysław Kołosowski was born in Poland. He has been working at Military University of Technology since 1952. In 1962 and 1978, he received the PhD and DSc degree respectively from Military University of Technology both in communications systems. He was given the title of professor in 1981. Professor Kołosowski

specialises in problems concerning the antennas fields, with analysis and construction of antennas on a dielectric layer as well as with the electromagnetic compatibility of communications systems. He has received three awards of the Minister of National Defence for his outstanding scientific achievements and practical application of their results. Prof. Kołosowski is a member of IEEE and of Armed Forces Communications and Electronics Association (AFCEA). He is a member of many research councils of Polish universities and of research industrial institutes



Dr Marek Amanowicz was born in Łódź, Poland, in 1946. He studied communications systems at Military University of Technology, Warsaw, Poland, where he received the MSc degree in 1970. In 1978 and 1990, he received PhD and DSc degree respectively from MUT both in communications systems. From 1993 to 1996

he held a dean of Electronics Faculty position in MUT. In 1996 he became a deputy rector of MUT. From 1994 he has been a professor at MUT. The main domain of his research work is communication theory with application to communication system modelling and its analysis. His current interests are in communications systems engineering and telegraphic analysis.

Dr. Amanowicz is a member of IEEE, New York Academy of Science and AFCEA of present the president of the Polish Chapter of AFCEA. He is a member of many research councils of the polish universities and research industrial institutes

VIII

EMC RELATED TO PCB AND IC

AN EFFECT OF FAR-END CROSSTALK COMPENSATION IN DOUBLE-LAYERED DIELECTRIC PCB INTERCONNECTS

T.R.Gazizov and N.A.Leontiev

Television Systems Department, Tomsk State University of Control Systems and Radioelectronics,
Lenin Ave., 40, Tomsk, Russia, 634050, phone/fax:+7(3822)423112, E-mail: talgat@tu.tasur.edu.ru

The problem of crosstalk reduction is considered. The possibility of far-end crosstalk compensation in cascaded sections of coupled inverted microstrip lines and coupled suspended microstrip lines of double-layered dielectric PCB is shown. Computer simulations of capacitive and inductive couplings and of far-end crosstalk waveform are performed to show an effect of complete far-end crosstalk compensation.

1. INTRODUCTION

The crosstalk reduction problem becomes one of most important an internal EMC problems being an obstruction for development of high-speed and high density digital electronic equipment. Particularly, the problem is very actual for PCBs with the long interconnects in nonhomogeneous dielectric filling. In this case, the magnitude of crosstalk at the far end of passive line may be much more than at the near end, as shown, for example, in well known paper [1].

The far-end crosstalk may be reduced by wider separation of coupled interconnects that is often impossible in case of high density interconnects. Another way consists in the placing of additional grounded traces between coupled interconnects, but it has the same drawback and, moreover, as shown in [1], sometimes has the negative effect. In [2] the crosstalk in double-layered dielectric PCB with interconnects formed by suspended and inverted microstrip lines was considered and it was shown particularly that the far-end crosstalk in coupled pairs of the lines may be eliminated. An advantage of the way is that the elimination is forceful for arbitrary length of coupled lines, because the capacitive and inductive couplings in the lines are equalized, but unfortunately it takes place only for certain choice of dielectric parameters of suspended line or inverted line.

The aim of this paper is to show an additional possibility for reduction of far-end crosstalk in interconnects of double-layered dielectric PCB.

2. THE PROPOSED METHOD

First of all, it would be noted that we shall consider here the cases of two coupled lines only, assuming for simplicity that the influence of other conductors is neg-

ligible. The main idea of the proposed method consists in the following.

As shown in [3, 4], the capacitive coupling of suspended or inverted microstrip lines may be more than, less than or equal to the inductive coupling in accordance with parameters of the lines. (Note that the capacitive coupling of usual microstrip line is always less than the inductive coupling for any parameters of the line.) Therefore, the far-end crosstalk being approximately proportional to the difference of capacitive and inductive couplings will have positive or negative polarity in accordance with parameters and type of the lines.

It is well known that for real PCB's layout the interconnects of neighboring signal layers are passed orthogonal so that a long interconnect consists, as a rule, of two, three or more cascaded sections of lines connected through via with each other. For double-layered dielectric PCB a high-speed signal propagates, for example, from driving output along inverted microstrip line and then through via along suspended microstrip line to receiving input. For considered case of coupled interconnects it is obvious to assume the following. If the difference of capacitive and inductive couplings in one section has a sign which is opposite to the difference of capacitive and inductive couplings in other section, the partial or complete compensation of far-end crosstalk is possible. To test this assumption the computer simulations of capacitive and inductive couplings and of far-end crosstalk waveform are performed for structure shown in Fig. 1.

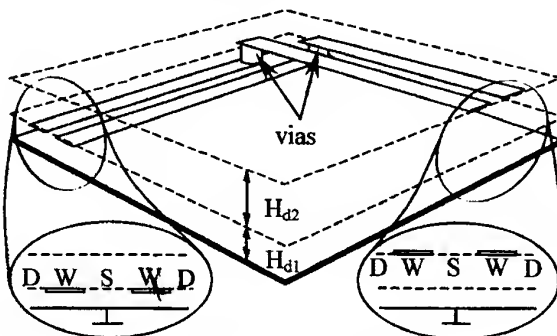


Fig. 1. Cascaded sections of coupled lines

3. COMPUTER SIMULATION OF CAPACITIVE AND INDUCTIVE COUPLINGS

First of all, the per unit length matrixes of capacitive coefficients [C] (in real dielectric filling), [C₀] (in air) and inductive coefficients [L] are calculated for both lines by program based on two-dimensional method of moments and described in [3, 4]. The relative dielectric permittivities of the first and of the second (from a ground plane) dielectric layers are $\epsilon_{r1}=2$ and $\epsilon_{r2}=5$, accordingly. An external dielectric is air. The relative permeabilities of all dielectrics are equal to unit. All strips have the same thickness (T) and the same width (W). These T and W are such that T/W=0.1. A distance between internal sides of coupled strips (S) and a distance from external sides of strips accounted for in calculations (D) are equal to W. The heights of the first and of the second dielectric layers (H_{d1} and H_{d2}) are such that $H_{d1}/W=0.5$ and $H_{d2}/W=0.01, \dots, 1$.

Then, using the calculated elements of matrixes [C] and [C₀] a capacitive coupling (K_C) and an inductive coupling (K_L) are obtained accordingly by following formulae.

$$K_C = \frac{-C_{2,1}}{C_{1,1}}; K_L = \frac{L_{2,1}}{L_{1,1}} \quad (1)$$

A difference ($K_C - K_L$) of capacitive and inductive couplings as a function of height of the second dielectric layer relative to width of strip (H_{d2}/W) is shown in Fig. 2 for both lines. Note that in $H_{d2}/W=0.09$ the value of function for inverted line changes a sign, while in $H_{d2}/W=0.28$ the values of both functions have the same magnitudes and opposite signs. According to proposed method of far-end crosstalk reduction it may be supposed the following.

For structure shown in Fig. 1 and consisting of two the same sections of coupled inverted and coupled suspended lines, the resultant value of far-end crosstalk is proportional to a sum of contributions of inverted and suspended lines. Each of these contributions in turn is proportional to value ($K_C - K_L$) of corresponding line. Therefore (see Fig. 2), when rising H_{d2}/W from 0.01 to 0.09 the resultant value of far-end crosstalk will decrease due to the contributions of both lines are decreasing. However, in $H_{d2}/W=0.09$ the contribution of inverted line becomes minimal. When rising H_{d2}/W from 0.09 to 0.28 the resultant value of far-end crosstalk will decrease due to the contribution of suspended lines is slowly decreasing, but mainly due to the contribution of inverted lines is increasing with opposite sign. Here the phenomenon of partial compensation of far-end crosstalk of suspended lines by far-end crosstalk of inverted lines will take place, while approximately in $H_{d2}/W=0.28$ an effect of complete compensation of far-end crosstalk would be observed. When rising H_{d2}/W from 0.28 to 1 the resultant value of far-end crosstalk will increase due to the contribution of suspended lines are slowly decreasing, but mainly due to the contribution of inverted lines are increasing with opposite sign. Here the phenomenon of overcompensation of far-end

crosstalk of suspended lines by far-end crosstalk of inverted lines will take place, resulting in change of polarity of resulting far-end crosstalk.

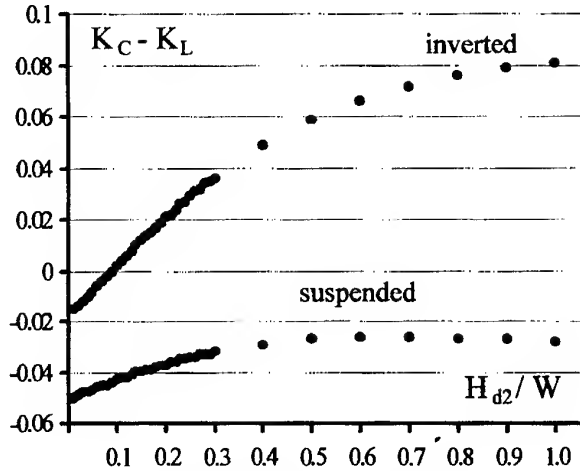


Fig. 2. The difference of capacitive and inductive couplings for considered lines

4. COMPUTER SIMULATION OF CROSSTALK WAVEFORMS

To test the analysis of far-end crosstalk's behavior with change of H_{d2}/W a computer simulation of far-end crosstalk waveform is performed. The even- and odd-mode method used in [5] is applied for case of cascaded sections of coupled lines shown in Fig. 1. The far-end crosstalk may be obtained using the following formula from [5]

$$V_f(t) = \frac{1}{2} (V_T^e(t) - V_T^o(t)), \quad (2)$$

where $V_T^e(t)$ and $V_T^o(t)$ are the transmitted signals calculated for case of single lines of the considered structure with parameters of even mode and odd mode, accordingly.

A simplified equivalent circuit for case of single lines of the considered structure may be presented as shown in Fig. 3, where Y_0, Y_1, Y_2, Y_3 and $\tau_0, \tau_1, \tau_2, \tau_3$ are the characteristic admittances and total signal delays of lines' sections, while C_d is equivalent lumped capacitance discontinuity.

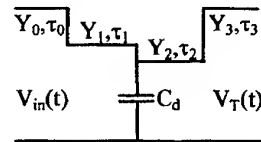


Fig. 3. A simplified equivalent circuit of cascaded sections of single lines.

For this circuit, using inverse Laplace transform the analytic expressions have been obtained recently by authors for transient response on ramp input signal $V_{in}(t) = (V_{in0} / t_r) [t U(t) - (t - t_r) U(t - t_r)]$, where $U(t)$ is a step function, and V_{in0} and t_r are the mag-

nitude and the rise time of the ramp step input. A detailed derivation of the expressions is presented in [6]. An expression for transmitted signal used here for calculation of far-end crosstalk by (2) is the following.

$$\begin{aligned} V_T(t) = & (V_{in0}/t_r) T_{10} T_{32} \\ & \cdot (d_1/a_1) \{ R(1, a_1(t - (\tau_1 + \tau_2))) \\ & - \Gamma_{10} [R(1, a_1(t - (3\tau_1 + \tau_2))) \\ & - (1 + a_2/a_1) R(2, a_1(t - (3\tau_1 + \tau_2)))] \\ & - \Gamma_{23} [R(1, a_1(t - (\tau_1 + 3\tau_2))) \\ & - (1 - a_2/a_1) R(2, a_1(t - (\tau_1 + 3\tau_2)))] \\ & + \Gamma_{10} \Gamma_{23} d_1 d_2 a_1^{-2} R(3, a_1(t - 3(\tau_1 + \tau_2))) \}, \quad (3) \end{aligned}$$

where

$$T_{10} = \frac{2Y_0}{Y_0 + Y_1}; T_{32} = \frac{2Y_2}{Y_2 + Y_3} \quad (4)$$

$$\Gamma_{10} = \frac{Y_1 - Y_0}{Y_0 + Y_1}; \Gamma_{23} = \frac{Y_2 - Y_3}{Y_2 + Y_3}, \quad (5)$$

$$a_1 = \frac{Y_1 + Y_2}{C_d}; a_2 = \frac{Y_1 - Y_2}{C_d} \quad (6)$$

$$d_1 = \frac{2Y_1}{C_d}; d_2 = \frac{2Y_2}{C_d}, \quad (7)$$

$$\begin{aligned} R(n, x) = & (1/a_1) [xP(n, x) - x_r P(n, x_r)] \\ & - (n/a_1) [P(n+1, x) - P(n+1, x_r)], \quad (8) \end{aligned}$$

where

$$P(n, x) = 1 - e^{-x} \sum_{k=0}^{n-1} \frac{x^k}{k!}, \quad (9)$$

$$x_r = x - a_1 t_r. \quad (10)$$

The even- and odd- mode characteristic admittance and total signal delay for sections of coupled inverted lines and coupled suspended lines are obtained from calculated (see paragraph 3) elements of [C] and [C0] matrixes by following formulae.

$$Y^e = c \sqrt{C^e C^{0e}}; Y^o = c \sqrt{C^o C^{0o}}, \quad (11)$$

$$\tau^e = \frac{\ell}{c} \sqrt{C^e / C^{0e}}; \tau^o = \frac{\ell}{c} \sqrt{C^o / C^{0o}}, \quad (12)$$

where

$$C^e = C_{1,1} + C_{2,1}; C^o = C_{1,1} - C_{2,1}, \quad (13)$$

$$C^{0e} = C_{0,1,1} + C_{0,2,1}; C^{0o} = C_{0,1,1} - C_{0,2,1}, \quad (14)$$

c — speed of light in vacuum,

ℓ — the length of section of according line.

5. RESULTS OF WAVEFORMS' CALCULATIONS

The parameters of first and last sections representing the terminating sections of matched lines or driving output and receiving input ($\tau_0=0$ and $\tau_3=0$) are the same for both modes accordingly. In order to minimize an influence of lines' mismatching, the both terminations were assumed 50 Ohms. A strict accounting for the value of capacitive discontinuity for both modes demands a comprehensive three dimensional electrostatic field cal-

culations, for example, by method of moments and is not in scope of this paper. Therefore, in order to minimize an influence of capacitive discontinuity, we assume $C_d=0.01$ pF for both modes. At last, the lengths of lines' sections is assumed here the same ($\ell=100$ mm) in order not to consider in this paper their influence on far-end crosstalk compensation. The magnitude of the ramp input $V_{in0}=10$ V and the rise time $t_r=10$ ps.

Far-end crosstalk waveform was calculated for a number of values of H_{d2}/W . A phenomenon of far-end crosstalk compensation is observed clearly from plots of these waveforms. Three examples of the plots are shown in Fig. 4. The first plot (a) calculated for $H_{d2}/W=0.01$ demonstrates the high negative magnitude of far-end crosstalk. An effect of complete far-end crosstalk compensation is observed clearly in the second plot (b) calculated for $H_{d2}/W=0.28$. The third plot (c) calculated for $H_{d2}/W=1$ demonstrates the high positive magnitude of far-end crosstalk, taking place due to the overcompensation of far-end crosstalk. An increasing mismatching between the lines' sections and at the terminations is observed also.

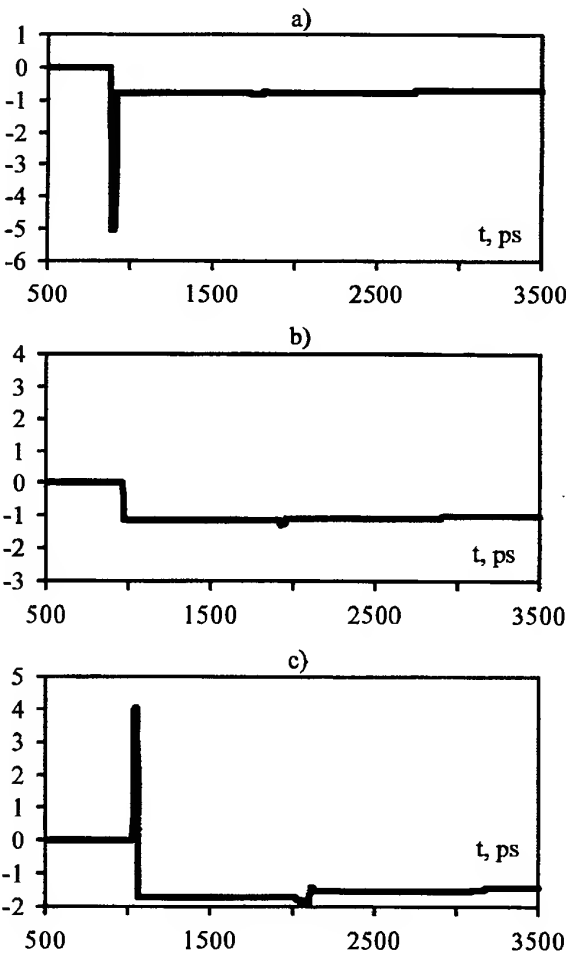


Fig. 4. The far-end crosstalk waveforms (in Volts) for $H_{d2}/W=0.01$ (a); 0.28 (b); 1 (c).

In conclusion it would be noted the following. A waveform calculated by (3) consists of the traveling wave and the terms undergoing two reflections before coming to the output, while the terms undergoing four, six and more reflections are not accounted for. It was shown in [7, 8] for periodic structures with large number of sections that for cases with large difference of the characteristic admittances and moreover of the total delays in different line sections the contributions of the terms not accounted for may be very significant. Therefore, the presented formula is accurate for almost matched cases, for example, for estimation of effect of admittance tolerance on the signal waveforms, while in other cases the accounting for the additional terms of the signal may be necessary.

However, it is seen clearly that for plots of Fig. 4 the main component of far-end crosstalk coming to output at time ($\tau_1 + \tau_2 \approx 1000$ ps) is specified by traveling wave only, while the other components of the waveform specified by terms undergoing two reflections come to output later and are negligible.

6. ACKNOWLEDGMENT

T.R.Gazizov thanks N.I.Bazenkov for enthusiasm on this work and A.V.Gazizova for great support.

7. REFERENCES

1. A.R.Djordjevic, T.K.Sarkar, and R.F.Harrington, "Time-domain response of multiconductor transmission lines," IEEE Proceedings, vol.75, no.6, pp.743-764, June 1987
2. T.R.Gazizov and N.I.Bazenkov, "On the crosstalk reduction in printed circuit boards", Proceedings of the 12-th Int. Wroclaw Symposium on EMC, June 28 - July 1, 1994, pp.550-553
3. T.R.Gazizov, "Computer simulation of electromagnetic coupling in interconnects of a double-layered dielectric PCB: parallel lines on one side of the layer", Proceedings of the 13-th Int. Wroclaw Symposium on EMC, Wroclaw, Poland, June 25-29, 1996, pp.230-234
4. T.R.Gazizov, "Computer simulation of electromagnetic coupling in interconnects of a double-layered dielectric PCB: parallel lines on opposite sides of the layer", Proceedings of the 6-th Int. Symposium on Antennas and Propagation, Chiba, Japan, September 24-27, 1996, pp.681-684
5. Q.Gu and J.A.Kong, "Transient analysis of single and coupled lines with capacitively-loaded junctions", IEEE Trans. Microwave Theory Tech., vol.MTT-34, pp.952-964. Sept.1986

6. T.R.Gazizov and N.A.Leontiev, "Analytical Expressions for Transient Response of Two Cascaded Transmission Line Sections" (in Russian), Trudy TUSUR, 1998, to be published
7. T.R.Gazizov and N.A.Leontiev, "Analytical Expression for Transient Response of a Periodic Structure Consisting of Two Kinds of Transmission Line Sections With Capacitively Loaded Junctions.", Proceedings of the 4-th Int. Symposium on Antennas and EM Theory, August 19-22, 1997, Xi'an, China, to be published.
8. T.R.Gazizov and N.A.Leontiev, "Transient Response of a Periodic Transmission Line Structure With Capacitively Loaded Junctions", Proceedings of the 1997 Sino-Japanese Joint Meeting on Optical Fiber Science and Electromagnetic Theory, October 14-16, 1997, Wuhan, China, to be published.

BIOGRAFICAL NOTES

Gazizov Talgat Rashitovich was born in 1963. He got his higher professional education on radioengineering in 1985 in the Tomsk Institute of Automatic Control

Systems and Radioelectronics. His research interest is the multi-conductor transmission lines' analysis and its application to digital systems. Now he is finishing his work toward Ph.D. degree with Television Systems Department of Tomsk State University of Control Systems and Radioelectronics.



Leontiev Nyurgun Anatolievich was born in 1974. He got his higher professional education on radiophysics and electronics in 1996 in Yakutsk State University. Now he is working toward Ph.D. degree with Television Systems Department of Tomsk State University of Control Systems and Radioelectronics.

EXPERIMENTAL VALIDATION OF A HYBRID METHOD TO PREDICT DIFFERENTIAL AND COMMON MODE RADIATED EMISSIONS

Emmanuel LEROUX*, Carla GIACHINO*, Razvan ENE*, Flavio CANAVERO**, Paolo FOGLIATI[†], Bernard DEMOULIN[°]

*High Design Technology
Corso Trapani 16
10139 Torino Italy

**Politecnico di Torino
Corso Duca degli Abruzzi 24
10100 Torino Italy

^CSELT
Via Reiss Romoli 274
10148 Torino Italy

[°]Université de Lille-LRPE
59655 Villeneuve d'ascq
France

The introduction of severe Electromagnetic Compatibility international standards had as a result the interest of manufacturers of electronic systems on optimizing their products, in most of cases Printed Circuit Boards, before the compliance tests. In this paper we present the validation of a hybrid approach aimed at predicting radiated emissions due to differential mode currents on boards traces and common mode currents flowing through attached cables.

1. INTRODUCTION

The introduction of severe international standards in the field of Electromagnetic Compatibility (EMC) in the last years had as result an increasing interest for computing the radiated electromagnetic fields from electronic products. In fact the manufacturers of electronic systems are interested in optimizing from EMC point of view their products before arriving to the compliance tests in order to reduce time to market and contain the costs. In most of the cases the electronic products are composed of Printed Circuit Boards (PCBs) and connection cables. The possibility of having a fast and reliable estimation of the radiated field of a PCB at design level is highly desirable.

In the first part of this paper, a numerical hybrid method is presented. It associates analytical techniques and numerical methods to predict the emissions radiated by differential mode currents on PCB traces and common mode currents flowing on attached cables.

In the second part an experimental validation using a specific test board is proposed. It permits to appreciate the realism of results and the trade-off with simulation time.

2. HYBRID METHOD FOR COMPUTING RADIATED EMISSIONS (RE) FROM PCB AND ATTACHED CABLES

First of all the method used to compute RE from PCB traces is presented. Then the calculation of the radiation of a cable whose shield is attached to the PCB ground plane is explained.

2.1 Green Dyadic for computing radiation from PCB traces

As dielectric layers can severely modify radiation patterns [1], it is important to take into account for each microstrip structure the actual medium existing between the metal plane and the air. A possible way to take into account dielectric layers in the RE calculation is to use the dyadic Green's function of the actual PCB medium.

The start point is the determination of the actual current distribution along each trace. The method just needs the knowledge of voltage and current on one of the two extremities of each rectilinear trace, information given by PRESTO™ environment [2]. Then the current waveform at any abscissa x on the trace is determined by means of the Transmission Line Theory (TLT) assuming that only the quasi-Transverse Electric Magnetic (TEM) mode is present along the trace. Then, the radiated field can be calculated using dyadic Green's function, which can be interpreted as a transfer function between the surface current distribution and the electric field.

With the assumption of being in far field conditions, the Green Dyadic can be substantially simplified. Fortunately this particular condition applies approximately at 10m in the whole frequency range (30MHz÷1GHz) described in EN55022 standard [3] used for Information Technology Equipment (ITE), which justifies the use of far field Green's function. Being difficult to directly calculate the electric field due

to the current density of a segment buried in dielectric layers, the far field method applies the same current source on the observation point where the EM field has to be calculated and exploits the theory of reciprocity [4] to transform the emission problem in a susceptibility one.

Then the method assumes that the field arriving at the air/dielectric interface is a plane wave which can be divided into two components, the transverse electric (TE) and transverse magnetic (TM) modes. With the use of Modal analogy, Transmission Line Theory (TLT) can be then applied to the propagation of these two modes in the embedded microstrip structure and two transfer functions are produced for the actual medium between the metal plane and the air.

2.2 An hybrid method for computing radiation from common mode currents on an attached cable

The finite dimension of the PCB local ground plane and the presence of the soil (ground) cause a Common Mode (CM) current flowing through the local plane itself. If a cable is attached to the plane, this current spreads along the cable too; the cable behaves like an antenna and radiates a CM electromagnetic field.

To model the CM ground noise, it is necessary to take into account inductive and capacitive couplings between the PCB and the metal floor of the chamber.

The key idea of the present method is to model the common mode current on the local plane as an equivalent noise voltage source, depending on voltages and currents on PCB traces [5], which stimulates the cable. Below is explained the algorithm for a trace:

Noise voltage on the cable can be seen as an effect of voltage and current on the PCB trace, respectively corresponding to a capacitive and an inductive term.

$$V_{\text{noise}} = \frac{C_{20}}{C_{10}} V_{\text{track}} + j\omega L_{\text{trans}} I_{\text{track}} \quad (1)$$

where

- C_{10} models the capacitive coupling between local PCB plane and metal floor;
- C_{20} models the capacitive coupling between trace and metal floor;
- L_{trans} is a transfer inductance depending on the mutual inductance between the PCB local plane and the trace.

Capacitances are evaluated by the means of Partial Element Equivalent Circuit (PEEC) method [6]. The transfer inductance is calculated by the means of a closed form formula using coupled flux [7].

If more traces are laying on the PCB local plane, the superposition of effects can be applied to obtain the equivalent voltage source.

This approach has a fundamental advantage: it allows to separately analyze PCB and cable equivalent circuits, through a "Thevenin-like" approach but the coupling by proximity between traces and cable is not taken into account.

Once the equivalent noise voltage source has been evaluated, CM current flowing through the cable can be calculated applying TLT to the cable itself. It is seen as

a Transmission Line above an infinite ground plane (the soil), with air as dielectric. This requires the minimum involved wavelength to be greater than the physical dimensions of the structure. The biggest involved dimension is typically the height of the PCB above the soil. The model can approximately apply up to about 300MHz for a PCB placed at 0.8m of distance from the soil. Fortunately this limit corresponds to the maximum frequency for which the RE due to the cable is predominant on the total RE for most of cable lengths used in RE tests for ITE equipment [3]. The method is so used until the maximum frequency defined by the height of the PCB above the soil.

The method calculates then the electromagnetic field radiated from CM current on the cable taken into account the soil (ground), seen as an infinite reference plane.

3. EXPERIMENTAL VALIDATION:

For the validation process different test boards were built. The board A used in this paper is presented in the figure 1.

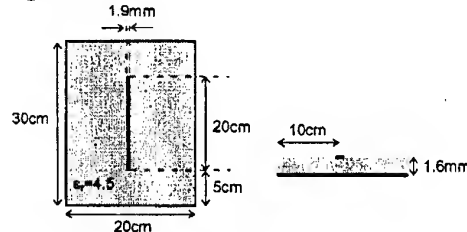


Fig.1: Board A: a microstrip with one rectilinear trace.

The measurement were made at the semianechoic chamber of CSELT (Telecom Research Center), Torino Italy. The facility allows to test equipment for European and International Standards for radiated emission (at 10 meters in full compliance of the ± 4 dB requirements of Normalized Site Attenuation (NSA)) and immunity. The soil (ground) is now referred to the metal plane of the semianechoic chamber. The experimental validation is divided in several parts. Each of them is aimed to verify a specific coupling.

Firstly the Green Dyadic formulation is verified using Board A. Two types of techniques are used to supply the board, a sine waveform generator and a digital oscillator. As it is important to provide the actual current distribution on the traces, driver models are firstly validated by the means of comparison with measurements. In order to cover a broad band of frequencies and technologies, two oscillators were used. The first one provides a 10 MHz frequency CMOS signal and will be used for the RE tests in the low frequency range (30÷200MHz). The second one provides a 68.8 MHz frequency ECL signal and will be used for the RE tests in the high frequency range (200MHz÷1GHz). In order to avoid unwanted couplings, both oscillators along with powering batteries were closed in a shielding box. The Green Dyadic formulation calculates RE due to differential

mode currents on PCB traces. So a metal plane of big dimensions has been connected to the ground plane of board A during the validations shown in § 3.3 and 3.4 to avoid creating common mode contributions.

The emissions estimation is based on the values of the current and voltage on the trace, so a good model is required both for oscillator and PCB. An accurate model of the trace and through holes was developed, among with a very good model for the oscillator.

3.1 Model of the ECL oscillator

Starting from the measured static and dynamic output characteristics, we obtain the equivalent circuit of fig. 2.

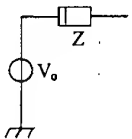


Fig. 2: Equivalent circuit of the driver.

V_o is the unloaded output voltage of the driver. To obtain the equivalent impedance Z , both the inductive and resistive effects have to be modeled. Impedance Z has been described starting from a Time Domain Reflectometer (TDR) characterization to obtain a Scattering S-parameter in time domain.

An accurate model must be guaranteed also in the working zone with varying R ; so a unique TDR measure is not in general enough to provide the complete model for Z . In this particular case, the used pull-down resistor (about 180Ω) that guarantees to always work in the zone with constant R , and the S-parameter is enough to model the complete equivalent impedance. The dynamic characteristic takes already into account the output resistance. Fig. 3 shows the comparison between the measured and simulated output of the ECL driver ended on a 50Ω resistor in the frequency domain. The ECL model is valid up to 894.4 MHz so it has been used for the RE tests in the high frequency range (200MHz+1GHz).

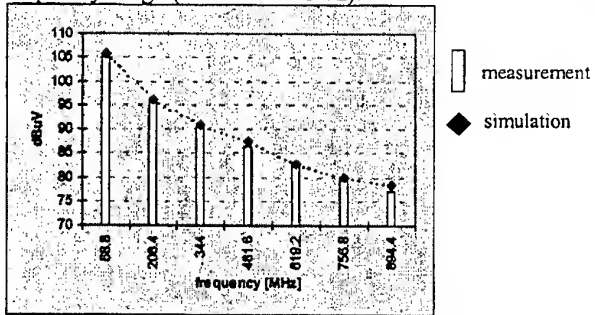


Fig. 3: Comparison between the measured and the simulated output of the ECL driver ended on a 50Ω resistor.

3.2 Model of CMOS oscillator

A shielded 10MHz CMOS signal generator has been modeled with the electrical circuit shown in fig. 4.

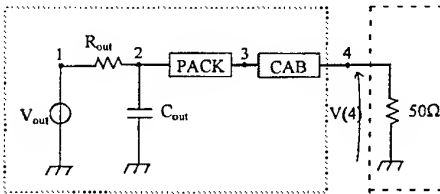


Fig. 4: Electrical Model of the CMOS driver.

- V_{out} is the measured unloaded output waveform of the driver.
- R_{out} is the 4Ω output resistance;
- C_{out} is the 25pF output capacitance;
- **PACK** is the model of the package of the integrated circuit and of the connections inside the oscillator shielding box; it is described through scattering parameters;
- **CAB** is the model of the coaxial cable connecting the test board to the oscillator connector; it is described through scattering parameters.

The 50Ω resistor models the input impedance of the measurement instrument.

In the ECL oscillator, **CAB** and **PACK** models were included in the Scattering description of Z impedance.

In fig. 5 the comparison between the measured and simulated output of the CMOS driver ended on a 50Ω resistor in the frequency domain is displayed. The CMOS model is valid from 30MHz up to about 450MHz. So the CMOS oscillator has been used for the RE tests in the low frequency range (30÷200MHz).

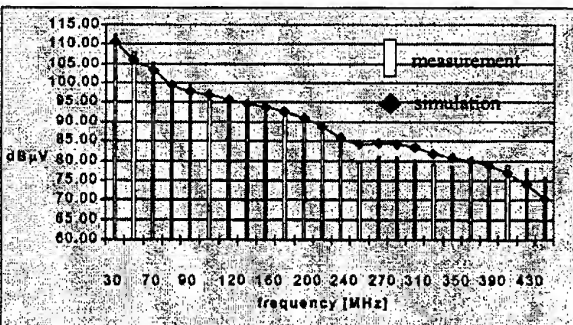


Fig. 5:Comparison between the measured and the simulated output of the CMOS driver ended on a 50Ω resistor.

3.3 Validation with sinusoidal signals

The first step of the validation process consists in the verification of the Green Dyadic formulation for the estimation of the RE by the tracks on the PCB. For doing this, Board A was powered by a sinusoidal generator placed outside of the chamber, and the radiated field was measured.

The board was connected to the generator via a 15m length cable, whose attenuation was taken into account. The test board has been vertically placed above the floor of the chamber. The metal plane of big dimensions has been used as a shield to limit RE from the portion of cable remaining in the chamber. In all the situations a

preliminary test has been made in order to quantify the contribution of the portion of cable on the total radiated field: measurements have been made with the cable not connected to the board, in order to measure only its effect. Measurements showed that the contribution of the portion of cable remaining in the chamber was really negligible (about 30-40dB lower than the total field). The first experimental setup is given in Fig.6 , while in Fig. 7. the measured and simulated field are plotted. The board is vertically placed above the metal floor of the chamber. The trace is horizontally placed, supplied with the sinusoidal oscillator and is ended on a 50Ω load. The antenna is polarized to have the maximum RE.

The frequency sweeps from 30MHz up to 1GHz.

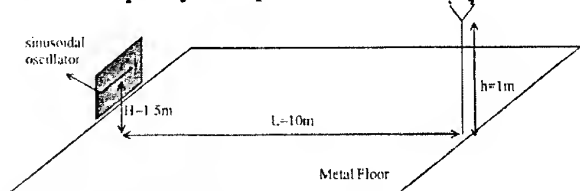


Fig.6: experimental setup

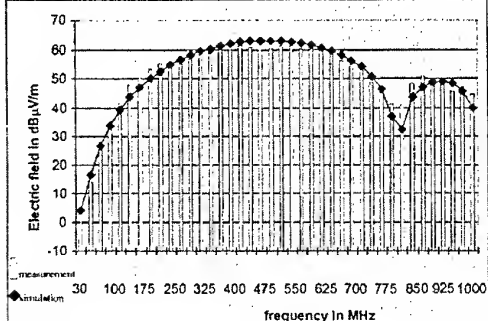


Fig.7:Comparison between measurement and simulation

The second experimental setup is given in Fig. 8, while in Fig. 9. the measured and simulated field are plotted. The board is vertically placed above the metal floor of the chamber. The trace is vertically placed, supplied with the sinusoidal oscillator and is ended on a 50Ω load. The antenna is polarized to have the maximum RE. The frequency sweeps from 30MHz up to 1GHz.

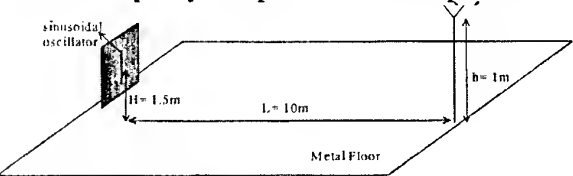


Fig.8: experimental setup

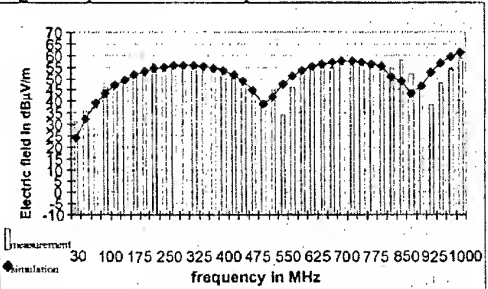


Fig.9:Comparison between measurement and simulation

3.4 Validation with ECL signals

The third experimental setup is given in Fig. 10, while in Fig. 11. the measured and simulated field are plotted. The board is vertically placed above the metal floor of the chamber. The trace is horizontally placed, it is supplied with the ECL signal generator and is not ended. The antenna is polarized at each antenna position to have the maximum RE, as requested from the standard [3].

h is varying from 1 to 4m, with a 0.5m step and the antenna is polarized at each antenna position to have the maximum RE, as requested from the standard [3]. The frequency range starts from 200MHz up to 1GHz. Only the harmonics that provide a maximum local radiated field are plotted because we are never sure to have both in measurement and in simulation exactly the same duty-cycle.

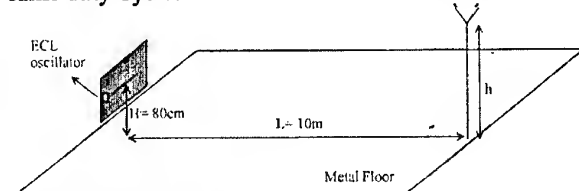


Fig. 10: experimental setup

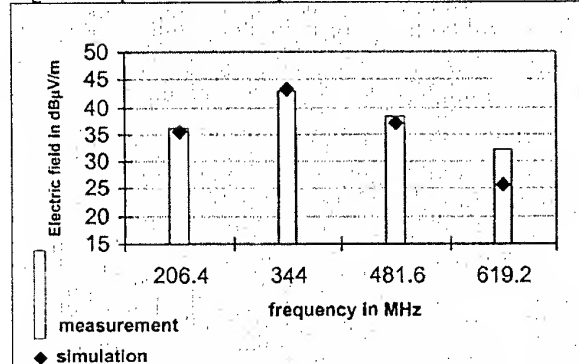


Fig. 11: Comparison between measurement and simulation

3.5 Validation with CMOS signals without and with the attached cable

For the validation of the evaluation of the radiated field with the attached cable, the PCB has always been driven with the CMOS oscillator. In the following an example is shown: the board is vertically placed above the metal floor of the chamber, it is not connected to the metal plane of big dimensions. The trace is ended on a 50Ω load, h is varying from 1 to 4m, with a 0.5m step and the antenna is polarized at each antenna position to have the maximum RE, as requested from the standard [3].

The fourth experimental setup is given in Fig. 12, while in Fig. 13. the measured and simulated field are plotted. The frequency range started from 30MHz up to 200MHz. The antenna is polarized to have the maximum RE.

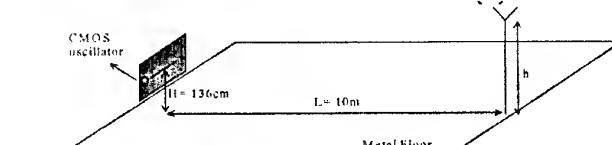


Fig.12: experimental setup

The same comparison has been performed with a 60 cm long cable whose shield is connected to the board, as shown in figure 14. The cable is open-ended. The comparison between measurement and simulation is shown in figure 15.

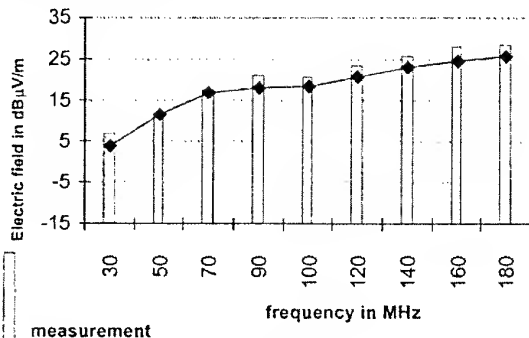


Fig.13:Comparison between measurement and simulation

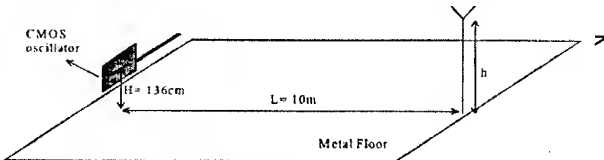


Fig.14: experimental setup

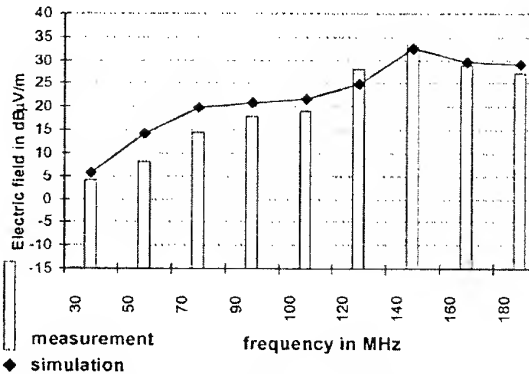


Fig.15:Comparison between measurement and simulation

The required simulation time on a HP750 workstation to obtain the radiated emissions results of a board which presents 6 nets and an attached cable is the following:

- PRESTO™ to obtain the current distribution on the nets: 4 s
- EmiR™ to obtain the differential mode radiated emissions from the nets: 2 s
- EmiR_CABLE™ to obtain the common mode radiated emissions from the cable: 15 s

4. CONCLUSIONS

The comparisons are good in most of the analyzed situations when the board is in vertical position: differences belongs to the $\pm 4\text{dB}$ range in the maximum field zone, while they are worse around the minimum. In a future paper results when the board is in horizontal

position will be presented. Some important considerations should be made about the simulation time: simulation were run on a HP750 workstation and took some seconds for each case. The presented solution for the prediction of radiated emissions of a PCB at post-layout level reaches a good trade-off between realism of results and computation time. It is so possible to simulate all the microstrips of a PCB for RE aspects in a reasonable simulation time: the tool can effectively be used in the CAD design flow. An experimental validation using an industrial board, put in vertical position, is presented in [8].

5. REFERENCES

- [1] E. Leroux, F. Canavero, G. Vecchi, "Prediction of radiated electromagnetic emissions from PCB traces based on Green dyadics", Proc. EURO-DAC, Brighton (UK), Sept. 18-22, 1995, pp. 354-359.
- [2] S. Fomo, S. Rochel, "Advanced Simulation and Modeling Techniques for Hardware Quality Verification of Digital Systems", EURO-DAC 1994, Grenoble France
- [3] EN55022, "Limits and methods of measurement of radio interference characteristics of information technology equipment", 1985
- [4] Monteath, "Applications of the Electromagnetic Reciprocity Principle", Pergamon Press, 1973.
- [5] J. R. Bergervoet, "EMC measurements and models connecting the system level with the module level", Philips Journal of Research, vol. 48, 1994, pp. 63-81.
- [6] A. E. Ruehli, "Equivalent circuit models for three-dimensional multiconductor systems", IEEE Trans. On Microave Theory and Techniques, v.MTT-22, march 1974, pp. 216-221.
- [7] F. B. J. Leferink, "Inductance calculations; methods and equations", IEEE symp. On EMC, Atlanta USA, pp. 16-22, 1995
- [8] E. Leroux, C. Giachino, R. Ene, F. Canavero, P. Fogliati, B. Demoulin, "Validation expérimentale d'une méthode numérique hybride pour la prédition des émissions rayonnées par les cartes à circuits imprimés", accepted paper at 9-ième Colloque International et Exposition sur la Compatibilité Electromagnétique, Brest France, 8-11 June 1998

BIOGRAPHICAL NOTES

Emmanuel LEROUX received the Engineering degree in Electronics from the Ecole Universitaire D'Ingénieurs de Lille in 1994. He is working toward the Ph.D. degree in ElectroMagnetic Compatibility field. He has been working for HDT since 1994 as EMC Applications engineer.

Carla GIACHINO was born in 1971 in Turin (Italy). She received the Engineering degree in Electronics from the Politecnico di Torino in 1996 with a thesis on PEEC method. She joined HDT in 1996. Her work mainly concerns Electromagnetic Compatibility.

Razvan ENE received M.Sc. degree in Applied Physics from Bucharest University in 1992. After research stages at Duisburg University and Warwick University, he is working toward Ph.D. in ElectroMagnetic Compatibility field at Politecnico di Torino from 1995, sponsored by HDT.

Flavio G. CANAVERO is a Professor of Circuit Theory and Chairman of the Department of Electronics of the Polytechnic of Turin. His research interests are in the field of Electromagnetic Compatibility, where he works on line modeling for signal integrity, field coupling to multiwire cables, and statistical methods in EMC. He is Associate Editor of IEEE Transactions on EMC, and a member of the Italian delegation to RTO/NATO Sensors and Electronics Technology Panel.

Paolo FOGLIATI received the Laurea degree in electronic engineering in 1986 from the Polytechnic of Turin, Italy. He works at CSELT since 1993 in the EMC group as expert in testing and in EMC design solving problems on Telecommunication equipment.

Bernard DEMOULIN received the M.S. and Ph.D. degrees from the University of Lille in 1971 and 1973, respectively. Currently, he is a Professor at the University of Lille. Since, he has been working at the Laboratoire de Radiopropagation et d'Electronique.

INFLUENCE OF ELECTROMAGNETIC FIELDS ON INTEGRATED MICROCIRCUITS.

Starostenko V.V., Glumova M.V., Taran Y.P., Grygoriev Y.V.
Simferopol State University, 4 Yaltinskaya St., Simferopol-333036, Ukraine
E-mail: gmv@ccssu.crimea.ua

The results of researches on the influence of electromagnetic fields on integrated microcircuits has been adduced. The distributions of electromagnetic fields near the integrated microcircuit are received. The physical model of degradation processes in integrated microcircuits placed in an electrostatic field is developed.

I. INTRODUCTION

Reliability of semiconductor devices and integrated microcircuits is one of the major factors of long-term operation of the radioelectronic equipment. The urgency of this problem is connected with influence of electromagnetic radiation of an artificial and natural high-power origin on elements of the radioelectronic equipment [1,2]. Influence of electromagnetic radiation is understood as large variety of kinds of influence, among which we shall allocate influence of pulse electromagnetic fields and electrostatic discharge [3].

The majority of researches on influence of electromagnetic and electrostatic fields was reduced basically to submission of a pulse of the higher voltage on leads of integrated microcircuits [3,4]. In this case the character of degradation processes was defined by values of the applied voltage and duration of an influencing pulse. The electrostatic influence was considered basically as contact of the operator who is taking place under large potential, with one of the leads of a microcircuit. In this case the development of degradation processes was determined by time of contact and potential, which the operator had [5,6].

Both in the first and in the second case dynamics of degradation processes was determined in parameters of external influence and parameters of the circuit, which was determined by topology of a microcircuit.

We've carried out researches of field influence of electromagnetic waves and electrostatic fields on integrated microcircuits. The physical model of degradation processes in integrated microcircuits placed in an electrostatic field has been developed.

2. INFLUENCE OF ELECTROMAGNETIC FIELDS ON INTEGRATED MICROCIRCUITS

The influence of electromagnetic fields on integrated microcircuits is especially urgent in connection with the occurrence of generators and sources of high-power radiation (10^9 W and more in a pulse). They can cause a complete failure of elements of the radioelectronic equipment or "to blind" elements on the certain time [1].

The influence of electromagnetic fields on integrated microcircuits essentially differs from the appendix of an additional pulse to leads of integrated microcircuits. In this case most urgent become not only parameters of external influence (amplitude of an electromagnetic field, duration of an influencing pulse), but also arrangement of an integrated microcircuit of a rather electromagnetic wave. Thus there are some circuits and voltage put to everyone of a circuit, is defined by an arrangement of leads of an integrated microcircuit of a rather electromagnetic field. In this case electromagnetic field can be enclosed on a feed of a microcircuit, as well as be sent on alarm leads.

The researches on the influence of an electromagnetic field on integrated microcircuits were carried out in closed waveguide transmission line on the length of the wave $\lambda \approx 10$ centimeter. Duration of a pulse $1 \dots 4 \mu s$, capacity ≤ 20 kW, relative pulse duration $Q = (0,25 \dots 1) \cdot 10^4$.

The carried out researches have shown, that the resistance of integrated microcircuits under the influence of an electromagnetic field essentially depends on orientation of a microcircuit concerning a field of an electromagnetic wave. Depending on orientation the threshold of the resistance of microcircuits on intensity of an electromagnetic field can differ on the order and more. In orientations, in which the integrated microcircuits are least stable, the threshold of resistance on intensity of an electromagnetic field makes $60 \dots 70$ kV/m. In some orientations microcircuits remain efficient even at intensity of an electromagnetic field 100 kV/m.

After the influence of electromagnetic fields the integrated microcircuits were exposed to level-by-level etching for the analysis of the reasons of a failure. The carried out analysis has shown, that about 90 % of microcircuits were out of order for the reason of metallization burn-out. Metallization has appeared the weakest part in an integrated microcircuit.

The metallization failure carried a local character - the certain sites of a metal path burnt out. The process "dot" metallization degradation is caused by heterogeneity of metallization and non-uniformity of metallization contact with the adjacent layers. It results in formation of "hot" channels and "local" degradation.

Degradation processes in integrated microcircuits are connected with the burn-outs of metallization or microsites of elements of a microcircuit. The researches have shown, that the threshold of degradation processes is one order less than a threshold of resistance of microcircuits for each of the orientations. For the orientation, in which microcircuits were least stable in intensity, the threshold of degradation processes made 4-7 kV/m.

Under the influence of electromagnetic fields on integrated microcircuits the voltage put to various circuits, depends on distribution of an electromagnetic field near the microcircuit. In approximation of a wave H_{10} the field of a falling wave was defined by the known parameters of the past and reflected of waves. During the researches the distribution of a field near the integrated microcircuit was received.

For theoretical account decomposite method was used. For the account of the fields near to a microcircuit and in its structure the microcircuit was submitted as a four-layer structure: 1-substrate, 2- oxide of silicon, 3- metallization, 4- oxide of silicon (fig.1). Thus the researches were carried out both in and without view of leads of a microcircuit.

In this method the whole structure of an integrated microcircuit was submitted as a set of the minimal independent blocks. For each block there was a matrix of dispersion S connecting vectors of the falling and reflected waves. After definition of matrixes of dispersion of all independent blocks with the help of recombination the common matrix of dispersion of the whole structure was determined. The accounts were carried out in view of 7 types of waves in waveguide.

The received data show, that the field near to a microcircuit and in the structure is determined in parameters of layered structure. Thus the essential influence on created potential in structure of a microcircuit is rendered by leads of an integrated microcircuit. It results that at the account of leads of a microcircuit there is a strong distortion of a field, that renders essential influence on dynamics of degradation processes in metallization of microcircuits.

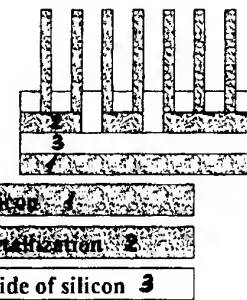


Fig.1. Layered structure of a microcircuit.

3. INFLUENCE OF ELECTROSTATIC FIELDS ON INTEGRATED MICROCIRCUITS

Researches on influence of electrostatic fields on integrated microcircuits was reduced basically to submission of an additional pulse on leads of a microcircuit [5]. We carry out researches on degradation of microcircuits placed in an electrostatic field. The physical model of development of dynamic processes in microcircuits which are taking place in an electrostatic field is developed.

For research of influence of an electrostatic field on integrated microcircuits the experimental plant was developed, which block diagram is given on fig.2.

The experimental plant consist of two section: 1 - working area, 2 - power area. In working area 1 through electrodes (3) there is an electrostatic field, in which the researched integrated microcircuit is located. The voltage submitted on electrodes (3), is developed by the power supply located in power area (2). It is possible to change a voltage submitted on electrodes (3), within the limits of 5-30 kV. The integrated microcircuits (7) were located in working area 1 with the help of stage (6), made of organic glass.

One of the electrodes (3) was mobile, that allowed to create a field inside working area 1 with the intensity of an electrical field from 10 up to 600 kV/m.

For the study of influence of an electrostatic field on integrated microcircuits the generator of rectangular pulses on a microcircuit was going. To a microcircuit a feed from power supply 4 is made, and the change of electrical parameters of an integrated microcircuit was defined with the help oscilloscope (5) (fig.2). To avoid inducing on wires, leading to an integrated microcircuit, they were located in shielded cable (8).

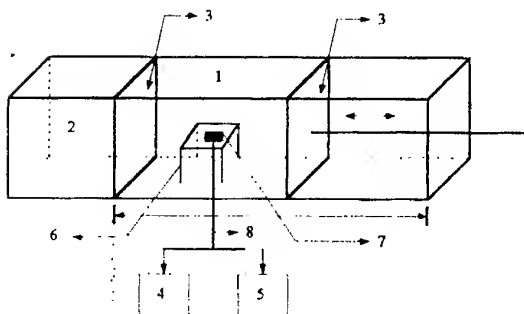


Fig.2. Experimental plant on electrostatic discharge.

The field mechanism of influence of an electrostatic field on the integrated microcircuits is connected with the production of displacement charge on elements of an integrated microcircuit. The values of the induced charge was defined by distribution of an electrostatic field near to a microcircuit and on its layers. For numerical definition of electrostatic fields the microcircuit was submitted as layered structure (fig.1). Metallization had island character - from this layer there were leads of a microcircuit that passed through a layer of silicon oxide. The account of an electrostatic field was done on the basis of the numerical decision of the two-dimensional equation of Puason. The account of layered structure of a microcircuit was made with the help of the following equation:

$$\epsilon_r \cdot |\Delta| F = 0 \quad (1),$$

where F - potential of an electrostatic field, ϵ_r - dielectric constant of layers of a microcircuit.

The analysis of the received results has shown, that the distribution of an electrostatic field in layered structure is defined not only by the properties of layers, but also by topology and distributing of metallization. The account of leads of a microcircuit essentially influences a picture of an electrostatic field, creating sites with a large gradient of potential. All this can result in occurrence of local degradation processes in places of the raised intensity of an electrostatic field.

The carried out experiment has shown, that the stationary field does not render influence on serviceability of integrated microcircuits at intensity of an electrostatic field up to 500 kV/m. It is connected with the fact that in experiment the influence of a "pure" statics without the account of processes taking place at an establishment of a static mode was investigated.

One of the factors, which influences the resistance of the integrated microcircuits in external electrical fields, is the speed of the establishment of an external field or its changes, that actually defines the values of the current of displacement in dielectric and the current of conductivity in metallization in a discharge circuit of an integrated microcircuit.

Irrespective of character of a static electricity the majority of constructive elements of integrated microcircuits are sensitive to capacity of dispersion connected with the course of a discharge current, caused by a static electricity. Such elements are the structures based on p-n junction, and metallization. To these elements are essential duration, the amplitude and form of a pulse of a discharge current, at certain combinations of which electric break-down of a discharge interval to transition in thermal break-down causing burn-out of p-n junction and burn-out of metallization.

The occurrence of degradation processes in integrated microcircuits placed in an external static field, is defined by intensity of an electrical field, and also mutual orientation of microcircuits both field and speed of change of an external field. The meanings of intensity of an electrical field exceeding discharge values on local sites of an integrated microcircuit, are defined by displacement charges collecting on the elements of a microcircuit. The values of these charges depend on values of an external field and mutual orientation of an integrated microcircuit concerning the field.

At discharge of an integrated microcircuit there is a discharge circuit, which equivalent circuit is given on fig.3. The following elements are included in a discharge circuit: C_B - capacity between leads of a microcircuit, R_0 - resistance of current conductive paths, C_0 - capacity of dielectric, R_{pr} - resistance of a discharge interval. The resistance of a discharge interval has nonlinear S-form voltage-current characteristic - up to discharge R_{pr} is great, after discharge it is small, but in any case $R_{pr} \gg R_0$.

The process of discharge is described as follows: at the increased intensity of a field near to an integrated microcircuit the voltage put to leads of a microcircuit (a voltage on C_B) and, hence, to C_0 is increased. If the a voltage of discharge is exceeded a discharge of dielectric, dividing the conductors occurs. At occurrence of discharge a circuit locks through currents of displacement arising as a result of transient in a discharge circuit. At discharge the resistance of discharge R_{pr} sharply falls. It results in a voltage reduction on capacity C_0 , that results in a voltage reduction on leads of an integrated microcircuit, causing the terminations of discharge. At the termination of discharge the voltage on leads of an integrated microcircuit again grows up to a discharge voltage and the process is repeated. The given circuit can be presented as a circuit with a source of a voltage controlled by a voltage of discharge, however there are also differences, which are connected with the fact that the external field does not depend on a circuit of the discharge - charge, or in other words, from an input - output.

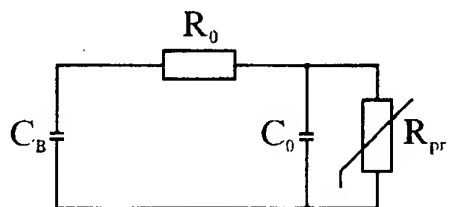


Fig.3. The equivalent circuit of a discharge circuit.

The characteristics of relaxation processes arising at discharge, depend on the speed of an establishment of an external field and the constants of the time of a discharge circuit (pic.3). In view of the form of a discharge current and its amplitudes there were carried out accounts of degradation processes in metallization on the basis of the analysis of thermal modes in an integrated microcircuit and the comparisons with the case of a constant discharge current have been carried out.

4. CONCLUSION

The carried out researches have allowed to establish thresholds of resistance of integrated microcircuits to influence of an external electromagnetic field depending on orientation of an integrated microcircuit. The character of degradation processes in an integrated microcircuit is established at the influence of an electromagnetic field. The meanings of intensity of an electromagnetic field resulting in occurrence of degradation of metallization are received.

The researches have shown, that degradation of integrated microcircuits placed in an electrostatic field, there is defined not only amplitude of an external field, but also time and character of an establishment of an external field. The developed mathematical model allows to describe physical processes arising at the influence of an external electrostatic field. On the basis of the given model the basic characteristics of electrostatic fields resulting in degradation and failure of integrated microcircuits are established.

5. REFERENCES

1. J.Benford, J.Swiegle High-Power Microwaves. Artech House, Norwood, MA, 1991, p. 412.
2. K.S.H.Lee EMP Interaction: Principles, Techniques and Reference Data. Hemisphere Publishing Corp., 1986.
3. Antinone J. Electrical Overstress Protection for Electronic Devices. 1986, New York. p. 387.
4. Wunch D.C., Bell R.R. Determination of Threshold Failure Levels of Semiconductor Diodes and Transistors Due to Pulse Power Voltage // IEEE Trans. Nucl. Phys., 1968, NS-15, N6. - pp.244-259.
5. Nailen R.L. Static charges - dinamic damage // Electrical apparatus. 1986. № 12, pp.26-27.
6. Welsher T.L., Blondin T.J. Etc. Design for electrostatic - Discharge (ESD) protection in telecommunication products // Technical Journal. 1990. Vol.69. № 3. pp.77-96.

DYNAMICS OF DEGRADATION PROCESSES IN METALLIZATION OF INTEGRATED MICROCIRCUITS UNDER THE INFLUENCE OF ELECTROMAGNETIC FIELDS.

Starostenko V.V., Glumova M.V., Taran Y.P., Grygoriev Y.V.
Simferopol State University, 4 Yaltinskaya St., Simferopol-333036, Ukraine
E-mail: gmv@ccssu.crimea.ua

The physical model of degradation processes in metallization of integrated microcircuits is developed under the influence of an external electromagnetic field. The temporary and spatial characteristics of degradation processes are received. The conditions of occurrence " of a mode with an aggravation " and formation of local degradation are revealed.

1. INTRODUCTION

Reliability of the radioelectronic equipment is defined by resistance of its elements to influence of the various external factors. Among plenty of kinds of influence on elements of the radioelectronic equipment the most dangerous is the influence of electromagnetic fields [1]. It is connected with the fact that the occurrence of an electromagnetic wave can be caused by both artificial, and natural sources of radiation [2,3]. Moreover, the electromagnetic wave can arise in the most radioelectronic equipment, that can result in the degradation of elements.

The researches on influence of electromagnetic fields on semiconductor devices and integrated microcircuits are carried out. The experimental data show, that the overwhelming number of failures of integrated microcircuits occurs because of defects of metallization - just they are mostly subjected to degradation [4]. It results in the necessity of research of the reasons and mechanism of metallization degradation.

In this work the mathematical model of the description of dynamics of development of degradation processes in metallization is given. The reasons of local metallization degradation are revealed, the temporary and spatial characteristics of degradation processes are received. The conditions of occurrence " of a mode with an aggravation ", resulting in instant "explosive" metallization degradation are received.

2. PHYSICAL MODEL, OF DEGRADATION PROCESSES IN METALLIZATION

The influence of electromagnetic fields on integrated microcircuits results in metallization degradation. The character of degradation processes is determined as parameters of an external electromagnetic field (amplitude, frequency), and orientation of an integrated microcircuit of a rather electromagnetic field.

The occurrence of dynamic processes in integrated microcircuits under the influence of electromagnetic fields is connected with the current induced on the leads of a microcircuit. The current induced on the leads of a microcircuit, becomes isolated through metal paths and a dielectric layer dividing them. In this case discharge circuit can be presented as the equivalent circuit given on fig.1. The equivalent circuit represents a RC-circuit, which includes resistance of metallization (R), capacity of a dielectric layer (C), resistance of a dielectric (R_0).

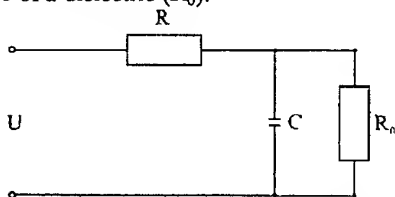


Fig.1. The equivalent circuit of a discharge circuit.

The voltage U is enclosed in the given equivalent circuit which in the first approach is determined by expression $U = E \cdot l$, where l - distance between the leads of an integrated microcircuit along a field.

The capacity of dielectric is defined by topology of an integrated microcircuit and depends on orientation of an integrated microcircuit concerning a field. It is connected with the fact that depending on orientation of an integrated microcircuit the voltage is put to different leads of a microcircuit. As a result there are different circuits, in which the circuit locks through a current of displacement. In this case the capacity of dielectric is

defined by the geometrical sizes of dielectric, which participates in the circuit formation.

Occurrence of a current in metallization and the formation of an electrical circuit results in occurrence of capacity of dispersion on metallization. The formed thermal field is distributed among structures of an integrated microcircuit. For the description of dynamics of the thermal processes in structure of an integrated microcircuit the crystal was submitted as 4 layers (fig.2): 1 - substrate (Si); 2 - dielectric (SiO_2); 3 - metallization (Al); 4 - dielectric (SiO_2).

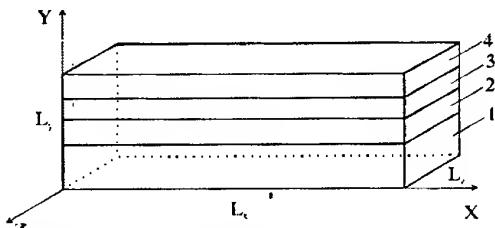


Fig.2. Structure of an integrated microcircuit.

The temperature field in layered structure was determined with the help of the two-dimensional non-stationary heat equation:

$$\begin{aligned} c_l \cdot \rho_l \cdot \frac{\partial T_l}{\partial t} &= \frac{\partial}{\partial x} \left[K_l(T) \cdot \frac{\partial T_l}{\partial x} \right] + \\ &+ \frac{\partial}{\partial y} \left[K_l(T) \cdot \frac{\partial T_l}{\partial y} \right] + q_l(x, y, t) \end{aligned} \quad (1)$$

where c_l - specific heat of a l-layer, ρ_l - density of a material, $K_l(T)$ - thermal conductivity, $q_l(x, y, t)$ - specific capacity of sources of heat, l - number of a layer.

The equation (1) represents a system of 4 equations for each layer of a microcircuit. On the border of the layers the condition of a continuity of a thermal flow and continuity of a temperature field was used. The thermal conductivity of layers were functions of temperature. The system of the equations (1) was nonlinear and for its decision the numerical methods were used.

In this work the character of a metallization degradation was investigated. For this purpose metallization was broken into homogeneous sites, within the limits of which its parameters (electrical conduction, heat conduction) were considered as constant values. During the investigation of degradation processes the homogeneous site was considered as one whole. Such representation is connected with the fact that metallization represents granular structure. The homogeneous site is a set of some grains.

To include such a structure of metallization in an electrical circuit (fig.1), it was submitted as a two-dimensional grid of resistance (fig.3). Each resistance represented a homogeneous site of metallization.

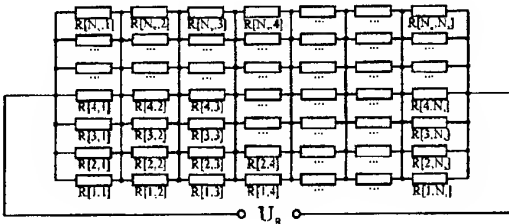


Fig.3. Metallization structure.

The expression for capacity allocated on a homogeneous site of metallization was received:

$$q(i, j) = \frac{I^2 \cdot \sigma(i, j)}{S^2 \cdot \left(\sum_{j=1}^{N_y} \sigma(i, j) \right)^2} \quad (2),$$

where I - current which is taking place through metallization, $S = h_y L_z$ - area of cross section of a homogeneous site (h_y - thickness of a homogeneous site), N_y - number of homogeneous sites along thickness of metallization (axis Y), $\sigma(i, j)$ - conductivity of a homogeneous site of metallization.

The two-dimensional heat equation (1) was solved with the use of the implicit circuit of variable directions. For this purpose the distribution of temperature was defined on half a temporary step, and then the meaning of the temperature on the whole temporary step was determined. It is the circuit of Peaceman-Rockford.

3. SPATIAL AND TEMPORARY CHARACTERISTICS OF DEGRADATION PROCESSES

The carried out numerical experiment has shown, that dynamics of degradation processes in metallization of integrated microcircuits under the influence of electromagnetic fields is defined by both parameters of an external field, and metallization structure. Metallization had non-homogeneous structure - homogeneous sites of metallization had different meaning of conductivity (fig.4).

The formation of heterogeneity is caused by the basic technological processes. The degree of heterogeneity of metallization especially is brightly displayed in places of contact of a metallization layer with other layers.

The researches were carried out for intensity of an electromagnetic field 5 kV/m and frequency 10^9 Hz.

Under the influence of an external electromagnetic field on non-uniform sites of metallization there is an allocation of heat and local warming up of these sites (fig.5). The values of the temperature on these sites is largely determined by a degree of metallization heterogeneity - the greater heterogeneity of metallization (the less meaning of conductivity), is the stronger the given site is warmed up. It is caused by the fact that in places of heterogeneity

there is "narrowing" of the path and formation of the "hot" channel.

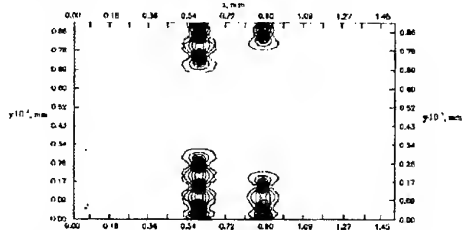


Fig.4. Distribution of metallization conductivity.

The process of distribution of heat carries a diametrical character - the heat dissipates in cross section of a crystal (fig.5). It is connected with the geometrical parameters of an integrated microcircuit - thickness is 3 orders less than length. Dynamics of thermal process carries anisotropic character along the section of the structure. It results in the local melting-down of metallization and can result in the short circuit of melting-down metal with a silicon substrate.

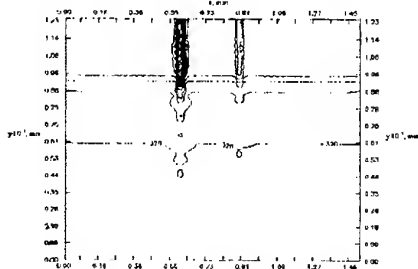


Fig.5. Distribution of levels of identical temperature on the structure of an integrated microcircuit.

The estimation of the temporary characteristics has shown, that the duration of the given degradation process makes about $10^{-10} \div 10^{-9}$ sec. The given type of the degradation is caused by the large density of a current ($10^7 \div 10^9$ A/cm²). Spatial degradation in this case makes about $5 \div 10$ μm .

At a strong degree of metallization heterogeneity the occurrence "of a mode with an aggravation" - the local allocation of heat on non-homogeneous sites is possible. This process is caused by nonlinear dependence on temperature of layers of an integrated microcircuit, and also nonlinearity of an external source. Such mode results in the formation of an "explosive" wave in places of heterogeneity. At the certain ratio of an external electromagnetic field and degree of heterogeneity the transition from usual time degradation to an explosive wave is possible.

In this work the researches of influence of parameters of an external circuit (fig.1) on dynamics of degradation processes are carried out. In particular, the influence of capacity of a dielectric layer on dynamics of thermal processes on non-homogeneous sites of metallization (fig.6) is investigated. It is established, that depending on capacity of a dielectric layer in a crystal

both local accumulation of heat (curve 1 on fig.6), and absence of accumulation of heat (curve 4) can be observed. Dynamic and degradation processes in layered structure of an integrated microcircuit depend on not only parameters of structure, but also on parameters of equivalent circuit, which is formed under the influence of an external electromagnetic field.

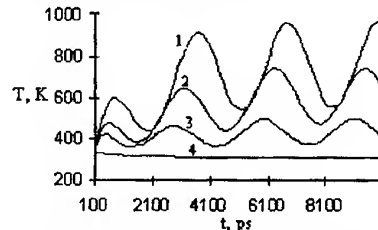


Рис.6. Dynamics of temperature of a non-homogeneous site of metallization depending on dielectric capacity.

4. CONCLUSION

On the basis of the developed model the reasons of local degradation of metallization are revealed under the influence of an external electromagnetic field. The temporary and spatial characteristics of development of degradation processes in metallization are received. During the realization of numerical experiment the ratio between parameters of an external electromagnetic field (amplitude, frequency) and degree of heterogeneity of metallization are established which result in occurrence "of a mode with an aggravation" - sharp growth of temperature on a non-homogeneous site.

Dynamics of degradation processes at non-homogeneous sites of metallization is investigated depending on the capacity of a dielectric layer. It is shown, that the development of degradation processes is determined in parameters of an external field, parameters of equivalent circuit and topology of an integrated microcircuit.

5. REFERENCES

1. Antinone J. Electrical Overstress Protection for Electronic Devices. 1986, New York. p. 387.
2. J.Benford, J.Swingle High-Power Microwaves. Artech House, Norwood, MA, 1991, p. 412.
3. K.S.H.Lee EMP Interaction: Principles, Techniques and Reference Data. Hemisphere Publishing Corp., 1986.
4. V.V.Starostenko, Y.V.Grygoriev, Y.P.Taran The influence of electromagnetic fields on resistance of integrated circuits // 6th International Crimean Microwave Conference «Microwave & Telecommunication Technology». Sevastopol. 1996. P.433-436.

IX

EMI REDUCTION TECHNIQUES

ABSORPTION PROPERTIES OF SIMPLE SHAPES

Berna Altay

S.S. Seker

Bogazici University
Department of Electrical and Electronic Engineering
Istanbul, Turkey

Absorption properties of any object is ruled by several major factors such as material parameters, the shape which is restricted by practical applications and the frequency range. Absorption is extremely difficult to analyze mathematically. The exact solution requires solving Maxwell's field equations for a three-dimensional shape.

A theoretical analysis of absorption can be applied precisely for a limited number of very simple geometric shapes and types of applied fields. It is practical to apply electromagnetic theory to the ideally-oriented shielding shapes. The absorption properties of geometric shapes such as cylinders and spheres can be useful for practical applications.

It is practical to apply electromagnetic theory to the ideally-oriented shielding shapes. The absorption properties of geometric shapes such as cylinders and spheres can be useful for practical applications. A theoretical analysis of absorption can be applied precisely for a limited number of very simple geometric shapes and types of applied fields.

The absorption effectiveness is defined in terms of absorbed power as the ratio of the absorbed power to the total power.

1. INTRODUCTION

The Rayleigh approximation deals with the general scattering characteristics of a small particle. The Rayleigh approximation sets the basis for investigating the absorption properties of simple shapes in most applications, but the energy conservation rule must be satisfied to evaluate the absorption effectiveness of simple shapes. The Rayleigh approximation does not satisfy energy conservation i.e.; the sum of the absorbed and scattered power is not equal to the total power extracted from the incident wave. In this study,

Improved Rayleigh approximation is used to satisfy energy conservation.

Absorption effectiveness is computed as the ratio of the absorbed power to the total power. Electromagnetic absorption properties of simple shapes such as spheres (Mie solution) and cylinders (Richmond and finite length solutions) also satisfy the energy conservation rule. Mie solution is the exact solution of scattering of a plane electromagnetic wave by an isotropic homogeneous sphere

The comparison of the Improved Rayleigh approximation with Mie solution for spheres and Richmond solution for cylinders satisfy energy conservation. The results of the Richmond and finite length solutions for thin cylinders are also compared. The absorption effectiveness of spherical and cylindrical shells are computed and compared with the results in the literature, and good agreement is found.

Some applications of Rayleigh approximation do not give acceptably accurate results. This is especially the case for material having low loss tangent values.

The scattered fields obtained via the Rayleigh approximation does not satisfy energy conservation rule [1-4], then an improved method should be used [2]. This is done by accounting for the multiply scattered fields inside the shape. An improved method which obeys the energy conservation rule also provides a great deal of information related with the absorption properties. In Section 2, the Improved Rayleigh approximation is reviewed and the extinction, absorption and scattering losses, absorption effectiveness are formulated. AE is formulated as the ratio of the absorption cross section and the total cross section for sphere and cylinders. AE of multilayered cylinders and spheres can also be defined using the solutions in literature.

In Section 3, the extinction efficiency and absorption effectiveness of spheres and cylinders are simulated numerically. The Rayleigh and Improved Rayleigh approximations and Mie theory for spheres and multilayered spheres are compared in terms of extinction efficiency and absorption effectiveness. Absorption effectiveness for a thin cylinder is obtained using the Improved Rayleigh approximation, Richmond and finite length cylinder solutions [5], and the results of these approaches are compared.

2. BACKGROUND FORMULATION

In this section, we will briefly explain the Improved Rayleigh approximation for arbitrary spheroids, the theoretical analysis of sphere, cylinder and derive the absorption effectiveness expression for such simple shapes. We will not go through the derivation of the solutions, but briefly explain them.

2.1. Electromagnetic Analysis of Arbitrary Spheroid

The scattering of electromagnetic waves by a finite dielectric body is important in various applications. A theoretical solution describing the electromagnetic scattering particles of high symmetry is well known. Here, we present a method to calculate absorption properties of dielectric bodies.

The Rayleigh approximation can be improved to satisfy energy conservation.[1-2]. We will use the Improved Rayleigh approach for the derivation of the inner field of the spheroid and evaluate the absorption effectiveness.

In Improved Rayleigh approximation, quasistatic approximation can be employed to find the field inside the spheroid. The improvement is represented by an equivalent polarizability tensor differing from that used in the Rayleigh approximation in two aspects: it is frequency dependent, and it gives a scattering amplitude tensor satisfying energy conservation [2]. Numerical calculations on spheres and ellipsoids indicate that the Improved Rayleigh extinction loss formulation has a wider validity range than the Rayleigh approximation. For a small shape where the scattered field inside the shape is accounted for and the phase variation over the scatterer is negligible, the internal field can be expressed in terms of incident field E_{inc} , equivalent polarizability tensor \bar{K}_{eq} , unit dyadic \bar{I} , polarizability vector \hat{q}_i , as

$$\bar{E}_{int} = \bar{K}_{eq} \cdot (\bar{I} - \bar{I} \cdot \hat{i}) \cdot \hat{q}_i E_{inc} \quad (1)$$

From [3], the equivalent polarizability tensor is

$$\bar{K}_{eq} = \sum_{t=1}^3 \zeta_{tt} \hat{x}_t \cdot \hat{x}_t = \sum_{t=1}^3 \frac{K_t}{1 + j \frac{k_0^3 V_p (\epsilon_r - 1) K_t}{6\pi}} \hat{x}_t \cdot \hat{x}_t \quad (2)$$

\hat{x}_t are spherical unit vectors in the principal frame and K_t values are given in [1] for different spheroids, V_p is the volume of the shape and

$k_0 = \omega \sqrt{\mu_0 \epsilon_0}$. This tensor accounts for the multiply scattered field inside the scatterer which has not been accounted for in the Rayleigh approximation. If the denominator of (2) is expanded:

$$\bar{K}_{eq} = \sum_{t=1}^3 K_{tt} \left(1 - j \frac{k_0^3}{6\pi} V_p (\epsilon_r - 1) K_{tt} + \left[\frac{k_0^3}{6\pi} V_p (\epsilon_r - 1) K_{tt} \right]^2 \right)^{-1} \hat{x}_t \cdot \hat{x}_t \quad (3)$$

The first term in this expansion, which is equivalent to the Rayleigh approximation stands for the direct incident field inside the scatterer. The other terms represent the first multiply scattered inner field. The Rayleigh approximation does not satisfy the boundary conditions, but this expression does [2].

Energy conservation requires that the energy lost by an incident wave is equal to the sum of the energy scattered and absorbed by the scatterer. The total dissipated, absorbed and scattered energies are represented by the extinction σ_{eq} , the absorption σ_{aq} , and the scattering σ_{sq} cross sections, respectively. Extinction (Total) cross section is the total energy abstracted from the incident beam by the shape. Absorption cross section is the energy lost within the shape or energy abstracted from the incident beam by absorption. Scattering cross section is the total energy scattered by a shape in all directions. We can write the extinction cross section as

$$\sigma_{eq} = k_0 V_p \left[\left(\epsilon_r'' + \frac{k_0^3 V_p}{6\pi} |\epsilon_r - 1|^2 \right) \sum_{t=1}^3 |\zeta_{tt}|^2 (\hat{x}_t \cdot \hat{q}_t)^2 \right] \quad (4)$$

The absorption cross section can be found as

$$\sigma_{aq} = k_0 V_p \epsilon_r'' \sum_{t=1}^3 |\zeta_{tt}|^2 (\hat{x}_t \cdot \hat{q}_t)^2 \quad (5)$$

The scattering cross section is

$$\sigma_{sq} = \frac{1}{6\pi} |k_0^2 V_p (\epsilon_r - 1)|^2 \sum_{t=1}^3 |\zeta_{tt}|^2 (\hat{q}_t \cdot \hat{x}_t)^2 \quad (6)$$

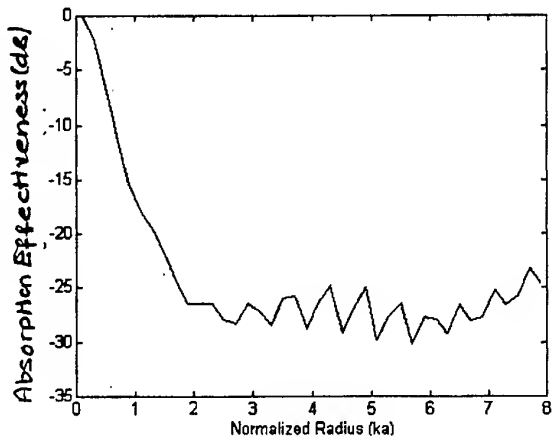


Fig. 2. The absorption effectiveness for a spherical shell (Mie solution) ($\epsilon_r = 4 - 0.1i$)

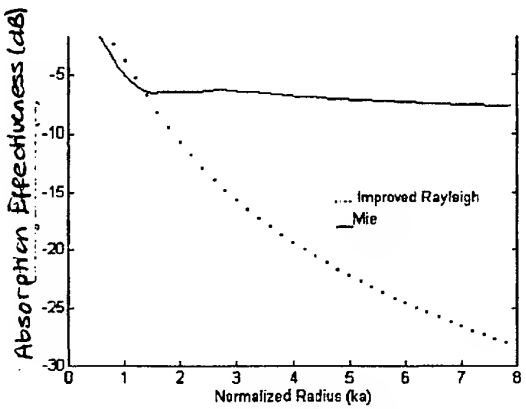


Fig. 3. The absorption effectiveness for a homogeneous sphere ($\epsilon_r = 4 - 2.74i$).

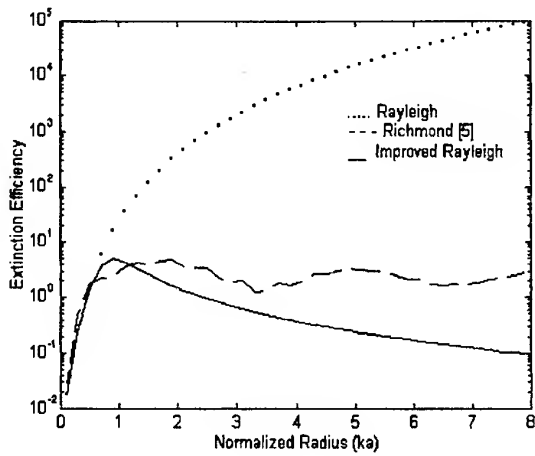


Fig 4. The extinction efficiency of thin cylinder (vertical polarization) as function of normalized radius (ka) ($\epsilon_r = 4 - 0.1i$).

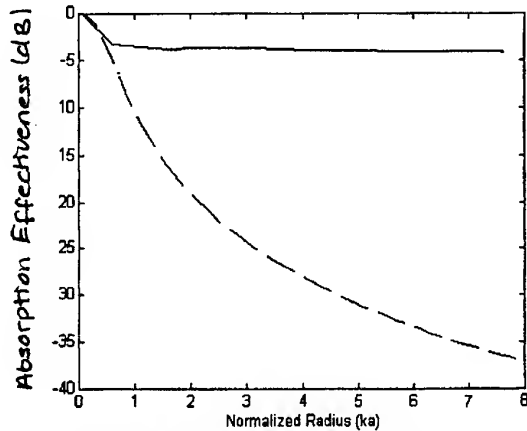


Fig. 5. Absorption effectiveness of thin cylinder (vertical polarization) ($\epsilon_r = 4 - 2.74i$)
- - Improved Rayleigh solution,
— Richmond solution [5].

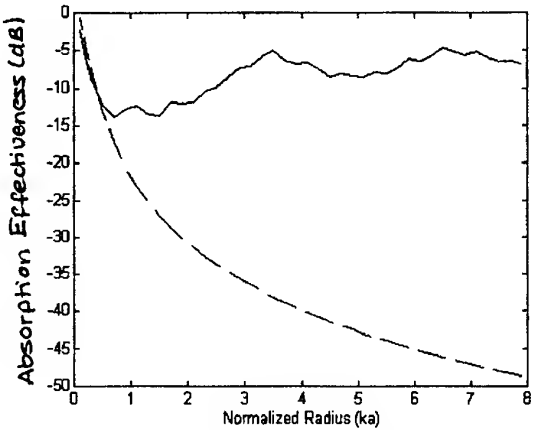


Fig. 6. Absorption effectiveness of thin cylinder (vertical polarization) ($\epsilon_r = 4 - 0.1i$)
- - Improved Rayleigh solution,
— Richmond solution [5].

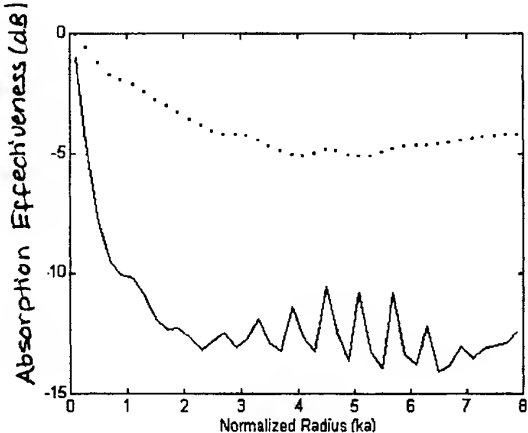


Fig. 7. The absorption effectiveness of a cylindrical shell (vertical polarization) as a - - - $\epsilon_r = 4 - 2.74i$,
— $\epsilon_r = 4 - 0.1i$.

The absorption efficiency can be calculated as

$$AE_{dB} = 20 \log \frac{\sigma_a}{\sigma_t}. \quad (7)$$

According to the forward scattering theorem [3], the extinction cross section given by (4) should be equal to the sum of absorption (5) and scattering cross sections (6).

2.2. Electromagnetic Analysis of Sphere

The extinction, scattering and absorption efficiencies of the multilayered sphere is:

$$Q_{ext} = \frac{2}{x^2} \sum_{n=1}^{\infty} (2n+1) \operatorname{Re}(a_n + b_n) \quad (8)$$

$$Q_{sca} = \frac{2}{x^2} \sum_{n=1}^{\infty} (2n+1)(|a_n|^2 + |b_n|^2) \quad (9)$$

$$Q_{abs} = Q_{ext} - Q_{sca} \quad (10)$$

The recursion formulae can be using the algorithm in [7] and the absorption effectiveness can be evaluated as follows:

$$\sigma_t = \pi a^2 Q_{ext} \quad (11)$$

$$\sigma_s = \pi a^2 Q_{sca} \quad (12)$$

$$\sigma_a = \sigma_t - \sigma_s \quad (13)$$

$$AE_{dB} = 20 \log \frac{\sigma_a}{\sigma_t} \quad (14)$$

2.3. Electromagnetic Analysis of Cylinder

Electromagnetic analysis of cylinder for scattering amplitudes and extinction, scattering and absorption cross sections [4-6]. Richmond solution [5] is a well known method for the evaluation of infinite length cylinder. Because the internal fields within the finite length cylinders are not known exactly, they are approximated by the internal fields within the infinite length cylinders of equal and respective diameters, permittivities and orientation [5-8].

The absorption cross section for cylinder is:

$$\sigma_{aq} = k_0 \epsilon_r \int |E_i|^2 dV \quad (15)$$

or

$$\sigma_{aq} = \sigma_{tq} - \sigma_{sq} \quad (16)$$

where \vec{E}_i is the internal electric field. Finally, using this information absorption effectiveness can be evaluated by using (16).

3. NUMERICAL RESULTS

In Figs 1, 2, and 3, the absorption effectiveness is calculated according to equation (16) for spheres. It must be noted that Fig. 2, can be used for simulating the absorption properties of a room that can be modeled as a spherical shell. It is clear that the higher loss tangent values (as in Fig. 3) give more accurate values for the Improved Rayleigh approximation when compared to the exact (Mie) solution for multilayered sphere.

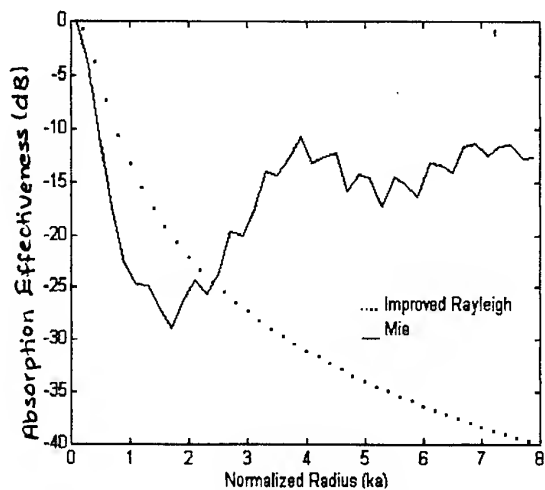


Fig. 1. The absorption effectiveness for a homogeneous sphere ($\epsilon_r = 4 - 0.1i$).

The extinction efficiency for a thin homogenous cylinder with radius $a=0.1$ m, height $h=1$ m is shown as a function of normalized radius (ka) in Fig. 4. It can be seen from Fig. 4 that the Richmond [5] solution in two dimensions and the Improved Rayleigh approximation for thin homogenous cylinder agree in the Rayleigh region.

In Figs. 5, and 6, the absorption effectiveness of thin homogenous cylinder for both Richmond solution and Improved Rayleigh approximation and both solutions agree in the Rayleigh region. The comparison of the Figs. 5 and 6 show that the contribution of the absorbed energy to the extinction cross section is higher in a high loss tangent material.

4. CONCLUSIONS

Absorption properties of simple shapes can be used for EMI reduction. Evaluation of electromagnetic absorption properties of various shapes and materials

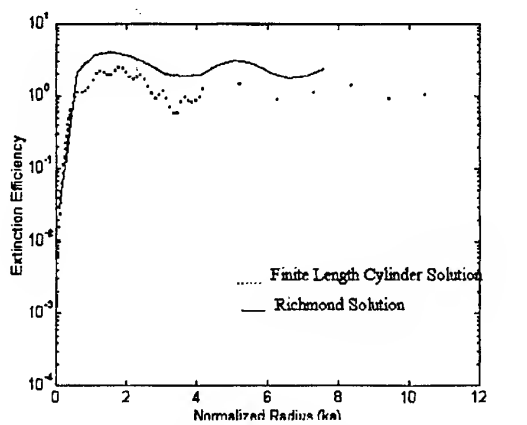


Fig. 8. The extinction efficiency of thin cylinder (vertical polarization), $\epsilon_r = 4 - 0.1i$.

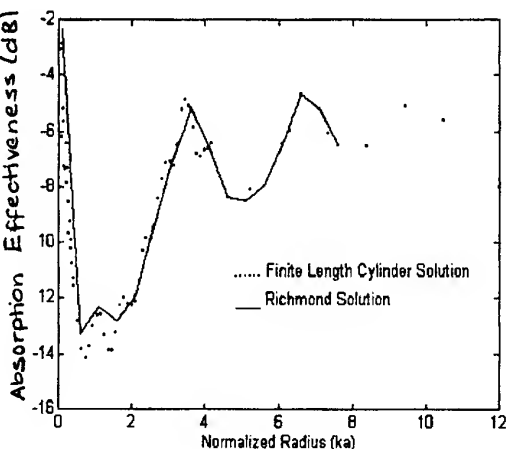


Fig. 9.. The absorption effectiveness of thin cylinder (vertical polarization, $\epsilon_r = 4 - 0.1i$).

usually depend on experimental techniques and hard to analyze mathematically. Electromagnetic properties of simple shapes can be computed using the techniques in literature.

Rayleigh approximation gives information about a number of shapes in aspect of their absorption and scattered losses, although it does not satisfy energy conservation. The Improved Rayleigh approximation satisfies energy conservation and is used to evaluate the electromagnetic absorption properties of simple shapes. In this work, the absorption effectiveness is defined as the ratio of the absorbed power to the total power extracted from the incident beam. Only a method obeying the energy conservation rule is suitable for the computation of electromagnetic absorption properties. The numerical results have shown that Improved Rayleigh approximation gives results as good as the exact solutions for the homogenous spheres and cylinders in the Rayleigh region. Improved Rayleigh approximation has a more simple algorithm than the exact algorithms for spheres (Mie solution) and cylinders (Richmond solution in two dimensions). For

the purpose of comparison the material properties of [2] are used. For spheres, it is obvious from the numerical results that the validity range of the Improved Rayleigh is greater than the validity range of the Rayleigh approximation. For cylinders, it is slightly accurate than the Rayleigh approximation. There are two algorithms for exact evaluation of cylinders which are extended to multilayered cylinder formulation.

One is the Richmond solution for infinite length cylinder and the other is the finite length cylinder solution.

In this work, these two exact solutions are compared and the evaluation of extinction efficiency and absorption effectiveness show good agreement.

5. REFERENCES

- 5.1. S.S. Seker, "Radar Cross-Section of Thin Dielectric Bodies", IEE Proceedings, Vol. 133, Pt. H., No.4, Aug. 1986, pp.305-307.
- 5.2. M.A. Karam, D.M. Levine, Y.M.M. Antar, A. Stogryn, "Improvement of the Rayleigh Approximation for Scattering from a Small Scatterer", IEEE Transactions on Antennas and Propagation, Vol. 43, No.7, July 1995, pp. 681-687.
- 5.3. A. Ishimaru, "Wave Propagation and Scattering in Random Media" - Volume1, pp.18, Academic Press, 1978.
- 5.4. Massoudi, H., Durney, C.H., Barber, P.W., Iskander, M.F., "Electromagnetic Absorption in Multilayered Cylindrical Models of Man", IEEE Transactions on Microwave Theory and Techniques, Vol. MTT-27, No.10, pp. 825-830, October 1979.
- 5.5. Bussy, W.E., Richmond, J.H., "Scattering by a Lossy Dielectric Circular Cylindrical Multilayer, Numerical Values", IEEE Transactions on Antennas and Propagation, Vol. AP-23 (9), pp.723-725, 1975.
- 5.6. Mackowski, D.W., Altenkirch, R.A., Menguc, M.P., "Internal Absorption Cross Sections in a Stratified Sphere", Applied Optics, Vol. 29, No. 10, pp. 1551-1559, April 1990.
- 5.7. Wu, Z.S., and Wang, Y.P., "Electromagnetic Scattering for Multilayered Sphere: Recursive Algorithms", Radio Science, Vol. 26 No. 6, pp. 1393-1401, Nov-Dec 1991.
- 5.8. Seker, S.S., Schneider, A. "Electromagnetic Scattering from a Dielectric Cylinder of Finite Length", IEEE Transactions on Antennas and Propagation, Vol. AP-36(2), pp. 303-307, 1988

BIOGRAPHICAL NOTES

BERNA ALTAY received her B.S. degree in electronics and telecommunications engineering in 1994 from Istanbul Technical University, Turkey, her M.Sc. degree in 1996 from Bogazici University, Istanbul, Turkey. She is currently Ph.D. candidate at Bogazici University. Her research areas include shielding, scattering and electromagnetic compatibility.

THE USE OF THE SPICE CIRCUIT SIMULATOR TO PREDICT SWITCHED-MODE POWER SUPPLY INPUT FILTER PERFORMANCE

John Kelly,
PEI Technologies,
Foundation Building,
University of Limerick,
Limerick,
Ireland

Tom Sorensen,
University of Limerick.
Limerick,
Ireland.

Peter Bardos,
Artesyn Technologies (formerly Computer Products),
Springfield,
Youghal,
Co. Cork,
Ireland

Abstract : Switched-mode power supplies are widely acknowledged as being among the major contributors to conducted emissions from modern electronic systems. In order to reduce these emissions, an input filter is used to attenuate the emissions conducted onto mains lines. The ability to predict the attenuation which this filter will provide is necessary in order to enable accurate prediction of conducted emissions. Furthermore, in order to give realistic information about filter performance under EMC test setup conditions, it is necessary to model accurately the attenuation provided in the presence of a Line Impedance Stabilisation Network (LISN) and a mains cable, which are standard elements of the conducted emissions test setup. This paper outlines techniques for modelling of the various filter and conducted emissions test setup elements. These models are used in conjunction with the SPICE circuit simulator to model the attenuation provided by a sample filter. The filter examined was used in a 40-watt AC-DC converter marketed by Artesyn Technologies (formerly Computer Products). Simulated attenuation results showed good agreement with measured results.

1. INTRODUCTION

Prediction of the conducted emissions from switched-mode power supply (SMPS) equipment is difficult to achieve but increasingly necessary in the light of the presence of world-wide EMC standards. A more realistic target is the prediction of the performance of the input filter used by SMPS equipment to suppress conducted emissions. Although most of the techniques used in input filters are relatively standard (e.g. the use of X-caps, Y-caps and common-mode chokes), the prediction of the attenuation provided by 'real-life' filters combining these circuit elements is an area

which has received relatively little attention. The fact that these 'real-life' filters also contain PCB tracks which must be modelled accurately in order to obtain useful results in the conducted EMI frequency range adds an extra level of complexity to the problem.

2. FILTER COMPONENT EQUIVALENT CIRCUIT EXTRACTION

2.1 General Filter Component Equivalent Circuit Extraction

At frequencies in the conducted EMI range (150 kHz-30MHz), the representation of discrete components such as resistors, capacitors etc. by their nominal value alone is not sufficient. A $1\mu F$ capacitor, for example, will have a series inductance and resistance as well as its nominal capacitance. Similar equivalent circuits exist for other filter components such as fuses, resistors, common-mode chokes, temperature-variable resistors etc. The acquisition of equivalent circuit parameter values for each of these filter components is necessary to obtain the overall response of the filter / line cord / LISN combination. Therefore, methods must be derived for the acquisition of parameter values for the equivalent circuit of various filter components.

Methods for the acquisition of these parameter values are relatively simple and well-known for many filter components : the series inductance of a capacitor, for instance, can easily be determined using an impedance analyser by isolating the parameter L in the well-

$$\text{known series resonance equation } f_r = \frac{1}{2\pi\sqrt{LC}}.$$

However, even the seemingly simple process of obtaining the equivalent circuit of a capacitor was complicated by the fact that the value of the resistor R in the series RLC circuit used as the capacitor

equivalent circuit was found to vary with frequency. The process of acquiring suitable functions of frequency to model the variation of the parameter R over the conducted EMI range, while necessary in order to accurately reproduce the variation of the capacitor's impedance in the conducted EMI range, is largely an exercise in mathematical modelling and is not presented here.

2.2 Common-mode Choke Equivalent Circuit Extraction

The equivalent circuit for a common-mode choke is shown in Figure 1.

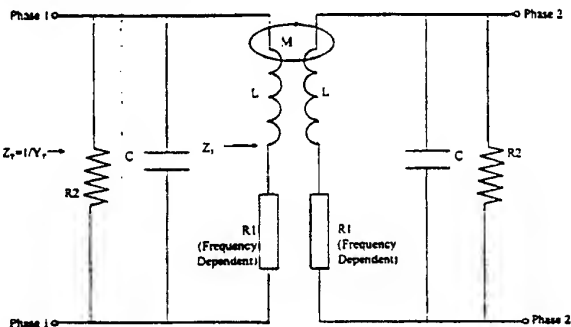


Figure 1 Common-mode choke equivalent circuit

The magnitude of the various parameters shown in the equivalent circuit in Figure 1 may be obtained from the frequency at which various resonances occur in the impedance plots of the common-mode choke. In order to acquire sufficient information to calculate all parameter values, it is necessary to plot the real and imaginary parts of the choke impedance for the following situations :

- (1) The impedance between both terminals which connect to the same phase when the terminals of the other phase are short-circuited.
- (2) The impedance between both terminals which connect to the same phase when the terminals of the other phase are open-circuited.

These impedance plots were taken using a HP 4194A Impedance / Gain-Phase Analyser. A description of the circuit analysis techniques required for the derivation of equations leading to the acquisition of the value of the various parameters in Figure 1 is outside the scope of this paper. However, the equations themselves are presented below.

$L = L_{inO/C}$ where $L_{inO/C}$ represents the inductance of one phase of the choke at low frequency with the other phase open-circuited

$M = \sqrt{L(L - L_{inS/C})}$ where $L_{inS/C}$ represents the inductance of one phase of the choke at low frequency with the other phase short-circuited

$C = \frac{1}{\omega_0^2(L + M)}$ where ω_0 represents the angular frequency at which the first resonant point occurs when measuring the impedance of one phase with the other

phase open-circuited (i.e. the first frequency point at which the imaginary part of the choke impedance is zero).

$R2 = 2Z_{RESONANCE}$ where $Z_{RESONANCE}$ represents the value of the impedance of a phase at the resonant frequency referred to above. This will be a totally real impedance.

$R1$ is a frequency dependent parameter due to the skin effect and hence is proportional to the square-root of frequency. The proportionality constant may be found by measuring the resistance of a phase at a number of different low frequencies and choosing a suitable proportionality constant which gives good agreement with each of the measured resistances.

3. CIRCUIT EXTRACTION OF MAINS CABLE AND ARTIFICIAL MAINS NETWORK

3.1 Circuit Extraction of Mains Cable

Many models of conducted EMI test set-ups (e.g. [1]) show the LISN connected to the equipment under test via a short-circuit. At frequencies in the conducted EMI range, however, it is necessary to incorporate a transmission-line model for the mains cable in order to yield the accurate model of the mains cable / LISN combination which is necessary to facilitate accurate prediction of input filter attenuation in a real conducted EMI test environment.

Figure 2 shows the equivalent circuit for a 1-metre mains cable used for connecting the power supply under test to the LISN. The value of C was easily obtained by measuring the capacitance between any two phases of the mains cable at low frequency : the acquisition of the values of L and M was a little more complex, however, and required the taking of a number of different readings in order to construct two simultaneous equations in L and M which yielded the required inductance and mutual inductance values.

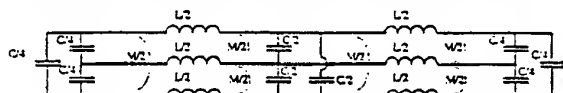


Figure 2 Equivalent Circuit of a 1-metre line

Note : In Figure 2, L, C and M are per-unit length parameters.

In addition, it was found that it was necessary to include a frequency-dependent resistor in series with each inductor in order to incorporate skin depth effects.

3.2 Circuit Extraction of Artificial Mains Network

The equivalent circuit of the artificial mains network (LISN) was modelled directly on the actual LISN components. This equivalent circuit is shown in Figure 3. It was assumed that at frequencies of 150 kHz and above, the impedance of the capacitors becomes negligible. It should be noted that the 51Ω resistor shown in Figure 3 would have been expected from quoted LISN component values to have had a value of

50Ω : its value had to be increased slightly to 51Ω to effect a closer agreement between measured results and SPICE simulation results.

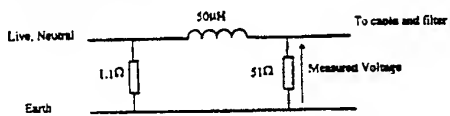


Figure 3 LISN equivalent circuit

4. MODELLING OF THE PCB

In modelling the PCB of the filter network, it was found necessary to consider the effect of the self-inductances of the connecting lengths of track and also the effect of mutual inductances involving loops with large relative areas. These self and mutual inductances were calculated using analytical formulae which have been derived at the University of Limerick. Obviously, analytical formulae are only useful for simple PCB geometries : in order to facilitate the modelling of the complex filter PCB layout using these formulae, the filter layout was reduced to a number of straight and orthogonal track sections which could then easily be analysed using the analytical formulae available.

5. TEST SETUP USED FOR EXPERIMENTAL MEASUREMENTS

In order to model the attenuation provided by the sample filter, a test PCB was constructed. This PCB reproduced the layout of the Artesyn Technologies power supply input filter, with additional tracking which facilitated injection of both a common-mode and differential-mode signal to the filter. This additional tracking was laid out in order to minimise its effect on the original system response.

The filter performance was observed by feeding a 0 dBm signal from the tracking generator output of a spectrum analyser into the signal injection section of the test PCB. The filter response could then be measured at the LISN connected to the phase under test (filter performance was measured for both phases). The test set-up used for the experimental measurements is shown below. A single-pole, double-throw switch is used to select between injection of a common-mode signal and a differential-mode signal.

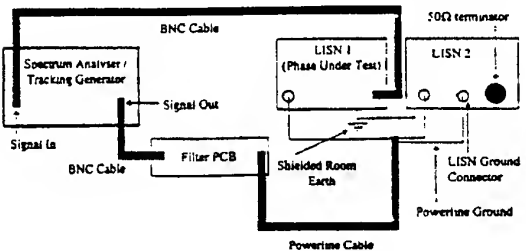


Figure 4 Generic Test Setup (Common-Mode and Differential Mode)

6. COMPARISON OF RESULTS

In order to assess the performance of the input filter, the response of a number of different configurations was measured. For each case, the measured response was compared with the simulated response obtained using SPICE. For each different configuration (e.g. different mains cable length, common or differential-mode signal etc.), the attenuation on both phases was measured : only the neutral phase has been shown here since attenuation on the live phase was almost identical in all cases.

Furthermore, the measured response for one of the configurations (1-metre cable from power supply to LISN ; common mode attenuation ; neutral phase) was compared with the simulated response for that configuration in the absence of PCB modelling : this comparison was carried out in order to emphasize the importance of PCB modelling if close agreement is to be obtained between measured and simulated results. This comparison is shown in Figure 5. It can be seen that up to 60 dB disparity is seen between simulated and measured results when PCB track models are not included.

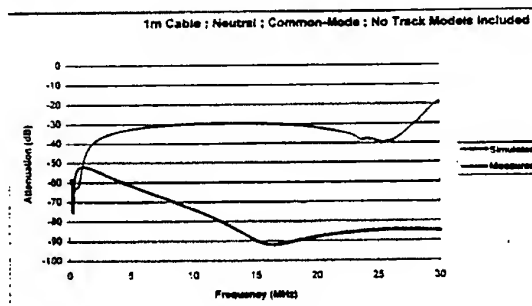


Figure 5 Effect of Omitting PCB Models

Figure 6 compares the simulated and measured attenuation provided on the neutral phase to a common-mode signal with a 1-metre mains cable from the power supply to the LISN. It can be seen that excellent agreement (maximum disparity of approximately 3 dB) is achieved between simulated and measured results, thereby verifying the accuracy of the modelling approach taken. There is, however, a relatively large disparity between simulated and measured results in the frequency region between approximately 27 MHz and 30 MHz. Disparities in this frequency region were seen for all configurations tested : considerable difficulty was encountered in obtaining reproducible test results in this area of the spectrum. These problems were thought to be due to a cable resonance or a resonance associated with the shielded room being used.

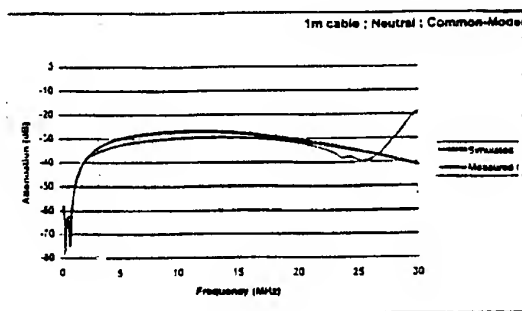


Figure 6 Comparison of Common-Mode Attenuation

Figure 7 compares the simulated and measured attenuation provided on the neutral phase to a differential-mode signal with a 1-metre mains cable from the power supply to the LISN. Once again, it can be seen that good agreement (within approximately 5 dB) is achieved between simulated and measured results.

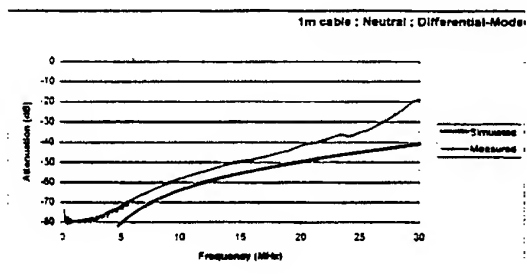


Figure 7 Comparison of Differential-Mode Attenuation
Figure 8 illustrates the effect of mains cable length on filter performance within the system. It can be seen that cable length has a significant effect on filter response within the system. Comparing Figure 8 with Figure 6, which shows common-mode attenuation with a 1-metre mains cable, it can be seen that there is a significant difference (both for simulated and measured results) between the attenuation provided in the 1-metre case and that provided in the 2-metre case : the 2-metre cable system provides more attenuation than the 1-metre system below 25 MHz but less from 25 MHz to 30 MHz. This shows the importance of accurate mains cable modelling when attempting to predict conducted emissions in a conducted EMI test environment.

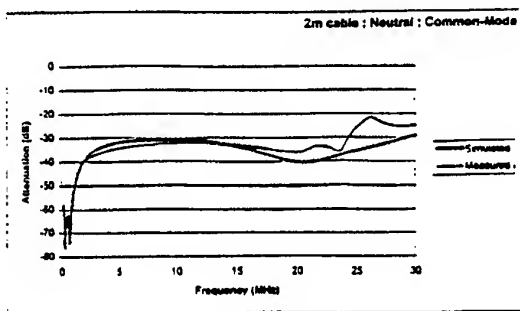


Figure 8 Effect of Cable Length

7. CONCLUSIONS

A set of techniques was developed which facilitated the acquisition of accurate models for the different elements affecting the attenuation provided by a switched-mode power supply input filter in a conducted EMI test environment. These models were used in conjunction with the SPICE circuit simulator to predict the attenuation provided by a sample filter for a number of different situations. It was found that in order to obtain accurate predicted results from SPICE, it was necessary to include accurate models of not only the filter components themselves but also of the PCB tracking and of the mains cable connecting the power supply to the LISN.

8. REFERENCES

- [1] Basso, C., "Spice Predicts differential conducted EMI from switching power supplies" *EDN Magazine*, pp. 191-204, February 3, 1997.

BIOGRAPHICAL NOTES

JOHN KELLY holds B. Eng and M. Eng degrees from the University of Limerick, Ireland. His principle research interests include PCB modelling techniques and power-supply EMI prediction. He is a research officer with PEI Technologies, a government-funded programme in advanced technology.

TOM SORENSEN holds B.E. and M.E degrees from University College Cork, Ireland. His principle research interests include radio-frequency design and radiated and conducted EMI prediction. He is a lecturer with the electronic and computer engineering department at the University of Limerick.

PETER BARDOS holds a B.Sc.(Eng) from London University. His principal research and technical interests include EMI control, magnetics, reliability, and engineer training. He is the Principal Engineer at Artesyn Technologies (formerly Computer Products) in Youghal, County Cork, Ireland.

SHIELDING OF THE DIELECTRIC BALL RESONATORS WITH WHISPERING - GALLERY MODES

S.N.Kharkovsky, Yu.F.Filipov, Z.E.Eremenko, V.V.Kutuzov, and A.E.Kogut

Usikov Institute of Radiophysics and Electronics National Academy of Sciences of Ukraine

Ulitsa Academika Proskury, 12, 310085. Ukraine

Tel: (0572)-448-593. Fax (0572) 441-105. E-mail:ire@ire.kharkov.ua

1. ABSTRACT

New results of the investigation of shielded dielectric ball resonator (DBR) with whispering gallery modes (WGM's) are represented. The characteristic relations TM and TE modes are obtained. The dependence of resonant frequencies and Q-factor of WGM's on resonator parameters have been calculated numerically. It is shown that the shielding of DBR provides the increasing modes Q-factor in ten times. A good agreement between theoretical and experimental results are obtained.

2. INTRODUCTION

Dielectric resonators with modes called traditionally whispering gallery modes (WGM's) [1,2] have recently become more popular [3-6]. In quasi-optical dielectric resonators ($D > 10\lambda_d$, where D is diameter of resonator, λ_d is the wavelength) these modes are formed by the grazing traveling waves inside dielectric with small incidence angles, their reflection factor being close to 1. Most of the modal energy is confined between the external and inner modal caustic. Near this region the electromagnetic fields are evanescent. That is why their electromagnetic field is localized in the vicinity of resonator's inner surface, as the result these modes have a high Q-factor, but also a dense spectrum of resonant frequencies. Various advantages of WGM's resonators suggest their utilization in microwave and millimeter wave devices such as directional filters, power combiners [7], bandstop filters [3], solid-state oscillators [8], sensors for study of various materials [9].

One of the most important limits of the wide usage in practice of dielectric resonators with WGM's is the problem of their electromagnetic compatibility with

other elements and devices because of their open nature and parasitic wave radiation. The open nature of the resonators leads to the system sensitiveness to the external medium and elements. It can display in non-control frequency and Q-factor oscillations and cross coupling with external circuits. One of this problem solutions is shielding of resonators [4,10].

During the calculation and experimental investigation of shielding cylindrical systems appears the difficulties through the limited axial side and dense spectrum of oscillations. There is an quite important problem such as an effective excitation of WGM's these resonators.

In this paper the shielding of the dielectric ball resonator (DBR) with WGM's is investigated. The choice of this system is determined that DBR modes can be analyzed by strict methods and are used in millimeter and optical techniques at the present time [9,11]. We first derive characteristic equations for shielded DBR modes. Then we calculated the resonant frequencies, the Q-factor (depending on dielectric, radiation, and conductor losses) for WGM's of the open DBR and at the presence of the metal shield. The resonant frequencies, Q-factor of open and shielded hemispheric dielectric resonator were measured experimentally.

3. THEORY

Consider the shielded DBR as a layered spherical resonator shown in Fig.1 (insect). In this resonator independence $TM(H_r = 0)$ and $TE(E_r = 0)$ resonant oscillations exist. Their electromagnetic field components are determined via potentials U and V , respectively, which are the solutions of wave equation ($\Psi = U, V$):

$$\left[\frac{\partial^2}{\partial r^2} + \frac{1}{r^2 \sin \theta} \left(\frac{\partial}{\partial \theta} \sin \theta \frac{\partial}{\partial \theta} + \frac{1}{\sin \theta} \frac{\partial^2}{\partial \varphi^2} \right) + \varepsilon(r) k^2 \right] \Psi = 0 \quad (1)$$

Divide the resonator into three areas (Fig. 1., insect), which are characterized by dielectric permeability $\varepsilon_1, \varepsilon_2, \varepsilon_3$. Here $\varepsilon_3 = \frac{4i\pi\sigma}{\omega}$, σ is the metal conductivity, ω is a resonant frequency. The depth of the field penetration into metal is small as compared with the thickness of metal shield. We can neglect the reflect wave from external metal side. The solutions of (1) in each area are

$$\Psi_j = R_{\psi_j}(r) P_n^m(\cos \theta) e^{im\varphi - i\omega t}$$

where n and m are polar and azimuth indices, $P_n^m(x)$ is the Legendre function

$$R_{\psi_1} = A_{\psi_1} j_n(\sqrt{\varepsilon_1} kr), \quad 0 \leq r \leq r_1$$

$$R_{\psi_2} = B_{\psi_2} j_n(\sqrt{\varepsilon_2} kr) + D_{\psi_2} \eta_n(\sqrt{\varepsilon_2} kr), \quad r_1 \leq r \leq r_2$$

$$R_{\psi_3} = L_{\psi_3} h_n^{(1)}(\sqrt{\varepsilon_3} kr), \quad r \geq r_2$$

$j_n(x)$, $\eta_n(x)$, $h_n^{(1)}(x)$ are spherical Bessel, Neumann, and Hankel functions for the first order, which connect with cylindrical function $J_{n+1/2}(x)$, $N_{n+1/2}(x)$, $H_{n+1/2}(x)$, respectively, in the

following correlation:

$$f_n(x) = \sqrt{\frac{\pi x}{2}} F_{n+1/2}(x),$$

$A_{\psi}, B_{\psi}, D_{\psi}, L_{\psi}$ are constants, which determinate via one from others at the satisfaction of boundary conditions at $r = r_1$ and r_2 . Using the continuity of tangential-field components on each layer surface of the resonator, we come to the characteristic relation, which determinate the resonant frequencies of TM and TE modes

$$\begin{aligned} & \left[\alpha_{\psi} \frac{j_n(\sqrt{\varepsilon_1} x_1)}{j_n(\sqrt{\varepsilon_1} x_1)} h_n^{(1)}(\sqrt{\varepsilon_1} x_1) - h_n^{(1)}(\sqrt{\varepsilon_1} x_1) \right] \\ & \cdot \beta_{\psi} \left[j_n(\sqrt{\varepsilon_2} x_1) \eta_n(\sqrt{\varepsilon_2} x_2) - j_n(\sqrt{\varepsilon_2} x_2) \eta_n(\sqrt{\varepsilon_2} x_1) \right] = \\ & = i(1 + i\beta_{\psi}) h_n^{(1)}(\sqrt{\varepsilon_3} x_2), \end{aligned} \quad (2)$$

where prime denotes derivative with respect to the argument.

$$\alpha_U = \sqrt{\frac{\varepsilon_2}{\varepsilon_1}}, \quad \alpha_V = \sqrt{\frac{\varepsilon_1}{\varepsilon_2}}, \quad \beta_U = \sqrt{\frac{\varepsilon_2}{\varepsilon_3}}, \quad \beta_V = \sqrt{\frac{\varepsilon_3}{\varepsilon_2}}$$

4. RESULTS

We study one of the most important situation: a teflon ball is inside of a copper spherical shield. The calculation have been obtained for TM_{nm1} and TE_{nm1} modes. The teflon dielectric losses tangent $\tan \delta$ and the conductivity of copper σ at the room temperature are $\tan \delta = 1.786 \cdot 10^{-4}$, $\sigma = 1.5 \cdot 10^{18} \text{ C}^{-1}$. The radius of the teflon ball r_1 is constant, but shield radius r_2 is varied, $\varepsilon_1 = 2.08$, $\varepsilon_2 = 1$.

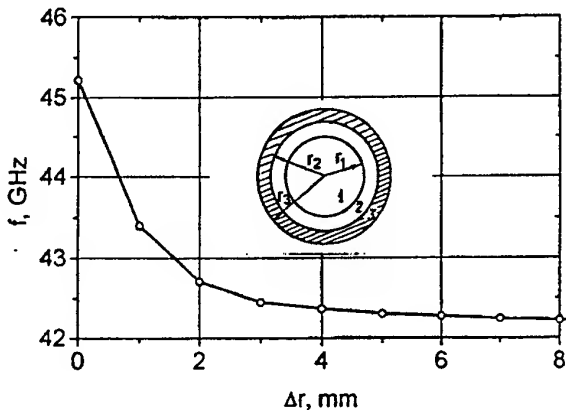


Fig. 1 The dependence of the resonant frequencies f of TE_{20m1} of the shielded DBR on the difference of the shield radius and dielectric ball one Δr ; $r_1 = 19$ mm. Insect: The schematic drawing of shielded DBR.

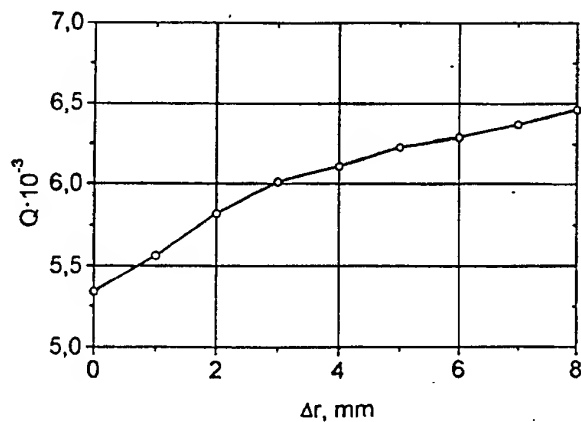


Fig. 2 The dependence of Q-factor of TE_{20m1} modes of shielded DBR on the difference Δr ; $r_1 = 19$ mm.

Fig. 1,2 show the influence of the metal shield radius on the resonant frequency and unloaded TM_{20m1} modes Q-factor for the dielectric ball with $r_1 = 19$ mm. It is shown that the resonant frequency increases at the increasing the gap value between the dielectric ball and the shield at $0 < \Delta r \leq 4$, where $\Delta r = r_2 - r_1$. This resonant frequency is constant at $\Delta r > 4$ and is equal the resonant frequency of open DBR. Q-factor has a little change near the $Q_d = (\tan \delta)^{-1}$ level. At $\Delta r = 0$, $Q \leq Q_d$ because of the conductor losses of shield, but at $\Delta r > 4$: $Q = \gamma Q_d$, where γ is the electric energy filling factor of the dielectric.

Let us noted that the area of dielectric ball oscillations and ring resonator ones interaction exists at the following increasing of the gap between the dielectric ball and the metal shield. Then the influence of the metal shield on the resonant ball frequency is not observed practically.

The value of TE_{20m1} modes Q-factor of the open dielectric DBR with $r_1 = 19$ mm is 400 [12], because of radiation losses. Thus the modes Q-factor increasing is observed in the shielding DBR. This Q-factor is 10 times more than in open DBR with the same radius. We can have such TE_{nm1} modes Q-factor in open DBR if the radiation losses are neglected as compared with dissipation losses in dielectric. For this purpose it is necessary to increase the polar index and the radius of the ball to keep the resonant frequency as a constant. The calculation carried out in our paper [12] show that TE_{nm1} radiation losses is neglected at $n > 40$. In this case the teflon ball radius must be 40 mm to allow 42 GHz resonant frequency.

The increasing of WGM's Q-factor in the shielded DBR is explained by the localization field effect in the dielectric ball at the determining system parameters. It confirms the dependence Q-factor on shield radius which we obtained from (2) at $\epsilon'' = 0$. It has non-monotone character at the gap deviation $0 < \Delta r < 10$ mm, approaching the value $Q_{\max} \sim 10^{10}$. It means that at such gap values in considering resonator the WGM's field is localized close the dielectric ball. The similar effect is observed in shielded cylindrical resonators with WGM's [4,10]. But at the shielded DBR the value of this effect higher than in cylindrical one, because of the resonant system is homogeneous and symmetrical. This property can be used to reduce the size and prize of DBR to provide the electromagnetic compatibility with other elements and devices.

The investigation of different WGM's shielded DBR has been carried out for the ball radius $r_d = 39$ mm. In considering frequency band the modes of the

resonator can have both high radiation losses and small ones, it depends on polar index. As the results the Q-factor of partial modes of open DBR are as following:

$$TM_{30m1} - 2.5 \cdot 10^3, TE_{30m1} - 3.05 \cdot 10^3,$$

$$TM_{40m1} - 5.6 \cdot 10^3, TE_{40m1} - 5.56 \cdot 10^3.$$

In Fig. 3,4 it is shown the dependence of the resonant frequencies of partial modes Q-factor in the shielded resonator on the gap value Δr . At the small Δr the metal shield has stronger influence on TE modes than on TM ones. In the area of «undisturbed» DBR Q-factor of TM modes higher than TE ones, and it depends on n more. In this case TM modes Q-factor is increased with decreasing n . Thus at the field

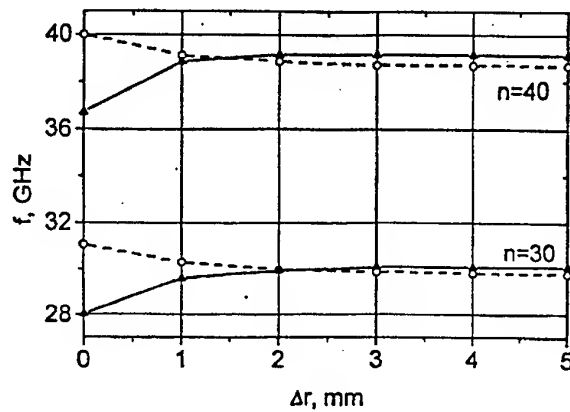


Fig. 3 The dependence of the resonant frequencies of TM_{20m1} (solid curves) and TE_{20m1} (dashed curves) modes of DBR on the difference Δr ; $r_1 = 39$ mm.

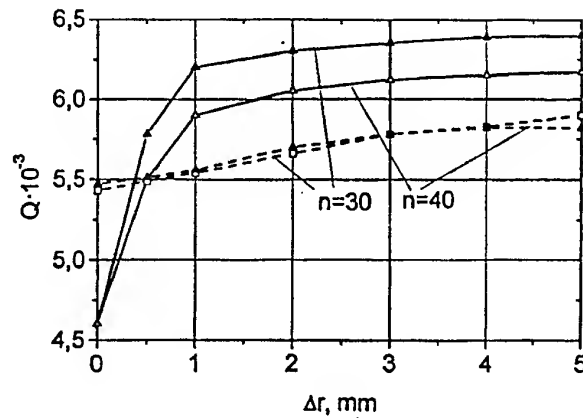


Fig. 4 The dependence of Q-factor of TM_{nm1} (solid curves) and TE_{nm1} (dashed curves) modes of DBR on Δr ; $r_1 = 39$ mm.

localization in the dielectric ball the part of the field is deflecting into the gap as in the open structure. The difference in the dependence Q on n TE and TM modes we can explain that TE modes in the ball have stronger wave slowing-down than TM ones [12]. Q-factor of TM modes in the shielded DBR at the increasing n will increase till the modes field reach to the metal shield.

At the experiment the one half of the resonator is flat mirror. WGM's of such hemispheric shielded resonator is provided by a empty metal waveguide via a split of coupling in this mirror. It is allowed to solve the problem of coupling with the field of shielded DBR localized close the dielectric ball. In the teflon resonator with $r_1 = 42$ mm the value of eigen Q-factor at the resonant frequency 39 GHz is $6.3 \cdot 10^3$. This value has a good correlation with the calculated one. Q-factor of open hemispheric resonator is $5 \cdot 10^3$ [12].

5. CONCLUSION

The shielding of the dielectric ball resonator with WGM's is necessary for solving the problem of electromagnetic compatibility this resonator with other devices. Obtained characteristic relations allow to calculate with sufficient exactness the resonant frequencies and Q-factor of different modes of shielded DBR. It is shown that at the definite parameters of the resonant system Q-factor of shielded DBR in ten times more than one of the open DBR. The physics of this phenomenon is the effect of field localization of the dielectric ball WGM's in the dielectric and the air gap nearby the latter. The original method was worked out for the excitation of the shielded resonator modes.

6. REFERENCES

- 6.1. Lord Rayleigh, «The problem of whispering gallery», Phil. Mag., Vol.20, 1910, pp.1001-1004.
- 6.2. J.R.Wait, «Electromagnetic whispering gallery modes in a dielectric rod», Radio Sci., Vol.2, N9, 1967, pp.1005-1007.

6.3. D.Gros, P.Guillon, «Whispering gallery dielectric resonators modes», IEEE Trans. Microwave Theory Tech., Vol.38, N11, 1990, pp.1667-1673.

6.4. E.N.Ivanov, D.G.Blair, V.I.Kalinichev, «Approximate approach to the design of shielded dielectric disk resonators with whispering-gallery modes», IEEE Trans. Microwave Theory Tech., Vol 41, N.4, 1993,pp.632-637.

6.5. J.Krupka, D.Cros, M.Aubourg, P.Guillon, «Study whispering gallery modes in anisotropic single of crystal dielectric resonators», IEEE Trans. Microwave Theory Tech., Vol.42, N1, 1994,pp.56-61.

6.6. Yu.F.Filipov, S.N.Kharkovsky, A.Ja.Kirichenko, «Whispering-gallery modes of nonuniform dielectric resonators», Microwave and Optical Tech. Letters, Vol.10, N2, 1996, pp.124-129.

6.7. X.H.Jiao, P.Guillon, Ph.Auxemery, Cros, «Dielectric resonators suitable for use in planar integrated circuits at short millimeter wavelengths», IEEE Trans. Microwave Theory Tech., Vol.37, N2, 1989, pp.432-437.

6.8. S.N.Kharkovsky, A.Ja.Kirichenko, A.E.Kogut, «Solid-state oscillators with whispering-gallery mode dielectric resonators», Microwave and Optical Tecn. Letters, Vol.12, N4, 1996, pp.210-213.

6.9. V.B.Braginsky, V.S.Ilchenko, K.S.Bagdasarov, «Experimental observation of fundamental microwave absorption in high-quality dielectric crystals», Phys.Letters A, Vol.120, N6, 1987, pp.300-305.

6.10. V.F.Vzyatyshev, V.I.Kalinichev, V.I.Kulinov, «Physical phenomena in shielded dielectric rod resonator and problem of its design», Radio Engineering and Electronic Physics, Vol.30, N4, 1985, pp.705-712.

6.11. E.M.Ganapolsky, A.V.Golik, A.P. Korolyuk, «Quasioptical method for measuring extremely low dielectric loss in condensed media at low temperatures» (in Russian), Fizika nizkikh temperatur, Vol.19, N11, 1993, pp.1255-1259.

6.12. A.E.Kogut, V.V.Kutuzov, Yu.F.Filipov, S.N.Kharkovsky, «Whispering-gallery modes of the quasioptical hemisphere dielectrical resonator» (in Russian), Izv.Vuz. Radioelektronika, Vol.40, N2, 1997, pp.19-26.



Sergei N. Kharkovsky was born in Mayskii, Kabardino-Balkaria republic, USSR in 1952. He graduated from Kharkov Institute of Radioelectronics (M.C.) in 1975, received Ph.D. from the Kharkov State University in 1985, and D. Sci .D. from the Institute of Radiophysics and Electronics National Academy of Sciences of Ukraine (IRE NASU) in 1994. Since 1975 he has been on the researcher staff of the IRE NASU. His area of interest is open and shielded non-uniform waveguide resonators, solid-state oscillators, the problem of their electromagnetic compatibility at microwave and millimeter waves and their applications for study of different materials.



Yuri Filippov was born in Leningrad, USSR in 1929. He graduated from the Kharkov State University in 1953. Since 1954 he has been associated with the Institute of Radiophysics and Electronics of National Academy of Sciences of Ukraine. In recent years his main area of interests is the theoretical methods of electromagnetic field theory in anisotropy non-uniform gyroscopic waveguides and resonators.



Zoya E. Eremenko was born in Kharkov, USSR in 1960. She graduated from Kharkov Aviation Institute in 1984, M.S. in Radio-engineering, received Ph.D. in Radiophysics in 1996 from the Institute of Radiophysics and Electronics National Academy of Sciences of Ukraine (IRE NASU). Since 1981 she has been in the researcher staff of the IRE NASU. Her main area of interests is the numerical investigation of the electromagnetic characteristics of open and shielded ball or cylinder resonators with anisotropy layered dielectrics or semiconductors.

Vladimir Kutuzov was born in Kharkov, Ukraine in 1966. He graduated from the Radiophysics Department of the Kharkov State University and post-graduate studentship of the Institute of Radiophysics and Electronics of National Academy of Sciences of Ukraine in 1990 and 1993, respectively. His main area of interests is the whispering gallery modes of resonators and their applications in millimeter wave length devices.



Alexander Kogut was born in Kharkov, Ukraine on 1970. He graduated from Radiophysics Department of the Kharkov State University and the post graduate studentship of this University in 1992 and 1997, respectively. He is scientific collaborator of the Institute of Radiophysics and Electronics of National Academy of Sciences of Ukraine. His main field of interests is the whispering gallery modes of dielectric resonator and their applications in millimeter wavelength devices.

FILTERING OF UNWANTED MICROWAVE RADIATION BY MEANS OF COMPOSITE GYROMAGNETIC THICK FILMS

Kitaytsev A.A.*¹, Koledintseva M.Yu., Shinkov A.A.

Moscow Power Engineering Institute (Technical University)

Krasnokazarmennaya, 14, Moscow, 111250 Russia

Tel. (095)362-79-58, fax: (095)362-89-38, e-mail: kitaitsev@b14s1nw.mpei.ac.ru

This paper is devoted to the investigation of frequency characteristics of waveguide sections with the positioned inside them single- and multi-layered composite gyromagnetic thick films for elaboration of filters of spurious electromagnetic radiation (filters of lower frequencies) with minimum losses in the pass-band, maximum abrupt slope of the amplitude-frequency characteristic and maximum possible losses outside the pass-band.

1. INTRODUCTION

Filtering of unwanted oscillations is the urgent problem for EMC of microwave apparatus and reduction of electromagnetic radiation [1]. For this problem solution various absorbing materials and coatings (of intererention, resistive type) are being elaborated [1,2]. Most of these materials and coatings absorb electromagnetic radiation only in a narrow frequency band and only at few certain modes. At the design of the corresponding filters there are problems connected with the forming of the desired amplitude-frequency characteristic. Elaboration of frequency-selective absorbers of unwanted and harmful radiation is an actual problem, because microwaves are being widely used nowadays in the systems of data transmission, radar technique, in technological installations and for other purposes. The most widely-spread way of the spurious radiation suppression in the microwave transmitting systems is the application of filters. The choosing of the filter type is determined by the demands to its frequency characteristic, matching of the filter with the main path, value of the induced attenuation on the frequencies of

spurious oscillations and on the main harmonic, electrical strength of the filter.

Filters, mainly applied nowadays, are of the reflecting type, and they as a rule don't satisfy the stringent demands to the mass and size parameters; their constructions are very complicated for technological reproduction, and including the filter into the path leads to the essential decrease of the electrical strength of the path. That's why it is urgent to develop filters of harmonics which get rid of the mentioned above shortcomings, and which satisfy the demands to the efficiency of the spurious oscillations suppression. Filter with the improved characteristics may be elaborated on base of the composite gyromagnetic material (CGM), where the phenomena of natural ferromagnetic resonance (NFMR) takes place.

The construction of the filter contains the waveguide section with inner walls covered by the CGM with frequency-selective magnetic losses. The CGM employed in the filter is the mixture of hexagonal polycrystalline ferrite powders distributed in the dielectric bond.

2. PECULIARITIES OF COMPOSITE GYROMAGNETIC MATERIALS AND FILMS ON THEIR BASE

Our investigations had shown that at the interaction of the particles of magnetouniaxial hexagonal ferrites with the electromagnetic wave there is efficient absorption of the microwave energy in the vicinity of the NFMR. In the frequency regions far from the NFMR interaction is practically absent. If the CGM is formed in such a way that its NFMR coincides with the

frequencies of the spurious radiation of the microwave source, it is possible to produce microwave transmission line with large losses at these frequencies and low losses in the main operating range.

The NFMR curve form as well as central resonance frequency depend on the chemical structure of hexagonal ferrites. Introduction of different doping ions into the main hexagonal ferrite allows to shift the central NFMR frequency to the side of its increase or, vice versa, decrease. The produced nowadays hexagonal ferrites have the NFMR at frequencies from 1 to 120 GHz. Using the combination of the powders of different hexagonal ferrites, it is possible to get composite materials with the desired amplitude-frequency characteristics.

The frequency characteristics of composite gyromagnetic thick films (CGTF) on base of the CGM have been studied. Single-layered CGTF is the layer of CGM from 0.2 to 2 mm thick. As required by spending to application of the films they can be placed on either metal or dielectric substrate.

Due to a number of physical features of hexagonal ferrites (absence of conductivity losses at resonance absorption of electromagnetic waves energy; high inner crystallographic anisotropy magnetic field; strong dependence of the crystallographic anisotropy field and the NFMR line width on the chemical formula of the powder), the films on their base have a number of advantages:

- resist high power levels ($P_{aver} \sim 1$ kW);
- don't need high fields of magnetization;
- allow to get the needed frequency characteristic by means of varying the chemical structure of powders, position and profile of the CGTF;
- have good matching with the waveguide transmission line.

The advantage of CGM is technological reproduction ability and simplicity of their production. It is possible to produce the filtering of unwanted oscillations, putting the CGTM on the waveguide inner walls of the existing microwave device without variation of its basic construction.

3. EXPERIMENTAL RESULTS AND DISCUSSION

Investigation of the CGTF were carried out on the waveguide section in the frequency range from 8 to 37.5 GHz. CGTF were placed on the walls of the waveguide, and the measurement of reflection and transmission coefficients for the waveguide with the film were carried out.

Fig.1a demonstrates the dependence of the microwave energy absorption in the

waveguide transmission line on the frequency at placing films on the narrow wall; and in Fig.1b there is shown the same dependence for the film on the wide wall.

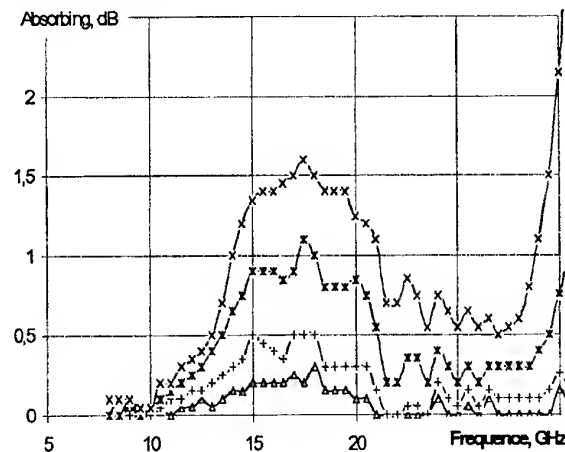


Fig. 1a

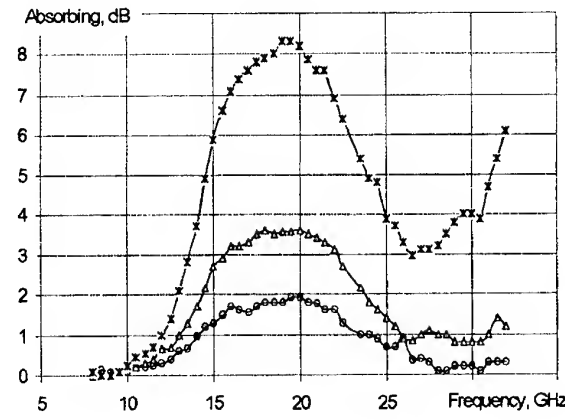


Fig. 1b

Using the mixtures of hexagonal ferrites with various NFMR frequencies, it is possible to control the frequency characteristic of the films absorption. In Fig.2 there is absorption of microwave energy in the waveguide with the film on base of a mixture of two hexagonal ferrites with different chemical structures. This film is placed on the wide wall of the waveguide.

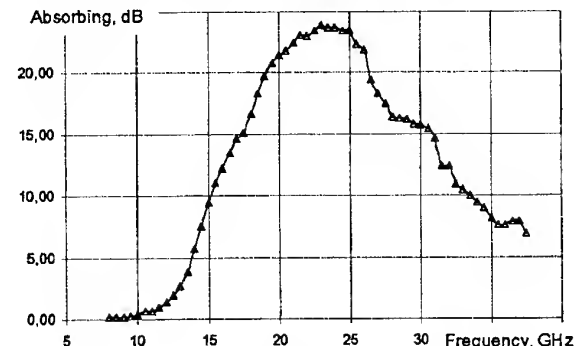


Fig.2.

For the increase of absorption in the waveguide with films the multi-layered composition gyromagnetic thick films were produced.

Multi-layered CGTF are the absorption structure consisting of layers of the CGM and dielectric slabs between these layers. Like in the case of single-layered films, the absorption in them is conditioned by presence of the doped barium hexagonal ferrites. But this class of materials has a number of peculiarities, giving them a number of advantages over the single-layered structures.

As a matter of fact, the multi-layered film is a combination of two single-layered ones with a dielectric layer between them.

In the investigations of multi-layered CGTF there were used special samples of multi-layered films as well as a packet of two single-layered with previously known characteristics.

First, investigation of the thickness influence of dielectric layer on the value of absorption in the multi-layered CGTF, was carried out. In this experiment between the ferrite films placed near the narrow wall of the waveguide dielectric slabs of different thickness were placed in turn. For CGTF with different dielectric slabs the dependence of absorption on the frequency are represented in Fig.3.

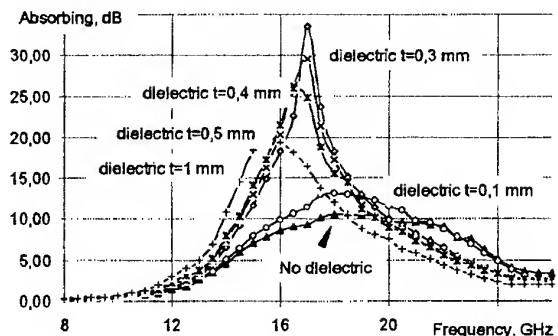


Fig.3

There is an optimum thickness of the dielectric layer. In the present case maximum absorption of the microwaves is observed at the dielectric slab having thickness 0.3 mm.

The laboratory samples of multi-layered CGTF were produced and absorption of microwaves was studied at the films positioned on the wide and narrow walls of the waveguide. Absorption characteristic with of fluoroplastic slab is represented in Fig.4.

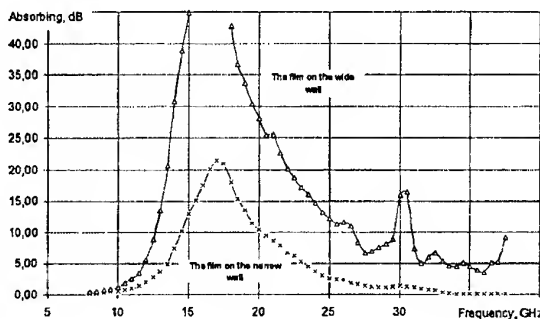


Fig.4

As it is seen from the obtained results there is increase of absorption in multi-layered film compared to the single-layered ones. There is also evident shift of the central resonance frequency at varying the dielectric thickness. Absorption in multi-layered films is essentially more than in the single-layered ones.

Multi-layered CGTF with frequency characteristic shown in Fig.4 provides suppression 30-40 dB in frequency range from 14 to 18 GHz. At frequencies 7-8 GHz losses don't exceed 0.2-0.3 dB.

3. CONCLUSION

Application of CGM and thick films on their base allows to produce filtering devices of absorbing type with the desired form of amplitude-frequency characteristic.

Technological simplicity, possibility to work at high power levels, efficient suppression of spurious oscillations in devices on base of the CGM and CGTF allow to use these materials for electromagnetic compatibility of microwave active devices without varying their basic construction.

REFERENCES

- [1]. Proc. 13 Int. Wroclaw Symp. EMC'96, June 25-28, 1996. Sections II, III.
- [2]. Proc. 12 Int. Zurich Symp. EMC'97, February 18-20, 1997. Sections H, J.
- [3]. Kitaytsev A.A. et al. Radioabsorbing composite magnetic materials and devices for ecological safety of electromagnetic fields sources (in Russian). Proc. of Russian Conf. 'Ecology'97', St.Petersburg, 1997, p. 58.

HETEROGENEOUS DIELECTRIC MATERIALS WITH HIGH PERMITTIVITY - ELECTRICAL PROPERTIES OF CARBON FIBRE - EPOXY COMPOSITES IN RADIOFREQUENCY RANGE 100 MHz - 1.8 GHz

V. Křesálek, Z. Římská

Department of Physics and Materials Engineering, Faculty of Technology Zlín
Technical University of Brno
T.G.M. 275, Postbox 183, 762 72 Zlín, Czech Republic

ABSTRACT

Electromagnetic interference is a specific kind of environmental pollution. Although metals can provide adequate shielding against EMI, conductive polymer composites are being increasingly used too. Structure and distribution of electroconductive fillers or their aggregates play the key role in the control of complex permittivity. Materials with short carbon fibres have very near threshold of percolation (≈ 4 vol.%). By means of the microencapsulation technology composite materials with high loading of short carbon fibres were prepared without reaching the threshold of percolation. Carbon fibres were coated with epoxy resin or PMMA (polymethylmethacrylate) and imbedded into epoxy resin as a polymer matrix. Electrical properties of these materials were studied.

1. INTRODUCTION

Absorption of electromagnetic waves is the irreversible conversion of electromagnetic energy into the heat. Material loss is the loss that occurs after the wave enters the material. The basic characteristic of this process is complex permittivity (for magnetic fillers complex permeability must be determined as well). The complex dielectric permittivity is usually defined by

$$\epsilon^* = \epsilon' - j\epsilon'' \quad (1)$$

where the real part (ϵ'), related to the storage of energy, is commonly known as the dielectric constant; the imaginary part (ϵ''), related to the energy loss of the system, is generally called the loss factor. The ratio of the imaginary to the real parts (ϵ'/ϵ'') is the dissipation factor, which represents $\tan \delta$, where δ is the angle between voltage and the changing current, i.e. the lag in the displacement current vector due to the presence of the dielectric [1].

The electrical conduction process in carbon fibre-polymer composites (or conductive filler - polymer composites in general) is complicated and dependent on

number of parameters, mainly on filler concentration. In addition to the amount of loading, particle size, geometry and structure, filler-matrix interactions (wettability) and processing techniques (disspergation) are the main factors in determining the electrical properties. The DC electrical conductivity of these composites was experimentally found to exhibit a threshold behaviour. For the low filler concentration the particles of conductive fillers are isolated to such extend that the resistance is large. The conductivity increases abruptly at a certain interval of concentrations of fillers reaching the so-called percolation threshold. It is a consequence of the appearance of the first conducting path through composite. The percolation theory predicts a conductivity above the percolation threshold by a simple power law [2,3]

$$\sigma = \sigma_0 (p - p_c)^t \quad (2)$$

where p is the conductive phase volume fraction, p_c is the conductive phase volume fraction at the percolation threshold, i.e. the volume fraction below which the conductivity falls to a very small value, σ_0 is the conductivity of the conducting filler, $t = 1.6$ to 1.9 [4]. The theoretical description of this complicated phenomena was developed for spherical and cylindrical shape of fillers. It gives a very rough estimation for practise and the model is valid mainly for DC current or low frequency range. Anisotropic percolation model has been studied for 2D composites with short fibres by means of Monte Carlo method [5].

For alternating current the problem is more complicated. The description of material must be done by complex permittivity and composite is modelled by a so-called effective medium theory. The satisfactory model is valid for spherical and cylindrical particles and for volume fraction below 0.3 [6].

In composites with conductive fillers the dependence of conductivity on frequency is qualitatively described by the model of an RC (resistor - capacitor) circuit (Fig.1). According to this model, the particles of the

conducting filler are approximated by resistors (R_F), and the resistance of contacts between two particles (which is a sum of the resistance of the interfacial boundary and the polymer layer between the particles) is modelled by a capacitor (C_M) and a resistor (R_M) arranged in parallel. Hence, a composite may be described by a set of RC circuits or by a single RC circuit with averaged parameters [7].

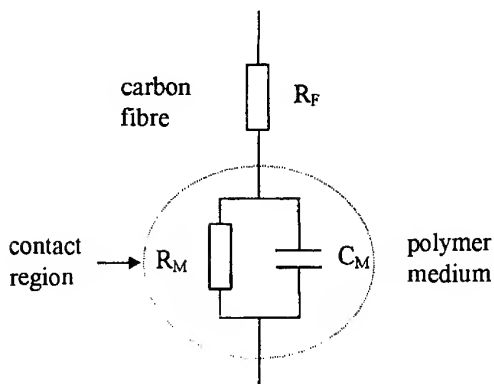


Fig. 1. Equivalent RC circuit in the contact region of carbon fibres

At low frequencies, the current flows through the contact resistance since it is blocked at the contact capacitance. The net resistance of the fibre in series with the contact region is $R_F + R_M$. At high frequencies, the impedance of the contact capacitance is much lower than the contact resistance and the current flows through the contact capacitance. Furthermore, since the capacitor's impedance is much lower than the fibre resistance, the net resistance at the high frequencies is equal to R_F , which is lower than the net resistance ($R_F + R_M$) for the low frequencies [8]. Thus, the conductivity of a specimen starts to rise from its DC value (σ_L) at a characteristic frequency and levels off at a higher value (σ_H) which is that of the carbon fibres alone.

Materials with good electromagnetic field absorption are distinguished for relatively high values of real and imaginary parts of complex permittivity (ϵ' , ϵ''). High values of permittivity can be reached by presence of high quantity of dipoles (in this case dipoles are represented by particles of electroconductive filler) in electrically non-conductive material [1]. As the material becomes electrically conductive for high volume fraction of electroconductive filler in the composite due to contacts of filler particles, it is necessary to protect the particles from connecting each other and creating an electrically conductive path in the material. This aim can be reached by coating the particles with thin insulating layer of non-conductive polymer. For this purpose microencapsulation technique can be used.

Microencapsulation is a process of enclosing small particles into the thin coat of film-forming material

(polymer). There are many methods of microencapsulation. The most widely used methods are physically - chemical methods [9]. The idea of fibre coating originated during our co-operation with the Chalmers University of Technology Gothenburg (Sweden) [10].

2. EXPERIMENTAL

2.1. Materials

Short carbon fibres, Bestfight, HTA - 7 - 12,000; PAN precursor, were produced by Toho Rayon Co.Ltd. (Japan). Parameters of the fibre: diameter $\varnothing = 7 \mu\text{m}$, length $l = 3 \text{ mm}$, density $\rho = 1,76 \text{ g/cm}^3$, electric volume resistivity $\rho_R = 18 \cdot 10^{-6} \Omega \cdot \text{m}$.

Polymethylmethacrylate, Akrylon, was manufactured by PCHZ Žilina (Slovakia). Parameters of PMMA: density $\rho = 1.17 \text{ g/cm}^3$, electric volume resistivity $\rho_R > 10^{13} \Omega \cdot \text{m}$.

Low temperature liquid epoxy resin, ChS Epoxy 531 and curing agent P11 (diethylenetriamine), produced in Spolek pro chemickou a hutni výrobu (Czech Republic), were used in present work. Parameters of the cured epoxy: density $\rho = 1.2 \text{ g/cm}^3$, electric volume resistivity $\rho_R > 10^{-12} \Omega \cdot \text{m}$.

2.2. Samples preparation

Many technologies of encapsulation were examined to get the coating on the fibre surface (polymerization, electropolymerization, coacervation, thermogelation, precipitation). The best results were obtained using the precipitation technology. Although the polymer layer on the fibre surface didn't have uniform thickness, the coating results were satisfying for our purpose. Carbon fibres were coated with PMMA or epoxy resin. The surface of carbon fibre was covered with a beads of polymer as spacers.

Encapsulated fibres were cut to the length of $10^1 - 10^2 \mu\text{m}$ and these particles were embedded in low temperature liquid epoxy resin. Composite samples with 7, 10 and 15 wt.% of carbon fibres and low temperature liquid epoxy resin as a matrix were prepared using press moulding.

2.3. Evaluation of Electrical Properties

The electrical conductivity and the dynamic electrical properties were measured through the vertical thickness of a round specimen of 15 mm in diameter. For the DC conductivity measurements, electroconductive rubber (Rhône Poulen) was used to ensure a good contact of the sample surface with electrodes. The DC electrical conductivity of the samples was measured using a KEITHLEY 617 Programmable Electrometer and the values varied over the range from $10^{12} - 10^7 \text{ S.m}^{-1}$. Dielectric properties (AC behaviour) of these materials were measured on Hewlett - Packard 4291 A Impedance and Material Analyser in the frequency

range 100 MHz - 1,8 GHz and the temperature range 20 - 160 °C.

3. RESULTS AND DISCUSSION

Figures 2 and 3 show real and imaginary parts of complex permittivity as a function of frequency (100 MHz - 1,3 GHz) and temperature (20 - 160 °C) for the sample with 10 wt.% of carbon fibres. It can be seen that ϵ' and ϵ'' are increasing with temperature. These values rise also with increased loading of composite samples. The values of dielectric loss, which represent the energy changed into heat in the material, are quite high.

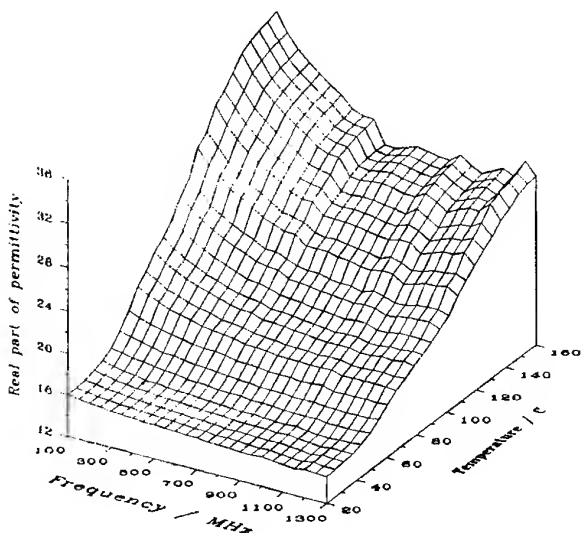


Fig. 2. Temperature dependence of real part of permittivity (dielectric constant) on frequency - 10 wt.% of carbon fibres

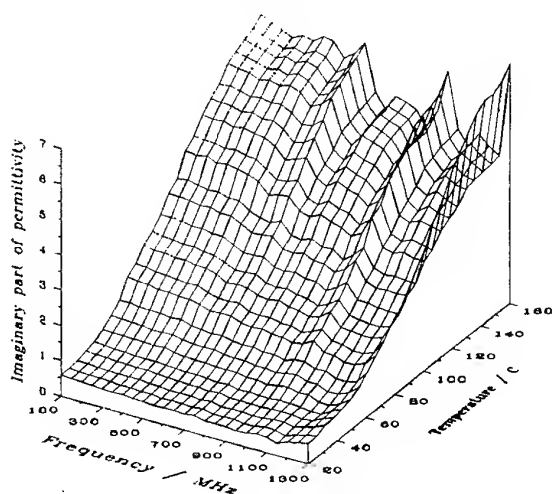


Fig. 3. Temperature dependence of imaginary part of permittivity (loss tangent) on frequency - 10wt.% of carbon fibres

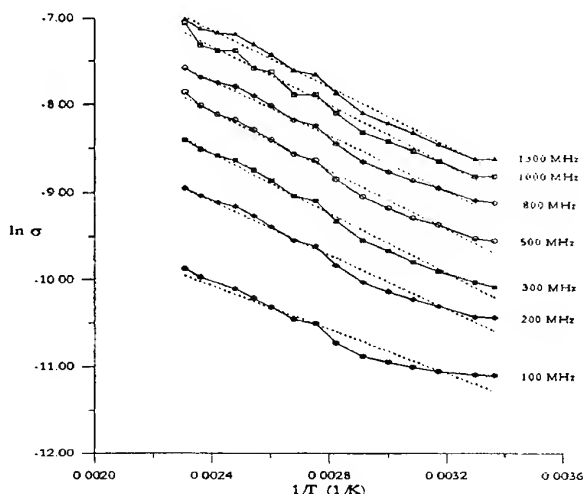


Fig. 4. Temperature dependence of AC conductivity - 7wt.% of carbon fibres

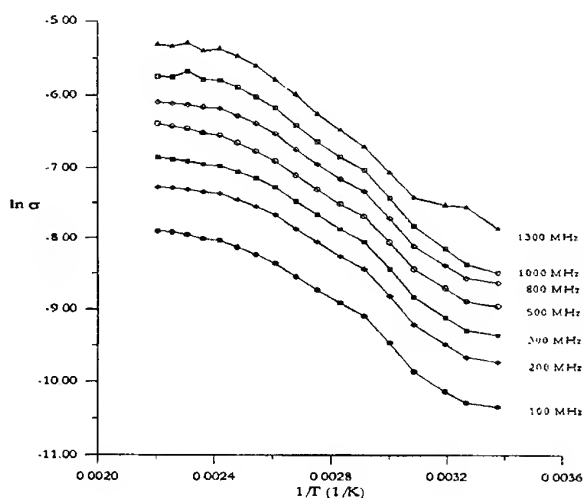


Fig. 5. Temperature dependence of AC conductivity - 10wt.% of carbon fibres

The AC conductivity was calculated from the dielectric loss and the values varied over the range from 10^{-3} to 10^0 S.m^{-1} . By plotting the electrical conductivity (its logarithmic values) against reciprocal temperature we expected to obtain a straight line according to the following equations:

$$\sigma = \sigma_0 \exp(-\Delta E/kT) \quad (3)$$

$$\ln \sigma = \ln \sigma_0 - \Delta E/kT \quad (4)$$

$$\ln \sigma_0 = a + b \Delta E \quad (5)$$

where σ is the conductivity, σ_0 is the pre-exponential factor, ΔE is an activation energy, k is Boltzmann's constant, T is the absolute temperature, a and b are constants.

This was true for low loading of carbon fibres (7 wt.% - Fig. 4.) but this assumption failed at higher loading (15 wt.% - Fig. 6.) and unexpected jump in conductivity occurred in the temperature range 82 - 112 °C. The origin of this behaviour is not fully understood and it is still under investigation.

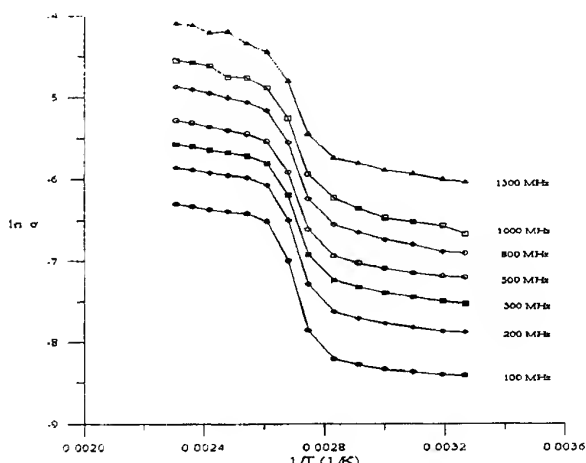


Fig. 6. Temperature dependence of AC conductivity - 15wt.% of carbon fibres

4. CONCLUSIONS

Our aim was to prepare material with high values of permittivity using methods of polymer engineering. The interest in such material derives from light weight, ease of processability of the polymer components, attractive mechanical properties, environmental stability and good thermal conductivity in concern with desired dynamic mechanical properties. Dielectric composite materials with relatively high loading of conducting particles from carbon fibres were prepared. As it was observed from the measurements of dynamic electrical properties, these materials have high dielectric loss and thus, good ability to absorb electromagnetic energy. This kind of material could be useful in the field of EMC or for the development of human body phantoms. Although ceramic materials (BaTiO_3 and others) showing high values of permittivity are already known, they cannot be used for all the purposes because of their brittleness and high weight.

5. REFERENCES

1. A.von Hippel, „Dielectric Materials and Applications“, Artech House, Boston - London, 1995.
2. Kirkpatrick, S., „Percolation and Conduction“, Reviews of Modern Physics, Vol.45, No. 4, 1973, pp. 574 - 588.
3. Stauffer, D., „Introduction to Percolation Theory“, Taylor & Francis, London and Philadelphia, 1985.
4. Ueda, N., Taya, N., „Prediction of the electrical conductivity of two-dimensionally oriented short fibre composites by a percolation model“, Journal of Applied Physics, Vol.60, No. 1, 1986, pp. 459 - 461.
5. Mamunya, E.P., Davidenko, V.V., Lebedev, E.V., „Percolation Conductivity of Polymer Composites Filled with Dispersed Conductive Filler“, Polymer Composites, Vol.16, No. 4, 1995, pp. 319 - 324.
6. Göktürk, H.S., Fiske, T.J., Kalyon, D.M., „Electric and Magnetic Properties of a Thermoplastic Elastomer Incorporated with Ferromagnetic Powders“, IEEE Transactions on Magnetics, Vol. 29, No. 6, 1993, pp. 4170 - 4176.
7. Chmutin, I.A., Ryvkina, N.G., Ponomarenko, A.T., Shevchenko, V.G., „Concentration Dependence of the Electrical Conductivity of Composites in High Frequency Plateau“, Polymer Science, Ser.A, Vol. 38, No. 2, 1996, pp. 173 - 177.
8. Medalia, A. I., „Electrical Conduction in Carbon Black Composites“, Rubber Chemistry and Technology, Vol. 59, pp. 432 - 454.
9. V.D. Solodovnik, „Mikrokapsulirovanije“, Chimija, Moskva, 1980.
10. Klasson, C., Kubát, J., private communication, Gothenburg, Sweden ,1993.
11. Jana, P.B., „Short Carbon Fibre Filled Polychloroprene Composites: Electrical Conduction“, Plastics, Rubber and Composites Processing and Applications, Vol. 20, No. 2, 1993, pp. 107 - 118.

BIOGRAPHICAL NOTES

Vojtěch Křesálek was born in 1952 in Czech Republic. In 1976 he finished his studies in Physics and in 1979 he received his PhD. degree in Physics from the University of Brno, Czech Republic. From 1979 until 1989 he worked in Military research and development institute where he created a laboratory for statistical optics and detection of weak light. Since 1989 he has worked at the Faculty of Technology in Zlín, Department of Physics and Materials Engineering. The area of his interest is dielectric spectroscopy of curing processes, electrical properties of polymers and composites.

Zdeňka Římská was born in 1972 in Czech Republic. She received her M.Sc. degree in Materials Engineering at the University of Technology Zlín, Czech Republic, in 1996. Now, she is working for her PhD. degree at the same University. She is carrying out research into the electrical properties of polymer composites.

THE EFFECT OF AGING ON THE SHIELDING OF ELECTROMAGNETIC FIELDS

George M. Kunkel
Spira Manufacturing Corporation
12721 Saticoy Street South
North Hollywood, CA 91605, USA

ABSTRACT

Shielding quality testing of EMI gasketed joints was measured on 24 samples of gasketed joints before and after the gasketed joints were subjected to a moisture/heat soak. The gaskets were stainless steel and tin-plated stainless steel using 3 resiliencies of each gasket. The joint surfaces were tin, nickel, chemical film and unplated 6061-T6 aluminum. The moisture/heat soak was performed per MIL-T-28800E. Plotted graphs and a tabular summary of the results are illustrated along with a summary of results and conclusion.

1. SUMMARY

1.1. The shielding quality of EMI gaskets is a function of the joint surface preparation, the gasket type and configuration as well as the force of the gasket against the joint surface. The shielding of a gasketed seam is known to degrade with time from oxidation (and sulfurization as related to the use of silver gaskets) of the gasket and joint surface due to the presence of moisture and heat as well as other environmental conditions such as salt fog, vibration, shock, thermal shock, etc.

1.2. The shielding quality of stainless steel and tin-plated stainless steel EMI gaskets was measured against tin-plated, nickel-plated, chemical film-plated and unplated 6061-T6 aluminum joint surfaces. Three resiliencies of the stainless steel and tin-plated stainless steel gaskets were used. The resiliencies (force of gasket against the joint surfaces) were approximately 2, 10 and 30 pounds per linear inch.

1.3. The results illustrated that the shielding quality of the gasketed joints is greatly dependent upon the joint surface preparation. The loss of shielding due to moisture soak can be significant. A

surprising result was that the stainless steel gaskets illustrated better shielding against the nickel-plated surface than the tin-plated gaskets. In all instances, the chemical film-plated surfaces produced the lowest level of shielding. The force of the gasket on the joint surfaces was not as significant a consideration as the other variables tested.

2. TEST CONDITIONS

2.1. Twenty-four (24) EMI gasketed joints were subjected to transfer impedance testing. The test sequence consisted of performing the transfer impedance testing, subjecting the gaskets to 164 hours of heat/humidity soak and re-running the transfer impedance testing.

2.2. The gaskets under test consisted of three resiliencies of stainless steel and tin-plated stainless steel gasket types. The force of the gasket exerted on the joint surface was approximately 2 pounds, 10 pounds and 30 pounds per linear inch.

2.3. The joint surfaces were constructed from 6061-T6 aluminum per QQ-A-200/8. The plating was electro-tin per MIL-T-10727, electroless nickel per MIL-C-26084 and chemical film per MIL-C-5541, Class 3.

2.4. The 164 hours of heat/humidity soak was performed in accordance with MIL-T-28800 for Class 2 equipment.

2.5. The transfer impedance testing was performed using the methodology of SAE-ARP-1705. The transfer impedance test results were converted to shielding quality data using theoretical shielding effectiveness conversion equations.

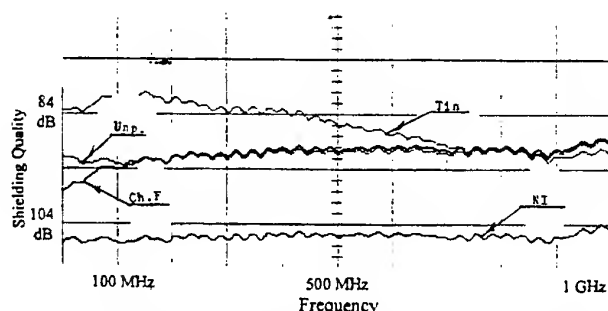


Figure 1. Shielding Quality of Stainless Steel Gasket exerting 2 pounds/inch force against Joint Surfaces before Moisture Soak

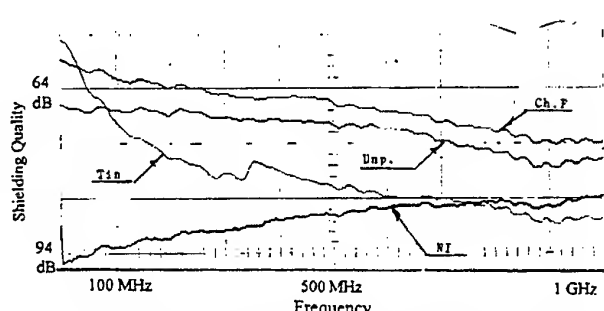


Figure 2. Shielding Quality of Stainless Steel Gasket exerting 2 pounds/inch force against Joint Surfaces after Moisture Soak

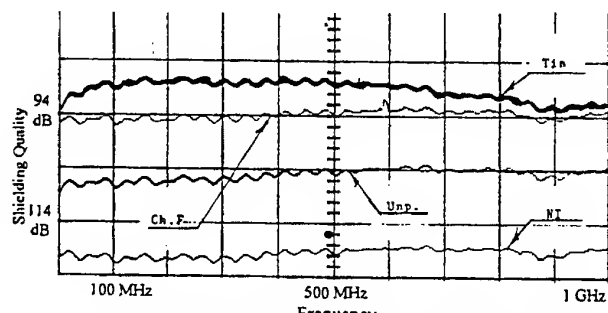


Figure 3. Shielding Quality of Stainless Steel Gasket exerting 10 pounds/inch force against Joint Surfaces before Moisture Soak

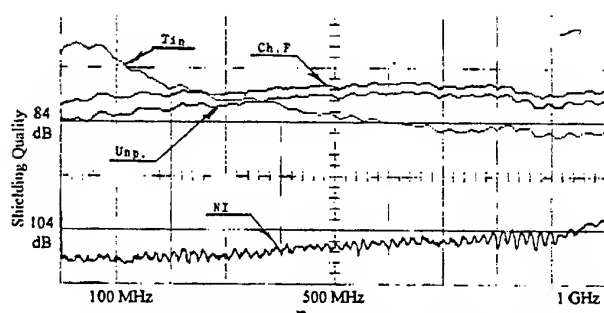


Figure 4. Shielding Quality of Stainless Steel Gasket exerting 10 pounds/inch force against Joint Surfaces after Moisture Soak

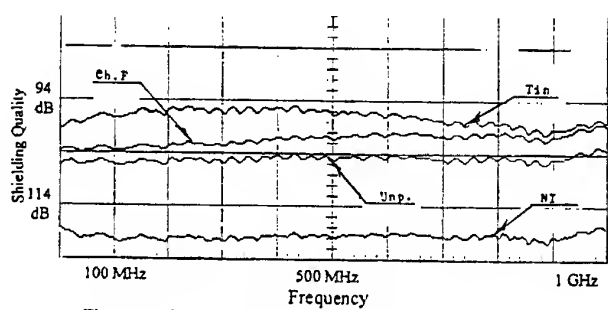


Figure 5. Shielding Quality of Stainless Steel Gasket exerting 30 pounds/inch force against Joint Surfaces before Moisture Soak

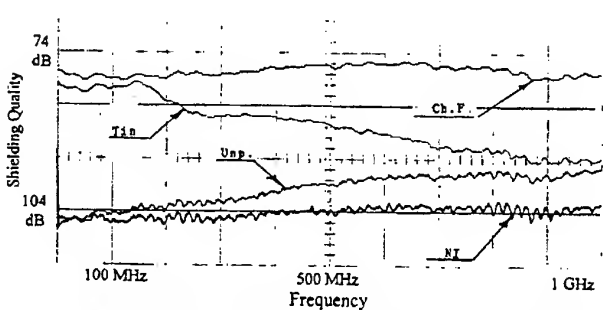


Figure 6. Shielding Quality of Stainless Steel Gasket exerting 30 pounds/inch force against Joint Surfaces after Moisture Soak

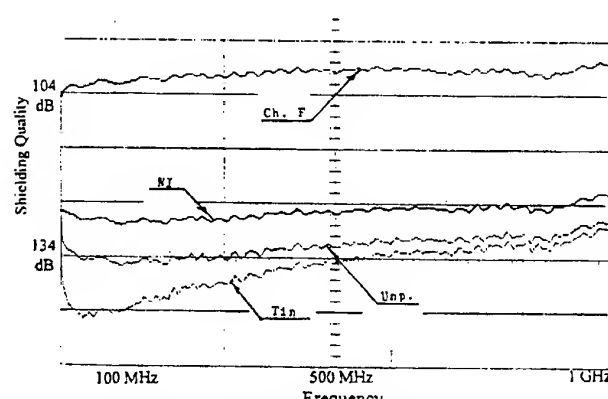


Figure 7. Shielding Quality of Tin Plated Gasket exerting 2 pounds/inch force against Joint Surfaces before Moisture Soak

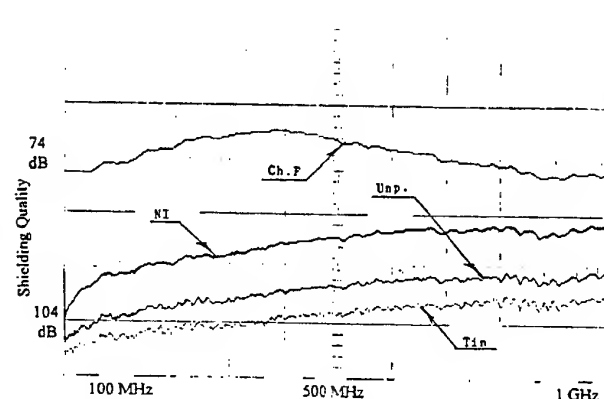


Figure 8. Shielding Quality of Tin Plated Gasket exerting 2 pounds/inch force against Joint Surfaces after Moisture Soak

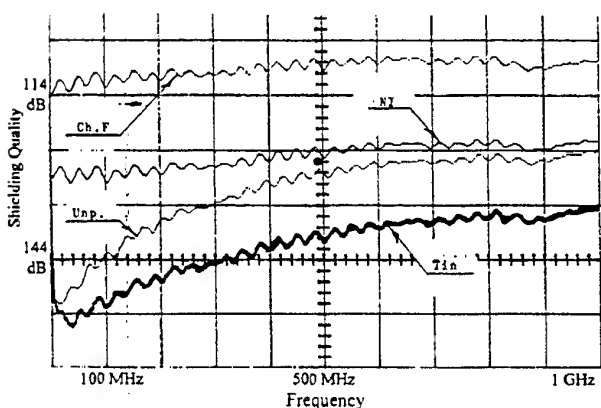


Figure 9. Shielding Quality of Tin Plated Gasket exerting 10 pounds/inch force against Joint Surfaces before Moisture Soak

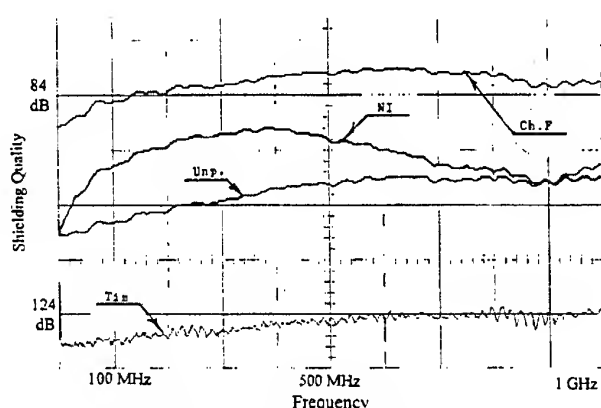


Figure 10. Shielding Quality of Tin Plated Gasket exerting 10 pounds/inch force against Joint Surfaces after Moisture Soak

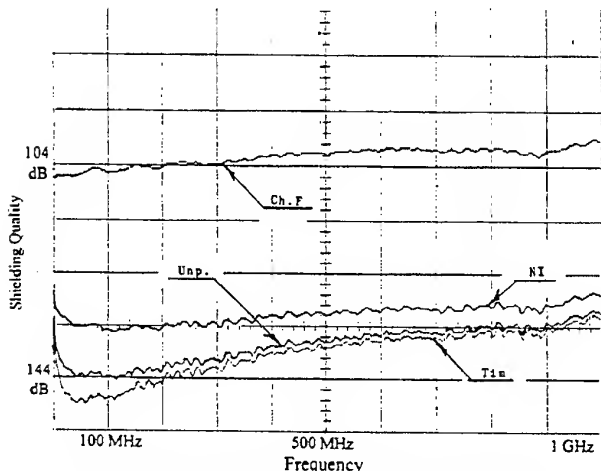


Figure 11. Shielding Quality of Tin Plated Gasket exerting 30 pounds/inch force against Joint Surfaces before Moisture Soak

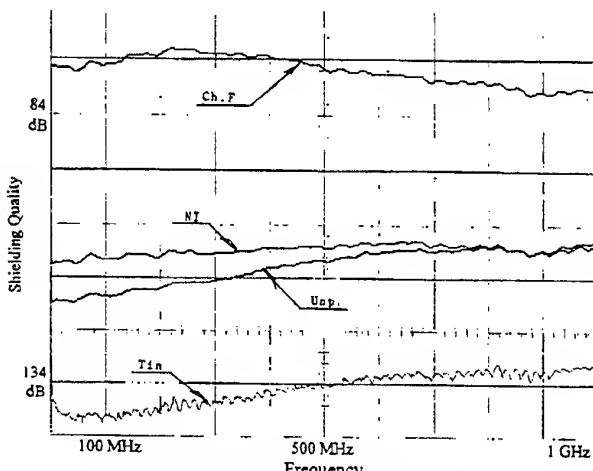


Figure 12. Shielding Quality of Tin Plated Gasket exerting 30 pounds/inch force against Joint Surfaces after Moisture Soak

Gasket	Joint Surface	Shielding Quality (dB)								
		100 MHz			500 MHz			1 GHz		
		Preparation	Before	After	Δ	Before	After	Δ	Before	After
Stainless Steel (2 lbs./in. of Force)	Tin	81	70	11	86	82	4	91	88	3
	Nickel	107	92	15	106	87	19	104	84	20
	Chem Film	94	62	32	91	67	24	89	74	15
	Unplated	94	68	26	91	71	20	89	77	12
Stainless Steel (10 lbs./in. of Force)	Tin	89	72	17	88	83	5	92	85	7
	Nickel	121	109	12	119	107	12	118	103	15
	Chem Film	95	80	15	93	78	15	93	78	15
	Unplated	107	83	24	104	80	24	104	80	24
Stainless Steel (30 lbs./in. of Force)	Tin	97	81	16	96	87	9	98	94	4
	Nickel	120	106	14	120	104	16	118	103	15
	Chem Film	104	79	25	101	76	25	98	77	21
	Unplated	106	104	2	105	99	6	103	96	7

Table 1. Test Results of Stainless Steel Gaskets

Gasket	Joint Surface	Shielding Quality (dB)									
		100 MHz			500 MHz			1GHz			
		Preparation	Before	After	Δ	Before	After	Δ	Before	After	Δ
Tin-Plated	Tin	144	107	37		135	102	33	128	99	29
Stainless Steel (2 lbs./in. of Force)	Nickel	127	96	31		126	88	38	123	86	37
	Chem Film	102	75	27		100	70	30	98	76	22
	Unplated	135	103	32		132	98	34	127	94	33
Tin-Plated	Tin	152	129	23		140	125	15	134	124	10
Stainless Steel (10 lbs./in. of Force)	Nickel	128	97	31		124	92	32	122	99	23
	Chem Film	111	85	26		108	80	28	108	81	27
	Unplated	144	107	37		128	100	28	124	97	27
Tin-Plated	Tin	148	141	7		138	134	4	132	131	1
Stainless Steel (30 lbs./in. of Force)	Nickel	135	111	24		132	108	24	128	107	21
	Chem Film	105	75	30		102	76	26	99	79	20
	Unplated	144	117	27		137	111	26	131	108	23

Table 2. Test Results of Tin-Plated Gasket

3. RESULTS

3.1. The results are illustrated in graphical form in Figures 1 through 6. They have also been put in tabular form and placed in Tables 1 and 2. The information in Tables 1 and 2 lists the shielding quality of the gasketed joints at 100, 500 and 1000 MHz before performing the moisture/heat soak, after performing the moisture/heat soak and the loss of shielding as a result of the moisture/heat soak for each of the 24 samples under test.

4. CONCLUSION

The information gained in the testing illustrated significant results (some expected, some not). A summary of these results are as follows:

4.1. General Conclusions

4.1.1. The shielding effectiveness of EMI gasketed seams or joints degrade due to aging as a result of moisture and heat which an electronic system is expected to encounter in its lifetime

4.1.2. Stainless steel (or monel) gaskets should be used if the joint surfaces are to be nickel-plated.

4.1.3. Chemical film plating of an aluminum surface significantly reduces the shielding of a gasketed joint.

4.2. Tin-plated stainless steel gaskets

4.2.1. The highest level of shielding was obtained using the tin-plated joint surfaces.

4.2.2. The degree of loss of shielding when using the tin-plated joint surfaces was less with the higher force gaskets.

4.2.3. The chemical film plating joint surfaces provided the lowest level of shielding of the joint surfaces under test

4.3. Stainless Steel Gaskets

4.3.1. The highest level of shielding was obtained using the nickel-plated joint surface.

4.3.2. Plating the joint surfaces with tin proved to be non-productive.

BIOGRAPHICAL NOTE

George M. Kunkel worked as an engineer in EMI, TEMPEST, EMP, lightning and RADHAZ design for 30 years. He holds numerous U.S. patents and is currently President of Spira Manufacturing Corporation. He received his BS and MS degrees in Engineering from UCLA. He has taught courses on applied electromagnetic theory for UCLA extension. He is also widely published and has chaired numerous IEEE symposium sessions on grounding, bonding, shielding and filtering.

ANALYSIS ON MICROWAVE ABSORPTION PROPERTIES OF M-TYPE HEXAGONAL FERRITES

Hiroyasu Ota, Masafumi Kimura, Risaburo Sato
*Electromagnetic Compatibility
Research Laboratories Co., Ltd.
6-6-3 Minami yoshinari Aoba-ku Sendai 989-3204,
Japan*

Katsumi Okayama ,Motofumi Homma
*Department of Material Science,
Graduate School of Engineering, Tohoku University
Aramaki Aoba-ku Sendai 980-77,
Japan*

The microwave absorption properties of M-type hexagonal ferrites were investigated. The complex permeability and permittivity were measured using a network analyzer. In the $\text{BaFe}_{12-x}(\text{TiCo})_x\text{O}_{19}$ system, the ferrimagnetic resonance frequency shifts down to the 1~20 GHz range, when x is increased. Due to the relatively high μ_r' value, thin matching thicknesses of 0.9~1.9mm were obtained in the 5~10 GHz range.

The frequency characteristics of μ' and μ'' were analyzed and simulated successfully using a parallel resonant circuit model based on the crystalline structure. Dual peak characteristics of μ'' were observed for a certain sintering temperature and duration, and a relative absorption bandwidth of 16 % was obtained. The simulation showed that a wider absorption bandwidth of 33 % may be possible.

1. INTRODUCTION

Metal-backed impedance matched absorbers made from spinel type ferrites, have good absorption properties in the hundreds of MHz range, and are widely used to prevent problems in VHF broadcasts, such as TV ghost images.[1] Recently, communication tools using the GHz frequency range have become popular, and so electromagnetic wave absorbing materials in the GHz range are needed to reduce EMI problems. The spinel ferrites, however, do not work well in the GHz range because of a decrease in permeability (μ_r', μ_r'').[2] A composite material with ferrite powder shows better absorption in this frequency range, but they have low μ', μ'' values and their frequency characteristics are determined by the size of the powder and by the mixture density. Therefore it is difficult to reduce the thickness and to widen the absorption bandwidth.

It is known that M-type hexagonal ferrites have a ferrimagnetic resonance frequency (f_r) of 50~60GHz.

And it is also known that the f_r can be shifted to a lower frequency by reducing the crystalline magnetic anisotropy. However, little work has been done on the analysis of the relationship between the ferrimagnetic resonance phenomena and the required conditions for microwave absorption.[3] In our previous work it was found that M-type Ba ferrite $\text{BaFe}_{12-x}(\text{TiCo})_x\text{O}_{19}$, in which Fe^{3+} is suitably substituted by $(\text{Ti}^{4+}\text{Co}^{2+})^{3+}$, exhibits ferrimagnetic resonance in the 1~20 GHz range.

The purpose of this study is to investigate the relationship between microwave absorption and the material constants in $\text{BaFe}_{12-x}(\text{TiCo})_x\text{O}_{19}$, and to determine the conditions required for a wide band absorber in the GHz range.

2. EXPERIMENT

M-type Ba ferrite $\text{BaFe}_{12-x}(\text{TiCo})_x\text{O}_{19}$ was prepared by the conventional powder metallurgy method. The starting materials (BaCO_3 , TiO_2 , CoO and $\alpha\text{-Fe}_2\text{O}_3$ purity>99%) were mixed in a planetary ball-mill, and compacted into $\phi 30 \times 10\text{mm}$ pellets. After the pellets were calcined at 1150°C in air for 3 hours, they were milled for 24 hours to produce a sub-micron powder. The powder was compacted into blocks with the size $20 \times 10 \times 10\text{mm}^3$, and then sintered in air at 1200~1350°C, for different times from 6 min to 100 hours. The sample for the measurement was cut and precisely polished into a toroidal shape with outer and inner diameters of 7.00mm and 3.04mm, respectively. The sample was inserted into a 7mm coaxial holder which is connected to a vector network analyzer HP8510C.

The complex permeability ($\dot{\mu}_r = \mu_r' - j\mu_r''$) and the complex permittivity ($\dot{\varepsilon}_r = \varepsilon_r' - j\varepsilon_r''$) were calculated from the values of S-parameters measured by the network analyzer. The reflection loss for normal incidence was obtained by measuring S_{11} with the back

3.3 Absorption conditions for μ'_r and μ''_r

Absorption boundary conditions with varying values of f and d , for certain given values of μ'_r , μ''_r , ϵ'_r and ϵ''_r , have been widely reported.[4] The upper and lower limits for μ'_r and μ''_r to achieve a -20dB reflection loss are calculated and plotted in Fig.5 and Fig.6 at thicknesses $d=1.9\text{mm}$ and 2.3mm , respectively. Fig.5 shows the data measured for a sample sintered for 10 hours, and the limit lines for μ'_r and μ''_r . The data of μ'_r fall between the upper and lower limit lines at 4.5-7.8GHz, and the data of μ''_r fall between the lines at 5.7-6.9GHz. This means that the metal-backed sample with thickness d should show good absorption at the common frequency range of 5.7-6.9GHz.

The μ'_r and μ''_r formed by a single resonant peak will cross the lines quickly, slightly below f_r , as shown in Fig.6. When two or more peaks are combined together, however, the resulting plateau gives a wider absorption bandwidth.

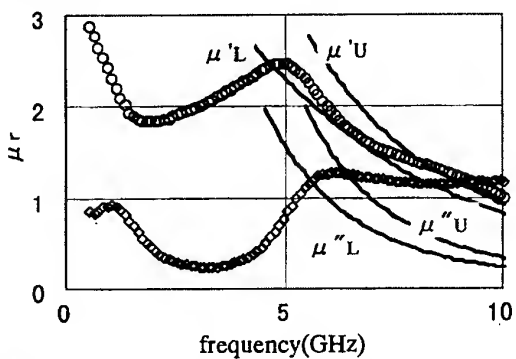


Fig.5 μ_r of the 10-hour sintered sample, with lines showing the lower and upper limits for μ'_r and μ''_r

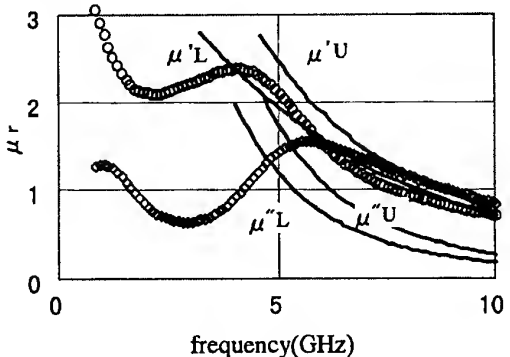


Fig.6 μ_r of the 1-hour sintered sample, with lines showing the lower and upper limits for μ'_r and μ''_r

4. SIMULATION

Ferrimagnetic resonance phenomena can be modeled using an electronic resonant circuit with some dissipation. Fig. 7 shows a circuit model that simulates the complex permeability μ_r . It consists of an L-R parallel circuit which expresses the domain wall

resonance, and a certain number (n) of L-C-R parallel resonant circuits which correspond to ferrimagnetic resonances in series.

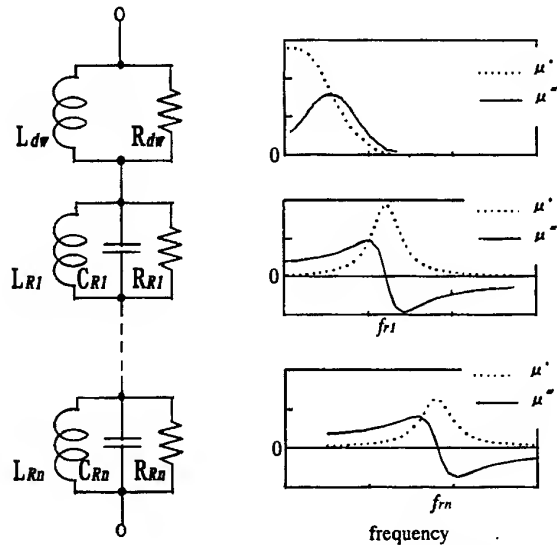


Fig.7 Parallel resonant circuit model

When the total impedance of the circuit Z is taken as a single inductor L_{eff} , the real part of L_{eff} corresponds to the real part of the permeability μ'_r , and the imaginary part of L_{eff} corresponds to μ''_r , as shown in the following equations.

$$Z = j\omega \cdot L_{eff} \quad (3)$$

$$L_{eff} = \frac{L_{dw}}{1+j(\omega/\omega_{dw})} + \sum_n \frac{L_{Rn}}{1-(\omega/\omega_{Rn})^2 + j\gamma_{Rn}(\omega/\omega_{Rn})} \quad (4)$$

where

$$\begin{aligned} \omega_{dw} &= R_{dw}/L_{dw} \\ \omega_{Rn} &= 1/\sqrt{L_{Rn}C_{Rn}} & \gamma_{Rn} &= \sqrt{L_{Rn}/C_{Rn}}/R_{Rn} \\ \mu_r' &= 1 + \operatorname{Re}(L_{eff}) & \mu_r'' &= \operatorname{Im}(L_{eff}) \end{aligned} \quad (5)$$

The measured data and the simulated curves of μ'_r and μ''_r are shown in Fig.7. Both curves agree very well even though only 3 parallel circuits were used in the modeling. The parameters ω_{Rn} , L_{Rn} and γ_{Rn} represent the resonant frequency, volume content and permeability and the quality of crystalline alignment, respectively.

Judging from the transition of the peak levels, each crystalline phase acts independently and exhibits its own resonance and dispersion characteristics. Therefore controlling the parameters (ω_{Rn} , L_{Rn} , γ_{Rn}) by altering the sintering conditions, and changing the composition, should make it possible to synthesize a thin wide-band absorber.

end of the sample electrically shorted by a conducting metal plate.

The air gaps between the sample and the coaxial holder were kept to less than $20 \mu\text{m}$ which causes an error of 1% in permeability and 20% in permittivity. The lengths of the ferrite samples were chosen to be between 0.7 and 3mm so as to avoid errors caused by multiple reflection within the sample.

3. RESULTS

3.1 Substitution amount X vs μ_r'' and reflection loss

In the $\text{BaFe}_{12-x}(\text{TiCo})_x\text{O}_{19}$ system sintered at 1300°C for 2 hours, the ferrimagnetic resonance frequency (f_r) shifts down from 14 to 6GHz when X is increased from 1.8 to 2.2, but almost the same frequency characteristics are exhibited in both μ_r' and μ_r'' . (Fig. 1)

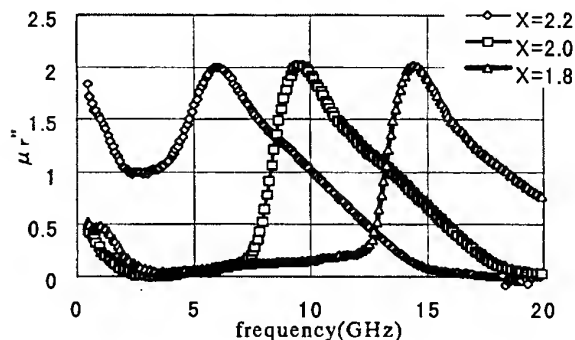


Fig. 1 Substitution amount X vs μ_r''

The maximum reflection loss Γ (dB) at the optimum matching thickness d is calculated using the following formulae.

$$\Gamma = 20 \log \left| \frac{z_{in} - z_o}{z_{in} + z_o} \right| \quad (1)$$

$$z_{in} = z_o \sqrt{\frac{\mu_r}{\epsilon_r}} \tanh \left(\frac{2\pi f d}{c} \sqrt{\epsilon_r \mu_r} \right) \quad (2)$$

where z_{in} : input impedance of absorber
 z_o : impedance of air
 c : velocity of light

The maximum reflection loss values reached $-25 \sim -35$ dB for the relatively thin matching thicknesses of $0.9 \sim 1.9$ mm. However, the relative absorption bandwidth $\Delta f/f$ exceeding -20 dB was limited to $5 \sim 8$ %. (Fig. 2)

Measured data using S_{11} shows good agreement with the calculated values. The values of permittivity ϵ_r' were $13 \sim 14$ in the range 3 to 20 GHz, almost the same as those of conventional spinel ferrites. However ϵ_r'' values were $1 \sim 1.5$ which is larger than for conventional spinel ferrites, and which helped to enlarge the absorption bandwidth.

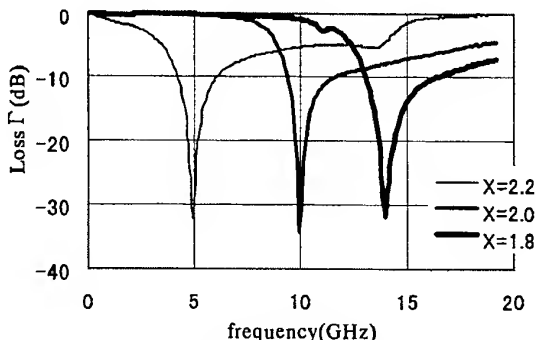


Fig. 2 Reflection loss vs X

3.2 Sintering time vs μ_r'' and reflection loss

Fig. 3 illustrates the transition of the peaks of μ_r'' with sintering time t from 1 to 100 hours, at a temperature of 1250°C . ϵ_r' values were $12.5 \sim 13$ over 3 to 20 GHz, which are slightly lower than the values for the samples sintered at 1300°C , due to their lower density. The reflection losses for samples with optimum thicknesses are shown in Fig.4.

The 10-hour sintered sample had double peaks of μ_r'' and showed a good relative absorption bandwidth of 16 %. The double peaks are considered to be caused by two different crystalline phases. The peak appearing at a lower frequency corresponds to the smaller grains pre-sintered at 1150°C , and the other peak is due to the crystalline grain growth that occurs at 1250°C .

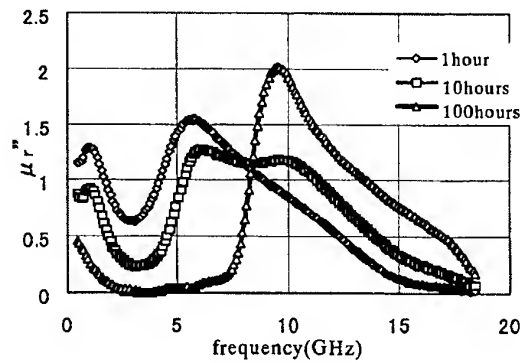


Fig. 3 Sintering time vs μ_r''

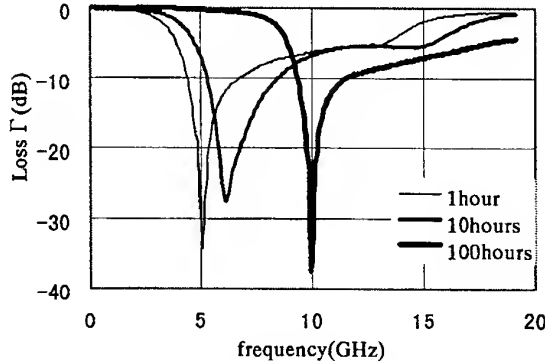


Fig. 4 Reflection loss vs t

sintering conditions.

6. REFERENCES

- [1] Y. Naito and K. Suetake, "Application of Ferrite to Electromagnetic Wave Absorber and Its Characteristics," IEEE Trans. Microwave Theory Tech., vol.19, no.1, 1971, pp.65-72.
- [2] J. L. Snoek, Physica, vol.8, 1948, p207.
- [3] W. Grunberger, B. Springmann, M. Schmidt and R. Janke, "Rubber Bonded Ferrite Layer as a Microwave Resonant Absorber in a Frequency Range from 3 up to 16GHz," J. Magn. Magn. Mater., vol. 101, 1991, pp.173-174.
- [4] H.M.Musal, Jr., and H.T.Hahn, "Universal Design Chart for Specular Absorbers," IEEE Trans. Magn., vol.25, no.5, 1989, pp.1462-1464.

BIOGRAPHICAL NOTES

Hiroyasu Ota received a M. E. degree from Tohoku University, Sendai Japan, in 1977. He joined Sony Corporation and was engaged in the design of switched mode power supplies. Since 1996, he has been a senior researcher at Electromagnetic Compatibility Research Laboratories Co., Ltd., Sendai, Japan. Presently he is engaged in research work on electromagnetic wave absorbers.

Masafumi Kimura is a General Manager at Electromagnetic Compatibility Research Laboratories Co., Ltd., Sendai Japan. He joined SANYO Electric Co., Ltd., where he was involved in developing audio-video products. He is currently engaged in research on installation environment technology, using electromagnetic wave absorbers and electromagnetic field simulation.

Risaburo Sato received a Ph.D. degree from Tohoku University, Sendai, Japan, in 1952. From 1961 to 1984, he was a Professor at Tohoku University, and he is presently Dean of the Faculty of Engineering of Tohoku Gakuin University, Tagajo, Japan. He is a life member of the IEEE and the president of Electromagnetic Compatibility Research Laboratories Co., Ltd.

Katsumi Okayama received a M. E. degree from Tohoku University, Sendai, Japan in 1996. He is currently a doctor course student in the Department of Materials Science, Graduate School of Engineering, Tohoku University. He has been engaged in research on electromagnetic wave absorption materials.

Motofumi Homma received a Ph.D. degree in engineering from Tohoku University, Sendai, Japan in 1964. After which he became a member of staff at Tohoku University and he is currently a Professor in the Department of Materials Science, Graduate School of Engineering. His research interests are primarily related to magnetic materials.

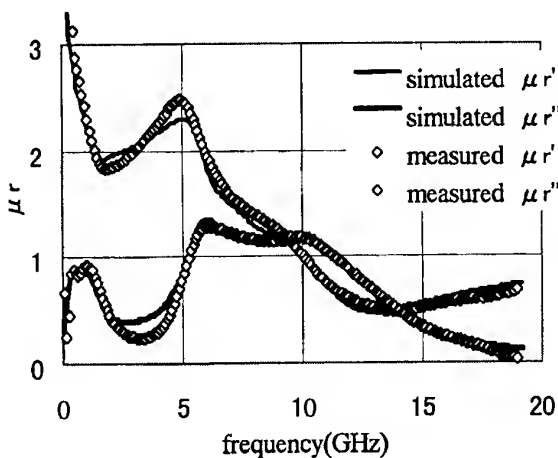


Fig.9 Measured and simulated μ

Fig 9 shows one example, in which an improved absorption bandwidth of 33 % was obtained by modifying L_{Rn} and γ_{Rn} . It may be that these parameters can be controlled by altering the duration of sintering.

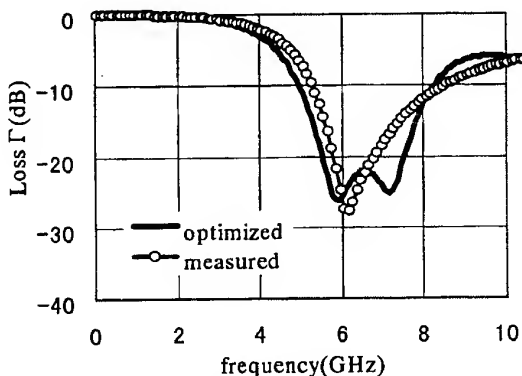


Fig.9 Optimized bandwidth

5. CONCLUSIONS

It was found that M-type ferrite $\text{BaFe}_{12-x}(\text{TiCo})_x\text{O}_{19}$ exhibits good microwave absorption characteristics in the GHz range, with thin matching thicknesses of 0.9 to 2.3mm.

The frequency characteristics of μ' and μ'' can be controlled by varying the composition, sintering temperature and sintering duration. The 10-hour sintered sample had double peaks of μ'' , which correspond to the difference in the crystalline configuration, and this sample exhibited a relative absorption bandwidth of 16 %.

The parallel resonant circuit model, based on multi-phased crystalline configuration, successfully simulates the frequency dependence of μ' and μ'' . The simulated model shows that it should be possible to enlarge the relative bandwidth to 33% by adjusting the

USE OF THE CASCADE MATRIX TECHNIQUE IN DETERMINATION OF THE PERFORMANCE OF MULTI-LAYER ABSORBING STRUCTURES BASED ON FERRITE TILES

Viktor Smieško – Karol Kováč – René Harfanský – Jozef Hallon

Department of Measurement, Faculty of Electrical Engineering and Information Technology, Slovak University of Technology, Ilkovičova 3, 812 19 Bratislava, Slovakia. E-mail: kkovac@elf.stuba.sk

Paper analyses the characteristics of multi-layer absorbing structures based on ferrite absorbers which are frequently used for suppressing the resonances in shielded chambers and creating anechoic rooms for EMC measurements. A combination of ferrites with dielectric layers or air gaps is frequently recommended to improve the frequency dependence of absorbing performance. Paper gives the exact analysis of the influence of the widths and permittivity of these layers upon the overall reflectivity of the absorber structure under the normal as well as oblique wave incidence.

Keywords: ferrite absorbers, reflectivity, wave impedance, multi-layer absorbing structures, normal and oblique wave incidence.

1. INTRODUCTION

Within recent times ferrite absorbers are frequently used for lining the shielded chambers to suppress resonances inside them and to create test sites complying with emission measurement and immunity testing requirements. Designing of such test rooms needs in perfect knowledge of absorber structure behaviour. As ferrite absorbers work well in relatively narrow frequency band, experts try to combine ferrites with dielectric layers to suppress the resonant character of ferrite absorbers reflectivity to wide up the frequency band of ferrites usage. There is lot of trials to describe the influence of additional dielectric layers upon the absorbing performance of so created two-layer or even multi-layer absorbing structure. But there are not a strict instructions as: what type of dielectric material to use, with what properties, how thick the dielectric layer has to be, which ferrite material can be supported with dielectric, under which conditions and which can not. There is still a lot of unanswered questions concerning this topic. Even one of the best and newest papers [3] dealing with absorber materials for semianechoic chamber building does not give a simple unambiguous answers to this set of questions.

This paper tries to bring an analytic analysis of the reflectivity of multi-layer absorbing structures based on the technique of cascade matrices introduced in [2]. Upon this theory the paper gives the results of evaluating the overall reflectivity of the structure in frequency band from 30 to 1000 MHz. The given analysis was made for several thicknesses of ferrite layer, as well as several thicknesses of dielectric layer and for normal as well as oblique incidence of TEM wave. The analysis was performed provided that the frequency dependance of material parameters ($\mu_\nu(f)$ and $\epsilon_\nu(f)$) is known. For all examples presented in this paper we used the parameter characteristics of F42 ferrite material given in manufacturer's data.

2. MULTI-LAYER ABSORBING STRUCTURE CHARACTERIZATION

For evaluation of overall characteristics of multi-layer absorbing structure one need to calculate the resulting reflection losses or reflectivity of such a structure. Obviously this problem was solved by gradually calculating the reflectivity of each layer substructure from the metallic wall to free space of the interior of the chamber. This technique was derived for normal incidence of TEM wave on the structure consisting of N isotropic linear homogeneous material layers. To calculate the resulting reflectivity one must know such material parameters of all layers as complex permittivity and permeability of the media, layer thickness, frequency and polarization of the incidence of the uniform TEM wave. Some of these parameters are frequency dependent specially for ferrite absorbers, for which the complex permeability and permittivity must be, otherwise they should not work in wide frequency range [1]. This gradual calculation is very cumbersome if one needs to analyze the influence of layer parameters on overall reflectivity. So the different method had to be found to describe the behaviour of the structure.

Characterizing a structure of several lossy layers concerning its reflection behaviour is a problem with a lot of degrees of freedom. A nice method was shown in [2]. It is based on the concept of cascade matrices as it is known from the transmission line theory. If the structure has N layers, each of the $N-1$ layers can be described by means of a cascade matrix A_ν

$$A_\nu = \begin{pmatrix} \cosh(\xi_\nu d_\nu) & \tilde{Z}_\nu \sinh(\xi_\nu d_\nu) \\ \frac{1}{\tilde{Z}_\nu} \sinh(\xi_\nu d_\nu) & \cosh(\xi_\nu d_\nu) \end{pmatrix}, \quad (1)$$

where d_ν stands for the thickness of the layer ν and \tilde{Z}_ν is effective medium impedance. It depends on polarization of the TEM wave and propagation constant ξ_ν . \tilde{Z}_ν is not identical with the wave impedance $\sqrt{\mu_\nu/\epsilon_\nu}$.

$$\tilde{Z}_\nu^{PE} = \frac{j\omega\mu_\nu}{\xi_\nu} \quad \tilde{Z}_\nu^{PH} = \frac{\xi_\nu}{j\omega\epsilon_\nu} \quad (2)$$

where μ_ν and ϵ_ν are permeability and permittivity of material in ν -layer, ω is circular frequency of incident wave, PE labelled incident TEM wave which E field is parallel to all media boundaries and PH analogous for H field. The propagation constant ξ_ν is known for TEM-wave propagation in a homogeneous medium ν

$$\xi_\nu = \sqrt{-\omega^2\mu_\nu\epsilon_\nu + \omega^2\mu_0\epsilon_0 \sin\Theta} \quad (3)$$

Θ is the angle of wave incidence measured from the z direction. According to [2] cascade matrix G of the whole structure is

$$G = A_1 \cdot A_2 \cdots A_{N-1}. \quad (4)$$

The reflection factor $\Gamma(z = z_1)$ at the boundary $z = z_1$ between medium 0 and medium 1 can be expressed by means of all four elements of matrix G . The full formula is given in [2]. If medium 0 is air and medium N is metal, then some simplifications can be made and resulting formula for reflection coefficient of PE wave is

$$\Gamma^{PE}(z_1) = \frac{G_{12}^{PE} - \frac{Z_0}{\cos\Theta} \cdot G_{22}^{PE}}{G_{12}^{PE} + \frac{Z_0}{\cos\Theta} \cdot G_{22}^{PE}} \quad (5)$$

Similarly for PH wave

$$\Gamma^{PH}(z_1) = \frac{G_{12}^{PH} - Z_0 \cdot \cos\Theta \cdot G_{22}^{PH}}{G_{12}^{PH} + Z_0 \cdot \cos\Theta \cdot G_{22}^{PH}} \quad (6)$$

where Z_0 is free space wave impedance and G_{ij} are elements of matrix G .

3. CALCULATION RESULTS

On the basis of shown method a lot of calculations of reflectivity of different layers combinations were performed. The basic combination of materials was ferrite - air - dielectric - air - metal. As the influence of

air gaps was very weak we continued only with ferrite - dielectric - metal structure. In all cases the ferrite layer represented the most absorbing part of them. Only the thickness of ferrite layer, the permittivity and the thickness of dielectric layer were changing. In all calculations the frequency dependance of reflectivity Γ was analyzed for PE orientation of incident wave. All calculations were made in *Mathematica* environment that way, which allowed us to simply change input parameters for calculation. A ferrite material (F42) with known permeability and permittivity was studied. The frequency characteristics of both parts of complex permeability of ferrite material are shown in figure 1. Real part of permittivity is almost constant and equal to 12, imaginary part can be neglected. It is clear that both parts of complex permeability are strongly frequency dependent.

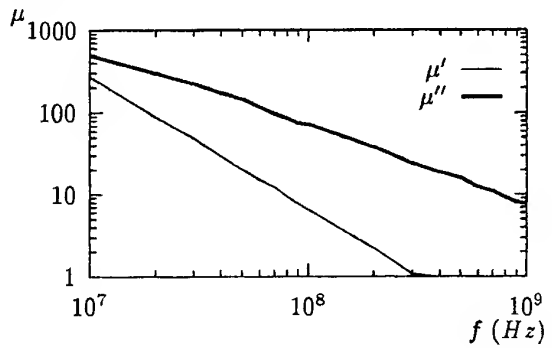


Figure 1: Permeability μ' and μ'' of used ferrite material

The first analysed situation was ferrite absorber placed directly on metallic wall. In this case the frequency dependencies of reflectivity (reflection factor expressed in dB) for different ferrite material thicknesses were calculated.

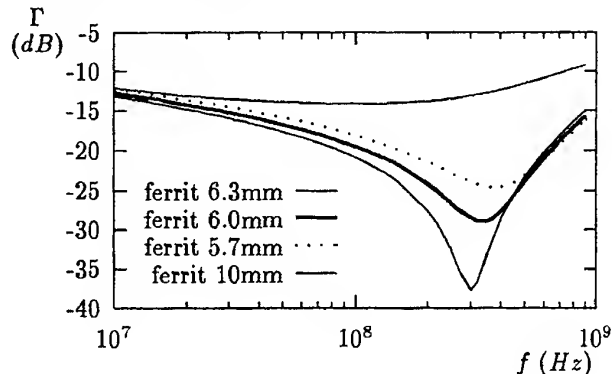


Figure 2: Frequency dependence of reflectivity for several ferrite layer thicknesses

The results for the most often used thicknesses and one unusual are shown in figure 2. It is evident that in all cases ferrite absorber has strongly resonant behaviour. The second evidence is that thin-

ner absorbers are less effective, minimum reflectivity is achieved at slightly higher frequencies, but the minimum value is higher. Also increasing the thickness above optimum value, which is 6.3 mm for this material, rises up the reflectivity (see the curve for 10 mm). This conclusion supports well known fact that ferrite absorbers are "tuned" or better written - the thickness of ferrite absorbers must be "tuned"¹. As some manufacturers recommend to use back di-

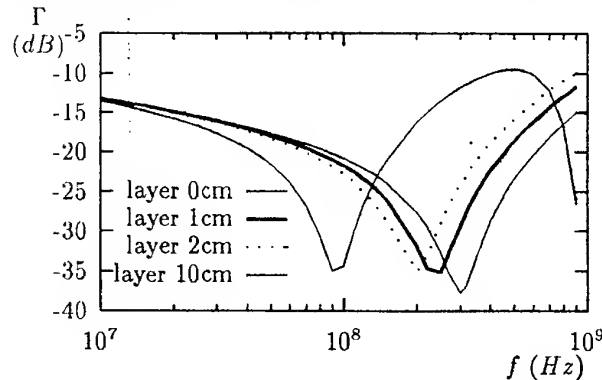


Figure 3: Reflectivity coefficient as function of dielectric thickness (dielectric permittivity $\epsilon_r = 2$, ferrite thickness = 6.3 mm).

electric layer to improve the frequency range of suitable reflectivity [3], the second analysed case was two layer absorbing structure. The backer layer material was plywood which is *synthetic material* with relative permittivity equal to $\epsilon_r = 2$ [3]. Figure 3 shows

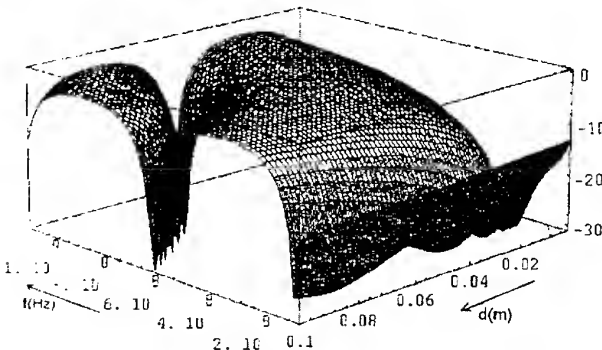


Figure 4: Reflectivity coefficient as function of dielectric thickness in 3D coordinates (dielectric permittivity $\epsilon_r = 8$ and ferrite thickness is 6.3 mm, normal incidence).

the influence of the thickness of this material on the structure reflectivity. In this case by increasing the dielectric thickness the position of the minimum is

¹Ferrite absorber is in its essence quarter length transformer, which transforms low impedance of conductive wall ($Z_N \rightarrow 0$) to wave impedance of open air ($\approx 377 \Omega$) to achieve the lowest possible reflection coefficient in the widest possible frequency range.

shifted to lower frequencies and the minimum value is slightly raised. This calculated result is in conflict with generally published statement, which says, that adding of dielectric layer causes shifting of the minimum frequency as well as of the whole characteristics to higher frequencies. As the changes in reflectivity are significant especially at higher frequencies, this behaviour can be used for "tuning" the absorber structure [3], i.e. to shift the minimum to required frequency, but only to lower frequencies. Of course this shift is limited and is tied with undesired increasing of minimum value. In our example for 2 cm thick dielectric layer the minimum was shifted to 2/3 in frequency and the minimum value was risen up 3 dB. By using dielectric backer layer with large relative permittivity and sufficient thickness the reflectivity minimum is significantly shifted to lower frequencies and at the same time second sharp minimum appears in frequency range of interest. For better explanation of this phenomenon figure 4 was prepared. It shows two dimensional dependence of total reflectivity upon dielectric backer layer thickness and frequency for 6.3 mm thick ferrite but the permittivity is higher. The diagram is oriented that way to show the shifting of the first and the second minimum with frequency and thickness of back dielectric layer. Overall increasing of reflectivity in wide frequency and thickness ranges is evident.

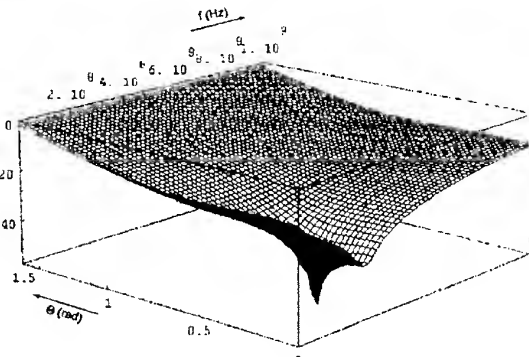


Figure 5: Reflectivity coefficient as function of angle of incidence and frequency in 3D coordinates (dielectric permittivity $\epsilon_r = 2$, thickness is 1 cm, ferrite thickness is 6.3 mm and PH wave).

In preceding text we dealt with normally incident wave. The fact, that there are differences in both denominators of eq.(5) and (6), could lead to situation when reflection coefficient can fall down to zero for some value of incident angle Θ . Similar preposition was done in [6], in which authors went out from much simpler formula for reflection coefficient calculation. This simpler formulation covered the frequency dependence of this behaviour, which could be discovered when using presented technique. So we analysed the

influence of angle of incidence on the reflectivity of our multi-layer absorbing structure. At first we studied the behaviour of ferrite material without dielectric spacer. For PE wave the reflectivity is monotonically rising with angle. But for PH wave the eq.(6) leads to a local minimum. The reflectivity in dependence on both incident angle and wave frequency is shown in figure 5.

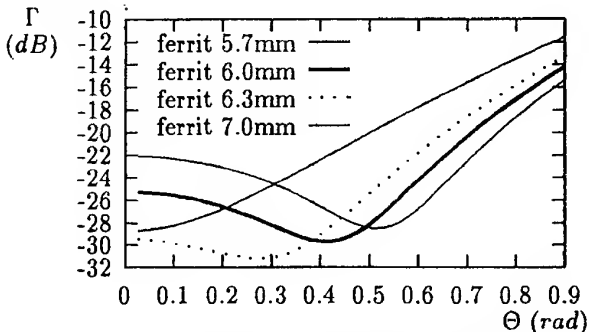


Figure 6: Dependence of reflectivity on incident angle for several ferrite layer thicknesses and frequency of 220 MHz (without dielectric backer layer)

The minimum value of reflectivity in this figure is more than 20 dB lower than normal incidence minimum. To see the shape of interesting dependence curves we added three more figures which are sections of the previous one. They show the reflectivity as a function of angle of incidence for interesting ferrite widths (fig. 6) at frequency $f=220$ MHz (which is

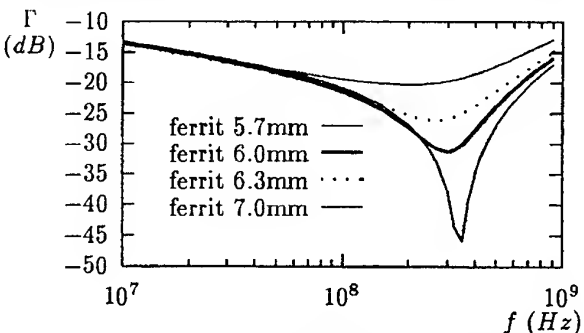


Figure 7: Frequency dependence of reflectivity for several ferrite layer thicknesses and $\Theta = 0.5$ (without dielectric layer)

slightly below minimum), then reflectivity as a function of frequency for the same ferrite widths and angle of incidence equal to half of the radian ($\Theta = 0.5$ rad) for structure without dielectric (fig. 7) and structure with $\epsilon = 2$ 0.5 cm wide dielectric (fig. 8). From given figures it is evident that:

1. At resonant frequency of the ferrite layer the reflectivity of PH wave falls down with rising the angle of incidence to minimum value. Then it rises up to 0.

2. Previous influence is observable only in close region about resonant frequency. This is almost unrecognizable at both ends of frequency band.
3. Last two figures illustrate that again the backer dielectric layer shifts the position of minimum to lower frequency while rising slightly the minimum value. The same influence as by normal incidence.
4. The backer dielectric layer slightly rises the reflectivity at high frequencies. This fact can be critical for absorber structures without foam absorbers in front of ferrite ones.

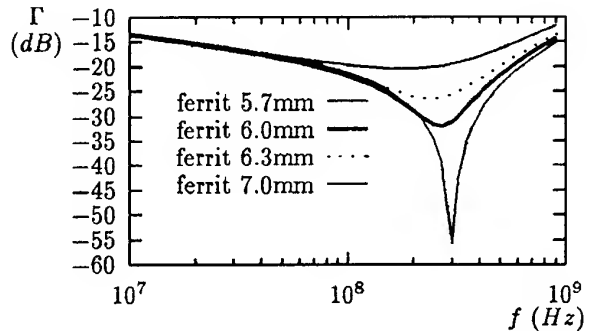


Figure 8: Frequency dependence of reflectivity for several ferrite layer thicknesses and $\Theta = 0.5$ (width $\epsilon_r = 2$, 0.5 cm dielectric layer)

4. CONCLUSION

Presented paper gave the analysis of the influence of ferrite layer thickness as well as the influence of the properties (permittivity and thickness) of backer dielectric layer upon the total reflectivity of two-layer absorbing structure. For this analysis cascade matrix method [2], known from the circuit theory and transmission lines theory, was used. This allows very simply to pick up the influence of particular parameters on total reflectivity. The reflectivity was calculated for both normal as well as oblique incidence of TEM wave. From the given analysis it is evident that parameters of ferrite absorbers and specially those of backer dielectric layer must be very properly chosen before anechoic chamber building. Otherwise the resulting behaviour of absorbing structure can be significantly deteriorated. Most of all this concerns the thickness of backer dielectric layer.

The calculations of the reflectivity under the oblique incidence show that at resonant frequency of ferrite tile the reflectivity of PH wave can be lower for small angles than for normal incidence. But this phenomenon is observable only in relatively narrow frequency range.

Sorrowly presented results could not be supported by measurements because our laboratory does not

have appropriate equipment. But they help us to select the technique for lining our shielded chamber and we consider them as useful for future users of ferrite absorbers.

5. REFERENCES

- [1] Halbach, L. - Kirschvink, M.: *Flat Ferrite RF Absorbers*, ITEM, pp. 116 - 121, 258, 266., 1996
- [2] Krause, J. - Mönich, G.: *New aspect of ferrite tile absorber optimization and corresponding measurements*, Symposium on EMC, pp. 341 - 346., Zürich 1997
- [3] Holloway, C. L. - DeLysen, R. R. - German, R., F. - McKenna, P. - Kanda, M.: *Comparison of Electromagnetic Absorber Used in Anechoic and Semi-Anechoic Chamber for Emissions and Immunity Testing of Digital Devices*, IEEE Trans. on EMC, vol. 39, pp. 33 - 47, February 1997
- [4] Kuester, E., F. - Holloway, C., L.: *A Low-Frequency Model for Wedge or Pyramid Absorber Arrays - I: Theory*, IEEE Trans. on EMC, vol. 36, pp.300 - 306, November 1994
- [5] *IEEE Recommended Practice for RF Absorber Performance Evaluation in the Range 30 MHz to 5 GHz*, Draft IEEE Standard, PAR - 1128
- [6] Liu, K.: *Analysis of the Effect of Ferrite Tile Gap on EMC Chamber Having Ferrite Absorber Walls*. Proc. of IEEE 1996 Int. Symp. of EMC, Santa Clara, Aug. 19-23 1996, pp.156 - 161.
- [7] Naito, Y. - Anzai, H. - Yamazaki, T. - Mizumoto, T.: *Criteria for Absorber's Reflectivity Lined in Semi-Anechoic Chambers Using Ray-Tracing Technique*. Proc. of IEEE 1996 Int. Symp. of EMC, Santa Clara, Aug. 19-23 1996, pp.140 - 142.

BIOGRAPHICAL NOTES

Viktor Smieško (Prof, Ing, CSc, MIEEE), was born in Zlatovce, Czechoslovakia, on June 7, 1948. He graduated with honors in 1970 and received the CSc (PhD) degree at the Faculty of Electrical Engineering, Slovak Technical University, Bratislava, Czechoslovakia. Currently, Full Professor Smieško is the Dean of the Faculty of Electrical Engineering and Information Technology, Slovak Technical University. His Research interests are in the areas of automated instrumentation and electromagnetic compatibility.

Karol Kováč (Ing, CSc) was born in Bratislava, Slovakia on June 9, 1952. He received the M.Sc. degree with honors in 1976 and then Ph.D. degree in electrical engineering from the Faculty of Electrical Engineering of the Slovak Technical University (FEE STU) in Bratislava. Since 1976 he has been with Department of Measurement of FEE STU. Now he is senior lecturer, he reads several EMC courses. His research interests are in the area of computer modelling and measurement of EMC phenomena.

René Hartanský (Ing) was born in Banská Bystrica on May 13th, 1969. He graduated in radioelectronics from the Faculty of Electrical Engineering of the Slovak Technical University of Bratislava in 1992. Since 1993 he has been a lecturer at Faculty of Electrical Engineering at the Department of Measurement. His research interests are electromagnetic field sensors and computer modelling of their properties.

Jozef Hallon (Ing) was born in Bratislava on Mart 16th 1963. He graduated in microelectronics from the Faculty of Electrical Engineering of the Slovak Technical University of Bratislava in 1987. During the years 1987 - 1992 he had been working as a research worker at Slovak Academy of Science. Since 1992 he has been working as a research worker at Faculty of Electrical Engineering at the EMC group of Department of Measurement.

IX

EMI REDUCTION TECHNIQUES

Architectural Shielding

Invited session organized by

Prof. J. A. Catrysse - Belgium

ARCHITECTURAL SHIELDING: FROM NEEDS INTO PRACTICAL REALISATIONS

Johan CATTRYSSE

KHBO, dept. IW&T, Zeedijk 101, B 8400 Oostende, BELGIUM

In this paper, some examples will be given where the need of large shielded rooms is needed. Examples can be mentioned as some medical installations in hospitals, measuring laboratories in the electronic industry, prohibiting eavesdropping of conference rooms, etc. ...

In all cases, a carefull analysis of the needs must be performed so that no extra-ordinary requirements are set for the shielding level needed. In most cases, a carefull use of the zoning concept will lead into reasonable requirements for the shielding effectiveness of the rooms.

Another important point in all this cases is that the user of the room may not have the impression to be in a shielded room. This is called the psychological effect, and precautions must be taken to have a 'normal' room impression.

Also, in many cases, these rooms must be realised within the existing building configuration. This retrofitting will also put extra requirements on the possible techniques and technologies for the realisation of these types of rooms. The global set of requirements and realisations is called architectural shielding.

1. INTRODUCTION

Architectural shielding is becoming an important topic, as well in relationship to EMC as to securing data and prohibiting eavesdropping of meetings and conferences.

It is clear that the required shielding level will depend on a number of parameters, which can differ from case to case. In order to prevent some sensitive measuring equipment from wrong measurements, shielding levels of only 20 or 40 dB will be sufficient. In other cases, in order to prevent reception from small wireless microphone at some distance, perhaps a global 'shielding' of 100 dB will be required. In this context, shielding is a wrong concept, and better is to introduce the overall attenuation from source to receiving point. This global concept has also been recognized recently by introducing the ZONING concept as a lower cost

alternative for the well-known TEMPEST requirements related to data security.

As a first conclusion, it can already be stated that the requested levels of shielding (or better: attenuation) in architectural applications, be directly depend on the application itself, and that appropriate methods and measures should be applies, in order to optimise both costs and performance.

2. ZONING CONCEPT.

In this section, the idea of the zoning concept is introduced related to the security requirements set by official agencies. In order to prevent the leakage of confidential data from computers and electronic data transfer systems, requirements were set by governments and official security agencies, and are known as the TEMPEST requirements. It means that there should be no possibility - using actual technology - to eavesdrop data from computers and electronic data equipment. These requirements were found at two levels: of the equipment itself, but also on installations. For the latter, shielding requirements were defined for enclosures, shelters and rooms. Well known shielding requirements were set by the American National Security Agency (NSA), and are known as the NSA 65-6 (high level) and NSA 73-2A (moderate level) specifications. These requirements are given in fig. 1.

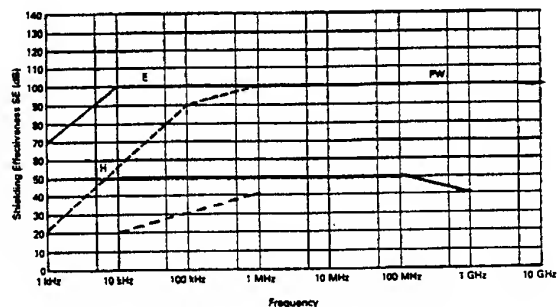


fig. 1. NSA specifications for shielding effectiveness

However, it has been observed that these requirements were very costly, and also not always needed for all applications involved. In order to reduce costs, the ZONE program has been introduced in 1993. It means that different zones are defined, in function of the activities, access control, security, ... Taking into account different effects, such as attenuation of electromagnetic fields due to distance, attenuation of the building structure itself, type of data and activities to be secured, etc. less severe requirements are set for both equipment and shielding.

An example of appropriate implementation is shown in fig. 2. where the Red Equipment Area is embedded within other equipment area's, with controlled access.

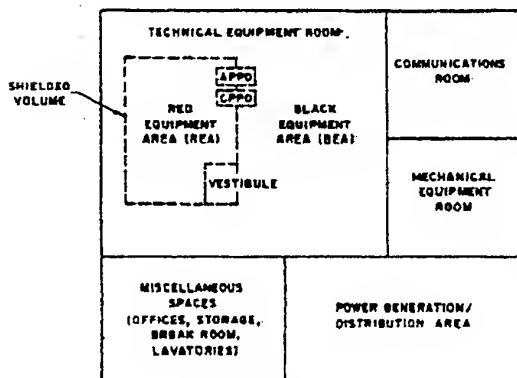


fig. 2. Zone planning for rooms.

It is clear that this concept of a combination of careful room planning, taking into account the environment, controlled access and the available shielding effectiveness offered by existing walls and building structures can also be applied to a lot of other applications. Some examples will be discussed in this paper as examples. It is clear that this concept will drastically reduce not only the shielding requirements, but also the costs of these installations.

3. BUILDING SHIELDING CHARACTERISTICS

Recently, some research and studies have been performed on the shielding characteristics of building structures and walls. It is also referred to one of the papers of this session. Other work has been published recently [3], showing an average attenuation of about 20 dB for reinforced concrete walls.

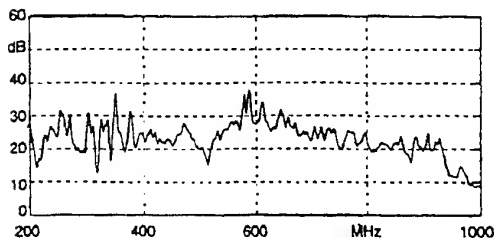


fig. 3. Typical SE of reinforced concrete walls

One remark should be made in this context: when applying shielding material on a reinforced concrete wall, only a few dB will be added to the shielding value of the applied material. But a wall at some distance from a shielded room, will add its dB's to the overall shielding.

4. EXAMPLES OF APPLICATION

In this section, some examples of combined zoning and shielding techniques will be discussed for different applications. Depending on the type of application, more or less severe shielding performance is required.

4.1. Application in hospitals.

Two typical applications in hospitals are the shielding of an NMR installation and the shielding for sensitive EMG and EEG measurements.

Concerning NMR, shielding is needed in order to avoid that the environment is highly disturbed by both the LF magnetic fields of the installation, and the frequency whereby the NMR is operated. The typical SE requirement for NMR facilities is shown in fig. 4.

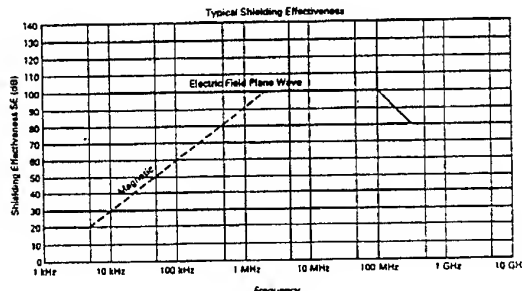


fig. 4. Required SE for NMR facilities.

Another application is the room where the measurements for EMG or EEG are performed. Typical signal levels for these measurements are in the μ V level and require very sensitive electronic equipment, especially the input amplifiers of the equipment. In order to perform correctly these measurements, a lot of precautions must be taken, including a high common mode rejection.

Although the electronic design of the medical equipment has made a big progress in this field, the ambient noise due to all kind of telecommunication systems (radio, TV, PCS, GSM and other mobile communications) and of electronic systems (PCs, other measuring equipment, physiotherapy, etc.) is coupling into the transducers and the leads of these EMG and EEG units. This can only be avoided by reducing the ambient noise level around the measuring unit, and consequently by appropriate shielding of these hospital rooms.

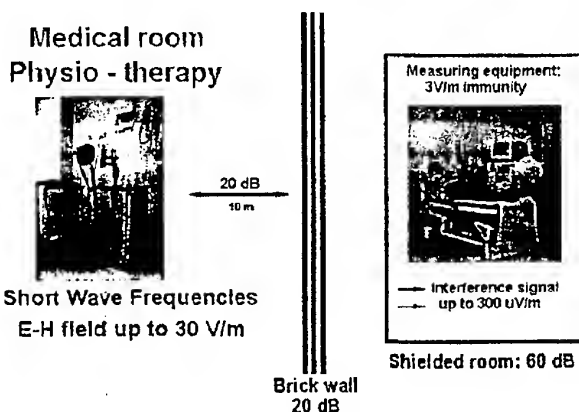


fig. 5. Example of medical application

It should be remarked that by a carefull design of the floorplan, and also by access control of authorised persons, the requirements on the shielding performance of the room itself can be drastically reduced. Reducing the overall cost of the installation.

4.2. Development laboratories in industry.

Some development laboratories in the electronic, and other industrial domains, suffer from the same problem concerning performing sensitive (analog) measurements. In these cases, a low level of ambient noise is required, and the same rules apply as in the medical examples.

Another situation encountered in industry is the problem of eavesdropping of new developments and designs. In this case, shielding will be required in order to avoid that electronic data can be captured at some distance. This problem is identical to the more general ones of data security.

4.3. Data security of computers.

Capturing data from computers can be done upto a distance of some hundreds of meters, simply by using appropriate receiving equipment as a directive antenna, a good receiver and a monitor or display. Data appearing on the screen of a PC can be reconstructed in this way. To avoid this type of spying, computers handling confidential data should be operated in a shielded room, and also by skilled personnel under controlled access to the computer rooms.

Two examples are given where the shielding requirements can be reduced, with respect to the overall requirements:

4.3.1. The computers are operated in a shielded room, and outside the room, other computers and equipment is operated, carrying no confidential handling and data. In this way, the critical data are embedded in the overall noise of the installation. By taking care that I/O lines - when needed - are appropriate shielded or implemented by optical fibers, the confidential data are

secured with respect to the outside environment.

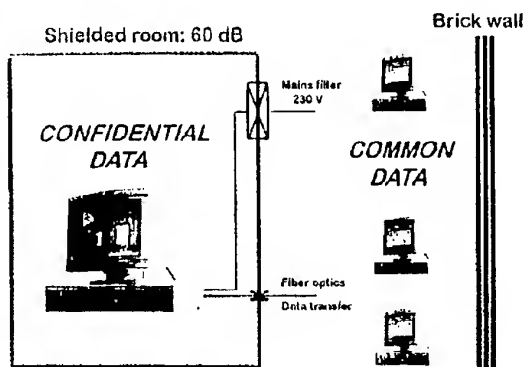


fig. 6. Data embedding in the ambient common noise

4.3.2. Another possibility for the reduction of the shielding requirements is by taking into account the attenuation of electromagnetic waves due to propagation distance. This situation is sketched in the next figure, showing an overall attenuation of 100 dB for a shielded room performance of 60 dB only.

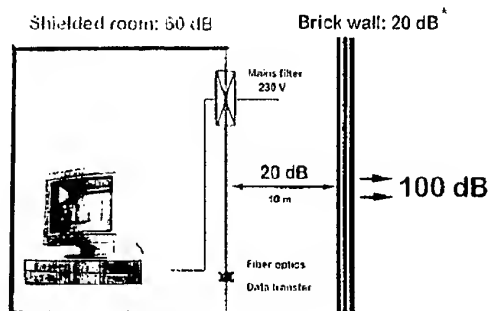


fig. 7. Propagation distance contributing in overall SE

4.4. Executive offices.

A confidential meeting is in progress in the executive offices of a large corporation. Spreadsheets and proposals involving new product development that may represent millions of dollars in research and development are displayed by computer screens. In the same way as described above, these data can be captured outside the building.

Other ways of eavesdropping executive and other meetings is by placing a (very) small wireless microphone in the meeting room. This microphone or electronic bug can than be captured at hundreds of meters outside the building. This can be avoided by shielding the executive rooms in an appropriate way. Other ways of eavesdropping is by the use of a laser beam pointed at the outside of the window of the

meeting room. The laser picks up the vibration of the glass, causing variations in the reflected beam. A converter can electronically reproduce the conversation.

5. DESIGNING THE FORTRESS

In this section, both architectural requirements and technical ones will be discussed.

5.1. Architectural requirements.

Architects need to be aware of the potential breaches in business security, medical applications and other technical requirements. Buildings not only house people, but must also shelter sensitive information. In the past, Faraday cages have been constructed for a lot of applications, but they often resemble vaults. These technologies cannot be used for these environments, where the appearance is of any concern.

The rating of protection against leakage is normally set to be 100 dB over a broad frequency band. This ensures nearly a theoretical loss of any information by 100%. In order to achieve this value, steel cabines with heavy doors and delicate copper finger stock seals are used.

With the rise in the sophistication and the intensity of threats to business security, the private sector needs also to secure their sensitive data. However, secure rooms have to meet the same criteria of attractiveness, cost efficiency, functionality, and design flexibility that businesses require of all their facilities, including the possibility to retrofit existing rooms and buildings. Research on the nature of emissions (equipment must already fulfill CE or FCC requirements at the emission level), and combining ZONING procedures, an attenuation of 60 dB will stop the information emanating from the electronic data processing apparatus. In this way, architects must be judicious in their selection of materials and must be aware of false claims of required shielding effectiveness.

5.2. Technical checklist.

Architectural shielding must be detailed very carefully since it is designed into the structure of a facility. It is very important that every penetration be defined and detailed since the overall shielding integrity is directly related to the quality of these penetrations.

Architectural checklist:

Layout: the floorplan of the space to be shielded should be laid out with consideration of the basic rules of zoning, and also to minimize the number of penetrations and shielded doors required.

Interior partitions: ensure that the design of the interior partitions does not compromise the floor and ceiling shielding.

Wall finishes: the wall finishes should be mounted on strips which have been glued to the surface. Nails and screws are not compatible with shielding since it is difficult to get a long-lasting metal-to-metal seal at each fastener location.

Electrical checklist:

Filters: all RF filters should be mounted in special cabinets, and a single penetration should be passed through the shield and clamped to the shield. The same acts for telephone filters and data filtering.

Electrical installation: All other electrical components as conduits, receptables, power outlets, light switches can be mounted on special mechanical supports, without disturbing or penetrating the shield.

Mechanical checklist:

Penetrations: all penetrations through the shielding surface must be mechanically supported. It should be recommended that all penetrations should be grouped using a common metal plate for the penetration. A good conductive contact must exist between each penetration (panel) and the shielding surface.

Joints: the junctions between the shielding surface and the other components are very critical for the overall SE behaviour of the room. To be mentioned are:

- air ventilation (using honeycomb structures)
- penetration of the heating system (hot water pipes)
- penetration of water pipes
- shielded door
- shielded windows

6. PSYCHOLOGICAL ASPECTS

A very important aspect in architectural shielding is the psychological aspect. In a lot of applications, people should not have any impression of being in a shielded room. It means that special care should be taken to the wall finishing, the floor covering and the ceiling. And also to create the opportunity that a 'normal' sight through a window is possible (without Moiré effects) when no shielding is required.

7. OVERVIEW OF THIS SESSION

In this session, the papers are discussing in detail typical aspects of architectural shielding and related topics:

- a study about the shielding offered by the (internal) walls of offices in a building, by Karacagil et al.
- a study on data protection, by Dobkowski
- a report on the implementation of low cost shielded rooms in a hospital environment, by Wolski & Barjack
- a report on low cost shielded rooms: from materials to practical realisations, by De Schacht & Hébert
- a proposal of practical approach for a measuring procedure to characterise shielded rooms, by Catrysse

[1] TEMPEST definitions, NSA specification

[2] ZONE program, NSA specification

[3] Schnettler et al., Schirmwirkung von Gebäuden, EMV Kompendium 97, pp. 181 - 183

[4] L. Hemming, Architectural EM Shielding Handbook, IEEE Press, 1992

[5] G. Wilson, Data security by design, Progressive Architecture, March 95, pp. 82-84

MEASURING METHODS FOR SHIELDED ROOMS: A PRACTICAL APPROACH

Johan CATTRYSSE

KHBO, dept. IW&T, Zeedijk 101, B 8400 Oostende, BELGIUM

An overview of well known standards as MIL STD 285, GAM T20, IEEE 299, will be given and the advantages and disadvantages of these methods will be discussed. Starting from this discussion, a practical approach will be formulated for the characterisation of shielded rooms under the architectural shielding constraints. Typical problems as unaccessible parts of buildings will be discussed and a global solution for the shielding characterisation in these cases will be presented.

The method will be discussed in detail, including the choice of antenna's, the possibilities of and the requirements for full automated, semi-automated and manually operated measuring systems.

Also, a method will be suggested for quick control measurements, in order to control the shielding quality over a longer time period, after installation and finishing the shielded room.

1. INTRODUCTION

The characterisation of the overall shielding behaviour of shielded rooms is a topic that can cause a lot of practical problems 'in situ'. Although since 1956, a military standard has been issued, a lot of discussions are still going on regarding this topic. It should be noted that the actual available standards - even the recently published new draft of IEEE 299 - causes problems when characterising shielded rooms under realistic circumstances (ex. a shielded room on the 10th floor at the streetside of a building, in the center of town).

Therefore, based on the principles of the existing standards, other practical procedures are presented in this paper.

2. EXISTING STANDARDS

2.1. MIL STD 285.

This specification written in 1956 "Military Standard Attenuation Measurements for Enclosures,

Electromagnetic Shielding, for Electronic Test Purposes, Method of". This document is a set of test methods for evaluating shielded enclosures, and no performance curves are given.

The method calls for the receiver to be located inside the enclosure, with the transmitter outside. The advantage is that the sensitive receiver is protected against possible strong fields at the outside (especially during calibration) and also that the received signals can 'easily' be detected over the low ambient noise inside the enclosure under test.

The method calls also for a calibration procedure using an external attenuator, so that the receiver is always operated in the same linear part of the operating range. The number and location of test points are left up to the tester at the time of the test. The result is that the quality of testing may vary considerably.

2.2. NSA 65-6.

This specification "National Security Agency Specification for RF Shielded Enclosures for Communications Equipment: General Specifications", specify both the performance curves required for the protection of communications equipment used in the transmission of intelligence information, and the test methods used for.

The test methods are essentially the same as MIL STD 285, with two notable exceptions. In the magnetic test, the loop antenna orientation is planar versus collinear, and the receiver is located outside the enclosure. The latter was chosen to simulate the classified emitter being inside and the eavesdropping receiver outside the enclosure. A set of test frequencies is given.

2.3. IEEE 299.

This specification "Standard Method for Measuring the Shielding Effectiveness of Electromagnetic Shielding Enclosures" is proposed to replace MIL STD 285 for non-military applications. It describes a set of measurement practices for different antenna configurations. No specifications are given and must be specified separately. The document points out the dif-

ficulties of performing reliable measurements in the lower frequency range from 20 upto 300 MHz (due to resonant effects inside the enclosures and the coupling of non-tuned antenna's with the conductive walls).

The standard specifies also test points at each wall, and extra ones at the location of each component, such as filter penetration panels, shielded doors, shielded windows, etc.

Care should be used when specifying this standard in that it is overkill in terms of the amount of testing required at each testing frequency. As an example, in order to overcome the uncertainty of measurements in the lower frequency range, it is specified to perform measurements at 5 testpoints, and to calculate an average over these points.

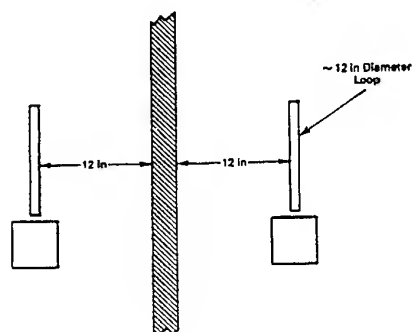


fig. 1. Magnetic field test

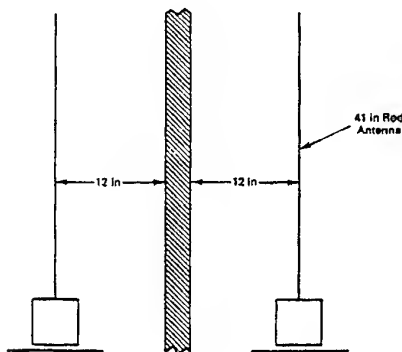


fig. 2. Electric field test

Magnetic field tests are performed upto 1 MHz and Electric field tests are performed upto 10 MHz, each time with distances from transmitting and receiving antenna to the shield of 12 inch or 30 cm.

For the higher frequency range, called the plane wave testing domain, the distances are changed into 72 inch for the transmitting antenna and only 2 inch at the receiving side.

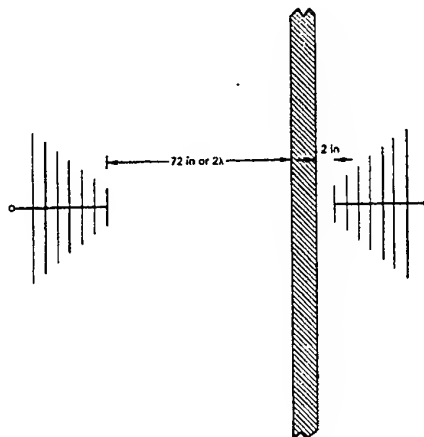


fig. 3. Plane wave test configuration

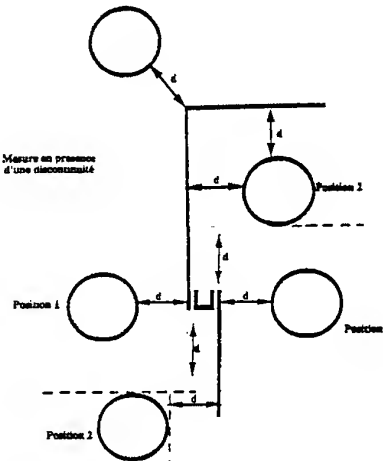


fig. 4. Typical example of test point locations

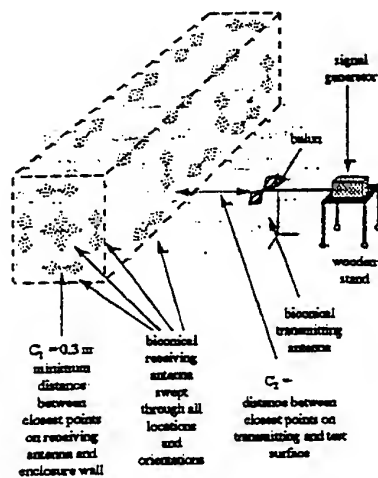


fig. 5. 5 point concept as defined in IEEE 299

3. PRACTICAL APPROACH

It is clear that the above mentioned standards are not applicable under realistic circumstances of architectural shielded installations.

In this section, 5 examples are discussed, where a rigorous application of the standards is not possible:

- accessibility of the room, the walls and the components. Consider a room to be shielded, located at the 3th floor (or higher?) of a building. The room has three windows and the shielding must be controlled.

In this case, the control of the antenna distance to the shield cannot be controlled in an adequate manner, neither it is possible to use a broadband antenna (bilog) at the outside.

- even inside the building, a wall touching the corridor, will cause a problem concerning the positioning of the antenna (width of the corridor is 1m, and the antenna length is 70 cm as for a logger antenna).

- the thickness of the existing walls of a room (when retrofitting), can only be estimated in some cases. Another problem is rising when a double wall is found, with water pipes, heating pipes, cable trays, etc. located in the empty space between the two walls.

- when performing the shielding measurements as a control during the installation of the room, in a lot of cases, the main power supply is not yet connected to the public network. Care must be used for battery operated measuring setups and the required power consumption (using power amplifiers at the transmitting side).

- people walking around in the vicinity of the measuring setup can influence the field distributions, and in this way the measured field strengths at a fixed point, and consequently will cause another shielding value. In practice, it is impossible to avoid this situation, especially in existing buildings and in buildings under construction. These effects must also be taken into account when defining a good procedure.

3.1. Basic requirements of the procedure.

The measuring procedure should be applicable in both situations where the shielded room is still under construction and the final installation is not yet done, and when the room has been finished (wall paper decoration, painting, etc ...) Solutions overcoming the problems mentioned as power supply requirements, people walking around, etc. ... should be implemented in the procedure.

3.2. Proposed procedure.

The procedure consist of 5 main points:

- control of the equipment, by connecting directly by cable the generator/amplifier configuration and the receiver. Control must be performed on the following:

- . control of the power amplification factor
- . control of linearity of generator/amplifier/receiver
- . control of frequency tracking generator/receiver

From these controls, the correct amplifier factor is set to the software, and also a frequency shift can be introduced in order to fit the frequency settings of both generator and receiver.

- reference measurement of the setup. The measured values of an antenna/antenna measurement are recorded and stored for further use as the 'empty' reference. By comparing these values with earlier recorded ones, the setup is controlled including antenna's, cabling and connectors.

The reference measurement is used for calculating the shielding values, given field strengths for a real measurement.

- a quick test is performed: without closing moving components as shielded doors, windows, etc ..., the normal background noise is measured. By closing all these components, the resulting background noise is measured. When the latter background noise is of the same order as the first one, a leakage is occurring. In this case, normally a critical moving component will be the cause, or another 'hole' in the shield.

Otherwise, the quality of the moving components is controlled very quickly by opening each time one of the components, and recording the measured noise levels.

- shielding measurements are now performed by placing the transmitting antenna outside the room, and the receiving antenna inside.

At least one point for each wall, floor and ceiling must be controlled, if technically and practically possible. This will give an evaluation on the average quality of the large surfaces. For the interpretation of the obtained values, care should be used by taking into account the possible effects of the existing attenuation of the walls or building construction itself.

Afterwards, all critical components as shielded doors, windows, penetration panels, heating pipes, honeycomb structures, etc. ... must be controlled.

In order to reduce the measuring time and the number of tests, only horizontal polarisation is used. Also, only one measurement per component is performed. Our experience learned that this is sufficient to characterise the shielding behaviour of these components, and that a leakage at the level of such a component is rising the overall noise level in the shielded room by 10ths of dBs, when a 'bad' component is illuminated with an electromagnetic wave.

Shielding values are obtained by subtracting these values from the reference measurements.

Basically, MIL STD 285, NSA 65-6 or IEEE 299 measuring setups are used, including the choice of antenna's, their positions, etc. ... These setups are then adapted to the practical situations, as already discussed above (as accessibility of the location, ...).

In principle, broad band antenna's are used, except in

the case where the size and/or the weight of the antenna is not practically useful. In this case, (tuned) dipole antenna's are used, because they are small and light weighted.

In order to overcome problems occurring from resonant effects (especially in the lower frequency range), a sweep around the center frequency of the tuned dipoles is performed. In fact, the same effect is obtained as by the 'space' sweep over 5 points as described in the IEEE 299 standard.

A typical example of SE is given in fig. 6.

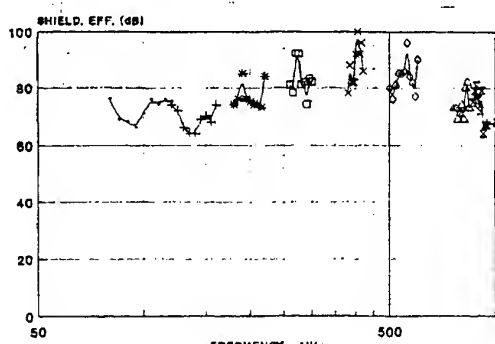


fig. 6. Example of SE, using tuned dipoles

Both antenna characteristics itself, coupling effects to the room and resonant effects are included in these measurements, and an interpretation of the obtained values is possible. Typically, normal averaging (called curve fitting) as available in each spreadsheet program can be done on these data, giving a good overall shielding effectiveness of the component under test.

- control measurements can be performed at regular intervals of time (ex. each year), in order to control the shielding effectiveness in function of elapsed time.

3.3. Implementation on PC.

The method discussed above can easily be implemented on PC. Depending on the possibility to implement a feedthrough connector on a penetration panel or not, different configurations must be implemented in the program:

- feedthrough connector available. In this way, the receiving antenna is inside the shielded room, but the receiver can be placed outside. In this way, both generator and receiver can easily be controlled over the typical IEEE 488 bus.

Depending on the possibility of using broad band antenna's, or a set of tuned dipoles, full automated measurements, or semi-automated measurements are performed. In the case of a set of tuned dipoles being used, each dipole can only be used within a restricted frequency range. Semi-automation means that each time, the set of two dipoles must be changed before

moving into the next frequency range.

When no feedthrough connectors are available, no coupled control between generator and receiver is possible. In this case, a full manually operated measurement is performed, switching manually from frequency point to the next one. Measured values can still be recorded and stored on PC, offering the possibility of easy handling of the measured data afterwards.

4. ALTERNATIVE METHOD

An alternative method to the previous one, is using a spectrum analyser. When broadband antenna's can be used, the generator is running in a free sweep, and the spectrum analyser is also set in a peak-hold repetitive measuring sequence. In this way, during the sweep of the spectrum analyser, the radiated signal is found at a higher level than the background noise, and is stored for further processing. Due to the nature of this setup, only a spectrum analyser can be used as receiver, requiring a high speed sweep.

The main disadvantage of this method is the use of a spectrum analyser, which holds a relatively high noise floor. It follows that a high transmission level is needed, compared with test setups using a measuring receiver. Given the same transmitted level, setups using receivers instead of spectrum analysers will have a dynamic range of 20 dB in more, and will thus enable to measure shielding effectiveness of 20 dB in more.

5. CONCLUSIONS

In this paper, a critical analysis has been done on existing standards for measuring the shielding effectiveness of shielded rooms, as MIL STD 285 or IEEE 299. Based on the principles of these standards, an appropriate measuring procedure has been presented, which overcomes all practical problems for the characterisation of shielded rooms under realistic constraints. The procedure is suitable for automated control using a PC.

It is hoped that this paper will contribute to the discussions concerning the characterisation of shielded rooms under architectural constraints, and to come to a handleable and practical measuring standard.

[1] MIL STD 285, Military Standard Attenuation Measurements for Enclosures, Electromagnetic Shielding, for Electronic Test Purposes, Method of - 1956

[2] NSA 65-6, National Security Agency Specification for RF Shielded Enclosures for Communications Equipment: General Specifications

[3] IEEE 299, Standard Method of Measuring the Effectiveness of Electromagnetic Shielding Enclosures, new draft proposal 1997

METHODS OF MAGNETOSTATIC AND ELECTROMAGNETIC SHIELDING OF DATA PROTECTION COMPARTMENTS

Jan T. Dobkowski

R&D Marine Technology Centre, Gdynia, Poland

Abstract

The article presents an evaluation of potential hazard posed to data carriers (MDC) by magnetic fields. The method and technical means to safe guard the data are discussed, and an original method is presented of examining magnetic field shielding efficiency by the use of large size generator of homogeneous magnetic field.

The presented results of experiments serve to evaluate the efficiency and range of the proposed method of magnetic data carriers protection against damage.

1. Introduction

Magnetostatic and electromagnetic fields can be destructive to magnetic data carriers (MDC) applied in electronic/computer techniques (floppy discs, hard discs and magnetic tapes). The destructive fields are generated by atmospheric discharges, shortings in electro-energetic networks or can be produced by portable generators as economic sabotage.

At present, there are technical means rendering possible registration of electro-magnetic signals produced during data processing in computers and networks, giving thus access of unauthorized persons to processed information. On the other hand, there are also means to safe guard the information against uncontrolled leakage or destruction of information carriers.

Problems related to MDC protection have a history of over 20 years. Some countries have successfully solved these problems by having adopted, to civilian employ, applications initially developed and verified to protect magnetic memory in computers used for cosmic or military purposes.

MDC protection is of vital importance in military service because of the potential threat that strong impulses of electromagnetic field (NEMP) can cause destruction or disablement of commanding units as well as other technical facilities operated by computers.

The standard „Standard ECEMA 59” sets the level of magnetic field intensity secure for magnetic data carriers (hard discs, floppy discs, magnetic tapes). It equals 4000A/m. In some instances the intensity of the field is given in equivalent terms of induction - 5mT. The author considers the Standard with some apprehension, because from his experiments it became evident that in modern magnetic data carriers, made of magnetic materials (with much stronger coercion), the limit of safety can be moved to 30mT.

On the other hand there have been developed protection methods against uncontrolled leakage of information or destruction of magnetic data carriers: magnetic data safes and shielded rooms.

The effectiveness of protection achieved by any of these facilities can be examined by experimental determination of shielding coefficients against magnetic and electromagnetic fields.

2. Concise technical characteristics of data protection facilities

MDC can be destroyed by high temperature, humidity or magnetic field. Facilities serving the purpose of MDC stores - called data safe (DS) - have installed heat screens and magnetic shielding. Large data processing centres are equipped with shielded rooms (SR) where the servers are operating.

Other problems occur with the construction of special shielded compartments for medical experiments (SMC). These rooms are used for research and highly sensitive bio-medical measurements with SQUIDS (measurements range down to 10^{-15} T).

The three types of technical facilities (data safe - DS, shielded room - SR and special medical compartment - SMC) represent variable designation, hence they have to comply with different technical requirements. Data safes, for data carriers storage, require efficient shielding against magnetostatic field and have to guarantee the damping/attenuation of the field inside the safe below 5mT, under unexpected circumstances (e.g. shortings in energetic circuits).

They have to be secure also against electromagnets, of the strength up to several kilowatts, which can be applied intentionally to destroy information on magnetic data carriers.

Different requirements are set in the case of shielded rooms installed at data processing centres. The applied shields have to safe guard against electromagnetic fields within the band from 10kHz to 40GHz. They protect magnetic memories of computers against destructive LEMP and NEMP impulses and also eliminate possible remote electronic listening-in.

The SRs require shielding coefficient for the field component E not lesser than 100 dB and for the H component of the field, the shielding coefficient should increase from 50dB for $f = 10\text{Hz}$ to 100 dB for $f > 10\text{MHz}$.

Medical laboratories using equipment with SQUID detectors to measure induction of neurocurrents should present excellent shielding coefficients against magnetostatic field and E-M field within the band (0.01÷1000)Hz. In practice, attenuation coefficients inside these compartments reach 80 - 120 dB, thus - inside - the geomagnetic field and its fluctuations are nearly completely eliminated as are the disturbances from industry.

The compliance with extreme requirements of MDC protection, i.e. protection of computing systems against magnetostatic and quasistationary electromagnetic fields, is achieved by the use of multilayer shields produced from materials of very good magnetic properties.

Electromagnetic shields are, at times, built of magnetic metal plates sandwiched with non-magnetic plates (copper).

The effectiveness of a shield depends on construction materials as well as on construction technology (welds, mechanical connections, number of technological openings). The shielding coefficient is determined experimentally.

3. Methods for shielding efficiency examination.

3.1. Shielding magnetostatic and quasistationary E-M fields.

Determination of shielding characteristics against magnetostatic and quasistationary E-M fields is essential in the case of data safe effectiveness evaluation and also in the case of special medical compartments, because the fields penetrate deep into the shield and for this reason protection is technically difficult.

DSs and SMCs shielding coefficients were studied in a special laboratory unit constructed by the author from non-magnetic materials and equipped with large generator of magnetic field. The generator consisted of 4 windings with current, having

dimensions of (3,5x3,5)m. The windings were set in mutually parallel planes (Fig.1), power input was 90kW.

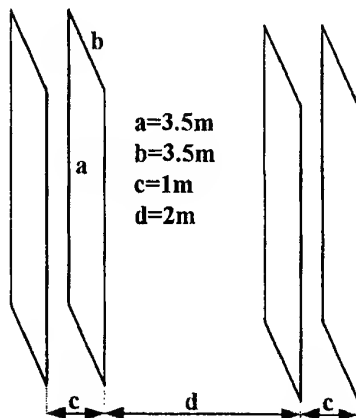


Fig.1. A diagram of winding in the generator of magnetic field.

Inside the generator a homogeneous magnetic field was produced, stationary or quasistationary with characteristic induction (in the air) changing from 0 to 100mT. This induction range proved sufficient to examine DSs in the full range of magnetization, including the magnetic saturation state.

Shielding coefficient was defined as a ratio between magnetic field component at selected internal point of the generator and this component at the same point measured inside the studied DS.

Geometric dimensions of the generator rendered possible the examination of shielding properties of data safes and server housings in small shielded rooms. The examination using a homogeneous magnetic field from the generator allowed very precise determination of shielding properties of the studied objects and an extensive evaluation of their shielding effectiveness.

Frequently, a simplified methods is used for the evaluation of shielding properties consisting in the application of portable magnets, equipped with cores of variable shape (cylindrical, C-letter). The magnets produce magnetic induction of (150÷500)mT. By comparing the intensity of electromagnetic field at the outer wall of the studied object with that at several internal points of the objects, the coefficient of magnetic field damping was determined. This coefficient is often mistakenly taken for the shielding coefficient. This simplified method is, to some extent, oppressive and less precise, though when examining large objects or under field conditions it's application was unavoidable.

3.2. Shielding electromagnetic field

The evaluation of E-M field shielding in the band $>10\text{kHz}$ is usually carried out according to the

standards MIL-STD-285, MIL-STD-461 and NSA 65-66.

The damping of E-M field by shielded rooms depends on magnetic permeability μ , conductance γ and the width g of materials used for the construction of the room. In low frequency range of the E-M field, with the dominating H component, the shielding is mainly influenced by physical properties of the building material μ and γ . While in the case of frequencies $f > 10\text{MHz}$, the E component becomes dominant and material of high conductance is necessary to obtain effective shielding, together with very tight connections between the elements of the shield.

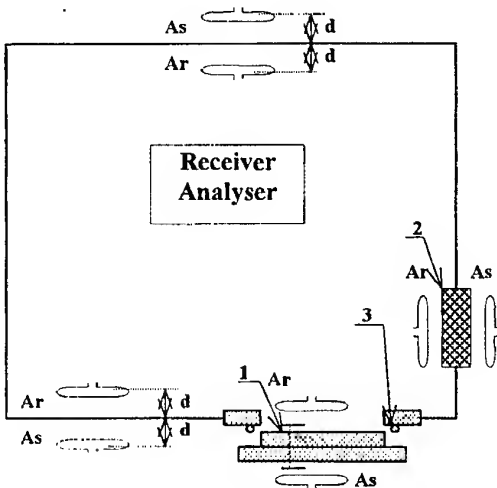


Fig.2. A diagram of shielding properties measurement system for shielded rooms;
1. door. 2. vent. 3. HF seal (A_s , A_r) aerials

The aerials, during the shielding examination experiments, were placed close to the walls of the studied object (0.3 ± 0.76)m, choosing vulnerable areas - joints, vents, cable channels, doors (Fig.2), where the shield efficiency was expected to fail.

The effectiveness of shielding was finally expressed by the coefficient damping of the filed components E and H given in dB.

4. Results of experiments

The measurements of the shielding against magnetic and electromagnetic fields carried out for some data safes and shielded rooms were performed on the basis of examination methods described above. Selected, representative results of these measurements are presented in the following section.

The examined DSs were built of steel plates, of ordinary quality, with double jacket in construction and $(1.5 \times 1.2 \times 1)$ m in size. The examination unit was

also used for large $(30 \times 80)\text{m}^2$ surface SRs evaluation. These were screwed constructions made of galvanized steel sheets, of (2 ± 2.5) mm width. Coefficient of field shielding was determined by placing the studied DS or small SR in the homogeneous magnetic field produced by the generator (Fig.1). The system allowed to determine simultaneously the threshold external field induction, where in the induction inside the DS exceeded the permissible value of 5mT (Fig.4).

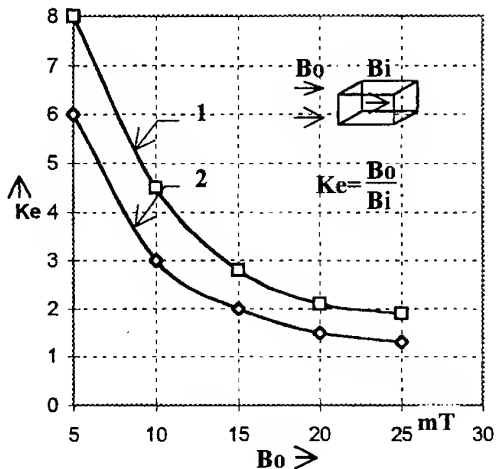


Fig.3. Shielding coefficient of magnetic field in DS as a function of external magnetic field;
1. B_o vector perpendicular to the side wall,
2. B_o vector perpendicular to the wall containing door.

Field shielding by a DS is not homogeneous; the walls with technological openings (doors, vents) demonstrate weaker shielding properties by c.a.30% (Figs.3 and 4).

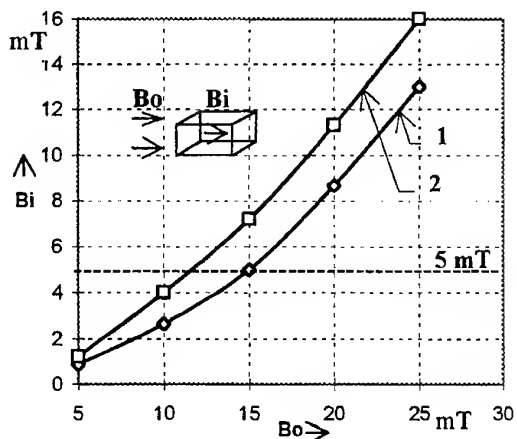


Fig.4. Induction inside DS as a function of homogeneous magnetizing field B_o ;
1. wall, 2. wall with door.

The shielding coefficient of DS declined fast with the growing induction B_o of the external magnetic field (Fig.3). Already, at induction $B_o > 10\text{ mT}$ the plates got magnetically saturated and shielding properties of the DS became very poor (inadequate).

Approximated evaluation of shielding properties was carried out using portable electromagnet, with cylindrical core, supplied from lighting installation. Placing electromagnet at the outer wall of the DS (Fig.5), served to determine the internal distribution of field induction. The measurements were carried out for 2 induction levels: 170 and 260 mT applied to the outer wall of the DS. Induction obtained inside the DS exceeded the threshold value of 5 mT in both cases at a distance $<(0.2 \pm 0.3)\text{ m}$ from the internal wall.

Relatively good protection against destructive influence of E-M fields and remote electronic listening-in of operating computers (servers) was obtained in SRs. The examine SRs, devoid of internal electricity installation, were characterised by E component attenuation amounting to $\sim 125\text{ dB}$ in the band $10\text{ kHz} - 1\text{ GHz}$, and the H component was attenuated to over 75 dB (Fig.6). When the servers installed inside the SR were switched on through energy filters, the shielding of E component decreased to 100 dB , this being an inherent feature of the applied filters - their shielding properties did not exceed 100 dB .

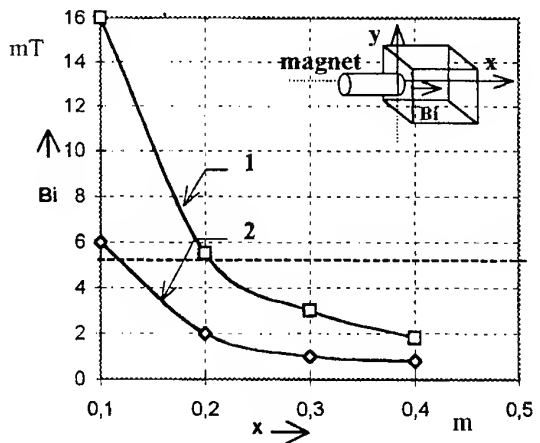


Fig.5. Distribution of B_i induction induced inside DS by portable electromagnet:

1. $B_{o(x=0, y=0)} = 170\text{ mT}$, 2. $B_{o(x=0, y=0)} = 260\text{ mT}$.

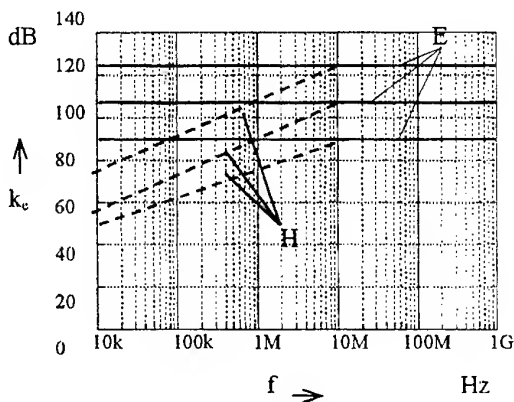


Fig.6. Shielding coefficients of E and H components of the field in SR;
 1. without electric network installation,
 2. complete,
 3. simplified HF tightening of the door.

It was found out during the experiments, that considerable effect of shielding properties of a given SR could be attributed to electromagnetic seals used to tighten doors, vents, screwing connections between the plates, etc. (Fig.6).

5. Conclusions

1. There are effective experimental methods to examine shielding properties of technical facilities designed to protect computers and magnetic carriers of information.
2. The safety of MDC in a DS or SR can be completely and precisely evaluated from results of their examination in a generator of uniform magnetic field. In some cases, when the high precision of evaluation is not necessary or when the evaluation is to be done under polygon conditions, the examination can be performed by portable electromagnet.
3. DSs as used up to date do not guarantee complete protection of MDCs stored inside. As shown by the experiments, a portable electromagnet supplied from lightning installation can easily destroy the information on MDC.
4. Good protection of data processing systems is obtained in SRs. These facilities are characterised by attenuation coefficients within the range $(80 \div 120)\text{ dB}$ for E component of the field and $(50 \div 80)\text{ dB}$ for the H component.
5. The shielding of magnetic field by SR is considerably influenced by their construction (assembly) technology.

LOW COST SHIELDED ROOMS; FROM MATERIAL TO PRACTICAL REALISATIONS

Laurence Hebert,
Johan De Schacht,

SCHLEGEL Bvba, Rochesterlaan 4, B 8470 Gistel, BELGIUM

In this paper, a description will be given of a low cost shielded room based on the use of a flexible metallized non - woven for wall covering and used in shielded components such as doors and windows.

The flexible material can both be applied in existing rooms as a retrofit and in new buildings.

The "turn key" system offers shielding solutions for all protrusions and apertures that may exist in a room that needs to be shielded.

The SE obtained with this system is sufficient for applications such as medical examination rooms, measuring laboratories in the electronics industry and industrial and military rooms where confidential data has to be secured against electronic eavesdropping.

The system allows a degree of finishing equal to that of regular rooms, so that the visual difference with non shielded rooms is almost non existent.

1. INTRODUCTION

The use of precision electronic devices, mobile, powerful and sophisticated telecommunication systems and ever higher-performance microprocessors increases the noise level exponentially. Characteristic examples can be cited to confirm the increasing risks of "electrosmog."

The protagonist of this technological evolution, i.e. the electronic industry, is concurrently becoming the prime victim of electronic interference. Can it afford to be exposed to electromagnetic interference risks (EMI), all the more so as European EMC standards on the matter are becoming very strict?

Consequently, the need to reduce the noise level by installing a system of architectural shielding often cannot be overlooked, in particular for development

and calibration standards, EMC measurement laboratories, medical electronics, etc.

The 60 dB minimum shielding efficiency attained by the Isowave® architectural shielding system are very satisfactory for numerous applications, not only in industry, but also for the security and protection of confidential information against electronic eavesdropping.

Industrial sites require extensive flexibility that traditional shielding systems cannot always offer. On the other hand, the "turnkey" architectural shielding system based on an electro-less copper plated non-woven and combined with components of highly innovative and unique shielding, will adapt to all types of premises, new or renovated, without affecting either the comfort or the appearance of the site.

2. "TURNKEY" ARCHITECTURAL SHIELDING SYSTEM

2.1. "Turnkey" concept

The Isowave® architectural shielding system provides a minimum shielding efficiency of 60 dB in the 50 MHz to 2 GHz range according to Mil-Std-285. This result is obtained by combining a very high-performance shielding material and shielding components developed especially to shield all apertures, large and small, through a global approach that comprises the study of the site to shield in consideration of all the specific characteristics of the premises, the production of customised components and their installation in optimal connection with the shielding material. Shielding efficiency measurements carried out by an independent EMC laboratory confirm the excellent level of shielding. The premises are then ready to be decorated with ease by following some rudimentary instructions.

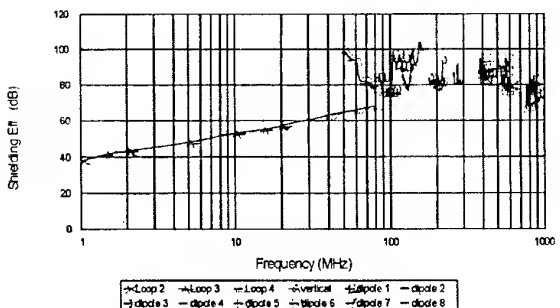


Figure no. 1: Shielding efficiency of the Isowave® architectural shielding system, complete and installed, measured according to Mil-Std-285.

2.2. The shielding material

The Isowave® system is based on the use of an electroless copper plated non-woven with excellent electrical characteristics and very low surface resistance (0.04 Ohm/□). The shielding efficiency of the material amounts to 75 to 80 dB in the electric

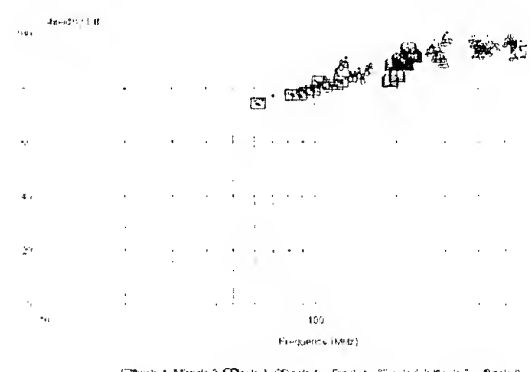


Figure no. 2: Shielding efficiency of the Isowave® material according to Mil-Std-285

field (see figure 2). The shielding material has undergone state-of-the-art development, which has made it possible -- by means of simulation in the near and far field and in practical cases (1) to improve its shielding efficiency and its unique anti-corrosion coating which ensures an excellent performance for the material in the accelerated ageing test according to Mil-Std-202. Furthermore, thanks to this coating, the material can be easily combined with various decorative materials using glue, paint, etc. Very thin (0.1 mm) and very light (60g/m²), the Isowave® shielding material offers great flexibility which is highly prized for industrial applications. Isowave® makes it possible also to reduce the costs for preparing the premises for shielding. No self-bearing structure is required nor any maintenance needed for the material. Isowave® is air-permeable and eliminates all risk of condensation. In laboratories requiring special measuring conditions on a continuous basis, engineers

rightly appreciate the comfort provided by the Isowave® system

2.3. components

The components have been specially designed to be combined with the Isowave® shielding material. Most of them in fact also use the Isowave® basic material themselves. Each of the components meets the flexibility requirement. They are thus highly innovative compared with traditional shielded cages and even conventional architectural shielding components. Each of the components required for an installation must be perfectly connected to the shielding material and installed by professionals. A single neglected detail could lower the shielding efficiency by at least 20 dB. The range of shielding components extends from shielded doors, to shielded window systems, shielded fastening systems, ventilation, filters, etc.

2.3.1. Isowave® shielded door:

The shielded door is made as a standard wooden door. The door is covered completely by Isowave® material. The door panel contains EMC gaskets, a material similar to Isowave® around a polyurethane foam. The EMC gasket of the door has been tested during 500,000 cycles, i.e. 250,000 openings and closings, with no change in shielding efficiency noted. The design and installation of the door, comprising the door, the door frame and the door step provide the same level shielding as the entire system with very limited door opening and closing forces. The latest generation of Isowave® door ensures a minimum of 60 dB shielding efficiency between 50 MHz and 2 GHz. The door step contains an EMC gasket too for the shielding, is only 10 mm high, and is sloped on either side so that trolleys can pass easily. The lock is specially designed so that the door can be closed on both sides. The installation of a card-key reader is also conceivable. Single or double-leaf doors can be used, turning inwards or outwards of the room. The different versions available include fire retardant doors.

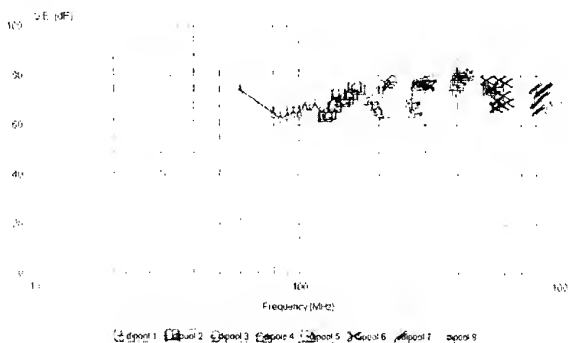


Figure No. 3: Shielding efficiency of the Isowave® door installed according to Mil-Std-285

2.3.2. Shielded window:

Three different types of shielding for windows have been developed. The most functional system is based on the shielded blind principle. This as a window shielding system mounted in front of an existing window. The existing window continues to be functional; opening, closing, cleaning, etc. The shielding contains an electrically driven roller of Isowave ® material. In the unrolled position, the window is shielded against EMI. The shielded window system offers excellent shielding, far superior to the 60 dB of the complete system.

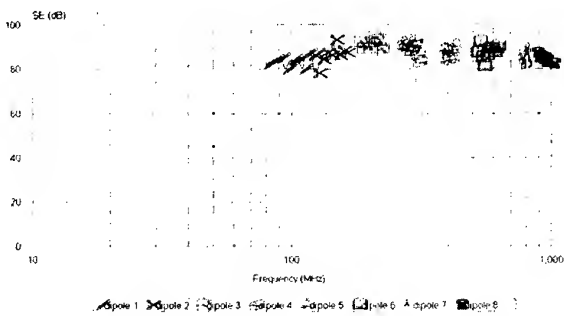


Figure no. 4: Shielding efficiency of the Isowave ® window installed according to Mil-Std-285

2.3.3. Shielded screw / plug system

All fixing devices for attaching light fixtures, electricity distribution conduits, false ceilings, shelving, etc. must be shielded. Standard plugs create perforations in the shielding, thereby opening a conductive path through the shielding that causes the shielding to deteriorate by 20 to 30 dB. Very low transfer impedance is ensured by means of stainless steel plates, so that the shielding does not deteriorate

2.3.4. Ventilation or air-conditioning panels:

a honeycomb system with mounting flange adapted on the Isowave ® non-woven has been developed for all ventilation or air-conditioning apertures.

2.3.5. Trap doors:

special panels that can be dismantled have been developed to cover all openings required for the maintenance and repair of equipment which are accessible only through shielded walls.

2.3.6. Shielded pipe

For a room with central heating and a washbasin, the connecting pipes through the shielded walls must be shielded too. Ducts have been developed for shielded pipes, and they provide a very low transfer impedance so that the shielding is not deteriorated by

the pipes. The pipe duct is equipped with a highly conductive flexible seal which provides superior shielding to the complete system, likewise under thermal cycle conditions as is the case at present for heating pipes.

2.3.7. Plate for BNC connectors, etc.

2.3.8 A special component has been developed for the optical fibre duct.

2.3.9. Electric filters

In order to filter all conducted interference, all cables (mains, telephone, data, etc.) entering or leaving the shielded room must pass through filters. All filters are grouped on a case which can be mounted inside our outside of the shielded room. The filter case is always electrically connected with the shielding of the room and serves as the central earthing point of the complete room. Electricity is distributed through metal or plastic ducts fixed thanks to the shielded screw/plug system.

2.3.10. Other components

The list is exhaustive. Other components can be integrated depending on the project: shielded system for liquid ducts, washbasin, shielded installation for the suspension of false ceiling and false floor, etc.

3. PRACTICAL CASE OF THE INSTALLATION OF AN INDUSTRIAL DEVELOPMENT LABORATORY

3.1. Situation

We can study the characteristic example of a laboratory for the development of electronic chips (for portable telephone) situated in front of a portable telephone relay antenna which is nonetheless located relatively far away. The interference levels are such that the desired measures cannot be carried out nor the results obtained relied upon.

3.2. Observation

A shielding level of 60 dB is required in the frequency band for the application of this company, i.e. between 800 MHz and 2.2. GHz.

The development laboratory is being renovated and must be configured in offices that already exist.

Emphasis has been focused on the comfort and working conditions of the engineers who refuse to work continuously in a shielded cage. The room must resemble the other offices of the site.

3.3. Installation

This installation must be carried out rapidly and adapted to the specific features of the premises. It must allow for flawless decoration on the walls, floor and ceiling as well as the components, identical with every other room. The room has numerous very interesting installations and components. The presentation and description of the installation will include the following elements: Isowave® non-woven on the floor, wall and ceiling, door, windows, filter case for mains, telephone data transfer, optical fibre duct, ventilation, connection panel, fixing systems and false ceiling suspension system, liquid duct, etc. The results of the measurements carried out by an accredited EMC laboratory reveal a very satisfactory shielding efficiency level once again. The shielding will be completely concealed by the decoration.

4. CONCLUSION

Developments carried out on the complete Isowave ® architectural shielding system are always intended to

meet the needs of industrial sites and maintain optimal working conditions at a reduced shielding cost that pays off quickly. Recent measurements carried out by reputable control organisations on concrete installations are excellent. The industrial application is not limited only to reducing the noise level for the use as a quiet room, but also for the protection of confidential information. To this end, BSI of Germany has already shown interest in the Isowave ® system. Their own measurements on a complete Isowave ® installation confirm the very satisfactory results of the system.

- (1) Catrysse J., A new test cell for the characterisation of shielding materials in the far field, 7 th Int. Conference on EMC, York, sept. 1990
- (2) MIL STD 285, Military Standard Attenuation Measurements for Enclosures, Electromagnetic Shielding for Electronic Test Purposes, Method of 1956

THEORETICAL AND EXPERIMENTAL SHIELDING STUDY OF OFFICES

P. KARACAGIL^{(1),(2)} S.S. ŞEKER^{(1),(2)} F. ÜSTÜNER⁽¹⁾ N. ARI⁽³⁾

(1) Marmara Research Center P.K. 21, 41470 Gebze-Kocaeli/TÜRKİYE

Tel: 0-90-262-6412300(3213), Fax: 0-90-262-6412309, e-mail: karaca@mam.gov.tr

(2) Boğaziçi University, Department of E.E. 80815 Bebek-İstanbul/TÜRKİYE

(3) Ingenieurschule Zurich, Lagerstrasse 45 Posfach 3021 CH-8021 Zürich/SWITZERLAND

In this work, the research has been carried out in two phases: shielding effectiveness of a building is calculated by using a multilayer model and compared with the measurements results inside building. Multilayer modeling enables us to obtain transmission and reflection coefficients of the layers, which are actually the rooms and/or floors that we are interested in. The second phase has been entered by making attenuation measurements by an automated measurement system. Two different situations have been tested. In the first one, the transmitting and the receiving antennas of the system have been located on the same floor of the building and the shielding effectiveness measurements have been carried out in the frequency range of 200 MHz -1000 MHz. In the second situation the receiver has been located one floor down and some single frequencies have been used during the measurements taken in various rooms at 952 and 937 MHz. The experimental results were found to be good agreement with theoretical results.

1. INTRODUCTION

Modelling of attenuation of electromagnetic fields by building structures is useful in a number of engineering applications. Because of the potential implementation of indoor wireless local area networks (LAN's) and personnel communication networks (PCN's), it is important to understand the propagation of signals inside buildings.

Indoor propagation study is more complicated than outdoor study. The environment inside a building consists of many obstructions, constructed from different materials, and these objects may be in close distance to the transmitter and receiver antennas of the measurement system during experiments. The space and height between furniture, architectural configurations, partition materials and even moving people can fluctuate the radio signals. Thus, the intensity of the radio signals varies from place to place inside a building.

Electromagnetic shielding properties of houses or

buildings are usually determined by measuring the signals generated by either portable equipments or by fixed equipments present in the vicinity. Smith [1] presented the results of an empirical investigation of the shielding properties of seven buildings ranging from a single family of detached residences to multistory office buildings. Both electric and magnetic field attenuations were measured in the frequency range of about 20kHz to 500 MHz. On site measurements are time consuming and expensive. One method to overcome this difficulty is to use a computer code, which calculates the attenuation of buildings as a function of its material characteristics, dimensions, room layout , frequency and the angle of incidence radiation.

Because of the presence of varying conditions, some approximation should be made for modelling the buildings. From the earlier studies in the literature, one may conclude that the approximations made in those researches can be classified into two main groups: In the first one, several measurements are made and then a formula is searched for modelling the measured data. The attenuation characteristics of the building is then approximated by the formula. Lafontaine and Lecours [2] examined the effects of the number of walls, number of floors, open and closed doors, corridors, windows present between anternas. In the other method, modeling takes the precedence: according to the architecture of the building a prediction formula is firstly proposed to estimate the attenuation characteristics of buildings. Then measurements are carried out to verify the assumed model.

Honcharenko, Bertoni, Diling [3],[4] studied on the propagation losses of the same and different floors inside a building. The research reported here contributes to their study by repeating the measurements to verify the multilayer model, and also not at a single frequency but for a range of frequencies. The propagation loss measurements have been carried out in two steps: in the first step, both the transmitting and the receiving antennas have been located on the same floor and the frequency range of 200MHz-1000MHz has been

scanned; where in the second step, the receiver has been moved one floor down and measurements have been repeated at the single frequencies of 937, 952 MHz. Measured data were obtained by using an automated measurement system which provides a synchronization between signal generator and receiver.

2. MULTILAYER STRUCTURES

2.1. Theory

The problem considered in this part of the study is the electromagnetic interaction (reflection and transmission) of a incident plane wave with multilayer.

Assuming that at any point (x, y, z) of a layer, reflection and transmission wave of the incident plane wave can be used to derive a set of two recursion formulas each of which is valid for an arbitrary layer number of multilayer structure and for arbitrary angle of incidence.

For the electric field intensity vector is parallel to the plane interfaces, two scalar quantities can be introduced by means of which the two recursion formulas can then be developed.

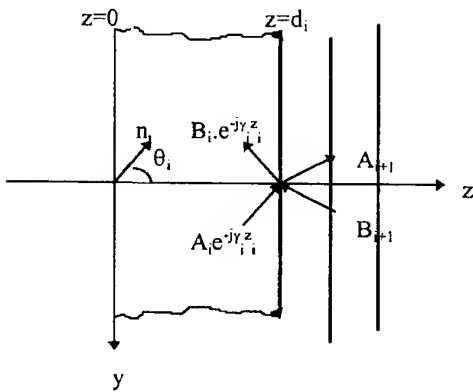


Figure 1. i.th layer of a multilayer structure

With reference to Fig. 1, A_i ; tangential E at left interface of i th layer, travelling from left to right, B_i ; tangential E at left interface of i th layer, travelling from right to left.

The exponential describing $e^{j\gamma_i z}$ these waves take into account both the attenuation and phase shift of the waves as they go through each layer. More precisely the wave travelling left to right is represented by an expression of the form $A_i e^{-j\gamma_i n_i r}$ where n_i is the two dimensional normal vector $n_i = -\sin\theta_i \mathbf{a}_y + \cos\theta_i \mathbf{a}_z$ and r denotes the usual position vector. Additionally, γ_i is the complex propagation constant for i th layer. For vertical polarization, continuity of the electric field intensity at $z=d$ gives the following relationships [5].

$$\begin{bmatrix} A_i \\ B_i \end{bmatrix} = \frac{1}{2} \begin{bmatrix} e^{k_i} A_{i+1} & e^{k_i} B_{i+1} \\ e^{-k_i} B_{i+1} & e^{-k_i} A_{i+1} \end{bmatrix} \begin{bmatrix} 1 + Y_{i+1} \\ 1 - Y_{i+1} \end{bmatrix} \quad (1)$$

$$Y_{i+1} = \frac{\cos\theta_{i+1}}{\cos\theta_i} \sqrt{\frac{\varepsilon_i(1-j\tan\delta_i)}{\varepsilon_{i+1}(1-j\tan\delta_{i+1})}} \quad (2)$$

where

$$\tan\delta_i = \frac{\sigma_i}{w\varepsilon_r\varepsilon_0} \quad w=2\pi f \quad (3)$$

$$\theta_{i+1} = \sin^{-1} \left[\frac{\gamma_i}{\gamma_{i+1}} \sin\theta_i \right] \quad (4)$$

$$k_i = d_i \gamma_i \cos\theta_i \quad (5)$$

$$\gamma_i^2 = -w^2 \mu_i \varepsilon_i + jw\mu_i \sigma_i \quad (6)$$

d_i is the thickness of the i . layer and θ_{i+1} is the complex angle of refraction in i . layer. Now in the region of the right of the multilayered slab, there is only a wave travelling from left to right whose amplitude can arbitrarily be set equal to unity. Therefore if we set $A_{N+1}=1$ and $B_{N+1}=0$, we can determine expressions for A_i and B_i , in sequence, by setting $i=N, N-1, \dots, 2, 1, 0$ in the recursion formulas given above. Obviously, A_0 is the incident wave on the left of the slab, and B_0 is the reflected wave. As a result, reflection coefficient R and transmission coefficient T are obtained as

$$R_V = B_0 / A_0, \quad T_V = 1 / A_0 \quad (7)$$

Finally

$$R_V^2 = [\text{Re}(B_0 / A_0)]^2 + [\text{Im}(B_0 / A_0)]^2 \quad (8)$$

$$T_V^2 = [\text{Re}(1 / A_0)]^2 + [\text{Im}(1 / A_0)]^2 \quad (9)$$

Shielding effectiveness is defined as for vertical polarization case.

$$SE_v = -10 \log |T_V|^2 \quad (10)$$

The same method could be applied in case of magnetic field shielding effectiveness.

2.2. Multilayer Model for a Single Floor

The model presented above gives us the transmission and reflection coefficients of the layers. The transmission coefficient of the multilayer can be used for calculating the shielding effectiveness (SE) of the layers.

We verify our computer code obtaining the same results as in [3-4]. Firstly, rooms housed through a corridor in the same floor can be modelled as a multilayer structure. (Fig. 2) This model can be easily adopted to the program. Parameters which are needed for calculating SE (μ_r , σ_r , ε_r and the distance for the measurement point) are known for the building. Under consideration theoretical results are obtained using this program for seven rooms at 200-1000 MHz. In order to carry out the measurement and get the data in a relatively short time, an automated measurement system can be used. When we apply this model in a building, we must also deal with some scattering and diffraction terms. For the same floor calculation, diffraction term is less significant than the reflection and transmission terms.

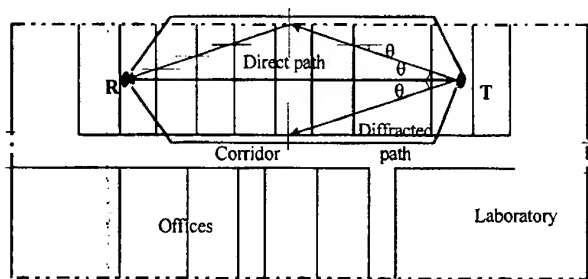


Figure 2. Multilayer structure of the rooms in the same floor.

Besides the basic building structure (walls, floors and ceiling), furnishings and people serve as scatterers. Because the many propagation paths from the transmitting to the receiving antenna resulting from the scattering objects, the paths exhibit many different starting directions at the transmitting antenna and many different directions of arrival at the receiving antenna. The resulting multipath structure causes the received signal to exhibit strong variations as either the transmitting or receiving antenna is moved over a distance on the order of $\lambda/2$. For propagation inside buildings traditional practice is to average the signal by moving the transmitter or the receiver over a spatial area having linear dimension of 10 to 20 wavelengths (often in a circular path) to remove the rapid variation. The result has been referred to as the sector average.

The vertical propagation space in which a signal can propagate depends on the environment of the building. Typical office buildings will have rooms filled with desks, chairs, file cabinets, low partitions etc. that define the lower boundary of the clear space through which the signal can propagate. The upper boundary of this clear space is defined by support beams, pipes, ventilation ducts, lighting fixtures. For a signal propagating through the rooms of an office building the vertical propagation space will be between the furniture and the ceiling features and it is typically 1.5 - 2.5m.

For propagation to distant points only the forward scattering through small angles is significant. Fields resulting from scattering that occurs at large angles will influence the local interference pattern. However to contribute at distant locations the fields would have to be rescattered through large angles thereby further reducing their amplitudes. Forward scattering is not sensitive to the shape of the object or boundary conditions. The change in excess path loss can be understood with reference to the width of the first Fresnel zone for the source and receiver antenna at the mid point of the clear space.

2.3. Multilayer Model for Separated Floors

In order to examine the propagation characteristics between floors of a building, the possible paths of

propagation must be determined.[4] The paths through the floors include the direct ray paths and the rays that are multiply reflected and transmitted at the walls and floors. These ray paths are contained entirely within the building perimeter. The diffracted ray paths involve transmission outside the building through windows and diffraction into paths that run along side the face of the building, propagating until they reach another window, at which the ray reenters the building at a different floor. Floors of a modern office buildings are typically constructed with precast concrete slabs, reinforced concrete or concrete poured over corrugated steel panels. UHF signals can propagate through the precast slabs and through reinforced concrete with a transmission loss at each floor. Floors constructed over a corrugated steel panels seriously limit the propagation through the floor.

3. MEASUREMENTS

In this section multilayer structures were applied to the building for the same and different floors. Propagation loss measurements were done in the first and second floors of TÜBİTAK Marmara Research Center Building. The structure of each floor and the placement of offices are the same.(Fig. 2) Each floor is divided by a corridor. 70 % of the outside walls of the offices are composed of glasses. Walls are concrete.

3.1. Automated Measurement System

The traditional measurement systems do not allow us to scan a particular frequency range. In order to examine more than one frequency, the synchronization between the transmitter and the receiver sites must be provided. Therefore several researchers have deal with this problem.

In this study, a synchronous test system has been used for the attenuation measurements of the building through the rooms in the same floor.

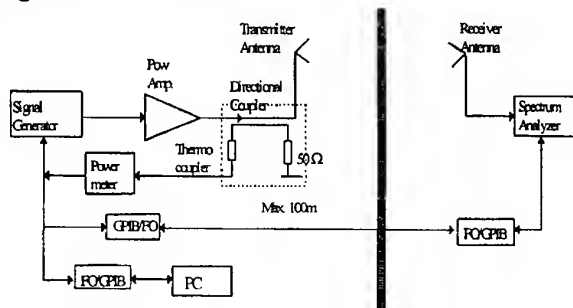


Figure 3. Automated measurement setup

The measurement setup shown in Fig.3. can be used to measure the shielding effectiveness of the building. This setup allows us measuring of any building automatically by using the IEEE 488 bus with GPIB (General Purpose Interface Board) control.

3.2. Measured and Calculated Results for Single Floor

Figure 4-7 shows the calculated and measured results of the different rooms on the same floor for 200 MHz-1000 MHz. Both of these results were obtained for 100 frequency step. The distance between the receiver and the transmitter seems to have significant effects on the calculated results. However the several factors effect the wave propagation such as reflection from the transmission media (ceiling, walls, floor, furniture etc.) Therefore some differences may occur between calculated and measured results although these effects were considered in the modeling with the incident angles. The results of the other rooms show similar behaviour as seen in Fig.4 but the magnitudes are different.

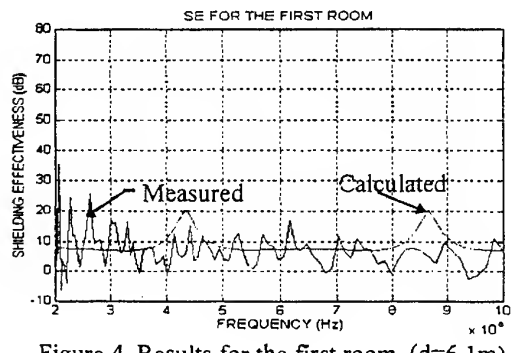


Figure 4. Results for the first room ($d=6.1\text{m}$)

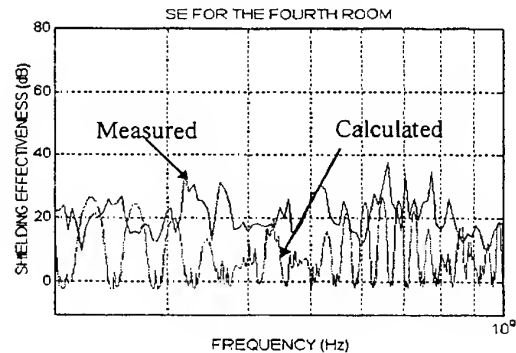


Figure 5. Results for the fourth room. ($d=20.9\text{m}$)

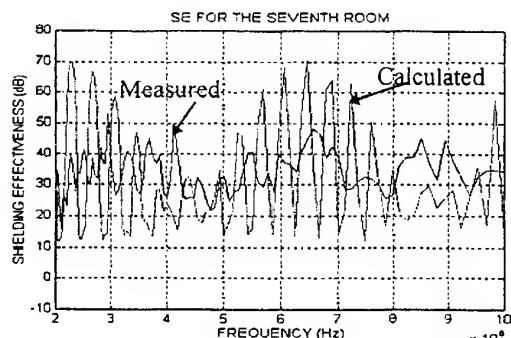


Figure 6. Results for the seventh room. ($d=28.3\text{m}$)

The peaks seen on the measured graph are the results of ambient radiation which are inherent in the propagation media because of the broadcasting radio stations, GSM systems and TV channels. In order to understand the attenuation characteristics of the building at a single frequency results were focused on the 937 and 952 MHz.

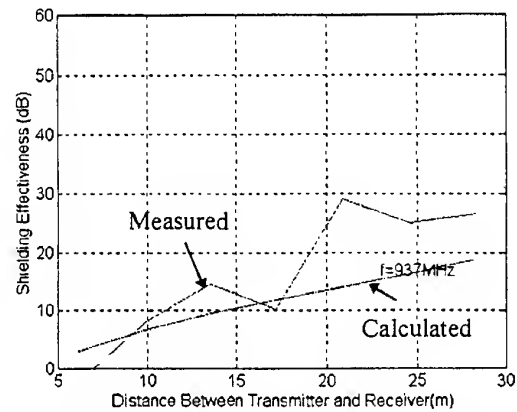


Figure 7. Receiver and transmitter are on the same floor(937 MHz)

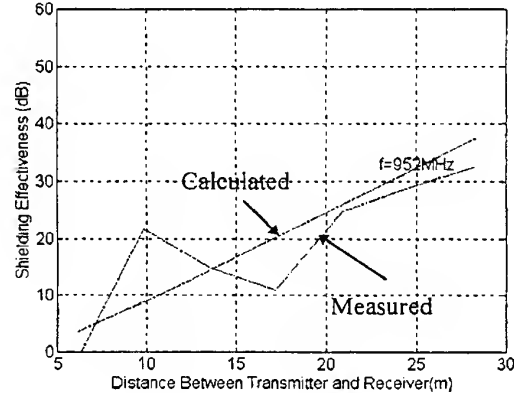


Figure 8. Receiver and transmitter are on the same floor(952 MHz)

For the same floor measurements shielding effectiveness results were normalized with respect to the first room result. A conical log spiral antenna was used as a transmitter antenna and a biconical antenna was used as a receiver antenna. Antenna directivity has an important role on the measurement. Because of the directivity of these antennas direct path is the most important components of the obtained results.

3.3. Measured and Calculated Results for Different Floors

SE calculation inside the building for different floors does not follow the same tends as in the same floor. Because of two aspects (1) direct path and (2)diffracted

path show different attenuation characteristics through floors. When the transmitter and the receiver antennas are located on the different floors it is expected that the direct ray has more effect for close distance while diffracted waves have more effects for large separation distances of the antennas.

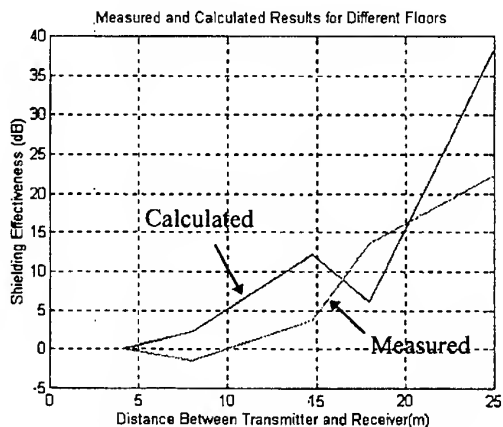


Figure 9. Receiver and transmitter are on the different floors (937 MHz)

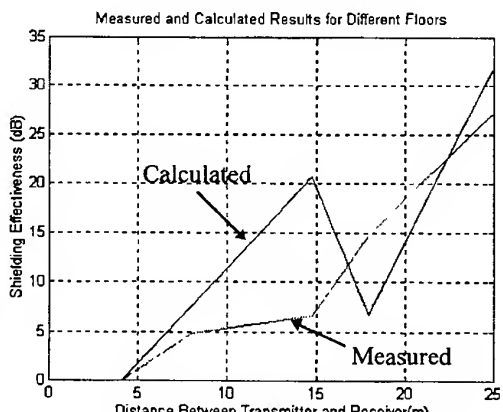


Figure 10. Receiver and transmitter are on the different floors (952 MHz)

In this study directive antennas have been used and the main lobes of their radiation patterns were not aligned to see each other. The results were normalized with respect to first measurement point which is the just beneath of the transmitter antenna. Diffracted ray path for the one floor down are not effective because of the antenna radiation pattern and the building characteristic. Figure 9 and 10 show the measured and calculated results for different floors and the different rooms through a corridor.

4. CONCLUSION

In this study the results of the measurements have been compared with the results obtained from the theoretical approach. We have seen that there is consistency especially for those frequency range where

the clear space distance falls into the Fresnel region for the same floor results. The different floor measurements were carried out at 937 and 952 MHz then found that they are close to the theoretical results while main lobes of the antennas cover the each other.

Multilayer model and the automated measurement system are an ideal case to examine building attenuation. We concluded that shielding effectiveness of an office building increases, depending on the building and antenna characteristics, approximately 10 dB for each room for the same and different floor.

5. REFERENCES

- Alberta A. Smith,JR., "Attenuation of Electric and Magnetic Fields by Buildings," *IEEE Transaction on EMC*, Vol. EMC-20, No.3, pp. 411-418, August 1978.
- Jean-Francois Lafourte and Michel Lecours, "Measurement and Modelling of Propagation Losses in a Building at 900 MHz," *IEEE Transaction on Vehicular Technology*, Vol. 39, No.2, pp.101-108, May 1990.
- Walter Honcharenko, Henry L. Bertoni, James L.Dailing, J Qian and H.D. Yee, "Mechanism Governing UHF Propagation on Single Floors in Modern Office Buildings," *IEEE Transactions on Vehicular Technology*, Vol. 41, No. 4, pp. 496 504 November,1992.
- Walter Honcharenko, Henry L. Bertoni, James L.Dailing, "Mechanism Governing Propagation Between Different Floors in Buildings" *IEEE Transactions on Antenna and Propagation*, Vol. 41, No. 6, pp. 787-790 June 1993
- Demetrius T. Paris, "Computer-Aided Radom Analysis," *IEEE Transactions on Antennas and Propagation*, Vol. AP-18, N0.1, pp. 7-15, January 1970.

ACKNOWLEDGEMENTS

The authors are grateful to facilities provided by TUBITAK MAM UEKAE EMC Lab. and they would like to thank the staff for their contributions during the measurements. They are particularly grateful to Dr. Temel YALÇIN, İbrahim ÖLÇER and Selçuk HELHEL for their helpful comments.

BIOGRAPHICAL NOTES

Piraye Karacagil has received her BS degree from Department of Electronics and Communication Engineering, Istanbul Technical University and MS degree from Department of Electrical Engineering, Bogazici University. She works as a researcher at TUBITAK National Electronics and Cryptology Research Institute and she has been involved in EMC tests and measurements for two years.

X

EMI SOURCES & COUPLING PATHS TO VICTIMS

MICROWAVE OVENS INTERFERENCE POTENTIAL BETWEEN 1 & 18 GHz AND ASSOCIATED STANDARDISATION ACTIVITIES IN CISPR

Bernard Després

France Télécom CNET DMR/RMC

38-40 rue du Général Leclerc 92 794 Issy Moulineaux Cedex 9 - FRANCE

Abstract : This paper describes a study conducted to characterise the radiation emitted by microwave ovens between 1 and 18 GHz, both inside and outside the oven allocated band (2.4 - 2.5 GHz). Results are presented in conjunction with the on-going work within CISPR Sub-Committee B which is currently defining emission limits for microwave ovens and other ISM equipment between 1 and 18 GHz, with the exclusion of the allocated ISM bands. The emphasis is on the frequency and time domain characteristics of this emission, by illustrating the significant difference between the peak and the average emitted level. Different weighting functions are discussed and the corresponding measured results are presented.

1. INTRODUCTION

More and more radio services are operating above 1 GHz, especially the new mobile radio systems (PCS in the USA, DCS 1800 in Europe, PHS in Japan...), and they will have to cope with the electromagnetic radiation produced by domestic microwave ovens. Some other systems such as the LEO (Low Earth Orbit) satellite systems or the RLANs (Radio Local Area Networks) are allocated inside the ISM band (2.4 - 2.5 GHz).

In the standardisation field, microwave ovens are classified as ISM (Industrial, Scientific and Medical) equipment and the radiated field emission limits are under the scope of Sub-Committee B of CISPR (International Special Committee on Radio Interference). At present, in the relevant standard [1] (CISPR Publication 11), limits between 1 and 18 GHz are under consideration except in the satellite broadcasting receiving band (11.7 to 12.7 GHz) where the oven effective radiated power (ERP) is limited to 57 dB(pW).

To try to improve this situation, CISPR/B has set up in 1994 an ad-hoc group (chaired by the author of this paper) to draft some emission limits between 1 and 18 GHz for all ISM equipment (except inside the allocated ISM bands 2.4 - 2.5 GHz and 5.725 - 5.875 GHz where the emission is unrestricted). A new draft amendment to CISPR 11 will be submitted for voting in the first half of 1998.

We will present in this paper results of measurement performed in our laboratory in France in conjunction with this standardisation activity. All data presented here was obtained using the measurement method defined by the CISPR ad-hoc group : measurement distance of 3 meters in a fully anechoic room, resolution bandwidth of 1 MHz and oven loaded with one litre of tap water.

2. FREQUENCY DOMAIN MEASUREMENTS

As the emission of an oven is highly fluctuating with time, measurements in the frequency domain are generally performed in max hold mode with a peak detector. This method obviously maximises the emission and is not representative of the level present at a given time, but enables to identify the frequencies of maximum emission for each oven.

Although every type of microwave oven has its own frequency « signature », it is generally around the same frequencies that these maximum occurs. We will give here a few examples of emission obtained between 1 and 18 GHz, based upon which some general characteristics can be deduced.

In general, out of band emissions between 1 and 2 GHz are rather limited. However, some of the ovens we have tested exhibited an emission peak at a frequency corresponding to half of the fundamental frequency (1.225 GHz), as shown on figure 1.

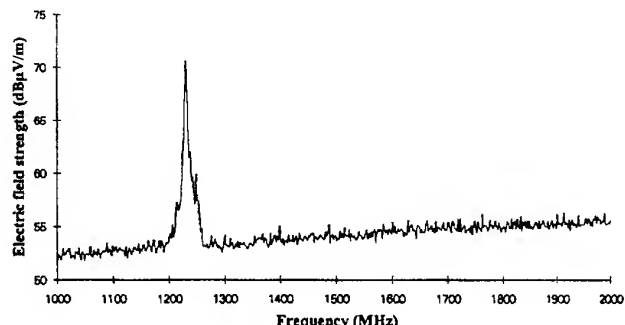


Figure 1 : Emission of a microwave oven between 1 and 2 GHz - Max hold during 2 minutes with a peak detector

Between 2 and 3 GHz, the emission is important only around the oven allocated band. In figure 2, we have shown only the part of this frequency range where some emission occurred above the noise level, i.e. between 2.1 and 2.8 GHz. The main characteristic here, that is common to every existing oven is that, although the oven allocation (without any limitation of the emission) is 2.4 - 2.5 GHz, the maximum emission occurs between approximately 2380 and 2480 MHz. This has two consequences :

- just below the allocated band, i.e. at 2.4 GHz, where CISPR has to set emission limits, the emitted levels are very high (between 100 and 110 dB μ V/m) and could disturb future mobile radio services that would be allocated here ;
- in the upper part of the allocated band, emissions are rather limited. For this reason and as new spectrum allocations become more and more difficult to find, the band 2483.5 - 2500 MHz has been allocated for MSS (Mobile Satellite Systems).

In addition, the lowest part of the oven band has been partially allocated to Radio Local Area Networks (RLANs). For example, in France they can operate only between 2446.5 and 2483.5 MHz. These systems use spread spectrum modulation techniques that are felt more immune to disturbances produced by microwave ovens than traditional modulation techniques. However, if they are used in close proximity to a microwave oven, they will experience interference that will at least increase the bit error rate and therefore prolong the transmission time, or even drop the link.

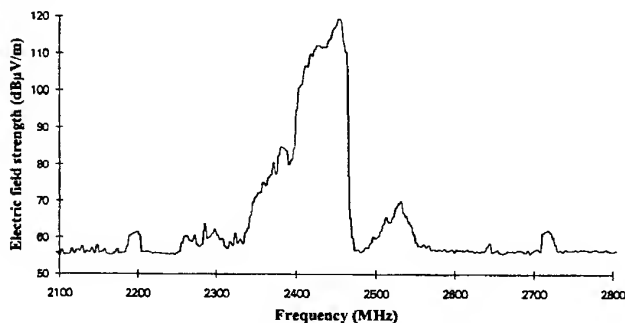


Figure 2 : Emission of a microwave oven between 2.1 and 2.8 GHz (including the allocated band 2.4 - 2.5 GHz)
Max hold during 2 minutes with a peak detector

Between 3 and 10 GHz, ovens generally show significant emission levels only in the frequency range shown on figure 3 above, i.e. between 3.6 and 8.2 GHz. As the oven second harmonic (4.9 GHz) and third harmonic (7.35 GHz) fall within this range, it is not surprising to register high emissions at these frequencies. More interesting is the fact that significant levels occur also at frequencies in between these harmonics ; they are different for each oven, an example is given on figure 3. They may be due to the changing of the load during the oven operation, and they are produced less frequently than the harmonics. Another characteristic is that the fourth harmonic (9.8 GHz), not shown here, did not appear above the noise level for all the ovens we have tested.

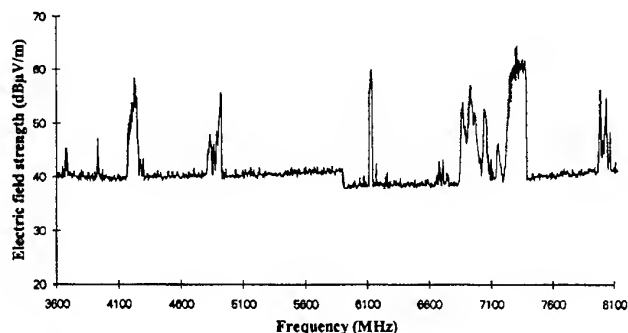


Figure 3 : Emission of a microwave oven between 3.6 and 8.1 GHz
Max hold during 2 minutes with a peak detector

Between 10 and 18 GHz (figure 4), three harmonics frequencies are met : 5th (12.25 GHz), 6th (14.7 GHz) and 7th (17.15 GHz). They all appear on the graph, but only the level of the sixth is significant. This is due to the fifth harmonic choke that is routinely installed on all magnetron to meet the only existing emission limit, that suppress the fifth and also the seventh harmonic, but that has the disadvantage to increase the level at other harmonics (especially the 6th).

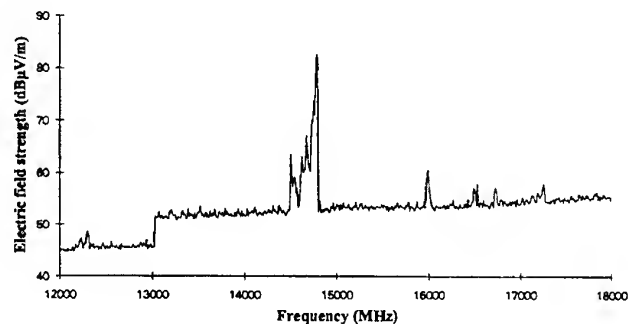


Figure 4 : Emission of a microwave oven between 10 and 18 GHz
Max hold during 2 minutes with a peak detector

3. TIME DOMAIN MEASUREMENTS

Due to the way the energy is produced inside a magnetron, the knowledge of the frequency spectrum is not sufficient to evaluate the interference potential of a microwave oven towards radio systems. For this reason, time domain measurements were also performed and results are presented here. They are obtained with a spectrum analyser set with a null frequency span.

Figure 5 show the time variations of the emission at the nominal operating frequency. The emission is present only half of the time (half wave rectified a.c.) and two main emission bursts appear during one mains cycle. If observed during a longer time, we would see that the maximum level of these bursts also change with time (for example between 100 and 120 dB μ V/m) depending on the variations of the load inside the oven.

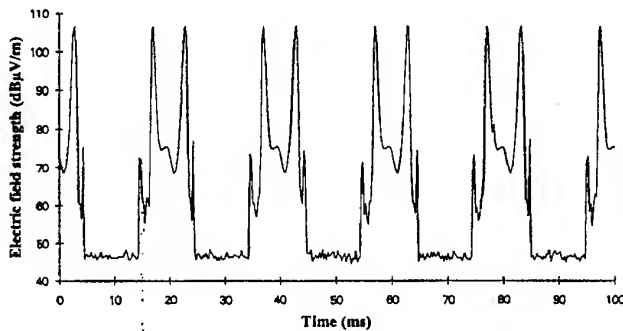


Figure 5 : Time domain measurement at 2450 MHz (oven centre frequency) during 100 ms (5 mains periods)

Figures 6 and 7 show the time variations at two randomly chosen frequencies, one above and one below the ISM band. It should be mentioned first that, at these frequencies not corresponding to a specific high emission (harmonic...) the levels encountered are very low and are in fact lower than the noise floor of the frequency domain measurements performed in max hold mode and presented before. Here again, the influence of the mains frequency modulation can be clearly seen, with also two bursts every mains period. But, additional randomly appearing bursts are also experienced (for example at 5 ms on figure 6 or at 90 ms on figure 7).

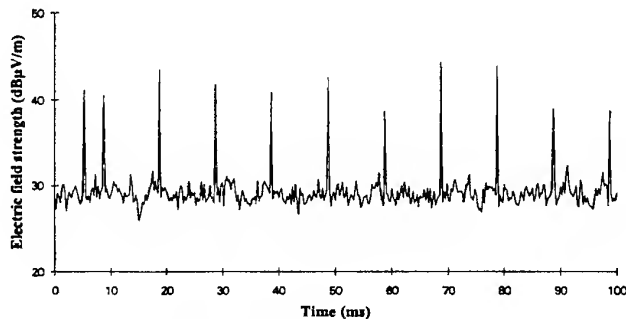


Figure 6 : Time domain measurement at 2000 MHz during 100 ms (5 mains periods)

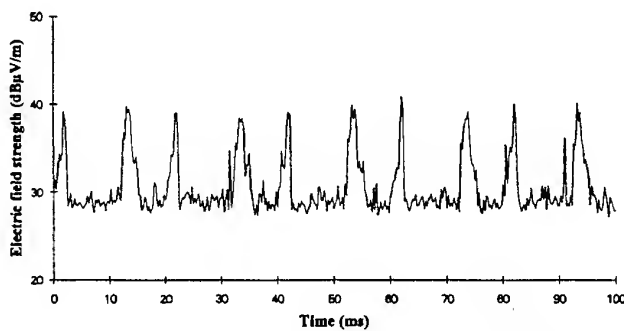


Figure 7 : Time domain measurement at 2600 MHz during 100 ms (5 mains periods)

In general, the time domain behaviour of a microwave oven can be summarised as follows :

- the emission is impulsive and « modulated » by the mains signal : 20 ms (50 Hz) periodicity of the emission ;
- around the operational frequency, the emission is nearly present half of the time, whereas, as we move away from this band, the emission becomes more and more scarce ;
- the amplitude of the pulses randomly varies with time.

The consequence is that, when frequency domain measurements are performed, the result very much depends on the type of detector used : the peak level is significantly higher than the average level, especially as we move away from the oven band. This has an influence on the interference potential towards radio systems : for the same peak level, microwave ovens are much less disturbing than a CW-like source (Information Technology Equipment for example).

For measurements above 1 GHz for all kind of non radio equipment, CISPR is currently defining the suitable detector, and the solution chosen is to use a peak detector that is quick and easy to use. But, for microwave ovens, the ad-hoc group concluded that there is a need for an additional measurement more representative of the average emission level.

4. DISCUSSION OF A WEIGHTING METHOD

The ad-hoc group deliberately investigated only weighting functions that would be easy to use and commercially available on most of the existing spectrum analysers. The aim was certainly not to design a new detector, as it was done in the past for the CISPR quasi-peak detector. For this reason, only the following options were considered :

- use of the trace (or video) averaging function : the displayed level is the average of a series of individual sweeps performed with a peak detector ;
- a reduction of the video bandwidth (VBW) on the spectrum analyser : it reduces and filters the brief isolated emissions and retains only the more permanent emissions.

For both of these methods, one drawback was identified : if the measurements are performed in logarithmic display (as it is the case for all the curves here), both the trace and the video bandwidth average the logarithmic levels and not the linear ones. As a consequence, for example if a square pulsed signal (half on, half off) at a level of 60 dB μ V/m is measured, the level indicated by both detectors will be 30 dB μ V/m, whereas the true average level would be 54 dB μ V/m. And, the measurement of a microwave oven emission in linear display is nearly impossible to perform. For this reason, the term « weighted » was chosen for this type of measurement rather than « average ».

Figure 8 shows the result obtained with the first method (trace averaging) as compared with a classical max hold result. As can be seen, the two curves drastically differ, illustrating once again the fluctuating nature of the oven emission. In fact, the same frequency is emitted so rarely

that, except in the middle of the allocated band, the « average logarithmic level » falls within the noise. Therefore, this method cannot be used to characterise the emission outside the oven band.

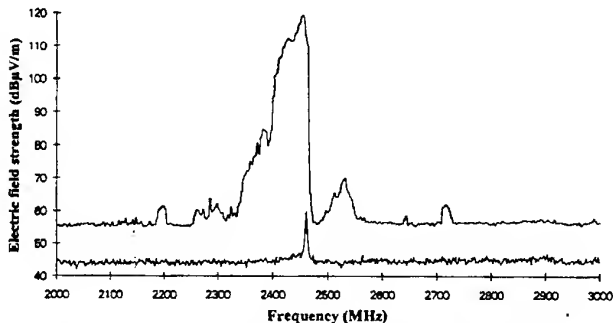


Figure 8 : Measurement of a microwave oven in the frequency domain with a peak detector in max hold mode (upper curve) and in trace averaging mode (lower curve)

Figure 9 show the result obtained with the second method (reduction of the VBW) as compared with a classical max hold result. The noise level is highly reduced by the weighting, as well as the frequency of emission of the oven, also showing that these emissions are not permanent (if the source was CW like the clock of an Information Technology Equipment, both methods would give nearly the same level). It can also be seen that this weighting technique is more useful to assess levels outside the allocated band.

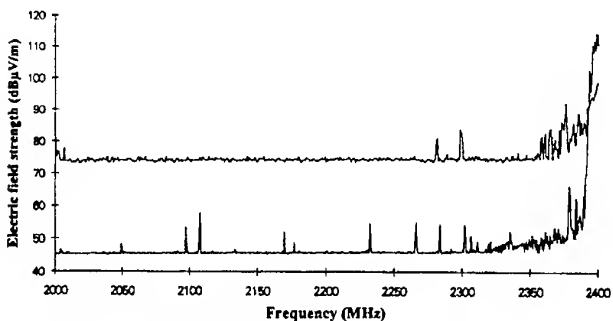


Figure 9 : Measurement of a microwave oven in the frequency domain with a peak detector (upper curve) and a reduction of the video bandwidth to 1 kHz (lower curve)

Based on these results, the reduction of the VBW was chosen as the weighting method for measurements of ISM. The ad-hoc group then discussed what value of the VBW was the most appropriate. Considering that the oven is modulated by the mains frequency (50 or 60 Hz), it was concluded that a value lower than the latter was needed in order to obtain the average (in logarithmic units) of the emission. For this reason, the value of 10 Hz was chosen.

5. CISPR/B PROPOSALS FOR LIMITS

This section summarises the content of the latest draft that will be distributed to the CISPR National Committees in the first half of 1998 proposing limits between 1 and 18 GHz. The rationale upon which the values of the limits themselves have been derived is not explained, only the main principles and the measurement technique to be used will be detailed.

We have seen that for microwave ovens, high peak levels can be tolerated, as the average emission level is very much lower. But, when elaborating the proposal, one element to take into account is that microwave ovens are only one specific kind of ISM (although the most widely spread) and that it may exist CW-like ISM sources (some prototypes are already under development), for which high peak levels would surely disturb the radio services to be protected above 1 GHz.

For these reasons, a two-tier approach was defined :

- a first measurement is performed in peak max hold mode. If all emissions between 1 and 18 GHz (except inside the ISM bands) are below a level of 70 dB μ V/m, then no additional measurement is necessary. If this level is exceeded (it is the case for all existing microwave ovens), then the measured result is compared to the limits given in Table 1 below. The equipment is declared compliant if these limits are met and provided that :
- a second measurement is performed with the weighted method discussed above (VBW reduced to 10 Hz) at two spot frequencies with regard to the limit given in Table 2 below.

To summarise, for CW-like sources, only one peak measurement is necessary and for fluctuating sources, one peak and one weighted measurement are required (and both Table 1 and Table 2 limits shall be met).

Table 1 - Electromagnetic radiation disturbance peak limits for Group 2 Class B ISM operating at frequencies above 500 MHz (peak measurements with a resolution bandwidth of 1 MHz and a video bandwidth higher or equal to 1 MHz)

Frequency range (GHz)	Field strength at a measurement distance of 3 metres (dB μ V/m)
1 - 2.3	92
2.3 - 2.4	110
2.5 - 5.725	92
5.825 - 11.7	92
11.7 - 12.7	73
12.7 - 18	92

Note : Limits of this table were derived considering fluctuating sources like magnetron driven microwave ovens.

Table 2 - Electromagnetic radiation disturbance weighted limits for Group 2 Class B ISM operating at frequencies above 500 MHz (weighted measurements with a resolution bandwidth of 1 MHz and a video bandwidth of 10 Hz)

Frequency range (GHz)	Field strength at a measurement distance of 3 metres (dB(μ V/m)) ; VBW = 10 Hz
1 - 2.4	60
2.5 - 5.725	60
5.825 - 18	60

To check the limits of this table, measurements need only to be performed around two centre frequencies : the highest peak emission in the 1005 MHz - 2395 MHz band and the highest peak emission in the 2505 - 17995 MHz band (outside the band 5720 - 5830 MHz). At these two centre frequencies, measurements are performed with a span of 10 MHz on the spectrum analyser.

6. CONCLUSION

Past standardisation efforts to set emission limits for microwave ovens have not been successful due to the following paradox : microwave ovens exhibited extremely high peak emission levels but, at the same time, when experiments of their effects on radio systems were made, very limited disturbances were experienced.

Since a few years, more in depth technical studies, as the one described in this paper, enabled to understand better the technical reasons of this paradox. As explained here, the main reason is the fluctuating nature of the oven emission with basically, at a given frequency, two major pulses emitted every mains period.

Therefore, the ratio between the peak and the average power is very high in the case of microwave ovens. The resulting effect on radio systems (nearly all digital above 1 GHz) very much depends on the maximum tolerable bit error rate of the latter : for systems like fixed links that can drop the link at error rates of 10^{-7} - 10^{-5} , interferences are likely to occur, whereas for modern mobile services like cellular telephones that can withstand error rates as high as 10^{-2} , the threat is in a great part reduced or will occur for a higher level of the interferer.

As it was not realistic to define a specific limit and measurement method (weighting detector) for each and every existing and planned radio service allocated between 1 and 18 GHz, the CISPR ad-hoc group in charge of this work choose a medium solution that is presented in the last part of this paper. We can reasonably hope that it should as a first step solve most of the potential interference situations outside of the allocated ISM bands. For systems allocated inside the oven band (Low Earth Orbit satellites and Radio Local Area Networks), further studies are necessary.

7. REFERENCES

- [1] CISPR Publication 11 : Limits and methods of measurement of electromagnetic disturbance characteristics of ISM radio frequency equipment, 1990
- [2] Radio disturbances in between 1 GHz and 18 GHz caused by microwave ovens - M. Vrolijk and B. Després - International Wroclaw symposium on EMC - June 1996

8. BIOGRAPHY

Bernard Després is head of the EMC and spectrum engineering group in CNET, the research centre of France Telecom. He is member of several standardisation committees on EMC : CISPR Sub-Committees A, B and G and CENELEC SC 110A, where he is convenor of several ad-hoc groups on the subject of limits and measurement methods above 1 GHz.

ELECTROMAGNETIC COMPATIBILITY FOR IMPRESSED CATHODIC PROTECTION SYSTEMS (ICCP)

K. DYMARDOWSKI, W. OBROCHTA, J. UCZCIWEK, R. ZAJĄC
R&D Marine Technology Centre, Gdynia – 62 Dickmana str., Poland

Corrosion of steel is recognised as one of the major problem of the Polish economy. The main modern method for corrosion protection is the Impressed Current Cathodic Protection (ICCP). The primary element of each ICCP systems are special controlled sources of direct current (rectifiers). ICCP systems are exposed on different electromagnetic influences. In the paper EMC requirements and test methods existing in actual standardised documents suitable for specific ICCP systems are presented. Selected results of testing of special marine ICCP system are showed too.

1. INTRODUCTION

Corrosion of metals costs the Polish economy more than one year's budget on defence, health service and education globally [1]. Corrosion of steel is recognised as one of the major contributors on these losses. The basic elements of steel constructions ventured on corrosion conditions are marine stable constructions such as piers and pilings, sailing objects i.e. ships and warships, underground pipe's systems, land constructions as bridges and roads etc. Approximately one-third of costs of corrosion could be reduced by application of the best corrosion-related technical practices, but not everybody realises necessity of corrosion protection. However there are seen changes in that area, for example Ministry of Communication have given instruction requiring to obligatory applying of standards in corrosion protection area by users.

The potential difference between the two metal surfaces, in ships between steel hull and bronze propeller, is the driving force of corrosion current flow. Corrosion current (ionic current) is cause of transportation of material from one electrode (anode-steel) to the other (cathode-bronze). The main modern method for corrosion protection is cathodic protection (CP). The decreasing of the corrosion potential of anode surface by applying a current is the basic of cathodic protection. An optimum polarisation level for steel is in the range from - 0.90 V to - 0.95 V (vs. Ag/AgCl seawater reference electrode).

Cathodic protection can be imparted by using either a sacrificial-anode systems or impressed-current cathodic protection (ICCP). Sacrificial-anode system bases on electronegative potential of anode's material. It provide adequate cathodic current to the attached structure by

gradually consuming the potential of the structure and maintaining it in the protective range. In ICCP systems cathodic current is generated by special system of direct current supplied anodes. The primary element of each ICCP systems are special controlled sources of direct current (rectifiers).

Protected structures are located in different areas with various corrosion hazards and operating conditions, so ICCP systems are exposed on different influences, among them on electromagnetic noise too. Today's switch - mode, digital controlled rectifiers are exposed on electromagnetic hazards of environment and are sources of damaging electromagnetic radiation.

Polish Ministry of Defence has given in 1997 order demanding certification for some main systems for warships among other CP systems. For ships electronic devices exist special needs in EMC area, they should have in general great level of EM immunity and low of EM noise emission [2] harmonised.

For certification there is needed reference document containing technical requirements of ICCP systems including EMC requirements. There exists several standards and other reference documents containing requirements on ICCP systems, especially in safety area [3+8] but they are incomplete. The European Directive on EMC - EEC/336/89 - sets requirements on both emission and immunity levels for EMC. In Poland several harmonised standards are already available, or are in discussion and development, or are under consideration but they aren't complete. So, it was necessary to complete specific EMC requirements for specific devices (ICCP-systems) used in specific environment (warship).

These works suggested to divide ICCP systems on several groups which differ specific environmental conditions of their using and to define basic EMC requirements for these groups of devices.

2. ICCP SYSTEM FOR MIDDLE SIZE SHIPS

Impressed Current Cathodic Protection system offers effective corrosion protection of submerged marine structures, so ICCP system (MPOK-2 type) intended for middle size ships is described in that chapter.

The schematic of that system is shown on fig.1. There exist two main units (subsystems) in that system. First is

the switch-mode rectifier (3) which can deliver smoother DC output than classic thyristor based rectifier.

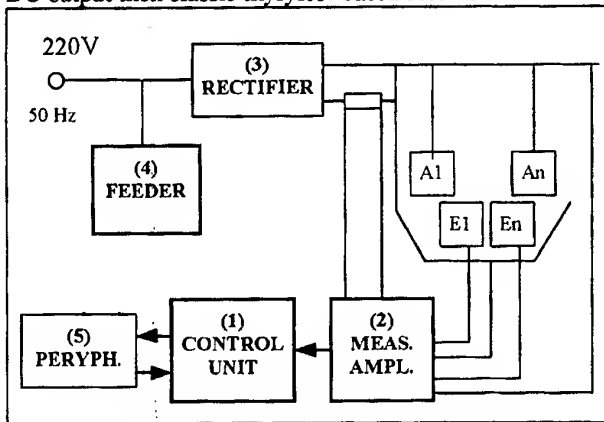


Fig 1. Block-diagram of ICCP - MPOK-2 type

It ensures better regulation, and the ability to accurately control of voltage and current from zero to maximum ratings too. The second of the main units of described system is control unit (1). Control unit acquires information from control electrodes (E1, E2, ..., En) by measurement amplifiers (2). From the other side operator has ability to set control parameters from keys (5) and to inspect parameters of work of protective anodes (A1, A2, ..., Am) by monitor. Because of great density of the electronic devices in ship engineering EMC must be taken into account during the design and concept phase of new apparatus and equipment and is becoming a basic requirement during the system design, at the same level as safety or cost - analysis.

3. PROPOSALS OF EMC REQUIREMENTS FOR ICCP-SYSTEMS

EMC is a necessity for disturbance-free operation of all electrical/electronic apparatus, systems and installations that are to be used in a common electromagnetic environment. Further, EMC is now also an important requirement for any electrical product being placed on different environmental conditions. The relevant legislation usually refers to standards that define both standardised test methods and certain minimum

EMC requirements. In Poland intensive efforts are devoted to developing suitable standards for all kinds of products, but it will take some times. In that communicate authors have tried to complete EMC requirements and test methods existing in actual standardised documents suitable for specific ICCP systems [9-14].

Because of their different application ICCP systems are used in different environmental conditions, so system is also categorised according to where it will be used and three-level classification scheme has been developed:

- industrial environment - closed industrial compartments,
- field, open area environment,
- vessels, ship environment - affect other closed marine structures too.

Proposals for Technical Regulations in EMC which should be reference document in performing ICCP equipment assessments in certification process is after-mentioned (table1 and table2). In table1 are mentioned requirements in immunity scope and in table2 in emission disturbances scope. There are called the main obligatory in Poland national and international standards and CISPR technical regulations as sources of needs and obligatory measurement methods.

4. RESULTS OF MEASUREMENTS

The results of EMC tests of MPOK-2 ICCP system is after mentioned. It was checked in laboratory condition only. During the tests real circuit was simulated by model reference electrodes, anodes and ship's hull in tank poured by sea water. The appliance was in operation state during testing. Total length of cables and power wires were less than 2 meters.

The purpose of the test was to check perform system which is produced by Polish industry, desired function without unacceptable degradation from or to the specified electromagnetic environment. The immunity to conducted interference or noise generated by radiated fields and disturbance emission were the main aim of tests. The limits of requirements parameters are specified in table 1 and 2.

Table 1 — Index of electromagnetic compatibility requirements in emission disturbances scope

Nr	Requirements	Basic Standards	Measurement methods	Environment of exploitation		
				Industrial	Field; open area	Vessels
1	2	3	4	5	6	7
1	Conducted disturbance for frequency bands 10 kHz to 10 MHz	MIL-STD 461D Requirement CE102	STANAG 4436	+	-	+
2	Radiated disturbance for frequency bands 30 Hz to 100 kHz	MIL-STD 461D Requirement RE101	STANAG 4436	+	-	+

Explanations to column 5, 6 i 7: "+" examination is performed; "-" examination isn't performed.

Table 2 — Index of electromagnetic compatibility requirements in immunity disturbances scope

Nr	Requirements	Basic Standards	Measurement methods	Environment of exploitation		
				Industrial	Field; open area	Vessels
1	2	3	4	5	6	7
1	Nuclear electromagnetic pulse NEMP	WPN-84/N-01003 Table 31	WPN-85/N-01007 p.6	-	+	+
2	Lighting electromagnetic pulse LEMP	EN 61000-4-5	EN 61000-4-5	-	+	-
3	Electro Static Discharge	PN-IEC-801-2	PN-IEC-801-2	+	-	+
4	Fast transient 5/50 ns induced in power line and In/Out circuits	PN-IEC-801-4	PN-IEC-801-4	+	+	+
5	High energy 1,2/50 µs pulse induced in power lines	PN-IEC-801-2	PN-IEC-801-5	+	+	+
6	Damped sinusoid test wave form 1 MHz	MIL-461c	MIL-461c	+	+	+
7	Radio-frequency electromagnetic field immunity test	PN-IEC 1000-4-3	PN-IEC 1000-4-3	+	+	+

Remarks to column 5, 6 i 7:
"+" examination is performed; "-" examination isn't performed.

The nuclear electromagnetic pulse and lightning electromagnetic test weren't done.

The purpose of the test was to check station resistance to the electrostatic discharge as may occur when personnel direct or indirect (by neighbourhood's devices) touch the appliance. First, the resistance of the system was to be checked, while generating discharges to the cover. Second the discharge was generated to the Horizontal Coupling Plane (HCP). Therefore, checked the product resistance to the pulse of short duration generated by switching contacts or short circuits in electric equipment and conducted to the product. The purpose of the test was to check station resistance to short-duration interference generated by switching contacts and short circuits and conducted to the equipment.

Furthermore purpose of the test was to check station resistance to discharge pulses existing in power lines indicated by nuclear explosive, atmospheric pulse lighting and switching inductive or capacitive contacts.

The latter three of the tests were made using coupling/decoupling network to AC line and capacitive coupling network to input line (reference electrode circuit) and output line (anode circuit).

The last immunity test was to check station resistance to electromagnetic field (E-field) indicated by radio and radar transmitters stations. The test signals are radiated by parallel plate lines powered by power signal generator (1 kW). The field intensity were measured using fibre optical to separate measuring devices. During the tests, station with models reference electrodes, anodes and ship's hull in tank poured by sea water was placed in area of parallel plate.

Electrical disturbance emission was the second group of tests. This test methods were used to verify that electromagnetic emission from the station do not exceed the specified conducted and radiated requirements showed in table 1.

Table 3 Results of measurements

Nr	Requirements	Test definition	Results of measurements
1	Electro Static Discharge: - indirect discharge to HCP - direct discharge to cover	6 kV 8 kV	Favourably *) Favourably
2	Fast transient 5/50 ns induced in: 1. AC line L 2. AC line N 3. PE line 4. Input line - reference electrode 5. Output line — anode circuit	Polarisation "±" 2.0 kV 2.0 kV 2.0 kV 0.5 kV 1.0 kV	Favourably Favourably Favourably Favourably Favourably
3	Damped sinusoid test wave form 1 MHz: 1. AC line L 2. AC line N 3. PE line 4. Input line - reference electrode 5. Output line — anode circuit	Polarisation "±" 1.0 kV 1.0 kV 1.0 kV 0.5 kV 1.0 kV	Favourably Favourably Favourably Favourably Favourably
4	High energy 1,2/50μs pulse induced in power lines L & N	Polar. "±" 2.0 kV	Favourably
5	Radio-frequency electromagnetic field immunity test: 1 MHz to 30 MHz	≥10 V/m	Favourably
6	Conducted disturbance for frequency bands from 10 kHz to 10 MHz	MIL-STD 461D Requirement CE102	Fig. 2
7	Radiated disturbance for frequency bands from 30 Hz to 100 kHz	MIL-STD 461D Requirement RE101	Fig. 3

*) Definition "favourably" it's mean that the test didn't make interrupts, obstructs, or otherwise degrades or limits the effective performance of station

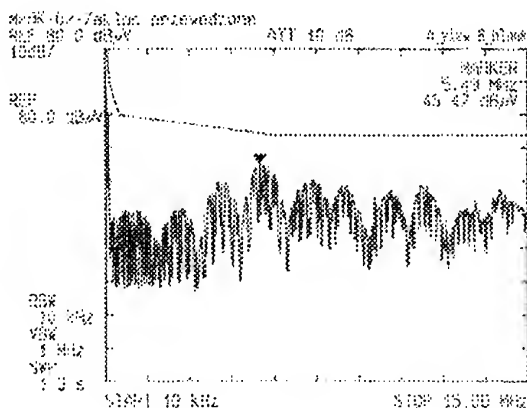


Fig. 2. Conducted disturbance generated by ICCP system for frequency bands from 10 kHz to 10 MHz

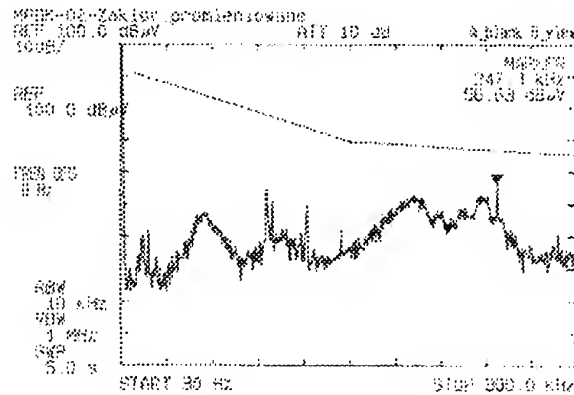


Fig. 3 Radiated disturbance generated by ICCP system for frequency bands from 30 Hz to 100 kHz

5. CONCLUSION

EMC is a necessity for disturbance-free operation of all electrical/electronic apparatus, systems and installations that are to be used in a common electromagnetic environment. ICCP systems are exposed on different influences, among them on electromagnetic noise too. It was necessary to complete specific EMC requirements for specific devices (ICCP-systems) used in specific environment. The results of EMC tests of MPOK-2 ICCP system used on warships have showed that using of compliance engineering in EMC during designing and manufacturing of that system allowed to obtain satisfactory results in immunity and emission.

6. REFERENCES

1. A.Sowa, K. Wincencik : Zabezpieczenie automatycznej stacji ochrony katodowej przed przepięciami. Ochrona przed korozjⁱ. 1994 - nr2.
2. STANAG 4436 Electro-magnetic compatibility testing procedure and requirements for naval electrical and electronic equipment (surface ship, non-metallic hull)
3. PN-E-06074:1974 (PN-74/E-06074) Zespoły prostownikowe bezpieczne - Ogólne wymagania i badania
4. PrPN-V-84000 Okrętowe systemy ochrony katodowej - Ogólne wymagania i badania
5. PN-E-05030-00:1990 (PN-90/E-05030/00) Ochrona przed korozją - Elektrochemiczna ochrona katodowa - Wymagania i badania
6. PN-E-05030-01:1990 (PN-90/E-05030/01) Ochrona przed korozją - Elektrochemiczna ochrona katodowa - Metalowe konstrukcje podziemne - Wymagania i badania
7. PN-E-05030-03:1981 (PN-81/E-05030/03) Ochrona przed korozją - Ochrona katodowa - Ochrona kadłubów statków i obiektów pływających
8. prEN 12473:1996 E General principles of cathodic protection in sea water
9. PN-IEC 801-2:1994 Kompatybilność elektromagnetyczna urządzeń do pomiaru i

sterowania procesami przemysłowymi - Wymagania dotyczące wyładowań elektrostatycznych

10. PN-IEC 801-4:1994 Kompatybilność elektromagnetyczna urządzeń do pomiaru i sterowania procesami przemysłowymi - Wymagania dotyczące serii szybkich elektrycznych zakłóceń impulsowych
11. PN-IEC 1000-4-3:1996 Kompatybilność elektromagnetyczna - Metody badań i pomiarów - Badanie odporności na pole elektromagnetyczne o częstotliwości radiowej
12. WPN-84/N-01001-01008 Aparatura, przyrządy, urządzenia i wyposażenie o przeznaczeniu wojskowym
13. MIL-STD-461D Requirements for the control of electromagnetic interference emissions and susceptibility
14. EN 61000-4-5 Immunity on Pulse Voltage (Surge)

BIOGRAPHICAL NOTES

Krzysztof DYMARKOWSKI received his M.Sc. degree in 1976 and Ph. D. degree in 1992 from the Technical University of Gdańsk both in electroengineering. His technical activity concerns in developing and designing corrosion protection systems.

Władysław OBROCHTA received the M.Sc. degree in 1974 in Technical Military University in Warsaw. His research interests include EMC testing of special marine electric and electronic devices.

Jerzy UCZCIWEK was graduated from the Technical Military University in Warsaw in 1975. He received the Ph. D. degree in 1996 from the Naval Academy in Gdynia. His research interests are in measurement and analysis of electromagnetic fields.

Ryszard ZAJĄC received his M.Sc. degree in 1970 and Ph. D. degree in 1978 from the Technical Military University of Warsaw. Now he is the head of department at the R&D Marine Technology Centre in Gdynia. His present scientific interests are all technical problems of EMC.

EVALUATION OF ELECTROMAGNETIC INTERFERENCE FROM ELECTROSURGICAL UNITS

Claudio A. C. Guimarães Jr, Renato Garcia O. and Adroaldo Raizer

Department of Electric Engineering of the Federal University of Santa Catarina (Brazil)
+ GPEB - Grupo de Pesquisas em Engenharia Biomédica

Departamento de Engenharia Elétrica
Universidade Federal de Santa Catarina
Florianópolis - SC
Caixa Postal 5199 - CEP 88040-970
Brazil
Tel: +55 48 331 9872
Fax: +55 48 233 4729

Abstract: The electrosurgical unit is one of the most harmful sources of electromagnetic emissions used during surgery procedures. Its emissions can interfere with other medical equipments installed in the same environment, like patient-connected devices, which are the most susceptible devices to electromagnetic interference -EMI- problems. These problems had or could have had life-threatening consequences for patients and medical staff, thus justifying the need for studying this subject. The main goals of this work are: to quantify with special equipments (spectrum analyser, antenna and a Line Impedance Stabilization Network -LISN) the electromagnetic emissions (conducted and radiated) of an Electrosurgical Unit -ESU-, to verify if these emissions are in accordance with the Electromagnetic Compatibility -EMC- standards for medical devices and, based on this analysis, to propose a set of alternatives do reduce the EMI generated by Electrosurgical Units. The results of the measurements of the electromagnetic emissions from an ESU prove that its emissions are greater than the emissions thresholds imposed by the EMC standards for medical devices.

1. INTRODUCTION

The operation of electronic equipments generates electromagnetic waves that spread for conduction, for radiation or for a combination of these two ways. The "electromagnetic pollution" produced by these emissions can interfere with other equipments which are near of the source of electromagnetic emissions. Depending on the number of equipments installed in the same environment, the problems of electromagnetic interference can become more hostile than those caused due to the operation of only one equipment.

Due to the growing use of electronic equipments in hospitals, the electromagnetic interference among

equipments is one of the most dangerous problems of electrical-nature that has been observed during surgery procedures. A study accomplished during three months with the professionals of a hospital located in São Paulo (a Brazilian state) showed that 47% of electrical-nature problems during surgery procedures are due to electromagnetic interference with equipments [1].

These problems had or could have had life-threatening consequences. Because of this, it is important that engineering and medical staff are aware of some of the complex interactions these devices can create. Managing this emerging problem should be a concern for the medical community and engineering staff should be able to communicate effectively with medical staff, patients, and visitors regarding potential interactions and how to recognize them and mitigate their consequences, thus justifying the need for studying this subject [2].

The great incidence of electromagnetic interference problems in surgery rooms is justified because in these environments are installed some devices which are the most susceptible to electromagnetic interference, like patient-connected equipments and other which are the most harmful sources of EMI, like electrosurgical units and perfusion machines. Because of this, it is important to evaluate the "electromagnetic pollution" generated by the devices installed in this environment in order to mitigate electromagnetic interference problems.

2. ELECTROSURGICAL UNITS

The electrosurgical units (Fig. 1) are devices used for cutting and coagulating human tissues during surgery procedures and they are harmful sources of electromagnetic interference because their operation generates high energy (300 watts of power for some procedures) and broadband emissions which can spread for conduction or radiation.

The cutting and/or coagulating of the tissues during electrosurgical procedures happens because of the 0.5-2 MHz radio-frequency current which is delivered to the tissue by a hand-held probe (active electrode in Fig. 1). The large-area passive electrode provides a safe return path for the electrosurgical current which spreads through the human body (a conduction path for electromagnetic emissions) [3].

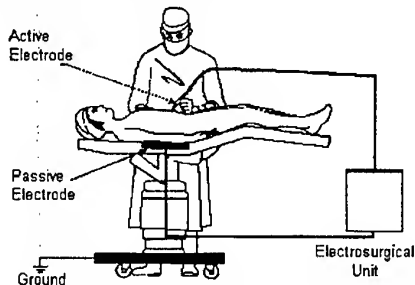


Fig. 1. Electrosurgical unit [3]

The cutting and coagulating of human tissues performed with electrosurgical units can be provided by selecting one of its modes of operation. These modes are: CUT, COAG and BLEND (a combination of cutting and coagulating).

When used in the CUT mode, the ESU which was evaluated produces a waveform that is almost a pure sinusoid, with a fundamental frequency around 500 kHz. When used in the COAG mode, the ESU produces a waveform that consists of short bursts of radio frequency energy. When used in the BLEND mode, the ESU produces a waveform that can be modeled as a 500 kHz sinusoid. Fig. 2 shows these waveforms.

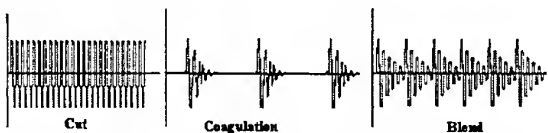


Fig. 2. Electrosurgical Emissions Waves [3]

3. ELECTROSURGICAL EMISSIONS

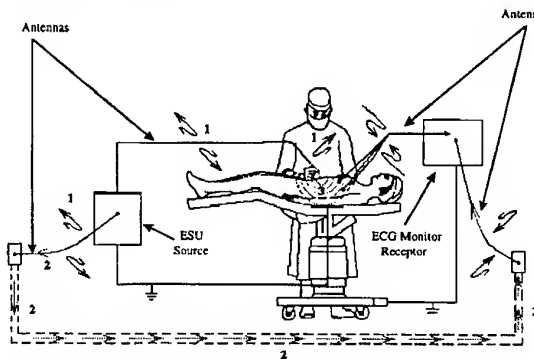
The Fig. 3 shows an electrosurgical unit during a surgery procedure and the ways its electromagnetic emissions can propagate and interfere with an electrocardiograph -ECG- monitoring equipment (a patient-connected device).

The ECG monitoring devices are used to monitor biopotential signals with small amplitudes (between 1mV and 10mV). These signals are captured by electrodes which are connected to the patient through cables attached to the monitor (see Fig. 3). The cables can act just like antennas¹, which means that they can capture the electromagnetic emissions radiated in the environment (like the one generated by the ESU).

Besides, the electrodes connected to the patient can capture, with the biopotential signals, the

electrosurgical signals generated because of the high frequency electrosurgical currents conducted through the patient body. These signals, as well as the one radiated through the air, after being received by the ECG monitor, can be misunderstood as biological signal, degrading the performance of the equipment. To solve this problem, the medical staff must keep the ECG electrodes as far as it is possible from the ESU active electrode. This same procedure can be adopted in relation to the position of the ESU, which must be placed far away from the most susceptible devices.

The AC network provides another conduction way for the propagation of electrosurgical emissions. These emissions can reach the ECG monitor through its AC cable and interfere with its performance. Because of this, it is recommended to design filters within the cables and to design independent circuits (AC network) to provide the energy for the most harmful sources of electromagnetic interference.



- 1 - Radiated Emissions from ESU
- 2 - Conducted Emissions from ESU Through AC Network
- 3 - Conducted Emissions from ESU Through Patient Body

Fig. 3. Propagation of the electromagnetic emissions of an ESU.

4. ELECTROMAGNETIC COMPATIBILITY

"Electromagnetic compatibility" is used to describe a condition wherein electrical and electronic equipments operate successfully together or in close proximity [3]. The best way of assuring the electromagnetic compatibility of medical devices is to guarantee that these devices comply with the EMC standards for medical devices, which determine thresholds for electromagnetic emissions and for the immunity of the equipments.

At the present time the IEC 601-1-2² is the most accepted standard for medical devices. Besides imposing thresholds for electromagnetic emissions and immunity, this standard proposes tests methods to verify the compatibility of the equipments and specifies the

² Recognized as "Medical Electrical Equipment - Part 1: General requirements for safety - 2. Collateral Standard: Electromagnetic compatibility - Requirements and tests" [5].

¹ Any conductor can act like an antenna if it is longer than 1/20 of the wave-length of the radiated signal [4].

devices that must be used to make the measurements of the electromagnetic emissions and immunity of equipments under tests.

When compliance tests are performed, there is an assumption that all laboratory accoutrements exist: a radio frequency -RF- isolated environment such as a screened room or an anechoic chamber, discrete frequency and amplitude-controlled RF sources and tests equipments [6].

5. SCOPE OF STUDY

The methodology employed in the following measurements of the electromagnetic emissions of an electrosurgical unit is quite different from those proposed for IEC 601-1-2, because the tests were not performed with all laboratory accoutrements. In spite of this, the measurements can be accepted as pre-compliance tests, whose results can qualify the electrosurgical unit as one of the most harmful source of electromagnetic interference.

Measurements are reported of the electric field strengths emanating by radiation and by conduction from an electrosurgical unit used in the Hospital of the Federal University of Santa Catarina in Brazil. The ESU considered in this study was the Model B-3600 A made by Deltronix, which is a Brazilian manufacturer. This device includes an electrosurgical generator unit and an electrode (electrosurgical knife). To simulate the tissue being operated on was used a bar of soap and the measurement antenna was placed about 1 m from both the active electrode of the ESU and the soap.

6. MEASUREMENT EQUIPMENTS

6.1. Radiated Emissions

Measurements of electromagnetic emissions radiated by the electrosurgical unit were performed with a broadband biconical antenna (EMCO Model nº 93110 B), which is calibrated for use over the frequency range of 30 MHz to 300 MHz. The antenna was placed 1 meter from both the active electrode of the electrosurgical unit and the specimen being operated on and 1 meter high.

To evaluate the largest field strengths emanated, measurements were made with the antenna in vertical polarization and in horizontal polarization (see Fig. 4).

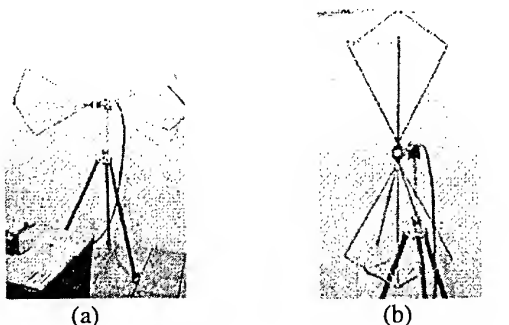


Fig. 4.(a) horizontal and (b) vertical polarizations.

The broadband biconical antenna (EMCO Model nº 93110 B) was used in conjunction with a Spectrum Analyser (Model HP 8591 EM) and a Pre-Amplifier (Model 8447 F POT H 64) to amplify the antenna signal. To evaluate the emissions radiated from the electrosurgical unit, measurements were made from 30 MHz to 300 MHz, which is the frequency range of operation of the antenna. This range was chosen because of the EMC standards for medical devices, which determine radiated emissions thresholds for this range of frequencies.

6.2. Conducted Emissions

The conducted emissions of the electrosurgical unit (ESU) were measured with a Line Impedance Stabilization Network -LISN- (Model 3810/2) in conjunction with a Spectrum Analyser (Model HP 8591 EM) and a Transient Limiter (Model HP 11947 A). The conducted emissions measurements procedure is shown in Fig. 5 and the frequency range of the measurements was from 150 kHz to 30 MHz.

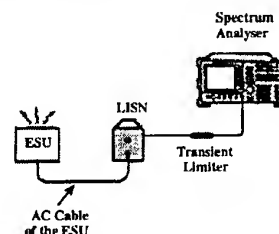


Fig. 5. Conducted emissions measurements procedure.

7. TEST ENVIRONMENT

The pre-compliance measurements were not performed in a surgery room since the intention of this work was to quantify only the ESU emissions, instead of measuring the electromagnetic emissions generated by other medical devices installed in the same ESU's environment. The measurements were made in the Electromagnetic Compatibility Laboratory, which is a 15 m² room, at the Electric Engineering Department of the Federal University of Santa Catarina, in Brazil. Fig. 6 shows the measurement environment, the test equipments and the ESU.

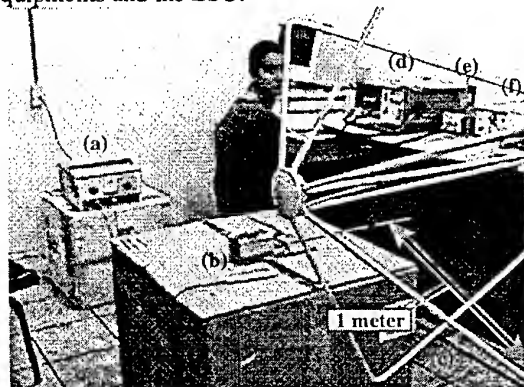


Fig. 6. (a) ESU; (b) specimen operated; (c) antenna; (d) spectrum analyser; (e) pre-amplifier; (f) LISN.

8. MEASUREMENT RESULTS

The ESU's emissions must comply with the emissions limits imposed by the EMC standard for medical device "IEC 601-1-2", which references CISPR 11 for emissions requirements, only when the equipment (ESU) is in the STAND-BY mode (energized but not cutting or coagulating tissues). Although, the electromagnetic emissions measurements were made for the STAND-BY (with cables attached), CUT, COAG and BLEND modes of the ESU.

Each of the three ESU operation modes can be used with different output power levels. Measurements were made for the CUT, COAG and BLEND modes of the ESU with two power settings³ used for each mode. The maximum power level is used for delicate surgery procedures (like during transurethral resection, an urological surgery), while the minimum power level is recommended for general surgeries.

8.1. Radiated Emissions

As mentioned above, the electromagnetic emissions radiated from the ESU (in STAND-BY, CUT, COAG and BLEND modes) were measured with an antenna placed 1 meter away from the specimen being operated. Measurements were performed with the antenna in vertical and horizontal polarization and the results were compared with the thresholds imposed by the EMC standard for medical devices (IEC 601-1-2).

The measurement results show that energy of the electromagnetic emissions radiated from the ESU are higher when the antenna is in the horizontal polarization. Besides, the highest levels of energy are observed when the ESU is operating in the CUT mode with the highest output power level (200 watts). Fig. 7 shows the spectral analysis of the test environment when the ESU was used in STAND-BY mode and Fig. 8 shows the analysis when the ESU was used in the CUT mode with the highest power level (200 watts). The flat lines in these figures are the electromagnetic emissions thresholds imposed by IEC 601-1-2 standard.

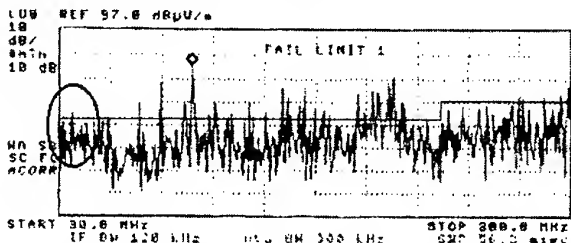


Fig. 7. Spectral analysis of the ESU's emissions in STAND-BY mode.

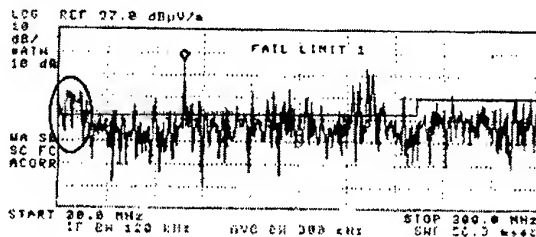


Fig. 8. Spectral analysis of the ESU's emissions in CUT mode with maximum power level (200 watts).

The circles in Fig. 7 and 8 show that spectrum changes are greater at lower frequencies which were captured by the antenna (around 30 MHz). Besides, the energy level of the electromagnetic emissions were greater when the ESU was used in the CUT mode.

8.2. Conducted Emissions

The electromagnetic emissions conducted from the ESU through the AC network were measured with a LISN device in conjunction with the Spectrum Analyser and the results were compared with the thresholds imposed by IEC 601-1-2, which references CISPR 11. Fig. 9 shows the CISPR 11 conducted thresholds and the spectral analysis of the conducted emissions of the ESU in STAND-BY mode, while Fig. 10 shows the same analysis with the ESU operating in the CUT mode with the highest power level (200 watts).

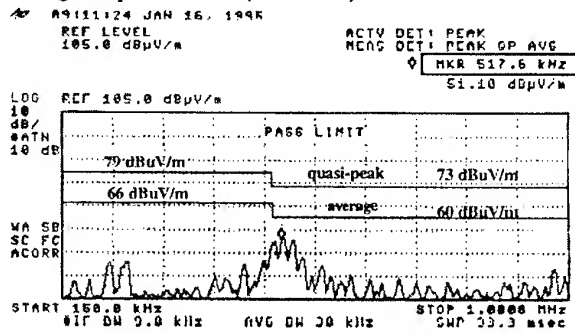


Fig. 9. Spectral analysis of the ESU's conducted emissions in STAND-BY mode.

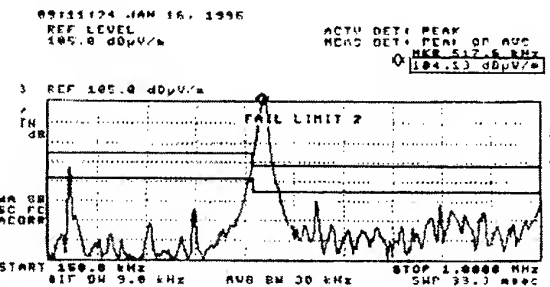


Fig. 10. Spectral analysis of the ESU's conducted emissions in CUT mode (200 watts).

According to Fig. 9, the evaluated ESU⁴ operates with a fundamental frequency of almost 520 kHz (see MKR in Fig. 9 and 10) and its emissions comply with

³ For the CUT and BLEND modes were used power settings of 200 watts (the maximum power chosen) and 30 watts (the minimum power chosen). For the COAG mode were used power settings of 70 and 50 watts.

⁴ Model B-3600 A manufactured by Deltronix.

the conducted emissions thresholds in the STAND-BY mode. In spite of this, this device does not comply with these thresholds when it is operating in the CUT mode (see Fig. 10). When operating in the CUT mode, the highest energy level is observed at the fundamental frequency of operation of the ESU (about 520 kHz).

The higher energy levels observed after the ESU activation (in CUT mode) suggest that the most harmful sources of electromagnetic interference (like the ESU) in hospitals must be energized by independent circuits (AC networks), instead of being energized by the same circuits of the most susceptible devices (like monitoring devices).

9. REDUCING EMI PROBLEMS

When dealing with any EMI problem, it is important to evaluate sources of electromagnetic emissions, receptors of these emissions and paths coupling these sources to the receptors. All three must exist for there to be a problem and, therefore, eliminating any one of these will eliminate the problem. But in any specific case, some solutions are more practical and less expensive than others [4].

To reduce the undesired effects of the electromagnetic interference among equipments both the source and the receptor of the emissions can be shielded. Although, this solution can be very expensive and, because of this, not practical.

Other solution can be provided by assuring an ineffective path between the source and the receptor of the electromagnetic emissions. This can be done by installing sources (like ESU) as far as it is possible from receptors (like monitoring devices) of electromagnetic emissions. The installation of filters within the AC cables of the equipments is another way of mitigating EMI problems, since they suppress emissions from the equipments and external interference [4].

The manufacturers of electrosurgical units suggest to use the lowest power indicated for each surgery procedure. This measure guarantees that the receptor will receive ESU's emissions with low energy, what will reduce the probability of occurring electromagnetic interference problems. Finally, the ESU must be energized by different circuits from those that energize the most susceptible equipments (like monitoring devices).

10. CONCLUSIONS

Measurements of electric field strengths of the electromagnetic emissions of an electrosurgical unit were made in the Electromagnetic Compatibility Laboratory of UFSC, in Santa Catarina, a brazilian state.

The results of the measurements (see Fig. 7, 8, 9 and 10) of the electromagnetic emissions (radiated and conducted) of an electrosurgical unit, when compared with the thresholds imposed by the EMC standard for medical devices "IEC 601-1-2", prove that electrosurgical units are harmful sources of electromagnetic interference. These devices are usually

installed in surgery rooms, which are places where the malfunction of an equipment due to the interference generated by the ESU's emissions can imply serious risks to the patients and medical staff safety. These results represent the first step to reduce EMI problems due to the operation of ESU, since after the evaluation of them the designers of these devices can propose a set of alternatives to reduce their emissions.

Due to the great number of equipments installed in this hospital environment, it is very hard to eliminate the problems of electromagnetic interference just by assuring the compliance of the electrosurgical units with the thresholds mentioned. It must be clear that the emissions thresholds imposed by IEC 601-1-2 do not guarantee the electromagnetic compatibility of harmful sources of EMI and that they must be used just like a basis for the elaboration of more demanding thresholds for these devices.

11. REFERENCES

- [1] Marcelo Hein, Sérgio Mühlen, "Electrical safety aspects in hospitals" (portuguese), Proceedings of the III National Forum of Science and Technology in Health, São Carlos, Brazil, 1996.
- [2] J. L. Silberberg, "Performance degradation of electronic medical devices due to electromagnetic interference", Compliance Engineering, vol. X, no 5, Fall 1993, pp. 25-39.
- [3] Leslie A. Geddes (ed.), "Handbook of electrical hazards and accidents", CRC Press, Boca Raton, 1995, ch. 5, pp. 129-164.
- [4] William Kimmel, Daryl Gerke, "Electromagnetic compatibility in medical equipment - a guide for designers and installers", Interpharm Press, Buffalo Grove, 1995.
- [5] Gary Fenical, "Current and proposed EMC tests for medical devices", ITEM - The International Journal of EMC, 1997, pp. 78-82.
- [6] W. David Paperman, Y. David, M. Martinez, "Testing for EMC in the clinical environment", Journal of Clinical Engineering, Quest Publishing Co., May/June, 1996, pp. 207-211.

BIOGRAPHICAL NOTE

Claudio A. C. Guimarães Jr was born in Rio Grande do Sul, Brazil in 1973. He received the degree in electrical engineering from the Federal University of Rio Grande do Sul -UFRGS- in 1996 and the M. Sc. degree in electrical engineering in 1998 from the Federal University of Santa Catarina -UFSC-, in Brazil.

Renato Garcia O. was born in Santiago, Chile in 1955. He received the degree in electrical engineering from USACH in 1981, the M.Sc. degree from the Federal University of Santa Catarina -UFSC- in 1986 and the Dr.Sc. degree from UFSC in 1992.

Adroaldo Raizer received the degree in electrical engineering from UFSC in 1985, the M. Sc. degree from UFSC in 1987 and Dr. INPG degree in Grenoble, France in 1991.

Measurement of Voltage Rising Part due to Gap Discharge in Air Using Distributed Constant Line System

Ken KAWAMATA

Department of Electrical Engineering, Hachinohe Institute of Technology,
88-1 Ohbiraki Myo Hachinohe-shi, 031 JAPAN

Shigeki MINEGISHI, Akira HAGA, and Risaburo SATO
Faculty of Engineering, Tohoku Gakuin University,
1-13-1 Chuo Tagajo-shi, 985 JAPAN

Abstract --- Very fast voltage rise curve due to gap discharge was considered in time domain. The measurement system consists of a distributed constant line system and a coaxial electrode, because the voltage transients are very rapid and fluctuations are complicated. The coaxial cables were used as distributed constant lines. The coaxial electrode has matched impedance for a characteristic impedance of the coaxial cables. The atmosphere around the coaxial electrode is normal air. This distributed constant line experimental system enables to measure the high speed and high voltage transients of about 100 ps. As a consequence of the experiment using this measurement system, the voltage rise time was slowed down from about 100 ps to about 400 ps due to increasing of source voltage from 510 V to 1450 V.

1. INTRODUCTION

It is well known that very fast voltage transients are generated at the make and break of switch gears. The voltage transients generate electromagnetic noise and surrounding electrical devices are affected [1]. Gap discharge at the contacts should be considered as a main factor of the electromagnetic noise source [2,3]. The switching phenomena have been studied extensively, but in almost all reports, phenomena at the electric contacts have been investigated from the viewpoint of the contact reliability and the contact materials. So, a great deal of effort has been made on the electromagnetic noise due to gap discharge. What seems to be lacking, however, is experimental results of the transients in order of picosecond time domain [4-9].

The voltage transient due to gap discharge was examined from viewpoint of EMI source as the making of electrical contacts. However, it was difficult to examine the voltage transients due to gap discharge in lumped constant system because the transients were very rapid and fluctuations were complicated. In the first place, we set up a measurement system using the distributed constant line system to observe the high speed transient due to gap discharge. Furthermore, the coupled transmission lines were used to detect the rising part and high frequency phenomena of voltage transients in more detail. Because the macroscopic voltage fluctuation was high voltage and the voltage variation superimposed on the macroscopic fluctuation were very fast, it was difficult to observe them using voltage probes [10-13].

The measurement system consists of a power supply, a coaxial electrode, a directional coupler as coupled transmission lines, coaxial cables as distributed constant lines, and voltage probes. A characteristic of the coaxial electrode, which has a matched impedance for the distributed constant line system, was investigated in the frequency range below 5 GHz. The voltage of power source in experiment was from 800 V to 1450 V.

In this paper, the characteristics of the voltage rise curves in precise observation of the voltage rising part are presented.

2. DISTRIBUTED CONSTANT EXPERIMENTAL SYSTEM

The experimental system using the distributed constant line system shown in Fig.1 was set up. The system consists of a power supply, a coaxial electrode, a

directional coupler (HP778D, 100MHz - 2GHz, 20dB) as coupled transmission lines, coaxial cables (50Ω) as typical distributed constant lines, and voltage probes

(TEKTRONIX P6009, DC-120MHz, 100:1). The directional coupler was used to observe the rise curve and the voltage variation in more detail. The coaxial electrode was connected to the coaxial cable and the directional coupler with the Type-N (50Ω , 11GHz) coaxial connectors. A voltage probe was connected between the contact of source side (①) and the ground, and another probe was connected between the contact of load side (②) and the ground. A BNC (bayonet coupling connector, 50Ω , 4GHz) to probe adapter (TEKTRONIX 013-0054-00) was used for the voltage probe connection so that the effect of the stray capacitance at the probe tip is reduced as much as possible. When the directional coupler was driven by 34ps rise time pulse, it had 39ps rise time (HP54121T, 18GHz).

Fig. 2 shows an axial sectional view of the coaxial electrode. The electrode consists of inner conductors, outer conductor, and the Type-N receptacle connectors. Each conductor was made of copper. The characteristic impedance Z_C is 50Ω . So, impedance matching between the cable and the coaxial electrode was accomplished. The two needle electrodes have radius of curvature of 0.1mm (type I), and 0.9mm (type II), respectively. The plane electrode has a diameter of 20mm.

Fig.3 shows the insertion loss of the electrode measured by a network analyzer (HP8510), where the needle and plane electrodes are connected mechanically. The combination of electrode of source side and load side is needle - plane, and the radius of curvature of needle electrode is 0.9 mm (type II). The insertion loss is within -3dB in the frequency range below 5GHz.

Voltage rise curves and times (10%-90%) at the instance of discharge were observed with a transient digitizer (TEKTRONIX SCD5000, 200GS/s, 4.5GHz). The voltage rise curves were observed at the output of directional coupler (③) through the coaxial attenuator of -20dB and -30dB (DC-12.4GHz), where the combination of electrode and the radius of curvature of needle electrode are changed. Furthermore, the voltage of power source was increased from 800V to 1450V to consider the relation between source voltage and voltage rise times.

3. EXPERIMENTAL RESULTS

Fig.4 shows the voltage rise curves at the instance of discharge, where the voltage of power supply is 800V. In

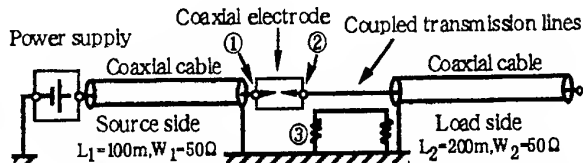


Fig. 1 Experimental system using distributed constant line system.

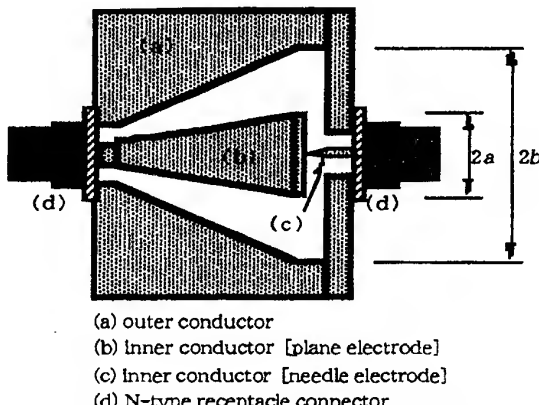


Fig. 2 Construction of the coaxial electrode.

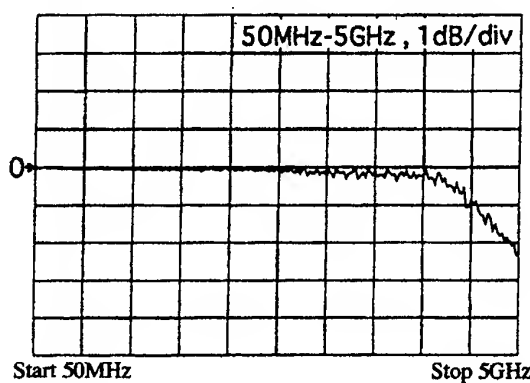
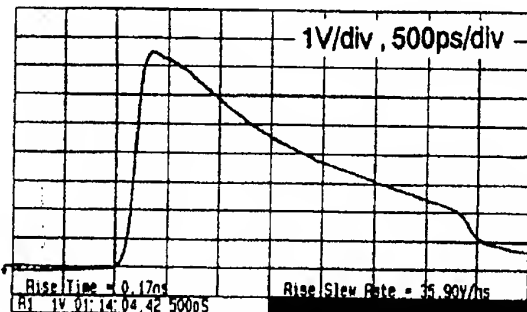


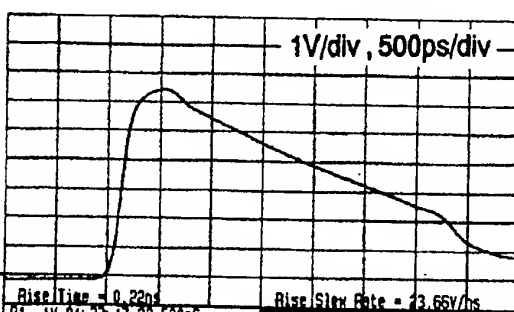
Fig. 3 Insertion loss of the coaxial electrode.

(Type II, 0.9mm needle to the plane electrode.)

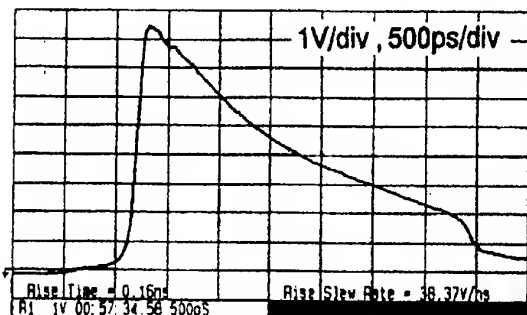
In this figure, the combination of electrode of source side and load side and the radius of curvature of needle electrode are as follows; (a-I) at needle of 0.1mm - plane, (a-II) at needle of 0.9mm - plane, (b-I) at plane - needle of 0.1mm, and (b-II) at plane - needle of 0.9mm. The voltage rise time (a-I), (b-I), (a-II), and (b-II) is about 0.17ns, 0.26ns, 0.16ns, and 0.17ns respectively. In figure (a-II), a small voltage fluctuation was observed prior to reaching a breakdown process. It may be that phenomenon of the small voltage fluctuation is corona discharge. Fig.5 shows a voltage waveform of rising part with the corona discharge in more detail. The combination of electrode is as follows; (a) needle of



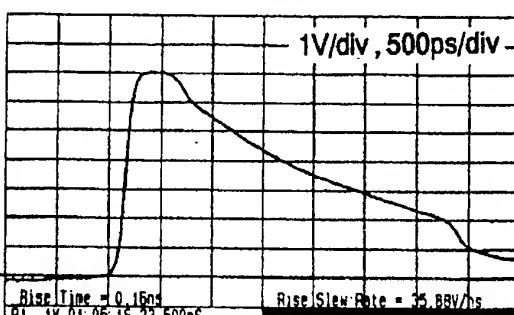
(a-I) Rise curve at needle of 0.1mm - plane.



(b-I) Rise curve at plane - needle of 0.1mm.



(a-II) Rise curve at needle of 0.9mm - plane.



(b-II) Rise curve at plane - needle of 0.9mm.

Fig. 4 Waveform of voltage rise curve at 800V.

0.9mm - plane (type a-II), and (b) plane - needle of 0.9mm (type b-II). When an electrode combination was type (a), a voltage fluctuation due to the corona discharge was observed with comparatively high probability. It is considered as this cause with the benefit that streamer shaped corona becomes easy to occur because a positive leader grows easily when a needle electrode is a positive pole. However, as for this experiment, the sufficient consideration to prove these causes is not present.

The voltage rise times due to increasing of source voltage from 800 V to 1450 V were considered in more precise observation. The relation between source voltage and voltage rise times are shown in Fig.6. The combinations of electrode of source side and load side and the radius of curvature of needle electrode are same as Fig.4. In these figures, a plot is shown by the minimum, maximum and average values of rise times obtained in thirty measurements. The relation between source voltage and voltage rise times (a-I), (b-I), (a-II), and (b-II) is from 250ps to 370ps, from 245ps to 440ps, from 270ps to 400ps, and from 290ps to 395ps respectively. The voltage rise times were slowed down due to increasing of source voltage. These results are different. However, a general trend of the relations between source voltage and voltage rise times is about

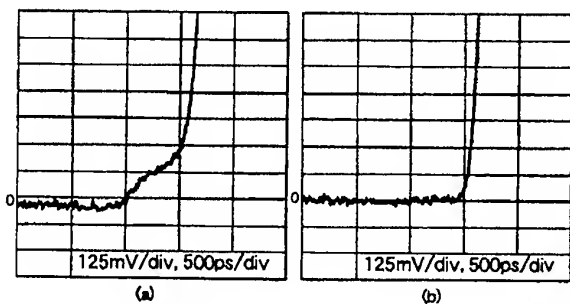
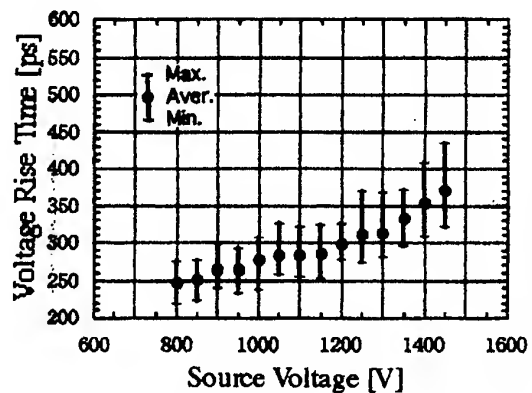
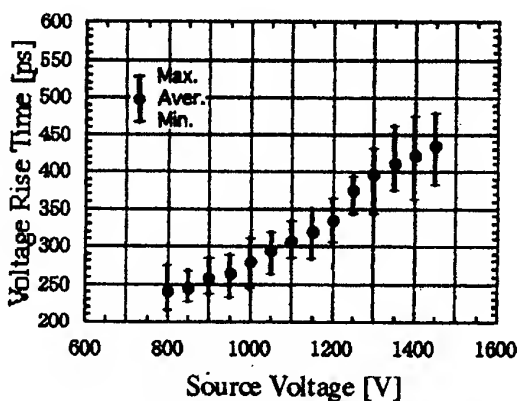


Fig. 5 Waveform of rising part with the corona discharge.
 (a) Combination of electrode is needle of 0.9mm - plane
 (b) Combination of electrode is plane - needle of 0.9mm

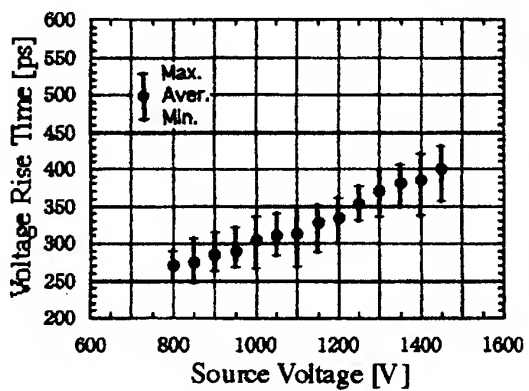
the same. Mutual relationship between source voltage and voltage rise times was sufficiently confirmed from the result of measurements. The cause of the mutual relationship is a relation between a gap distance of electrode and a forward speed of discharge. It is clear that the forward speed of the discharge is almost constant about this electrode of short distance. Voltage rise time is slowed down in proportion to gap distance. These experimental results agree qualitatively with the theory of the forward speed in the nonuniform spark gap discharge.



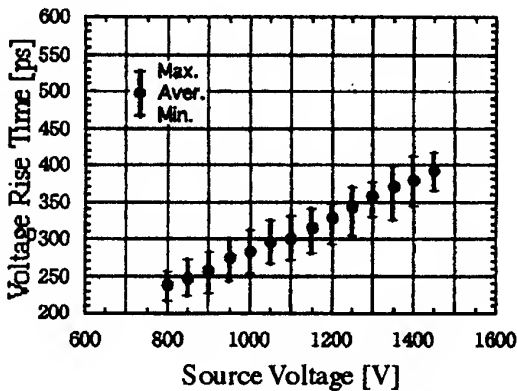
(a-I) Rise time at needle of 0.1mm - plane



(b-I) Rise time at plane - needle of 0.1mm



(a-II) Rise time at needle of 0.9mm - plane

(b-II) Rise time at plane - needle of 0.9mm
(average value of the rise times obtained in thirty measurements)

4. CONCLUSIONS

The very fast voltage rise curve due to gap discharge was considered in time domain using the coupled transmission lines in distributed constant line system.

As a consequence of the experiment using this measurement system, the voltage rise time was slowed down from about 250 ps to about 400 ps due to increasing of source voltage from 800 V to 1450 V.

Mutual relationship between source voltage and voltage rise time was sufficiently confirmed from the result of measurements. The cause of the mutual relationship is a relation between a gap distance of electrode and a forward speed of discharge. It is clear that the forward speed of the discharge is almost constant about this electrode of short distance. Voltage rise time is slowed down in proportion to gap distance. These experimental results agreed

qualitatively with the theory of the forward speed in the nonuniform spark gap discharge.

REFERENCES

1. Donald R. J. White : "EMC Handbook", 1,2,3,4,5, Don White Consultant, Inc. 1973.
2. E.K.Howell: "How Switches Produce Electrical Noise", IEEE Trans. EMC-EMC-21, 3, pp.162-170, Aug. 1979.
3. C.R.Paul: "Introduction to Electromagnetic Compatibility", John Wiley & Sons, Inc. 1992.
4. D.Klapas, R.H.Apperley, R.Hackman and F.A.Benson: "Electromagnetic interference from electric arcs in the frequency range 0.1-1000MHz", IEEE Trans. on Electromagn. Compat., vol.20,no.1,pp.198-202, 1978.
5. R. Wallace: "6GHz time Domain Measurement of Fast Transient Events", Proc. of 1992 IEEE Int'l Symp. on Electromagn. Compat., pp.460-463, Aug. 1992.

6. B.Daout and H. Ryser: "The reproducibility of the rising slope in ESD testing", Proc. of 1986 IEEE Int'l Symp. on Electromagn. Compat., pp.467-474, Aug.1986.
7. K.Arai, W.Janischewskyj and N.Miguchi : "Microgap Discharge Phenomena and Television Interference ", IEEE Trans.Power Appar.& Syst., PAS-104, No.1, 1985.
8. L.M.MacLeod and K.G.Balmain: "Compact Traveling-Wave Physical Simulator for Human ESD", IEEE Trans. on Electromagn. Compat., vol. 39, no. 2, pp. 89-99, May 1997.
9. E.J.M. van Heesch, M.H.P. Dagelinckx, F.M. van Gompel and P.P.M. Blom :"Surge Corona Propagating Along a Transmission Line", 9 th Int'l. Symp. High Voltage Eng. (ISH), 2793, Sept. 1995.
- 10.Y. Kami and R. Sato: "Circuit-Concept Approach to Externally Excited Transmission Lines", IEEE Trans. on Electromagn. Compat., vol. 27, no. 4, pp. 177-183, May 1985.
- 11.S. Frankel: "Multiconductor Transmission Line Analysis", Artech House, Inc. 1997.
- 12.G.Wanninger: "Antennas as Coupling Devices for UHF Diagnostics in GIS", 9 th Int'l. Symp. High Voltage Eng. (ISH), 5625, Sept. 1995.
- 13.D.Wenzel, U.Schichler, H.Boris and E. Gockenbach: "Recognition of Partial Discharge on Power Units by Directional Coupling", 9 th Int'l. Symp. High Voltage Eng. (ISH), 5626, Sept. 1995.

BRIEF BIOGRAPHY OF AUTHORS

Ken Kawamata was born 1965, in Japan. He received the B.S., and M.S., degree in engineering from Tohoku Gakuin University in 1987, and 1989, respectively. He joined Tohoku Electric Power Co. in same year. He has been a Research Associate in the Faculty of Engineering, Hachinohe Institute of Technology since April 1992. He has Doctor of Engineering degree. He research discharge noises in electrical contacts and application of distributed constant system in connection with the electromagnetic compatibility.

Dr. Kawamata is member of the Institute of Electronics, Information and Communication Engineers of Japan; and the Institute of Electrical Engineers of Japan.

Shigeaki Minegishi was born 1951, in Japan. He received the B.S., M.S., and Doctor degree in engineering from Tohoku Gakuin University in 1976, 1978, and 1981 respectively. He became a Research Associate in April of same year; and after served as a Lecturer, he has been an Associate Professor since April 1989 at the Faculty of

Engineering, Tohoku Gakuin University. He research measurement method of transient processes in interrupting of current, discharge noises in electrical contacts and application of distributed constant system in connection with the electromagnetic compatibility.

Dr. Minegishi is member of the Institute of Electronics, Information and Communication Engineers of Japan; and the Institute of Electrical Engineers of Japan.

Akira Haga was born 1944, in Japan. He received the B.S., and M.S., degree in engineering from Tohoku Gakuin University, and Yamagata University in 1968, and 1970, respectively. He joined Technical Research Laboratory of Citizen Watch Co., Ltd in April of same year. He became a Research Associate in April of 1972; and after served as a Lecturer, Associate Professor, he has been a Professor since April 1992 at the Faculty of Engineering, Tohoku Gakuin University. He has Doctor of Engineering degree. He research on magnetic application and connection with the electromagnetic compatibility.

Dr. Haga is member of Japan Applied Magnetism Society; Institute of Electronics, Information and Communication Engineers of Japan; and the Institute of Electrical Engineers of Japan.

Risaburo Sato was born 1921, in Japan. He received the B.S. degree in engineering from Tohoku University in 1944. After served an Associate Professor, he became a Professor in 1961 at the Faculty of Engineering, Tohoku University. He retired from the Tohoku University in March 1984. He has been a Dean of the Faculty of Engineering, Tohoku Gakuin University since April of the same year. He has Doctor of Engineering degree.

He has been engaged in research and education on high-frequency transmission. The contents of research cover many branches such as distributed constant circuits, instrument transformers for communications, antenna design, electromagnetic compatibility, satellite-utilized computer networks, etc. For these researches, he has received Papers Awards from the Institute of Electronics, Information and Communication Engineers of Japan (IEICE of Japan); and the Institute of Electrical Engineers of Japan (IEE of Japan); Institute of Television Engineers of Japan (ITE of Japan); and IEEE-MITS.

He has served as a member of Radio Technology Council; Vice President of the IEICE of Japan; and a member of Science Council of Japan. For these distinguished services, he has received a Commendation of Minister of Posts and Telecommunication; an Achievement Award of the IEICE of Japan; and an Achievement Award of IEEE.

Dr. Sato is member of Institute of the IEICE of Japan; the ITE of Japan; and the IEE of Japan. He is a Fellow of IEEE EMC-S.

A Study on Evaluation Method of Showering Noise

- From the Viewpoint of the Circuit Malfunction due to Showering Noise in Consideration of the Number of Contact Operations -

Shuichi NITTA, Atsuo MUTOH, Kiyotomi MIYAJIMA

Faculty of Technology

Tokyo University of Agriculture & Technology

2-24-16 Naka-cho Koganei Tokyo 184-8858, JAPAN

The authors describe that the malfunction conditions (due to the showering noise which generates when relay contact is turned off) of digital IC change with the number of contact operations, and what parameters featuring the showering noise waveforms influence the digital IC's malfunction, and propose the evaluation index of showering noise and proves the proposed index is effective.

1. INTRODUCTION

Many research results have been reported about showering noise generated when relay contact is turned off. Most of the researches have described the relationship between the contact material and the showering noise[1][2], the measurement results of frequency spectrum of showering noise[3] and the noise induced in circuits due to showering noise.[4][5][6]

However, the above researches have neglected the influence of the number of contact operations on the showering noise's characteristics such as waveforms. While, the authors clarified that the surface conditions of contact and the showering waveforms change with the number of contact operations[7][8], but didn't clarify the influence of the number of contact operations on the noise induced in circuit by showering noise and the method to evaluate the showering noise from the viewpoint of the circuit malfunction due to the induced noise.

In this paper, the authors show that the malfunction conditions (specially, due to the noise induced in circuit by

capacitive coupling with showering noise) of digital IC change with the number of contact operations, and what parameters featuring the showering noise waveforms influence the digital IC's malfunction, and propose the evaluation index of showering noise and prove the proposed index is effective for evaluating the showering noise.

2. THE INFLUENCE OF THE NUMBER OF CONTACT OPERATIONS ON THE DIGITAL IC'S MALFUNCTION

The experimental apparatus shown in Fig. 1 is composed of two loop antennas standing vertically ② and lying horizontally ① (connected to clock terminal of counter) to receive the noises radiated from the relay contact which is opening, the noise generator made up of relay contact, inductive load, DC power supply and the counter IC (CMOS M4040B) to count the number of malfunctions due to noise radiated from the noise generator for one-time opening operation of relay contact, and has high susceptibility for noise coming to clock terminal since the impedance of clock terminal is high ($1\text{ M}\Omega$) and the loop area of antenna is large (50mm x 60mm), and the impedance of DC power supply terminal is low and the loop area of power supply wiring is small.

Fig. 2 shows the relationship between the number of contact operations and the number of circuit's malfunctions. In Fig. 2, C1 and C2 show the number of malfunctions due to the noise induced on antenna ① and due to the noise

induced on antenna ②, respectively, where, the number of malfunctions shows the number stored in counter for one-time showering noise.

Fig. 3 (a) and (b) show typical examples of noise voltage waveform observed at clock input terminal received by antenna ① and ②, respectively. Fig. 3 (a) shows the same voltage waveform as the showering noise voltage (refer to Fig. 4) observed across relay contact which is opening. However, the waveforms specified by "mark A" are observed in Fig. 3 (b). This noise waveform synchronizes with impulsive arc discharge current which flows across relay contacts synchronously with dielectric breakdown of relay contact which is opening. It can be understood from Fig. 3 and

the direction of electric/magnetic field generated by showering noise that antenna ① receives the capacitive coupling noise with showering noise and antenna ② receives the inductive coupling noise mainly. The noise voltage in Fig. 2 (a) is about 1/100 of showering noise voltage across contact.

From the above investigation of Fig. 3 and the fact that the number of malfunction of circuit connected to antenna ① is many in comparison with the number of malfunctions of circuit connected to antenna ②, it is said that the capacitive coupling noise to antenna ① dominates the circuit malfunction.

3. THE RELATIONSHIP BETWEEN THE NUMBER OF CIRCUIT'S MALFUNCTION AND THE PARAMETERS FEATURING THE SHOWERING NOISE

Fig. 4 shows the definition of the parameters featuring the showering noise waveforms which change with the number of contact operations.

Fig. 5, 6, 7 and 8 show the relationship between the parameters of continuous time Tt of showering noise, discharge time Td of making/breaking, number d of making/breaking

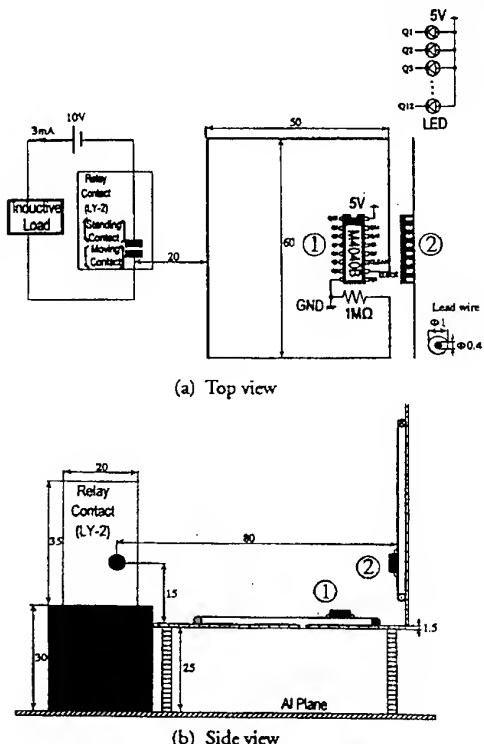


Fig. 1 Experimental apparatus

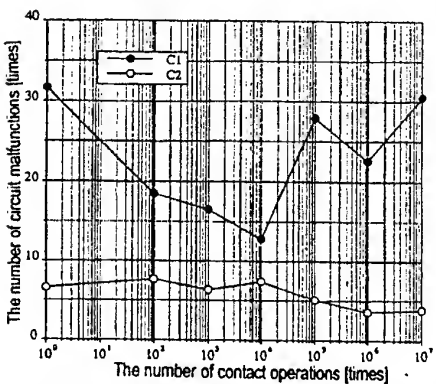
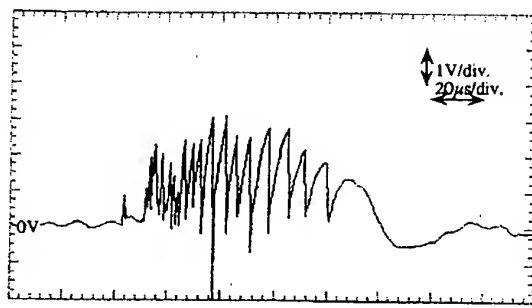
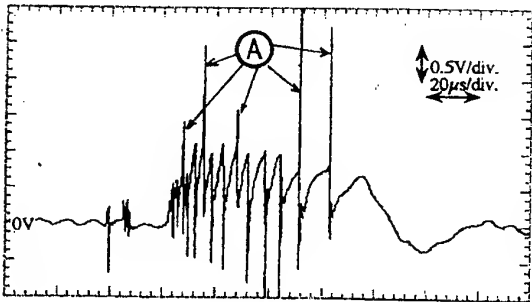


Fig. 2 The relationship between the number of contact operations and the number of circuit malfunctions



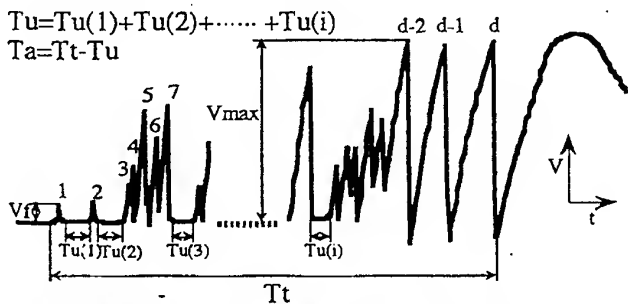
(a) Received waveform by antenna ①



(b) Received waveform by antenna ②
Fig. 3 Noise voltage waveforms

breaking and maximum discharge voltage V_{max} and the number of circuit malfunction, respectively. From Fig. 5, 6, 7 and 8, the number C_2 of circuit malfunctions due to induced noise on antenna ② has no relation to these parameters representing the showering noise waveforms. In Fig. 5 and 6, it looks like that the number C_1 of circuit malfunctions due to induced noise on antenna ① increases with T_t and T_a , but the correlation of T_t and T_a to C_1 is not clear. In Fig. 7, C_1 and d are mutually correlated at significant level 0.01. In Fig. 8, C_1 has a tendency that C_1 decreases with the increase of V_{max} .

From the above, it is concluded that C_1 is related to d , and C_2 is not related to showering noise waveforms. In Fig. 7, C_1 is larger than d . This phenomenon is due to the cause that the count of C_1 was done at different time from the measurement of showering noise waveforms and the showering noise would be suppressed by connecting the probe of oscilloscope to relay contact at measurement.



- The number of times of short circuit being formed (the number of condition) i : The number of times of generation of the phenomena that contact forms short circuit again after voltage between anode and cathode goes up during contact's being open. It is supposed that these phenomena are caused by the formation of short circuit between anode and cathode due to arc-discharge.
- Continuous time of showering noise: T_t
- Discharge time of making/breaking: T_a
- Time forming short circuit: T_u
- The number of making/breaking discharge phenomena: d
- First firing potential: V_f

Fig.4 The definition of the parameters featuring the showering noise waveforms

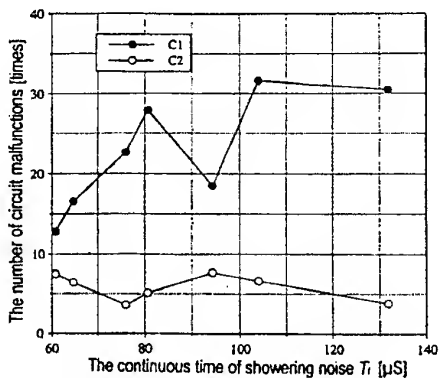


Fig.5 The relationship between the continuous time of showering noise and the number of circuit malfunctions

4. PROPOSAL OF EVALUATION INDEX

Fig. 9 shows an example of the showering noise waveforms observed by digital oscilloscope. Point • shows a sampled voltage stored in memory of oscilloscope. From the above results shown in chapter 3, the authors propose the following evaluation index L for showering noise, referring to Fig. 9.

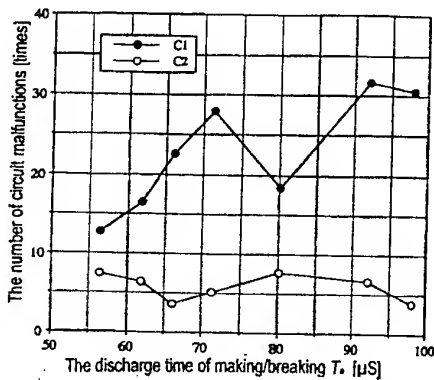


Fig.6 The relationship between the discharge time of making/breaking and the number of circuit malfunctions

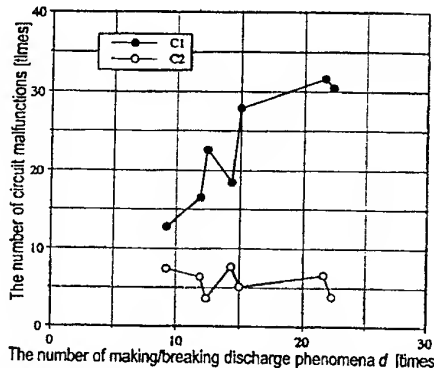


Fig.7 The relationship between the number of making/breaking and the number of circuit malfunctions

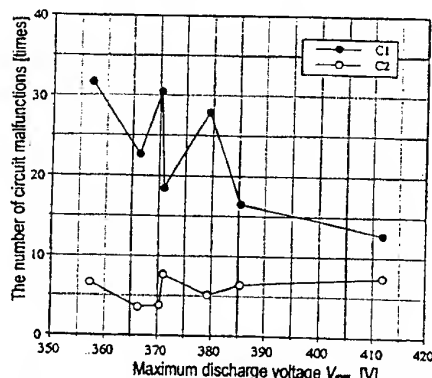


Fig.8 The relationship between the maximum discharge voltage and the number of circuit malfunctions

$$L = \sum_{n=1}^N \sqrt{\left\{ \frac{f(t_n + dt) - f(t_n)}{V} \right\}^2 + \left(\frac{dt}{T} \right)^2}$$

where, N : The number of sampling (times)

V : Measurable voltage range of
oscilloscope (V)

T : $N \times dt$ (sec.)

$f(t)$: Voltage recorded in oscilloscope
memory at time t (sec.)

L represents the distance from one sampled point to next sampled point, as shown in Fig. 10. That is, as the amplitude of noise is larger and the frequency of noise is higher, as L should be bigger. In order to confirm the above characteristics of L , the relationships between the evalua-

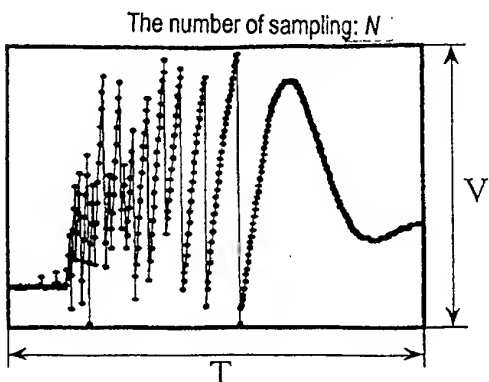


Fig.9 An example of showering noise voltage waveforms

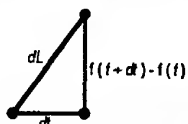


Fig.10 The principle of evaluation index

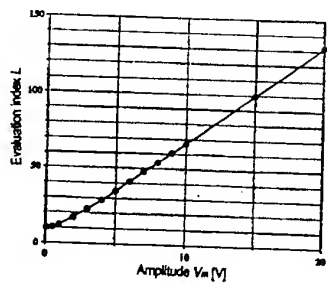


Fig.11 The characteristics of L for amplitude of sinusoidal voltage

tion index L , and the amplitude, the frequency and the phase angle of sinusoidal voltage are calculated and shown in Fig. 11, 12 and 13, respectively. From Fig. 13, it is understood that phase angle doesn't influence the malfunction of victim circuit so much, although we know this fact by experience. From Fig. 11 and 12, it is understood that L represents the degree of the influence of showering noise on malfunction of victim circuit.

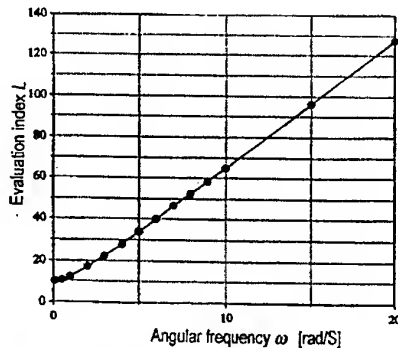


Fig.12 The characteristics of L for angular frequency of sinusoidal voltage

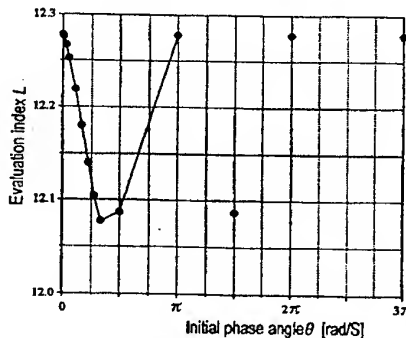


Fig.13 The characteristics of L for phase angle of sinusoidal voltage

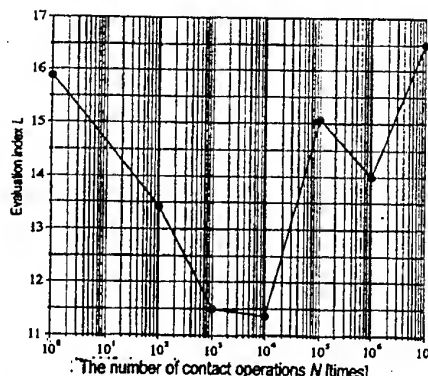


Fig.14 The relationship between the number of contact operations and the evaluation Index L

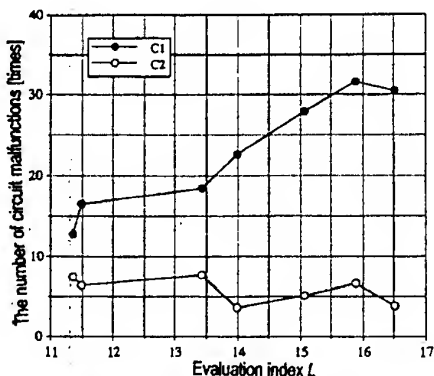


Fig.15 The relationship between the evaluation index L and the number of contact malfunctions

Fig. 14 and 15 show the relationship between L , and the number of contact operations and the number of circuit malfunctions, respectively. In Fig. 15, the number C1 of circuit malfunction is in proportion to L and these two factors have correlation in significant level of 0.001. And, L shows better agreement with the number C1 of circuit malfunctions than T_a in Fig. 6. However, the number C2 of circuit malfunction and L have no correlation. This shows that the circuit malfunction C2 can't be evaluated by showering noise waveforms.

5. CONCLUSIONS

From the above mentioned, it is concluded that the influence of showering noise on circuit's malfunction changes with the number of contact operations and the our proposed evaluation index is effective for evaluating the influence of showering noise on circuit's malfunction.

Future issue is to propose the index of showering noise to evaluate the influence of showering noise on C2 (inductive coupling noise).

References

- [1] K. Uchimura, T. Aida and T. Takagi, "Showering Arcs in breaking Au, Ag, Pb and W contacts and radio noise caused by these arcs," Proc. 1984 Int'l Symp. on EMC, Tokyo, Japan, pp.91-96, 1984
- [2] H. Sone and T. Takagi, "Role of the metallic phase arc discharge on arc corrosion in Ag contacts," IEEE Trans. Components,

- Hybrids & Manuf. Technol., vol.13, no.1, pp.13-19, March 1979
- [3] S. Minegishi, H. Echigo and R. Sato, "Frequency spectra of the arc current due to opening electric contacts in air," IEEE Trans. EMC., vol.36, no.3, pp.244-247, 1994
 - [4] T. Takagi and H. Inoue, "Induced Electromagnetic noise from contact discharge measurement and statistical characteristics," Proc. IEEE Symp. on EMC, pp.345-350, 1980
 - [5] K. Uchimura and H. Fujita, "Induced noise properties caused by circuit interruption with electric contacts," IEICE Trans. Electron., vol.E-74, no.7, pp.1935-1940, 1991
 - [6] T. Aida, K. Uchimura, T. Noguchi and S. Ogata, "Effect of alloying elements on the radio noise characteristics of silver based alloy contacts," Proc. 1984 Int'l Symp. on EMC., Tokyo, Japan, pp.79-84, 1984
 - [7] S. Nitta, A. Mutoh and K. Miyajima, "Generation mechanism of showering noise waveforms - Effect of contact surface variations and moving velocity of contact -," Trans. IEICE, vol.E-79B, no.4, Apr. 1996, pp.468-473
 - [8] K. Miyajima, S. Nitta and A. Mutoh, "A proposal on contact surface model of electromagnetic relays - Based on change in showering arc waveforms with the number of contact operations -," Trans. IEICE, vol.E81-B, No.3, Mar. 1998

Biography

Shuichi Nitta received B.S.E.E. from Kyoto University, Kyoto, Japan, and Ph. D. from the University of Tokyo, Tokyo, Japan, in 1960 and 1978, respectively. After working for electrical industry as system engineer and quality assurance manager in the area of process computer from 1960, he is currently a professor at Tokyo University of Agriculture and Technology since 1985. His research interests are EMC, System maintainability and safety. Dr. Nitta is a member of IEEE, IEEJ, IEICE, SICEJ, REAJ, JSME, JSFE and AFSMI.

Atsuo Mutoh was born on April 5, 1966 in Fukushima, Japan. He received B.E., M.E. and Ph.D. degrees from Tokyo University of Agriculture and Technology, Tokyo, Japan in 1989, 1991 and 1994, respectively. He is currently a research associate at Tokyo University of Agriculture and Technology since 1994. His research interest is EMC. Dr. Mutoh is a member of IEEE, IEEJ, IEICE, SICEJ and ISOC.

Kiyotomi Miyajima was born on September 19, 1972 in Osaka, Japan. He received the B.E. and M.E. degree from Tokyo University of Agriculture and Technology, Tokyo, Japan in 1995 and 1997, respectively. He currently works for Central Research Institute of Electric Power Industry. Mr. Miyajima is a member of IEICE.

DISTURBANCE VOLTAGE ON MAINS TERMINALS OF THE EQUIPMENT USED IN CABLED DISTRIBUTION SYSTEMS FOR TELEVISION AND SOUND SIGNALS

Anushka Stantcheva, Stanislav Petrov, Bisser Stantchev

Institute for Scientific Research in Telecommunication, 8, Haidushka Poliana Str., 1612 Sofia, Bulgaria

1. ABSTRACT

With regard to the European Community Council Directive on Electromagnetic Compatibility (EMC) 83/336 EEC all products, including equipment of cabled distribution systems for television and sound signals, have to meet requirements, such as RF emission and immunity.

All companies will meet those requirements when developing new products. They would be taken into account during the product design, also preliminary tests should be performed during development.

Equipment of cabled distribution systems are subject to the EN 50083-2. The EMC performances of such equipment are closely correlated with quality of the distributed television signals.

The level of disturbance voltage on mains terminals of the equipment was investigated and statistically estimated.

As a result appropriate conclusions about the compliance were made.

2. INTRODUCTION

Distribution of signals in cabled distribution systems for television and sound signals (CATV) is carried out in frequency bands, which cover both the frequencies of the television ranges and the frequencies used from different amateurs, civil and special radioservices.

The problem of decreasing of disturbances, due to unwanted emission from CATV, impose introducing of norms and developing of methods for

measurement of disturbance voltage, injected into the mains by the CATV equipment.

In this paper the investigations of the mains terminals disturbance voltages of CATV equipment is discussed. Some details, concerning the measurement conditions and frequencies in which the measurements would be made are stated.

3. MEASUREMENT METHOD

The equipment under test (EUT), artificial mains networks, signal generator and measuring receiver (quasi-peak) are disposed and connected in accordance with the set ups, shown in figures 1 and 2.

The measurements have been done according to the method, developed on CENELEC and CISPR recommendation base [1], [2] and author's personal experience.

The following test conditions should be fulfilled:

a) Equipment under test and signal generator should be placed on non-metallic support with height of 0.8 m;

b) Measuring receivers and all other metallic objects should be situated in a distance not shorter than 0.8 m from the EUT;

c) The mains lead of the EUT should be arranged vertically, following the shortest possible path between the EUT and the artificial mains network placed on the ground.

d) The measurements should be carried out twice- with and without an earth connection made to

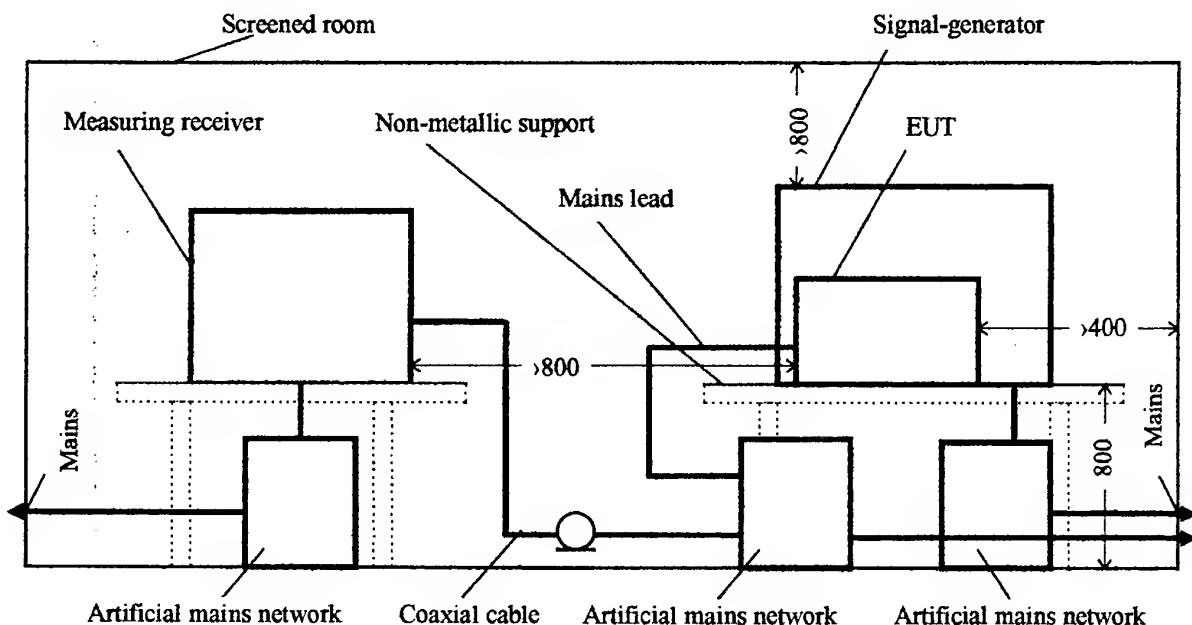
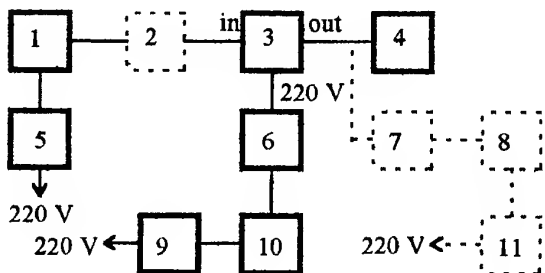


Fig. 1 - Test set-up for measurement of the radio-frequency disturbance voltage injected into the mains



1 - Signal generator; 2 and 7 - Matching network; 3 - EUT; 4 - Screened load resistor; 5, 6, 9 and 11 - Artificial mains network; 8 and 10 - Measuring receiver

Fig. 2 - Bloc-diagram of measuring set-up

the outer conductor screen of the coaxial radiofrequency input connector of the EUT;

- e) The signal generator and the measuring receivers should be powered through the artificial mains networks, placed on the ground.

4. OPERATING CONDITIONS

The equipment under test shall be operated in accordance with the manufacturer's recommendations and tested under conditions which maximise the disturbance voltage. During the test the maximum rated input level shall be used. That is the level which is declared by the manufacturer, stated on the equipment or

accompanying data sheet. All adjustable controls (if any) of the equipment under test shall be set to optimum position for its normal operation. All radiofrequency terminals, which are unused during the test, shall be terminated with their nominal impedance by means of non-radiating loads directly connected without any cabling. The supply voltage shall be set to a value within the specified by the manufacturer rating for tested object.

5. MEASUREMENT PROCEDURE

During the measurement the peculiarity and differences of the individual CATV equipment are taken into account. For example, in the case of the single channel equipment and frequency converters the test signal generator shall be set to the vision carrier frequency of the TV channel, for which the equipment is designed (input vision carrier frequency of the frequency converter). The measuring receiver at the output of the EUT shall be adjusted to:

- the input signal frequency in the case of single channel equipment
- the relevant output frequency in the case of frequency converters

The signal level at the signal generator output shall be such, that the output level measured by measuring receiver corresponds to the maximum rated value for the equipment operating range. The measuring receiver is disconnected and the output of the equipment is terminated by a screened load resistor. Then the measuring test set-up shown in fig. 2 is

realised; the measuring receiver is connected to the RF output of the artificial mains network. The frequency of measuring receiver is varied smoothly from 0.15 to 30 MHz. The frequency and the level of the observed disturbance voltages are noted. This procedure shall be repeated for position 1 and 2 ("phase" and "0") of the artificial mains network switch.

The highest of all registered values for mains disturbance voltage at each frequency is accepted as a measurement result.

The measurement procedure for the wideband equipment is analogical to the above described one, but in this case measurements of the disturbance voltages are carried out for the input signals with frequencies equal to the lowest, medium and the highest frequency of the vision carrier signal at the rated frequency range of the equipment.

After fulfilling the whole test conclusions about the EMC performance of the equipment can be made.

6. EXPERIMENTAL RESULTS

There have been examined the disturbance voltage, injected into the mains by the following CATV equipment:

- cable amplifier 1CAS 25 M;
- cable amplifier SCA 94 F;
- frequency converter TM 200.

The most important experimental results, statistically evaluated in accordance with CISPR recommendation, are summarised in Tables 1 to 3.

Table 1

EUT	Cable amplifier N 1	
Type	SCA 94F	
Manufacturer	"Mikroelektronika"	
Parameters		
Frequency range	40 to 800 MHz	
Max. amplification	20 dB	
Max. output level	115 dB/ μ V	
Input/output impedance	75 Ω	
Test condition:		
Input signal	106 dB/ μ V	
Output signal	115 dB/ μ V	
Frequency	780 MHz	

continue table 1

Frequency [MHz]	Results	
	with an earth connection to the artificial mains network	without an earth connection to the artificial mains network
0,220	66,5	67,5
0,490	57,5	57,5
7,960	35,5	25,5
9,840	21,0	24,5
13,515	23,5	23,5
20,990	18,5	18,5
22,510	25,0	22,5
24,020	24,5	25,5

Table 2

EUT	Cable amplifier N 2	
Type	1 CAS 25M	
Manufacturer	"Samel - 90"	
Parameters		
Frequency range	47 to 470 MHz	
Max. amplification	25 dB	
Max. output level	115 dB/ μ V	
Input/output impedance	75 Ω	
Test condition:		
Input signal	100 dB/ μ V	
Output signal	115 dB/ μ V	
Frequency	470 MHz	
Results		
Frequency [MHz]	Disturbance voltage U [dB/ μ V]	
0,160	68,5	68,5
0,220	57,5	57,5
0,513	48,5	47,5
0,855	37,5	37,5
0,920	34,5	34,5
1,700	22,5	22,5

continue table 2

6,145	17,5	17,5
7,970	20,5	20,5
8,200	25,5	25,5
8,800	20,5	20,5
9,500	22,5	22,5
10,790	21,5	21,5
13,600	24,5	24,5
15,300	27,5	27,5
16,650	24,5	24,5
19,140	22,5	22,5
24,400	24,5	24,5
28,400	18,5	18,5

7. CONCLUSIONS

On the basis of the present investigation can be asserted, that the lower part of the test frequency range is more critical for the tested CATV equipment. At these frequencies they don't fulfil the requirements of the EN 50083-2 for limits of mains disturbance voltages. The frequency converters show better EMC performance.

8. REFERENCES

1. pr. EN 60728-2/Ed.1 "Cabled distribution systems for television and sound signals - Part 2: Electromagnetic compatibility of equipment"
2. CISPR 13 "Limits and methods of measurement of radio interference characteristics of sound and television broadcast receivers and associated equipment"
3. Hawker P. "EMC and Cable TV", Radio Communication, Vol. 61, N 5, 1985, pp 357.

BIOGRAPHICAL NOTES

Anushka Stantcheva received PhD in EMC and radio interference measurement in 1990. Now she is a senior research associate and head of the EMC Division at the Institute for Scientific Research in Telecommunications, Sofia, Bulgaria. Her main interests are in the field of study, measurement and monitoring of the radio signals and interferences.

Stanislav Petrov is a research associate of the EMC Division at the Institute for Scientific Research in Telecommunications, Sofia, Bulgaria. His main interests are in the fields of signal processing, measuring and computer modelling of radio signals and interferences.

Bisser Stantchev is a research associate of the EMC Division at the Institute for Scientific Research in Telecommunications, Sofia, Bulgaria. He is interested in the Problems of EMC in Telecommunications.

Table 3	
EUT	Frequency converter from 10 TV channel to 8 TV channel
Type	TM - 200
Manufacturer	"Kwarta"
Test condition:	
Input signal	SW signal, vision carrier frequency 207,25 MHz, level 80 dB
Output signal	Vision carrier frequency 167,25 MHz, level 92 dB
Results	
Frequency [MHz]	Disturbance voltage U [dB/ μ V]
0,15	19,5
0,42 to 0,48	12,5
8,048	8,5
8,194	9,5
17,395	28,5

X

**EMI SOURCES &
COUPLING PATHS TO VICTIMS**

EMC in Amateur Radio Service

Invited session

chaired by C. M. Verholt - Denmark
organized by Prof. H. Trzaska - Poland

RESIDENTIAL BROADBAND NETWORKING AND CONCOMITANT EMC PROBLEMS

Hilary Claytonsmit

RSGB HQ, Lambda House, Cranborne Road, Potters Bar, Herts, EN6 3JE, United Kingdom

ABSTRACT

This paper looks at the developing line transmission techniques being proposed for use in the domestic environment in the UK and potential EMC problems which could arise from advances in broadband networking. These issues will be looked at from the point of view of one group of users of the lower h.f. spectrum where the reception of weak signals is of significant importance - amateur radio operators.

The desire to provide high speed access to services such as the Internet, Home Shopping and Video-on-Demand has caused new digital techniques to be developed with the object of utilising existing delivery systems such as the telephone network and more recently, the mains electricity supply, to carry high speed data.

Although innovative and exciting, these new techniques may also generate interference problems. In particular leakage of RF energy in frequencies at the lower end of the h.f. band could cause a serious problem.

Emphasis will be placed on Digital Subscriber Line techniques, especially ADSL, VDSL and a system which has been in the development stage for some 3 years and which will provide Internet access ten times faster than current ISDN links, utilising the mains electricity supply infrastructure.

This latter technology is due to be launched in April 1998. At the time of writing this paper the hard facts are veiled in commercial confidentiality. It is hoped that the fears regarding the possible EMC problems which might arise from such a system are unfounded!

1. 'AMBIENT NOISE FLOOR' ON THE LOWER H.F. FREQUENCIES

Natural radio frequency noise falls into two broad categories, natural and man-made noise. The first of these can itself be divided into two categories, terrestrial and galactic (sometimes called cosmic) noise. Natural terrestrial noise comes mainly from lightning strikes taking place in locations of high thunderstorm activity and propagated over long distances by ionospheric reflections. Galactic noise increases as the frequency decreases but in practice, at lower h.f. frequencies, it is difficult to distinguish between galactic noise and man-made noise, even in a "quiet" rural location.

Official figures gathered world-wide show that, in temperate regions, the 'ambient noise floor' is determined by the man-made / galactic noise level for a considerable part of the time. At these times, natural terrestrial noise falls well below this level and can be ignored. In temperate regions, man-made noise governs the minimum level of signals which can be received on the h.f. bands and sets the 'bottom line' to radio performance.

Monitoring signals on 3.5 or 7.0MHz in a quiet location, where there are no arcing contacts or similar impulsive interference generators, reveals a reasonably quiet band with a minimal 'noise floor'. This ties up with figures in official publications such as CCIR 322. It is important to note however, that the low 'noise floor' is not always readily apparent when measuring in the 9kHz "CISPR" bandwidth. Band occupancy is so high in many parts of the h.f. spectrum that it is difficult to find a band 9kHz wide which is free from intentional signals! If the output of a suitable antenna tuned to a frequency in the lower h.f. band is examined on a spectrum analyser, it will be seen to consist of a floor of noise, with peaks of discrete signals. These may be genuine, intentional, signals, or emissions from oscillators in electronic equipment, or possibly intermodulation products. Transmissions which use very narrow bandwidth, such as CW Morse code, or other slow speed data modes, can often operate in between discrete signals, permitting communication to take place under circumstances where casual observation might indicate that such signals would be completely drowned in the noise.

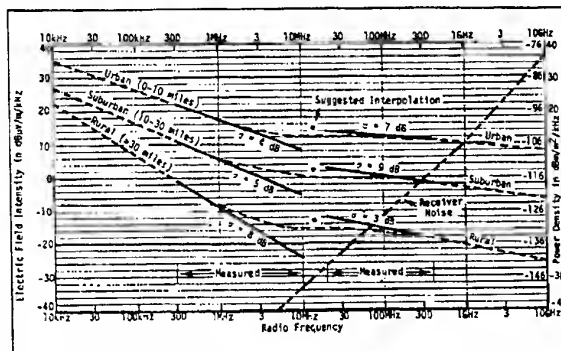


Fig 1 Model of Median Incidental Man-Made Noise Based on Lossless Omni-directional Antenna Near Surface [6.1]

It may be thought that the increasing use of satellite communications has made long distance h.f. communications a thing of the past. This is not the case. This portion of the h.f. spectrum is used by distress and safety traffic, aeronautical search and rescue, the Coast Guard and Government agencies. An increase in the 'noise floor' would affect reception of signals in these areas, as well as on the amateur bands.

2. ADSL / VDSL

The idea of working remotely from the office at home is becoming more attractive and with the new advances in line transmission techniques, becoming a reality. Asymmetric Digital Subscriber Line (ADSL) which operates up to 1.1MHz, has been promoted for this use in the US as well as for Video-on-Demand in the UK. Digital data can be transmitted at 2Mbit/sec in one direction (to the subscriber) on the existing telephone wires without disrupting ordinary telephone calls. By using advanced digital compression techniques it is possible to transmit TV pictures digitally at 2.048Mbit/sec with high quality definition. However, it is believed that this may not be commercially viable at present, due to the high capital cost of the computer equipment needed at the exchange to make the service available. Concern has been expressed that there will be leakage from the street furniture, but this should be remediable by using good engineering techniques.

Very high speed Digital Subscriber Line (VDSL), whilst providing similar facilities to the customer, presents somewhat of a different picture. It permits transmission rates of up to 12-26Mbits/sec downstream and 2Mbits/sec upstream on frequencies up to 10MHz. There will be optical fibre links from the telephone exchange to Optical Network Units (ONUs) in the street which will service around 200 customers using the existing telephone wire network, some lines being 1km long.

Concern was expressed by the EMC Committee of the Radio Society of Great Britain (RSGB), the national body for radio amateurs and following discussions between the RSGB and the UK's major telephone company, comprehensive tests were carried out. An h.f. receiver and antenna system, typical of those used by radio amateurs, was set up at a measured distance from a test line carrying simulated VDSL signals. During one trial the effect of reducing the power density in the amateur bands by using a digital notching technique was observed. The results suggested that VDSL transmissions with flat in-band power density on overhead cables presented a threat of interference to some users of the h.f. spectrum with unacceptable levels in the lower h.f. amateur bands. In the trial where notching of the amateur band was switched in and out, a reduction of more than 20dB was observed. The radio frequency interference (RFI), from the overhead drop-wire carrying a full power spectrum VDSL signal could produce an S8 signal strength at a distance of 20m. ('S' units are a method used by radio amateurs for measuring received signal strengths and are defined in 6dB

steps. They range from S1, which is 'barely perceptible' to S9 which is 'extremely strong'). For anyone listening on the amateur bands this would sound like white noise, but could in fact be 25dB higher than the noise floor previously mentioned. It is therefore hoped that the upstream channel does not transmit on amateur frequencies as this may render these frequencies unusable.

As a result of these tests, it was suggested that the maximum transmitted launch power of -60dBm/Hz up to 30MHz, should be reduced to -80dBm/Hz on the amateur frequencies and also that this requirement should be applied to the ONU in the street and at any units at the subscriber's premises.

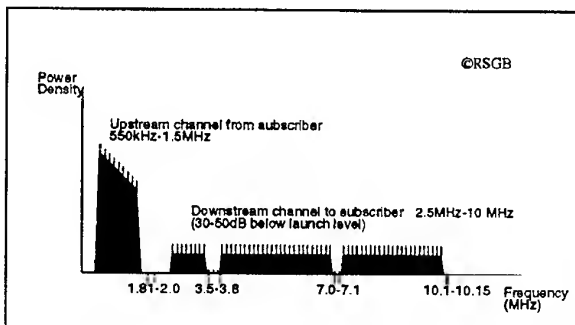


Fig. 2 Possible Frequency Allocation for VDSL Signals at User's End of Telephone Line Avoiding Amateur Bands

VDSL emissions are one problem, but r.f. pickup of h.f. amateur transmissions in the vicinity, on to the telephone wires, could cause problems for VDSL subscribers, especially in areas where homes are served by overhead 'drop wires' from telephone poles. It is believed that the UK's major telephone provider is hoping to achieve a specification for modems used with VDSL which would be sufficiently immune to r.f. pickup. However radio amateurs are concerned that, if such systems become widespread, with a number of competing providers, commercial pressures may cause systems with relatively poor immunity to be used. In the long run this could lead to the radio amateur being penalised. The RSGB EMC Committee is watching the development and application of standards with interest (standards will be discussed later) and suggests that any emerging standards should consider the following:

- The shaping of the VDSL frequency spectrum to incorporate deep notches at 1.81-2.0MHz, 3.5-3.8MHz and 7.0-7.3MHz.
- That the upstream channel should use frequencies below 1.8MHz to avoid transmissions from subscribers into the amateur bands.
- That the downstream channel should use higher frequencies, with the amateur bands notched (see Fig.2).
- That Time Division Duplexing (TDD) should not be used unless the notches in the amateur bands can be made deeper than the 20 - 24dB achievable by TDD.
- That Power Spectral Density (PSD) should be tailored to allow for poorer balance of cables at higher frequencies.

- That 'Power Back-off' should be used to reduce launch power on shorter cable runs.
- That a VDSL transmitter should 'power down' when the line is idle.

3. THE NEXT PHASE

Competition is high to provide faster and faster access to Internet-based applications such as electronic commerce, telemarketing with broadcast media and Internet telephony. To be viable, costs will have to be kept low; hence the utilisation of existing networks.

Nortel (Northern Telecom) and Norweb Communications have developed a new technology that allows data to be transferred over electricity power lines into homes at speeds of over 1Mbit/sec. It is believed that the system uses Minimum Shift Keying techniques with a $\pm 500\text{kHz}$ bandwidth at a power of 50 mW on two frequencies, 2.9MHz and 4.3MHz. These frequencies are not 'cast in stone', but frequencies in the range up to 8MHz or possibly 10MHz are being considered.

The High Frequency Conditioned Power Network (HFCPN), part of which is shown in Fig. 3, supplies in the region of 150 domestic customers, 50 on each of the three phases. The majority of the UK's Low Voltage Electricity Distribution Network (LVEDN) uses underground cables. There are three separate three-phase LV distributor cables which leave the substation (as shown in Fig. 3). The cable lengths vary between 250m and 600m. The service cable feeding each house carries a single phase supply. Conditioning Units (CU) containing filtering may be fitted to connect the LVEDN to a HFCPN. CUs could be placed on the consumer side of the substation and the subscriber-to-mains side of the meter. However, filtering at these frequencies is costly and it is thought that filtering where the supply enters the consumers premises will be minimal or non-existent. It is possible that this might be considered an asset, since customers could connect their PCs etc. via Ethernet-style adapter cards directly into the 13 Amp sockets via a local filter unit.

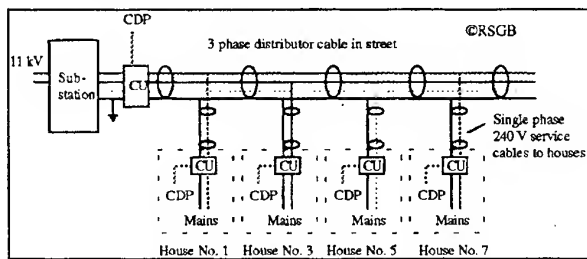


Fig. 3 Block diagram showing part of a High Frequency Conditioned Power Network

Although a commercially exciting project, signalling down the mains could signal a significant increase in the already rising 'noise-floor' on the lower h.f. frequencies.

There are many areas of concern, but the main one is radio frequency interference RFI.

Leakage of signals out of the HFCPN is more than likely, with the potential for coupling into the house wiring. It is presumed that the signals will be present at all houses supplied with electricity from this source, whether there is an uptake or not. This will mean that any cable emerging from the underground distribution system is a potential radiator of RFI. The magnitude of the radiation will depend on the disposition of the cables and the balance of the system, both of which could vary widely, and which would be very difficult to model. Unless all outlets are filtered as they emerge from the underground system, it is difficult to see how severe emission problems can be avoided. The modulation techniques used in HFCPN could be of a similar type to those used in digital audio broadcasting, where there are many carriers with overlapping sidebands. All these carriers could approach MPT 1520 limits, with a resultant broadband noise effect which could cover a whole amateur radio band rather than just spot frequencies.

The mains infrastructure is of indeterminate quality and age. Even though the underground LV cables look like coaxial cable, they are not designed to have high shielding effectiveness at r.f. However, as has already been said, the real problem will be radiation from the above-ground cabling. It is believed that during trials, broadband emissions with a field strength as high as 57dB μ V/m have been measured.

Leakage will occur from above-ground wiring connected to underground cables, but where there is overhead LV distribution there would be direct pickup and radiation from the distribution system itself. In an urban environment there are many more, less-elevated conductors which will make effective unintentional radiators, the most obvious ones being lamp posts. Unlike interference which originates from a single source where the radiated field falls off in a predictable way, mains signalling data is deliberately disseminated over a wide distribution area and radiation will take place from all connected wiring. Each lamp post could act as a potential vertical antenna and with others, would form part of a radiating antenna system which could increase the risk of interference to other radio services. The problem could be overcome by filtering each lamp but the overall costs would then increase.

Taking a simplistic view, that a very large number of small leakages could be added in terms of power, the possibility of long-range ionospheric propagation of the resultant noise would also have to be considered. This is a 'worst case' scenario, with the assumption that the system has these inherent problems and that it is developed on a large scale.

As with VDSL, there is the possibility that the multi-carrier modulation techniques used could be configured to take account of frequencies used by the amateur service in

their sector of the spectrum. The immunity of the system to transmissions from other users of the lower h.f. frequencies must also be addressed.

4. STANDARD PROTECTION

Because technology is moving so quickly and because the procedures for making and implementing standards is so protracted, it is possible that the 'Generic' standards would be used as a stop-gap. Most standards relating to emissions from electronic equipment were devised to cater for situations relating to analogue techniques. The emergence of digital techniques means that broadband emissions at the maximum permissible level will extend over a wide bandwidth making large chunks of the lower h.f. spectrum unusable.

Existing EU EMC standards, such as EN55022 do not call for radiated emission limits below 30MHz. Above this frequency, only conducted emission limits are specified. The current standard that applies to mains signalling is IEC 61000-3-8 which deals with emissions in the 3kHz to 525kHz range. There is no specific standard for emissions from mains-borne communications systems at m.f. or h.f. so it appears that MPT1520 will be applied in the UK. This however, deals with cable-to-cable TV systems operating below 30MHz.

As far as VDSL is concerned, a Draft Standard exists :- DTS-TM-06003-1 "Transmission and Multiplexing (TM); access transmission systems on metallic access cables; Very High Speed Digital Subscriber Line (VDSL); Part 1 Functional Requirements" - but as yet it is not in the public domain.

Mains communication, being somewhat of a hybrid system, does not fit comfortably within existing standards. It is feared that it may fall into the gap between the WT Act and the EMC Regulations. Is the technology classed as a large installation or a system, as far as the EMC Directive is concerned? Until an engineering specification for the system is seen, together with any EMC analysis and proposed route to conformity, it is difficult to assess how it will comply with

the essential requirements of the EMC Directive.

The EMC Regulations Statutory Instrument SI 1992 No 2372 Part 1 Protection Requirements Section 5 Clause 4 states "..... the electromagnetic disturbance generated by relevant apparatus shall -

- a) not exceed a level allowing radio and telecommunications to operate as intended and"

This offers a small degree of comfort!

5. CONCLUSION

In the commercial race for faster data delivery systems which push the frontiers of technology, it must not be forgotten that as well as financial interest, there should also be an interest in protecting all users of the spectrum.

Existing emission standards allow emissions which are large in relation to weak signals in the amateur bands. There is no limit to the number of different frequencies which equipment may emit, provided none of these exceed the limits set. With broadband digital communications coming on stream, the risk of RFI generated on a large scale cannot be discounted. The resulting compounded cacophony could mean an increase in the 'noise floor' resulting in obliteration of weak signals on the lower h.f. bands which could effect national interest or just eliminate portions of the amateur bands used by the Amateur Service.

6. REFERENCES

- 6.1 D.R.J.White, "A Handbook Series on Electromagnetic Interference and Compatibility", Vol 3, Don White Consultants, Inc., Germantown, MD, USA, p 2.42.

BIOGRAPHICAL NOTE

Hilary Claytonsmit is a Director of the Radio Society of Great Britain and Vice Chairman of the RSGB EMC Committee and Founder Member of the RAKE (Radio Activated Key Entry) Group. She is also Secretary of the IARU Region 1 EMC Working Group.

THE EMC PROBLEMS FACING AMATEUR RADIO COMMUNITY IN THE POST COMMUNIST SOVIET REPUBLICS AND THEIR EFFECT ON THE FUTURE GROWTH OF THE AMATEUR RADIO POPULATION

By Victor V. Goncharsky US5WE/K1WE/SO9WE/S21ZM, P.E.
p.o.box 41, Lvov, Ukraine 290000, Europe

INTRODUCTION

It seems quite obvious that the recent changes in the CIS countries have had affected everyone's life greatly. Hams, as the most technically advanced multicultural group, were affected by the mentioned changes in several ways.

As the Ukrainian representative I am going to give the broad picture of the problems we are facing in Ukraine. No doubt our experience could be interpolated over the most of the C.I.S. countries

Firstly - most of the hams lost their technical jobs and have been forced to look for something else to survive. This resulted in drastic decrease in ham radio activity within the former Soviet Union.

Secondly - availability on the legal and black markets of the new and used ham gear, which is the cheapest one to get. This resulted in immediate appearance of a lot non-licensed commercial stations on the VHF ham bands. These stations cause a lot of interference to the amateur, fixed and broadcast services. As usual, amateurs are first to be blamed for the mentioned interference.

Thirdly - several modern commercial communication techniques were introduced in Ukraine lately. They include: pager broadcast, trunking, cellular and long range cordless telephones, commercial repeaters and some other. The transmitters on sites are mostly running excessive power and sometimes supervised by non qualified, poorly paid personnel. This results in misalignment and a lot of out of band interference. For example, the 300 W paging transmitter completely blocks the packet frequency of 144.650 in some parts of Lvov.

Fourthly - another serious EMC problem for the apartment dwellers, who most of the Ukrainian hams are, is cable television. The typical installation is done by stringing long runs of low grade (cheap) coax between the blocks and along the roofs to the satellite dish sites. These installations are susceptible to all kinds of HF and VHF interference. What is even worse that according to the local regulations one of the cable

TV subbands falls within the amateur 2 m band. Therefore operation of the 5 watts HT blocks the reception on this channel for the whole neighbourhood.

Fifthly - the mass "invasion" of the cheap low end electronics from the Far East presents another EMC problem to the Ukrainian Hams and can potentially eliminate, especially in the law-less situation that exists in most of the CIS countries, a lot of active hams from the air. Examples of the RFI/TVI situations involving TV-sets, satellite systems, VCR's, digital telephones, etc. are given. **Sixthly** - local import and manufacturing regulations do not even mention EMC standards for the home electronic devices. Therefore the Ministry of Communication has no legal authority to justify amateur's rights to operate his properly aligned station in case of the RFI/TVI complaints from the owner of such a device.

Let's examine the mentioned problems and find out what could be done to reduce the possible negative effects on ham radio activities in the post Soviet countries.

1. EXPERIENCES FROM THE PAST

As in most of the Eastern European countries hams were concentrating in urban areas mainly surrounding the huge industrial agglomerations. This was a forced solution since both land and apartment buildings belonged to the State and one could not buy the piece of land to built the house with antenna tower in the backyard. Therefore RFI and TVI problems with hams involved were quite common those days. Fortunately "hamwise" only few official state-run TV channels were available giving hams chances to find the EMC solutions on their end. Different kinds of TVI filters were quite popular and ferrite cores were cheap and easy to find on almost every electronic "black market".

RFI EMC problems involving shortwave broadcast reception were rare since the electromagnetic energy levels from the jammer stations located in all major cities were so high that they effectively eliminated the possibilities of such receptions themselves. The side effect was inability for hams to use some of the bands during

some parts of the day. For instance, in Lvov, Ukraine the use of the 40 meter band was almost impossible from 1500 GMT to 0500 GMT due to the jammers fighting Radio Tirana that was transmitting within the amateur band. Harmonics from the mentioned jammers were heard on 20 and 15 meters effectively reducing one's ability to hear weak signals. The jammer's signals were so strong that it was rectified by the poor relay contacts, bad or corroded antenna connections making hamming in the cities a real nightmare.

Another problem that remains from the past is so called "wire broadcasting". This system remains unchanged since World War II and uses open wire lines string between the blocks to transmit several radio programs. This system causes the following EMC effects: pickup by grounding wires, coaxial cable shields, microphone and headphones cords and finally heavy QRM on several 160 meter frequencies. All these forced hams to learn a lot to find the proper solutions to every EMC problem.

2. THE RECENT SITUATION WITH AMATEUR RADIO IN UKRAINE

Hams in Ukraine are very proud of a new regulations adopter by the Ukrainian Justice ministry and Ministry of Communication on November 27, 1997 No 564/2368. Putting aside all the details of this document let's look on the EMC part of it to see if it contains any potential danger for hams. Actually only one paragraph, i.e. 8.3.10 deals with EMC saying: "It is prohibited to operate the Amateur Radio Station during the TV - hours if such ARS creates TVI QRM on a commercially made TV-set which operates according to its specifications and is connected to the commercially made outdoor antenna." Looks great, isn't it? But let's analyze this regulation more closely.

Firstly, we need to see if there were any changes in the living conditions of the inhabitants in general and hams in particular. The answer is definite NO. Most of the hams remain in cities, but in majority lost their jobs and provisions for better life.

Secondly, there is a huge amount of the cheap electronics from the Far East being brought into the country by all possible means. This equipment is not only bad in general but is making an impression that it's designers never heard about EMC and made their boxes to be intentionally susceptible to all kinds of interference. These include:

- TV-sets in the fancy plastic boxes which are not only jumping down from their pedestals after the first transmitter key-down but also creating noise intensities compared to the "good-old" Russki jammers mentioned above. These units have almost no front-end selectivity due to the lack of input RF filtering;

- VCR players and recorders that have no shielding at all and, as we found here, having the unique property to be RFI susceptible in accordance to the reverse relationship, i.e. the lower the transmitting frequency the stronger the RFI at the VCR site. Putting the ferrite chokes on AC and video cables does not help at all and we believe this is a most difficult EMC problem at the moment due to the fact that a lot of consumers connect their TV-sets through these recorder units that makes the "dreadful" combination;

- Cheap digital telephones which are excellent RF energy rectifiers, having in mind the length of the "antennae" connected to them. These telephones are the amateur's nightmare. In fact we never had problems with the old rotary dial phones.

Thirdly, as we're entering the computer era it's quite obvious the computers and ham gear would have start to interfere with each other. Again, as with the items mentioned before, most of the computer hardware that get's on CIS markets is of the cheapest "yellow" brand. I want to a few examples of the noticed EMC compatibility problems.

1. Bad keyboards that show two major EMC problems: rectification through the keyboard cord - no ferrite beads both on computer and keyboard sides of the cord and rectification through the hand/keyboard capacitance (the worst case) that forces keyboard to generate random symbols when one's typing or just approaching the fingers to the keyboard when transmitter is on. I'll address this situation more closely when analizing the EMC situation while running the PLX multimode mailbox.

2. Processor Unit's problems. The major EMC problems concerning the processor units from the ham standpoint are: the noise from power supply, data cables, phone line connected to the internal and external modems and unshielded twisted pair network cables. Grounding the unit can partly cure the noise generated by the power supply and data cables inside the cabinet but has no noticeable effect on the outside cables. Most of the networking in this country is done by using the cheap (again) unshielded twisted pair resulting in high levels of RF noise generated by such networks. Telephone modems are capable to generate even more noise due to unbalanced status of the open two wire lines, bad interconnections and extremely long runs. Needless to say that reciprocity law can result in ham ruining some big company's network by simply transmitting on, say 20 meter sideband. If the company owner belongs to mafia (which is quite common nowadays), this poor ham is in real trouble.

3. Videomonitors and other external devices are the source of all kinds of noise as well. The colour SVGA ones from BY, VS6, BV, etc. are extremely

"loud" while the multimedia AF sets are "ideal" to receive and rectify any RF enrage nearby. I tested these boxes with a 5 watt HT and found that the latter makes them useless - good news, one can't simultaneously listen to "heavy metal" and talk to local repeater.

3. SANITARY INSPECTION - ANOTHER THREAT TO CIS HAMS

Recently another serious threat to the CIS hamming community appeared to be the Sanitary Inspection. This government institution not only defines standards on electromagnetic radiation levels which is it's duty but recently announced that every user of the radioelectronic transmitting device has to have certification by the mentioned inspection. This procedure is not only time consuming but also costs up to \$100 per unit. What is even worse that according to the recent Ukrainian Sanitary regulation N190 adopted by the Justice Ministry the non-certified unit can be confiscated or put under arrest until the certification is completed. Hams simply can't afford paying this much and UARL is working trying to change this regulation. The recent admissible levels of radiation according to national standards N39 01.08.96 are presented in a table below.

Frequency MHz	Level Volt/meter
1.8	15
3.5	5.8
7	4.9
10	4.4
14	4.0
18	3.7
21	3.5
24	3.3
28	3.1
50	3.0
144	3.0
432	2.2

4. CABLE TELEVISION - THREAT TO LOCAL 2 METER ACTIVITY.

Another problem the hams are facing in big cities is cable television. One can object to this by saying that, ideally, cable television reduces or even eliminates the TVI complaints possibility. Not in this country! The coax cables are "low grade - less braid" kind, amplifiers use cheap low signal FET's and one of the channels transmitted falls within the limits of the amateur 2 meter band! This makes it hard to use even the HT with the outdoor antenna in the evening in some parts of the city of Lvov. Packet activity is also affected. No solution has been found to this EMC problem since cable TV companies don't want to make their systems EMC compatible.

All the listed facts show how difficult the ham life became during the last few years. In the next part I'll try to show what ham can do to reduce these negative effects.

5. SOLUTIONS TO THE EMC PROBLEMS BY THE URBAN UKRAINIAN HAMS

Followed is a discussion of several amateur set-ups and how the arising EMC problems are being solved.

Setup 1 - AMTOR/PACTOR/PACKET scanning mailbox. Frequencies of operation : 3.5,7,10,14 MHz HF, 144 MHz VHF.

This U5WF mailbox is operating near the center of the city of Lvov for more than 3 years now and represents a kind of extreme case due to 24 hour schedule, amount of frequencies used and high percentage of key-down in Pactor mode.

EMC problems found: keyboard RF pickup on 80 and 30 meters, TVI complains from VCR users when MBO is transmitting on 80 meters and those located in front lobe of 40 m yagi antenna, two meter transceiver squelch randomly opening when MBO was transmitting on 20 and 80 meter bands. Equipment used: "Kenwood TS-930S" using the parallel scanning scheme and recently "Ten-Tec Paragon" using serial scanning scheme, output power 100 watts HF bands;

Icom IC281 FM transceiver, output power 10/50 watts VHF;

Antennae: 80 m - shunt fed Omega matched mast with 20 and 40 meter yagis as top hat, 16 meter high;

40 m - 2 element yagi - split driven element, direct 50 Ohm feed, symmetry by coaxial choke according to Cushcraft instructions;

20 m - 5 element monoband yagi direct 50 Ohm feed through 2 quarterwave coaxial transformers, symmetry by coaxial choke as on 40 meters;

2 meters HB9CV two element antenna, vertical polarization, at first located on the same mast as other antennae;

Computer: "Wise Decision 20-SX".

To solve the mentioned EMC problems the following actions has been taken:

The ferrite chokes were put on a keyboard cord, all signal cables outside the computer to Pactor, Amtor, Packet controllers and scanning/switching box and transceivers. The 2 meter antenna was moved to another mast 6 meters from the main one. These cured all EMC problems within the mailbox itself while VCR RFI situation could not be solved.

Setup 2 - VHF amateur repeater UR0WVC in Lvov, Ukraine.

Equipment used: Hamtronics 2 meter repeater 25 watts output, WACOM duplexer 92 dB isolation

between receive and transmit frequencies channels tuned to repeater channel R2. There was NO interference between this repeater and two other installations in the same building:

1. The commercial 4 channel trunking system using the "Motorola" GM300 transceivers and duplexers.
2. The commercial no-duplexer separate receiver/transmitter antennae repeater system.

Both commercial installation were operated in the 150 - 170 MHz range with vertically polarized antennae installed on the same roof measuring 20 x 40 meters.

Setup 3 - The multichannel Lvov DXCluster VHF/UHF node US5WE.

The 4 channel node operates on three 2 meter frequencies of 144.675 MHz, 144.950 MHz -1200 bps, 144.850 MHz- 2400 bps and 430.600 MHz RX/438.200 MHz TX 9600 bps packet.

Simple front-end filtering is used on all 2m channels by means of spiral resonators. The 70 cm "K-Net" transceiver has no additional filtering. There are two other VHF communication systems in the same building - commercial 50 Watts FM voice operating on 156/160 MHz and high power SINAQ telephone operating on 260/300 MHz range. No interferences to or from these services were noticed on the packet system. No interchannel interference was noticed between 144.675 and 144.850 MHz channels using the same vertical polarization and 30 meter separation between antennae. Both were using 5 watts output Yaesu FT23R transceivers. The 144.950 MHz is a backbone channel to Ternopol and uses stacked 10 over 10 horizontally polarized yagi driven by Motorola M10 25 watts transceiver. No interference to other channels from this one was noticed as well. On the other hand, SINAQ telephone is interfering with 156/160 MHz commercial system which uses Alinco DR130 transceiver with no front-end filtering.

5. CONCLUSION

The presented examples clearly show that ham radio activities present no serious EMC

problems to other communication services in this and other CIS countries due to the fact that these services use high grade equipment which generally is being properly installed by qualified and well-trained personnel. The vast majority of EMC problems for hams comes from interfering with low quality home electronic devices and systems installed by unqualified technicians. Serious efforts are made by the Ukrainian Ham community to improve the communications laws in this country to include the European EMC standards into the local regulations. Ukrainian hams are needing international support and seeing the participating in this Conference as an important move in that direction.

BIOGRAPHY

Technical director J V "Safe Guard - Ukraine"; Chairman of the Digital Communications Committee of the Ukrainian Amateur Radio League (UARL);

Director for the European Operations Foundation For Amateur International Radio Service (FAIRS) - planning, coordination and implementation of the \$24,873 "Eurasia Foundation" grant "Ukrainian Digital Amateur Radio Network"

Educational Background:

Lvov Polytechnic Institute, Radio Engineering Department, graduated 1978, specialized in radioelectronic equipment design.

Virginia Polytechnical Institute and State University IBM computer Interfacing and Control Workshop, Oct. 1990, Lvov Ukraine.

Peace Corps of the United States of America
The Small Project Design and Management Workshop, March 1994, Lvov Ukraine.

Languages: Native speaker of Russian. Fluent in Ukrainian, English and Polish.

Ham Radio Experience:

Licensed Ukrainian Amateur Radio Operator since 1967, Highest class of licence with the callsign US5WE(ex UB5WE).

US FCC Extra class amateur licence K1WE since 1990. Bangladesh amateur radio licence S21ZM since 1993.

EM ENVIRONMENT IN APARTMENT HOUSES

Hubert Trzaska

EM Environment Protection Lab., ITA Techn. Univ. of Wroclaw
Wyspianskiego 27, 50-370 Wroclaw, Poland

The work presents the role of Amateur Radio Service in the electromagnetic environment of apartment houses and other inhabited areas. Some interference may be caused by the service, however, presently it is rather a victim of interferences generated by other services and devices than primarily responsible for their presence, especially while good professional equipment and correctly designed antennas are in use. Briefly are discussed problems with interferences which result from presence of harmonic frequencies in power frequency rectifiers and regulators, power devices applied in TV and VDU devices, environment in the vicinity of cable TV networks and the role of resonant effects in the proximity of local FM and TV stations.

1. INTRODUCTION

Members of the Amateur Radio Service (ARS), both CB enthusiasts and the hams, have been installed in apartment houses or dwelling ones. With no regard to the type of a house, they are usually located in areas where the population density is extremely large. Thus, the experience of ARS, as regards its 'cohabitation' with neighbours as well as problems of the mutual interference, is the longest and the largest. It is not by haphazard that a pretty large number of people professionally involved in EMC has more or less interests to the ARS. The point may be confirmed by the inclusion of the problem 'EMC in ARS' to international EMC symposia.

The area, till now occupied monopolistically by the ARS, is more and more often entered by professional services as well. The trend has been initiated by wide spread implementation of electric and electronic devices applied in house-holds which are applied for 'technological' or medical purposes, e.g.: microwave oven, inductive cooker, apparatus of d'Arsonval, for work and pleasure purposes, e.g.: TV- and video sets and installations, computers and ending on devices for remote control, toys, etc. Then different types of transmitting devices were installed on the roofs of the tallest buildings. Starting from BC and TV transmitters to a variety of types of base stations, radiotelephone centers and cellular phone stations. Presently a global explosion of the cellular phones' use penetrates the environment the strongest.

The wide spread of these devices has caused that the EM environment, especially that in apartment houses, is more and more dense and its pollution is incomparable to any other one; even with no exclusion of the majority of ISM environments. Every type of device may be a source of the interference and, some time simultaneously, a victim of it. Apart from the human exposure it means that every type of device, applied in the environment, must be more and more immune against the EMI. The 'system' seems to be 'overloaded' now. The best example here is practical impossibility to listen to LW BC stations or even to the local MW stations. As a result the problems faced till now by the ARS only are more and more essential for other services and institutions. Here is the reason why hams' experience is important and their opinions are of concern not only for themselves.

2. POWER FREQUENCY DEVICES

We won't discuss here sparks discharges or similar phenomena in power substations and transmission lines. They generate quite strong EMI, however, they usually are located at a distance from the environment discussed. In household one uses widely different types of thyristor regulators, lamps, power converters and others that may create EMI in wide frequency range [1, 2, 3]. The basic frequency content in the full-wave thyristor controller is shown in Fig. 1 versus current flow angle. In this case the basic frequency is the same as the input one, however, in multi-phase rectifiers and regulators it may be its multiple as shown in Fig. 2 for the full-wave rectifier, while Fig. 3 presents current spectrum of a 15 W GE lamp [4, 5].

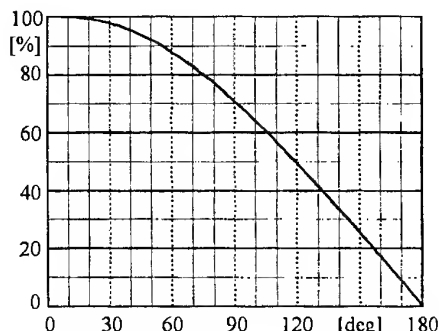


Fig. 1 First harmonic in a full-wave thyristor regulator

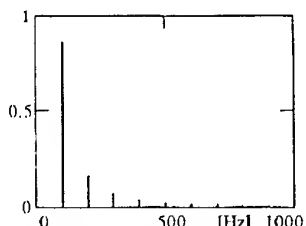


Fig. 2. Harmonic fringes at output of full-wave rectifier

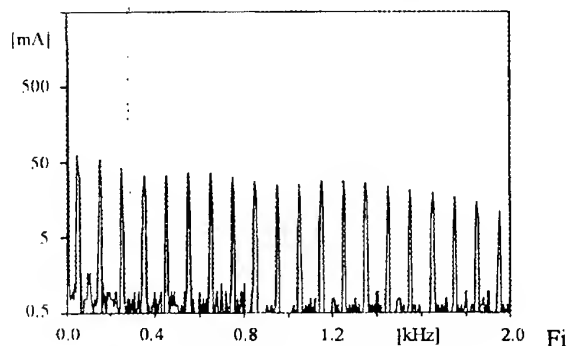


Fig. 3 Current spectrum of a 15 W GE lamp

We should add here that due to high current, especially in ISM type devices, the harmonics may be of remarkable intensities even at RF. By the way we may notice that the phenomenon creates significant legal problems that may be summarized in the question: what does power line frequency mean? [6]

The above mentioned phenomenon results, in majority, in EMI. At the same time the newspapers frequently bring 'revelations' on the cancer cases due to HV overhead lines and even home power installations. The author's experience, supported by numerous measurements performed in the neighbourhood of local power substations (some time located on the ground floor of apartment houses) and HV lines, shows that in no flat EMF exceeds this of a typical floor for home installation. However, years before these installations were placed inside the Bergmann's tubes. This forgotten technique assured remarkable reduction of EMFs radiated from the power installation.

3. VDUs

Analysis, similar to the above, should be devoted to countless types of power sources containing pulsed stabilizers or/and based upon frequency conversion which are widely used, e.g.: in TV and VDU devices. We would not discuss here the problem of the hazard, created by these devices to their users. We will focus our attention only on EMI radiated by them that, in fact, have excluded the possibility of LW, and even MW, reception in their proximity. The ARS, working with signal levels much below these of applied in BC or TV reception, has with them problems at SW as well. Wide spread applications of these devices causes EMI in almost every apartment house. However, here is a certain hope that the technology development and the trend to limit power consumption will lead to flat

displays' use in VDUs that should remarkably limit the EMI in real future. It is a unique example while a technological trend is identical with the ecological one.

In order to illustrate the scale of the problem in Fig. 4 is shown measured EMI level within LW and MW range in a typical apartment house and caused in the majority by the VDUs. Contrary to other works [7] spectral distribution of fringes is emphasized. It is evident that the measured values may be different in different local environments and it is a function of the 'devices density' as well as their quality. We should remind here that an important role in the EMI increase may be played by home-born 'inventors' and other 'reformers'. Fortunately, as a result of general economical development and availability of necessary spare parts, this kind of problems is less serious now when compared to the past.

The measurements were performed with the use of a spectrum analyser equipped with a small size wide-band active antenna working within frequency range 100 kHz - 110 MHz. Its AF \approx 0 dB.

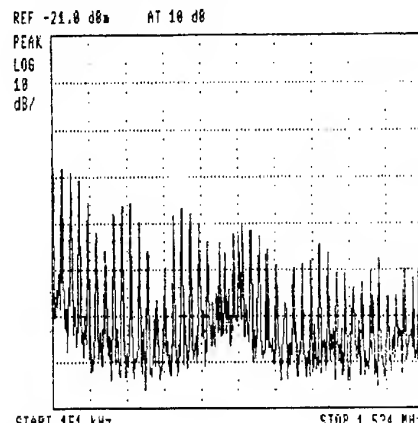


Fig. 4 EMI level within LW and MW.

Another factor, specific for TV receivers, is the radiation of its local oscillator and other HF fringes that include signals at a receiver's input frequency and its harmonics. The former is well illustrated in Fig. 5 (right fringe appears at a TV RCVR LO frequency while it was tuned into channel 7 and the left one a signal of a local ham station). The latter were presented

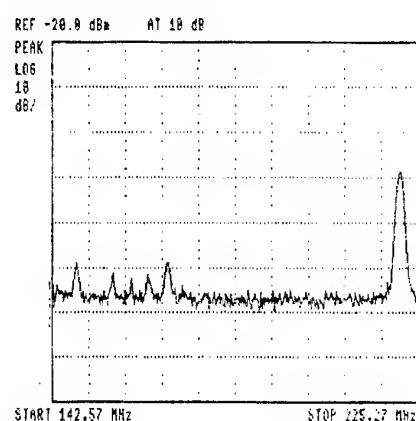


Fig. 5 LO radiation from a TV receiver

in [8] on the ground of a standard [9] which is a subject of protests of the IARU. Apart from less important interference to ARS within 420 MHz band it creates real possibility of cross-channel interference for other TV receivers, even connected to a cable network. The latter may be often seen in the local cable TV.

4. CABLE TV NETWORKS

Firstly the problem with radiation from cable networks and video recorders was mentioned in [10]. That measurements were performed more than ten years ago, but they lose none of their immediate importance till now. In Fig. 6 is compared signal from a recorder (right) with that of a local ham station (left).

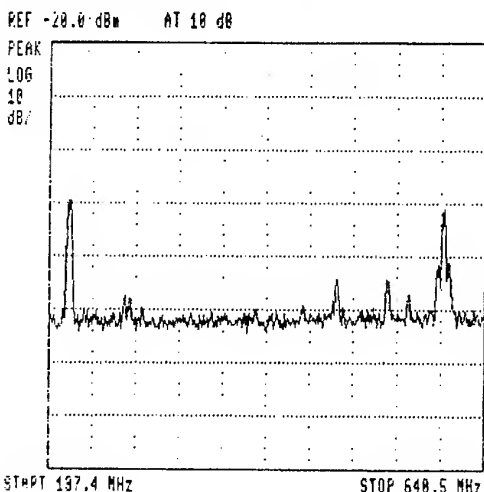


Fig. 6 Radiation from a tape recorder

The measurements were repeated lately in several local environments in Wroclaw. The measurements were performed with the use of a spectrum analyzer with a small size antenna which $A_F \approx -20$ dB and its frequency response flatness was estimated at the level of about ± 4.5 dB within the measuring range. The differences of EMF strength measured in different places have quite exceeded possible errors due to the unaccuracy of the set applied. An example of results of the measurements is shown in Fig. 7. We would not like to comment these results. Instead we will cite the regulation for a local TV cable network users [11]: *the operator is not responsible for the interference caused by a local TV station*. It is possible to confirm that the network is so 'transparent' to external EMI that direct reception of local TV is possible even without an antenna. Fortunately, the channels of local TV are not used in the network. However, this 'transparency' acts in opposite direction as well. As a result not only ARS 70 cm band and other radio and radar services working within the same frequency range are jammed but also direct reception of farther TV stations, in our case these are Czech stations located near the Polish border, i.e.: on Mt. Jasted, about 130 km west of Wroclaw, and Mt. Praded located about 120 km south of Wroclaw, is interfered.

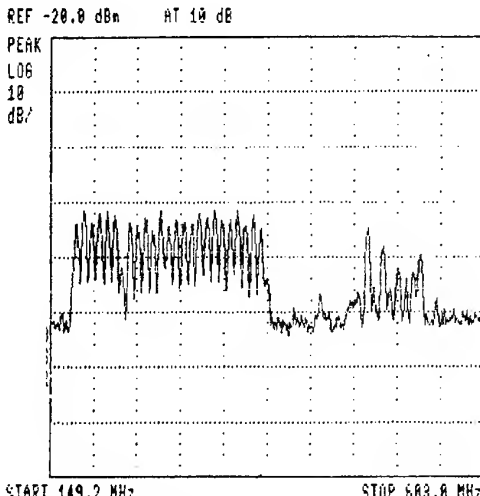


Fig. 7 EMI radiated by a cable network

5. EM RADIATION HAZARD

The most typical effects of interference, caused by ARS, are distortions in BC and TV reception, jamming of remote control and protection systems, voices may be heard in intercom installations and in audio devices - the latter are usually caused by CB-ists, which exceptionally were allowed to use AM [12]. We won't repeat here thousands of possibilities to interfere ARS. However, conflicts with neighbours may be minimized using known methods and solutions [13, 14], especially while a good will between both sides exists. Much worse problems are created when real or even imaginary exposure to EM radiation exceeds (or not) permitted levels. It was shown many times that well installed and well working ham's transmitter does not create any hazard in its proximity, even in the light of more restrictive Eastern exposure limits. Only one exception may be mentioned, i.e.: while high gain antennas are in use [15]. The point is still valid, however, circumstances were changed. EM phobia has come to this country as well. We may cite here an example with Polish LW station, where, after its antenna collapse, local committee has stopped the possibility to reconstruct the station in the same place. The problem with power line radiation was mentioned above. A lot of people visit our Lab in order to consult their problems with exposure created by mysterious devices installed by MI6, MOSSAD, KGB and other secret services, by their neighbours to damage them or even by Martians [16]. A part of these problems possibly could be explained on the ground of 'hypersensitivity', but not all of them. It shows the possibility of much more emotional approach to them as compared to interference. First examples are known. Several hams faced problems with their neighbours that accuse them of their health problems starting from cancer throughout headaches till variety of mysterious illnesses. It is necessary to add that in many cases the doubts of the people are groundless and resulted from their persecution mania or similar reasons. However, in

many cases the EMF intensity may really exceed permitted levels.

To repeat: with some exceptions no protection limits are exceeded by a well installed and well working ham's antenna system. It may be said that in majority cases these limits are exceeded due to the resonant phenomena and secondary radiation from accidental passive radiators. The problem of passive EMF 'amplification' has already been discussed [17]. In order to illustrate the phenomenon in Fig. 8 is shown standing wave on the power cord of a hanging lamp. The measurement has permitted to identify the source of radiation. Fig. 9 shows standing waves on a metal hand-rail in a terrace on the highest floor of an apartment house located at distance of about 150 m from a local FM/TV transmitting center.

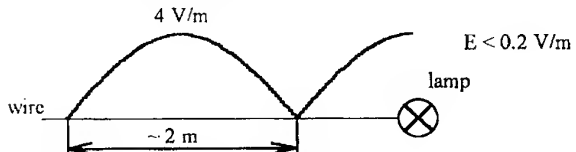


Fig. 8 EMF 'amplification' by the cable of a lamp

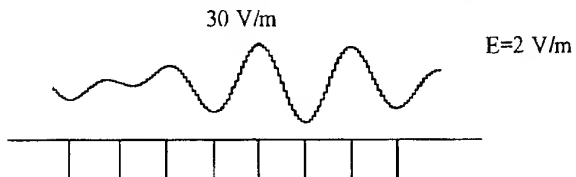


Fig. 9 Standing waves on a hand-rail

6. FINAL COMMENTS

The ARS, apart of many professional services, seems to be still very important and necessary service for the society. Its usefulness has many times been confirmed in the most difficult situations. The point was again fully confirmed during 'the flood of the millennium' in Poland last year.

Because of its location the service is the most experienced in interfered environments and is the first victim of the interference, especially in inhabited areas, where the level of the interference is one of the highest. In the same time the ARS, as often suspected to be a source of any possible troubles, is not allowed to install its antennas (examples from USA) or the antennas are used to confirm these troubles faced by neighbours. Paradoxically, a higher installed and more sophisticated antenna system on one hand creates a possibility to some separate the service against the environment and they protect the neighbours against discussed problems from the other hand.

We may formulate the final conclusion that the ARS, contrary to the past - while it was the only service using transmitters installed in inhabited areas and due to the 'long wire' type antennas applied - could have been the main source of the interference in the areas and presently may be responsible only for very small part of the interference. It results from the professional

equipment use and perfection in antennas' construction. As it may be seen from the presentation the biggest role is played here by a variety of devices and installations applied in house hold and it's surroundings now.

BIBLIOGRAPHY

- [1] G. Gardi, I. Montanari, U. Reggiani – Effects of power controller parasitic components on conducted EMI. Proc. Intl. EMC Symp., Zurich 1997, pp. 499–504.
- [2] M. Lutz – Oberwellen "Harmonics". EMC Kompendium 1998, pp. 210–213.
- [3] H. Endress, J. Pautz – Elektromagnetische Felder im Bedienungsbereich von Elektrowaermegraetik in Haushalt. ETA No. 46/1988, pp. 117–124.
- [4] A. Siwik, A. Gula, Z. Hanzelka, A. Jaglarz, R. Pietrucha – Higher harmonics in installations of communal customers (in Polish). Natl. Konf. on Electricity in Civil Engineering, Krakow 1997, pp. 40–46.
- [5] M. Rejmer – Problems of current and voltage harmonics in power installations (in Polish). Ibid. pp. 47–58.
- [6] H. Trzaska – 50 Hz? (in Polish). Polish Radiation Res. Assn. Natl. Meeting, Siedlce 1998.
- [7] H. A. Jordan, R. V. Gomez, L. H. Vazquez – Electromagnetic environment in a PC's room. Proc. Intl. EMC Symp. Sendai 1996, pp. 187–170.
- [8] J. Kusig, D. Hansen – CE requirements for modern television receivers. ITEM 1997 Up, pp. 24–29.
- [9] EN 55013 prA14 Final Draft
- [10] G. Schwarzbeck – Sensitivity of television video recorders to radio frequency fields. Proc. Intl. EMC Symp. Wroclaw, 1984, pp. 1037–48.
- [11] Regulation of the cable network users (in Polish). Telemozaika No. 6/98, p. 59.
- [12] Radio transmitters and home security systems. RSGB, Sept. 1996.
- [13] Guidelines for improving television and radio reception. The Radiocommunications Agency, Mar. 1997.
- [14] H. Cichon, H. Trzaska – Immunity improvement of home entertainment electronic devices. Proc. Intl. EMC Symp. Wroclaw 1984, pp. 1015–20.
- [15] H. Trzaska – ARS and EM-radiation hazard. Proc. 1994 Intl. EMC Symp. Sendai, pp. 191–194.
- [16] H. Trzaska – Hypersensitivity? Proc. COST-244 on EM Hypersensitivity, Graz 1996, pp. 106–117.
- [17] H. Trzaska – EMF near passive radiators. 1995 USNC/URSI Meeting, Newport, CA, p. 59.

BIOGRAPHICAL NOTE

Prof. H. Trzaska was born in Wilno (Poland) in 1939. His. M.Sc., Ph.Dr. and D.Sc. degrees completed at the Tech. Univ. of Wroclaw in 1962, 1970 and 1988 resp. Head of the EM Env. Prot. Lab., involved in labour safety and environment protection against EMF. Active ham radio SP6RT.

EMC Work in IARU

Christian M. Verholt
IARU EMC Adviser & Chairman of Reg. 1 EMC WG
Graekenslandsvej 140
DK - 2300 Copenhagen S
Denmark

General: This presentation will present the status of the work within the International Amateur Radio Union - IARU - Region 1 EMC WG, and gives views on the development in EMC, both in relation to technology and standards.

1. Introduction

1.1 Radio amateurs and EMC

As radio amateurs are heavy users of the radio spectrum, EMC problems has always been a major problem. Radioamateurs share the domestic environment with other users of electrical and electronic equipment and the compatibility problem includes both immunity and emission aspects.

This has been the case for more than 70 years giving the radio amateurs an outstanding experience with causes of interference, the social and physiological interactions, solutions of interference and the responses of authorities and manufacturers.

1.2 EMC work within IARU

The members of IARU are national amateur radio societies all over the world. Most national societies have formed their own EMC group giving advice to the individual radio amateur. Furthermore, many societies publish magazines where amateur relevant technical information including EMC relevant information is presented.

The main task of the IARU EMC working group is to gather and distribute information and to influence legislation and standardisation on an international level. IARU is a member of CISPR and is active in most EMC committees.

2. Concerns in relation to EMC

EMC is a matter of compatibility. Most manufacturers and importers of electronics tend not to consider the broad perspective of compatibility and customer

satisfaction, but focus on fulfilment of mandatory requirements. The European EMC Directive specifies mandatory compliance with the essential requirements expressed in broad terms as the equipment shall work satisfactorily in it's environment. However, manufacturers and importers focus on compliance with harmonised standards which may or may not give the desired compatibility. Some standards include a statement regarding mitigation methods and manufacturers should consequently be prepared to provide the necessary mitigation hardware when requested. If this is not the case then the main objective of compatibility has not been achieved. Anyone in doubt of how this works in practice should enter a radio-TV shop and ask for guidance on how to solve an EMC problem !

2.1. Will manufacturers fulfil the requirements

Experience has shown that some manufacturers meet the requirements, but a large number of manufacturers in the Far East - and the importers - sell products which does not fulfil the requirements. It is therefore essential that the enforcement of the national authorities is kept on a high level. This will secure fulfilment of the requirements, support the manufacturers who comply with the legislation and strengthen the trust in European regulation.

2.2. High speed data

The development in high speed data systems goes in the direction of use of higher and higher data rates on existing unshielded twisted copper-pairs originally installed for analogue telephones. The interference potential of the broad-band signal covering several MHz and the radiation properties of these "old" cables give rise to major concerns for users of the radio spectrum. The present standards were not developed with this kind of emitters in mind. The emitted signals, the emitted levels and the distance between emitter - equipment and

cable is different. ITE equipment and networks are now used in close proximity to telecommunications equipment incorporating radio receivers and transmitters.

3. The electromagnetic environment

3.1. Emission

Previously, electric motors generated broad-band noise and oscillators generated narrow band noise on discrete frequencies. The space between the narrow band signals are now being filled by "spread spectrum" signals and consequently the "noise floor" rises. There are only three ways to manage this interference problem e.g.: to increase the distance between source and victim, increase the wanted radio signals by increasing the transmitter power or keep the unwanted emission levels below the appropriate levels.

3.2. Immunity

The rapid increase in usage of cordless equipment increases the emitted radio signals to levels up to 30V/m depending on type and distance. Most people will expect electronic equipment to work without annoying interference at a distance of more than 1 meter. Some kinds of equipment are used in situations where distances may be smaller as e.g. when a user of wheel chairs uses a mobile telephone.

The average fields from radio amateur transmitters are typically in the range of 1 to 10V/m at the place of neighbours' electronic equipment. However, the levels may be up to 100V/m (peak value) under certain conditions.

The constraint on the height and placements of antennas and masts is a major cause of some of the high field strengths.

4. Trends in technology

4.1. General

The change of technology sometimes changes the EMC properties of equipment. A good example is the GSM mobile telephone system, where the resulting interference from the pulsed carrier is just as annoying as any other AM modulated interference.

The use of SMD components improves the immunity of equipment because of their more ideal - non parasitic - properties.

The larger integration reduces the sizes of PC boards and the number of boards which is beneficial with respect to both immunity and unwanted emissions.

The technology used by radio amateurs is - from an interference perspective - virtually unchanged. The receivers have become more sensitive and at the same time more immune to overloading by large signals. The

latest technology in digital signal processing reduces some of the negative effects from other interfering sources.

The transmitted signals from radio amateur transmitters will still be dominated by AM-like signals.

4.2. Broadcast radio and TV

Broadcast radio and television becomes more and more digital and the difference between computers and other kinds of video/audio equipment will diminish. This may improve the immunity of video and audio equipment, but the emissions compared to purely analogue equipment will increase both in frequency and levels.

4.3. Digital technology

The clock speed in computers increases and so is the number of peripherals. The boxes and other things which have an influence on the emission level have not changed significantly which this results in an increase of interference above 200MHz. The number of computers and other kinds of equipment incorporating high speed CPU's is increasing in huge numbers. Anyone carrying a VHF receiver moving through a normal residential area with small shops, petrol stations, amusement centres etc. will experience interference on almost any frequency. Lately police and fire-fighters are sometimes without secure radio communication because of interference from office machinery.

5. Trends in standardisation

5.1. General

The role and usage of international standards increase because of the change of legislation towards a more international regime, and this has shifted the setting of limits from national authorities to a forum dominated by manufacturers. We fear that this will result in standards with an inadequate level of protection offered to radio services.

5.2. Emission

Emission limits are kept uniform for most equipment, but there is an increasing number of standards where exceptions allow more or less free unwanted radiation. This development should be monitored in IEC by ACEC and in CENELEC by TC210. It is our hope, that this supervisory function is done properly and on an objective basis.

5.3. Immunity

Immunity requirements should also be based on environmental considerations where radio services used in the environment and the typical configuration e.g. protection distances are taken into account.

Furthermore, the interference susceptibility of the receiving system should be taken into account. At present the new digital radio services have not been evaluated properly and therefore this work should be performed as soon as possible.

5.4. Test methods

Measurement methods are simplified and unified whenever possible, but the difference between direct radiation and indirect radiation from attached cables should be recognized and accepted. Radio amateurs have many years of experience on how to cure emission problems, and we have experienced that radiation from cables and radiation from cabinets are two different things without real commonality.

7. Future work in IARU

The IARU Region 1 Working Group will continue to:

- monitor and participate in the EMC work
- prepare technical information to both professionals and radio amateurs
- support the EMC work in national societies
- distribute technical information
- give recommendations regarding acceptance of draft standards
- be a forum within the radio amateur community for EMC related discussions

8. Conclusions

8.1 The radio amateurs are very concerned with regards to protection of radio services. We hope that the users of the radio spectrum together with national authorities and manufacturers will acknowledge the need for adequate protection of radio services. We are especially concerned with the rapid introduction of high speed telecommunication services on existing unshielded cables.

The work of the EMC WG is of great importance to the radio amateurs because of the international development of limits and regulation. The individual radio amateur can not do this on their own, nor can the national society.

The IARU EMC WG shall continue to influence the professional and commercial EMC work to the benefit of the radio amateurs.

Support from all WG members and national societies is vital for the success of the work..

BIOGRAPHICAL NOTE

Christian M. Verholt

Radio amateur since 1970 as OZ8CY. Project manager of an EMC test lab in Jutland Telephone Company, Denmark, 1977 to 1990. Active in EMC standardisation since 1982 and a member of IEC TC77, TC77B, TC85, CISPR (S, E, G); CENELEC TC210, SC210A, TC211, SC211B.

XI

ESD, LIGHTNING, EMP

COMPUTER SIMULATION OF ACTION OF LIGHTNING CURRENT ON THE CONSTRUCTION OF ANTENNA MASTS

Gennadij G. Chavka, Karol Aniserowicz

Technical University of Białystok, ul. Grunwaldzka 11/15
15-893 Białystok, Poland

A new modification of a full, precise and detail time- and frequency analysis of current and voltage distribution along the construction of antenna masts and their arbitrary chosen elements during the lightning strike is described in this paper. The received results may be used for EMC tests and protection circuits design of existing and modernising antenna masts under the conditions of lightning action.

1. INTRODUCTION

A proposed modification of the computer simulation of the lightning current action on antenna mast is based on the studying of a spectrum of the lightning current pulse and on the full analysis of some frequency characteristics of the different parts of the mast regarding the influence of the mutual coupling and the second radiation of the construction. These are: the cross-admittance and the current transmittance from the lightning strike point to an arbitrary given element of the construction; the distribution of these characteristics and current-voltage spectrum along the chosen element of the mast. Resonant properties of the above characteristics are discussed. The Discrete Fourier Transform is used to obtain the current and voltage distribution in the time domain.

2. TIME AND SPECTRAL CHARACTERISTICS OF LIGHTNING CURRENT PULSE

There are different mathematical models of the lightning electromagnetic pulse [1-3,5]. The often used double-exponential model (DEXP) of the lightning current pulse is taken under considerations:

$$i_l(t) = I_m k (e^{-\alpha t} - e^{-\beta t}) = I_m k i(t) \quad (1)$$

where I_m - the pulse maximum, α and β - pulse parameters, k - scaling coefficient :

$$k = 1/i(t_o), \quad t_o = \ln(\beta/\alpha)/(\beta - \alpha), \quad (2)$$

t_o - time of maximum (Fig. 1). It is known that β factor

determines basically a pulse front-time, and α factor - a half-delay time of the lightning current pulse; in this case $\alpha < \beta$. In this paper, it is accepted a standard IEC lightning current pulse model with the maximum value $I_m=100\text{kA}$, the front-time $1.2\mu\text{s}$ and the half-delay time $50\mu\text{s}$ for which: $\alpha = 1.466 \times 10^4 \text{ s}^{-1}$, $\beta = 2.469 \times 10^6 \text{ s}^{-1}$, $k = 1.0373$, $t_o = 2.089\mu\text{s}$ (Fig.1) [1,3].

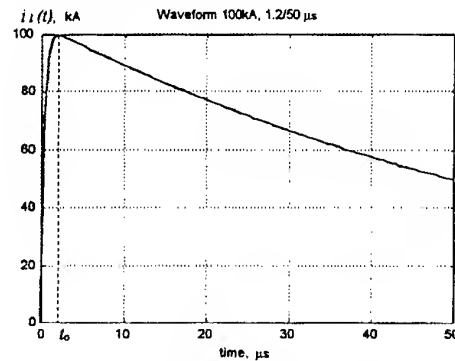


Fig. 1. Lightning current pulse

The spectral characteristics $I_{light}(j\omega)$ of the lightning current pulse (1) for the above-mentioned parameter values obtained by the Fourier Transform are shown in Fig. 2. It is significant that the spectrum modulus has a monotone form, but the phase has a wave type.

For the precise computer simulation it is important to formulate a criterion of the reconstruction quality of the time domain characteristics from the pulse spectrum samples. A process of synthesis of the waveform $i_l(t)$, using the Discrete Fourier Transform (DFT) was analyzed. In particular, it was determined that the frequency step must be $\sim 2\text{kHz}$ and the maximum frequency of a spectrum $\sim 1\text{MHz}$ for a level $\sim 60\text{-}70\text{dB}$ from the value $I_{light}(0)$ (the synthesis error $\sim 1\text{-}2\%$).

The influence of α and β factors on the width and the form of the spectrum was analyzed. In particular, there was determined that the width of the lightning current pulse spectrum depends almost not at all on value of the front-time of the current pulse.

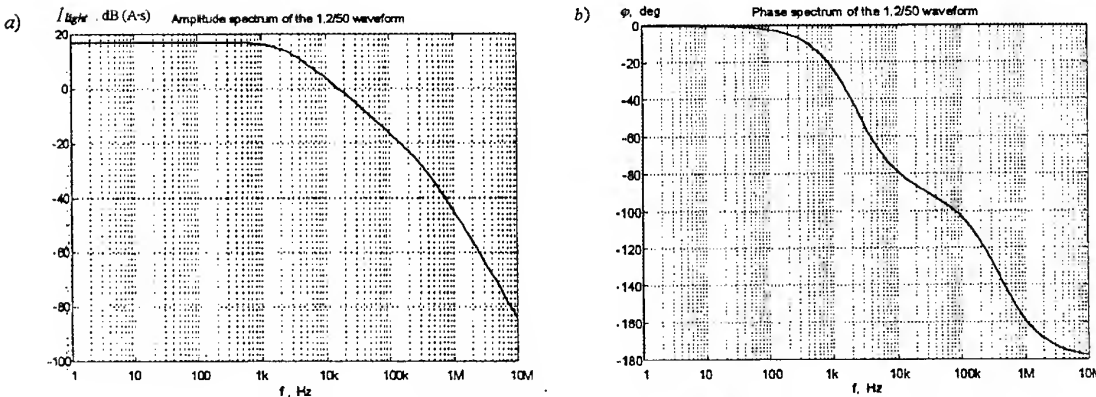


Fig. 2. Spectrum of the lightning current pulse: modulus (a), phase (b)

3. A METHOD OF COMPUTER SIMULATION

The computer simulation of the action of the lightning current pulse on the antenna tower is based on the analysis and modification of some frequency characteristics of the different parts of the mast construction. A somewhat another approach to this task is described in [6]. The considered antenna mast consists of the tower and of six guys in two levels (Fig. 3). It is used a simplified model of the lightning strike as an apex drive by an ideal 1V frequency independent voltage generator connected between the top of the mast and an additional short monopole. Then the distribution of currents along the mast and guys is calculated in the frequency domain basing on the mixed-potential equations combined with the method of moments for the polynomial approximation of the current [4].

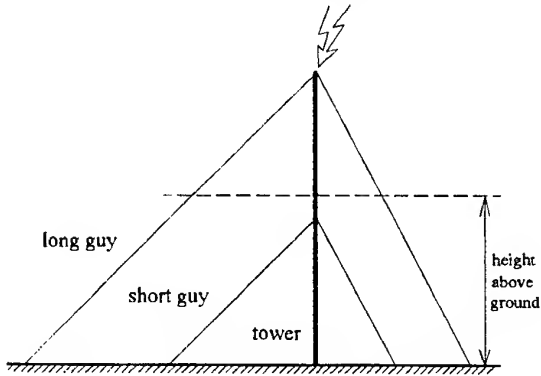


Fig. 3. Guyed antenna mast (two levels of guys)

Here follows the algorithm of computer simulation:

- calculation of the input admittance and the cross-admittance from the top of mast to an arbitrary given element (segment) of the construction, for drive of 1V; these are numerically equal to the input current $I_{inpV}(j\omega)$ and the current distribution $I_{sV}(j\omega)$ along the segments;

- determination of the current transmittances of the different segments of the mast:

$$T_s(j\omega) = I_{sV}(j\omega) / I_{inpV}(j\omega); \quad (3)$$

these are equal to the current distribution along the segments for the driving by the 1A frequency independent current source on the top of the mast;

- calculation of the spectrum of the segment's current for given spectrum of the lightning current pulse $I_{light}(j\omega)$ (Fig. 2):

$$I_s(j\omega) = T_s(j\omega) \times I_{light}(j\omega); \quad (4)$$

- determination of the voltage spectrum distribution along the segment:

$$U_s(j\omega) = I_s(j\omega) \times j\omega L, \quad (5)$$

where L - a lumped inductance of the short (lower) part of the segment;

- use of DFT to obtain the current $i_s(t)$ and voltage $u_s(t)$ segment distribution in the time domain.

All of the above-mentioned frequency characteristics depend on the position of the observation point along the analysed segment and they have an information about resonant or aperiodic properties of the different elements of the antenna mast.

The influence of radiation of the construction and the mutual coupling between metal parts is taken into account automatically during formulation of the integral equations.

The analysis of the influence of distributed power losses in metal parts may be included into the algorithm. There may be also modeled relatively small details of the construction as equivalent lumped reactive or complex elements.

4. FREQUENCY CHARACTERISTICS OF THE ANTENNA MAST

Consider the mast consisting of the tower and of two levels of guys (Fig. 3). In the example below the height of the mast is 100m, all the angles between the guys and the ground are 45°, the angles between the guys are 120°. The perfect ground is assumed.

The analysis of the cross-admittance and the current transmittance as the 3D functions of frequency and of height above ground was performed during computations. The results of the analysis are shown in Fig. 4-7.

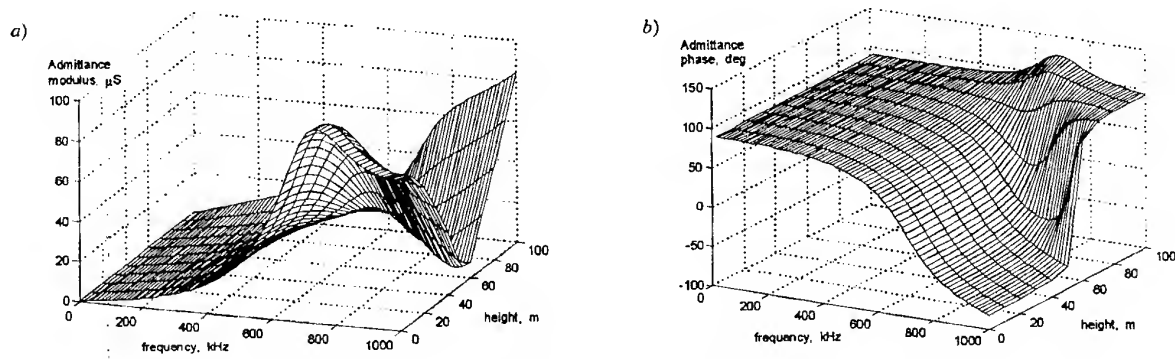


Fig. 4. Distribution of the modulus (a) and phase (b) of the cross-admittance along the long guy

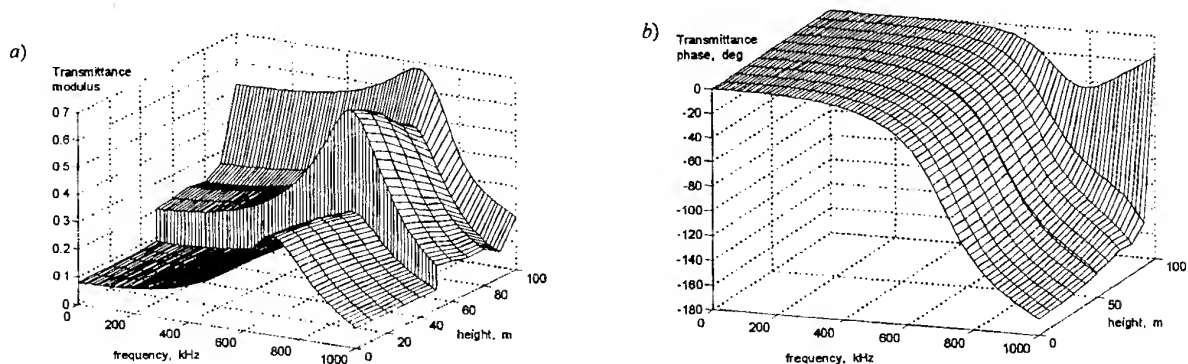


Fig. 5. Distribution of the modulus (a) and phase (b) of the current transmittance along the tower

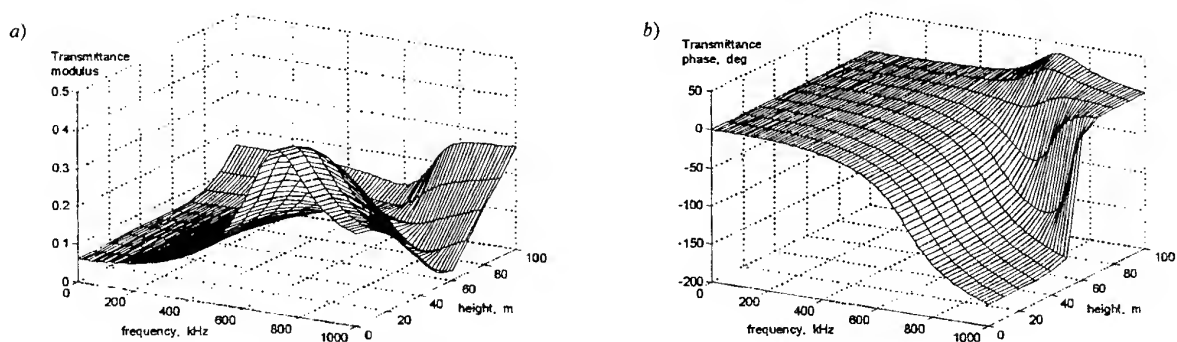


Fig. 6. Distribution of the modulus (a) and phase (b) of the current transmittance along the long guy

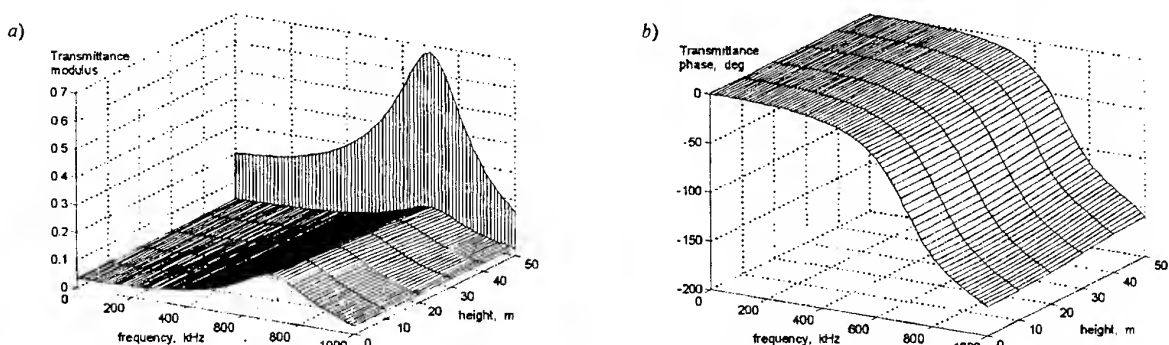


Fig. 7. Distribution of the modulus (a) and phase (b) of the current transmittance along the short guy

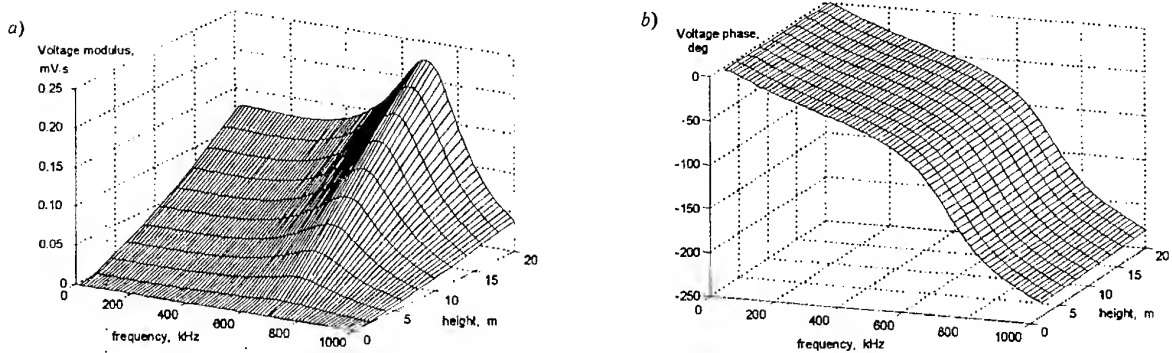


Fig. 8. Distribution of the modulus (a) and phase (b) of the voltage spectrum near the bottom of the tower

There was also analysed the distribution of the voltage spectrum near the bottom of the tower (Fig. 8).

These 3D figures comfortably show a dependence of the currents or the voltages from the frequency for the given point of the construction as its dependence from height above ground for chosen frequency. The resonant character of the structure is expressed in these figures.

The analysis of the spectral characteristics is very advantageous because it leads to the formulation of the criterion of how wide range of the spectrum should be taken into account during return to the time domain. From many numerical experiments it follows that at least first resonance should be included for objects as large as antenna towers. For the example presented in this work the spectrum range of 1 MHz was analysed.

Including next resonances gives small changes to the results shown in Fig. 9 because of relatively small amount of lightning energy above 1 MHz (see Fig. 2).

5. TIME DOMAIN CURRENT AND VOLTAGE CHARACTERISTICS

The results of computations of the current and voltage 3D distribution along the elements of the construction are presented in Fig. 9. It is shown that the current intensity decreases while going down from top to the bottom of the mast. The discontinuous current changes (see Fig. 9a and 9c) are because of the division of the current between the tower and the guys due to the Kirchhoff's law.

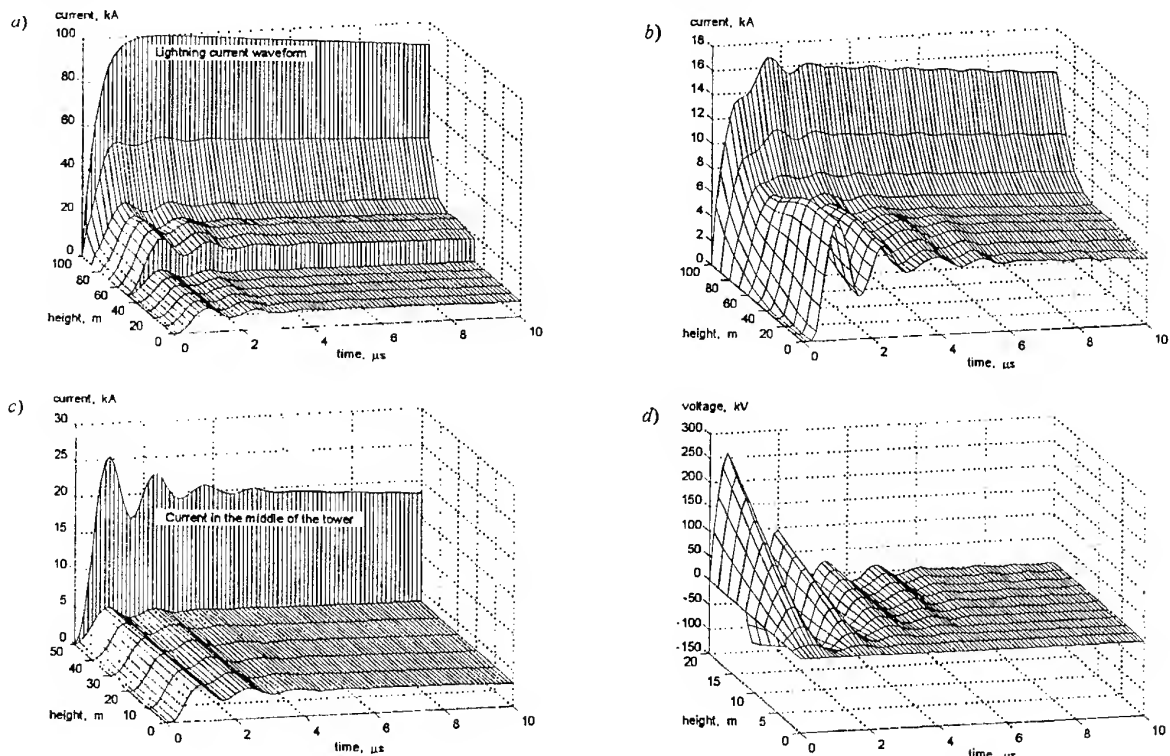


Fig. 9. Distribution of the lightning current along the tower (a), the long guy (b) and short guy (c) (in the background of (a) and (c) the lightning current and the current in the middle of the tower is shown, respectively). Voltage distribution near the bottom of the tower (d)

The continuous current decreasing while going down the mast may be explained by the electromagnetic radiation, as well as damping of the oscillations in the function of time. The oscillations are growing while going down the construction due to the changes of the current transmittance.

The period of the oscillations is adequate to the dimensions of the structure. The changes of the current along the long guy are much more significant than along the short one because the short guys are 'encapsulated' by the construction.

The voltage between the ground and the chosen point of the tower grows to some hundreds of kilovolts vs. the height above ground. The computations of the voltage changes higher than several meters above ground may not have any sense because of the lumped inductance used in the model of the electric circuit.

6. CONCLUSIONS

The paper presents a new modification of a full and detail time- and frequency analysis of current and voltage distribution along the construction of antenna masts and its arbitrary chosen segments during the lightning strike. The method of computations is based on the studying of the spectrum of the lightning current pulse and the full analysis of frequency characteristics of the different parts of the mast with due regard for the influence of the mutual coupling between the elements and the second radiation of the construction.

The example of computations of the simplified model of antenna mast is given. From the included quasi-3D figures in the frequency and time domains it is seen that the electrical properties of the segments of the mast vary in the function of height above ground. The resonant character of the mast is much more significant near the bottom than near the top.

The full analysis in the frequency domain is very important before proceeding the inverse Fourier transform. It helps to make the proper choice of the width of the spectrum and the step of computations in the time domain. At least first resonance of the structure should be included during numerical analysis.

The considered spectrum range depends on the pulse current parameters and on the dimensions of the mast. The proposed algorithm may be generalised to any lightning current waveform and any construction.

7. REFERENCES

1. R.B.Standler, "Protection of Electronic Circuits from Overvoltages", J. Wiley & Sons, N.Y., 1989.
2. D.J.Bem (ed.), "Electromagnetic Pulse Overstress", (Polish), Wrocław Techn. University, Wrocław, 1994.
3. V.I. Kravchenko, "Lightning protection of radio-electronic equipment", (in Russian) Radio and Communication, Moscow, 1991.

4. A.R.Djordjević, M.B.Baždar, T.K.Sarkar, R.F.Harrington, "Analysis of Wire Antennas and Scatterers (AWAS)", Artech House, London, 1995.
5. A. Karwowski, "Time- and frequency-domain characteristics of LEMP", Proceedings of the 13th Int. Wrocław Symposium on Electromagnetic Compatibility EMC'96, pp.489-493.
6. A. Karwowski, "Use of the impedance matrix interpolation technique in numerical modelling of lightning protection systems", Proceedings of the 13th Int. Wrocław Symposium on Electromagnetic Compatibility EMC'96, pp.175-178.

ACKNOWLEDGEMENTS

The authors would like to acknowledge the support of this work by the State Committee for Science Research of Poland under Grant 8 T11D 008 14 (G.C.) and under Rector's Project W/WE/2/95 (K.A.).

BIOGRAPHICAL NOTES



Gennadij G. Chavka was born in Russia in 1942. He received M.Sc., Ph.D. and D.Sc. degrees from Saint-Petersburg State Electrotechnical University, Russia in 1965, 1969 and 1987 respectively. Since 1988 he is Professor of a.m. University, and since 1993 he is Professor of Electrical Engineering, Technical University of Białystok too. He is a member of Institute of Electrical and Electronics Engineers, USA. The main interests are: radiocommunication, antennas and antenna arrays, network synthesis, broadband radiotransmitters, multiport transmitting and receiving subsystems, CAD of radio equipment. He is the author of 6 books, 25 patents, some 130 papers and conference presentations.



Karol Aniserowicz was born in Białystok, Poland, in 1955. He received the M.Sc. degree in electronic engineering from the Warsaw University of Technology, in 1979 and the Ph.D. degree in electrical engineering from the Technical University of Szczecin, in 1987. Since 1979, he has been with the Department of Electrical Engineering, Technical University of Białystok. He was one of the founders of the Center of Protection from Overvoltages and Electromagnetic Interferences in Białystok, established in 1995. His research interests include electromagnetic compatibility, industry applications of microwaves, and numerical methods applied to the theory of electromagnetic fields.

THE OCCURRENCE OF TRANSIENT FIELDS AND ESD IN TYPICAL SELECTED AREAS

Stephan FREI

Technical University Berlin, Institute of Electrical Power Engineering
Einsteinufer 11, 10587 Berlin, Germany
e-mail: frei@ihs.ee.tu-berlin.de

The occurrence rate of Electrostatic Discharges (ESD) depends extremely on the environment. Several parameters influence ESD and the severity of this interference. A special measurement system to measure the transient fields of ESD was designed. Measurements were done in different environments. A theoretical model was developed, helping to predict and to evaluate the severity level of an environment towards ESD.

1. INTRODUCTION

Electrostatic Discharges (ESD) can cause temporary disturbances or even lasting destruction of electronic devices. The critical components of an ESD-event are both the current and the always associated transient E- and H-Field. The short rise times of the ESD-current can cause strong, steep-rising fields even at larger distances from the discharge location.

Due to the stochastic nature of ESD it is very difficult to determine the currents and the fields of ESD occurring under practice conditions. Many parameters influence the occurrence rate and the intensity of real ESD.

The direct environment of a device and the activities which happen in the environment determine the ESD threat. Each environment has its own average hazard potential. In the test standard IEC 1000-4-2 there are little considerations concerning the environment dependency of the ESD threat: It is however desirable to improve the ability to differentiate better the actually possible extent of the environmental hazard potential. If it is sure, that a certain threshold of a disturbance variable does not or only occur with infinitesimal probability, in certain cases the protection level can be reduced. However, only with knowledge of the occurrence rates and the intensities a decision can be made.

In reality ESD pulses can have a higher disturbance intensity than even the strongest pulses, which are prescribed with a test to meet the IEC 1000-4-2

standard. In the standard a negligible occurrence frequency of these strong disturbances is assumed. This is hardly provable so far.

Apart from study [1] published at the beginning of the 80's, there is no detailed information about ESD in practice so far. The mentioned study examined only two different environments and did not consider the fields of ESD. Due to the small number of examined environments and the disregard of the ESD field effects, the results of this investigation are incomplete and cannot be generalized.

In order to increase the knowledge base concerning the occurrence rate and the intensity of ESD events that really occurs in practice, long-term measurements of the transient fields at three different places were made by means of a new developed, complex measurement system [2]. The large variation of ESD and the necessity for further tools to determine the occurrence of ESD under practice conditions was confirmed.

A universal stochastic model of ESD can be helpful. It has to consider the substantial parameters of ESD, and it should be able to characterize ESD with a few, simple measurements and general considerations of the environment.

With the help of a stochastic model it would be possible with little effort to receive the ESD hazard potential that is possible in an environment. The stochastic model helps to determine suitable test procedures and also to select the really necessary protection measures.

A stochastic model for the occurrence rate of ESD considering the intensity distribution is presented here.

2. EXPERIMENTAL METHOD

The developed and applied measurement system consists of a specially designed circuit for the evaluation of fast transient pulses. The measurement system is

equipped with several field sensors. It is optimized for ESD long term measurements. The E- and H-fields are measured separately. This system automatically registers the amplitude of impulsive fields within the range of 20 V/m up to 1000 V/m or 0.05 A/m up to 2.7 A/m. The pulse width can thereby be smaller than 1 ns. Apart from the pulse amplitudes the system records important frequency components, environmental conditions (temperature, relative humidity) and time. The maximum repetition rate is higher than 25 kHz. A detailed description of the developed measurement system can be found in [2].

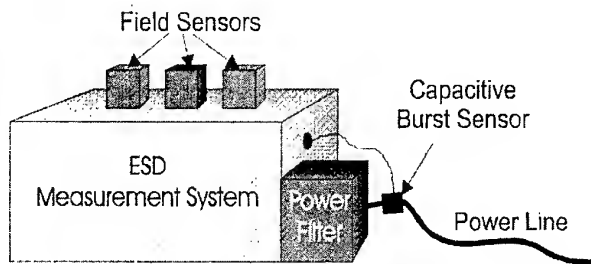


Fig. 1: Capacitive sensor connected to the power line for burst detection

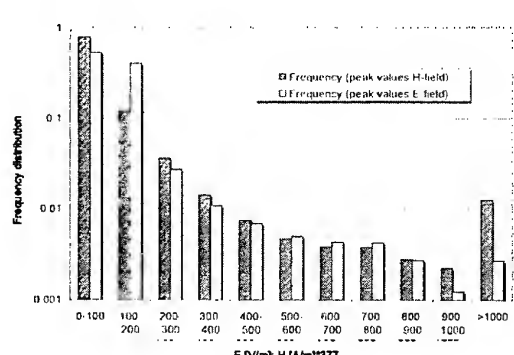
The often occurring burst fields (switching actions propagated by the power lines) can be mistaken for ESD events. For this reason a differential measurement method was implemented. Burst pulses were detected by a capacitive sensor placed on the power line of the

measurement system. If this burst sensor measures a pulse at the same time with the field sensors and a certain relation between the signals is exceeded, the measurement system rejects this event. With this method, the measurement of ESD by the observation of the transient fields is possible.

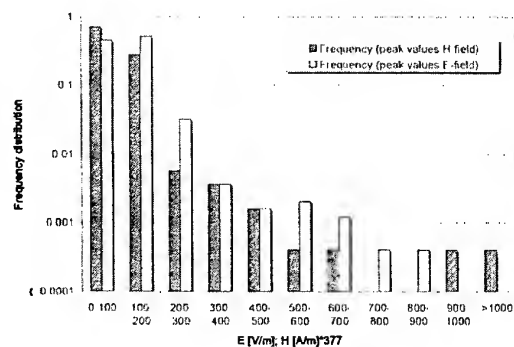
The measurements presented here were done without this burst sensor. The criterion for Burst rejection was the level of the pulses.

3. EXPERIMENTAL RESULTS

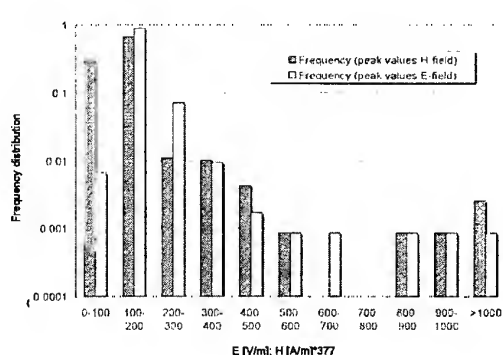
By means of three identical measurement systems at three different measuring locations long-term measurements of the impulsive fields were done. One location, the university library of the Technical University Berlin, was selected due to ESD promoting conditions there. ESD occur there very often. The device was placed in an arbitrarily chosen book shelf. The second measuring location was under a workstation, on the floor in a student electronics laboratory. The students there work with a lot of ESD-sensitive electronic components. The system was located in the middle of the room. The third location was a computer room equipped with 8 PCs. Here the device was placed in the middle of the room on the floor. The relative humidity during the entire measuring period ranged between 30% and 40%, the temperature was nearly constant with approx. 20°C.



a)



b)



c)

Fig. 2: Frequency and intensity of impulsive field events in three different environments

- a) Library; duration of measurement 20 days; 18620 events;
- b) Computer room; duration of measurement 14 days, 2488 events
- c) Electronics laboratory, duration of measurement 9 days, 1162 events

Histograms of the results of the measurements can be found in figure 2. The histograms show the relative frequency of the field pulses as a function of the amplitude. As expected in all three cases the weak field pulses occurred substantially more frequently than the stronger pulses.

Among the many impulsive events, which were recorded by the system, also many Burst (switching) actions can be found. Even though the ESD fields often differ from the fields generated by switching actions (frequency spectrum, repeating rate), nevertheless in practice it is very complex to execute this differentiation. The limited dynamic range of the used measurement setup and interference with the environment cause problems. With larger field strengths the necessary dynamic becomes available. In normal environments in larger distances large field strengths can be produced only by ESD. A minimum distance of 1 m was ensured between the measuring instruments and other electrical equipment. From investigations it could be determined that the switching actions occurring in the environments cause field strengths of less than 250 V/m or $250/Z_0$ A/m. With the described differential measurements or an evaluation of the data with neural networks, a better distinction would be possible.

In the examined library an ESD promoting carpet is laid. A high activity of students and staff further promotes the frequent occurring of ESD. Here an average number of 931 pulses per day was measured. In the computer room and the electronics laboratory an older linoleum floor is laid. This floor does not particularly promote ESD. Also less activities generating triboelectricity can be found there. Only 178 (computer room) or 129 (electronics work space) impulsive events per day could be measured in average. A lot of the pulses are generated by switching actions.

Site	Number of pulses/day	Number of pulses >500 V/m/day	Number of pulse >500/377 A/m/day	notes
library	931	19	28	-many activities -flooring
computer room	178	0,9	0,4	-less discharge locations
electronic laboratory	129	0,7	0,8	-less critical activities

Table 1: Comparison of the average number of strong field pulses in the different sites

The higher frequency of large H-field amplitudes measured in the library compared to the frequency of E-field amplitudes can be explained by the fact that most

of the strong discharges were probably caused by a discharge in a door handle located in a distance of approximately 2 m from the measurement instrument. The E-field probe was shielded in this direction by a metal book shelf.

In table 1 the environments are compared. In the university library an average number of 19 to 28 ESD serious events per day occur, which cause a field strength of more than 500 V/m or 500/377 A/m at a quite arbitrarily selected measuring point. In the other environments less than 1 serious ESD event could be measured in average per day. The ESD promoting conditions in the library like the floor and the activities caused such big differences.

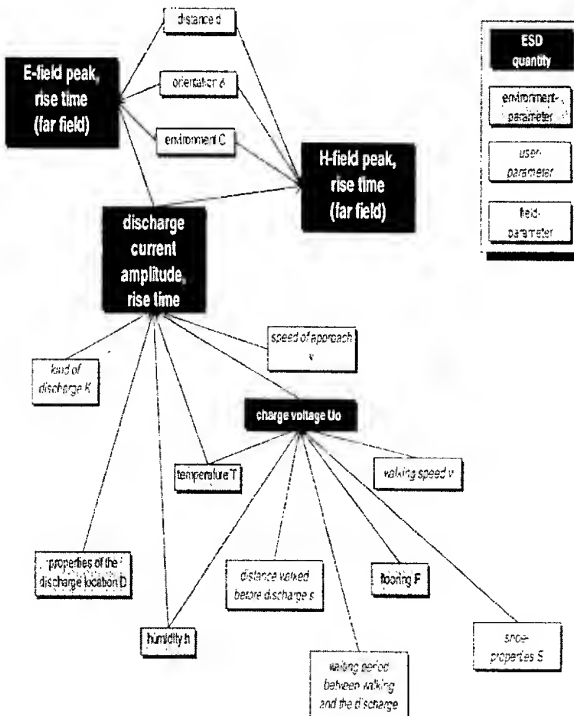


Fig.3: Dependency of ESD from the 'environment'

3. A STOCHASTIC MODEL OF THE OCCURRENCE OF ESD

The actually interesting parameters of ESD are the currents and the fields, but the always preceding charging process can be characterized by the generated charging voltage. To describe the severity of an ESD, the charging voltage is however an unsuitable quantity. For the same charging voltage, e.g. the amplitudes of the currents can vary to up to three orders of magnitude. The current derivatives, the amplitudes and the derivatives of the fields can vary even up to three orders of magnitude [3].

Parameter	Abbreviation	Example	Possible Probability Density Function	f0
1 distance walked before discharge	s	0-20 m	Exponential Distribution	
2 walking speed	v _L	0-1 m/s	Normal Distribution	
3 flooring	F			
4 shoe-, garment properties furniture properties...	S			
5 delay between walking and the discharge	t			
6 rel. humidity	h	10-90%	Normal Distribution	
7 temperature	T	0-35°C	Normal Distribution	
8 charge voltage	U ₀	0-20 kV	Exponential Distribution	s,v _L ,F,S,t,h,T
9 kind of discharge	K	finger, metal piece		
10 speed of approach	v		Normal Distribution	
11 properties of the discharge location	D	impedance Z of the current path		
12 discharge current	i _{max} , $\frac{di}{dt}_{max}$		Exponential Distribution	U ₀ ,h,T,K,v,D
13 distance	d	0-3m	Exponential Distribution	
14 orientation	ϕ	0-90°	Normal Distribution	
15 environment	C	reflection		
16 E-field (far field)	E _{max} , $\frac{dE}{dt}_{max}$		Exponential Distribution	i,d,ϕ,C
17 H-field (far field)	H _{max} , $\frac{dH}{dt}_{max}$		Exponential Distribution	i,d,ϕ,C

Table 2: Parameter influencing the occurrence rate and the intensity of ESD (assumption: electrification by walking)

With some additional assumptions statements concerning the severity level of ESD can be derived from the charging voltage distribution.

ESD depends on many parameters. The table prepared by Ryser [4] was extended in table 2 with further important parameters. In figure 3 the dependencies are presented graphically. It must be kept in mind that it is impossible to consider all influencing parameters. Only the most important ones are specified here.

The generation of charge and the charging voltage mainly depend on the parameters specified in table 1, line 1-7. The exact functional dependencies between the parameters and the value of the charging voltage can hardly be determined by analytical calculation, since the conditions are too complex. However based on measurements the necessary dependencies can be determined. By measurements a table can be made with the approximate charging voltage as a function of the individual parameters. A function:

$$U_0 = f(s, v_L, F, S, h, t)$$

can be generated from this table, which determines U₀.

The occurrence of each single parameter, specified in table 2, is determined by the respective probability density distribution for each environment.

4.1 Calculation of the resulting probability function from the individual probability functions

If the probability density functions $f(x_i)$ of the individual parameters are known, the total probability function can be determined by simple multiplication of the functions (1), due to the stochastic independence of the individual ESD influencing parameter:

$$f(x_1, x_2, \dots, x_n) = \prod_{i=1}^n f(x_i) \quad (1)$$

An area of the n-dimensional density function may represent, e.g. the probability of a certain current amplitude.

In many cases the distribution function is of special interest, i.e. the function, which determines the probability that a disturbance quantity $g(x_1, \dots, x_n)$ is bigger than a certain threshold g_0 . If a constant distribution of the densities is assumed, the distribution function can be determined (2):

$$F(g_0) = P(g \geq g_0) =$$

$$\iint_{g(x_1, x_2, \dots, x_n) \leq g_0} \dots \int f(x_1, x_2, \dots, x_n) dx_1 dx_2 \dots dx_n \quad (2)$$

5. DISCUSSION

The measured distributions in figure 1 can be approximated by an exponentially dropping function. This correspond with the assumption that the different charging voltages occur with an exponential distribution (acceptance; the walking distances are exponentially distributed and on the average are the charging voltage is a function of the distance). This dependency was already determined empirically in [1]. It is also obvious that ESD events far away from the measuring point appear more often than ESD events close to the measurement system (uniform distribution of the discharge locations assumed). This is just determined by the available space. Even if an exponential distribution is assumed here, the resulting function is again an exponential distribution.

The measured dependency can thus be explained by theoretical considerations. Considering ESD as a complex stochastic process it is possible to determine the intensity and frequency of the ESD in an environment with a few measurements and observations. A necessary prerequisite is the knowledge of the individual dependencies.

Even if the accuracy of such an estimation will not be very well in many cases, this will cause less problems. The variations that occur with almost all measurements concerning ESD, they do not influence a stochastic model. As long as the kind of distribution, the expected value and the variance correspond, the result does not change or it changes only insignificantly. This agreement can be achieved with some measurements and basic considerations.

6. CONCLUSION

At selected locations measurements of the transient fields were done. A stochastic model for ESD was presented. With some measurements and basic considerations the average intensity and frequency of ESD can be determined.

A lot of the data, which is necessary for the modeling of ESD as a stochastic process, does unfortunately not yet exist. This will be an important aspect of our future work. Further a simulator program, which describes an environment concerning its ESD behavior, will be developed.

ACKNOWLEDGMENT

The author wishes to thank the German Research Foundation (DFG) for the financial support of this project.

7. REFERENCES

- [1] R. B. Simonic, "Electrostatic Furniture Discharge Event Rates for Metallic-Covered, Floor-Standing Information Processing Machines", IEEE International Symposium on EMC, 1982
- [2] S. Frei, D. Pommerenke, "A Study of the Impulsive Field Occurrence Rate and Intensity", IEEE International Symposium on EMC, 1997
- [3] S. Frei, D. Pommerenke, "Wirkung von transienten Feldern auf digitale Systeme", EMV '96 Karlsruhe, 1996
- [4] H. Ryser, "The Relationship Between ESD Test Voltage and Personnel Charge Voltage", EOS/ESD Symp., 1990

BIOGRAPHICAL NOTES

Stephan Frei was born in 1966 in Hanau, Germany. He received his diploma in Electrical Engineering in 1995. He is now a research assistant in EMC at the Technical University of Berlin, Institute of Electrical Power Engineering. There he works on a long term study sponsored by the German Research Foundation (DFG) concerning the occurrence rate of ESD in typical environments. Another research interest is the sensitivity of electronic systems to fields of ESD.

APERTURE PENETRATION OF FIELDS RADIATED BY ESD

R. Jobava, R. Zaridze, P. Shubitidze, N. Adzinba, D. Karkashadze,
R. Beria, M. Sukhiashvili, S. Frei*, D. Pommerenke**

Laboratory of Applied Electrodynamics, Tbilisi State University 3 Chavchavadze Ave.,
Tbilisi, 380028, Georgia, Tel & Fax: +995 32 290845, e-mail: lae@resonan.ge

*Technical University of Berlin, Germany

**Hewlett Packard, Roseville, USA

Abstract - Numerical study of aperture penetration of transient fields related with indirect Electrostatic Discharge (ESD) is presented. Computer simulation of ESD from spheroid is performed to model human hand discharge. Computed ESD fields are in a good agreement with experimental data. Such realistic fields are used as incident fields to investigate two-dimensional cavities. Time domain analysis of shielding effectiveness of rectangular cavity with aperture is done using FDTD method.

1. INTRODUCTION

Usually the metallic shields are used to prevent equipment, sensitive electronic parts and systems of which can be disturbed or even destroyed by transient EM fields. The propagation of energy inside the enclosures occurs principally via transmission lines, transmission line-like structures and different kind of apertures, realized for cooling purposes and cable connections.

This paper presents numerical study of the coupling of transient fields radiated during ESD into the metallic enclosure with aperture. Computer simulation of ESD is done using an electrodynamic method based on the Method of Moments in time domain for the discharging bodies of revolution, located near the grounded plane [1-4]. For the discharging structure like spheroid, that models human/hand related ESD, calculated arc currents and fields were compared with experimental data and showed sufficient for EMC applications accuracy of the developed technique [1-4]. Such realistic fields are used as incident fields to investigate aperture penetration into two-dimensional cavities. Time domain analysis of shielding effectiveness of rectangular cavity with aperture is done using FDTD method.

2. MATHEMATICAL MODEL OF ESD

In this Section we describe briefly the mathematical model of ESD.

In the moment before discharge the static charge distribution $\rho_{\text{stat}}(\vec{r})$ is known on all metallic surfaces. During the discharge this distribution will be disturbed. Let us denote this disturbed part of charge by $\rho_{\text{trans}}(\vec{r}, t)$. The whole charge density in any point on the surface of the body or on the plane is $\rho(\vec{r}, t) = \rho_{\text{stat}}(\vec{r}) + \rho_{\text{trans}}(\vec{r}, t)$. The current density $\vec{J}(\vec{r}, t)$ deals with transient part of charge density. So the transient problem can be stated as the problem of defining the surface current densities $\vec{J}(\vec{r}, t)$ and arc-current density $\vec{J}_{\text{arc}}(\vec{r}, t)$. By these quantities all charges and fields can be calculated. Mathematical model for $\vec{J}(\vec{r}, t)$ and $\vec{J}_{\text{arc}}(\vec{r}, t)$ can be formulated as follows.

1. On the perfectly conducting surfaces $\vec{J}(\vec{r}, t)$ satisfies Integral Equation for Magnetic Field (IEMF):

$$\vec{J}(\vec{r}, t) = 2\hat{n} \times \vec{H}^{\text{arc}}(\vec{r}, t) + \frac{1}{2\pi} \hat{n} \times \int_s \left\{ \frac{\vec{J}(\vec{r}', \tau)}{R} + \frac{1}{c} \frac{\partial}{\partial \tau} \vec{J}(\vec{r}', \tau) \right\} \times \frac{\vec{R}}{R^2} d\vec{s}, \quad \vec{r} \in S \quad (1)$$

2. In each point of the arc the current density satisfies Ohm's differential law:

$$\vec{J}_{\text{arc}}(\vec{r}, t) = \sigma(\vec{r}, t) \cdot \left\{ \vec{E}_{\text{stat}}(\vec{r}) + \vec{E}_{\text{trans}}^{\text{arc}}(\vec{r}, t) + \vec{E}_{\text{trans}}^{\text{surf}}(\vec{r}, t) \right\}, \quad \vec{r} \in V_{\text{arc}} \quad (2)$$

3. Initial values are written as follows:

$$\forall \vec{r}, t \leq 0: \begin{cases} \vec{J}(\vec{r}, t) = 0; \\ \vec{J}_{\text{arc}}(\vec{r}, t) = 0; \\ \rho_{\text{trans}}(\vec{r}, t) = 0. \end{cases} \quad (3)$$

Let us consider terms of these expressions. In the equation (1) $\vec{H}^{\text{arc}}(\vec{r}, t)$ is magnetic field obtained on the metallic surface. This field is radiated by arc-current. S is the area of surface of the body and of its image. \vec{r} is the point of observation, \vec{r}' is the point of integration, τ is the delay time: $\tau = t - R/c$; $R = |\vec{R}|$, and $\vec{R} = \vec{r} - \vec{r}'$. c is the speed of light, \hat{n} is the outer normal of the surface. In equation (2) $\vec{E}_{\text{stat}}(\vec{r})$ is electrostatic field produced by static charge distribution before discharge. This field initiates the spark. $\vec{E}_{\text{trans}}^{\text{arc}}(\vec{r}, t)$ and $\vec{E}_{\text{trans}}^{\text{surf}}(\vec{r}, t)$ are transient electric fields, radiated by the arc and the surface and their mirrors.

Arc conductivity $\sigma(\vec{r}, t)$ in equation (2) is the function of electric field in the channel. In this work this conductivity is calculated by empiric model of Rompe and Weizel. According this model arc resistance is function of time [6]:

$$R(t) = \frac{2h}{\sqrt{2a_R \int_0^t I_{\text{arc}}^2(t') dt'}} \quad (3)$$

where $R(t)$ is arc resistance ([Ohm]), $2h$ is length of arc and its image ([m]), $I_{\text{arc}}(t)$ is arc current ([A]), a_R is empiric constant ($[m^2/V^2 \text{sec}]$), t is time ([sec]).

The equation (1) coupled with nonlinear equation (2) is solved by time domain Method of Moments. Algorithm allows the calculation of transient fields and simulation of whole electrodynamical process of discharge. The results are compared with measurements and show good agreement [2-4].

3. FIELDS RADIATED BY ESD

The question how the discharging body radiates into the space is of great importance because the answer gives hints about the region where sensitive apparatus might be disturbed.

In the Fig. 1 the geometry of discharging structure is shown. Metallic spheroid of semi-axes $a=31$ cm and $b=5$ cm is chosen in order to model human hand discharge.

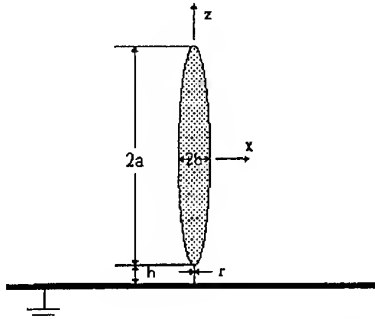
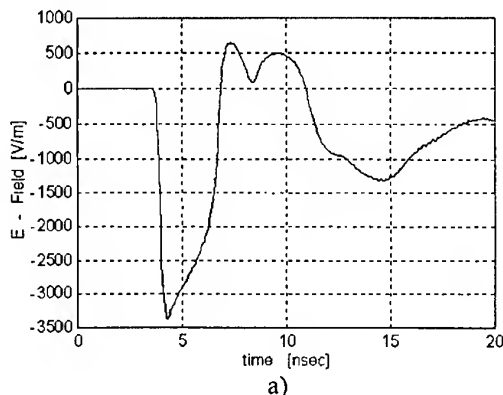
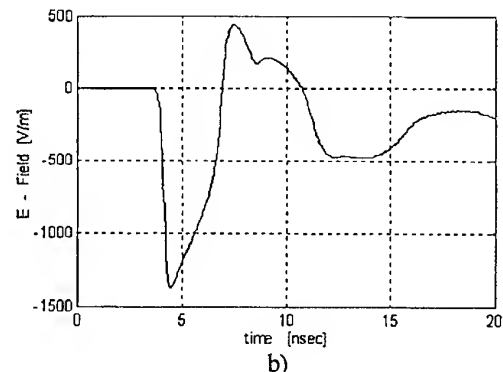


Fig. 1 Geometry of discharging body.

Fig. 2 shows radiated electric fields for two different cases: a) $V=5$ kV, $h=0.6$ mm; b) $V=10$ kV, $h=1.2$ mm. Observation point is located on the grounded plane. The distance to the point of observation from the location of arc is 1 m.



a)



b)

Fig. 2. E-field radiated by ESD from spheroid 0.31 m and 0.05 m semi-axes: a) $V=5$ kV, $h=0.6$ mm; b) $V=10$ kV, $h=0.6$ mm.

Fig. 3 shows maximums of radiated electric fields for different arc lengths and different voltages of spheroid. Observation point is located on the plane in 1 m from the arc. One can observe monotonic drop of maximums of fields as arc length is increasing while the voltage is fixed.

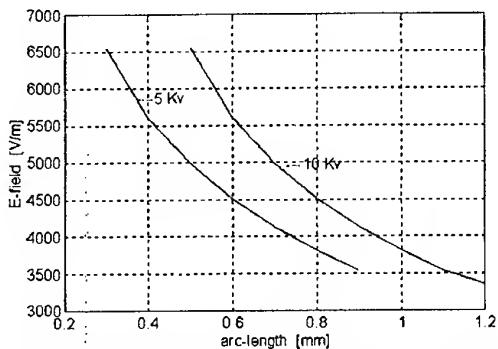


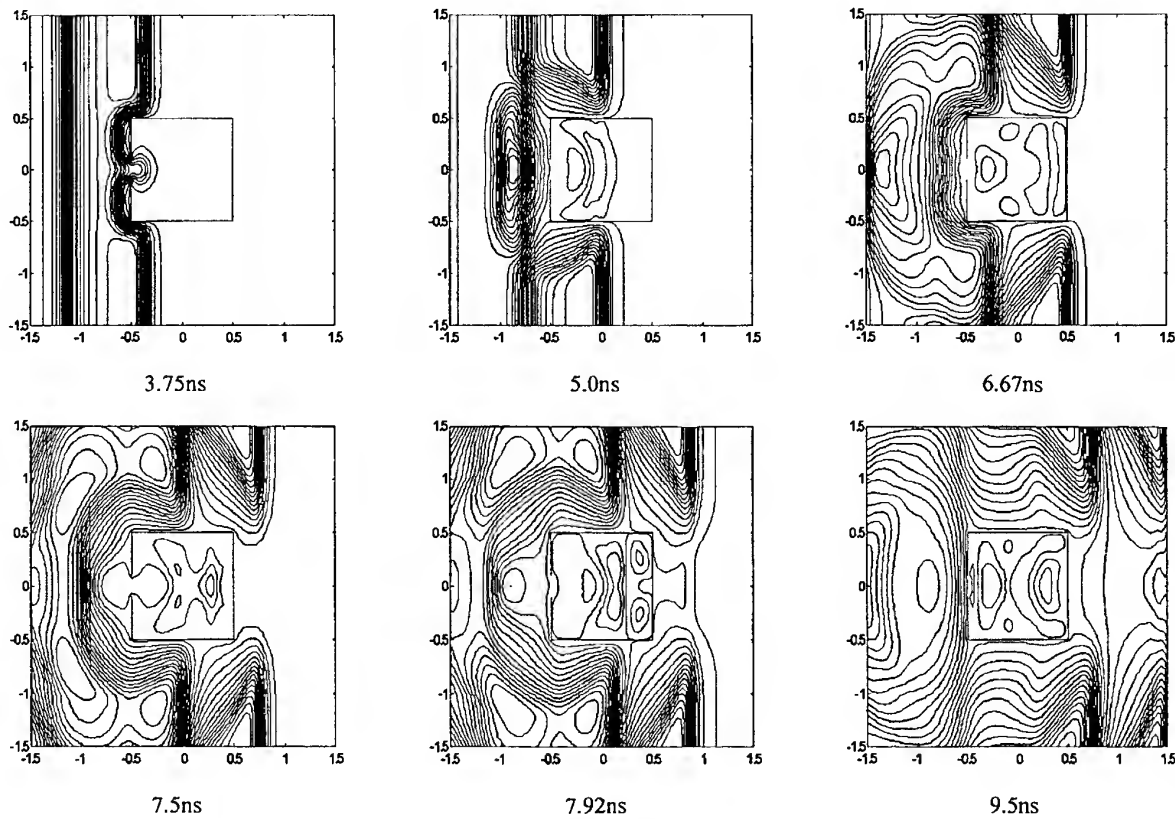
Fig. 3. Maximums of electric fields, radiated during ESD from spheroid.

Electric fields calculated in this section are then considered as incident fields for metallic enclosure with aperture.

4. TIME DOMAIN ANALYSIS OF SHIELDING EFFECTIVENES

In this section infinite perfectly conducting cylinders with rectangular cross sections are investigated under illumination of the plane wave having the same time-dependence and magnitude, as a transient field of ESD in some distance near the discharging body.

The method of investigation is Finite-Difference Time-Domain Method (FDTD) [5]. This method gives possibility to determine the complete electromagnetic field in the space surrounding the cylinder for all times of interest. This wealth of information can be displayed in a manner to enhance our understanding of the fields coupling phenomena. For this purpose we present the graphs in Fig.4. These graphs show the electric field in the space near and inside the rectangular cylinder of 1×1 m for different moments of time. In Fig. 4, for the moment $t=3.75\text{ns}$ the incident pulse just approaches to the cylinder and first part of energy begins to penetrate the aperture. The next graph shows the cylindrical wave inside the cavity with the center located on the aperture. This field propagates with small reflection from the walls. Reflection can be detected via curvatures in the lines of field near the walls. Graph on the Fig. 4 for $t=6.67\text{ns}$ shows the moment when field reaches the right wall of the cylinder. After this field begins to reflect from the wall and due to the geometry it behaves like the field in the resonator. For the quite a big aperture incident field is penetrating inside and all graphs in Fig. 4 can be explained by consideration of pulse propagation inside the cavity.



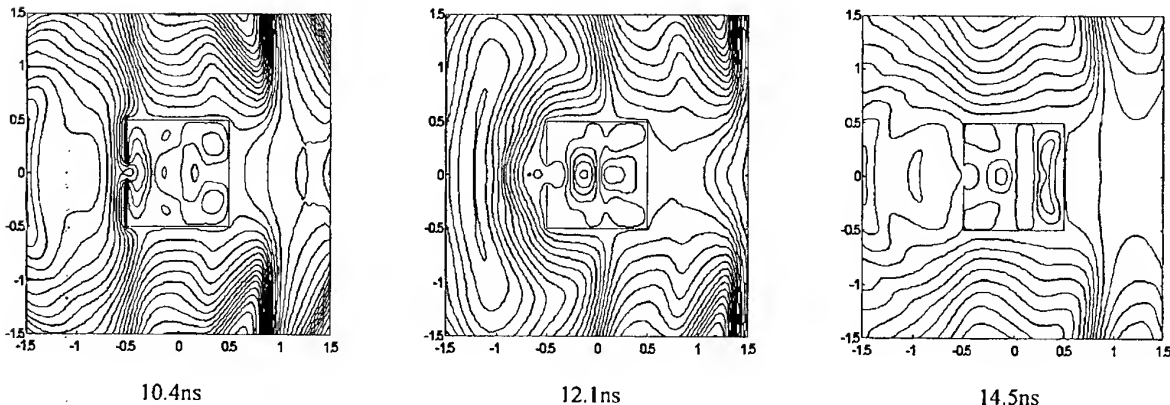


Fig.4 Time-history of the field inside the cavity. Cylinder 1×1 m, size of aperture 0.2m, ESD field from spheroid (0.31m by 0.05m semi-axes), charged by 5kV. Arc length 0.6mm.

To estimate shielding effectiveness of the screen we calculate the value

$$S = \frac{\int_{\text{Area}} \max |\vec{E}^{\text{total}}| ds}{\int_{\text{Area}} \max |\vec{E}^{\text{inc}}| ds} * 100\% \quad (4)$$

Here "Area" denotes the area of the cavity. Maximums of fields are calculated for each point inside the cavity during all time of observation. In the Fig.5 the shielding effectiveness of rectangular cylinder is shown for two cases: a) V=5 kV and b) V=10 kV.

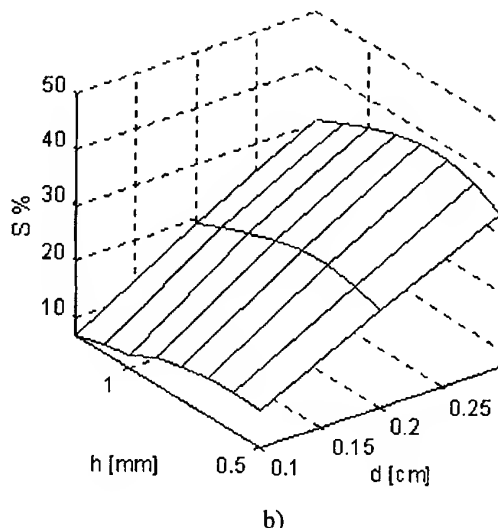
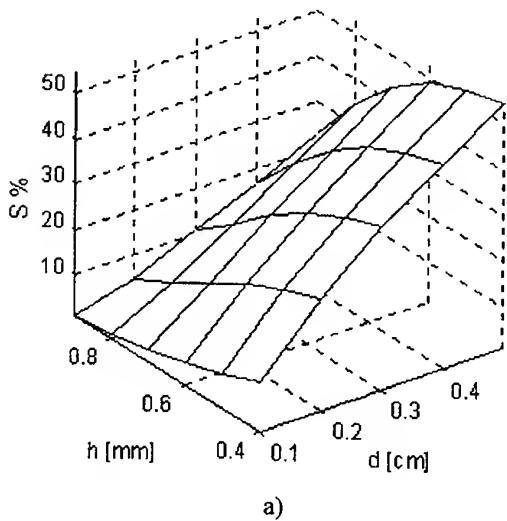


Fig.5. Shielding effectiveness of rectangular cylinder as function of arc length h and size of aperture d . ESD from a) $V=5$ kV and b) $V=10$ kV.

To demonstrate how maximums of fields are distributed inside the cavity we present Fig.6. One can see that maximums of electric fields that penetrate in the aperture are located near aperture and have smaller values in the inner part of cavity. Shielding effectiveness, calculated by formula (4) gives possibility to estimate average value of fields maximums shown in Fig. 6.

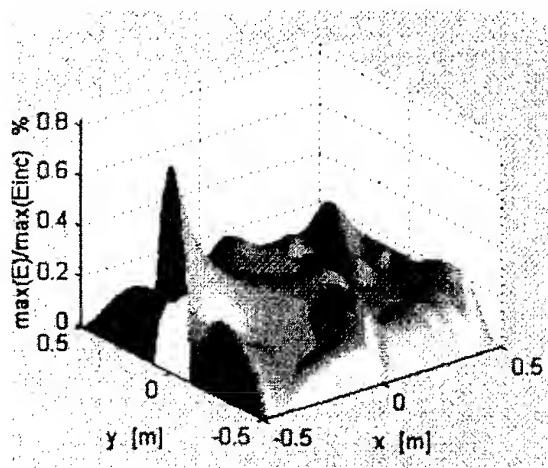


Fig. 6. Normalized maximums of electric field inside rectangular cavity. ESD from spheroid, V=5 kV, h=0.6 mm, d=20 cm.

3. ACKNOWLEDGMENT

This work was supported by Volkswagen Foundation.

4. REFERENCES:

- 4.1. R.Zaridze, D.Karkashadze, R.Jobava, D. Pommerenke, M.Aidam. "Calculation and Measurement of Transient Fields from Voluminous Object," EOS/ESD Symposium Proceedings, Phoenix, USA, 1995, pp. 2.6.1-2.6.6.
- 4.2. R.Zaridze, D.Karkashadze, R.Jobava, D. Pommerenke, M.Aidam. "Numerical Calculation and Measurement of Transient Fields from Electrostatic Discharge ". IEEE Trans. on Components, Packaging and Manuf. Technology Part C: Manufacturing. Vol. 19, No. 3, July 1996 , pp 178-183.
- 4.3. R.Jobava, D.Karkashadze, R.Zaridze, P.Shubitidze, D.Pommerenke, M.Aidam. "Numerical Calculation of ESD". EOS/ESD Symposium Proceedings, Orlando, Florida USA, 1996, pp. 203-210.

4.4. R.Jobava, D.Karkashadze, P.Shubitidze, R.Zaridze, G.Bit-Babic, D.Pommerenke, M.Aidam. "Computer Simulation of ESD". EMC Symposium, Zurich, 1997.

4.5. K.S. Yee, "Numerical solution of initial value problems involving Maxwell's equations in isotropic media". IEEE Transactions on Antennas and Propagation, vol. AP-14, pp.302-307, May 1966.

BIOGRAPHICAL NOTES

Roman G. Jobava was born in Sukhumi, Georgia (FSU), on October 14, 1965. He received M.S. in Radiophysics in 1987 from Sukhumi University and Ph.D. in Radiophysics in 1990 from Tbilisi State University. Since 1996 he is docent (Associate Professor) of Sukhumi University. He is member of Laboratory of Applied Electrodynamics of Tbilisi State University. His research covers computer simulation of transient electromagnetic phenomena, especially in EMC applications.

Revaz S. Zaridze was born in Tbilisi, Georgia (FSU), on May 8, 1938. He received M.S. and Ph.D. in 1962 and 1973 respectively from Tbilisi State University and the degree of Doctor of Sciences in 1984. Since 1985 he is professor of general Physics in Tbilisi State University. He is chief of the Laboratory of Applied Electrodynamics. The Laboratory is researching problems of scattering of EM waves, waveguide and resonator problems, antenna design, transient processes, EMC problems.

Phridon I. Shubitidze was born in Kochara, Georgia (FSU), on January 20, 1975. He received M.S. in Radiophysics in 1994 from Sukhumi University and Ph.D. in Radiophysics in 1997 from Tbilisi State University. He is member of Laboratory of Applied Electrodynamics of Tbilisi State University. His research covers computer simulation of transient electromagnetic phenomena, especially in EMC applications.

Distance Characteristics of Electromagnetic Fields Caused by ESD Above a Ground Plane

In-ho Kang, Osamu Fujiwara*

Dept. of Radio Science & Engineering Korea Maritime
University #1 Dongsam-Dong Yeongdo-Ku Pusan, Korea 606-791
* Dept. of Electrical and Computer Engineering Nagoya Institute of
Technology Gokiso-Cho, Showa-Ku, Nagoya 466, Japan

Summary: Serious troubles may occur in electromagnetic equipments due to electrostatic discharge (ESD). The number of the damaging incidents has been significantly increasing with increased use of integrated semiconductor elements with lower operation power. In this paper, the electric field intensities will be examined both experimentally and analytically with respect to the distance from the ESD point when the ESD occurs above a ground.

1. Introduction

Advanced electronic equipment employing highly-integrated digital-IC with low dissipation power is more fragile to electrostatic discharge (ESD). This is mainly because the immunity of high-tech equipment to the transient electromagnetic noises caused by the indirect ESD event has been degraded. For the electromagnetic interference of this kind, following strange cases^{[1],[2]} are well-known as a peculiar phenomenon of unknown origin. Indirect ESD occurring at the location distant from an equipment

causes the stronger electromagnetic interference than direct ESD does.

In this paper, the electric field intensities will be calculated with respect to the distance from the ESD point when the ESD occurs above a ground plane. From the result of the calculation, it will be verified that the electromagnetic interference level is not always proportional to the inverse of the distance.

2. Theory

The portion right after the ESD has occurred can be modeled as a current dipole with the length of ℓ through which the ESD current $i(t)$ flows, as shown Figure 1 (a). In this case the occurrence electromagnetic fields can be theoretically derived in terms of a function of the ESD current. Figure 1 (b) shows dipole current. The current peak value is denoted by I_m , the nominal duration period by τ . Then the ESD current $i(t)$ can be expressed as:

$$i(t) = I_m \times F(t/\tau) \quad (1)$$

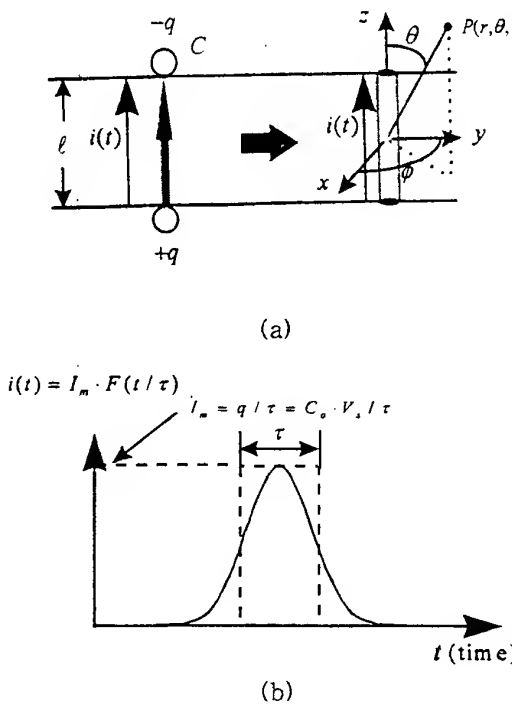


Figure. 1 (a) Electric dipole moment and dipole model
 (b) ESD dipole current

where $F(\cdot)$ is a dimensionless function representing the ESD waveform^[3] and following relation holds:

$$\int_{-\infty}^0 F(x) dx = 1 \quad (2)$$

Here, we can drive $F(\cdot)$ in a closed form from solving the equation for the electrical behavior of a capacitance discharge circuit through a spark gap. For spark resistance, the Rompe-Weizel's formula could quantitatively explain the spark process^[4]. From the capacitance discharge circuit and Rompe-Weizel resistance formula, the following equation is derived:

$$I_m = \frac{C_o V_s}{\tau} = \frac{C_o V_s (a/p)(V_s/\ell)^2}{3\sqrt{3}} \quad (3)$$

$$F(t/\tau) = \frac{3\sqrt{3}}{2} \exp \left\{ 3\sqrt{3} \left(\frac{t}{\tau} - x_o \right) \right\}^{-1.5} \cdot \left[1 + \exp \left\{ 3\sqrt{3} \left(\frac{t}{\tau} - x_o \right) \right\} \right] \quad (4)$$

$$\frac{\partial F(t/\tau)}{\partial(t/\tau)} = \frac{27}{4} \exp \left\{ 3\sqrt{3} \left(\frac{t}{\tau} - x_o \right) \right\}^{-2.5} \cdot [1 + \exp \left\{ 3\sqrt{3} \left(\frac{t}{\tau} - x_o \right) \right\}]^{-2.5} \cdot [2 - \exp \left\{ 3\sqrt{3} \left(\frac{t}{\tau} - x_o \right) \right\}] \quad (5)$$

where x_o is an integral constant, ℓ is the spark length, a is a spark coefficient determined by the gas pressure, nature and temperature, p is pressure. The stray capacitance across the gap before ESD occurs is denoted by C_o , and the spark voltage V_s . Figure 2 shows a dipole

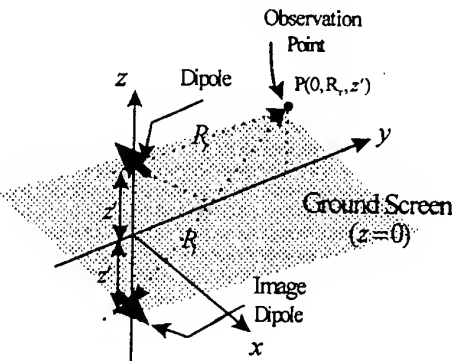


Figure. 2 Dipole model of ESD on the perfect ground

model of ESD on the perfect ground plane. At a point P , the radiation components of the electric fields are expressed as follows:

$$\overline{E_{re}} = -\overline{a_y} \cdot \frac{I_m \mu_0 \ell}{4\pi} \cdot \frac{1}{\tau R_r} \cdot \frac{\partial F(t/\tau - R_r/c\tau)}{\partial(t/\tau - R_r/c\tau)} \quad (6)$$

$$\overline{E_{im}} = \overline{a_y} \cdot \frac{I_m \mu_0 \ell}{4\pi} \cdot \frac{1}{\tau R_i} \cdot \frac{\partial F(t/\tau - R_i/c\tau)}{\partial(t/\tau - R_i/c\tau)} \quad (7)$$

where R_i is the distance between the observation point P and the dipole on the plane and R_i is one from the image dipole.

3. Experiment

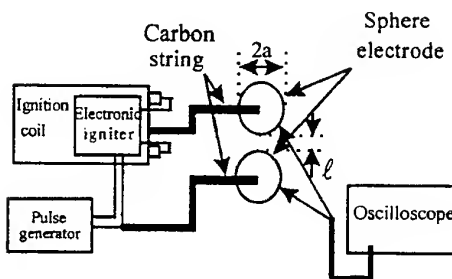


Figure. 3 The configuration of experimental setup and ESD detection

Figure 3 shows the configuration of experiment setup and ESD detection, indicating the top view. The ignition coil controlled by an electronic circuit can generate a high voltage, which is applied through carbon strings(250 Ω /m, 70 cm \times 2) to sphere electrodes (radius: $a=15$ mm) for producing a spark. The carbon strings are used to prevent the spark current from flowing into the portion except the gap. An ESD event can simply be detected with a commercially available ESD detector. The ESD detector was placed at a distance r from sphere electrodes as shown in Figure 3. The spark was generated at a two seconds

interval and then simultaneous measurements of the ESD detection frequency and the spark voltage were made for fifty sparks. Figure 4 shows the detection rate on observation distance r .

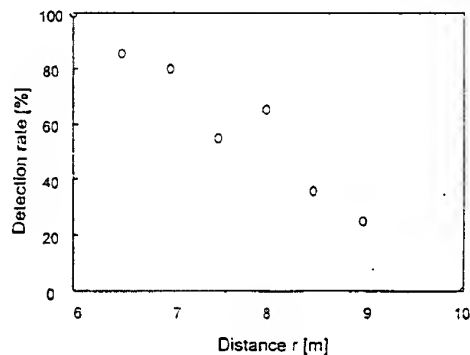
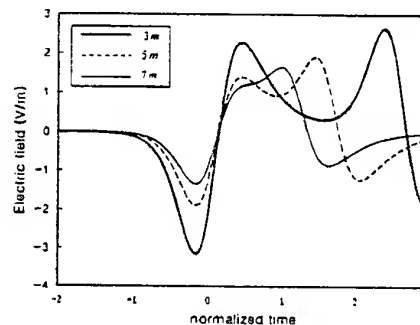
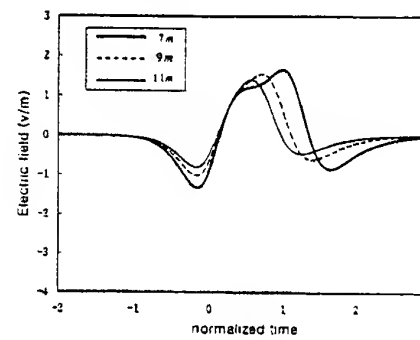


Figure. 4 The detection rate at observation distance r .



(a) distance $r=3, 5, 7$ (m)



(b) distance $r=7, 9, 11$ (m)

Figure 5. The waveform of the summed electric fields

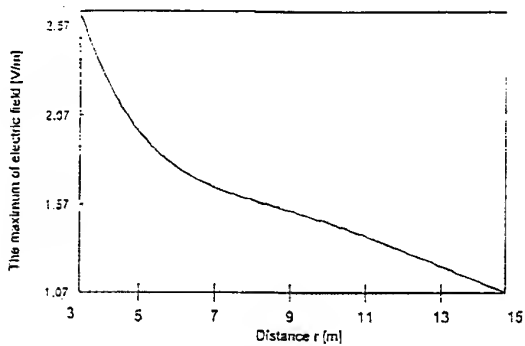


Figure 6. The peak radiated electric field calculated with respect to the distance r

Figure 5 is the waveforms of the summed electric fields. Figure 6 shows the peak electric field at distance r . The frequency rate can be compared with the peak electric field because it is proportional to the peak value of the electric field. From the Figure 4, 6 it is verified that the peak electric field is not always decreased as the observation distance is increased. The above strange phenomenon is resulted from the phase difference between the propagating wave and the reflected wave from the ground plane.

4. Conclusion

An ESD event has been modeled using a simple elementary dipole above a ground plane. It has been verified that radiated field is not always proportional

to the inverse of observation distance. The cause is based upon the fact that the phase difference between the directly propagating wave and the reflected wave change the field waveform according to the variation of the observation distance.

References

- [1] M. Honda, "A new threat-EMI effect by indirect ESD on electronic equipment", IEEE Trans. Ind. Appl., vol.25, no.5, pp.939-944, 1989.
- [2] W.D. Greason, "Indirect effect of ESD: modeling and measurement", Proc. 11th Int. Zurich Symp. Tech. & Exh. on EMC, 116R1, pp.613-618, March 1995.
- [3] O. Fujiwara, "An analytical approach to model indirect effect caused by electrostatic discharge", IEICE. Trans. Commun., E79-B, no.4 1996.
- [4] I.H. Kang, O. Fujiwara, J. Wang, "An analytical approach to the spark resistance formula caused by electrostatic discharge", Elect. Lett., Vol.33 no.14 3rd July 1997.
- [5] O. Fujiwara, Y. Amemiya, "Calculation of ignition noise level caused by plug gap breakdown", IEEE Trans. Electromagn. Compat., vol.24, no.1, pp. 26-32, Feb. 1982.

HAZARD FOR ELECTRONIC SYSTEMS DUE TO EFFECTS OF LIGHTNING ELECTROMAGNETIC IMPULSES

C. Mazzetti,
University of Rome "La Sapienza"
Via Eudossiana 18, 00184 Roma, Italy

and

Z. Flisowski, B. Kuca
Warsaw University of Technology
ul. Koszykowa 75, 00-662 Warszawa, Poland

The paper deals with a simplified method of the hazard assessment for electronic systems due to lightning electromagnetic impulses (LEMP). The main idea of the method is presented in which the immunity level of the considered system is to be correlated with the statistical distribution of overvoltages appearing inside the protected structure. On the base of this correlation the way for risk and frequency of possible damages of the system under consideration is discussed and evaluated.

1. GENERAL APPROACH TO HAZARD ASSESSMENT

Every structure equipped with conducting installations is endangered - in greater or less degree - by lightning overvoltages caused by direct and nearby strokes. Hazard due to overvoltages for such installations depends, of course, on parameters of lightning discharges [2] but not only on them. The failures in the installations depend also - and even in greater degree than on the lightning parameters - on their resistibility or immunity to overvoltages [9].

Only direct strokes and very limited number of nearby strokes, close to the structure, may be dangerous for common electrical installations due to relatively high resistibility or high level of their withstand voltages. In the case of equipment such as electronic systems with, usually, low level of immunity to overvoltages even very far lightning strokes may be dangerous.

To assess the hazard for such installations the level of expected overvoltages should be correlated with the threshold of resistibility or immunity of the installation system and its components. However, due to random nature of lightning overvoltages as well as withstand voltages of the components the assessment of the hazard should be considered as statistical one [2]. It means that the statistical withstand characteristics of installation should be taken in account on the background of statistical distribution of all possible overvoltages that may penetrate the installation. The probability of appearance of overvoltages with peak values greater than the withstand voltage of the equipment should be accepted as probability of its

damage due to one lightning stroke. Annual probability of equipment damage depends additionally on annual number of lightning strokes, which may cause overvoltages exceeding immunity level. This number of strokes together with the probability of the damage due to one stroke result in the annual frequency of the damage [5].

In the case for which the damage frequency is greater than its acceptable level, the measures for protection of the structure and its installation against overvoltages should be taken in account [6]. The efficiency of such measures becomes a very important parameter for the hazard assessment.

2. PENETRATION OF EQUIPMENT BY LIGHTNING OVERVOLTAGES

All possible cases of lightning stroke influencing the structure with sensitive equipment should be taken in account. As it is shown in Fig. 1 they are associated with different parts of considered arrangement.

Lightning strokes intercepted by the structure and by incoming overhead lines [4] are associated with equivalent areas A_1 limited by the distance

$$d_1 = 3 h \quad (1)$$

where: h - height of the structure or line.

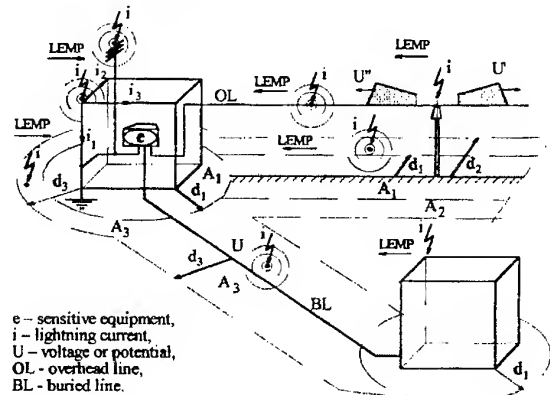


Fig. 1. Possible cases of lightning influence on the sensitive installation of the structure

The equivalent area A_2 associated with nearby strokes inducing overvoltages in the overhead line [5]

is limited on both its sides by distance d_1 and by distance

$$d_2 = \frac{30 k_v I_L h}{U_c} \quad (2)$$

where: I_L – lightning current peak value, U_c – level of voltage immunity, k_v – coefficient depending on the velocity of induced wave ($k_v \approx 1,1$).

The equivalent area A_3 associated with nearby strokes increasing ground potential around the structure and along incoming buried lines or other conducting elements [5] is limited between the distances d_1 and

$$d_3 = \frac{I_L \rho}{2\pi U_c} \quad (3)$$

where: ρ - ground resistivity.

For example the distances corresponding with real values of: $h = 10 \text{ m}$, $I_L = 30 \text{ kA}$, $\rho = 500 \Omega \cdot \text{m}$, $U_c = 2 \text{ kV}$ and $k_v = 1,3$ are as follows: $d_1 = 30 \text{ m}$, $d_2 = 5000 \text{ m}$ and $d_3 = 1200 \text{ m}$.

Sensitive installation inside the structure may be penetrated by lightning overvoltages in different way [3].

According to Fig. 1 it is possible to distinguish the overvoltages due to:

- direct lightning strokes into different parts of overhead incoming lines (direct overvoltages);
- magnetic coupling of the nearby lightning channel with incoming overhead lines (induced overvoltages);
- electrical coupling of nearby lightning ground currents with incoming buried lines or other conducting elements (growing of ground potential);
- partial lightning currents flowing into the ground through the conducting elements of the structure or LPS (resistive and inductive voltage drops);
- direct (by LEMP) magnetic coupling of nearby lightning channel with the circuits of internal installations of the structure without LPS and equipped with it;
- direct magnetic coupling of the conducting elements of structure or LPS with internal circuits of installation at lightning stroke into the structure (induced voltages).

At direct lightning stroke to a line, three cases (Fig. 2) should be taken in account: stroke into the single conductor, stroke to one of two parallel conductors and stroke to the conducting support of the conductor.

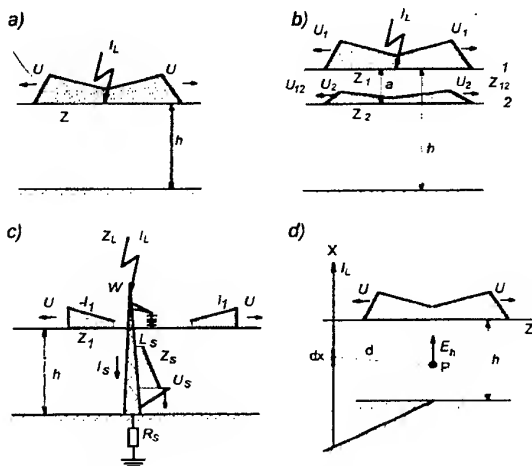


Fig. 2. Lightning stroke into: a) the single conductor, b) one of 2 conductors, c) conducting support, d) the ground near the conductor.

In the first case of the stroke into a single conductor of incoming line (Fig. 2a) the overvoltages may be expressed by relation

$$U = 0,5 Z I_L \quad (4)$$

in which: Z – conductor wave impedance, I_L – peak value of lightning current. It confirms a very great value of U in this case. For example, when: $Z = 450 \Omega$ and $I_L = 30 \text{ kA}$, then $U = 6,75 \text{ MV}$.

In the second case of the stroke to one of two parallel conductors (Fig. 2b) and at the assumption that $h \gg a$ the overvoltages between the conductors may be expressed by relation

$$U_{12} = 30 I_L \ln \frac{a}{r}; \quad (5)$$

where: a - distance between conductors, r - conductor radius.

In the third case of the stroke to the top of conducting support of the conductor (Fig. 2c) the overvoltages, just after breakdown from the support to the conductor, may be expressed by the relation

$$U = \frac{Z_1 Z_s}{Z_1 + 2Z_s} I_L \approx 0,2 Z_1 I_L \quad (6)$$

in which: Z_1 – wave impedance of the conductor, Z_s – wave impedance of the support.

Overvoltages induced in the incoming lines, according to the Fig. 1 (area A_2) and Fig. 2d, may be expressed by simplified relation as follows

$$U = \frac{30 k_v I_L h}{d} \quad (7)$$

where: h - height of the line conductor; d – distance, according to relation (2), between the overhead line and lightning channel, k_v – coefficient, as in relation (2).

Ground potentials and voltages caused by electrical coupling of nearby lightning strokes into the ground surface (equivalent area A_3 in Fig. 1) with incoming buried lines (cables) or other conducting

elements may be expressed by simplified relation as follows

$$U = \frac{I_L \rho}{2\pi d} \quad (8)$$

where: ρ , I_L , - as in relations (2) and (3), d - distance between the buried conductor and lightning channel. Quantitative relation between U and d according to (8) is shown in Fig. 3. It is evident that significant values of U may appear within a distance d of a range of 1000 m.

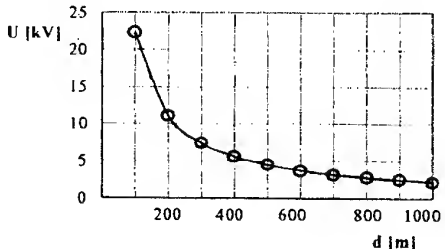


Fig. 3. Relation $U = f(d)$ at $I_L = 30$ kA and $\rho = 500 \Omega \cdot m$.

Resistive and inductive voltage drops due to partial lightning currents flowing into the ground through the conducting elements of the structure or LPS at direct strokes result adequately from simple relations:

$$U_R = R \eta I_L \quad (9)$$

$$\text{and} \quad U_L = L \eta s_L \quad (10)$$

where: R - grounding resistance, L - conductor or circuit inductance, η - coefficient for evaluation of a part of lightning current, I_L - lightning current, $s_L = (di_L/dt)_{\max}$ - its maximum steepness.

Induced voltages due to direct magnetic coupling of nearby lightning channel with the circuits of internal installations of the structure without LPS (Fig. 4a) may be evaluated from the following simple relation [7]

$$U = \frac{\mu_0}{2\pi} \frac{di_L}{dt} l \ln \frac{d+b}{d} \quad (11)$$

where: μ_0 - magnetic permeability, $4\pi \cdot 10^{-7}$ (V·s/A·m); d , b , l - dimensions (m) explained in Fig. 4;

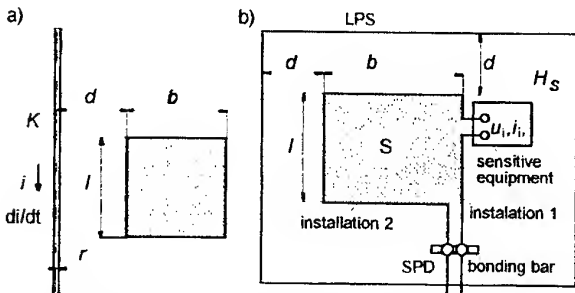


Fig. 4. The loop $L \times b$: a) without LPS (K - lightning channel), b) with LPS at direct stroke.

At the equality $\frac{di_L}{dt} = 2\pi d \frac{dH}{dt} \approx 2\pi d \frac{H_m}{T_1}$ and at the condition $d \gg b$ (nearby strokes) the expression $\ln \frac{d+b}{d} \approx \frac{b}{d}$ and relation (11) takes the form as follows

$$U = \mu_0 S_{lb} \frac{H_m}{T_1} \quad (12)$$

where: S_{lb} - loop surface (m^2); H_m - maximum magnetic field in the structure (A/m); T_1 - front time of current and field waves (s).

The induced voltages - according to this relation - may reach some hundred volts. For instance, at the surface $S_{lb} = 1 \div 10 m^2$, magnetic field $H_m = 400 A/m$ and the front time $T_1 = 5 \cdot 10^{-6}$ s, it yields the voltage $U = 100 \div 1000 V$.

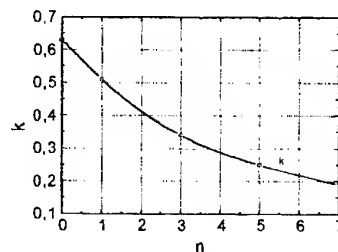


Fig. 5. Relation between coefficient k and number n of down conductors for 10 m cubic model cage.

In the case of the structure equipped with LPS the induced voltages are adequately reduced [1] and their values given by relation (12) should be multiplied by the coefficient

$$k = \frac{1}{SF} = \frac{H_s}{H} = \frac{U_s}{U} \quad (13)$$

in which: SF - shielding factor; H , H_s - magnetic fields and U , U_s - induced voltages respectively before and after LPS application. The coefficient k is different in different places [1]. Its average values for the LPS model cage with n down conductors are given in Fig. 5. Distribution of SF values along the horizontal diagonal line in the cage [3] is shown in Fig. 6.

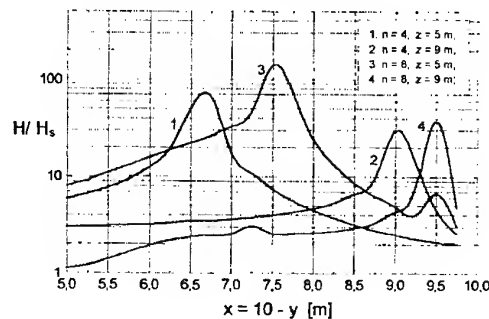


Fig. 6. Distribution of shielding factor along the diagonal line of cubic cage; z - height of line, n - number of down conductors.

At direct lightning stroke into the LPS the voltages induced in the open loop $b \times l$, due to its magnetic coupling with conducting elements of gridlike spatial LPS, may be expressed in volts [7] by relation

$$U = \frac{\mu_0 I_L}{40 T_1} l \ln \left(\frac{d+b}{d} \right) \quad (14)$$

where: d , b , l , I_L , T_1 - as in relations (11), (12) and in Fig. 4b.

Relation (13) involves shielding features of LPS. The distance d between the loop and a structure wall with LPS conductors may differ from that between the loop and a structure roof. In such a case the distance with less value should be accepted for calculation of induced voltages. For structure equipped with common LPS the voltages may reach some thousand volts. For instance, at assumption that $d = l = b = 3$ m, $I_L = 200$ kA, $T_1 = 5 \cdot 10^{-6}$ s and $\mu_0 = 4\pi \cdot 10^{-7}$ H/m it yields $U = 2,6$ kV.

In order to assess the hazard caused by lightning overvoltages, their values should be compared with the immunity of equipment and, if the latest is exceeded, the application of protection measures, surge protection devices (SPD) and shields, should be considered. SPD are adequate as measures against overvoltages incoming from external lines and against voltage drops. Shields are adequate as measures against induced voltages. Selection of the measure should result from the assessment of risk of damage due to lightning.

3. RISK ASSESSMENT

The risk of damage or malfunction of sensitive equipment due to lightning influence to the structure may be expressed by general relation [2] as follows

$$R = (1 - e^{-Np})^{\delta} \quad (15)$$

where: N - annual number of direct and indirect strokes influencing the structure equipment, p - probability of equipment damage or malfunction due to one lightning stroke, δ - economical or social consequences of the damage or malfunction of equipment.

From the technical point of view the product Np , expressing the damage frequency or the level of the risk of equipment damage, is of essential meaning so that it is here considered as a first basic step for eventual further economical considerations involving consequences represented by different values of δ . Assuming that $\delta = 1$ and $Np \ll 1$ the risk R (or frequency of damage may be expressed by the relation

$$R = Np \quad (16)$$

The probability p results from the distribution of overvoltages, which may appear in open circuits of the equipment, and from the distribution of withstand voltages of the circuits or their immunity levels [9]. In other words the probability p may be obtained from the relation as follows

$$p = \int_{-\infty}^{+\infty} g(U_s) P(U_s) dU_s \quad (17)$$

where: $g(U_s)$ - density function of distribution of induced voltages; $P(U_s)$ - cumulative distribution of voltages causing a damage or malfunction of the equipment. Graphical explanation of this relation is shown in Fig. 7.

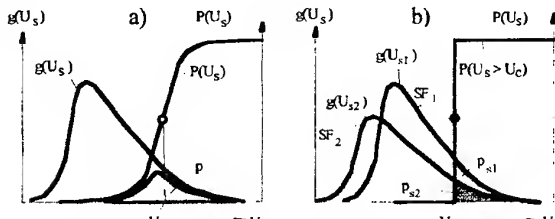


Fig. 7. Distribution of voltages induced and causing damages: a) $\sigma_u \neq 0$; b) $\sigma_u = 0$;

According to relations (4) – (11) and (14) the density function $g(U_s)$ corresponds with the density function $g(I_L)$ for lightning current, which is lognormal. Hence

$$g(U_s) = \frac{1}{\sqrt{2\pi}\sigma_u U_s} \exp \left(-\frac{1}{2\sigma_u^2} \ln^2 \frac{U_s}{U_{s50}} \right) \quad (17)$$

where: U_s - overvoltage under consideration, U_{s50} - its expected value, σ_u - standard deviation of its distribution.

The distribution $P(U_s)$ results from the characteristic of the equipment. Assuming that this distribution is normal one it is possible to write

$$P(U_s) = \frac{1}{\sqrt{2\pi}\sigma_u} \int_0^{U_s} \exp \left[-\frac{1}{2} \frac{(U_x - U_c)^2}{\sigma_u^2} \right] dU_x \quad (18)$$

where: U_c - average (critical) value of withstand voltages (immunity level of equipment), U_x - variable of integration, U_s - voltage as co-ordinate, σ_u - standard deviation of withstand voltages (experimental value).

Because of difficulties with σ_u assessment a simplification of the relation (18) is proposed. Namely, assuming that $\sigma_u = 0$ one gets $P(U_s > U_c) = 1$ and $P(U_s \leq U_c) = 0$. At this assumption relation (17) may be expressed as follows

$$p = \int_{-\infty}^{+\infty} g(U_s) P(U_s \geq U_c) dU_s = \int_{U_c}^{+\infty} g(U_s) dU_s \quad (19)$$

It is graphically explained in Fig. 7b. Value U_c results from equipment features [9] and for defined cases it is fixed so that equipment damages or its interference depend on distribution of overvoltage $g(U_s)$. This distribution depends, between others, on:

- the distribution of lightning currents,
- the distance between lightning channel and structure equipment, as well as its dimension and position in the structure,
- the shielding efficiency (factor SF) of LPS.

When the equipment in the structure is fixed then the lightning current, the distance between lightning channel and equipment and the shielding factor are decisive for the level of overvoltages.

It should be noted that according to relations given in section 2 of this paper there is a direct relation between critical value I_C of lightning current I_L and the critical value U_C of withstand voltage. For nearby strokes (relation 12) it yields

$$I_c = \frac{2\pi}{\mu_0 S_{lb}} d T_1 U_c SF \quad (20)$$

where: d , S_{lb} , T_1 - as in relations (11) and (12). According to relation (13) the shielding factor is defined by

$$SF = \frac{U}{U_s} \quad \text{or} \quad SF_{dB} = 20 \log \frac{U}{U_s} \quad (21)$$

Influence of SF on the density function $g(U_s)$ and therefore on the probability p_S is evident from the data given in Fig. 7b. The curve $g(U_s)$ at greater value of SF is shifted into the direction of lower values of U_s . To assess this dependence quantitatively new Fig. 8 has been arranged on the base of data given in section 2 of this paper and on the base of relations given in the document [8]. Moreover, according to [8] it has been assumed that $T_1 = 10 \mu s$ for first lightning stroke, what corresponds with the frequency $f = 0,025 \text{ MHz}$, and that $T_1 = 0,25 \mu s$ for subsequent strokes, what corresponds with the frequency $f = 1 \text{ MHz}$.

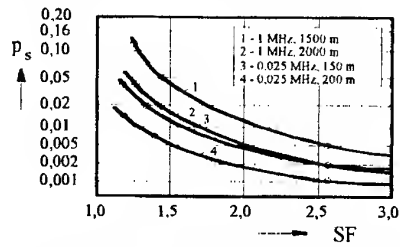


Fig. 8. p_S versus SF for different values of frequency f and distance d

The probability $p \approx p_S$, corresponding with the critical current I_C , is to be assessed directly from the lightning current distribution $g(I_L)$ given adequately for first and subsequent strokes.

Distance $d = d_3$ (relation 3) around the structure limits the ground surface from which the lightning strokes may be dangerous with probability $p \approx p_S$ for equipment inside the structure. The number of these strokes

$$N = N_g \pi d^2 \quad (22)$$

where N_g - the average annual density of the strokes, which should be obtained from local data. For the aim of this paper it is assumed to be equal 1 stroke per 1 km^2 and 1 year.

Taking in account the relation (16) and the data given in Fig. 8 together with the number N of relation (22) it is possible to calculate the risk of equipment damage or interference. An example of the calculation gives results as shown in Fig. 9.

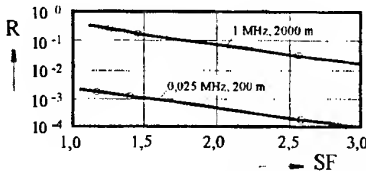


Fig. 9. Risk R versus SF for different f and d values

It should be noted that the number N increases with second power of d and at the same time the probability p decreases with d according to relation (20) and lightning current distribution. For small distances increment p is much greater than reduction of N so that the actual risk values may be a little greater than those of Fig. 9. More exact calculations need the product Np to be integrated as a function of d .

4. CONCLUSION

From obtained results it is possible to conclude that:

- assessment of the risk of damages is a proper way for selection of measures of protection against induced overvoltages;
- a distinction between distributions of first and subsequent lightning strokes is very important for the risk assessment;
- passage from the distribution of first strokes to that of subsequent strokes causes a very great increase of the risk of damage;
- first strokes are dangerous for sensitive equipment in a distance of a range of hundred meters whereas the dangerous distances d at subsequent strokes may reach some thousand meters;

5. REFERENCES

- 5.1. Z. Flisowski, B. Stańczak, B. Kuca, C. Mazzetti, A. Orlandi, M. Yarmarkin: "Induced currents and voltages inside LPS models due to lightning current", Proceedings of 23rd ICLP, Florence, Italy, Sept. 23 - 27, 1996, pp.527-532.
- 5.2. C. Mazzetti, M. Pompili, Z. Flisowski: "Review of application problems of probabilistic approach to the lightning hazard assessment", Proceedings of 23rd ICLP, Florence, Italy, Sept. 23 - 27, 1996, pp. 707-712.
- 5.3. C. Mazzetti, A. Orlandi, M. Yarmarkin, Z. Flisowski, B. Kuca: "Shielding properties of LPS under LEMP", 10th International Symposium on High Voltage Engineering (ISH'97), Montreal, Canada, August 25-29, 1997.
- 5.4. IEC 1024-1-1, International Standard, First edition, 1993-08: "Protection of structures against lightning", Part 1: General principles. Section 1: Guide A - Selection of protection levels for lightning protection systems.
- 5.5. IEC 1662. Technical Report 1995: "Assessment of the risk of damage due to lightning" and Amendment N° 1 Annex C: "Structures containing electronic systems".

5.6. IEC 1312-1, International Standard, First edition 1995-02: "Protection against lightning electromagnetic impulse (LEMP)". Part 1: General Principles.

5.7. Draft IEC 1312-2, Technical Report Type 2 on: "Shielding of structures, bonding inside structures and earthing relating to LEMP" prepared by TC 81 WG 3 TF 2, November 1996

5.8. Draft IEC 61312-2: Protection against lightning electromagnetic impulse (LEMP) – Part 2: "Shielding of structures, bonding inside structures and earthing". Committee draft for vote 81/105/CDV, 25-07-1997.

5.9. IEC 1000-4-5, 1995: Electromagnetic compatibility of electrical and electronic equipment. Part 5: Surge immunity requirements.

BIOGRAPHICAL NOTES

Carlo Mazzetti: born (1943) in Rome, Italy; graduated (1967) from Electrical Engineering Department of Rome University "La Sapienza" and joined it in 1967; associate professor (1970), professor (1986) and director of Department (1986 -89) of the University; director of the High Voltage Group (HVG) of the

Italian National Research Council (1989); president of ICLP (1996) author and co-author of more than 100 scientific papers. His main interests: HV transient analysis and measurement, electrical insulation, lightning electromagnetic fields and lightning protection. His membership: the Italian Electrical Committee (CEI/81) and the International Electrotechnical Commission (IEC/81) on Lightning Protection.

Zdobyław Flisowski: born (1931) in Brzeźno/B, Poland; graduated from Electrical Engineering Faculty of Warsaw University of Technology; joined it in 1952; associate professor (1971), professor (1987), head of High Voltage Technique Division (1991); prorector of the University (1988-92); author or co-author of 6 books and above 110 scientific papers. His main interests: HV technique and lightning protection. His memberships: the Polish Committee on Lightning Protection (president 1972), the Scientific Committee of International Conference on Lightning Protection (vicepresident 1996), Fellow IEE (1993).

VOLTAGES INDUCED ON SWITCHING EQUIPMENT BUS CABLES BY A DIRECT LIGHTNING STRIKE

Masaji Sato*, Shigeo Chikai*, Satoshi Sakaida*, Syouichi Kuramoto**, Masaru Kanazawa**

*NTT Technical Assistance and Support Center **NTT Multimedia Networks Laboratories

3-9-11 Midori-Cho, Musashino-Shi, Tokyo 180, Japan

Abstract This paper analyzes damage to the switching equipment bus circuits caused by a direct lightning strike to a telecommunications center, and describes the measures taken to prevent future damage.

Based on the current observed at the antenna tower leg, the distributed lightning currents in the columns and girders, and the potential difference induced in the damaged bus circuits, were estimated by using a linear building model and vector potential methods. The discharge trace on the damaged circuit was also analyzed by comparison with the tested discharge traces. Consequently, the estimated potential difference matched well with the analysis of the discharge traces.

To suppress the induced voltages on the bus circuits, the mesh-grounding and the zinc oxide variable resistors were added to the reference ground and the bus circuit.

1. INTRODUCTION

Direct lightning strikes to a building can seriously damage telecommunications equipment. Several papers have reported the results of simulated lightning current distribution and the induced voltages on wires in a building [1]-[2], but few reports have described actual examples of induced lightning surges on signal cables and how the surges damage equipment circuitry. In this paper we report on the damage to digital switching equipment bus cable interface circuits caused by a direct lightning strike on December 16, 1995 to a telecommunications center located on the shore of the Japan Sea.

Direct lightning current was observed at a leg of the antenna tower. The lightning current distribution in the building and the induced voltages on the bus cable interface circuits were estimated by applying vector-potential methods to the currents in the building columns and girders. The discharge traces on the circuits were analyzed by applying experimental lightning surges to the circuits. The calculated voltages agreed well with the results of the cir-

cuit immunity tests and the discharge traces on the damaged circuits.

Following the lightning strike, a mesh-grounding was added to the switching equipment and protectors were placed on the bus interface circuits to suppress induced voltages.

2. DAMAGED CIRCUITS

When the lightning struck the antenna tower on the four-story telecommunications building, the digital switching

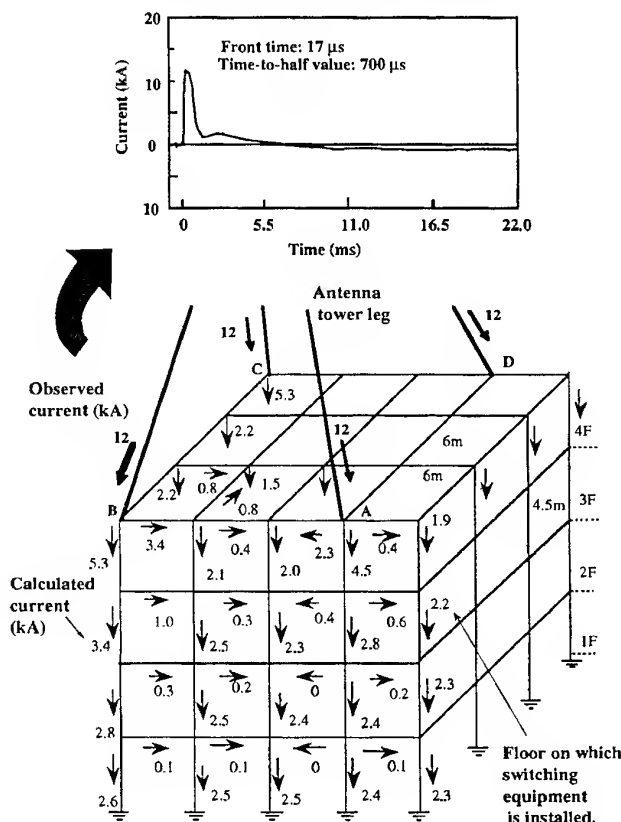


Fig. 1. Observed current at an antenna tower leg and the calculated current distribution in the building.

equipment bus cable interface circuits were damaged. According to the lightning positioning and tracking system, the lightning current flowing into the antenna tower had a peak value of approximately 100 kA. As shown in Fig. 1, the peak value of the current observed at the tower leg was 12 kA. Based on other observed cases of direct lightning strikes to this building, the total current can be assumed to be more than 80 kA because the antenna tower has four legs, stairs, and dozens of waveguides.

An overview of the damaged bus cable interface circuits is shown in Fig. 2. The damaged transistors, marked A in Fig. 2, were located between the signal ports and the reference ground of each device. They were connected in a row with bus cables and grounding wires. The damaged circuits were more vulnerable to positive surges between the signal port and reference ground than to negative surges because diode B in Fig. 2 protects against negative surges.

The damaged bus cable interface circuits had a single grounding point at the rectifier, and had no direct connection to the subscriber lines, AC mains, or conductive structures of the building. Therefore, the potential differences between the bus cables and grounding wires induced by the lightning current were assumed to be the main cause of the damage.

3. INDUCED VOLTAGES ON BUS CABLE AND GROUNDING WIRES

3.1 Induced voltage calculation methods

Based on the current observed at the antenna tower, the lightning current distribution in the building was calculated using the linear building model shown in Fig. 1. The relations between the currents in the columns and girders and the potential difference between their joints can be represented as follows [3].

$$\begin{aligned} v_1 - v_2 &= z_{11} i_1 + z_{12} i_2 + \dots + z_{1n} i_n \\ v_2 - v_3 &= z_{21} i_1 + z_{22} i_2 + \dots + z_{2n} i_n \\ &\dots \end{aligned} \quad (1)$$

Here, i_n represent the currents of column and girders, v_n are the potentials of joints, z_{mn} are the impedances of column and girders, z_{mn} are the mutual impedances between those currents. Equation (1) can be rewritten in matrix form.

$$[v] = [z] [i] \quad (2)$$

Therefore, current matrix $[i]$ can be obtained by calculating the inversion of the impedance matrix $[z]$.

$$[i] = [z]^{-1} [v] \quad (3)$$

The induced potentials of the bus cables and reference grounding wires were estimated as shown in Fig. 3 by applying vector-potential methods to the calculated currents in the building columns and girders. Vector potential A_x in the X direction at position P , generated by current I_g in the girder, is given by the following equation.

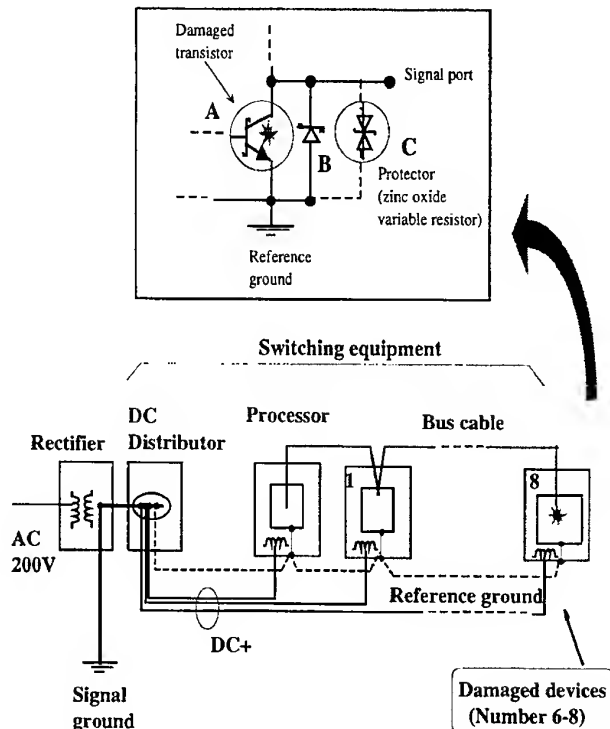


Fig. 2. Overview of the damaged devices and circuits.

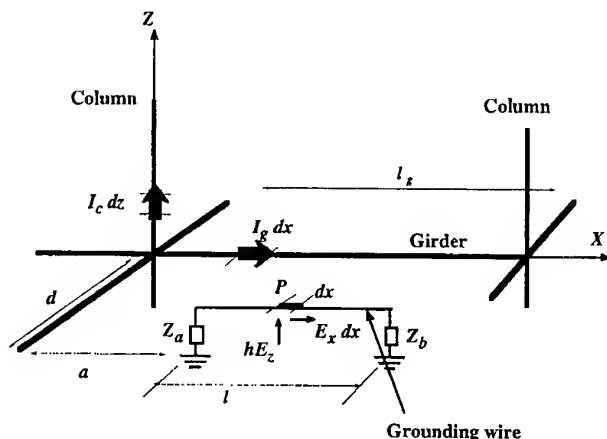


Fig. 3. Locations of current in column and grounding wire.

$$A_x = \int_0^{l_g} \frac{\mu_0 I_g(x,t)}{4\pi r} dx \quad (4)$$

Here, μ_0 : Permeability,

l_g : Length of girder, and

$$r = \sqrt{(l_g - (x + a))^2 + d^2}$$

The electric field strength E_x in direction X is given by the next equation.

$$E_x = - \frac{d A_x}{dt} \quad (5)$$

The field strengths in directions Y and Z , generated by the current in the girders, are individually given by considering the inductor-current positions, directions, and magnitudes.

The transmission line equations for the grounding wire short section with fields strengths under E_x and E_z are given as follows [4].

$$-\frac{dV_x}{dx} = z_0 \frac{dI_x}{dt} + E_x ,$$

$$-\frac{dI_x}{dx} = y_0 \frac{d}{dt} (V_x - h E_z) \quad (4)$$

Here z_0 and y_0 are the primary impedance and the primary admittance of the grounding wire. As the maximum length of the grounding wire is at most several dozen meters, the frequency of the lightning surge is at most several hundred kHz, and the height h of the grounding wire is approximately zero because it is installed on the floor, we estimated the induced voltage at the open end of the grounding wire by using the following simplified equation [5].

$$V_x = \int_0^l E_x \, dx \quad (5)$$

Since there are several girders that generate electric field, the induced voltage at the end of the grounding wire is determined by integrating each voltage induced by the individual girders as follows.

$$V_0 = \sum_{i=1}^n \int_0^l E_i d l \quad (6)$$

Here E_i is the field strength generated by currents in each girder. The induced voltages on the bus cable can be calculated by applying above equations because the bus cables are usually installed in the same way as grounding wires.

Since a lightning surge is described in the time domain as shown in Fig. 1 and the wire impedance is described in the frequency domain, we applied the Fourier transformation to the lightning surge and calculated equations (1)-(6) in the frequency domain. We then inverted them to produce the time-domain voltages.

3.2 Calculated induced voltages

The lightning current distribution of building columns and girders are shown in Fig. 1. The current in columns under the antenna tower leg is larger than that in other columns, and the current in girders is almost one-tenth of the current in columns. Figure 4 shows the peak values of lightning current in the third floor girders. The current in outside girders is larger than that in girders located at the

center part of the floor.

Figure 4 also shows the locations of bus cables and grounding wires. The route of the bus cable starts at the processor and connects devices 1 to 8 in a row, while reference grounding wire A starts at the DC distributor and connects the devices 3, 4, 7, and 8. The reference ground of the processor and devices 1, 2, 5, and 6 were connected by another grounding wire.

Figure 5 shows the calculated induced voltage peak values on bus cables and reference grounding wires at each devices. The calculated results show that the potential differences of the damaged devices reached more than 40 V.

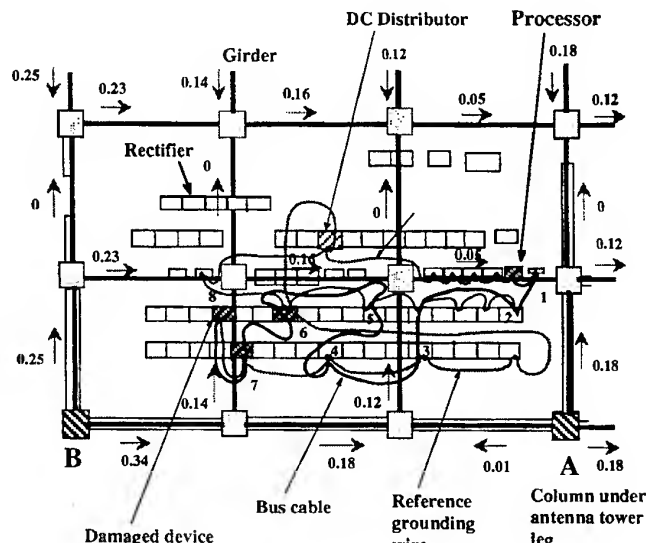


Fig. 4. Calculated current distribution in girders on the third floor and locations of bus cables and grounding wires.

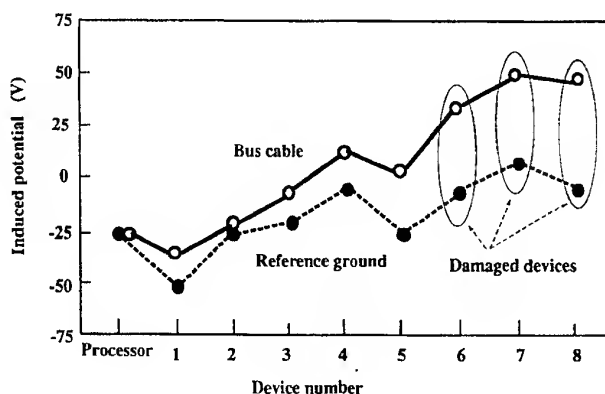


Fig. 5. Calculated potential difference between bus cables and reference grounding wires.

and had a positive polarity between the signal port and reference ground, while those of the undamaged equipment were less than 30 V.

3.3 Immunity level and discharged trace of the damaged transistor

The tested immunity level of the circuit against lightning surges is shown in Fig. 6. When a positive surge was applied to the signal port, the transistor in the bus circuit, marked A in Fig. 2, broke down at 20 V, and it became completely impossible to output signals at 40 V, while the circuit had an immunity level of more than 100 V against negative surge due to the diode marked B in Fig. 2. We applied three kinds of surge waveforms to the circuit, but the circuits immunity level did not change with these test waveforms as shown in Fig. 6.

Figure 7 shows the discharged trace of the damaged transistor, making clear that induced surge had discharged between the collector and emitter which were directly connected to the bus cable and reference ground as shown in Fig. 2.

Figure 8 shows the discharged traces tested at the voltage of 30, 46, 60, 100. The discharged trace in Fig. 7 matched well with that of the circuits tested at 46 V.

The damage is thus attributed to the induced potential difference of 40-60 volts between the bus cables and reference ground, which was more than twice the allowable voltage of the circuits.

4. INDUCED VOLTAGE SUPPRESSION USING MESH-GROUNDING AND ARRESTORS

To suppress the induced voltages on the grounding wire, typical wiring methods, such as single-wiring, star-wiring, and mesh-wiring, were experimentally studied[5]. Based on these experiments, mesh-wiring was added to the switching equipment reference grounding wires, as shown in Fig. 9. Additionally, bus cables were installed along the mesh-grounding wires.

Figure 10 shows the calculated induced voltages on the bus cables and reference grounding wires in the case of a direct lightning strike of 100 kA. We assumed that the induced potential difference was reduced by about half by adding mesh-grounding.

For additional protection, considering a direct lightning strike of over 100 kA, a zinc oxide variable resistor, marked C in Fig. 2, was added to the bus cable interface circuit. The resistor strengthened the circuit immunity level by more than five times, as shown in Fig. 6.

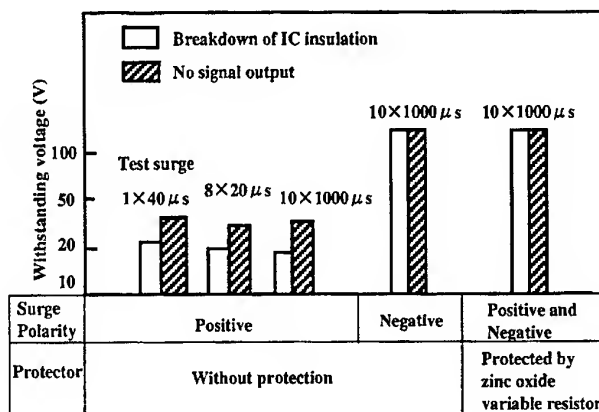


Fig. 6. Tested immunity level against lightning surges.

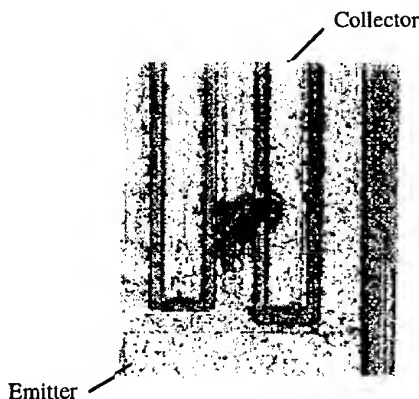


Fig. 7. Discharge trace on the damaged transistor.

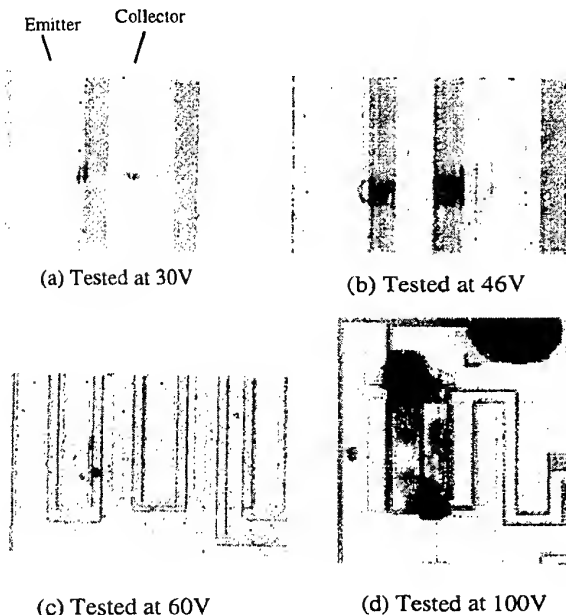


Fig. 8. Discharge traces on the tested transistors.

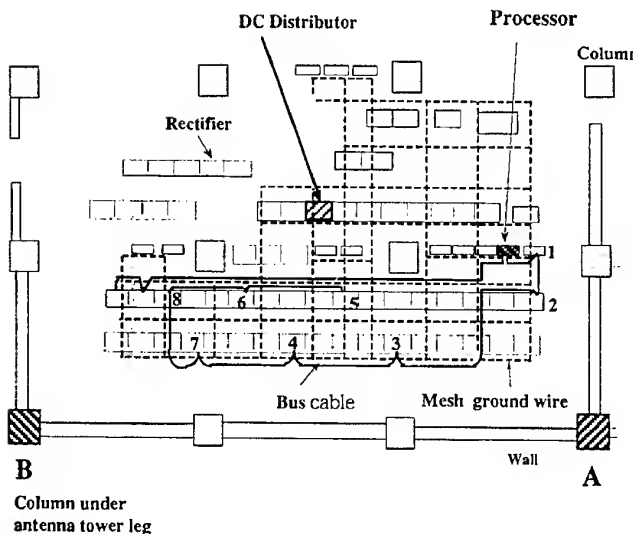


Fig. 9. Mesh-grounding used to suppress induced voltages.

5. CONCLUSION

We have described the damage caused to the digital switching equipment bus cable interface circuits by a direct lightning strike to a telecommunications center, the estimated voltages on the bus circuits, and the measures taken to prevent future damage.

The direct lightning current was assumed to flow into the antenna tower with a peak value of 80-100 kA. The distributed lightning current in the columns and girders induced a potential difference of more than 40 V between the signal port and reference ground, as estimated using a linear building model and vector potential methods. The discharge trace on the damaged circuit matched well to that of the circuit tested at 46 V.

The mesh-grounding added to the reference ground reduced the induced potential difference by about half. The zinc oxide variable resistors added to the circuit strengthened the circuit immunity level by more than five times.

REFERENCES

- [1] E. Montandon and W. Hardrian, "Neuartiges Blitzschutzkonzept eines Fernmeldegebäudes," Sonderruck auss dem Buletin des SEV/VSE, Bd75, pp. 3-11, 1984.
- [2] Andjzef Sowa, "Lightning Overvoltages in Wires within the Building," IEEE 1991 International Symposium on EMC, pp. 99-102, NJ.
- [3] Masaji Sato and Shoichi Kuramoto, "Surge Current Distributions in Telecommunication Building Caused by Direct Lightning Strike," 9th International Zurich Symposium on EMC, pp. 251-256, Mar. 12-14, 1991, Switzerland.

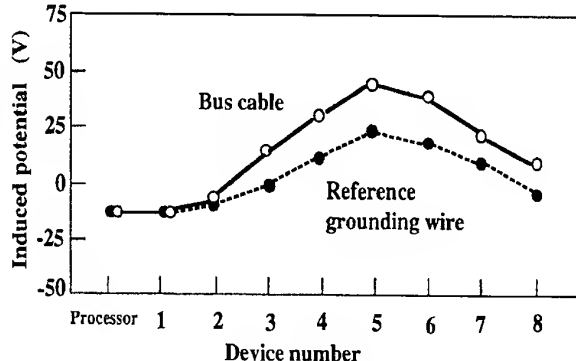


Fig. 10. Improved induced potential difference.

[4] H. Koga, T. Motomitsu, and M. Taguchi, "Lightning Surge Waves Induced on Overhead Lines," Trans of IECE of Japan, Vol. E62, No. 4, pp. 216-223, 1979.

[5] Masaji Sato and Tsuyoshi Ideguchi, "Overvoltages in Telecommunications Equipment Grounding Wires Induced by Direct Lightning Strikes," EMC '96 ROMA International Symposium on EMC, pp. 707-712, Sept. 17-20, 1996, Rome, Italy.

BIOGRAPHY

Masaji Sato is a Senior Engineer in the EMC Group of Technical Assistance & Support Center, NTT, Japan. Since joining NTT in 1972, he has been engaged in research on design of overvoltages protection, and grounding systems for telecommunications equipment.

Shigeo Chikai is an Engineer in the EMC Group of Technical Assistance & Support Center, NTT, Japan. Since joining NTT in 1964, he has been engaged in research on design of telecommunications terminal equipment and overvoltages protection.

Satoshi Sakaida is an Engineer in the EMC Group of Technical Assistance & Support Center, NTT, Japan. Since joining NTT in 1976, he has been engaged in switching equipment operation and maintenance.

Shoich Kuramoto is a Senior Research Engineer in the Multimedia Networks Laboratories, NTT, Japan. Since joining NTT in 1987, he has been engaged in research on design of grounding systems for telecommunications equipment.

Masaru Kanazawa is an Engineer in the EMC Group of Multimedia Networks Laboratories, NTT, Japan. Since joining NTT in 1986, he has been engaged in telecommunications outside plant maintenance and customer service.

COMPUTER SIMULATION OF ESD FROM OBJECT WITH SURFACE RESISTANCE

P. Shubitidze, R. Jobava, D. Karkashadze, D. Pommerenke*, R. Zaridze

Laboratory of Applied Electrodynamics, Tbilisi State University 3 Chavchavadze Ave.,
Tbilisi, 380028, Georgia, Tel & Fax: +995 32 290845, e-mail: lae@resonan.ge;
*Hewlett Packard, Roseville, USA

Abstract - *Electrostatic discharge of the body with different surface resistance is investigated. Influence of the surface resistance on the current in the arc and on the radiated by the body fields is studied. The problem is formulated in the terms of surface integral equation for magnetic field. The equation is solved by the Method of Moments in time domain. Results are given for spheroid with different surface resistance. It is shown that for some kind of distribution of surface impedance the level of radiation from electrostatic discharge can be reduced.*

1. INTRODUCTION

As the complexity and sensibility of digital systems increase, there is an increasing need to better understand basic phenomena associated with Electrostatic Discharge (ESD) and its effect on electronic systems [1]. The basic ESD event is direct ESD, whose discharge current flows inside electronic equipment and interferes its work. The other type of ESD is the indirect ESD that can be analyzed as a form of electromagnetic interference, caused by transient fields or electromagnetic pulses (EMP) radiated by ESD. Computer simulation of such kind of phenomena raises interest to development of efficient numerical techniques for solving appropriate problems. To determine the severeness of ESD and predict possible malfunctions the transient fields must be known in the near and in the far zones [2,3]. The objective of this work is to investigate these fields within the electrodynamical model of discharge phenomena for objects with surface resistance.

2. NUMERICAL METHOD

Let us consider ESD from voluminous conducting objects. The boundary value problem for this case can be transformed into a magnetic field integral equation (MFIE) [4]:

$$\bar{j}_s(\vec{r}, t) = 2\vec{n} \times \bar{H}^{inc}(\vec{r}, t) + \vec{n} \times \frac{1}{2\pi} \left\{ L[\bar{j}_s(\vec{r}', \tau)] \times \frac{\bar{R}}{R^2} \right. \\ \left. + \frac{\epsilon_0}{R} \cdot \frac{\partial \bar{M}(\vec{r}', \tau)}{\partial t} + L[H_n(\vec{r}', \tau)] \cdot \frac{\bar{R}}{R^2} \right\} dS' \quad (1)$$

$$L[f] = \frac{f}{R} + \frac{1}{c} \frac{\partial f}{\partial t};$$

where \bar{J} is the current density on the surface of the body, $H^{inc}(\vec{r}, t)$ is the field radiated by the arc (for the discharging body this field is considered as an exciting field), \vec{r} is the point of observation on the surface of the body, t is the time of observation, \vec{r}' is the point of integration, $\bar{R} = \vec{r} - \vec{r}'$, $R = |\vec{r} - \vec{r}'|$ is the distance between the point of observation and integration, $\tau' = t - R/c$ is the retarded time, \bar{M} is magnetic current density on the surface of the body, H_n is normal component of the magnetic field on the surface of the body, \vec{n} is the normal to the surface and c is speed of the light.

For the computer simulation of the ESD the following model can be formulated: we suppose the existence of a channel with time dependent conductivity $\sigma(t)$ in the gap. Therefore we have boundary conditions:

$$\sigma(t)\bar{J}(t) = \bar{E}_{self}(t) + \bar{E}_{body}(t) \quad \text{in the channel}$$

and

MFIE on the surface of the body,

where $\bar{E}_{self}(t)$ is electric field produced by channel and $\bar{E}_{body}(t)$ is electric field produced by discharging body, located near the ground plane.

We assume that the surface S is described by the parametric equations: $\vec{r} = \vec{r}(u, v)$ and we further assume that these coordinates are orthogonal, that is, that the tangent vectors $\vec{r}_u = \partial \vec{r} / \partial u$ and $\vec{r}_v = \partial \vec{r} / \partial v$ satisfy equation $\vec{r}_u \cdot \vec{r}_v = 0$.

In the following discussion our attention will be limited to axial excitation of rotational bodies. Equation (1) can be rewritten for this case:

$$J_u = -2H_v^{inc} - \frac{1}{2\pi} \int_s \left\{ \frac{J_u}{R} G_{vu} + \frac{1}{c} \frac{\partial J_u}{\partial \tau} [G_{vu} + G'_{vv}] \right\} ds \quad (3)$$

where $G_{vu} = \frac{\tilde{R} \cdot [\tilde{n}_v \times \tilde{n}_{u'}]}{R^2}$, $G'_{vv} = \frac{Z}{120\pi} \frac{\tilde{n}_v \cdot \tilde{n}_{v'}}{R}$
with $\tilde{n}_u = \frac{\tilde{r}_u}{|\tilde{r}_u|}$; $\tilde{n}_v = \frac{\tilde{r}_v}{|\tilde{r}_v|}$; Z is surface impedance.

Solution of the equation (3) coupled with the equation for arc can be done with the well-known Method of Moments (MOM) directly in the time domain [2,3].

Let us consider some computational problems arising at numerical realization of the MOM algorithm. The first stage of this algorithm is segmentation in both the space and time coordinates. The simplest scheme of discretisation is based on the uniform discretisation ($\Delta l \times \Delta l \times \Delta t$, where $\Delta l = c\Delta t$). Since an integration is performed in the space coordinates, subsectional collocation with a δ -pulse approximation in space can be used. Using Galerkin method [5] we can write discrete analogue of equation (3):

$$J_u(i, j) = (-2H_v^{inc}(i, j) - \frac{1}{2\pi} \sum_{k=1}^{N_s} \int_{\Delta S_k} \left\{ \frac{J_u(k, \tau)}{R} G_{vu}^{(k, i)} + \frac{1}{c} \frac{\partial J_u(k, \tau)}{\partial \tau} [G_{vu}^{(k, i)} + G'_{vv}^{(k, i)}] \right\} dS_k) \frac{1}{1 - \beta_i} \quad (4)$$

Here i is used for number of belt (we assume that body is divided into N_s belts), j is used for time moment, ΔS_k is the area of k -th belt. Each belt in addition is divided into M_k patches. M_k depends on the number of belt k . Coefficients β_i take into account self-influence of i -th patch [5].

In general case $\tau = (n + \gamma)dt$, where n is an integer and $0 \leq \gamma < 1$. So it is necessary to provide some kind of interpolation for currents between the integer time-steps. We are using interpolation:

$$J(\tau) = \frac{J_{n-1} + J_{n+1} - 2J_n}{2dt^2} (\tau - t_n)(\tau - t_{n+1}) + \frac{J_{n+1} + J_n}{dt} (\tau - t_{n+1}) + J_{n+1}, \quad (5)$$

where $t_n = dt(n - 1)$.

The main problem in numerical algorithm is the coupling of the arc to the body. The electric field in the gap must be known accurately as the highly non-linear arc current depends on its value due to the ionization process. The arc models by Rompe and Weisel [6] and the model by Mesiats [7] are usable for ESD as they can reproduce the influence of the arc length on the current rize [1]. Presently the Rompe and Weisel model is used in our algorithm. According this model the arc resistance is represented by formula [6]:

$$R(t) = \frac{2h}{\sqrt{2a_R \int_0^t I^2_{arc}(t') dt'}} \quad (6)$$

where $R(t)$ is the arc resistance [Ohm], h is the arc-length [m], $I_{arc}(t)$ is an arc-current [A], $a_R = 10^{-4} [m^2 / V^2 sec]$ - is some experimental constant.

Validation of the algorithm was done both theoretical and experimental way. The code was tested against literature data in the linear scattering problems in time domain [5,8-10] and in frequency domain [11]. For the discharge problem the fields were tested inside the body (inside the perfectly conducting body the field should be zero). It was tested also if the calculated transient electric field approaches the negative value of the electrostatic field for a long calculation times.

From the other hand currents and fields were compared to measured data in the case of perfectly conducting bodies. While the current on the body can hardly be measured, the discharge current can [1]. Measured data compared with calculations show high

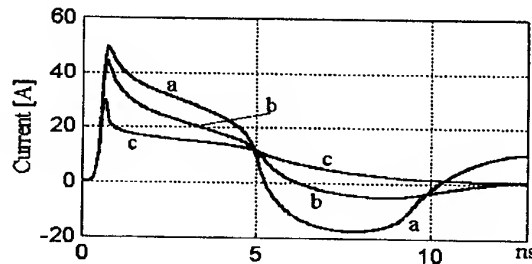


Fig.1. Arc currents from spheroid with semi-axes: $a=0.31$ m, $b=0.05$ m, static voltage: $V_0=5$ kV, arc-length: $h=0.3$ mm, a-perfectly conducting body, b - homogeneous distribution of surface resistance: $Z=37.7$ Ohm, c - inhomogeneous: $Z=1/L$ Ohm, where L is distance along the generating line.

accuracy of the developed algorithm [3].

Let us consider the influence of surface resistivity on the behavior of discharge phenomena. From the resistive boundary condition we have relation:

$\tilde{M} = -\hat{Z}[\tilde{n}, \tilde{j}]$, where $\hat{Z} = Z/120\pi$ is surface impedance. Due to the axial symmetry $H_n=0$. Calculations were proceeded for the prolate spheroid with semi-axes: $a=0.31$ m, $b=0.05$ m. This spheroid is quite a good model for the human arm. If resistance is chosen $Z=0$, the algorithm turn into algorithm for perfectly conducting objects [2-3].

Fig.1 represents the time dependence of arc current for different arc resistances. It can be seen that with increasing the surface resistivity arc current drops in magnitude. This conclusion is done for the homogeneous resistance. It can be chosen such a distribution of surface

resistance, that not allows the redischarge of the body at all due to the losses of energy.

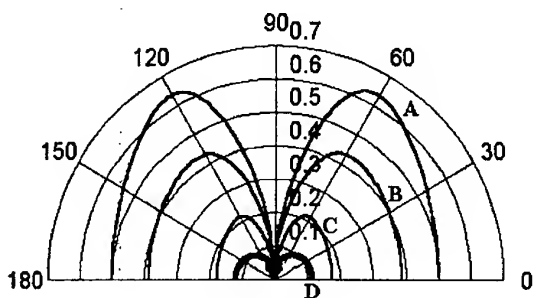


Fig. 2. Distribution of maximums of radiated H-fields of ESD from spheroid: $a=0.31\text{m}$, $b=0.05\text{m}$, static voltage $V_0=5\text{kV}$, arc length $h=0.3\text{ mm}$, A - perfectly conducting body, B, C - homogeneous impedances $Z=37.7\text{ Ohm}$, 377 Ohm , C - inhomogeneous distribution: $Z=1/L\text{ Ohm}$, where L is distance along the generating line.

Fig.2 represents distribution of maximums of radiated H-fields of ESD from spheroid: $a=0.31\text{m}$, $b=0.05\text{m}$, for the fixed moment t and for different values of surface impedance, the arc-length in this case is equal $h=0.3\text{ mm}$. In case of perfectly conducting spheroid the maximum of the pattern can be seen at angle $\theta = 30^\circ$. From this we can made conclusion that scattered field consists of high frequency components. While the value of surface impedance arises, the magnitude of scattered field drops and pattern has tendency to change to circle shape. That means that high frequency components are not radiated from the lossy surface.

3. CONCLUSION

Developed algorithm gives possibility to carry out computer simulation of electrostatic discharge from perfectly conducting as well as from resistive objects. Former objects are interesting for the problem of modeling of discharge from parts of human body (hand, for example). Algorithm is tested in scattering problems against literature data. In case of perfectly conducting bodies, comparison with experimental data shows sufficient accuracy of the method. Using this algorithm for ESD modeling we have found that surface impedance can reduce radiated during discharge fields and change the shape of radiated pattern. This information is very useful for reducing malfunctions of electronic equipment by ESD.

4. ACKNOWLEDGMENT

We want to thank the Volkswagen Foundation for sponsoring this work.

5. REFERENCES

- 5.1. D. Pommerenke, 'ESD: transient fields, arc simulation and rise time limit', Journal of Electrostatics 36 (1995), pp. 31-54
- 5.2. R. Zaridze, D. Karkashadze, R.G. Djobava, D. Pommerenke, M. Aidam, 'Calculation and measurement of transient fields from voluminous objects', EOS/ESD Symp., Phoenix, Arisona, USA, 1995, pp.95-100
- 5.3. R.G. Jobava, D. Karkashadze, R. Zaridze, P. Shubitidze, D. Pommerenke, M. Aidam, 'Numerical Calculation of ESD', EOS/ESD Symp., Orlando, Florida, USA, 1996, pp.203-211
- 5.4. H. Mieras, C.L. Bennett, 'Space-time integral approach to dielectric targets', IEEE Trans. Antennas Propagat., Vol. AP-30, pp. 2-9, 1982
- 5.5. A.J. Poggio, E.K. Miller, 'Integral equation solutions of three-dimensional scattering problems' in 'Computer Techniques for Electromagnetics', Oxford: Pergamon Press, 1973, pp. 159-264
- 5.6. Meek and Craggs, 'Electrical Breakdown of Gases', New York: J. Wiley&Sons, 1978
- 5.7. Bennett C. L., 'Time Domain Solution of Transient Problems. In: Lectures on Computational Methods in Electromagnetism' (Ed.: Harrington R. F., Wilton D. R., Butler C. M., Mittra R., Bennett C. L.), St. Cloud, SCEEE Press, 1981
- 5.8. R. Mittra, 'Integral equation methods for transient scattering' in 'Transient Electromagnetic Fields' by L.B. Felsen, Berlin: Springer Verlag, 1976, pp. 73-126
- 5.9. G. A. Mesyats, 'Physics of pulse breakdown in gases', Moscow, Nauka Publisher, 1990, ISBN 5-02-014173-9 in Russian.
- 5.10. J. Mautz, R. Harrington, 'Radiation and scattering from bodies of revolution', Appl. Sci. Res. June 20 1969, pp. 405-434
- 5.11. M. Belkina, 'Radiation characteristics of the prolonged ellipsoid of rotation', Electromagnetic waves diffraction by the bodies of revolution, Moscow, 1957, pp. 126-174, in Russian

BIOGRAPHICAL NOTE

Phridon I. Shubitidze was born in Kochara, Georgia (FSU), on January 20, 1975. He received M.S. in Radiophysics in 1994 from Sukhumi University and Ph.D. in Radiophysics in 1997 from Tbilisi State University. He is member of Laboratory of Applied Electrodynamics of Tbilisi State University. His research covers computer simulation of transient electromagnetic phenomena, especially in EMC applications.

XII
IMMUNITY

METHOD OF CALCULATING FACSIMILE IMAGE QUALITY FOR IMMUNITY TESTING

Yoshiharu HIROSHIMA*, Ryoichi OKAYASU**, Toshiko TOMINAGA*, and Nobuo KUWABARA*

*NTT Multimedia Networks Laboratories, **NTT Technical Assistance and Support Center
9-11 Midori-Cho 3-Chome Musashino-Shi, Tokyo 180-8585 Japan

The proposed method for evaluating the image quality of facsimile output reduces evaluation time and cost. The quality calculated from five parameters obtained from the original and evaluated images was compared with that judged by 40 subjects. The results for immunity testing indicated a positive correlation.

1. INTRODUCTION

Improved immunity testing is required for evaluating the performance of information technology equipment. Immunity testing is done by injecting the equipment under test (EUT) with various electromagnetic noises and measuring the degradation in performance. In immunity testing, the methods for injecting noise are standardized[1], [2], but no methods for measuring the degradation in performance have been developed yet.

In immunity testing of facsimiles we measure the errors in operation and the degradation in output image quality. While operation errors are easily measured, measuring image-quality degradation requires determining the mean opinion score (MOS) of many subjects. A simple, inexpensive method is needed to determine this subjective MOS.

In this paper, we have developed a method for measuring the immunity of facsimiles by calculating the MOS from the differences between the original image and the evaluated image.

2. PROPOSED METHOD

A method for measuring the transmission characteristics of a communication line and facsimile by calculating the MOS from the differences between the original page and the evaluated image has been reported[3]. Here, the evaluated image was facsimile output. However it is difficult to use this method for measuring the immunity of facsimiles, because it cannot separate the degradation caused by communication line transmission characteristics,

facsimile transmission characteristics and various electromagnetic noises. So a new method for measuring the immunity of facsimiles independent of the communication line transmission characteristics and facsimile transmission characteristics is needed.

In our proposed method, MOS is calculated from the differences between the original image and the evaluated image. Here, the original image is the facsimile output without added noise and the evaluated image is the facsimile output with added noise. Since the original and evaluated images both have the same degradation caused by transmission characteristics of the communication line and facsimile, the differences between the images are caused by various electromagnetic noises.

The flow of the MOS calculation is shown in Fig. 1. The arrows express the transmission of control signals and data. The facsimile output page is scanned by an image scanner whose resolution (600 dpi) is set higher

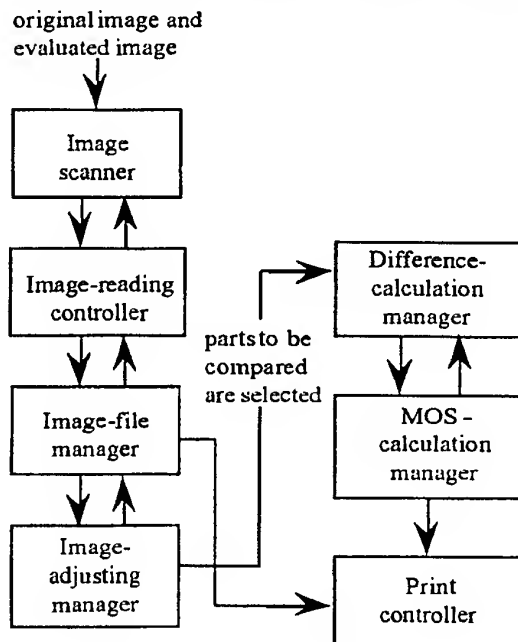


Fig. 1 Flow of MOS calculation

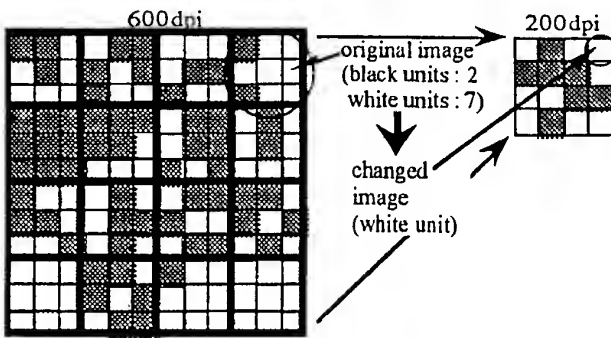


Fig. 2 Reduction of resolution

than that of the facsimile output (200 dpi) to reduce read errors during scanning. The resolution is then reduced to that of the facsimile output by an image-reading controller. The method of resolution reduction is shown in Fig. 2. When more than half of the units in a 3×3 group in the higher resolution image are black, then the unit of lower resolution is set to black. Otherwise it is set to white. Both the original image and the evaluated image are stored in memory by an image-file manager.

The position of the evaluated image is adjusted to that of the original image by an image-adjusting manager. And sections for comparison (called the compared sections) are then selected from the evaluated image.

Noise creates black areas in the evaluated images; several sections containing these areas are among those selected for comparison.

The differences between the original and evaluated images are calculated for the compared parts by a difference-calculation manager. Five parameters are used to evaluate the calculated MOS:

N : number of compared sections;

L : for each compared section, the maximum vertical

- width of the black area;
 W : for each compared section, the maximum horizontal width of the black area;
 B : for each compared section, the value expressed as $B = (B_1 - B_2)/B_2$, where B_1 is the number of black image units comprising the desired image, and B_2 is the number of black image units in the same section of the original image;
 K : for each compared section, the self-correlation coefficient between neighboring image units in the same section of the original image expressed as

$$K = \frac{\sum_{t=1}^m (I_0(t) - \frac{1}{m} \sum_{t=1}^m I_0(t)) \cdot (I_0(t+1) - \frac{1}{m} \sum_{t=1}^m I_0(t+1))}{\sqrt{\sum_{t=1}^m (I_0(t) - \frac{1}{m} \sum_{t=1}^m I_0(t))^2 \cdot \sum_{t=1}^m (I_0(t+1) - \frac{1}{m} \sum_{t=1}^m I_0(t+1))^2}} \quad (1)$$

where $I_0(t)$ is the t -th image unit ($I_0(t)=0$ when the unit is white and 1 when the unit is black) and m is the number of image units per scanning line.

The MOS-calculation manager calculates the MOS using Eqs. (2) and (3).

At $N=1$,

$$\text{MOS} = a_0 + a_1 \log L + a_2 \log W + a_3 \log B + a_4 \log K, \quad (2)$$

$N > 1$,

$$\text{MOS} = b_0 + b_1 \log \text{MOS}(\min) + b_2 \log N, \quad (3)$$

where MOS(\min) is the minimum MOS calculated for each compared part. The coefficients $a_0, a_1, a_2, a_3, a_4, b_0, b_1$, and b_2 are determined so as to minimize the deviation between the calculated MOS and the subjective MOS, where the subjective MOS data used to determine the coefficients is obtained independently from the subjective MOS for experiment.

3. EXPERIMENTAL RESULTS

The test setup we used to measure the immunity of facsimiles is shown in Fig. 3. One of the original

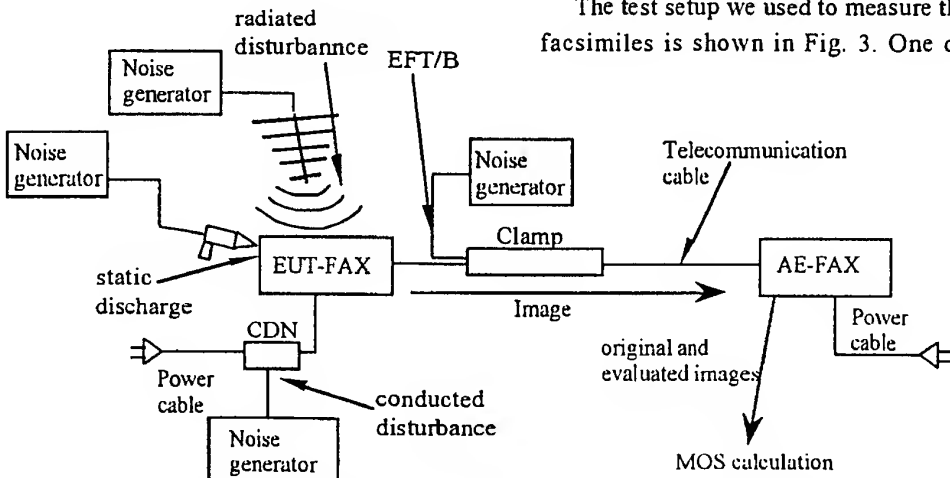


Fig. 3 Experimental setup used to measure performance of MOS calculation

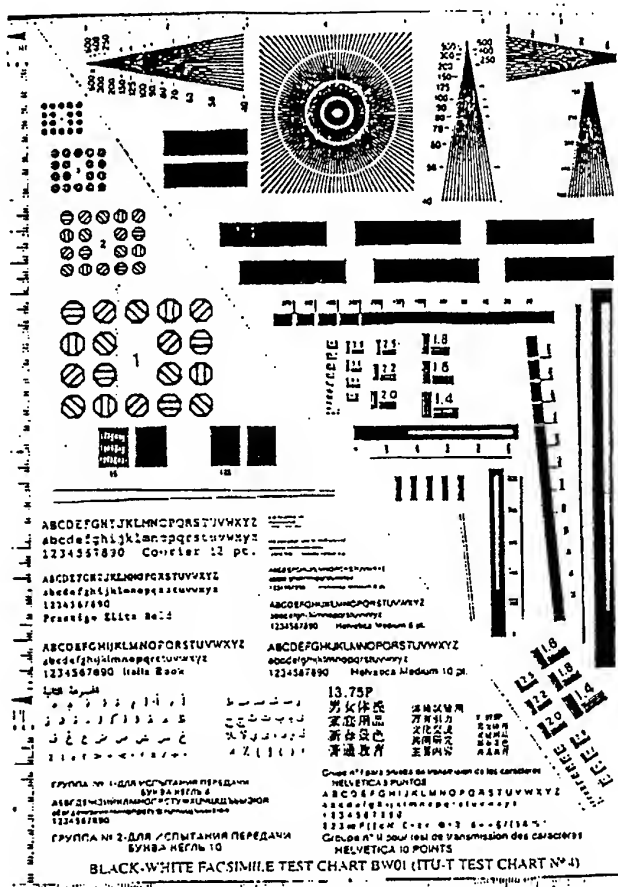
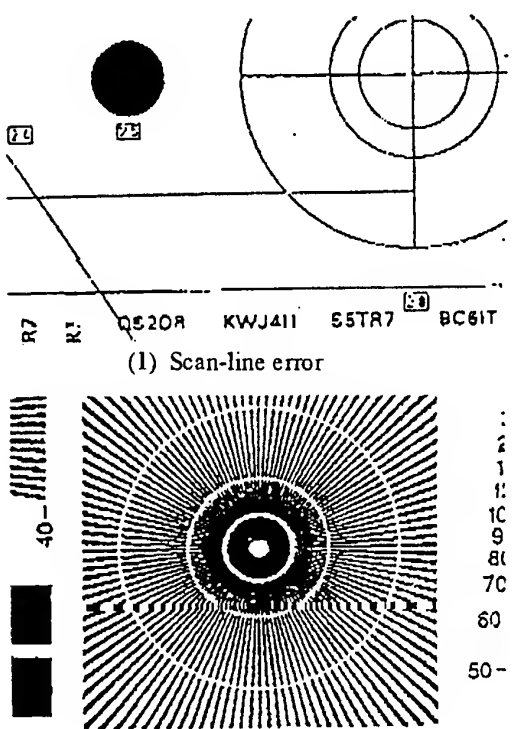


Fig. 4 Original image to be measured

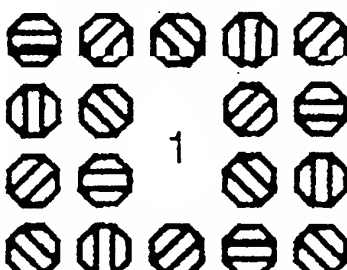


(3) Print previous line error

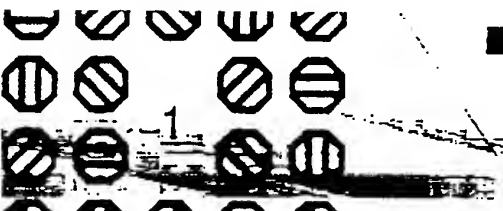
images to be measured is shown in Fig. 4. Four different original A4 images were used (three facsimile test charts and one newspaper page).

There were two types of electromagnetic noise: one was directly injected into equipment like a radiated disturbance or static discharge, and the other was injected into equipment through power cable or telecommunication cable like a conducted disturbance or electrical fast transient burst (EFT/B) noise. In Fig. 3 radiated disturbance and static discharge were directly injected into the facsimile under test (EUT-FAX). The conducted disturbance was injected into EUT-FAX through the power cable. EFT/B noise was injected into EUT-FAX through the telecommunication cable. They were injected separately. And the subjective MOS for the facsimile output by the auxiliary facsimile (AE-FAX) was compared with the calculated MOS. This subjective MOS was given by 40 non-expert subjects.

Various types of degradation of the facsimile output are shown in Fig. 5: (1) a scan-line error, (2) a line deletion error, (3) a print previous line error, and (4) other types of error. Radiated disturbance causes all types of degradation at almost the same rate. Static discharge makes line deletion and print previous line



(2) Line deletion error



(3) Print previous line error



(4) Other types of error

Fig. 5 The various types of degradation of the facsimile output

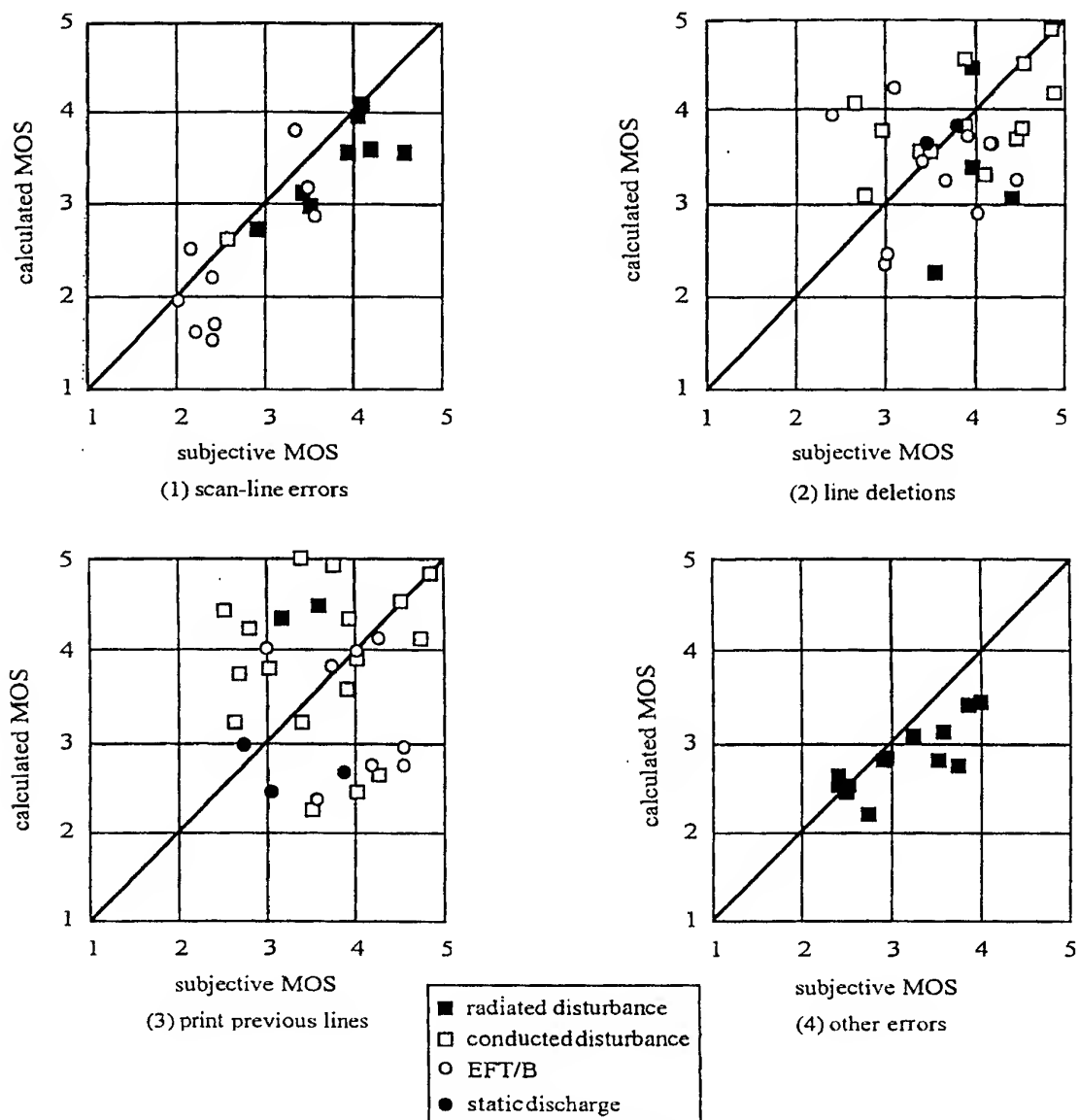


Fig. 6 Correlation between subjective MOS and calculated MOS

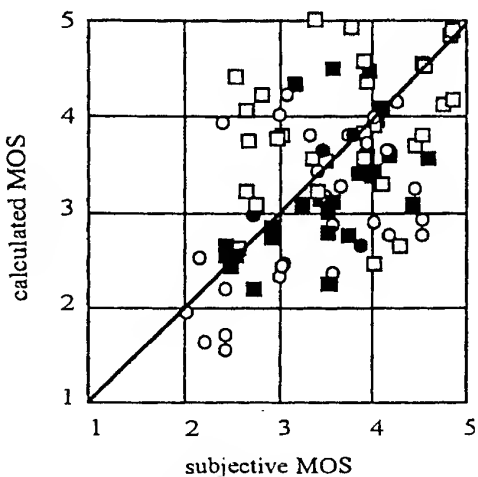


Fig. 7 Correlation between subjective and calculated MOS for all errors

errors at almost the same rate. Conducted disturbance makes line deletion and print previous line errors. Most of the degradation caused by EFT/B noise is scan-line errors.

Correlation results between subjective MOS and calculated MOS for each degradation are shown in Fig. 6. In this figure, (1) shows the correlation for scan-line errors, (2) for line deletion errors, (3) for print previous line errors, and (4) for other errors. Among the calculated, 15 became more than MOS 5, so these were removed from Fig. 6. Also data whose subjective MOS was under 2 were removed from Fig. 6, because there is no need to evaluate an image that is clearly distorted, while if the MOS of the data is above 3, they are difficult to evaluate. In this figure, the horizontal line shows the subjective MOS and the vertical line shows the calculated MOS. The black squares show the correlation for radiated disturbance, the black circles for static discharge, the white squares for conducted disturbance, and the white circles for EFT/B noise.

For (1) and (4) the correlation factors were 0.88 and 0.81 respectively, which indicate strong positive correlation. For (2) the correlation factor was 0.30, which indicates weak positive correlation. And for (3) the correlation factor was -0.05, which indicates almost no correlation.

The correlation results between subjective and calculated MOS for all degradations are shown in Fig. 7. The overall correlation factor was 0.41,

4. CONCLUSIONS

Our new method for evaluating the image quality of facsimile output reduces evaluation time and cost. The quality calculated from five parameters obtained from the original and evaluated images was compared with that judged by 40 subjects. The results for immunity testing show that this method can be used for measuring the immunity of facsimiles for some types of degradation. Future work should investigate a method of objective evaluation which has a higher correlation.

5. REFERENCES

- [1]IEC 61000-4-2: "Electrostatic discharge immunity test", Jan. 1995.
- [2]IEC 61000-4-4: "Electrical fast transient/burst immunity test", Jan. 1995.
- [3]NTT, AT & T, and CPRM-Marconi: "International Verification Test Results on the NTT Model for Evaluating Facsimile Image Quality", ITU-Telecommunication Standardization Sector, Q.2/SG2, Manila meeting, July 18-23, 1996.

BIOGRAPHICAL NOTE

Yoshiharu HIROSHIMA was born in Akita, Japan in 1962. He received the B.E. and M.E. degrees in electrical and communication engineering from Tohoku University. He is currently a Research Engineer in Electromagnetic Environment Research Group of Multimedia Networks Laboratories, NTT. Since joining NTT, he has been engaged in research and development on immunity measurement for telecommunication systems.

EFFECTS OF ELECTROMAGNETIC INTERFERENCES ON OPERATIONAL AMPLIFIERS *

Jerzy F.Kołodziejski

Institute of Electron Technology, 02-668 Warszawa, Al. Lotników 32/46, Poland
tel. (22) 847 26 61, fax (22) 847 06 31, e-mail : jekolo@ite.waw.pl

Marek Skorupski

Technical-Agriculture Academy, Telecommunication and Electrotechnical Department, Poland
85-796 Bydgoszcz, ul. Kaliskiego 7, tel. (52) 340 83 97, fax (52) 340 83 10

Abstract. In the work some results of simulation and experimental investigations are given, concerning the susceptibility of operational amplifiers (OpAmps) to electromagnetic interferences (EMI). The effects of EMI, mainly hf (out-of-band) in the form of short pulses, on the inputs of OpAmps and on their power supply lines are considered. Conventional (voltage dependant) and current feedback amplifiers (FCAs) are taken into account. Final conclusions embrace some practical recommendations.

1. INTRODUCTION

Operational amplifiers like any other elements and electronic circuits are very often exposed to undesired effects of disturbing signals. Particular type of these signals represent hf interferences which are mainly spread out as electromagnetic waves. As their sources one can point out radio and TV stations, radars, telecommunication transmitters etc. Electromagnetic radiation may induce variable currents of respective frequencies in the lines and cables connected to electronic equipment. In the case of electromagnetic field of high energy, the induced voltage levels can be so high that they could be able to disturb the function of amplifier and cooperating circuits. Transistor in the amplifier input stage works as a detection diode. Interferences coming to the input are then rectified and can pass to the next stages of the amplifier [6, 7, 16, 18].

Various kind of high speed digital circuits can also be recognized as possible and dangerous sources of unwanted hf signals. Interferences produced by digital circuits have usually the form of random or periodic pulses. They can reach the circuits with operational amplifiers through direct couplings of conductive or capacitive character. As an example it can be shown that TTL switching signals coupled through 0.5 pF capacitance to 1 MΩ resistor may induce voltage pulses of nearly 5 V amplitude and duration about 100 ns [6].

The presence of electromagnetic interferences with frequencies higher than the specified bandwidth of operational amplifier creates the real threat for reliable work of the amplifier. It is well known that such signals induce constant voltage of the significant level at the output of amplifier [6, 7, 8, 14, 15, 16].

Equally undesired influence may have interferences appearing on the supply lines of operational amplifier. They produce additional variable signals at the amplifier output. The disturbance of amplifier response can result from short step-like changes of supply voltage, which generate voltage pulses of relatively high amplitude [15].

Although the majority of OpAmps are designed to work with harmonic (sinusoidal) signals, it is not justified to regard only this signal category during the investigations of amplifiers susceptibility to electromagnetic interferences. The effects of hf (wideband) interferences are sufficiently specific and significant to be considered as well.

2. PULSE INTERFERENCES AT OPAMP INPUTS

It could seem that the signals with frequencies exceeded the frequency f_i , corresponding to the unity gain of the amplifier, should not be transferred throughout the circuit but rather strongly suppressed. However, it is commonly known that this kind of signals produce relatively high steady voltage at the output of the amplifier, even in the case the average (mean) value of the input signal is equal zero [7, 14, 15, 16, 18]. As a basic reason of this phenomena the asymmetry between the slopes of raising and falling edges of the output voltage is given: $|SR^+| \neq |SR^-|$.

When $|SR^+| > |SR^-|$ the steady voltage at the output is positive and when $|SR^-| > |SR^+|$ - negative.

Taking the above explanation into account one could conclude that it would be possible to avoid the generation of additional steady voltage using the amplifier with equal values of $|SR^+|$ and $|SR^-|$.

*Partially supported by KBN, project nr 8T11B 06710

However, the detailed investigations and computer simulation not allow to accept this assumption as a sufficient condition.

Let consider the response of noninverting circuit stimulated by the voltage pulse of amplitude U_i and duration t_i . In the case of ideal circuit, output voltage would have the form of voltage pulse with the amplitude $U_o = G U_i$ and duration t_i , where G means the circuit gain. But in practice the amplifier bandwidth is limited by frequency f_c what causes that the change of output voltage follows exponential curve with the time constant $\tau_c > 0$

$$\tau_c = 1/2\pi f_c \quad (1)$$

where $f_c = R_c/C$.

Also the second factor should be regarded, namely the limitation of current which charges the inherent capacitance C_k designed for compensation amplifier frequency characteristic. It confines the output voltage raising rate to certain maximal value SR^+ .

The circuit response will then change in the following way:

- initially the voltage raises linearly with the slope equal SR^+

$$U_o(t) = SR^+ t \quad (2)$$

right for the range of time $0 < t \leq t_x^+$

where

$$t_x^+ = \frac{U_i G}{SR^+} - \tau_c \quad (3)$$

- afterwards linear time dependence is followed by exponential one

$$U_o(t) = U_i G - SR^+ \tau_c \exp\left(-\frac{t-t_x^+}{\tau_c}\right) \quad (4)$$

right for the range of time $t_x^+ < t \leq t_i$.

After the time interval of t_i , output voltage reaches the value of $U_o(t_i)$. It is worth to notice that in the case when $t_x^+ < 0$ the output voltage will change exponentially already from the starting point t_0 , with the time constant τ_c .

The process of falling the output voltage begins at the end of stimulating pulse. Similarly like above, the initial part can be approximated by straight line with the slope SR^-

$$U_o(t) = U_o(t_i) - SR^- t \quad (5)$$

right for the time range $t_i < t \leq t_x^-$

where

$$t_x^- = \frac{U_o(t_i)}{SR^-} - \tau_c \quad (6)$$

Further fall of output voltage can be described as

$$U_o(t) = [U_o(t_i) - SR^- t_x^-] \exp\left(-\frac{t-t_x^-}{\tau_c}\right) \quad (7)$$

for $t \geq t_x^-$.

The considered process of changing the output voltage of noninverting amplifier circuit is illustrated in Fig. 1.

If time constant τ_c is significantly greater than t_i , the output voltage at the moment t_i reaches the value $U_o(t_i) < G U_i$. In this case, even when $|SR^+| = |SR^-| = S$,

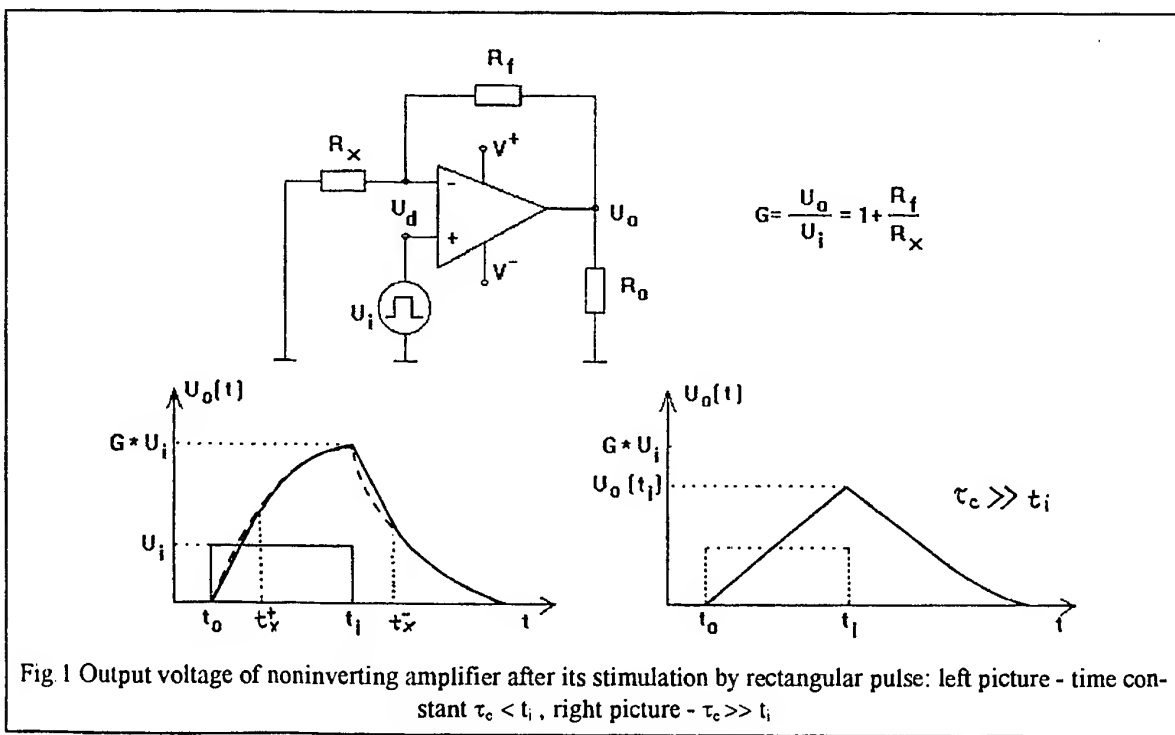


Fig. 1 Output voltage of noninverting amplifier after its stimulation by rectangular pulse: left picture - time constant $\tau_c < t_i$, right picture - $\tau_c \gg t_i$

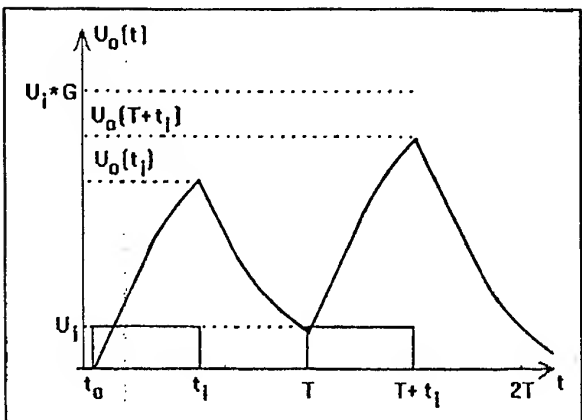


Fig. 2 Output voltage of operational amplifier stimulated by two short pulses

the time necessary for output voltage U_o to fall to zero is longer than t_i , Fig. 2.

There is a difference between the time interval needed for output voltage to rise from initial value of zero to the value of $U_o(t_i)$ and the time interval needed for output voltage to return again to zero. The difference results from the fact that circuit gain G forces faster rise of output voltage (up to the theoretical level GU_i) than could have the falling process, which begins at the end of input pulse. If a next pulse occurs at the input, before the output voltage falls to zero, it stops the fall and causes the repeated rise of the voltage - but this time from the initial value $U_o(T) > 0$. Since that, after the time interval t_i , output voltage achieves higher level than in the case of duration of previous pulse: $U_o(T + t_i) > U_o(t_i)$. The phenomenon will be repeated with each subsequent pulse and will be more pronounced for smaller value of $|SR^+|$ as well as at higher frequency of input signal.

More complicated situation we experienced when the hf pulse signal (with $f \gg f_i$) is given to the input of operational amplifier. In this case the duration of single pulse is considerably shorter than the time of linear work of the amplifier circuit $t_i \ll t_s$. Hence, the output voltage increases or decreases linearly. The short duration of disturbing pulses has also another consequence. Integrating circuit, responsible for the correction of amplifier frequency characteristic, can not keep up with the fast changes of output voltage ($t_i \ll \tau$). Input signal oscillates around the steady component which simultaneously rises exponentially with certain time constant τ' . In this manner, integrated steady component of the signal is transferred from the input to the output amplified by G . Output voltage will be then composed of the amplifier responses to the hf pulses as well as to steady component of the input signal, which is proportional to its repetition rate α (where $\alpha = t_i/T$, $0 < \alpha < 1$). Because the output voltage can not rise faster than at the rate determined by the slope of output voltage S , the presence of steady component has no influence on the speed of rise. However, it contributes to the

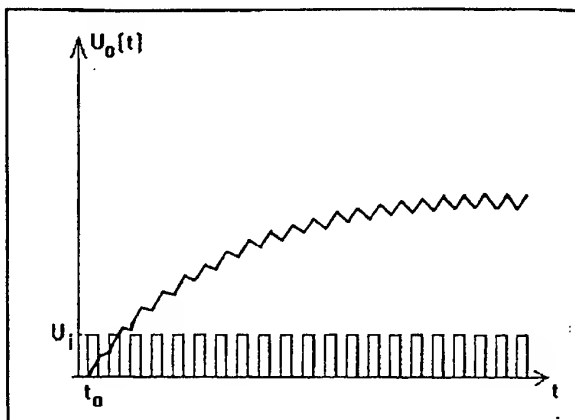


Fig. 3 Output voltage of operational amplifier stimulated by hf interferences : input signal is integrated ; steady component of output voltage tends exponentially to value U_{ODC} ; variable component oscillates around U_{ODC} with constant peak-to-peak value.

decreasing of output voltage falling rate during the intervals between disturbing pulses.

The final effect is expressed as gradual increase of the output voltage proceeded up to the moment the steady component reaches the value of $G U_{i av}$, Fig. 3. On its way to the saturation output voltage oscillates around the value of $G U_{i av}$ with the amplitude $S t_i$.

The described behaviour of operational amplifiers was confirmed by the results of computer simulation with the help of PSPICE programm. Three amplifiers - bipolar OP 77 and two other with current feedback - AD 844 and AD 8001 were analyzed in details. The last two amplifiers, with the equal slew rates $SR^+ = SR^-$, were configurated as the voltage followers.

OpAmp OP 77 has rather small slew rate - measured value was equal $0.21 \text{ V}/\mu\text{s}$. When stimulated by train of pulses with amplitude $U_i = 1 \text{ V}$ and frequency about few tens kHz (closed-loop bandwidth BW specified by manufacturer is equal 400-600 kHz), the amplifier exhibits a tendency to integrate the input signal. The time characteristic of output voltage can be taken as typical for the effect of interferences with out-of-band frequencies. Evidently, the characteristic results not from the asymmetry of SR^+ and SR^- but from their small values, which reveal their influence already at relatively low frequencies. The observed limitation of output voltage raising rate may be used to suppress short disturbing pulses. In the time of pulse duration the output voltage comes only to the value of $S t_i$, what reduces the interference influence on the output voltage.

CFAs have usually broader bandwidth than conventional (voltage) amplifiers and are more immune to hf interferences. The integration of amplified hf input signals, having its place at the output of amplifier, proceeds similarly like in the case of voltage amplifiers but at the higher frequency level. The large values of slew rates provide additional practical advantage of CFAs. CFAs have the specific feature: their parameters related to frequency band depend on the value of co-

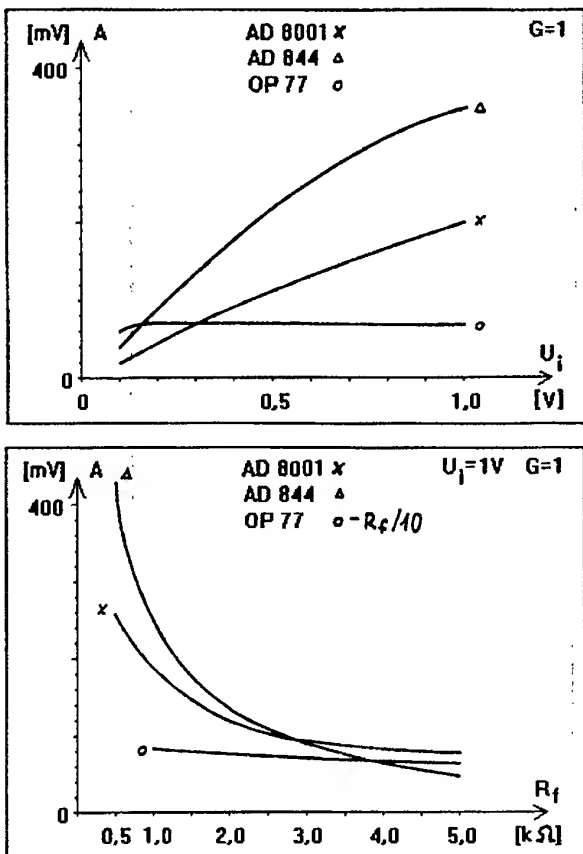


Fig. 4 Peak-to-peak voltage (amplitude) of variable component at the amplifier output versus: a) amplitude U_i of input interfering signal ($R_f = 1 \text{ k}\Omega$ for CFAs and $R_f = 10 \text{ k}\Omega$ for OP 77), b) value of resistor R_f for 3 OpAmps working as voltage followers ($U_i = 1 \text{ V}$).

uppling resistor R_f . 3 dB frequency band is determined by the expression $f_{3\text{dB}} = 1/2\pi C_T R_f$, where C_T means the amplifier transfer capacitance (transcapacitance).

CFAs gain for inverting and noninverting configurations depends only on R_f and R_x resistors and can be evaluated with the same equations like for the conventional OpAmps. The circuit stability is also dependent upon R_f [20]. There is a certain minimal value below which the amplifier becomes unstable. Since that, even for voltage follower R_f value must be greater than zero. Too small R_f values may increase CFAs susceptibility to EMI. Let take as an example AD 844 amplifier ($f_t = 100 \text{ MHz}$, $\text{SR} = 2000 \text{ V}/\mu\text{s}$) in noninverting configuration. After stimulation its input with hf signal ($f = 100 \text{ MHz}$, amplitude = 1 V), we observe the oscillation of output voltage around certain value $U_{o\text{DC}}$, which is the function of mean value of input signal and circuit gain. For determined G and R_f , large value of SR is the reason that the amplitude of output voltage oscillations rises linearly with increase of input signal, Fig. 4a. Instead, for determined G and U_i , amplitude of oscillations decreases nonlinearly with the rise of R_f , Fig. 4b. As can be seen from the figures these dependencies are valid only for CFAs. At large slew rate $\approx 2000 \text{ V}/\mu\text{s}$

during the time $t_s = 5 \text{ ns}$ (it corresponds to frequency $f = 100 \text{ MHz}$ and $\alpha = 0.5$), output voltage could rise up to 10 V ($U_o = \text{SR } t_s$). But the raising rate of output voltage is limited by time constant τ , which increases proportionally to R_f , what in turn slows down the process of raising the output voltage. When input pulse duration is confined, it results in weaker oscillations.

3. INTERFERENCES SUPERIMPOSED ON POWER SUPPLY LINES

It is well known that to assure proper functioning of OpAmp its supply voltages should be symmetrical and stable. OpAmps designers apply some measures to prevent transfer of supply voltages changes to the amplifier output. The effect of these efforts is reflected by the value of PSRR - power supply rejection ratio. Nevertheless, some disturbing phenomena like temporary loss of symmetry caused e.g. by fast step-like changes of one or both supply voltages still remain threatful. Asymmetry in supply voltages limits the circuit dynamic features and contributes to an increase of offset voltage $U_{o\text{off}}$. Another effect of jumps in supply voltages is generation of voltage pulses of relatively

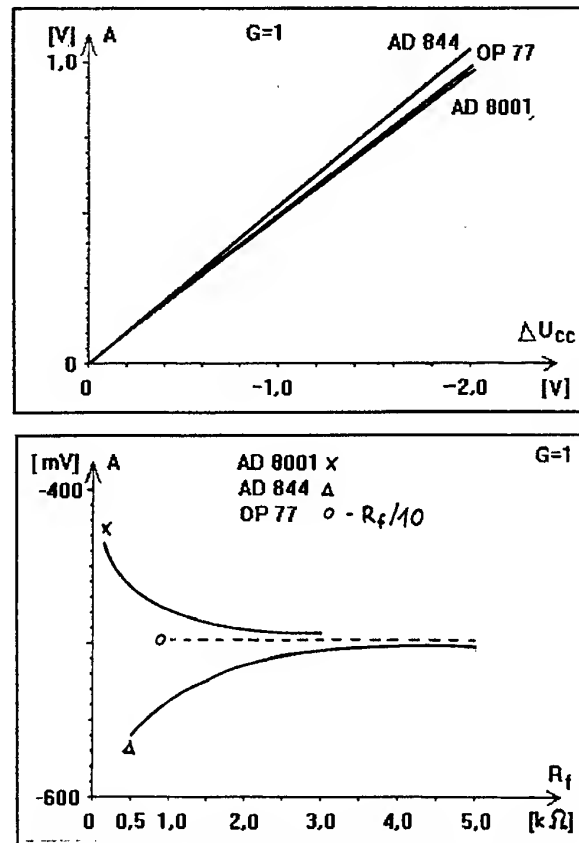


Fig. 5 Output pulse of voltage follower caused by jump of supply voltage $+ U_{cc}$ versus : a) magnitude of jump ($R_f = 1 \text{ k}\Omega$ for CFAs $R_f = 30 \text{ k}\Omega$ for OP 77), b) value of R_f resistor ($\Delta U_{cc} = -1 \text{ V}$).

high amplitude at the amplifier output. The pulse amplitude depends on the jumps magnitude. Pulses are positive for raising edges (increase of V^+ or decrease of V^-) and negative for falling edges. The pulse amplitude can be partially reduced by heavy load. It was found that at the moderate loading of OpAmps, the values of pulse amplitude were in the range of 450-550 mV on every 1V change of supply voltage, independently of circuit configuration, gain and R_f value (for voltage amplifier). For CFAs the R_f value was significant. The values of output pulse amplitude versus the magnitude of supply voltage changes and the value of R_f resistor are given in Fig. 5a and 5b, respectively.

Step-like changes of supply voltage cause the change of amplifier offset voltage, what influences the output voltage level in proportion to magnitude of changes and R_f value (the test was performed with input terminals connected to zero level point of supply lines).

4. CONCLUSIONS

We have been striving to show that the effect of integration of input pulse signals, with frequencies exceeded 3 dB amplifier band, is caused above all by real (limited) parameters of OpAmps like C_k , f_t , SR. Consequently, if we expect the presence of hf interferences, to avoid generation of additional steady output voltage, it is advisable to use OpAmp with greater bandwidth. When circuit time constant is smaller than pulse duration, hf signal is induced at amplifier output, although without any amplified steady component. If the circuit is expected to be exposed to disturbing short pulses (glitches) it is recommended to chose OpAmp with small SR values.

CFAs are more immune to hf interferences (but with $f < f_t$). Value of R_f should be select with care: smaller values can extend amplifier bandwidth but simultaneously they rise the amplitude of oscillation at the output.

Proposed installation of low pass filter at the amplifier inputs [24] can prevent only the disturbing effect of harmonic (sinusoidal) interferences with the mean value equal zero. Otherwise, e.g. for the pulses shorter than time constant of filter circuit, the steady voltage component with the level proportional to the repetition rate of input pulse train will be induced at the amplifier output.

5. REFERENCES

1. J.J.Solomon: The Monolithic OpAmp. A Tutorial Study. IEEE Journ. of Solid-St. Circuits vol. 9, no.6, Dec. 1974
2. G.Krajewska, F.E.Holmes: Macromodeling of FET/Bipolar Operational Amplifiers. IEEE Journ. of Solid-St. Circuits vol. 14, no.6, Dec. 1979
3. M.Nadachowski,Z.Kulka: Analog integrated circuits (in Polish). WKif Warszawa 1980
4. W.Nowakowski: Basic electronic circuits. Pulse circuits (in Polish). WKif Warszawa 1982
5. B.Perez-Verdu, J.L.Huertas, A.Rodriguez-Vazquez: A New Nonlinear Time-Domain Op-Amp Macromodel Using Threshold Functions and Digitally Controlled Network Elements. IEEE Journ. of Solid-St. Circuits vol. 23, no. 4, Aug. 1988
6. C.Rudnicki: Integrated operational amplifiers as the amplifiers of variable signal (in Polish). Elementy pol-przewodnikowe i układy scalone, PIE W-wa 1/1989
- 7.D.Golzio et al.: EMI induced failures in integrated circuits operational amplifiers. Proc. 8th Symp. on Reliability in Electronics, Budapest, Hungary 1991
8. S.Graffi, G.Masetti, D.Golzio: New Macromodels and Measurements for the Analysis of EMI Effects in 741 Op -amp Circuits. IEEE Trans. on EMC vol.33, no.1 1991
9. C.Coughlin, F.F.Driscoll: Operational Amplifiers and Linear Integrated Circuits. Prentice Hall 1991
10. E.Bruun: Constant-Bandwidth Current Mode Operational Amplifier. Electronics Letters vol. 27, no. 18, 29 Aug. 1991
11. T.Vanisri, C.Tomazou: Wideband and High Gain Current-Feedback OpAmp. Electronics Letters vol. 28, no. 18, 27 Sept. 1992
12. A. Guziński:Linear electronic analog circuits (in Polish). WNT Warszawa 1993
13. J.Dostal: Operational amplifiers. Butterworth-Heinemann 1993
14. G.Masetti et al.: Failures induced on analog integrated circuits conveyed electromagnetic interferences. Proc. ESREF Conf., Bordeaux, France 1993
15. H.Lestienne et al.: Rapport sur: L'étude de la perturbabilité des amplificateurs opérationnels soumis à des parasites transistoirer. Université de Lille 1994
16. A.S.Poulton: Effect of conducted EMI on the DC performance of operational amplifiers. Electronics Letters vol. 30, no.4, 17 Febr. 1994
17. A.Filipkowski: Analog and digital electronic circuits (in Polish). WNT Warszawa 1995
18. S.Graffi et al.: Criteria to reduce failures induced from conveyed electromagnetic interferences on CMOS operational amplifiers. Proc. 10th Symp. on Reliability in Electronics, Budapest, Hungary 1995
19. L.Hasse et al.: EMI in electronic equipment (in Polish). Radioelektronik Sp. z o.o. Warszawa 1995
20. R.Wojtyna: Operational CMOS amplifier with current feedback and 3 V supply voltage (in Polish). Proc. VIII National URSI Symp., Wrocław, Poland 1996
21. M.Skorupski: Susceptibility of operational amplifiers to EMI (in Polish). Elektronizacja 3/1997
22. S.Kuta, G.Krajewski, W.Machowski: Current feedback OpAmps in CMOS technology. Proc. 4th International Workshop MIXDES'97, Poznań, Poland 1997
23. M.Neag, O.Mc Carthy: Current Feedback Op-Amp Based Voltage Amplifier and Integrator Analysis Using a Two-Poles Model. ditto
24. P.Studziński: Susceptibility of instrumentation and operational amplifiers to high frequency interferences (in Polish). Elektronizacja 1/1997
25. J.Rahbek: Comparison of the RF immunity of operational amplifiers. Proc. International Zurich Symp. on EMC, 18-20 Febr. 1997.

THE IMMUNITY OF WROCŁAW TOWN HALL TOWER FIRE DETECTION SYSTEM TO ATMOSPHERIC DISCHARGE

Andrzej E. Sowa Rafał Zdunek

Wroclaw University of Technology
Institute of Telecommunication and Acoustics
Wybrzeze Wyspianskiego 27
50-370 Wroclaw, Poland

phone: (+4871) 3203276
fax: (+4871) 223473; 3203189

This paper presents the use of the computer simulation for analysing the immunity of exemplary system to atmospheric discharges. The equivalent circuit model of the system was constructed. The model made it possible to compute the system response to arbitrary input. The model was verified by comparing the calculated and measured results. The verification proved to be satisfactory.

The effective ways of increasing the immunity to atmospheric discharges were developed with the help of the model.

1. INTRODUCTION

Atmospheric discharges are one of the most significant threats to electrical/electronic equipment and can cause considerable damage to equipment and systems. This is as a result of the limited immunity of the equipment and systems to electromagnetic surges which reach them mainly by signal, control and power lines. Adequate lightning protection needs to be ensured.

The intuitive use of standard countermeasures often proves ineffective. Computer modelling of the system of interest, including its coupling to the lightning channel, may be an effective way of finding efficient protection. Computer simulation allows the mechanism of damage caused by lightning to be defined and the effectiveness of proposed protection measures to be examined. The method of analysing the immunity of an exemplary system to lightning, described in this paper, may serve as an example of the effective use of computer simulation for developing lightning protection.

The exemplary system used for the computer simulation was the Wroclaw Town Hall Tower fire detection system. In the past, thunderstorms occurring over Wro-

claw Market Square often damaged a fire detection system protecting Wroclaw's famous Town Hall. The Town Hall's 60m high tower, the highest building in the Square is particularly prone to lightning. To increase the immunity of the system, standard lightning protection measures as used for systems with signal and power lines were employed.

This method of protection did not work as expected and therefore the task of constructing an exact model of the system was undertaken. This model is to enable the immunity of the system to lightning to be investigated. For the construction of the model circuit theory methods of analysis of the system were employed. The use of circuit theory methods of analysis instead of field theory methods (e.g. [1], [4], [5]) simplifies the calculations necessary. An equivalent circuit representation of the coupling between the fire detection system and the lightning conductor can be employed because the system is situated close to the lightning conductor (of course only for the limited frequency spectrum of lightning [3]).

2. WROCŁAW TOWN HALL TOWER FIRE DETECTION SYSTEM

The lightning protection system of the Town Hall Tower consists of two vertical conductors running parallel to the tower.

To simplify the calculation it was assumed that the lightning current flows along a single path i.e. along one lightning conductor. It was also assumed that the lightning conductor was a part of lightning channel.

The fire detection system consists of several signal lines, some of which run parallel to the lightning conductors for a significant length. These cables go from the top of the tower to a control module on the ground floor.

The fire detection system may be divided into three main parts:

- sensors which detect the increase of smoke and temperature levels and transform the information into electric signals,
- dual signal lines connecting sensors with a control unit,
- control module which reads information from signal lines and generates alarm signals; it also supplies power to sensors using the same lines,

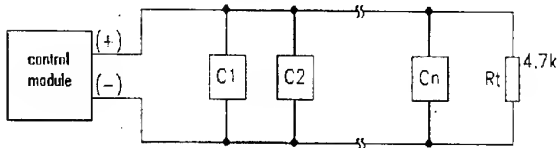


Fig. 1. Simplified block diagram of the system.

A single signal line parallel to a lightning conductor was chosen to analyse the system immunity. This signal line goes from the top of the Tower to the control module placed at the bottom of it. The average distance from the nearest lightning conductor is approx. 5 m.

Sensors are connected in parallel to this signal line, every 2 m. Their positioning to the lightning conductor is random. Up to 32 sensors are connected to one signal line. Fig. 1 shows a simplified block diagram of the fire detection system.

3. SIMPLIFIED SIMULATION MODEL

Faithful modelling of the system together with the lightning conductor requires exact modelling of every element of the system and every coupling path between the system and the lightning conductor.

The control module [6] is represented by the model of its input circuits shown in Fig. 2.

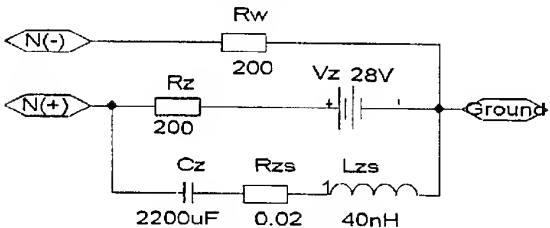


Fig. 2. Simplified diagram of the control module.

A coupling between the fire detection system and lightning conductor was modelled using an equivalent circuit representation. The coupling paths were represented by additional elements included into the model. Their values were obtained both by simple calculations and simple measurements.

Fig. 3 shows an equivalent circuit diagram of a single section of the coupling between the fire detection system and the lightning conductor. The section is 1 m long.

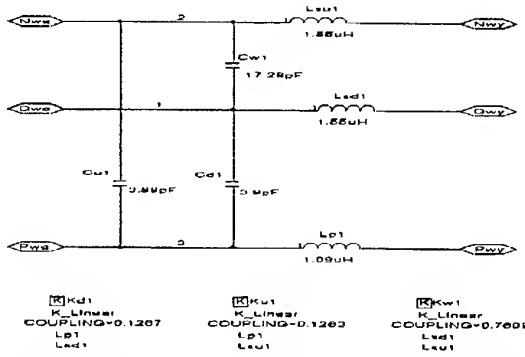


Fig. 3. Single section of the coupling between the signal line and the lightning conductor.

Fig. 4 shows a complete model of the sensor [6]. A direct coupling between the lightning conductor and certain elements of the sensor was taken into account. Particularly important is the coupling (represented by Cs) of the screen of the ionisation chamber with the lightning conductor, because of the size of the element. All additional elements are shown on the drawing.

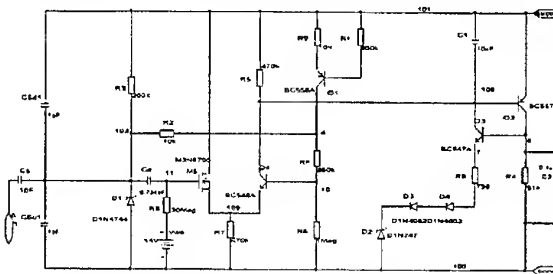


Fig. 4. Model of the sensor with additional coupling elements.

Fig. 5 shows a block diagram of a coupling of a system with 8 sections (Fig. 3) with the lightning conductor.

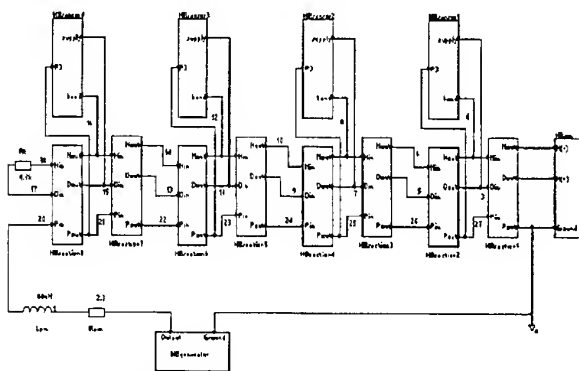


Fig. 5. Block diagram of the model.

Symbols used:

HBsection – a single section of a signal line; the diagram of this section is shown in Fig. 3,

HBsensor – a sensor with additional coupling elements; the diagram of this sensor is shown in Fig. 4,

HBcm – a simplified control module; the diagram of this module is shown in Fig. 2,
 HBgenerator – a generator of lightning current,

4. MODEL VERIFICATION

The model was verified by comparing the calculated and the measured results. The excitation was achieved by a source of current surge. For verification purposes the system was driven by a 1.2/50 8/20 μ s surge generator [2]. The real waveform of the driving current was measured and then reproduced exactly in the simulation.

A single line consisting of 14 sections (Fig. 3) with 7 sensors and loaded by the control module equivalent circuit was measured. The distance between the line and the wire carrying the surge current was approx. 0.5 m. The measurement was taken at the input terminals of the third sensor (as counted from the control module). Common and differential voltages were measured. The result for the common component measured at positive terminal of the sensor is shown in Fig. 6.

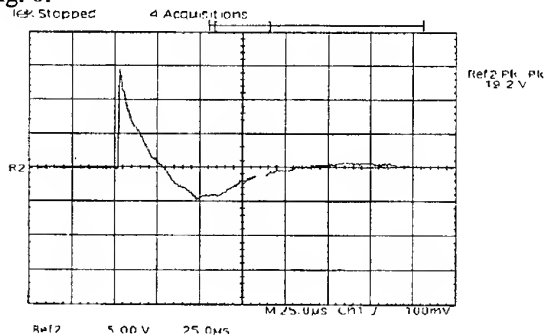


Fig. 6. Common voltage component measured at the positive terminal of the third sensor for the positive polarisation of the driving pulse (amplitude 50 V/div, time 25 μ s/div).

Fig. 7 shows the result of measurement of differential component.

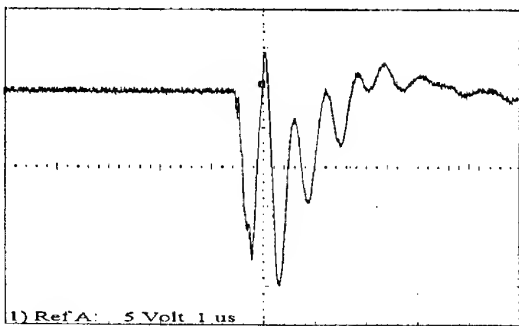


Fig. 7. Differential voltage component measured across the input terminals of the third sensor for the positive polarisation of the driving pulse (amplitude 10 V/div, time 1 μ s/div).

The computer simulation was conducted for the line consisting of 8 sections using PSPICE. Selected results are shown in Fig. 8 to 10.

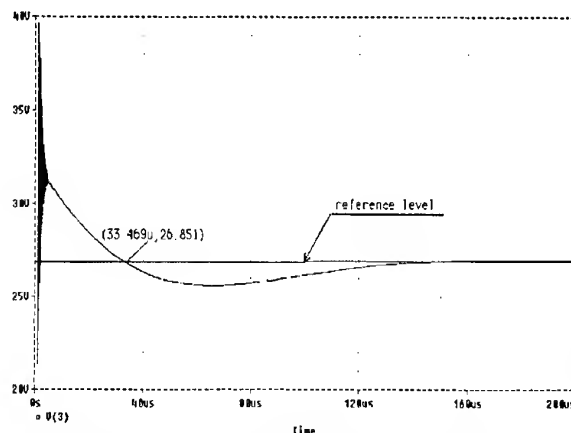


Fig. 8. Common voltage component at the first sensor (as counted from the control module).

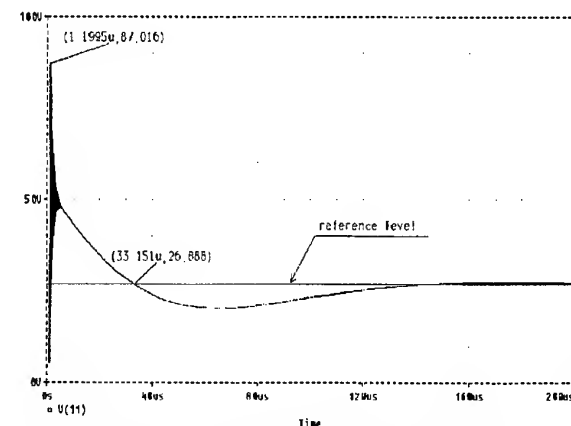


Fig. 9. Common voltage component at the third sensor.

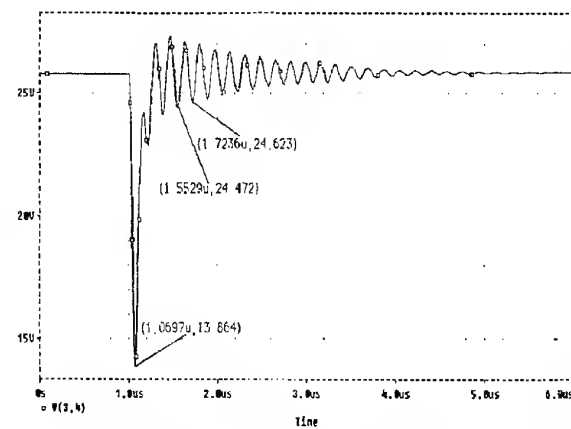


Fig. 10. Differential voltage component at the first sensor.

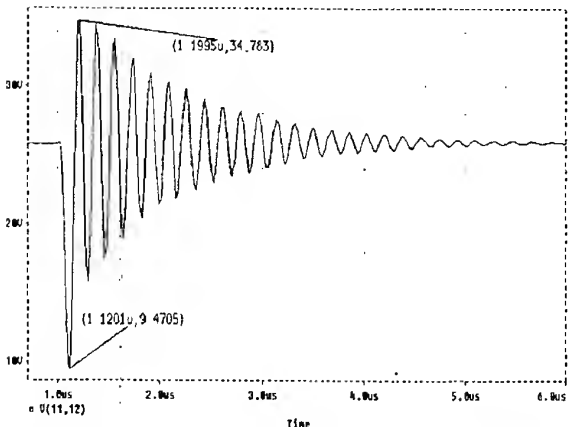


Fig. 11. Differential voltage component at the third sensor.

A comparison of measured and computed results shows that they are adequately compatible. The differences are caused mainly by the limitation of the computer model used for the simulation to 8 sections while 14 sections were used for the measurement. The limited accuracy of the model may be another source of error.

5. USE OF THE MODEL FOR INCREASING THE IMMUNITY OF THE SYSTEM TO ATMOSPHERIC DISCHARGE

The constructed model was employed for computer simulation of a real system with the distance of 5 m between the signal line and the lightning conductor. Two sections (Fig. 3) and one sensor were used for the simulation. Fig. 12 shows the driving current waveform as used for the simulation.

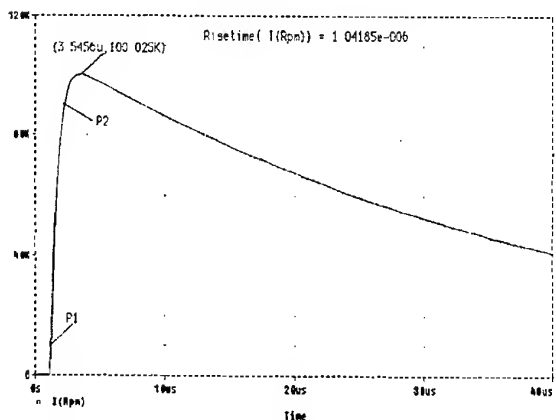


Fig. 12. Waveform of the current surge used to drive the system in computer simulation.

Fig. 13 and 14 show the differential and common voltage components computed at the sensor input terminals. Additionally, Fig. 15 shows the waveform computed at the screen of the ionisation chamber.

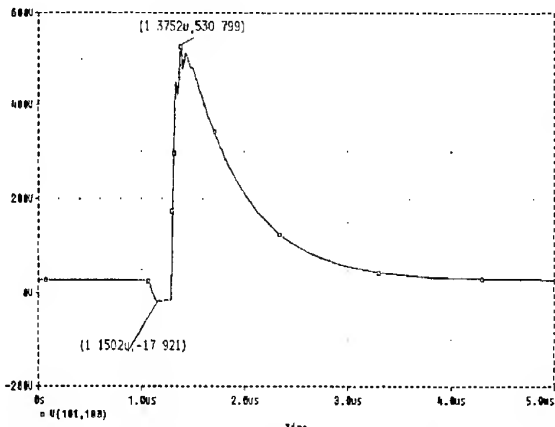


Fig. 13. Computed differential voltage component across the sensor input terminals.

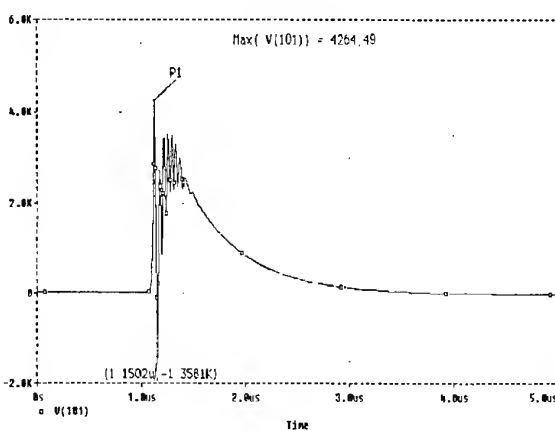


Fig. 14. Computed common voltage component at the positive terminal of the sensor.

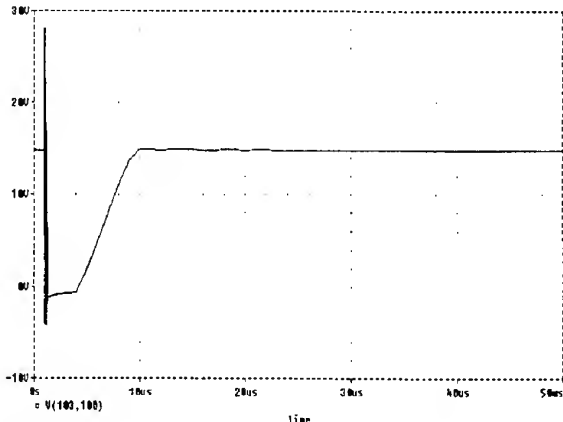


Fig. 15. Computed voltage at the screen of the ionisation chamber (the voltage between the screen and the bond of the sensor).

The computer simulation proved that the differential component occurring in consequence of signal line asymmetry was the main cause of sensor and control module damage during atmospheric discharges.

The line asymmetry can be easily reduced by symmetrization of the control module input made in the way shown in Fig. 16.

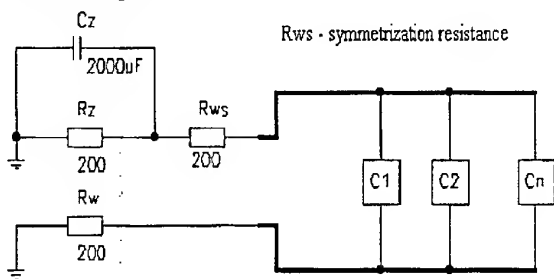


Fig. 16. Illustration of line symmetrization.

To improve the symmetry an additional resistor R_{ws} was incorporated. The value of R_{ws} was equal to the value of R_w in the control module simplified diagram. The solution effectiveness was checked with use of the two section model. Fig. 17 shows the computed differential voltage component across the sensor input terminals.

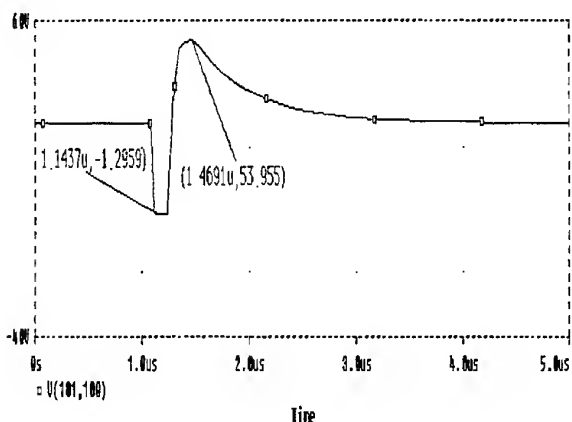


Fig. 17. Differential voltage component across the sensor input terminals after the symmetrization.

The result obtained indicates that the symmetrization gives significant reduction of the differential components level. Low price and simplicity of the solution are self-evident. But apart from symmetrization additional means of the signal line protection should be employed. The use of screened twisted pair of wires which are adequately earthed may be recommended.

The simulation made it possible to define the effectiveness of transient suppressors connected to sensor and control module input terminals. The simulation proved that even the use of the effective protection of the sensor input terminals did not give the full protection of the sensor. This happened because of the previously mentioned relatively strong capacitive coupling between the screen of the ionisation chamber and the lightning conductor. The use of the adequate means

limiting the effects of this coupling is necessary to obtain high immunity of the system to atmospheric discharge.

6. CONCLUSIONS

It can be concluded that the model describes faithfully enough the reaction of the analysed system to selected pulse excitation. For calculations aimed at finding the immunity of the system to lightning, current surges with parameters typical of a lightning main stroke should be used. Transient analysis computed for a model driven by a current pulse whose parameters are similar close to the real lightning pulse (adequate waveform and amplitude of a current surge) allows elements potentially causing system damage during thunderstorms to be identified and the effectiveness of potential countermeasures to be defined.

If atmospheric discharges occur rarely it may not be possible to carry out research of a real system and computer simulation may prove to be the only way to recognise the mechanism of damage. This solution has obvious economic advantages and allows research into the immunity of equipment and systems to be carried out quickly.

7. REFERENCES

- [1] Canavero F., Salio S., Vecchi G., „Voltage induced on a line by a nearby lightning stroke with a tortuous channel”, 12th International Symposium on EMC, Zurich, 1997, 81L8, pp. 425 – 430,
- [2] IEC 1000 - 4 Electromagnetic compatibility (EMC), Part 4: Testing and measurement techniques. Section 1: Overview of immunity tests. Basic electromagnetic compatibility publication,
- [3] Karwowski A., „Time - and frequency - domain characteristics of LEMP”, 13th International Symposium on EMC, Wroclaw, 1996, pp. 489 – 493,
- [4] Omid M., Kami Y., Hayakawa M., „Analysis of field coupling to nonuniform transmission lines”, 12th International Symposium on EMC, Zurich, 1997, 76L3, pp. 397 – 402,
- [5] Sowa A., „Numerical calculation of lightning voltages induced within transmission cables”, International Symposium on EMC. Wroclaw, Poland, 1982, pp. 485 – 493,
- [6] Technical documentation of the control module T8/SC and the sensor DIO 31 – 2, issued by POLON Bydgoszcz, 1991

XIII

NATURAL AND MAN-MADE EM ENVIRONMENT

LOW FREQUENCY EMISSIONS ONBOARD "INTERCOSMOS" SATELLITES RELATED TO RING CURRENT SPACE VARIATIONS

Larkina V.I.

IZMIRAN, Troitsk Moscow Region, 142092 Russia

It is established, that at an average, the VLF/ELF emission intensity linearly grows with an increase Dst variations. The connection of low frequency noise amplitude with Dst variations reflects an growth of particle quantity in the radiation belts causing to increase of a ring current energy and the VLF/ELF emissions excitation.

In this work we examine the space-temporary variation of the ELF/VLF emission intensity and the particle flows of a ring current during moderate magnetic storm by results of supervision of "Intercosmos 5" (noises) and "Explorer 45" (ring current particles) satellites simultaneous flights. The joint consideration of the two given satellites has allowed to make some conclusions:

- area, where the emission amplitude is maximum and where these emissions probably excited, coincide or are very close to the area of a ring current,

- during the geomagnetic disturbance similar space movement of these areas occur,

- by estimations movements of the VLF emission generation areas it is possible to judge changes of average radius of the ring current and the speed of this change.

It seems that in process of the ELF/VLF emission excitation in the plasmasphere some mechanisms will be realized. Listed above facts permit to make the assumption about an opportunity of generation of a part of registered on "Intercosmos 5" satellite low frequency emissions by the ring current

electrons at their interaction with a plasmasphere cold plasma.

The results of the wave space experiments had shown that received on board the "Intercosmos" satellite noises are the plasmaspheric hiss emissions, advantage. They are generated near the equatorial plane of the plasmasphere, i.e. in the "shot" between the inner and outer radiation belts of the magnetosphere and in the region of equatorial ring current. The unique position of the generation region enables us to investigate the effect of geomagnetic storms on the characteristics of the noise. During geomagnetic storms the low frequency emission generation region tends to move inwards, similar to the inward motion of the plasmapause [1].

A comparison of the data on wave emissions and energetic particle fluxes reveals characteristics relationship between these two phenomena. On the fig.1 we have the typical distribution of the quasi-trapped electron ($E_e \geq 40$ kev) flux and emission amplitude at 170 Hz in the daytime along some orbits of the "Intercosmos 5" satellite in different phase of the storm of 16-17 December 1971. These data were measured concurrently during three orbits of "Intercosmos 5" passing approximately over the same area (the southern hemisphere, day time, the apex of the trajectory over Australia).

On 16 December 1971, prior to the storm, a slot was recorded in the electron flux ($L \sim 3.8$) between the inner and outer radiation belts. During the storm on 17 December 1971 ($K_p = 3+$),

the slot considerably narrowed and shifted to $L = 3.2-3.3$. The electron fluxes increased markedly, especially in the outer radiation belt. On 20 December 1971, when the storm had died down ($K_p=0$), the electron fluxes at $3 < L < 4.5$ still remained high. The spatial structure of the electron fluxes observed during the post-storm-time on 20 December 1971 was very complicated, with several maxima and minima in the inner radiation belt ($L <$

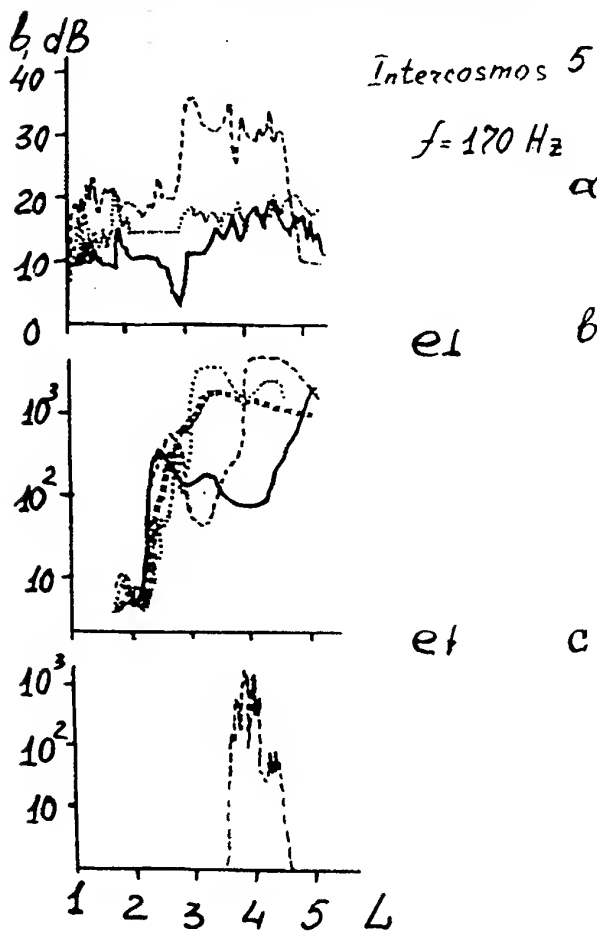


Fig.1.

Distributions of the emission amplitude at 170 Hz (a), the flux of quasi-trapped (e₁) electrons (b), and precipitation electrons (e_↓) in the daytime along some orbits during the storm of 16-17 December 1971.

- December 16, before the storm,
- December 17, during the storm,
- December 20, after the storm,
- *** December 21, after the storm.

3). The slot between the radiation belts was not distinct and was probably located at $L \sim 4$. (These changes in the fluxes of the energetic particles are ascribed to inward radial diffusion).

The amplitude of low frequency noise also undergoes considerable variations (fig. 1 a). Prior to the storm, the maximum emission intensity was observed, as usual, in the region $3.8 < L < 5$. This region coincides with the slot and the inner edge of the outer radiation belt. On 17 December 1971 the emission amplitude increased markedly (up to 40 dB) during the storm; the region occupied by the noise widened and moved towards the Earth. As prior to the storm, noise was intense in slot and at the inner edge of the outer radiation belt. In addition intense fluxes of precipitating electrons were recorded in the same region (see fig. 1. c).

On 20 December 1971, after the storm the noise intensity decreased, the position of their maxima shifting to $L \sim 4.5-5$. Even if we assume that the relative minimum of the large electron fluxes at $L \sim 4$. At that time corresponds to a new position of the slot between the radiation belts, the position of the slot corresponds with the maximum amplitude of the emissions as described above.

We suppose that at moderate altitudes (several hundred kilometres) the maximum of the emission amplitude is at the L_{max} that coincides with or is very close to the position of the emission generation region. This enables us to identify the emissions.

Our investigations can be categorized into two general classes, those using a case study and those using a statistical approach.

The emission amplitude increases linearly with growing Dst on average. The rate of the amplitude change with Dst increases with increasing L-shell crossed by the satellite. This increase is frequency dependent, i.e. the rate of increase is less at 2500 Hz than at 170 or 500 Hz (see fig. 2).

Among the indices of geomagnetic disturbance, Dst is the most useful parameter to characterize the intensity and position of the generation region of plasmaspheric noises because these emissions are generated in the equatorial ring current region, with the result that both its amplitude and the equatorial ring current depend on the flux of particles in the outer radiation belt.

Maximum of the quasi-trapped electrons (by "Intercosmos 5" satellite) and maximum of the emission amplitude are some displacement. It put us into one's head to study the ELF/VLF emission variations in the dependence on ring current particle.

In fig.3 we have geophysics situation (Dst - variations) for 23-29 February 1972. The storm of February 24, 1972 (SSC at 6.42 UT) began at the very quiet background. This was a classical magnetic storm. A deep Dst decrease during the main phase reached -86γ , Kp-reached 5+. It was the simplest one. In the bottom part of the figure we pointed out the "Intercosmos 5" orbits

(vertical lines). Vertical lines (in the middle part one) represents the distribution of the low frequency (500 Hz) emission intensity along the revolutions. We see from fig.3, that noise emission intensity maximum before the storm was take place at the $\Phi^{\circ} = 60^{\circ}$ - 65° , then ones invade the low (invariant latitude) region during the main phase, the maximum intesity was being at $\Phi^{\circ} = 50^{\circ}$ - 52° .

During the recovery phase the storm the emission maximum shift to $\Phi^{\circ} = 58^{\circ}$ - 61° (February 26) and $\Phi^{\circ} \geq 60^{\circ}$ (February 29). After the storm the emission intensity maximum is localized near $\Phi^{\circ} = 61^{\circ}$ - 65° . The area, where the emission amplitude is maximum repeated or are very close to the Dst variations or ring current, and during the geomagnetic disturbance they have similar space movement.

By experimental results received on board "Intercosmos 5" satellite it is difficult to separate the ring current particles from the radiation belt one. "Intercosmos" satellites did not cross of

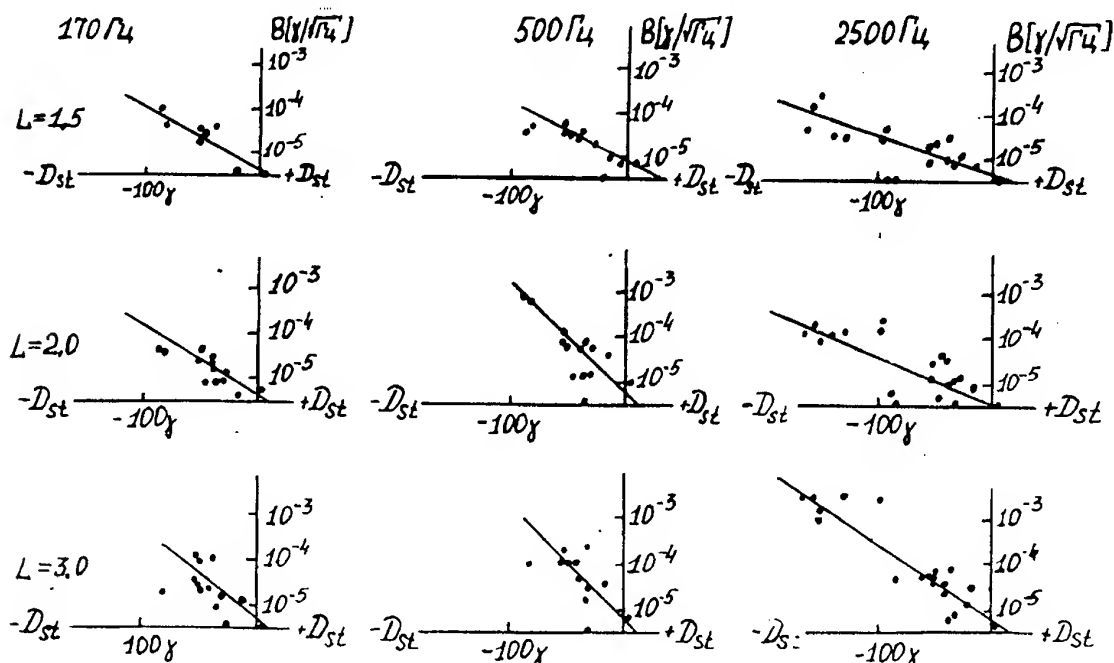


Fig.2.

Emission amplitude vs Dst variations. The horizontal axis represents Dst in units of γ and the vertical axis amplitude in units of $\gamma/\sqrt{\text{Hz}}$.

the equator regions of the ring current ($R_e \sim 5\text{--}8$). They are existing on the ionospheric altitude. Simultaneously, it was observed the ring current particle variations onboard "Explorer 45" satellite.

"Explorer 45" satellite was launched into an elliptical orbit. "Intercosmos" was launched into orbit having a perigee of 200 km, an apogee of 1200 km and 48.4° inclination to equatorial plane, ~98 min orbiting period [2]. Table 1 lists the characteristics of the parameters of the "Explorer 45" and "Intercosmos 5" satellite orbits.

	"Explorer 45"	"Intercosmos 5"
launched	November 15, 1971	December 2, 1971
on		
apogee	5.24 R_e	1200 km
perigee	222 km	200 km
inclination	3.6°	48.4°
period	7h 49m	98 m

We choose the events when the "Explorer 45" satellite was in the equatorial region and "Intercosmos 5" was at the same L-shell, but near Earth and when the local time at the satellite orbits was the same [3-7].

In the bottom part (fig.3) we presented the "Explorer 45" orbiter by horizontal lines. Vertical point lines show the ring current boundaries by "Explorer 45" data. We used the data on the distribution variations for the low-energy protons from 20 to 50 keV [7].

Before the storm the ring current boundaries by "Explorer 45" we observed at $\Phi = 60^\circ\text{--}65^\circ$ (orbit 314). In the beginning of the recovery phase the boundary was registered at $\Phi = 52^\circ\text{--}55^\circ$. During the recovery one the boundary carry at $\Phi = 57^\circ\text{--}60^\circ$ (February 25) and $\Phi \geq 60^\circ$ (February 27 and 28). Variations of the emission amplitude coincides or very close the ring current one.

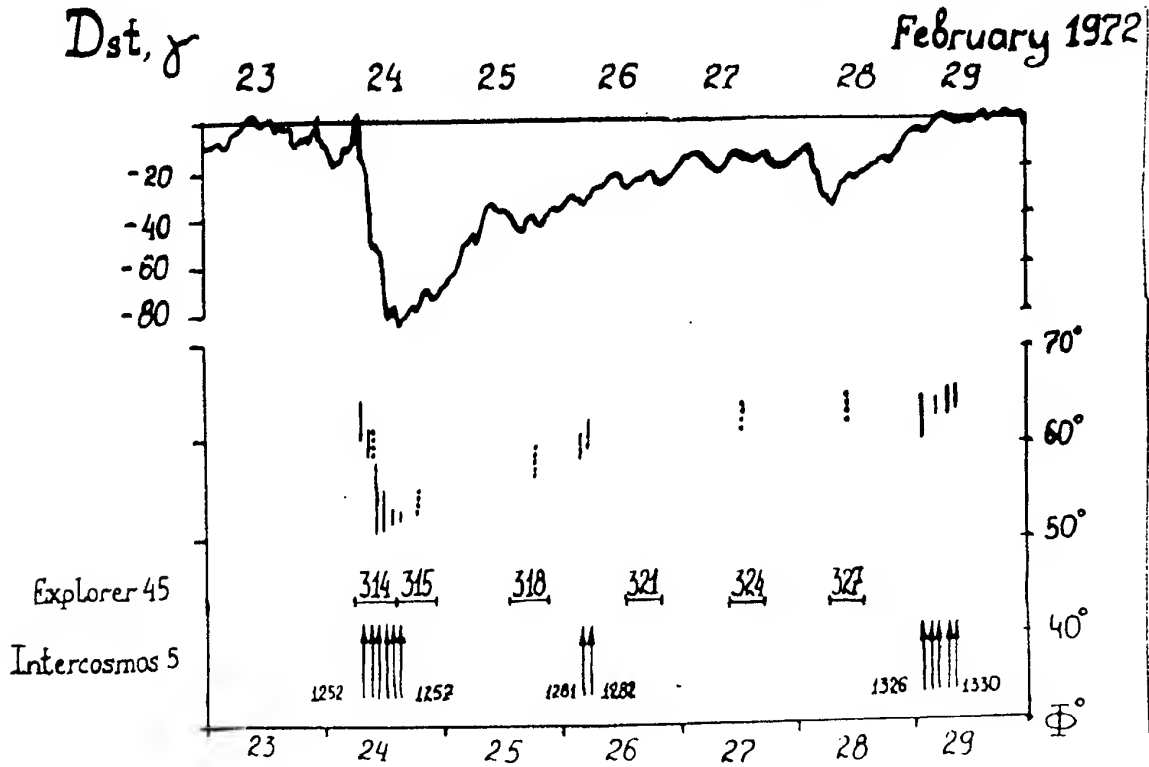


Fig.3.

Geophysics situation (D_{st} - variations) for 23-29 February 1972 and ring current variations by "Explorer 45" (vertical point lines) and low-frequency emission amplitude variations (vertical solid lines) by "Intercosmos 5". In the bottom part we pointed out the satellite orbits: "Intercosmos 5" - vertical lines, "Explorer 45" - horizontal lines.

We had information for 4 geomagnetic storms from two satellites "Intercosmos 19" (VLF/ELF emissions). Table 2 lists the characteristics of these storms. The results was like. But using the results of the low frequency (ELF/VLF) emission observations on board these satellite, we could to draw some conclusions about low frequency emission generation proceses.

Table 2.
Max

Data	UT	Kp	-Dst	AE
December 16, 1971	SSC	19.06	7+	-167 1375
January 21, 1972	SSC	11.51	6-	-79 1239
January 28, 1972		10.00	5+	-56 907
February 24, 1972	SSC	6.42	5+	-86 986

Conclusions:

-Area, where the emissions amplitude is maximum and where these emissions probably excited, coincide or very close to the area of a ring current,

-During the geomagnetic disturbance similar space movement of these areas occur,

-By estimations movements of the ELF/VLF emission area it is possible to judge changes of average radius of a ring current and of the speed of this change.

It seems that in process of the ELF/VLF emission excitation in the plasmasphere some mechanisms will be realized. Listed above facts permit to make the assumption about an opportunity of generation of a part of registered on "Intercosmos 5" satellite low frequency emissions by the ring current electrons at their interaction with a plasmasphere cold plasma.

References:

1. Larkina V.I., Likhter Ja.I. Storm-time variations of the plasmaspheric ELF hiss // J.Atm. Terr. Physics. 1982. Vol.44, N5. P.415-423.
2. Longanecker G.W., Hoffman R.A. S3-A Spacecraft and Experiment Description // J.Geophys. Res. 1973., V.78. P.4711-4717.
3. Parady B., Cahill L.J. ELF Observations during the December 1971 Storm // J.Geophys. Res. 1973. V.78., N22. P.4765-4770.
4. Hoffman R.A. Particle and Field observations from Explorer 45 during the December 1971 Magnetic Storm Period // J.Geophys. Res. 1973., V. 78, N22. P.4771-4777.
5. Taylor W.W.L., Parady B., Cahill. L.J. Explorer 45 observations of 1 to 30 Hz Magnetic Fields Near the Plasmapause during Magnetic Storms // J.Geophys. Res. 1975. V.80, N10. P.1271-1285.
6. Parady B., Ebereiein D.D., Marvin J.A. et al. Plasmaspheric Hiss observations in the Evening and Afternoon Quadrants // J.Geophys. Res. 1975.V.80, N16. P. 2183-2198.
7. Smith P.H., Hoffman R.A. Ring Current Particle Distributions during the Magnetic Storms of December 16-18 1971 // J. Geophys. Res. 1973. V.78, N22. P4731-4738.

Vera Larkina graduated from Moscow Aviation Institute. In 1979 she defended (protected) candidate dissertation, in 1997 - doctor one. Today she works for Laboratory of Active Experiments in the Space of IZMIRAN. Her interests lay in the field of experimental investigations of natural ELF/VLF signals, seismogenic effects in the Earth plasmasphere.

RESEARCH of the BARENTS-KARA SEA SHELF by using LOW FREQUENCY EMISSION SATELLITE MONITORING

Migulin V.V., Larkina V.I.,

IZMIRAN, Troitsk Moscow Region, 142092, Russia

Sergeeva N.G.,

Polar Geophysical Institute, Murmansk, 183010, Russia

Senin B.V.

Research Institute of Marine Geophysics, Murmansk, 183025, Russia

Results of the supervision low frequency emissions (0,1 - 20 kHz) onboard "Intercosmos" satellite are involved for the research of the Earth's crust fault in the region Barents-Kara sea. Use of the global satellite monitoring method of the natural ELF/VLF noises has allowed to reveal the large-scale areas of the fault. The attraction of statistical methods of the mathematical analysis permits us to investigate a thin structure of the low frequency emissions above a tectonic fault zone and to display an opportunity of the observe satellite result use for the control at a condition earthly crust.

Introduction.

In 1979 on "Intercosmos 19" satellite phenomenon of sharp increase of the low-frequency electromagnetic noise emissions in the upper ionosphere was found out when the satellite passed over the zone of future or occurring earthquakes with the magnitude of 5 numbers and higher [1, 2]. This phenomenon has called a

large interest at geophysics. It is confirmed by numerous supervision on other space crafts [3, 4] and stimulates ground supervision over condition of the ionosphere above the areas with active seismic processes [5].

The set of results of these researches permits to consider, that the ionosphere, as a whole, and the processes proceeding in it are indicators of certain processes in the lithosphere, though the gear (mechanism) of observable effects cannot be considered established [6,7].

The data processing results presented below, also received on "Intercosmos 19" satellite give additional acknowledgement of the electromagnetic phenomenon on the existence of the lithosphere processes in the upper ionosphere. Thus, it revealed in the given work that electromagnetic processes are unequivocally connected not with catastrofic manifestations of the seismic activity, but with current processes, occurring in the lithosphere.

Experimental data

We considered data about 20 "Intercosmos 19" orbits over the Barents and Kara seas in quiet days on March 15, 1979, on June 14, 1979, on December 7, 1979 and on November 20-21, 1980. The H - Components magnetogrammes of the high-latitude observatories Loparskaya ($\varphi=68.15^\circ\text{N}$, $\lambda=33.05^\circ\text{S}$) and Lovozero ($\varphi=67.59^\circ\text{N}$, $\lambda=35.05^\circ\text{S}$) were looked up for this purpose (supervision of the Polar Geophysical Institute). The active storm was observed on March 9, 1979 and the active period was on 10-11, March. The period of positive Interplanetary Magnetic Field (IMF) followed the storm was accompanied by appreciable decrease of geomagnetic activity down to March 17, 1979, when the next substorm arises. In June 1979 a long period of moderate activity was observed, basically, at positive IMF till June 15. The intensive storm was observed on December 4. The following days are weakly disturbed or are quiet till December 8. In November 1980 an intensive disturbance begins on November 15 and the high activity is saved up till November 11 (up to the end of a positive pulse of IMF). The inclusion of a short negative pulse has an effect for downturn of the activity.

At the crossing of deep faults of the considered region by the "Intercosmos 19" satellite

trajectory changes in the electrical and magnetic components of the VLF emissions are observed, that was marked in other our works [8-10]. In figure 1 sites of "Intercosmos 19" satellite trajectories are put, where the intensity VLF emissions variations on emptiness from 100 up to 20 000 Hz were observed. In this figure a drawing of the stretching areas and the compression areas in the lithosphere are put, between which "channels" of the material-power exchange take place. These ones connect the deep bowels of the Earth to its surface. From this figure it is clear, that the VLF emission intensity variations are observed over these channels, except for the region of the Novaya Zemlya. The high concentration radioactive garbage of the nuclear explosions and other pollution are so far contained in the bottom soils of this region. Probably, the changes in the VLF emissions can be caused (called) by two sources: a natural one in the lithosphere and an artificial source, called by the residual pollution of nuclear explosions.

Besides, two orbits on March 15 and on June 14, 1979 were chosen, they took place very closely over the same area of the Barents sea. The analysis of the VLF emission data has shown the stability of the effect discovered earlier in space and time [11].

Results of the correlation analysis.

We have received the items of information on the similarity of the emission burst form, having executed the correlation analysis of simultaneous bursts of the magnetic and electric component intensity of the low-frequency emission field (see table 1).

Table 1
Variations of the correlation coefficient (R) between magnetic and electrical component intensity of the field bursts

F, Hz	$R_{233, H=580 \text{ km}}$	$R_{1537, H=941 \text{ km}}$
140	0,6518	0,8738
450	0,6914	0,4764
800	0,7846	0,3474
4650	0,1526	0,4010
15000	0,6310	0,4204

More than likely, the measured wave field represents a mix of electromagnetic and electrostatic waves. On the orbit 233 (the satellite height is 580 km) the observable emissions are predominant electromagnetic. The correlation coefficient on all frequencies, except 4650 Hz, exceeded 0,63. On the orbit 1537 (the satellite height was a little higher and was 940 km) electrostatic waves prevailed, correlation coefficient was 0,5. The exception was only for the emissions on the frequency 140 Hz, where $R = 0,87$.

Thus, the correlation analysis has shown, that the emission on various frequencies

reacts to the processes in the lithosphere differently. At the lower heights (see orbit 233, satellite height of 580 km) the emissions were predominant electromagnetic. At large heights (900 km) the emission is transformed into electrostatic one.

The conclusion.

The presented in the work results of the VLF emissions measured onboard "Intercosmos 19" satellite have allowed to reveal the large-scale areas of the faults in the considered region. In [11] we have received the experimental evidence of the existence of electromagnetic phenomenon of the lithosphere processes in the upper ionosphere and consequently use of monitoring of supervision of the VLF emissions is one of the possible methods of the control of processes, occurring in the lithosphere.

References:

1. Mugulin V.V., Larkina V.I., Molchanov O.A. et al. Discovery of earthquake influence effects on VLF-ELF noises in outer ionosphere //Preprint IZMIRAN N25 1982. 28p.
2. Larkina V.I., Migulin V.V., Nalivaiko A.V. et al. Observation onboard the "Intercosmos 19" satellite of VLF emissions associated with seismic activity // Geomagn. i Aeronom. 1983. V.23. N5. P.842-845.

3. Electromagnetic Forerunners of Earthquakes // Ed. Sadovsky M.A. M.: Nauka, 1982. 68 p.

4. Gokhberg M.B., Morgunov V.A., Pohotelov O.A. Seismoelectromagnetic phenomena. M.: Nauka. 1988. 173 p.

5. Fatkullin M.N., Zelenova T.I., Legen'ka A.D. On the Ionospheric Effects of Earthquakes //Phys. Earth. Planet. Inter. 1989. Vol.57. P.82-85

6. Larkina V.I., Migulin V.V., Molchanov O.A. et al. Some Statistical Results on Very Low Frequency Radio Wave Emissions in the upper Ionosphere over Earthquake zones //Phys. Earth. Planet. Inter. 1989. Vol.57. P.100-109

7. Migulin V.V. Ionosphere as Indicator of Disturbances in the Lithosphere //Proceedings of the 1992 STEP Symposium/5-th COSPAR Colloquium Laurel Maryland. U.S.A. P.519-521.

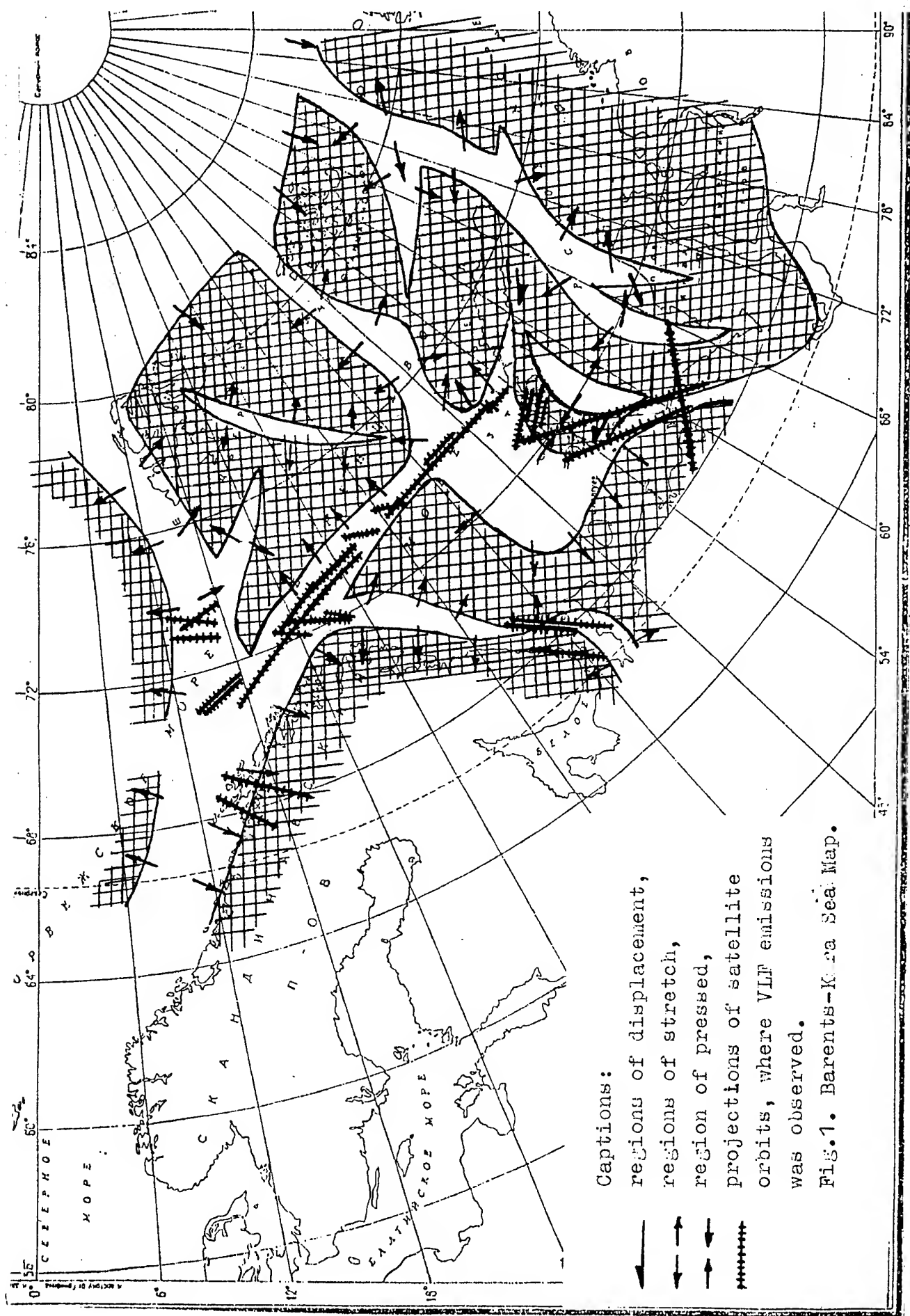
8. Larkina V.I., Sergeeva N.G., Senin B.V. Regional structure reflection on the Barents-Kara shelf in the electromagnetic emission satellite data // Abstracts of the

International Symposium "Satellites researches of ionospheric and magnetospheric processes" M., IZMIRAN, 1995, p.37-38.

9. Migulin V.V., Larkina V.I., Sergeeva N.G., Senin B.V. Regional structure reflection of lithosphere in the satellite observations of electromagnetic emissions //Dokl. Akad. Nauk. 1997, V.357, №2. C. 252-254.

10. Migulin V.V., Larkina V.I., Sergeeva N.G., Senin B.V. Regional structure reflection on the Barents-Kara shelf in the electromagnetic emission satellite data. //Proceedings of the International Conference on Marine Electromagnetics. 1997 London, UK The Defence Evaluation and Research Agency, Imperial College of Science, Technology and Medicine P.6.1

11. Larkina V.I., Sergeeva N.G. and Senin B.V. Electromagnetic Emissions over the Deep Fault of the Lithosphere by Satellite Measurements. // Proceeding of the Wroclaw International Symposium on Electromagnetic Compatibility. Wroclaw. 1998.



LOCAL LOW-THRESHOLD INDUCTIVE SENSORS FOR INVESTIGATION OF NATURAL ELECTROMAGNETIC ENVIRONMENT

Vitalij Nichoga, Petro Dub

Karpenko Physico-Mechanical Institute of National Academy of Sciences of Ukraine
5 Naukova str., Lviv, 290601, Ukraine

Large loop inductive sensors are used in investigation of natural electromagnetic environment to measure low-frequency magnetic field which have various origins. The possibility of changing such loops by local active low-threshold inductive sensors is considered in the paper. The methods which allow to achieve low discrimination threshold by sensors with small dimensions are discussed. The main characteristics of designed sensors are given.

1. INTRODUCTION

When carrying out the investigation of electromagnetic environment the large stationary inductive sensors (IS) with dimensions 50 x 50 m, 100 x 100 m and even more are used to measure low-frequency natural magnetic field caused by various sources. Such dimensions are necessary because of very low level (less than 1 nT) of measured magnetic field in 0,01÷1000 Hz frequency band. And if frequency is less than 0,01 Hz induction can come down to hundredths and thousandths of nT. Although such stationary sensors can measure only vertical field component they provide high signal-to-noise ratio and correspondingly high accuracy of measurements exactly in the frequency band below 0,01 Hz.

At the same time stationary IS has some defects and first of all great size and big mass, low mobility, necessity of considerable work to place the loop, especially in complicated physics-geographical conditions (crossed relief, wood, bog). Besides, it is necessary to choose relatively even horizontal plots with large area to decrease the measurement error, caused by horizontal field components. On the other hand, exploitation of unwieldy sensors leads to impossibility of horizontal component measuring and of further increasing of sensitivity by using summing of signals from several sensors situated on a large area (composite frame sensors or array). So it is clear that loop IS with mentioned dimensions are useless for such measurements. The urgency of designing the high sensitive IS with less dimensions is evident.

2. BASIC REQUIREMENTS AND CALCULATION EXPRESSIONS

IS is a principal part of the whole data-measuring for natural magnetic field investigation. This device is also responsible for system quality. The basic requirements to the IS for investigation of natural magnetic fields are as follows: linear and high-accuracy conversion of the measured magnetic field, high sensitivity, wide-band performance, high temperature and time stability, quick availability for service, wide dynamic range, simplicity of service and exploitation, high spatial resolution, short recovery period after high pulse overloads, high reliability during exploitation, low energy consumption. Additional requirements to amplitude-frequency (AFC) and phase-frequency (PFC) characteristics are formulated if minimal distortions are needed.

It is worthwhile to introduce some parameters to characterize IS [2]. Its sensitivity $G(\omega)$ can be determined by the following ratio:

$$G(\omega) = \frac{U_S}{B} = \omega w S K_i K_{PA}, \quad (1)$$

where U_S - input signal, B - measured magnetic induction, $\omega = 2\pi f$ - signal frequency, w - turn number, S - area, enclosed by IS loop or frame, K_i - coefficient of electromotive force transformation from IS to preamplifier (PA), K_{PA} - amplification coefficient of PA. Coefficient K_i can be written as:

$$K_i = \frac{K_0}{\sqrt{(1 - \omega^2 T^2)^2 + 4\omega^2 \eta^2 T^2}}, \quad (2)$$

where K_0 - direct current transformation coefficient, T - time constant of oscillation network, formed by IS and PA, η - relative damping factor of this network. These values can be expressed by input network parameters in the following way:

$$K_0 = \frac{R}{R+r} , \quad (3)$$

$$T = \sqrt{\frac{LCR}{R+r}} , \quad (4)$$

$$\eta = \frac{L + CRr}{2\sqrt{LCR(R+r)}} , \quad (5)$$

where L, r - inductance and pure resistance of IS, C - total capacity, R - pure input resistance of PA. L, C, R, r depend, in their turn, on constructive parameters of IS and PA (core dimensions, turn number, wire diameter and others). Sensors with linear frequency response are mainly used in geophysical practice. It must be mentioned that relative damping factor is used usually equal to 1 or some what less than 1. In such cases the transient period is the shortest.

Within linear band, where $K_i=K_0$, reduced sensitivity are often used:

$$G_f = \frac{G}{f} = 2\pi wSK_0K_{PA} . \quad (6)$$

Also equivalent area S_e is a convenient parameter:

$$S_e = wSK_0K_{PA} . \quad (7)$$

Some other requirements to IS are as follows: phase shift must be linear and discrimination threshold can't exceed permissible level. We interpret discrimination threshold as magnetic induction value with which signal-to-noise ratio is equal to 1, that is

$$B_m = \frac{\sqrt{S_n}}{2\pi f wSK_0K_{PA}} , \quad (8)$$

where S_n - PA output spectral density, which is a complicated function of electrical and constructive parameters of IS.

Thus, when designing local IS its S_n must be not smaller than that of large loop, K_i must be frequency independent in all operating range, B_m of local IS must not exceed that of large loop.

3. REALIZATION OF LOCAL INDUCTIVE SENSORS

Designing of local IS causes two main problems: realization of required AFC and PFC and obtaining of sufficiently low threshold of sensitivity. The first is needed in order to have the useful signal, which pass through IS with minimal distortions, the second - in order to have signal which can not be lost in IS and PA own noise. These requirements are often contradictory and their realization is usually complicated.

IS with linear sensitivity which is traditionally used can be realized when IS resonance frequency is considerably higher than upper frequency of researched signal spectrum. In such case IS itself may be considered as differentiator of useful signal. We consider mainly such IS although wide possibility of digital processing allow to use non-linear AFC because non-linearity can be taken to account while signals are processed.

The substitution of large loop by small (local) one with the same equivalent area may be realized either by increase of turn number or by application of additional preamplifier. In first case the needed equivalent area can be achieved but the required frequency characteristics can not be realized because of essential growth of sensor inductance and capacity. Compromise variant when insufficient number of turns is compensated by introduction of supplementary preamplifier is better. New source of noise (preamplifier own noise) and necessity of supplementary feed source appear in this case. Nevertheless the small sensor which enable to substitute large loop can be created when sufficiently qualitative low-noise preamplifier is designed and correct choice (called noise adjustment) of structural parameters is realized to minimize discrimination threshold. The creation of such IS named local active low-threshold inductive sensors (LANID) has been successfully provided in Physico-Mechanical Institute of National Academy of Science of Ukraine during 80-ths and 90-ths [1,2,3].

Theoretical analysis and experimental researches have allowed to create the series of LANID sensors that satisfy the mentioned earlier requirements in 0,001-1000 Hz band. They were introduced into the practice of measuring of electromagnetic environment in several states (Russia, Kirghizstan, Turkmenistan, Uzbekistan, Tadjikistan). Comparative testing in Australia confirmed that LANIDs can successfully compete with the best foreign analogues. The exploitation of LANIDs shows that they can substitute large loops with dimensions 50×50 and 100×100. The main parameters of LANIDs made in Physico-Mechanical Institute are given in the table.

Sensors LANID-1, LANID-2 and LANID-3N are manufactured as loop on the base of special multicore cable and LANID-4 as multturn sectional rigid frame with electrostatic shield. Dimensions of such sensors are within range 1,5-9 m.

The sensor preamplifiers are also different: LANID-1 has modulator-demodulator preamplifier with magnetic modulator, LANID-2 - with semiconductor modulator, LANID-3N and LANID-4 have preamplifiers with direct amplification. Some measures to decrease external noise (screen, differential schemes etc.), zero thermal drift and thermal electromotive force are taken in these sensors.

Parameters of LANID sensors

Sensor Parameter \ Sensor	LANID-1-9	LANID-1-5,7	LANID-2-2	LANID-2-6,7	LANID-3N	LANID-4
Type	loop	loop	loop	loop	loop	frame
Form and dimensions, m	circle D=9	circle D=5,7	circle D=2	circle D=6,7	square 4 × 4	square 1,6 × 1,6
Equivalent area with preamplifier S_e, m^2	$8,6 \cdot 10^6$	$3,5 \cdot 10^6$	$1,2 \cdot 10^6$	$10,6 \cdot 10^6$	$2 \cdot 10^5$	10^5
Reduced sensitivity $G_f, V/(T \cdot Hz)$	$54 \cdot 10^6$	$22 \cdot 10^6$	$7,5 \cdot 10^6$	$66,6 \cdot 10^6$	$1,26 \cdot 10^5$	$6,82 \cdot 10^5$
Frequency range, Hz	$10^{-3} \div 20$	$10^{-3} \div 20$	$10^{-3} \div 150$	$10^{-3} \div 150$	$0,1 \div 2 \cdot 10^3$	$0,1 \div 2 \cdot 10^3$
Discrimination threshold $B_m, nT \cdot Hz^{-0,5}$						
0,01Hz	$1 \cdot 10^{-2}$	$1,58 \cdot 10^{-2}$	$1,13 \cdot 10^{-1}$	$1,07 \cdot 10^{-2}$	$2 \cdot 10^{-1}$	$4,9 \cdot 10^{-1}$
0,1Hz	$3,8 \cdot 10^{-4}$	$6,3 \cdot 10^{-4}$	$6,4 \cdot 10^{-3}$	$7,16 \cdot 10^{-4}$	$5 \cdot 10^{-3}$	$1 \cdot 10^{-2}$
1Hz	$2,9 \cdot 10^{-5}$	$5,2 \cdot 10^{-5}$	$4,36 \cdot 10^{-4}$	$5,6 \cdot 10^{-5}$	$3 \cdot 10^{-4}$	$8 \cdot 10^{-4}$
10Hz	$3,1 \cdot 10^{-6}$	$5,9 \cdot 10^{-6}$	$3,5 \cdot 10^{-5}$	$4,9 \cdot 10^{-6}$	$4 \cdot 10^{-5}$	$5 \cdot 10^{-5}$
100Hz	-	-	$3,1 \cdot 10^{-6}$	$4,8 \cdot 10^{-6}$	$4 \cdot 10^{-6}$	$5 \cdot 10^{-6}$
1000Hz	-	-	-	-	$4,6 \cdot 10^{-7}$	$1,5 \cdot 10^{-6}$

4. CONCLUSIONS

Thus, the creation of LANID sensors gives the possibility to increase the Earth magnetic field measuring efficiency and in LANID-4 case to realize three-dimensional measurements.

LANIDs also can be used for forecast of earthquakes, measurements of fields, caused by lightning discharges and for electrical prospecting of minerals.

5. REFERENCES

1. V.A. Nichoga, "Very Weak Low Frequency Magnetic Fields Measurements in Geophysical and Space Researches" (Russian), Selection and Processing of Information, Vol.9, 1993, pp.70-77.
2. A.S. Gnatyuk, P.B. Dub, V.A. Nichoga, A.S. Yasinovy, "Large Geophysical Loop Inductive Sensors And The Possibility of Changing Them by Local Active Sensors" (Russian), Geophysical Instrumentation, Vol.98, 1994, pp.31-38.

3. V.A. Nichoga, P.B. Dub, G.R. Trokhym, "Manufacturing of Instrumentation and Procedure of Operative Magnetic Monitoring" (Ukrainian), Proceedings of the Conference on Automatic Control, Sevastopol, Ukraine, 9-14. 09. 1996, Vol. III, pp.168-170.

BIOGRAFICAL NOTES

Vitalij Nichoga is a leading scientific researcher and the manager of laboratory of primary measuring transducers of Karpenko Physico-Mechanical Institute of National Academy of Sciences of Ukraine. He graduated Radio Engineering Faculty of State University "Lvivska Politehnika" in 1960, obtained his Dr. ing. degree in 1966 and Dr. hab. degree in 1996.

Petro Dub is a leading engineer of the same Institute. He graduated Automatics Faculty of State University "Lvivska Politehnika" in 1977.

Investigation of electromagnetic fields and manufacturing of instrumentation for their measuring are both V. Nichoga and P.Dub main scientific interests.

ELECTROMAGNETIC SPACE DISTURBANCES REPRODUCED BY THE METHOD OF SATELLITE RADIOTOMOGRAPHY

Razinkov O.G., Kunitsyn V.E., Ruzhin Yu. Ya., Kolomiitsev O.P., Cherkashin Y.N., Shagimuratov I.I.

IZMIRAN, Troitsk, Moscow Region, 142092, RUSSIA

Fax.: 007 (095) 334-01-24, Tel.: 007 (095) 334-02-91

The possibilities and main advantages of the satellite radiotomography method for monitoring and investigation of electromagnetic (EM) disturbances in the space near the Earth are discussed. The results of experimental tomographic reconstructions of the electron density distribution along the line Moscow-Arkhangelsk are submitted. It is shown that such two-dimensional cross-sections of the ionosphere are very useful for the forecast of EM environment properties in the space near the Earth in particular in presence of various «cloud/hole» type inhomogeneities in the ionospheric plasma density distribution. Such data allow the complex HF radio waves trajectories to be calculated. Examples of such calculation are shown.

1. INTRODUCTION

To investigate the EM compatibility problems it is very important to know in details the properties of media in which the processes of generation, propagation and impact of EM disturbances occur. Because the majority of processes concerning the problem of EM compatibility take place in the space near the Earth, particularly in the ionosphere, it is very important for investigator to have an effective method that allow the continuous or operative monitoring and forecast of ionospheric plasma properties to be made. Such forecast is very important for normal operation of orbital and ground-based transmitter facility. For this purposes we propose the method of satellite computerized radiotomography.

2. SATELLITE RADIOTOMOGRAPHY

Methods of satellite radiotomography of the ionosphere have been developed intensively in the last decade. These methods combines well developed during several tens of years the measurement technique and advanced technical base of methods of remote sounding with opportunities of modern computer facilities, allowing during small of time to manipulate gigantic arrays of data using very complex numeric algorithms. Method of the satellite radiotomography allows during a short interval of time (15-20 minutes) to get the global information on structure of the ionosphere as sections of distribution

of electronic density and collision frequency up to satellite orbit height and on distances in a few thousands kilometers.

Typical geometry of the radiotomographic experiments is shown on Fig.1. Several receivers are located on the Earth in the plane of satellite orbit. This method is cheap enough because it uses the sounding two-frequency signals from satellites of existing navigation systems like «Cicada» (Russia) and

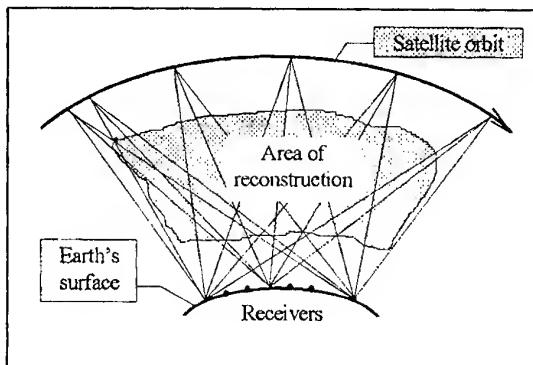


Fig.1. The scheme of radiotomographic experiments

«Transit» (USA). The moving satellites and receivers network give a possibility to probe the medium in various directions and to restore the structure of nearspace environment. The first radiotomographic sections of subauroral ionosphere were obtained near spring equinox during various levels of magnetic activity [1]. For quiet conditions classic structure of the main ionospheric trough is well defined.

Russian-American tomographic experiment with the radar of incoherent scattering, made in 1993, confirmed high quality of radiotomographic reconstructions of the ionospheric structures [2].

To solve the reconstruction problem we use the phase-difference tomography method because it eliminates possible considerable errors in absolute phase signal detection and improve the quality of tomographic reconstruction [3]. For the phase-difference tomography, both a complete theoretical simulation and many experimental measurements have already been carried out. It was shown that the reception of satellite signals even at three ground-based points located along the orbit projection on the

Earth's surface gives a good quality data for the reconstruction of a two-dimensional section of electron density variations, in particular, the structure of the EM disturbances in the ionosphere [4].

3. EXPERIMENTAL RADIOTOMOGRAPHIC RECONSTRUCTIONS

Now we have a lot of data about the distribution of electron concentration in the region along the Moscow-Arkhangelsk radiotomographic route obtained in the series of experiments that were carried out during the several last years. This route was prepared by IZMIRAN in 1993 to investigate the subauroral ionosphere by the method of satellite radiotomography. Specially designed new facility for digital registration, algorithms and software for data collection and ionosphere section tomographic reconstruction are used in these experiments. Unlike previous such experiments our system includes also two vertical sounding ionosondes, established in Moscow (55.5°N , 37.3°E) and Arkhangelsk (64.6°N , 40.3°E). Bottomside N(h) - profiles calculated by means of IRI model was used as a prior information for iterative reconstruction algorithm. One of the main goals of our experiments was to detect and to trace the evolution of local natural and artificial EM disturbances in middle-latitude and subauroral ionosphere.

Many experimental data contain the information about wave-like disturbances in the electron density at latitudes of tomographic route. It was shown by the analysis of tomographic reconstructions containing such quasiperiodical inhomogeneities that they are well-known traveling ionospheric disturbances (TIDs) caused by propagation in the thermosphere of middle-scale internal gravity waves. One of TID structure reconstructions obtained in the series of experiments in December 1993 is presented on Fig.2. The picture have clear wave structure with wavelength about 300 km and period about 15-20 minutes. TIDs have been studied very extensively by a variety of techniques since they were first identified as ionospheric signatures of atmospheric gravity waves in 1960. But only the radiotomographic methods gives the opportunity to obtain directly a two-dimensional spatial image of the wave structure in latitude versus height plane.

In other series of tomographic experiments a number of reconstructions contain the local inhomogeneities of "cloud/hole" type that were found below the main ionospheric maximum height. From our point of view the formation of such structures can caused not only by natural reasons but also artificial ones, that is, by human activities [5].

Some reconstructions contain other types of EM space disturbances with original features. In [6] the example of reconstruction with slope weak through of

ionospheric electron density is shown, the nature and properties of this plasma structure are discussed. Such structures was detected also in the Russian-American tomographic experiments [2] approximately at the same geomagnetic latitudes.

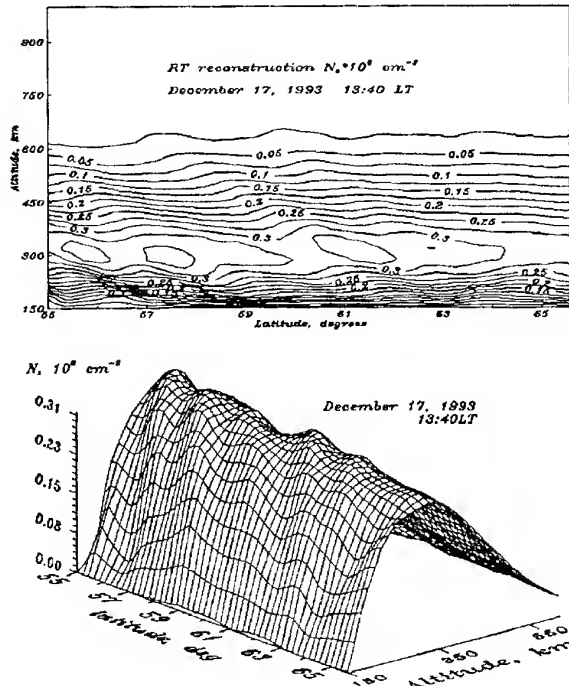


Fig.2. Tomographic reconstruction of TIDs along Moscow-Arkhangelsk line: a) isolines of 10^6cm^{-3} units; b) fragment of electron density surface. December 17th, 1993.

4. IONOSPHERIC HOLE-TYPE DISTURBANCES AND PROPERTIES OF EM ENVIRONMENT

The ionospheric disturbances of «cloud/hole» type mentioned above and detected by the method of satellite radiotomography are of the great scientific and practical value in relation to the problem of EM waves propagation in the ionosphere. The large number of papers devoted to construction of radio wave propagation trajectories at various ways of environment parameters setting is published enough - simulated or experimentally observed. However, today only the radiotomographic method gives the possibility to obtain the section of the ionosphere on routes 1000-2000 km practically in real time. Therefore the numerical modeling of radio wave propagation and distribution in environment which is similar to real one is very important because such simulation gives the possibility to investigate the real modes and ways of propagation.

Some interesting examples of numerical simulation of HF radio wave propagation on routes crossing ionospheric holes are shown in this part. Calculations are made in approach of geometrical

optics [7]. The basic environment properties for simulation are set using radiotomographic cross-section of ionospheric electron density along the line Moscow-Arkhangelsk obtained in May 1993 [6].

The example of focusing of HF radio waves is shown on Fig.3. This phenomenon observed in the wide range of frequencies from 10 up to 16MHz by sounding in north direction. The vertical angles of exit of ray trajectories arrived actually to the focus point are in the range of six degrees. This wide range of angles provides the high degree focalize, that is, sharp irregularity of distribution of field along the route.

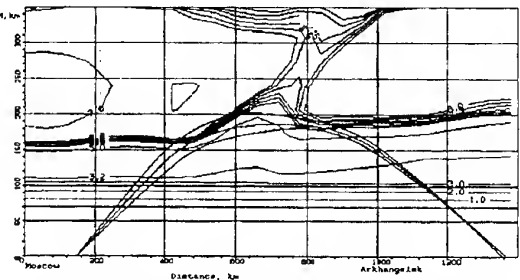


Fig.3. Focusing of HF (14 MHz) radio waves by sounding in the north direction.

The results of simulation of quasi-vertical sounding, that is, practically direct to hole are shown on Fig.4. Whole set of various ray trajectories (hop, trapezoid, passed through the hole, captured by hole) is obtained by the following sounding conditions: exit points are located on distance 600-730 km from Moscow; vertical angles of exit are in range 74-78 degrees with direction of sounding to north.

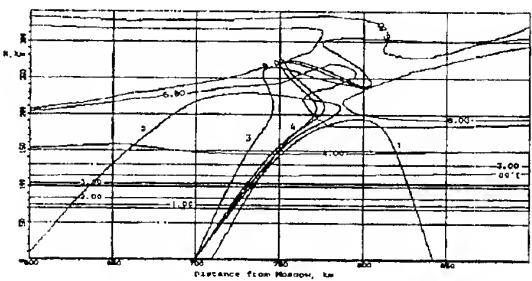


Fig.4. The set of typical ray trajectories for sounding directly to hole: 1-hop, 2-trapezoid, 3-passed through the hole, 4-captured by the hole. Frequency 6 MHz.

Captured trajectories are of the great value of interest. They oscillate inside the hole and come back near the point of exit. The delay of such trajectories exceeds the delay of usual vertical sounding trajectories in 2-10 and even more times.

5. CONCLUSION

The radiotomographic approach prepared and tested on the Moscow-Arkhangelsk route allowed

many interesting results on the ionospheric plasma structure of subauroral ionosphere in the global scale to be obtained. The local plasma inhomogeneities and disturbances that can strongly influence the operating of different navigation, radar and communication systems were reconstructed during the series of radiotomographic experiments and were analyzed. Examples of calculation of radio waves trajectories passing through the ionospheric irregularity of «hole» type reconstructed by the method of satellite radiotomography are analyzed. It was shown that some original results can be obtained in this case such as unexpected focusing of radiowaves in space, capture phenomenon, creation of local patches of high intensity EM radiation. These examples demonstrate the impact of such plasma inhomogeneities on space EM environment and possibilities to forecast the level of EM disturbance near the Earth surface.

The cheap and effective method of satellite computerized radiotomography make it possible to carry out continuous monitoring of EM media in the space near the Earth that can be successfully used in solving the problems of EM compatibility.

6. REFERENCES

- 6.1. Andreeva E.S., Galinov A.V., Kunitsyn V.E. et al., «Radiotomographic reconstruction of ionization trough in the plasma near the Earth», JETP Lett, 1990. V.52, N3, P.145-148.
- 6.2. Foster J.C., J.A. Klobuchar, V.E. Kunitsyn, E.D.Tereshchenko, E.S. Andreeva, M.J. Buonsanto, P. Fougerre, J.M. Holt, B.Z. Khudukon, W.Pakula and T.D. Raymund, «Russian-American tomography experiment», Int. J. Imaging Syst. Techn., 5, 1994, pp.148-159.
- 6.3. Kunitsyn V.E., Andreeva E.S., Tereschenko E.D., Razinkov O.G., «Phase and phase-difference ionospheric radiotomography», Int. J. Imaging Syst. Technol. V.5, 1994, p.128-140.
- 6.4. Kunitsyn V.E., Tereschenko E.D. «Radio tomography of the ionosphere», IEEE Antennas and Propagation Magazine, V.34, N5, 1992, P.22-32.
- 6.5. Oraevsky V.N, Kunitsyn V.E., Ruzhin Yu.Ya., Razinkov O.G. and Shagimuratov I.I. «Ionospheric structures of anthropogeneous origin by radiotomographic diagnostics», Adv.Space Res, V.15, No.11, 1995, p.145-148.
- 6.6. V.N.Oraevsky, V.E.Kunitsyn, Yu.Ya.Ruzhin et al. «Radio tomographic cross-sections of the subauroral ionosphere along the Moscow-Arkhangelsk corridor», Geomagnetism and aeronomy, V.35, N.1 August 1995. P. 87-91.
- 6.7. I.B.Egorov, O.P.Kolomiitsev, Yu.Ya. Ruzhin, Y.N.Cherkashin, «Modeling research of the influence holes in the ionosphere on conditions of HF radio wave propagation», IZMIRAN press, Moscow, N.9(1105), 1997.

XIII

**NATURAL AND MAN-MADE
EM ENVIRONMENT**

**Terrestrial Electromagnetic
Environment**

URSI Commission E sponsored session

Invited session organized by

Prof. M. Hayakawa - Japan

ELECTRIC FIELDS FROM MODEL LIGHTNING DISCHARGES

A. P. Nickolaenko,

*Institute of Radio Physics and Electronics, Ukrainian National Academy of Sciences
12 Acad. Proskury St., Kharkov 310085, Ukraine*

M. Hayakawa,

The University of Electro-Communications, Chofugaoka, Chofu-city, Tokyo 180, Japan

Time domain electric field from the model lightning discharges in the neutral atmosphere is computed and its modifications due to geometrical changes of the stroke are examined. A standard model of the return stroke is used as a basic one. The current waveform at the stroke base is a sum of four exponential terms. Current wave moves upward with an exponentially decaying velocity. Static, induction and radiation field components were computed. The model was modified then to describe the electric fields from: (i) the powerful vertical return stroke, (ii) the positive stroke that initiates from the ground or from the cloud, (iii) the 'broken' discharge, (iv) the 'spider' stroke.

Combined effect of the motion of the current wave and the tortuosity of the lightning channel results in multiple pulses. Vector of the electric field acquires transient vertical, inward/outward and sideways components. The relevant field 'scans' the sky. Disturbances above the storm may lead to the air density and temperature fluctuations that facilitate modification of the plasma in the lower ionosphere.

The time domain electric field produced by a model lightning discharges in the neutral atmosphere is computed and its modifications are examined arising due to changes in the stroke geometry. A standard model of the return stroke is used as basic one. The current waveform is presented as a sum of four exponential terms.

$$I(t) = \sum_{k=1}^4 I_k \cdot e^{-\frac{t}{\tau_k}}, \quad t \geq 0 \quad (1)$$

Here, I_k is the amplitude of an individual current term, and τ_k is the relevant time constant describing the temporal decay of the current. The following values are used in the basic model:

$I_1 = -28.45 \text{ kA}$, $I_2 = 23.0 \text{ kA}$, $I_3 = 5.0 \text{ kA}$, $I_4 = 0.45 \text{ kA}$, and $\tau_1 = 1.66 \mu\text{s}$, $\tau_2 = 33.33 \mu\text{s}$, $\tau_3 = 500 \mu\text{s}$, $\tau_4 = 6800 \mu\text{s}$.

The current moves upward (see Fig.1) with an exponentially decaying velocity having the initial value of 1/4 of the speed of light.

Progress of the Current Wave in the Standard Model of the Return Stroke

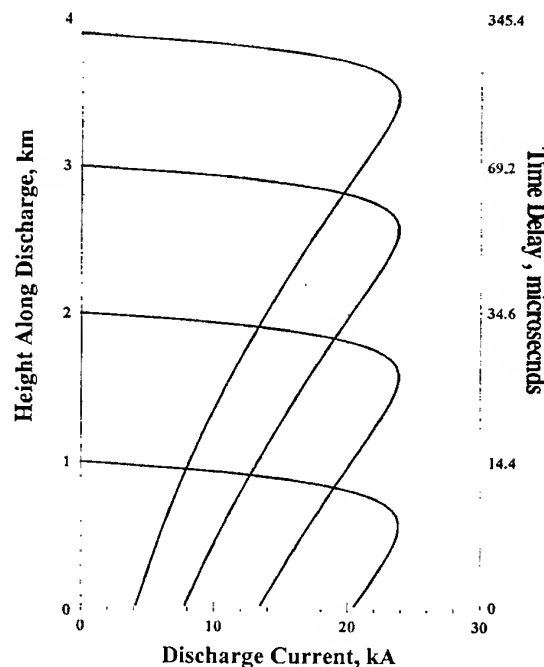


Fig. 1. Motion of the current wave along the channel in the basic return stroke model.

Fig. 1 depicts four successive positions of the current wave along the vertical channel of the stroke. The stroke current in kA is shown along the horizontal

axis. The height or vertical length of the channel is plotted along the left ordinate in *km*. The lowest curve in Fig. 1 demonstrates an early stage of motion (14.4 μ s after the stroke initiation). The highest curve corresponds to the final stage, when the current wave ap-

proaches the end of lightning channel of 4 *km* length (approximately 340 μ s from the beginning of the return stroke). Time delay is shown along the right ordinate. Its scale became logarithmic, since the velocity $V(t)$ of the current wave decays exponentially in time.

Observer Altitude 50 km

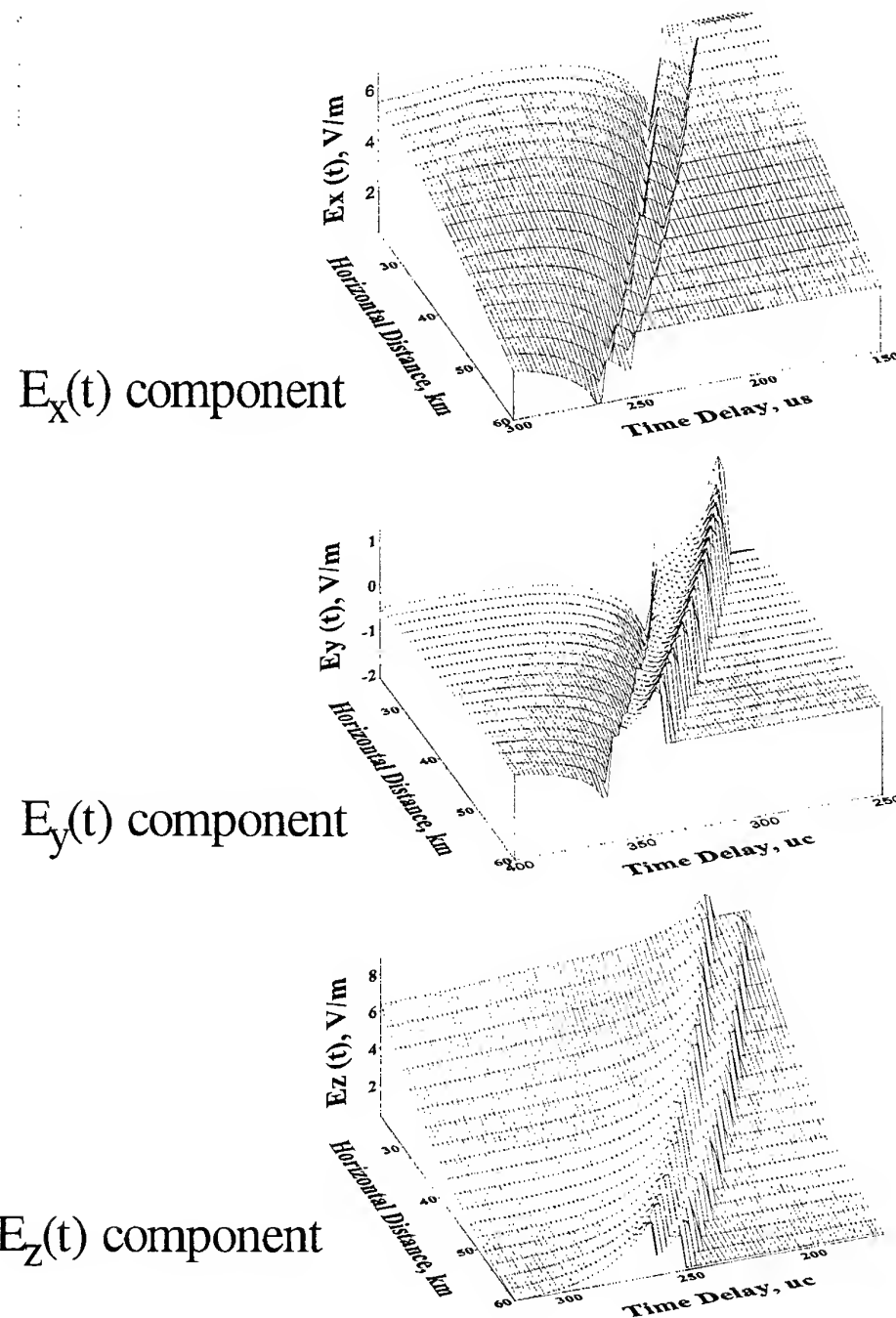


Fig. 2. Relief of the electric field components above the distance-delay plane. The altitude in neutral atmosphere is 50 km above the model perpendicular broken stroke of lightning.

The basic model of vertical lightning stroke was modified then to obtain the electric fields from:

- powerful vertical return stroke,
- positive stroke that is initiated either from the ground or from the cloud,
- 'broken' or tortuous discharge,
- 'spider' stroke.

Computations show that the combined effect of the onset of the current wave (direction of its propagation) and the tortuosity of the lightning channel may result in multiple pulses of the atmospheric electric field. The effects are weak at the ground surface, and 'pulse breeding' could not be observed here.

Electron Driving by Broken Stroke $H=50 \text{ km}$, $\psi = \pi/2$

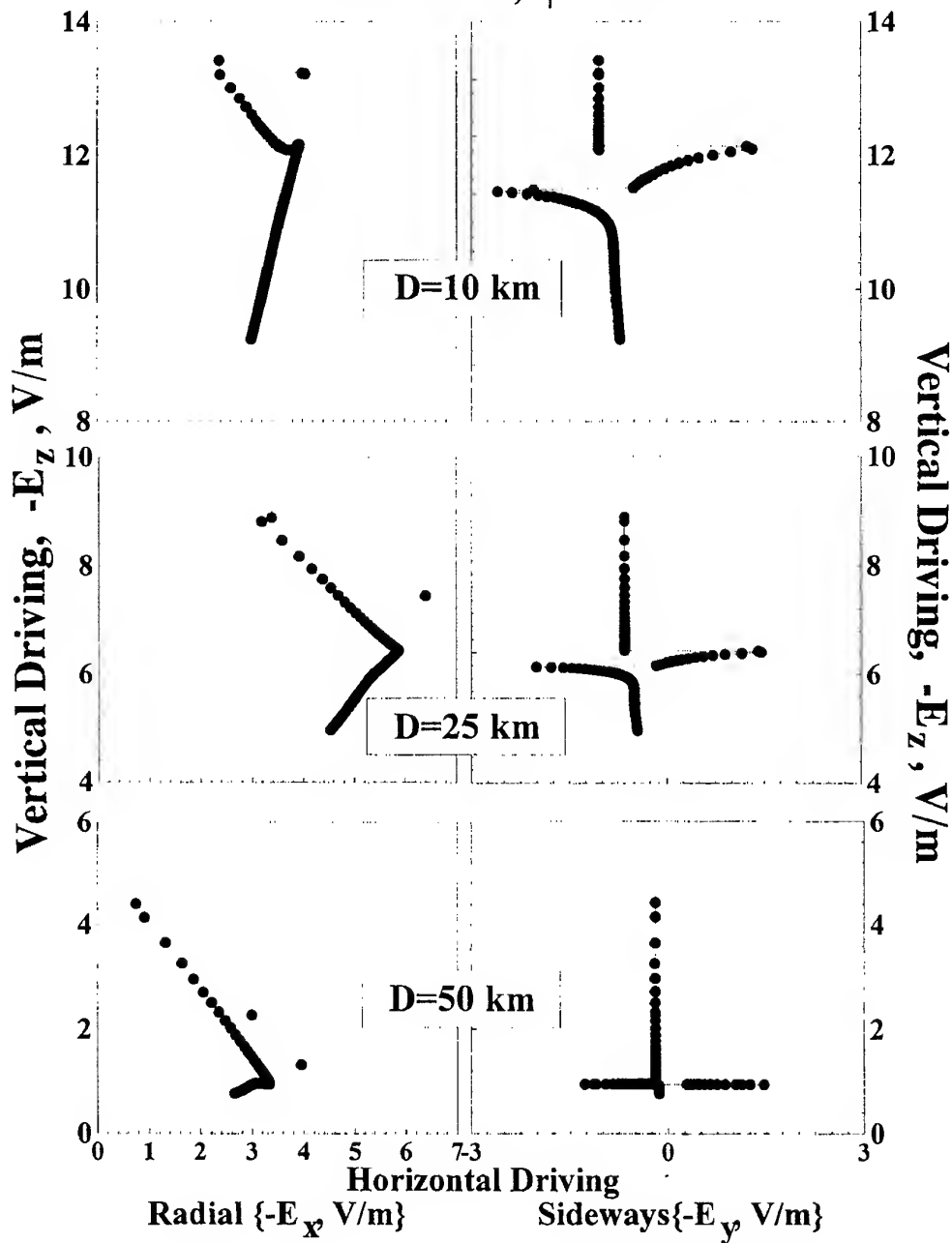


Fig. 3. Temporal variations in the electron driving force produced by a perpendicular broken stroke of lightning. Radial cross-section of the driving is shown in the left plots and the sideways force is depicted in the right frames.

Electric field in a neutral atmosphere above the lightning stroke acquires the transient vertical, inward/outward and sideways components and therefore 'scans' the sky (see Fig.2). Fields from powerful strokes of lightning are of the level that enables them to initiate the plasma process in the atmosphere.

In the model of a tortuous or 'broken' stroke presented in Figs.2 and 3, we apply the standard current model (1) of four exponential terms. Current wave starts from the ground vertically and turns in a horizontal direction after the altitude $z_k = 5 \text{ km}$ is achieved. The whole length of the lightning channel equals 10 km. Initial velocity of the current column remains equal to $V_0 = 8 \cdot 10^7 \text{ m/s}$ and its decay factor is $\omega_0 = 8 \cdot 10^3 \text{ s}^{-1}$. The observer is situated in the atmosphere at the 50 km altitude and is displaced from the discharge in horizontal direction by a distance D in such a way that the horizontal part of the lightning stroke is perpendicular to the direction observer-base of the stroke (a perpendicular displacement with $\psi = \pi/2$).

Three components of the normalized electron driving forces are depicted in Fig. 2 over the horizontal distance - time delay plane produced by a perpendicular broken discharge.

The figure demonstrated dynamics of the propagation of the electromagnetic pulses through the atmosphere. Static, induction and radiation field components were included into computations. It is clear that dual pulses may cause the focusing of the charges particles in the atmosphere.

Sample cross-sections of electron driving forces produced by the same discharge are depicted in Fig. 3. Left column of the plots shows the radial cross-section of the driving force, i.e. $-E_z(t)$ versus $-E_x(t)$. The right frames demonstrate the transverse cross-section that is $-E_z(t)$ against $-E_y(t)$. Time t is a parameter, and each dot in Fig.3 plots represents the fields computed with the 2 microsecond step. Results are shown for three horizontal distances of 10, 25, and 50 km.

As Fig. 3 shows, the electrons are accelerated upward and towards the discharge axis at the pulse onset in a broken stroke. Sideways motion is seen in the right column of the frames in Fig.2 begins after radial driving returns to the 'initial' position. This example shows that the fields from a broken stroke drive electrons 'to scan' the sky above the lightning. Such a scanning may facilitate finding a 'hole' in the atmosphere, say, of lower local density and initiating the sprite or jet.

Atmosphere disturbances above the storm themselves may lead to the air density and temperature fluctuations that modify the electron collision frequency. The pertinent fluctuations and the scanning electric field may contribute to the sprite and jet structure. Since both the effects are enhanced at the periphery of a thunderstorm, the luminous structures may be expected at some distance from the parent stroke.

In our report, we analyze different models of lightning strokes, arriving to the following conclusions:

- Positive cloud-to-ground discharge initiated from the top of the lightning channel produces dual pulses in the atmosphere.
- Broken or tortuous lightning multiply reproduces radiation pulses. Substantial transverse transient field appears that depends on orientation of the horizontal section of the channel. Vertical part of the stroke is responsible for the static field. This field persists until the vertical charge dipole moment is present. Horizontal branch generates the intense pulses that contribute to the transient electric field.
- Combination of vertical and horizontal currents in a lightning source increases the amplitude of the transient electric field observed in the atmosphere.
- Branching of the stroke results in overall decrease of radiation from the horizontal currents due to interference between individual pulses. This is why the horizontal part of a symmetrical 'spider' stroke does not radiate.
- Transient fields vanish at the ground surface or right above the stroke. Therefore, the high altitude airborne observations should be used to detect the above features performed at distances of tens of kilometers from the discharge.
- Pulse component of the field substantially modifies the electron driving force. Vector of the force acquires vertical, horizontal radial and sideways components at the onset of the pulse. Horizontal distance where electron focusing may occur lies between 25 and 75 km from the stroke.
- Density and temperature disturbances in the atmosphere above a thunderstorm may contribute to the initiation of the plasma process. Both the disturbances and electron focusing are enhanced at the periphery of a storm, so the luminous structures must be expected at some distance from the parent discharge.

Biographical notes:

NICKOLAENKO Alexander Pavlovich was born in Kharkov, the Ukraine in 1944. He graduated from the Kharkov State University in 1966 and got his Ph.D. from the same University in 1972. A.P. Nickolaenko got the Doctor (full Prof.) degree in 1988 from the Kharkov state University. Now, he is a Leading Scientist of the Institute of Radiophysics and Electronics of the Ukrainian National Academy of Sciences.

HAYAKAWA Masashi was born in Nagoya Japan in 1944. He got his BS and MS degree from the Nagoya University in 1963 and 1968 correspondingly. In 1974, M. Hayakawa got a Ph.D. from Nagoya University. Prof Hayakawa worked for the Sheffield University (UK) in 1976 and for the Centre de Recherches in Physique de l'Environnement (France) in 1980-1981. Now, he is the Head of Electronic Engineering Department of The University of Electro-Communications, Tokyo, Japan.

SPECTRA AND WAVEFORMS OF NATURAL ELECTROMAGNETIC PULSES IN THE ELF RANGE

A.P. Nickolaenko

*Institute of Radio Physics and Electronics, Ukrainian National Academy of Sciences
12 Acad. Proskury st. Kharkov 310085, Ukraine*

Electromagnetic waves are studied in the extremely low frequency range where single zero-order radio wave propagates. We apply the well known solution for the spherical Earth-ionosphere cavity. Relevant time domain fields are obtained using the FTT algorithm. The field distribution had been obtained both in frequency-distance and in time-distance domains.

Relief of the amplitude of the natural radio signal over the frequency-distance plane is a system of summits and depressions. The maximum energy lies at hundreds of Hz when the source-observer distance is small. This explains an effectiveness of the nearby discharge location using the slow tail atmospheric technique. The high frequency signal rapidly decays when the distance grows, and from some megameter distance, amplitude reaches its maximum in the Schumann resonance (SR) frequency band. This is why the global lightning location is a success based on the SR techniques.

Natural ELF pulse travels within the Earth-ionosphere guiding system with a constant velocity and 'bounces' from the source and its antipode. The pulse width gradually increases along the propagation path due to natural filtration of the high frequency components. Meanwhile, distance dependence of the pulse amplitude depends on both the geometrical focusing of the signal in a spherical cavity and the high frequency absorption.

ELF radio wave propagation from the natural source of radiation in the Earth-ionosphere waveguide is analyzed. We introduce the vertical electric dipole as the natural EM source of radiation that models the lightning return stroke. The spectrum radiated is supposed to be independent of frequency (a delta-pulse in the time domain). The extremely low frequency (ELF) spectral components of an electromagnetic wave are described using the mode theory for the spherical Earth-ionosphere waveguide:

$$E_r(\omega) = \frac{i\nu(\nu+1)}{\omega} \cdot \frac{M_c(\omega)}{4a^2 h \epsilon} \cdot \frac{P_\nu[\cos(\pi - \theta)]}{\sin \pi \nu} \quad (1)$$

Here $\nu(\omega)$ is the propagation constant of the ELF radio wave, ω is the circular frequency, $M_c(\omega)$ is the current moment of the source, θ is the angular distance between the source and observer, a is the Earth's radius, h is the effective height of the ionosphere, ϵ is the dielectric constant of the free space, $P_\nu(x)$ is the Legendre function.

The following model parameters are specified: $a = 6.4 \text{ Mm}$, $h = 60 \text{ km}$, and $M_c = \text{const} = 10^8 \text{ Am}$. Main emphasis is made in the work to the vertical electric field E_r component. An heuristic frequency dependence was introduced for the ELF propagation constant

$$\nu(f) = (f-2)/6 - j f/100 \quad (2)$$

based on the experimental coherent SR data which we extrapolated to the higher frequencies.

When computing the fields we applied the zonal harmonic series representation for the Legendre functions in the SR frequency range from a few Hz to 250 Hz and accelerate the convergence. At higher frequencies the asymptotic expansions are used: the cosine asymptotic first, and the exponential expansion then ($f > 1700 \text{ Hz}$).

ELF spectra were computed for the source-observer distances (SOD) up to the source antipode $D = 20 \text{ Mm}$ in the frequency range from 4 to 1700 Hz. A survey of the computed data is shown in Fig. 1. Here a 3-D view of the ELF 'highlands' is shown. The amplitude of the vertical electric field component is plotted over the frequency-distance plane in this figure. Source-observer distance (SOD) in megameters is shown along the abscissa. Value of the extremely low frequency is shown along the ordinate in logarithmic scale [the numbers correspond to $25 \cdot \ln(f)$]. The vertical electric field amplitude is plotted along applicata axis in $mV/m \text{ Hz}^{1/2}$.

Frequency-Distance Profile for the ELF Pulse Signal

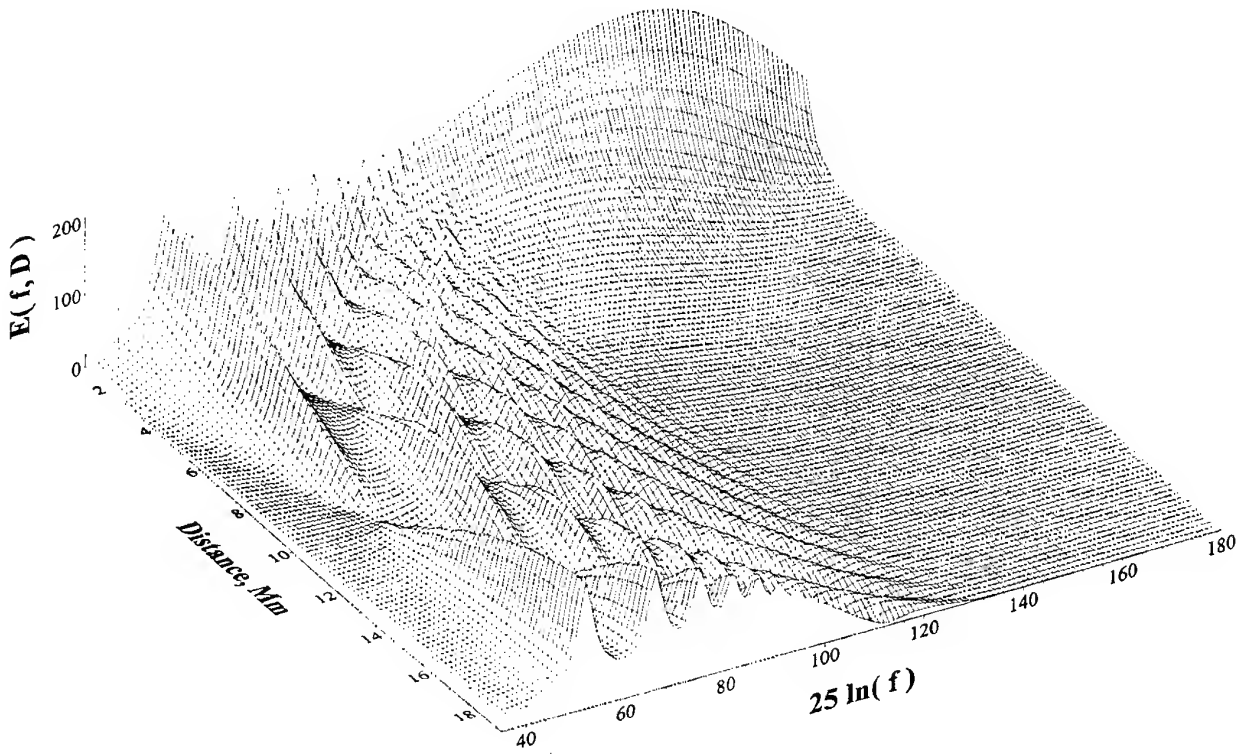


Fig. 1. 3-D map of the E_r amplitude above the frequency-distance plane.

Fig. 1 actually presents the profile of the Green's function for the electromagnetic problem, since the model source used in computations is a delta-source both in time and space. The SR peaks are seen in the field profile at the lower frequencies having resonance pattern that depends on the interaction between the direct and antipodal waves. This pattern is used to establish the SOD when studying the ELF transient events or Q-bursts.

Two crests are seen above the source and its antipode divided by a wide valley centered around 10 Mm distance. The side transverse ridges descend into the valley depicting the individual modes of the Schumann resonance. Each ridge is not smooth, it consists of a series of summits and depressions. Bottom of the valley is not smooth as well, it is covered with a system of regular peaks that tend approach the antipodal ridge. The valley descends and becomes more uniform when the frequency increases. Spectacular feature of Fig.1 is the system of 'side canyons' representing the ELF field nodal lines. One of such gullies starts from the 10 Mm

distance (the node of the first SR mode) and moves towards the source and antipode crests. The system of canyons corresponds to the family of hyperbolic curves, when a linear frequency scale is applied along the ordinate.

A broad spectral maximum is seen over the short source-observer distances. This peak occupies frequencies around some hundred Hz thus indicating the range of the slow tail atmospherics. When the distance increases, the peak rapidly decays due to absorption in the ionosphere that grows with frequency.

We obtained the $E_r(t)$ waveforms after applying the FFT procedure to the spectral data. Direct and antipodal pulses were examined. The last pulse grows with increasing distance and is not seen at short distances. For the considerable distances, the Earth-ionosphere waveguide works as a low-pass filter, and the signal at higher frequencies attenuates rapidly. Amplitudes of direct and antipodal waves become close to each other when the SOD grows and coalesce in one pulse at the source antipode $D=20 Mm$.

ELF Pulse Bounce From the Source Antipode

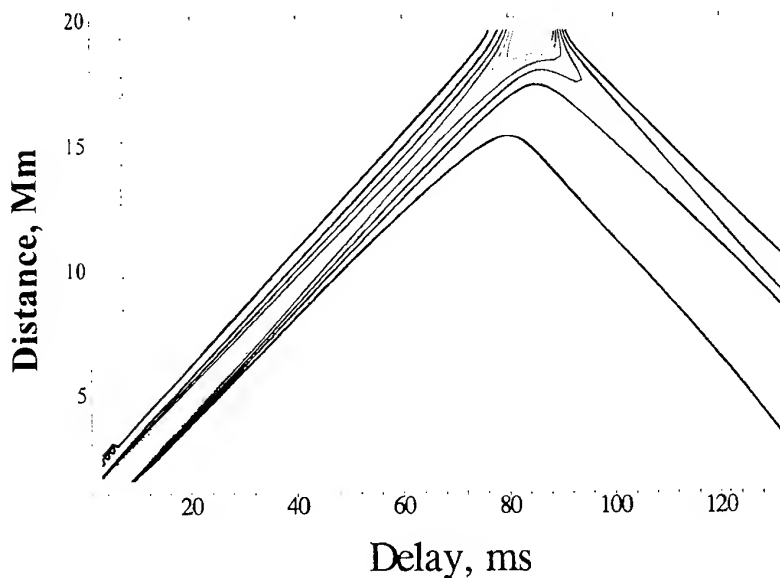


Fig. 2. Reflection of the ELF pulse from the source antipode.

The 'plane geometry' pertinent to the time delay of the direct and antipode waves is demonstrated by Fig. 2. Dominant role of the shortest distance between the source and observatory is rather straightforward, since it determines the shortest time delay of the EM pulse arriving to the observer. The role of antipodal path is not so evident in a spherical cavity, since this is the largest distance from the source. Both the distances form a great circle path 40 Mm long. We see that these two arcs determine the delay of the pulses. A 'perfect reflection' is observed from the source antipode. Meanwhile, the role of the wave guide sphericity is seen in the modifications the pulse amplitudes, e.g. in antipodal enhancement of the field.

Figs. 1 and 2 explain two existing measurement techniques applied in the ELF range. The first is used in the Schumann resonance range and allows for the global location of the sources of powerful ELF transient events or Q-bursts. This technique is based on the variations of the resonance patterns observed for different source-observer distances. Fig. 1 demonstrates that such an approach works at frequencies lower than 100 Hz or within the SR band.

The second approach is based on the slow tail atmospherics. It works at the distances where a broad high frequency spectral maximum is observed (see Fig. 1).

Relevant slow tail pulse width of both the positive and negative half-waves gradually increases with the distance. This feature allows for evaluating the SOD through comparing the mutual delay between positive and negative half-waves in the arriving ELF pulse, provided the spectrum of the source is 'white' within the analyzed frequency range.

Fig. 3 demonstrates the pulse amplitude versus the source-observer distance. The whole propagation path length (the circumference of the globe) is shown along the horizontal axis, and the relevant pulse amplitude is plotted along the ordinate in logarithmic scale measured in millivolts per meter. The computed range dependence of the pulse amplitude is shown with dots.

Sphericity of the guiding system shows itself in the field amplitude. Geometrical enhancement of the field around the source and antipode has been discussed for a long time in the literature. This is why we show additional lines in the plot to compare our results with 'approximating' amplitude variations often used for the monochromatic signals. An exponential attenuation of 3 dB/Mm for the plane wave predicts the amplitudes that vary in a linear way within the co-ordinate system applied. The inverse distance dependencies fit the pulse amplitudes in a better way (especially the $1/D^{3/2}$ function) but these have nothing to do with the field enhancement around the source and its antipode. The asterisks in Fig. 3 denote the results calculated for a classical narrow band representation of the field when one accounts for both the attenuation (0.8 dB/Mm) and the focusing. In the case, the amplitude of the field varies as

$$\exp\{-\alpha\theta\}/(\sin \theta)^{1/2},$$

with θ being the angular SOD.

Fig. 3 demonstrates how far the simple distance dependencies are from the broad-band pulse amplitude. The reason lies in the spectra modifications that occur for the real signal when the source-observer distance varies. Meanwhile, the pulse delay depends on the pure geodetic distances between the source, observer and the source antipode. It varies in a linear fashion with the SOD.

Pulse Amplitude vs Propagation Path

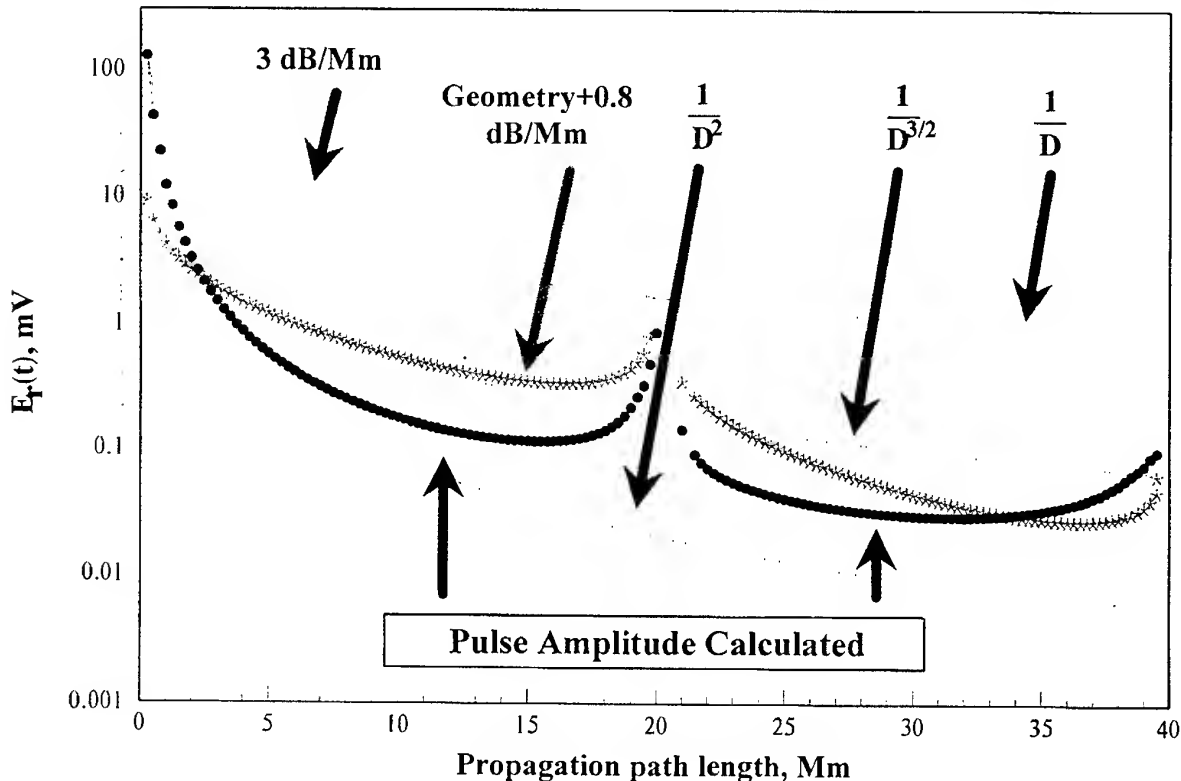


Fig. 3. Distance variations of the slow tail amplitude

The following conclusions are made in the report:

- Relief of the natural pulse signal over the frequency-distance plane resembles the 'ELF highlands' having regular ridges, peaks and depressions. Peaks and depressions form the chain structures extended over hyperbolic lines in the frequency-distance plane. The relevant lines become the straight ones over the distance-period plane.
- The electromagnetic power is concentrated over higher extremely low frequencies (some hundred Hz) when the source-observer distance is small. This explains an effectiveness of the nearby source location using the slow tail atmospherics. Beginning from some Mm distance, the 'high frequency' component vanishes, and the energy shifts into the SR band. This is why the Schumann resonance supports the global location of the powerful lightning discharges.
- Radio pulse moves with a constant velocity in the time domain. A 'bouncing' occurs in the time domain from the source antipode (and the source it-
- self). The pulse width grows monotonously with the propagation path length.
- The distance dependence of the natural wide band pulse amplitude is conditioned by two factors. The first is the field focusing around the source and the source antipode due to spherical geometry of the guiding system. The second is the spectra modifications due to absorption in the ionosphere. Attenuation of the higher frequencies governs the dependence of a pulse amplitude versus propagation distance.

Biographical notes:

NICKOLAENKO Alexander Pavlovich was born in Kharkov, the Ukraine in 1944. He graduated from the Radiophysical Department of the Kharkov State University in 1966 and got his Ph.D. in radio physics from the same University in 1972. A.P. Nickolaenko got the Doctor (full Prof.) degree in 1988 from the Kharkov state University. Now, he is a Leading Scientist of the Institute of Radiophysics and Electronics of the Ukrainian National Academy of Sciences.

MID-LATITUDE MULTI-PATH WHISTLER INCLUDING A NON DUCTED WHISTLER

Kenji Ohta, Tomomi Kitagawa, Akihiro Tanaka

Department of Electronics Engineering, Chubu University, Kasugai Aichi, 487 Japan
(e-mail: ohta@isc.chubu.ac.jp).

Masashi Hayakawa

Department of Electronic Engineering, The University of Electro-Communications, Chofu Tokyo, 182 Japan
(e-mail: hayakawa@aurora.ee.uec.ac.jp).

R. L. Dowden

Department of Physics, University of Otago, POB 56 Dunedin, New Zealand
(e-mail: dowden@physics.otago.ac.nz).

Abstract

This paper reports on a new type of mid-latitude multi-path whistlers based on the observations at Hobart, Australia and Dunedin, New Zealand. Though a majority of whistler elements are ducted, this new type includes a non-ducted whistler as well. The study is based on the detailed comparison of the field-analysis direction finding results with the nose-extension and ray tracing computation ones. Important findings have emerged from this study are summarized as follows. (1) The majority of whistler elements are ducted, (2) at least one whistler element was experimentally convinced to be a non-ducted PL (prolongitudinal) whistler, (3) the whole life of propagation path seems to be of the order of 6 hours, with including cyclic occurrence and decay.

1. Introduction

Mid-latitude whistlers in the magnetosphere are generally considered to be attributed to the propagation trapped in field-aligned ducts [1], but some authors have suggested the presence of non-ducted mode of propagation [2]. However, the finer details of propagation characteristics of mid-latitude

whistlers are not still well understood.

The purpose of this paper is to provide the characteristics of mid-latitude whistlers on the basis of VLF observations Australia and New Zealand, and the coordinated comparison of direction finding (DF), nose-extension analysis results and ray tracing computation.

2. VLF observations

VLF observation were carried out at Hobart (geographic coordinates; 42.8° S, 147.4° E; geomag. lat. 51.4° ; $L=2.92$), Australia and at Dunedin (geographic coordinates; 45.9° S, 170.5° E; geomag. lat. 50.4° ; $L=2.77$), New Zealand for about two weeks from August 16 to 31, 1994. Fig. 1 illustrates the location of observation stations. Wideband VLF/ELF signals in a frequency range from 1 to 8kHz were recorded by means of digital audio tape recorders (DATs) for the three field components (two horizontal magnetic field components and vertical electric field component) [3]. In this paper we will report only the analysis results of Dunedin, because the occurrence rate and strength of whistlers are higher than that of Hobart.

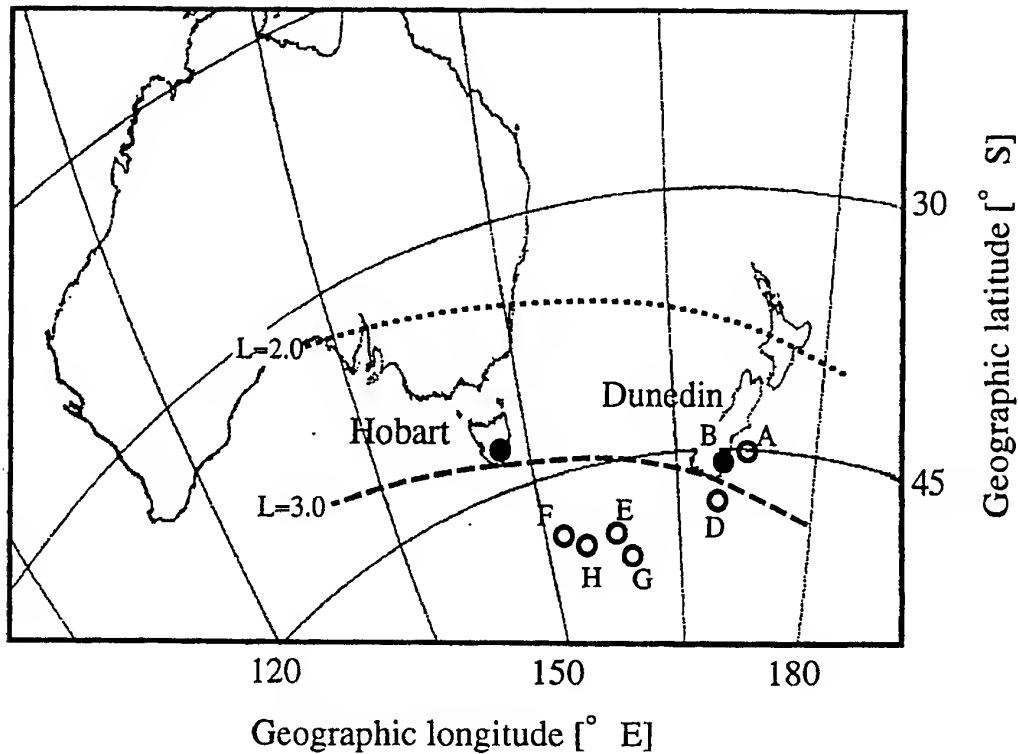


Figure 1. Location of VLF observation stations of Dunedin and Hobart, and the results on the locations of ionospheric exit regions of different whistler elements (A~H). Only ducted whistlers are plotted in.

3. Analysis results based on the direction finding and nose extension methods

General structure of frequency spectra of a group of whistlers (normally called "multi-path" whistlers originated from a sferic, as illustrated in Fig.2) is found to be rather stable for our observation period (6 hours) from 22hLT (at Dunedin) on August 30 to 4hLT on August 31. The number of whistler elements in the group varies from time to time, and this might imply that the ducts are formed and decay with a small cyclic time (of the order of hour) [4],[5],[6]. But, the whole life of a duct seems to be at least 6 hours of our observation period. In Fig. 2 elements of these multi-path whistlers are tentatively labeled, such as A ~ H. Whistlers E ~ H are easily identified as nose whistlers, and so they must have penetrated through the ionosphere at higher latitude. The whistler elements, A ~ D are considered to be mid-latitude ones, whose characteristics will be examined here in details.

The results on wave polarization of the three

whistlers A and B are summarized as follows, which is based on our field-analysis DF by using three field components [3],[7],[8]. The polarization parameters (u,v) are based on the information at different frequencies (every 25Hz) for each whistler. The definitions of (u,v) is given in Okada et al. [7], and $(u,v)=(0,-1)$ indicates the polarization of whistler-mode waves (right-handed circular polarization). The distributions of (u,v) for B is broadly peaked around $(u,v)=(0,-1)$, which means that this whistler B is nearly right-handed circularly polarized. An additional information for B is its small incident angle (i) from the ionosphere to the free space. The results of these directions finding indicate that whistler B has exited the ionosphere very close to the observing station of Dunedin. Another hand, the distribution of (u,v) for whistler A shows left-handed polarization (v is mainly positive). This kind of left-handed polarization was found by Ohta et al. [9]. This fact suggests that the ionospheric exit region of this whistler A is not so close to the observing station, as compared to whistler B.

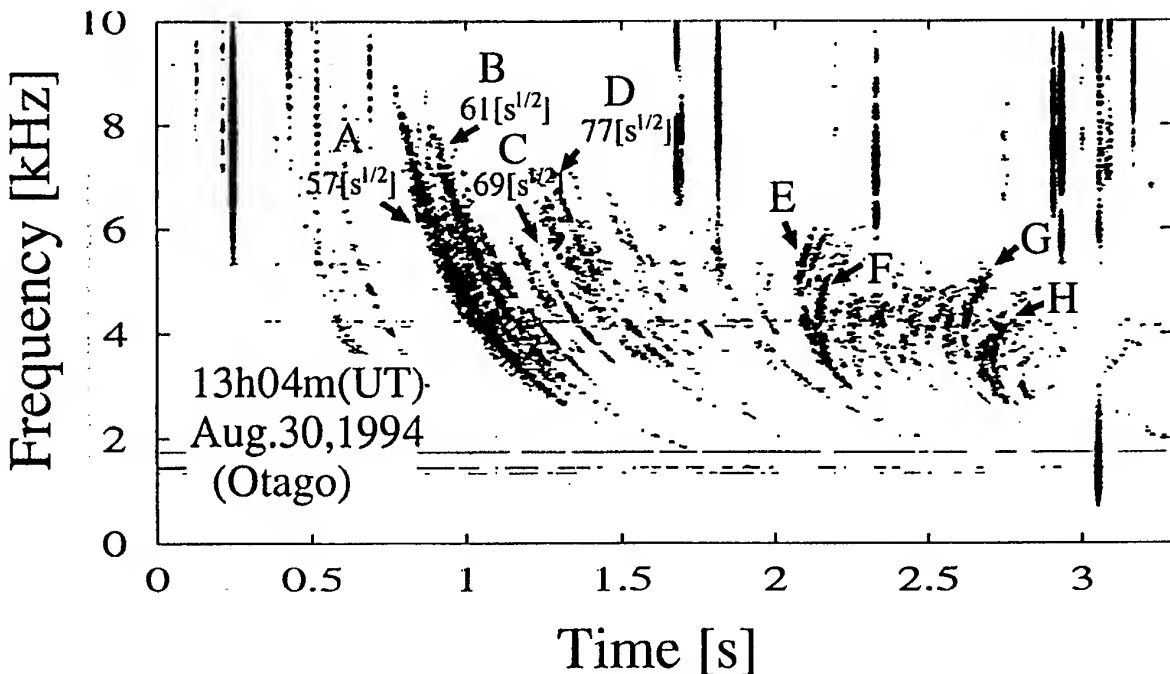


Figure 2. An example of a train of multi-path whistlers observed at Dunedin at 13h04m46s UT (Local time =UT+12h) on August 30, 1994. Whistler elements (of course, not all) are tentatively labeled A~H.

While, we describe the corresponding characteristics of whistlers C and D. The polarization of whistler C is shown to be generally distributed around $(u,v)=(0,-1)$. The polarization of whistler D $(u,v)=(0.8,-1)$ is found to be more linear than that of whistler C, which indicates their propagation in the Earth-ionosphere over great distances [10].

We now perform the analysis of path latitude (L value), equatorial electron density N_{eq} (cm^{-3}) and the dispersion of whistler ($D;(\text{s}^{1/2})$) by means of the nose-extension method [11]. The dispersion of each whistler labeled from A to D is shown in Fig. 2. The L value for whistler B estimated by the nose-extension method is found to be $L=2.829 \pm 0.018$ ($N_{eq} = 1112 \pm 21 \text{ cm}^{-3}$, $D=61 \text{ s}^{1/2}$), very close to that of the ionosphere, as based on the field-analysis DF. This indicated that the duct of whistler B has extended down to the ionosphere (probably F region) sometimes found at mid latitudes [9][12], at least, during this observation period. The ionospheric exit points of whistlers labeled from A to H except C by means of the nose-

extension method and our field-analysis DF are marked in Fig. 1. Now we discuss the properties of whistler C and its interpretation. The polarization of whistler C, $(u,v)=(0,-1)$ has already indicated that whistler C has exited the ionosphere relatively close to the observing station of Dunedin (of course, not so close as compared with whistler B), but its L value estimated by the nose-extension method is $L=3.327 \pm 0.022$ ($N_{eq} = 641 \pm 6 \text{ cm}^{-3}$, $D=69 \text{ s}^{1/2}$), being very different from the station. If we assume ducted propagation, the L value should be just ≈ 2.8 . So that, we reasonably consider that the apex altitude of the propagation path for whistler C is much higher than the corresponding apex for its ducted propagation path, but the exit latitude is definitely confirmed by the DF to be relatively close to the observation station. The most promising possibility of non-ducted propagation mode is PL (pro-longitudinal) mode of propagation [13], which is characterized by a non-ducted propagation, but being approximately symmetrical about the equator due to the presence of

the suitable ionospheric magnetospheric density profiles. No doubt we could find a PL mode of propagation by assuming an appropriate latitudinal gradient, on the basis of previous ray-tracing computations [9], so we consider it unnecessary to

repeat such ray-tracing computations here.

The propagation paths of ducted, non-ducted and PL mode whistler, penetrate through the ionosphere very close to the observing station of Dunedin are shown in Fig. 3.

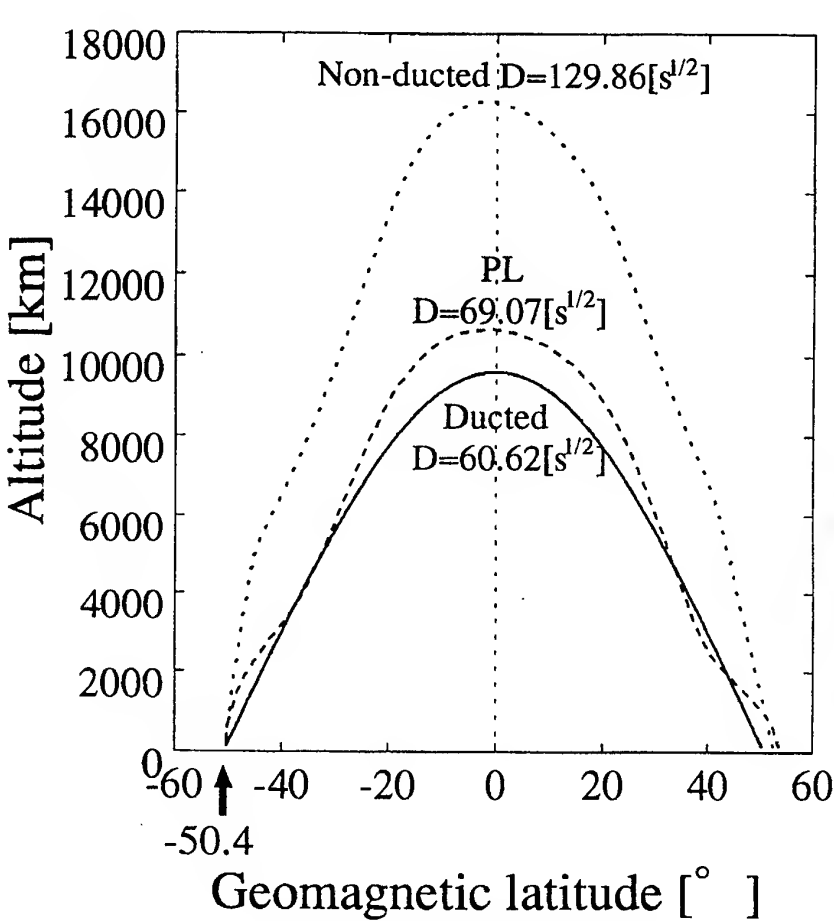


Figure 3. The propagation paths of ducted, non-ducted and PL mode whistler penetrate through the ionosphere very close to the observing station of Dunedin are shown. The dispersions of whistler are computed using the ionosphere/magnetosphere electron density model given by nose-extension method.

4. Conclusions

The wideband VLF measurements of three field components at two stations in middle latitudes have made it possible to perform the DF measurement on and apply the nose-extension and ray-tracing results have yielded a new type of multi-path whistlers including non-ducted whistlers. The most important

finding of this paper is to have provided convincing experimental evidence on non-ducted whistler propagation. We can expect the following research such that a particular large-scale horizontal gradient supports a non-ducted PL mode of propagation at some specific initial and final latitudes, and that many small-scale ducts are superimposed on such a large-scale inhomogeneity.

5. References

- [1] Helliwell, R. A., Whistlers and Related Ionospheric Phenomena, Stanford Univ. Press, 1965.
- [2] Thomson, R. J., and R. L. Dowden, Simultaneous ground and satellite reception of whistlers, I. Ducted whistlers, *J. Atmos. Terr. Phys.*, 39, 869, 1977a.
- [3] Ohta, K., M. Hayakawa, and Y. Tanaka, Ducted propagation of daytime whistlers as deduced from the ground-based direction finding, *J. Geophys. Res.*, 89, 7557, 1984.
- [4] Hayakawa, M., Y. Tanaka, and T. Okada, Time scales of formation, lifetime and decay of whistler ducts at low latitudes, *Ann. Geophysics*, 1, 515, 1983.
- [5] Balmforth, H. F., M. A. Cliverd, and A. J. Smith, A case study of storm commencement and recovery plasmaspheric electric fields near $L=2.5$ at equinox, *Ann. Geophysics*, 12, 625, 1994.
- [6] Hansen, H. J., M. J. Scourfield, and J. P. S. Rash, Whistler duct lifetimes, *J. Atmos. Terr. Phys.*, 45, 789, 1983.
- [7] Okada, T., A. Iwai, and M. Hayakawa, The measurement of incident and azimuthal angle and the polarization of whistlers at low latitude, *Planet. Space Sci.*, 25, 233, 1977.
- [8] Hayakawa, M., Whistlers, in *Handbook of Atmospheric Electrodynamics*, Ed. By H. Volland, Vol.II, p.155, CRC Press, Boca Raton, 1995.
- [9] Ohta, K., T. Kitagawa, N. Shima, M. Hayakawa, and R. L. Dowden, Characteristics of mid-latitude whistler ducts as deduced from ground-based measurements, *Geophys. Res. Lett.*, 23, 3301., 1996. Res
- [10] Shimakura, S. M. Hayakawa, and Y. Tanaka, The relationship between the polarization of whistlers and their dispersion, *J. Geophys.*, 59, 140, 1986.
- [11] Tarcsai, G., Routine whistler analysis by means of accurate curve fitting, *J. Atmos. Terr. Phys.*, 37, 1447, 1975.
- [12] Takahashi, O., K. Ohta, and M. Hayakawa, On the structure of ducts for mid-latitude whistlers and their ionospheric transmission as deduced from the ground-based direction finding, *Pageoph*, 140, 519, 1993.
- [13] Thomson, R. J., PL whistlers, *J. Atmos. Terr. Phys.*, 25, 1037, 1977.

BIOGRAPHICAL NOTES

Kenji Ohta graduated from Department of Communications Engineering, Shinshu Univ. in 1966 and received the Doctor of Engineering from Nagoya Univ. in 1987 and he is a Professor of Chubu University. His main interests are the development of measuring systems of natural radio waves including whistlers, tweeks and emissions associated with earthquakes. He is a member of the Society of Atmospheric Electricity of Japan and was awarded its Society Prize in 1991.

Masashi Hayakawa was graduated from Nagoya Univ. in 1966, where he obtained a master's degrees in 1968. In 1970 he obtained a Dr. of Eng. degree and became a Professor of The Univ. of Electro-Communications in 1990. In 1983 he was awarded the Tanakadate Prize, and in 1989 the Society Award of the Atmospheric Electric Society.

LASER TRIGGERED LIGHTNING IN FIELD EXPERIMENTS

Shigeaki Uchida, Zen-ichiro Kawasaki

Institute for Laser Technology
2-6 Yamada-oka, Suita, Osaka, 565-0871 Japan
e-mail:uchida@ile.osaka-u.ac.jp. Fax:06-878-1568

Department of Electrical Engineering
Faculty of Engineering, Osaka University
2-1 Yamada-oka, Suita, Osaka, 565-0871 Japan
e-mail: zen@pwr.eng.osaka-u.ac.jp. Fax:06-879-7724

1. INTRODUCTION

Laser triggered lightning is a technique to actively discharge electrical charges in thunderclouds to a safe place using laser produced plasmas conductivity, thereby protecting important facilities such as power transmission lines.

The authors' research group had been conducting field experiments for four years and reached a significant milestone in technological developments. verification of a scientific feasibility of the technique. In the course of the experiments, triggered lightning phenomena were observed with various lightning diagnostics data showing that laser plasmas trigger natural lightning.

This report describes the overview of the field experiments and UHF (Ultra High Frequency) interferometer data which show both temporal and spatial correlation between laser plasma generation and lightning initiation. These are the first observations of natural lightning being triggered by laser plasmas.

A concept of laser triggered lightning is depicted in Fig. 1. The basic idea of the concept is to induce, so called, "triggered lightning", occasionally observed in nature. Natural triggered lightning starts from a top of a conducting structure such as towers. Top of a tower is usually covered by corona charges due to high electric field concentration which reduces leader initiation. Natural triggered lightning is considered to occur when corona charges are quenched for some reasons such as abrupt change of electrical fields under thunderclouds and thus an electrical leader starts. Laser triggered lightning is to artificially create this condition using electrical conductivity of laser plasmas and to initiate electrical leader propagation. Laser plasmas are created by focusing intense laser beams to the top of a lightning tower through focusing mirror.

There are four critical issues for successful laser triggered lightning experiments:

- (1) understanding discharge induced process,
- (2) characterization of laser transmission in air
- (3) formation of effective plasma channels
- (4) determination of timing of laser irradiation.

The first two have been discussed in previous reports [1, 2], while the last two issues will be described in this report.

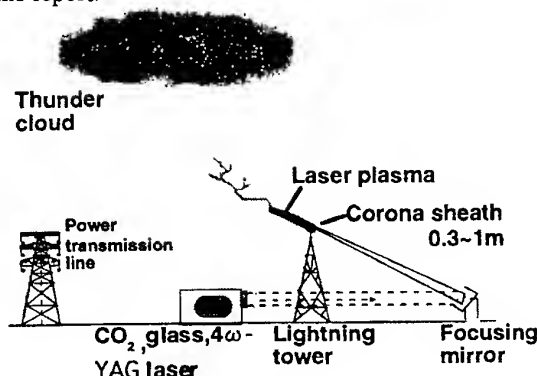


Fig. 1 The concept of laser triggered lightning

2. FIELD EXPERIMENTS

There are two types of thunderstorms in Japan, the summer thunderstorm and the winter thunderstorm. An important difference between them is its electrical field strength observed at the ground. Since altitude of thunderclouds is determined by ground temperature, the height of winter thunderclouds are lower than that in summer and thus exhibit stronger electrical field on the ground (typically 10 kV/m). Strong fields are preferable to laser triggered lightning studies; therefore, an experimental site was chosen on the Japan

seacoast where possibility of being attacked by winter thunderstorms is high [1].

The experimental station (see Fig. 2) consists of five principal facilities, laser systems, focusing telescopes, lightning tower, operation house, and thunderstorm/lightning diagnostics. The site configuration is shown in Fig. 1. The site is located on a 200-m high hill on the seashore of Japan sea.

The laser system is consisted of CO₂, Nd:glass and Nd:YAG lasers. The CO₂ laser is a two-beam system and delivers 1 kJ energy in 50 ns pulse duration per beam from an unstable cavity (210 mm² × 3600 mm). The glass laser is a MOPA (Master-Oscillator Power-Amplifier) style system and delivers 600 J in 50-ns pulse duration. The oscillator has a 60-mm² rod in an unstable cavity. The oscillator pulses are amplified by a three-pass amplifier with two 100-mm² rods. The pulse train from the YAG laser is converted to the 4th harmonic (100 mJ/70 Hz) and produces weakly ionized plasma channels far above the target to guide a leader towards thunderclouds.

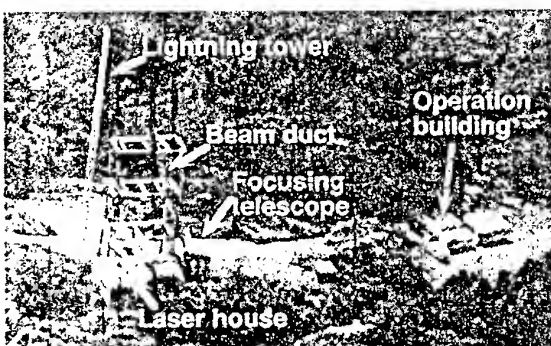


Fig. 2 Laser triggered lightning field experimental site

These laser pulses are focused to the top of the lightning tower to produce laser plasma (see Fig. 3). Two Cassegrain type telescopes (1000 mm² and 500 mm² aperture size) are used to focus CO₂ laser pulses.

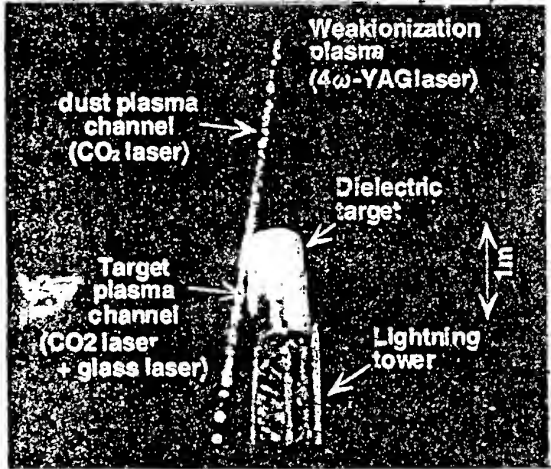


Fig. 3 Laser plasma channel at the dielectric target at the top of the lightning tower

One arm of the system is focused using a cylindrical reflector to generate a plasma channel on a dielectric target at the top of the tower. The glass laser pulse is also focused by a cylindrical lens.

The dimensions of the dielectric targets are 600 mm¹ × 600 mm². The target provides a stable source of plasma even in a strong wind or corona discharge where aerosols as a plasma seed are strongly depleted. Laser pulses with a line focus irradiate the target and produce strong enough plasma to initiate an electrical leader. Another arm of CO₂ laser produces a 2-m long plasma channel over the target to guide the leader out of the corona region.

The thunderstorm diagnostics include electrical field meter (Field Mills, FM), corona current probes (CP), meteorology radar systems, broad band capacitive antennas (Slow Antenna, SA) [3] and UHF interferometers[4]. The FMs and CPs compose a thunderstorm monitoring network with 6 observation stations around the site. The stations are distributed in the north-west of the site, a typical direction of cloud approach. Using the network and the radar system, motion and height of thunderclouds were monitored in real time basis and thus the laser system was prepared for shots. There are two types of interferometers, one is designed for detecting a direction of UHF pulse in a short range (of the order of few kilometers) and another, called SAFIR® system, is for long range (up to a hundred kilometers) detection [5]. The SAFIR system consists of three antenna each separated by 100 km and maps the location of the UHF source. The short range interferometer is located 5 km south east of the site. The SAs and the interferometer were used to map out lightning discharge paths with a microsecond time resolution.

It is crucial to determine the shot timing for laser triggered lightning. Since an electrical leader initiated by laser plasma needs to propagate from the top of the plasma channel to a thundercloud, certain electrical fields needs to exist along the leader progression. The right timing of laser irradiation is when a thundercloud starts to discharge its charges and can be determined using phenomenon called preliminary breakdown (PB), a precursor of lightning discharges in thunderclouds. The discharge process in a thundercloud lasts a few hundred milliseconds, while laser can be triggered within microseconds.

A novel technique, called PB trigger system, to determine precise timing of laser irradiation has been developed [2]. The schematic of the system is shown in Fig. 4. The system detects PB signals and gives precise laser shot timing. The system has a capability of triggering lasers faster than thundercloud response based on the fact that a whole process of a typical lightning discharge lasts a few hundreds ms [6], while the laser has a response time of 17 μs. Using this time scale difference, laser plasmas can be produced at right

timing. When a PB starts in a thundercloud, signals are detected by an SA or a CP current monitor. Criteria on frequency, number and amplitude of PB pulses are preset to distinguish them from noise pulses.

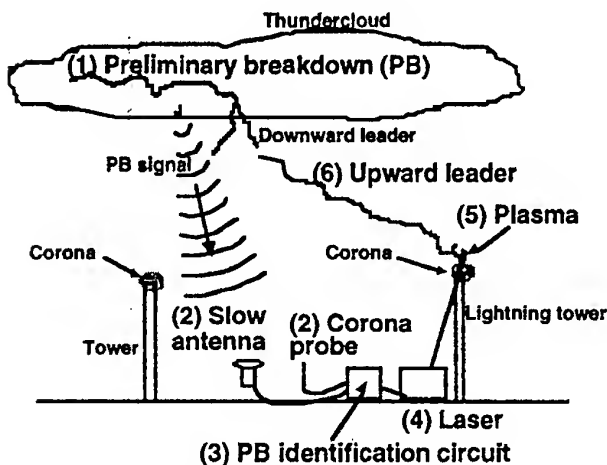


Fig. 4 Schematic of the PB trigger system

3. RESULTS

Two laser triggered lightning incidences were observed with extensive data set. Leader progression was recorded for the first triggered lightning event (see Fig. 5). The time elapse of the leader development from the lightning tower was recorded with a 33-ms resolution. It can be seen that the leader branches upward indicating that it was triggered from the tower top and progressed toward a thundercloud.

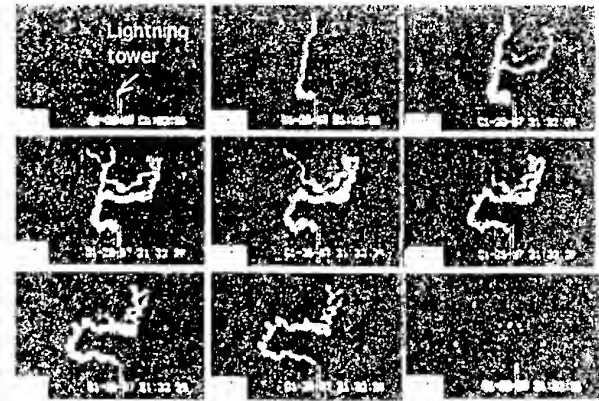


Fig. 5 An upward leader triggered by a laser plasma. Each frame is 33 ms duration, a CCD camera frame.

Tower currents of this leader propagation was recorded by a Rogovskii coil installed on the tower. The current rising is lead by plasma generation by 2 μ s. This time lag was observed in our laboratory

experiments and explained by plasma channel decay time for which plasma species is dominated by O₂⁺ ions acting as a charge source for leader propagation.

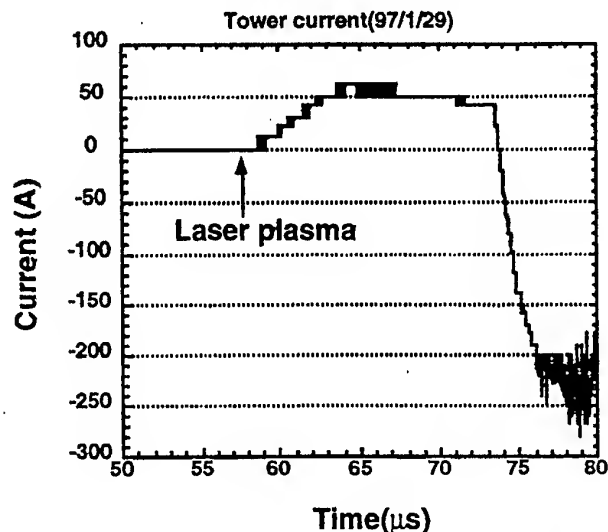


Fig. 6 Timing of laser plasma and current through the lightning tower.

Figure 7 shows UHF radiation (top) and tower currents (the second) detected by the interferometer and the Rogovskii coil, respectively. The lower two are the mapping (elevation and direction) of UHF sources as a function of time. As shown in the UHF plot, there is a UHF pulse detected 17 μ s after the laser trigger indicating that the pulse was generated by a leader triggered by plasma. The mapping shows that the source of the signal exists in the direction of the site. The SAFIR system also detects pulses at the experiment site.

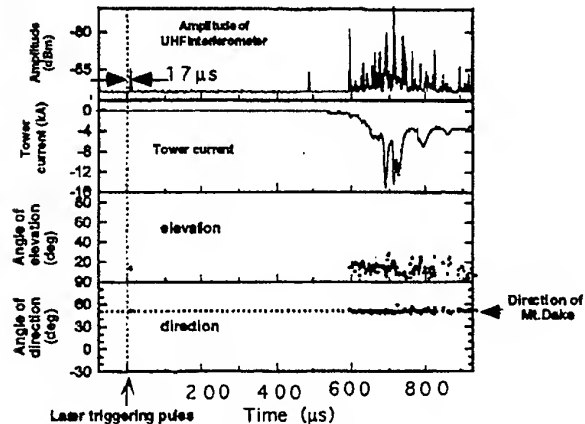


Fig. 7 UHF radiation and tower current triggered by laser plasma

The UHF pulses detected by the interferometer carry only directional information, however, their

origin being at the lightning tower is confirmed by the SAFIR data. Both the temporal and spatial coincidence of the UHF pulse at the plasma production indicates that an electrical leader and consequently lightning were triggered by a laser plasma.

This lightning event observed return strokes with a peak current of 35 kA and total discharge of about 3C. These are typical number for Japan winter thunderstorm. As shown in Fig. 8, most of the strong

field region above the site disappeared after the triggered lightning indicating that the most of the charges in the cloud were lowered by the triggered lightning. Assuming that the size of this strong field region is same as that of charge region, single shot of laser triggered lightning is able to neutralize at least 2 km of thundercloud in diameter.

4. SUMMARY

The combination of the laser systems are used to produce the plasma channels effective to laser triggered lightning. They enhances the plasma life time, laser triggering and guiding effects. The PB triggering system is developed to take advantage of fast response of laser systems. This new technique of triggering the laser system according to the thundercloud conditions was successfully employed in the field experiments and triggered natural lightning. The UHF interferometers, SAFIR system, slow antennas and tower current measurements were used to obtain consistent data which show the leader initiation triggered by laser plasmas.

ACKNOWLEDGMENTS

This study was supported by Kansai Electric Power Co. and Japan Ministry of Education.

REFERENCES

- [1] D. H. Wang et al., "The Study of the Possibility of Lightning Triggering by means of a Laser", *J. Atmos. Electr.*, 14, 49 (1994).
- [2] S. Uchida, Y. Shimada et al., "The field experiments of laser triggered lightning", *The review of laser engineering*, 24 547(1996).
- [3] T. Ushio et al., "Synchronized multipoint measurements of lightning electric field changes". *Trans. of IEE of Japan*, 114-B 1160 (1994).
- [4] J. Onuki et al., "Imaging of lightning channel in three dimensions using interferometer", *Trans. of IEE of Japan*, 116-B 475 (1996).
- [5] Z. Kawasaki et al., *Geophys. Res. Lett.*, 21 1133 (1996).
- [6] A. M. Uman, "The Lightning Discharge". Academic Press, Inc., (1987).

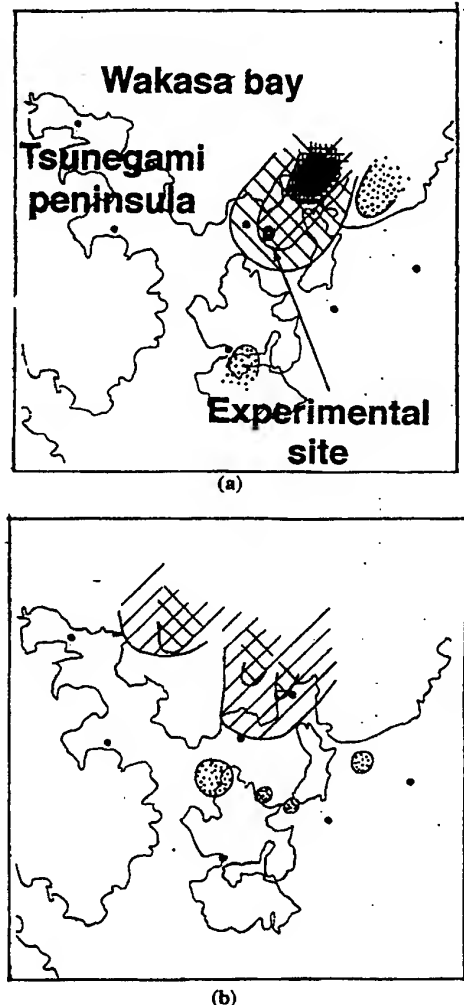


Fig. 8 Electric fields mapping in the vicinity of the field experimental site before (a) and after (b) the lightning discharge.

XIII

**NATURAL AND MAN-MADE
EM ENVIRONMENT**

**EM Emissions in High and Low
Frequency Ranges Related to
Earthquakes**

URSI Commission E sponsored session

Invited session organized by

Prof. T. Yoshino - Japan

LARGE-SCALE SEISMOIONOSPHERIC PLASMA STRUCTURES AND ANOMALOUS LOW-LATITUDE WHISTLERS

Depueva A.Kh., Ruzhin Yu.Ya.
IZMIRAN, Troitsk, Moscow Region, 142092, Russia

Electron density temporal and spatial variations before two strong earthquakes with their epicenters located at different latitudes were analysed. It was shown that low-latitude ionosphere reaction on the forthcoming earthquake is not similar to that observed at middle and high latitudes. The attempt is made to explain anomalous whistlers prior to and after the low-latitude earthquake by means of severe ionosphere modification close to the region of whistlers entrance into the magnetospheric ducts.

1. INTRODUCTION

Earthquake preparation processes in the lithosphere manifest themselves at ionospheric heights in a different way. It was stated that before strong earthquakes with $M > 5$ ionosphere electron density profile modification exists at the height range of 100-1000 km. As a rule, the electron density of the main ionospheric peak N_m over the epicenter located at middle and high latitudes some days before the main shock is greater than after it, exceeds N_m median value, and it is increased in comparison with N_m measured outside of the preparation zone boundary. Above-said effect manifest itself best at night and it is assumed to be one of the seismoionospheric precursors. Low-latitude ionosphere reacts on the forthcoming earthquake in a different way. Over the epicenter located in the vicinity of the dip equator some days before the earthquake N_m values are decreased in comparison with expected simulated values and those measured far from the epicenter. N_m spatial redistribution inside the earthquake preparation zone radius exists as well [7.1].

Nevertheless seismoionospheric phenomena at equatorial ($\pm 5^\circ$ off the magnetic equator) and low ($\pm 20-30^\circ$ off the magnetic equator) latitudes are not so far sufficiently clear.

The aim of the presented paper is to study reaction of the ionosphere on isolated earthquake with its epicenter situated at low latitude.

2. ELECTRON DENSITY VARIATIONS FOR EARTHQUAKE AT LOW LATITUDE

We have analysed retrospective ionosonde data for the earthquake occurred on October 1, 1971, with its epicenter located near Vanimo (New Guinea) $\varphi=3.1^\circ$ S, $\lambda=139.17^\circ$ E, dip= -18° . Its magnitude was $M=8.1$. As it have been shown in [7.2] the earthquake preparation zone dimension at the F layer height is the same as on the Earth's surface, radius of the preparation zone being estimated by the following relation: $R=e^M$, where M is the earthquake magnitude. Preparation zone dimension is in the case under consideration ≈ 3200 km.

In Fig.1 the location of the earthquake epicenter (asterisc), its preparation zone (circle with radius 3200 km), and mutual position of observation points are shown.

In Fig.2 F layer critical frequency (f_c) diurnal dependences are presented for Vanimo ($\varphi=2^\circ 42' S$, $141^\circ 18' E$, over the epicenter of the earthquake), Townsville ($\varphi=19^\circ 18' S$, $\lambda=146^\circ 44' E$, outside the preparation zone of the earthquake but close to its boundary), and Brisbane ($\varphi=27^\circ 32' S$, $\lambda=152^\circ 55' E$, too far from the epicenter) some days prior to the earthquake. Dashed curves are ones calculated by means of the International Reference Ionosphere [7.3].

N_m corresponds to the measured by ionosondes F layer critical frequency f_c as $N_m=1.24 \times 10^4 f_c^2$, where N_m is scaled in el/cm^3 and f_c is scaled in MHz.

The definite effect of the earthquake preparation is seen at Vanimo. Daytime f_c values are enhanced, and nighttime ones are reduced in comparison with calculated f_c values by 20-30%. At the same time at Townsville diurnal behavior is slightly disturbed, f_c being 10% reduced in daytime and enhanced in evening. At Brisbane f_c variation is similar to simulated one. According to aforesaid we can assume that the southern slope of the equatorial electron density anomaly is modified some days before the event, the main

perturbation being observable at the southern crest which coincides with the epicenter location. Unfortunately, there are no Port Moresby data just before the earthquake but monthly medians for this place confirm the latter idea.

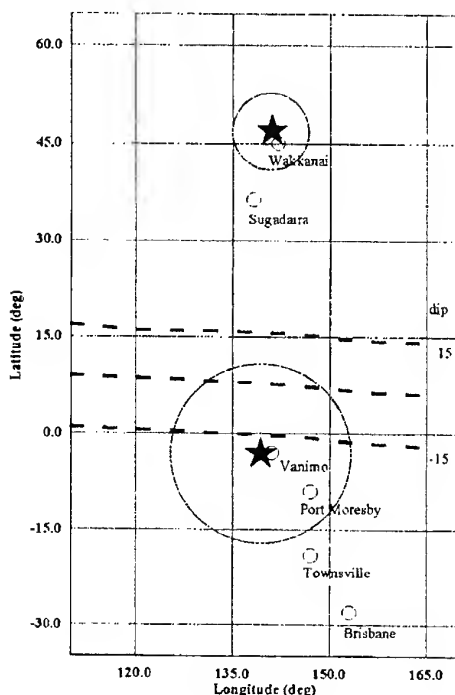


Fig.1. Mutual locations of bottomside ionosondes and Sugadaira whistler observatory. Earthquakes epicenters are pointed by asterisks.

We have compared the ionosphere reaction on the earthquake close to Vanimo with the second one occurred a bit earlier on September 6, 1971, with its epicenter located near Wakkai (Japan) $\phi=45^{\circ}23' N$, $\lambda=141^{\circ}41' E$, $dip=+60^{\circ}$. Epicenter location is marked in Fig.1 by asteric: $\phi=46.5^{\circ} N$, $\lambda=141.1^{\circ} E$.

The opposite kind of f_0 deviation but worse pronounced is observed over the epicenter before the event in the high latitude region (Fig.2, bottom panel). The result confirms already known fact about increased N_m in nocturnal hours. The smaller deviation relatively to that observed over Vanimo may be due to smaller earthquake magnitude $M=7.2$, ($R=1221$ km).

Thus, preparation processes of isolated identical earthquakes with different epicenters positions influence the ionosphere in a different way.

3. LOW-LATITUDE ANOMALOUS WHISTLERS DURING THE EARTHQUAKE

It was shown in [7.4] that anomalous propagation of magnetospheric whistlers at low latitudes (geomagnetic lat. $20\text{--}30^{\circ}$) is the other consequence of an earthquake preparation process.

An anomalous whistlers with dispersions of $D > 60 \text{ sec}^{1/2}$ and $D = 100 \text{ sec}^{1/2}$ were detected at Sugadaira (Japan) $\phi=36^{\circ}31' N$, $\lambda=138^{\circ}19' E$, $L=1.33$ on 25 and 29 September 1971, six and one day before the former of earthquakes under consideration. (The dispersion value is the characteristic of time delay of a whistler during its propagation in field-aligned duct and wave frequency). Such anomalous whistlers continued to be detected for a few days after the event (namely, on 2 October). Short whistlers also appeared beginning from 29 August.

In this connection we have to note the follows. Whether the low latitude ground whistlers are of the ducted mode or the non-ducted mode remains a question not yet solved. Authors of [7.4] believe in ducted propagation in the case.

The earthquake took place relatively close to the region of entrance of the whistlers into the magnetospheric duct and its epicenter was located under a magnetic field line between Sugadaira and its conjugate point.

4. DISCUSSION

As it was pointed out in Section 1 the modification of the ionosphere over the epicenter occurred some days before the former earthquake. Namely, 25 and 29 September were characterised by severe diurnal variation over the epicenter with f_0 enhancement during the daytime and fall during evening hours. The same picture but not so good emphasized is seen on 2 October, just after the earthquake. On 28 September when anomalous whistlers were absent there were an increased f_0 values even in the evening (Fig.2).

So, at the waveguide entrance place one can observe sharp electron density temporal gradients followed by anomalous whistlers appearance.

Epicentral zone where the ionosphere disturbance is observed coincides with the equatorial anomaly crest region, so any plasma density changes there have to lead to the plasma redistribution in the whole equatorial anomaly area. Spatial modification of the electron density over the preparation zone of the forthcoming equatorial earthquake was observed by means of

topside ionosondes [7,1]. In our case of the low-latitude earthquake electron density spatial variation is also really observable on the southern slope of the equatorial anomaly. Such kind of horizontal gradient of ionization associated with the equatorial anomaly can lead to some favourable conditions for duct trapping at its entrance.

The aforesaid modification of the ionosphere can effect on non-ducted propagation as well.

When discussing the equatorial earthquake consequences we have proposed [7,1] that plasma spatial redistribution before the event can be due to the same mechanism as it is in the case of natural equatorial anomaly. Instead of horizontal electric field of electrojet origin we take in mind electric field horizontal component of lithospheric origin. The same mechanism is not valuable if the epicenter departure from the magnetic equator is more than $\pm 5^\circ$.

In order to stay in frames of our position we have to suppose the electric field of lithospheric origin generation not only exactly over the epicenter but also over some additional area. In our case it is approximately 15° apart the epicenter, i.e. inside the scale of the preparation zone.

It seems that the latter earthquake preparation does not lead to anomalous whistlers appearance at a conjugate point because there is no evidence of plasma spatial redistribution close to its epicenter. Unfortunately, now we have no experimental confirmation of this idea.

5. CONCLUSION

There are some difference in seismoionospheric reaction between earthquakes with their epicenters located at low (including equatorial) and high latitudes.

Now we have a reason to suppose that sufficiently severe time and space gradients of electron density over the preparation zone of the low-latitude earthquake can influence on the duct trapping conditions and, as a consequence, lead to anomalous whistlers appearance before and after the event at low latitudes of the opposite hemisphere.

6. ACKNOWLEDGEMENT

This research was supported by the Russian Foundation of Basic Research No 96-05-65473.

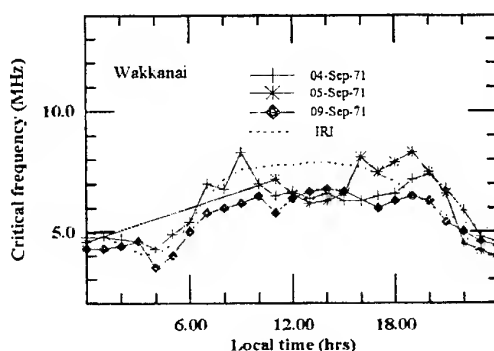
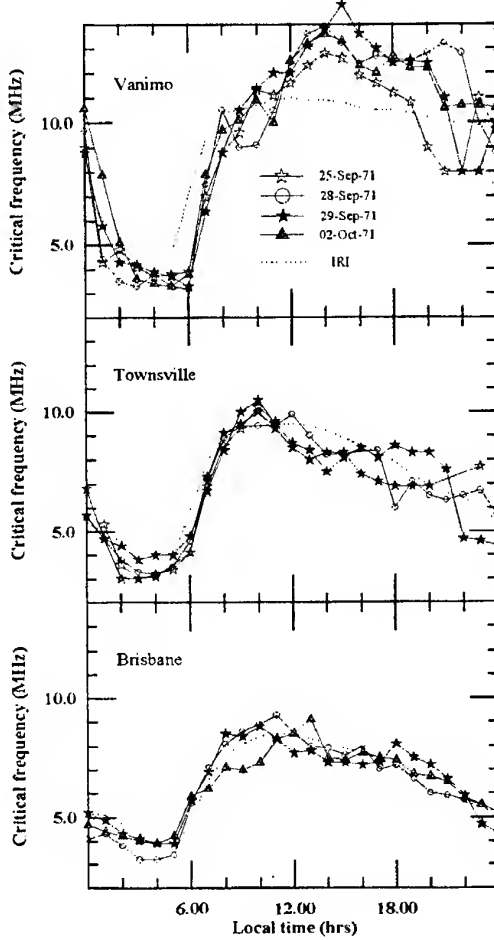


Fig.2. Diurnal F layer critical frequency variations before and after the two considered earthquakes.

7. REFERENCES

- 7.1. A.Kh.Depueva, Yu.Ya.Ruzhin, "Peculiarities of earthquake forerunners at low-latitude ionosphere" (English), Proceedings of the International Workshop on Seismo Electromagnetics, Tokyo, Japan, 1997 March 3,4 and 5, pp.202-206.
- 7.2. Yu.Y.Ruzhin and A.Kh.Depueva, "Seismoprecursors in space as plasma and wave anomalies" (English), Res. Lett. Atmos. Electricity, Vol.16, No.3, 1996, pp.271-288.
- 7.3. D.Bilitza, "International Reference Ionosphere 1990" (English), NSSDS-90-22, Greenbelt, Maryland, USA, 1990.
- 7.4. M.Hayakava, T.Yoshino and V.A.Morgounov, "Low-latitude magnetospheric whistlers and earthquakes" (English), Res. Lett. Atmos. Electr., Vol.12, No.3, 1992, pp.253-273.

8. BIOGRAPHICAL NOTES

A.Depueva graduated as Radio Electronics Engineer from Moscow Power Engineering Institute, in 1971. In 1977 she joined IZMIRAN where she received her Candidate of Science Degree. Now she is a senior scientific researcher at the same Institute. Her particular scientific interests lie in low latitude ionosphere and ionospheric inhomogeneities.

Yu.Ya.Ruzhin has a background in physics from the Kazan State University. His Doctor of Geophysics Thesis was on active experiments in space plasma. Now he deals with ionospheric disturbances such as ionospheric ones.

ELECTROMAGNETIC EMISSIONS over DEEP FAULTS of the LITHOSPHERE by SATELLITE MEASUREMENTS

V.I. Larkina

IZMIRAN, Troitsk Moscow Region, 142092, Russia

N.G. Sergeeva

Polar Geophysical Institute, Murmansk, 183010, Russia

B.V. Senin

Research Institute of Marine Geophysics, Murmansk, 183025, Russia

Changes in magnetic and, especially, in electrical component of the low-frequency emission field, registered on board satellite are found out, when its trajectory crosses the contrast forms of the "Solid Earth" topography mid-oceanic ridges, zones of continental slope, island and mountain massifs, hights and ets.

The presented results of data processing of the wave experiment on "Intercosmos 19" satellite give confirmation of existence electromagnetic lithosphere process manifestations in the upper ionosphere. Electromagnetic processes revealed in the work are unequivocally connected not to catastrophe manifestations of the seismic activity, but to current processes, occurring in the lithosphere. Interpretation of the received results is given.

1. Introduction

Variations of intensity of the electromagnetic emission are registered by satellite "Intercosmos 19" when it passes over deep faults of the lithosphere of the Barents and Kara Seas [1-3].

2. Experimental data

In this paper the electromagnetic emission data of two near orbits 233, 1537 "Intercosmos 19" satellite over the Barents and Kara Seas in quiet days: on March 15 1979,

on June 14 1979 ($K_p = 2 \div 3$). These experimental data give us the possibility to verify the stability of discovering phenomenon recently [1-3] (relative to time and space).

The electric and magnetic component VLF emissions in 10 minutes of four frequencies from 140 Hz to 15000 Hz of 233 and 1537 orbits has been considered for a detail comparison. The satellite trajectories have crossed the contrasted forms of the Earth crust: the Medvezhinsko - Nadezhinsky graben system, the Central massif of Svalbard microplate, the Nordkap graben, the Finnmark massif, the East Barents graben, the Novaya Zemlya microplate. All these forms are limited or are divided by deep faults of sufficiently ancient origin which keep their activity during the long period of the last 1 - 2 million years. In the eastern region of the Barents Sea the deep faults are broad zones with crack systems in the near-surface structure of the bottom and with fault-flexures within sedimentary cover and others. This indicates that they function in the regime of common stretch of the region.

The projection of orbits 233 (shade line) and 1537 (solid line) to the Earth surface is shown in *Figure 1a*. The driving of the intensity electric

component of the electromagnetic emission is shown in *Figure 1b*. The Earth crust section in the Barents - Kara Sea region is shown in *Figure 1c*. The magnetic component of VLF emission is not considered here. The variations of magnetic component intensity over the deep faults are shown in *Figure 2b* for orbit 1537.

The comparison of electromagnetic emission data with the Earth crust section permits us to mark the following particularities. We pick out several typical zones of the variation intensity VLF emission which are marked in *Figure 1b* as zones *a, b, c, d, f, g*.

The decreasing field of the electromagnetic emission (the zone *b*) is observed over the relatively stable crystalline massif - the Central massif of Svalbard microplate. The solidity of the massif is a possible reason of that. The decreasing field of the electromagnetic emission is observed over a very big depression with the thick cover of sediments too (the zone *f* over the East - Barents graben). The absorption in this zone is a possible reason of that.

The increasing field of VLF emission is observed over the Finnmark massif (the zone *d*). The field increase may be connected to the fact that the massif is small, the graben's zones are close to each other and that is why the common background is increased.

The disturbed electromagnetic emission zones are closely connected with the border deep faults, which limit the deep grabens. The spades of the electromagnetic emission intensity over the Nordkap graben's faults and over the deep fault system (the zone *c* and *e*) are good examples of that.

The location of the spades and their configuration is just the same in some cases on both orbits. For

example: the variations of the intensity of VLF emission over the Medvezhinsky system (the zone *a*), over fault "system 42 E" (the zone *e*) and the western zone of Novaya Zemlya (the zone *g*). Besides, the configuration of the spades of VLF emission intensity is just the same, when the intensity is increased over the Medvezhinsky fault system (the zone *a*) and over the western Novaya Zemlya system (the zone *g*) and the intensity is decreased over the border faults "system 42 E" (the zone *e*).

It should be noted, that the high - frequency spades are occurred over the deep fault system. They are not observed in the data of other orbits or are observed weakly. The intensity spaces of VLF emission on frequency 15000 Hz over the deep faults (the zone *g*) and over the deep faults of the inside region of the East - Barents graben (the zone *b*) confirms this fact.

You can see the simultaneous intensity variations of VLF emission on two orbits 233 and 1537 in *Figure 1b*, too, where the satellite passes over the deep fault system.

3. Results of correlation analysis

Coefficients of the correlation for the curves of VLF emission (magnetic and electric components) on two orbits 233 and 1537 are received from a correlation analysis (Table 1).

Table 1. Correlation coefficients between intensity VLF emission burst curve for magnetic and electrical components on two orbits (233 and 1537).

f , Hz	R_{magn}	R_{electr}
140	0,6443	0,9218
450	0,0904	0,4893
800	0,4467	0,1981
15000	0,2317	0,5585

On the frequency 140 Hz the correlation coefficient for electrical and magnetic components is more 0,5. On the frequency 15000 Hz the correlation coefficient for electrical component is more 0,5, too. On the frequency 450 Hz one for electrical component is very close to 0,5 ($R=0,4893$). On other frequencies the correlation coefficients are less 0,5. We explain it, that one curve maximum is late to the second curve maximum and the reason of that is different heights of these orbits.

4. Conclusion

The conformity of the Earth crust structure to the peculiarities of VLF emissions has been found from the experimental data analysis. It should be noticed, that one of the possible mechanisms of this conformity is the following. The examined border (edge) faults are long - living deep zones. They separate the large Earth crust blocks and are characterized by high warm streams and high permeability of bowels of the Earth. This high permeability provides the possible circulation of activity water and gas solutions along the deep faults. Thus, they are peculiar channels or "vertical conductions" which connect the deep bowels of the Earth with its surface and the atmosphere and can introduce a determined contribution in the structure of electromagnetic emission in the upper ionosphere.

We conclude that:

1. The prominent simultaneous variations of electric component of the VLF emission intensity on all frequencies of the spectrum are observed when satellite "Intercosmos 19" (orbits 233 and 1537) passes over the deep faults.
2. The stability of the measured parameters of VLF emission on two

orbits 233 and 1537 is observed over one and the same region with a three months' interval.

3. The data measured by satellite "Intercosmos 19" have given an experimental evidence of the electromagnetic phenomenon existance of the lithosphere processes in the upper ionosphere.

Acknowledgments.

The authors wish to express their thanks to collaborators IZMIRAN Acad. V.V. Migulin and Prof. Yu.Ya. Ruzhin for their suggesting, discussions and encouragement during the preparation of this paper.

References:

1. Larkina V.I., N.G. Sergeeva, and B.V. Senin, Regional structure reflection on the Barents-Kara shelf in the electromagnetic emission satellite data, Abstracts of the International Symposium "Satellites researches of ionospheric and magnetospheric processes"(in Russian), Moscow, IZMIRAN, 1995, pp.37-38.
2. Migulin V.V., V.I. Larkina, N.G. Sergeeva, and B.V. Senin, Regional structure reflection of lithosphere in the satellite observations of electromagnetic emission (in Russian), Dokl Akad. Nauk, v.357, №2, 1997, pp.252-254.
3. Migulin V.V., V.I. Larkina, N.G. Sergeeva, and B.V. Senin, Regional structure reflection on the Barents-Kara shelf in the electromagnetic emission satellite data, Proceedings of the International Conference on Marine Electromagnetics. The Defence Evaluation and Research Agency, Imperial College of Science, Technology and Medicine, London, UK, England, 23-26 june 1997, P. 6.1.

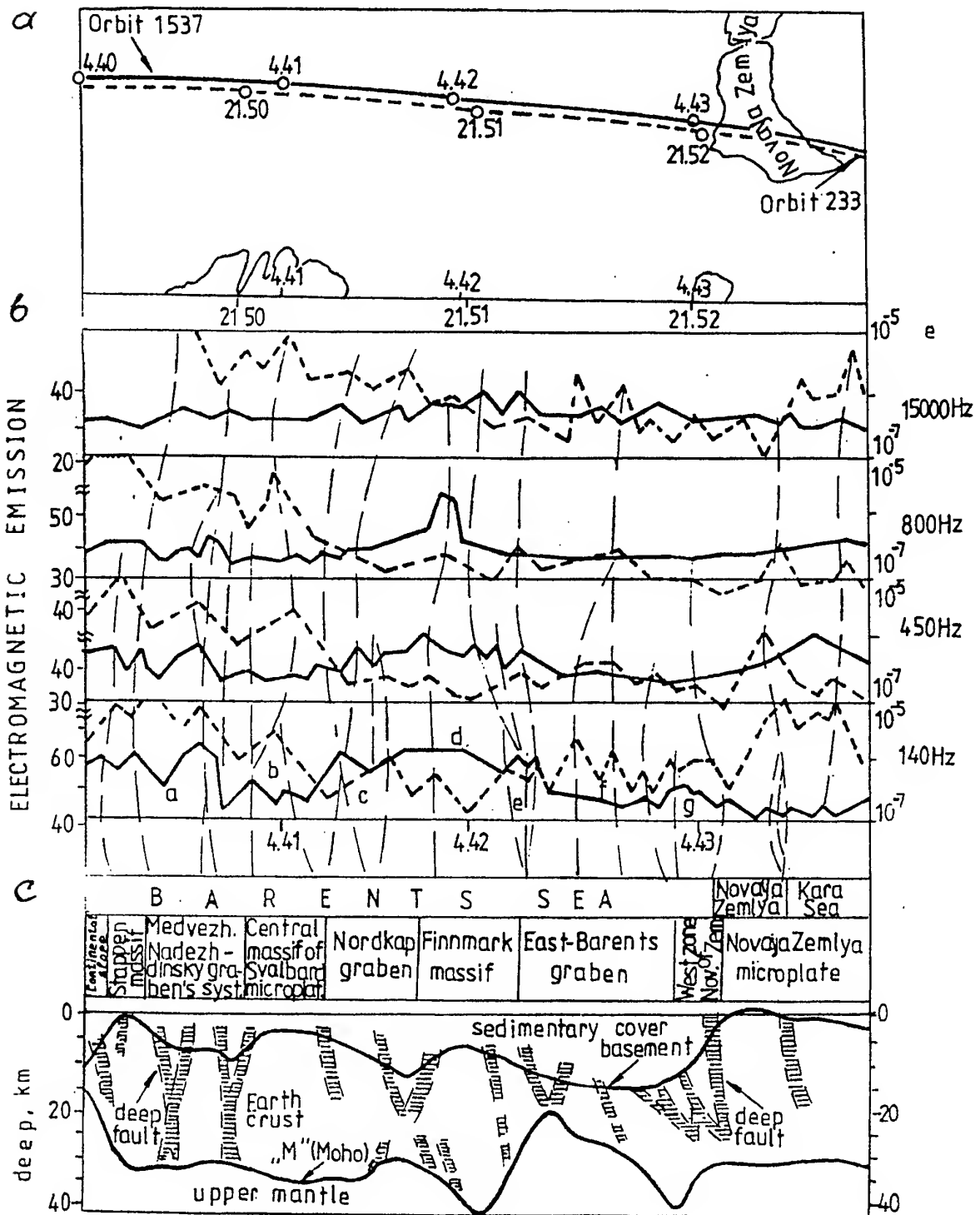


Fig.1. Experimental data of the VLF emissions and tectonical structures of the lithosphere.

- a. trajectories of "Intercosmos 19" satellite (orbits 233 and 1537) over the Barents - Kara Seas.
 - b. electrical component of VLF emission on two orbits: 233 (shade line), 1537 (solid line).
 - c. tectonical section of the Earth crust along satellite trajectories.

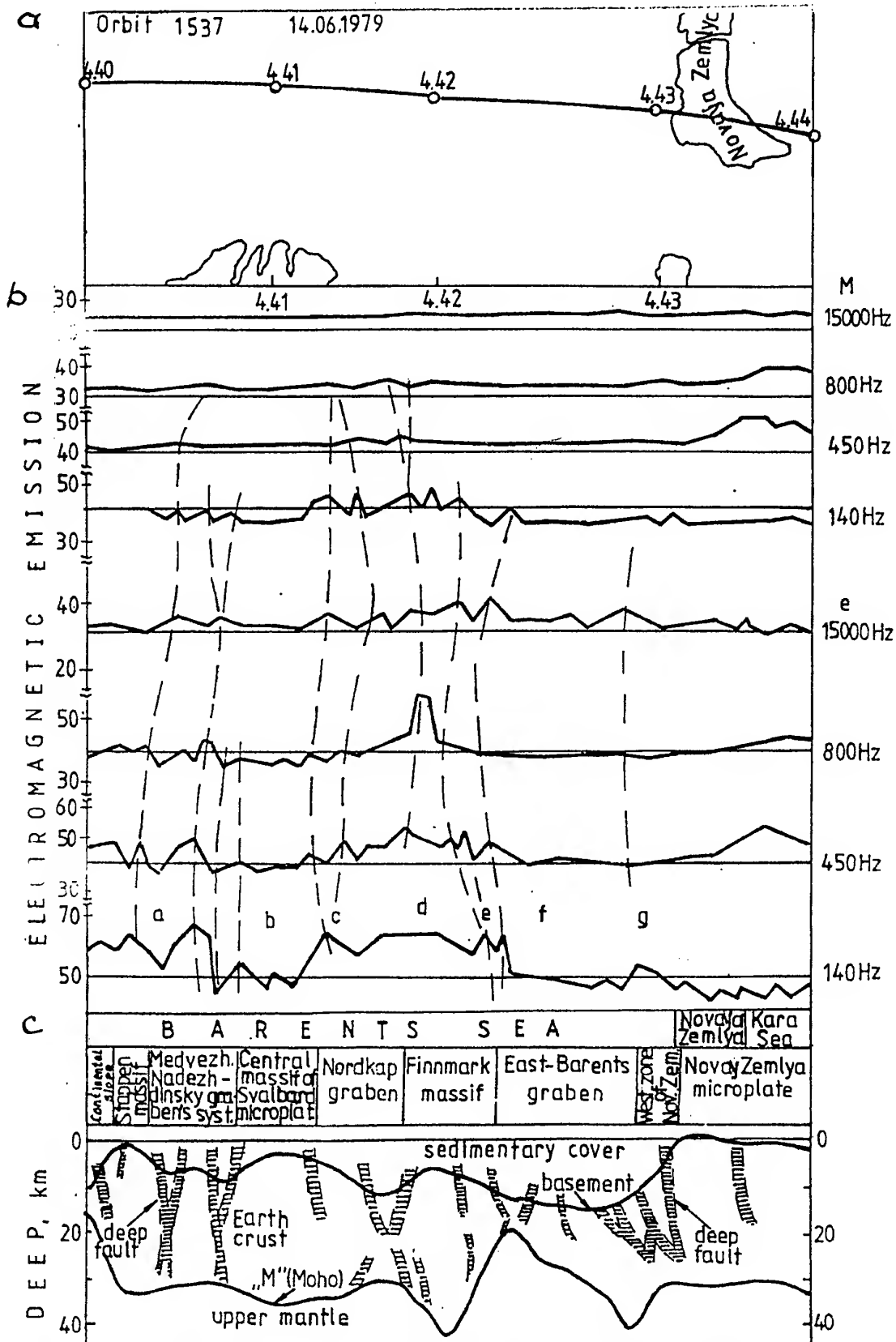


Fig.2. Experimental data of VLF emissions on orbit 1537 and tectonical structures of the lithosphere.

- trajectory of "Intercosmos 19" satellite over the Barents - Kara Seas.
- magnetic (m) and electrical components (e) of VLF emission.
- tectonical section of the Earth crust along the satellite trajectory.

REGIONAL (LOCAL) MANIFESTATION OF SEISMOPRECURSOR SPACE ANOMALIES

Ruzhin Yu.Ya. and Depueva A.Kh.

IZMIRAN, Troitsk, Moscow Region, 142092, RUSSIA
Fax.: 007 (095) 334-01-24, Tel.: 007 (095) 334-02-91

It is shown and motivated that two main groups of the earthquake precursors exist in near-Earth space. There are plasma anomalous structures which appear above the epicentral area of future earthquake at full range of ionospheric heights and so-called "noise" belts in VLF band registered at both hemispheres by low-orbit satellites.

For the both types of space precursors it was claimed that they have their local image which depends strongly on epicenter location and on time and geographical position of precursors observations.

1. INTRODUCTION

Earthquake preparation processes in lithosphere manifest themselves not only on the Earth's surface, but also in the ionosphere, and the whole complex of various physical phenomena in near Earth environment are observable [1-4].

Amongst them we have to take in mind ionospheric plasma density reaction. Particularly, in the majority of recent publications electron density at 300 -1000 km enhancement over the preparation zone of the future earthquake 1 - 3 days before the event is emphasized. This effect is observable at night hours and assumed as one of the seismoionospheric precursors. Changes depict not only in regular ionospheric structure but also in the irregular one [1]. Some days before the earthquake ionosondes often register E- and F-spreading, E_s appearance, anomalous traces like stratifications, crescent disturbances (kinks) etc. All of them testify the presence of different scale inhomogeneities during earthquake preparing stage [4].

VLF precursors which appears at satellite orbits some hours before the earthquake are localized close to magnetic shell corresponding to future earthquake epicenter and have a belt-like structure (longitude aligned on more than some tens thousands kilometers) [5]. There are some progress in investigations of space plasma precursors of earthquake - the magnetic conjugation of ULF preseismic emission on satellite orbits was found [6] in both hemispheres. It means that some signature of precursor could be found inside the geomagnetic flux tube (shell) connected both conjugated midlatitude ionospere regions ($L=1.5-1.75$) where the ULF

precursors on satellite orbits were registered. $L=1+h_e/R_0$ is MacIlwain parameter. Here h_e is equatorial height of magnetic field line connected with epicentre and R_0 - is the Earth radius.

Based on the quantitative characteristics of seismionospheric precursors and their comparison with atmospheric potential disturbances parameters and preparing zone dimension on the earth's surface it is concluded [2-4] that the anomaly of the atmospheric electric fields created by the lithospheric processes (including possible modification of atmospheric electricity redistribution due to the radioactive or/and aerosol emanations) before earthquakes may be the reason for the generation of seismo-ionospheric disturbances as space earthquake precursors even in magnetically conjugate region.

The difference in earthquake preparation processes manifestation at ionospheric heights can be caused by unsimilar physical processes in low and higher latitudes. In our opinion the electric field of lithospheric origin which by one or another way penetrate up to ionosphere play an important role anywhere. So, we have now some reasons to believe that earthquake epicenter location play an important role as to differences in electron density modification over the preparation zone and VLF anomalies observation.

2. PLASMA STRUCTURE OF IONOSPHERE IN RELATION TO LOCAL POSITION OF EPICENTRE

Numerous evidences of increasing electron concentration over the epicenter some days before the future earthquake have been published in recent years (see [1] and references there in for example). Consecutive two days before the day of earthquake F-and E-layers critical frequencies over the epicentral region increase by 1-1,5 MHz. It means that F-layer penetration frequencies (foF2) measured both by bottomside and topside ionosondes before the earthquake are greater:

- than after it,
- in comparison with (foF2) measured outside the preparation zone,
- in comparison with median value of (foF2) at the same location.

Nevertheless, when analysing the ALOUETTE1 ionosphere data [7], we came across with the phenomenon opposite to usually observed: (foF2) values before earthquakes were less than after them, less than (foF2) measured outside the preparation zone boundary, and comparatively to median values.

In our mind the absence of correspondence between our results and usual point of view is not random. We have analysed ALOUETTE topside ionospheric data obtained some days before and during equatorial earthquake with magnitude of $M=6.9$ on April 13, 1963 with an epicenter 600 km to N-W of Huancayo, Peru. It was noticed that the F-layer critical frequency (foF2) dependence against magnetic inclination shown in Fig.1 had a pronounced minimum (deep plasma trough) close to magnetic equator and two maxima in both hemispheres one day before the earthquake although they were absent during two weeks before and after it. The regional ionospheric model doesn't predict the existence of this kind of equatorial anomaly.

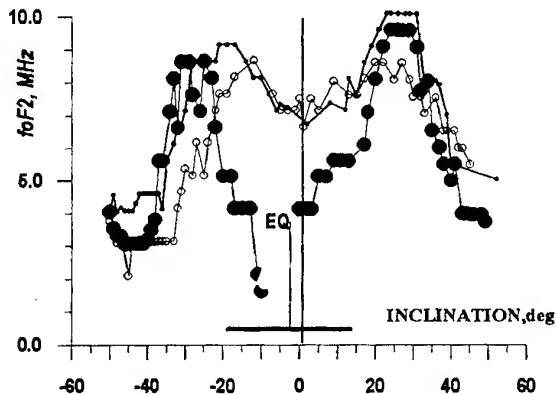


Fig.1. The plasma structure in the ionosphere one day before the pending earthquake 12.04.1963 (big black circles). The rest two lines are foF2 values more earlier and after the earthquake. Thick horizontal line is the estimated earthquake preparation zone dimension (the zone radius $R=\exp M=898$ km [2-3]). By EQ sign the epicenter position is shown.

It is proposed that the generation of anomalous eastward electric field at the epicenter of future earthquake together with Earth's magnetic field at ionospheric level may cause the upward vertical ionospheric plasma drift over the epicentral zone known as 'fountain effect'. One can conclude that the electric field of the precursor has to be less or compatible with the electric field of natural origin leading to the 'fountain-effect' and Appleton anomaly. So, the electric field magnitude of the precursor which is sufficient for this aim could be less than one mV/m also at ionospheric heights.

In order to decide if the originality (distinction) of our results is denoted to earthquake epicenter location near the magnetic equator we have compared ionospheric data for equatorial

earthquake occurred on October 1, 1971, $M=8.1$ near Vanimo (New Guinea), dip= -20° and the second earthquake occurred on September 6, 1971, 05.35 UT, $M=7.2$ close to Wakkanai (Japan) dip= $+60^\circ$, high latitudes. Preparation zone dimensions $R=\exp M=3200$ km and $R=1221$ km respectively. In Fig. 2 foF2 daily variations for "disturbed" (before the earthquake) four days are presented in comparison with month median for ionosondes situated inside the preparation zone of the first earthquake. In Fig.3 the analogous dependences for ionosonde situated in Wakkanai before and after the second earthquake are presented.

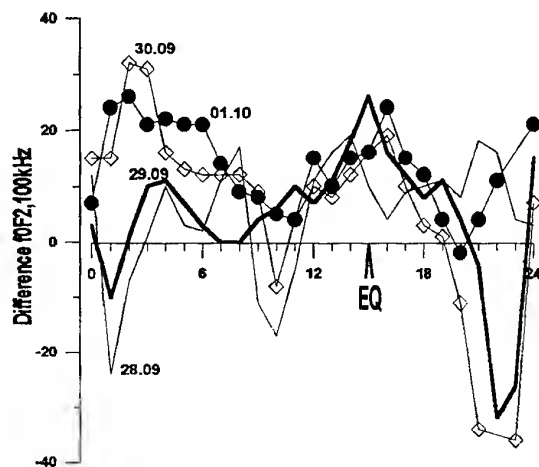


FIG.2. The difference of foF2 for four days before the earthquake. It is seen very well the premidnight MIN (deviation more than 3 MHz) for 29-30.09 and presunrise MAX 1-2 days before. The ALOUETTE data also show deep plasma trough at 22 LT.

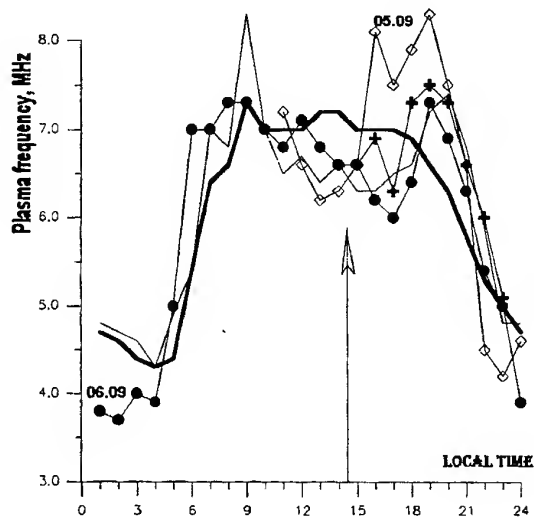


FIG.3. Daily variation and premidnight MAX of foF2 before the midlatitude Wakkanai earthquake. Thick line is month median.

Without going into details we make a conclusion that definite effect is seen in morning and evening hours consisting in "disturbed" foF2 values relatively to month median foF2 values as to the first earthquake. Besides, as the distance between epicenter and ionosonde increase this difference is less pronounced. The opposite reaction is seen in Fig.3 (premidnight MAX) in the case of the second earthquake: foF2 values before the event are larger than median. The same result was obtained in [8] by means of ionospheric data Milcovo ($L=1.71$) situated not far from Wakkai ($L=1.43$) to North, but for another earthquake of the same magnitude ($M=7.3$). Thus, we have some reasons to conclude that earthquake epicenter location play an important role as to differences in electron concentration modification over the preparation zone. So, one can observe electron concentration reduction instead of midlatitude enhance (see Milcovo and Wakkai events) in the case of equatorial earthquake.

3. SEISMOIONOSPHERIC VLF-EFFECTS IN CONJUGATED HEMISPHERES

It was shown [5] that the onboard satellite registrations of the VLF-ELF noise in ionosphere permits detection of the spatial-temporary behavior of the zone dimensions where the intensive low frequency bursts (over epicentral region) were observed. The reliability of this observed precursor effect was estimated on the basis of experimental data to be about 85 to 90%. The appearance of low frequency noises (emissions), so-called "noise belts" in the upper ionosphere was associated with the longitudinal drift of the energetic seismo-particle of the inner radiation belt.

The high conductivity along geomagnetic field line provides hard electromagnetic coupling of conjugate ionosphere regions of both hemispheres and ionosphere disturbances over the earthquake preparation region (or precursors) have to form their definite images in magnetically conjugate region. INTERCOSMOS-18 and ALOUETTE satellites data were analyzed from this point of view. Conjugate earthquakes precursors were found in very low frequency (VLF) emission and F2 peak plasma parameters [6].

It is necessary to note that the VLF signals measured on satellite board (500-1000 km) are characterized by so large amplitudes (comparable with the same band burst amplitudes measured on the Earth's surface) that they can't be assumed as a consequence of originated on the Earth's surface signals propagation.

We have showed [6] that aforesaid signals observed inside the centered around the epicenter of the future earthquake longitudinal "belt" were followed by ones existing in the magnetically conjugate (to the satellite orbit) region in the opposite hemisphere. They are in turn also localized inside the

longitudinal "belt" which, as it became clear, is a projection of the VLF precursor zone surrounding the epicenter on the appropriate magnetic field line ($L=1.5-1.75$).

We also succeeded in detection of energetic particles corresponding bursts registered on board of the same satellite appeared to be to a large extent correlated with VLF bursts both in their shape and localization.

The aforesaid facts, namely:

- high signal magnitude in the vicinity of the satellite;
- longitudinal extent, or 'belt-like' structure centered around epicenter;
- good magnetic conjugation with signals measured at the opposite hemisphere;
- conjugated VLF signals magnitudes comparability;
- high degree of VLF bursts correlation with energetic particles flux bursts

allows to confirm that VLF earthquake precursors discovered more than 15 years ago [5] and so far intensively studied source is the anomalous fluxes of energetic particles originated in the epicentral (preparation) zone. The hypothesis was proposed even in [5] and were studied from the theoretical point of view in details latter.

Nevertheless we succeeded in finding of new experimental convincing evidence of the leading role of energetic particles in VLF earthquake precursor generation. Taking in mind the above mentioned we can propose some topology model of VLF-precursors in nearest Earth space. The description of our VLF space earthquake precursor model is as follows:

Originated above epicentral zone anomalous energetic particles fluxes reflect from the mirror magnetically conjugate points (for $L=1.5-1.75$) and drift in longitudinal direction making VLF signal "belts" (due to beam-plasma interaction). So, the VLF-belts are caused by energetic particles (during anomalous fluxes) and ionospheric plasma interaction in the vicinity of flying satellites. Thus, the precursors global volume appears (in space: ionosphere-magnetosphere) as cupola-shaped shell (which is defined by geomagnetic field line topology) and symmetric one relatively to geomagnetic equator. The highest shell (cupola) points are elongated in east-west direction above the magnetic equator. Such a cupola props up on longitudinally extended "belts" where intensive VLF precursors are generated, one of the "belts" being without fail centered around the future earthquake epicenter.

So, such type of precursor can be very sensitive to geographic position of future earthquake epicenter and status of geomagnetic activity.

4. CONCLUSIONS

Taking into account everything of above mentioned it is not surprisingly that investigations of different ionospheric plasma precursor images and

space VLF seismo-emission show the remarkable peculiarities which depend on geographical location of earthquakes epicentre (equatorial or midlatitude event).

The first kind of precursors are nocturnal ionospheric anomalies in plasma density distribution which appear over the earthquake preparation region some days before the main shock of the earthquake and can be caused by local changes of the electrical parameters of the spherical condenser (capacitor) formed by the two high conductive shells: Earth's surface and lowest ionosphere plasma boundary. It is shown that such variations of the atmosphere electricity cause appropriate electric field at the ionospheric heights, which being added to existing natural field may both increase or decrease its action on the ionospheric plasma characteristics: drifts, aeronomy, plasma chemistry, ion composition etc. Anomalous variations appear inside whole ionosphere volume from the lowest boundary of Earth's plasma shell (80-100 km) up to 1000km and higher. Under fortunate coincidence precursor electric field can generate natural phenomena, 'fountain-effect' for example [7] leading to Appleton anomaly in the equatorial ionosphere over future earthquake position. Estimation of electric field magnitude necessary to generate observing event was made. It was shown that the electric field less than one mV/m must be generated in the ionosphere.

The second type of precursors are VLF emission registered by satellites at the height range of 500-1000km. Electromagnetic emission (radiation) anomalies are concentrated in longitude-aligned belt orientated along the geomagnetic shell passed over the future earthquake epicenter. It is shown that during a satellite crossing this 'noise' belt the VLF bursts and correlated in time and space energetic particles flux bursts could be registered not only over the preparation zone but also in magnetically-conjugated region [6]. If a satellite intersect the corresponding magnetic shell to the epicenter at the too large heights in the magnetosphere then only the anomalous energetic particles fluxes alone will be registered (monitored). In the intermediate height range and as well over and under this magnetic shell ('cupola' above the geomagnetic equator) weak VLF radiation can be registered due to both processes: generation and propagation. The wideness of belt or latitudinal size R define by simple relation ($R = \exp M$) with magnitude M of future earthquake. So, it may be assumed as parameter for prediction the danger of earthquake or its power.

There are a lot of separate information concerning precursor type anomalies in energetic particles fluxes, but so far there is no complete theory of this event. This fact confirm the lithosphere-ionosphere-magnetosphere interrelation mechanism complexity before the earthquake. It also pointed out to further experimental data accumulation validity, model and theoretical conception development, and,

possibly, organized aimed monitoring of plasma anomalies on the satellite orbits.

5. REFERENCE:

1. Liperovsky V.A., Pokhotelov O.A., Shalimov S.L. *Ionospheric earthquake precursors*. Moscow. Nauka. 1992. 304 p.
2. Oraevsky V.N., Ruzhin Yu.Ya., Depueva A.Kh. Seismoionospheric Precursors and Atmospheric Electricity. *Turkish J. of Physics*, 1994.V. 18. N.11. P.1199-1204.
3. Ruzhin Yu.Ya. and Depueva A.Kh. Seismoprecursors in Space as Plasma and Wave Anomalies. *J.Atmosph.Electr.* 1996 . V.16. N3. P.251-288.
4. Ruzhin Yu.Ya. and Depueva A.Kh. Preseismic Response of Earth Space Environment. *Proceed.of London Marelec '97 Conference*, 1997. N4.2, 5P.
5. Larkina V.I., Migulin V.V., Nalivaiko A.V. et al. Observation Onboard the "Intercosmos 19" Satellite of VLF Emissions Assosiated with Seismic Activity // *Geomagn. i Aeronom.* 1983. V.23, N 5. PP. 842-845
6. Ruzhin Yu.Ya., Larkina V.I. Magnetic Conjunction and Time Coherency of Seismoionosphere VLF Bursts and Energetic Particles. *Proceed.13th Wroclaw EMC Symposium (URSI)* , 1996. PP.645-648
7. Depueva A.Kh., Ruzhin Yu.Ya. Seismoionospheric Fountain-Effect as Analogue of Active Space Experiment. *Adv. Space Res.* 1995. V.15. N12. PP.(12)151-(12)154.
8. Depuev V., Zelenova T. Electron Density Profile Changes in a Pre-earthquake Period. *Adv. Space Res.* 1996. V.18. N6. PP.(6)115-(6)118.

BIOGRAPHICAL NOTES

Ruzhin Yury, Male, Age 54, M.S. of Kazan University in 1970, Ph.D (1980) and D.S. (1992) of Institute of Geomagnetism, Ionosphere and Radiowave Propagation , Vice-Director of IZMIRAN Division. Fields: Space Plasma Physics, Active Space Experiments and Space Seismoprecursors.

A.Kh.Depueva graduated from Moscow Power Institute, she is Candidate of Science. Her scientific interests are ionosphere and ionospheric inhomogeneities.

THE ANOMALY INTERFERENCE OF MF BROADCAST SIGNALS IN THE VLF RECEIVERS BY LUXEMBURG EFFECTS OF IONOSPHERE AS ONE OF THE SEISMOGENIC PHENOMENA

Takeo Yoshino and Masashi Ohtsuka
Fukui University of Technology
3-6-1 Gakuen, Fukui 910, Japan.
(Tel/Fax: +81-33397-5577)
e-mail: yoshinot@nisiq.net

Abstracts:

Today, the most observatories of seismogenic emissions to purpose of earthquake prediction are used below VLF frequency range in the world. But usually natural and man-made noise levels of ELF, VLF and LF frequency ranges had been increased gradually entire the earth after 1990. And the detection for earthquake prediction signals (so called seismogenic emission) is becomes to impossible for the difficulties of separation of seismogenic signals and other noises under the low S/N ratio. The authors are started an experiment of the modulation signals of MF broadcast stations are able to receive by the VLF receivers as interference signal prior to earthquakes. This phenomena will be able to explain by the effect of anomaly electromagnetic modulation of disturbance of E or F layers of ionosphere by MF broadcast station signal of the Luxemburg effects above epicenter area. The last December 22nd, 1997 at 22:10 JST, a earthquake ($M = 4.6$, $D=10\text{km}$) was generated at sea bottom of north of Awara observation point of Fukui Univ. of Tech., were frequently detected anomalous BC signals between one day before and few minuits before the shock without any impulsive noise signal interference.

1. INTRODUCTION

The author had been moved my position from a professor of University of Electro-Communications to Fukui University of Technology at April in 1996, for my retirement of UEC by the age limit. The Fukui University of Technology is one of the private university and the location is in the Fukui city, about 600km by railway of northwest of Tokyo.

The Author is building the latest research and the observation facility for the space science and the seismogenic electromagnetic emissions (SEE) research. The location of facility is in Awara town of the northern Fukui prefecture. The back ground noise levels through VLF to MF range around this observatory is one of the most quite area in Honshu island rank with former Sugadaira observatory of Univ. of Electro-Communications. The facility buildings are set on the island in the large Kitakata Lagoon.

Today, the almost observatories of SEE to purpose of earthquake predictions in the world are observed below VLF frequency ranges. But, since 1990, the average back ground natural and man-made noise levels over the earth were increased around 10 dB or more higher than 1980 decade, and to obtain the clear signal for the detection of very weak signals of SEE is became to impossible by the difficulties of the separation betteeen seismogenic signals and other noises.

The last December 22nd, in 1997 at 22:09 JST, the earthquake ($M = 4.6$, Depth = 10 km) were generated at sea bottom of northern off shore of Fukui prefecture. the distance between epicenter and our observatory of Awara is approximately 50 km, and the VLF observation sensor detected anomalous BC signals clearly between two days before and until few minutes before the main shock, without any disturbance of impulsive noise interference

We were started an experiment and an investigation of the source mechanism about modulation interference signal of MF broadcasting stations could be detected by VLF receivers as cross-talked type interferens just prior to earthquake. This phenomena will be able to explain as the effect of may-be similar to "luxembourg" phenomena on the top of the earth-

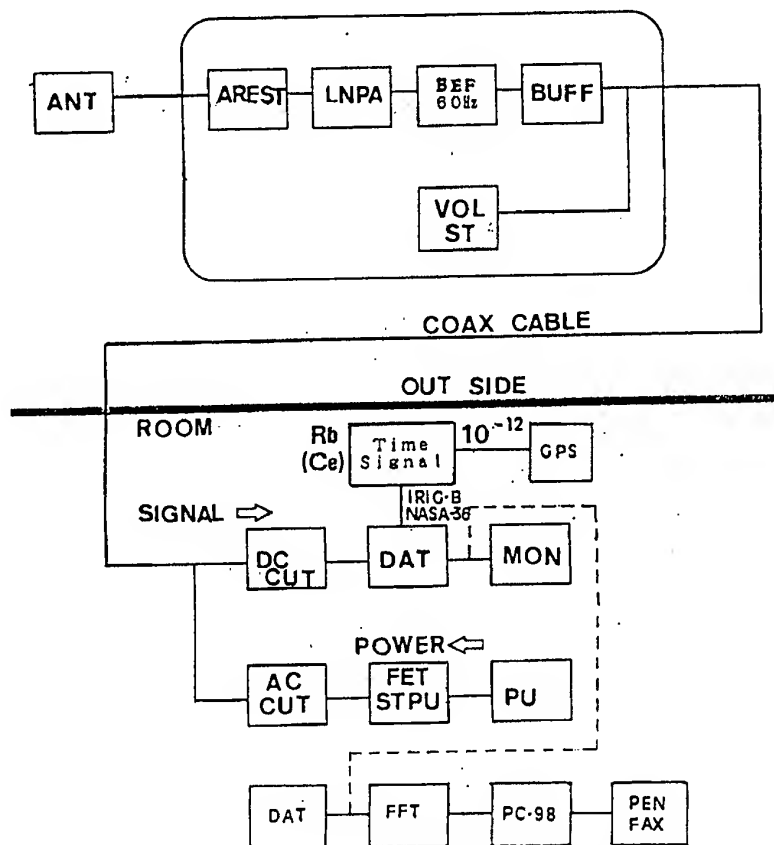


Fig. 1. A Block diagram of VLF wave receiver built at Awara obs.

quake epicenter area, which is generated by the anomaly electromagnetic modulation of electron density disturbance in E and lower of F layers according to the AM modulation energy of the broadcast.

2. New observation facility of Awara

Fig. 1 shows a block diagram of our new observation facilities. The original purpose of this facility is a routine observation for the plasma wave and whistler wave phenomena in the magnetosphere, but, of course, it will be useful to use as the detector of observation for electron density disturbance related by the earthquake effects in the ionosphere. The sensor is consisted of a large one-turn delta loop antenna with an electrostatic shield, and this size is 20 meter high, 39 meter width and 351 square meter area as shown in Fig. 2. The effective heights of this loop is 4 cm at 10 kHz. The impedance matching characteristics for receiving frequency of this antenna is almost flat from 15 Hz to 1 MHz, and we can take out any desirable observation frequency in this range, and now we connected the lower band circuit between 10 Hz and 20 kHz.

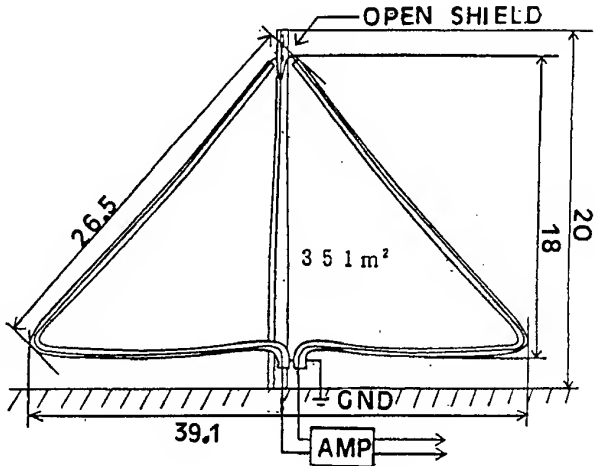


Fig. 2. An antenna of Awara observatory.

A Rubidium and Cecium atomic time standard clock and time code generator with time comparator of GPS satellite are used to the time standard system for this observatory. Then the accuracy of time stability are always kept to 1 pico seconds. Two time code signals that is IRIG-B and NASA 36 Bits are supplied from this time code generator.

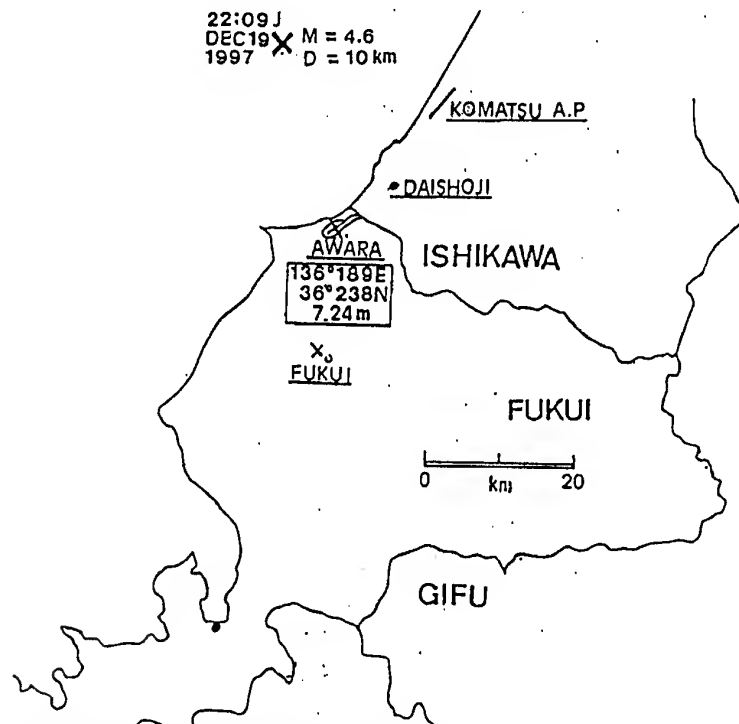


Fig. 3. The position of Awara observation point and the location of epicenter of the earthquake at 22:09 JST of December 19th in 1997.

3. The MF broadcast signal cross-talk observed at Awara obs.

In December 19th, 1997, at 22:09 J (JST), an earthquake (M = .4.6, Depth = 10 km) attacked an areas of northern Fukui and southern Ishikawa prefectures. The location of Awara observation point and the epicenter of this earthquake are as shown in Fig. 3. About 5 hours prior to this earthquake, the VLF receiver of Awara observatory had registered the quite strange cross-talked audio voice and music signals of several MF broadcast

stations in the 50 km of northeastern area. The level of interference was increased gradually until the level to cirtificate the contents of several MF broadcasting stations in Kanazawa area and erased them after 10 minutes of main shock as shown in Fig. 4. The frequencies and transmission power of these stations are 1107 kHz 5kw, 1224 kHz 10kw and 1386 kHz 10kw.

As the primary stage of research about such phenomena, the author made following two scenarios such as;

[1] The receiving field intensity of

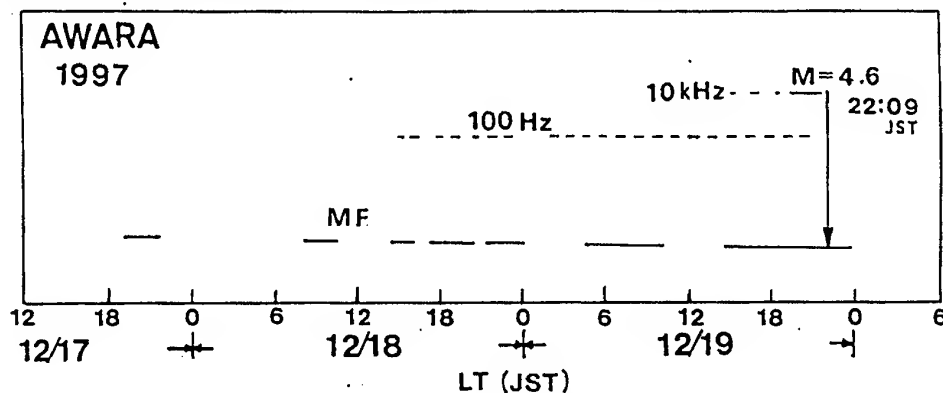


Fig. 4. The time of appeared the cross-talk signal of MF broadcast stations observed at Awara of the earthquake of December 19th in 1997. Black line shows the duration of cross-talk appearance, and the dotted line shows the time of back ground noise level.

the MF broadcasting station when they reflect at E layer is amplified to anomalous levels by the electron densities disturbances on the top of epicenter area of the earthquake during precursor. And the stronger field of the MF signals penetrated into the VLF receiving equipment will be demodulated at the nonlinear portions of some circuits. Although this recent scenario is becomes to popular, but this explanation included many difficulties for reasonable theoretical analysis.

[2] The radio wave of MF broadcasting stations are radiated from antenna on the ground, and a portion of transmitted power will be influenced to the intensity modulation of the electron densities in accordance with the contents of AM signals in the E and the lower portions of F layer of ionosphere. When the SEE electromagnetic wave is generated at this disturbed electron density regions, the VLF receiver will be received this AM modulated SEE wave. The audio output of this receiver will be contained of cross-talked signals according to the modulation of the broadcast stations. This is famed as "Luxembourg" effect.

At the start of the radio broadcasting by the LF band in the early 1920, when the french or belgium listeners wish to receive the german stations signal which was reflected at the ionosphere on the top of Luxembourg, they were suffered by a strong cross-talked signals of Luxembourg station was mixed in the german signal in spite of the different frequencies each other. But, today, the frequency of usually Broadcast stations were shifted from LF to MF band and this effects is reduced by the improvement of vertical radiation pattern of broadcast antennas as the Anti-fading antenna.

Although in the past intermodulate signal received at just prior to earthquake at Awara is impossible to an explaination perfectly as Luxembourg effect, the VLF SEE signal are modulated by electron density disturbance of ionosphere at they generate on the top area of epicenter area. The epicenter area in the past earthquake at offshore of Ishikawa is located about 50 to 60 km from transmitting antenna of BC station in Kanazawa city. This is just distance which reached to the transmitting power of the first high angle lobe of the vertical radiation pattern of usually BC anti-fading antenna. The reasonable transmission power reached to the lower ionosphere and the electron density will be able to modulate on the top area of epicenter of ionosphere [Yoshino et.al. 1993].

If this explanation process is correct, the SEE observatories by using ELF, VLF and LF bands which are suffering by the decline of the SEE detection levels to the rise of the threshold level of natural and man-made background noise since 1990, have produced by the new detection system without the effects of noise level increasing using the modified Luxembourg phenomena.

The Author and the research group will studies this effect by using the data obtained at Awara, to progress the investigate of the generation mechanism and to progress of the possibility of SEE detection systems without the rise of noise level.

4. The observation the HF fading characteristics related the earthquake

The Author is planning the build of a new research system for the HF dopplar phenomena observation which observed to an ionospheric responce according to the change of plasma waves at the magnetospheric region by means of the fading characteristics variation. Then we are building the HF multi-direction fading characteristics observation facility in the Awara campus. By this equipments, it seems to effected of possibility the HF fading characteristics variation against the effected to critically on the propagation mode of internal gravity waves of earthquake phenomena. If this idea is correct, we have to be a new possibilities about an ionospheric responce by an earthquake phenomena which have the different style of research such as above mentioned "Luxembourg" phenomena.

This observation system for Awara observatory is consisted of the eight or more receivers tuned to HF stable transmission stations of the radio navigation signals from radiusly to eight different directions as shown in Fig. 6. And the levels of AGC voltages of each receivers will be recorded as the timely variations of electron densities of the ionosphere along the wave propagation path by the detect of the fading characteristics of each directions..

Although, this equipment is not complete at today by the financial problem. As an example of observation results of HF fading characteristics at November 16th in 1997 obtained at the pretest of this system at Awara observatory is as shown in Fig. 7. For this observation, we are building a receiving system for the several different HF frequencies and we also are planning the build of two points with several 10km separation distance

interferometer system in near future. This research has one of the great expectation item for us in future.

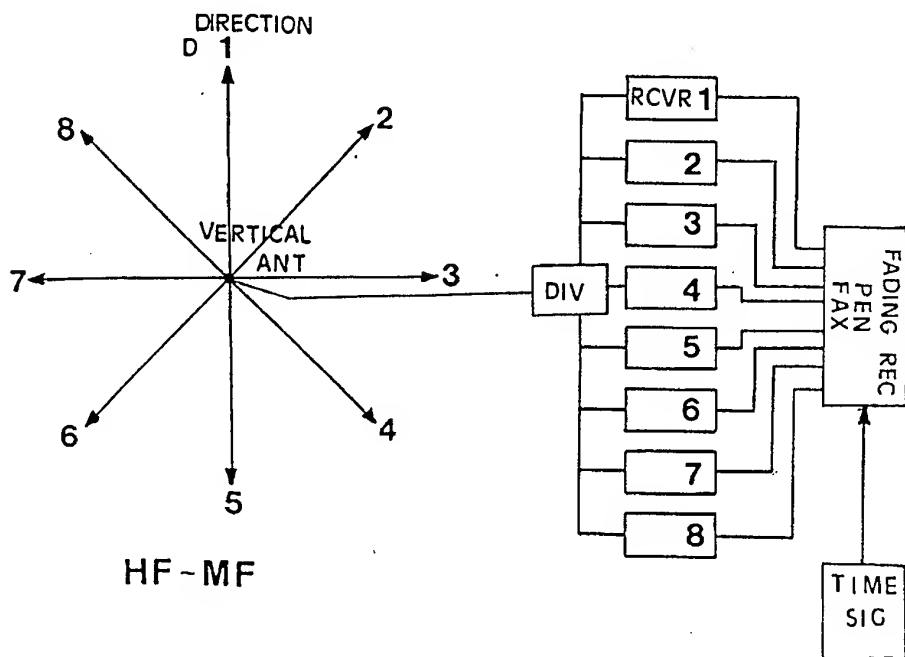


Fig. 5. HF fading characteristics observation equipment with 8 directional receivers under construction at Awara.

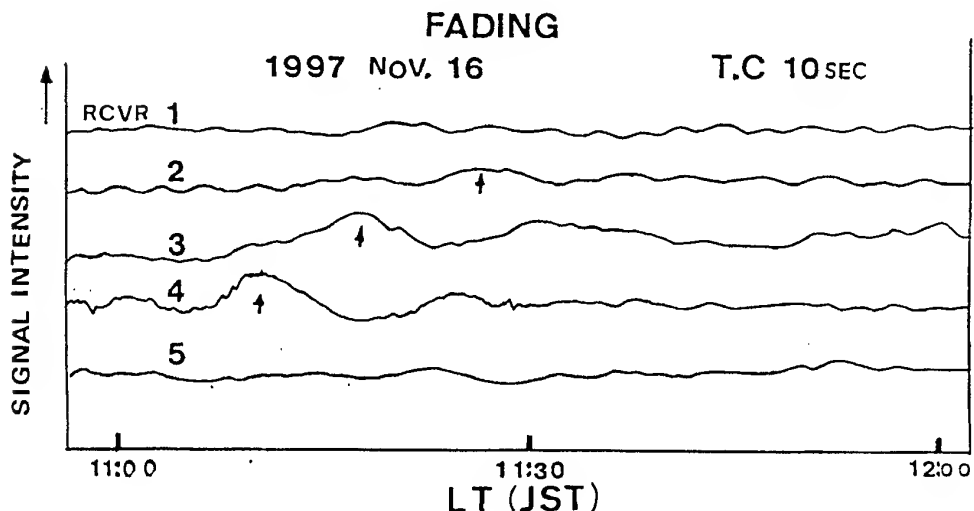


Fig. 6. A example of HF fading observed at Awara during a testing time.

6. Conclusion

The observation that the authors group started at Awara campus as one of the pioneer works in the world is as follows;

(1) By the "Luxembourg" effects that the electron density variation in the ionosphere are modulated according to the contents of the AM sideband modulation by the MF broadcasting station which transmitted from an antenna on the ground, are received as the cross

talk signal at the VLF receiving site. This cross-talk signal were received at Awara observation point as a prior to earthquake of off-shore of Ishikawa prefecture on February 19th in 1997. Today, the investigation of the phenomena of this crosstalk signal of MF broadcast station were received by the VLF receiver, is only stand on the starting line. At the Awara observation point will continue this research until the build up of the effective observation system of the earthquakes prediction to obtain the advance points of this cross-talk phenomena against the groval increasing of the strong level of natural and man-made noise in the ELF, VLF and LF bands. Also, we will continue the observation and investigation to obtain the physical mechanism of the details of this phenomena by using the observation data of Awara.

(2) At Awara observation point will extend the research of co-relation between the earthquakes and HF fading characteristics, the investigate of the physical effects of the electromagnetic earthquake precursor phenomena influenced to the ionosphere. And the author wishes progress to the investigation about the strong emission of HF band noise generation observed as Hyogo-ken Nambu earthquake (Kobe earthquake) [Maeda et.al 1996], [Yoshino 1996a, and 1996b] and the anomaly propagation characteristics on the VHF-FM wave, prior to earthquake observed at southern Yatsugatake observatory [Kushida 1997].

References

- Kushida.Y.,(1997) "Observation of earthquake prediction of plasma density variation in the ionosphere", 1997 the transaction on the Japan Earth and Planetary Science Joint Meeting; G12-P03, 434, 1997.(Japanese)
- Maeda.K., N.Tokimasa,(1996) "Decametric radiation at the time of the Hyogo-Ken Nanbu earthquake near Kobe in 1995". Geophys. Res. Lett.,23, 2433.
- Yoshino.T., I.Tomizawa, T.Sugimoto, (1993) "The results of statistical analysis of seismogenic emissions as precursors to the earthquake and volcanic eruptions", Phys. of the Earth and Planetary Interiors, 77, 21-31.
- Yoshino,T.(1996a)"Energy transmission from focus to epicenter and radiation mechanisms at epicenter for seismogenic emission",13th Wroclaw Sympo. on EMC, 13, 649-653.
- Yoshino,T. (1996b)"The anomaly higher frequency seismogenic missions observed at "Kobe earthquake",13th Wroclaw Sympo. on EMC, 13, 654-658.

XIV

**SPECTRUM MANAGEMENT,
ENGINEERING, SHARING
AND MONITORING**

MANAGEMENT OF THE RADIO FREQUENCY SPECTRUM: TOWARDS STRUCTURED APPROACHES FOR NATIONAL AND INTERNATIONAL POLICY

Ronald Hes and Daniëlle Wille

Delft University of Technology, Faculty of Systems Engineering and Policy Analysis
PO Box 5015, 2600 GA Delft, Netherlands

Jan Gerrit Schuurman

University of Maastricht, Section of Cognitive Psychology, PO Box 616, 6200 MD Maastricht
CICT, Faculty of Mathematics and Physics, University of Amsterdam, Netherlands

ABSTRACT

As radio frequencies are becoming a scarce resource, governments are redesigning their national assignment policies. Next to technical(EMC-) criteria, also economical, social and cultural aspects are being integrated in the process. This paper argues that international spectrum allocation must follow these changes, aiming at new procedures that are both flexible in time and acceptable to the community of spectrum users at large. Meeting these criteria is possible if the spectrum is no longer regarded as a 'common resource' but rather as an 'open resource'. Open resource allocation methods promise to solve the problems inherent in the established methods.

1. REGULATING THE RADIO SPECTRUM: ASSIGNMENT AND ALLOCATION

This paper discusses how the use of the radio spectrum is currently regulated. Two levels of regulation will be distinguished here: *assignment* of the radio spectrum, which is the responsibility of individual nations, and *allocation*, the designation of parts of the spectrum for certain types of use at an international level. Instead of approaching spectrum management as a strictly technical or EMC-problem, we treat it as a public policy issue with a strong technical dimension. The public character of this problem stems from the properties of the radio spectrum as a 'global common' and, at the national level, as a 'public good'. [1][2] Historically, the role of governments has been primarily to prevent unwanted interferences, often with the specific aim to protect military and emergency services. As the use of the spectrum increased, especially for broadcasting and telecommunications purposes, other than technical (EMC-) considerations had to be considered: the economic value of spectrum became apparent, as well as the importance of controlling the content of the transmitted messages. This prompted

governments to distribute the benefits derived from the radio spectrum between private and public interests. Consequently political, social and cultural issues have entered the process of spectrum distribution.

In our description of the policy process we assume the following structure: 1. definition of goals, 2. formulating policy options, 3. evaluating options, 4. implementation and, 5. measuring of effects and feedback. The increasing demand for spectrum urges national regulators in many countries, acting at the operational level, to implement new policies for spectrum assignment. We note, on the other hand, that international spectrum management is still in the policy formulation stage: options are being explored for strategic changes in the allocation process, which are to be applied on medium to long term.

In this paper we investigate the first three stages in the policy process: which goals should be achieved, what are the proposed and applied policy options, both at national and international levels, and against which criteria can these be systematically evaluated? We have chosen the perspective of national governments, which play a pivotal role in spectrum assignment, by co-ordinating the national spectrum policy, either directly or by means of an independent regulatory body, and in international spectrum allocation, by assembling delegations for various gremia.

2. ASSIGNMENT OF THE RADIO SPECTRUM

First we discuss the assignment of spectrum at a national level. It was noted that initially frequency assignment policies were rather straightforward. There was no shortage of required frequencies, and therefore most frequency requests could be granted.

The main goal of frequency assignment was to promote the public interest, as perceived by the government. There were basically two important methods (or options) for frequency assignment: *priority rights* and '*first come, first served*'.¹

Because of the relatively simple goal, few different issues were considered when evaluating frequency assignment options. Those considerations were mainly of a technical and administrative-legal nature.

Technical considerations:

- prevention of interference

Administrative-legal considerations:

- minimizing assignment costs;
- achieving some degree of social acceptability. Because of the public interest goal, legitimacy of policy was needed. In practice this meant reaching agreement with the few parties involved in frequency assignment.

Having sketched the methods and criteria in use for spectrum assignment, we turn to the question how these have developed in a changing environment, where demand for spectrum has become much higher and more diverse.

3. SETTING GOALS FOR SPECTRUM ASSIGNMENT: AN INTEGRATED APPROACH

Established national frequency assignment policies have lately been criticized for two main reasons. Firstly, most applied policies have been, or still are, far from transparent. Secondly, frequency scarcity has rapidly become an important issue. Due to many developments, in particular the growth of mobile telecommunications, the demand for certain frequencies has exceeded the supply by far.

To increase the *supply* of frequencies is an EMC problem: this can for instance be achieved by enabling the use of higher frequencies, or by developing more efficient frequency sharing technologies. It is noteworthy that, from the engineering point of view, the emphasis shifts from merely preventing interference to the design of more efficient uses of bandwidth.

To limit the *demand* for frequencies, however, assignment policies can be used. This possibility to

alleviate the pressure on the spectrum through assignment policies, has raised the interest in new options, the *public tender* and the *auction*.

The *public tender*, also known as the 'beauty contest', became of interest when spectrum scarcity occurred. Theoretically, this can be considered a market based approach to spectrum management, but in practice it may not work out, since the evaluation of competitive proposals can be based on highly subjective criteria. Currently, because of the economically oriented approach to spectrum management, the *auction* is a popular policy instrument. Several countries have recently used the auction to assign frequencies.

With the demand for frequencies exceeding supply, several other, mostly economic considerations became important in frequency assignment [3]:

- economically efficient use of spectrum (assigning bands to those who value them most)
- stimulation of competition
- generation of financial revenues for government
- restriction of influence on consumer tariffs (governments do not stimulate a raise in consumer tariffs, because this harms the public)

It is striking that the evaluation of several options for frequency assignment still is quite imbalanced. Where initially some technical, and administrative-legal issues were considered, now the economic issues predominate.

We promote a more integrated approach to frequency assignment in which, additional to the technical, economic and administrative-legal issues already mentioned, the following issues are also considered.

Administrative-legal considerations (additional):

- minimizing transition problems;
- predictability of policies/legal security;
- transparency to parties involved.

Technical considerations (additional):

- technical dynamics, e.g. when a new technology is introduced, spectrum is reserved for parallel use of both old and new technology;
- technically efficient use of spectrum.²

It can be observed that the early methods for frequency assignment meet with most of the administrative-legal considerations, whereas the use of auctions meets with most of the economic considerations. For a more elaborate approach on this see [3].

¹ Frequencies can be used for a great variety of purposes, which can generally be divided into four categories: i) state security use and defense, ii) commercial use, iii) broadcasting, and iv) miscellaneous. Priority rights were often used for frequency assignment to state security and defense services, whereas 'first come, first served' was used for other assignments.

² Although technically efficient use is considered important in many countries, solid definitions appear to lack. See for an EMC-related approach [4].

We argue here that the assignment process, and its design, should ideally address most of the criteria. To achieve such an integral approach to frequency assignment just choosing between 'first come, first served', or (a specific design of) auctions will not be sufficient.

First of all, the interference and technical dynamics considerations need to be considered prior to the actual assignment. Secondly, the economic and administrative-legal considerations have to be dealt with in the assignment process. This goes beyond choosing an assignment method. Necessary to accomplish a balanced integral approach are, for instance, specific licence conditions that go with the assignment, and special rules for specific market players (like former monopolists).

The successful auction of PCS-frequencies in the USA illustrates this point. [5] This success should partly be credited to: i) the 10 year licence term, long enough to stimulate investments by licence owners, but also flexible enough to enable future modifications of assignment policies, ii) network build-out requirements, which assure a rapid service delivery to the public, iii) spectrum caps for cellular licence owners, to prevent them from acquiring spectrum for anti-competitive purposes, and to promote a great diversity of licence owners.

Thirdly, the technically efficient use of spectrum can only be measured during the actual use of the spectrum, i.e. after the assignment. To enforce technically efficient use of the spectrum, it is possible to charge a fee to spectrum users: the more efficient the use of the spectrum, the smaller the fee. The possibility of such regulatory control after the assignment, in the feedback stage, is often neglected.

Resuming, successful spectrum management is more likely if the complete range of aspects is taken into account, and all steps in the assignment process are being considered.

4. ALLOCATING THE RADIO SPECTRUM IN A CHANGING ENVIRONMENT

While the approaches to *assignment* of spectrum at the national level are rapidly being adapted to the changing environment, certain boundary conditions will, at least in the near future, still be determined by the *allocation* of spectrum through international institutions. As the flexibility of assignment mechanisms increases, the need for more versatile international allocation schemes also becomes more explicit.

An obvious need for *international* management of the radio spectrum comes from the fact that radio waves travel across national borders or even between different continents. The role of the radio spectrum as 'fuel' or 'resource' for global telecommunications should also be emphasised. The demand for spectrum is growing dramatically, in particular because of the fast technical progress in mobile communications coupled with the opening of deregulated and liberalised telecommunications markets. Access to spectrum across national borders will be a key factor for participation in the future world economy. Investments in world wide mobile communications satellite systems reveal the monetary value of the spectrum: the most ambitious plan so far, the Celestri system announced by Motorola Inc. in the summer of 1997, involves an investment of no less than \$13 billion. [6]

Traditionally, the allocation of radio spectrum has been a task of the International Telecommunication Union (ITU). In the early years of this organisations' history the approach to spectrum issues was clear-cut: preventing interference was the main objectives of establishing the International Telegraphy Union in 1865, converted into the ITU in 1932. Allocations of spectrum have traditionally, and formally, been the outcome of lengthy negotiations among delegates from nation states at the World Radio Conferences (WRC). With increasing scarcity of the spectrum, these negotiations have become extremely complex and politically charged. The current path towards decision-making is such that smaller interest groups may find themselves disabled in defending their interest in spectrum, while industrial consortia backed by powerful investors seem to become more influential. To speak with Lee (1996), inequality has become institutionalised in the current system. [7] Moreover, the process of negotiations towards consensus decisions, is far too slow to respond to the continuous introduction of new technologies and services with decreasing time-to-market and the accompanying demand for rapid allocation of spectral bands. The unsatisfactory outcome of this situation is the emergence of parallel processes, e.g. in other gremia like the World Trade Organisation. This entails the risk that more influential spectrum users circumvent the negotiations with less influential parties. [8]

To illustrate the nature of conflicts over spectrum, we refer to two recent cases. Several world-wide networks of non-geostationary satellites will soon be established, either for mobile telephone services, or for wireless broadband and multimedia services. These new systems, backed by large industrial consortia, have been allocated considerable blocks

of radio spectrum, some in already congested bands, e.g. around 1.6 GHz. Harmful interference is expected by other spectrum users who have vested interests in these bands. Scientific use of these frequencies by radio astronomers e.g., is projected to be seriously hampered, leading this small non-commercial user group to protest vigorously. [9] Likewise, at the most recent WRC a conflict surfaced between the vested interests of transmissions from geostationary satellites and the proposed plans for new mobile satellite systems. [10]

Essential is that, while in principle these problems have a technical (EMC-) origin, their resolution cannot be achieved by a technical approach only. The broader 'design requirements' we derived for spectrum management can be summarized as acceptability and flexibility. The first refers to the achievement of solutions that maximise benefits to the user community as a whole, the second to the necessary adaptivity to a rapidly changing environment.

Several proposals have been made to address these problems facing international policy. Two approaches for reform of the current allocation are:

- recurrent re-definitions of (away from traditional service separation);
- enforcing the jurisdiction of the international institutions, in particular the ITU.

These two options may fail to meet the requirements because they are still rooted in a traditional approach to *common-resource* allocation, with characteristics:

- a well defined institutional structure, with one authority holding the management rights;
- well defined user-groups who obtain user-rights from the distributor;
- a division of the radio spectrum into distinct spectral bands.

The traditional methods provide rigid answers to the questions: who, to whom, what?³ In the last part of this paper we argue, referring to developments in spectrum assignment policies, that a long-term solution to international spectrum allocation needs to address these three questions in an integrated way.

5. POLICY OPTIONS FOR THE FUTURE: TOWARDS STRATEGIC SOLUTIONS

As the established schemes for spectrum distribution fail to work in the presence of

increasing demand for frequencies and conflicts among user groups, adaptations have been made, like the introduction of market mechanisms. These shift the authority away from the central institutions, towards the users themselves. Government control in the process to achieve certain policy goals can be enhanced by modifying the design of the methods, e.g. provisions for applicants from minority groups in the PCS-auctions in the United States. [12]

Limitations inherent in the traditional methods, however, urge for solutions which are fundamentally different in the way they address the three mentioned characteristics. Such options consider the spectrum as an *open-access resource*. It is essential that in these proposals members of the user-community determine the access to spectrum themselves, abandoning for a large part the existing institutional structures and traditions.

Sketches of such new paradigms have been presented by e.g. Struzak and Noam. [11,13] The essence of these approaches is their self-regulatory nature. Roughly the new approaches can be classified as:

- open access solutions;
- open access coupled with price mechanisms.

Struzak sketches a network of coupled computers with a world-wide spectrum allocation system, somewhat comparable to the current system for airflight-ticket reservations. [14] Users would book the needed spectrum, whereby the allocation would be done on strictly technical (EMC-) criteria, independent of the user or the message content. Ultimately this would render the current administrative procedures superfluous. Control of the actual spectrum use, by monitoring stations, is a key element of this proposal. Such a system would certainly overthrow the traditional methods with central authority, fixed user groups and rigid slicing of the spectrum. [15]

It is questionable, however, whether this would solve the problems associated with spectrum scarcity: the solution fails to address the question how the users with competing interests can all have management and user rights at the same time.

Noam (1997) presents an adaptation: open-access coupled with a price mechanism. In this system all users would have equal rights to apply for spectrum, and the access price at a given time would be determined by demand and supply. Obviously, when old allocation authorities and procedures are abandoned, some authority must be charged with the levying of access charges. Noam suggests the erection of non-governmental 'clearing houses' for

³Noam (1997) uses the expression 'licensed exclusivity' for these characteristics [11]

this purpose, where determination of access prices is done in an objective and unpolitical manner. Open-access is an extremely flexible solution, independent of a particular configuration of users or allocating authorities, independent of the functional use of the spectrum, and adaptable in time. Moreover, it is adjustable to the scale of the spectrum problem: local spectrum issues will only have to be dealt with locally and no longer need to be regulated on a larger scale than necessary. The redundancy currently present in spectrum distribution methods will be reduced.

This leaves, however, an acceptability problem because groups requiring spectrum for unprofitable, yet socially desirable, purposes may be barred due to financial limitations. Acceptability can be improved if the proceeds from the spectrum pricing are partially returned to these groups as a compensation. A different option is the a priori reservation of fractions of the spectrum. Interestingly, the system has built-in incentives for innovative use of the radio spectrum as uncongested bands will be cheap or free to use.

The promise of the new options is resource management which balances the conflicting interests of the segments of the user community. It is only by renewing the institutional structure that the necessary flexibility can be achieved, thus providing strategic solutions that facilitate global wireless networking.

6. SUMMARY

Increasing demand for radio spectrum and emerging conflicts between user groups, require that this public good is being distributed in different ways. National governments have therefore started to reform their assignment policies. Motivated by the apparent deadlock in international allocation, we argue that the reforms at national levels should be accompanied by changes in the international allocation policies. Based on the lessons learned from new assignment methods, new options should aim at an integrated approach, incorporating technical, economic, cultural and social factors.

Instead of making adjustments to the current methods, it appears a better strategy to develop fundamentally different methods in which the institutional structure is modified. Open-access methods provide a valuable framework for such a reform.

7. REFERENCES

- [1] Wijkman, P. M., 'Managing the Global Commons', in: International Organisation, Vol. 36, 1982, p. 3
- [2] Arnbak, J. C., 'Managing the radio spectrum in the new environment', in: Telecom Reform: Principles, Policies and Regulatory Practices, ed. W. Melody, CTI, Technical. Univ. of Denmark, Den Private Ingeniorfond, 1997, p. 139
- [3] Wille, D., de Bruijn, H. A., 'An integral approach to spectrum management: design requirements for frequency assignment', in: Communications and strategies, Euro CPR, Vol. 26, 1997, p. 101
- [4] Janssen, G. J. M. Arnbak, J. C., 'A theoretical model for the assessment of spectrum occupation efficiency', Delft University of Technology, Internal Report, 1996
- [5] FCC Report to Congress on Spectrum Auctions, FCC Wireless Telecommunications Bureau, 97-353, WT-Docket 97-150
- [6] Foley, T., 'New hybrid systems aim to compete with Teledesic', in: Communications Week International, Vol. 187, 1997, p. 6
- [7] Lee, K., Global Telecommunications Regulation, Pinter, London, 1996, p. 107
- [8] Molony, D., 'Does the ITU know the score?' in: Communications Week International, Vol. 196, 1996, p. 20
- [9] Thompson, A. R. et al., 'Interference and radioastronomy', in: Physics Today, Nov. 1991, p. 41
- [10] Foley, T., 'Spectrum clash looms at WRC', in: Communications Week International, Vol. 193, 1997, p. 1
- [11] Noam, E., in: Telecommunications Policy, Vol. 21, 1997, p. 461
- [12] McMillan, J., in: Telecommunications Policy, Vol. 19, 1996, p. 191
- [13] Struzak, R., in: Pacific Telecommunications Review, Vol. 18, 1996, p. 2
- [14] Struzak, R., in: Proceedings of Commsphere 97, URSI, Lausanne, 1997
- [15] Hes, R., Schuurman, J. G., 'Managing natural resources: global management of the radio frequency spectrum', Proceedings of World Multiconference on Systemics, Cybernetics and Informatics, Ed. N. Callaos, Vol. 2, 1997, p. 319

BIOGRAPHICAL NOTES

Ronald Hes is educated in physics and astronomy and obtained a Ph. D. in 1995 at Groningen State University, Netherlands. Currently he is working at Delft University. His research interest is in telecommunications, especially in resource allocation.

Daniëlle Wille graduated as electrical engineer in 1995 at Delft University. Her Ph. D.-research is on frequency assignment policy. She focuses on issues and options for an integrated approach to frequency assignment.

Jan Gerrit Schuurman is trained as psychologist and currently finishing a Ph. D. at Univ. of Maastricht on knowledge transfer by means of educational technology. He has a particular interest in educational ICT-applications.

REVIEW OF ITU SPECTRUM MANAGEMENT STUDIES

Robert J. Mayher
Chairman ITU SG 1
SMILE Associates
168 Cardamon Dr.
Edgewater Md. 21037
United States of America

Study Group 1 (Spectrum Management), of the Radiocommunication Sector of the International Telecommunication Union, is responsible for spectrum management and long term strategies for effective spectrum use. In addition the Study Group provides assistance to developing countries in cooperation with the Telecommunication Development Sector. The Study Group also studies a limited number of specific urgent Questions concerning inter-service sharing and compatibility referred to it by the Radiocommunication Assembly.

1 GENERAL

The Study Group (SG) is responsible for the overall development of principles and techniques for spectrum management. The chairman and vice-chairman of Study Group 1, except for Mr. Agrawl, were re-elected at the 97 Radio Assembly. Mr. Agrawal who served as vice-chairman of the Study Group and Chairman of Working Party 1C (monitoring) for a number of years was elected as Chairman of the Special committee on Regulatory/Procedural matters of the Radiocommunications Bureau (BR).

In 1997 the SG formed Task group1/6 to develop a new Recommendation concerning Appendix 28(S7) in coordination with Study Groups 4 & 9. The work of this Task Group is also being coordinated with other study groups concerned with coordination between their radio service and the satellite service.

The SG is investigating on an urgent basis "Economic Approaches to National Spectrum Management." The SG completed the first phase of this task and a report has been completed that answers many of the questions that were originally asked. The report describes economic approaches that promote economic, technical, and administration efficiency and can also help fund a national spectrum management system.

Task Group 1/4 (Phase 2), on 'Electronic Exchange of Spectrum Management Information" has completed a draft Radiocommunication Data Dictionary (RDD) that should serve as a guideline for future spectrum management computer systems. This was a very large task and required the cooperation of many experts.

The past period was a very successful one in which many new Recommendations and other documents were approved by the SG. The largest attendance at a meeting of Study Group 1 and its Working Parties was held in 1996. The interest in activities of spectrum management has continued to increase during this period. The requirements for improved and effective spectrum management procedures around the world continue to drive the work of the study group.

2 ORGANIZATION

The SG was organized into three Working Parties and three Task Groups during the past period.

Working Party 1A is responsible for the development of engineering principles and techniques, including computer analysis for effective spectrum management.

Working Party 1B is responsible for the studies concerning principles and techniques for spectrum sharing criteria and methods with concerned study groups. A Special Rapporteurs Group was established to complete the report on Spectrum Economics for the Radio Assembly.

Working Party 1C is responsible for all aspects of spectrum monitoring for a national spectrum management system.

The three Working Parties form an effective working structure and the SG sees no reason to change this other then to clarify the definition of the tasks for 1A and 1B where they overlap.

Task Group 1/4(Phase 1) completed its work with the adoption of a Recommendation on "Electronic Exchange of Spectrum Management Information." Task Group 1/4 (Phase 2) on the Radiocommunication Data dictionary (RDD) completed a draft Recommendation that was circulated for review by all concerned study groups and the BR.

Task Group 1/5 on "Unwanted Emissions" is continuing the work of Task Group 1/3 (Spurious Emissions) and has just begun its work to develop a Recommendation on "Out of Band Emissions and maintain or modify Satellite spurious emission limits" by the 99WRC. This will be a difficult task because of the conflict between spectrum efficiency concerns and the cost and practicality of developing hardware.

Task Group 1/6(Appendix 28(S7)) has just begun it's work and effective and timely cooperation between all concerned Study Groups is required to complete this task by the 99WRC.

3 ASSISTANCE TO COUNTRIES

The SG has continued to provide assistance to developing countries in cooperation with the ITU-D that was endorsed by the 93RA. This assistance is in the form of Recommendations, Handbooks, Reports and direct assistance.

During this period a Draft New Recommendation on "Design Guidelines for an Advanced Spectrum Management System" was approved by the SG for adoption by the 97 Radiocommunications Assembly. This Recommendation should help companies building these systems and countries buying these systems to develop or obtain the most cost-effective system in a minimum time.

Members of Study Group 1 in cooperation with the BDT continue to train countries on the use of the Basic Automated Spectrum Management System (BASMS). The BDT has also developed an improved multi-language version of BASMS in Windows (WINBASMS) with the assistance of members of Study Group 1. The first training on the use of WINBASMS was in Thailand in September 1997. The next training session is scheduled for Senegal in April 1998. Future training sessions will be in the Caribbean, Eastern Europe and the Far East

The Study Group just completed a report on "Economic Aspects of Spectrum Management" that is primarily for developing countries. This is the first report on economics of spectrum management and contains a summary of past actions as well as new information on this subject. I would appreciate comments about this report and other information that you wish to be developed on this important subject.

The Study Group has conducted studies about the requirements of developing countries in Spectrum Management in the past. The results of two CCIR/BR studies (1992 and 1993) were previously reported to Study Group 1 in Doc. 1/22 (January 1995). Since then survey information from a special meeting of SG1 and BASMS training meetings was evaluated and reported to the Study Group in July 1997. This Report describes the status of thirty-six developing countries concerning the "Functional Requirements of Spectrum management" and is contained in the 97 Radio Assembly Document 1/1001 Annex 1.

The SG previously developed an action plan to assist developing countries and is continuing to follow up on this plan. The SG is presently developing a new spectrum management booklet and a brochure describing spectrum management information available from the BR.

4 HANDBOOKS

The SG previously developed handbooks on "Monitoring" and "National Spectrum Management" that have been well used by administrations. A handbook on "Computer Aided Techniques" in Spectrum Management has just been completed. This handbook will describe the What and How of computer techniques for spectrum management. The following sections outline the report.

Chapter 1-Introduction

Chapter 2-Spectrum Management Data

Chapter 3-Computer Techniques

Chapter 4-Electronic Exchange of Information for Spectrum management

Chapter 5-Examples of Automation for spectrum management

Annex 1-Decission 119

Annex 2-Spectrum Management Data Tables

Annex 3-WINBASMS

Annex 4-Examples of ASMS Systems

5 NEW AND REVISED DOCUMENTS

A total of 19 new and revised Recommendations were adopted during the past study period following the provisions of Resolution ITU-R1-1. Seven new and revised questions and two Resolutions were approved. This includes critical Questions and Resolutions on the task groups on Appendix 28(S7) and unwanted

emissions. The following briefly describes the work of all SG 1 groups.

5.1 Task Group 1/4 (Chairman: Mr. David Baacon, UK)

TG 1/4 met in Geneva in July, 1997 to continue preparation of the Radiocommunication Data Dictionary (RDD). Document 1/51, Preliminary draft new Recommendation ITU-R SM. (AA1-4), Radiocommunication Data Dictionary was completed and was reviewed by all study groups and the Radiocommunications Bureau. The Task Group met during May and completed the review of the data fields and produced a draft RDD to be reviewed and possibly approved by Study Group 1 in July 1998.

5.2 Task Group 1/5 (Chairman: Mr. Dhamarat, UK)

Meetings of TG 1/5 were held in Geneva in July, 1997 and January 1998. Twenty-seven input papers and one information document were submitted to the July meeting about spurious emissions and out-of-band emissions. Seventy-four delegates participated in the meeting of TG 1/5 and five drafting groups were formed. Initial work on the limit values for spurious emissions for space services and out-of-band emissions needs to be completed for the 1999 WRC.

5.3 Task Group 1/6 (Chairman: Mr. Gerry Chan, Canada)

The first meeting of TG 1/6 was held in Geneva in 1997. This meeting concerned the planning for the development of a Recommendation concerning the determination of the coordination area around earth stations was highly successful. A draft document is to be completion by October 1998 that should be considered at WRC-99.

5.4 Working Party 1A (Chairman: Mr. Terry Jeacock, UK)

WP 1A met in Geneva in July 1997. This meeting addressed engineering principles and techniques, including computer-aided analysis for effective spectrum management. New activities for WP 1A, including the impact of digital technology on spectrum management, software requirements, investigations of the principles and benefits that make certain types of equipment suitable for organizing on a global scale, and the effects on other equipment of the introduction of large scale hand-held mobile networks were discussed.

Draft revision of Recommendation ITU-R SM. 855, Multi-service telecommunication systems (Question ITU-R 45-3/1) was modified and sent to publications. It was decided that in the future it would be useful to

define multi-service systems and to present examples of such systems.

Draft revision of Recommendation 853, Necessary bandwidth, was adopted with editorial changes and approved by the "second method".

Draft new Recommendation ITU-R SM. (Document 1/25), Design guidelines for developing an advanced automated spectrum management systems (ASMS) (Question ITU-R 68/1), was adopted with editorial changes and was approved by the "second method."

Draft revision of Recommendation ITU-R SM. 328-8, Spectra and bandwidth of emission, was adopted and approved by the 1997 Radiocommunication Assembly.

5.5 Working Party 1B (Chairman: Mr. Alex Pavliouk, Russia)

WP 1B met in Geneva in July 1997. This meeting concerned principles and techniques for spectrum planning and sharing and economics aspects of spectrum management. Important work was performed on Document 1/53 concerning economic aspects of spectrum management but no new input material was submitted in other areas under the terms of reference of WP 1B.

Because new material is being submitted with respect to economic aspects of spectrum management, revisions to Document 1/53 will likely be required at the next meeting of SG 1. Attention of telecommunications regulatory agencies should be brought to Document 1/53, and to request that these agencies provide SG 1 with any information concerning their experiences in introducing various economic methods of spectrum management.

Document 1/2 (Revision 1), Draft revision of Recommendation ITU-R SM. 337-3, Frequency and distance separations (Question ITU-R 72/1), was adopted by the Study Group and later approved by the 1997 Radiocommunication Assembly.

Draft addition to Recommendation ITU-R SM. 1046 (Document 1/4), Definition of spectrum use and efficiency of a radio system (Question ITU-R 47/1), was adopted and later approved by the 1997 Radiocommunication Assembly.

Draft addition to a new Recommendation ITU-R (1B/AA, Document 1/5), Efficient spectrum utilization using probabilistic methods (Question ITU-R 45/1), was adopted and later approved by the 1997 Radiocommunication Assembly.

5.6 Working Party 1C (Chairman: Mr. Kisrawi, Syria)

WP 1C met in Geneva in 1997. The meeting concentrated on digital broadcasting signals and monitoring of the radio coverage of land mobile networks to verify compliance with a given license. There is significant future work to be done in WP 1C with respect to digital technologies. Guidelines for developing a basic automated monitoring system should be developed.

6 NEW AND REVISED QUESTIONS

A Draft new Question on the Development of method(s) for the determination of the coordination area around earth stations, was adopted by the SG and later approved by the 1997 Radiocommunication Assembly.

A Draft new Question ITU-R (AA/1A), Technical and operating parameters and spectrum requirements for short-range devices, was adopted by the SG and later approved by the 1997 Radiocommunication Assembly.

A Draft revision of Question ITU-R 205/1, Long term strategies for spectrum utilization, was adopted by the SG and later approved by the 1997 Radiocommunication Assembly.

A Draft revision of Question ITU-R 45-3/1, Techniques and technical criteria for frequency sharing, was adopted by the SG and later approved by the 1997 Radiocommunication Assembly.

A Draft revision of Question ITU-R 71-1, The use of spread spectrum techniques, was adopted by the SG and later approved by the 1997 Radiocommunication Assembly.

A Draft new Question ITU-R (AB/1C), Monitoring of digital broadcasting signals, was adopted by the SG and later approved by the 1997 Radiocommunication Assembly.

A Draft new Question ITU-R (AC/1C), Monitoring of the radio coverage of land mobile networks to verify compliance with a given license, was adopted by the SG and later approved by the 1997 Radiocommunication Assembly.

7 STATUS OF QUESTIONS, OPINIONS, RESOLUTIONS AND DOCUMENTS

Draft Resolution (Document 1/68), Further studies concerning unwanted emissions, was adopted by the SG and later approved by the 1997 Radiocommunication Assembly.

Draft new Decision (Document 1/45), Development of method(s) for the determination of the coordination area around earth stations, was approved by the SG.

Draft revision of Resolution ITU-R 11-1, Development of automated spectrum management systems, was adopted by the SG and was later approved by the 97 Radio Assembly

8 FUTURE STUDY GROUP ACTIVITIES

Future activities of the SG were discussed and a plan of possible future activities was developed. The members of SG 1 are encouraged to consider these long-term future activities and their relationship with other ITU Study Groups and develop appropriate documents. These activities include the following;

- Changes in spectrum management resulting from new technology and priorities of Administrations,
- Approaches to spectrum management that allow the user greater flexibility to manage the radio spectrum,
- Technical and legal aspects of alternative approaches to spectrum management,
- New computer-based tools for technical and administrative applications in spectrum management,
- Impact of the limitations of advanced computer analysis models, propagation, engineering and databases,
- Impact of computer networking and decentralizing spectrum management functions,
- Interference criteria between digital and analogue systems,
- Techniques for monitoring non-GSO systems,
- Implications for sharing and other aspects of multiple function communication systems (e.g. the signal structure and sharing criteria for digital signals is independent of the information being carried),
- Measurement of quality indicators to assess the effectiveness of "spectrum management organizations",
- New "vertical dimension" sharing techniques for space or stratospheric-based systems,
- Assignment techniques and other aspects of wireless local loop systems,
- Further application of Monte Carlo techniques to spectrum management,
- Role and tasks of monitoring in a liberalized environment,

- Identification of frequency bands where it would be suitable to place certain types of equipment, e.g. short range devices.
- Investigation of the principles and benefits that make certain types of equipment suitable for organizing on a global scale,
- Global investigation of current and future uses of the spectrum taking into account changes in the technological and regulatory environment.

9 CONCLUSIONS

More effective use of the radio spectrum is required to meet the ever increasing requirements in radio communications. This increase in effective use can only come from applying more effective techniques in managing the spectrum. Study Group 1 has in the past developed techniques and procedures that lead to more effective spectrum use. It is up to all countries to use these techniques and to continue to improve them. The future work of the SG requires the assistance of all countries to develop these new techniques and procedures. Key areas of future development include, Advanced (automated) Spectrum Management Systems, economical methods of spectrum management, new monitoring techniques, and new methods of spectrum management that allow the user of the spectrum greater flexibility.

BIOGRAPHICAL NOTE

Mr. Robert J. Mayher (Bob) is president of SMILE (Spectrum Management, International Licensing and Engineering) Associates and International Chairman of Study Group 1 (Spectrum management) of the Radiocommunication Bureau of the International Telecommunications Union (ITU). He was formerly Director of Spectrum Planning and Policy for the National Telecommunications and Information Administration (NTIA) of the United States. Before this Mr. Mayher was chief of the Spectrum Engineering and Analysis Division of NTIA. Mr. Mayher is an expert in spectrum planning, spectrum engineering, interference criteria and is knowledgeable in all aspects of SG1. He has written over 100 reports on various aspects of spectrum management.

WUEFEM – COMPUTER PROGRAM FOR SIMPLE, FAST ANALYSIS OF INTERMODULATION INTERFERENCE IN FM RADIO BROADCASTING IN THE CITIES

Tomasz Niewodniczanski – Institute of Telecom, Wroclaw Branch, Swojczycka 38, 51-501 Wroclaw

tel.: (+48) 71 728868, fax: (+48) 71 729375, e-mail: tnie@il.wroc.pl

Marek Slowinski – Bank Zachodni SA we Wroclawiu – Centrala, Rynek 9/11, 50-950 Wroclaw

tel. (+48) 71 723138 w 1597, e-mail: PK.ZP@bzc.BZ.x400.net.pl

Increase in supply of the radio receivers to the market in Poland, caused the situation in which there is at least one radio receiver per household. Licences are available to applicants who want to establish commercial radio stations working in both FM bands i.e. 66 – 74 MHz and 87,5 – 108 MHz. Emission of numerous signals creates increased probability of interference, and important problem to be solved is to avoid combinations of frequencies causing intermodulation effects in receivers. Therefore, the proper selection of dynamic parameters of input circuits and stages, in other words their quality, is of particular importance, reducing the number of cases of intermodulation and easing limitations for frequency planners. Unfortunately, only a limited number of types of receivers meet the quality requirements. A series of receivers available on the market has been examined [1,2] recently in the Wroclaw Branch of the Institute of Telecom and the conducted measurements allowed for establishing the dynamic parameters of computer models for these receivers. These models were used to prepare a computer program analysing intermodulation interference in FM broadcasting reception in the cities i.e. in the situation when the input stages of the receiver are attacked by many

strong signals. The program includes a data base containing the above mentioned models of radio receivers, models of popular transmitting antennas and maps of the selected cities.

The most important features of the program are:

- evaluation of receiver performance in a given geographical location in the presence of numerous radio signals;
- analysis of possible intermodulation products in a chosen receiver model located in a specified area (for such areas, radio signals at the receiving point are determined, based on information regarding transmitter location, frequency, kind of antenna, and output power).
- simulation analysis of the situation in which one can check the intermodulation interference originating from the new, hypothetical station or from the existing station, but with changed parameters;
- simulation of the situation in which one type of receiver is replaced by another one or some parameters in a given type are changed (e.g. the attenuation in antenna input).

The figures 1 to 5 illustrate the results of analyses for some cases (| - signal, ▨ - intermodulation)

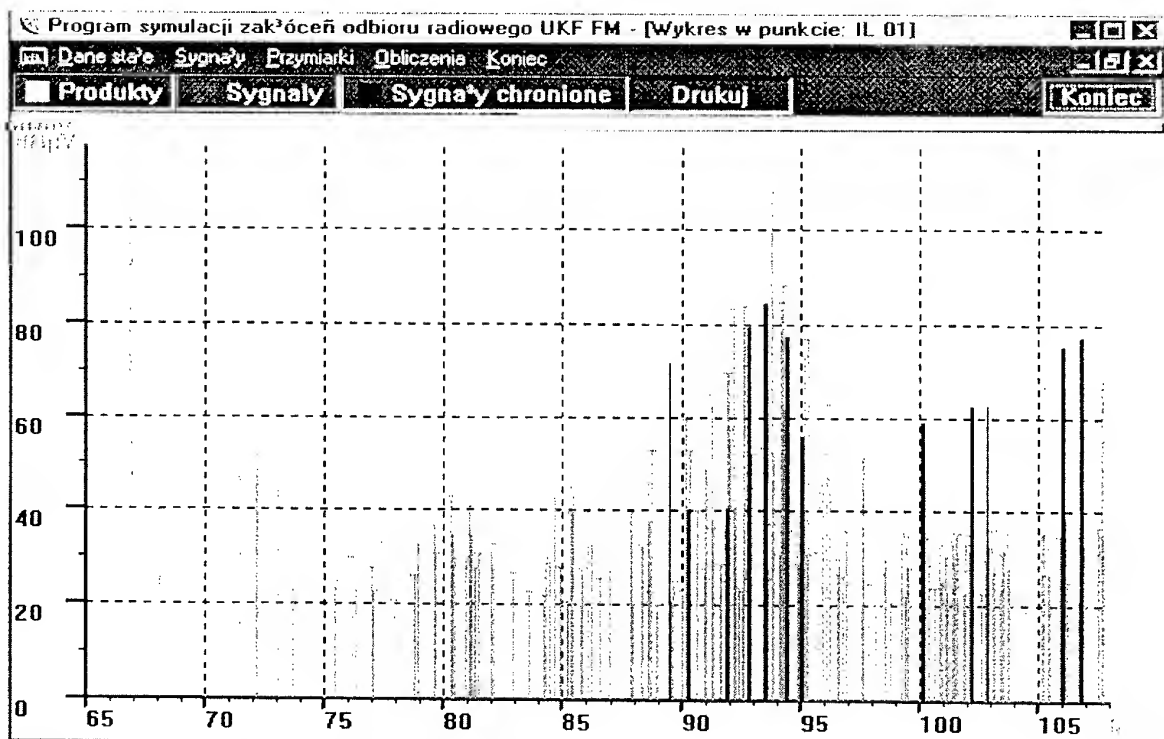


Fig. 1 - Intermodulation interference, originating in a popular, low quality receiver.

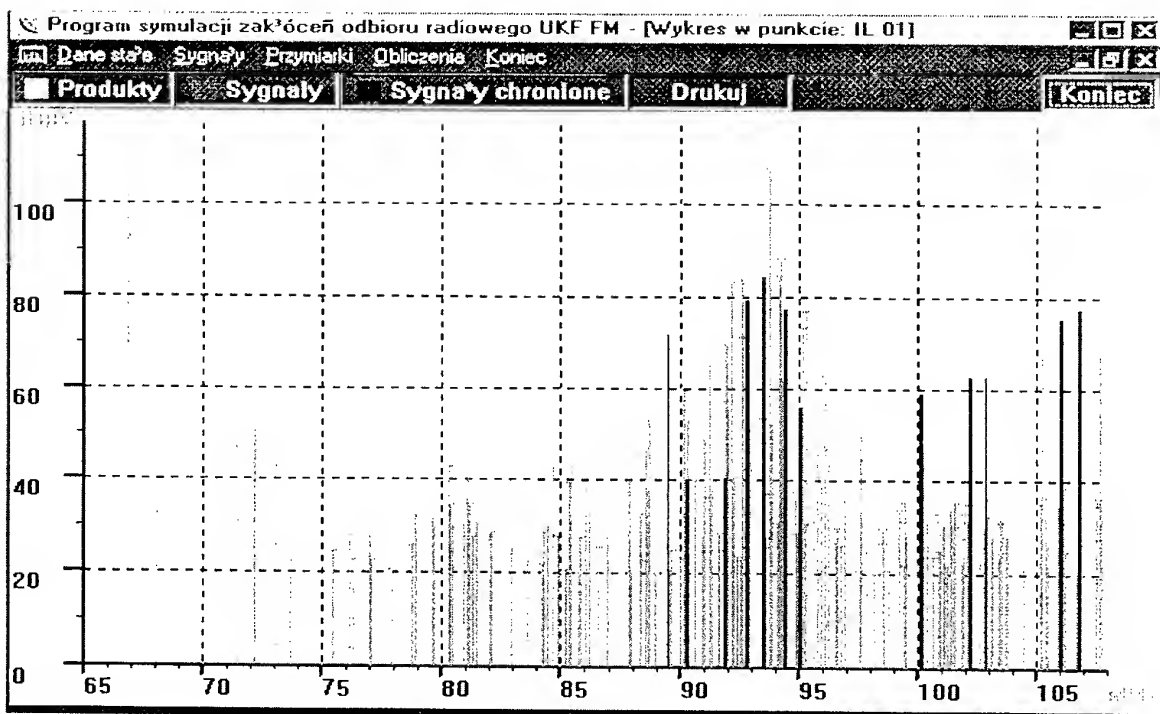


Fig. 2 - Intermodulation interference originating in a high quality receiver. Situation as in Fig. 1

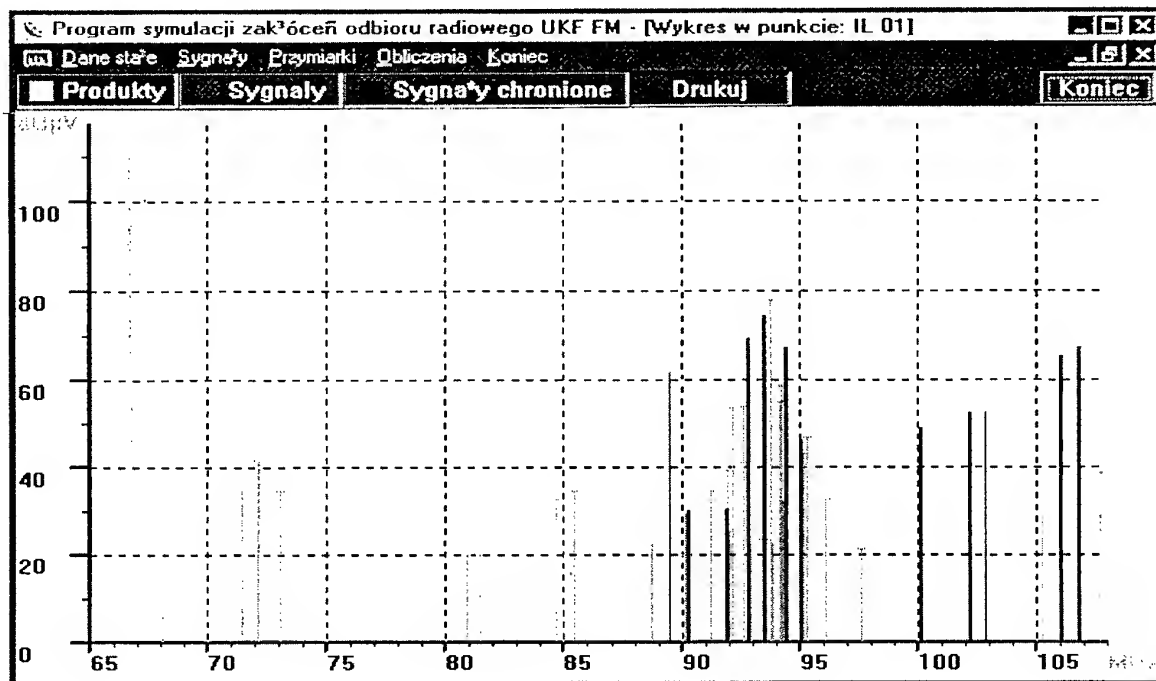


Fig. 3 – The same receiver and situation as in Fig 1, but with addition of 10 dB attenuation in receiver antenna input.

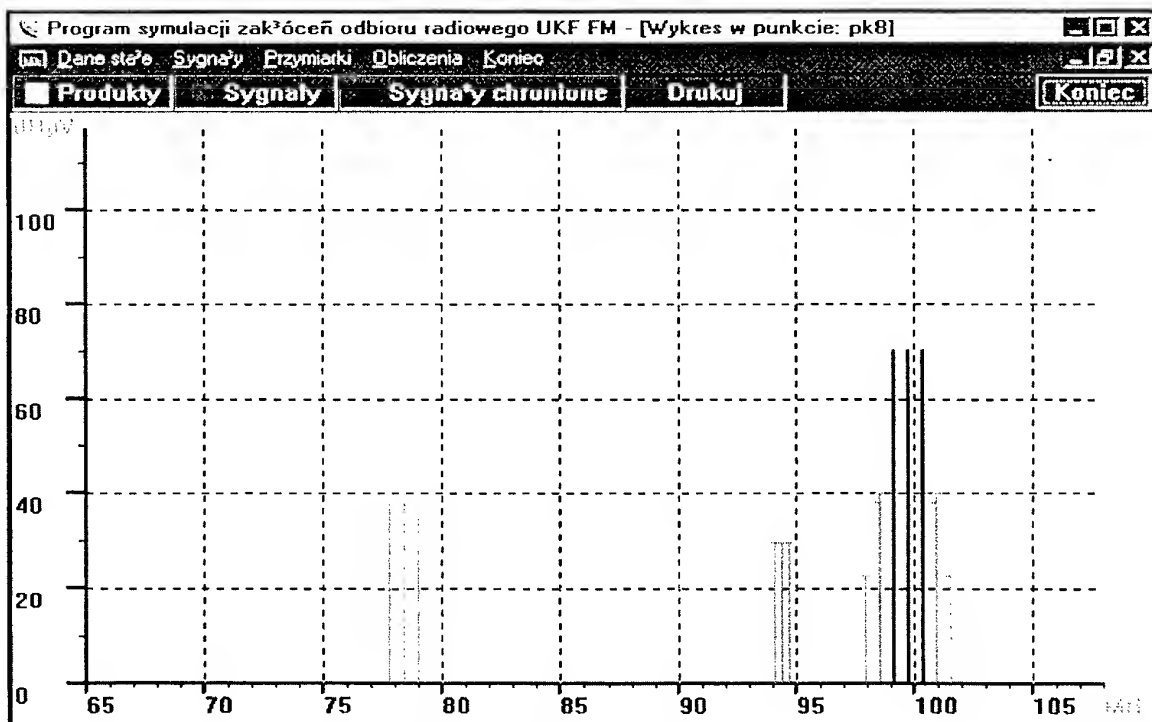


Fig. 4 - Real life example, in which three high power stations are working with frequency separation of 600 kHz from each other.

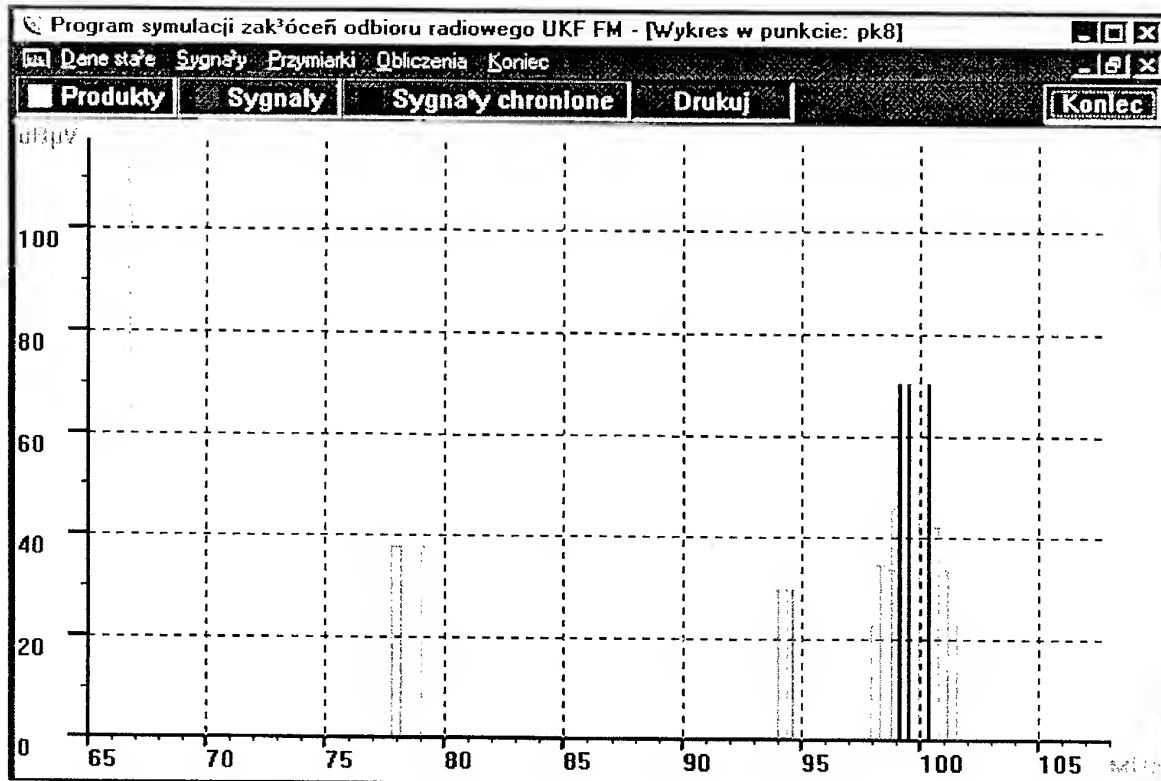


Fig. 5 – The example the Fig. 4 but the frequency of the station which has the frequency in between of two others has been changed by 200 kHz.

One may conclude from the above that in the situation of many FM stations placed especially in big cities, it is important to consider the intermodulation phenomena during the detailed frequency planning for these cities.

The receiver and antenna data bases should be continuously updated and propagation model refined, to maintain the usefulness of the program.

References:

1. Pietranik Miroslaw, Niewodniczanski Tomasz – Recommendations for limitations in frequency assignments for FM broadcasting stations in the cities resulting from intermodulations phenomena in the receivers. – Report Z21/21.3.02.1/419/91 of the Wroclaw Branch of the Institute of Telecom (in Polish)
2. M. Pietranik, L. Stasierski, T. Niewodniczanski, R. Zarko, M. Kaluski – EMC of FM radio broadcasting reception resulting from the simultaneous use of 66-74 MHz and 87,5 - 108 MHz. – Report 124/43/92 of the Wroclaw Branch of the Institute of Telecom (in Polish)

INTERNATIONAL STUDIES OF ECONOMIC ASPECTS OF SPECTRUM MANAGEMENT

Alexandre PAVLOUK

State Radio Research & Development Institute (NIIR)

16, Kazakova str., NIIR, Moscow, 103064, Russia

Tel. + 7 095 261-18-41, Fax: + 7 095 267-52-68,

E-mail: EMC.DEP@g23.relcom.ru

More and more attention of telecommunication administrations of many countries, developed and developing ones, is recently paid to economic aspects of radio spectrum management.

Following this interest, International Telecommunication Union (ITU) through its Radiocommunications Sector (ITU-R) and European Conference of Postal and Telecommunications Administrations (CEPT) through its European Radiocommunication Committee (ERC) have began in-depth studies in this field. Latest results of these studies are shortly discussed.

1. INTRODUCTION

The increasing use of new radio technologies through new spectrum applications has produced tremendous opportunities for countries to improve the telecommunications infrastructure and through it - the country's economy as a whole. These developments, though often making spectrum use more efficient, have spurred greater interest and demand for the limited spectrum resource. Thus, the efficient and effective management of the spectrum, while crucial to making the most of the opportunities that the spectrum resource represents, grows more complex. Improved data handling capabilities, engineering analysis methods and expanding radio monitoring activities previously have generally met requirements for accommodating the number and variety of users seeking

access to the spectrum resource at exclusive or shared basis.

However, under circumstances of continuously increasing of the frequency band congestion in many developed countries, further introduction of new spectrum applications, keeping sufficient spectrum use efficiency, by only convenient administrative and technical measures become more and more difficult. Moreover, large attention, which until recently was given to questions of introduction of the specialized frequency assignments databases, and also significant improvements in automation of radio monitoring and frequency assignment procedures with use of the improved radio propagation models based on digital topographical map utilisation, have resulted in creation, in many developed countries, advanced automated systems of spectrum management working in aggregate with wide automated radio monitoring networks [1], [2]. Thus, in a number of developed countries the technical means of the further improvement of their spectrum management systems, at the given stage of engineering development, have appeared basically exhausted.

As a result, telecommunication administrations have begun to display the increasing interest to alternative methods of increase of spectrum use efficiency and first of all - to economic methods. Therefore at the given stage of development, modern radio spectrum management is associated with economic measures, rather than with technical ones [3].

The developing countries, at which the frequency band congestion though while does not cost is so sharp, recently also have begun to display the increased interest to economic aspects of spectrum management in hope to find sources of financing of their programs of development of modern spectrum management systems.

In spite of the fact that in many developing countries license fees regime has already been implemented, their tariff systems in many cases are somewhat haphazard and in some way technically and economically non- reasonable. In some countries the tariffs extremely low and can not cover even administrative costs, not speaking about an opportunity of accumulation of resources for appropriate technical support of national spectrum management system including radio monitoring network. In other countries, on the contrary, the rates, at least for radio transmitters of some services, are rather great, and that in the certain degree constrains development of a radio communication and, at the end, development of a national economy. Besides, in a number of the countries all income from licence fees, which basically would be sufficient for phased creation of a national spectrum management system, wholly goes to the national budget of the country and are used for other purposes, which are considered to have more priority. It, in particular, occurs also due to insufficient knowledge of government circles on importance of radio communications and their appropriate administrative regulation, supported technically, for development of country economy.

A number of countries which nowadays are carrying out transition from rigid planned to market-oriented economy, meets specific difficulties in introduction of license fees regime. They will be mentioned below.

Thus, there is a large interest of various countries, both developed, and developing, to economic aspects of spectrum management, that could result in a wish to have some international recommendations or guidance in the given area.

2. MAIN RESULTS OF ITU-R ACTIVITIES

Following requirements of many administrations to have an international recommendations on the given problem, the Radiocommunication Sector of the International

Telecommunication Union (ITU-R) at its Radiocommunication Assembly 1995 (RA-95) through Study Group 1 (SG 1) "Spectrum management" has launched a study program in this new for the ITU-R field of activity. It consists of three interrelated Questions:

-Question 206/1 Strategies for economic approaches to national spectrum management and their financing,

-Question 207/1 Assessment, for spectrum planning and strategic development purposes, of the benefits arising from the use of radio spectrum,

-Question 208/1 Alternative methods of national spectrum management.

SG 1 has charged these researches to Working Party 1B (Principles and techniques for spectrum planning and sharing), which, in turn, has created special Reporter's Group on the given subjects. During 1996 - 1997 the Group has carried out extremely large work on generalisation of available materials, including results of the works which have been carried out within the framework of activity of the ITU Telecommunication Development Sector (ITU-D), (particularly [4] should be mentioned) and also experience of various countries. In result, the Group has managed to prepare a draft of a rather extensive Report (ITU-R [1/53]) "Economic Aspects of Spectrum Management", which was discussed and consistently adopted and approved by WP 1B and GS 1 meetings, which were held in Geneva at the end of July 1997. In a final form, issued in English, French and Spanish languages, the Report under number SM.2012 [5] was officially published by the ITU to the opening of RA-97, Geneva, October, 1997.

The Report being the first consolidated international material on the given urgent subjects, in more or less details answers all three Questions put forward by RA-95.

In this short paper it is not possible at all to make a summary of the Report in all variety of its issues. Let us only mention that the Report contains four chapters which cover the following main issues.

Chapter 1, Introduction to economic considerations, is an introductory one and

covers the main subjects of spectrum management at national and international levels and specify needs for introduction of economic means of spectrum management. Various legal, socio-economic, and technical infrastructure considerations in the application to spectrum management are shortly discussed.

Chapter 2, Strategies for economic approaches to national spectrum management and their financing, describes different economic aspects with their application to spectrum management and its financing: traditional national budget financing, spectrum use fees, spectrum usage comparative hearings, lotteries and auctions. Advantages and disadvantages of these approaches are discussed and some general suggestions on their implementation in different situations are presented. Transferable and flexible spectrum rights are also discussed. Experience of different administrations (of developed countries) with auctions, transferable spectrum rights and license fees is shortly discussed.

Chapter 3, Assessment of the benefits of using the radio spectrum, cover variety of issues connected with assessment of importance of radiocommunication for the economic development of different countries and assessment of direct benefits of using radio spectrum. If modern economic approaches, covered in previous Chapter of the Report, with more or less detail can be found in many other papers (bibliography to [4] contains 50 entries), material of Chapter 4 in such generalised form applicable to modern radiocommunication development, can be considered as an unique and very important one.

Chapter 4, Alternative support for national spectrum management, discusses possibilities to use alternatives to the traditional centralised, government operated and funded national spectrum management systems. Though national spectrum management remains a primarily governmental effort, alternative approaches using resources outside the national spectrum manager to perform or fund certain spectrum management functions can enhance the efficiency and effectiveness of the national effort. A number of administrations have made use of spectrum management resources outside the national spectrum manager including: communication groups with

a direct interest in spectrum such as advisory committees, trade associations, professional organizations, and quasi-governmental associations; frequency coordinators (and coordination groups) and designated spectrum managers; and spectrum management consultants, and support contractors. Application of this approach in developing countries is shortly discussed too.

As it was mentioned above a number of countries which nowadays are carrying out transition from rigid planned to market-oriented economy, meets specific difficulties in introduction of license fees regime. In particular, they are caused by the fact that in a system of a rigid planned economy, when the state was the unique exclusive operator and, simultaneously, all-round regulatory body, frequency assignments to radio stations and frequency bands to radio systems were provided to the users practically free-of-charge. It was quite logical and well-grounded economically in the given social-economic system. On this basis, there was (and still, on inertia, there is) an opinion, that frequency resource, provided to a society, "in former good times was free-of-charge"; and recent measures, have been undertaken within the framework of new social-economic conditions on formal introduction of spectrum pricing, are identified as an introduction of a new indirect tax on the whole population of a country. In result some opposition to these measures is observed and in a number of cases it creates one of main obstacles on a way of reforms in the given sphere.

It is obvious that all reasoning that the spectrum use was previously free-of-charge have no real justifications. The state (society) spent and continues to spend huge resources for activities on providing radio channels to be free from non-acceptable interference as the major condition of the availability of radio communications.

Therefore the transferring of burden of this payment on shoulders of the real spectrum users means not the introduction of new taxation but more appropriate method of distributing the costs of spectrum management to those who actually use the spectrum and receive benefits. On basis of Russian contribution [6] to Reporter's Group work this important provision was included in

section 2.2 "Underlying approaches with respect to financing national spectrum management" of the Report SM.2012 [5].

3. MAIN RESULTS OF ERC ACTIVITIES

Studies of economic aspects of radio spectrum management with application to CEPT countries have been started by Radio Regulation Working Group (WG RR) of ERC in 1992 when special Project Team RR8 "Harmonisation of fees and charges" was created. As it is clearly seen from the name of the Team its final goal is to study and propose measures which would lead to harmonisation of spectrum use fees and charges throughout CEPT countries.

It happened, that RR8 has completed its "Report on introduction of economic criteria in spectrum management and the principles of fees and charging in the CEPT" [7] almost simultaneously with above mentioned ITU-R Report [5] and almost in the same volume. However, the content of RR8 Report [7] is somewhat different, more oriented to in-depth study of spectrum pricing issues and related matters including administrative ones (such as managing transition period, spectrum refarming etc.), so those both Reports are very well supplementing each other. In January 1998 Report [7] was presented for approval by WG RR and then by ERC.

A short overview of Report [7], based on material of its Chapter 2, can be presented in the following way.

Chapter 1, Introduction, presents background and a short history of the work, refers on CEPT policy, reports and recommendations on the subject and makes reference to ITU-R Report [5].

Chapter 3, The principles of financing spectrum management, describes the various methods that have traditionally been used for funding spectrum management. These methods range from state funding to cost recovery and gives a breakdown of the distribution of fees across radio users. The chapter also presents alternative methods, to charging fees, that are used by some administrations for providing spectrum management services and manpower resources.

Chapter 4, Licensing mechanisms, covers the licensing mechanisms that have been used with the funding methods. This includes the main licensing mechanisms like "first come first served" to the newer mechanisms like "lotteries".

Chapter 5, Spectrum pricing, discusses some difficulties facing a number of administrations from rising spectrum congestion and the increased competition for scarce spectrum has led to the introduction of spectrum pricing. Spectrum pricing is the term given to funding and licensing mechanisms that bring economic factors into spectrum management. This includes on one hand the possibility to use fees for influencing the behaviour of users (administrative pricing) and on the other hand the introduction of new frequency allocation procedures, like auctions.

Chapter 6, Spectrum rights, explains that the introduction of spectrum pricing has raised a number of issues on the rights a licence confers on a licensee, the level of control retained by the administration and the licensee's spectral obligations to other radio users.

Chapter 7, Spectrum pricing - further considerations, shows that the introduction of spectrum pricing allows some of the spectrum management problems caused by limitations in administrations funding to be resolved, allowing them to develop their spectrum management facilities. This chapter examines some of the uses to which additional funding could be put and some of the associated spectrum management problems that spectrum pricing may help to resolve.

Chapter 8, Managing the transition, states that all major changes to spectrum management need to be planned and implemented carefully. Spectrum pricing is no exception and this chapter highlights some of the key areas administrations need to take into consideration when changing their funding or licensing methods, particularly if this leads to changes in the way radio administrations are financed.

Chapter 9, International perspective, shows that spectrum pricing and some of the problems it has been introduced to resolve are being studied in a variety of international fora.

This chapter presents reports from some of these debates and the work in progress.

Chapter 10, Conclusions and proposals for further work, presents conclusions on spectrum pricing and recommendations for further work, including identifying where further work on harmonisation within CEPT countries may be possible and how this may be taken forward.

The Report contains 8 Annexes:

- Recommendations ERC PT8 Report;
- Recommendations DSI I and II (Detailed Spectrum Investigation, Phase 1 [8] and 2 [9]);
- Spectrum management functions;
- Examples of charging systems in certain administrations;
- Administrative pricing applied to different services;
- Developments with regard to spectrum pricing in individual administrations;
- A glossary of spectrum pricing;
- Spectrum refarming issues.

4. CONCLUSIONS

The International telecommunication community has started in-depth study of economic aspects of spectrum management aiming to assist administrations of different countries, developed and developing ones, to further increase efficiency of spectrum use in developed countries and to identify sources and procedures of financing of programs of modern spectrum management system creation in developing countries.

Nevertheless, in view of extremely fast progress in the given new sphere of ITU-R activity and due to rather compressed terms of preparation, there is a real opportunity to further expand available international Reports [5] and [7] on the matter and to fill them up by newest results. Particularly, sections of Report [5] concerning experiences of different countries, including developing ones, can be considerably extended. Therefore ITU-R SG 1 intends to continue work on the given subjects during the next Study Period 1998 - 1999. Proposals for future work are identified in Report [7] too.

5. REFERENCES

1. ITU-R Handbook on National Spectrum Management. Geneva, 1995.
2. ITU-R Handbook on Spectrum Monitoring. Geneva, 1995.
3. W. Webb. Modern Radio Spectrum Management. 1997 International Forum on Spectrum Management, London, June 1997 (IBC Technical Services Ltd).
4. ITU-D. Study on Spectrum Pricing. Report RAS/94/013 by Dr. Z.E. Kalman and M.K. Nunas. Geneva, 1994.
5. ITU-R SM Series Reports. Report SM.2012. Economic Aspects of Spectrum Management. Geneva, 1997.
6. ITU-R Radiocommunications Study Groups. SG1 Reporter's Group on Spectrum Economics. Doc. 4. June 1997. Russian Federation. Some Aspects of a Problem on Spectrum Economics in Countries, Carrying out Transition from Planned to Market Economy.
7. WG RR of the ERC. Doc. RR(97) 135(rev 1). Report on the Introduction of Economic Criteria in Spectrum Management and the Principles of Fees and Charging in the CEPT.
8. ERC/CEPT. Results of the Detailed Spectrum Investigation. First Phase - 3400 MHz to 105 GHz. 1993.
9. ERC/CEPT. Results of the Detailed Spectrum Investigation. Second Phase - 29.7 - 960 MHz 1995.

BIOGRAPHICAL NOTE

Alexandre P. Pavliouk received the Ph. D. Degree from Radio Research and Development Institute (NIIR) in 1972. General scientific worker of the NIIR. He is an expert in fields of radio measurements and monitoring, frequency planning and radio spectrum management. He is the author of about 100 technical papers on the above subjects, including about 40 contributions to different CCIR and recently ITU-R Study Groups (SG) and their working organs. Vice-Chairman of the ITU-R SS 1 and Chairman its Working Party 1B. ITU-D Senior Expert on spectrum management and radiocommunications development.

SPECTRUM EFFICIENCY IN UNIVERSAL MOBILE TELECOMMUNICATION SYSTEM (UMTS)

Halina Uryga

Francc Télécom Mobiles

41-45. boulevard Romain Rolland, 75672 Paris cedex 14 - FRANCE

Abstract: This paper addresses some key issues concerning the efficient use of the spectrum for the Third Generation system. It covers some results of the ongoing work in European fora- in particular UMTS Forum Spectrum Aspect Group - to determine how to make the best use of the UMTS/IMT-2000 spectrum allocated by WARC-92 and how to estimate the additional spectrum needed which could be allocated by the next World Radiocommunication Conference (WRC-99). The Extension Bands should be identified to meet the predicted increase in traffic demand by 2010.

The Third Generation mobile system will deliver an extensive range of high-performance wide-band wireless and personalised multimedia services with a better spectral efficiency than the Second Generation mobile systems. UTRA - UMTS Terrestrial Radio Access - the new European radio interface confirms the possibility of better use of the spectrum resources and guarantee the quality of services provided.

The increase of the spectrum efficiency could be found in the improvements of the radio transceiver technology, the applications and services technology, the traffic management and the radio channel access management. Some other factors such as : wider channels, Adaptive Antenna Arrays, Hierarchical Cell Structure, Multi-User Detection, fast Power Control are crucial too.

Although the technical improvements are essential, if the spectrum is to be used efficiently, it is also critical to ensure the best frequency allocation (high flexibility for operators) and the frequency management at both international and national level.

I. INTRODUCTION

The European approach concerning the Third Generation Mobile System consists of widespread availability of wireless networks capable of supporting a wide range of traffic types mixing many services with different requirements in the system. UMTS/IMT-2000 will enable consumers to access multimedia communication devices, capable of sending and receiving voice, data, graphics,

images and video regardless of physical location of the user. The adaptive multi-mode/multi-band terminals will ensure world-wide roaming. The market predictions by the UMTS Forum indicate about 32 million European mobile multimedia users among 200 million mobile users by 2005 . [1]

In order to meet this demand it is essential to dispose of the sufficient spectrum allocation. The WARC-92 has allocated 230 MHz - for IMT-2000 - in the following frequency bands :

- ♦ 1885 - 1980 MHz, 2010 - 2025 MHz, 2110 - 2170 MHz *for terrestrial applications,*
- ♦ 1980 - 2010 MHz, 2170 - 2200 MHz *for satellite component.*

This initial allocation will only accommodate predicted traffic levels for the start up in the year 2002-2005.

The first estimates of the additional amount of the spectrum needed were done by UMTS Forum Spectrum Aspect Group, by Task Group 1 of European Radiocommunication Committee of the CEPT and by Task Group 8/1 of ITU-R (Table 1). We agree with these results and support the idea that the WRC-99 should allocate Extension Bands of about 380 MHz for the terrestrial component.

YEAR	UMTS	ERU	ITU-R
	SAG	TCI	REC-196
2005	400 MHz	360 MHz	
2010	580 MHz	550 MHz	550 MHz

Table 1 - First estimates of the total spectrum needed for terrestrial component

The existing spectrum designated for the second generation mobile services may be refarmed and integrated into the allocations for UMTS/IMT-2000 if both, the national regulator and the licensed operator agree. The second generation licensed operators should be able to organise their transition to the Third Generation networks according to their own time-table.

2. THIRD GENERATION'S SPECTRUM EFFICIENCY

One of the goals of UMTS system will be to meet a balance between the users demand for world-wide mobile applications and the scarcity of spectrum resources. The spectrum should be used more efficiently than in current systems because of the importance of the traffic to be handled with.

ETSI SMG2 defines spectrum efficiency [2] as the system load where any of the services has exactly x_2 % satisfied users, whereas the rest of the services have at least x_2 % satisfied users each. This is shown in Figure 1 below.

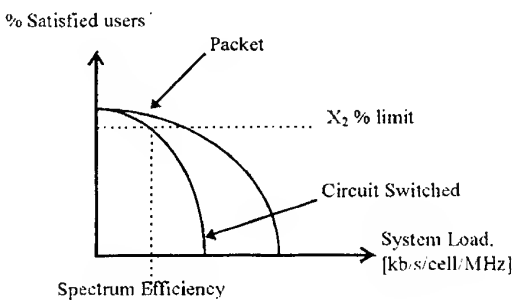


Figure 1 - Example of spectrum efficiency for a mixed service scenario.

The spectrum efficiency should be given for up-link and down-link respectively and for terrestrial and satellite environments. For terrestrial environment two entries are considered :

- Traffic capacity (Erlang/MHz/cell) for FDD and TDD mode.
- Information capacity (Mbps/MHz/cell) for FDD and TDD mode.

Traffic capacity is the total traffic that can be supported by a single cell which is part of an infinite set of cells in a uniform two or three dimensional pattern.

Information capacity is the total number of user-channel information bits that can be supported by a single cell which is part of an infinite set of cells in a uniform two or three dimensional pattern. Information capacity is the instantaneous aggregate user bit rate of all active users over all channels within the system on a per cell basis.

Both *traffic capacity* and *information capacity* must be specified at a stated spectrum allocation, quality and grade of service, assuming an appropriate propagation model. These metrics are valuable for comparing systems with identical user channel requirements.

To set up UMTS's spectrum efficiency data, both FDD and TDD mode are to be considered. Wide-band Code Division Multiple Access (W-CDMA) has been selected by ETSI for Frequency Division Duplex (FDD) and Time Division-Code Division Multiple Access (TD-CDMA) for Time Division Duplex (TDD).

As example we take in table 2 some results obtained by Concept Group Alpha [3], [4] simulations concerning the

W-CDMA FDD mode cell capacity and spectrum efficiency.

Service [kb/s]	Environment and speed	Cell capacity		Spectr. efficiency [kbps/MHz/cell] UL/DL
		Erlang/MHz/cell	UL/DL	
Speech 8	Outdoor to indoor and pedestrian 3 km/h	159/204		127/163
Speech 8	Vehicular 120 km/h	123/98		98/78
LCD 384	Vehicular 120 km/h	1.8/1.1 5.3/3.2 1.8/2.8 5.3/6.6		138/85 204/123 138/211* 204/250*
UDD 384	Outdoor to indoor and pedestrian 3 km/h			470/565
UDD 2048	Indoor office 3 km/h			300/230 300/500*
Mixed speech + UDD	Indoor office 3 km/h	6.3/4.2 6.3/9.3*		315/207 315/460*

UL = up-link, DL = down-link

LCD = Long Constrained Delay Data Services

UDD = Unconstrained Delay Data Services

* DL antenna diversity

Table 2 - Some of W-CDMA/FDD simulation results

This results show that the performance for speech is between 78-163 kbps/MHz/cell. The result depends on the radio propagation case and vehicle speed. These figures are higher than for GSM.

For a 384 kbps service for vehicular 120 km/h the simulated performance is between 85-250 kbps/MHz/cell depending on whether antenna diversity is used or not in the down-link.

For a packet service in pedestrian environment and with traffic characteristics of 384 kbps the performance is 470-565 kbps/MHz/cell.

For indoor packet services with 2048 kbps the performance is between 230-500 kbps/MHz/cell depending on whether or not down-link antenna diversity is used.

3. EFFICIENT SPECTRUM USE AS A RESULT OF TECHNOLOGICAL IMPROVEMENTS

Diverse technological improvements regarding efficient spectrum use will be implemented in UMTS network. High spectrum efficiency for typical mixture of services could be obtain. We will highlight some essential spectrally efficient factors such as :

- wider bandwidth (5 MHz)
- joint multi-user detection
- modulation technology, channel coding and interleaving
- adaptive antennas
- MAC and LLC protocols

UMTS will use wider channels as Second Generation Systems. Increasing the bandwidth translates into enhanced performance due to improved interference averaging. A wider bandwidth improves also frequency diversity effects and therefore reduces the fading problems. The fading resistance in most environments will give the additional gain in spectrum efficiency. Due to less fading effects in a wider channel, the power control accuracy will be improved too.

The other new feature which increases the spectrum efficiency of a cellular network is a joint multi-user detection. Its application will eliminate the interference within a cell and improve the capacity detecting more than one transmission in the radio system. Joint detection is used to remove either intracell or intercell co-channel interference or both.

The use of higher efficiency channel codes, more adapted to the particular propagation, of deeper interleaver, and of higher modulation levels will increase the system efficiency. This increase is balanced by an increase in complexity, a longer delay for some services and a reduction of the cell size.

The deployment of adaptive antennas in the MS as well as BS will give also the possibility to use the spectrum more effectively. Adaptive Antenna Arrays (AAA) will optimise the antenna pattern for each individual mobile. AAA is a technique in which an antenna beam is directed to each user. It could be very effective in the particular areas where limited radio spectrum is available for wideband deployment.

For UMTS network efficiency the improvements concerning main sub-layers - *logical link control (LLC)* and *medium access control (MAC)* - on layer 2 are crucial. The MAC and LLC protocols should be designed to be as efficient as possible.

MAC will provide very flexible means to combine different variable-rate real-time and non-real-time services with different Quality of Service (QoS) requirements to the same physical channel. LLC sets up a logical link over the radio interface and minimises the amount of data that has to be transmitted for the given channel bit error characteristics. The MAC and LLC should allocate resources to user services and to control channels so as to minimise the total power transmitted whilst simultaneously maintaining spectral efficiency.

4. EFFICIENT SPECTRUM USE AS A RESULT OF ADEQUATE ALLOCATION

In spite of the technological progress there are a lot of factors limiting the maximum achievable spectrum efficiency of UMTS/IMT-2000. Very important aspects of efficient radio resources use are its allocation, planning and management. From the technical point of view the UMTS operators will be able to exploit very efficiently their part of the spectrum. The full technical potential of

the Third Generation networks could be deployed only if the frequency allocation is adequate and corresponds to the operator's needs i.e. traffic asymmetry, service flexibility.

The expected efficiency and capacity requirements should be considered from the initial planning stage. One way which might be proposed to achieve improved spectrum use is to adopt the most efficient spectrum allocation scenario. A flexible asymmetrical band allocation adapted to the UMTS operators needs is required.

For UMTS deployment in 2002-2005 Europe will dispose of 155 MHz for terrestrial component (T) from the initial WARC-92 allocation (Figure 1).

1900 (MHz)	1980	2010	2025	2110	2170
UMTS terrestrial (T)		T			T

Figure 2 - UMTS frequency allocation (WARC-92)

The UMTS Forum traffic forecast confirms that there will be a larger demand for capacity on the down-link than on the up-link. On this basis we propose three spectrum allocation scenarios assuming three operators are granted a 40 MHz UMTS licence to use up to 35 MHz in the down-link and 5 MHz in the up-link. A total bandwidth of 155 MHz will be allocated to the three operators : 120 MHz in the first step, 30 MHz will be split between three operators as extension band of 10 MHz each one and the remaining 5 MHz could be used for the unlicensed applications.

Both TDD and FDD modes will be used for UMTS. It is expected that the terminals will be TDD/FDD dual-mode. Three possible allocation scenarios presented in Figures 4, 5, 6, below propose some solutions mixing the TDD and FDD modes in order to plan the spectrum the most efficiently.

This paper shows a possible frequency allocation for three operators with separate frequency assignment in both : paired (2110 - 2170 MHz, 1920 - 1980 MHz) and unpaired (1900 - 1920 MHz; 2010 - 2025 MHz) spectrum. In all scenarios the upper band of 60 MHz is used for the down-link and is split between three operators (Figure 3).

2110	2130	2150	2170
A	B	C	
DL	DL	DL	

Figure 3 - Allocation of the upper band common for all scenarios

The different allocations are proposed for two remaining bands. In each scenario 5 MHz are available for unlicensed private use (P) in TDD mode.

4.1 - Possible UMTS Core Band allocation N°1

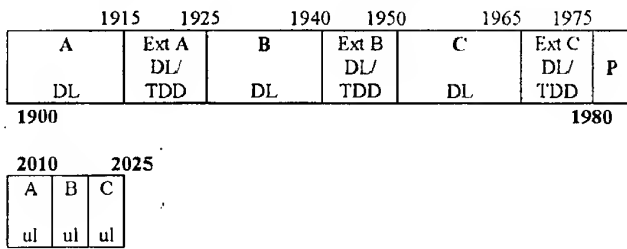


Figure 4 - Scenario N° 1

This scenario provides a sufficient ratio of asymmetry : 35 MHz (15 MHz + 20 MHz) for down-link and 5 MHz for up-link. It is possible to use the FDD mode in all bands and the TDD mode in the lower paired band. The extension bands are available on the lower part of the spectrum and could be used in FDD down-link or TDD mode.

4.2 - Possible UMTS Core Band allocation N°2

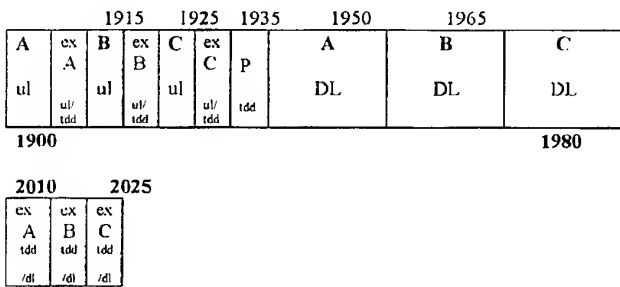


Figure 5 - Scenario N° 2

The total band is first divided between up-link and down-link transmissions and then each part is split between the three operators. A 20 MHz duplex separation is available allowing a use either in TDD or FDD mode. Extension bands could be used in TDD or FDD up-link (lower part of spectrum) and FDD down-link (middle part of spectrum).

4.3 - Possible UMTS Core Band allocation N°3

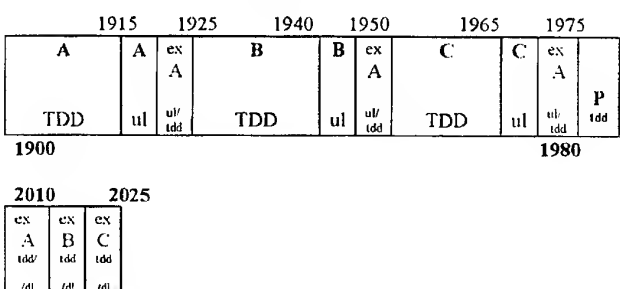


Figure 6 - Scenario N° 3

An alternative solution is to split the lower part between three operators and then to divide between up-link and down-link transmissions. The duplex separation in the lower part is too small to allow the usage of the FDD mode in down-link. Therefore the TDD mode has to be used for the down-link traffic with a small up-link return channel. Extension bands in the lower part could be used in TDD or FDD up-link mode and in the middle part in TDD or FDD down-link.

With the second and third scenarios the TDD mode use would allow each operator to adjust the level of asymmetry to the traffic situation. It should also be possible to use more FDD mode for the up-link traffic.

Further studies on guard bands are required.

All these scenarios allow the optimum utilisation of available radio resources. We think that the adoption of one of these scenarios will be a better solution to allocate spectrum efficiently. Currently there are significant differences in the bandwidth allocated to each operator in various countries so the spectrum is not used in the most efficient manner.

5. CONCLUSION

UMTS will provide world-wide new additional services on the basis of IMT-2000 Core Band and Extension Bands which allocation we expect during the next WRC-99.

The UMTS success will depend on the efficient use of the adequate amount of the spectrum. New technological features, new allocation and management policy will allow spectrum use in the most efficient manner. It is critical to plan today tomorrow's communications.

6. REFERENCES

- [1] 'Spectrum for IMT 2000', UMTS Forum, October 1997
- [2] UMTS : Selection procedures for the choice of radio transmission technologies of the UMTS. UMTS 30.03 version 3.1.0, ETSI, 1997
- [3] Concept Group Alpha. Wideband Direct-Sequence CDMA : Evaluation Summary, ETSI SMG#24, Tdoc 903/97, December 15-19, 1997
- [4] Concept Group Alpha, Evaluation document 3.0, ETSI SMG#24, Tdoc 905/97, December 15-19, 1997

BIOGRAPHY

Halina Uryga is deputy head of spectrum management group in France Telecom Mobiles. She is involved in the work of a number of international fora developing UMTS IMT-2000, such as UMTS Forum SAG, CEPT-ERC/TG1, ETSI/ERM/RM, ETNO/FM, ITU-R TG81.

XIV

**SPECTRUM MANAGEMENT,
ENGINEERING, SHARING
AND MONITORING**

**Co-existance of Radio Services
after 2000, a "Passive" View**

**ESF Committee on Radio Astronomy
Frequencies (CRAF) sponsored session**

Invited session organized by

T. A. Spoelstra - The Netherlands

LAST MINUTE INFORMATION : UNKNOWN SATELLITE TRACED

T.A.Th. Spoelstra

Netherlands Foundation for Research in Astronomy
and

ESF - Committee on Radio Astronomy Frequencies
P.O.Box 2, 7990 A.A.Dwingeloo, The Netherlands

Phone: (+31)521-595100, Fax: (+31)521-597332, e--.mail: spoelstra@nfra.nl

Since about 1992, radio observations done in the 322.0 - 328.6 MHz band suffer harmful interference from an unknown space station. The interference still exists at a level not different from its initial detection. In the frequency band 322.0 - 328.6 MHz the Fixed, Mobile and Radio Astronomy services enjoy a primary (shared) allocation.

Radio astronomers in the Netherlands and India were the first to report the existence of this unknown space station of which several characteristics were derived from careful analysis of the radio astronomical measurements. The radio astronomy observations were confirmed by the Leeheim Satellite Monitoring Station of the German administration. The Dutch administration filed a formal complaint at the ITU in Geneva, the ITU brought this to the attention to a.o. the USA and Russian administrations.

CRAF was informed by the Russian administration that it could be excluded that the space station is a Russian one. In the meantime the US administration (NTIA) and the spectrum manager of the US National Science Foundation, dr.T.Gergely, put much effort into this issue attempting to solve it.

At the 43rd meeting of the Committee on Radio Frequencies of the US National Research Council, CORF, in Washington (13-14 May 1998), dr.Gergely reported that now the space station is known: the TEX satellite.

1. THE TEX SATELLITE

The TEX satellite was built by Defence Sciences Inc (DSI) which is now part of Orbital Sciences Corp (OSC), as a part of an experiment built by Rockwell International, now part of the Boeing Company. It was launched on April 11,1990 and its service ended in June 1991.

The satellite moves in a polar orbit (90 degr. inclination). Its mean altitude is 372 Nmi (~689 km). Its decay is 0.005 Nmi per week or about 1 NMi each 4 years (~0.01 km and 1.85 km, respectively). The orbital period is 100 minutes, which implies about 14 revolutions around the Earth each 24 hours. The satellite visits every place on the Earth's surface at least twice each 24 hours, while the frequency of "in view"

events increases with latitude (e.g. in view of the North Pole on all 14 revolutions per day).

2. ILLEGAL FREQUENCY

The interference is caused by the "Beep Receive" transmissions of the satellite. TEX uses the UHF frequency of 328.25 MHz. However, given the ITU-R Radio Regulations the use of this frequency for space applications is illegal and therefore the satellite must be maintained in "quiet" mode. The satellite uses a two-way command and control link which transmits and receives on 328.25 MHz. In the communications with the ground control station, the downlink is used for satellite telemetry and the uplink for commands and schedules.

The satellite attitude control relies on a gravity gradient boom. This implies an about 3 kG mass on a 7 meter boom. The satellite attitude is driven to maximize difference in altitudes of satellite mass and boom mass. It may become stable "right side up" or "up side down". A "Z" coil provides controlled magnetic torque to invert the satellite if necessary.

The following event occurred: the TEX gravity gradient boom did not deploy correctly: it is deployed after the satellite is on orbit. During the extension the boom became bent and flexible. Therefore, it cannot hold the satellite attitude. DSI developed a control procedure to maintain the correct attitude. However, its success was moderate.

3. NO OFF-SWITCH

The current problem is that the UHF link was, and is still functioning. The system has no "off" switch to prevent fatal unintentional shutdown, and it can still receive commands and download telemetry.

The satellite was designed to be robust: if the power system bus voltage falls below a threshold, protective circuits operate to shed satellite loads, to restart the computer when the batteries have been recharged and to initiate the beep receive mode to re-establish communication with the ground station. If the flight computer "hangs up", a watchdog timer operates to reset the computer, clear the memory, restart the control program and initiate the beep receive mode.

The UHF link expects regular scheduled contact with the ground control station, which executes normally two or more scheduled exchanges per day. It enters the beep receive mode if no schedules are seen for 72 hour.

The schedules can become absent if the operator has neglected to uplink updated schedules, if timely schedule uplink was not heard by the satellite, and if the flight computer "watch-dog" timer initiates reset.

The beep receive mode is the interfering mode. The UHF link transmits a 2-second burst of status and telemetry every 72 seconds and listens for a reply. It is attempting to re-establish contact with the ground control station. The beep receive mode continues until valid schedules are received from the ground control station. The operator must recognize the beep receive mode in order to take action. He cannot execute corrective action in absence of the beep receive mode since that would overflow the satellite command buffer, lose visibility of future schedules events in telemetry and initiate possible watch-dog timer reset. The beep receive potential is expected to continue until the solar panels cannot collect sufficient energy to sustain the system (the system cannot restart after a recharge period), the flight computer hangs up and the watchdog timer has failed, or the satellite's transmitter fails.

4. ACTIONS

To keep the UHF link "quiet" requires regular operator effort and regular communication of the ground station with the satellite. An accompanying problem is that the satellite uplink appears to be degraded due to the following reasons:

- * The satellite receiver may be losing sensitivity because to aging of the components, exposure to space environment and increased ambient noise.
- * Or, the satellite is upside down, so that the antenna is less effective in this inverted attitude.

Boeing is maintaining the TEX satellite and has set up a program for daily monitoring and work on the problem solution. The ground station has employed operator manpower and installed equipment to keep the satellite "quiet". OSC has a backup station for assistance when required.

Boeing began monitoring TEX on 5 September 1997. TEX had probably been in continuous beep receive mode up to that time since it has no possibility to turn it "off" at end of mission. After several Boeing activities the beep receive ended on 21 September 1997. From 21 September 1997 to 8 May 1998 (= 230 days) TEX has been in beep receive mode for 43 days only. Of these 43 days, 15 days turned out to be "avoidable" and 28 days were "spontaneous" due to malfunction of the satellite system).

The following ongoing actions are distinguished:

- * Maintain beep silencing through Boeing/ground station

- * Improve the link margin by increasing the ground transmitter power, installing a tracking antenna at OSC /backup facility
- * Improve spacecraft control reliability
- * Interface to radio astronomy community (beep log from USAF, TEX pass data from USAF and interference report log from radio astronomers).
- * Pursue permanent deactivation (the risk assessment requires radio astronomy input).

5. DEDUCTIONS

The events with the TEX satellite show that the harmful interference results from a series of mishaps.

Among those are:

- [a] the frequency used by the satellite which is illegal according to the ITU-R Radio Regulations (see its Article S5, the Table of Frequency Allocations).
- [b] the satellite has no "off" switch. The reasons for this are known and it is CRAF's understanding that later satellites are required to have such a switch. However, the absence of this facility in the TEX satellite implies great difficulty to make it silent.

CRAF assumes that deduction [a] is not an intentional error but the result of insufficient or inaccurate communications or misunderstanding, somewhere between the parties involved in the frequency selection and coordination process for this space station. CRAF considers this a serious issue because of its possible consequences: The harmful interference event hurts currently the Radio Astronomy Service. Another event with a different space station might cause interference to other users of radio, e.g. the safety of life communications. And when the space station does not have the facility to kill the interference (as in this case), the consequences can be much more catastrophic.

A case as the harmful interference from the TEX satellite is therefore extremely important. CRAF trusts that the lessons which have to be learned from this case by regulatory authorities, operators, system designers, and industry lead to adequate regulatory, procedural, and technical improvements to prevent similar cases in future.

Knowing the details about the TEX satellite, it has to be investigated in which way, and to which extent the interference problem can be alleviated.

6. ACKNOWLEDGEMENTS:

CRAF thanks the administrations of the Netherlands, Germany and the USA (NTIA) for their supportive help. We also thank the ITU-R Radiocommunications Bureau for its actions, the US Department of Defence, the NSF Spectrum Manager, and the Boeing Company to bring clarity on this issue.

THE CLOUD RADAR, A PROBLEM FOR THE PASSIVE USERS OF THE mm-WAVE SPECTRUM. TESTS ON A PROPOSED FILTERING STRUCTURE

V. Natale (*), G. Tofani (*), G. Tomassetti (**), V. Dainelli (***)
C. G. M. Van't Klooster (****)

(*) CAISMI - CNR Largo E. Fermi, 5 I-50125 Firenze

(**) IRA - CNR Via Gobetti 101 I-40129 Bologna

(***) OERLIKON-CONTRAVES Via Affile, 102 I-00131 Roma

(****) ESTEC, Nordwijck, The Netherlands

After a recollection of the scientific aims and of the proposed hardware for its implementation, the Authors describe the behaviour of a novel band-stop filter working at 95 GHz, designed and manufactured by Oerlikon-Contraves in the optics of a profitable collaboration between science and industry.

The results of the measurements of the filter at 78K and 4K are also presented and discussed.

1. SCIENTIFIC GOALS

A global warming monitor may become the measurement of the three-dimensional distribution of clouds which effectively govern the earth radiation budget.

The large scale air circulation and the vertical distribution of radiative and latent heating are also largely dependent on the vertical cloud profile. The cloud profiling cannot be fully ascertained by optical means due to the cloud's opacity at very short wavelengths.

However the reflectivity of clouds at microwave frequencies can be profitably used to "see" their inside and if the microwave stream comes from above e.g. from a radar orbiting at the proper height, its multi-layer structure down to ground level can be evaluated.

The use of a low earth satellite (LEO) carrying a suitable radar device has been envisaged in order to carry out this task in a relatively simple fashion.

It has been estimated that one kilowatt of millimetre-wave power and a 2 meter diameter parabolic dish, nadir looking, flying in a polar orbit some 400 km above ground would be just enough in the first phase of the proposed research.

Modern technology gives the right answers to most of the problems involved in the design of such a flying structure but open questions still remain e.g.:

- i) the choice of a suitable frequency;
- ii) the interference caused to other services (largely dependent on the previous choice).

As a matter of fact radars located on space stations, according to Radio Regulations, were supposed to operate within 78-79 GHz, but meteorologists opposed this confinement and suggested the use of a small sector close to 95 GHz for two important reasons:

- i) a technical one: existing high power radar devices at 95 GHz are readily available while nothing of that sort is to be found at 78 GHz;
- ii) a scientific one: the back scattering coefficient of clouds is inversely proportional to the fourth power of wavelength making a worthwhile improvement in the radar sensitivity (3.4 dB) the choice of 95 GHz instead of 78 GHz.

The choice of a sector close to 95 GHz is today agreed to by the majority of the scientific community (WRC 97 has just allocated 94.0-94.1 GHz) the only objections coming from radioastronomers and remote-sensing scientists who fear the consequences of a high power transmitter crossing either the main beam or side lobes of their ground-based sensitive millimetre-wave receivers.

It has been shown that an SIS receiver can be destroyed or suffer heavy overloading depending on the position of the flying radar overhead.

2. DESIGN AND MEASUREMENTS

Aware of these problems, the European Space Agency (ESA) have let a contract to Oerlikon-Contraves to make a "Study of Protective Measures for mm-wave Radio Telescopes against Interferences Generated by Spaceborn Cloud Radar".

The results of the preliminary "Study" were presented by Oerlikon-Contraves during the March 1997 meeting at ESTEC.

The proposed solution consists essentially in the introduction of a suitable band-stop filter before the input of the mm-wave receiver.

The aim of the design of the protective structure was the integration of the filter between the mixer/bolometer waveguide mount and the feedhorn which collects the radiation from the telescope antenna. Usually, at mm-waves in particular, these components operate at cryogenic temperatures, typically between 4K and 70K. The filter structure was designed as a cascade of cavities, made either with slots or rings in circular waveguide.

Both solution imply severe technological problems which have been analysed in great detail by Oerlikon-Contraves. The two options have been manufactured by electroforming techniques and tested at ambient temperature.

Owing to the physical complexity in the structures, only the electromagnetic characterisation was possible and, from the derived parameters, a comparison between theory and measurements was carried out considering nominal dimensions of the filter and random error tolerances effects.

The results indicate that the ring-loaded filter is the one which meets more easily the required specifications. A cross-section of the filter is shown in Fig. 1.

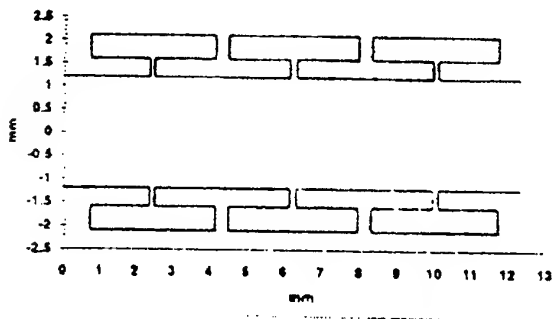


Fig. 1. Cross-section of the selected three section ring loaded filter.

In the prosecution of the program, the impact of the cryogenic temperature on the filter response and on the measurements procedures was carefully analysed.

The expected major effects of very low temperatures on the filter, concern the dimensions and the electromagnetic parameters changes in the metal itself. A review of the properties of solids at cryogenic temperatures, therefore, has been carried out in order to predict the behaviour of the filter near 4K.

The actual measurements of the electrical parameters of the prototype unit needed its fixing on the cold plate of a proper dewar as sketched in Fig. 2.

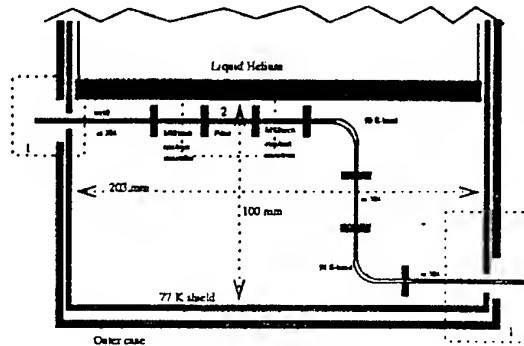


Fig. 2. Cross-section of the lower side of the dewar. The DUT is screwed on the thick copper plate.

Stainless steel waveguide lengths solved the thermal isolation problem between the device under test (DUT) and the ambient temperature window protected by a 10 mil thick Mylar membrane, shown in Fig. 3.

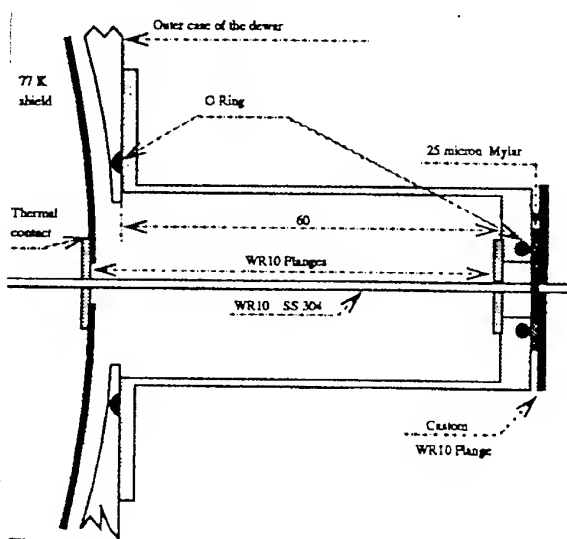


Fig. 3. Detailed section of the input/output windows of the dewar.

The actual filter response was measured in terms of S-parameters using a HP8510 test system at Oerlikon-Contraves facilities. The measurement procedure was the standard substitution method where the DUT is removed in order to calibrate and store the measurement set up, interface transitions included.

A lengthy and cumbersome calibration-substitution-measurement had to be performed at ambient, 78K and 4K temperatures. The filter true performance was then finally obtained by subtraction.

An alternative measurement procedure, more appropriate considering the peculiarity of the application of the filter, could be the radiometric method (RATEP WP2000, 1997) but its complexity (need of a broad

band highly stable receiver at 95 GHz and of a high resolution spectrometer) and the expected lower accuracy (noise measures) suggested to favour the S-parameter approach.

3. RESULTS

The main parameters to be measured in the prototype filter unit were:

- i) its ability to withstand a sudden temperature stress;
- ii) the insertion loss variation vs. temperature;
- iii) the "depth" in dB of the rejected band vs. temperature;
- iv) the frequency shift of the band-stop centre frequency vs. temperature.

The first point was implemented by simply dipping the filter in liquid nitrogen. As this test was well taken, the unit was located in the dewar for further investigations. The second point, the out of band insertion loss variation with cooling, results difficult to quantify: the computed loss of the filter is 0.13 dB at 300K. The expected improvement of this already small quantity was well detected at 78K and 4K but being so close to the accuracy of the test gear is difficult to quote it with confidence. An estimate figure could be 0.05 dB, equivalent to 5K noise temperature.

The shape, position and depth of the stop-band response are easily determined because displayed on the monitor of the test set-up.

Fig. 4 shows the response of the filtering structure at ambient temperature.

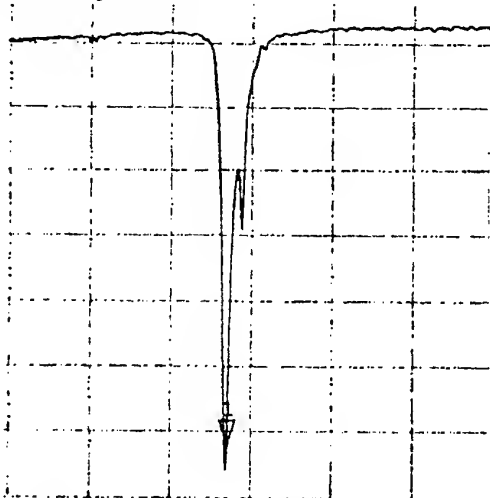


Fig. 4. The filter response at ambient temperature. On the horizontal frequency scale the resolution is 3.5 GHz; the vertical scale reads 5 dB/.

The loss of the rejected band is greater than 30 dB. The band effectively "occupied" (pedestal of the whole

response on the frequency axes) is of the order of 3 GHz.

The results of the test at 78K are not commented because they are so close to those obtained at 4K.

Fig. 5 shows what's happening when the physical temperature drops down to 4K (actually the effective working temperature was measured to be 7K). The improvement in the depth of the resonance is about 10 dB.

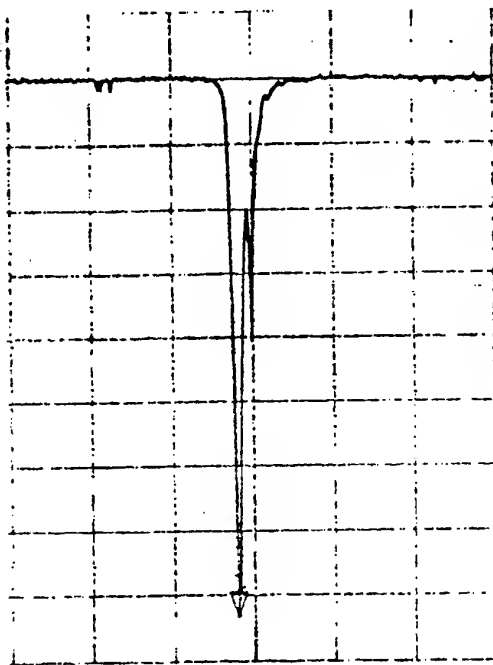


Fig. 5. Filter behaviour at 4K. Note the improved depth of the resonance and the shift upwards of the centre frequency.

Finally the graph of Fig. 6 shows the measured linear trend of the band stop dip towards higher frequencies for temperature dropping from ambient to 78K. Only a marginal change of this parameter is detected when the physical temperature swings from 78K to 4K. The computed slope in the linear region is 1.56 MHz/K.

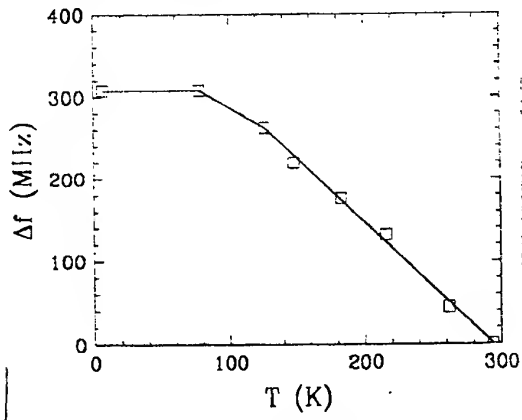


Fig. 6. The shift of the stop-band centre frequency vs. temperature.

4. REFERENCES

- 4.1. Proceedings of RATEP Program final meeting, ESTEC, Nordwijck, The Netherlands, March 24 1997.
- 4.2. C.C. Linn, P. Ingmann, "A cloud profiling radar for studying the earth radiation processes and budget", ESTEC, The Netherlands.
- 4.3. J.E.B. Ponsonby, "Notes on the proposed 94.5 GHz space based cloud profiling radar and its impact on mm-wave radioastronomy", Jodrell Bank, UK
- 4.4. "Spaceborn cloud radar measurement at 95 GHz band and preliminary sharing considerations", Radiocommunication Study Group, Document WP7C/-E.
- 4.5. "Preferred frequency band, technical characteristics and sharing considerations for a spaceborn cloud radar", ITU-R Fact sheet: Study Group JWP 7-8R.
- 4.6. T. Spoelstra, "CRAF Newsletter", 1997/2.
- 4.7. D. Morris, A. Winnberg, "Enhanced protection of the mm Radio Astronomy bands".
- 4.8. Proceedings of ESA Workshop on rain/cloud radar, 1993.
- 4.9. V. Dainelli, K. Van't Klooster, G. Figlia, "Protective devices for ground based mm-wave radiotelescopes against satellite cloud profiling radar operation", 20th ESTEC Workshop on mm-wave antenna technology and antenna measurements, ESTEC, Nordwijck, The Netherlands, 1997.

BIOGRAPHICAL NOTES

V. Natale received his laurea in physics from Torino University, Italy in 1966. He is presently in the research staff of CAISMI - CNR (Centro per l'Astronomia Infrarossa e lo Studio del Mezzo Interstellare del CNR). Since 1990 he is involved in the design and construction of submillimetre wave receivers for astronomical observations.

G. Tofani received the laurea in electronic engineering from Pisa University, Italy. Currently he is senior astronomer at the Arcetri Astrophysical Observatory and Director of the Institute for Infrared Astronomy of the CNR. His main research interests are on radioastronomy techniques and star formation astrophysics. Dr. Tofani is an Italian delegate of URSI (Comm. J) and vice-president of the Italian URSI Commission.

G. Tomassetti is the physicist in charge of the microwave lab of the IRA - CNR (Istituto di Radioastronomia, Bologna). He designed and supervised the installation of the early receivers of the "Northern Cross" and afterwards of the VLBI cooled front-ends in Medicina and Noto. Today is very active in the task of protecting the radioastronomy bands as the Italian representative in the CRAF.

V. Dainelli joined Oerlikon-Contraves in 1976. He acts as project manager in the microwave and mm-wave development of military and space applications. He is the project manager of the ESA contract: "Study of Protective Measures for mm-wave Radio Telescopes against Interferences Generated by Spaceborn Cloud Radar". The 95 GHz filter described in this paper was designed, manufactured and tested at ambient and cryogenic temperature under his supervision.

At the Limits - Radioastronomical Observations with the Effelsberg 100m Telescope

K. Ruf, E. Fürst, and W. Reich

Max-Planck-Institut für Radioastronomie

Auf dem Hügel 69

D-53121 Bonn, Germany

tel.: +49 228 525255, fax.: +49 228 525229, e-mail: kruf@mpifr-bonn.mpg.de

Abstract: Radioastronomical observations require the maximum possible sensitivity to detect weak signals of cosmic origin. Interference by active services limits the sensitivity or makes observations impossible at all. We describe the actual and expected interference situation at the Effelsberg 100m telescope.

1. Introduction

The Effelsberg 100m telescope (see Fig. 1) is still the largest fully steerable single dish radio telescope in the world. Continuously improved over its 25 years of operation, it is a very flexible instrument, used for a wide range of scientific applications over a wide range of frequency bands. Located in a narrow valley, it is

and announced satellite networks, however, constitute a major threat for the future.

2. The Frequency coverage of the Effelsberg radio telescope

Initially designed for decimeter and centimeter wavelengths up to a frequency of 10 GHz the Effelsberg 100m telescope is today used at a highest frequency of 86 GHz. Astrophysically important information can be gathered at all frequencies, not only within the bands, which the ITU has allocated to radio astronomy. Therefore, full frequency coverage up to 50 GHz is aimed for. (86 GHz is used presently for interferometric observations (VLBI) only.)

An updated list of receivers is available at <http://www.mpifr-bonn.mpg.de/w3/technik/rxlist.html>. Specifications, such as RF-filtering and system temperatures, can be found there as well.

3. Radioastronomical frequencies

Radio astronomy is treated as a radiocommunication service by the ITU, which means that a series of frequency bands are allocated to radio astronomy. Additionally, use of certain subbands for radioastronomical observations is indicated by a footnote in the table of frequency allocation. Another footnote contains a list of passive bands, where all emissions are prohibited. The fraction of spectrum allocated to radio astronomy is increasing with frequency:

below	1 GHz :	2.2%
below	10 GHz :	3.1%
below	30 GHz :	4.0%
below	100 GHz :	9.0%
below	275 GHz :	22.5%

However, below 10 GHz most of the allocation is secondary, and radio astronomy has formally to accept interference by active services with a primary allocation, although no useful measurement can be made. 2/3 of the radio astronomy allocation below 100 GHz fall into the

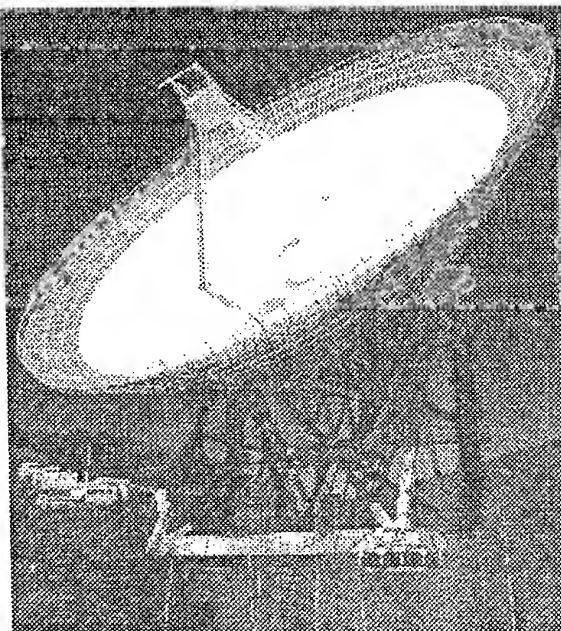


Fig. 1 The 100m radio telescope of the Max-Planck-Institute für Radioastronomie

reasonably well shielded against interference from terrestrial transmitters. The large number of planned

band 86 - 92 GHz, which is of limited use for the Effelsberg radiotelescope only.

4. Sensitivity and Interference limits

Radio astronomy is the radio service with the highest sensitivity and hence the lowest interference threshold values. Tables with interference threshold values for all frequency allocations to radio astronomy can be found in the ITU-R literature together with their derivation and assumptions [1].

The basic assumptions are: The interfering power should stay below 10% of the noise fluctuation of the measuring system after detection given by the system noise. In other words, the sensitivity of the radioastronomical system should not be reduced by more than 10%. This sensitivity is derived for the different frequency bands as a function of the receiver noise temperature, minimum antenna temperature, observing bandwidth, and an integration time of 2000 sec. Bandwidth is taken to be the width of the allocated band in the case of continuum observations, and as channel bandwidth corresponding to a Doppler broadening of 3 km/s for spectroscopy. These values are just sample values and not at all representative for the best in sensitivity that can be reached today. Also some of the assumed receiver noise temperatures are a bit outdated.

4.1 „On the fly“ measurements.

The Effelsberg radiotelescope is sensitive enough to measure some of the stronger spectral lines „on the fly“. In this observing mode, the telescope is moved continuously, scanning a field in the sky, rather than taking a spectrum on a source position and subtracting the spectrum of an off-source position, as is the more common observing mode in spectroscopy. As the integration time one may, in that case, take the time interval in which the main beam of the telescope slews over a fixed point in the sky. An example of such an „on the fly“ measurement is given in figure 2, a spectrum of a SO-line at 30.001 GHz. The equivalent integration time is 30s and the line flux density is 1.6 Jy.

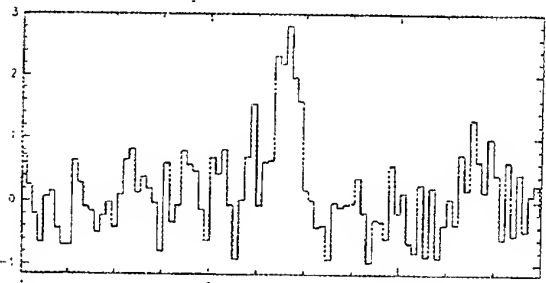


Fig. 2 Spectrum of the SO line at 30.001 GHz, observed in the dark cloud L1512 (D. Muders, private communication) Brightness temperature (K) is plotted against velocity (km/s)

4.2 Deep spectra.

At the other end of the sensitivity scale long integrations result in spectra of very weak spectral lines. As an example (Fig. 3) a spectrum of the very rare isotope ^3He at 8.6 GHz is given. The determination of the abundance ratio of the rare isotope ^3He to the ^4He isotope and its spatial distribution are of greatest cosmological importance. Presently only the Effelsberg radiotelescope is sensitive enough to take ^3He spectra. The given example is the result of 21 hours of integration time, and the line flux density is 4.5 mJy.

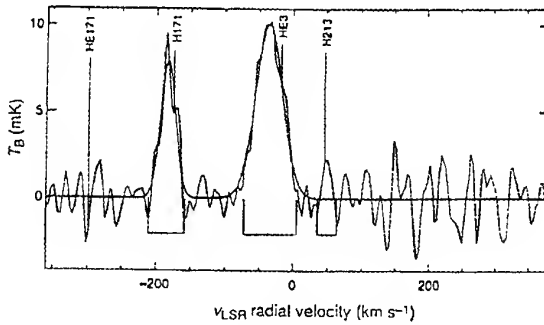


Fig. 3 Spectrum of the ^3He line at 8.6 GHz, observed in NGC3242. The weak Hydrogen line (H171) is also displayed.[2]

5. Interference examples.

5.1 GLONASS.

The first case of a loss of a complete radioastronomical band to interference happened a couple of years ago. The reason was the Russian global navigation satellite system GLONASS, which rendered the frequency band 1610.6 - 1613.8 MHz useless, where a transition of the OH radial (Hydroxyl) is observed. This event did, of course, affect all radiotelescopes in the world. Therefore, IAUCA, the Inter-Union-Commission for the Allocation of Frequencies, started negotiations with the GLONASS administration. The negotiation resulted in a coordinated experiment first, and later in an agreement to remove the interference in a step by step approach. Until the year 2005, the transmissions of the GLONASS satellites into the radio astronomy frequency band will be suppressed to below the interference threshold values of ITU-R RA.769. (i.e. -238 dB(W/m².Hz)). Also the Effelsberg telescope has taken part in the coordinated GLONASS experiment, the results have been presented [3].

5.2 ASTRA 1D.

The second case of the destruction of a whole radio astronomy band is constituted by the TV satellite ASTRA 1D of the Luxemburg based company SES.

Radio astronomy has a primary allocation in the band 10.6 - 10.7 GHz, the upper part of which, 10.68 - 10.7 GHz even being a purely passive band („all emissions are prohibited“). However, the adjacent band 10.7 - 11.7

GHz is allocated to the fixed satellite service for space-to-earth transmissions. ASTRA 1D now (ab)uses the lowest channel of that FSS allocation to broadcast direct-to-home TV. The situation is best illustrated by the spectrum given in Fig. 5, which the satellite monitoring station Leeheim of the German administration has taken. The sensitivity of their system (12m antenna, uncooled receiver) was not sufficient to detect signals at the interference threshold levels of ITU-R RA.769, nevertheless, the power flux density of the TV programme is well above the noise floor of the Leeheim spectrum analyser through the upper part of the radio astronomy band. This noise floor corresponds to a flux density of 30 dB above the recommendation ITU-R RA.769 threshold value, where, additionally, another 15 dB of extra protection against transmitters in the geostationary orbit is asked for, because the assumption of 0 dBi of sidelobe level for the receiving antenna is not valid in a large circle around the satellite transmitter.

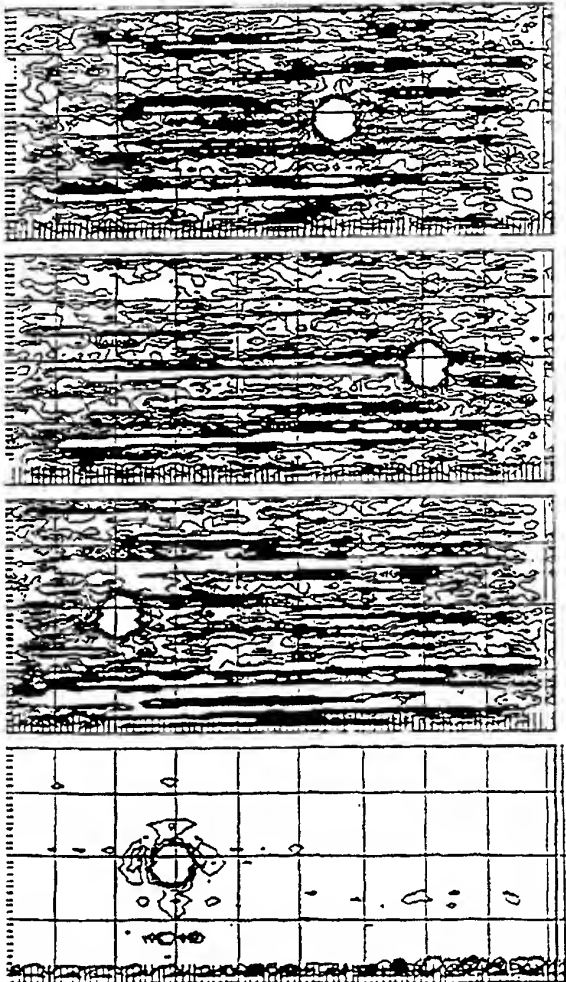


Fig. 4 Test measurements on a strong point source, 20° away from the ASTRA position, with channels A to D (bottom to top) of the 10.7 GHz receiver.

This effect could be clearly shown in test measurements with the Effelsberg telescope. The 2.8cm receiver has a 4-horn 8-channel frontend. For the test observations, represented in Fig. 4, channel A was equipped with a steep bandpass filter and tuned to a lower frequency. Channel B was also tuned to lower frequencies by 100 MHz, but without additional filtering. Channels C and D remained unmodified, i.e. optimized to observe the radio astronomy band. The measurement was taken at a position in the sky, 20 degrees away from the ASTRA position. Clearly, only channel A delivered useful data. Now, all 4 channels are retuned and filtered, and a frequency band is observed, which is allocated to other services. This is in general acceptable for continuum observations, but the filters reduce the sensitivity a bit, and in case of interference by the services, to which this band is allocated, there is no basis for complaints.

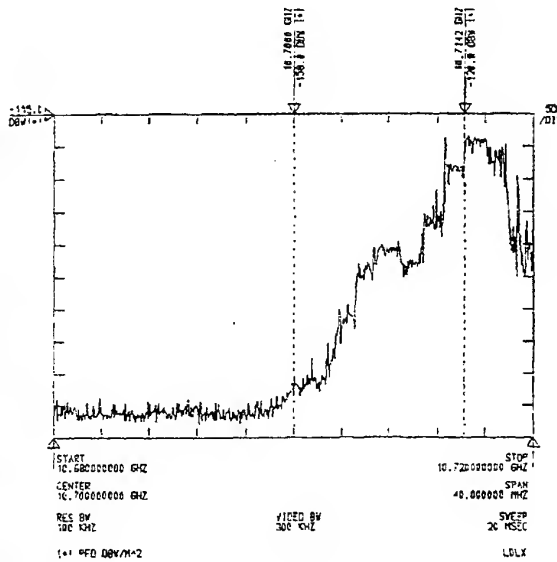


Fig. 5 Calibrated spectrum of ASTRA 1D, taken by the satellite monitoring station Leeheim. The dashed line at 10.7 GHz is the border line between the radio astronomy and the fixed satellite allocation

5.3 Fixed link networks.

As an example for an ongoing coordination process the setup of the mobile phone networks may be considered. The frequencies at which the mobile phones are operating are not under discussions here, the potential danger comes from the associated fixed link networks. Their preferred frequency band in Germany is 23 GHz. A few years ago, interference at such a high frequency was beyond imagination, today fixed links are being installed at frequencies even above 30 GHz.

In the spectrum region of the 23 GHz fixed service, radio astronomy has two allocations with primary status: 22.21 - 22.5 GHz and 23.6 - 24.0 GHz, for observations of interstellar water and ammonia. Three further sub-

bands are protected by footnote S5.149 in the radio regulations of the ITU-R for spectroscopic observations: 22.01 - 22.21 GHz, 22.81 - 22.86 GHz, and 23.07 - 23.12 GHz. Additionally, a lot of other spectral lines are observed in that part of the spectrum with the Effelsberg telescope outside the allocated bands. The mobile phone companies as well as the German regulating authority use modern computer tools for network planning and licensing. During that process it appeared that some of the fixed links would produce power flux densities at the site of the Effelsberg telescope, which could be tens of dB above the interference threshold levels. At that point, radio astronomy, mobile phone companies, and regulating authority came together and started a coordination process, which is still ongoing.

The companies very cooperatively opened their plans and even participated in test measurements. Again, the common problems showed up: measurements with regular monitoring and control instruments are not sensitive enough. The very sensitive Effelsberg radiotelescope, however, is not able to point at a terrestrial transmitter, due to its location in a valley, even if there is line of sight from the transmitter to the limb of the telescope protruding over the hills. Also, an antenna diagramme, like the technical specifications of e.g. the small dish antennas of the fixed service, cannot be obtained for the 100m telescope. On top of it, the interfering transmitters are in the near field, which makes predictions of the sidelobe level and distribution even more vague.

In fact, during test observations performed with a fixed transmitter at one of the critical sites, which was pointed in the direction of the Effelsberg telescope for test purposes, a relative maximum power level happened to be detected with the telescope pointing at 15° elevation and 36° offset in azimuth. A later, more systematic measurement showed the sidelobe level of the near field antenna beam pattern in reasonable agreement with the far field model antenna response with possibly a few dB extra margin due to the shielding by the surrounding hills. (There was line of sight to part of the telescope aperture, only.) So, the Effelsberg telescope is continued to be protected to the interference threshold levels of Recommendation ITU-RA.769 in the bands allocated to radio astronomy. Negotiations with the involved companies have even shown the willingness to protect the Effelsberg telescope in a more general manner even outside the allocated bands, in the case of very nearby fixed stations. Technical solutions discussed are connection of the sites by cable, or implementation of a switching capability, in order to allow sensitive observations in each part of the spectrum on request. Details have to be worked out, how

ever, the interference situation is still very good.

6. Conclusions

The observations of the two spectral lines (SO and ^3He), described in part 4, were made at frequencies where there is no allocation to radio astronomy, and which are not contained in footnote S5.149 of the radio regulations. Nevertheless, excellent and scientifically high ranking measurements are possible.

The 10.7 GHz band has been an important continuum band for polarisation and pulsar observations. The allocation has always been a bit narrow, but it was well placed in the spectrum, at about octave distance to the 5 GHz band below and the 22 GHz band above. It is completely destroyed by one satellite.

The GLONASS-IUCAF agreement is up to now followed by the Russian administration, and OH observations in the affected band are again possible, at least on the stronger maser sources. However, some of the mobile satellite systems, which are presently prepared, aim at exactly this band with their difficult to coordinate mobile frequencies. In fact, the Iridium system, which is the most advanced of these systems, plans to use a nearby portion of the frequency spectrum for their downlink transmissions.

In the 23 GHz FS band negotiations with interested active users of the spectrum has so far resulted in a very favourable situation. However, the before mentioned mobile satellite system Iridium plans to use the band 23.1925 - 23.3675 GHz for their intersatellite link, in analogy to the fixed network of the mobile phone systems. This subband is very close to the before mentioned band 23.07 - 23.12 GHz, for which the radioastronomical interest and use is notified in footnote S5.149 of the radio regulations. In this case it must be strongly doubted that there is the possibility and the willingness to protect observations with Effelsberg or any other radio telescope in this part of the spectrum, which is very rich in spectral lines.

Alltogether, the interference situation at the Effelsberg telescope with its unique scientific possibilities is not very clear cut. Two trends, however, are evident: interference is occurring at higher and higher frequencies, and the advantage of the valley location is more and more lost due to satellite transmissions.

7. References

- [1] Handbook on Radio Astronomy, 1995, ITU, Radiocommunication Bureau, Geneva
- [2] R.T. Rood, T.M. Bania, and T.L. Wilson, 1992, Nature, 355, 618
- [3] K. Ruf, 1994, Kleinheubacher Berichte 37, 541

10 years CRAF - an evaluation

T.A.Th.Spoelstra

ESF - Committee on Radio Astronomy Frequencies

P.O.Box 2, 7990 AA Dwingeloo, The Netherlands

Phone: (+31)521-595100, Fax: (+31)521-597332

e.mail: spoelstra@nfra.nl, WWW homepage: <http://www.nfra.nl/craf>

Man-made interference of various kinds has an increasingly negative impact on passive services and scientific applications of radio. The key to the problem is due to the different characteristics of "passive" and "active" spectrum applications. By nature these are not compatible. Sophisticated hardware and software tools have to be developed to cope with interference effects. In cases where this is not sufficient other solutions have to be found. The pressure from commercial and industrial applications of radio is increasing exponentially. Facing this development, scientists - radio astronomers in particular - are confronted with the question how they could proceed beyond for instance the year 2050. This paper reviews the activities of European radio astronomers during the last decade to keep their radio windows clean. It is considered that from this basis radio astronomy will remain a healthy science doing frontline research while taking the developments adequately into account.

1. INTRODUCTION TO CRAF

The compatibility between radio applications of a passive and an active radiocommunication service is a key question of the issue of sharing the same radio frequency band. Daily experience of the vulnerability of passive radio use for harmful radio interference lead in 1988 to the formation of the Committee on Radio Astronomy Frequencies, CRAF, under the umbrella of the European Science Foundation, ESF (Strasbourg France). CRAF coordinates the European efforts for the protection of radio spectrum bands used by the Radio Astronomy Service, RAS, and other passive applications. At present 16 European countries are member of CRAF. Also the European organisations ESA, EISCAT (European Incoherent Scatter Scientific Association) and IRAM (Institut de Radio Astronomie Millimétrique) are member of CRAF.

The technological development has enabled all kinds of advanced astrophysical research, but at the

same time it threatens to render it impossible from the surface of the Earth. Terrestrial, airborne and space-borne transmissions are generated in ever increasing numbers for a multitude of purposes. The starting point of CRAF is not only that the frequency protection should be maintained at least to the level passive applications of radio enjoyed until now, but also to enable scientific use of radio for the next generation of scientists.

An important part of its work is to assist the International Union Commission on the Allocations of Frequencies for Radio Astronomy and Space Research, IUCAF. This body is a joint commission of the International Union of Radio Sciences, URSI, the International Astronomical Union, IAU and the Committee on Space Research, COSPAR. These three are amongst the many international scientific unions which under the International Council of Scientific Unions, ICSU, devolve from UNESCO.

For the protection of the Radio Astronomy Service within Europe, CRAF attempts to coordinate the representations made to the various national and supranational radio regulatory bodies. It operates both at an administrative and at a technical level, so that it is for instance also concerned with setting up programmes of interference monitoring and seeks to develop technical means for the protection of radio astronomical observations. It has an educational role in making other radio spectrum users aware of the sensitivity and consequentially the need for protection of the RAS. This function is being fulfilled by e.g. the publication of its Handbook for Radio Astronomy [1] which is intended to be widely available, particularly to system designers and to Spectrum Managers. Furthermore, CRAF regularly publishes a Newsletter, which is available on the WorldWideWeb (URL address: <http://www.nfra.nl/craf>) and as a hardcopy publication. The CRAF information on the WorldWideWeb also contains detailed information about the relevance of all frequency bands used by radio astronomy in Europe, a brief summary of the interference status and a review

of those applications which have impact on radio astronomy by their interference.

Since January 1, 1997, CRAF employs a full time pan-European radio astronomy Spectrum Manager.

The division of the activities of the organizations working on the protection of radio astronomy frequencies is as follows: IUCAF considers global issues. CRAF addresses European regional issues. In the USA and China radio astronomers have their local organization. An Asia-Pacific regional body for this work will soon become operational as well.

2. SHARING BETWEEN RADIO ASTRONOMY AND OTHER SERVICES.

Radio astronomy is a "passive" radiocommunication service: a *receiver-only radiocommunication application*. It is not able to influence the transmitting source: the celestial radio source which transmits its radio waves at the frequency it likes and at the time it prefers. All other services use both a transmitter and a receiver, both of which man can manipulate. They are called "active" services.

Passive frequency use is most vulnerable for pollution. This is particularly true for the radio signals relevant for scientific research. The science which is the best example of passive frequency use is radio astronomy. By its extremely sensitive sensing techniques it enables mankind to access physical conditions in the universe which are impossible to attain in a man-made laboratory. Radio astronomy does not give merely a description of the universe; it is providing tests for the laws of basic, fundamental physics. The results of radio astronomical research have often opened new directions in other sciences and technology. This opening of new perspectives can only be achieved when certain frequency bands are 100% free of interference. These bands can not be selected at will, but are set by Nature itself.

Radio astronomical signals are about 9 orders of magnitude weaker than those used by active services. This difference is a major cause of the vulnerability of radio astronomy to man-made interference.

This interference introduces a "radio-climate" with parameters depending on frequency, transmitted power, spatial coordinates and time. Furthermore, this interference can be either intended or unintended, legal or illegal, which implies that the problem has a dynamic character. To answer this, a dynamic solution is required, which needs adequate system design on the one hand and cooperation with administrations, active spectrum users and radio astronomers on the other hand. The different characteristics of passive and active spectrum use implies a multidimensional regulatory approach.

The radio spectrum is scarce natural resource. This implies that it is unavoidable that different radiocommunication services share the same frequency bands.

To enable this, complicated coordination work is often required. The fundamental difference between active and passive services implies that, unless the contrary has been proven by a thorough coordination study, in general no sharing is possible. This holds especially for radio astronomy with respect to active users of the spectrum.

In some cases sharing might be possible between terrestrial applications of radio and radio astronomy, e.g. by geographical "shielding". But spaceborne application can in no way share with radio astronomy, since radio telescopes cannot be shielded against spaceborne transmissions [2].

The number of resolutions adopted World Radiocommunication Conference 1997, WRC97, in which studies are asked to investigate this problem in various frequency bands does support this fact. Furthermore, most of the sharing problems radio astronomers has with spaceborne transmissions are due to the fact that this difficulty was not understood adequately during previous WRCs and World Administrative Radio Conferences, WARCs.

3. ISSUES OF THE PAST - ISSUES OF THE FUTURE.

In the past, e.g. more than a decade ago, the majority of the interference issues in radio astronomy had a terrestrial origin: e.g. broadcasting, military applications, civil users of radio, traffic (one of the many EMC problems).

However, the space era which started with the launch of the Russian SPUTNIK in 1957, showed an enormous development of space applications of radio. Administrations and terrestrial radio frequency users had to change their minds: terrestrial applications of radio could be considered in a relatively local context (possibly coordination with a neighbouring country was needed, which placed the issue in a regional context), but space applications have a global impact because of the transmitters fly all around the world (except for geostationary stations) and the footprints of their transmitters cover very large areas.

Reference documentation of the Radiocommunication Sector of the International Telecommunication Union, ITU, addressing protection and sharing issues have been developed mainly before the space applications became mature systems. The effort to adjust these references adequately to deal properly with space issues is slowly taking shape (apparently too slowly).

This implies that without reducing the effort to work on terrestrial issues, the space issues became of major importance as can be learned from the many interference cases radio astronomy experienced of various systems: e.g. GLONASS [3], ASTRA [4], IRIDIUM [5] and a decade ago with GEOSTAR and LOCSTAR [6]. New systems are coming which also may have strong impact on radio astronomy when no

sufficient precautions are taken.

Another development concerns the application of spread spectrum modulation techniques. Very wide frequency ranges are used for transmissions using this kind of modulation. When we consider that only the central main lobe of the spectrum carries the information, the sidelobes manifest first order spectrum pollution. It has been shown that [a] this is another major threat to radio astronomy, and [b] that by applying the proper modulation schemes much can be done to reduce the spectrum pollution [7]. It has also been recognized that ITU-R definitions for e.g. bandwidth, spurious and out-of-band emission have to be readdressed. Work on this is in progress in ITU-R TG1-5.

4. THE ROLE OF CRAF IN EUROPE.

CRAF acts on several fronts to protect the Radio Astronomy Service. It communicates and cooperates the Conférence Européenne des Postes et des Télécommunications, CEPT, and its off-shoot the European Radiocommunications Office, ERO, to ensure the continued good management of the radio spectrum. It participated in the preparation of a European Common Allocation Table which should come into force in the year 2008.

CRAF participates also in various CEPT SE project teams:

- SE17 PT concerning the compatibility between the MSS uplink and other radio systems in the 1610-1626.5 MHz band. With respect to radio astronomy the report of the project team compared the required separation distances between a radio astronomy observatory and a Mobile Earth Station, using different propagation models taking into account in-band as well as out-of-band emission from the MSS applications.
- SE21 PT concerning Spurious Emissions.
- SE27 PT concerning Terrestrial Digital Video Broadcasting, T-DVB.
- SE28 PT concerning MSS technical standards, operations, and compatibility issues (such as: the protection of primary services sharing the band or operating in adjacent bands (Radio Astronomy, MSS,...) and the protection of the Radio Astronomy Service at 5 GHz (second harmonic of the band 2483.5-2500 MHz).
- FM PT33 concerning the harmonization of frequency bands above 105 GHz.

CRAF also communicates and cooperates with European national administrations (both civil and military) on local issues with impact on European radio astronomy. It also has good contacts with the European Commission and NATO.

In addition, CRAF communicated with industry and operators in cases of interference problems: e.g. with the Société Européenne des Satellites in Luxemburg

and the German administration to solve the problem of out-of-band emission from the GDL-6/ASTRA-1D satellite in the radio astronomy band 10.6 - 10.7 GHz. The ASTRA satellite operating in the Fixed Satellite Service at frequencies just above 10.7 GHz, causes harmful interference in the subband 10.69 - 10.7 GHz. The band 10.6 - 10.7 GHz is heavily used by Effelsberg observatory in Germany.

Finally CRAF draws attention in various publications of its members to the effects of man-made interference on radio astronomical observations. In this context, it contributes also to radio and TV programs.

5. WHAT HAS BEEN ACHIEVED?

In general, CRAF has become a well-known organization in Europe which addresses the issue of protection of radio astronomy frequencies. Often administrations and the CEPT keep CRAF informed about developments and ask for advice.

In some cases a frequency band could be safeguarded for radio astronomy: e.g. CRAF corresponded with the UK Radiocommunications Agency concerning the possible use of television channel 38 (608-614 MHz). As a result channels 35 and 37 have been allocated to television transmitters but in the UK channel 38 is being kept free for radio astronomy.

In Italy, CRAF supported Italian radio astronomers in their communication with the Italian administration. This resulted in a much improved relationship between Italian radio astronomers and the Italian national administration. Also the communication with the Italian military authorities could be improved. This development resulted in activities to reduce the interference to radio astronomy in Italy. However, many issues still await a solution in Italy, especially related to private TV-networks which made it impossible to protect channel 38 in Italy. Also an radar interference issue at the radio observatory near Noto, Sicily, in the 1400-1427 MHz hydrogen line band (in which "all emissions are prohibited" according to the ITU-R Radio Regulations) awaits a solution.

CRAF acted as consultant under contract in an ESA - Oerlikon-Contraves (Italy) project to develop filtering techniques to protect radio astronomy for interference from cloud radar applications at 94 GHz. This resulted in the development of a bandstop filter with very promising characteristics [8].

CRAF contributed to the NATO-Committee on the Challenges of Modern Society, CCMS, by investigating the possibilities for more alert administrative control of frequency allocation and management, and possibly obtaining international judicial support. Report No. 213 on "The Passive Use of the Frequency Spectrum" [9] of this commission is a result of this effort.

The Nançay Radio Observatory in France maintains a European database on events of harmful interference

suffered by European radio astronomy observatories. Software tools are presently under development to query this database from the CRAF WWW pages. Nançay has also installed a dedicated monitoring facility to serve CRAF with adequate experimental data.

6. NECESSARY FURTHER DEVELOPMENTS.

Basically two items need to be addressed in the near future:

[i] the frequent WRCs (currently with 2 year interval) require a continuous effort and monitoring of related regulatory and technological developments. To achieve this, radio astronomers need to update their understanding of activities in other services continuously in order to anticipate further developments.

[ii] the increasing commercialization of telecommunication affects also the strategy of the ITU. The power of the market-perspective implies a major threat to non-commercial users of the spectrum. Non-commercial users of radio, radio astronomy in particular, should actively cooperate to react adequately to this "aggression". Nobody has more rights in the radio spectrum than anyone else. This "chapter" in effort coordination should become better developed.

In practice this means that the understanding of the radio climate needs to be improved. For that reason the CRAF EMI database at Nançay Radio Observatory will be a useful tool. Joint projects of radio astronomers and other spectrum users similar to the cloud radar project mentioned above are an important activity to achieve better interference protection and mutual understanding between different spectrum users. Many problems occur because of insufficient mutual understanding.

Of course actions to solve specific issues remain to take place, but an open eye to future developments requires flexibility, coherence in opinion among radio astronomers, and an assertive attitude. To assist, CRAF is considering preparing a handbook explaining the nature of frequency management, the role of regulatory bodies and the legal status of their products and a guide with recommendations for solving problems.

However, all these efforts only take place in the prevailing regulatory and legal framework.

7. IMPROVEMENTS OF THE REGULATORY METHODOLOGY NEEDED.

The principles of frequency allocation are laid down in the 1947 Atlantic City WARC of the ITU. To appreciate the mechanism and the results of these meetings an insight in the history of the ITU is very helpful [10]. The purpose of the ITU is based on the following principles:

International cooperation for the improvement and

the rational use of telecommunications of all kind, promotion of the technical facilities and harmonization of actions of nations.

With respect to the frequency allocation this means: Allocation of radio frequencies and registration of frequency assignments in order to avoid harmful interference between radio stations of different countries, and to coordinate efforts to eliminate harmful interference between radio stations of different countries and to improve the use made of the radiospectrum.

The changing "radio climate" (see above), the current modern technological developments, improved scientific understanding of radio wave propagation and changes in social interests, imply that the regulatory effort is of a "multi-dimensional" nature. In allocating use of radio frequencies one has to consider more than in the past in this regulatory process, geographical conditions, the use of time-slots and the allocation of transmitter power levels (maximum/minimum/operational). This further elaboration obviously depends completely on the considered radiocommunication service. The ITU needs to initiate and direct the development of adequate regulation methodology suited for today's conditions taking into accounts trends or future developments. This activity should be a combined effort of ITU-T and ITU-R. We note that in this case the ITU can already profit from the work started in Europe. The current regulatory effort is, in our opinion, not suited to respond to "overall development", it is too much limited to a simple dividing-a-cake-into-slices-procedure in which everyone likes to have the most tasty piece. This methodology may work in many cases, but in others it holds at its root a conflict when frequency sharing between e.g. active and passive services is required without adequate physical understanding and technological means to ensure whether this sharing is indeed possible. An example is the current sharing difficulty in between active and passive services in the 1.6 GHz frequency domain: allocations space-to-Earth have been given to the mobile-satellite service (although on a secondary basis) while a passive primary service (radio astronomy) for which the frequency of interest is given by Nature cannot be protected properly yet. The WRC-97, recognizing this kind of problem, did adopt some resolutions and footnotes to deal with the protection of radio astronomy, but until now this kind of action is too much an ad-hoc fix of a problem: it is not a structural aspect inherent to the overall allocation methodology of the ITU. Scientific users of radio experience a one-sided openness of the ITU for commercial, financial and industrial interests. This is enhanced by the "first strategic objective" for the ITU Standardization Sector: "adopting a market-oriented approach to standardization". If primarily commercial interests lead the interests of standardization, this will have enormous consequences for the work of ITU-R

(note the emphasis on "market"): in this case, the "standard" restricts regulation. [11]

9. CONCLUSIONS

The radio spectrum is a unique natural phenomenon. Active and passive frequency use have always been closely associated. In daily practice, active and passive services find themselves more in competition than cooperation. Mutual cooperation, however, is mandatory for the survival of vulnerable frequency use. This may result in joint technological developments and in agreements with the status of international law.

On the other hand the technical progress in both kinds of services is of mutual interest and benefit. It may help to find ways to escape the more and more pressing interference problems which is acute not only for radio astronomy but a fact of life for all applications of radio.

CRAF is contributing in a constructive manner to improve this cooperation and to stimulate this technological development. Although in other parts of the world organizations with similar interest operate at a local, regional or global scale, during the 10 years of its existence CRAF turned out to be the most productive one. The strong support of the ESF enables CRAF to address all upcoming issues in an assertive and flexible way.

CRAF started from scratch a decade ago. After a decade with restauration efforts and consolidation, CRAF has now entered an phase of cooperation with all interested parties. The aim is to live together in telecommunication country after 2050 or later. This can only be achieved when the radio windows are properly clean [12].

10. REFERENCES

- [1] "Handbook on Radio Astronomy", International Telecommunication Union, Radiocommunication Bureau, 1995
- [2] CRAF Handbook for Radio Astronomy, CRAF secretariat, P.O.Box 2, 7990 AA Dwingeloo, The Netherlands, 1995.
- [3] R.J.Cohen, "The GLONASS-Radio Astronomy Joint Experiment". Proceedings of the 12th International Wroclaw Symposium on Electromagnetic Compatibility, Wroclaw, June 28 - July 1, 1994. editors: J. Janiszewski, W. Moron and W.Sega, p.530-533.

[4] CRAF Handbook for Radio Astronomy, CRAF secretariat, P.O.Box 2, 7990 AA Dwingeloo, The Netherlands, 1995, p.98.

[5] T. Feder, "Iridium Satellite System Poses Threat to Radio Astronomy", Physics Today, November 1996, p.71-73.

[6] CRAF Handbook for Radio Astronomy, CRAF secretariat, P.O.Box 2, 7990 AA Dwingeloo, The Netherlands, 1995, p.96f.

[7] J.E.B.Ponsonby, "Modulator and form of modulation suitable for digital communications achieving low far-out side-bands levels without the use of filters: proposed as a modification to the Global Satellite Navigation System GLONASS", Proceedings of the International Wroclaw symposium on electromagnetic compatibility, Wroclaw, Poland, June 28 - July 1, 1994, editors: J. Janiszewski, W. Moron and W.Sega, p.578-582.

[8] G.Tomassetti and G.Tofani (see elsewhere in this book).

[9] "The Passive Use of the Frequency Spectrum", Final Report, Report No.213, NATO Committee on the Challenges of Modern Society, 1996.

[10] R.L.White and H.M.White, "The Law and Regulation of international Space Communication", Artech House, 1988.

[11] T.A.Th.Spoelstra, "Science, Development and Radio", Global Communications Africa '98, editor: R.G.Struzak, Hanson Cooke Ltd, London, 1998 (in press).

[12] D.McNally (ed.), "The Vanishing Universe", Cambridge University Press, 1994.

BIOGRAPHICAL NOTES

Dr.T.A.Th.Spoelstra is secretary and frequency manager of the Committee on Radio Astronomy Frequencies of the European Science Foundation. His research experience is related with polarization studies of cosmic radio waves, cosmic magnetic fields, radio wave propagation through ionized media, systematic philosophy and philosophy of science. He has served the Netherlands Foundation for Research in Astronomy as Head of Operations of the Westerbork Radio Observatory. He can be reached at: CRAF, NFRA, P.O.Box 2, 7990 AA Dwingeloo, The Netherlands [tel.: +31-521-595100, telefax: +31-521-597332, email: spoelstra@nfra.nl].

NEW RADIO WINDOWS: MM-WAVE ASTRONOMY

Anders Winnberg
Onsala Space Observatory, S - 439 92 Onsala, Sweden

The radio bands at frequencies above 60 GHz have properties which make this region of the electromagnetic spectrum quite different from the region at lower frequencies. This is the transition region to the infrared spectral parts and the absorption by the atmosphere is a complicated function of frequency and is very high in some frequency bands. The passive radio service, Radio Astronomy (RAS), has enjoyed relatively interference-free access to the millimetre-wave range for three decades. This situation will not last much longer. There are plans for many active services in this part of the radio spectrum, as for example a satellite-borne cloud radar and several commercial satellite systems. The present paper discusses the uniqueness of the millimetre-wave region for astronomy and points out possible methods to help reducing the impact of interference from the active services.

1. UNIQUENESS OF THE MILLIMETRE-WAVE REGION

Natural radiation in the millimetre-wave region carries information about the cold parts of the universe. It enables us to map interstellar dust clouds through their thermal Planck radiation and it contains spectral lines of a multitude of molecules inside such clouds from which stars are formed. By analysing such lines astronomers can deduce the physical properties of the molecular cloud medium. Also a new branch of astronomy has arisen due to the molecular lines: Astrochemistry. No other wavelength range of the electromagnetic spectrum can give us the same information about the chemistry inside cold interstellar molecular clouds.

Recently millimetre-wave astronomy has also proven to be an invaluable tool in observational cosmology - a science which deals with the large-scale structure of the universe and its evolution in time. Due to the expansion of the universe, distant galaxies seem to be receding from us with velocities which are proportional to their distances. This has been proven at optical and at centimetre wavelengths by measurements of the increase of the wavelength of radiation from distant galaxies. This so called 'redshift' phenomenon is one of the most important instruments in observational cosmology. Redshifted, i.e. 'frequency-decreased', line emission from carbon monoxide and from several other species has been detected from many distant galaxies. This fact has given us the possibility to study the mo-

lecular content and star formation rates of galaxies in the early universe. Millimetre-wave astronomy might thus turn out to be the most sensitive technique to study matter close to the limit of the observable universe.

The faint echo from the creation of the universe (the Big Bang) is detectable as an omnidirectional blackbody radiation at a temperature of 3 K. This Cosmic Background Radiation can be studied with great accuracy at a wavelength of about 2 mm. Small deviations from isotropy in this emission gives information about creation of matter when the universe was very young.

Millimetre-wave astronomy delivers new knowledge about celestial objects from comets and planetary atmospheres in our solar system to the most distant galaxies at the dawn of the universe.

2. EMISSION AND ABSORPTION OF THE ATMOSPHERE

The species dominating the emission and absorption of microwave radiation in the terrestrial atmosphere are water vapour (H_2O), oxygen (O_2), and nitrogen (N_2). Scattering by aerosols generally can be neglected for these frequencies. The resulting microwave transmission is characterised by some 20 strong spectral lines superimposed on a continuum.

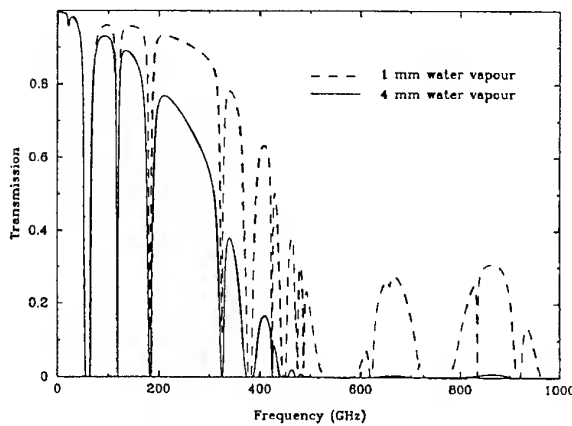


Fig. 1 The atmospheric transmission for two values of water vapour abundance (4 and 1 mm). Absorption lines of oxygen and water vapour divide the spectrum into several 'atmospheric windows'.

Figure 1 depicts a model of the atmospheric transmission for two values of precipitable water vapour (4 and 1 mm). 4 mm of water vapour is a good value for sea-level conditions and 1 mm water vapour only occurs at high altitudes. The atmosphere divides the spectrum into several 'windows' due to absorption lines of oxygen and water. The windows at frequencies higher than about 500 GHz 'open up' only at high-altitude sites.

3. THE NEED FOR BROAD-BAND FREQUENCY PROTECTION

Although ITU allocations to the RAS have been made for some of the stronger spectral lines this limited protection will not be sufficient in the future.

The justification for this statement is based on recent discoveries. The millimetre-wave spectral lines from distant galaxies mentioned above can appear in any part of the atmospheric windows, depending on the exact redshift. Furthermore the continuum emission from dust in these objects and in our own Galaxy can be detected using wide-band bolometer detectors which for the highest sensitivity utilise a whole atmospheric window.

Also modern mixer receivers use so called Superconductor - Insulator - Superconductor (SIS) mixers which are extremely sensitive and inherently broadband. This fact, in combination with the fact that filters with high Q-factors and low insertion losses have not yet been designed, makes it extremely difficult for the RAS to share mm-wave bands with active radio services or even to operate in bands adjacent to active services.

4. POSSIBLE SOLUTIONS

4.1 Limits for harmful interference

ITU has defined the limit for 'harmful interference' for the RAS in its recommendation ITU-R RA.769-1. For the mm-wave range the spectral power density threshold for a radio telescope operating alone (as opposed to a radio interferometer consisting of many telescopes) varies in the range -213 to -222 dBWm⁻² Hz⁻¹. This might be regarded as a very low value, but one should keep in mind that it is no problem whatsoever for modern radio astronomy equipment to detect such weak signals. One should be aware also of the fact that these limits are referred to an antenna with isotropic gain. For a typical radio telescope this gain is reached at about 19° from the main beam. Therefore, it is quite possible to encounter interfering signals several degrees of magnitude stronger than the above mentioned limits but still fulfilling the ITU recommendation.

4.2 Ground-based transmitters

4.2.1 The classical method to distribute radio resources is to divide the electromagnetic spectrum into bands of varying width. This method becomes increasingly unrealistic with increasing frequency, because the re-

quirements on filters (Q factors, insertion loss) often exceed present-day technical feasibility. Whereas research and development in this area deserve high priority, it is reasonable to propose a more cautious way of applying this classical frequency allocation method in the near future. There are at present several cases of unfortunate (for RAS) allocations in the mm-wave range. One of the worst cases is an allocation to the Broadcasting Satellite service from 84 to 86 GHz adjacent to the very important RAS band from 86 to 92 GHz. Fortunately this service is not yet in operation.

From the viewpoint of the RAS it would be desirable to get access to comparatively broad bands close to the centres of the main atmospheric windows. These bands should be surrounded by 'guard bands' in which no space-borne services should be allowed. In addition, narrower bands centred on the rest frequencies of the main oxygen and water vapour lines should be set aside to the RAS for future space-borne observations of these molecules in outer space.

4.2.2 Instead of the classical way of dividing up the electromagnetic spectrum into bands one should, in addition, consider a geographical protection of mm-wave observatories. Such establishments are often situated in remote areas on high mountains in order to minimize the water vapour above them. Therefore it should be possible to create Quiet Zones around such observatories inside of which all ground-based emissions should be forbidden.

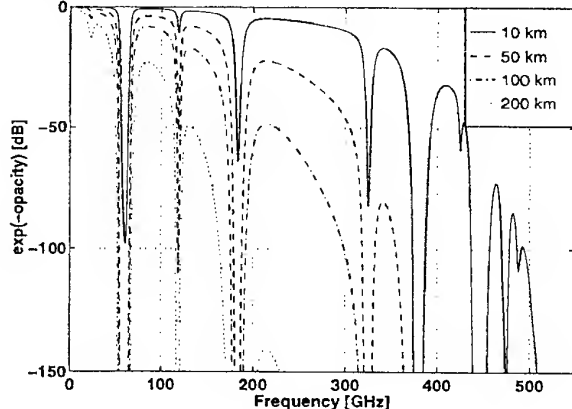


Fig. 2 The total atmospheric transmission for a signal transmitted at sea level at a distance of 10, 50, 100, and 200 km from a mm-wave observatory at an altitude of 4000 m. The relative humidity is assumed to be 30% at sea level and the water vapour mixing ratio to vary exponentially. The US Standard Atmosphere is assumed

The atmosphere is an efficient protective medium at mm-wavelengths. Figure 2 shows the atmospheric transmission (excluding the $1/r^2$ dependence) for a signal transmitted at sea level at various distances (10, 50, 100, and 200 km) from an observatory at a mountain top with an altitude of 4000 m. The relative humidity at sea level is taken to be 30% with an exponential variation with altitude. The attenuation exceeds 100 dB for a

signal transmitted at 200 km distance for frequencies higher than about 170 GHz, even when neglecting the strong spectral lines of oxygen and water vapour. The corresponding limiting frequencies for the other distances are 300 GHz for 100 km, 355 GHz for 50 km, and 490 GHz for 10 km. The geometrical dilution of the signal of course improves the situation. These considerations could be taken into account when planning future Quiet Zones surrounding mm-wave observatories. The establishment of such Quiet Zones would fall under the jurisdiction of the country in which the observatory is situated (and possibly neighbouring countries), further simplifying the process.

4.3 Space-borne transmitters

Space-borne radio services of many kinds, e.g. navigation, broadcasting, and communication, are becoming more and more common. Emissions from such satellite transmitters constitute a much more serious threat to the RAS than ground-based transmitters, because neither the topography nor Quiet Zones around the observatory can protect from interference.

4.3.1 There are essentially two types of satellite orbits: geo-synchronous (GSO) and low-earth orbit (LEO). For GSO-type satellites it should be possible in most cases to avoid illuminating radio astronomy observatories in remote areas. Thus, the idea of Quiet Zones could be implemented also in this case albeit in a very different way. However, in the case of LEO-type satellites such a simple scheme is not possible.

Most existing and all planned LEO satellite systems, however, are and will be equipped with accurate navigational instruments so that the position of every individual satellite is known at any given moment. Therefore such systems can be designed to switch off the transmitter whenever the satellite is above an observatory. This will, for example, be the case for the planned ESA cloud radar satellite operating at 94 GHz. In this way it should be possible to create yet another type of Quiet Zones around remotely situated mm-wave observatories.

4.3.2 Some LEO-type systems might allow time sharing with the RAS if the transmitters operate in a time-synchronized ‘burst mode’. Although less attractive from the viewpoint of radio astronomy it certainly offers a solution in some cases.

4.3.3 This paper has so far discussed the coordination problem with active radio services in terms of restrictions and concessions on the part of the active services. Surely this is unavoidable, since we are dealing with a passive service (which by definition cannot interfere!)

and active services producing signals vastly stronger than the signals detected by the passive service.

However, radio astronomers have to adapt their techniques to a changing world, in which the radio spectrum becomes increasingly used for the benefit and convenience of modern society. There are two areas in which such adaptation is possible. Development of filter technology for mm-waves has been mentioned already. Such technical development has started only recently and it is very uncertain whether it will lead to practical results. The other area of adaptation lies in radio telescope design. Radio astronomers are interested in getting high angular resolution. Radio telescope reflectors therefore are illuminated with this goal in mind which inevitably creates higher side lobes than for a less efficient illumination. In addition, off-axis designs may get a greater attention.

5. CONCLUSIONS

Millimetre-wave astronomy is a field of astronomy based on front-line techniques, delivering new knowledge of the universe, and offering a great potential for the future. It has operated for 30 years without any serious hampering from man-made interference. This situation will not last much longer because several active radio services are being planned and prepared for the mm-wave region. It will be a complicated task to coordinate these active services with the RAS. Such coordination will have to be made in a way which deviates from the traditional way of just dividing the radio spectrum into allocation bands. Quiet Zones around remotely situated mm-wave observatories should be established to protect from ground-based interference. This does not need the involvement of the ITU. Some important frequency bands, however, still need the full traditional protection but they should not be adjacent to active satellite services. The possibility of switching off the transmitters of LEO-type satellite services, whenever a satellite is above a mm-wave observatory, should be studied. The RAS itself, however, has to adapt to a changing radio world. Technical research and development in the fields of filter and telescope design has to be intensified.

BIOGRAPHICAL NOTES

The author is an Associated Professor at Onsala Space Observatory, Chalmers University of Technology, Göteborg, Sweden. He got a PhD at Chalmers in 1970 and worked at the Max-Planck-Institut für Radioastronomie in Bonn, Germany, in the 1970ies. His scientific interests lie in the areas of late-type stars, galactic structure, comets, and the earth atmosphere. He is a member of the ESF Committee for Radio Astronomy Frequencies (CRAF).

XIV

**SPECTRUM MANAGEMENT,
ENGINEERING, SHARING
AND MONITORING**

**Factors and Methods of Radio
Frequency Assignment**

Invited session organized by

J. Finnie - UK

THE ROLE OF RADIOWAVE PROPAGATION MODELS IN SPECTRUM PLANNING

K.H.Craig

Radio Communications Research Unit,
Rutherford Appleton Laboratory,
Chilton, Didcot, OX11 0QX,
United Kingdom

Radiowave propagation plays an important role in spectrum planning. The paper gives an overview of the relevant propagation effects and models. Emphasis is given to planning tools being developed for broadband millimetrewave cellular services.

1. INTRODUCTION

Radiowave propagation plays an important role in radio frequency assignment and spectrum planning. Indeed interference between radio systems is the reason that frequency assignment is required at all, and the magnitude of the interference problem is strongly determined by the radiowave propagation between the radio systems.

The market requirement for higher data rate services is forcing the pace for the adoption of millimetric frequencies in fixed link and point-to-multipoint applications, and these frequencies are even under consideration for mobile broadband services. The effects of the atmosphere and terrain features on the propagation of radiowaves are very different at these frequencies than at UHF and the lower microwave frequencies.

This paper discusses the important propagation mechanisms and how these are modelled. For illustration purposes, it will be convenient to concentrate on cellular services. At the lower (UHF) end of the spectrum lie the traditional mobile and personal communication cellular services, while at the higher (millimetrewave) end, broadband cellular access systems are being planned above 40 GHz.

The reader is referred to the radiowave propagation literature for a more detailed discussion of the propagation issues. A recent general text is [1], while prediction tools and decision aids are discussed in [2].

2. PROPAGATION EFFECTS

2.1. System model

Fig 1 shows a simplified model of a radio network. The T_i represent radio transmitters, and the P_i the propagation channels between the transmitters and a

receiver. The suffix 0 is used to represent the "wanted" transmitter, while the suffices 1, 2, ..., N represent "unwanted" or interfering transmitters. These unwanted transmissions may be co-channel or adjacent channel to T_0 .

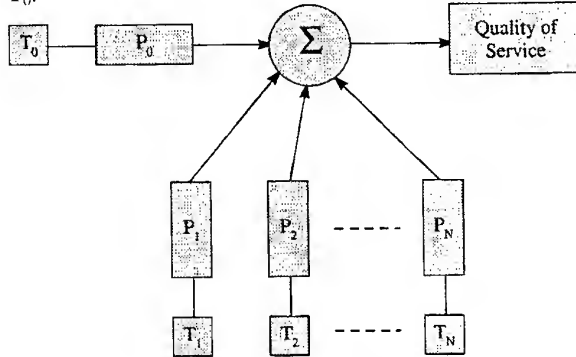


Fig 1: Simple model of a radio network

In this simple picture, the receiver antenna sums together in Σ the wanted and unwanted transmissions and the receiver's detection circuitry outputs (an approximation to) the reconstructed signal transmitted by T_0 . What is required in spectrum planning tools, of course, is not the signal itself, but some indication of the quality of service as shown in Fig 1.

The determination of a suitable quality of service measure depends on many systems issues apart from propagation, and a full discussion is outside the scope of this paper. For digital systems, the ratio of carrier to noise powers is a useful criterion when interference is negligible; when interference is important and the interference is incoherent (noise-like) the carrier to interference plus noise ratio, $C/(I+N)$, is used. Lower system noise figures, and the drive to greater spectrum occupancy (maximising spectrum efficiency) has led to a desire to design networks to operate in the interference-limited regime.

Although "higher level" indicators of quality of service (such as bit, frame or cell error rates) are often used, the $C/(I+N)$ ratio is a simple and adequate indicator for frequency assignment modelling.

Note that the way in which the signals are combined at the receiver in Σ depends on system parameters (such as antenna beamwidths and polarisation).

We now consider the effects that need to be included in the propagation blocks P_i in Fig 1. The propagation mechanisms that give rise to these effects, and the way in which they are modelled, are discussed in the next section.

2.2. Attenuation

The power of the received signals will be much less than that of the transmitted signals. The main cause is of course the free-space spherical spreading of the electromagnetic waves, giving rise to an inverse distance squared reduction in power. However, the non-free space propagation environment strongly modifies this path length dependence.

The propagation medium itself (the atmosphere) can give rise to excess attenuation (absorption by atmospheric gases and absorption and scatter by rain and other hydrometeors) and reduced attenuation (refractive focusing and trapping by atmospheric layers). The surface of the Earth can also strongly affect the signal (reflections from the surface, diffractive losses due to path obstruction, absorption and scatter by surface clutter such as trees and buildings).

Since the relative strengths of the wanted and unwanted signals is the main determining factor in the quality of service estimation, the modelling of attenuation is the most important component in the P_i .

2.3. Delay

The finite speed of propagation means that the signal suffers a delay between transmission and reception. The delay is determined by the "optical" path length between transmitter and receiver; this is slightly longer than the physical path length, and variable in time, due to the refractive index of the propagation medium. However, the absolute delay is not really an issue for frequency assignment models. The important thing is the relative delay between the different P_i . Generally, the P_i will have sufficiently different delays that the received signals are uncorrelated. For digital systems this means that the *powers* (rather than the *amplitudes*) of the interfering signals can simply be added to each other and to the system noise in determining their effects on the system.

2.4. Multipath

The P_i do not necessarily represent a single propagation path between transmitter and receiver. Obstructions (such as buildings and the ground) can cause reflections that add to the direct signal (see Fig 2). These added "multipath" signals will have different amplitudes and delays from each other.

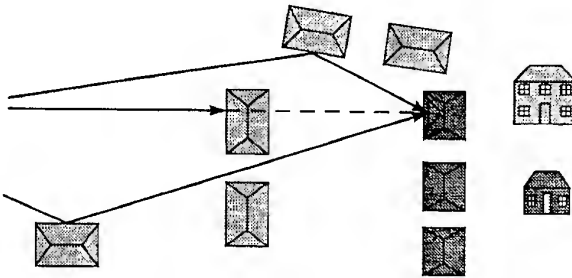


Fig 2: Illustration of diffraction, reflection and multipath in an urban environment

Unlike the signals from different transmitters, these multipath signals will be highly correlated (because of the common signal source and the small relative path delays), and will interfere with each other coherently. The effect will be to give rise to a received signal whose amplitude varies with time and across the bandwidth of the signal.

Multipath can also be caused by reflection and refraction by atmospheric layers. The effects of atmospheric multipath on the received signal are similar but occur less frequently. Atmospheric multipath is important on long fixed link paths, but is of minor consideration for cellular systems.

It is a convenient approximation to represent multipath as a block within the propagation channel P_i . In practice, the significance of multipath depends on such system parameters as the receiver antenna beamwidth (narrower beamwidths reducing the importance of secondary paths). If these effects are to be taken fully into account the model of Fig 1 could be extended by including a separate P_i for each propagation path and extending the summation Σ to include these.

2.5. Dispersion

This is the effect on the signal of the frequency dependence of the propagation channel. If the frequency dependence is small within the signal bandwidth, the channel is referred to as "flat", whereas if the effect is large, the channel is referred to as "frequency selective". Narrowband systems will be less affected than broadband systems. Intrinsically, most propagation mechanisms produce little dispersion. One unavoidable source of dispersion is multipath, and this can be significant. However, systems that operate in a strongly multipath environment (such as GSM) have been designed with countermeasures against these effects.

2.6. Independence

A further simplification in Fig 1 is that the different P_i are assumed to be independent. This assumption depends on the type of model used to represent the P_i . In a statistical model, the amplitude variation within different P_i may not be statistically independent; for example the statistics of rain fading are highly correlated on neighbouring paths. This can be a significant issue in

network design, especially when diversity is used as a countermeasure against propagation degradations.

2.7. Time variability

Most propagation impairments are time variable. The timescales to be modelled range from micro- or milliseconds for mobile radio networks where the movement of the transmitters and receivers are the prime cause, to variations on the scale of minutes or days where atmospheric effects dependent on the weather are concerned. This time variability can be modelled in various ways, but for network planning, statistical models are usually used.

3. PROPAGATION MECHANISMS AND MODELS

3.1. Types of propagation models

In principle, a model for any electromagnetic wave propagation problem is provided by a solution of Maxwell's equations. Such a model is deterministic in the sense that if the propagation medium is characterised exactly, the solution would also be an exact description of the propagation conditions at the given time.

In practice, approximations and simplifications are required, and different methodologies are required for different propagation mechanisms and frequencies. Both analytical and numerical solutions are used. Deterministic models are particularly relevant when a prediction of the performance of a specific system is required at a specific location and time. Of course, the accuracy of the prediction critically depends on the fidelity of the real-time environmental data available; the (lack of) availability of such data is a serious constraint on the usefulness of deterministic models.

For network design applications, predictions for a specific time are not appropriate, and the time-variability of the propagation environment must be taken account of in a statistical manner, based on historical data. Most of the established methods for calculating the availability or outage of a radio link are empirical or semi-empirical, based on the underlying physical mechanisms, but taking account of a statistical nature of the environment. (See, for example, [3].)

3.2. Clear-air atmosphere

"Clear air" refers to those aspects of the Earth's troposphere (the lower atmosphere) that are due to its gaseous constituents, and excludes clouds, rain, etc. Electromagnetic waves are refracted and scattered by variations in the radio refractive index n . The value of n is determined by the molecular constituents of the air, and can be expressed in terms of the meteorological quantities pressure, temperature, and water vapour pressure.

Certain weather conditions give rise to strong gradients of temperature and water vapour, and these can cause "anomalous" propagation. The most significant impact on frequency assignment is the

increased risk of interference due to the over-the-horizon ranges of transmissions at certain times due to radio ducting. Atmospheric subsidence and advection can produce ducting on the mesoscale, while nocturnal inversions can be of localised significance on land paths. On overwater paths the low lying evaporation duct has dominant effect on near-surface propagation. Much work has gone into measuring and modelling the effects of ducting, and deterministic and statistical models are available (see for example [3], Rec P.452-7). The effects of refraction and ducting are strongest at UHF and microwave frequencies.

Significant attenuation caused by gaseous absorption is limited to specific, narrow frequency bands (for example, water vapour absorption at 22 GHz and oxygen absorption at 60 GHz). At these frequencies, the effects can be extremely severe. For example the absorption rate at 60 GHz exceeds 10dB/km; note that the reduction in received signal power due to any absorption mechanism depends *exponentially* on the path length through the medium. However, for most frequencies of interest to frequency assignment models, gaseous absorption is relatively small, and easily modelled.

3.3. Rain

The presence of rain and snow on a propagation path can cause severe attenuation at microwave and millimetrewave frequencies. The processes are largely well understood, and deterministic and statistical methods are available for predicting their effects (see [2], lecture 7).

The significance of rain attenuation depends on frequency, rainfall rate and climate. Below 3 GHz, rain attenuation can generally be ignored. (The attenuation rates are less than 0.01 dB/km for all but intense rain). Above 10 GHz the attenuation rate can be several dB/km and for millimetrewave cellular systems, rain is the dominant factor in defining the maximum cell size.

It is important to remember that rain is not spatially homogeneous. The most intense convective rain occurs in rain "cells". When designing a network, account has to be taken of the likelihood of fading on the wanted link occurring at the same time as an unfaded interfering link.

A more direct source of interference can be coupling of an unwanted signal into the receiving antenna via rain scatter. This will occur if there is rain in the "common volume" defined by the intersecting beam patterns of the transmitter and receiver antennas. Rain scatter is intrinsically stronger at higher frequencies, but this is offset to some extent by the narrower antenna beamwidths at these frequencies which result in a reduction of the size of the common volume.

3.4. Terrain

If the path between transmitter and receiver is line-of-sight, the ground will not affect the propagation as

long as the path is sufficiently clear of the ground (by at least one Fresnel zone), and the ground is not illuminated by the main beam of either antenna. If the ground intrudes into the first Fresnel zone, and in particular, if the path is obstructed by the terrain, the signal will suffer additional diffraction loss.

For a given path geometry, the diffraction loss is greater at higher frequencies. At the highest frequencies under consideration (millimetre waves) the first Fresnel zone is extremely small (a few metres) and the diffraction losses are very high. In this case the propagation is effectively optical and to a first approximation terrain blockage cuts off the signal completely. However, at UHF and lower frequencies, the loss due to diffraction may be much smaller, and significant interference may occur from transmitters that are obscured by terrain. There are well-established (deterministic) models that account for terrain diffraction (see [3], Rec P.526-4). To a very high degree of accuracy, only diffraction in the vertical plane need be considered; two-dimensional models are therefore adequate, resulting in efficient models.

If the ground is illuminated by the antenna beams, reflection and scatter from the ground also needs to be considered. This gives rise to multipath propagation.

3.5. Buildings and other surface clutter

The effects of ground clutter depends on frequency and terminal heights. At the lower VHF and UHF frequencies, buildings may be semi-transparent to radiowaves; at the higher microwave and millimetre-wave frequencies, they become opaque. Transmission (with attenuation) through obstacles needs to be modelled. Diffraction over and round obstacles can deliver signals to the "shadow zone" behind an obstacle, as can reflections from the ground and other obstacles.

At the frequencies of interest, ground clutter on a terrain obstacle can be modelled adequately as an increase in the terrain height. For antennas that are located within the clutter different approaches are required depending on application. At VHF and UHF, semi-empirical methods are often adequate, as the effect of the clutter is "smeared out" on the large scale, and the spread about the "average" is not too large. The "two-slope" model of Fig 3 is a common example of this type. At short ranges the received power falls off with distance d as d^2 , but at longer ranges this increases to d^n , with n in the range 2–4. The value of n and the range at which the slope changes depends on clutter type, antenna heights, etc.

At higher frequencies, the measured received powers become much more site-specific, and a simple empirical model for the trends with distance becomes less tenable. Fig 4 shows the trend obtained from 42 GHz measurements in the city of Oxford. A two-slope model is hard to justify here.

Although it is hoped that useful empirical models may become available for millimetric networks in the future, at the present time three-dimensional ray tracing

methods are the main source of urban predictions. Three-dimensional modelling is the only way of obtaining propagation channel predictions since off-axis reflections can be important in the urban multipath environment.

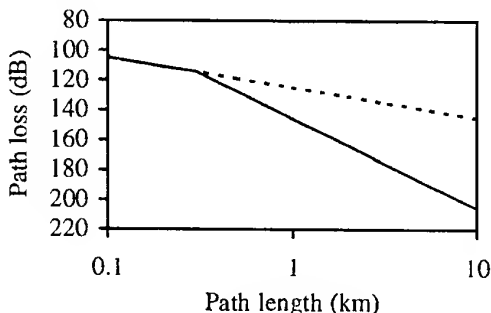


Fig 3: Low frequency, two-slope model

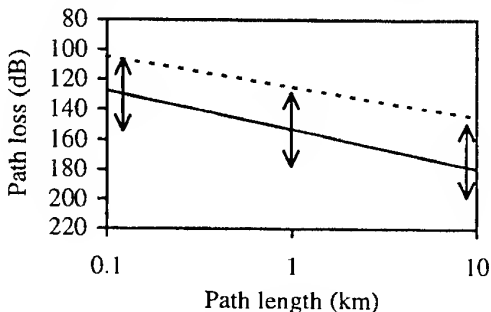


Fig 4: Trend of urban measurements at 42 GHz

3.6. Vegetation

Trees are a particular problem at microwave and millimetre wave frequencies. Fig 5 shows that the attenuation of a typical tree can be high at 42 GHz. Note that tree attenuation depends greatly on tree type, moisture content, etc. The shape of the curve is due to the multiple scatter nature of the propagation through the tree. The initial steep slope is caused by the attenuation of the coherent component of the electromagnetic wave. The flatter (high attenuation) portion occurs when multiple scattered energy dominates over the (highly attenuated) coherent component. For point-to-point links vegetation should be avoided, but this is not always possible for cellular network services to the home.

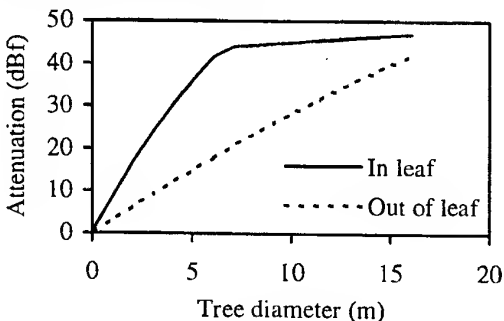


Fig 5: Tree attenuation at 42 GHz

4. CELLULAR NETWORK PLANNING

Traditionally, cellular networks have evolved in two phases. In the early stages of deployment, available spectrum exceeds demand, and a conservative frequency re-use can be tolerated without the risk of interference. As demand increases, and extra capacity is provided within the network, the probability of interference increases and the need for careful planning is required to minimise interference. In the later stages, the network may be interference-limited, but this progression is unlikely to result in an optimum configuration of the resulting network.

The high demand for spectrum nowadays means that it is now necessary to plan for interference-limited networks from the outset. This approach is being encouraged by legislative procedures (for example, spectrum pricing in the UK).

For the millimetric cellular systems, tools are being developed within the EU ACTS project CRABS ("Cellular Radio Access for Broadband Services") that should aid in the process of optimisation of coverage and interference simultaneously. These model

developments are supported by measurement campaigns in several countries. Fig 6 shows an example of contours of (a) terrain, and (b) the corresponding $C/(I+N)$ for a typical millimetrewave video distribution system at 42 GHz. The tool includes deterministic models for rain, atmospheric gases, terrain, and buildings, and also statistical models for rain and surface clutter. In Fig 6, a statistical rain model was used (99.7% availability). Note the high degree of shielding from interference provided by the range of hills. The three centres of population can be adequately covered with single frequency re-use. The reason is the low system margin requirement for this service, and the narrow beamwidth of the receiving antennas (less than 3°).

5. CONCLUSION

This paper has given an overview of the propagation effects and models that are relevant to spectrum planning. As new, higher frequency, interference-limited networks are introduced the need for good propagation models and tools will increase.

6. ACKNOWLEDGEMENTS

The author expresses his thanks to his colleagues in the CRABS consortium at RAL and Telenor, and in particular to Tim Hayton and John Biddiscombe for the planning tools and to Mike Willis and Andy Seville for the 42 GHz clutter measurements.

The work has been funded partly by the European Union ACTS programme and partly by the UK Radiocommunications Agency as part of the National Radiowave Propagation Programme.

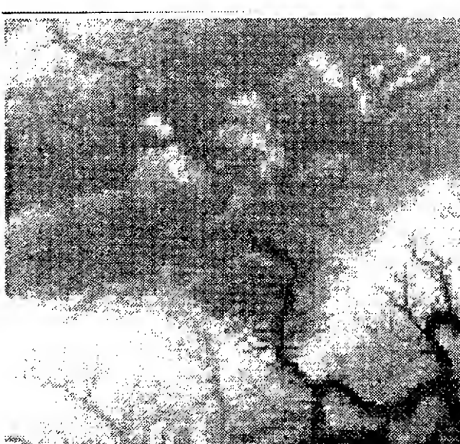
7. REFERENCES

- [1] MPM Hall, LW Barclay and MT Hewitt (eds), "Propagation of radiowaves", The Institution of Electrical Engineers, London, 1996, ISBN 0-85296-819-1.
- [2] KH Craig (ed), "Propagation modelling and decision aids for communications, radar and navigation systems", AGARD Lecture Series, AGARD-LS-196, Neuilly-sur-Seine, 1994, ISBN 92-836-1004-0.
- [3] Recommendations of the ITU-R, Geneva, 1996, ISBN 92-61-05961-9.

BIOGRAPHICAL NOTE

The author is Head of the Radio Communications Research Unit at Rutherford Appleton Laboratory and is responsible for several experimental and theoretical radiowave propagation programmes. His main interest has been numerical modelling of propagation, in particular the parabolic equation method. He leads the propagation workpackage of the CRABS project.

He has a BSc from the University of Glasgow and a DPhil from the University of Oxford and is a Fellow of the IEE.



(a) Terrain



(b) $C/(I+N)$

Fig 6: A 3-cell 42 GHz MVDS network

MATHEMATICAL METHODS IN RADIO FREQUENCY ASSIGNMENT

Robert A. Leese

Mathematical Institute, University of Oxford, Oxford OX1 3LB, UK

The aim of this paper is to provide a short informal review of mathematical methods developed over the last few years in the area of radio channel assignment. It is directed at the general radio community, who may not have been previously aware of such work. The ideas described in the paper are the subject of ongoing research programmes in several university departments in the United Kingdom, with the active support of the Radiocommunications Agency. More detailed treatments are the subject of an URSI Commission E Workshop at this Symposium.

1. INTRODUCTION

As new radio systems are brought into service and existing ones extended, radio spectrum is becoming increasingly valuable, prompting the introduction of new pricing structures in various parts of the world. The incentive to find new ways of using spectrum efficiently is therefore also increasing. One aspect of spectrum efficiency concerns the hardware used when implementing radio systems; advances in technology lead to new generations of equipment, which increase the traffic that can be carried by a given piece of spectrum. This paper is concerned with a second aspect of the problem, namely the possible ways of assigning radio channels to individual transmitters once the hardware specification has been agreed.

The channel assignment problem deals with the competing wishes to provide sufficient radio coverage while at the same time avoiding unacceptable interference between groups of transmitters. The problem specification must therefore include information about the requirements for spectrum across the system, and also a set of constraints, designed to limit the interference levels, that a channel assignment should respect. In the version of the problem used most widely in practice, the spectrum requirements are given by specifying the number of distinct channels that each transmitter site requires. So, for instance, if there are n transmitter sites, called T_1, T_2, \dots, T_n , then we have a corresponding set of demands m_1, m_2, \dots, m_n , where site T_i requires the

assignment of m_i distinct channels.

The most useful specification of constraints is somewhat less clear. The most usual route, which reflects the use of protection ratios in the radio community, is to have a set of constraints each relating to either a single transmitter site (called co-site constraints), or a pair of transmitter sites (called inter-site constraints). To be explicit, suppose the channels are labelled by integer values, corresponding to their positions in the frequency spectrum. Then the co-site constraints require that if $f_1^{(i)}$ and $f_2^{(i)}$ are different channels both assigned to some transmitter site T_i then

$$|f_1^{(i)} - f_2^{(i)}| \geq c_i$$

for some specified minimum channel separation c_i . Likewise, the inter-site constraints require that if $f^{(i)}$ and $f^{(j)}$ are channels assigned to two different transmitter sites T_i and T_j , respectively, then

$$|f^{(i)} - f^{(j)}| \geq c_{ij}$$

for some specified minimum channel separation c_{ij} (equal to c_{ji}). The constraints are therefore completely specified by the numbers c_i and c_{ij} , which are usually written in the form of a matrix, called the constraint matrix. The c_i make up the diagonal entries and the c_{ij} the off-diagonal entries. Although this formulation is the most common, it has recently come into question, following case studies indicating that it can be over-restrictive, in a sense to be described shortly.

The final part of the problem specification is the objective, for which there are two natural choices. The first and most widely studied to date is the *minimum span problem*, in which the aim is to find an assignment satisfying all spectrum requirements and all interference constraints, for which the span, defined as the difference between the highest and lowest channels used, is as small as possible. This would tend to be the concern of spectrum regulators and system designers. The second possibility is the *fixed spectrum problem*, in which a maximum span is given (corresponding to the amount of spectrum available)

and the aim is to assign channels to as many spectrum requirements as possible, within the given span and without violating any constraints. This would tend to be the concern of system operators, as they attempt to manage existing services. A variant on the fixed spectrum problem would assign channels to all spectrum requirements and try to minimize the number of violated constraints.

The above specification assumes that the transmitter locations and powers are fixed (they are effectively taken account of by the constraint matrix). More general formulations could have locations and powers as extra variables, to be optimized along with the channels, but there has been very little theoretical work on such problems to date.

Before moving on, it is useful to mention the way in which the constraint matrix can be over-restrictive. First, it is important to realise that any mathematical model of the channel assignment problem represents an attempt to capture the practical requirements of radio engineers. The success or otherwise of the whole enterprise is largely determined by the accuracy of translation from the engineering specifications into mathematical specifications. As far as avoiding interference is concerned, the radio engineer generally requires that the signal-to-interference or signal-to-noise ratios should be sufficiently high at all receiver positions where radio coverage is desired. There is no mention of *pairs* of transmitters, but simply a requirement that the combined effects of *all* sources of interference are sufficiently low. If there are single dominant interferers then a constraint matrix is likely to be a reasonable mathematical model, but more generally it will be difficult to translate the engineering specification into a matrix form. Putative constraint matrices will then tend to be either too 'loose', in which case they fail to ensure the desired coverage, or too 'tight', in which case they lead to assignments using more spectrum than necessary. These issues are discussed in the contribution by Bater, Jeavons and Cohen [1] in these Proceedings. For the moment, constraint matrices remain in widespread use.

2. COMPLEXITY

The channel assignment problem, even in the basic form given in Section 1, has exercised many researchers over many years, but why should it be so hard? (In fact we shall see later some evidence that certain types of problems are not so hard as might first be expected, but for the moment we keep the discussion general.)

The standard formulation includes, as a special case, the celebrated *graph-colouring problem*. A graph in this context is a collection of abstract 'nodes', some pairs of which are joined by 'edges'.

The colouring problem is to attach a colour to each node in such a way that a pair of joined nodes should receive different colours and the total number of colours used should be as small as possible. The smallest number of colours needed is called the *chromatic number* of the graph. If we think of the nodes as transmitter sites and the colours as channels then we have precisely a minimum span channel assignment problem, in which all the m_i are 1, and the c_{ij} are 1 if the nodes T_i and T_j are joined and 0 otherwise. (Since only one channel is required at each site, the values given to the co-site constraints c_i are immaterial.) In physical terms, we are modelling only co-channel interference, with the edges in the graph indicating the rough location of potential coverage blackspots. Figure 1 shows a graph with chromatic number 4, along with a possible valid colouring. (Note that our conventional definitions mean that the span is one less than the chromatic number.)

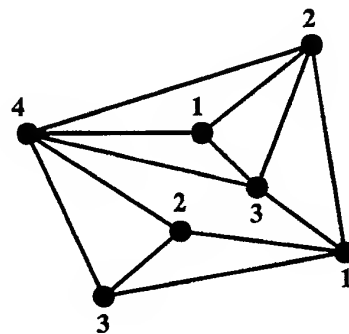


Figure 1: A small graph with chromatic number 4.

Algorithms for graph-colouring have been extensively studied and so making this contact can shed light on channel assignment. In fact, graph-colouring was one of the first problems identified as NP-complete, about 25 years ago. NP-completeness is a technical property in the study of algorithms (an excellent introduction is given in [2]). What it means in practice is that it is extremely unlikely that any efficient algorithm exists for determining the chromatic number. The term 'efficient' here is also used in a precise sense: an efficient algorithm is one that runs in a time increasing only polynomially (as opposed to exponentially) with the size of the problem specification. Even restricted cases of graph-colouring are NP-complete. For example, if we look only at *planar* graphs, meaning graphs that can be drawn on a piece of paper without any edges crossing (as in Figure 1), then the famous 4-colour theorem says that

the chromatic number can be no larger than 4, but finding it is still NP-complete! (It is easy to check whether 1 or 2 colours will do; the difficulty comes, if more than 2 colours are needed, in deciding whether 3 or 4 are necessary.)

Hopefully the above comments go some way to justifying the familiar claim that channel assignment is a difficult problem. They highlight some of the limitations that must be borne in mind when designing algorithms.

3. ALGORITHMS FOR CHANNEL ASSIGNMENT

Despite the complexity of NP-complete problems, algorithms do exist for solving them, generally through some exhaustive search of all possibilities, but they have execution times that increase exponentially with the size of the problem. For channel assignment, such considerations limit tractable problems to a total spectrum requirement, *i.e.* the sum of the requirements of all transmitter sites, of just a few tens of channels. Since real problems often involve a total requirement of a few thousand channels, there is clearly a need for alternatives.

There are several so-called meta-heuristic techniques that seem well-suited to attacking discrete optimization problems such as channel assignment. They operate by trying to limit the portion of the 'search space' that is explicitly considered. The search space is the set of all possible configurations in the problem. For channel assignment, a configuration is simply a possible assignment of channels to transmitter sites, without regard for how many constraints might be violated. Meta-heuristics evaluate assignments using some objective function, which for illustrative purposes can be taken as number of violated constraints. Fixed spectrum problems involve minimizing the objective. Minimum span problems can be treated as a sequence of fixed spectrum problems, beginning with sufficient spectrum so that an assignment with zero objective (in this illustration no constraint violations) is known or easily found. The available spectrum is then decreased one channel at a time, effectively discarding the highest channel at each stage, until the algorithm can no longer find a configuration of zero objective.

A software package called FASoft has been developed by the Cardiff/Glamorgan research group, implementing three different meta-heuristics in the context of channel assignment, namely simulated annealing, tabu search and genetic algorithms. Full details of these methods appear in [3]. Here we simply mention the different approaches that these algorithms take to avoiding the problem of being caught in a local minimum of the objective function. Simulated annealing is a stochastic procedure in which

progress through the search space tends to move through successively lower objective values, but with some positive probability of making a move to higher values, thereby giving scope for climbing out of local minima. As time progresses, the probability of such moves decreases. Tabu search addresses the issue by keeping a list of forbidden (tabu) moves based on the recent history of the search. Genetic algorithms take a very different approach, in which a whole set of configurations, called a population, is maintained and updated in parallel.

Experience to date suggests that simulated annealing and tabu search are somewhat more promising than genetic algorithms, although there is plenty of scope for fine-tuning of the parameters that govern detailed operation. Historically, some authors have also attempted to use neural networks for the channel assignment problem, but these seem rather less successful.

4. INTEGER PROGRAMMING AND LOWER BOUNDS

A line of enquiry complementary to meta-heuristics starts with a more direct treatment of the problem. The specification given in Section 1 can be recast in the language of mathematical programming. For the minimum span problem, the variables would be the span, S , and the set of all channels assigned at each site, written $\{f_r^{(i)} : i = 1, 2, \dots, n, r = 1, 2, \dots, m_i\}$. Here, $f_r^{(i)}$ denotes one of the m_i distinct channels assigned to transmitter site T_i . It is mathematically convenient to remove the modulus bars in the constraints, using the following 'trick'. Replace the variables $f_r^{(i)}$ with new variables

$$u_{rs}^{(ij)} = \max(0, f_r^{(i)} - f_s^{(j)})$$

and

$$v_{rs}^{(ij)} = \max(0, f_s^{(j)} - f_r^{(i)})$$

The channel assignment problem may then be written in the following form.

$$\begin{aligned} & \text{Minimize } S \\ \text{subject to } & u_{rs}^{(ij)} + v_{rs}^{(ij)} \geq c_{ij} \quad \text{for } i \neq j \\ & u_{rs}^{(ii)} + v_{rs}^{(ii)} \geq c_i \quad \text{for } r \neq s \\ & 0 \leq u_{rs}^{(ij)} \leq S \\ & 0 \leq v_{rs}^{(ij)} \leq S \\ & S, u_{rs}^{(ij)}, v_{rs}^{(ij)} \quad \text{all integer-valued.} \end{aligned}$$

The details of this rewriting are not important. They are included only to show that channel assignment may be treated as an *integer programming* problem, characterised by the optimisation of a linear objective function subject to linear constraints,

over variables restricted to integer values. Such problems are also well known to be NP-complete (after all, the complexity cannot be changed simply by rewriting). The point of the exercise is to note that by removing the restriction to integer values, a *linear programming* problem is obtained, for which good algorithms have been known for 50 years.

The dropping of the restriction to integer values is known as *relaxation*. It clearly leads to reductions in the minimum span S (or possibly no change in certain special circumstances). The other variables, corresponding to the assigned channels, would then also generally be non-integers. Hence the relaxation is of limited use for generating explicit assignments (although see [4] elsewhere in these Proceedings for a variation on this theme which does work).

The power of this approach lies in the observation that the reduced value of S , calculated relatively easily after relaxation, provides a lower bound on the true minimum span. The most promising methods for lower bounds [5, 6] actually go a stage further and effectively drop some of the constraints in the linear program altogether; this reduces S still further, but can make the calculation much shorter.

It should be clear that meta-heuristics (or any other assignment method) provide upper bounds for the minimum span. One hopes that the best upper and lower bounds are not very different, so giving a small interval in which the true value must lie. In fact, experience indicates that for channel assignment problems based on cellular systems, the upper and lower bounds can often be made to match precisely. The exact value of the minimum span is then known, along with a corresponding assignment, and the problem can be reasonably said to be 'solved'. In contrast, problems arising from radio links seem rather more difficult.

5. CONCLUDING REMARKS

We have seen that channel assignment is closely related to graph colouring and to integer programming, both of which are well-known NP-complete problems. In fact, for the chromatic number of a general graph, it is also NP-complete to calculate good approximations ('good' in the sense of to within a constant multiplicative factor). These observations might lead to undue pessimism, but recent work seems to indicate a much better state of affairs, with several benchmark problems previously thought to be difficult now completely solved [3].

One interpretation of these results is that channel assignment problems arising in practice have special properties, which are not captured explicitly by the problem specification, but which can be successfully exploited implicitly by well-designed algorithms. A main aim for future research should be trying to un-

derstand these properties more precisely. This would naturally lead to a means of classifying channel assignment problems according to difficulty.

Qualitatively, it would seem that both the distribution of spectrum requirements and the underlying geometry play a role. To take an extreme example, many spectrum planning exercises take place with uniform requirements on regular lattices, where the explicit exploitation of geometry is crucial [7, 8, 9] and meta-heuristics generally struggle to find good assignments. An easier situation occurs when there is a small cluster of transmitters sites with high requirements, which can often determine the minimum span on their own, especially in cellular systems, where interference constraints are imposed locally over relatively short geographical distances.

This work was carried out under a research contract between the Radiocommunications Agency and St. Catherine's College, Oxford.

6. REFERENCES

- [1] J.E.Bater, P.G.Jeavons and D.A.Cohen, *Non-binary modelling of frequency assignment leads to significant reduction in predicted spectrum requirements*, these Proceedings.
- [2] M.R.Garey and D.S.Johnson, *Computers and intractability: a guide to the theory of NP-completeness*, W.H.Freeman, New York (1979).
- [3] S.Hurley, D.H.Smith and S.U.Thiel, FASOFT: *a system for discrete channel frequency assignment*, Radio Science, Vol. 32, No. 5 (1997) 1921–1939.
- [4] R.A.Leese, *Structural features in the construction of good channel assignments*, these Proceedings.
- [5] J.Janssen and K.Kilakos, *Tile covers, closed tours and the radio spectrum*, London School of Economics research report LSE-CDAM-97-08 (1997).
- [6] N.Dunkin and S.Allen, *Frequency assignment problems: representations and solutions*, Royal Holloway (University of London) and University of Glamorgan research report (1997).
- [7] C.McDiarmid and B.Reed, *Channel assignment and weighted colouring*, University of Oxford and CNRS (Paris) research report (1997).
- [8] J.van den Heuvel, *Radio channel assignment for 2-dimensional lattices*, in preparation.
- [9] R.A.Leese, *A unified approach to the assignment of radio channel on a regular hexagonal grid*, IEEE Transactions on Vehicular Technology, Vol. 46, No. 4 (1997) 968–980.

COMPUTING TOOLS IN SUPPORT OF RF SPECTRUM MANAGEMENT

Ryszard Struzak

Member, ITU Radio Regulations Board

Co-Chair, URSI WGE1 on Spectrum Management and Wireless Telecommunications¹
Route du Boiron 45, CH-1260 Nyon, Switzerland <ryszard.struzak@itu.int>

Management of the radio frequency spectrum and geostationary satellite orbit resources includes national and international coordination to assure their rational use and to avoid mutual interference. A huge amount of data needs to be exchanged and processed and complex computations are required for that purpose, which, in turn, requires efficient computing tools. The text reviews key issues involved.

1 INTRODUCTION

The status of spectrum management tools contrasts sharply with the progress made recently in computing and communication technology. And it is in spite of criticism of the present spectrum management, both national and international, for being costly, inefficient, and not adapted to the current needs. According to official estimates, the spectrum management activities of ITU headquarters in Geneva cost about 20 million Swiss francs per year [Doc. PP94-176]. But it is only "a top of iceberg" as most of the work is done far away from Geneva, and the total costs are much greater. The ITU staff only checks if the international agreements are not violated, and the substantial work is done by national spectrum management agencies in each of ITU member countries before the international notification/ verification process can start.

Of equal (or even greater) importance are delays involved by spectrum management processes. Such delays are especially harmful during and after disasters when the time factor is crucial. In many cases the information which frequencies can be used and where is not available when needed. In addition, various national regulatory procedures may paralyze all efforts to replace the destroyed telecommunication network by its new wireless substitute. But even in normal situations such delays may have calamitous effects. Space systems may serve as example. The ITU notification process of such systems introduces up to two years of delay. The 1998

plan of the ITU-R Sector states: "...in spite of the measures taken and the resulting higher rate of productivity, delays in treatment of material represent a continuing problem." (Doc. RAG98-1/1E). Several years may be required until the system receives the national and international authorizations to operate. It contrasts sharply with the 18-month life span of electronic technology generations. A space system may easily become out-of date waiting for authorization by spectrum managers. If it has been modified during the waiting time to keep pace with the technological developments, it may be required to restart the coordination process with the competing systems that might appear on the scene in the meantime. This perspective is difficult to accept in the competitive, market-driven environment.

Continuing attempts have been undertaken to improve the spectrum management. These go in two directions: reviewing basic policies and improving computing tools. However, the tools available in ITU and in majority of its member countries are inadequate. The number of various space systems submitted to ITU for notification increased by 600% from 1993 to 1997, and the complexity of systems also increased dramatically. It has not been accompanied by appropriate upgrading of the computing tools. In his letter (CR/84 of 2/2/98), the Director of ITU-BR wrote: "The ITU-R has not yet adapted any methodology nor algorithm [to perform required computations]. Also, there is no established and internationally recognized software..." It should be noted that such a methodology and algorithms may require reviewing mathematical foundations on which the present approach is based. A special URSI WGE1 Workshop organized at this symposium is devoted to that topic.

2 SPECTRUM ENGINEERING

With the progress in electronic and space technologies, and with the increasing wealth of nations, an enormous

¹ Opinions expressed in this paper are those of the author and do not engage the ITU, URSI, or any other entity.

growth of communication and other applications of radio applications is observed. However, that growth is hampered by the apparent shortage of spectrum/ orbit resources necessary for wireless systems to operate. The problem has been discussed at various occasions. At the previous session of this symposium it was suggested that the deficit of spectrum/ orbit resources could be decreased, among others, by improvements in spectrum management.

The central issue here is spectrum engineering and electromagnetic compatibility, "EMC". Both terms have received a wide international acceptance after the IEEE report "Spectrum engineering - the key to progress" was published in 1968. At that time, engineers and scientists from government, academy, and industry, were concerned with the potential disruption of vital wireless services due to radio interference. Since then EMC has been the basis for rational use of the spectrum/ orbit resources. EMC involves two complementary aspects. The first one is a correct operation of a system in hand under the influence of the environmental stimuli, intended and unintended. The second aspect involves non-interfering with the environment. Also here the intended and unintended interactions have to be taken into account.

Spectrum management usually involves a compromise between parties making incompatible use of the spectrum/orbit resources. A rational approach involves an evaluation of the interference threat implicated. As such an evaluation inevitably contains some assumptions and approximations, usually one party claims that the interference threat is underestimated whereas the other one maintains that it is overestimated. In such cases when traditional computing results are questioned, experimental evidence remains a valid argument. But "real world" experiments may require special measuring campaign. Such campaign may require too much time, or may be too expensive. For instance it may require a full-scale satellite system to be deployed. In such situation more advanced computing tools have to be used.

One difficulty with computing support of spectrum management is that interaction models are not well defined and that exact values of variables are often unknown. On the one hand, the rigorous theoretical models are available for the simplest structures only. On the other hand, "experimental" models have limited applications. The unintended interactions are usually ignored in the planning, design and production processes. Consequently, these are poorly documented, if documented at all. Another difficulty that spectrum engineering encounters results from the dimension of the problems that may make them intractable by rigorous approach. The performance of a communication system depends on the performance of its component transmitter-receiver links during a given time period. It is the state-space, or test-domain - the set of all states the system might occupy. For instance, with aeronautical and satellite systems all expected locations of stations, varying in space and in time, have to be taken into account as test domain. It

may require a great number of computations. A quick order of magnitude analysis illustrates this point. On the one hand, the test domain should be large enough to embrace all significant elements of the system and their behavior in time. On the other hand, the resolution of the results has to be fine enough to capture the smallest scales that are relevant. The test domain contains, therefore, $N = (D_{\text{Max}} / D_{\text{Min}})^4$ points, where D_{Max} and D_{Min} denote the largest and the smallest distances involved in the four-dimensional space-time test domain. If $D_{\text{Max}} / D_{\text{Min}} = 10\,000$, then there are 10^{12} points.

Frequency planning can serve as another example illustrating the size of the problems involved. A frequency plan is a function that assigns operational characteristics to transmitting stations. It may be the frequency channel, polarization, power, antenna location, its radiation pattern, time of operation, etc. Even with a moderate number of transmitters and operational parameters, the number of EMC computations required to select the best variant of the plan by an exhaustive inspection is enormous. Take for example a plan of small point-to-multipoint wireless network that consists of 10 transmitting stations, each linked with 10 receiving stations. Every transmitter can use one of 20 frequencies, and one of 5 power levels available. To simplify, all other parameters, such as location etc., are fixed, and all environmental signals can be ignored. The complete set of EMC computations would require of 10^{22} tests. Even if each would take only 1 microsecond of computer time, the job would not be finished in 10^9 years! Most often, frequency planners and spectrum managers have to abandon such impractical rigorous approaches and have to rely on approximations justified by their intuition and past experience. But such "approximate" solutions do not warrant the best use of the resources that would be (theoretically) possible.

2.1 COMPUTER SIMULATION

One of advanced tools that may be helpful in spectrum management is computer simulation. It is an experiment run inside the computer instead of the "real world". Its aim is to imitate modifications to various parameters of the system, or its environment, or both, and to examine their effects to obtain information about the system, about modifications to the system or about several competing systems.

There are two approaches to simulation: deterministic and probabilistic. The first one involves deterministic models and variables. In this approach, a simulation "scene" is generated and analyzed. The trial is done only once. There is no need to repeat the trials with the same set of input variables because, with deterministic relationships and data, each trial gives the same result (within a small computation error). In the probabilistic simulation, random elements are introduced. With random components, the system performance is subject to statistical dispersion and each trial may give a different result. Flipping a coin is a good example. Although the laws of physics allows to predict exactly its position

(given the initial position, velocity, spin, etc), it is practically impossible to determine in advance whether the coin lands on heads or tails. To obtain results that are statistically significant, the simulation experiment has to be repeated a number of times. The probabilistic simulation is thus based on a repetition of many trials and collection of statistics representing the global, or most probable, result. That approach was first proposed by Stanislaw Ulam (1909-1984), a Polish mathematician who later played a major role in the development of the hydrogen bomb at Los Alamos. Ulam had a number of specialties, including the probabilistic simulation theory, named also "Monte-Carlo".

The sample size (the number of tests to be performed) determines the uncertainty with which the statistical performance measures of the system are estimated. Here, we have to differentiate between "population mean" and "sample mean" of a variable. The population mean relates to all possible tests involved, whereas sample mean is associated with the sample, i.e. with a limited set of tests actually made. Because of the limited size of sample, the sample mean (Mean_s) may differ from the population mean (Mean_p) and, in order to obtain valid simulation results, the difference must be kept small. The probability (P) that the difference lies within a small error (Err) depends on the sample size (n), and is subject to the Tchebycheff's inequality:

$$P\{|\text{Mean}_p - \text{Mean}_s| < \text{Err}\} > 1 - [(\text{Var} / \text{Err})^2 / n],$$

where Var is variance. By selecting a sufficiently large sample, n , the probability that the sample mean will fall within a small error interval about the population mean can be made as near to unity as desired. If, for instance, the acceptable error is $\text{Err} = 0.1\%$ of the variance and probability $P = 99.9\%$, than the sample size should not be less than $n = 10^9$. In practice, rarely such a precision is needed and much smaller samples are sufficient. A smart design of simulation experiments can decrease the number of simulation runs.

3 COMPUTING TOOLS

In view of the problems indicated earlier, the development in computer technologies will have an immense impact on spectrum engineering and spectrum management. One of the driving forces is a growing need to determine the performance of increasingly complex systems in their increasingly congested electromagnetic environments. The ideal approach would combine computation, simulation, measurement, and analysis, so that system assessment can be achieved to a needed accuracy at acceptable cost and within acceptable time limits.

3.1 COMPUTERS

In 1965, Gordon Moore, who later co-founded Intel, examined the price/ performance ratio of integrated circuits and predicted that the capacity of a computer chip would double every year. Nobody believed that this rate

of improvement would last long. But his forecast proved true until now with one correction: the average doubling period is not twelve but eighteen months. This regularity has been referred to as Moore's Law.

The Toshiba laptop computer I am using is ten thousand lighter, hundred thousand faster, and has four hundred thousand more memory than Eniac, its grandfather. In addition it is five hundred times less expensive. It is build around a single Intel Pentium MMX processor that runs 10^7 instructions per second (10 MIPS). Just when I bought it, Intel announced a prototype of a multi-processor computer that combines nine thousand Pentium-Pro processors and runs 10^{12} float-point operations per second. My laptop operates at 150 MHz, and almost seven times faster processors running 1GHz have been announced in 1998. Technological innovations make the computing costs declining. The price index, about \$1/MIPS in 1975, dropped 10^4 times by 1995, making computing costs insignificant in comparison with other costs. This trend will continue. We will be able to solve bigger computing problems much faster and much cheaper.

3.2 COMPUTER NETWORKS

The most important change in computing environment since the Eniac times come with computer networks. A computer network offers a multi-user, multi-task environment in which information and tasks can easily be shared, subject to system access control. One computer can use data on disks attached to other computers and share tasks by initiating, executing and communicating with other computers. The tasks can optimally be distributed within the network to minimize the time required, amount of information exchanged, etc. The first experimental DARPA project launched in seventies connected only a few computers. By the year 2000, projections indicate that about 180 million computers will be connected to an Internet constituting 4 million networks dispersed around the globe. In 1997, more than 10 million hosts were connected to Internet in the USA alone, and the number of interconnected computers increased with a rate of 170% a year. The ITU TIES system is following a similar trend, following Kyoto Resolution 66 and Resolutions ITU-R 19 and 20. It offers electronic access to a growing number of documents available earlier only on paper.

The Internet has supported thousands of different applications including a trillion dollars a year of transactions. It is becoming a substantial part of collaborative aspects of our activities, reshaping institutional, business, financial, and political boundaries. Many analysts are of the opinion that this phenomenal growth has been possible because regulatory constraints were minimal and there has been no central administrative body of Internet. Could that approach be applied in spectrum management?

3.3 ELECTRONIC DOCUMENTS

Our decision-taking processes, engineering, administrative, and financial have been paper-based. Anything requires a paper document that usually has to be submitted for comments and/or approval. The process may involve a number of persons, sometime at distant places, and each may introduce modifications, annotations and comments. Coordinating that process with paper documents it is difficult, error-prone, time-consuming, and expensive.

With paper documents, we have been forced to order information linearly, one after another. To facilitate the search, we have been using tables of contents, indexes, and cross-references, but these have also been organized linearly. Digital documents can be faster and easier to work with than paper as the logical structure and physical arrangement of data in electronic form can be kept separately. The needed information can be searched, identified, and retrieved almost instantly.

With powerful computer database technologies, documents, texts, formulas, numbers, images, and sounds can easily be indexed, retrieved, or linked with related subjects. The content can be restructured easily by date, time, or by any other index. Data are easier to find, to copy, and to distribute. Bill Gates of Microsoft predicts that within a few years the digital document, complete with authenticatable digital signatures, will be the original, and paper printouts will be secondary and a significant percentage of documents will not even be fully printable.

Most engineering, financial and administrative documents are superior in digital form. More and more engineering tasks base on electronic documentation. The case of Boeing can serve as good example. Earlier, paper documentation was used and full-scale mock-ups of the airplanes were built. The mock-up was necessary to make sure that every part of the airplane, often designed and produced by different teams, actually fit together correctly.

With its 777 jetliner Boeing replaced it by a gigantic electronic document to hold all relevant information. The document contained digital models of all the parts together with all necessary information on how they should work together. By using such digital documents, Boeing was able to make significant savings and assure required product quality.

With such an electronic documents, planners and designers could work with the same data, track modifications at computer terminals, identify any incompatibility immediately, and correct it if necessary. The document could be updated automatically and modifications shared among all those involved, with annotations who made them, why, and when - something that would be very difficult on paper. The same approach could be applied in spectrum engineering and management, national and worldwide. The analogy with fitting service areas of wireless systems is evident.

3.4 DATABASES

A spectrum management database is a set of objects representing the world in the form of electronic document. It is used to organize, warehouse, retrieve, and manipulate information relevant to spectrum-related activities. Such a database integrates three major components: position, time, and attributes or properties of the objects. These components define what is the object, where is it, how is it related to other objects, and what is its history. Position refers to the fact that each radio station has a geographical location and orientation that must be specified in a unique way. It is employed in combination with a frame of reference with its position, orientation and scale. Time is important since the real world is changing with time. Attributes, often termed "non-spatial data", represent all other features that essentially do not depend on location and time.

Spectrum management database represents the real world as it really is and also a "virtual" world of objects that do not exist in reality but are declared, such for instance as "paper satellites" discussed at the recent World Radiocommunication Conference WARC 97. These virtual objects can be created, modified, and annihilated at will by the users. Problems with such objects were discussed at previous occasions. Usually, different applications require different subsets of data derived from the database, or different "user views". Sharing a database by several applications instead of each having independent databases results in reduction of data redundancy and inconsistencies.

3.5 GIS

Geographic Information Systems or GIS are specialized database management systems developed to facilitate handling spatially related data. They include data structuring and manipulating systems that may be useful in spectrum management applications. They all base on few primitive types of geometric entities used to encode spatial data: points, lines, polygons and surfaces. Points are 0-dimensional objects, lines are 1-dimensional (length), polygons are 2-dimensional (length and width), and surfaces are 3-dimensional (length, width and height).

The spatial distribution of points, lines, and surfaces may be represented in raster and in vector models. Raster or cellular organization of spatial data is one of the simplest. It involves the grid and other regular tessellation, nested tessellation or irregular tessellation. In the grid tessellation, square, triangular and hexagonal cells are used. The most widely used is the square grid. The smaller the piece of land represented by each cell, the higher the spatial resolution of the data. However, the size of the file increases with resolution. Since the file size is related to the area, it increases by the square of the increase in resolution. In the nested tessellation model, cells are recursively subdivided into smaller cells of the same shape. The most common model is the quadtree based on recursive decomposition of a square

grid. The area under consideration is first enclosed within a square, which then is subdivided into four subquadrants. The subdivision process is repeated until a predetermined resolution level is achieved. The quadtree approach provides a more compact raster representation by using a variable-sized grid, with finer subdivisions in areas where finer resolution is required. Irregular tessellation can be adjusted to the irregular character of data. The triangulated irregular network (TIN), was developed in early 1970s to create a digital elevation model (DEM) basing on a set of irregularly spaced points on the Earth surface. It is an alternative to the DEM based on a regular grid (raster). Raster models have a regular data structure that makes overlay and combination of mapped data easier than with vector (irregular) models as the same set of grid cells are used for several variables. It makes also simulation calculations simpler.

3.6 DATA WAREHOUSING

One of important tasks of spectrum management is exchanging and archiving or warehousing of large amounts of information. Until recently, the whole human knowledge has been stored and exchanged as paper documents. But the role of paper as a vehicle of preserving and distributing information is changing. All information documents can easily be stored and exchanged in an electronic digital form. CD-ROM multimedia encyclopedias are good example. For instance, Microsoft Encarta includes 9 million words of text, 7'000 graphical illustrations, 800 maps, 250 interactive charts and tables, 8 hours of sounds, and 100 animations and video clips. And all this is packed in a disk, 12 cm in diameter, 1 mm thick, cheap and easy to store and to transport.

In comparison with paper-based technology, electronic storage is more practical and less expensive. Storing one megabyte of data on a hard disk drive in personal computers costs about \$0.15, and about ten times less on CD-ROM. That cost is actually the cost of renting as the storage space can be reused - something impossible with the paper. Note that one megabyte holds about 700 pages of text. The SABRE airline reservation system stores more than 4×10^{12} characters on computer hard disks. It is a giant electronic document or database containing information on flights, fares, bookings, seat assignments, and billing for hundreds of flights a day. If that information were copied into a hypothetical paper reservation book, it would require more than 2 billion pages.

Storage is getting cheaper, and hard disk prices have been dropping by about 50 percent per year for the last several years. The hard disk in my laptop has 1.35GB capacity, an equivalent of 9'000 pages of text. In January this year, IBM has announced a new technology that allows storing about ten times more (16.8GB) in the same volume. Such disks will be introduced in this year's laptop and desktop computers. Huge data collections and immense documents related to spectrum man-

agement can thus be stored, copied and distributed easily and cheaply. Copies can be made on different servers and one disk-based server is able to serve simultaneously a number of users. The extra cost for each user is simply the cost of using the disk storage for a short period of time and the communication charge. And that is becoming extremely cheap. Some ITU publications have been available in electronic format. In 1998, the International Frequency List, terrestrial frequency assignment plans, and the list of Space Radiocommunication Systems with all specific data (including graphical data) will be published on CD-ROM. Similarly, the Weekly Circular and HF Broadcasting Schedules and Summary of Monitoring Information will be published. The disks will also contain some software packages of interest to frequency managers. A CD-ROM of all ITU-R recommendations in force will also be published.

4 ONE SPECTRUM, ONE MANAGEMENT SYSTEM

There is one frequency spectrum shared by all users around the world. Consequently, one should expect one management system to avoid chaos and assure its rational use. However, the present spectrum management, seen from a global perspective, resembles a patchwork rather than an integral structure. Because of historical reasons, the world has been divided into many countries and the principle of sovereignty combined with competition dominates over the globalization trends. The ITU covers only a part of spectrum management activities necessary to assure global compatibility. It bases on a voluntary approach and on consensus negotiated at international meetings and conferences. Traditionally, each such conference is limited to issues raised by individual countries seeking their own interests, and nobody wants to resign from sovereignty.

The inefficiency of that approach has been evidenced by the delays mentioned earlier, and also by a large number of meetings. The 1998 schedule includes about hundred regular meetings of ITU-R Study Groups, Working Parties and Task Groups. And it is on the top of other meetings by two other ITU Sectors and such gatherings as the World Telecommunication Development Conference, Plenipotentiary Conference, World Telecommunication Policy Forum, Radiocommunication Assembly, etc. To that, one should add conferences organized by other organizations such as UN conference on emergency communications, WTO negotiations on trade in telecommunications, etc. Participation in all these gatherings constitute a heavy burden especially for countries far away from Geneva. A common system of videoconferencing and common computing tools could reduce that burden and make the cooperation more efficient.

The fragmentation of the present spectrum management system imposes severe barriers in cross-border exchange of services and goods. When moved from one country to another, the wireless communication systems/equipment are required to pass through a series of

costly and time-consuming administrative clearing processes. Due to differences in national spectrum management requirements, such as frequency allocations, the equipment has often to be redesigned before it can be authorized to operate. This became a substantial administrative obstacle in the development of global services and global systems, otherwise feasible technically and economically.

4.1 ITU COMPUTING TOOLS

Computers have been used heavily in the ITU headquarters. However, the ITU hardware and software has been tailored to fulfil only the tasks that specifically have been defined at relevant conferences. Consequently, only a few of ITU computing tools could found a wider application outside Geneva. When the headquarters moved to the personal computers, more tools could be used also at national level. Over the years, several ITU members have requested specialized software to support their spectrum management activities. In late eighties, this author organized in then-ITU-CCIR a library of such computing tools. The idea has been supported and the catalogue of software library ITU lists today about a hundred programs, including copies of electronic notification tools created for use within the ITU. However, the software offered for that library is fragmented and of limited practical use outside the offering administration. These are separate pieces of programs, written in different languages, to solve partial problems, not easily transportable. The only exception is BASM, or Basic Automated Spectrum Management System developed to fulfil basic needs of the developing countries. A more sophisticated system, and spectrum management data dictionary, are under development. Computing tools of greater practical value have not been offered for common use because of unsolved copyright and intellectual property problems.

Although there have been several ITU resolutions concerning the wider utilization of modern electronic communication and computing tools, and some progress is visible, the status of computing tools is still much below what modern technology can offer. None of ITU conferences addressed explicitly the issue of integration of national spectrum management systems into one global system, and the need for common "groupware" computing tools.

5 CONCLUDING REMARKS

We have no control over the pace of innovation. Every day we see new ideas, new products, new applications, and new services. The innovation process develops following its own rules, pushed by the ingenuity of individuals, competition, and market demand. The national spectrum management systems and supporting computing tools have been created to serve local needs. To a large extent, they ignored transnational aspects of use of

the spectrum/ orbit resources. Now separated, in future they will be interconnected and integrated into one global system. Common standards for "open system interconnection" will enable messages and data flow easily from one to another. The system will be "intelligent". It will do the work required to access various information sources. Software agents will "understand" the information needs of individual users and automatically seek out, retrieve and process the needed information. It will be able to perform various complex tasks mixing multimedia, data, text, image, sound, and video with computing.

Opinions have been expressed at several occasions that the material gathered in the framework of ITU, including data and computing tools, should be made accessible in electronic format via Internet, free of charge for ITU members, researchers, etc. The argument is that the material has been produced using public money and in-kind contributions and, consequently, it should remain in public domain. The current ITU copyright and pricing policy does not follow that rule which creates additional obstacles in promoting the rational use of spectrum - orbit resources. It is especially detrimental in the case of developing countries, where flow of information is not so efficient as in rich countries and where more and more universities and other entities are connected to Internet. The current ITU pricing policy is seen by many as incompatible with the purposes of the organization. It is my belief that in the future this policy will change.

To conclude, I would like to quote Vice President Al Gore, who said at the ITU Development Conference, Buenos Aires, 1994: "...we now have at hand the technological breakthroughs and economic means to bring all the communities of the world together. We now can at least create a planetary information network that transmits messages and images with the speed of light from the largest city to the smallest village on every continent. [...] And it will greatly promote the ability of nations to cooperate with each other..." It is up to us when we will use these means to create a new worldwide spectrum management system.

BIOGRAPHICAL NOTE. Ryszard Struzak was elected a Member of Radio Regulations Board at the Plenipotentiary Conference of International Telecommunication Union (ITU) in Kyoto in 1994, and the Co-Chair of WG on Spectrum Management and Wireless Telecommunications at the General Assembly of International Union of Radio Science (URSI) in Lille in 1996. He has received two international awards and many other professional awards and decorations. He is co-founder of International Wroclaw Symposium on Electromagnetic Compatibility (EMC) that has continued since 1972, and served as Chairman at several international conferences and workshops

XIV

**SPECTRUM MANAGEMENT,
ENGINEERING, SHARING
AND MONITORING**

**New Trends in Computer Support
for Frequency Spectrum Management**

Invited session organized by

T. Cesky - Denmark

Databases for frequency spectrum management systems

BAQUIAST Laurent
PASTOR Robert

CRIL INGENIERIE
Le Newton 25,27 Rue Jeanne Braconnier
F-92 360 Meudon La forêt (France)
tel : 33 (1) 40 83 52 52 fax : 33 (1) 40 83 52 53
E-mail : crilid@cril-ing.fr

1. Overview

Studies throughout Central and Eastern Europe have highlighted the importance of establishing and developing adequate telecommunications.

In the particular area of radio communications, an harmonised regional approach is of utmost importance due to the necessary international co-ordination required by the operation of radio services.

1.1 PHARE 9511

This paper is associated with the PHARE 9511 project which focuses on the frequency spectrum management.

Main objective of the project is to implement a standard interface software in order to permit exchange of data and frequency management software between participating countries.

Expressed in a different way, one could say that, with the P-Interface, Administration A can use its own compatibility software on data received from administration B and also use software received from administration B in its own environment.

The so called P-Interface layer :

- offers its services to spectrum management applications,
- masks underlying databases,
- provides communications services between National Spectrum Management systems.

P-interface allows to see the set of national databases as a virtual unique data base.

1.2 Reason for data exchange

Primary reason for data exchange between administration is the co-ordination process.

This particular exchange of information is a necessity for technical reasons such as radio interference calculations but also for other regulatory issues such as mutual recognition of frequency assignments.

1.3 Problem of data exchange

It is obvious that efficient exchange of information necessitates a common language, common measurements units, common way to describe radio communications objects.

Variations in data definitions across the different radio communications services and the different frequency bands complicate the data exchange process.

Unique identification of data elements throughout participating countries makes it easier for all administrations to understand the definition of terms regardless of the original language used to define them.

1.4 Sharing of common software

One of the major benefit of the P-Interface will be to implement the same compatibility calculation program in different administration.

A compatibility calculation software, developed for one administration will be portable to all other administration.

One example of this common compatibility software is the Harmonised Calculation Method (HCM). HCM access to radio communication data

for transmitter definition and to DTM data for calculation of propagation losses.

Software certification is possible thanks to the presence of a unique Application Programming Interface. It is obvious that only software which is not specific to a particular Computer System can be effectively certified.

In doing so, the software development burden will be shared among participating administrations.

1.5 Expected benefits

Computer assistance will :

- assure that information exchange is complete and consistent,
- improve the accuracy of data supplied by administrations.

Direct data exchange between administrations will shorten the co-ordination process with the final objective to facilitate radio services growth while reducing harmful interference risks.

2. Proposed concept

2.1 Client / Server

The technology proposed for the solution is based on the Client / Server concept where the relevant data in national systems for spectrum management will be accessible via server services.

2.2 Container

With a standard interface to the server, data can be seen as being placed inside a container with an unambiguous way to access it.

The internal structure of the data and data storage thus become irrelevant and invisible for the client application.

2.3 Advantages

P-Interface masks underlying database in a such way that each application could access to its own radio communications data and those belonging to foreign countries in the same way.

As an extension of the presented architecture, databases could be physically distributed among a Wide Area Network and logically integrated under the P-Interface without any modification for the client application.

2.4 Database access

When developing a client / server application in an heterogeneous environment, it is first important to understand what will be the low level approach to each database.

As an implementation of the software is foreseen in eleven countries in Central and Eastern Europe, it was crucial to minimise specific developments.

ODBC (Open Data Base Connectivity) has been chosen as a Standard Interface to each database.

2.5 ODBC

The ODBC application programming interface (API) provides a set of functions intended for use from different application environments that query a database server using Structured Query Language (SQL).

In ODBC, the user does not have to learn a database vendor's proprietary API. He can use the ODBC API to access any data source for which an ODBC driver is available.

3. Principles

Principles of the P-interface are an harmonised approach on the following aspects :

- utilisation of a unique data dictionary,
- definition of a common radio communications database structure,
- utilisation of a common map server.

3.1 Data dictionary

As stated previously, one of the main problem in data exchange is the unique identification of data elements.

In order for electronic data exchange to be successful, the data to be exchanged between Administrations must first be agreed.

Data elements used by the P-Interface will be those defined by the ITU-R Task Group 1/4.

Every administration will be able to adequately and correctly identify frequency management information.

3.2 Common database structure

Each data element will be affected as a database attribute to a radio communication entity managed by the P-Interface.

This database structure will integrate latest results of TG 1/4 and could be the reference towards which each administration could evolve.

This organisation is adapted to take into account the needs of compatibility calculations.

3.3 Common map server

Diverging co-ordinates system are in use among participating countries. To solve this

problem, P-Interface will expose a common interface to Digital Terrain Data.

P-Interface has retained World Geodetic System 1984 (WGS84) as the reference co-ordinates system.

P-Interface will offer conversion services between native co-ordinates systems and the WGS84.

In this first version, associated terrain database will use no projection system and P-Interface will deal only with elevation information. A future extension of the Digital Terrain Model (DTM) services will allow to :

- manage other maps such as morphology, road, ...
- implement projected data in different coordinate system in order to calculate terrain cuts through borderlines.

4. Transport Containers

4.1 Purpose

One of the basic tasks of the P-Interface is the data exchange between foreign administrations. In the proposed concepts, data exchange becomes a simple act of sending a transport container to a foreign administration.

Transportation of Container will be based on Internet.

4.2 Transport container

Typical scenario is that data is forwarded in the transport container. This container is connected to the user's database. On the client side of the P-Interface no distinction is seen whether the particular data element is taken from the transport container or from one of the local containers.

4.3 Content

In this first version, a Transport Container will contain only co-ordination data. In future extension, digital terrain data could be exchanged by the same way.

4.4 Stand alone database

In small administrations, a Data Container could behave as a native database allowing the administration to operate only with Data Containers in a stand alone configuration.

4.5 Backward compatibility

Throughout the whole life of the P-Interface, the software will present a series of incremental versions.

If successive versions should modify the structure of a radio communications object or the structure of a container and its associated transport files, these should remain compatible with earlier versions.

Attempts to read a container stored by a previous version may fail because of these different structure.

In order to prevent backward compatibility, P-Interface will check its own version and compare it to the version of the P-Interface who creates a transport container.

5. Specific problems to deal with

5.1 Internationalisation

Handling multilingual data includes how to input, display, sort and store multi lingual texts, manage date and time, etc.

P-Interface behaves like a server application. Client applications and native database could not be able to manage wide characters set such as UNICODE. To solve this problem, it is foreseen to implement a specific character set conversion method in each country. This conversion method will translate the specific characters in the national character set into pure ASCII codes exploitable by the foreign client applications.

5.2 Heterogeneous environment

The P-Interface should be designed in such a way which allows for efficient implementation on different databases in a mixed Unix-Windows environment.

In the PHARE 9511 project, it is assumed that an administration will deploy the transport containers on a Windows 32 bit platform. This will lead to develop the P-Interface as a Windows server which offer its services to an Unix or Windows client application.

For the P-Interface, the retained solution is based on CORBA. CORBA approach let us describe the P-Interface API in a common portable language : IDL (Interface Definition Language). IDL provides a standardised representation of an object through its methods and attributes. The object remains consistent regardless of language or platform implementation.

The central component of CORBA is the Object Request Broker (ORB). An ORB allows objects to interact in a heterogeneous, distributed

environment, independent of the platforms on which these objects reside and techniques used to implement them.

The basic functionality provided by the ORB consists of passing the requests from clients to the object implementations on which they are invoked. In order to make a request, the client can communicate with the ORB through the IDL stub. The stub represents the mapping between the implementation language of the client and the ORB core. Thus the client can be written in any language as long as the implementation of the ORB supports this mapping. The ORB Core then transfers the request to the object implementation which receives the request as an up-call through an IDL skeleton.

6. Database encapsulation

6.1 Encapsulation

P-Interface should encapsulate the user's database in the way that the client sees the "Standard P-Database" which contains information important for frequency co-ordination and compatibility calculations.

P-Interface must be capable of encapsulating of a number of data containers in one database session.

6.2 Flexibility

Encapsulation has no impact on the native database structure. So the native databases remain compatible with all existing programs.

It is indispensable that the encapsulation is achieved in a flexible manner.

Minor modification of the native database as changing a table or a column name, adding a new column, etc. should be achieved without rewriting code and so without a software release.

It is believed therefore that information relative to the native database diagram should correspond to input parameters of the P-Interface.

6.3 Mapping between classes and tables

The P-Interface works in the object model. All underlying databases are relational ones. P-Interface therefore must do Object Oriented versus Relational transformations.

Mapping between the P-Interface object model and the underlying relational model is performed at different levels :

- first mapping level corresponds to mapping between classes and tables. In general, a class is mapped to one table. In the case where one class is mapped to several tables, it is necessary to define a join operation between these tables.
- second mapping level corresponds to the mapping between object members and columns. One object member is generally mapped to one column of a table.
- third level corresponds to mapping between data types in the object and in the relational model,
- last level corresponds to the mapping between units. Data should be convert in the target unit before applying type conversion.

7. Conclusion

Due to the number of techniques involved, the problem addressed by the P-Interface is considered as very ambitious and is further complicated by considerable differences in the implementation of native databases across participating countries.

Achievement of such a project within its deadlines could be possible only if all participants throughout concerned countries work tightly together.

New requirements and trends in computer support for frequency spectrum management

Tomas CESKY

EUROPEAN RADIOPHYSICS OFFICE

Midtermolen 1, DK-2100 Copenhagen, Denmark

E-mail : cesky@ero.dk

1. Introduction

Frequency spectrum management (FSM) is a key element in the rapidly developing world of radiocommunications. Advanced tools for frequency spectrum management have to be used in order to accommodate requirements of all users of the spectrum and to maintain a mutual electromagnetic compatibility between radiocommunication systems in operation. Most, if not all, methods used for interference assessment and frequency co-ordination are based on common agreed procedures and algorithms; however, their implementation in a particular system seems to be a unique undertaking. Resources required for "re-inventing the wheel" tend to exceed justifiable limits in many administrations.

2. Major factors

Frequency spectrum managers operate in a turbulently changing environment. Factors having a significant impact on FSM are:

- Congestion of many parts of the frequency spectrum;
- deregulation;
- new telecommunication services and new technologies.

The rapid development in all of the above areas poses new requirements on FSM concepts and presents a challenge in implementing up to date FSM techniques. The computer support for frequency management together with powerful computation techniques play a very important role here.

2.1 Spectrum requirements

The amount of information to be communicated is constantly increasing. The typical pattern is that when there is not enough spectrum available to satisfy certain needs a solution is sought by means of enhancing or changing the transmission technology, by regulatory means and in many cases by shifting the service paradigm. Usually when an acceptable solution is found an additional spectrum need is already on the table.

One of the tasks of FSM in this process is to ensure mutual compatibility between services sharing the spectrum or occupying adjacent frequency bands without unnecessary portions of spectrum being wasted. The availability of inter-system compatibility analysis, based on non-trivial assumptions, is one of the prerequisites of the efficient FSM.

2.2 Deregulation

Deregulation in telecommunications is the most significant trend from the point of view of frequency management. The roles of the regulator and operator are being consistently divided. The equilateral triangle with balanced roles for the regulator, operators and the manufacturing industry is a generally acknowledged model. This arrangement is considered to be optimal in general and appropriate for the end of this century.

From the point of view of FSM there are a number of serious consequences to this trend. Frequency management must be based on a set of rules agreed between all parts of the triangle. This set of rules tends to be quite complex and the radio

frequency spectrum aspects are only one of many facets.

For the efficient use of spectrum under these conditions it is essential that the regulator has a good engineering insight backed by appropriate computer support.

2.3 New services and technologies

Implementation of services and technologies has an ambivalent effect on FSM. On the one hand it helps to satisfy more communication needs with existing resources but on the other requires complex activities centred around inter-system compatibility and coexistence problems. Whilst the intra-system compatibility is guaranteed by the system design, the inter-system compatibility can be achieved by appropriate defined system standard and by the frequency management procedures.

The particular difficulty in including the spectrum efficiency requirements and inter-system compatibility elements into the standard for a new system is the usual unavailability of real-life experience with any system comparable with the proposed standard. Similarly the strategic decision of the regulator on frequencies for a new service is required prior to deeper experience with the system.

A considerable amount of simulation and modelling tools tailored for FSM is necessary in order to implement new systems in an orderly manner and to ensure spectrum efficiency also in a longer term.

3. Computer support

Inappropriate computer support is necessary for all three parties of the above mentioned triangle *industry-operator-regulator*. Unfortunately their requirements differ fundamentally and lead to the need for specialised software. The system manufacturer, the system integrator and partly the operator need to simulate their system in great detail with a possibility to study virtually every internal aspect of the system, however, the inter-system compatibility part is of lesser interest. In the latter case usually the only issue is the conformity with relevant standards.

For frequency management purposes the model of the radio environment is needed. The simulation of a particular system in this model need not be as deep as in the previous case and the emphasis is on the completeness of the model and on inter-system compatibility issues.

3.1 Ideal system

An ideal system for computer support of frequency management would be built around a National Frequency Register database. This register should be scalable and able to supply the information ranging from a National Allocation Table at one end up to assignments for certain services at the other end. Also a very important part of such a register is data on licenses. The register would be augmented by additional databases including topographic and cartographic data. User programmes would be clients utilising a number of servers for access to data and servers performing basic functions e.g. protection ratio estimations, radio propagation calculations, cartographic transformations, etc.

The interface for clients should be using a Client/Server machinery standard for the platform, e.g. COM on Wintel platforms as shown in the diagram (Fig 1).

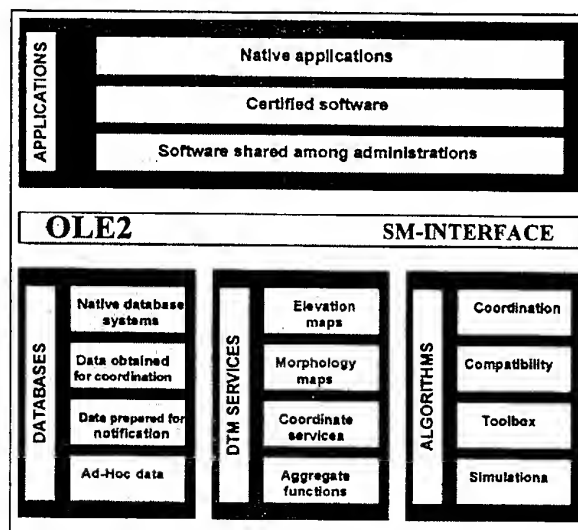


Figure 1: Example of Client/Server system

The data and services should be accessible to a number of users, local and remote, with different levels of information accessible. The system must be suitable for exchange of data with other parties e.g. in the process of international frequency co-ordination. In the ideal system the data subject to exchange should be seamlessly integrated into the data server.

3.2 Data encapsulation

Encapsulation of data along the lines suggested above is seen as essential for computer systems for FSM.

Experience shows that the diversity of FSM applications and their implementations in practice makes it impossible to maintain one coherent data model across all implementations of one system. As a consequence a number of diverse databases in different formats is in use even within one organisation together with an unavoidable overhead of conversion programmes. A good, scaleable, encapsulation of data alleviates this problem completely.

Encapsulation plays an even greater role in co-operation between various systems for FSM. It is not feasible to require a universal common data model in all relevant systems and even if it were it would be counterproductive. By means of encapsulation of various a virtual database with a uniform data model can be produced.

One of benefits of the encapsulation, which is most apparent, is their suitability for exchange of data for instance between administrations for international co-ordination. Standard encapsulation has the potential to remove the need for agreeing data formats for every type of co-ordination.

3.3 Shared software

The need to share engineering software among different players on the FSM field is quite obvious and is likely to increase with the introduction of new advanced communication systems. In particular small administrations do not have enough resources to develop the required software in house and the software is usually not available commercially.

A number of catalogues of engineering software for FSM exist, e.g. the ITU-BR Catalogue of Software to name the most important one. The major difficulty with such catalogues is that all but trivial programmes require access to some database. In order to utilise programmes from a general catalogue it is usually necessary to re-write the data part of the software. This makes programmes from the catalogue less appealing.

As far as a lack of commercial software is concerned the reasons for this situation are very much the same.

It is believed that a suitable standard for the data encapsulation can be defined to enable the use of software for FSM regardless of the structure of underlying data.

3.4 Software certification

The possibility to use engineering software for FSM tasks independently of the data format makes possible the certification of this software by some recognised authority. As mentioned in the introduction the interaction of various players in the radiocommunications arena is based on a number of formal rules.

Procedures dealing with the compatibility are typically in the form of a recommendation (ITU-R, CEPT, ...). The implementation of such procedure usually involves software development. Once the software is certified it could become part of a recommendation including all implications.

4. Implementations

4.1 Computer platforms

The concept of an "ideal system" for FSM suggested above corresponds very well with current trends in computer technology. It suggests a multi-tier architecture with suitably thin clients.

The example in Figure 1 shows a typical situation for the Win32 platform where the Client/Server communication is based on OLE2/COM standard. The implementation in a simple environment is straightforward. Also considering DCOM a full functionality in a distributed environment can be foreseen.

The biggest hurdle in turning existing PC system for FSM into this architecture is a proper encapsulation of the database.

In a pure UNIX environment a complete analogy to the example in Figure 1 could be developed using object brokers such as CORBA. However, the potential of exchanging encapsulated data and of sharing software in a UNIX environment does not seem high enough to encourage the development.

The most difficult situation to be encountered in FSM practice is probably a mixed UNIX/Win32 environment with databases on UNIX servers, most users with Win32 clients and with power users utilising UNIX workstations. Recent studies indicate that a feasible implementation could be a Win32 middleware communicating with UNIX clients through a CORBA layer. In the near future also a COM is expected to be able to work between these two platforms.

The rule that the UNIX environment is more suitable to mission critical applications and for

large systems whilst Windows platforms fit for small-scale applications is no longer indisputable. The current trend "Windows everywhere" will probably not be sustained in the longer term, however it gives a straightforward indication when developing a new system from scratch.

The most important fact from the FSM computer systems point of view is that the architecture of either system (components and objects) is compatible with the concept presented.

4.2 Large UNIX data-oriented systems

One archetype of national system for FSM that can be found in bigger countries is using a large database distributed over a network of UNIX computers. A couple of hi-tech engineering applications, which are available on workstations, usually does not suffice and therefore a number of Win32 clients are also installed for engineering applications.

The development of such a system is a substantial undertaking with a considerable inertia. It is believed that data encapsulation and the introduction of a common interface could considerably speed up and enhance the development of the engineering part of the system without substantial impact on the data part.

4.3 Redesigned PC systems

A number of MS-DOS based systems developed in the eighties are now being redesigned for the Win32 platform. Quite naturally in most cases the result is component-oriented and more or less corresponds to Figure 1.

Experience shows that the overhead of completing such systems with standard encapsulation is not serious and that the encapsulation can be accomplished in the course of an upgrade.

4.4 Terrain data aspects

The inclusion of topographical and geographical (DTM) data into engineering FSM applications is necessary for all but the most trivial tasks. While the data model of DTM is simple and more or less identical in virtually all implementations, complications arise from the use of numerous geodetic systems and projections and from differing spatial resolution.

Despite considerable efforts to standardise DTM data formats, at least for certain applications, the prospects for embarking on a region-wide homogenous database are low. The promising solution is the virtualisation of terrain data by encapsulating "maps" into DTM servers with a standard interface. This encapsulation presents a programming challenge because of the performance requirements. Recent implementation of a DTM server demonstrates that neither its architecture, nor its performance, need to be compromised.

4.5 Multinational environment

A study investigating the suitability of encapsulated data for data and software exchange between administrations was performed within the PHARE programme.

An implementation of the software encapsulating existing databases in 11 participating countries from Central and Eastern Europe into data containers and combining them with "transport" containers is in progress.

The encapsulation of existing databases in a way which is completely transparent to all existing applications presented a real challenge for software designers, but the requirement for a non-invasive solution was indisputable.

In order to allow the connection of one or more transport containers to one or more local data containers, machinery combining data containers into a coherent database was worked out. It turned out that the usefulness of such "multi-container oriented database" goes far beyond the original objective.

5. Conclusion

This review of the current situation in FSM with respect to the computer support suggests that a computer technology is available which has a considerable potential and which might help to fulfil enormous tasks FSM is facing. The concept of data encapsulation is presented, which can address a number of problems stemming from the specific role of FSM in a de-regulated environment.

Component-based Architecture for Frequency Spectrum Management Software

Jiří Filčev

CRC Data, spol. s r.o.

U krčské vodárny 26, Prague, CZ 140 00, Czech Republic
E-mail : filcev@crcdata.cz

Increasing number of radiocommunication services (mobile, DAB, DVB,...) and stronger and wider co-operation requirements in 90' lead to new activities in frequency spectrum management software.

New software technologies (OLE, DCOM, component-based multi-tier applications) bring new possibilities in software development – building scalable, distributed systems from components, encapsulating low level implementation (database engine), functionality (relational data structure, SQL) and/or standardised algorithm implementation (Vienna...). Rapid Application Development techniques based on powerful server components enables more effective building FSM software and easy tracking system requirement changes and extensions.

Advantages of new software architecture presented on set of components for accessing DTM data (Digital Terrain Model) and related services will be presented together with performance results and shorts demonstration of component usage from MS Excel VBA environment.

1. Introduction

Frequency Spectrum Management systems (FSM) are complex software systems that should solve several complex and computation intensive problems: database task (radiocommunication data management, other related data storage and management – terrain data, morphology, measured/estimated field strength etc.), computation task (large interference scenarios, network planning,...) and need to be equipped with powerful visualisation tools to see computed results (radiocommunication objects, terrain profile,

coverage curves, field strength, quality criteria e.t.c.) in context of terrain data, morphology and/or raster or vector map data. Such systems consume much computer resources (CPU, memory, disk space and video operations). In the past – in MS-DOS days, UNIX platform with SUN like workstations was typical platform having enough capacity and computation power for these systems with graphic capabilities for requested visualisation systems.

Now, typical PC workstation equipped with PentiumPro od PentiumII CPU, 64M RAM or more, powerful graphic subsystem running Windows NT offers comparable computational power and resource capacity, comparable software environment (networking, multiprocessing, multi-user, virtual objects...) for a significantly lower price.

Another important point is current state of software technologies. Win32 development platform brings the solution of nearly all important requirements, which were not implemented or not robust enough on MS-DOS or Win16 systems: flat memory model (no 64K segments), virtual memory management, symmetrical multiprocessing, security, networking and others. After general adoption of Win32 platform with Windows NT release, OLE technologies (Object Linking and Embedding) became the engine of further software technology development.

Why OLE technologies are so important? OLE as a part of operating system brings large support for solving very general software problems:

- object orientation in large sense

OLE promoted OOP (Object Oriented Programming) techniques from development environment frame (classes in C++) into binary objects even distributable on network. Mutual object communication (client-server communication) is now not restricted into one application, one programming language, one workstation.

- development platform independence

OLE components can be created in many popular development environments and languages (Microsoft and Borland C/C++, Visual basic, Turbo Pascal, Delphi, Java, ...). OLE components can be driven from scripting languages, too. Simple tasks can be solved using VBA in MS Office applications or using VB script in HTML document..

- system scalability

Scalability means the way to reconfigure, extend or (the worst case) rewrite whole system to support more users, more data requests, more computations, distributed environment etc. Current support for multi-tier applications (Microsoft Transaction Server) allows component distribution over the network without any modifications in component code.

2. DTM services in FSM systems

Following services are generally used by most FSM systems:

- get point – station oversee height
- get profile – attenuation computing, field strength computing
- get set of profiles – group of profiles starting from the same point - effective height, delta h computing
- get square data – data in rectangular (or pseudo-rectangular) area
- profile visualisation (graph) with signal propagation (Fresnel curve)
- square data visualisation (topographic map)

There are several levels of DTM service access differing in the amount of accessed data

- single transmitter field strength evaluation with no interference – one set of profiles (typically 360 profiles in 1deg increment)
- interference evaluation – typically 10 to 100 interferes x 360 profiles
- network with interference – 100 interfered transmitters

It is obvious that there is a big influence of DTM subsystem performance on whole computation time and so there is strong requirement on profile constructing performance.

3. DTM server

DTM server is a key component of whole architecture, strong performance requirements lead to a request to optimise following problems:

3.1 Input data storage

HCM files (TOPO data) cannot be used for direct data access keeping performance on requested level (data block is too big for efficient caching, file format and directory structure need further processing for DTM data access), DTM data from HCM files were converted into database. Optimum DTM data block (tile) was found by dividing 1 x 1 deg square. Microsoft Access 8.0 and DAO 3.5 (Data Access Objects) were used as physical database representation.

3.2 Data caching

The most time consuming operation in the whole profile constructing process is reading data from its storage. Keeping DTM data blocks in memory can significantly improve server performance, especially for typical task reading set of profiles starting from the same point (for field strength evaluation). Neighbouring profiles are usually stored in the same tiles and so no database access is required, when appropriate number of tiles resides in cache memory.

3.3 Profile evaluation

The input data are organised into rectangular matrices (tiles) containing elevation data in raster 3 x 3 seconds (below 50 degrees Lat) or 3 x 6 seconds (above 50 degrees)

Profile evaluation consists from following steps:

- creating the main circle crossing profile end points
- creating set of equidistant profile points
- evaluating elevation values by compiling data from tiles covering requested profile

From practical point of view, nearest value from DTM data matrix is taken as appropriate profile value.

4. Computation server

This component encapsulates computation algorithms commonly used in FSM systems:

- Field strength evaluation (broadcasting problem)
- Signal propagation attenuation (microwave links)
- terrain statistics computation – effective height, clearance angle, delta h, visibility e.t.c.

Computation server (RA) database contains sampled propagation curves and other algorithm constants, which are expected to change in the future.

5. DTM subsystem architecture

DTM server described in previous chapter implements core functionality on DTM data. Because of existence of HCM data, there is no problem with connecting different blocks of DTM data presented in different formats and different co-ordinate systems. This is not true for morphology data, where different data sources in different co-ordinate systems can be expected.

Whole architecture is presented on following picture:

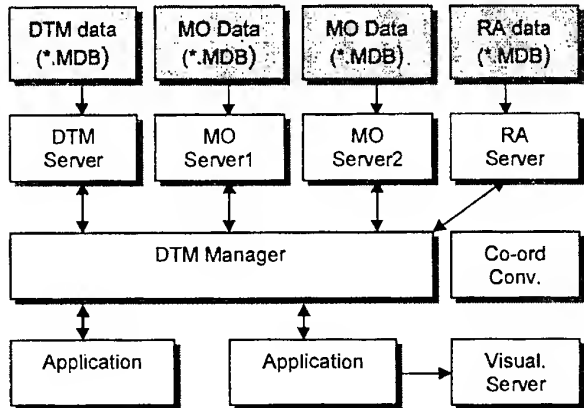


Fig. 1 – DTM Subsystem Architecture

First level servers are encapsulated into DTM Manager object, which is the main interface with client applications. DTM manager is responsible for following services:

- co-ordinate transformation between input co-ordinate system (e.g. S42 LonLat) into DTM native co-ordinate system (WGS84) or native co-ordinate system used by morphology data servers.
- co-ordinate transformation between input co-ordinate system and services implemented in Algorithm server (e.g. GetFieldStrength(...) method)
- compilation of morphology data from servers operating on different data sources
- local (InProc) interface for distributed installation

DTM Manager is implemented as InProc OLE server with dual interface for minimum OLE communication overhead.

DTM and MO servers are typical client/server components – for a simple request (definition of 2 points), a large amount of data should be processed (tiles reading, profile constructing) and small amount of data (typically square root of the amount of processed data) is returned.

Distributed configuration shown in Fig. 2 is a good example of a component based system scalability. Clients on remote PCs can use all DTM services in the same way as for single PC configuration saving local disk space for large DTM databases and saving local CPU time for profile constructing.

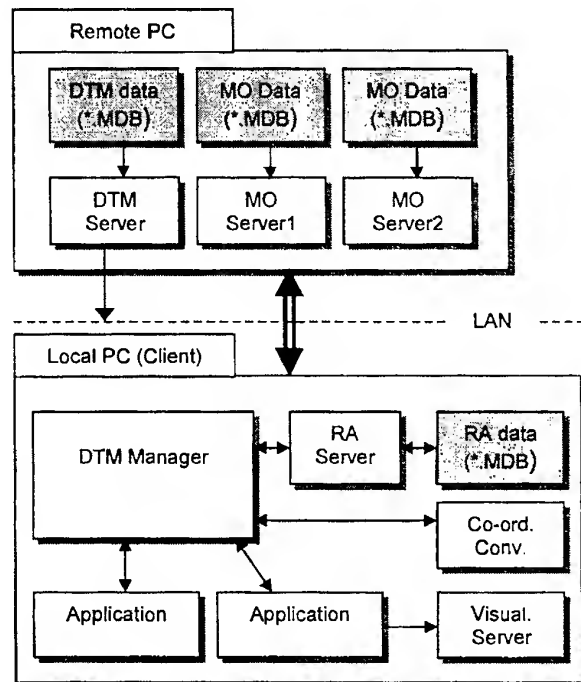


Fig. 2 – DTM Subsystem Distributed Architecture

6. Performance results

Performance results were measured for 5 typical tasks – single profile (20 and 50 km long) with 100 m step and set of profiles (20, 50 and 100 km long) starting from the same point with azimuth incremented by 1 degree. First and successive profile read were evaluated separately to demonstrate power of DTM caching algorithm.

Results for three system configuration are presented in following tables. In Tab. 1, DTM components are running in client application address space with minimum OLE communication

overhead. Results for DTM components running in separate address space in Microsoft Transaction Server but on the same computer are presented in Tab. 2. Finally, results for distributed solution, where DTM components are running in MTS on server computer are summarised in Tab. 3.

Tested profile	First read	Next read
Single 20 km/100m step	5 ms	1 ms
Single 50 km/100m step	8 ms	2 ms
Set 20 km/100 m/1 °	1643 ms	441 ms
Set 50 km/100 m/1 °	3155 ms	921 ms
Set 100 km/100 m/1 °	18436 ms	1823 ms

Tab. 1 – DTM server in client address space

Tested profile	First read	Next read
Single 20 km/100m step	3 ms	2 ms
Single 50 km/100m step	9 ms	4 ms
Set 20 km/100 m/1 °	1392 ms	901 ms
Set 50 km/100 m/1 °	2914 ms	1412 ms
Set 100 km/100 m/1 °	17145 ms	2363 ms

Tab. 2 – DTM server in MTS on client PC

Tested profile	First read	Next read
Single 20 km/100m step	6 ms	5 ms
Single 50 km/100m step	9 ms	6 ms
Set 20 km/100 m/1 °	2083 ms	1532 ms
Set 50 km/100 m/1 °	3866 ms	2133 ms
Set 100 km/100 m/1 °	16484 ms	4426 ms

Tab. 3 – DTM server in MTS on server PC

DTM components were tested on 180 MHz PentiumPro PC with 64M RAM running Windows NT Workstation 4.0. The same PC configuration was used as a server PC (for distributed configuration) connected by 100 MHz Ethernet.

Performance results illustrates scalability feature of DTM components: average 50km profile access time 2.5 ms in local installation is increased slightly more than 2 times (6 ms) by moving DTM components on server computer.

Following lines illustrates profile accessing from VBA (MS Excel 97).

```

Dim oDTMMgr As Object 'object variable
Dim vaProfile As Variant 'profile variable
...
Set oDTMMgr = New DTMMManager.clsMgr 'create
object
...
Call oDTMMgr.SetInputCoordSystem(1) '1 = S42 LonLat
Call oDTMMgr.GetProfile(15, 50, 15.1, 50.1, 100, vaProfile)
...
For i = 0 To UBound(vaProfile)
    Range("Profile").Offset(i) = vaProfile(i) 'display profile
    values
Next i

```

8. Conclusion

Component-based approach can bring a real benefit for creating FSM systems on Win32 platform especially in development speed, performance, component reusability and system scalability in comparison with traditional approach.

7. DTM service usage

DTM server, similar to all OLE components can be easily accessed from most popular development environments – Microsoft Visual C++, Borland Delphi, Microsoft Visual Basic, VBA from Microsoft Office applications, VB script on HTML pages and others.

Experience with frequency management programs based on a component architecture

PAVELKA Čeněk

TESTCOM
Hvoždánská 3
CZ-148 01 PRAHA 4 (Czech Republic)
tel : 420 (2) 79 92 153 fax : 420 (2) 79 34 588
E-mail : pavelka@testcom.cz

1 Introduction

The Czech Telecommunication Office (CTO) which is charged with regulation of radiocommunications in a rather small-size country employs, in national frequency spectrum management (FSM), exclusively PC compatible computers. The PCs are capable to fully cover all current and foreseen requirements. As far as relevant software is concerned, the conditions change quite dramatically. The CTO, until recent past, was employing a number of single-purpose software products running under MS-DOS which had weak mutual system coupling. Fast deployment of existing telecommunication services, together with the implementing of new services, has forced basic software innovations, the description of which along with first observations of applying them are the contents of this contribution.

2 The new generation of FSM software

2.1 Structure of the FSM software

The new generation of FSM software is designed in Win32 environment and is composed of components in the Client-Server architecture. This solution is updated to the maximum extent possible; it brings, on the one hand, initial investment which is really bulky but, on the other hand, in the long-term outlook, is utmost rational and brings considerable expense reduction. When implementing new services, it only takes to extend the functions of relevant servers to new elements not used by then, which are typical for the service in question. Realising new applications based on

stand-by components is rather easy then, and thus less costly.

In designing the software, conclusions of ERC-PT13 "Computer support for spectrum management" were taken into account. The principles set down in the preparatory phase of the PHARE 9511 Project the objective of which is to realise a software product implementing the common interface to FSM data, so called P-Interface were also fully respected from the outset.

In 1995, the development of an entirely new system for microwave links had begun. In 1996, realisation of the software for broadcasting services called KoPRT had started and its Version 1.6 has just been completed.

2.2 Components

Individual components which constitute the system are designed in such a way that they can be used utmost universally in the framework of the system while not excluding their stand-alone applications.

2.2.1 Data Server

Data server is capable of autonomous functioning and includes all functions related to administering and utilisation of the databases. The data structure is rather complex. The data server of the new system makes it possible for every new transmitter to keep several sets of parameters (unlimited in number) e.g. data co-ordinated in parallel with actual operational data of the transmitter. For example, actual antenna radiation diagrams and ERPs within a certain set could differ considerably from those which have been co-ordinated. Each parameter in the database also bears its history, i.e. information on its previous values is saved together with the date and reason of the change.

The Data Server co-operates with the DTM Server in inserting topographic heights of given sites and in calculations of effective heights and roughness factors of the terrain. In addition, it is interconnected with the Map Server by means of which any transmitter can be displayed on the map and its geographical co-ordinates edited.

An important feature of the Data Server is the possibility of sorting and selection according to chosen parameters, furthermore forming various sets of transmitters (e.g. according to the program transmitted or SFN network) and displaying them by means of the Visualisation Server. The Data Server also caters for printing output printouts and co-ordination forms as well as for data export for other purposes (e.g. export of TV transmitters data into the CEPT database according to the Chester 97 agreement).

2.2.2 DTM Server

The DTM Server operates on the basis of topographic data transferred from TOPO-files as defined in the Vienna Agreement. The Czech Administration has at its disposal topographic data of all of its neighbouring countries with which it had exchanged the data. The DTM Server opens its clients access to topographic data; moreover, it provides a number of functions related to terrain analysis. As a rule, the client directly applies for the analysis of the terrain profile, effective height in given direction, signal attenuation etc. The DTM issue is dealt with in another contribution.

2.2.3 Map Server

The basic function of the Map Server is working out tasks on topographic maps in raster format u (BMP). The Server offers to display a given site or the line connecting two sites (radio relay link) in the map, to change positions of the sites and to transfer new co-ordinates into a given application. At present, a set of military topographic maps of the Czech Republic (scale: 1:100 000) is in use, with the possibility of zooming the scale in the range from 1 : 25 000 do 1 : 200 000. It is foreseen to open the possibility of other scale values (in addition, maps in scales 1:50000 to 1:200000 are available), however, it is felt that this is not necessary because the maps having the scale 1 : 100 000 fully meet given purpose and required precision. Users highly appreciate including the Map Server into the system because it fully replaces former working with maps printed on paper.

2.2.4 Visualisation Server

Visualisation Server is a universal tool for displaying input data and results of calculations. Several layers can be displayed: transmitter sites, coverage curves, results of calculations of

coverage from individual transmitters or by an entire network; the data displayed may become an overlay over topographic or morphologic data. Boundaries of countries, administrative units, co-ordinates network etc. can also be displayed. It is possible to overlay a map with the results of several calculations at the same time.

2.2.5 Functionality Server

This Server offers its clients a number of services above all of computing nature. As an example, the calculation of electromagnetic field strength may be carried out using four various methods, including the HCM (Vienna Agreement) method, the choice depending on the user

2.3 The KoPRT Program

The KoPRT Program is a typical representant of the new computer system. It is intended for broadcasting and serves in projecting and international co-ordinations of transmitters and networks of analogue and digital television and FM radio. Extension for T-DAB is foreseen to be completed soon. Its basic calculation functions are:

- calculation of interference of a given transmitter by other transmitters in the network
- influence of changes to a transmitter or of including a new transmitter on remaining transmitters in the network
- calculation of coverage of a territory with a transmitter network
- project and analysis of SFN networks (in preparation)

The attached figure shows an example of graphic output of the calculation of the coverage of a simple TV network.

3 Experience with the new component based system

Experience with replacement of existing frequency management programs with a new component based system run by the Czech Administration can be divided in two parts: the influence of the new system on its user, and its influence on the concept of frequency management itself.

3.1 The influence of the new system on its user

Users of computer systems are relatively conservative, and are not in favour of changes even when the changes aim at getting things better, regarding mastering the system and its functionality. In designing new systems, this reality is to be regarded, and co-operation with future users is strongly recommended. Among great advantages of new systems is the intuitiveness of their control. The position of the user who has

basic knowledge in using e.g. MS Office is fairly facilitated here.

The users got acquainted with the new system very quickly and started its immediate application. The authors of the system keep close contact with its users and respond quickly on their observations and suggestions as for the system management and its functions. However, a certain danger occurs here. Users of such a sophisticated system tend to require from the computer support even solutions of such tasks which come under their decision making competency. It should be borne in mind that the mission of computer support is to facilitate the work of frequency managers but computer support can never replace them. The idea of an undergraduate girl-clerk equipped with top level software who would master complex tasks in planning frequencies is entirely wrong.

3.2 Influence on the concept of frequency management itself

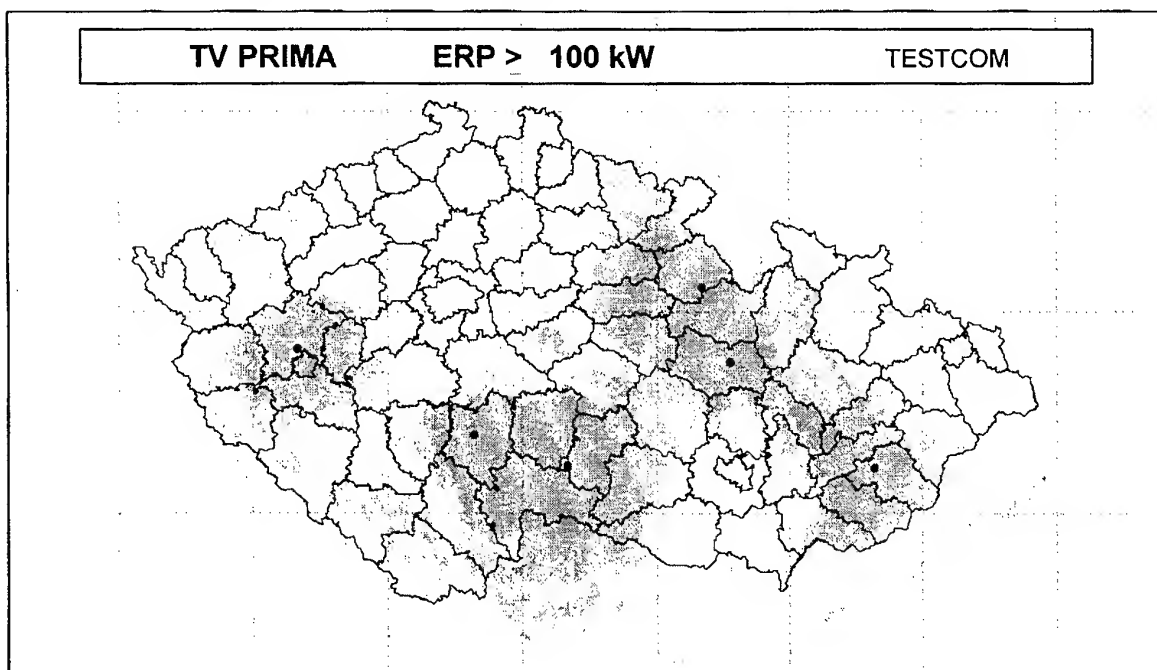
More relevant is the influence of the new software on the concept of frequency management itself. New software is designed to work in a network; all applications are interconnected and share all data which is determined to be common. Problems begin to emerge here. The old software used to store data for individual services in autonomous databases. Therefore, we often met, as a typical example, the case when certain transmitter site, physically one and the same, had two different names for TV and for FM, and, which case was even worse, its dual geographical co-ordinate differed from each other. Checking all databases, unification of names, co-ordinates and other common data appeared to be the primary

precondition for implementation of the new system. There is no need to underline that this work is pretentious and lengthy. However, the result is a consistent database containing a minimum of erroneous data.

Implementing new software brought with it, no doubt, a number of organisational changes and changes of run-in procedures in frequency management. However, with the system being in operation for some time, one may clearly see that the implementation of the new software system has a deep influence on ameliorating the procedure in its entirety, and made it possible to work with new services as e.g. DVB which the ancient system would not master at all.

4 Conclusion

It may be stated as a concluding observation that the experience with utilising new software for frequency spectrum management are fairly good. Above all, the users appreciate very efficient tools for database management including all visualising utilities and working with maps. In the day-by-day practice, the user spends much more time on data organising than on calculations themselves. At present, this holds prevailingly with respect to DVB planning process based on the CHESTER 97 Agreement. A further major step forward will be the implementation of the P-interface and data containers supplied in the framework of the PHARE 9511 Project which will make an easy data exchange possible and, as case may be, make possible software exchange among administrations. The concept has been realised, and theoretical assumptions have been confirmed.



DEPLOYMENT OF A LARGE UNIX-BASED SYSTEM AT THE POLISH ADMINISTRATION

Zbigniew Wizimirski

NATIONAL RADIOPHYSICS AGENCY

Kasprzaka 18/20, Warsaw, Poland

E-mail : Z.Wizimirski@par.gov.pl

1. INTRODUCTION

A frequency management system is something that *de facto* exists in any national radiocommunication regulating institution. The level of automation in such system may be varying widely, from a paper-based one to a comprehensive computer-based system, supporting virtually all relevant tasks and activities of such institution. The problem of building a computer-based system for this purpose becomes more complex as the amount of work to be supported increases and when the radiocommunications technology itself evolves.

2. FREQUENCY MANAGEMENT VS SPECTRUM ENGINEERING

A national Frequency Management System is the tool designed to support essential activities of the radiocommunications national regulator. It has to be stressed that the regulator's tasks although seem to be similar to frequency engineering performed by a radiocommunications operator are in fact quite different.

2.1. Operator's needs

For the operator the most important aim of computer support is to aid for system planning, operability analysis, assessment of coverage, quality of signal. Once the service is running the cost and resources management, system maintenance and upgrades become the crucial tasks, put aside the billing system which is usually very complex.

In some, rare cases the operator has the responsibility of co-ordinating his service with other domestic or neighbour country spectrum users.

Broadly speaking the operator is interested mainly in engineering tasks and in management of internal resources.

2.2. Regulator's needs

On the other hand the regulator's responsibility is built around the licensing process. The database gathering the information of spectrum use in all radiocommunication services has to be complemented with a comprehensive database of spectrum users and issued licences. The regulator is interested in many non-technical aspects as the user's legal status, the user's activities in other fields of radiocommunication, different kinds of business information regarding financial relations between the regulator and spectrum users. To assess the possibility of issuing a licence the regulator needs also the relevant type approval information.

3. REQUIREMENTS FOR A NATIONAL COMPUTER-BASED FM SYSTEM

3.1. General requirements

There are features which have to be required for any fairly big business-supporting system. Required for a national FM system they influence the choice of its proper technical architecture: The most important of them are:

- robustness,
- scalability,
- multi-user support,
- trackability of important data changes,
- support for distributed environment (central and regional functions and data, data consistency),
- well defined interfaces to some other applications (in this case to spectrum engineering software and for input of spectrum users' requests),
- well defined interfaces to other systems (in this case to foreign radiocommunications regulating bodies and the ITU notification system),
- extendibility when new tasks emerge.

3.2. Specific business requirements

While assessing the compatibility of a new transmitter or network there is more and more probable that different radiocommunications services have to be taken into account. Therefore, first of all the information of all spectrum use has to be accessible and then the appropriate engineering procedures and algorithms have to be implemented to help inter-service co-ordination. This situation seems to be more and more common nowadays and is one of main reasons of decreasing usefulness of disparate spectrum engineering systems separately build for particular services.

The specific tasks of regulator put forward licensing, billing and document management to be as important as frequency co-ordination itself. The legal environment is specific to a particular country and may change quickly. Automatic issuing of all relevant documents for assignment and licensing processes in accordance to recent legal regulations becomes the substantial requirement for the information system.

The regulator's organisation may be fairly large and complex. In the case of Polish National Radiocommunication Agency it means several hundred people grouped in 17 cities. The system not only has to be multi-user but has to address the workflow control and role management issues. It's also important to understand that a system having several hundreds of users does not mean simply multi-user but must be based on a DBMS designed especially for such use.

Receiving and issuing large number of documents relevant to the licensing and billing process makes document tracking quite a task; this problem should also be addressed.

There is always a dilemma, how much freedom should be given to the system users to disregard some bureaucratic principles. In a big system one system administrator who is given the power of performing some restricted operations may not be enough. Therefore some other „power user” roles should be designed. On the other hand some rules should never be violated and it may be feasible to implement them on the database level.

The billing and bookkeeping subsystem could be the most sensitive one. There are two reasons for that. First, the money handling is always sensitive; second, there are typically (as in Poland) specific regulations setting additional requirements on such software.

The last but not least is the problem of managing the changes.

It is quite common that regulator's tasks have to be modified because of radiocommunications' technology changes or, in some cases rapid legal changes. This has to be taken into account while building the automated system. As we have seen, the business rules have to be implemented and forced; on the other hand they are prone to

changes. To resolve this contradiction it is required to be able to quickly implement these changes. This puts some requirements on the programming technology which should be used. The requirements (rules, state regulations, document's form and contents) may change quite rapidly - even during the process of software build. Therefore the whole software process has to have the built-in procedures of requirements' changing. Also the coding tools have to be sophisticated enough to enable quick and efficient changes.

Besides, because of this or other reasons sometimes a business rule has to be violated. Some exceptional procedures should be built into the system to allow for this.

3.3. The human perspective

Some operational requirements for a National Frequency Management system are natural to any big business-supporting system. Such systems should be:

- user friendly (sticking to some well-known user interface standards),
- resilient to human errors,
- highly adjustable (configurable), allowing for implementation of rapid business rules changing,
- allowing for exceptional decisions and procedures.

Let us explain these requirements in some detail:

Ease of use and low costs of training can be achieved if the user's interface follows some well known standards. In today's environments this most probably will mean the MS Windows (95) conventions. The application programmes in this environment will be event-driven but one has to be careful not to allow simultaneous use of too many sub-modules and to many event-based scenarios. The multiplicity of non-modal dialogue windows should be rather avoided. The screen forms should be simple and containing not too many objects; tabbed forms are recommended for complex tasks. The delay in performance should be always clearly communicated to the user. The success or failure of data modification should be notified or shown.

It is obvious that any user can make mistakes and sometimes even very serious ones. Once the database is modified this mistake propagates to all users i.e. wrong data can be seen and used by all other users. Any simple withdrawal from this situation is virtually impossible. This means that such mistakes should almost never happen and if one has happened some extraordinary procedure and programmatic means should be foreseen to deal with it. It may require a special role within the system and special rules for 'mending' the data. To make such situations exceptional means

forcing any user to follow business rules, notifying unlikely data values i.e. by using data value dictionaries like towns, streets, names and whatever is feasible, implementing domain ranges for certain attributes, implementing automated cross-checking if some dependencies are common enough, persuade users to double-check the input data when the mistake may have serious consequences. These means are costly in terms of programmers' effort but the data deficiencies and inconsistencies may be much more costly in terms of the regulator's efficiency and credibility.

3.4. The data perspective

The data is the core of the system. The overall system usability depends on data quality. Proper data modelling is a fundamental requirement. It is true that many contemporary FM systems don't use a coherent data model. This is partly because building such a model is a complex task and seems to be impossible to be accomplished without a CASE tool, but first of all the reasons are historical, going back to the times, when inter-service co-ordination seemed unnecessary. The data encapsulation may be helpful in such cases but one has to keep in mind that some data categories like e.g. spectrum user are in such system duplicated or multiplied which means that the discrepancies are inevitable. To make encapsulation relay work one has to unify the duplicated data categories and use only one instance of it. Unifying should be 'vertical' and 'horizontal' i.e. the attributes should be merged leading to one coherent structure and then the tables should be merged by eliminating duplicates. This is in fact re-designing the system. The simple encapsulation works smoothly only on data which do not overlap, as for example engineering data for different radiocommunication services. When building a new comprehensive system the data model should be, of course coherent throughout the whole business. The most critical part is the national frequency register, the spectrum user model and billing information. On the other hand the technical aspects of the radiated signal and of its emitters and receivers are better suited to encapsulation, which gives the possibility to share the engineering programs developed according to some standards. One has, however to keep in mind how his data would be related to this 'standard' data model. The question is very difficult if this 'standard' model does not exist. In this context it is worthwhile to recognise the first international 'standard' data model worked out by the ITU Study group 1, Task Group 4, so-called Radiocommunication Data Dictionary (RDD). Its scope is limited to co-ordination and notification aspects only but even this gives a good foundation for proper semantics of data sharing and data encapsulation. The PHARE P.-interface project

follows these lines building its data model around RDD.

4. THE SOFTWARE PROCESS

As we can see from the above analysis building a comprehensive nation-wide system is not a simple task. So there is a need for some software process management requirements. Let us point out some of them:

- the possibility to pass system requirements in an unambiguous way to a software house which wants to build a system,
- the possibility to keep up with requirement changes throughout the full life cycle of software,
- sufficient documentation to allow for system maintenance in changing circumstances (this in fact requires the use of a very high level and reasonably widely known programming tools).

It is feasible to use CASE tools in order to fulfil these requirements.

4.1. How to proceed

To successfully build a national FM system several steps have to be made:

- understanding of needs,
- defining strategy,
- agree on priorities,
- understanding limitations (funds, platforms currently used, 'subculture' - influencing peoples behaviour, software currently used - influencing future acceptance of the system),
- agree on technical assumptions following this analysis,
- perform market analysis (software and software houses, similar solutions e.g. in other countries),
- establish internal management structures for the project,
- acquire a team for performing or supporting systems requirement analysis,
- perform the analysis identifying the requirements hierarchy (critical requirements),
- approve requirements specification in the frame of project management structure,
- define the rules for the production phase,
- approve the rules (plans) for product testing, allocate assets for this process,
- define the way existing data will be migrated to the new system,
- set up a contract for building the system (this requires conforming to legal bounds, sometimes very restrictive). The contract should include procedures for quality management and changes management and reasonably detailed plan of implementation. Choosing the partner is very important, because the life-cycle of the system may be

very long and support requirements are usually very high. Acceptance criteria for the software should be clearly agreed - the use of metrics is recommended.

The list above stresses the role of preparatory steps. These steps should not be neglected, because erroneous definition of needs and priorities may result in acquiring software of very limited use and even not worthwhile of making efforts to deploy it. The amount of work needed for implementation of such a system is very substantial and must pay off to be successful.

Incremental build and deployment of the system should be based on agreed priorities and critical requirements. A pilot project, prototyping and incremental build requirements are highly recommended.

5. THE POLISH NATIONAL SYSTEM

The National Radiocommunications Agency decided to build a comprehensive system in 1995. This was a consequence of adopting the Information Strategy for NRA which was developed in years 1993 -1994. The first step was to perform a thorough analysis of essential NRA needs with respect to information processing, existing information processes and data flow. Then three logical models have been constructed: Requirements Model, Process Model and Data Model. For the analysis and modelling the CASE tool has been used, namely the Systems Engineer from LBMS. To meet the requirements formulated in the Requirements Model several solutions have been adopted. These solutions may be regarded as a general characteristics of the future system. The most important decision following this step was choosing the operating system and database platform for the future information system. Thanks to the aid through a PHARE programme NRA was able to acquire a number of UNIX hosts to serve as the platform for the INFORMIX ON LINE Database Management System. This choice enables us to develop the application software as CLIENT-SERVER or even 3-layer/multilayer/com-

ponent based if such solution would be cost-effective.

To check the feasibility of this approach and identify possible caveats and technological problems the pilot application using client-server architecture and INFORMIX database has been developed. This application supports management of the information about incoming and outgoing documents and may be utilised either as a stand-alone application or be integrated in the future with the main information system. Important lessons have been learned from this pilot project, as well on the technical as on organisational matters. We believe that these lessons will enable us to avoid failure while starting the construction of the main application.

To closer define the future system the so-called user objects have been defined, showing the activities to be supported for different services and for different categories of employees, the data to be processed and the results (outputs) to be obtained. The approach used is commonly called quasi-object and is considered appropriate for client-server applications based on a Relational Database Management System. The true object approach is also possible in this situation but one has to remember that the underlying database is relational and appropriately represent it in the model.

The choice of client-server technology and industry standard SQL database system gives us the chance to build a really country-wide and robust system. The risk of building the whole system in one go is fairly high; fortunately the chosen platform allows us for incremental build. So as the first step we have chosen the modules for land-mobile services but the database schema should be extendible to allow for encompassing all other services in next phases. Having the requirement model and the comprehensive data model we can expect that the Land-Mobile subsystem, following these directives will be easily extended and some its functions will be adaptable to other subsystems.

XV

EMC MANAGEMENT

Interference Control for IT Installations — a practical approach —

Dave Sawdon BSc CEng MIEE

EMC Consultant

IBM Global Services

MP131 Hursley Park, Winchester, SO21 2JN, UK

Virtually all individuals and businesses now rely on Information Technology Equipment in some form, reliable operation of IT installations is therefore essential. This paper discusses some basic theory and then uses case histories to provide practical guidance on how to ensure that the electromagnetic immunity of an installation is maximised and that the operating environment is electromagnetically suitable.

1. Introduction

Virtually all individuals and businesses now rely on ITE (Information Technology Equipment) in some form, reliable operation of IT installations is therefore essential. Unfortunately all electronic equipment is a potential victim to electromagnetic interference, the only question is *how susceptible* it is. All electronic equipment, electrical equipment and cabling is also a potential threat as it radiates electromagnetic energy, the only question is *how much* it radiates. If we can arrange that any potential victim is only operated in an environment where the sum of the fields from all the threats is less than its susceptibility level we have a condition of EMC (Electromagnetic Compatibility) and a reliable system. The art of achieving this state could be called *Interference Control*.

Compliance with certain EM (electromagnetic) emission and immunity performance standards must be demonstrated during product development. The tests used are, of necessity, based on standardised configurations and layouts, they therefore do not reflect the real world performance of an installation. It is almost always the case that the EM immunity performance of an installation is worse than that for a single piece of equipment, largely because of cables. It is therefore necessary to consider cabling during the *Interference Control* exercise.

In practise, controlling the emission and immunity levels of an installation is only part of the story; it is also necessary to provide a suitable EM environment for the installation to operate in. The design of a building, together with its support systems and location, defines this environment.

If ITE (Information Technology Equipment) is operated in an unsuitable EM environment the symptoms can include hardware failures, losses of system function, loss of data and (the most common problem) image jitter and/or flicker on visual displays. One answer may be thought to be that manufacturers should build their equipment to be capable of operating in any electromagnetic environment. In many instances it is either impossible to define the actual field strengths that will be encountered or impractical to make commercial equipment immune to such "worst case" levels.

Because of the points listed earlier it is essential that EMC is considered in the design, fitting-out and management of all buildings and installations. The threats that need to be considered include lightning, electrostatic Discharge (ESD), mains quality, electric fields and magnetic fields. Lightning protection and the control of ESD and mains quality are generally well understood, in this paper I will discuss electric and magnetic fields. Areas that I will not be covering are the assessment of personnel exposure, health effects and design to withstand a deliberate EM attack; I can be contacted separately about these by anyone who has a specific interest.

The fundamental message is that IT installations require the early consideration of EMC. This will help prevent or solve problems that, if found later, would otherwise lead to project delays and expense.

2. A little theory

2.1 Electric and magnetic fields

Before delving into examples and cures it is necessary to introduce some terminology and a little basic theory.

- An Electric field is generated around a conductor whenever a voltage is present on it, a Magnetic field is generated whenever a current flows.
- At distances greater than about one sixth of the signal wavelength from the source the magnetic field can be predicted from measurements of the electric field (and vice versa). At shorter distances the magnetic and electric fields must be considered and measured separately.
- The initial strength of the field depends upon the magnitude and frequency of the voltage or current causing it, together with the electrical and physical characteristics of the conductor and its' surroundings.
- The rate of decay of field strength with distance from the source depends on the characteristics of both the source and the space between the source and the potential victim.

2.2 Field decay with distance

As a general rule Electric fields tend to decrease linearly with distance:

$$\text{Field decay proportional to } \frac{\text{voltage}}{\text{distance}}$$

The magnetic field around a single conductor varies in direct proportion to the current flowing but inversely with distance:

$$\text{Field decay proportional to } \frac{\text{current}}{\text{distance}}$$

If two conductors are arranged to lie parallel, with equal and opposite currents (such as twin core mains cable) the magnetic field, at a distance which is much larger than the conductor separation, varies directly with conductor separation and current but inversely with the SQUARE of the distance away:

$$\text{Field decay proportional to } \frac{\text{current} * \text{separation}}{\text{distance}^2}$$

The magnetic field around a transformer or solenoid varies in direct proportion to the current flowing but inversely with the CUBE of the distance away:

$$\text{Field decay proportional to } \frac{\text{current}}{\text{distance}^3}$$

In practise, the field decay characteristic from a real world magnetic source is a composite of the three shown above.

3. The arsenal

The field strength experienced by a potential victim can be reduced using one of the following techniques.

- **Modifying the source.** By making changes to the source it may be possible to eliminate or reduce the unwanted emissions or to increase their rate of decay with distance. These changes may be as simple as decreasing the separation between cables carrying load and return currents.
- **Shielding.** Electric fields can be attenuated by virtually any thin grounded conductive layer whereas Magnetic field shielding must possess magnetic permeability. The degree of attenuation depends on the frequency of concern, the distance from the source and the detailed design of the shield. Electric field shielding is frequently used and, particularly if the source is outside the building, can sometimes be the only solution. Magnetic shielding is much more difficult and is usually only successful for very small volumes.
- **Cancellation.** A field can be deliberately generated such that it is equal in magnitude and orientation to the interfering field but in anti-phase to it. This cancellation field subtracts from the interfering field and, ideally, produces a zero resultant at the victim. This technique is very limited in practise but can be useful for dealing with some problems.
- **Changing the installation layout.** The area containing the victim can be electromagnetically surveyed to map the areas of particularly high or low field strength. The victim(s) can then be moved into an area of lower field strength. This can be the simplest and cheapest option if the source cannot be modified and the field distribution is suitable.
- **Procedural changes.** Sometimes the victim can most economically be protected from the source by administrative measures. Examples of this are controlling the use of mobile phones and other radio transmitting equipment, either hand held or vehicle mounted, close to ITE.

These are all useful techniques for solving EMC problems but the principles can also be used to avoid problems. As always in life, prevention is better than cure and in almost every case it is simpler and cheaper to perform an EMC

assessment before an installation takes place rather than track down and fix problems afterwards, particularly as these EMC problems are often subtle.

4. Preventing interference

Think about EMC from the start of an IT project.

1. **EM environment.** Is the proposed building close to any obvious RF threats such as Radar, transmitting antennae, heavy industry, etc? Is the site on raised ground? Are there any adjacent IT installations which have a history of unexplained problems? If the site is not totally and obviously benign then consider a Radio Frequency (RF) survey to determine the actual ambient field strengths, anything over 1 V/m is a cause for concern.
2. **Electrical infrastructure.** Are there any adjacent power cables (underground or overground)? Does the Neutral conductor of your lighting or ring wiring follow a different path to that of the Line conductor? Do you have any large (more than about 2 A) earth currents? Do any site processes generate large magnetic fields? Is there a sub-station near? There is a risk of image jitter or flicker on display screens if the answer to any of these questions is YES and a magnetic field survey should be performed to determine the actual field strengths and locations, anything over about 500 nT is a cause for concern.
3. **Changes to the EM environment.** Ensure that there are controls on the use of mobile radios and phones near the proposed installation and that site changes are approved by the IT department.
4. **Equipment.** Does it comply with the EMC Directive? If not, can the manufacturer give any information about the immunity levels to which it was tested?
5. **Data cables.** Ensure that the data cables are shielded. Running cables in steel trunking is helpful but will not give the same EM performance as shielded structured cabling.

5. Case histories

5.1 Case histories: Problem avoidance

Many organisations now invest in an EMC survey prior to installing IT equipment in a new location, during a major refurbishment or, sometimes, prior even to purchasing a site. An EMC survey can check right across the frequency spectrum or can be highly selective and assess threats from obvious

sources, such as local Radio transmitters, or power lines.

Here are some examples where the electromagnetic environment was assessed prior to installation and appropriate changes made to the plans, when appropriate.

A surprise cable. The client was considering the construction of a new IT centre at an existing site, fortunately an EMC survey was recommended by the equipment supplier. During the survey the following problems were found:

- An unexpected high voltage cable directly beneath the floor of the area proposed for the computer suite,
- An adjacent substation generated magnetic fields in the area proposed for the operator suite that would have caused severe image jitter, and
- The car park outside the building was commonly used by van drivers with mobile radios. We measured the field strength from one of these radios and it would have made the system unreliable if no mitigation steps were taken.

The client was able to modify the proposed design to take account of the EMC threats.

Another surprise cable. The client was considering occupying a new factory unit and, as a result of an earlier encounter with EMC problems in buildings, commissioned an EMC survey. There were strong magnetic fields above a power cable that ran beneath an area that would have housed several Visual Display Units (VDUs).

The proposed layout was changed to use the area over the cable for non-VDU work.

A change of building use. A site was being considered for redevelopment into house offices and a Data Processing centre but the prospective developer was concerned about the possible impact of a nearby antenna tower. We surveyed the area and were able to confirm that the tower did not present a threat. The developer concluded the deal for the site.

A known cable in a shopping area. The client was considering updating a shopping area with new Point-Of-Sale equipment but was concerned about a buried power cable shown on the plans. We were able to plot the position of the cable, measure the fields around it and to provide appropriate advise on the positioning and type of new equipment to avoid any performance degradation from the fields.

An IT centre in a factory. The client was consolidating several functions onto one site, this involved building an IT centre directly over a factory floor. The equipment supplier was concerned about

interference and recommended an EMC survey. The plant in the factory was checked and assessed as not posing an EMC threat.

5.2 Case histories: EMC problems

The examples earlier included problems that were avoided by the consideration of EMC at the outset of a project. Unfortunately, when expanding a business or changing the usage of space within a building, EMC is not traditionally a subject that is considered. Here are some examples that are typical of the relatively common problems that we have dealt with as a result. In each case, considerable disruption and expense would have been avoided if EMC had been considered at the outset.

It will rapidly become apparent that magnetic fields cause the most real world problems as they can result in VDU image jitter which is noticeable by the lay user and often gives rise to questions about the risk of adverse health effects.

VDU image jitter in an office (1). The clients' sales office needed to expand, so they decided to adapt what had previously been a store room next to the main sales office. The necessary structural changes were made but it was found that VDUs in the new area suffered from image jitter that was so severe that staff refused to use them. After a long period of trial and error the client contacted us and we quickly determined that the problem was caused by magnetic fields from the main building power feed that ran directly beneath the new office. Several solutions were suggested to the client, the one that they chose was to dig-up the car park and re-route the power cable.

VDU image jitter in an office (2). The client had recently taken over the management of a tower block. Prior to finalising the contract they discovered that some staff were unhappy with the Front Of Screen performance of their VDUs. A quick check confirmed that jitter was the problem. When we performed a Magnetic field survey it revealed that the problem only existed on one floor, close to some internal studding walls. Further investigations revealed that the ring main Neutral was broken, causing a current imbalance in the mains wiring and a potential safety problem. The imbalance was the cause of the large Magnetic field (see the section on field decay, above).

VDU image jitter in an office (3). The clients' drawing office employed high resolution VDUs but, because of jitter, these could not be used at some workstations when the room lighting was switched on. Visual investigation above the suspended ceiling revealed that the wiring was unstructured and just lay on the ceiling panels. Further investigation revealed that two separate electrical contractors

had installed the wiring, one had attempted to keep the Line and Neutral cables close to one-another whereas the other had not. The second contractor had run the Line wire from the distribution panel to the light switches and then to the various light units, the Neutral went direct from the distribution panel to the lights. The recommended solution was to re-wire the lights in a structured way with Line and Neutral currents flowing next to one another, preferably in twin cable. This maximises the magnetic field cancellation and removes the problem.

VDU image jitter in an office within a factory. The client had a high-current product test lab directly beneath their sales office. The magnetic fields from the lab were so large that it was impossible to use the VDUs, so the testing had to be performed at night. The automated test system was unreliable and a single test typically took 6 months because of this and the night-only operation. When we were asked to help, we redesigned the test so that the magnetic fields were effectively cancelled-out. A further refinement was possible by performing a magnetic field survey of the office area and changing the desk layout to avoid the areas with a high residual field strength. The redesigned test brought several incidental benefits and the test time was cut as a result.

VDU image jitter in a factory. At apparently random times of the day, a newly installed VDU (used for monitoring a manufacturing process) became unusable due to severe image jitter. Over an extended period the service engineers replaced several items of equipment and the end user threatened legal action against the supplier. After all other avenues had been exhausted it was agreed to consider the possibility of an EMC problem and we were contacted. Investigation identified the source as being a pipe! Pipes are often used to carry ground currents which can be the source of magnetic fields but, in this case, the pipe was being electrically heated as it carried a chemical which froze at room temperature. Since the current was controlled by a thermostat there was no obvious pattern to the timing of the fields being generated and it therefore took some time to track down. The solution required localised screening being applied to the VDU.

Image jitter caused by under-floor heating. There are two ways to install under-floor electric heating. The costs and performance are identical but one way produces very large magnetic fields whereas the other produces virtually none. Since the guidance notes to installers do not discuss magnetic fields we are in the lap of the Gods as to which way they lay the cable. If, as is common, they choose the "wrong" way there is a major problem because the mistake is literally "cast in concrete".

The solutions are to dig up the concrete and re-lay the heating, to raise the floor level so that a cancellation cable can be laid on top of the existing floor, to use a more expensive (non-CRT) display technology or to install a different heating system - none are particularly pleasant options.

Mysterious system failures. Mobile phones and other radio transmitters generate electric fields which can easily interfere with computers and other electronic systems if they are operated close enough to them. The only practical solution is to instigate a ban on their use close to computer systems - but what is a computer system? Recently we became aware of problems with a sophisticated telephone system which had a microprocessor in each handset, this is disrupted if security radios are used nearby. The only solution is to ban the use of radios in offices.

6. Summary and Recommendations

The EMC management of an installation is not just about product conformance to standards. It also includes consideration of the electromagnetic environment that's caused by power lines, mobile phones, building wiring, radio and radar transmitters. All of these present potential problems that cannot accurately be forecast and, as with most problems in life, the earlier they are discovered the cheaper and simpler they are to overcome.

Installation EMC problems are not usually apparent for what they are. They may manifest themselves as screen jitter, decreased system performance or as a general lack of system reliability. Because the end-user perceives a system problem and not an EMC problem, a lot of time, energy and money can be expended before the EMC option is explored.

The only way to minimise (or even to quantify) the risk is to contact a competent EMC Consultant and ask for advice at the planning stage, he or she will probably recommend an EMC survey. Few Laboratories and Consultants have the expertise and equipment to perform a 50 Hz magnetic field survey yet this is the parameter that causes most difficulty with IT installations in buildings, ensure that 50 Hz is included in any survey.

7. In conclusion

EMC problems with installations can be expensive to track down and solve if precautions are not taken at the planning stage. Thinking **EMC**, and spending a little money at the start of a project can save a lot of money in the longer term.

The only way to avoid these very common pitfalls is to consider EMC every time that IT equipment is

introduced into a new location or when a change is made to an environment that is known to be satisfactory.

About the author

Dave Sawdon graduated in Electronic Engineering in 1976 and joined IBM in 1982. His work has included a wide range of analogue and digital development projects; until 1991 he was a user of EMC services but now provides them. He holds 9 patents in areas such as power supply design, fibre optics, interface protocols and emission reduction and has produced many technical papers for both internal IBM and international conference consumption.

Dave is the IBM Corporate Project Authority for "near field phenomena", the UK expert on the Swedish Electrical Commission (SEK) display emissions standards committee and chairman of the Federation of Electronic Industries (FEI) project group dealing with aspects of human exposure to non-ionising radiation. He has an accredited laboratory for the measurement of low frequency display emissions and susceptibility (MPR2, MPR3, TCO, EN61000-4-8).

IBM Global Services provide a product testing service for displays in addition to EMC site surveys, on-site EMC problem resolution and general EMC consultancy services. Dave can be contacted by email: dave_sawdon@uk.ibm.com, phone: +44-1962-816120 or by fax +44-1962-842327.

XV

EMC MANAGEMENT

NATO Naval Approaches to EMC

**NATO Special WG10 "EM Environment Effects"
sponsored session**

Invited session organized by:

Capt. R Azzarone - Italy

Capt. A. Simi - NATO HQ

S. Beaton - NATO HQ

Chaired by:

Capt. R. Azzarone - Italy

ARMAMENTS COOPERATION AND ELECTRO-MAGNETIC COMPATIBILITY

Captain Raffaele Azzarone, Italian Navy
Technical Director, Naval Shipyard
(MARINARSEN)
Viale Amendola, 11911 La Spezia, Italy

Phone: 39 187 782 512, Fax: 39 187 782 326

Captain (r) Arcangelo Simi
Head, Naval Armaments Section
Defence Support Division, NATO Headquarters
1110 Brussels, Belgium

Phone: 32 2 707-4294, Fax: 32 2 707-4103
Email: simi@hq.nato.int

Within the structure of NATO's Conference of National Armaments Directors, Special Working Group 10 on Naval Electro-Magnetic Environment Effects was instituted by NATO national naval armaments authorities to address the problems of both intra- and inter-ship electro-magnetic interference. The aim continues to be to work collectively towards the enhancement of electro-magnetic compatibility in ships at sea so as to maximize operational capability. To this end, the Group has developed NATO Standardization Agreements and Allied Naval Engineering Publications, developed a frequency management tool, and conducted sea trials, among other activities. Special Working Group 10 has pursued working relations with Partnership for Peace navies through symposia, and in conjunction with EMC '98, will hold a meeting with Partner experts.

1. ORIGINS

Since the establishment of the Alliance, extensive coordination and cooperation in the field of armaments has taken place among the 16 NATO nations. Even if the ultimate responsibility for equipping and maintaining military forces rests with the member nation itself, in most spheres, research, development and production of equipment are organised by each nation in accordance with both its national requirements and its commitments to collective defence in NATO.

NATO's forum for naval armaments planning authorities, the NATO Naval Armaments Group (NNAG) was formed by the North Atlantic Council to harmonize national naval armaments requirements and to pursue collaboration in their development. NNAG formed six "Naval Groups" to address all aspects of naval armaments planning, from above water warfare to ship design and everything else in between.

2. CONFERENCE OF NATIONAL ARMAMENTS DIRECTORS

Some time after it was formed, NNAG was placed under the control of the newly-established Conference of National Armaments Directors (CNAD), the forum for senior national authorities responsible for the development and acquisition of military materiel. The current organization is as depicted in Fig. 1.

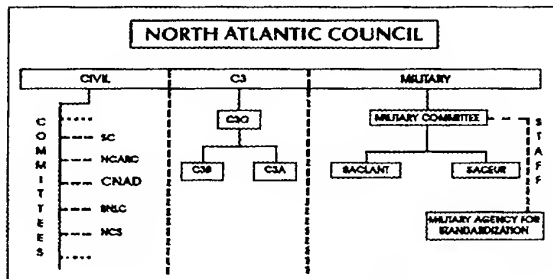


Fig. 1. NATO Organization

The NATO structure is divided into three main parts:

- the so-called military side of the house, led by the Military Committee and including the Command Structure of the Alliance;
- the civil side of the house, concerning all other committees; e.g., political, administrative, scientific, and so on; and
- a combined military and civil organization dealing with what is called Consultation, Command and Control (C3).

CNAD meets on a regular basis every six months to consider political, economic and technical aspects of the development and procurement of equipment for NATO forces. As

well as the navy's NNAG, the other two services also have Main Armaments Groups: the army's *NATO Army Armaments Group* (NAAG) and the air force's *NATO Air Force Armaments Group* (NAFAG). All three Main Armaments Groups are responsible for the areas concerning relevant services as shown in Fig. 2.

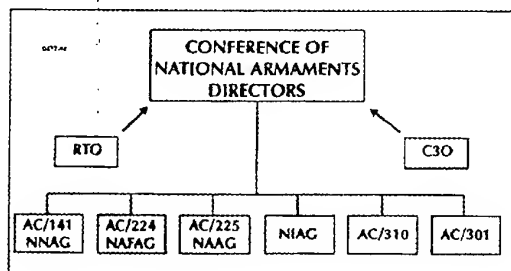


Fig.2. Main Armament Groups

Advice and assistance on industrial matters is provided by CNAD's *NATO Industrial Advisory Group* (NIAG). This Group enables the CNAD to benefit from industrial advice on how to foster government-to-industry and industry-to-industry cooperation, and it assists the Conference in exploring opportunities for international cooperation. Other groups under CNAD are active in fields such as defence procurement policy and acquisition practices, codification, quality assurance, test and safety criteria, and materiel standardization.

Within the CNAD structure, project groups, panels, working and *ad hoc* groups are established to promote cooperation in specific fields. The overall structure enables member countries to select the equipment and research projects in which they wish to participate and facilitates exchange of information on operational concepts, national equipment programmes and technical and logistics matters where cooperation can be of benefit to individual nations and to NATO as a whole.

3. ELECTRO-MAGNETIC ENVIRONMENT

The domain of the electro-magnetic environment and its impact on equipment cooperation and overall military operational capability is quite large. Fig. 3 lists the six groups currently active in this area.

The two groups under the Military Agency for Standardization (MAS) -- the *Radar and Radio Radiation Hazards Working Group* and the *Air Electrical and Electro-Magnetic Considerations Working Group* -- are mainly focussed on policy, procedures, terminology. The four other groups are under CNAD. AC/301 -- the *Group on Standardization of Materiel and Engineering Practices* -- has a sub-group addressing environmental conditions and test procedures. AC/310 -- the *Group on Safety and Suitability for Service of Munitions and Explosives* -- has a sub-group that deals with environmental safety testing. AC/225 is the NAAG, and its Land Group 7 on *Nuclear, Biological and Chemical Defence* has a Technical Sub-Group (TSG) addressing tri-service technical aspects of nuclear survivability.

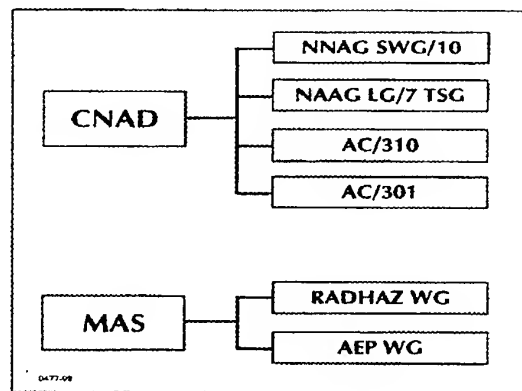


Fig. 3. NATO Groups Working in the Electro-Magnetic Environment

Standardization of Materiel and Engineering Practices -- has a sub-group addressing environmental conditions and test procedures. AC/310 -- the *Group on Safety and Suitability for Service of Munitions and Explosives* -- has a sub-group that deals with environmental safety testing. AC/225 is the NAAG, and its Land Group 7 on *Nuclear, Biological and Chemical Defence* has a Technical Sub-Group (TSG) addressing tri-service technical aspects of nuclear survivability.

This brings us to AC/141, which is NNAG, and its Subordinate Group, Special Working Group 10 on the *Naval Electro-Magnetic Environment Effects*.

4. SPECIAL WORKING GROUP 10

From time to time, important topics arise which cross the lines between the various Naval Groups, and which demanded a more general approach. To address such topics, the NNAG formed what are called Special Working Groups.

In 1987, after concerns were raised in a Naval Group, NNAG formed Special Working Group 10 to address the problems of electro-magnetic interference in and between ships. Initially, the major concern was that such interference would inhibit the full capability of shipboard weapons systems, their sensors, electronic warfare devices and communications. But more recently the Group has expanded its mandate to include most electro-magnetic environment effects, both intra- and inter-ship.

Currently, the Group is chaired by an Italian Navy Captain, and thirteen NATO nations send experts in the naval electro-magnetic environment to twice-yearly meetings. A representative of the Supreme Headquarters Allied Powers Europe (SHAPE) also participates. Administrative support is

provided by the Naval Armaments Section in NATO's International Staff.

5. OBJECTIVE

The principal objective of the Group is to enhance the operational potential of NATO naval ships by the minimization of electro-magnetic interference. In the Group's Terms of Reference, however, NNAG specifically excluded some areas of interest because they are being adequately addressed by other NATO fora. These include the effects of nuclear electro-magnetic pulse (EMP), hazards from electro-magnetic radiation to ordnance (HERO), radio and radar radiation hazards (RADHAZ), and communications security (TEMPEST).

If one visualizes the superstructure of a modern warship, one will immediately note the multitude of active and passive sensor, communications and weapon control emitter and receiver antennae, operating across the whole spectrum and at all levels of power, but all located in close proximity to one another. It is in this environment that the Group conducts its business.

6. TASKS

NNAG has tasked the Group, firstly, with the exchange of national information on intra- and inter-ship EMC matters. A core business at meetings is the discussion of each nation's plans, research and development and programmes in the naval electro-magnetic environment. Such information exchange fuels subsequent collaborative action, and results in the development and promulgation of NATO Standardization Agreements (STANAGs) and Allied Engineering Publications (ANEPS). A STANAG is a standard that, once ratified by a nation and promulgated by NATO, commits that nation to implementing it in national programmes. An ANEP is a less strict standard that only provides guidance to nations in their programmes.

To date, the Group has developed and promulgated three STANAGs on the EMI/EMC aspects in the design of metallic hull and non-metallic hull surface ships, and submarines. Another STANAG, dealing with standard attenuation measurements for naval enclosures, is in the final stages of development.

Three ANEPs have either been promulgated or are under development: one on EMI in glass-reinforced plastic (GRP) vessels, another on EMI incident analysis, and a third on procedures for conducting an EMI survey in naval ships.

With respect to inter-ship EMC, the Group has been addressing ways to counter inter-ship EMI in multi-national maritime forces. NATO navies have long operated in multi-national task groups, but the recent Allied emphasis on such task groups has brought to the fore the problem of frequency management of all the various emitters so as to avoid EMI. To address this problem, Special Working Group 10 has developed what is called the NATO EMI Operational Programme and Data Base, abbreviated to "NEOP".

NEOP is a frequency management data base with software to de-conflict to potential sources of EMI within a task group. This work is getting close to completion. To validate NEOP, as well as to explore other facets of EMI and test possible remedies, the Group occasionally participates in sea trials.

Under its Terms of Reference, Special Working Group 10 is also undertaking to address matters like the relationship between ship design and the resultant EMI problems that arise and subsequently need fixing. An obvious consideration is that the electro-magnetic environment should be taken into account early in the ship design process. The Group is currently deciding on how to approach the NNAG Naval Group 6 on Ship Design in this respect.

An important issue now in the forefront of NATO armaments development is harmonization between military and commercial standards. Special Working Group 10 is looking into this for the naval electro-magnetic environment. The idea, of course, is to reduce duplication of effort and, in the end, to save money.

Another area just being opened up in the Group is the potential for numerical modelling, simulation and virtual prototyping in EMC programmes. A final aspect that the Group wishes to address is the potential for a more "joint" (that is, multi-service -- navy/army/air force) approach to common EMC matters. This effort is just getting underway. Related to this is an initiative to rationalize and codify the electro-magnetic terminology used by the three services and other interested NATO bodies.

7. PARTNERSHIP FOR PEACE

A very important aspect of the Group's way ahead is its working relationships with EMC experts from Partnership for Peace navies. In 1996, in cooperation with the University of Florence in Italy, the Group participated in an EMC Symposium to which the Partners were invited. On the margins of this meeting, the Group also held a meeting with

Partners to discuss items of common interest. Fundamentally, this was mostly just an introduction for Partners to the work of the Group, but there was general agreement to exchange and discuss respective EMC standards.

On the two days either side of the EMC '98 Symposium, Special Working Group 10 will once again be inviting Partner experts to discussions. The longer term aim is to make Partner invitations to such Group meetings a regular event. In this regard, Partners will be invited to the next regular meeting of the Group, expected in early 1999. In NATO, the feeling is that we have a lot to learn from each other.

8. CONCLUSIONS

NATO has a well-established structure that effectively addresses most aspects of armaments and industrial cooperation. Within this structure, the nations represented in Special Working Group 10, in collaboration with other interested NATO bodies, have been working hard to develop standards and otherwise resolve problems associated with the naval electro-magnetic environment.

This work will continue. And the Group looks forward to working in this area with Partner navies.

BIOGRAPHICAL NOTES

Captain Raffaele Azzarone.

Captain (Naval Armaments) AZZARONE was born in Rome on 24th May 1948.

After completing his studies in Scientific High School in Rome he entered the Naval School in Livorno in 1967 and after completing the four-year course he attended the University of Torino (Polytechnic) where in 1974 he achieved his Doctorate in Electronic Engineering.

After almost four years, in which he was employed on board of ships the Cruiser (CC) "DORIA" and the Guided Missile Destroyer (DDG) "ARDITO", as a technical expert in the Operations Department, he was sent to the Italian Research & Development Institute on Radar and Telecommunication ("MARITELERADAR") where, as Chief of the Telecommunications Department, he studied, designed and gained experience in new generation transceivers, satellite terminals, EPM equipments, modems and crypto-voice devices.

Starting from 1979 he participated as national representative to the NATO Tri-Service Groups

concerning maritime communications, electronic countermeasures and modem interoperability.

In 1989, he began work at the Naval Shipyard in La Spezia, as Chief of the Electronics Section, and later as Deputy Vice Director for Armaments Components.

From 1992 to 1996 he was appointed to the Ministry of Defence in Rome as Chief of the Telecommunications Division in the General Directorate (NAVALCOSTARMI). Currently, he is again in the Naval Shipyard in La Spezia, as Technical Director, where one of his main responsibilities is Electro-Magnetic Interference reduction, especially in Glass-Reinforced Plastic (GRP) vessels.

In Spring 1997, he was elected Chairman of NATO's Special Working Group 10 on Naval Electro-Magnetic Environment Effects.

Captain(R) Arcangelo Simi

Arcangelo SIMI is currently the Head of Naval Armaments Section and EW Coordinator within the Defence Support Division of the International Staff in NATO HQ, Brussels. He is a graduate of the Italian Naval Academy class of 1963, where he received a formal education in engineering.

He served at sea on board several ships, including submarines, minesweepers and cruisers, with jobs related to operations (Navigator, CIC Director, Signal and EW Officer, etc). He graduated as a "Radar and Combat Information" specialist.

In August 1975, after attending the Italian Navy War College, he was appointed as Chief, Maritime Section of the Electronic Warfare Branch in SHAPE. In this position he promoted the launch of the Maritime (nowadays Multi-Service) Electronic Warfare Support Group (MEWSG) Programme and its implementation.

Thereafter he achieved the advanced qualification in "Communications and Electronics (TES)" and was assigned as Chief of "Radar and Surveillance Branch" to the Navy General Staff.

Subsequently he attended the NATO Defence College.

After a period of sea duty as Commanding Officer of a Minesweeper Oceanic Squadron, in 1984 he was promoted Captain.

Captain SIMI served in Rome on the General Defence Staff as Chief, "Electronic Warfare and Electronics Branch" for five years, in this position he authored the "Manual for employment of lasers on open ranges" and chaired the NATO Project Group (AC/141-PG/30) on NATO EW System for MPAs and Helicopters" and the Italian Defence committees on EW (GLIGE), on Infra-red (GLLASIR) and Electro-Magnetic compatibility (CAICE).

On 1st June 1987 he retired from active service in order to assume his present post.

Captain Simi has been a member of the Association of Old Crows for about 20 years.

EMI ANALYSIS OF HIGH FREQUENCY ANTENNAS ON NAVAL PLATFORMS

Professor Mario Calamia

Department of Electrical Engineering

University of Florence

Via Lombruso 6/17, I-50734 Florence, Italy

A software package is presented for the Electro-Magnetic Compatibility (EMC) and Electro-Magnetic Interference (EMI) analysis of transmitting and receiving devices, installed in electro-magnetically complex environments. As an example of its capabilities the software is applied to the EMI analysis of some devices typically found on naval platforms.

In EMC studies of radiating systems in complex environments it is usual to limit the analysis just to the antenna-antenna coupling, without considering the characteristic of the underlying transmitters (Tx) and receivers (Rx) connected to the antennas.

Recently at the Electrical Engineering Department of the University of Florence, a software package has been developed to further this aim. ACE (Antennas in Complex Environments [1] allows for EMI [2] analysis, taking into account both the antenna-antenna coupling in the complex environment and the contribution due to the internal functionality of the various devices. In particular the codes are able to provide the user with the antenna patterns; the antenna-antenna couplings; the Interference Margin (IM) between the various Tx-Rx couples. The IMs provide an estimation of the quantity by which the disturbing power received is above the sensibility of the receiver. Taking into account user definable security margins it is possible to obtain a global evaluation of the EMC/EMI situation which could not be achieved with the bare antenna-antenna coupling.

The block diagram of the ACE code will be shown in Fig. 1. The code is highly modular since the various modules used by the *Central Processor* (CP) can be easily modified or integrated with new modules, so as to allow easy extensions of the class of the problems which can be dealt with.

The CP executes the EMI analysis of antennas and devices placed on complex platforms. In particular it computes the radiation patterns both in near and far

field. The antenna-antenna couplings both in near and far field and the IMs with the relative evaluation of EMI/EMC. The CP uses four modules each of them specific to a particular simulation: antennas, structure, Tx and Rx. These modules use their own databases, six databases altogether, four of which provide a way to store numerical models for antennas, scenarios, transmitters and receivers, and two containing statistical data relative to the most common transmitting and receiving devices. These last two databases provide data to carry on analysis when real data are difficult to find.

The Antenna Simulation module simulates the antennas in free space both resorting to the main radiation parameters (main lobe angle, side lobe level, etc.) and resorting to radiation patterns provided by the user in one of two ways: by analytical function or by points on the principal radiation planes.

The Structure Simulation module provides the CP with the simulation of the complex scenario where the antennas are placed by resorting to canonical geometries such as polygonal plates and elliptical cylinders.

The Transmitter Simulation and the Receiver Simulation module simulates the inner behaviour of the devices by resorting to their technical specifications (Tx output power level and Rx receiving sensibility, frequency bands, etc.). These simulations are specific to the determination of the transfer functions of the transmitters and receivers in and out of their bands. Of course the accuracy of these simulations is heavily dependent on the quantity and quality of available data. When such data is not available the statistical database can be used instead.

To compute the fields radiated by the antennas once they are placed in the complex environment, the CP resorts to techniques which are related to the dimensions of structures and antennas with respect to

the wavelength. In particular, in the high-frequency region the analysis is based on the Uniform Geometrical Theory of Diffraction (UTD), while in the low frequency region the analysis is based on the solution of integral equations solved with the Method of Moments (MoM) procedure.

For the evaluation of the IM, defined as the difference between the power the victim receives and its sensibility in dB, inside and outside its working bands, the CP considers; the antenna-antenna coupling, by applying the reaction integral; the transfer functions of the Tx and Rx evaluated by the relative modules. Finally the discrimination between EMI and EMC is made by comparing the IM with a user-defined Safety Margin (SM). If $IM < SM$ we possibly have EMC, if $IM > SM$ we possibly have EMI, otherwise we are in an uncertain situation where EMI and EMC are equally possible.

Furthermore, ACE exhibits a graphical interface for input/output which is very useful, both in the scenario numerical modelization phase and in the visualization of results. This interface has been developed in the Tcl/Tk [3], a very flexible interpretative language designed for creating windows-based graphical interfaces. The main characteristic of this language is that of being multi-platform. The same Tcl/Tk code can run, without any modifications, on UNIX, Windows (95 and NT) and Macintosh platforms. The *Pre-Processor*, with dialogue windows and graphical output, allows the user to easily enter all the antennas, structures, Tx and Rx data. This data is then elaborated to the standard required by the four simulation modules. The *Post-Processor*, on the other

hand, is still in an early stage of development. Its purpose is to elaborate the results of the four module simulations and present them in graphical form (polar and Cartesian radiation patterns, solids and 3D maps of radiation, curves at equal field and hazard curves, coupling, IM and EMI/EMC tables).

To show the functionality of the software package an EMI analysis of some simple Tx and Rx devices on a realistic naval environment has been performed. The real radiation patterns, antenna-antenna coupling and IM have been investigated. Results will be shown in the oral presentation.

References:

- [1] A. Naldini, G. Pelosi, C. Pochini, S. Salleri & L. Vigna "ACE: UN *Virtual Lab* per l'analisi di prestazioni di antenna su piattaforme satellitari", Alta Frequenza-Rivista di Elettronica, Vol.9, n. 6, pp 12-15, Novembre-Dicembre 1997.
- [2] D. R. J. White. "EMI control method and techniques", in *A Handbook Series on Electromagnetic Interference and Compatibility*, Vols. 1,2,3,4,5, Germantwowa (MD), Don While Consultants Inc., 1973.
- [3] J. K. Ousterhout "Tcl and the Tk Toolkit," Addison-Wesley Professional Computing Series, Redwood City (CA), 1994,

ELECTROMAGNETIC COMPATIBILITY IN THE ROYAL NAVY

A C MITCHELL

DGSS/SS625, MoD(PE) Abbey Wood#54
Stoke Gifford, Bristol
BS34 8JH, UK

This paper reviews how EMC is achieved and maintained in the United Kingdom Royal Navy and the policy that supports it.

1. INTRODUCTION

The achievement of EMC in design and production is a subject often addressed at conferences, however for many organisations the maintenance of EMC in the field is equally as important. The UK Ministry of Defence (MoD) and the Royal Navy (RN) is one such organisation and this paper reviews how EMC is achieved and maintained in the RN and looks at the policy which supports it. In addition the current and possible future EMC acceptance philosophy for ships is discussed. Finally as an example of achieving EMC, the techniques used to optimise the location of communication aerials are reviewed. However as an introduction, the Naval Environment is first considered.

2. NAVAL ENVIRONMENT

There are many features of a modern warship which tests the skills of the electromagnetic engineer; the number and power of transmitters; the high density of equipment fitted within the ship and the problem of not having a test chamber big enough to test it. When these are considered alongside special military considerations, the result is a variety of considerations which may be collectively termed the Electromagnetic Effects (EME).

- Electromagnetic Compatibility
- Tempest
- Electronic Warfare
- Radiation Hazards (Radhaz)
- Frequency Management
- Signature Control
- Electromagnetic Survivability - Electromagnetic Pulse (EMP)
- Electro Static Protection

It is the role of the Electromagnetic Engineering Sections in MoD and the RN to ensure that the

requirements for each of these disciplines is balanced and integrated

To conclude this section on the naval environment it is worth reminding the reader that war can magnify the consequences of any electromagnetic interference (EMI) seen in peace time. The most notable example of this is HMS SHEFFIELD in the Falklands Campaign, where EMI contributed to her loss.

3. NAVAL EMC POLICY

The RN and MoD as an organisation responsible for both the procurement and operation of warships has an EMC policy which pays equal importance to maintaining a state of electromagnetic compatibility as well as achieving it in build. To this end a policy has been produced which does not solely concentrate on standards, but instead considers the broader issues of:

- Organisation
- Management
- Technical
- Education & Training

What the main policies are in each of these four areas are will be discussed later, however the main point to note is that each describe the principles by which EMC is achieved and not the detail of how this is carried out. Siting below this policy are a further series of documents tracking how each numbered policy statement is implemented eg by Naval Engineering Standards or Operational Procedure etc.

This has allowed a rationalisation and consolidation of standards, practises and procedures which historically had been developed by a bottom up approach.

3.1 Organisation

Within a large organisation, any broad based programme must have Senior Management support and provide technical expertise, advice, investigate and engineer solutions. In the case of EMC, the level of EMI

in the RN is regularly reviewed by a senior committee known as the Mutual Interference Steering Group (MISG) which is chaired at Director or 1 Star level. The MISG maintains a database of the predicted and reported instances of interference in the Fleet and through its Working Groups reviews interference on each class of ship; classifies the operational significance of each report and co-ordinates the development of techniques to predict and solve interference problems.

In addition to this, it is now common practise for each ship programme to run a Electromagnetic Engineering Working Group which co-ordinates the EM disciplines in order to achieve an electromagnetically optimised design.

Finally two specialised EMC sections exist, looking after Platform (SSA/ME252) and Combat System (DGSS/SS625) EMC to provide in house assistance to Ship/Equipment projects. These in turn are supported by the Defence Evaluation and Research Agency (DERA) and Industry to undertake EM Research, Development and Testing.

3.2 Management

There are two aspects of management which need to be considered: Responsibilities and Techniques. Addressing the first of these, it is vital that across the spectrum from Project Managers in procurement to naval staff in operational platforms that there are nominated and identifiable points of contact who have a responsibility for EMC.

Looking at techniques, firstly management plans on how EMC is to be achieved in the design/production need to be produced and these are well defined in Defence Standard 59-41 Electromagnetic Compatibility [1]. Secondly, the documentation must be managed. With new equipment always being added or updated it is important that our documentation gives us the big picture and be not just a collection of individual equipment EMC reports with no synergy.

Finally a clear and defined reporting system must exist. Often EMI is either not recognised or is incorrectly reported resulting in many EMC problems never being addressed. To complement this reactive process it is also valuable to have a regular proactive investigation which can look for EMI. These are usually subjective tests based the serial energisation of equipment. However they are cost effective, simple and often can be carried out by ships staff.

3.3 Technical

The general technical EMC philosophy applied to warships is fundamentally the same that most commercial or military systems adhere to, namely

defined susceptibility and emission criteria. The fundamental difference with a warship is the need to address EMC at two distinct levels, equipment and platform. Ideally the platform should be defined as a high level equipment, however this distinction is needed due to the way that equipment is procured usually across many platforms and because we cannot objectively EMC test a platform in a test chamber or open site.

The second factor that has shaped how EMC is addressed is environment. In steel ships there are two distinct electromagnetic environments Above Decks and Below Decks. In the first we have an environment which is relatively high and dominated by own ship emissions. Below Decks we have a passive controlled environment which is similar to a light/heavy industrial environment.

All this has resulted in the development of four main groups:

- Below Decks Equipment
- Below Decks Platform
- Above Decks Platform
- Above Decks Equipment

3.4 Below Decks Equipment/Platforms

In this relatively benign environment EMC is usually achieved through equipment compliance with Defence Standard 59-41 and installation procedures defined in Naval Engineering Standards (NES).

3.5 Above Decks Equipment /Platform

In contrast with the below decks situation, standards alone do not achieve EMC. Instead an optimised topside layout has to be achieved based on modelling and experience. This is specifically true for the aerial systems whose performance can be significantly altered by its position relative to its neighbours and masts. In such cases the coupling/isolation between aerials need to be predicted as do how the VSWR and polar plots are affected by the surrounding super structure. The current and future modelling tools which support this activity are discussed latter in the paper.

3.6 Through Life Testing

EMC assessment of warships is carried out in a subjective, but systematic manner. Firstly all equipments are expected to meet the EMC specification contracted to, primarily Def Stan 59-41. Hull and Compartment shielding requirements are defined in NES 1027 [2] and for each ship EMC Precaution Schedules are raised to classify the shielding level each compartment is to be built to. Detailed guidance on how the equipment is installed is also provided in NES 1027 and is reviewed in the Ships Final Electrical Inspections (FEI). In

addition to this certain marine equipment in situ emission test or audits of certificates may be carried out.

For submarines the main marine and combat systems are systematically energised and any interference noted. For surface ships the main area of concern are the aerials and weapon systems. To identify interference in these systems an Enhanced Weapon Mutual Interference Trial (EWEMIT) is carried out which follows the systematic approach applied to the submarines to detect the existence and source of interference.

Although they do not provide absolute levels of interference, in the case of the EWEMIT, it allows the performance of the ship and the Class to be baselined in order for any degradation in performance to be identified as the trial is completed every 4 to 5 years or following any major equipment update or refit.

This policy of through life testing for combat system equipment is also applied to certain marine equipment.

3.7 Education

Compatibility once achieved is very vulnerable to degradation through wear out and failure mechanisms, unauthorised modifications or failure to follow procedures. The first is managed through regular maintenance and through life testing. The last two rely on education.

EMC and MI is lectured on at the RN Training schools and Fleet documentation provides guidance to ships on its achievement. Awareness campaigns including posters and leaflets are directed to fighting units and every effort is made as part of the through life testing programme to educate ship staff of the importance of EMC and the vital role they play in maintaining it. One important aspect of this is the reporting of interference. Reporting mechanisms exist, but all too often personnel do not recognise the defect as interference or just assume that someone else has reported it.

Equally Project Staff must be educated on the need to pay attention to EMC during the requirement stage and review it through the life of the project. With the collocation of MoD(PE) to Abbey Wood in Bristol, EMC specialist from the Sea, Land and Air Systems are now drafting management guidance to provide a common framework for all project staff to work to.

4. FUTURE DEVELOPMENTS

The policy as described evolved from the historical separation of platforms and equipment and the difficulty As might be expected, the disadvantages of this process is the cost of producing the model and the fact that it can only be carried out once the overall ship design is

in objectively assessing the EMC performance of a warship. However the development of "Whole Ship Procurement" has changed our focus to the demonstration of EMC at the platform level.

To aid us in this aim, we are looking at two main whole ship tests. The first will be based on existing combat system trials which require the serial energisation of equipment to identify sources of EMI. The second will define and measure the coupling requirements of internal systems with the outside environment i.e. measuring the shielding effectiveness of the EMC Citadel.

Another area of consideration is the concept of zones. If a number of zones can be defined on the ship then it may be possible to relax the need for defence standards and have some of them replaced with commercial standards. Such zones could cover domestic, light industrial, heavy industrial, communication offices and above decks and be separated by EMC Citadels with defined and measurable performance requirements.

5. EMC AND AERIAL INSTALLATION

For each of the three main communication bands (HF, V/UHF and Satcom) a typical medium size ship will have six or seven aerials ranging in powers from a few watts to several kilowatts. When deciding on the location of these aerials the ship designer has to consider many constraints such as Mutual Interference, Radhaz, Signature Control and transmission performance. To aid them in this task a set of techniques have been developed.

During the early stage of the design they may rely on guidance documentation such as the System Weapons Engineer Guidebook which gives typical separation distances and the isolation requirements between aerials in dBs or from previous problems reported in the MI database. For satcom systems simple power density predictions can be calculated, however for HF systems physical modelling is required before the aerial system can be defined.

Most HF systems rely on a mixture of monopole whips and wire broadband aerials. Due to the complexity introduced by the near field the design is optimised for Isolation, Voltage Standing Wave Ration (VSWR), Impedance and Polar Plots by the construction of a 1/50th scale copper model of the ship. This is placed on a large ground plane and swept with a boom at scaled frequencies allowing the performance of the design to be established.

established. To improve this situation MoD are developing prediction codes to replace copper

modelling and also to provide more accurate analysis of the aerial systems at microwave frequencies.

6. CONCLUSION

EMC can be achieved through the application of standards, techniques and procedures, however it must be carried out within the framework of a clear policy, an agreed testing programme extending through the life of the product, a supportive organisation and an education programme.

These aspects have been brought together in the RN to combat electromagnetic interference, however whilst the framework exists, it relies on continual effort to build and strengthen the elements of the policy to ensure that compatibility is maintained.*

7. REFERENCES

1. Defence Standard 59-41 Electromagnetic Compatibility.
2. Naval Engineering Standard 1027 Electromagnetic Compatibility Requirements for Installations in Ship and Submarines.

BIOGRAPHICAL NOTE

Alex Mitchell is responsible for Combat System EMC in the Royal Navy and works for the Ministry of Defence Procurement Executive. He studied Electronic Engineering at King's College London and has been in his current post for two years.

© CROWN 1998

* The views expressed in this paper are those of the author and do not necessarily reflect those of the Ministry of Defence.

THE NATO EMI OPERATIONAL PROGRAMME & DATA BASE (NEOP)

Mr. Fred M. Stewart

Space and Naval Warfare Systems Command, attn.: Code 051-2E
4301 Pacific Highway, San Diego, California, USA 92110-3127

Voice Tel: USA (619) 524 7230; Fax Tel: USA (619) 524 7896; e-mail: stewartm@spawar.navy.mil

The NATO Naval Armaments Group (NNAG) Special Working Group Ten (SWG/10) on Naval Electro-Magnetic Environment Effects (E3) is developing the NATO EMI Operational Programme and Data Base (NEOP) that will automate those tasks associated with the management of the electromagnetic spectrum. The US Navy's Automated Spectrum Planning, Engineering, Coordination, and Tracking System (ASPECTS) was used as a baseline system. The software has been modified to incorporate tasking and format specific to the NATO alliance. The NEOP is composed of standard electromagnetic engineering algorithms that can speedily compute potential electronic system degradation due to electromagnetic environmental effects. The NEOP contains the international tables of allocation with applicable footnotes for each of the three regions, and provides for the addition of national tables of allocation if desired.

1. BACKGROUND

Electromagnetic Interference (EMI) presents a considerable threat to electronic system performance, and in extreme cases can be responsible for the total loss of these systems. Inter-platform EMI problems have occurred between ships of the NATO alliance. These incidents will become more frequent as the new force structure of the alliance moves towards expanded Multi-National Naval Formations. Advances in technology, which have introduced such techniques as frequency agility and spread spectrum, further increases the likelihood of EMI by placing greater demand on the already overcrowded spectrum.

SWG/10 has participated in Multi-National trials and exercises which have demonstrated a need for an automated tool to coordinate the use of multiple emitters and receivers across the communications and radar frequency bands.

2. OPERATIONAL CONCEPT

The concept is to allow Multi-National forces to minimize the effects of electromagnetic interference as much as possible during the planning stages of a deployment. This includes the development of the communications and radar frequency plans, as well as providing advice on ship and aircraft positioning to minimize EMI to weapons and sensors. The NEOP will contribute to every facet of maritime warfare as it pertains to the use of electromagnetic emitters and sensors.

In order to meet the operational concept, as described above, it is essential that the NATO EMI Operational Programme & Data Base (NEOP) be capable of:

- A. Determining potential EMI issues prior to, and during the deployment of forces using:
 1. Force composition
 2. Force disposition
 3. Geographic area
 4. Platform electronic system suites
 5. Electronic system parametric data
 6. Meteorological conditions, and
 7. Sea State or terrain conditions
- B. Modifying frequency plans to accommodate the addition of new platforms; re-analyzing the EME; and distributing a new frequency plan.
- C. Operating aboard ship. The NEOP must be designed such that it can be used in a shipboard environment with a high degree of reliability.
- D. Calculating EMI predictions for a 50 platform force in one hour or less.

3. ARCHITECTURE

In order to function as a planning and operational tool, it was determined by SWG/10 that the NEOP software must be hosted on a computer system capable of being used shipboard. Therefore, the Personal Computer (PC)

was chosen as the host hardware because of its standard features, i.e., it is relatively the same anywhere in the world and is easily maintained.

3.1. Hardware considerations

The power of PC system hardware is changing at a rapid rate, and thus software engineers are developing new software, and modifying older software programs, to take advantage of this new found power. Today's recommended *minimum* hardware requirements to run the NEOP are:

- A. STORAGE: 3.5in Disk Drive; CD-ROM drive; and 500 MB hard drive.
- B. PROCESSOR: Pentium CPU
- C. MEMORY: 16 MB RAM
- D. I/O Devices: Keyboard, printer

3.2. Software considerations

The NEOP software is designed for a Common Operating Environment (COE) running on a PC system to maximize portability and to eliminate the need for special hardware or operating systems. The basic considerations are:

1. Developed in a High Level language
2. User friendliness
3. Minimizing software upgrade cost as new versions are developed
4. Modular design made up of a Communications Planning Module (CPM), a Frequency Management Module (FMM), and a Radar Module
5. OS: Windows 95 or NT
6. Year 2000 compliant

3.3. Database considerations

In order to perform the planning, management, and analysis functions, the NEOP contains information specific to each of these functions. Specific data requirements are discussed later as we investigate each of the modules.

4. NEOP SYSTEM OVERVIEW

SWG/10 approved the use of the US Navy's ASPECTS program as the NEOP Initial Capability system (NEOP IC). Many of the features of the ASPECTS software were retained as part of the NEOP to eliminate duplication of effort, i.e., to take advantage of features already developed. The NEOP consists of three modules:

- (1) Communications Planning Module (CPM);
- (2) Frequency Management Module (FMM) , and
- (3) Radar Module.

5. NEOP MODULE DISCUSSION

Many of the features of the NEOP Initial Capability system (NEOP IC) are based on the US Navy's ASPECTS software. All modules are "stand alone", i.e., they may be used independently of

each other. The CPM and the FMM can work together on the same computer to identify communication requirements and then browse records to find suitable assignments. The NEOP RADAR module is used solely for radar and weapon system frequency plans. It is capable of transferring frequency assignment data to the FMM.

5.1. Communications Planning Module (CPM)

Communications planning and the management of radio frequency assignments to support the plan is a continuous planning and modification effort. The NEOP CPM provides communications planners with the capability to quickly and accurately develop and modify detailed communication plans. Based on user input, the CPM will:

1. Determine frequency requirements based on required bandwidth
2. Perform band overlap and basic engineering analyses to ensure compatibility
3. Generate a frequency request message to higher authority
4. Perform harmonic and intermodulation analyses on frequencies assigned by higher authority
5. Generate the communications plan in message or letter format for immediate distribution to fleet units

The CPM must have access to specific platform equipment, and operational information in order for the user to obtain maximum benefit. This includes, but is not limited to:

1. Ship or platform name, call sign, communications suite, warfare mission area and embarked staffs
2. Operation name, start date, end date, area of operation and communication net data.

5.2. Frequency Management Module (FMM)

The FMM was developed to assist frequency managers ashore and afloat. It quickly identifies available frequency resources, assigns frequencies to support force communication plans, and maintains a record of all frequency requests and assignments for each operation.

The FMM extracts potential assignments from a database of frequency records. Once the CPM identifies the number of frequencies required by band and modulation type, the FMM may be used to browse the database of frequency records in search of suitable frequencies.

The ability of the FMM to assist with the nomination of frequencies is dependent upon the assignment request data provided. Specific data required includes:

1. Emission characteristic data, i.e., necessary bandwidth, power required, etc.

2. Date and Time the frequency is required
3. Transmitter and receiver system, to include antenna characteristic data

The FMM selects suitable frequencies to support the request received from the user, providing use constraints, if any, that apply to each assignment. Prior to releasing the frequencies for assignment, the user can perform harmonic and intermodulation analyses on the assignments to ensure compatibility.

5.3. NEOP RADAR Module

The objective of the NEOP RADAR module is to minimize radar and weapon system antenna-to-antenna coupled interference. It considers all force radars and honours international air traffic control and other commercial frequencies that may be in use by littoral nations adjacent to the area of operation.

The latest version of the module is designed to allow the coordination of radar and weapon systems manufactured anywhere in the world, provided characteristic data is available. It uses a combination of measured data and data obtained from resident engineering models to analyze the expected radar electromagnetic environment and provide compatible assignments. Specifically, the NEOP RADAR module will:

1. Analyze the force's radar electromagnetic environment
2. Identify EMI source/victim pairs
3. Suggest operational alternatives to alleviate residual EMI
4. Identify and calculate reassignment of offending radar frequencies
5. Develop radar and NAVAID frequency plans
6. Generate correspondence for the distribution of the radar frequency plan

The NEOP RADAR module calculates potential EMI for non-measured source/victim radar and weapons system pairs through the application of predictive models. Although the models will calculate and use default data where system parametric data are unknown, every attempt should be made to obtain actual characteristics. The accuracy of this module is highly dependent upon the accuracy of the data used for the calculations. The RADAR module is designed for multi-national naval deployments, however, it can also be used to assist amphibious operations to achieve EMC. The module is designed to consider shore facility and air platform radar equipment thereby making it a versatile radar EMC tool.

Once the analysis is completed the module displays the cumulative affects that the composite EME will have on each system.

XVI WORKSHOPS

Mathematical Methods in Frequency Planning

URSI Commission E WGE 1 Workshop

Organizers:

Dr. J. Finnie - UK

Dr. R. Leese - UK

Prof. R. G. Stružak - Poland

We wish to thank the United States Air Forces European Office of aerospace research and development for their support which contributed considerably to the success of this event.

SOLVING FREQUENCY ASSIGNMENT PROBLEMS

S. M. Allen, S. Hurley, D. H. Smith and W. J. Watkins

The importance of efficient frequency planning is increasing as the demand for spectrum use increases. Modern meta-heuristic techniques can be successfully applied to the problem to generate good quality assignments.

There are two main types of channel assignment problem of importance:

- **Minimum span frequency assignment.** Given a required level of service quality to be met at all possible reception points in a network, generate an assignment that minimises the range of channels used (usually called the *span*, $f_{\max} - f_{\min}$).
- **Fixed spectrum frequency assignment.** For a given network and a specified allocation of available channels, generate an assignment that maximises some measure of service quality.

The channel assignment problem is NP-complete and to generate best possible solutions is impractical for non-trivial networks. Meta-heuristic algorithms do not guarantee optimal solutions, but generate near optimal solutions in reasonable time.

Most current solution methods model the problem as a set of frequency separation constraints between pairs of transmitters. For example, two transmitters at the same site may be required to have frequencies that are at least three channels apart. The quality of the assignment can be measured by the number or amount of constraints violated.

Tabu search and simulated annealing are two meta-heuristics that have proved successful when applied to frequency assignment problems [2,3]. Both use improvement methods based on local search. Firstly, an initial solution is selected. At each step a new solution is selected from a neighbourhood of similar solutions (for example, all assignments which differ at exactly one transmitter). In its simplest form, local search selects the best solution from each neighbourhood.

However, this is likely to lead to a solution that is a local minimum but not a global minimum. Tabu search and simulated annealing use rules to counteract this.

Since meta-heuristics are not guaranteed to produce optimal solutions it is important that good lower bounds can be generated to assess the quality of solutions. Techniques based on the Travelling Salesman Problem have proved successful [1,4,5]. An important aspect of lower bounding is the identification of critical areas of the problem that capture most of the difficulty of the whole problem. These regions can also be used to aid the assignment procedure [3,6,7].

The use of lower bounds has shown tabu search and simulated annealing, as described in [2,3], to give optimal solutions for many realistic problems. Over a range of realistic cellular coverage type problems the solution is on average within 3.7% of the lower bound. Optimal solutions are sometimes obtained.

REFERENCES

- [1] S. M. Allen, D. H. Smith and S. Hurley, Lower bounding techniques for frequency assignment, *Discrete Mathematics*, to appear.
- [2] S. Hurley, D. H. Smith and S. U. Thiel, FASoft: A system for discrete channel frequency assignment, *Radio Science*, Vol. 32, No. 5, 1997, pp. 1921 – 1939.
- [3] S. Hurley and D. H. Smith, Metaheuristics and channel assignment, In *Radio Channel Assignment*, edited R. Leese, OUP, to appear.
- [4] D. H. Smith, S. M. Allen and S. Hurley, Lower bounds for channel assignment, In *Radio Channel Assignment*, edited R. Leese, OUP, to appear.
- [5] D. H. Smith and S. Hurley, Bounds for the frequency assignment problem, *Discrete Mathematics*, Vol. 167/168, 1997, pp. 571-582.

- [6] D. H. Smith, S. Hurley and S. U. Thiel, Improving heuristics for the frequency assignment problem, European Journal of Operational Research, to appear.
- [7] S. M. Allen, S. Hurley, D. H. Smith and S. U. Thiel, Using lower bounds in minimum span frequency assignment, Proceedings of 2nd International Conference on Metaheuristics, Sophia-Antipolis, France, 1997, to appear.

S. M. Allen and D. H. Smith,
Div. of Maths. and Computing,
University of Glamorgan,
Pontypridd,
Mid Glamorgan CF37 1DL,
U.K.
[{smallen, dhsmith}@glam.ac.uk](mailto:{smallen,dhsmith}@glam.ac.uk)

S. Hurley and W. J. Watkins,
Dept. of Computer Science,
University of Wales, Cardiff,
P.O. Box 916,
Cardiff CF2 3XF,
U. K.
[{S.Hurley, W.J.Watkins}@cs.cf.ac.uk](mailto:{S.Hurley,W.J.Watkins}@cs.cf.ac.uk)
<http://www.cs.cf.ac.uk/User/Steve.Hurley>.

Non-binary modelling of frequency assignment leads to significant reduction in predicted spectrum requirements

J.E.Bater, P.G.Jeavons and D.A.Cohen

Royal Holloway, University of London, Egham, Surrey, TW20 0EX, UK

Methods for generating binary re-use distance constraints on a network of randomly placed Tx are considered. We demonstrate that even "very good" binary constraint solutions are easily outperformed by global constraints. We argue that binary constraint modelling inherently fails to capture the requirements of a good solution: adequate coverage and minimum span.

1. INTRODUCTION

The frequency assignment problem (FAP) is a genuine hard problem of practical importance to both civil and military administrations. The FAP can, according to its particular definition, encompass one of a number of possible tasks. We are particularly concerned with coverage problems in dense networks, such as those existing for mobile telephone networks.

The essential characteristic of these is that a frequency must be assigned to each transmitter (Tx) in such a way that the signal-to-noise ratio (SNR) at every receiver (Rx) in the region to be covered is greater than some specified acceptable value. (How we calculate SNR is described in Section 2.)

$$\forall \text{Rx}, \exists \text{Tx}_{\text{desired}} : \text{SNR} \geq \text{SNR}_{\text{acceptable}}$$

Coverage tasks can take a number of guises. Two common such coverage-type tasks are:

1. Minimize the spectrum requirement, by finding a satisfactory assignment which uses the smallest number of distinct frequencies.
2. Maximize the solution quality, by finding an assignment using a given fixed allocation of frequencies that provides the best possible coverage (there are many possible optimisation criteria).

The work described here concerns the first of these tasks and investigates some of the assumptions commonly made when modelling this kind of FAP. Specifically, we question the assumption made in

many previous studies that binary constraints (constraints which restrict the values on pairs of transmitters) are sufficient to specify the problem effectively [7, 9, 10, 11].

To carry out the study described here, a small network of transmitters and receivers was modelled, emulating the propagation characteristics of a mobile telephone network (GSM). Binary constraint solutions (generated with different techniques) were compared to the solutions obtained by expressing the original system requirements as a global constraint.

We found that global constraint solutions were consistently more spectrally efficient than binary constraint solutions. This remains true even after optimisation of these binary constraints. Furthermore, an examination of the requirements for good binary constraints suggests that this type of constraint inherently leads to solutions which do not minimise span.

2. THE MODEL EMPLOYED

In the land-mobile service radio networks are typically designed with a cellular structure in which each transmitter provides the signal for all receivers in its neighbourhood [1, 3].

Our model contained a fixed set of Tx sites placed at random (uniform distribution) on a 100 by 100 matrix of Rx sites which is referred to as "Pinkville" (such an approach has been used before [4]), each Rx position was "scaled" by a factor of 50, Pinkville is thus notionally a 5km by 5km region. We randomly generated 50 Tx locations, and then generated problem instances with n transmitters by simply using the first n of these Tx locations (for n in the range 20-50). The positions of the first 20 transmitters are shown in Figure 1.

The propagation model used was as follows:

1. Tx were assumed to operate with uniform effective radiated power. That is, all transmitting

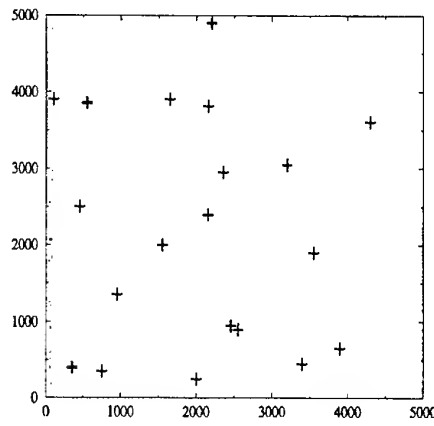


Figure 1: Positions of first 20 transmitters in Pinkville

powers were equal, and propagation was omnidirectional

2. Free-space loss was assumed to be the only cause of signal attenuation. This was modelled using an inverse fourth power law:

$$P_{Rx} = \frac{P_{Tx}}{d^4}.$$

3. Cells were defined by assuming that the desired signal at each Rx was received from the nearest Tx (equidistant Tx were chosen arbitrarily).
4. Frequencies were assumed to be chosen within discrete channels. Adjacent channel rejections followed the GSM specification [5, 6]:

offset	interference	rejection
0	C/Ic	(none)
1	C/Ia ₁	-9dB
2	C/Ia ₂	-41dB
3	C/Ia ₃	-48dB
≥ 3		(total)

5. Multiple interfering signals at the same receiver were combined using power-summation:

$$\text{Total Interference} = \sqrt{\sum_{i=1}^n \text{Interference}_i^2}$$

6. Signal-to-noise ratios are thus calculated:

$$\text{SNR} = \frac{\text{Signal}_{\text{desired}}}{\sqrt{\sum_{i \neq \text{desired}} \text{Signal}_i^2}}$$

3. CHOOSING BINARY CONSTRAINTS

Although the various specifications of radio services suggest no particular approach to choosing frequencies [5, 6, 7, 13], a graph theoretic approach is commonly used. In this approach, the FAP is considered to be analogous to GRAPH K-COLOURING, or GRAPH T-COLOURING [4, 9, 11, 15].

When the problem is tackled using this graph-theoretic approach, the requirements on the desired assignment are described by specifying constraints on the frequencies that may be assigned to certain pairs of transmitters. These constraints typically take the form:

$$f(\text{Tx}_i) - f(\text{Tx}_j) \geq k$$

meaning that the frequencies assigned to Tx_i and Tx_j are required to be $\geq k$ channels apart in order to avoid excessive interference at any Rx.

This raises the question of how the original requirements for an adequate SNR at each Rx may be translated into these binary constraints between pairs of transmitters. In our experience, the data sets made available to many researchers are often already in binary constraint form, so this question has not received the attention it deserves. This problem is particularly acute when attempting to find solutions which minimise the number of frequency channels used, because the choice of binary constraints must then satisfy two opposing criteria:

1. *minimum spectrum* The binary constraints chosen must be sufficiently loose. If they are too restrictive, then the solutions found will use an unnecessarily large number of frequency channels.
2. *adequate coverage* The binary constraints chosen must be sufficiently tight. If they are not restrictive enough, then at least some of the solutions found will not satisfy the coverage requirements.

One common way to obtain suitable binary constraints, at least in theoretical studies, is to introduce the notion of "re-use distances" [4, 7]. The re-use distance, d_0 , specifies the geographic distance that two Tx must be apart before they may operate on the same frequency channel. Similarly, d_1 is the distance that two Tx must be apart before the first adjacent channel may be used, and so on for d_2, d_3 , etc. Once these distances are chosen, constraints are imposed on every pair of transmitters that are nearer than d_i to each other to ensure that they use frequency channels that are more than i channels apart. Clearly, as the re-use distances are increased the corresponding binary constraints become more restrictive and the number of distinct frequency channels required to satisfy them all will increase.

Binary constraints, or the underlying re-use distances, may be chosen in a number of different ways:

1. ESTIMATION: The re-use distances, d_0, d_1, \dots , can be estimated from engineering "common sense" (e.g. [2, 10, 13, 14]).
2. CALIBRATION: The estimated re-use distances d_0, d_1, \dots can all be multiplied by a suitable scale factor (found by some search procedure) in order to obtain the smallest possible values which still achieve adequate coverage.
3. TRADE-OFF: The relative sizes of d_0, d_1, \dots can be adjusted to reduce the number of frequency channels required whilst maintaining adequate coverage [12].
4. SEARCH: The values of d_0, d_1, \dots can be adjusted separately for each Tx using some computational search technique (e.g. evolutionary algorithms, simulated annealing, etc.).
5. OMNISCIENCE: Given an optimal solution, a set of binary constraints can be derived which obtain exactly that solution (unfortunately this approach is rather impractical).

In the two experiments reported below, we demonstrate that the most straightforward of these methods, ESTIMATION and CALIBRATION, lead to very poor estimates of the number of frequencies required for the problems considered here.

4. RESULTS

4.1. Experiment One

In the first experiment, we used the method described by Withers [14, pp.231–232] to generate constraints on the Pinkville instances. This method estimates the re-use distance d_0 as $D1 + D2$, where $D1$ is the distance from a Tx which gives minimum acceptable signal quality (GSM mobile stations have a reference power sensitivity of -104dBm [8]), and $D2$ is an additional distance which should be sufficient to prevent excessive co-channel interference (i.e. a further 10dB fall off in signal strength). Other re-use distances are calculated in a similar way, taking into account the channel rejections. This method resulted in the following re-use distances for the propagation model used in these experiments:

$$\begin{aligned} d_0 &= 7399 \\ d_1 &= 4407 \\ d_2 &= 701 \\ d_3 &= 467. \end{aligned}$$

Once the binary constraints were defined for the Pinkville instances, solutions (and lower bounds) to these constraints were found using the software package *FASoft* [9]. This software provides a facility to calculate a lower bound on the number of frequency

channels needed for a solution, based on "cliques" in the constraint graph. For each problem instance, these lower bounds were calculated, and then an attempt was made to find a solution using this minimal number of channels. If no solution could be found using the default search options, then this channel allotment was incremented until a solution was found. In all cases the number of channels used in the solutions obtained was very close to the lower bound, only involving adding 4 or 5 more channels.

The binary constraint solutions were then compared to *global constraint solutions* produced by a simple backtracking search through all possible assignments, checking each one directly against the propagation model described above. Each assignment was checked by calculating the SNR at each Rx and rejecting assignments for which this value was less than the desired value, 9 dB, at any Rx. The number of channels made available to the search procedure was equal to the number of Tx in the instance. No attempt was made to optimise the solution, rather reported solutions are the *first* solutions returned.

Examination of SNR distributions on the results shows that the solutions obtained from the binary constraints have a SNR at many receivers which is much larger than required (See Figure 2). This suggests that the binary constraints used were too restrictive, and therefore very inefficient in terms of the number of frequencies used. This is confirmed by comparing the solutions obtained from the binary constraint formulation with the solutions obtained from the global constraint formulation (Figure 3).

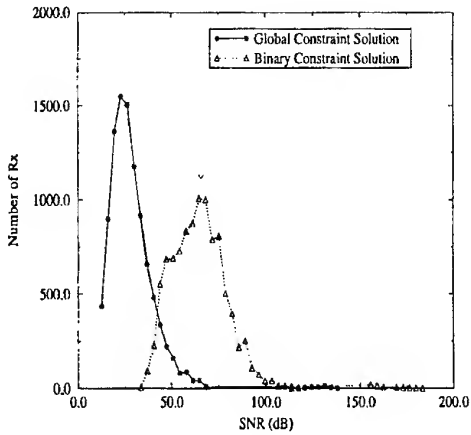


Figure 2: Distribution of SNR results on the 50 Tx Pinkville Instance

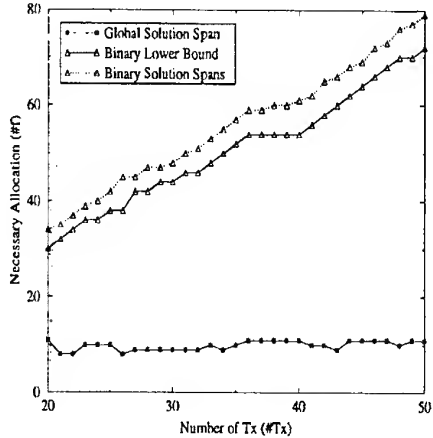


Figure 3: Comparison of Pinkville Instance Solutions

4.2. Experiment Two

In the second experiment, we attempted to reduce the number of frequency channels required by choosing a less restrictive set of binary constraints. To do this we used the CALIBRATION method, described above, to scale down the re-use distances chosen in Experiment 1.

To do this, the reuse distances were gradually reduced from the distances used in Experiment 1, and for each value new binary constraints were calculated, and the resulting set of constraints was solved by FASoft. The coverage achieved by this solution (that is, the proportion of receivers for which the SNR was greater than 9 dB) was then plotted, as shown in Figure 4. Using this information, it was possible to estimate the minimal possible values for the reuse distances such that the coverage on the resulting assignments was 100% at the 9dB SNR level (the same solutions were also checked at the 12dB and 15dB levels at which coverage was typically $\geq 95\%$ but $< 100\%$). The values for the re-use distances obtained in this way were as follows:

$$\begin{aligned} d_0 &= 2959.6 \\ d_1 &= 1762.8 \\ d_2 &= 280.4 \\ d_3 &= 186.8 \end{aligned}$$

Using these smaller re-use distances resulted in much less restrictive binary constraints, and hence in solutions using fewer frequency channels, as shown in Figure 5. However, it is clear from this Figure that even after optimising the reuse distances in this way, the number of frequency channels required to solve the corresponding binary constraints is still considerably larger than the number found by a simple search

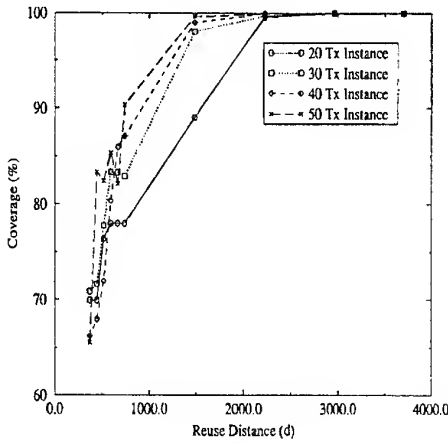


Figure 4: Calibrating Binary Constraints on the Pinkville Instance

procedure.

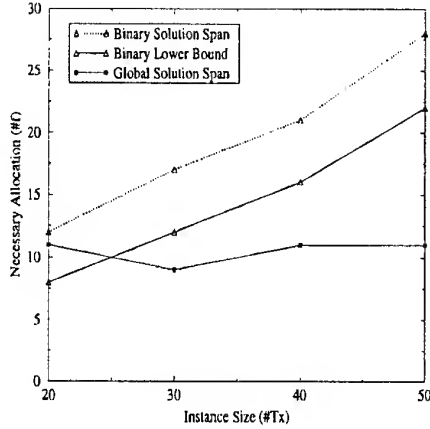


Figure 5: Solution Spans for Calibrated Binary Constraints

5. CONCLUSIONS

The results presented above lead to two significant conclusions. First, lower bounds obtained from a collection of binary constraints do not necessarily provide a reliable lower bound for the number of frequencies required for a given network of transmitters.

We have shown that even when binary constraints are "calibrated" from initial "common sense" settings, global constraint solutions easily outperform these bounds.

Secondly, the setting of binary constraints is widely believed to be on a sliding scale, and that it is only a matter of "fine tuning" to get the "right" constraints. This work suggests that in some cases there is no optimal point on the scale, since binary constraints that are loose enough to allow *minimum spectrum* solutions may fail to ensure *adequate coverage*.

References

- [1] M.S. Appleby. The UK cellular system. In Macario, R.C.V., editor, *Personal & Mobile Radio Systems*, chapter 9, pages 192–207. Peter Peregrinus, Stevenage, United Kingdom, 1991.
- [2] J-F. Arnaud. Frequency planning for Broadcast Services in Europe. *Proceedings of the IEEE*, 68(12):1515–1521, December 1980.
- [3] D.M. Balston. The pan-European cellular technology. In Macario, R.C.V., editor, *Personal & Mobile Radio Systems*, chapter 14, pages 290–319. Peter Peregrinus, Stevenage, United Kingdom, 1991.
- [4] L.A. Berry. Potential contribution of optimum frequency assignment to efficient use of the spectrum. In *Proceedings of the IEEE International Symposium on Electromagnetic Compatibility*, pages 409–412, 1990.
- [5] ETSI. *European digital cellular telecommunications system (Phase 2); Radio network planning aspects (GSM 03.30)*, February 1995.
- [6] ETSI. *Digital cellular telecommunications system (Phase 2); Radio transmission and reception (GSM 05.05)*, November 1996.
- [7] W.K. Hale. Frequency assignment: Theory and applications. *Proceedings of the IEEE*, 68(12):1487–1514, December 1980.
- [8] L. Hanzo and J. Stefanov. The pan-European digital cellular mobile radio system - known as GSM. In R. Steele, editor, *Mobile Radio Communications*, chapter 8, pages 677–678. Pentech Press, London, United Kingdom, 1992.
- [9] S. Hurley, D.H. Smith, and S.U. Thiel. Fasoft: A system for discrete channel frequency assignment. *Radio Science*, 32(5):1921–1939, 1997.
- [10] A. Knälmann and A. Quellmalz. Solving the frequency assignment problem with simulated annealing. In *Proceedings of the Ninth International Conference on Electromagnetic Compatibility*, pages 233–240, 1994.
- [11] R. Leese. Tiling methods for channel assignment in radio communication networks. In *Proceedings of the 3rd International Conference on Industrial and Applied Mathematics*, 1995.
- [12] R. Leese and R. Gower. The sensitivity of channel assignment to constraint specification. In *EMC97 Symposium*, Zurich, 1997. To appear.
- [13] R.G. Stružak. Optimum frequency planning: a new concept. *Telecommunications Journal*, 49:29–36, 1982.
- [14] D.J. Withers. *Radio Spectrum Management*. Peter Peregrinus, Stevenage, United Kingdom, 1991.
- [15] J. Žerovník. Experiments with a randomized algorithm for a frequency assignment problem. Technical Report 97-27, Ecole Normale Supérieure de Lyon, September 1997.

STRUCTURAL FEATURES IN THE CONSTRUCTION OF GOOD CHANNEL ASSIGNMENTS

Robert A. Leese

Mathematical Institute, University of Oxford, Oxford OX1 3LB, UK

Recent work on the channel assignment problem has produced various benchmark problems for which optimal assignments are known. The solutions to cellular problems exhibit a structure which can be used to motivate the design of faster algorithms, opening the way to finding good solutions to large problems in no more than a few seconds. One such possibility is described here.

1. INTRODUCTION

Over the last few years there has been a considerable research activity among mathematicians and computer scientists directed towards the design of effective algorithms for radio channel assignment in large radio systems. Mathematical interest in these problems is heightened by their close relation to the notorious NP-complete problems of combinatorial optimization, and in particular to the graph-colouring problem.

Specifications for the channel assignment problem tend to come in a small number of standard forms, all of which describe, in some fashion, a set of demands (or requirements) for channels and a set of constraints on the overall assignment, designed to capture the physical need to avoid interference. The transmitter sites and powers are generally fixed in advance. In the most common specification, constraints take the form of minimum allowed differences between pairs of assigned channels, either both at the same site (co-site constraints) or one each at two distinct sites (inter-site constraints). Such constraints may naturally be written as a matrix. (It has recently been suggested that the constraint matrix may not be the most suitable form in which to couch interference constraints, but it is certainly the most commonly used, capturing similar information to sets of protection ratios.)

Depending on the objective, the channel assignment may be treated as either a *minimum span problem* or a *fixed spectrum problem*. In the former, all

demands must be satisfied and all constraints must be met, using as few overall channels as possible (the span is conventionally defined as the difference between the highest and lowest channels used). In the latter, the amount of spectrum available is given beforehand, and the objective is to satisfy as many channel requests as possible, again without violation of constraints. Most work to date has concerned minimum span problems. Extensions of these two basic problems incorporate variations in the quality of assignment, by allowing some violation of constraints, but we will not consider such possibilities here.

As work has progressed, there have emerged several sets of benchmark problems, which have been used to test and compare various algorithms. The most valuable benchmarks are those for which exact answers are known, *i.e.* for which no further improvement is possible. For some minimum span problems, this has been achieved by using lower bound techniques (see, for example, [1]).

Experience of working with particular problems leads to the qualitative view that some are easier than others. The translation of this experience into a quantitative classification of problems remains one of the most important open questions. However, some hints can be found by looking at the assignments produced by software packages such as FASoft [2]. Cellular systems, especially, often generate assignments showing a degree of local regularity, which may be seen by looking at the sequence of channels assigned to individual sites. To take a random illustration, FASoft generated the sequence 52, 132, 142, 152, 162, 172, 185, 190, 198, 204, 210, 216, 222 for a particular cell of demand 13 as part of an optimal solution to the common 'Philadelphia' benchmark (E3 in Table 1 below). The striking features are the regular spacing of 10 channels near the start and 6 channels near the end. (All the differences must, of course, be at least as large as the corresponding co-site constraint, which here is 5 channels.)

2. SPECTRAL BLOCKS

The appearance of regular increments, not imposed by the software that generates them, suggests a possible design for faster algorithms. The idea is construct small pieces of the overall assignment, using small sets of consecutive channels and covering just a subset of the sites. Laying down several copies ‘end-to-end’ in the frequency spectrum will produce the regular pattern seen above. The original small piece is called a *spectral block*. A complete assignment is built up from several spectral blocks, each in general repeated different numbers of times. Each site will be served by some, but generally not all blocks. The size of a spectral block is the number of consecutive channels one repetition takes up, and naturally determines the increments seen in individual cells. For example, the above sequence could arise from using (among others) spectral blocks of sizes 10 and 6.

Algorithms based on this technique were first implemented as part of an MSc project in Oxford [3]. A small example was subsequently discussed in [4]. It is attractive to treat spectral blocks in an object-oriented setting, and therefore a new implementation has recently been developed in C++, from which preliminary results are presented below.

The algorithm first constructs a collection of spectral blocks, of various sizes, and then decides how the blocks will be assembled into an overall assignment. The interference constraints are dealt with during block construction, *i.e.* transmitters sites can only be assigned to blocks in ways that satisfy the interference constraints. Currently, the blocks are constructed using fast sequential techniques, governed by ordering the sites in various ways. At this stage, no attempt need be made to assess the ‘quality’ of blocks as far as assembling efficient overall assignments is concerned. Think of the block construction as filling a toolbox with a collection of tools (the blocks), some of which will eventually be used for solving the particular problem at hand. The ones that are not suitable will be left in the box. The second stage constructs an overall channel assignment by choosing some of the spectral blocks constructed previously. It is only now that the spectrum requirements are considered. The repetitions of the chosen spectral blocks are determined by a linear program, as outlined in [4]. It is possible to treat both minimum span and fixed spectrum problems in the same setting.

Table 1 presents preliminary minimum span results for variants of the ‘Philadelphia’ benchmark. These problems have the advantage that they have been solved to optimality, and so give an absolute measure of performance. They are referred to in the table by the labels E3–E6, E8 and E9, as used in [2]. The sequence of channels generated in the same cell of E3 as given earlier for FASoft, is 156, 162, 168, 174,

180, 186, 192, 198, 207, 212, 217, 222, 429. The precise numbers are unimportant, but there are again two regular increments that dominate, this time 6 and 5. For this particular example, Janssen and Kilakos [5] have given an optimal assignment in which only the increment 6 appears.

Example (see [2])	Minimum span (from FASoft)	Span found using spectral blocks
E3	426	428
E4	426	427
E5	257	261
E6	252	257
E8	855	857
E9	1713	1714

Table 1: The spans obtained using spectral blocks on the benchmark problems discussed in [2].

These results are very encouraging, and they are also calculated extremely quickly (each in fractions of a second on a Pentium processor). The execution time will increase as the number of sites increases, but is insensitive to changes in the demands at each site. In fact, there are mathematical reasons why the algorithms should perform better as the demands increase. Moreover, the algorithm requires neither fine-tuning of internal parameters nor any external guidance dependent on the input data. It is intended to carry out further tests to determine more fully for which types of channel assignment problem the regular structure of spectral blocks is useful.

This work was carried out under a research contract between the Radiocommunications Agency and St. Catherine’s College, Oxford.

3. REFERENCES

- [1] S.M.Allen, D.H.Smith and S.Hurley, *Lower bounding techniques for frequency assignment*, University of Glamorgan research report (1997).
- [2] S.Hurley, D.H.Smith and S.U.Thiel, FASOFT: *a system for discrete channel frequency assignment*, Radio Science, Vol. 32, No. 5 (1997) 1921–1939.
- [3] H.J.Pung, *Designing a channel assignment algorithm using spectral blocks*, MSc thesis, University of Oxford (1996).
- [4] R.A.Leese, *Fast channel assignment in irregular radio systems*, Proceedings of the IEEE International Symposium on Electromagnetic Compatibility, Beijing, China (1997) 426–429.
- [5] J.Janssen and K.Kilakos, *An optimal solution to the Philadelphia channel assignment problem*, London School of Economics research report, LSE-CDAM-96-16 (1996).

COLOURING AND LABELLING OF PLANAR GRAPHS

(Extended Abstract)

J. VAN DEN HEUVEL*

Centre for Discrete and Applicable Mathematics, Department of Mathematics
London School of Economics, Houghton Street, London WC2A 2AE, U.K.

S. MC GUINESS

Department of Mathematics, University of Umeå, Umeå, Sweden

Graph colouring and labelling has been an important tool in the mathematical study of Frequency Assignment Problems (FAP's). The underlying idea is that a collection of transmitters or base stations and their mutual interference can be represented by a graph. This graph has the collection of transmitters as its vertices and two vertices are connected by an edge if their mutual interference is large. A further assumption in this model is that the distance of two transmitters in the graph (the length of the shortest path between the two vertices) gives a good indication of the mutual interference between the two transmitters.

When the FAP originates as a problem in a cellular network, with the cells being regions in the plane, the graph obtained as above is very likely to be a planar graph or a graph that is "close" to being planar. Because of this it is surprising that no research on labelling with distances has been done specifically for planar graphs. The aim of this note is to start filling this gap.

1. INTRODUCTION AND NOTATION

Suppose we are given a cellular network in which the base stations for each cell need to be assigned a certain frequency. This assignment needs to be done so that the quality of reception everywhere in every cell is above a certain minimal level. An im-

portant ingredient that determines this quality is the mutual interference between stations, especially from stations that are broadcasting on frequencies close together on the spectrum. This interference will be strong from cells that are neighbouring the cell under consideration, but also from cells further away the interference might be significant enough to prescribe a certain minimal distance between the frequencies used.

In this note we model the above situation as follows. The cells in the network will become the vertices of a graph (see further in this section for definitions), where two vertices are connected by an edge if they have a border in common (see Figure 1). If the cells have roughly the same size and form, then the distance between two cells in the plane will be roughly proportional to the distance between the corresponding vertices in the graph. Hence from now on we will assume that the minimum required separation between the frequencies used in two cells is determined by the distance in the graphs of their associated vertices.

A particular property of a graph obtained in the manner above is that it is *planar*, i.e., it can be drawn in the plane in such a way that edges do not cross. The problem to assign frequencies to a network as sketched above hence becomes equivalent to finding a *labelling of a planar graph* satisfying certain properties.

*Supported by the U.K. Radiocommunications Agency.

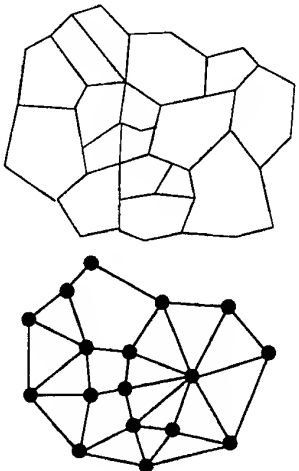


Fig. 1. A cellular network and its associated graph.

We will now sketch a more formal mathematical setting of the problem. A graph $G = (V(G), E(G))$ is a (finite) collection of vertices $V(G)$ together with a collection of edges $E(G)$. Each edge consists of a pair uv of vertices and we only allow at most one edge for each pair. If u, v are two vertices such that an edge $uv \in E(G)$ exists, then we say that u and v are neighbours or adjacent. The degree of a vertex $u \in V(G)$, notation $d_G(u)$, is the number of neighbours of u in the graph. The maximal degree over all vertices is denoted by $\Delta(G)$.

A path $P = u_0u_1u_2\dots u_m$ in G is a sequence of different vertices such that for each $i = 0, 1, \dots, m - 1$ there is an edge u_iu_{i+1} . The length of the path is the number of edges in the path (which is m in the notation above). A graph is connected if there exists a path between any two vertices. If a graph is connected, then the distance $\text{dist}(u, v)$ between two vertices u, v is the minimum length of a path between u and v . Note that this means that $\text{dist}(u, u) = 0$, and $\text{dist}(u, v) = 1$ if and only if u and v are adjacent.

A labelling of a graph G is a function $\varphi : V(G) \rightarrow \{0, 1, 2, \dots, n - 1\}$ for a certain n . A colouring is a labelling φ such that if $uv \in E(G)$, then $\varphi(u) \neq \varphi(v)$. For integers $p, q \geq 0$, a labelling φ of a graph is called an $L(p, q)$ -labelling if it satisfies that whenever $\text{dist}(u, v) = 1$, then $|\varphi(u) - \varphi(v)| \geq p$, and whenever $\text{dist}(u, v) = 2$, then $|\varphi(u) - \varphi(v)| \geq q$. The p, q -span of a graph G , notation $\lambda(G; p, q)$, is the minimum n for which an $L(p, q)$ -labelling exists.

2. $L(p, q)$ -LABELLINGS FOR PLANAR GRAPHS

The problem to determine $\lambda(G; p, q)$ for certain graphs or certain classes of graphs (or at least to find

good lower bounds for the span) has been studied before, see e.g. [4, 5, 6, 7, 11]. The Frequency Assignment Problem is often mentioned as a motivation for studying the $L(p, q)$ -labellings of graphs. But most of the specific graph classes studied in the literature are not the kinds of graphs that would arise from FAP's. As described in the previous section, when the interference graph of an FAP arises from a problem on a cellular network, the interference graph will have certain planarity properties. This is why we will consider planar graphs only in this note.

The problem to find an $L(1, 0)$ -labelling of a graph is equal to finding a proper colouring of a graph. This means that for planar graphs we have the famous Four Colour Theorem, which can be stated in our notation as follows.

Theorem 1 [1, 2]

If G is a planar graph, then $\lambda(G; 1, 0) \leq 4$.

For general p it is easy to show that this gives the following.

Corollary 2

If G is a planar graph, then $\lambda(G; p, 0) \leq 3p + 1$.

We now start looking at the case $q \geq 1$. A straightforward argument shows that if G is a graph with maximum degree Δ , then an $L(p, q)$ -colouring of G needs at least $q \cdot \Delta + p + 1$ labels. Since planar graphs with arbitrarily large maximum degree exists, we can no longer expect to be able to find a constant upper bound on the p, q -span of planar graphs as we were able to do for the case $q = 0$ in Corollary 2. In fact, it is not too hard to construct planar graphs G with $\lambda(G; p, q) = \frac{3}{2}q \cdot \Delta(G) + c_1(p, q)$, where $c_1(p, q)$ is a constant depending on p and q only.

As far as upper bounds for $\lambda(G; p, q)$ are concerned, in [4] it is shown that $\lambda(G; 2, 1) \leq \Delta(G)^2 + \Delta(G)$. This suggest that for graphs in general the best possible upper bound for $\lambda(G; p, q)$ will be of the order $q \cdot \Delta(G)^2$. Our main result shows that for the case that G is planar, we can reduce the order of magnitude of the upper bound.

Theorem 3

If G is a planar graph with maximum degree $\Delta \geq 12$, then

$$\lambda(G; p, q) \leq (4q - 2) \cdot \Delta + 10p + 38q - 23.$$

Since we don't believe the dominant term $(4q-2)\cdot\Delta$ to be best possible, no effort has been made to find the best possible additive constants.

Theorem 3 has some interesting connections with known problems on graph colourings. This is since the special case $p = q = 1$ can be seen as a graph colouring problem. In order to find a $L(1, 1)$ -labelling, we are looking at a labelling φ of a graph G such that $\varphi(u) \neq \varphi(v)$ whenever $\text{dist}(u, v) = 1$ or 2. This is equivalent to colouring the square G^2 of G : G^2 is the graph defined by $V(G^2) = V(G)$ and two vertices u, v are adjacent in G^2 if $\text{dist}(u, v) = 1$ or 2 in G .

The question to find the best possible upper bound for the chromatic number of the square of a planar graph can be found in the literature. The problem seems to be posed for the first time by G. Wegner in 1977 (see [9, Section 2.18]). Wegner conjectures the following, when described in the notation introduced in the previous section.

Conjecture 4

If G is a planar graph with maximum degree Δ , then

$$\lambda(G; 1, 1) \leq \begin{cases} \Delta + 5, & 4 \leq \Delta \leq 7; \\ \lfloor \frac{3}{2}\Delta \rfloor + 1, & \Delta \geq 8. \end{cases}$$

Wegner also gives examples of planar graphs that show the upper bounds in the conjecture are best possible.

As far as we know, not much seems to be known about Conjecture 4. As a consequence of Theorem 3 we obtain the following result, which goes some way towards establishing the truth of the conjecture.

Corollary 5

If G is a planar graph with maximum degree $\Delta \geq 12$, then

$$\lambda(G; 1, 1) \leq 2\Delta + 25.$$

3. SKETCHES OF PROOFS AND ALGORITHMIC ASPECTS

The proofs of many results on planar graphs, including our Theorem 4, rely heavily on the property that planar graphs can be shown to obtain certain small, so-called unavoidable, configurations. For instance, it is well known that a planar graphs has a vertex of degree at most five. This fact was used by Heawood [8] to prove the weaker version of Theorem 1 that every planar graph is five colourable. The proof

of the Four Colour Theorem used a very large number of unavoidable configurations (see the beautiful collection of 633 unavoidable configurations in the Appendix of [10]).

For our proof of Theorem 4 we need a somewhat more involved structural result. The proof of the following lemma is based on discharging arguments as can be found in, e.g., [3].

Lemma 6

Let G be a planar graph. Then at least one of the following is true:

- (a) there exists a vertex in G with degree at most two;
- (b) there exists a vertex v in G of degree three such that if the neighbours of v are $\{u_1, u_2, u_3\}$ with $d_G(u_1) \leq d_G(u_2) \leq d_G(u_3)$, then $d_G(u_1) \leq 11$;
- (c) there exists a vertex v in G of degree four such that if the neighbours of v are $\{u_1, u_2, u_3, u_4\}$ with $d_G(u_1) \leq \dots \leq d_G(u_4)$, then $d_G(u_2) \leq 11$, $d_G(u_1) \leq 7$ and the edge vu_1 is contained in a triangle;
- (d) there exists a vertex v in G of degree five such that if the neighbours of v are $\{u_1, u_2, u_3, u_4, u_5\}$ with $d_G(u_1) \leq \dots \leq d_G(u_5)$, then $d_G(u_3) \leq 11$, $d_G(u_2) \leq 9$, $d_G(u_1) \leq 6$ and the edge vu_1 is contained in a triangle.

The existence of the specific vertices in Lemma 6 makes it possible to obtain an inductive proof of Theorem 4. The inductive step used is not the normal removal of a vertex, but the contraction of an edge. We'll leave the details, because they are not really enlightening.

The idea to reduce the labelling of a planar graph to that of the labelling of a smaller planar graph obtained by contracting an edge of the graph has an interesting counterpart if we look at the cellular network the graph originated from. Contracting an edge in the associated graphs corresponds to removing the border between two cells in the network. Thus the algorithm which underlies the proof of Theorem 4 can be paraphrased as follows in the cellular network:

Step 1: find a cell with a small number of neighbours and such that its neighbours also only have a relatively small number of neighbours, similar to the vertices in the lemma above;

Step 2: join the cell found in Step 1 with its neighbouring cell of smallest degree;

Step 3 : find a labelling of the smaller network (e.g. by repeating the algorithm);

Step 4: restore the border between the cells joined in Step 2, and give the original label of the large cell to the cell which is the neighbour of the cell found in Step 1;

Step 5: greedily assign a label to the cell without a label which was formed in Step 4.

The algorithm above will be able to finish the labelling if the number of labels is at least the number of labels given by the bound in Theorem 4. Of course, this bound assumes a worst case scenario, so in many cases a significant smaller number of labels will be enough. Also, because of its greedy structure it is unlikely that the algorithm will give a best possible labelling. Nevertheless, it seems an interesting problem to explore if the approach can be generalised to cellular networks in which the interference structure is more complicated than the one we have assumed in this note.

4. REFERENCES

- [1] K. Appel and W. Haken, "Every planar map is four colourable. Part I: Discharging", *Illinois J. Math.*, Vol. 21, 1977, pp. 429–490.
- [2] K. Appel, W. Haken and J. Koch, "Every planar map is four colourable. Part II: Reducibility", *Illinois J. Math.*, Vol. 21, 1977, pp. 491–567.
- [3] O.V. Borodin, "Structural properties of plane graphs without adjacent triangles and an application to the 3-colouring", preprint, 1994.
- [4] G.J. Chang and D. Kuo, "The $L(2,1)$ -labeling problem on graphs", *Siam J. Disc. Math.*, Vol. 9, 1996, pp. 309–316.
- [5] J.P. Georges and D.W. Mauro, "Generalized vertex labelings with a condition at distance two", *Congressus Numerantium*, Vol. 109, 1995, pp. 141–159.
- [6] J.P. Georges and D.W. Mauro, "One the size of graphs labeled with a condition at distance two", *J. Graph Th.*, Vol. 22, 1996, pp. 47–57.
- [7] J.R. Griggs and R.K. Yeh, "Labelling graphs with a condition at distance 2", *Siam J. Disc. Math.*, Vol. 5, 1992, pp. 586–595.
- [8] P.J. Heawood, "Map colour theorem", *Quart. J. Pure Appl. Math.*, Vol. 24, 1890, pp. 332–338.
- [9] T.R. Jensen and B. Toft, "Graph Coloring Problems", John-Wiley & Sons, New York, 1995.
- [10] N. Robertson, D. Sanders, P. Seymour and R. Thomas, "The Four-Colour Theorem", *J. Comb. Th.*, Vol. 70, 1997, pp. 2–44.
- [11] D. Sakai, "Labeling chordal graphs: Distance two condition", *Siam J. Disc. Math.*, Vol. 7, 1994, pp. 133–140.

BIOGRAPHICAL NOTES

Jan van den Heuvel has a Ph.D. from the University of Twente, Enschede, The Netherlands. Before his present position he has worked in Vancouver, Canada and in Oxford.

Sean McGuinness has a Ph.D. in Mathematics from the University of Waterloo, Canada. Before joining the University of Umeå he had positions in Lyngby and Odense, both in Denmark.

Research interest of both authors include discrete mathematics in general, with emphasis on graph theory, matroid theory, and algorithmic aspects.

XVI
WORKSHOPS

**European Union EMC Directive
in Practice**

Workshop Organizer:

M. C. Vrolijk - The Netherlands

EU EMC DIRECTIVE IN PRACTICE ANALYSIS OF THE IMPLEMENTATION OF THE EMC DIRECTIVE AFTER 2 YEARS BY A EUROPEAN COMPETENT BODY

Dr. Diethard Hansen
EURO EMC SERVICE (EES) Dr. Hansen GmbH, Germany
homepage: <http://www.euro-emc-service.de>

1. Introduction

Reporting from the first year after the implementation of the EMC directive, we concluded, nothing is perfect at the beginning and regulations need time to be optimised regarding their actual procedures. We also pointed out "Besides competition the market policing plays an important role to ensure fair competition and reduced barriers to trade." Although much progress has been made in the enforcement of the EMC in Germany (BAPT is now re-organised and called Reg. TP, which is reporting to the ministry of economic affairs since 1998-01-01), however the market place with the overwhelming majority of small and medium size companies still try to get a way doing nothing but affixing the CE mark and issuing a conformity declaration. Nobody says that testing is mandatory but how is a company going to prove due diligence in court without proper evidence to support their case. Prosecution in the UK (October 1997) already demonstrated to a computer assembler, CE + CE + CE is not CE, in spite of the fact that the new EMC guideline by the commission, June 1997, says so. If the testing of each individual CE marked component would have been done with due consideration of a later system integration, the legal formula could be correct.

2. European Association of Competent Bodies

The new set of guidelines is a very useful document, which was created among others, with the help of the Association of Competent Bodies (ACB). This started in Rom at the EMC conference in September 1997 and went all the way to the end. It is important to know, that this document has no legal status. Overall, the number of CBs has grown over 100 throughout the EU with the highest number in the UK and directly followed with about 30 in Germany. At the beginning of 1998 the EC-commission has initiated the formation of the ECACB. This organisation is no longer funded by its members (700 XEU per year). The new organisation works in co-operation with EOTC which will normally provide the administration, funded by the EC-commission. ECACB is similarly structured

as the equivalent Notified Body association. In this respect, mainly dealing with radio transmitters and TTE equipment, the legal situation is undergoing dramatic changes following the general trend of deregulation. ACBs major achievement is the harmonisation of CB decisions in Europe due to the technical working group's, technical guidance notes (TGN). About 7 representatives throughout Europe are working as technical experts (the author represents Germany). Some new TGNs (No. 13 - 20) deal with the following issues:

13. Testing frequency converters
14. Testing to EN 61000-3-2 (1995)
15. Conformity declarations including deviations from standards
16. EN 61800-3
17. Immunity failures within the TCF
18. CE + CE = ?
19. Application of generic standards where product specific standards exist
20. Manufacturers of Desk Top PCs, etc...

For the future it is not ruled out that ACB and ECACB will lead to a peaceful and fruitful coexistence. The ACB has furthermore given many professional presentations to educate the users of the directive around the world.

3. Still unresolved problems

Although the institution of the CB was originally more of a temporary nature, the CB are slowly but surely gaining acceptance both by the authorities as well as the clients. This is because they professionally fill an existing gap and help bridging an inherent, technical deficiency in some (harmonised) standards. This is to say in the field of product variances and deviations from the standards for technical or economical reasons, the TCF 3-rd party route by the Competent Body can lead to substantial cost savings. It goes without saying CBs can give the highest level of assurance in meeting the protective requirements of the directive. This comes at a higher

level of justification to have done everything as just the presumption of conformity under the self declaration route. CBs are nationally appointed legal entities which must have professional liability insurance. In most countries including Germany, market enforcement is entirely supported by tax payer's money. There are 54 field offices and more than 100 enforcement officers and some specialised EMC government labs. It is difficult to understand, why Germany does not involve those professional EMC Laboratories and CBs which their own accreditation office has successfully assessed. Does this mean, the Reg. TB does not trust their own accreditation effort? Other countries naturally do the opposite. Sometimes, the in principle admirable efforts of the German EMC market enforcement appear questionable in efficiency and drive. The PTT ministry change of the Reg. TB to the equivalent of the British DTI in Germany leads some German people and politicians to believe that the action against violations of the German EMC act are not fully taken serious. However, since recently the new Reg. TB can issue financial enforcement sanctions of up to 1 Mio. DM. Unfortunately this news doesn't really penetrate the market place. Consequently there are very many black sheeps which get a way with almost nothing. Very often the enforcement agency uses a totally unacceptable argument of "We can't be too harsh with the manufacturers in economically difficult times". Thinking this through, reveals exactly the opposite, namely a blank cheque to unfair competition. Unfair competition is introduced by those manufacturers, doing nothing in comparison to those fulfilling the requirements of the law and spending considerable money to get their products compliant.

Aside from the CBs there are more than 100 accredited EMC laboratories in Germany. EMC however, is not the only directive, which means the trend in the labs goes to one-stop-shopping in order to attract and keep customers. The accreditation is slowly but surely tightening the reaccreditation conditions for the laboratories to help sorting out the black sheeps from the white sheeps. How can a laboratory fulfil the required test time as given by the standards, while only asking for 30 % of the regular fees? There is a lot of unfair competition but the market forces and the clients

will certainly in the long run appreciate correctness, professionalism and reliability. An other trend may lead to outsourcing of services. This however, is not as popular as in North America and Asia.

4. Future perspectives

The never ending story of the conflict between overdoing the market surveillance or just letting go will certainly continue. There is always a need for professional services which are competitive and competent. Looking into the Crystal ball of global EMC, it becomes clear, compliance is more and more important to meet economical and regulatory constraints with due consideration of time to market. On the other hand it is pretty clear, testing is somehow local. The mutual recognition agreement (MRA) will certainly have an impact on the EMC business in Europe. Namely, the MRA with USA seems to be helping the US companies rather than the European side because export figures in electronics are much higher from the US to Europe than vice versa.

References

- [1] G. Jeromin, *EMV von Geräten*. Köln: Bundesanzeiger Verlag, 1996, 1th edition.
- [2] Unruh, Zeller, *CE-Kennzeichnung von Medizinprodukten*. VDE-Schriftenreihe 76. Berlin: VDE-Verlag, 1996.
- [3] D. M. Imeson, "The EU EMC Directive - The EU Competent Bodies" in *Workshop Notes IEEE 1996 Int. Symp. on EMC*, Santa Clara, August, 1996.
- [4] D. Hansen, "Situation for In-Situ Testing/Certification of Large Apparatus and Systems" in *Workshop Proc. EMC'96 Roma Int. Symp. on EMC*, Roma, Italy, Sept., 1996, WS No. 3.
- [5] W. A. Poggi, "EMC Laboratory Accreditation" in *ITEM UPDATE 1996*, pp. 7-9
- [6] *Proc. of the Reverberation Chamber and Anechoic Chamber Operators Group Meeting*, 5 - 7 Dec. 1995, NSWC Dahlgren, VA USA, March 1996
- [7] D. Hansen, D. Ristau, M. Loerzer "Analysis of the implementation of the EMC Directive after one Year by a European Competent Body" *Workshop, EMC 97*, Zurich, Supplement, Page 3 W1 ff.

ENFORCEMENT OF THE EMC DIRECTIVE IN GERMANY: TWO YEARS EXPERIENCE WITH MARKET SURVEILLANCE

Dipl.-Ing. Gerd Jeromin,
Regulatory Authority for Telecommunications and Posts (Reg TP)
Canisius Str 21, Mainz, Germany

Article 3 of the EMC-Directive 89/336/EEC determined, that Member States shall take all appropriate measures to ensure that all apparatuses covered by the directive and placed on the market bears the CE marking provided for in Article 10 indicating its conformity to the EMC protection requirements.

The German Competent Authority for enforcement of the EMC Directive (89/336/EWG) and the Telecommunications Terminal Equipment Directive (91/236/EWG), the Federal Office for Posts and Telecommunications (BAPT) started in 1995 their policing activities concerning market surveillance. The provisions concerning the testing of equipment on the market which have to be complied with in Germany are not only based on the EMVG (German EMC Act) but also on the Telecommunication Act (TKG) which transposed the TTE Directive into national law.

The German market for equipment covered by the EMC Directive contains about 250 million units per year. This is approximately 30% of the European market. Specifically, this includes:

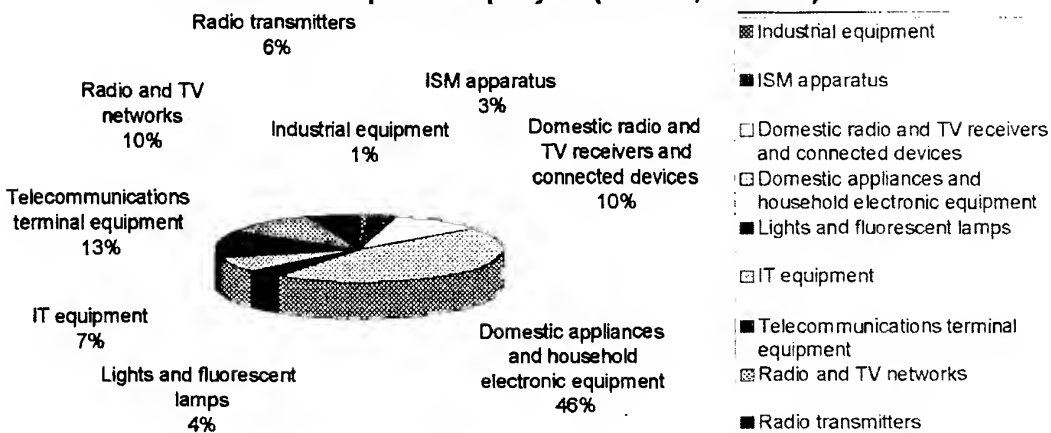
- 200 million apparatus per year
- 50 million components performing a direct function per year, comprising approximately
- 65,000 different types of equipment, placed on the market by
- 50,000 individuals and handled by
- 100,00 product providers and/or trade companies.

In 1997 the civil servants of the BAPT checked approximately 37,000 electrical products.

The result of this market surveillance and the system developed for this goal will be presented in the lecture.

Reg TP Measurement Strategie

Measurement quantities per year (total : 9,600 units)



Results of EMC market surveillance in Germany in 1997 by the Bundesamt für Post und Telekommunikation

In view of the vast number of items placed on the German market every year (approximately 200m. pieces of equipment, 50m components and 65,000 new equipment types) it is neither feasible nor envisaged to carry out tests on every single item. Hence a rating system based on the relevant product standards and market volumes was used for selecting 37,600 items which were then subjected to a visual inspection.

The tests were carried out for the first time on the basis of a new market surveillance strategy, using a newly developed software tool.

The results for 1997 revealed as many as 1,100 cases involving shortcomings in the CE marking, corresponding to 3% of all tested products.

A total of 4,410 EC declarations of conformity had to be presented, of which 2,498 did not meet requirements or were not submitted before the specified deadline.

1,535 of the 37,600 individual items, i.e. roughly 4% of the tested products, were placed on the market by other EEA Member States as shown in the table below.

Belgium	92 items	6%
Denmark	53 items	3%
France	141 items	9%
Great Britain	174 items	11%
Italy	399 items	27%
Netherlands	422 items	28%
Austria	139 items	9%
Other EEA countries	115 items	7%

In the second half of 1997 a total of 119 defects were identified in items placed on the market by the "Other EEA countries".

In 51 cases the marking obligation requirements had not been met.

In 48 cases shortcomings were discovered in the EC declaration of conformity.

In 20 cases the EMC protection requirements had not been satisfied.

In all cases the competent authorities were notified of the findings to enable them to take corrective measures.

Tests on several production models in a series (i.e. excluding single measurements on unique products) yielded the following results.

Product Categories			
Product category	Tested items	Nonconforming	Percentage
1 Domestic appliances	1556	285	18%
2 Electr./electronic eq.	1180	379	32%
3 Illumination facilities	262	109	42%
4 IT/office equipment	178	50	28%
5 Consumer electronics	203	103	51%
6 Telecoms app.	153	25	16%
7 Radiocomms equip.	5	0	0%
8 Industrial equip.	65	10	15%
9 Medical devices	5	0	0%
10 Scientific equip.	10	5	50%
11 Wiring mat./access.	35	5	14%
12 Other	40	5	13%

In the above table, "nonconforming" means that the EMC protection requirements had not been fulfilled.

In 120 cases administrative fines proceedings were instituted against the parties who had placed the items on the market. The administrative fines varied between DM 100.- and DM 30,000.-. In addition, charges in accordance with the EMC Cost Ordinance were levied in 100 of these cases.

In 23 cases the item was no longer permitted to be placed on the market and the safeguard clause in the EMC Directive was invoked, i.e. the Commission was notified of the restriction in the placing on the market. In such cases the Commission informs the other EEA countries of the sanctions imposed.

EMC 98

**INTERNATIONAL WROCŁAW SYMPOSIUM
ON ELECTROMAGNETIC COMPATIBILITY
WORKSHOP**

**IMPLEMENTATION OF THE EU-EMC DIRECTIVE:
ADDED VALUE OF THE EMC GUIDELINES**

E. Santiago, European Commission, DGIII
Brussels, Belgium

Materials available during presentation

THE EMC DIRECTIVE: A MANUFACTURER'S PERSPECTIVE

S.P. Scott, IBM (UK) Ltd., Greenock, Scotland

Abstract: The paper outlines a manufacturer's experience of the EMC Directive from its draft consultation stage, through its publication in the "Official Journal", its transition period, and finally during its first two years as a mandatory requirement. An outline is presented of the evolution of this manufacturer's approach to compliance and the assessment of conformity. Some of the encountered difficulties are discussed and some solutions suggested. The paper concludes by looking to the immediate future and offering advice on how manufacturers might become more pro-active in their approach.

1. INTRODUCTION

Although the EMC Directive has been mandatory since January 1 1996, many manufacturers' experience of it goes back somewhat further; in the UK, the Institution of Radio and Electronic Engineers held a colloquium on the (then draft) EMC Directive in February 1988. For the 400 or so attendees, it was the their first acquaintance with the draft text. The original Directive was published in the "Official Journal of the European Communities" on May 23 1989. The Directive was in fact mandatory on January 1 1992, until the issuing of the amending Directive on April 28 1992 provided for the transition period.

2. THE APPROACH TO CONFORMITY

It was obvious from the outset that EN 55022 would be the emission standard for ITE, and compliance with this standard became a design objective for our products around 1988; as CISPR 22 it was also becoming a legal requirement in some countries around that time. Five emission standards in the EN 550XX series were listed in the "Official Journal" on February 19 1992.

2.1. Technical construction file approach

For most product types, no immunity standard existed on January 1 1992. EN 50082-1, the generic immunity standard for residential, commercial and light industrial environments was published by CENELEC later that month and was listed in the "Official Journal" in April 1992. Strictly, therefore, the Technical Construction File (TCF) was the only method of demonstrating conformity until that date, although the UK Department of Trade and Industry stated informally that they would take no action on products for which conformity was based on EN 50082-1 and the appropriate emission standard.

In fact, although the three immunity tests specified in EN 50082-1 were widely anticipated, few products already on the market before 1992 had been designed to comply with them, and in reality the TCF was the only alternative for many manufacturers. The EMC community in my own company had already agreed a format and content for a TCF for our products; it was based on compliance with a set of company standards on immunity, developed over many years in response to EMC problems in the field. The appointment of competent bodies was, quite reasonably, assumed by the competent authorities of the Member States to be their responsibility (although the EMC Directive does not state this); but in early 1992 none of the Member States had enacted the national legislation giving their competent authorities the legal instrument to do this. Fortunately, however this did not seem to present a problem in the Netherlands, and we were able to use the services of competent bodies appointed in that country early in 1992.

2.2. Harmonised Standards approach

In the latter part of 1991, as the immunity requirements under the harmonised standards approach began to emerge, products entering the design phase had these requirements included in their design

objectives. Since the design principles needed to comply with our broadly-similar company EMC standards were already embodied in the products, the major effort was in purchasing new test equipment and/or adapting existing test equipment to perform the new tests. By mid-1992, we were able to place on the market product types complying with the applicable harmonised standards, and have continued to do so since then, while keeping aware of the continuously-evolving standards situation.

2.3. Company standards

During the last five years, answering queries from all parts of the company, as well as discussing broader issues in an industry-wide forum, has enabled me to crystallise my ideas on how and if the Directive applies in various situations, and on how to approach the assessment and attestation of conformity. These ideas have been embodied in a company standard which draws together the general information contained in the Directive itself, in the European Commission guideline to the application of the EMC Directive, and in the lists of standards published in the "Official Journal". The information is tailored to express it in a way relevant to the company's products and reflecting my interpretation, where necessary. It specifies the scope of the Directive, as far as is relevant to our products, outlines the applicable technical requirements under the harmonised standards and Technical Construction File approaches, and specifies how we have chosen to address the conformity assessment procedures and filing requirements. Reference is made to other company standards, which specify in detail the test methods and performance requirements for each test.

I consider it a worthwhile effort to write these standards and keep them up to date, rather than to direct people to the appropriate CENELEC product, generic and basic standards. In the company standards, the technical requirements of the CENELEC standards are tailored to apply to our product range. Where the CENELEC standard is ambiguous or unclear, the company standard reflects my interpretation. For example, the operating conditions and performance criteria in the generic immunity standards are necessarily of a very general nature. The company standards can be much more specific.

By having one standard for each test, it is possible, in the case of the immunity standards, to draw together the test levels for that test for the two environments covered by the generic standards, with the test method from the appropriate basic standard, and performance criteria expressed in a way relevant to the company's products. Future changes to the CENELEC standards, still in the draft stage, are included in the company standards as Annexes for information only.

2.4. Joint EC Declarations of Conformity

Until 1995, most EC Declarations of Conformity addressed only the EMC Directive, and were processed by the EMC Laboratory. From 1995, by virtue of the so called "CE Mark Directive", it became optional, for most products, to include the Low Voltage Directive on the Declaration. From 1997, it became mandatory to do so. We have developed a format for the Declaration in which the Directives are listed on a front sheet with a signed statement of conformity. For each Directive, a schedule is attached, listing the harmonised standards applied under that Directive, and details, where applicable, of any notified or competent bodies which were involved in the conformity assessment.

The assessment of conformity with the Low Voltage Directive is undertaken by a separate Product Safety function; the EMC Laboratory co-ordinates the assessments and processes the Declaration.

As more Directives become applicable, and as the product range diversifies so that some products fall within the scope of other Directives, this co-ordination will become much more difficult.

3. ADDRESSING THE ISSUES

3.1. Customer awareness

The high level of customer awareness of the EMC Directive was quite unexpected. We receive many queries concerning compliance with EMC standards; sometimes the queries concern draft or inapplicable standards, so that the answer is not straightforward. Customer demand for copies of EC Declarations of Conformity has been overwhelming. At the peak of the demand in 1995, my site alone was dealing with five or six requests per day, some requesting lengthy lists of Declarations. This led the company to establish a corporate database of compliance documents, where the site processing a certification loads an image of the documents onto the database. Any person needing a copy of a Declaration, in order to respond to a request from a customer or from a national authority, can access the database and print the image at his own location.

Most of the company EMC laboratories now have web sites on the company Intranet, from which images of the EC Declarations processed by that laboratory are available. Test reports (which are generally too large for the compliance database) can be accommodated at the web sites; these are frequently needed for national certifications in various countries, and may be accessed by company officers in those countries for that purpose.

3.2 Components

During 1995 and 1996, there was much discussion on the extent to which components were covered by the EMC Directive, insofar as separate conformity assessment and CE Marking was required. At the same time, the Commission were debating the same subject in meetings with government and industry experts, so that it could be addressed in the EMC Directive guidelines. The new criterion for applicability (for components "placed on the market" within the meaning of the Directive) is the performance of a "direct function for the end user". Even this is open to different interpretations, particularly as applied to CPU and memory modules. I have suggested that the IT industry associations should establish an industry-wide agreement on which of its components satisfies this criterion, in the interests of keeping a level playing field. My personal preference would be for the Directive to apply to all components capable of generating a disturbance (and which are placed on the market); this is a much easier concept to understand. Since all components will have been included in the configuration for the testing of at least one product type (usually several), there is no need to perform a test specifically for a component. To reduce the burden of processing Declarations of Conformity for hundreds of components, where possible we group them into families of similar components, and issue one Declaration for the whole family (e.g. parity single inline memory modules). The Declaration has an Appendix listing all the part numbers in the family and identifying the product type in which they were tested. Each test report routinely includes the component list by part number for the product which was tested, so this provides a cross-reference in the conformity documentation.

3.3 The harmonics debacle

By far the most cost in expense and man-hours were incurred over the harmonics standard EN 61000-3-2. This issue merits description in some detail, not least because of the chaos it has caused. In order to understand the problem, it is necessary to understand how revisions to standards are implemented by CENELEC. Each standard includes a foreword, which specifies a "date of withdrawal" which is the latest date by which any conflicting standards must be withdrawn, and some forewords also include a "certification clause". CENELEC have a Memorandum No. 6, under which certification clauses allow voluntary product certifications to the previous version of a standard to be valid for a limited period after that version has been withdrawn. At the time, in the absence of any contradiction from the European Commission, it was assumed that certification clauses were also valid for the purposes of the EMC Directive.

EN 61000-3-2 was a more complex case; its scope was very much enlarged from that of the earlier standard EN 60555-2, which covered only household appliances. EN 61000-3-2 had been some years in the making in IEC (the CENELEC version had been approved at the final draft stage in a parallel vote with the IEC version) and most companies were aware of it. However, its publication in May 1995 caused widespread alarm. Although the certification clause was understood as allowing products certified to EN 60555-2 before January 1 1996 to continue in production until January 1 2001, it was assumed that products outside the scope of EN 60555-2 had to comply with EN 61000-3-2 (if using the "harmonised standards" approach) by the specified date of withdrawal, July 1 1997, a date which most manufacturing industries considered to be unachievable. Although the "date of withdrawal" strictly has no meaning for such products, there being no conflicting standard to withdraw, I verbally confirmed the above interpretation with the Chairman of the responsible CENELEC committee.

Worse was to follow. It was soon realised that, unlike its companion EN 61000-3-3 on voltage fluctuations and flicker, the foreword did not explicitly provide for any delay in application for products which were outside the scope of the earlier standard, and could be construed as implying that the new standard applied immediately to these products. The matter was raised with CENELEC, and at a meeting in September 1995, attended by representatives of the electricity supply industry (the driving force behind the production of the standard), and various manufacturing industries, it was agreed that CENELEC would propose an amendment (A12) changing the date of withdrawal to June 1 1998, and explicitly exempting products outside the scope of EN 60555-2 until that date. The amendment was subsequently approved by the national committees.

Within a week of the September meeting, however, EN 61000-3-2 and EN 61000-3-3 had been listed in the "Official Journal", and the Commission were reported to have said that since the foreword was not legally part of the standard, it was applicable immediately. The logic of this is difficult to follow, because an amendment to EN 60555-3 was listed in the same table in the "Official Journal", and following this reasoning, EN 60555-3 should have been made obsolete by the listing of EN 61000-3-3!

The matter was debated at great length at meetings of the Commission with government and industry experts in November and December 1995. The Commission acknowledged that manufacturers would not be able to comply with the standard for some time, but insisted that some alternative action would have to be taken from January 1 1996 when the Directive

became mandatory. The use of a Technical Construction File (TCF) was discussed, but the fact is that many products produce harmonics because compliance with harmonics limits was never in their design objectives as it was not a requirement at that time, and no TCF can alter that fact. A TCF might be used for product types which are in service in very low numbers and low geographical concentrations, thus presenting a low risk of interference; but a consultation within the IT industry showed that there were still large numbers of products to which this argument did not apply. In any case, the industry representatives at the meeting objected in principle to being forced to use a TCF from the moment a standard was changed, if the product was unable to comply with it immediately. The implication is that this would be necessary every time a new or revised standard is published.

Another suggestion was to apply the generic emission standard EN 50081-1. This specifies no harmonics or flicker requirements for products outside the scopes of ENs 60555-2 and -3.

Applying EN 50081-1 causes another problem; it requires compliance with the Class B limits of EN 55022 at radio frequencies (150 kHz - 1 GHz), even for an industrial IT product, which would generally comply only with the more relaxed Class A limit. Even more absurdly, it would require ISM or professional lighting equipment to comply with the EN 55022 Class B limit. Of course, these products have product-family standards (EN 55011,

EN 55015) with completely different limits (generally much more relaxed than EN 55022 Class B), and these take precedence over EN 50081-1. Applying these standards would mean that

EN 50081-1 were being applied only in part (i.e. at frequencies covered by harmonics and flicker standards), and the product-family standards were being applied at radio frequencies. At the time, I verified with CENELEC that generic standards are not intended to be used in this way. In any case, it is not possible for an EC Declaration to make reference to part of a standard. On the other hand, there is also a difficulty in claiming that a product-family standard covering only radio frequencies takes precedence over a generic standard which covers a wider frequency range. A standard cannot strictly take precedence over another unless it covers the same frequency ranges or disturbance types.

In 1997, the situation was considered in the wider context of the general principle for the transitional arrangements for new and revised standards under the EMC Directive, which is discussed in detail below. At one point the problem appeared to be resolved by a proposal to include notes with the references to ENs 61000-3-2 and -3 in the "Official

Journal", stating explicitly that compliance under the harmonised standards approach for products outside the scope of the old ENs 60555-2 and -3 would be required from June 1 1998. Further ENs in the 61000-3-X series are planned, specifying harmonics and flicker limits for products with input current greater than 16 A. It is intended that these also provide alternative means of compliance for products which are unable to comply with ENs 61000-3-2 and -3 (by allowing connection on a conditional basis). Because there was no likelihood of these new standards being completed until well after June 1 1998, the CENELEC Technical Board (BT) decided to change the dates of withdrawal for ENs 61000-3-2 and -3 to January 1 2001, so that manufacturers could avoid expensive redesigns of their products which would no longer be necessary when the alternative methods of compliance, provided by the new standards, became available. They also deleted the aforementioned notes from the standards list to be forwarded to the European Commission for publishing in the "Official Journal", throwing the situation for products newly in the scopes into confusion once again. There were many different interpretations of the situation expressed in various sectors of industry.

In July 1997, the BT initiated a vote to withdraw the amendment A12, and this was approved by the national committees. Corrigenda were issued to the forewords of ENs 61000-3-2 and -3, in which the dates of withdrawal were confirmed as January 1 2001, but deleting the explicit delays in application for products outside the scopes of the earlier standards.

Later the BT, in conjunction with the Commission, produced an "informative letter", attempting once more to clear up the confusion, and distributed it to the national committees. The letter was vague and difficult to follow, but it seemed to suggest (though not explicitly) that either the generic emission standard EN 50081-1 or the Technical Construction File provided the solution. These were precisely the arguments which had been debated in 1995, i.e. progress had been set back two years!

The Commission have subsequently issued a discussion paper which confirms the EN 50081-1 alternative. Their intention to delay the mandatory application of ENs 61000-3-2 and -3 under the harmonised standards approach is clear, even if the method of reaching this conclusion is problematic. The IT industry therefore agreed that it would regard January 1 2001 as the mandatory date for compliance with ENs 61000-3-2 and -3.

The problems with EN 61000-3-2 were not just related to its effective date; several technical ambiguities have been discovered, which mean that different laboratories may test in different ways and obtain different results on the same product, and different test equipment would yield different results on

the same product. A CENELEC Working Group continues to try to resolve these problems, but meanwhile the CENELEC BT complain about what it calls the "unceasing pressure on EN 61000-3-2." This is a disappointing response. Standards which define limits for such a vast range of different products are always going to be fraught with difficulty. The concerns raised by the IT industry have had a particularly high profile, but the UK national committee for low-frequency EMC have also considered concerns raised by the lighting, refrigeration, heating and ventilation industries that low-frequency emission limits will exclude some of their products from the market. Surely, it makes no sense for a limit to apply to an enormous diversity of product types which have greatly differing potentials for causing interference because of, for example, the differing numbers in service and differing degrees of simultaneity of use. Interestingly, the Introduction which appears in all the IEC 1000 / EN 61000 series of standards implies that there is a possibility of product committees setting their own immunity limits, but not their own emission limits. Perhaps the view is that the consequences of excessive emissions are more serious, and therefore product committees are not to be trusted to set their own limits. However, in CISPR, several product subcommittees set their own RF emission limits, and these have proved perfectly adequate for the protection of the RF spectrum.

3.4 Transitional arrangements for standards

The harmonics issue finally brought to a head the problem of transitional arrangements for new and revised standards. It is clear that the certification clauses cannot be included in standards which confer on a product the presumption of conformity with a New Approach Directive; in the Commission's words, "... a standard cannot give exemptions from requirements regarding the placing on the market of products covered by New Approach Directives ...". CENELEC are taking steps to delete the certification clauses from all standards which have been listed in the "Official Journal" in connection with New Approach Directives. In most cases, the date of withdrawal has been amended to coincide with the date specified in the former certification clause.

Fortunately, the Commission do acknowledge the need for sufficient time for manufacturers to adapt product designs to new standards and to continue manufacturing to old designs until the new ones are ready. They have agreed on a method of presentation of standards in the "Official Journal" in which a "date of cessation" of the presumption of conformity conferred by the old standard is specified. This date will normally be the same as the date of withdrawal specified in the foreword. At the time of writing, however, this presentation fails to address two important cases, in

which there is no superseded standard, and for which the date of cessation of presumption of conformity therefore has no meaning:

1. The case where a new standard supersedes no previous standard, e.g. the European versions of the future IEC 1000-3-9 and 1000-3-10.
2. The case where a new standard supersedes a standard with a narrower scope; for products outside the scope of the previous standard, there is no superseded standard. This is the precisely the "EN 61000-3-2" problem.

In these cases the presentation in the "Official Journal" must include a statement giving meaning to the date of cessation of presumption of conformity, i.e. it must state explicitly that a product newly in the scope of the standard, but which does not comply with it, may continue to enjoy the presumption of conformity with the essential requirements until the specified date of cessation, provided of course that it complies with all other applicable standards whose dates of cessation have passed.

As noted above in the discussion of the EN 61000-3-2 problem, this solution, in the form of notes annotated to the "Official Journal" references for ENs 61000-3-2 and -3, has been considered, but seems to have been rejected. The probable reason is the Commission's view, expressed during the deliberations on the EN 61000-3-2 problem, that since the new standard represents an essential requirement, a product must still conform to the essential requirement even if it is exempt from the standard.

This leads to an impossible scenario. The essential requirements cover all frequencies and all disturbance types capable of causing interference. This implies that until there are standards for all such frequencies and disturbance types, a TCF must be used. The standards committees are producing more and more new standards (see the discussion below on the proliferation of standards); how will we know when the process is complete? It shows no signs of ever being complete. Most manufacturers do not know about a standard, and certainly have not seen its contents, until it is published. Until then, it is unlikely that a product will have design objectives to limit emissions at frequencies covered by new emission standards and certainly it will have none to establish immunity to disturbances covered by new immunity standards. As noted in the harmonics case, a TCF is no help.

But the above scenario is inconsistent with the fact which has allowed us to claim conformity with the Directive since 1992; that compliance with the applicable harmonised standards, which cover only emissions in the 150 kHz - 1 GHz range and immunity to three types of disturbance, nevertheless confers the presumption of conformity on our products.

These problems could be solved, together with those arising from trying to apply only part of EN 50081-1 as a way out of the EN 61000-3-2 problem, if all the product and product-family standards at present covering radio frequencies had their scopes extended to cover all frequencies. For radio frequencies, the limits should be unchanged. For harmonics and flicker (50 Hz - 2 kHz), they could invoke ENs 61000-3-2 and -3. For other frequencies, they could either specify "no limits" or "limits under consideration". The revised product and product-family standards could be given dates of withdrawal of January 1 2001.

There would then be no doubt that ENs 61000-3-2 and -3 are not mandatory until January 1 2001, and no need to try to apply some parts of the generic standard but not others in order to reach this conclusion.

It would only be necessary for two standards to apply to a product; one emission standard and one immunity standard. Each could be either a generic, product, or product-family standard. Standards such as ENs 61000-3-2 would only apply when invoked by a generic, product or product-family standard.

In order to introduce limits at frequencies where previously there were none, e.g. those specified by the European versions of the forthcoming IEC standards 1000-3-9 (limits for interharmonics between 50 Hz and 2 kHz) and 1000-3-10 (limits at frequencies between 2 kHz and 9 kHz), the generic, product and product-family standards should be amended to invoke the new limits; the amendment should be listed in the "Official Journal" with an associated date of cessation, until which the unamended standards, without the new limits, would still confer the presumption of conformity on products. This would correspond exactly to the way in which new immunity requirements are introduced today; there is no justification for any difference.

This method would also resolve the paradox, discussed above, about having to use a TCF for frequencies not at present covered by standards.

3.5. Proliferation of standards

One might have expected work on the development of EMC standards to decline as 1996 approached; in fact the reverse appears to be true. The IEC 1000-4-X series of test method basic standards (parallel voted and published by CENELEC as EN 61000-4-X) now has seventeen parts either published or in draft, specifying immunity tests to various types of disturbance (and several more parts specifying test equipment and facilities). Each immunity test is a potential candidate for inclusion in the generic immunity standards. It is difficult to argue against their inclusion there, because those standards cover such a wide range of equipment that, for each phenomenon, it

may be possible to conceive of a situation where some type of product may be affected.

In addition to the conducted and radiated emission tests required by the appropriate radio-frequency emission standard, the great majority of products are also subject to the requirements of IEC 1000-3-2 and -3-3, and in future, those of 1000-3-9 and -3-10 also. It is therefore not inconceivable that at some future time, products will have to undergo a total of 23 tests, possibly more if further new standards projects continue to be initiated. There is no technical justification for the burden that this would place on manufacturers, and no commercial justification for the cost which would be ultimately borne by the consumer, with no tangible benefit for him. Although the existing overview of immunity tests in EN 61000-4-1 (1992) does little to alleviate these concerns, a draft amendment is more explicit in stating which immunity tests are relevant to which environments; some, indeed, are designed only for special cases. IEC have confirmed this view in correspondence with IT trade associations. However, some of the CENELEC national committees hold the view that a standard cannot confer the presumption of conformity unless it addresses all these types of disturbance.

In the interests of striking a balance between the immunity of a product and the cost which is added by the testing, it is the author's opinion that after the current revisions to the generic immunity standards are complete, there should be a standstill on new standards for at least two years, after which an evaluation should be made of the EMC situation, and consequently of the need or otherwise for further standards. In the interim, the standards bodies might review their existing standards for technical and editorial improvements. After the standstill, standards projects should only be initiated as required to address real-life EMC problems.

3.6. Reconfigured equipment

The question of the applicability of the Directive to second-hand equipment, in service before the Directive's mandatory date, if that equipment is then reconfigured and then re-sold, was raised late in 1995. The Directive itself says nothing about second-hand equipment, whether modified or not. The definition of "placing on the market" in the Commission 1993 guideline excludes second-hand equipment which has already been made available in the EU, but does not consider modified equipment. The UK Regulations implementing the Directive exempt second-hand equipment, except that which has been reconditioned or modified so as to substantially change its EMC characteristics. This has a potentially serious impact on the reconditioning business, which is worth billions of dollars annually. The matter was considered by the Commission with government and industry experts in November 1996. The outcome was that the Directive is

considered to apply to a product which has already been placed on the market in the EU, and which is re-sold after modifications which are such that its performance becomes equivalent to an "as-new" product. However, a product which has only been placed on the market outside the EU, and which is then reconfigured and placed on the market in the EU, is subject to the requirements of the Directive whether or not it is "as new".

4. CONCLUSION

The Commission published a new EMC Directive guideline in 1997. This clarifies many matters left unclear or not addressed in the 1993 guideline, and reflects a more pragmatic approach. Although it is not a legal instrument, the competent authorities of the fifteen Member States participated in its production, and manufacturers can therefore feel fairly safe in following its advice.

However, the scope of the EMC Directive is so wide-ranging that it would be naive to expect any guideline to answer every possible question about every possible situation. Inevitably, situations will still be found where the manufacturer will have to interpret the available information and make a decision about what to do. So long as this is defensible, based on sound common sense and is well-documented, there should be little chance of falling foul of a national authority to the extent of prosecution, if the authority should have a different interpretation; the authority's view will take precedence as far as the product is concerned, but it is

to be hoped that the manufacturer will be considered to have been acting in good faith.

Various European industry associations were invited to participate in the drafting of the guideline. This emphasises the importance for manufacturers to participate in such associations; they are also a more general vehicle for manufacturers to make their views known to the Commission.

Participation in national trade associations is also important. Apart from being a vehicle for lobbying, they are the base level at which manufacturers participate in the standards-making process; recognised trade associations send delegates, with voting rights, to the national EMC committees which decide the national input to the IEC, CISPR and CENELEC standardisation process.

February 1998

The author wishes to point out that the views expressed herein are his own, and not necessarily those of his employer.

Steve Scott
Standards Project Authority, European EMC Requirements

EUROPEAN UNION EMC DIRECTIVE IN PRACTICE TELECOMMUNICATIONS EQUIPMENT

Christian M. Verholt
Danish Standards Association
Kollegievej 6
DK - 2920 Charlottenlund
Denmark

General: This presentation will present the status of EMC standards applicable to telecommunications equipment.

1. Introduction

The EMC Directive gives the manufacturer or importer of non-radio communications equipment three ways to validate compliance with the essential requirements: Compliance with National standards, harmonised standards or technical files. All three options have a special set of conditions which can be found in the Directive (ref.1) or in the published guide (ref.2). Telecommunications equipment designed for transmission of radio communications shall, as stated in the EMC Directive Clause 10.5, be type approved by a notified body so that the provisions of the EMC Directive are met.

2. Radio communications equipment

The notified body will normally use EMC standards developed by ETSI or other relevant documents giving the presumption of conformity to the essential requirements.

At present, the following standards have been published by ETSI:

ETSI 300 127 Radiated emission testing of physically large telecommunication systems

ETSI 300 162 Radiotelephone transmitters and receivers for the maritime mobile service operating in VHF bands

ETSI 300 279 ElectroMagnetic Compatibility (EMC) standard for Private land Mobile Radio (PMR) and ancillary equipment

ETSI 300 329 Electro-Magnetic Compatibility (EMC) for DECT equipment

ETSI 300 339 General electromagnetic compatibility (EMC) for radio communications equipment

ETSI 300 340 Electro-Magnetic Compatibility (EMC) for European Radio Message System (ERMES) paging receivers

ETSI 300 342-1 Electro-Magnetic Compatibility (EMC) for European digital cellular telecommunications system

ETSI 300 342-2 Electro-Magnetic Compatibility (EMC) for European digital cellular telecommunications system

ETSI 300 385 ElectroMagnetic Compatibility (EMC) standard for digital fixed radio links and ancillary equipment

ETSI 300 386-1 Public telecommunication network equipment Electromagnetic Compatibility (EMC) requirements;

ETSI 300 386-2-2 Telecommunication network equipment; Electro-Magnetic Compatibility (EMC) requirements;

ETSI 300 386-2-3 Public telecommunication network equipment Electromagnetic Compatibility (EMC) requirements

ETSI 300 386-2-4 Public telecommunication network equipment Electromagnetic Compatibility (EMC) requirements;

ETSI 300 445 Electro-Magnetic Compatibility (EMC) standard for wireless microphones and similar

ETSI 300 446 Electro-Magnetic Compatibility (EMC) standard for second generation Cordless Telephone (CT2) apparatus

ETSI 300 447 ElectroMagnetic Compatibility (EMC) standard for VHF FM broadcasting transmitters

ETSI 300 673 ElectroMagnetic Compatibility (EMC) standard for 4/6 GHz and 11/12/14

GHz Very Small Aperture Terminal (VSAT)

ETSI 300 680-1 ElectroMagnetic Compatibility (EMC) standard for Citizens' Band (CB) radio and ancillary equipment

ETSI 300 680-2 ElectroMagnetic Compatibility (EMC) standard for Citizens' Band (CB) radio and ancillary equipment

ETS 300 682 ElectroMagnetic Compatibility (EMC) standard for On-Site Paging equipment
ETS 300 683 ElectroMagnetic Compatibility (EMC) standard for Short Range Devices (SRD)
ETS 300 684 ElectroMagnetic Compatibility (EMC) standard for commercially available amateur radio equipment
ETS 300 717 Electro-Magnetic Compatibility (EMC) for analogue cellular radio communications equipment
ETS 300 741 ElectroMagnetic Compatibility (EMC) standard for wide-area paging
ETS 300 826 ElectroMagnetic Compatibility (EMC) standard for 2,4 GHz wide band transmission systems
ETS 300 827 ElectroMagnetic Compatibility (EMC) standard for Trans-European Trunked Radio (TETRA)
ETS 300 828 ElectroMagnetic Compatibility (EMC) for radiotelephone transmitters and receivers
ETS 300 829 ElectroMagnetic Compatibility (EMC) for Maritime Mobile Earth Stations (MMES)
ETS 300 830 ElectroMagnetic Compatibility (EMC) for Receive Only Mobile Earth Stations (ROMES)
ETS 300 831 ElectroMagnetic Compatibility (EMC) for Mobile Earth Stations (MES)
ETS 300 832 ElectroMagnetic Compatibility (EMC) for Mobile Earth Stations (MES) providing
ETR 077 Spurious radiation limits to and from satellite earth stations, Very Small Aperture Terminals (VSATs)
ETR 108 GSM Electro Magnetic Compatibility (EMC) considerations (GSM 05.90)
ETR 127 Electrostatic environment and mitigation measures for Public Telecommunications Network (PTN)
ETR 151 Electromagnetic Compatibility (EMC) testing of telecommunication equipment above 1 GHz
ETR 238 for the development of Harmonized Standards related to Electro-Magnetic Compatibility (EMC) in the field of TTE
ETR 357 GSM Electro Magnetic Compatibility (EMC) considerations (GSM 05.90 version 5.0.0)

For ports where the manufacturer finds that the ETSI standards do not offer adequate test levels and/or test methods, it is possible to use other standards e.g. the generic standards or the ITE standards prepared by IEC CISPR G (CISPR 22 and CISPR 24).

3. Telecommunications Terminal Equipment

Telecommunications equipment incorporating processing devices - micro processors - shall comply with EN55022 which is the emission standard for ITE equipment.

Telecommunications equipment not incorporating micro-processors, shall comply with the generic

standards EN50081-1 or EN50081-2 depending on the intended place of use.

For most telecommunications equipment there is no harmonised immunity standard and consequently the generic standards shall be used.

At present an European modification is being developed on the basis of IEC CISPR 24. When finished and harmonised EN55024 can be used.

4. Telecommunications Network Equipment

The Guide to the EMC Directive addresses the problem of installations in clause 6.5.2. The conclusion is that the installations shall fulfil the essential requirements, but if the installation is not put on the market as a single unit, it is not required to affix a CE-label on the installation. In practise, most networks consist of a number of individual equipment often from different manufacturers, and therefore it is normal practice to require that each individual equipment is CE-labelled. ETSI is developing standards for equipment for telecommunications network intended for use in switching stations. At present, none of the published standards have been harmonised.

5. Future

The European Commission is presently working on a major modification of the TTE Directive. One of the changes is an introduction of manufacturers self declaration as we know it from the EMC Directive Clause 10.1. The draft Directive includes both radio and non-radio based terminal equipment.

6. References

1. Council Directive 89/336/EEC of 3 May 1989 on the approximation of the laws of the Member States relating to electromagnetic compatibility.
2. Guidelines on the application of Council Directive 89/336/EEC of 3 May 1989 on the approximation of the laws of the Member States relating to electromagnetic compatibility, published 1997.

BIOGRAPHICAL NOTE

Christian M. Verholt

Project manager of an EMC testlab in Jutland Telephone Company, Denmark, 1977 to 1990. Active in EMC standardisation since 1982 and member of IEC TC77, TC77B, TC85, CISPR (S, E, G); Cenelec TC210, SC210A TC211, TC215.

Project manager in Danish Standards Association since 1995 with responsibility for standardisation of EMC and telecommunications equipment.

EXPERIENCES OF INDUSTRY WITH THE EMC DIRECTIVE

M.C. Vrolijk

Corporate Standardization Department

Nederlandse Philips Bedrijven B.V.

P.O. Box 218, 5600 MD Eindhoven, Netherlands

1. Introduction

The entering into force of the EMC Directive on the 1st January 1996 was already postponed for four years due to the lack of product standards on emission and on immunity for a great number of products and due to the lack of knowledge of manufacturers of the immunity characteristics of their products.

To cover a variety of products the approach of generic standards was invented related to the intended product environment. However, the generic standards are in many respects too vague for application to a variety of products. The performance criteria in the immunity standard leave open many options for product specifications. Therefore the transition time was used to prepare a number of product specific EMC standards.

2. Published standards in the OJEC

On the 1st of January 1996 five lists of EMC standards and/or amendments have been published in the Official Journal of the European Communities (OJEC):

C44	dated 1992-02-19	related to 9 standards;
C90	dated 1992-04-10	related to 2 standards;
C49	dated 1994-02-17	related to 13 standards;
C241	dated 1995-09-16	related to 11 standards;
C325	dated 1995-12-06	related to 5 standards;

followed by the next publications:

C60	dated 1996-02-29	related to 2 standards.
C37	dated 1997-02-06	related to 10 standards.
C270	dated 1997-09-06	related to 39 standards.

The 8 publications contain standards and their modifications, but also standards which have been outdated by newer issues and which have been withdrawn by CENELEC. The manufacturer is supposed to have sufficient skill to find his way through these eight lists and to compose a package of standards and amendments relevant for his products.

3. Transition periods for standards

For all new or modified EMC requirements forwarded in draft standards or draft amendments, the technical standardization committee has investigated:

- 1) the expected influence on the electromagnetic compatibility between apparatus used at close distance, and on the other hand

- 2) the economic impact that the new requirement or modification will have on the products concerned.

With that in mind new technical requirements in standards are accompanied with a "latest date of withdrawal of conflicting standards" (d.o.w.). Industry has so far understood that products concerned, put on the market before the d.o.w., need not yet to be in conformity with the new requirements and can still have the presumption of conformity with the essential requirements of the EMC Directive (for instance if all the requirements are met as formulated in the other applicable standards published in the OJEC).

It is obvious that the economic impact of new requirements is heavier for equipment at the end of the development or for those already in running production. To enable an earlier general application of new requirements a distinction was made in a number of standards between new products after a certain date and equipment in running production on that date. This so-called certification clause is declared to be illegal by DGIII.

An agreement has been reached between DGIII and CENELEC to publish a new list of all EMC standards in the OJEC while for each standard or amendment a date is added at which the presumption of conformity to the essential requirements of the Directive cease to exist for the superseded standard. The intention is to adopt for harmonized standards the latest date, either the d.o.w. or the date in the certification clause as the date of cessation. This new list will overrule the 8 earlier publications.

Awaiting this new list, industry has no alternative than to act as if the published d.o.w. and certification clause in the standard are representing the legal dates of applicability (of course without having any influence on the possibility of the technical file route as described in art. 10.2 of the Directive).

4. Multistandards equipment

One of the problems which manufacturers have faced since 1 January 1996 is to know which standards are applicable to their products. The matter is even more complicated if the equipment incorporates more than one function, covered by different standards. An example is the cooker extractor hood with a fan motor (EN 55014 for emission) and a luminair for fluorescent

lighting (EN 55015 for emission). Luckily these two standards prescribe that the measurements should be carried out in isolation, with the other functions switched off.

Unfortunately such multifunction indications are not given in other standards. For instance for multimedia equipment where information technology, telecommunication and broadcast functions are combined, it is not easy to define a reasonable combination of functions during the test according to the several (single) standard specifications.

5. Under consideration in standards

In a number of harmonized standards the limit or measuring method for specific phenomena are still under consideration for certain products. It concerns in most cases apparatus for which in practice no complaints on emission (or immunity) occur (examples are: radiation from battery powered household appliances when not connected to the mains for recharging, radiation from A.M. receivers, no immunity requirements exist yet for portable broadcast receivers with no external power connection).

Manufacturers have interpreted the rules that the manufacturer's declaration may be made for this equipment, making reference to the standard concerned (as the equipment is covered by the scope).

It is well understood that some public authorities are becoming impatient for these cases and that on short notice the gaps in standards need to be filled in.

6. Equipment for specific applications

Some apparatus exist which as such cannot fulfil the requirements as formulated in the standards. For instance, electromicroscopes are highly sensitive to 50 Hz magnetic fields and need to be installed in specific rooms. Also magnetic resonance imaging equipment (medical) have specific installation instructions. These apparatus are installed by the manufacturer and are guaranteed for electromagnetic compatibility after installation. In fact the screened enclosure and/or mitigation measures during the installation form a part of the conditions for which the apparatus can meet the requirements.

Similar practices were developed for sub-assemblies which do not need to be CE-marked if they are intended to be incorporated in the equipment. An example is a power converter for which big purchasers insisted on the affixing of the CE marking. This was granted at surplus cost, but related to the application inside the enclosure for which the power converter was designed.

7. Measurement uncertainty

In view of the ISO 9000 certification of testing institutes and manufacturers laboratories the question of measurement uncertainty was raised with respect to the approval or rejection of products, comparing the measured values with the required limit in the standard. It is recognized that repetition of tests on one or more equipment gives an impression on the repeatability of

the test method and can indeed lead to decrease the measurement uncertainty, but systematic errors may remain undetected. In all CISPR emission standards the limits have been derived on a probabilistic basis, taking into account the statistics of an acceptable number of complaints, while the verification of the measurement values with the limits is carried out with measurement tools (e.g. V-network, measuring receiver, test-site) with characteristics with well-defined tolerances.

Subtracting of the measurement uncertainty from the limits would mean for these standards that the measurement uncertainty is taken into account twice, first in the establishment of the limits and secondly in the application of the limits. To have a uniform interpretation of test results for all standards, EMC experts in test houses and laboratories have therefore adopted the procedure that equipment under test (EUT) is approved if the measured values are below the emission limits and for immunity if the EUT continues to operate as intended under phenomena adjusted to their nominal value. Condition is that the measurement equipment is well within the specified tolerances.

8. Use of alternative measuring methods

It is impossible for manufacturers to investigate emission and immunity during the development of a prototype of a new apparatus in accordance with the official measurement method. The expensive anechoic rooms would have been overbooked if the influence on all trial-and-error changes had to be verified there. Several alternative measurement methods have been developed, for instance small rod and loop antennas of a few centimetres with which at printed wiring board level the radiation and immunity can be investigated. For some apparatus manufacturers have found a good correlation between the measuring results of these alternative methods and the results with the official method according to the standard.

It is of course depending on the confidence of the manufacturer in his test results whether he still performs an official test on the finalized apparatus. The aim is however: meeting the EMC requirements, but at minimum costs!

9. Biographical note

The author completed his study in physics at the Technical University Delft in 1967. He is Senior Physicist in the staff of the Philips Corporate Standardization Department in Eindhoven. In his function he is responsible for external standardization on radio interference, electromagnetic compatibility and safety.

He participates in many national and international committees, is chairman of CENELEC 210A, chairman of CISPR-B and secretary of CISPR-F.

For further information contact the author:

M.C. Vrolijk

Telephone +31-40-2732 834

Telefax +31-40-2737 357

E-mail w.zuidinga@nl.cis.philips.com

XVI
WORKSHOPS

**EMC Quo Vadis - What Standards
Will We Need in the Future**

Workshop Organizers:

P. J. Kerry - UK
Dr. B. Szentkuti - Switzerland

Industry's view on EMC requirements

Philips Semiconductors
Systems Laboratory Eindhoven
Mart Coenen
P.O. Box 218, Bld. BE-3
5600 MD Eindhoven
The Netherlands
mart.coenen@ehv.sc.philips.com

Abstract

Over the last few years, many new EMC norms and standards have been developed for a variety of electronic products. On the one hand, we have the RF emission standards that are there to protect the environment for not getting too polluted by EM-smog. On the other hand, products have to be able to withstand a great number of EM threats.

There is one thing in common, which is not commonly implemented in the standards yet and that is the place of use; domestic, office, light industry or an industrial environment.

With CENELEC, now taken over by IEC, the generic 61000-6-x series [5.1 – 5.8] have been developed to put and end to this situation. These standards make reference to other "Basic" standards, which are there to define a common method of measurement for a given phenomenon.

These generic standards assume that the basic standards referred to are unambiguous and always applicable which unfortunately is not the case.

Based upon an agreement between the product family standard writing committees and the "umbrella" organisation (e.g. DG-III, ACEC), these committees are NOT allowed to divert from the measuring methods in the

basic standard unless there is an explicit need to do so. The criticality of the application of the product may set test levels and severity criteria. The product (family) standards committees should set these special requirements for their group of products.

This convergence in measurement methodology may not affect the product manufacturer so much but is of the utmost importance for the semiconductor supplier who is willing to support design-in for a large variety of market segments: PC, telecom, audio and video, automotive and last but not least commodity electronic products.

1. Introduction

All EMC legislation is created to achieve a common agreement on requirements either applicable for one country; like a national standard; e.g. FCC47 Part 15, or a common agreement between several member states, like in Europe: CENELEC.

Standards are an indispensable tool to take reference to. But one should always bear in mind that these norms and standards can not be a full guarantee for Electro magnetic compatibility in every area of application.

These standards should be used as reference with (some) common sense in mind.

In the next paragraphs, topics, which have lead to misunderstanding and differences in interpretation, are given together with some examples.

2. Inconsistencies in the standards

2.1 Ambiguity

The EMC requirements, either for RF emission and immunity, have to be unambiguous and the measurement uncertainty with those measurements has to be within close limits to allow mutual acceptance and recognition of test results.

These two requirements are necessary to assure that a product approval at one test site will give close to the same results as in another location.

However, practice shows that this is not always the case. The measurement uncertainty of a whole measurement system can be defined within tight ranges but the effect of the EUT, its exact location, the cable length, the cable diameters and cable routing have a great impact on radiated RF phenomena like RF emission and immunity to RF fields.

2.2 Costs

Another issue is the need to reach EMC at minimum cost. This not only involves EMC standards and the required test facilities but also the philosophy that has to be followed during the design phases of product development and system concept.

Minor changes (selection) at the component level or even PCB layout may have a great impact on the measures to be taken at the system level.

Unfortunately, meeting the EMC requirements of certain Norms and Standards is something different from achieving system EMC.

Measures may need to be taken for certain requirements which are useless for the EMC system approach and measurements may or must be carried out without a specific need as the prove of being compliant can be given on a theoretical basis e.g. the emission of mains frequency harmonics.

Another aspect of a measurement standard is the cost involved for the information gathered.

For example, immunity to RF-fields, like in IEC 1000-4-3 is a burden to many manufacturers, because the investments involved are too high for smaller companies who become dependent on test houses and therefore privilege the larger companies who can afford it themselves.

Looking at the frequency range of concern: 80 MHz to 1 GHz (or even 1.89 or 2.45 GHz to cover also DECT and wireless LAN sources) is just a single aspect out of the at maximum 7 phenomenon which are of common interest, see also 2.8.

Defining an homogenous field intensity over a surface area which will never be equal to the actual threat; being a portable transmitter, just for the sake of reproducibility makes such an investment even more debatable.

Alternatives, like using worst-case "dummy" transmitters at GSM frequencies, as proposed as an amendment to EN55020, make more sense as they represent the real threat at minimum cost.

2.3 Consistency

From the EMC point of view, EMC requirements should be based on the approach that a system build from compliant products would give a compliant system:

$$(CE + CE + \dots = CE ?? !!)$$

Even on a macro scale, this approach should be independent on whether this is at product or at the component level as long as the measurement methods are consistent and unambiguous.

This requires that a product related EMC standard characterise the full EMC behaviour of the products including their interfacing cables.

Another pre-requisite is that EMC requirements should be equally to a range of products used in the same EM-environment (like the generic EMC requirements). It is unacceptable to have less severe requirements for one product compared to

another when the same environment defines the EMC threats.

A topical area of concern is the merge of audio and video products into the information technology equipment (ITE) area.

The integration of test and measurement functions into a PC environment gives a conflict, not only at EMC but also at the product safety level. For this one has to compare the insulation requirements between IEC 950 and IEC 1010.

2.4 Fair competition

To remain competitive, an equal burden of requirements should be placed or rest on the shoulders of all manufacturers and not just a specific group that is of less interest for the decision making party involved.

As an example: the spurious RF-emission from cordless telephone may be 20 to 40 dB higher than the spurious emission from any other electronic device in that same frequency range.

Another example is that for television receivers, no RF emission requirements are set for frequencies above 30 MHz other than for the local oscillator and its harmonics [5.10]. Some TV sets, however can be used as a monitor and therefore become "ITE" [5.13].

2.5 Incompleteness

Technical problems arise with, for example, immunity tests, where for instant the immunity test to ESD phenomena for portable and ungrounded equipment is NOT defined at all in the present version of the standard: IEC 1000-4-2. However, manufacturers, test houses and even the generic standards assume that it is all well defined and reproducible and that it can be addressed.

Another example again is that battery operated products are excluded from some EMC measurements e.g. games, portable radio's, toys.

Doing a tolerance analysis on the several EMC measurement systems and calibration procedures reveals that most of the frequently used standards suffer from incompleteness

and inaccuracies, for which a local correction or interpretation is given (either by a product manufacturer or an EMC test house).

2.6 Through-put-time

With standardisation, through-put-time with EMC measurements and their procedures have never been optimised in this respect.

For example the use of the Quasi-Peak detector with RF emission measurements is just one example of how time consuming measurements can be. This Quasi-peak detector is still there in the qualified EMC measurement equipment but commonly just used in case of dispute.

Another example is the fact that almost every measurement procedure requires another set-up of the equipment under test, different measurement heights and other accessories, like networks: artificial mains networks, impedance stabilising networks, coupling/decoupling networks, current clamps, absorbing clamps, ...

2.7 Relevance

We believe that it is absolutely necessary to have unambiguous measurement standards as a reference, but why is it necessary to use these reference measurement standards with every measurement again.

For example: a spring rule is as good as a yard stick a so many millions of wavelengths of a Caesium lamp when it concerns compliance with the elementary rules of the EMC Directive.

2.8 Simplification

Last but not least is the present burden of the variety of measurement procedures, as shown above, that exist for all the products in which the semiconductors are being used.

This does not only claim an investment in a large variety of measurement systems but also claims test facility area and knowledge of all the measurement systems and the according measurement procedures.

The 7 most useful immunity phenomena have recently been described in the draft version, third edition of IEC 1000-4-1. These phenomena are:

ESD	Part 2
Immunity to RF fields	Part 3
EFT	Part 4
Surge	Part 5
Conducted RF	Part 6
Voltage dips on the mains	Part 8
Mains-frequency magnetic fields	Part 11

For other immunity phenomena, more than 20 extra standards are available or being prepared. These standards will be useful under some circumstances but not suitable for 95 % or more of all electrical and electronic products to be sold on the market.

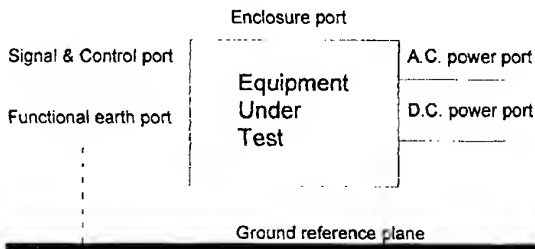


Fig. 1 Example of ports

With the Generic EMC standards, both for emission as well as for immunity, ports have been defined for the equipment under test. Up till now, only a few pulsed immunity requirements have been set. For telecom ports RF emission requirements at the lower frequencies ($f < 30$ MHz) have been set. With wired applications, the cables connected are the main cause for emission problems. Using CDNs, as defined in IEC 1000-4-6, can help to measure the available RF power at each port at minimum cost, at least compared to the cost of an an-echoic chamber.

As a manufacturer of semiconductors, being involved in the design-in of ICs, these inconsistencies place a burden on the designs as applications need to be modified upon the EMC requirements for that product to be fulfilled.

3. Conversion problems

When carrying out pre-compliance EMC measurements the problem arises of how reliable this pre-compliance information is with respect to the requirements of the official standard.

Most of the radiated measurement methods are hard to convert into conducted measurement methods. This also means that the radiated EMC requirements defined are hard to be converted into "conducted" circuit analysis tools.

In this respect, the use of the MDS-clamp, as defined in IEC publication CISPR 14 [5.11], to be introduced in other standards has carried out in many attempts.

Recently, the use of CDNs has shown close relation with the RF emission results obtained by using the MDS clamp which has to be moved up and down a 4.2 metre long mains line to locate the maximum available RF-power from a small radiating device.

Other new measurement methods, which also uses CDNs, are under development for lighting devices for frequencies between 30 and 300 MHz to eliminate the need for radiated measurements.

By a conversion of the radiated emission or radiated immunity problems into conducted problem, by using current (injection) probes, the problem of termination of the multi-port network, being the equipment under test is the main cause for this inconsistency.

4. Conclusions

Most of the electric and electronic products now sold in Europe bear the CE-mark with it. Whether systems build with individual products each complying with the present Norms and Standards is questionable, due to the inconsistency of these standards or the way these standards are interpret.

Too many standards have been developed for no good reason. It would be better to improve the existing, frequently used standards in this respect and to change these such that system EMC can be guaranteed when using compliant products. As defined in the EMC Directive, the products just need to have the presumption of conformity.

No matter how good EMC norms and standards are and even when products fulfilling the requirements are used, it will always be possible that an EMC problem may occur when building several products together to a larger system.

EMC standards need to be updated to improve them on several points:

- Ambiguity,
- Costs
- Consistency
- Fair competition
- Incompleteness
- Through-put-time
- Relevance
- Simplification

5. References

5.1 European standard EN 50081-1, Electromagnetic compatibility – Generic emission standard, Part 1: Residential, commercial and light industry. CENELEC, Brussels 1992

5.2 European standard EN 50081-2, Electromagnetic compatibility – Generic emission standard, Part 2: Industrial environment, CENELEC, Brussels 1993

5.3 European standard EN 50082-1, Electromagnetic compatibility – Generic immunity standard, Part 1: Residential, commercial and light industry. CENELEC, Brussels 1992

5.4 European standard EN 50082-2, Electromagnetic compatibility – Generic immunity standard, Part 2: Industrial environment, CENELEC, Brussels 1995

5.5 International standard 61000-6-1, Electromagnetic compatibility – Part 6: Generic standards, Section 1: Immunity for residential, commercial and light-industry environments, Geneva, 1997

5.6 Draft International standard 61000-6-2 (77/177/CDV), Electromagnetic compatibility – Part 6: Generic standards, Section 2: Immunity for industrial environments, Geneva, 1997.

5.7 International standard 61000-6-3, Electromagnetic compatibility – Part 6: Generic standards, Section 3: Emission standard for residential, commercial and light-industry environments, Geneva, 1996

5.8 International standard 61000-6-4, Electromagnetic compatibility – Part 6: Generic standards, Section 4: Emission standard for industrial environments, Geneva, 1997.

5.9 EN 55011, Limits and methods of measurement of radio disturbance characteristics of industrial scientific and medical (ISM) radio -frequency equipment, CENELEC, 1989

5.10 EN 55013, Limits and methods of measurement of radio disturbance characteristics of broadcast receivers and associated equipment,

5.11 EN 55014, Limits and methods of measurement of radio disturbance characteristics of electrical motor-operated and thermal appliances for household and similar purposes, electric tools and similar electrical apparatus, CENELEC, 1993.

5.12 EN 55020, Electromagnetic immunity of broadcast receivers and associated equipment, CENELEC, 1994

5.13 EN 55022, Limits and methods of measurement of radio disturbance characteristics of information technology equipment, CENELEC,[CISPR 22: 1993]1992

Biographical notes

Mart Coenen received his grade in Electrical Engineering in 1979 at the Polytechnic University of Breda in the Netherlands. Since 1986 he is involved in EMC standardisation, first with IEC TC65-WG4, later with IEC TC 77A-WG-6, TC77B-WG-3 and CENELEC TC 210 and 210A. With TC65A he was the secretary of the taskforce responsible for IEC publication 1000-4-6. Since 1996 he is chairman of the National Electro-technical Committee for basic and generic EMC standards. In 1994 he founded the Dutch EMC Society of which he was chairman for 2 years. Yet he is still member of the board of this Society. He is also member of the technical paper committee of the Zurich EMC symposium since 1993 and session chairmen since 1995 on various topics. He has written over 50 technical papers as company notes and in technical magazines.

THE RESEARCH ENVIRONMENT AND ITS ROLE IN DEVELOPING EMC STANDARDS

Alwyn Finney

ERA Technology Ltd, Cleeve Road, Leatherhead, Surrey, KT22 7SA, England

Abstract

The publication of the EMC Directive (and subsequent European legislation to enforce the Directive) has required that the development of electronic systems shall take the objectives of the Directive into account. This is best carried out by compliance to published standards.

Before standards can be published for use by manufacturers, there is a considerable period of time when the requirements are being established. This is a period for research into what are reasonable requirements for emission or immunity levels, what measurement methodology or equipment set up should be used and in certain cases, the development of suitable measurement equipment.

This paper describes some of the research elements used to determine the requirements that will ultimately be used in standards. The paper considers research related to a measurement tool used for showing compliance to an EMC standard, emission measurement methodology for large systems, and finally, some of the elements that will need to be considered if standards are to be developed for newly emerging services on existing networks.

1. THE EMC DIRECTIVE

The publication of the EMC Directive (and subsequent European legislation to enforce the Directive) has required that the development of electronic systems shall take the objectives of the Directive into account. That is, designs of such systems shall be such that its taking into use will not cause interference to other equipment and it will have an adequate level of immunity. Systems can be demonstrated to comply if they are tested using the methods specified and meet the levels set out in published harmonised standards or by use of a Technical Construction File (TCF).

Directives relating to EMC conformance are being issued in many countries around the world. In order

that the cost of compliance can be minimised, administrations are introducing regimes whereby manufacturers can self declare. Self declaration requires that the manufacturer should have performed tests to a requirement stated in a standard or alternative requirements which enable conformance to be demonstrated via the Technical Construction File route.

Before standards can be published for use by manufacturers, there is a considerable period of time when the requirements are being established. This is a period for research into what are reasonable requirements for emission or immunity levels, what measurement methodology or equipment set up should be used and in certain cases, the development of suitable measurement equipment.

In obtaining committee consensus in order to publish a standard dealing with requirements, the testing methodology or measurement equipment, and the original objective of the essential requirements may have been lost. It is important therefore to focus on the original purpose of the standard, such that a range of experience and expertise is input into the initial drafts. This requires research into understanding the techniques that are to be used, as well as measurement experience and resources to carry out related research topics.

Research into EMC phenomena is wide and varied. What will be described in the next sections are examples of approaches taken on measurement tools, a measurement methodology and an example of where the existing boundary of requirements is being extended and further research is needed in order to ensure continuing compatibility.

2. DEVELOPMENT OF EXISTING STANDARDS

2.1. Existing standards

The Generic Standards (EN50081/2-series) have been developed in order that they can be used for testing the majority of electrical and electronic equipment. Principally the Generic Standards can

be used for proving compliance for equipment which will fit on the Open Area Test Site (OATS) as described in CISPR Publication 16, or into a reasonable sized anechoic screened room for immunity testing. Each of the Generic Standards refers out to published "Basic Standards" which in a number of cases are standards that have been published by the IEC. These basic standards address both immunity and emission requirements.

In addition, other standards institutes are publishing standards, which set EMC requirements at system level. These are known as Product Standards. Although these are applicable to systems, which can be tested in the "normal" test house, some systems, for example, large complex telecommunication network installations do need special consideration. This particularly applies when two large systems have to inter-work and the conflicts between meeting EMC requirements and appropriate earthing, have to be resolved.

2.1.1 Emission Standards

The limits for emission and the test method to be applied are covered in a number of international standards. Although these standards exhibit differences in the emission levels at selected frequencies, in principle the methodology is based on CISPR Publications 22 and 16 for an open area test site. CISPR Publication 22 has been utilised in the harmonised standard EN55022 but its application can only be successfully applied to systems (equipments) which are physically compatible with the dimensions of the test site.

As an example of a system which has only just been addressed by standards, consider the testing of large systems which are assembled from independent operating sub-units. Research, backed up by practical measurements has been performed in order that a testing methodology could be developed which could then be written into standards. This methodology has had to take into account the complexity of the sub-systems as well as the wide variety of ports available for connecting cables e.g. pairs, multi-pairs, screened twisted pairs, coaxial, optical fibre, all in large quantities.

2.1.2 Immunity Standards

Immunity requirements have been set in the Generic Standards, and these refer out to "Basic Standards" for the test methods. Again these rely on standards which have been produced by the IEC. Such standards address various phenomena, e.g. fast transients (IEC 1000-4-4), surges (IEC 1000-4-5), and magnetic fields (IEC 1000-4-8). Each of these requirements need to be addressed and considered especially when there may be conflicting requirements e.g. earthing and bonding of equipment from both a safety and EMC point of view. Conflicting

requirements may be resolved via research. For example, the provision of one common bonding point (to suit EMC requirements) versus the provision of a multi-point grounding system for earthing purposes.

2.2. EMC measurement tool

The Line Impedance Stabilisation Network, (LISN) is usually applied in EMC tests for the measurement of conducted emissions from virtually all types of apparatus. It permits the measurement of RF conducted emissions from the EUT or the injection of disturbances into the EUT; it stabilises the impedance for the EUT power and/or signal port; and it provides filtering for power supplies or signal sources. The calibration of LISNs comprises measurement (without power applied) of the impedance of each line to ground and the insertion loss of each coupling network. The measured impedance characteristic is required to be within the stated parameters of the relevant standard for each device and is usually stated as impedance as a function of frequency with a tolerance in ohms or percentage terms. Many test laboratories perform an additional test of insertion loss between the input port and output connector to doubly ensure that there are no unquantified losses in the measurement paths.

The greatest difficulty encountered in LISN calibration is associated with the provision of suitable test jigs to interface with the EUT port where unwanted interference can adversely affect the result, unless sufficient care is taken. When calibrating the impedance, it is necessary to make up a special calibration jig for the EUT connection to interface to the measuring instrument.

Generally, in measurement mode the LISN has a nominal 0 dB voltage correction factor; however the presence of additional attenuators and pulse limiters fitted internally will result in a different correction factor. For measurements below 150 kHz, a further correction factor for the coupling capacitor is also required. The difficulties encountered in measurement usually relate to inadequately filtered noise at low frequencies and random or poorly specified mains cable layouts, which can result in significant variation in the 10-30 MHz range where transmission line effects begin to be observed.

CISPR publication 16-1 defines the methods for calibrating most LISNs and states the performance requirements to be attained. Defence EMC standards such as DEF STAN 59-41 also state methods and procedures for the LISNs referred to in the standard. It is important that the dependence of the LISN characteristics on the coupling jig, the measurement instrumentation performance and ancillary equipment etc. are well understood such that the contribution of each to the overall uncertainty budget can be determined.

Although the LISN is a regular tool in use by Test Houses, there is a need to thoroughly understand the issues elaborated above, in order to understand how improvements in calibration technique, instrumentation, and LISN design etc. could be achieved. Some of the elements where research continues to be applied is to the LISN calibration uncertainty value. This value is one line in the conducted emissions uncertainty budget, but there are many factors, which can affect overall variations. These include the following:

- coupling between coils (phase to phase)
- transmission line effects of the EUT mains lead
- bonding methods to the ground plane
- supply filtering, especially at low frequencies
- incorrect correction factors
- marginal compliance with the specification for the LISN

These, and other contributions, need to be assessed practically by variation and repetitive test using swept signal sources and display where appropriate. A thorough understanding of the above is required in order that the best performance from the LISN is achieved in the practical measurement situation. This understanding is best achieved in the research environment.

2.3 Emission testing standard for large systems

Large telecommunication systems are based on functional units known as sub-systems, which provide the specialist facilities needed to perform the overall system function. In order that systems can be installed which comply with EMC requirements, a representative system concept has had to be developed which requires that the system so defined can be tested on a free field site and/or sufficiently large semi-anechoic chamber, followed by characterisation of the sub-system modules in a suitable shielded anechoic room.

Operational telecommunication systems are physically large, made up of many sub-units and equipment suites, and only become functional when installed and cabled on site. Such systems need to be on a sufficiently large open area site and/or in a suitable semi-anechoic chamber. By developing a suitable methodologies and incorporating them in a harmonised standard it is possible to show verification of the system to EMC Directives. A number of stages were needed to achieve a suitable method, and these are outlined below.

2.3.1 Representative System

In order to achieve compliance, a minimum representative system is defined which is suitable for testing. A minimum representative system is defined as one which includes all equipment connected

together for the duration of the operational life of the large system and is thus unique to the site on which it is installed. Thus the equipment connected together is the minimum configurable operational system and is the minimum requirement for an Equipment Under Test (EUT) to be used for compliance testing.

2.3.2 Equipment Configuration

The minimum representative system includes all equipment connected for the operational life of an actual system; it exclude any equipment connected for the purpose of monitoring or system measurements, and which are connected for a temporary period. In addition, the EUT consists of the minimum number of sub-units which are needed to produce an operational system, it should be the minimum configuration of any product that is offered for sale, and should include at least one of each sub-unit to be used in the actual installation. There exists for representative systems a minimum set of interface lines which is required for the operation of the system and this number must be defined for each representative system.

The sources of maximum emission should be identified by initially measuring each rack on an individual basis and where appropriate, assembling the representative system in such a way that emissions are maximised. The system configuration will be arranged so as to maximise emissions such that noisy sources within equipments are not shielded by periphery equipments.

2.3.3 Test Methodology

The test methodology in current standards applies in the main to physically small systems which may be assembled from like units. To apply this concept to physically large systems, which are assembled from a variety of different units and are only operational when in combination, could lead to the adoption of an in-situ testing approach. However, significant measurement errors are associated with this approach for a variety of reasons:

To establish a suitable test method then the requirements of the test site need to be defined. Generally the test site layout and conditions shall conform to the principles set out in EN55022 and CISPR Publication 16. The test site should be flat, and free from nearby reflecting structures, particularly vertical structures. It shall be sufficiently large to permit antenna placement at the specified distance and provide adequate separation between antenna, test unit and reflecting structures.

Since such a site is much larger than those specified in the above standards then the ground plane should be laid so as to extend at least 2m beyond the measurement antenna wherever the antenna may be

placed (i.e. at any radial measurement point). The ground plane should have no voids or gaps that are a significant fraction of a wavelength at the highest measurement frequency of 1GHz. The recommended minimum mesh size is 30mm.

Having laid out the ground plane then a site attenuation measurement is required. The result of the measurement should be such that the test site conforms to the site attenuation characteristics as defined in CISPR Publication 16, with measurement being made in both horizontal and vertical polarisations using balanced dipoles

2.3.4. Representative System Tests

To assemble a practical representative system requires considerable attention to detail, not least, that of selecting sub-systems which are representative of those that are used on actual customer sites. The practical matters of whether the representative system will be assembled on site or taken on a platform need evaluation as well as preparation of the actual test site.

All of the above issues were addressed and satisfied as to their practical application before a standard could be prepared and issued.

3. EXTENSION TO EXISTING STANDARDS

The use of the mains cables and lines to transmit signals has been with us for many years. Up to the 1970s, it was largely used by utilities for circuit protection and to control system loading. In the UK, the preferred operating frequencies for power line carrier systems in the 1960s and 1970s, were in the range 70 - 489 kHz and 511 - 1000 kHz. At the other end of the spectrum, ripple control, using low audio frequencies, was used around 1913 in Leatherhead for tariff switching. During the 1980s, there was an upsurge of interest in using the mains for more complex information and data transmission, using very low frequency (VLF) radio frequencies (10 kHz - 150 kHz) to signal between points connected by the low voltage network. To prevent these VLF signals interfering with broadcast radio and other users of the radio spectrum, such as aircraft navigation, the UK Home Office asked that transmissions be limited to the frequency bands 40-90 kHz and 110-140 kHz. By 1986, a British Standard has been drafted that further sub-divided the allowed frequency bands and allocated them to specific applications, such as the supply authority, private installations, alarm systems etc. British Standard 6839 was first published in 1987. The standard recognised signalling at frequencies as low as 3 kHz.

Standardisation in Europe later progressed with the introduction of CENELEC standard EN 50065, dealing with signalling on low voltage electrical

installations. The frequency range remained 3 kHz to 148.5 kHz.

3.1. Supply of new services on power line cables

Outdoor lines, primarily used for power and/or low frequency communications are to be employed for the transmission of high rate digital signals. The new signalling protocols will generate signals which will occupy the frequency band from approximately 600 kHz up to 10 MHz, i.e. at frequencies considerably greater than the upper limit of 140 kHz used currently. This frequency range is occupied by LF, MF and HF radio frequency transmissions, thus there exists a great potential for interference to be caused to broadcast services.

Conversely, broadcast services have the potential to cause interference to the new services. Spread spectrum techniques are planned to be used, in order to achieve the larger transmission distances needed to make the services economic to provide. As well as the potential interference from the fundamental signal, unwanted harmonics from the transmitted signal could exist up into the 10s or 100s of MHz, thus extending the range of potential interference complaints.

Given the desire to utilise the installed power supply network for services which are to be transmitted at frequencies not intended in the original concept of the system, there is an urgent need to develop a model through research which will permit the estimations of radiated emissions from power and telephone lines such that consideration can be given to the development of suitable standards.

Broadband RF signals such as those used for video on demand, can occupy a bandwidth with an upper frequency of around 10 MHz, harmonics of the signals can extend to 100s of MHz. It is clear that coupling to and from the emerging transmission systems is of concern for two reasons;

- a) Radiated emissions from the transmission lines can interfere with other users in the designated frequency spectrum.
- b) Radiated susceptibility of the transmission line can result due to radio transmissions currently present within the designated frequency spectrum.

Power distribution cabling and telephone cabling was not originally designed to transmit high frequency signals over long distances. In addition to high cable attenuation and hence restricted transmission distances, electromagnetic compatibility becomes an issue. With regard to high voltage power distribution lines, control of radiated emissions has been exercised through the application of standards such as CISPR 18 (BS 5049 in the UK) and EN 50083-1

for mains signalling. The latter specifies a maximum level of applied voltage to the power line at frequencies in three bands with an upper limit of 140 kHz. The use of higher frequencies and much wider bandwidths is likely to result in efficient radiation from any overhead line that is not perfectly balanced.

3.2. Elements of a research programme

The development of a model capable of predicting the effects of high frequency transmissions on the power network needs to take account of a number of factors.

In the case of the mains distribution network, the prediction of radiated emissions has to consider a variety of scenarios and models which encompass typical 'tree and branch' networks. The transmission and radiation properties of power cables at high frequencies have not been thoroughly characterised, although similar theoretical principles can be applied to power cables as those used for telecommunication cables. The major difference is that power cables are inherently unbalanced and will be more effective at generating common-mode emissions.

For the prediction of radiation from mains communication systems, a number of real life scenarios will need to be analysed. The network should be modularised into elements with defined radiation properties. For instance, a 'lamp-post' radiator is likely to exhibit a different radiation pattern and field polarisation to overhead distribution cables, which in turn will determine whether their respective emission would affect, for example, domestic radio receivers or air traffic communications. Also, in the case of multi-occupier buildings, the effects of multiple radiation sources has to be considered due to the possibility of constructive field enhancement.

Techniques for predicting the radiated emission levels from VDSL transmission systems on telephone subscriber lines (twisted pair cables) have already been published. It has been shown using simple formulae and worst-case assumptions that the disturbance voltage received in an antenna operating in-band due to a collocated VDSL transmission line could be of the order of 20 µV, a level likely to cause interference to amateur radio users. Parameters of the transmission systems identified as critical in the calculations are;

- The power spectral density of the transmission signal.
- The balance of the transmission line (or longitudinal balance)
- The method of termination of the transmission line

- The perpendicular distance from the transmission line to the receive point.

Attempts have been made to characterise the transmission properties of power distribution network in terms of the attenuation losses as a function of frequency, up to a frequency of 20 MHz. It was shown that at high frequencies the attenuation in the power network is affected strongly and randomly by the number of users (loads) and hence the particular time of day.

The VLF schemes currently use a range of transmission modes and signal types. Both common mode and differential schemes are used on single phase and three phase systems.

The modularisation of the mains network will allow estimations to be made of the level of radiated emissions for a variety of real-life networks and installations. Worst-case assumptions regarding the interaction of the emission levels from the various models will form the basis for determining acceptable radiation limits.

Finally all the above elements will need to be included in a standard which would be used to control the emissions from such systems.

4. CONCLUSION

This paper has outlined some of the research elements which are involved in the development of standards. Even for well established measurement methods and equipment, there is a need research in order to improve measurement accuracy. Research is even more important to define acceptable EMC requirements when new, high speed systems are planned to be connected to an installed infrastructure.

BIOGRAPHICAL NOTE

Alwyn Finney joined ERA Technology as Manager of the Advanced Project Department. He has been responsible for the introduction of EMC screened practices into a telecommunication company and has represented that industry on European standards making institutes. His current responsibilities include amongst others, investigations into how cables should be screened and bonded for best EMC performance and how large systems can achieve compliance to the EMC Directive. He is a Member of the IEE.

EMC QUO VADIS - WHAT STANDARDS WILL WE NEED IN THE FUTURE? WORKSHOP CONTRIBUTION: TESTHOUSE VIEW

Dr. Diethard Hansen,
EURO EMC SERVICE SERVICE (EES) Dr. Hansen GmbH, Germany,
homepage: <http://www.euro-emc-service.de>

Introduction:

Since the start of the EMC directive many things have changed in a positive as well as in a negative way. The enormous amount of new harmonised standards by the EC and the latest Guidelines could possibly help the manufacturer world wide under the self declaration route. EMC however, seems to stand for "even more confusion" and CE is in some parts of Asia interpreted as Chinese export. The testhouse and certification agency - Competent Body customer still needs a lot of guidance, information and finally professional help. This is why EES decided to put valuable information on the homepage for downloading free of charge. CE Marking is by far no more limited to EMC but rather electrical safety, medical, telecommunications, radio, machinery and many other directives. The automotive EMC problems are dealt with separately and will lead to e1 certification. This means, the trend in testing and certification clearly goes to one-stop-shopping for the client. A reliable, fast and cost effective service based on a strong international competence is mandatory to become successful in this new market. The market is on the one hand side very much locally oriented and many testhouses popped up in the last 3 years. not all of them are necessarily experienced. Consequently some people believe price is the only issue. This could back fire, thinking of product liability and time to market. On the other hand testing and certification including approvals is a global issue in the major markets North America, Europe and Far East. A reaction to the European EMC legislation is a world wide trend of national legislation in order to negotiate mutual recognition agreements (MRAs). This means a niche market is slowly developing into a real world wide market, including East Block Countries and e. g. China.

An other consequence is the strong need for efficient and cost effective test standards.

Achievements, trends and deficiencies of today's EMC standards

An often misunderstood concept of standards under the self certification route using harmonised standards which are published in the official journal of the European Union is disregarding to meet the essential protective requirements as defined in the various directives. Using the harmonised route means the manufacturer declares conformity and the presumption of conformity is based on meeting the harmonised standards. However, this may lead in some cases to severe problems if standards are wrongly interpreted. One of the typical problem areas is the legal formula $CE+CE=CE$, when it comes to system integration. Recent prosecution in the EU has technically clearly denied this approach, because in each and every declaration case (self certification or third party, accredited testlab or Competent Body) the ultimate goal is to meet the protective requirements. In the actual presentation technical examples will be given from the various parts of our testhouse and certification activities.

Even correctly interpreting the standards and being an expert in the field, many questions about standards and their pure consistency become apparent. Why are emission and immunity, LISN and CDNs and other coupling networks using different impedances (50 Ohm and 150 Ohm)? Is there any difference in physics? Why do we use different EUT layouts of cables for conducted and radiated tests? Why do we define different heights for the same cables under emission and immunity? What is happening to the length of the exposed EUT cables? Why are the locations of measurement points different? Can anybody reasonably explain why radiated emission sites are totally different from immunity sites? Is historical development of the standards the only justification why alternative radiated test sites are probed by volumetric testing while radiated immunity sites are only probed in 16 points of a 1,50 m x 1,50 m

plane area? What is done to test and certify systems and installations in a physically meaningful, reliable and still cost effective procedure? In the actual presentation the author is trying to point out to some realistic solutions by not necessarily playing the devil's advocate in favour of military standards. The presentation will conclude with the authors experience as an official testhouse and Competent Body auditor in the German accreditation system. How accurate, repeatable and traceable are the measurements of some "accredited EMC labs" operating in a price range which clearly indicates they are using a fraction of the prescribed test and dwell time as specified in the

corresponding standards. What is next after having converted the black sheeps into white sheeps by the market forces and the clients? Who is able to bring together the world wide scattered experts which have the practical experience and the theoretical background to finally create global harmonisation and unification of EMC standards which will make almost everybody happy? This is a very demanding challenge which should quickly get industry, government enforcement agencies and universities to co-operate effectively as soon as possible to eliminate international trade barriers.

CISPR Standards Present and Future

Peter J Kerry, Radiocom. Agency, UK
President of IEC - CISPR

1. INTRODUCTION

CISPR was formed in 1934 to protect radio reception. In those days, the main concern was the protection of Broadcast services, from the electrical devices that were beginning to become a part of everyday living. Today the expectations of radio users have increased, and CISPR has risen to meet these expectations. The use of radio has greatly increased in recent years, especially the use of mobile and satellite services. Also the number of other electrical products has greatly increased, and now most of these products contain electronic controls of some form. These developments greatly increase the opportunity for EMC problems. It must also be recognised that in addition to protecting the reception of radio services, people expect other electrical equipment to be immune from radio transmissions.

CISPR has successfully evolved to meet these demands, and will need to continue to evolve as these demands change in the future.

2. WHY STANDARDS?

EMC standards have often been considered to be primarily a matter of national concern. However, this can lead to the creation of technical barriers to trade. With the present world trade situation, it is essential that a product from country A and one from country B will both function third countries, without suffering from problems associated with EMC. To achieve this, technical barriers need to be removed by the adoption of common standards - this was one of the driving forces behind the adoption of the EMC Directive in the European Union. This move has given EMC Standards in Europe a legal status. Unfortunately this has also created some legal problems which we are working to overcome. However, the desire to have fully international standards in Europe has led to the use of a parallel voting procedure with the IEC, so that international standards can be adopted as soon as possible.

3. CISPR STANDARDS

Many of the CISPR standards are well known, but as with other standards, they continually need to be updated, and new ones added. Table 1 indicates the current range of CISPR Standards. This list of EMC Standards shows that the CISPR activities have primarily been concentrated on emission standards, which have been based on individual product areas. However, at the bottom of the list are two Generic Standards. These are different from the other standards, in that their scopes are based on particular EMC environments, and not on particular products. It will be noticed that these last two standards have "IEC" numbers instead of "CISPR" numbers. This change was agreed by the CISPR Steering committee in order for the emission standards to be in the same series as the IEC Generic Immunity Standards. Also if these Generic Emission standards are studied, it will be seen that they contain limits below 9kHz. This is an area that is the responsibility of IEC TC77, but it was considered that users would benefit from having the limits in a single document.

4. THE STANDARDS HIERARCHY

To fully understand the standards situation there is a need to be aware of the standards hierarchy. Essentially, standards fall into one of three categories:

- **Basic Standards** address a particular EMC phenomenon, the appropriate test method(s), and a suggested range of limits.
- **Generic Standards** address all the relevant EMC phenomena for a particular EMC environment, and define the necessary test levels. To do this, the Generic Standards make reference to the appropriate Basic Standards.
- **Product Standards** define specific EMC requirements and test procedures dedicated to

specific families for the environment in which they are intended to operate. Note: The term *Product Standard* is used in this paper to also covers the term *Product Family Standard*.

In these three categories it needs to be recognised that the Product Standards are at the top of the standards hierarchy. Hence, there is a demand by product committees to have their own Product Standard, rather than try to apply the Generic Standards. Whilst this is an understandable request, there is also a need to ask the question; "Is this in the best interests of protecting the use of the radio spectrum?"

4. PRESENT PRODUCT STANDARDS

In general, CISPR Product Standards have served their purposes well, and have assisted in ensuring that EMC problems remain at a manageable level. However, if the individual standards are studied in any depth, becomes apparent that there are significant differences between them. For instance, not all Product Standards test over the same frequency range. In general most standards require testing up to 1GHz however, some only test up to 300MHz. It is also apparent that similar types of products fall into the scopes of different standards, with different EMC requirements, although they operate in the same EMC environment. Such discrepancies have to a great extent arisen due to the advances in technology that have taken place since the earlier standards were developed. To give two examples:

- An electronic typewriter now bears a greater resemblance to a PC than the electro-mechanical device envisaged by CISPR 14.
- The difference between a VDU and a television is becoming increasingly blurred, yet the present EMC requirements are vastly different.

Advances in technology, requires EMC standards to be reviewed ever more frequently. In particular faster switching speeds necessitate testing for emissions at ever-higher frequencies, and the merging of technology requires the scopes of the Product Standards to be redefined.

The above scenario poses a dilemma regarding how to balance the need for the continual updating of standards against the requirement of industry to have some stability in the standards. This is essential to allow industry to development and market their products. Against this background there is a need for EMC standards to protect the EM environment to enable the ever-growing use of radio services.

It is this changing world of EMC that needs to be carefully managed if CISPR is to continue to have effective EMC standards that enable products to function in the same environment as radio services. How can CISPR standards continue to balance these apparently conflicting requirements?

5. STANDARDS FOR THE FUTURE

CISPR standards have proved their usefulness over a period of time, and despite their inconsistencies, are generally effective and easy to use. Against this, the developing and merging of technology requires them to be updated ever more frequently.

The primary purpose of CISPR standards is to protect the use of the radio spectrum. With the changes in technology that we are experiencing, the traditional division of standards into different product areas is becoming increasingly difficult to justify. The need for a more consistent relationship between product emission limits and the radio environment is becoming increasingly apparent. If CISPR standards are to continue to succeed in their role in the EMC standards process, they will need to remove some of the present inconsistencies. I believe that of necessity standards will have to move closer towards some form of reference standard, such as the Generic Standards.

From the point of protecting the EM environment, this has to be considered a good thing, as it is anomalous to have two products in the same location having different levels of EMC emissions. The future of CISPR standards is seen to lie in applying the requirements of the Generic Standards to particular products so that industry can produce and test their products economically and effectively. A move towards adopting the values in the Generic Standards will assist the radio authorities to develop their new services against this common reference, knowing that EMC will be achieved.

6. SUMMARY

CISPR standards have served their purpose well, but the present continually changing environment in which they now find themselves poses both problems and challenges for the future. If CISPR is not to lose its way, it will need a clear reference against which to develop product standards. At present, the prime candidates for that reference are the Generic Standards. Moves towards a reference of this nature will not only greatly benefit the planning of future radio systems and services, but to ensure that EMC is achieved for the benefit of all

Table 1
Current CISPR Standards

Scope	Reference Number	Emissions/ Immunity
Industrial, Scientific and Medical (ISM)	CISPR 11	Emissions
Vehicles, Motorboats etc.	CISPR 12	Emissions
Radio, Television etc. - Emissions	CISPR 13	Emissions
Domestic Appliances, Tools etc. - Emissions	CISPR 14	Emissions
Domestic Appliances, Tools etc. - Immunity	CISPR 14-2	Immunity
Lighting	CISPR 15	Emissions
Measuring apparatus	CISPR 16-1	
Measurement Methods	CISPR 16-2	
Filter Measurements etc.	CISPR 17	
Overhead Power Lines etc. (3 parts)	CISPR 18	Emissions
Microwave Ovens Measurements	CISPR 19	
Radio, Television etc. - Immunity	CISPR 20	Immunity
Mobile Radio interference	CISPR 21	
Information Technology Equipment - Emissions	CISPR 22	Emissions
ISM - Determination of Limits	CISPR 23	
Information Technology Equipment - Immunity	CISPR 24	Immunity
Protection of Mobile Receivers	CISPR 25	Emissions
ISM In-band Emissions	CISPR 28	Emissions
Generic Emissions for Residential Areas etc.	IEC 61000-6-3	Emissions
Generic Emissions for Industrial Areas etc.	IEC 61000-6-4	Emissions

EMC STANDARDS TODAY: STARTING POINT INTO THE FUTURE

Bàlint T. Szentkuti

Swisscom Ltd., Corporate Technology

CH - 3000 Bern 29, Switzerland

Phone: +41 31 342 5258, Fax: +41 31 342 3917,
e-mail: balint.szentkuti@swisscom.com

The structures, concepts and contents of current EMC standards are reviewed. They are the starting point to future standards that should further implement new technologies and improve benefit/cost optimization when specifying and testing EMC. The paper gives some details on the standards of IEC TC 77: EMC.

1. INTRODUCTION

EMC standardization has started at the very beginning with product standards, dealing with particular technologies and with a rather limited number of electromagnetic (EM) phenomena. Test methods for similar phenomena but for different products might have been quite different. The following developments and events have given the most significant impacts to EMC standardization:

- The ever increasing use of electrical and electronic technology, especially the omnipresence of power- and micro-electronics and of mobile communication,
- The EMC Directive of the EU.

As a consequence, new technical and management structures and new specification concepts emerged, resulting in better coordination and faster development of standards. The structures are well established and the most important standards are available. Although there are still needs for filling gaps, improving standards and considering emerging new technologies, there is a solid basis for future development. This paper aims to describe the current situation, which is the starting point into the future. It concludes with some views on further steps.

2. STRUCTURES FOR COORDINATION: BASIC / GENERIC / PRODUCT STANDARDS

A significant step towards better coordination and management of the development of EMC standards has been done by the application of the clear concepts of Basic / Generic / Product or Product Family Standards and by the attribution of responsibilities for setting emission limits [1].

2.1 Basic EMC Standards

Basic EMC Standards or Publications give general and fundamental conditions and rules and serve as reference documents for product committees. Examples: test methods (without requiring specific limits) or publications on the EM environment.

2.2 Generic EMC Standards

Generic EMC Standards specify a set of essential requirements on emission and immunity for a given environment. They cite the Basic Standards as test methods and specify emission and immunity limits. They may be applied where no Product (Family) Standards are available for a certain product.

2.3 Product (Family) EMC Standards

Product (Family) EMC Standards specify EMC requirements for defined products (or product families), giving detailed operating conditions and performance criteria for EMC testing. These standards cite basic standards as test methods, and specify immunity limits according to the environment where the equipment should operate and also according to the intended quality of the equipment.

2.4 Responsibilities

2.4.1 Basic standards are usually developed by the horizontal committees: by IEC TC 77 for immunity and for low frequency (LF) emission and by CISPR for high frequency (HF) emission.

Note: In EMC terminology the "high frequency" refers to frequencies $f > 9 \text{ kHz}$, i.e. to radio frequency, RF.

2.4.2 Generic standards are in the responsibility of TC 77 and CISPR, whereby they have been voted and issued through CISPR (Standards 61000-6-3 and -4).

2.4.3 Product Standards and Product Family Standards are in the responsibility of the product committees, however:

2.4.4 Emission limits are specified by the responsible EMC committees with horizontal function, taking into consideration the needs of the product committees. TC 77 is responsible for low frequency (LF) and CISPR for high frequency (HF) emission limits. This responsibility of the horizontal committees guarantees the coordination of the emission limits in order to optimize EMC performance and costs.

3. REINVENTED: BLACK BOX WITH PORTS

An important step towards better technical concepts and structures is the new view that considers basically each equipment as a "black-box" having number of physical "ports" (AC and DC power ports, signal and telecommunication ports, earth port). These ports and the equipment enclosure are assumed to interact with the environment (see e.g. the Generic Immunity Standard IEC 61000-6-1). Using this specification structure, most equipment can be tested with the same test methods, i.e. the same Basic Standards can be used for measurement and testing of nearly all products.

4. CONCEPT OF EM ENVIRONMENT

Further structures and basis for optimum specifications have been introduced by distinguishing relevant EM phenomena, see table 1. Publications on the EM environment are the basis for setting emission and immunity limits. The respective publications on the EM environment either give a description or classification of the environment or they specify compatibility levels. "Compatibility level" is a key quantity in EMC planning. It is defined as the specified electromagnetic disturbance level used as a reference level for coordination in the setting of emission and immunity limits. Note: By convention

the compatibility level is chosen so that there is only a small probability that it will be exceeded by the actual disturbance level.

5. STRUCTURES WITH CONTENT: STANDARDS OF IEC TC 77

The publications of IEC TC 77 and sub-committees appear in the series IEC 61000-x-y (formerly numbered 1000-x-y), according to the structure given in table 2. Tables 3 and 5a offer a complete overview on what is available and what is going on in TC 77. The part and section numbers which are in brackets, indicate that there is only a project but not yet a printed publication available.

The main aim of Table 5 is to show which EM phenomena are covered by which type of publication or project in TC 77. Not all phenomena are equally important and therefore, not all of them need to be covered by an EMC specification.

Further important IEC standards are published by CISPR (either as basic HF emission test methods or as HF emission limits or as product standards). A great deal of product standards is published by the appropriate Product Committees of IEC.

CENELEC is usually adopting the standards of IEC. For legal reasons, there was an urgent need for the Generic Standards in Europe. Therefore they have been first developed by CENELEC. IEC has adopted the CENELEC Generic Emission Standards in the fast track procedure. The Generic Immunity Standards of IEC are nearly identical to the CENELEC versions. Some further international organizations are developing product EMC standards, e.g. ITU-T, ISO, OIML etc.

Hint: A visit to the IEC web site, <http://www.iec.ch>, is recommended for obtaining the most recent information on publications and projects.

6. THE GENERIC STANDARDS: A KEY ROLE

These standards specify EMC requirements related only to essential EM phenomena and serve as guidance for drafting Product Standards. Therefore they have a key role, they tell us

- which are the essential phenomena to be measured or tested and
- which levels or limits should generally be applied.

The Generic Standards are in a rather mature stage. All EM phenomena which are currently considered as essential, are covered. Therefore it is worth noting the phenomena and levels in table 4.

7. WHAT NEXT ?

- **Essential phenomena:**

As already mentioned, the essential EM phenomena are rather well covered with basic standards and requirements, they are included in the Generic Standards. Some small gaps have to be filled (LF emission limits for $I > 16$ A). Test and measurement methods for further phenomena are near to completion or in steady progress.

- Further important ongoing work in IEC TC/SC 77:

- EMC and functional safety
- Power Quality
- HEMP concepts and protection methods, not necessarily restricted to HEMP (shielding, filtering, testing large systems etc.)
- New technologies:
New methods and requirements may be imposed by the extension of frequency ranges of specification for both, low and high frequency phenomena: LF requirements up to 9 kHz, HF requirements well above 1 GHz.

- Physically large systems, installations:

EMC testing is poorly defined in the Basic Standards for such systems. More guidance and standards are required for

- in situ testing
- assessment of large systems and installations (see also some concepts in the projects on HEMP and on EMC and functional safety)
- EMC requirements, based on EM environment and experience: EMC standards are widely used. In many countries they are applied by legislation. Therefore, further optimization of the EMC requirements is necessary. This requires:
 - better and more accurate description of the environment (statistics) for setting optimum limits. Compatibility levels for voltage dips and short interruptions in the LV public network have 1st priority in the LF range

- more experience with equipment behavior, related to optimized limits, in order to optimally minimize the number of phenomena to be tested.
- EMC measurement and test methods:
Also the test procedures should be further optimized for the aforementioned reasons. This means:
 - drafting standards of better quality
 - new, innovative cost and/or time saving test methods
 - coordination of emission and immunity testing: Increased cooperation CISPR / TC77, e.g.: Joint Task Forces for "TEM cells", "Mode stirred chambers"
 - strong consideration of feedback from product committees, who are applying the Basic and Generic Standards,
 - improved cooperation of the horizontal EMC committees of the IEC (CISPR and TC77) with the product committees in IEC and with committees outside IEC (ISO, ITU etc.)
- Priority of Product Standards:
While essential standards and requirements are at a mature stage in the horizontal EMC committees, the drafting of Product Family or Product Standards obtains high priority. Therefore, more technical guidance should be given to product committees in this field.

8. REFERENCES

- [1] IEC GUIDE 107 (1998-01), "Electromagnetic compatibility - Guide to the drafting of electromagnetic compatibility publications" IEC, Geneva, 1998
- () Numbers in round brackets refer to IEC publications with the same number

BIOGRAPHICAL NOTE

Bàlint T. Szentkuti has obtained his diploma in electrical engineering and his Ph.D. degree from the Federal Institute of Technology Zurich, Switzerland. He has first been with the Microwave Laboratory of the same Institute. In 1978 he has joined the Swiss PTT R&D Division, now called Swisscom - Corporate Technology, where he is manager in Environment and EMC. He is active in standardization, currently being the chairman of IEC TC 77: EMC.

ABBREVIATIONS AND DEFINITIONS			
Ai	amendment No i,	DC	direct current
Ai / fj:	Amendment i, fragment j	EM	electromagnetic
AC	alternating current	EMC	electromagnetic compatibility
APUB	document approved for publication	FDIS	final draft international standard
BPUB	document being published	(pr)EN	(draft) European standard
CD	Committee draft	ENV	European prestandard
CDV	committee draft for voting	IEC	International Electrotechnical Commission
2CD(V)	second committee draft (for voting)	HF	high frequency;
CENELEC	European Committee for Electrotechnical Standardization	LF	low frequency; in this context usually $f < 9 \text{ kHz}$
CLC	= CENELEC	PPUB	printed publication
CISPR	International Special Committee on Radio Interference	RF	radio frequency, $f > 9 \text{ kHz}$
CRT	cathode ray tube	SC	subcommittee
		TC	technical committee
		TR	technical report
		WG	working group

Table 1: Principal EM phenomena

Conducted low-frequency phenomena
- Harmonics, interharmonics
- Signaling voltages
- Voltage fluctuations
- Voltage dips and interruptions
- Voltage unbalance
- Power-frequency variations
- Induced low-frequency voltages
- DC in AC networks
Radiated low-frequency phenomena
- Magnetic fields
- Electric fields
Conducted high-frequency phenomena
- Induced CW voltages or currents
- Unidirectional transients
- Oscillatory transients
Radiated high-frequency phenomena
- Magnetic fields
- Electric fields
- Electromagnetic fields
. Continuous waves
. Transients
Electrostatic discharge phenomena (ESD)
High altitude nuclear electromagnetic pulse (HEMP)

Table 2: IEC 61000-x-y series publications

Part 1: General
- General considerations (introduction, fundamental principles)
- Definitions, terminology
Part 2: Environment
- Description of the environment
- Classification of the environment
- Compatibility levels
Part 3: Limits
- Emission limits
- Immunity limits (in so far as they do not fall under the responsibility of the product committees)
Part 4: Testing and measurement techniques
- Measurement techniques
- Testing techniques
Part 5: Installation and mitigation guidelines
- Installation guidelines
- Mitigation methods and devices
Part 6: Generic standards
- Immunity
- Emission
Part 9: Miscellaneous
- (empty)
Each part (x) is further subdivided into sections (y) which are to be published either as international standards or as technical reports

Table 3: List of IEC 61000-x-y publications and projects (Fall 1997)

Notes:

1. Part and section numbers -x-y in brackets indicate projects (no printed publication available)
2. In case of existing publications, the document numbers in brackets indicate the last versions of ongoing amendments or revisions, if any
3. In case of projects, the document numbers in brackets indicate the last draft

61000: Electromagnetic compatibility (EMC) - Part 1: General -

- 1-1: Application and interpretation of fundamental definitions and terms, TR3
- (-1-2): Methodology for the achievement of functional safety of electrical and electronic equipment (77/182/CD)

61000: Electromagnetic compatibility (EMC) - Part 2: Environment -

- 2-1: Description of the environment - Electromagnetic environment for low-frequency conducted disturbances and signalling in public power supply systems, TR3
- 2-2: Electromagnetic compatibility (EMC) - Part 2: Environment - Section 2: Compatibility levels for low-frequency conducted disturbances and signalling in public low-voltage power supply systems (77A(Sec.)85/NP)
- 2-3: Description of the environment - Radiated and non-network-frequency-related conducted phenomena, TR3
- 2-4: Compatibility levels in industrial plants for low-frequency conducted disturbances, (77A(Sec.)112/NP)
- 2-5: Classification of electromagnetic environments, TR2
- 2-6: Assessment of the emission levels in the power supply of industrial plants as regards low-frequency conducted disturbances, TR3
- 2-7: Low-frequency magnetic fields in various environments, TR3
- (-2-8): Voltage dips, short interruptions and statistical measurement results (Report), (77A/121/NP)
- 2-9: Description of HEMP environment - Radiated disturbance. Basic EMC publication.
- (-2-10): Description of HEMP environment - Conducted disturbance. Basic EMC Publication (77C/43/CDV)
- (-2-11): Classification of HEMP environment. Basic EMC Publication (77C/41/CD)
- (-2-12): Compatibility levels for low-frequency conducted disturbances and signalling in public medium-voltage power supply systems. Basic EMC Publication (77A/174/CDV)

61000: Electromagnetic compatibility (EMC) - Part 3: Limits -

- 3-2: Limits for harmonic current emissions (equipment input current \leq 16 per phase) (77A/185/FDIS, Amd. 1 Ed. 1.0, 77A/186/FDIS, 77A/217/FDIS, 77A/166/CD, 77A/164/CD)
- 3-3: Limitation of voltage fluctuations and flicker in low-voltage supply systems for equipment with rated current \leq 16 A (77A/140/NP)
- (-3-4): Limitation of emission of harmonics for equipment with rated current greater than 16A, TR2 (77A/169/CDV)
- 3-5: Limitation of voltage fluctuations and flicker in low-voltage power supply systems for equipment with rated current greater than 16 A, TR2

-3-6:	Assessment of emission limits for distorting loads in MV and HV power systems - Basic EMC publication, TR3
-3-7:	Assessment of emission limits for fluctuating loads in MV and HV power systems - Basic EMC publication
-3-8:	Signalling on low-voltage electrical installations - Emission levels, frequency bands and electromagnetic disturbance levels
(-3-9):	Limits for interharmonic current emissions (equipment with input power \leq 16 A per phase and prone to produce interharmonics by design) (77A/196/CD)
(-3-10):	Emission limits in the frequency range 2 ... 9 kHz (77A/122/NP)
(-3-11):	Limitation of voltage changes, voltage fluctuations and flicker in public low-voltage supply systems for equipment with rated current \leq 75 A and subject to conditional connection (77A/193/CD)
61000:	Electromagnetic compatibility (EMC) - Part 4: Testing and measurement techniques -
-4-1:	Overview of immunity tests. Basic EMC Publication (77/188/CD)
-4-2:	Electrostatic discharge immunity test. Basic EMC Publication; (77B/216/FDIS, 77B/189/NP, 77B/190/NP, 77B/191/NP)
-4-3:	Radiated, radio-frequency, electromagnetic field immunity test (77B/203/CDV, 77B/204/CDV, 77B/212/CD, 77B/215/CD)
-4-4:	Electrical fast transient/burst immunity test. Basic EMC Publication (77B/193/CD)
-4-5:	Surge immunity test (77B/152/NP, 77B/192/INF)
-4-6:	Immunity to conducted disturbances, induced by radio-frequency fields
-4-7:	General guide on harmonics and interharmonics measurements and instrumentation, for power supply systems and equipment connected thereto (77A/197/CD)
-4-8:	Power frequency magnetic field immunity test. Basic EMC Publication
-4-9:	Pulse magnetic field immunity test. Basic EMC Publication
-4-10:	Damped oscillatory magnetic field immunity test. Basic EMC Publication
-4-11:	Voltage dips, short interruptions and voltage variations immunity tests
-4-12:	Oscillatory waves immunity test. Basic EMC Publication (77B(France)3/NP)
(-4-13):	Harmonics and interharmonics including mains signalling at a.c. power port, immunity tests. Basic EMC publication (77A/215/CD)
(-4-14):	Test for immunity to voltage fluctuations, Immunity test - Basic EMC Publication (77A/214/CDV)
-4-15:	Flickermeter - Functional and design specifications (BPUB: 77A/187/NP)
(-4-16):	Test for immunity to conducted, common mode disturbances in the frequency range 0 Hz to 150 kHz (77A/201/FDIS)
(-4-17):	Ripple on d.c. input power port, immunity test. Basic EMC publication (77A/207/CDV)
(-4-20):	TEM cells. Basic EMC Publication: 77B/153/CD (see also -4-3)
(-4-21):	Test for immunity to radiated electromagnetic fields in mode stirred chambers (see also -4-3)
(-4-22):	Guide on measurement methods for electromagnetic phenomena (77(Sec.)134/NP)
(-4-23):	Test methods for protective devices for HEMP radiated disturbance (77C/38/CD)
-4-24:	Test methods for protective devices for HEMP conducted disturbance - Basic EMC Publication
(-4-25):	HEMP requirements and test methods for equipment and systems. Basic EMC Publication (77C/46/CD)
(-4-26):	Calibration of probes and associated instruments for measuring electromagnetic fields (77B/150/NP)
(-4-27):	Unbalance, immunity test (77A/176/CD)
(-4-28):	Variation of power frequency, immunity test - Basic EMC Publication (77A/157/CD)
(-4-29):	Testing and measuring techniques - Voltage dips, short interruptions and voltage variations on d.c. input power ports, immunity tests - Basic EMC publication (77A/206/CD)

(-4-30): Measurement of power quality parameters. Basic EMC Publication (77/183/NP, 77/187/NP)
(-4-31): Measurements in the frequency range 2 kHz to 9 kHz. Basic EMC publication (77A/198/CD)

61000: Electromagnetic compatibility (EMC) - Part 5: Installation and mitigation guidelines -

- 5-1: General considerations - Basic EMC publication, TR 3
- 5-2: Earthing and cabling, TR3
- (-5-3): HEMP protection concepts (77C/39/CD)
- 5-4: HEMP - Specification for protective devices against HEMP radiated disturbance. Basic EMC Publication, TR2
- 5-5: Electromagnetic compatibility (EMC) - Part 5: Installation and mitigation guidelines - Section 5: Specification of protective devices for HEMP conducted disturbance. Basic EMC Publication
- (-5-6): Mitigation of external influences, TR3 (77B/154/CD, reactivated)
- (-5-7): Degrees of protection against electromagnetic disturbances provided by enclosures (EM Code) (70(France)23/NP)

61000: Electromagnetic compatibility (EMC) - Part 6: Generic standards -

- 6-1: Immunity for residential, commercial and light-industrial environments
- (-6-2): Immunity for industrial environments (77/195/CDV)

CISPR 61000-6-3: Emission standard for residential, commercial and light-industrial environments

CISPR 61000-6-4: Emission standard for industrial environments

61000: Electromagnetic compatibility (EMC) - Part 9: Miscellaneous -

(empty)

Table 4: Generic EMC Standards**Table 4a: Overview¹⁾ of the Generic EMC Immunity Standards**

Phenomenon Basic std	Port	Test specification		Comments
		resid., commerc., light-industrial 61000-6-1 ≈ EN 50082-1:1997	industrial environment draft 61000-6-2 77/195/CDV	
power freq. magn. field, <i>IEC 61000-4-8</i>	enclosure	3 A/m	30 A/m	acceptable jitter on CRT screen specified at 1 A/m
radio freq. EM field, AM <i>IEC 61000-4-3</i>	enclosure	carrier: 3 V/m	carrier: 10 V/m ⁵⁾	carrier f ²⁾ : 80 - 1000 MHz, with AM 1 kHz, 80 %
radio freq. EM field, keyed carrier <i>ENV 50204⁴⁾</i> ("GSM")	enclosure	carrier: 3 V/m	no requirement	carrier f: 900 MHz, on/off rate: 200 Hz (only in Europe)
ESD <i>IEC 61000-4-2</i>	enclosure	4 kV / 8 kV	4 kV / 8 kV	air / contact discharge
radio freq. induced current <i>IEC 61000-4-6</i>	signal, control DC input, output AC input, output functional earth	carrier: 3 V, e.m.f.	carrier: 10 V, e.m.f. ⁵⁾	carrier f ²⁾ : 0.15 - 80 MHz with AM 1 kHz, 80 %, 150 Ω source
fast transients, "burst" <i>IEC 61000-4-4</i>	signal, control DC input, output AC input, output functional earth	... 0,5 kV. ... 0,5 kV ... 1,0 kV ... 0,5 kV	... 1 kV ... 2 kV ... 2 kV ... 1 kV	
"surges" <i>IEC 61000-4-5</i>	signal, control DC input, output AC input, output	... no requirement ... 0.5 / 0.5 kV ... 2 / 1 kV	... 1 kV ... 0.5 / 0.5 kV ... 4 / 2 kV ³⁾	... line-to-earth [line-to-earth/ line-to-line]
Voltage dips & <i>IEC 61000-4-11</i>	AC input	30 %, 0.5 periods 60 %, 5 periods	30 %, 0.5 periods 60 %, 5 & 50 periods	... reset allowed
Voltage interrupt. <i>IEC 61000-4-11</i>	AC input	> 95 %, 250 periods	>95 %, 250 periods	... reset allowed

1) This table does not contain significant details. See further information in the original documents!

2) In some non-European countries the transition frequency between conducted and radiated RF tests (61000-4-6 and -4-3) is optional within 26 and 80 MHz.

3) With external protection elements, if their use is required in the equipment's manual

4) Required only in European countries, according to the pre-standard ENV 50204. This standard will probably be withdrawn

5) In the ITU broadcasting bands only 3 V/m or 3V, respectively is required

Table 4b: Overview¹⁾ of the Generic EMC Emission Standards

Phenomenon Basic std	Port	Test specification		Comments
		resid., commerc., and light-industr. CISPR 61000-6-3 ≡ EN 50081-1:1992	industrial environment CISPR 61000-6-4 ≡ EN 50081-2:1992	
radio frequency EM fields: <i>CISPR 22, 11</i>	enclosure	30 - 37 dB(µV/m) at 10 m	30 - 37 B(µV/m) at 30 m	f: 30 - 1000 MHz
Harmonics <i>IEC 61000-3-2</i>	AC	0.05 - 2.3 A	no requirements	f: 0 - 2 kHz
Volt. fluct. & flicker <i>IEC 61000-3-3</i>	AC	see Standard	no requirements	
radio frequency voltages <i>CISPR 22,11,14,</i>	AC	46 - 66 dB(µV)	60 - 79 dB(µV)	f: 0.15 - 30 MHz (also "clicks")

1) This table does not contain significant details. See further information in the original documents!

Table 5 : Cross reference of publications and projects 61000-x-y versus EM phenomena (Fall 1997)

Notes:

1. The first column refers to the EM phenomena, the others to publication 61000, part x. The numbers in the cells refer to section y.
2. Section numbers in brackets indicate projects (no printed publication available).
3. * means that amendment or revision is in progress.

4. Essential phenomena referenced in Generic standards are highlighted 
5. Additional abbreviations

cal	calibration	HV	high voltage
CL	compatibility levels	ind	industrial
class	classification	MV	medium voltage
con	conducted	pr	protective device
CW	stationary wave	rad	radiated
desc	description		

principal EM phenomena	61000-1-General	61000-2-Environment	61000-3-(Emission) Limits	61000-4-Test & measurement methods	61000-5-Install. & mitigation guidel.	61000-6-Generic Stds (see also tables 4)	Emis-sion
EM phenomena, generally	-1, (-2)	-3 desc -5 class		-1*	(-22) -1 general -2 earth/cabl. (-6) ext. influ.		Immuni-tiy
Conducted low frequency phenomena					(-30) power quality		

principal EM phenomena	61000-1- General	61000-2- Environment	61000-3- (Emission) Limits	Test & measurement methods		61000-5- Install. & mitigation guidel.	61000-6- Generic Stds (see also tables 4)
				Immunity	Emission		
- Harmonics,			≤16A, LV (-4) >16A, LV -6 MV, HV (-10) 2-9 kHz	(-13) (-17) ripple on DC	(-31) 2 - 9 kHz		3
Interharmonics			(-9) ≤ 16A, LV (-10) 2-9 kHz	(-13)	-7* (-31) 2 - 9 kHz		
- Signaling voltages			-8	(-13)			
- Voltage fluctuations			≤ 6A, LV -5 >16A, LV -7 MV, HV (-11) ≤ 75A, LV	(-14)	15*		3
- Voltage dips and interruptions			(-8) desc		AC (-29) DC		-1 (-2)
- Voltage unbalance					(-27)		
- Power-frequency variations					(-28)		
- Induced low-frequency voltages					(-16)		
- DC in AC networks							
Radiated low frequency phenomena							
- Magnetic fields			-7 desc		CW -9 pulse -10 oscill		1, (-2)
- Electric fields							

principal EM phenomena	61000-1-General	61000-2-Environment	61000-3-(Emission) Limits	Test & measurement methods	61000-4-Immunity	61000-5-Install. & mitigation guidel.	61000-6-Generic Stds (see also tables 4)	Emiss-ion
					Emission	Immuni-tiy		
Conducted high frequency phenomena								
- Induced CW voltages or currents			6	CISPR 11, 22		1 (-2)	-3, -4	
- Unidirectional transients				-4** burst 5** surge		1 (-2)		
- Oscillatory transients			-12*			1 (-2)		
- "clicks"					CISPR 14		3, -4	
Radiated high frequency phenomena								
- Magnetic fields								
- Electric fields					3** (-20) TEM (-21) mode stirr.	CISPR 11, 22 (-26) cal of probes	(-7) enclosure	1, (-2)
- Electromagnetic fields								3, -4
-- Continuous disturb.								
-- Transients								
Electrostatic discharge (ESD)					2*			1, (-2)
High altitude nuclear electromagnetic pulse (HEMP)			-9 rad (-10) con (-11) class		(-23) pr rad -24 pr con (-25)		(-3) concepts -4 pr rad -5 pr con	

XVI
WORKSHOPS

**Practical Solution for Frequency
Planning and Spectrum Management**

Workshop Organizers:

L & S Hochfrequenztechnik - Germany
in cooperation with
Rohde & Schwarz - Austria

Practical Solutions for Frequency Planning and Spectrum Management

Daniel Lautenbach, L&S Hochfrequenztechnik GmbH

Im Gewerbegebiet 31, D-77839 Lichtenau, phone: +49 7227 95350

1. SPECTRUM MANAGEMENT

Spectrum Management is an extremely wide field of work. Starting from the Monitoring, which is highly important to know about the present situation, it delivers large numbers of data which need to be administrated. The data has to be compared with the actual situation according to the existing licenses. Due to that, a countrywide spectrum database, accessible from every relevant co-worker in dedicated security levels, needs to be available. For the daily work like data access, project tracing, licensing, EMC and interference checking, statistics and visualization of data on a map are important tools for cost effective work.

The highly specialized procedures for national and international coordination in today's communication services make it necessary to have service specific tools besides the global functionality. If also a full or partial check of an existing or a new planning approach needs to be done, additional engineering tools for the different services need to be available.

Spectrum management software solutions incorporate all these issues in a modular way. Common start-up software can contain toolmodules for almost all of the daily work. For the very specialized tasks planning or coordination software can be started from the interface. Specialized tools, for e.g. data integration and compression gained out of monitoring activities, can also be accessed.

Due to the very specialized tasks, the individual packages are needed for, they have very individual data structure. To make data comparable, systems also incorporate a Browser Database, being identical in data structure for all services and frequencies. State-of-the-Art software packages have the facilities to update the common Browser whenever a change in the service specific database has been carried out. Consequently data

from different sources stay comparable and every user has permanently the most important data available directly at his desk.

A basic idea is the modularity. It can be configured totally individual in the most helpful and cost efficient way for the user. Only the needed toolmodules and software packages are combined under one shell and can work together in the way described above.

Step by step the system can be enlarged by adding other software packages or toolmodules to upgrade functionality.

The following toolmodules are necessary to reach the high tasks for spectrum management.

1.1. Data Access

Data Access is a linking module towards the Spectrum Database. It manages all the linking and querying towards the database and makes the data available inside the environment for all other toolmodules.

1.2. List Visualizer

Checking data, making queries, visualizing tables is the job of a List Visualizer. The data can be viewed and edited (depending on the user level and the specialties of the data). E.g. browser data is always read only type, because it is an extract of the other databases.

1.3. Archive Data

Outdated information and calculation results need to be removed from the database in order to increase the working speed. On the other hand, especially in administrations such data needs to be traceable even after years. For that purpose an Archive Data module is helpful. It allows to clean up databases and to move outdated information towards a storage media like a tape, CD or a background hard disc. A special movement list is

created and controlled by the Archive Data module which allows to retrieve such data it is needed later on again.

1.4. Statistics

Statistics is a very important mean to show the activity of an organization and to get an overview about tendencies of the customers (e.g. license applicants). General and individual statistic research can be carried out using a Statistics module. It allows to check daily, weekly, monthly, quarterly or yearly activities for a special task or a compound task being carried out from a department. Standard deviation, mean value, variance and other characteristic figures can be produced within no time. Information is displayed as piegraph, bargraph, table or can be exported into an Excel format for instance.

1.5. Map Handler

Using a Map Handler, one gets additional GIS functionality into the system. The Map Handler allows to load maps and binary data matrices and is able to visualize them on the screen. The actual cursor position is permanently shown on the screen and operations like length measurements can be carried out directly. In binary data profiles can also be derived. Maps can be printed in scaled proportions.

1.6. Net Visualizer

To visualize a net configuration, e.g. of a broadcast provider a Net Visualizer is an important addition to the Map Handler. It enables the user to display all stations within a specific area or a frequency range. Selections of an area can be carried out graphically.

1.8. Vector Handler

To present vectorized data within the system, a Vector Handler is the appropriate tool. It allows to overlay such data over the Map Handler worksheets and to present data in different colors and ways like numbers, location points, piegraphs or nets. Vectors can be edited graphically or in list form. Also new vectors can be generated easily by hand.

1.8. Project Tracer

A very important matter is the actual stage of a project like a licensing or a coordination request. A project tracer helps to overcome this problem. It consists of a project database which incorporates the stage of each single task being presently under

work in the organizations. All changes of the project status are recorded and the person or department, actually working on the task is visible. The system also allows to set and trace deadlines. The one who has to obey the deadline is warned and also a supervising instance can be informed early enough. For organizations like authorities a Project Tracer is a guarantee for efficient, smooth working.

1.9. Licence Check

To cross-check licensing situations, to trace licence deadlines and to incorporate or retrieve additional licence data like e.g. licence related measurement results or Photographs of a site, a Licence Check tool is needed.

1.10. Licence Billing

The most important tool in terms of cash flow is a Licence Billing tool. For every administrative service a billing procedure can be individually created which includes billing dates, licence rates, penalty fees and upgrades for quarterly or monthly payments. The payment tracing for all existing licences gives a high level of security.

1.11. Licence Printing

A special print facility takes care of the different types of licences in the different services. With an included special configurator, a TIFF picture being created in a drawing or painting software e.g. also in the map handler, can be integrated as form sheet for a special licence type.

1.12. IF Checker

To cross-check between existing licences and the results of the monitoring measurement, an IF Checker tool is extremely helpful. A relation, between measured results and existing licences inside and outside the country, is set up. The functionality allows to carry out simple propagation checks and interference analysis in order to get a rough idea about the real interference situation. The results can be compared with monitoring data.

1.13. EMC Checker

In order to trace Electro Magnetic Compatibility (EMC) problems, an EMC Checker can be included. If a problem has occurred, the EMC situation of a location can easily be analyzed with simple models. Such a list of possible problem causing candidates can be created to assist the people of measurement department.

2. STAND ALONE SOFTWARE PACKAGES

2.1. Planning Tools

Engineering tools for planning all kinds of services are a helpful extension to previous described spectrum management system. Common for all is a graphical user interface and a high grade of linking between map graphics and the database. Stations can be positioned and visualized in the maps and all calculation results can be overlaid to any type of map and data. All tools are stand alone solutions which can be used for the individual work without adding anything else and can work under the spectrum management system environment.

2.2. Coordination Tools

Especially during the implementation phase of a new network large numbers of license requests occur. It may easily amount a thousands of requests a month which have to be checked in terms of data integrity and coordinability. This is the task of coordination tools. They allow to carry out the coordination check procedure which is agreed for specific services in specific regions (e.g. the Vienna Agreement). All coordination tracing and data exchange with the operators is done within these packages. Actually such tools are available for all kinds of services.

2.3. Monitoring Package

The link to the Data Access System of the monitoring Stations and Drive Measurements. The following functions are typically requested:

- comparison of technical output parameters (monitored against licensed)
- verification of spectrum occupation (monitored against licensed; monitored actually against monitored previously)
- visualization of DF results and search for most likely licensed emitter
- cross-check of measurements and licensed behavior and detection of discrepancy
- triggering of monitoring process in those cases where discrepancies have been detected
- compressing of data by statistical means like mean value, elimination of worst X percentage, integration of data from a definable tile
- administration of results via monitoring database
- linking of data to specific stations (sites)
- searching the most likely station for a monitoring result and allocating it
- visualization of data on a map
- visualization of data in a spreadsheet
- visualization of data as diagrams (bar, pie)
- export of data to Excel, ASCII files and dTIFF (Pictures)
- creation of measurement tasks command strings

XVI
W O R K S H O P S

**Transients Immunity Tests on Different
Ports, Flicker and Harmonics
Measurements on Power Line Port**

Workshop Organizer:

EMC PARTNER AG - Switzerland

EMC 98

INTERNATIONAL WROCŁAW SYMPOSIUM ON ELECTROMAGNETIC COMPATIBILITY WORKSHOP

TRANSIENT IMMUNITY TESTS ON DIFFERENT PORTS, FLICKER AND HARMONICS MEASUREMENTS ON POWER LINE PORT

Martin Lutz
EMC PARTNER AG
Baselstrasse 160
4242 Laufen Switzerland

Phone: ++41 61 763 01 11
Fax: ++41 61 763 01 15

1. ACTUAL STATUS INTERNATIONAL (IEC)

Within the International Electrotechnical Commission (IEC) the technical committee TC 65 began early in the eighties with the publication of the 801-x product family standard. The technical committee 65 is responsible for the area industrial process measuring and control equipment. Therefore the documents 801-x series are product family standards. Also in the eighties the IEC established an other technical committee 77. The committee TC77 is responsible for the electromagnetic compatibility within IEC. In addition to own basic EMC standards the TC 77 has taken over, at the beginning of the nineties, the technical content of the existing 801-x documents and published them as basic standards with the number 1000-4-x. In the future both series 801-x as product family standards and the 1000-4-x as basic standards will be available and used. The information in the table below represents the status of the 61000-4-x series in January 98.

Standards IEC	Standards EN	Content, title	Revision within the next 3 years?	Status
61000-4-1 1992	EN61000-4-1	Overview	yes	IS
61000-4-2 1995	EN61000-4-2	ESD	no, amendments	IS
61000-4-3 1995	ENV 50140	EM field	no, amendments TEM cells, reverberation chamber, digital radio	IS
61000-4-4 1995	61000-4-4	EFT	no, amendments	IS
61000-4-5 1995	61000-4-5	SURGE	no	IS
61000-4-6 1998	61000-4-6	Conducted disturbances, induced by radio-frequency fields	no	IS
61000-4-7 1991	-	Harmonics measuring	yes	IS
61000-4-8 1993	61000-4-8	50/60 Hz Magnetic field	no	IS
61000-4-9 1993	61000-4-9	SURGE Magnetic field	no	IS
61000-4-10 1993	61000-4-10	Oscillatory Magnetic field	no	IS

61000-4-11 1994	61000-4-11	Voltage dips and interruption	no,	IS
61000-4-12 1995	61000-4-12	Oscillatory waves	no, amendment >1MHz	IS
61000-4-13		Harmonics, Interharmonics, Main Signalling	77A/215/CD	CD
61000-4-14		Voltage fluctuations, unbalance, variation of the power frequency	77A/214/CDV	CDV
61000-4-15 1997		Flicker measurement	no, amendment verification	
61000-4-16 1996		Conducted disturbance in the range of DC to 150 kHz	no	IS
61000-4-17		Ripple on DC power supply	77A/207/CDV	CDV
61000-4-18		free		
61000-4-19		free		
61000-4-20		TEM cells Alternative method to 61000-4-3	77B/153/CD	CD
61000-4-21		Reverberation chamber Alternative method to 61000-4-3	77B/.../CD	CD
61000-4-22		Guide on measurement methods for electromagnetic phenomena	Status D	NMI
61000-4-23		Test methods for protective devices for HEMP radiated disturbance	77C/36/CD	CD
61000-4-24 1998		Test methods for protective devices for HEMP conducted disturbance	no	IS
61000-4-25		HEMP requirements and test methods for equipment and systems	77C/55/CD	CD
61000-4-26		Calibration of probes and instruments for measuring electromagnetic fields	77B/150/NP	NMI
61000-4-27		Unbalance in 3phase mains	77A/178/CD	CD
61000-4-28		Variation of power frequency	77A/235/CDV	CDV
61000-4-29		Voltage dips and interruption on d.c.	77A/206/CD	CD
61000-4-30		Measurement of power quality parameters	77A/183/NP	NP
61000-4-31		Measurement in the frequency range 2 kHz to 9 kHz	77A/198/CD	CD

Legend:

- CD Committee draft of comment
CDV Committee draft for vote
DC Draft for comment
DIS Draft international standard
DV Draft for voting
IS International standard
NCP National Committee proposal
NP New work item proposal
RV Result of voting
RVC Result of vote on CDV
RVD Report of voting on DIS
RVN Report of voting on NP
WG Working group membership list

2. ACTUAL STATUS IN EUROPE (EN)

The European Community EC has issued an EMC directive mandating that all electronic products must have a certain immunity and overpass not a certain emission limit. These requirements are scheduled to become effective January 1, 1996. In the transition period whereas no IEC or EN product standards are available the EC normalisation organisation CENELEC (European Committee for Electrotechnical Standardisation) has published the so called „Generic standards“. The different immunity tests and emission measurements in the generic standards are based on the IEC documents 1000-4-x. In December 1996 the IEC and the ISO have allocated themselves blocks of publication numbers from 60'000 to 79'000 for IEC. Therefore the numbers of the standards are equal between the IEC and CENELEC.

IEC IEC 61000-4-X	CENELEC EN 61000-4-x
----------------------	-------------------------

As long as the IEC product committees has not worked out EMC product standards, or in the existing product standards the EMC aspects are not covered, all the electronic equipment must be tested in accordance with the generic standards to pass the EC border after 1st January 96.

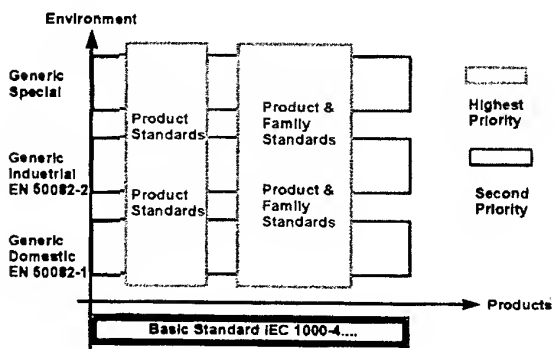
Generic Immunity Standard

- EN 50082-1 Part 1: Residential, commercial and light industry
- EN 50082-2 Part 2: Industrial environment

Generic Emission Standard

- EN 50081-1 Part 1: Residential, commercial and light industry
- EN 50081-2 Part 2: Industrial environment

3. RELATION BETWEEN BASIC, GENERIC AND PRODUCT STANDARD



From the above diagram it can be derived that the product or product family standard has the highest priority and must be used, when they are

published. To understand better the different among the three standards very briefly the contents of the three types will be described.

4. BASIC STANDARDS

The content of the basic standard is:

- definition and description of the phenomenon
- detailed test and measurement methods
- test instrumentation
- basic test set up
- range of test levels

not included:

- prescribed limits
- performance criteria
- product specific test arrangements
- test sequences

As a consequence of the content of the basic standards, EMC immunity test can not carry out alone with the basic standard. To run EMC test additional information are needed. The additional information is given either in the generic or product standards.

Most of the basic standards work are finished in TC77. Only about two to three basic immunities basic documents are still in the pipeline of TC77.

Electrostatic Discharge ESD, electrical fast transient EFT, SURGE and DIPS are the most important transient's interference sources. An overview about the different important parameter as defined in the basic immunity standards are given in the table followed:

Characteristics	Static discharge	Switching operations	Lightning	Power trip o
	"ESD"	"EFT Burst"	"Surge"	"DIPS"
Voltage U	up to 15 kV	up to 4 kV	up to 6 kV	supply voltage
Energies at maximum charging voltage	below 10 mJ	300 mJ	300 J	-
Repetition rate	Single impulse	multiple pulses 5 Idz	maximum 8 Impulses / Min	related to the power frequ
Application Equipment under Test	Metal parts, which can be touched by persons	Power-, Signal-, Measuring- and Data-lines	Power-, Signal-, Measuring- and Data-lines	power supply a dc
Upper frequency limit	Approx. 1 GHz	Approx. 100 MHz	Approx. 350 kHz	Approx. 100 k
Waveforms	ESD	EFT	SURGE	DIPS
	IEC 1000-4-2	IEC 1000-4-4	IEC 1000-4-5	IEC 1000-4-

5. GENERIC STANDARDS

The generic standards are only important for the transition time up to the publication date of product standard.

Basically two environments can be differ:

61000-4-3 or part 20 or 21

Residential, commercial and light industry

Locations that are characterised by being supplied directly at low voltage from public mains are considered to be residential, commercial or light industry.

- residential properties, e. g. houses, apartments
- retail outlets, e. g. shops, supermarkets
- business premises, e. g. offices, banks
- areas of public entertainment, e. g. cinemas, public bars, dance halls
- outdoor locations, e. g. petrol stations, car parks, amusements and sports centres
- light-industrial locations, e. g. workshops, laboratories, service centres.

Industrial environment

Current and associated magnetic fields are high

- industrial, scientific and medical (ISM) apparatus
- heavy inductive or capacitive loads are frequently switched

The generic standard refers to the basic standards.

Phenomena Basic standard	Tests	Residential and light industrial	Industrial	Special e. power pls
61000-4-2	ESD	g.a.	g.a.	g.a.
61000-4-3	Radiated electromagnetic field >80MHz	g.a.	g.a.	g.a.
61000-4-4	EFT/Burst	g.a.	g.a.	g.a.
61000-4-5	SURGE	g.a.	g.a.	g.a.
61000-4-6	Conducted disturbances induced by radio-frequency fields <80MHz	g.a.	g.a.	g.a.
61000-4-7	General Guide on harmonics and inter-harmonics measurements and instrumentation	n.i.s.	n.i.s.	n.i.s.
61000-4-8	50/60 Hz Magnetic field	may	may	g.a.
61000-4-9	SURGE Magnetic field	g.n.a.	g.n.a.	g.a.
61000-4-10	Oscillatory Magnetic field	g.n.a.	g.n.a.	g.a.
61000-4-11	Voltage dips and interruption	g.a.	g.a.	g.a.
61000-4-12	Oscillatory waves „ring wave“	may	may	may
61000-4-12	Oscillatory waves 1MHz	g.n.a.	may	g.a.
61000-4-13*	Harmonics, Inter-harmonics, Main Signalling	g.n.a.	g.n.a.	g.n.a.
61000-4-14*	Voltage fluctuations	g.n.a.	g.n.a.	g.n.a.
61000-4-15	Flickermeter	n.i.s.	n.i.s.	n.i.s.
61000-4-16	Conducted disturbance in the range of DC to 150 kHz	g.n.a.	may	g.n.a.
61000-4-17	Ripple on DC power supply	g.n.a.	may	g.n.a.
61000-4-18	free			
61000-4-19	free			
61000-4-20*	TEM cells	2	2	2
61000-4-21*	Reverberation chambers	2	2	2
61000-4-22	free			
61000-4-23*	Test methods for protective devices for HEMP radiated disturbance	g.n.a.	g.n.a.	g.n.a.
61000-4-24	Test methods for protective devices for HEMP conducted disturbance	g.n.a.	g.n.a.	g.n.a.
61000-4-25*	HEMP requirements and test methods for equipment and systems	g.n.a.	g.n.a.	g.n.a.
61000-4-26*	Calibration of probes and instruments for measuring electromagnetic fields	n.i.s.	n.i.s.	n.i.s.
61000-4-27*	Unbalance in 3phase mains	no	maybe	maybe
61000-4-28*	Variation of power frequency	no	maybe	maybe
61000-4-29*	Voltage dips and interruption on d.c.	may	may	may
61000-4-30*	Measurement of power quality parameters	n.i.s.	n.i.s.	n.i.s.
61000-4-31*	Measurements in the frequency range 2 kHz to 8 kHz	n.i.s.	n.i.s.	n.i.s.

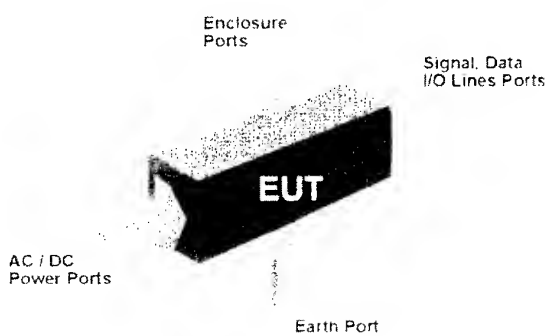
Legend:

- n.i.s. Not an immunity standard
- g.a. Generally applicable except in special cases
- may May be applicable in certain circumstances
- g.n.a. Generally not applicable except in special cases
- * The document is in progress but not finally published
- 2 Special alternative test method. Application range see

In addition to the basic standard the following information and questions are included the generic document. The question must be answered to run EMC tests.

Applicability of the generic standards

- The applicability of the test depends on the particular apparatus, its configuration, its ports, its technology and its operating conditions.
- Test shall only be carried out where the relevant ports exist
- It may be determined by characteristics and usage that some of the test are inappropriate and therefore unnecessary. The decision and justification not to test shall be recorded in the test report.



Condition during testing

- Test shall be made in the most susceptible operating mode.
- The configuration of the test sample shall be varied to achieve maximum susceptibility
- If the apparatus is part of a system with auxiliary apparatus then it shall be tested with the minimum representative configuration of auxiliary apparatus.
- When external protection devices are clearly specified in the user manual, then the test may be applied with the external protection devices.
- The configuration and mode of operation shall be precisely noted in the test report. The most critical mode operations shall be selected.
- If the apparatus has a large number of similar ports a sufficient number shall be selected to simulate actual operating conditions.
- Test condition shall be within the operating ranges of temperature, humidity, pressure etc.

Immunity test requirements

- Test shall be conducted in a well defined and reproducible manner.

- The test shall be carried out as single tests in sequence.
- The sequence of testing is optional.
- Test generator, test method, test set up is given in the basic standards.
- Modification and additional information needed for the practical applications of the tests are given in the product standard.

General test requirements

- Reliability of the test results:**
 - number of shots
 - test time
 - polarity
 - phase angle
 - synchronisation with EUT operating sequence
 - etc.
- Statistical aspects**
- The personnel safety must be guaranteed during the immunity test.

Performance criteria

- The variety of the apparatus makes it difficult to define precise criteria.
- As a result of the application of the test the apparatus becomes dangerous or unsafe as a consequence the test failed.
- Definition of performance shall be specified in a test plan and noted in the test report.

Three general performances can be used as a guide:

- A) No loss of function is allowed below and equal the test levels**
- B) No loss of function is allowed after test. During the test, degradation of performance is allowed**
- C) Temporary loss of function is allowed.**

6. PRODUCT STANDARDS

All the questions in the generic standard should be answered in the product standard.

Phenomena Basic standards	Tests	AC- power	DC power	Enclosure	Signal Data	Earth
1000-4-2	ESD	- ³	g.n.a.	g.a.	g.n.a.	g.n.a.
1000-4-3	Radiated electromagnetic field >80MHz	g.n.a.	g.n.a.	g.a.	g.n.a.	g.n.a.
1000-4-4	EFT/Burst	g.a.	g.a.	-	g.a.	g.a.
1000-4-5	SURGE	g.a.	may	g.n.a.	may	may
1000-4-6	Conducted disturbances, induced by radio-frequency fields <80MHz	g.a.	g.a.	no	g.a.	g.a.
1000-4-7	General Guide on harmonics and inter-harmonics measurements and instrumentation	n.i.s.	n.i.s.	n.i.s.	n.i.s.	n.i.s.
1000-4-8	50/60 Hz Magnetic field	-	-	may	-	-
1000-4-9	SURGE Magnetic field	-	-	may	-	-
1000-4-10	Oscillatory Magnetic field	-	-	may	-	-
1000-4-11	Voltage dips and interruption	g.a.	-	-	-	-
1000-4-12	Oscillatory waves, ring wave*	may	g.n.a.	-	may	g.n.a.
1000-4-12	Oscillatory waves 1MHz	may	may	-	may	may
1000-4-13*	Harmonics, Inter-harmonics, Main Signaling	g.n.a.	-	-	g.n.a.	-
1000-4-14*	Voltage fluctuations	g.n.a.	-	-	-	-
1000-4-15	Flickermeter	n.i.s.	n.i.s.	n.i.s.	n.i.s.	n.i.s.
1000-4-16	Conducted disturbance in the range of DC to 150 kHz	g.n.a.	g.n.a.	-	g.n.a.	-
1000-4-17*	Ripple on DC power supply free	-	may	-	-	-
1000-4-18	free					
1000-4-20*	TEM cell	2	2	2	2	2
1000-4-21*	Reverberation chamber	2	2	2	2	2
1000-4-22	free					
1000-4-23*	Test methods for protective devices for HEMP radiated disturbance	g.n.a.	g.n.a.	g.n.a.	g.n.a.	g.n.a.
1000-4-24	Test methods for protective devices for HEMP conducted disturbance	g.n.a.	g.n.a.	g.n.a.	g.n.a.	g.n.a.
1000-4-25*	HEMP requirements and test methods for equipment and systems	g.n.a.	g.n.a.	g.n.a.	g.n.a.	g.n.a.
1000-4-26*	Calibration of probes and instruments for measuring electromagnetic fields	n.i.s.	n.i.s.	n.i.s.	n.i.s.	n.i.s.
1000-4-27*	Unbalance in 3phase mains	may	-	-	-	-
1000-4-28	Variation of power frequency	g.n.a.	-	-	-	-
1000-4-29*	Voltage dips and variation on d.c.	-	may	-	-	-
1000-4-30*	Measurements in the frequency range 2 kHz to 9 kHz	n.i.s.	n.i.s.	n.i.s.	n.i.s.	n.i.s.
1000-4-31*	Measurements in the frequency	n.i.s.	n.i.s.	n.i.s.	n.i.s.	n.i.s.

Legend:

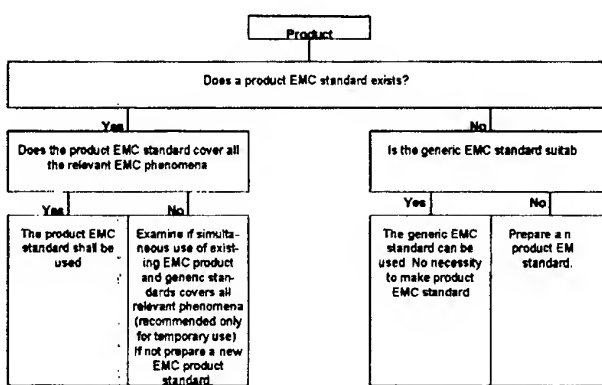
- | | |
|--------|---|
| n.i.s. | Not an immunity standard |
| g.a. | Generally applicable except in special cases |
| may | May be applicable in certain circumstances |
| g.n.a. | Generally not applicable except in special cases |
| * | The document is in progress but not finally published |
| 3 | Application not possible |

Within IEC more than 200 working group are discussing EMC aspects for their products.

7. CE MARK

The electronic equipment must be labelled with the CE mark for free circulation within the EC from 1st January 96 on.

To stick the CE mark onto an equipment, different immunity test and emission measurements must be made in accordance with the generic or product standards. Today the standards are in a transition period from generic to product standard. For manufacturers of electronic equipment it is very difficult to get the actual information about the status of the product-standard related to theirs product. Report R110-001:1993. The flowchart below is a copied from the CENELEC report R110-001:1993 and can be of help for taking decision.



The manufacturers of electronic equipment will consequently be compelled to conduct immunity tests. This will lead to an increased test volume. Large companies will automate their existing test equipment and will have to integrate their EMC tests into their quality assurance systems. Small and medium companies will most likely have to rely for their test needs on test houses and official test authorities.

One solution for the performance of fast, economic and well-documented EMC tests may be the use of automated test systems. EMC PARTNER AG has developed the TRANSIENT 1000 system, which allows the quick automation of the four most important transient immunity tests.

For a great number of electronic equipment all four immunity tests are required. If you need any further information about pulsed immunity test contact the authors.

8. REFERENCES:

K.Feser

Mikroelektronik, EMP-Phänomene und EMV-Probleme in unserer Technischen Gesellschaft.
Paper delivered at EMC-Symposium UNI Stuttgart/Germany 1988.

A. Rodewald / M. Lutz

Interference generated by switching operation and simulation.

Paper delivered at EMC Symposium Tokyo 1984

M. Lutz

The determination of the immunity to low energy transients ns-impulses (Burst) with the EFT Generator.

Syllabus for Technische Akademie in Esslingen / Germany

M. Lutz

The determination of the Immunity to high energy transients μ s-Impulse (SURGE) with the CWG Combination Wave Generator.

Syllabus for Technischen Akademie in Esslingen / Germany

M. Lutz

Determination of the immunity to electrostatic discharges ESD

Standards:

- IEC TC65 drafts and standards 801-x
- IEC TC77B drafts and standards 1000-4-x
- CENELEC TC 110 EN drafts and standards 61000-4-x; EN 50082-x

ABOUT THE AUTHOR:

Martin Lutz has over 20 years' experiences in the EMC domain and has served on various technical committees within the IEC and the Swiss national standardisation.

Martin Lutz is author of different technical EMC articles partly presented at IEEE EMC symposiums and co-author of EMC books. He holds a grad. Electrical Eng. of the Engineer University of Biel Switzerland.

Today Martin Lutz is president of EMC PARTNER AG Switzerland, one of the leading EMC equipment manufacturer in the world.

XVI WORKSHOPS

New Era of Communications Technologies - EMC Aspects

Workshop Organizer:

H. Kimball - USA

Speakers:

A. Rinker, Orbcomm - USA

P. Towler, Iridium - USA

T. Hayden, Teledesic - USA

Ch. Patuskey, Sky Station - USA

Information available during the Workshop

XVI
WORKSHOPS

EMC from Hewlett Packard

Workshop Organizer:

Hewlett Packard

Speaker: **B. Dougall**

Information available during the Workshop

XVI
W O R K S H O P S

**Penetration of EM Field Through
Shielding Materials and Components**

Workshop Organizer:

SPIRA Manufacturing Corp. - USA

Speaker: **G. M. Kunkel**

Information available during the Workshop

LIST OF EXHIBITORS

ABC ELEKTRONIK Sp. z o.o.

Kolejowa 10, PL-38-300 Gorlice, Poland
Phone: +48 18 3536 665, Fax: +48 18 3536 833

ASTAT Sp. z o.o.

Dąbrowskiego 461, PL-60-451 Poznań, Poland
Phone: +48 61 84 88 871, Fax: +48 61 84 88 276

DASAP POLSKA Sp. z o.o.

Obozowa 20, PL-01-161 Warsaw, Poland
Phone: +48 22 632 8146, Fax: +48 22 632 3716, E-mail: waw@dasap.pol.pl

ECOMP GmbH

Kloster-Langen-Strasse 22, D-26723 Emden-Wybelsum, Germany
Phone: +49 4921 9687-0, Fax: +49 4921 6032

ELSINCO-POLSKA Sp. z o.o.

Dziennikarska 6, PL-01-605 Warsaw, Poland
Phone: +48 22 396 979, Fax: +48 22 394 442, E-mail: elsincow@bevy.hsn.com.pl

EMERSON & CUMING MICROWAVE PRODUCTS N.V.

Nijverheidsstraat 7A, B-2260 Westerlo, Belgium
Phone: +32 14 562 500, Fax: +32 14 562 501, E-mail: ecmwprod@innet.be

HEWLETT-PACKARD POLSKA Sp. z o.o.

Jerozolimskie 181, PL-02-222 Warsaw, Poland
Phone: +48 22 608 7839, +48 22 608 7700 Fax: +48 22 608 7564

INSTITUTE OF TELECOMMUNICATIONS

WROCŁAW BRANCH

Swojczycka 38, PL-51-501 Wrocław, Poland
Phone: +48 71 483 0501, Fax: +48 71 729 375, E-mail: hlug@il.wroc.pl

PHOENIX CONTACT Sp. z o.o.

Szewska 3, PL-50-053 Wrocław, Poland

Phone: +48 71 343 9755, Fax: +48 71 343 9661,

E-mail: phoenixcontact@phoenixcontact.pl

ROHDE UND SCHWARZ OESTERREICH

Sonnleithnergasse 20, A-1100 Vienna, Austria

WARSAW OFFICE

Stawki 2, 00-193 Warsaw, Poland

Phone: +48 22 860 6490 to 6498, Fax: +48 22 860 6499

RST Sp. c.

Grunwaldzka 11/15, PL-15-893 Białystok, Poland

Phone: +48 85 455 400, Fax: +48 85 455 433

SCHROFF GmbH

Feldrennach, Langenalberstr. 96-100

D-75334 Straubenhardt, Germany

Phone: +49 70 82794-0, Fax: +49 70 82794-2 00

TECHTRONIC

Grabiszyńska 85, 53-503 Wrocław, Poland

Phone: +48 71 342 5856, Fax: +48 71 342 5021

UNIVERSAL ELEKTRONIK IMPORT GmbH

WARSAW OFFICE

Lektykarska 25/4, PL-01-687 Warsaw, Poland

Phone: +48 22 8330 716, Fax: +48 22 8331 059, E-mail: uei_war@uei.com.pl

UNITRONEX POLAND Sp. z o.o.

Grzybowska 87, PL-00-844 Warsaw, Poland

Phone: +48 22 631 2643, Fax: +48 22 632 7559

E-mail: kazikg@unitronex.com



PLUS GSM - TELECOMMUNICATION REVOLUTION

There are few inventions in the world which found their application in Poland so quickly. After merely five years from the launch of the first GSM network in Europe, results of the tender for construction of such network were announced in Poland. Polkomtel S.A., operator of Plus GSM network, came first receiving license number 1.

GENERALLY AVAILABLE AND OF HIGH QUALITY

Coverage

Today, that is only two years after receiving the license, Plus GSM has almost 400 thousand subscribers. The network operates on 70% of the territory of Poland and 80% of the Polish population may use its services. Several hundred cities and thousands of kilometers of roads connecting those cities are covered. By the end of 1998 we plan to extend our coverage to 85% of the territory of Poland and 90% of its population. We assume that by the turn of the century more than a million subscribers will be using Plus GSM network.

Roaming

International roaming, the service determining the global nature of the GSM system, is expanding at a really record speed. Within 8 months from commercial launch Plus GSM network offered roaming with 50 foreign operators, and within less than eighteen months with as many as 50 countries. These achievements are two world records. In April 1998 the Plus GSM network offered its subscribers the possibility of using their own handsets and SIM cards in 61 countries in Europe, Asia, Africa, Australia and Oceania and USA. This is the broadest roaming offer on the Polish telecommunication market.

Services

Since the beginning of its operations the Plus GSM network has offered its subscribers a wide range of value added services and expanded it systematically. Subscribers may use voice mail, conference calls, SMS, data and fax, calling line identification presentation, call hold, barring calls, etc. New services will be launched soon offering information services (the first service of this type was provided last year during Tour de Pologne), closed user groups, etc. The scope of grows systematically and in near future will involve internet, multimedia, various forms of cooperation between telecommunication systems and computer networks. Plus GSM network provides its subscribers with an effective information tool whose widespread in Poland entails serious civilization, economic and cultural consequences. A measure of Plus GSM success is customer satisfaction resulting from the fact that they receive services they need and where they need them. A sign of our care about the subscriber is also the Customer Operations Department available 24 hours a day, 365 days a year. Consultants who work there are able to help subscribers and solve their problems related to using Plus GSM network. Also "Plus GSM Magazine", a publication designed to improve information exchange between subscribers and the operator, provides some useful guidance. It contains descriptions of new services and equipment, practical advice, updated information on coverage and roaming, etc. Every subscriber receives a copy "Plus GSM Magazine" free of charge together with the bill.

Prices and pricing plans

Plus GSM offers several pricing plans with varying levels of monthly access fee and call prices. Market research revealed that within the target group of potential customers three subgroups could be distinguished depending on the

intended usage of the telephone. As a logical consequence of such findings of the survey three pricing plans were introduced: Contact, Business and Prestige. Their names clearly identify the plan with the target subgroup. The structure of prices and pricing plans adopted by Plus GSM is undoubtedly most transparent for potential customers who are comparing competitive offers. Simplicity of estimating costs before the actual purchase of a SIM card and a telephone, combined with competitiveness of the offer itself was appreciated by the market and facilitated decision-taking to hundreds of subscribers. Each pricing plan offers lower charges for calls between mobile telephones owned by the same person (or firm) and for calls to voice mail.

Sales

Services of Plus GSM network are offered through 9 company shops located in major Polish cities and though more than 450 points run by comprehensively trained Authorized Representatives. They offer our subscribers assistance and professional advice. Long term network roll-out strategy adopted by Plus GSM proved to be effective. It is also to a significant extent thanks to our reliable business partners, who create the right conditions for display of services, that the growth of the subscriber base is so dynamic and that our subscriber number increased sixfold in 1997.

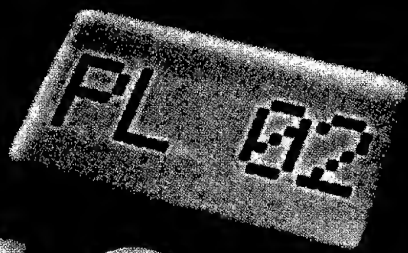
State-of-the-art technology

Capital, however necessary for such an immense investment as GSM network construction, is only one of the elements determining the present and the future of Plus GSM. People who create this network and service it are equally important. They cooperate with vendors providing most modern world technologies and computer hardware. They develop extremely complex software adjusted to the continually expanding range of services available through the GSM system. Many of these developments are still at the stage of preparations and testing as we are still at the beginning of the information civilization age. By installing the most modern infrastructure and by investing in people, Plus GSM wants to be an operator who will be able to immediately implement latest telecommunication solutions, i.e. it takes care of every aspect of what is included in the definition of an operator providing widest range of top quality services. Cooperation of Plus GSM network with world leading manufacturers and vendors of equipment and software serves this purpose. Among our partners there are Nokia Communications, which is the main vendor of technical infrastructure, Lucent Technologies, Digital, Hewlett Packard, IBM, AMS and others. Thanks to cooperation with those partners the network was provided with state-of the art equipment for network maintenance center, software for customer operations department, and our voice mail and billing systems are among the most efficient in Europe. This, combined with the open nature of the GSM standard, guarantees smooth functioning for many years and will enable us to connect further hundreds of subscribers.

----- * -----

Plus GSM strive for perfection in its operations on the Polish GSM market was recognized by the Polish business community. Recently, in the presence of President of Poland and NATO's Secretary General Javier Solana, Polish Business Club awarded Polkomtel S.A. the title of the company of the year 1997. The justification stated that this is a dynamic company, professionally managed and contributing immense benefits to the Polish economy.

Your network choice



it's like
being there



Era GSM, the leading network operator, is pleased to welcome foreign visitors coming to Poland to freely use their GSM telephones and enjoy the quality of Era GSM network. You will be pleased with the service you receive from us. Just click your mobile to Era GSM by selecting **PL 02 or 260 02**.

Our current Era GSM users can also take their telephones abroad and have the ability to speak freely in Andorra, Australia, Austria, Azerbaijan, Bahrain, Belgium, Bosnia-Herzegovina, Bulgaria, Croatia, Cyprus, Czech Republic, Denmark, Estonia, Finland, France, Georgia, Germany, Gibraltar, Greece, Guernsey, Hong Kong, Hungary, Iceland, Indonesia, Ireland, Italy, Kuwait, Latvia, Lebanon, Lithuania, Luxembourg, Macau, Macedonia, Malaysia, Monaco, Netherlands, New Zealand, Norway, Portugal, Romania, Russia (Moscow, St Petersburg), Serbia, Singapore, Slovakia, Slovenia, South Africa, Spain, Sri Lanka, Sweden, Switzerland, United Kingdom, Ukraine, USA (New York, New Jersey), Taiwan, Thailand, Turkey and Yugoslavia just to name a few... For your convenience, your billing will also be in PLN via Era GSM.

Era GSM is the first operating Polish GSM network.
Call customer hotline anytime on 0 800 22 900 or from Era GSM phone: 602 900.
Internet: <http://www.eragsm.com.pl>



EMERSON & CUMING

MICROWAVE PRODUCTS



Nijverheidsstraat 7A - 2260 Westerlo - Belgium Tel. 32-14-562500 Fax 32-14-562501

Head Office
Germany
Potsdamer Str. 18A
D-14513 Teltow
(near Berlin)
Tel: +49 3328 430 141
Fax: +49 3328 430 142

EURO EMC SERVICE®



Dr. Hansen GmbH

Branch Offices
Europe
North America
Asia
Australia

Approval & Testing
EMC
Telecom / Radio
Product Safety
Low Voltage Directive (LVD)
Automotive Testing (e Mark)



Mail Order Service
Cost effective, fully automated,
speedy testing of your
smaller products.
Send your products to EES by
express delivery and we will
start testing immediately.

ELECTROMAGNETIC COMPATIBILITY

<http://www.euro-emc-service.de>

Internet

CERTIFICATION EES TESTING

e-mail

euro.emc.service@t-online.de

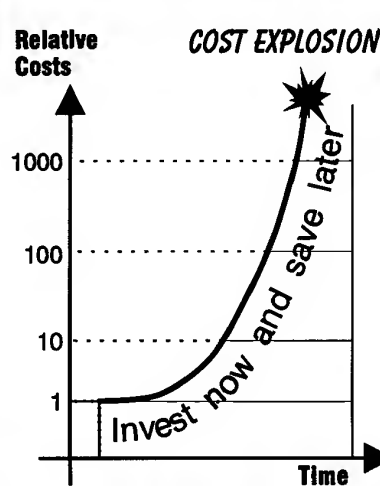
FIXING & MODIFICATION SERVICE

Certification

**Electronic & Electrical
Products
Large
Installations & Systems**

**Competent Body assesses a
TCF under art. 10.2 of
89/336/EEC if:**

- No harmonised standards
- Standards in part only
- Standard not practical
- Product variants exist
- Foreign certificates exist



Testing

**EMC Directive
89/336/EEC
Mandatory
1 January 1996**

- Our test laboratories are accredited for all sectors in accordance with EN45001
- We operate a 3 shift, 24 hour testing service
- We can audit your test results on-site: save transport costs!
- OATS: 10, 30, 100 & 300m



**EMC
Competent Body**

**EMC Accredited
Test Laboratory**

